

AD-A235 006



MINUTES OF THE TWENTY-FOURTH EXPLOSIVES SAFETY SEMINAR

Volume II



DTIC

APR 1 1991

C

D

**Adam's Mark Hotel
St. Louis, Missouri
28-30 August 1990**

EX-100 COPY

**Sponsored By
Department of Defense Explosives Safety Board
Alexandria, Virginia**

91 4 09 1,10

**MINUTES OF THE
TWENTY-FOURTH EXPLOSIVES SAFETY SEMINAR**

Volume II

**Adam's Mark Hotel
St. Louis, Missouri**

28 - 30 August 1990

Accession for	
Serial	<input checked="checked" type="checkbox"/>
Index	<input type="checkbox"/>
File	<input type="checkbox"/>
Journal	<input type="checkbox"/>
By	
Director	<input type="checkbox"/>
Assoc.	<input type="checkbox"/>
Dist	
A-1	

Sponsored by

**Department of Defense Explosives Safety Board
Alexandria, Virginia 22331-0600**

Approved for public release; distribution unlimited

TABLE OF CONTENTS

VOLUME II

SESSION - KLOTZ CLUB UNDERGROUND TESTING I

Moderator: Arnfinn Jenssen

**Shallow Underground Tunnel/Chamber Explosion
Test, Executive Summary of Results.....1193**
Charles E. Joachim

**Tunnel Pressure and Emergent Blast Calculations
for the Shallow-Buried China Lake Test.....1215**
Charles Needham, K. Schneider, J. Crepeau, L. Kennedy

**Accidental Detonation in Underground Munitions
Storage Magazines: Prediction of Cover
Rupture Overpressures.....1227**
Charles E. Joachim

**Ejecta Hazard Ranges from Underground Munitions
Storage Magazines.....1241**
Charles E. Joachim

SESSION - LIQUID EXPLOSION HAZARDS

Moderator: Mel Hudson

**Mixing of Liquid Cryogens in the Simulation
of Liquid Hydrogen/Liquid Oxygen
Explosion Hazards.....1265**
T. S. Luchik, K. M. Aaron, E. Y. Kwak,
P. Shakkottai, L. H. Black

**Hot Spot Mechanism in Bubble Sensitized
Commercial Explosives.....1291**
S. K. Chan, Kuo K. Feng

**Explosive Safety Testing at New Mexico Tech:
The Brower Adiabatic Compression Test.....1315**
K. R. Brower, D. B. Olson, P. A. Persson

SESSION - EXPLOSION PROPAGATION TESTS

Moderator: Carl Halsey

**Propagation and Fire Tests Conducted on a Secondary
Steel Container Designed for Movement of Chemical
Agent Artillery Projectiles.....1333**
Daniel B. Hill

Mass Detonation Hazard Assessment from Violently
Deflagrating Munitions.....1363
M. Chick

SESSION - KLOTZ CLUB UNDERGROUND TESTING II

Moderator: N. J. M. Rees

Continued Klotz Club Tests.....1385
Bengt E. Vretblad

Pre- and Post-Test Calculations for the
Aelvdalen 5000-kg Tests.....1405
Lynn W. Kennedy, K. D. Schneider, J. E. Crepeau,
C. Needham

Loads Prediction Program for Accidental Explosions
in Underground Munitions Storage Facilities.....1417
Arnfinn Jenssen, C. Canada, C. Needham, L. Kennedy

SESSION - EXPLOSION HAZARDS REDUCTION

Moderator: Phil McLain

Understanding the Risk of Ammunition Kickout
from Explosion Suppressive Structures.....1429
Richard B. Shipe

Test Data on the Storage of Mixed Munitions in
Conex Containers.....1449
William Lawrence

The Blast and Fragment Resistant Construction System
(BFR) for Ammunition Quickload Program.....1487
Yaakov Yerushalmi

SESSION - LIGHTNING PROTECTION II

Moderator: John Eddy

A Microphysical Model for the Electrostatic
Discharge Susceptibility of Solid
Rocket Propellants.....1493
Ronald W. Larson, R. A. Perala, M. F. Gyure, P. Beale

Operational System for Advanced Lightning Warning.....1513
Philippe Richard

Development of a DoD Handbook on Inspection and
Testing of Lightning Protection
and Grounding Systems.....1521
Mitchell A. Guthrie

TABLE OF CONTENTS

VOLUME II

SESSION - KLOTZ CLUB UNDERGROUND TESTING I

Moderator: Arnfinn Jenssen

Shallow Underground Tunnel/Chamber Explosion
Test, Executive Summary of Results.....1193
Charles E. Joachim

Tunnel Pressure and Emergent Blast Calculations
for the Shallow-Buried China Lake Test.....1215
Charles Needham, K. Schneider, J. Crepeau, L. Kennedy

Accidental Detonation in Underground Munitions
Storage Magazines: Prediction of Cover
Rupture Overpressures.....1227
Charles E. Joachim

Ejecta Hazard Ranges from Underground Munitions
Storage Magazines.....1241
Charles E. Joachim

SESSION - LIQUID EXPLOSION HAZARDS

Moderator: Mel Hudson

Mixing of Liquid Cryogens in the Simulation
of Liquid Hydrogen/Liquid Oxygen
Explosion Hazards.....1265
T. S. Luchik, K. M. Aaron, E. Y. Kwak,
P. Shakkottai, L. H. Black

Hot Spot Mechanism in Bubble Sensitized
Commercial Explosives.....1291
S. K. Chan, Kuo K. Feng

Explosive Safety Testing at New Mexico Tech:
The Brower Adiabatic Compression Test.....1315
K. R. Brower, D. B. Olson, P. A. Persson

SESSION - EXPLOSION PROPAGATION TESTS

Moderator: Carl Halsey

Propagation and Fire Tests Conducted on a Secondary
Steel Container Designed for Movement of Chemical
Agent Artillery Projectiles.....1333
Daniel B. Hill

Mass Detonation Hazard Assessment from Violently
Deflagrating Munitions.....1363
M. Chick

SESSION - KLOTZ CLUB UNDERGROUND TESTING II

Moderator: N. J. M. Rees

Continued Klotz Club Tests.....1385
Bengt E. Vretblad

Pre- and Post-Test Calculations for the
Aelvdalen 5000-kg Tests.....1405
Lynn W. Kennedy, K. D. Schneider, J. E. Crepeau,
C. Needham

Loads Prediction Program for Accidental Explosions
in Underground Munitions Storage Facilities.....1417
Arnfinn Jenssen, C. Canada, C. Needham, L. Kennedy

SESSION - EXPLOSION HAZARDS REDUCTION

Moderator: Phil McLain

Understanding the Risk of Ammunition Kickout
from Explosion Suppressive Structures.....1429
Richard B. Shipe

Test Data on the Storage of Mixed Munitions in
Conex Containers.....1449
William Lawrence

The Blast and Fragment Resistant Construction System
(BFR) for Ammunition Quickload Program.....1487
Yaakov Yerushalmi

SESSION - LIGHTNING PROTECTION II

Moderator: John Eddy

A Microphysical Model for the Electrostatic
Discharge Susceptibility of Solid
Rocket Propellants.....1493
Ronald W. Larson, R. A. Perala, M. F. Gyure, P. Beale

Operational System for Advanced Lightning Warning.....1513
Philippe Richard

Development of a DoD Handbook on Inspection and
Testing of Lightning Protection
and Grounding Systems.....1521
Mitchell A. Guthrie

SESSION - ACCIDENTS I

Moderator: Carlo Ferraro

Safety Management in the Explosives Industry.....1543
G. E. Williamson

**Investigation of an Explosive Accident Using
Simulation as a Tool.....1551**
J. F. Drolet, G. Couture, R. Farinaccio

**Ammunition Accidents - Their Causes,
Investigation and Prevention.....1565**
Lt Col A. J. Morley, Maj D. C. Hewitt

**Report on the Peterborough Explosion -
Blast Damage and Injuries.....1573**
Roy Merrifield

SESSION - EXPLOSION CONTAINMENT

Moderator: Paul Price

**Totally Contained High Explosive Test
Facility Site 300.....1597**
C. F. Baker

Test and Evaluation of a 1-kg Storage Magazine.....1625
A. Weston and E. L. Lee

Autoclave Explosion and Protection Analysis.....1659
Kathy H. Spivey

**"Designing for Explosive Safety" The Explosive
Components Facility at Sandia
National Laboratories.....1669**
William A. Couch

Vented Suppressive Shielding.....1681
Dr. D. J. Katsanis

SESSION - UNEXPLODED ORDNANCE CLEARANCE

Moderator: Michael M. Swisdak, Jr.

**Application of Risk Assessment Techniques to Evaluate
Public Risk and Establish Priorities for Clean-up of
Ordnance at Formerly Used Defense Sites.....1693**
C. David Douthat

**Remediation of Ordnance Contamination at the
Tierrasanta Community, San Diego, California.....1709**
Bill Chaffin

Overview of the Mandatory Center of Expertise and
Design Center for Explosive Ordnance Engineering.....1719
Robert G. Wilcox

SESSION - ACCIDENTS II
Moderator: Eric Olson

Results of an Accidental Explosion in a Propellant
Process Building.....1729
Boimel Arie

Magazine Fire - Hawthorne Army Ammunition Plant -
9 August 1989.....1761
Robert A. Loyd

Blast Yield Estimation for the PEPCON Ammonium
Perchlorate Accidental Explosions.....2481
Wilfred Baker, Quentin Baker, Kathy Spivey

SESSION - DEBRIS HAZARDS I
Moderator: Fred Krach

Scaled Debris Throw Tests of Norwegian/US
Aircraft Shelters.....1813
Patricia Bowles, K. A. Marchand, J. W. Strybos

Joint Australian-UK Stack Fragmentation Trails,
Phase 4 Preliminary Report.....1829
Jon Henderson

TRAJ - A Two Dimensional Trajectory Program for
Personal Computers.....1853
Paul E. Montanaro

SESSION - SITE PLANS AND SURVEYS
Moderator: John Byrd

Data Management/Communications.....1881
John R. Thompson

Explosive Safety Siting of Corps of Engineers
Standard Igloo Designs.....1929
Earl H. Williams, Adib Farsoun, Wallace Watanabe

World-Wide Port Survey.....1945
Gary W. Abrisz

Air Force Logistics Command Automated Explosive
Site Planning.....2011
William E. Rieder

Explosive Safety Training.....2025
Barbara J. Overton

SESSION - EXPLOSIVES MANUFACTURING CONSIDERATIONS

Moderator: Ken Siler

Twin Screw Extruder Safety Demonstration Tests.....2073
David R. Dillehay

Special Study of Safety in Pyrotechnics Manufacturing.....2081
John A. Johnson

**Design, Installation, and Maintenance of Ultra High
Speed Deluge Systems for Ordnance Facilities.....2101**
Robert A. Loyd

Pyro Suit System-Review and Update on Field Use.....2139
Stephen J. Asthalter

SESSION - DEBRIS HAZARDS II

Moderator: J. E. Meyers

**Procedures for the Analysis of the Debris Produced by
Explosion Events.....2159**
Michael M. Swisdak, Jr.

Building Debris Hazard Prediction Model.....2177
Patricia Bowles, Charles J. Oswald

**Development of Predictive Methods from Test Data for
Breakup of Building Components and Debris Roll.....2191**
Charles Oswald

Building Debris Hazard Evaluation Test Program.....2207
Patricia Bowles, Luis M. Vargas, Charles J. Oswald

SESSION - SPACE VEHICLE EXPLOSIVE HAZARDS

Moderator: Wayne Frazier

**The Hazard of an Explosion of the ARIANE 5 Launcher
The Risks for the Astronauts Sitting on the
Ejector Seats.....2227**
Michel Rouze

SESSION - CONCRETE RESPONSE TESTING

Moderator: Sam Kiger

**Critical Failure of Concrete Slabs Due to
Contact Charges.....2243**
R. J. M. van Amelsfort, J. Weerheijm, G. Opschoor

**Experiments Used for Comparison of Blast Damage to Full
Scale and One-Fourth Scale Reinforced Concrete
Structures.....2263**
Rickard Forsen

Behaviour of Concrete on High Velocity Impact.....2277
R. A. Goel, S. Chandra, U. C. Chandola,
A. K. Abrol, R. Kumar

**Vulnerability Assessment of Structurally Damaging
Impulses and Pressures.....2301**
Frank B. Tatom, John W. Tatom

**Charge Calculation for Underwater Blast Demolition
and Its Application.....2317**
He Chengzhi, Li Zheng, Wang Zhongqian

SESSION - FAR-FIELD AIRBLAST EFFECTS

Moderator: R. Lorenz

Noise Abatement at FMC Hollister Site.....2333
Kathy H. Spivey, Wilfred E. Baker

Prediction of Acoustic Focusing Hazard in the Atmosphere...2247
Gil Smith

**An Operational Prediction for Far-Field Airblast
Effects: Practical Experience at Caepe2259**
J. Sauvel, J. Vermorel

**Program "BLASTO" for Weather-Dependent Airblast
Predictions.....2281**
Jack W. Reed

SESSION - FRAGMENT HAZARDS

Moderator: John Rodriguez

**Drag Coefficient Measurements for Typical Bomb and
Projectile Fragments.....2393**
Miles C. Miller

Fragment Mass Distribution of Debris.....2403
Manfred Held

A Comparison of Two Personnel Injury Criteria Based on Fragmentation.....	2423
Frank McCleskey	
An Investigation of Fragment Stopping Barricades.....	2443
Frank McCleskey	
Blast Yield Estimation for the PEPCON Ammonium Perchlorate Accidental Explosions.....	2481
Wilfred Baker, Quentin Baker, Kathy Spivey	

APPENDIX A

I. CLOSING REMARKS

A. Colonel Jack Mathews, Chairman.....	2491
Department of Defense Explosives Safety Board	
B. Brigadier Robin C. Armstrong, Chairman, Explosives Storage and Transport Committee (ESTC) ..	2493

II. ATTENDANCE LIST.....2501

SHALLOW UNDERGROUND TUNNEL/CHAMBER EXPLOSION TEST

Charles E. Joachim
U.S. Army Engineer Waterways Experiment Station
Vicksburg, Mississippi

INTRODUCTION

A considerable amount of research has been performed in the last two decades to develop a technical data base and methods to predict the airblast and ejecta/debris hazards from accidental explosions in underground magazines. Much of the work was concerned with detonations in magazines so deep that venting of the detonation through the magazine cover rock does not occur. The effect of cover venting on the reduction of external airblast from the entrance portal has been demonstrated in small-scale tests performed in the United Kingdom (Millington, 1985). The Shallow Underground Tunnel/Chamber Test Program was designed to provide large-scale airblast and ejecta/debris effects from a detonation of 20,000-kg (net explosive weight) in a shallow underground magazine.

The test program was primarily funded on an equal share basis by three organizations: the U.S. Department of Defense Explosives Safety Board; the Safety Services Organisation of the Ministry of Defence, United Kingdom; and the Norwegian Defence Construction Service. Additional funds were provided by the Pyrotechnie Saint Nicolas, France; the Royal Swedish Fortifications Administration, Sweden; and the Amt fur Bundesbauten, Switzerland, to expand the scope of blast instrumentation and debris measurements.

This paper summarizes the hazard analyses (Joachim, 1990) based on the technical data acquired during the test.

OBJECTIVE

The overall objective of the test program was to determine the hazardous effects (debris, airblast, and ground shock) produced by a simulated accidental detonation of explosive stores which ruptures the overhead cover of the underground chamber. The results will be used to evaluate and validate quantity-distance (Q-D) safety standards for underground storage of munitions.

DESCRIPTION OF TEST

The Shallow Underground Tunnel/Chamber Explosion Test Program involved the detonation of a 20,000-kg charge of Composition B explosive, simulating the accidental explosion of ammunition stored inside an underground magazine in granitic rock. A large-scale storage chamber and access tunnel were constructed for this test at a selected site on the Naval Weapons Center test range at China Lake, CA (Halsey, et al, 1989). For the TNT-equivalent (1.1 equivalence factor) 20,000-kg net explosive weight (NEW), the chamber loading density was 66.4 kg/m^3 . The storage chamber (with the 20,000-kg explosive charge) and access tunnel are shown in plan and profile in Figure 1. Active measurements included (1) internal chamber and access tunnel airblast pressures, (2) free-field overpressure along the 0, 30, 45, 60, 90, and 180-degree azimuths, measured from the tunnel portal, (3) beta densitometer/general purpose blast stations at the 75-m range along the 15, 30, and 60-degree azimuths, and (4) ground motion measurements along the 0, 90, and 180-degree azimuths (note: the 0-degree azimuth is the extension of the tunnel axis beyond the portal). Passive airblast and ejecta/debris measurement devices consisted of blast cubes, wire drag gages, smoke puffs, and artificial missiles. In addition, an ejecta collection study was performed and motion picture film analyzed to quantify the ejecta missile ranges.

AIRBLAST INHABITED BUILDING DISTANCE

The distances required for protection of inhabited areas from airblast and debris depends, to a large degree, on the depth of overburden over the storage chamber. The chamber cover depth for the Shallow Underground Tunnel/Chamber Explosion Test ranged from 9.4 to 13.7 m (scaled cover depth from 0.34 to $0.49 \text{ m/kg}^{1/3}$). The minimum scaled cover depth required to ensure containment of the explosion (except for gas venting through the access tunnel), and to ensure that no significant surface disruption occurs, is $1.4 \text{ m/kg}^{1/3}$ in the current DOD Explosives Safety Standards (DOD 6055.9-STD) and $0.2 \text{ m/kg}^{1/3}$ in the Manual on NATO Safety Principles (NATO AC/258). For overburden depths less than this, the Standards require consideration of both airblast and debris effects. When the actual scaled overburden depth is less than $0.2 \text{ m/kg}^{1/3}$, the Standards state that the airblast at large distances may

not be appreciably reduced from that of a surface burst. Thus, the scaled cover depth for this test fell between these limits, and the Standards (DOD 6055.9-STD) require that airblast and debris projection must be considered in the Q-D hazard analysis. However, the scaled cover depth exceeded the NATO AC/258 minimum scaled cover depth. Therefore, the NATO criteria require consideration of debris and ground shock hazards for the Tunnel/Chamber test.

The present DOD Standards use two different airblast pressure criteria to define Inhabited Building Distances--5 kPa (0.73 psi) for underground storage, and 6.2 kPa (0.9 psi) for open or other above-ground storage. For the 22,000-kg NEW detonated in the Shallow Underground Tunnel/Chamber Explosion Test, the distances to these two pressure contours as given in the present Standards (DOD 6055.9-STD) are shown in Figure 2. For comparison, Figure 2 also shows the actual distances to the 5 and 6.2 kPa pressure contours that were defined by measured pressures on the Tunnel/Chamber Test. Since overpressures were not measured along the 120-degree radial on the test, the distance to the 5 and 6.2 kPa contours along the 120-degree azimuth were assumed to be the same as on the 180-degree azimuth.

As also shown in Figure 2, the distance along the extended tunnel axis to the 6.2-kPa overpressure level indicated by the test data is close to the airblast Inhabited Building Distance specified by the present Standards for above-ground storage ($20 Q^{1/3}$). The off-axis distance to the measured 6.2-kPa level is approximately two-thirds the distance specified by the Standards for above-ground storage at 30 degrees, 61 percent at 60 degrees, 50 percent at 90 degrees, and 20 percent at 180 degrees.

Figure 3 compares the Inhabited Building Distances, derived from the Standards and from test data, as a function of azimuth. The measured distance to the 5-kPa peak pressure on the Tunnel/Chamber tests falls well within the airblast Inhabited Building Distance specified in the Standards. The measured distance to the 5-kPa pressure level was 75 percent of the distance the Standards call for along the 0-degree azimuth, 58 percent at 30 degrees, 71 percent at 60 degrees, 88 percent at 90 degrees, and 68 percent at 180 degrees. Thus, except over the arc that extends from 120 degrees to approximately 150 degrees, the present airblast Inhabited Building Distance can be seen to be generally conservative for underground magazines with

geometries and loading densities similar to the Shallow Underground Tunnel/Chamber Explosion Test.

In 1987, a 4,540-kg ANFO charge (3,815-kg TNT-equivalent NEW) was detonated in a KLOTZ Club test in an underground tunnel/chamber test facility at Alvdalen, Sweden (Vretblad, 1988). Figure 4 shows the measured distances to the 5 and 6.2-kPa overpressure contours for this test. Also shown are the 5-kPa contour specified by the present Standards (DOD 6055.9-STD) for underground storage of the 3,815-kg NEW tested at Alvdalen, and the 6.2-kPa contour specified by the Standards for above-ground storage of the same NEW.

Along the extended tunnel axis (0-degree azimuth), the measured distance to the 5-kPa pressure was 85 percent of the distance specified by the Standards. Off-axis (Figure 5), the measured distance was 80 percent of the current Standard at 45 degrees from the tunnel axis, 41 percent at 75 degrees, 13 percent at 110 degrees, and 11 percent at 180 degrees. The comparison in Figure 4 also shows that the measured distance to the 6.2-kPa overpressure for the Alvdalen test is far less than that specified by the current Standards for Inhabited Building Distance from above-ground explosions.

In Figure 6, the Inhabited Building Distance (distance to the 5-kPa overpressure level) derived from the Shallow Underground Tunnel/Chamber test data is plotted versus loading density, where loading density is the NEW in the chamber divided by the total volume (chamber plus access tunnel). The Alvdalen test in Sweden was conducted in an underground complex containing two chambers, as depicted in Figure 4. The overburden depths were sufficient to prevent rupture of the detonation chamber. Total volume for this tunnel/chamber system was taken as the volume of the loaded chamber, plus the volume of the access tunnel through which the airblast exited to the portal (disregarding the volume of the second empty, chamber).

Table 1 compares the Inhabited Building Distances for airblast specified by the current Standards with those indicated by the Tunnel/Chamber test and Alvdalen tests. Note that, as a maximum, the hazard area indicated by the test data is less than half that required by the Standards.

A series of model tests were conducted at WES on small-scale munition storage magazines. The WES model (Smith, et al, 1989) consisted of a small-

scale (1:75 scale) tunnel and magazine cast into a large concrete block. Since there was no rupture of the concrete block (simulating the magazine overburden) over the range of loading densities tested (Figure 6), no venting through the chamber cover occurred. This resulted in higher free-field airblast overpressures from the tunnel entrance, which gave significantly greater Inhabited Building Distances than implied by either the Norwegian model or the full-scale Tunnel/Chamber Test, both of which vented through the cover.

GROUND MOTION HAZARD RANGE

For the Shallow Underground Tunnel/Chamber Test, the measured compressional wave velocity of the rock mass in the region of the explosive storage chamber ranged from 944 to 1,526 m/s, with an average value of 1,309 m/s (Halsey, 1989). These values are more typical of compressional wave velocities in soil, rather than in solid rock, and indicated that the rock at the Tunnel/Chamber site was heavily jointed and weathered. The plot of the ground motion arrival time recorded on the test (Figure 7) indicates a higher compressional wave velocity (2,166 m/s), implying the existence of less weathered, more competent rock at depth. This value is within the compressional wave velocity range for material described in the Standards as soft rock.

Data points for maximum particle velocity vectors measured on the Tunnel/Chamber Test are plotted in Figure 8 as a function of slant distance from the center of the chamber. The velocity curve given by Vretblad (1988) falls slightly below the measured data along the 0-degree azimuth (i.e., the extended tunnel axis), but closely matches the far-field data in other directions.

The gages beyond the 100-m range along the 0-degree azimuth in the Tunnel/Chamber Test were emplaced in desert alluvium soil in the valley floor in front of the tunnel, while the gages in other directions were emplaced on the rock surface. Using the criterion of 6.1 cm/s and the equation given in the Standards (Section G.4.d.(1)) for soft rock, the calculated Inhabited Building Distance for ground shock should be 160 m. Based on an interpolation of the data, the Tunnel/Chamber test results indicate that the 6.1 cm/s level

occurred at a distance of 580 m. For the 90 and 180-degree azimuths, the test measurements indicate a range of 155 m.

The NATO (AC/258) Inhabited Building Distances for ground shock are also displayed in Figure 8. The NATO criteria specifies levels of damage that occur at certain peak particle velocity thresholds--5 cm/s (threshold of no damage), 14 cm/s (minor damage), and 19 cm/s (major damage). These values are independent of velocity direction or earth media. The NATO Inhabited Building Distances for major damage from a detonation corresponding to the Shallow Underground Tunnel/Chamber Explosion Test are 300 m in soil (0-degree azimuth) and 120 m in rock.

There are two dominant factors associated with the Tunnel/Chamber Test that may explain the discrepancies between the predicted and the measured ranges to the 6.1-cm/s level of ground shock along the 0-degree azimuth. The first is the fact that the gages along the 0-degree azimuth were emplaced in soil, rather than rock. Since the detonation chamber was surrounded by rock, the use of the relation for soil in the Standards is obviously inappropriate. On the other hand, the use of the relation for soft rock does not take into account the effect of the soil layer overlying the bed rock along the 0-degree radial, in front of the tunnel opening.

The second factor is the apparent fact that the ground motions recorded by the gages on the 0-degree azimuth were predominately induced by airblast issuing from the tunnel portal. This is indicated by the arrival times of the ground motions at the gage locations, which match the arrival times recorded by the airblast gages along the 0-degree azimuth. Thus, it is obvious that the direct-induced motions transmitted to the gages in front of the tunnel, through the bedrock initially and then through the overlying soil, were completely obscured by the strong airblast-induced motions.

Figure 8 also shows a prediction curve from NATO AC/258 that does account for airblast-induced motions. This curve is based on the equation

$$v_v = P / \rho c_p \quad (1)$$

where v_v is the vertical velocity of motion, m/s

P is the airblast overpressure at the location of interest, Pa
 ρ is the density of the material, kg/m³
and c_p is the wave velocity of the material, m/s
In NATO AC/258, c_p is defined as the seismic velocity of the material.
However, Hadala (1973) found that the stress wave velocity is actually the controlling parameter in regions where the airblast-induced motions outrun the direct-induced ground shock. Using a typical stress wave velocity for desert alluvium and the overpressures measured on the Tunnel/Chamber Test, a prediction curve for airblast-induced ground motion velocity based on Equation 1 is shown in Figure 8. While the curve obviously overpredicts the close-in motions directly in front of the tunnel portal, it comes within 50 percent or so of matching the measured velocities on the 0-degree azimuth at the distances of interest for ground shock hazard definition.

A final comparison made in Figure 8 is with the curve established for ground shock velocity by Vretblad (1988), based on the results of the Alvdalen tests in Sweden. Vretblad's equation provides a better fit to the off-axis ground shock data at the ranges of interest for the Tunnel/Chamber Test, but still underpredicts the motions measured at the most distant gages.

In summary, the NATO AC/258 equation for airblast-induced motions provides the best fit to the data along the 0-degree azimuth for the Tunnel/Chamber Test, at the ranges of interest for defining the Inhabited Building Distance. For other off-axis directions, the NATO AC/258 equation for direct-induced motions and Vretblad's equation both closely predict the motions measured on the Tunnel/Chamber Test at ranges of interest. In all cases, however, the values predicted by these methods should be increased by a factor of two to provide a safe upper bound of the motions measured on the test.

EJECTA/DEBRIS HAZARDS

The DOD Explosives Safety Standards and the NATO AC/258 debris hazard criteria consider two sources of hazardous debris--material blown through the access tunnel portal and rock thrown by the overburden rupture. The Explosives Safety Standards require an Inhabited Building Distance for debris of 610 m along and 15 degrees either side of the extended access tunnel

centerline. The NATO AC/258 debris Inhabited Building Distance is 600 m over the same 30-degree arc.

The current Explosives Safety Standards (DOD 6055.9-STD) criterion for debris hazard range is the distance to a fragment or debris density of one hazardous particle per 56 m². Analysis of the debris on the motion picture records of the Tunnel/Chamber Test indicates that almost all debris seen on the film is potentially lethal (kinetic energy greater than 79 J), and thus considered hazardous. As shown in Figure 9, a debris density of one missile impact per 56 m² occurred at a distance of 656 m. For debris originating from rupture of the cover, the Standards give a hazard range of 236 m. Similarly the NATO AC/258 criteria predict a hazard range of 246 m from cover rupture.

The debris and ejecta collection on the Tunnel/Chamber Test was concentrated within a sector extending 45 degrees each side of the extended tunnel axis; therefore the effect of azimuth on debris range can only be based on data within this sector. These data are shown in Figure 9, where curves are drawn to approximate the debris limits at 0, 20, and 40 degrees. As shown here, the distance to a debris density of one strike per 56 m² is 656 m, 447 m, and 287 m along the 0, 20, and 40-degree azimuths, respectively. For the Tunnel/Chamber Test configuration, Figure 10 compares debris hazard range, as a function of azimuth, based on criteria given in the Explosives Safety Standards and NATO AC/258, with ranges derived from the actual debris data collected on the test. As shown in the comparison, both sources slightly underpredict the hazard ranges in front of this tunnel/chamber geometry and loading density.

CONCLUSIONS

The Inhabited Building Distances for airblast given in the current DOD Explosives Safety Standards are very conservative for the area in front of the access tunnel portal (azimuths from 0 to 90 degrees and 270 to 0 degrees), as shown in Figure 2. Over an arc from 90 degrees to 270 degrees (Figure 3), the distance specified by the manual provides a reasonable upper bound of the data measured on the Shallow Underground Tunnel/Chamber Test.

The manual sets damage criterion for airblast pressure against inhabited

buildings as 5 kPa (50 mb). As shown in Figure 2, the 5-kPa overpressure level measured during the Shallow Underground Tunnel/Chamber Explosion Test occurred at approximately the same distance that the Standards specify as the airblast Inhabited Building Distance for open storage of a 20,000-kg Composition B charge. The airblast Inhabited Building Distances specified in the Standards for underground storage are even more conservative when compared to the results of tests at Alvdalen, Sweden, as shown in Figure 4. The airblast Inhabited Building Distance is strongly dependent on the explosive loading density (charge weight divided by the volume of the access tunnel plus storage chamber) of the magazine, as shown in Figure 6.

Using a peak pressure criterion of 5 kPa (0.73 psi) for airblast Inhabited Building Distance, the test data indicate that the actual Quantity-Distance ($Q-D_{ib}$) is 25 percent less, and the $Q-D_{ib}$ area some 50 percent less than the values specified by the current Standards for underground storage. If the same damage criterion for inhabited buildings (6.2 kPa or 0.9 psi) used for above-ground storage is applied to underground storage, the test results indicate that the actual $Q-D_{ib}$ for underground storage is approximately equal to the $Q-D_{ib}$ specified in the Standards for above-ground storage, but the $Q-D_{ib}$ area is only one-third that specified for above-ground storage.

The Inhabited Building Distances for ground shock given by the Explosives Safety Standards and the NATO AC/258 yield reasonable results for shock transmitted through rock. For the case of a soil layer over bedrock, however, such as existed at the Tunnel/Chamber Test site, the Standards and NATO AC/258 both severely underestimate distances to the particle velocity levels used as criteria for Inhabited Building Distance to protect against ground shock.

The results of the Shallow Underground Tunnel/Chamber Explosion Test indicate that Inhabited Building Distance for ejecta/debris along the extended tunnel axis (0-degree azimuth) is underestimated by the NATO AC/258 guidance. The data indicate (Figure 9) that the Inhabited Building Distance for debris decreases with angle from the 0-degree azimuth, and approaches the distance specified by the standards and NATO AC/258 at an azimuth of 45 degrees.

RECOMMENDATIONS

Additional data are needed to evaluate the effect of storage loading density and cover depth on the Inhabited Building Distance for airblast. Previous data from WES model tests, shown in Figure 6, indicate that a non-linear relation exists. These data, from fully-contained storage magazine models, provide an upper bound for airblast Inhabited Building Distance as a function of loading density. Additional tests, where the extent of venting is varied over a range of cover depths (and other factors held constant), are needed to isolate this effect.

Computer model studies can also help define the effect of venting on external blast hazards, after a reliable material is established that simulates the response of the rock surrounding the magazine chamber.

The Shallow Underground Tunnel/Chamber Test demonstrated that current Inhabited Building Distance criteria for ground shock in a layered geology (with soil over rock) is inadequate. Improved methods must be developed to better predict these distances in complex geologies.

The Inhabited Building Distance that is currently specified in the Standards for debris expelled from the access tunnel should be reevaluated and corrected. Recent work in Sweden indicates that the large distances to which debris was thrown out the access tunnel on the Tunnel/Chamber Test could be reduced by a barrier outside the tunnel portal. Additional study is needed to evaluate such methods, and their most effective design, to reduce the external debris hazard.

ACKNOWLEDGEMENT

We gratefully acknowledge permission from the Chief of Engineers and the sponsors to publish this paper.

REFERENCES

Department of Defense, 1984, "Ammunition and Explosives Safety Standards," DOD 6055.9-STD, Assistant Secretary of Defense (Manpower, Installations, and Logistics), Washington, D.C.

Hadala, Paul F., 1973, "Effect of Constitutive Properties of Earth Media on Outrunning Ground Shock from Large Explosions," Technical Report S-73-6, U.S. Army Engineer Waterways Experiment Station, Vicksburg, MS.

Halsey, Carl C.; Durbin, William F.; and Berry, Sharon L.; 1989, "KLOTZ Underground Magazine Trial, Data Report," NWC TM-6562, Naval Weapons Center, China Lake, CA.

Joachim, Charles E., 1990, "Shallow Underground Tunnel/Chamber Explosion Test Program, Summary Report," in publication, U.S. Army Engineer Waterways Experiment Station, Vicksburg, MS.

North Atlantic Treaty Organization, 1977, "Manual on NATO Principles for Storage of Ammunition and Explosives, Part III," AC/258-D/258, Group of Experts on the Safety Aspects of Transportation and Storage of Military Ammunition and Explosives (AC/258).

Millington, Charles, 1985, "The Ernesettle Report," Preliminary AWRE Report UK(ST)IWP 205 0/1/85, AWRE (Foulness), Ministry of Defence, United Kingdom.

Smith, Dennis R.; Joachim, Charles E.; Davis, Landon K.; and McMahon, Gordon W.; 1989, "Effects of Explosions in Underground Magazines," Technical Report SL-89-15, U.S. Army Engineer Waterways Experiment Station, Vicksburg, MS.

Vretblad, Bengt, 1988, "Data From The 1987 Klotz Club Test In Sweden," Report C3:88, Royal Swedish Fortifications Administration, Eskilstuna, Sweden.

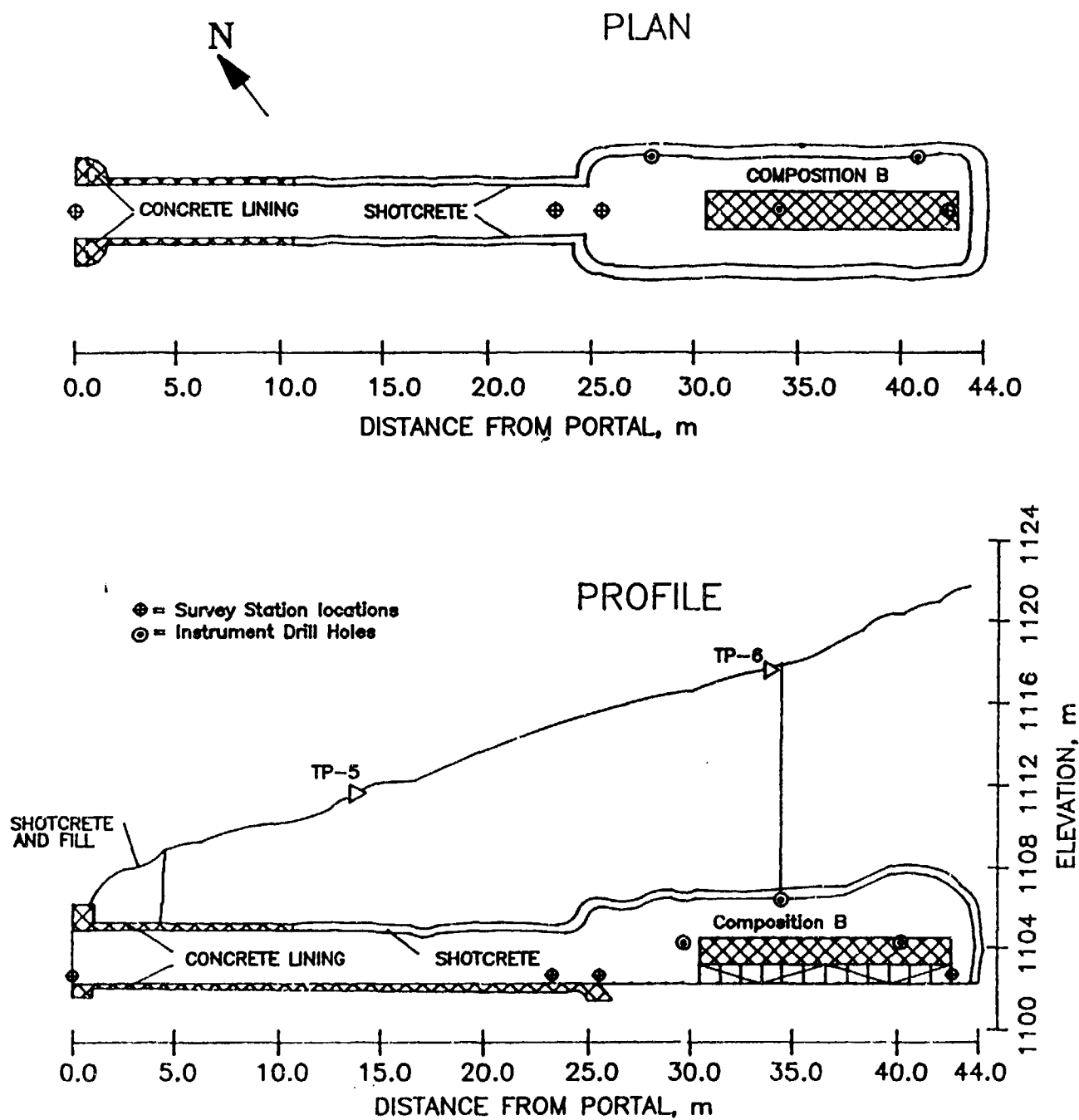


Figure 1. Location of 20,000-kg Composition B explosive charge for Shallow Underground Tunnel/Chamber Explosion Test Program (plan and profile).

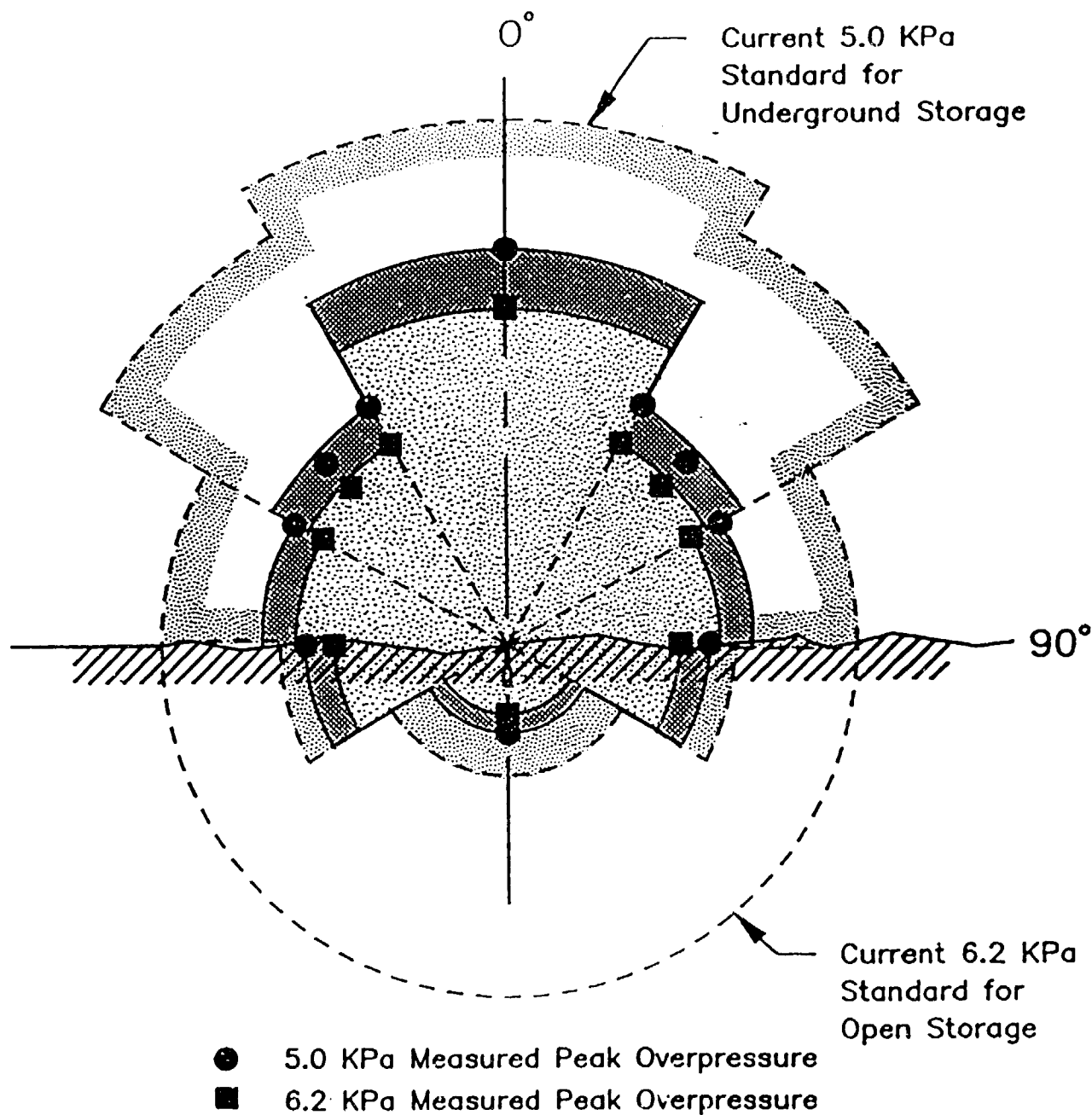


Figure 2. Airblast Inhabited Building Distances specified by Explosive Safety Standards (DOD 6055.9 STD) for open and underground munitions storage, compared to 5.0 and 6.2 kPa distances measured on Shallow Underground Tunnel Chamber Explosion Test (20,000 kg, Composition B, 66.4 kg/m³ (TNT equivalent) loading density).

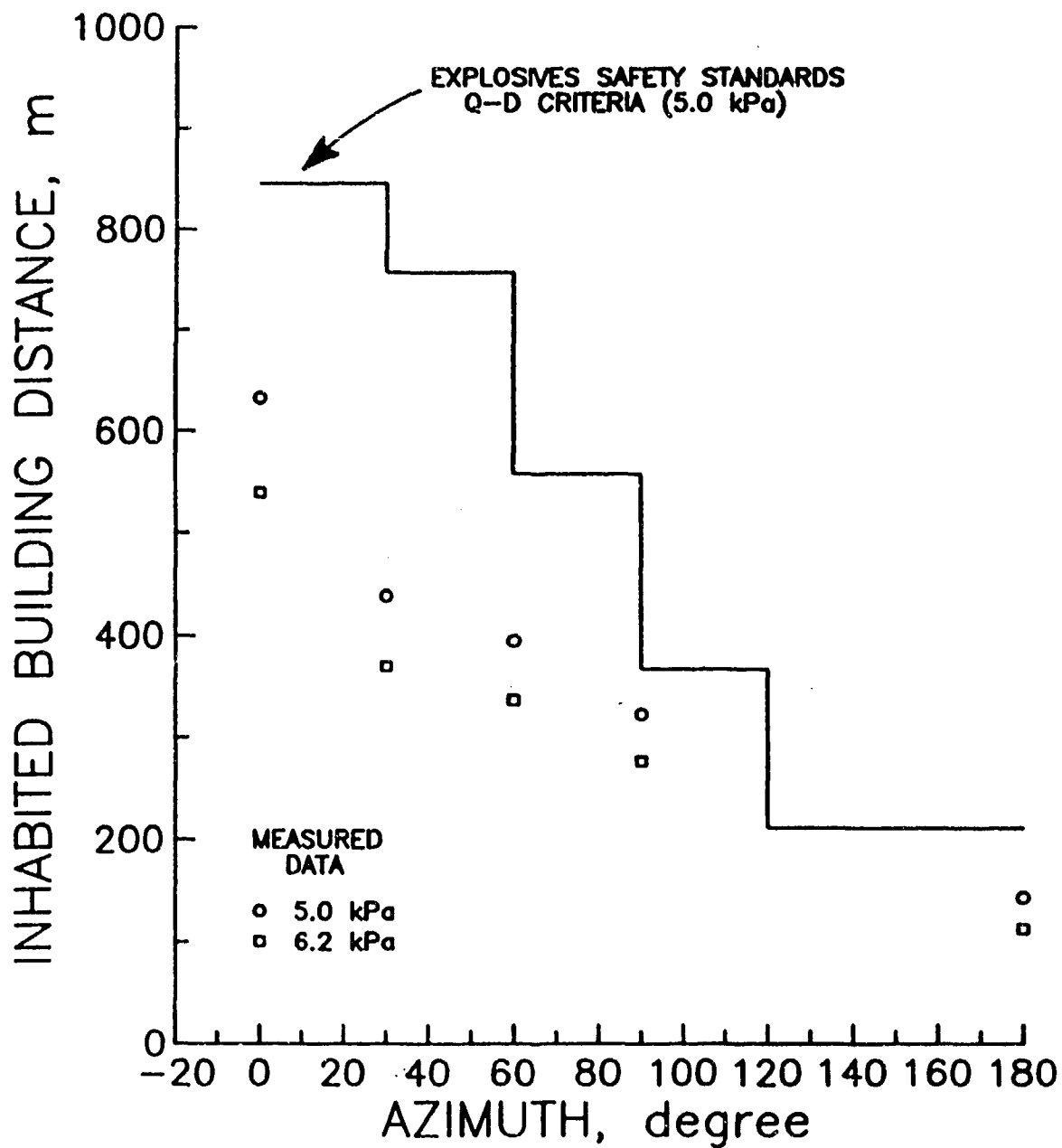


Figure 3. Airblast Inhabited Building Distances specified by Standards (DOD 6055.9-STD) compared to measured distances to 5.0 and 6.2 kPa pressure levels for the Shallow Underground Tunnel/Chamber Explosion Test (20,000 kg, Composition B, 66.4 kg/m³ (TNT equivalent) loading density).

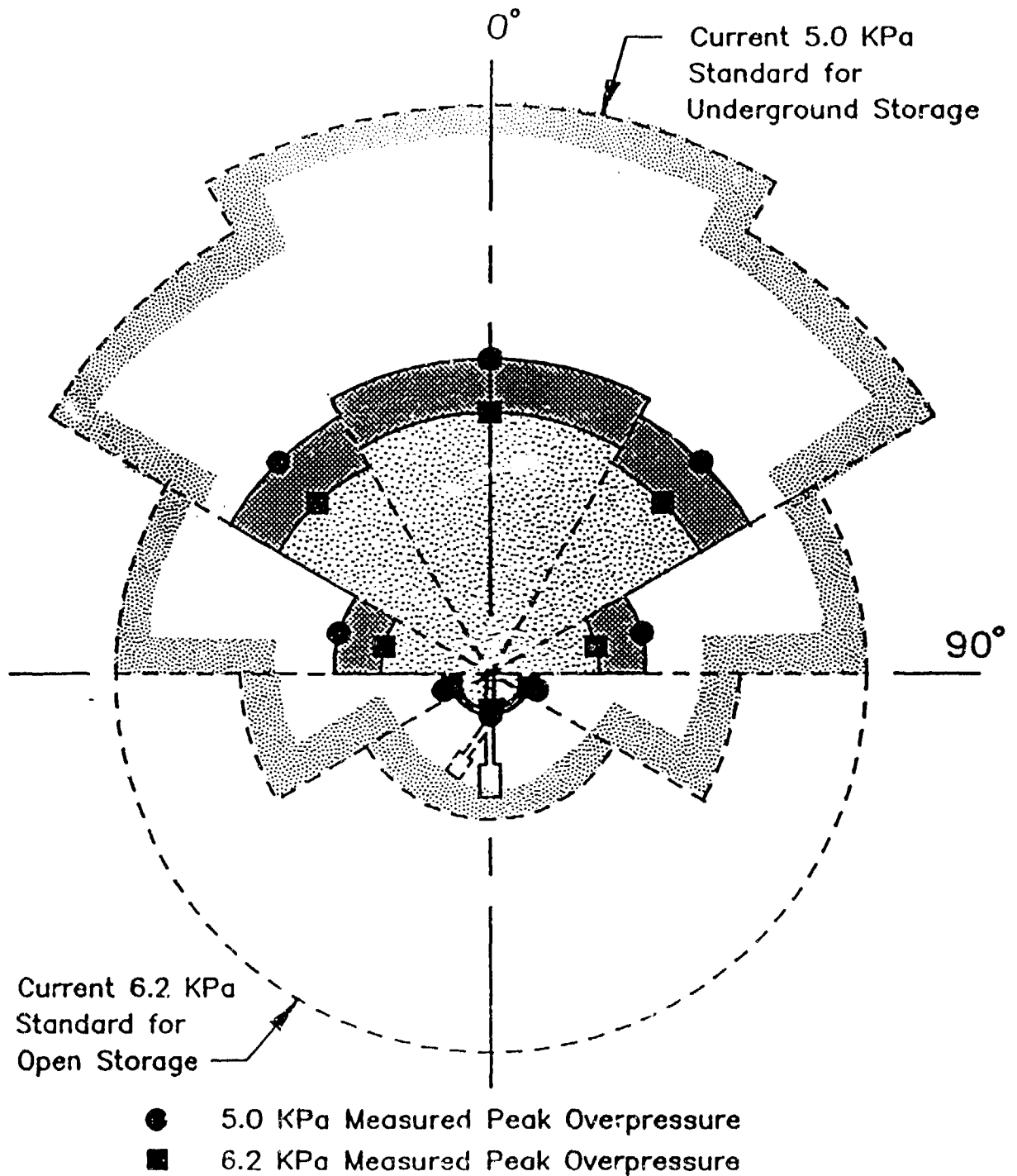


Figure 4. Airblast Inhabited Building Distances specified by Standards (DOD 6055.9-STD) for open and underground munitions storage, compared to 5.0 and 6.2 kPa distances measured in 1987 KLOTZ Club Test 8 at Alvdalen, Sweden (4540 kg ANFO, 12.7 kg/m³ TNT equivalent) loading density.

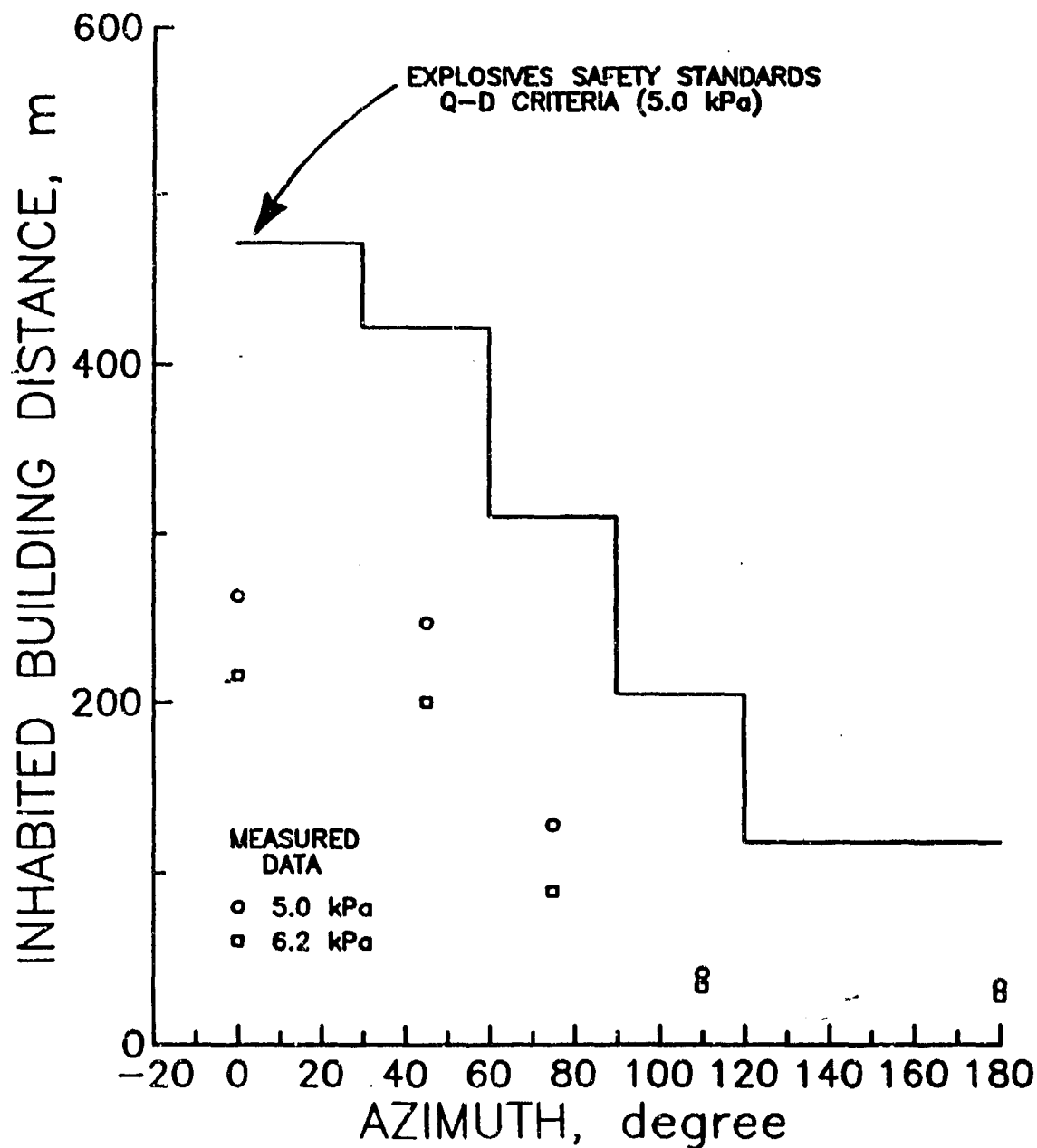


Figure 5. Airblast Inhabited Building Distances specified by Explosives Safety Standards for underground munitions storage, compared to measured distances to 5.0 and 6.2 kPa pressure levels, for 1987 KLOTZ Club Test 8 at Alydalen, Sweden (4540 kg ANFO, 12.7 kg/m³ (TNT equivalent) loading density).

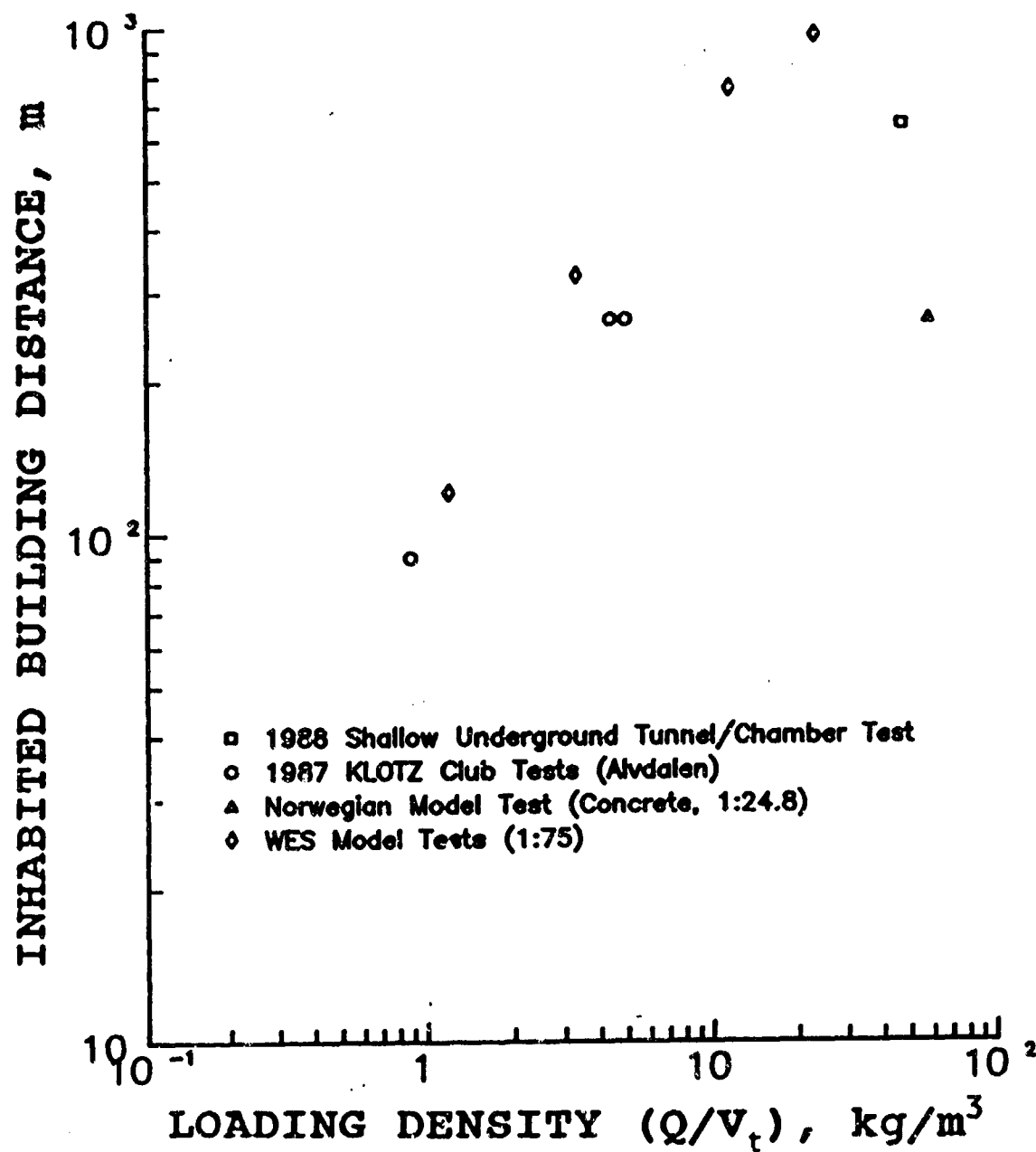


Figure 6. Airblast Inhabited Building Distance along the 0-degree azimuth (extended tunnel axis) as a function of loading density, as indicated by full-scale and model test data. (Note: Loading density is defined as charge weight, Q , divided by total volume, V_t , which is volume of the chamber plus the tunnel portion between the chamber and the portal).

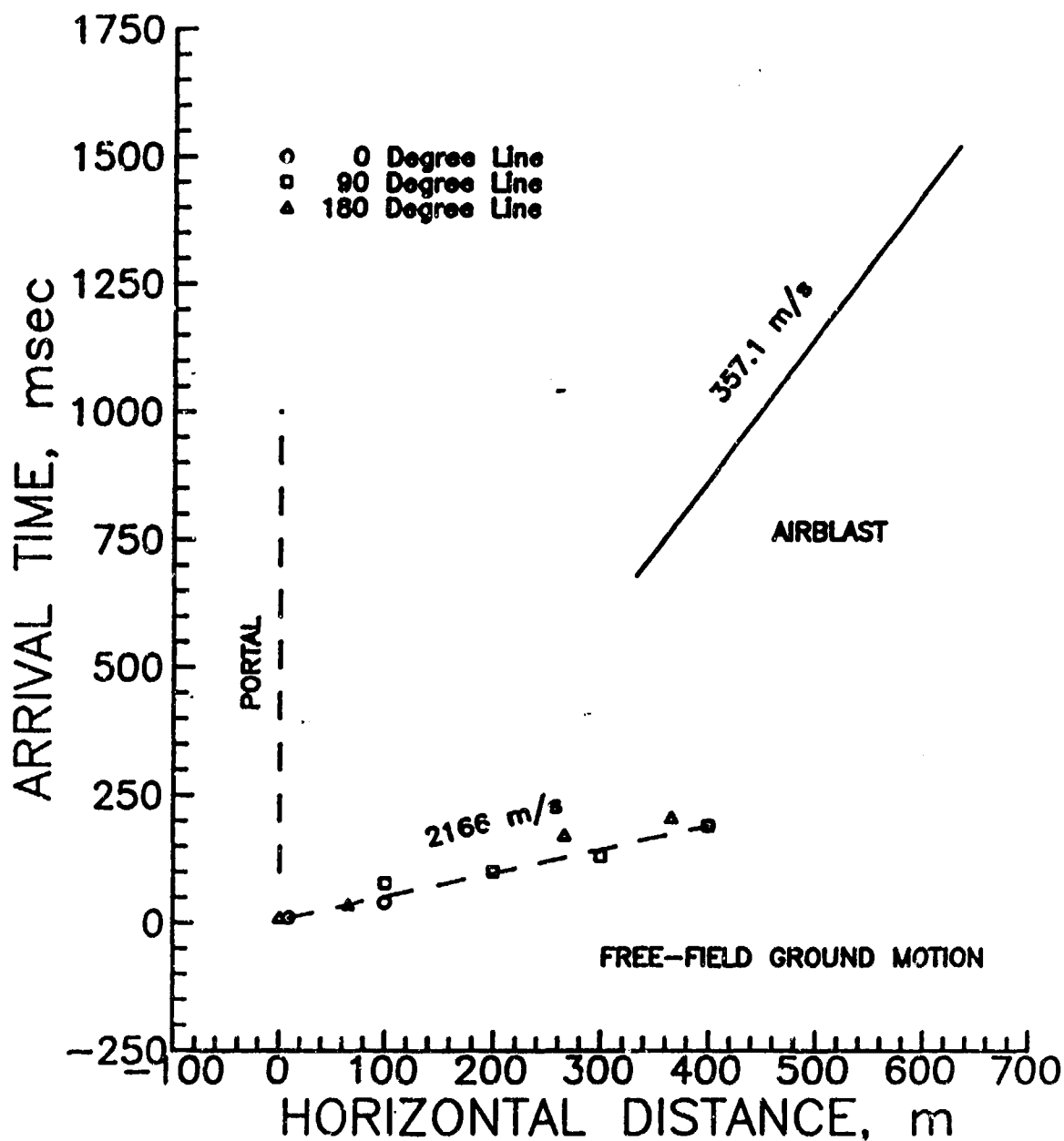


Figure 7. Free-field ground shock arrival time versus distance from center of chamber, Shallow Underground Tunnel/ Chamber Explosion Test. Long-range free-field airblast arrival along 0-degree line is shown for comparison.

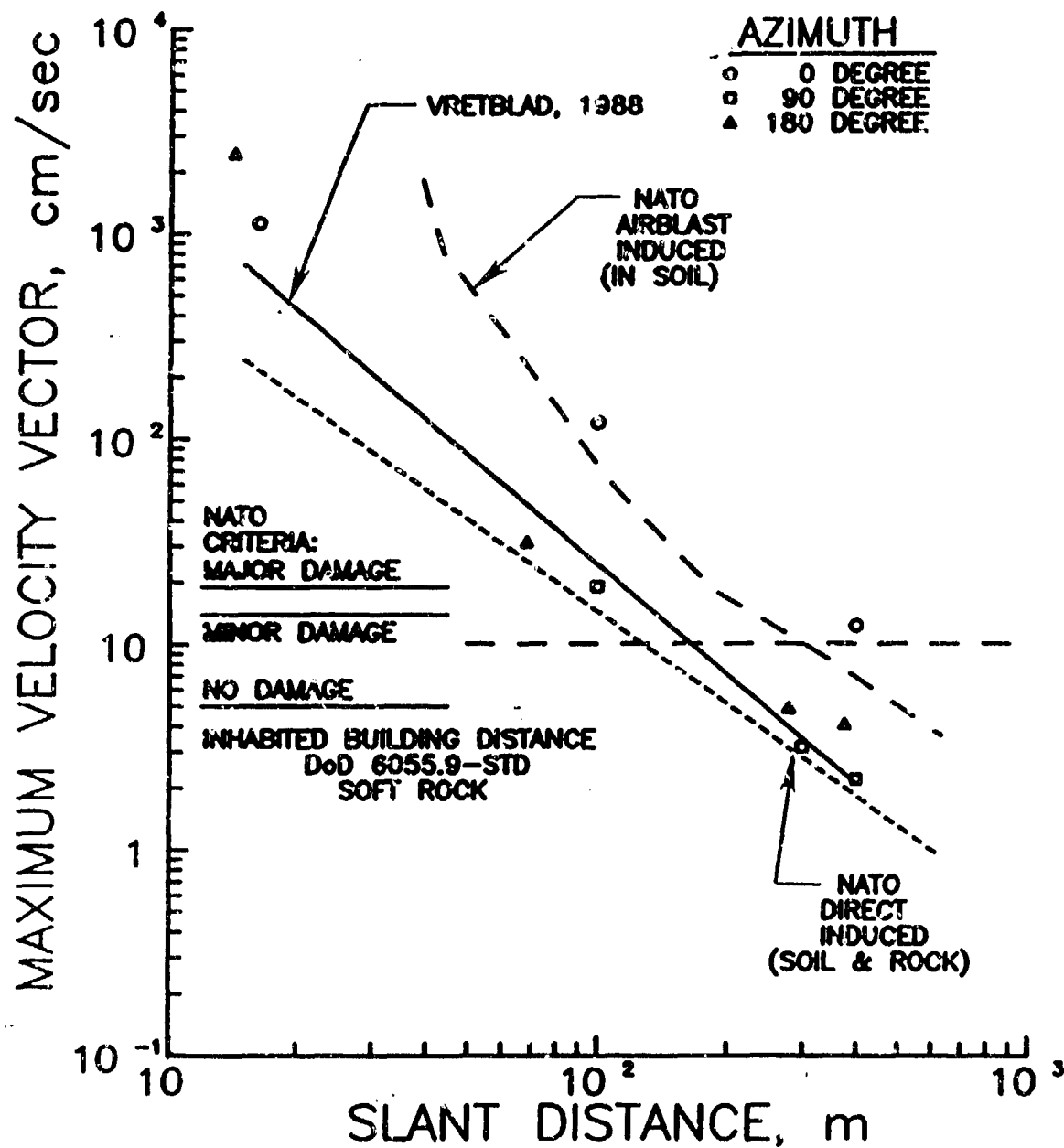


Figure 8. Maximum velocity vector versus slant distance from center of the charge; comparison of prediction curves with data from 0, 90, and 180-degree azimuths on Tunnel/Chamber Test.

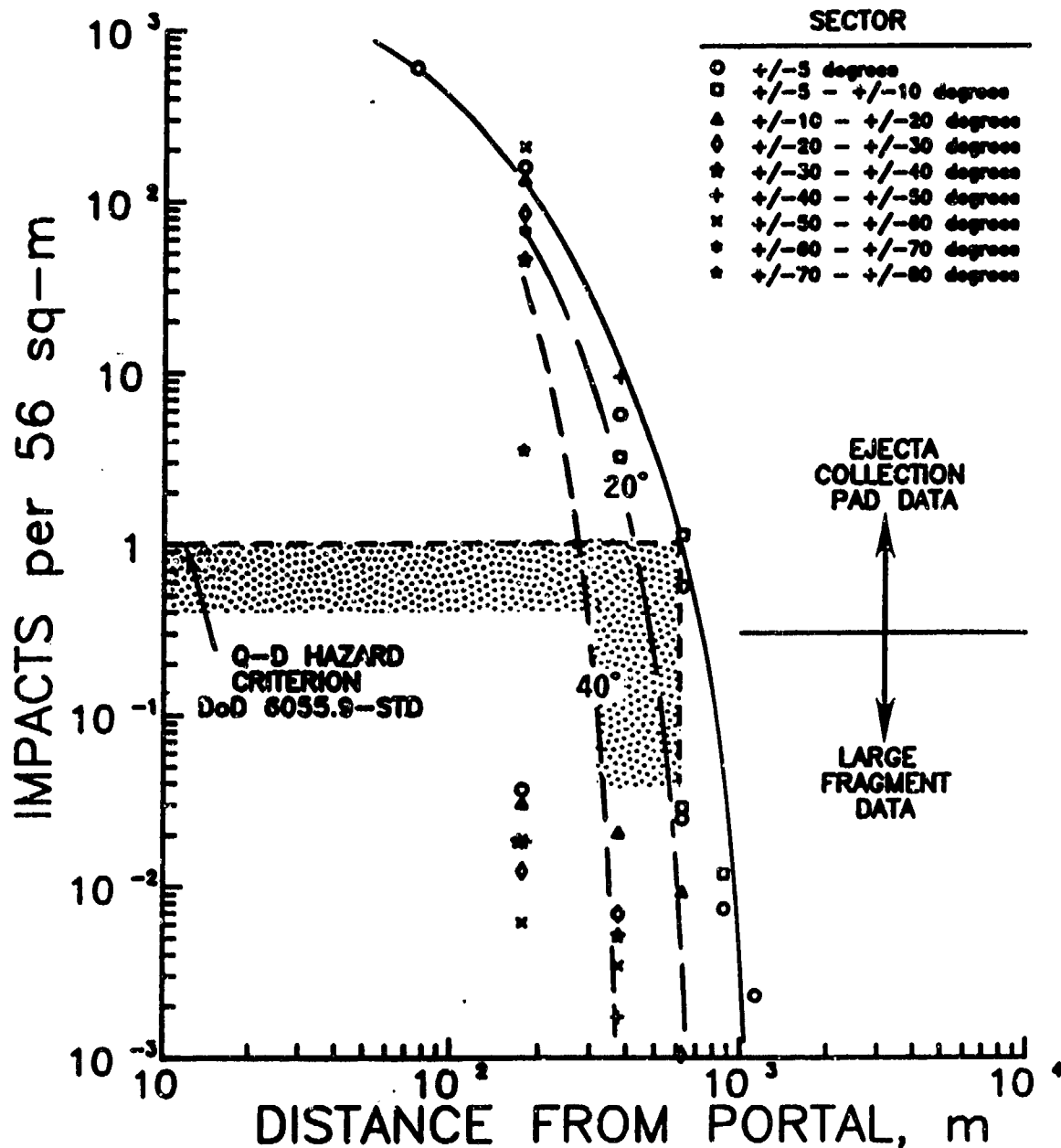


Figure 9. Ejecta/debris missile impact density versus distance from the portal, Shallow Underground Tunnel/Chamber Explosion Test. Curves show general limits of missile density ranges along extended tunnel axis (0-degree azimuth) and with ± 20 degree and ± 40 degree sectors.

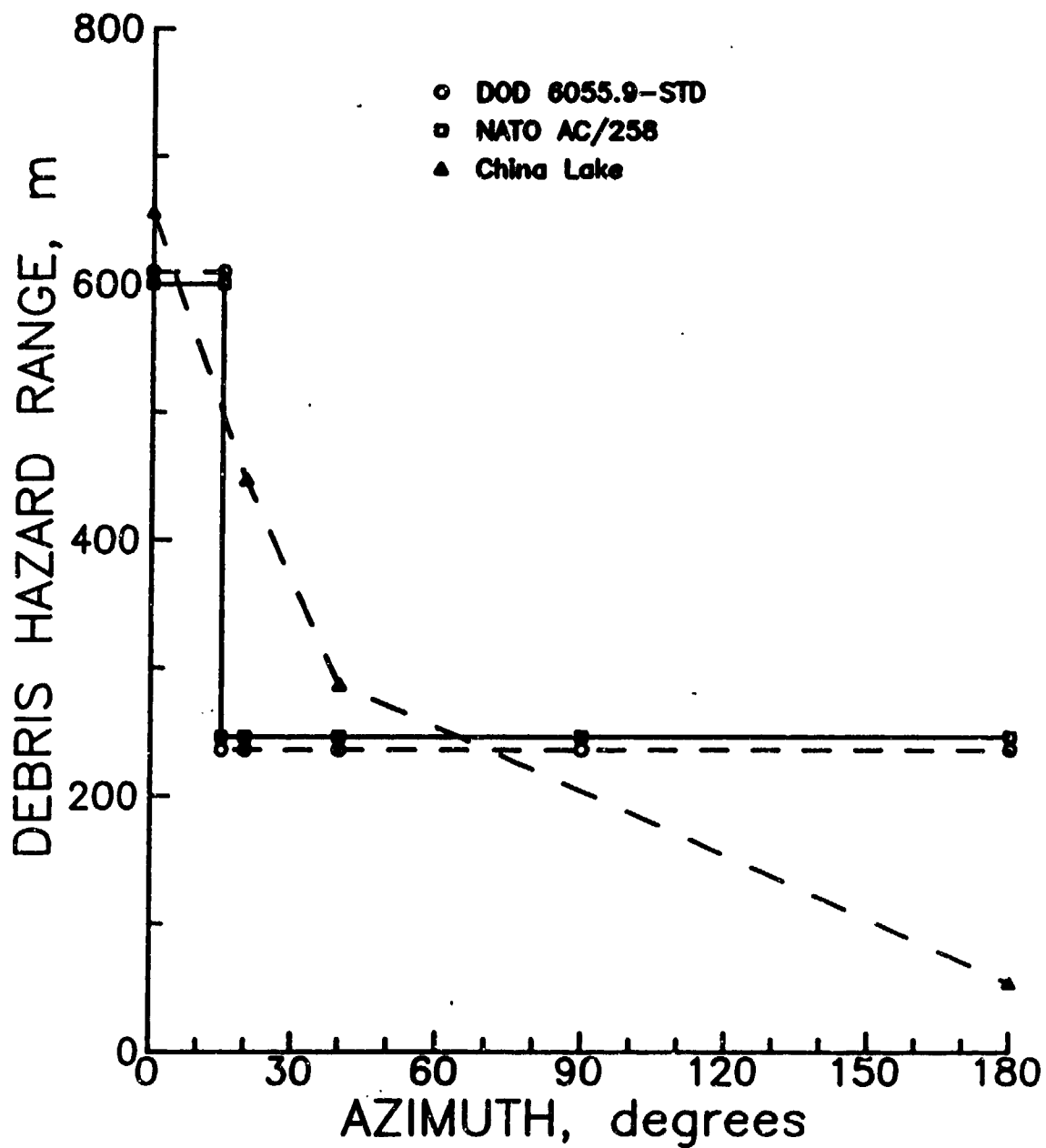


Figure 10. Inhabited Building Distances from debris hazards specified in the Explosives Safety Standards and NATO AC/258 for a 20,000-kg detonation, compared to ranges indicated by data collection on the Shallow Underground Tunnel/Chamber Explosion Test.

Table 1. Comparison of Airblast Inhabited Building Distances for 22,000 kg NEW; Current Standards versus Measured Distances (in metres).

Source	Hazard Zone ¹					Percent of Current Standard	Hazard Area (m ²)	Percent of Current Standard
	D ₅ 0°-30°	D ₄ 30°-60°	D ₃ 60°-90°	D ₂ 90°-120°	D ₁ 120°-180°			
FOR 5.0 kPa (0.73 psi)								
Current Standards (DOD 6055.9-STD) for UNDERGROUND storage	845	756	557	366	211	100	952,000	100
Measured Distances, Shallow Underground Tunnel/Chamber Test	632	438	394	322	143	75	467,000	49
Measured Distances, Alvdaalen Test (Vretblad, 1988) Scaled to 22,000 kg NEW	471	444	229	73.0	61.5	56	254,000	27
FOR 6.2 kPa (0.9 psi)								
Current Standards, (DOD 6055.9-STD) for ABOVE-GROUND storage	540	540	540	540	540	100	916,000	100
Measured Distances, Shallow Underground Tunnel/Chamber Test	539	369	336	276	112	100	336,000	37
Measured Distances, Alvdaalen Test (Vretblad, 1988) Scaled to 22,000 kg NEW	388	358	159	59.7	50.4	72	145,000	16

Note: ¹ See Figure 98.

Tunnel Pressure and Emergent Blast Calculations for the Shallow Buried China Lake Test

Charles Needham
Kenneth Schneider
Joseph Crepeau
Lynn Kennedy

Maxwell Laboratories, S-CUBED Division
Albuquerque, New Mexico

ABSTRACT

S-CUBED has performed a number of calculations in support of the 20,000 kg underground storage magazine explosive test detonated in August, 1988, at the Naval Weapons Center, China Lake, California. These calculations were done with our second-order hydrodynamic code, SHARC. They include two- and three-dimensional interior tunnel calculations, using several different materials to represent the overburden. The first two-dimensional calculation included rigid walls; subsequent calculations included equations-of-state for sand and then granite to calculate the response of the overburden. Specifics for the overburden response were found to be significant for a large yield test like that at China Lake. The granite, which provided the best correspondence to the experimental data in the two-dimensional case, was also used for a three-dimensional interior calculation. This latter calculation reproduced the tunnel shape and the depth of the overburden accurately. Artificial debris was also modeled with drag sensitive particles.

Two exterior calculations were also performed, a two-dimensional calculation over a flat exterior surface and a three-dimensional calculation including terrain modeling. The two-dimensional calculation was carried out to an overpressure level of 50 mbar.

Results of these calculations will be presented. Comparisons of calculated and measured results will be included.

SECTION I. TWO-DIMENSIONAL CALCULATIONS.

I.A. Initial Conditions.

A calculational mesh was established in cylindrical coordinates with the axis of symmetry on the center line of the floor of the tunnel. The explosive was placed in the chamber in the configuration described in the experiment (Figure 1). Detonation was initiated at the end face of the explosive nearest the tunnel opening.

The original purpose of the calculation was to provide gage ranging information to the experimenters (Figure 2). In the first calculation, the tunnel and chamber walls were treated as perfectly reflecting and non-responding (Figures 3 and 4). We felt that the

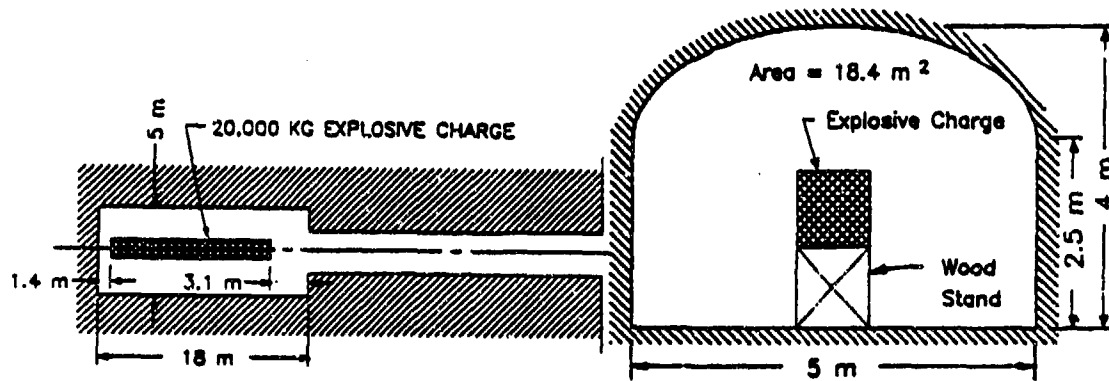


Figure 1. Plan view and cross-section showing explosive placement diagrams are not at the same scale).

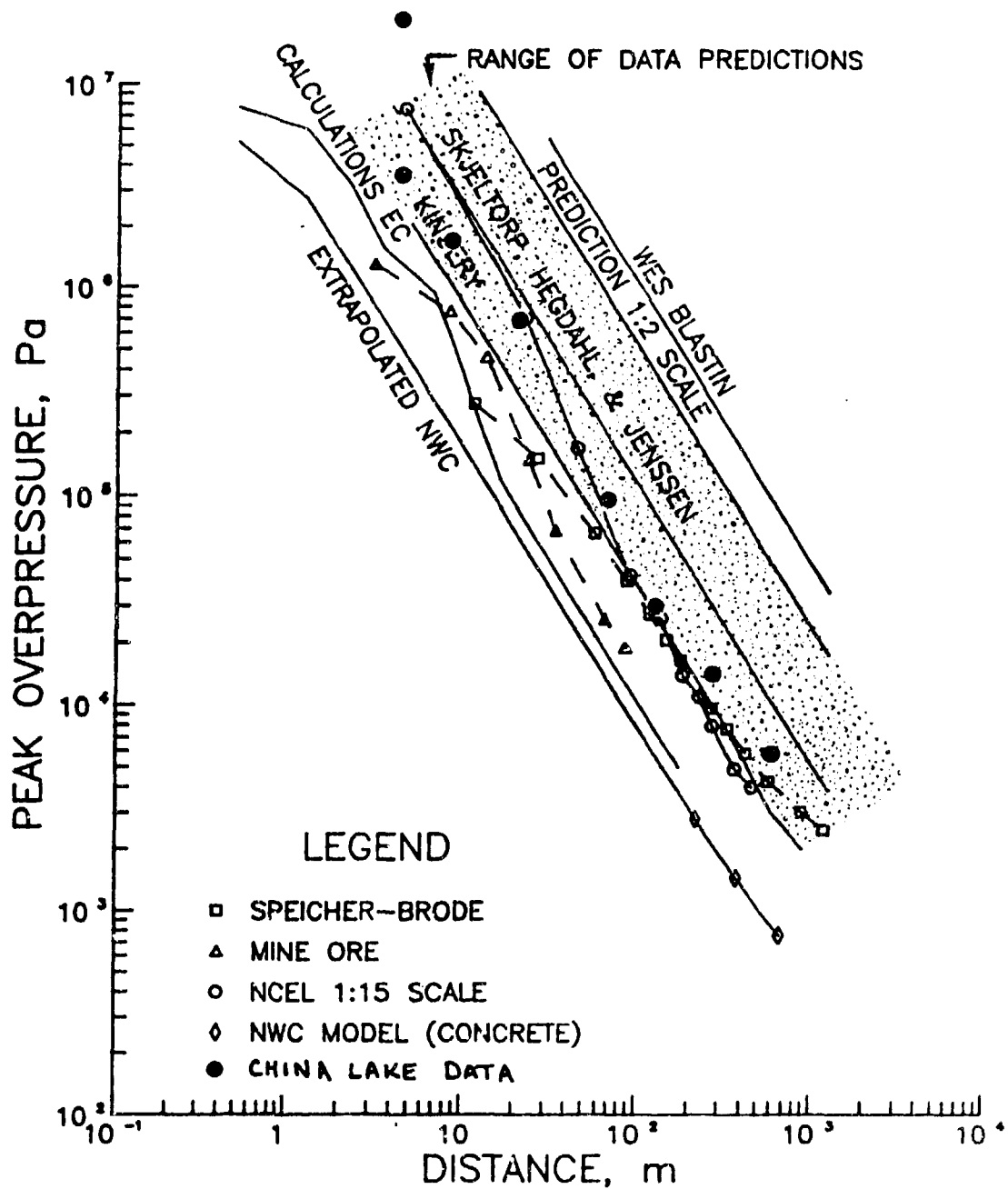


Figure 2. Several early predictions of pressure as a function of range from the tunnel exit.

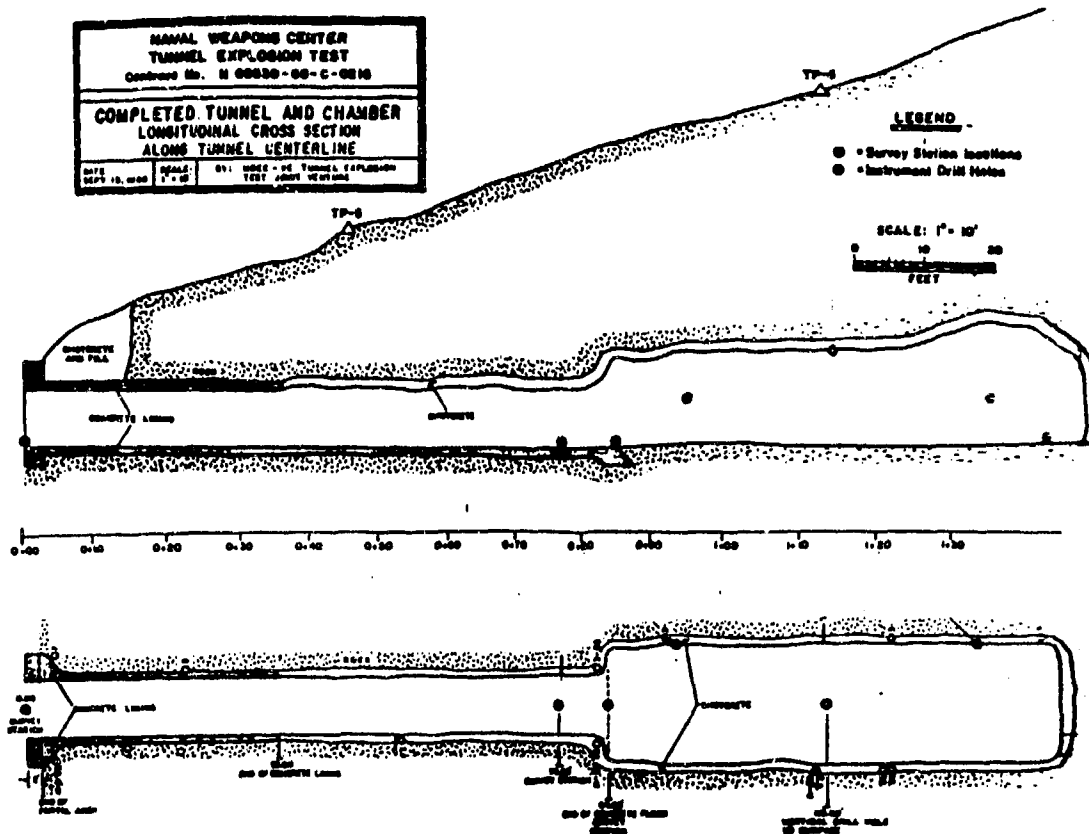


Figure 3. Longitudinal cross-section and plan view of as-built tunnel and chamber.

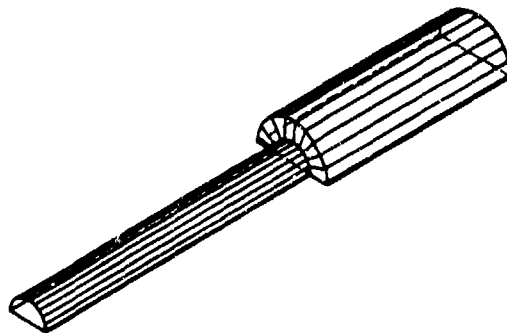


Figure 4. Calculational configuration in cylindrical symmetry.

perfectly reflecting case would provide the maximum possible exit pressure. The overburden was expected to be blown away during the experiment.

This fact made it obvious that a significant fraction of the explosive energy was absorbed by the overburden. We repeated the calculation with an overburden of highly compressible sand. The equation-of-state for sand was available and the calculation could be run without delay or expense. The argument here was that the sand would absorb a maximum amount of energy, thus giving a lower bound to the expected exit pressure.

A third two-dimensional calculation was made with an equation-of-state for porous granite. The compressibility model was based on density data taken from the test site. The equations-of-state used for sand and granite were compared. The results of this comparison are given in Figure 5.

I.B. The Detonation Process and Shock Propagation.

The detonation was modeled by releasing energy as a function of space and time. The detonation velocity is calculated as a function of local hydrodynamic conditions. The energy released is proportional to the mass engulfed by the detonation front in each zone during each time step. The material is converted from solid to gas and the appropriate equation-of-state is used. The expanding detonation products accelerate the air, creating the air shock. The shock strikes the wall of the chamber prior to completion of the detonation process and reflects toward the center. The artificial cylindrical geometry of the calculation tends to overestimate the formation of an axial jet of detonation products. This jet exists experimentally but dissipates more rapidly than in the calculation.

The intersections of walls, floors and roofs create re-entrant corners for shock reflections. The peak pressures (other than in the detonation) are found in these regions well after initial reflection. Sites which produce high pressures are the intersection of the back wall and the floor, and the intersection of the chamber roof with the front wall above the tunnel opening.

The reflection above the tunnel opening is important in the responding wall calculations because this corner reflection causes significant motion of the chamber roof and wall (Figure 6). The shock transmitted through the solid causes downward motion of the tunnel roof near the chamber. This motion has the effect of choking the flow into the tunnel. The timing is such that the shock has exited the tunnel entrance prior to blockage near the chamber (Figures 7 and 8).

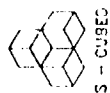
The shocks reflecting from the walls, roof and floor of the chamber interact in complex patterns creating complex waveforms propagated through the tunnel.

Internal waveforms are compared at a location 2.2 meters from the tunnel portal (Figure 9). The non-responding walls overestimate the pressure; sand walls underestimate the pressures and the porous granite walls in general also slightly underpredict the pressure.

I.C. External Blast Propagation

The external blast characteristics are very dependent on the time histories of dynamic pressure and overpressure near the tunnel exit. These parameters determine

JC 17:55 29MAR80



JC 17:58 29MAR80

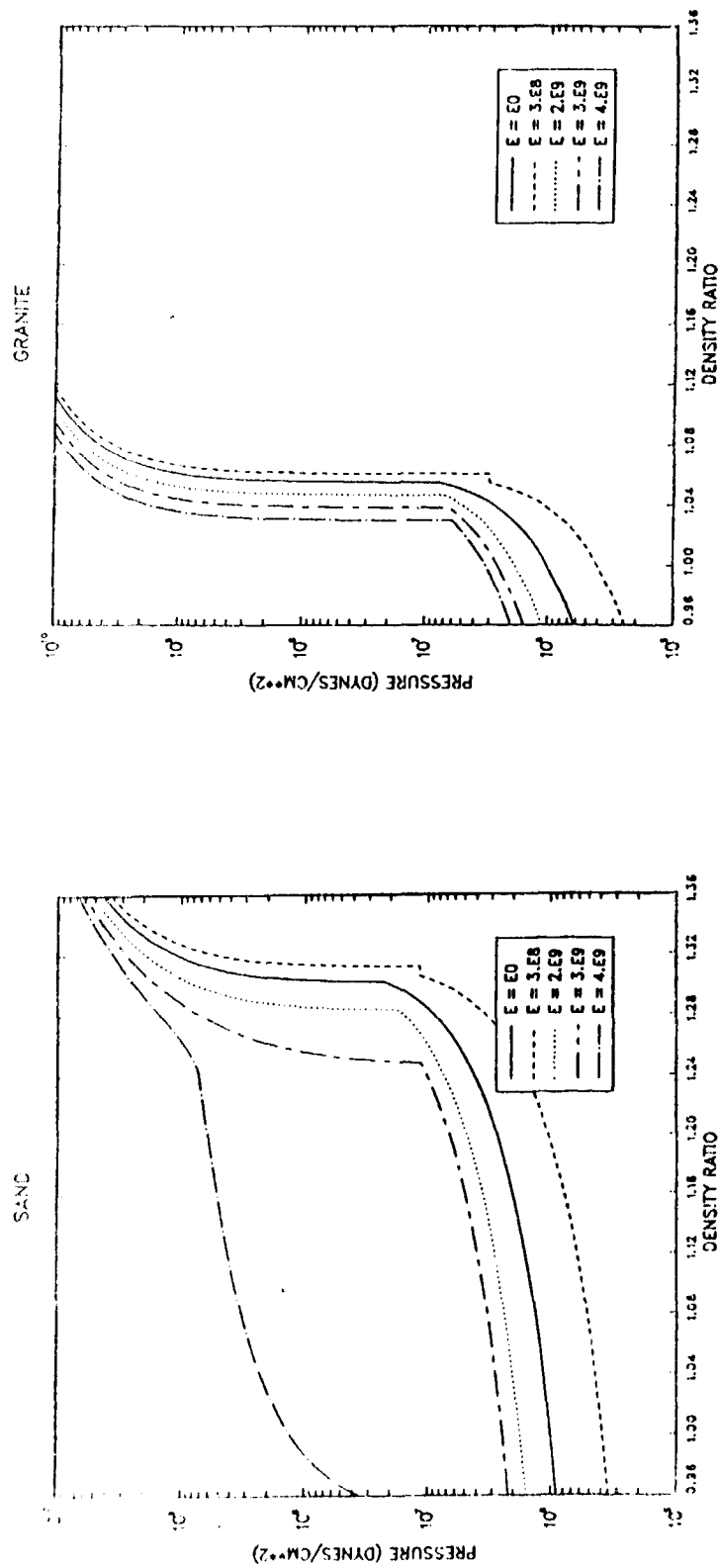
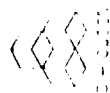


Figure 5. Comparison of sand and granite equations-of-state.

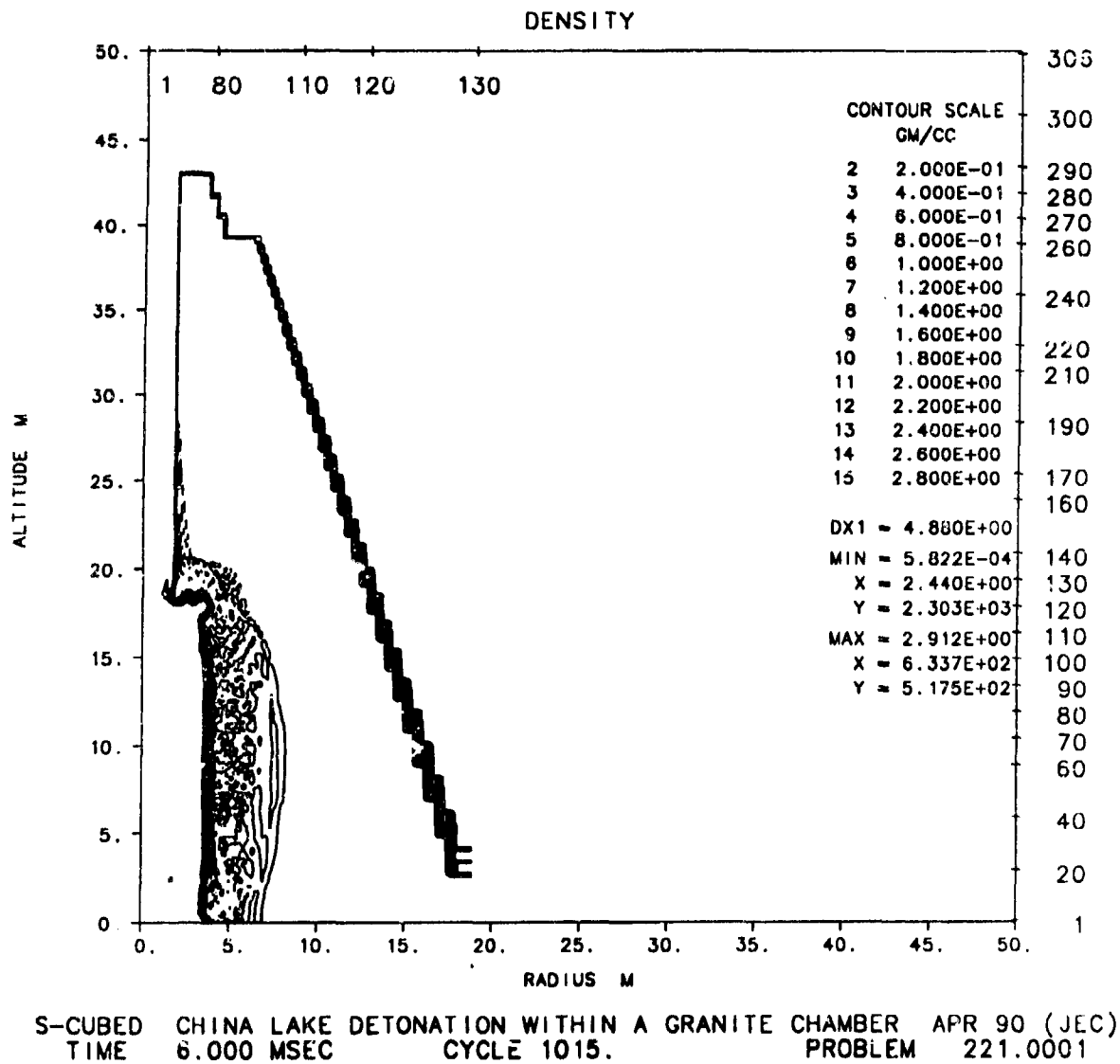
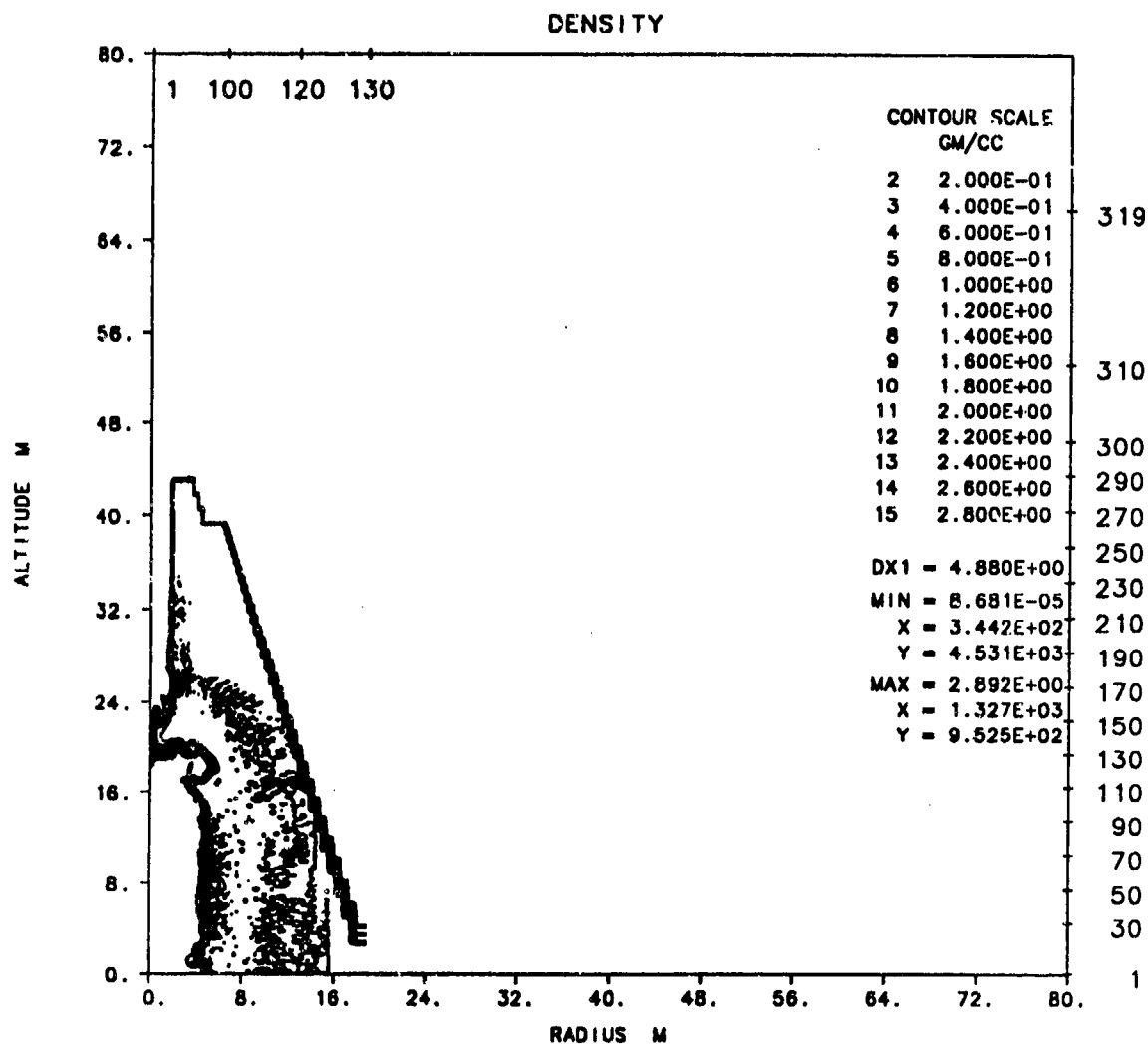
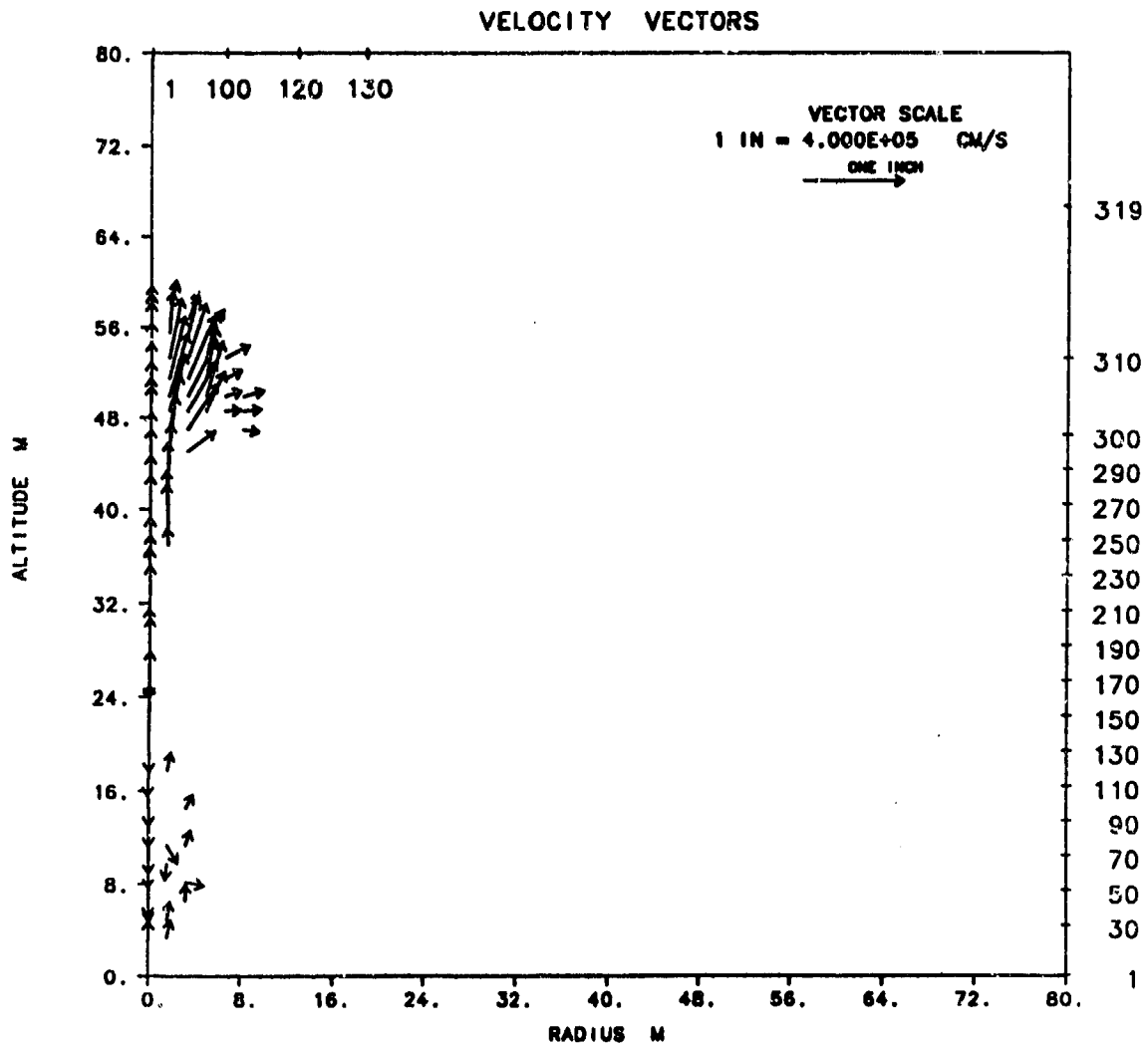


Figure 6. Tunnel cross-section at 6 ms.



S-CUBED CHINA LAKE DETONATION WITHIN A GRANITE CHAMBER APR 90 (JEC)
TIME 21.000 MSEC CYCLE 2137. PROBLEM 221.0001

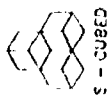
Figure 7. Tunnel cross-section at 21 ms.



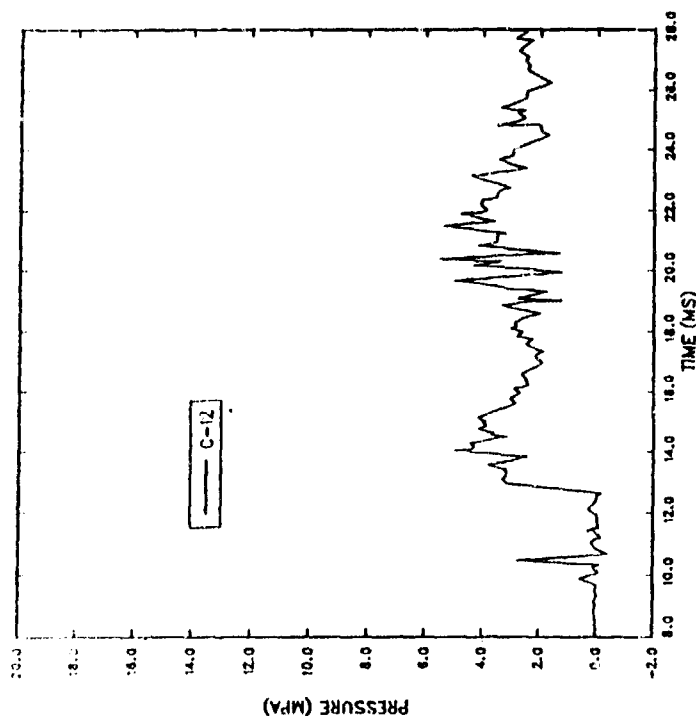
S-CUBED CHINA LAKE DETONATION WITHIN A GRANITE CHAMBER APR 90 (JEC)
 TIME 21.000 MSEC CYCLE 2137. PROBLEM 221.0001

Figure 8. Flow velocity vectors at 21 ms.

MS 14:28 18APR00

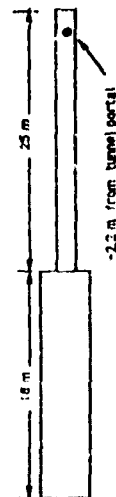


CHINA LAKE
CALCULATION, EXPERIMENTAL COMPARISONS
OVERPRESSURE VS. TIME

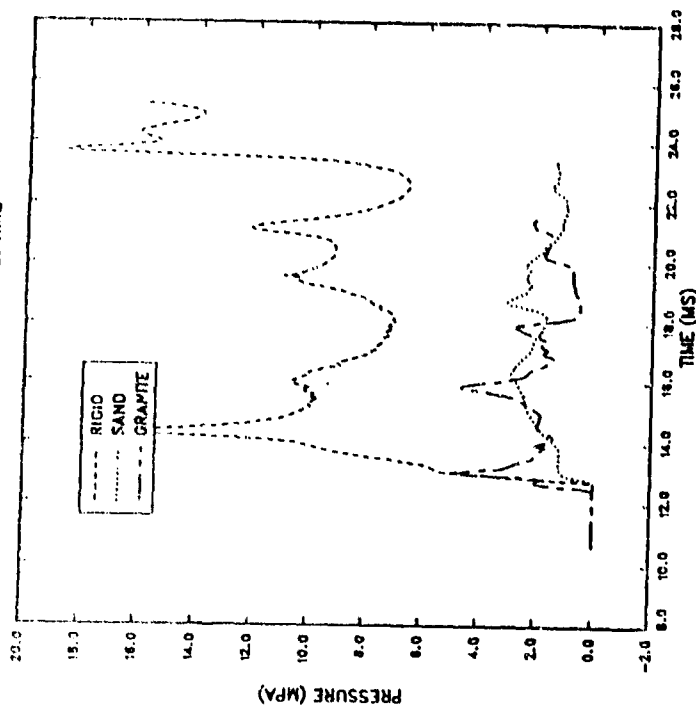


CHINA LAKE C-12 COORD: -2.2 M TOA: ?

ACCESS TUNNEL PRESSURE



CHINA LAKE
CALCULATION, EXPERIMENTAL COMPARISONS
OVERPRESSURE VS. TIME



2.5 9 COORD: -2.5 M TOA: 9.44 MS DTOA: +3.21
2.51 9 COORD: -2.5 M TOA: 11.23 MS DTOA: +1.42
221.0001 9 COORD: -2.7 M TOA: 11.3 MS DTOA: +1.00

ACCESS TUNNEL PRESSURE

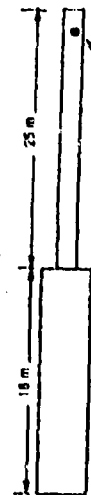


Figure 9. Comparison of experimental overpressure with three calculations.
Position 2.2 meters inside tunnel.

the angular distribution and decay rate of the external air blast. The high velocity and relatively cool detonation products form a jet from the mouth of the tunnel. The mixing of the jet with the external air determines the rate of energy and momentum exchange. The slowing of the jet converts momentum (a vector) and dynamic pressure (quasi vector) to overpressure (a scalar). After the jet has slowed, the expansion becomes more spherical. The blast wave may, therefore, have an apparent origin at some distance outside the tunnel.

At a pressure of about 30 psi, (two bars) when a negative phase has formed, the blast propagation and decay are independent of the source. Simplified methods may be used to predict the further decay.

Terrain effects must be considered for exterior blast propagation. Pressure has units of energy per unit volume. Thus any increase in volume gives a lower overpressure. A downslope outside the tunnel entrance gives a larger volume for expansion of the blastwave. The greater expansion results in lower peak pressures and more rapid decay. An upslope has the opposite effect.

Forests or other obstacles in the flow tend to retard the flow. The initial reaction of the blastwave is a conversion of dynamic pressure to overpressure. The longer distance effect is an overall reduction in pressure and impulse caused by a combination of shock reflection (an irreversible process) and absorption by exchange of energy with the intervening material.

SECTION II. THREE-DIMENSIONAL CALCULATIONS.

II.A. Initial Conditions.

The full three-dimensional structure of the tunnel was modeled. Some simplification was necessary for computational efficiency. A vertical symmetry plane was placed along the centerline of the tunnel. The bottom (floor) of the tunnel and back wall of the chamber were made perfectly reflecting. The walls were initially smooth and clean.

Massive, drag sensitive particles were placed in and near the tunnel to model the artificial debris in the experiment. Additional massive particles were placed in the overburden to track the trajectories of large particulates. The overburden was modeled using the same equation-of-state for granite that had been used for the two-dimensional calculations of Section I.

Monitoring stations were placed in and around the chamber and tunnel complex to provide time histories of all hydrodynamic variables. Positions were chosen to correspond to and supplement the experimental gage array.

Because of the large number of zones required for three-dimensional calculations, the resolution of the three-dimensional was significantly reduced from that of the two-dimensional calculations.

II.B Detonation and Early Shock Propagation.

The three-dimensional configuration very closely modeled the experimental geometry. The detonation was initiated at a point on the center of the face of the charge nearest the tunnel opening. The detonation process required about 1.88 ms. The

realistic three-dimensional representation of the charge more closely modeled the early shock wave formation than the two-dimensional approximation.

At 2 ms, the entire shocked region of air is contained in the storage chamber. The shock in the granite overburden has reached less than 2 meters from the interior surface and is nearly symmetric about the charge.

The agreement between the calculated and experimental waveforms inside the tunnel provides some assurance that the calculated energy partition between air and granite is approximately correct. A typical overpressure comparison is shown in Figure 10.

As the shock approaches the tunnel exit, the experimental data indicates a dramatic slowing of the shock front and a corresponding increase in overpressure. We believe this is caused by the constriction of the cross-sectional area of the tunnel in the region coated by shotcrete. The cross-sectional area decreased by 16 percent in a distance of 3 meters and then stayed nearly constant over the remaining 10 meters to the exit. Such a constriction was not modeled in either the two-dimensional or three-dimensional calculations. Our calculated peak exit pressures were therefore somewhat lower than measured.

SECTION III. EXTERNAL BLAST CALCULATIONS.

Both two-dimensional and three-dimensional preliminary results are available. The calculations are continuing at this time. The comparisons at 5-, 10-, and 25-meter ranges outside the tunnel show good to excellent agreement between calculation and experiment.

SUMMARY

When this project was started, a number of estimates of exit pressure were made. Some simplified methods overestimated the exit pressure by two orders of magnitude, most were high by a factor of 10 or 20. The initial S-CUBED rigid wall calculation was high by about a factor of three. The responding granite wall two-dimensional calculation came within 30 percent or so of the measured data. The full detailed three-dimensional calculation is generally within 20 percent of the experimental data.

To obtain better theoretical results, more detail of the tunnel construction must be included. The 20 percent differences noted for the three-dimensional calculation correspond to about 20 percent variations in the exit tunnel cross-sectional area.

ACCIDENTAL DETONATIONS IN UNDERGROUND MUNITIONS STORAGE MAGAZINES: PREDICTION OF COVER RUPTURE OVERPRESSURES

Charles E. Joachim
U.S. Army Engineer Waterways Experiment Station
Vicksburg, MS 39180-6199

INTRODUCTION

The Shallow Underground Tunnel/Chamber Explosion Test provides the only known airblast overpressure data produced by venting of the overburden cover from a decoupled high explosive detonation in a large-scale underground munitions storage chamber. A limited amount of overpressure data are available from fully-coupled underground high explosive detonations in alluvium (Buckboard 11 and 12, Stagecoach II and III, and Scooter events (Snell et al, 1971)), two recent tests in a recompacted soil media (Midnight Hour I and II), and small-scale Norwegian model tests in sand (Jenssen, 1979). This paper describes procedures used to develop prediction curves for overpressures produced by airblast venting through the rupture of the cover rock over an accidental explosion in an underground magazine.

TUNNEL/CHAMBER VENT PRESSURE

Hopkinson scaling is typically used when airblast overpressures from different explosives quantities are compared. Scaled distances are calculated by dividing the measured distance by the cube root of the explosive charge weight. A comparison of peak overpressures from the Shallow Underground Tunnel/Chamber Explosion Test (Joachim, 1990) and the NOL spherical surface burst curve (Swisdak, 1975) is shown in Figure 1. The peak data from the Tunnel/Chamber test decrease as a function of azimuth from the extended access tunnel centerline. The higher peak pressures, along the 0-degree azimuth, are the result of the jetting through the access tunnel portal.

A pressure-time history from a measurement point along the 180-degree azimuth gage line (Gage A-29) is presented in Figure 2 (Halsey et al, 1989). This gage was located on the ground surface 50 m behind the tunnel portal and 7 m behind a vertical projection of the rear wall of the explosives storage chamber. The wave form combines pressures expelled through the access tunnel portal as well as pressures vented through the ruptured overburden above the chamber. As shown in Figure 2, the airblast shock wave vented through the access tunnel

portal arrived at this gage position 165 msec after detonation. The blast pressure wave vented through the overburden arrives 100 msec later at this gage station.

Peak pressures were from the overburden venting obtained by estimating the difference between the peak shown in Figure 2 and the exponentially decaying waveform from the early arriving pressure from the tunnel portal. In Figure 3, the estimated peak vent pressures are plotted versus horizontal distance from the source (i.e., horizontal distance from the gage to the vertical projection of the nearest chamber boundary). As shown in Figure 3, the peak vent pressure at the closest gage (7 m from the vertical projection of the rear wall of the chamber) is less than the airblast level that defines the Inhabited Building Distance (5.0 kPa).

COUPLING FACTOR

The DOD Explosives Safety Standards (1984) gives the following relation for computing the Inhabited Building Distance for ground motion effects:

$$D_{ig} = C f_g W^{4/9} \quad (1)$$

where D_{ig} is the Inhabited Building Distance, ft

C is constant for a particular earth material type

W is the weight of the explosives in the storage chamber, pounds.

and f_g is the decoupling factor, where

$$f_g = (4/15) w^{0.3} \quad (2)$$

where w is the chamber explosive loading density, pounds per ft³. Since we are using Hopkinson scaling (cube root), some manipulation of the decoupling factor is required. Assuming that the equivalent charge weight is

$$W_e = f_g W^{4/9} = f_c W^{1/3} \quad (3)$$

where f_c is the equivalent decoupling factor for Hopkinson scaling, in metric units. After some algebraic manipulation, we find that

$$f_c = f_g^{3/4} \quad (4)$$

$$\text{so} \quad f_c = 0.2 \, q^{9/40} \quad (5)$$

where q is the chamber loading density, kg/m^3 . The decoupling factor for a loading density of $66.4 \, \text{kg/m}^3$ (used on the Shallow Underground Tunnel/Chamber Explosion Test) is 0.514.

VENT PRESSURE DATA

A comparison of the NOL curve for blast pressure from spherical-surface burst charges, vented pressure data from fully-coupled detonations in desert alluvium, and the decoupled Tunnel/Chamber test are presented in Figure 4. As shown here, the overpressure curve from the cover venting of the Tunnel/Chamber test plots in the vicinity of the Buckboard 12 and Scooter data for buried charges in alluvium. The minimum cover depth for the Tunnel/Chamber test was 9.4 m, giving a minimum scaled cover depth of $0.335 \, \text{m/kg}^{1/3}$, compared with the 0.495 and $0.496 \, \text{m/kg}^{1/3}$ depths of burst for the fully coupled events in alluvium. The scaled charge radius of a spherical TNT charge is approximately $0.053 \, \text{m/kg}^{1/3}$. Thus, a $0.495 \, \text{m/kg}^{1/3}$ depth of burst provides approximately $0.44 \, \text{m/kg}^{1/3}$ overburden depth above the buried charges. The comparison presented in Figure 4 shows reasonably consistent agreement for the variations in cover depth (or equivalent depth of burst) considering that two very different media were involved--weathered granite and desert alluvium for the fully-coupled events.

A similar comparison of vented overpressures is shown in Figure 5 between the NOL curve, small-scale Norwegian model tests in sand, and the Tunnel/Chamber decoupled detonation. As shown here, vented pressures from the small-scale charges at a depth of burst of $0.50 \, \text{kg/m}^{1/3}$ (cover depth approximately $0.44 \, \text{m/kg}^{1/3}$) are an order of magnitude less than those measured from the decoupled Tunnel/Chamber detonation. Thus, the small-scale tests in sand do not model large decoupled detonations in granite.

Lines of estimated fit were drawn through the data for fully-coupled, buried charges in alluvium in Figure 4 to provide a means of estimating scaled horizontal distances to the vented overpressure levels of interest (ranging from 50 to 240 mb). Least square fits were calculated for the Midnight I and II, and

the Stagecoach II and III data, with the results used to estimate curve fits for the remaining data. The resulting data fits are shown in Figure 6.

The curves for peak vent pressure versus scaled distance developed in Figure 6 were used to obtain the overpressure contours presented in Figure 7. As shown here, the scaled horizontal distance to the 50-mb contour (airblast criterion for Inhabited Building Distance) decreases rapidly as the scaled overburden depth is increased from 0 to $0.15 \text{ m/kg}^{1/3}$. The scaled horizontal distance to the 50-mb overpressure contour for a cover depth of $0.15 \text{ m/kg}^{1/3}$ is $10 \text{ m/kg}^{1/3}$.

DISCUSSION

The use of the vented overpressure curves in Figure 7 are best illustrated with a few examples. Assume that a chamber is loaded with 113,500 kg (250,000 lb) of explosives at a loading density of 100 kg/m^3 . The coupling factor for this loading density is 0.564. The equivalent coupled charge is computed to be $0.564 \times 113,500 \text{ kg} = 64,000 \text{ kg}$. The cube root of the 64,000-kg explosive weight in the chamber is $40 \text{ kg}^{1/3}$. The 50-mb vented overpressure occurs at a horizontal distance of $0.4 \text{ m/kg}^{1/3}$ (16 m) for a cover depth of $0.44 \text{ m/kg}^{1/3}$ or 17.6 m, as compared to the K19 distance of 365 m computed in the current Standards. Next, consider the same total explosive weight (113,000 kg) and chamber loading density (100 kg/m^3), but with a scaled overburden depth of $0.14 \text{ m/kg}^{1/3}$ (5.6 m). The airblast Inhabited Building Distance (50 mb) is 404 m, compared with the same K19 distance (364 m) for this explosive quantity. Thus, the airblast Inhabited Building Distance to the rear of an underground magazine (180-degree azimuth) specified by the current Standards is greater than hazard distance actually produced by cover venting, when the scaled cover is relatively thick. Additional analysis is required however, to determine the level of overpressure venting through the overburden when the scaled cover thickness is less than $0.2 \text{ m/kg}^{1/3}$ for this explosive quantity and chamber loading density.

Based on an airblast criterion of 50 mb, the Inhabited Building Distance for overpressure from overburden venting (Figure 7) on the Shallow Underground Tunnel/Chamber Explosion Test (22,000 kg, (TNT equivalent). with a chamber loading density of 66.4 kg/m^3 , and a scaled cover depth of $0.34 \text{ m/kg}^{1/3}$, is 32.7 m. The airblast gage at a horizontal distance of 7 m from the back wall of the

chamber recorded an estimated vent pressure of 40 mb. Thus, the vented airblast pressure contours shown in Figure 7 are conservative.

CONCLUSIONS

The overpressure prediction curves developed in this analysis (Figure 7) indicate that a scaled cover depth of $0.5 \text{ m/kg}^{1/3}$ is sufficient to contain all hazardous airblast overpressure (greater than 50 mb) vented through the ruptured chamber overburden. The analyses also indicate that the 50-mb pressure criterion for Inhabited Building Distance will occur at a horizontal distance of $0.4 \text{ m/kg}^{1/3}$ for typical underground magazine explosive quantities. This restricts the hazardous overpressure distance from cover venting to the immediate vicinity of the storage chamber. Therefore, it is suggested that the maximum scaled depth of overburden (C_c) specified in DOD 6055.9-STD (Section G.4.d.2) for which overpressure venting must be considered should be changed to a value consistent with the NATO hazard criteria for ejecta/debris, namely $C_c = 0.8 \text{ m/kg}^{1/3}$ for hard rock and $C_c = 1.0 \text{ m/kg}^{1/3}$ for soft rock. The data presented in Figure 3 indicates that these values would be conservative as far as hazardous venting overpressures from rupture of the chamber cover are concerned.

As the scaled cover depth decreases from $0.2 \text{ m/kg}^{1/3}$, the scaled horizontal distance to the 50-mb overpressure level increases at a slower rate for all the cover venting overpressure curves plotted in Figure 7. The vented overpressures from chamber cover rupture are approximately one-tenth of the overpressures predicted by surface detonations of the same yield; at this scaled cover depth the vented pressures will increase rapidly, however, as the scaled cover depth decreases. Therefore, the value of $0.2 \text{ m/kg}^{1/3}$ for the minimum scaled cover depth given in the present Standards appears reasonable.

RECOMMENDATIONS

A series of decoupled buried explosive tests is needed to more accurately define the venting pressures and explosive energy equivalence for detonations in shallow underground magazines.

ACKNOWLEDGEMENT

We gratefully acknowledge permission from the Chief of Engineers and the sponsors to publish this paper. We also gratefully acknowledge permission from the Defense Nuclear Agency for use of the MIDNIGHT HOUR (I and II) vent pressure data in this paper.

REFERENCES

Department of Defense, 1984, "Ammunition and Explosives Safety Standards," DOD 6055.9-STD, Assistant Secretary of Defense (manpower, Installations, and Logistics), Washington, D.C.

Halsey, Carl C.; Durbin, William F.; and Berry, Sharon L.; 1989, "KLOTZ Underground Magazine Trial, Data Report," NWC TM-6562, Naval Weapons Center, China Lake, CA.

Joachim, Charles E., 1990, "Shallow Underground Tunnel/Chamber Explosion Test Program, Summary Report," in publication, U.S. Army Engineer Waterways Experiment Station, Vicksburg, MS.

Jenssen, Arnfinn, 1979, "Fortifikaterick Notat" Nr 132/79, Norwegian Defence Construction Service, Oslo, Norway.

Snell, Charles M., and Oltmans, Dennis L., 1971, "A Revised Empirical Approach to Airblast Prediction," EERO Technical Report No. 39, U.S. Army Engineer Waterways Experiment Station, Explosive Excavation Research Office, Livermore, CA

Swisdak, Michael M., 1975, "Explosion Effects and Properties, Part I, Explosion Effects In Air," NSWC/WOL/TR 75-116, Naval Surface Weapons Center, Silver Spring, MD.

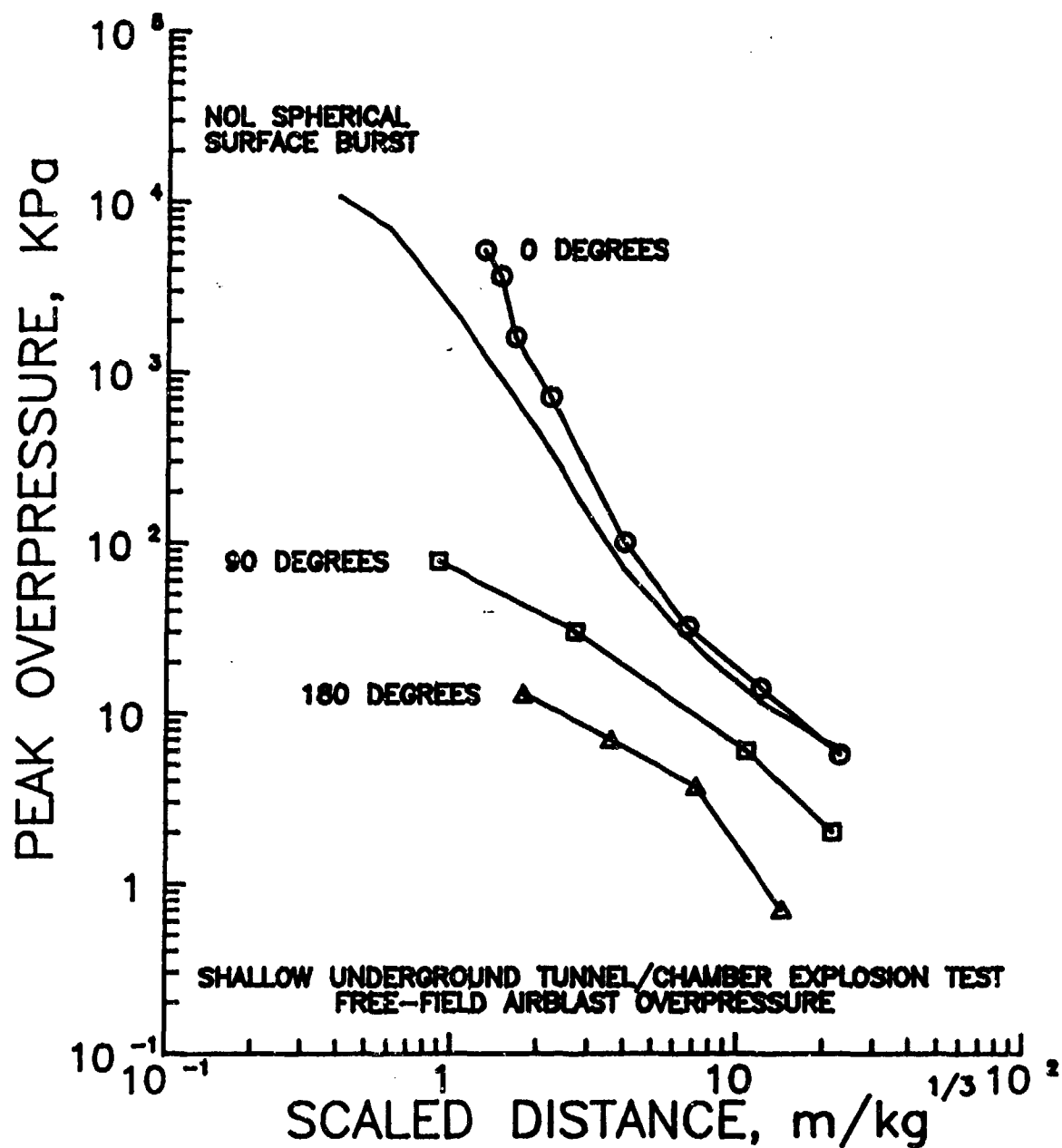


Figure 1. Comparison of free-field airblast overpressures from NOL spherical surface burst calculation and the Shallow Underground Tunnel/Chamber Explosion Test (0, 90 and 180-degree azimuths).

EXTERNAL AIRBLAST PRESSURE

0 m 150 m

Array Size: 200050
 F4 Low Pass 2000. HZ
 Init Time -4.9
 Start at 158
 Stop at 1420
 Cal val 1.03
 Deflection -727

SUTCET A-29-DUAL
 X5970 Track 23

50 KHZ 5-JUL-90

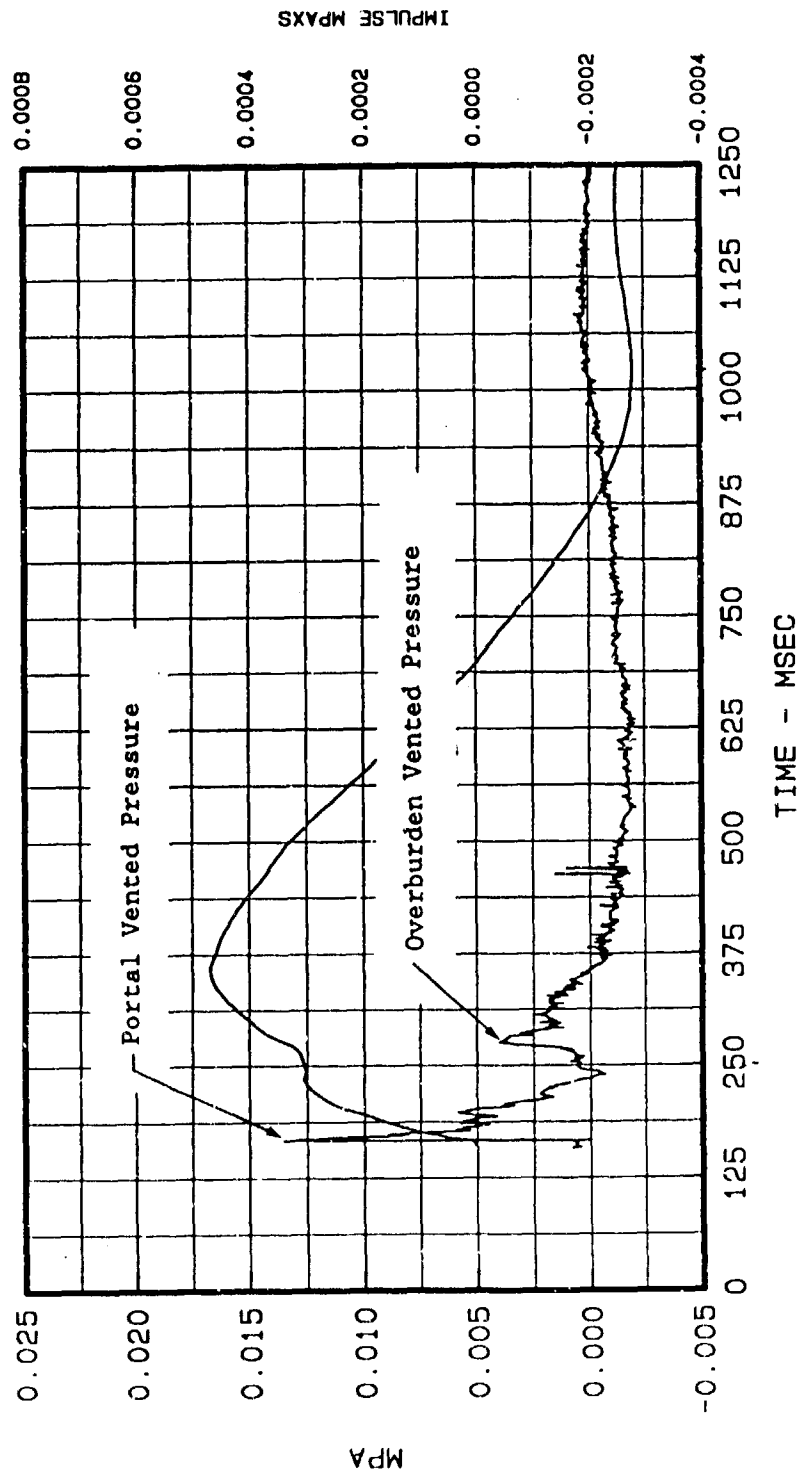


Figure 2. Portal and overburden airblast overpressure and impulse wave forms at Gage A-29, from decoupled detonation (Shallow Underground Tunnel/Chamber Explosion Test). Gage is located along 180-degree azimuth, 50 m from access tunnel portal (7 m from vertical projection of nearest chamber wall).

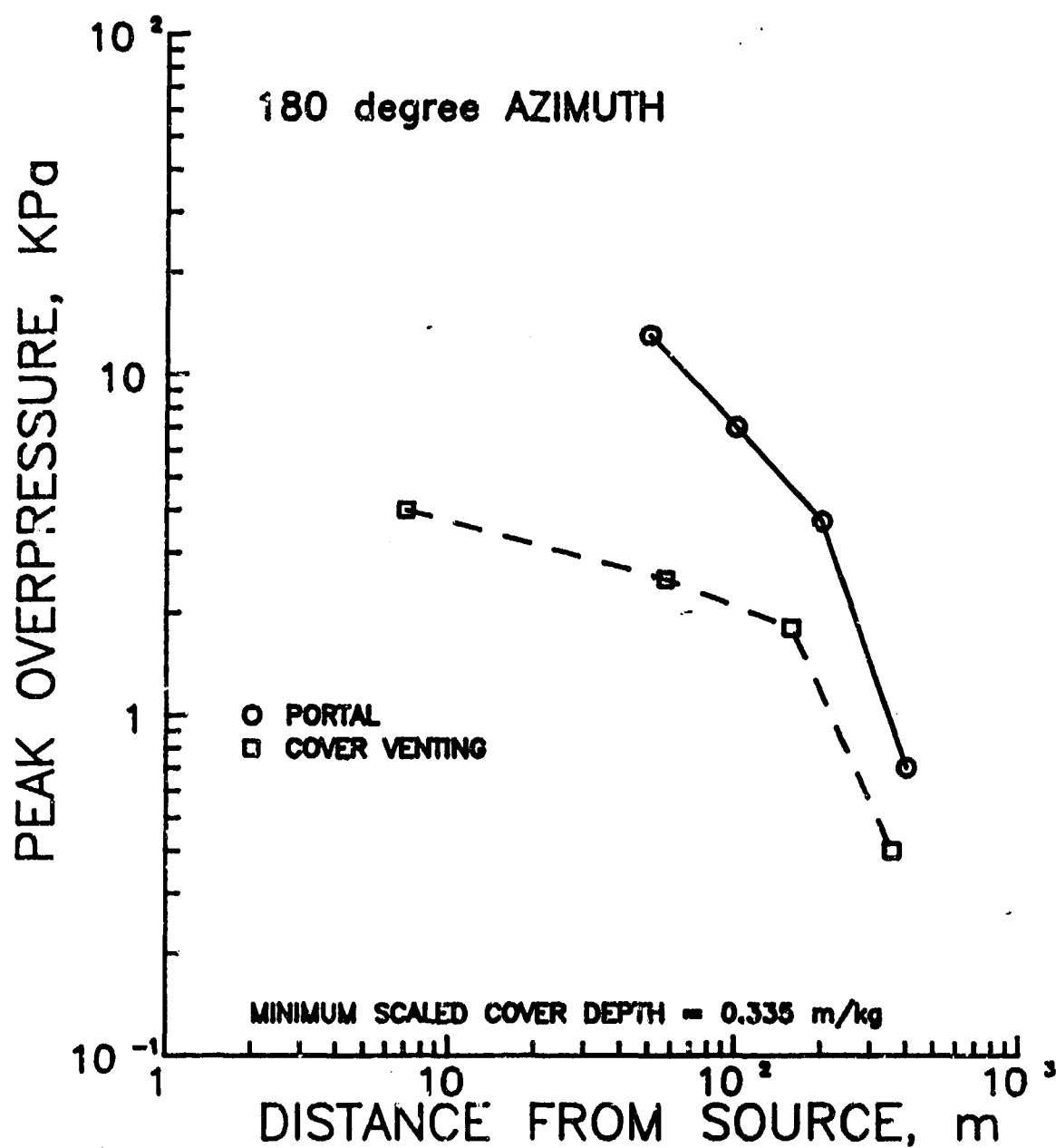


Figure 3. Comparison of portal and overburden vented overpressures along the 180 degree azimuth, Shallow Underground Tunnel/Chamber Explosion Test.

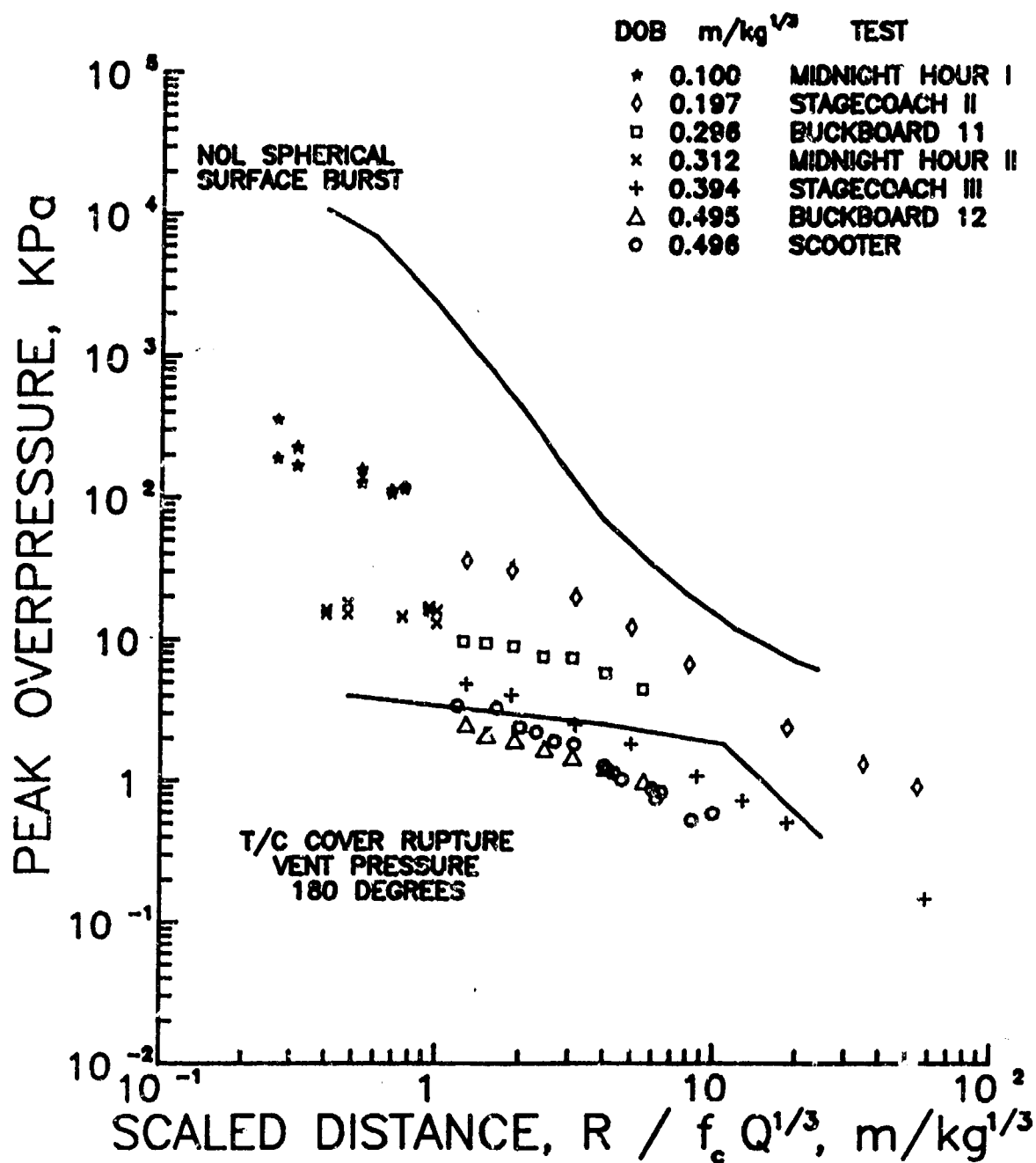


Figure 4. Comparison of vented airblast overpressure data from fully-coupled, buried detonations in desert alluvium with the NOL calculated pressure for spherical surface bursts and measured vent pressures from the decoupled Tunnel/Chamber test.

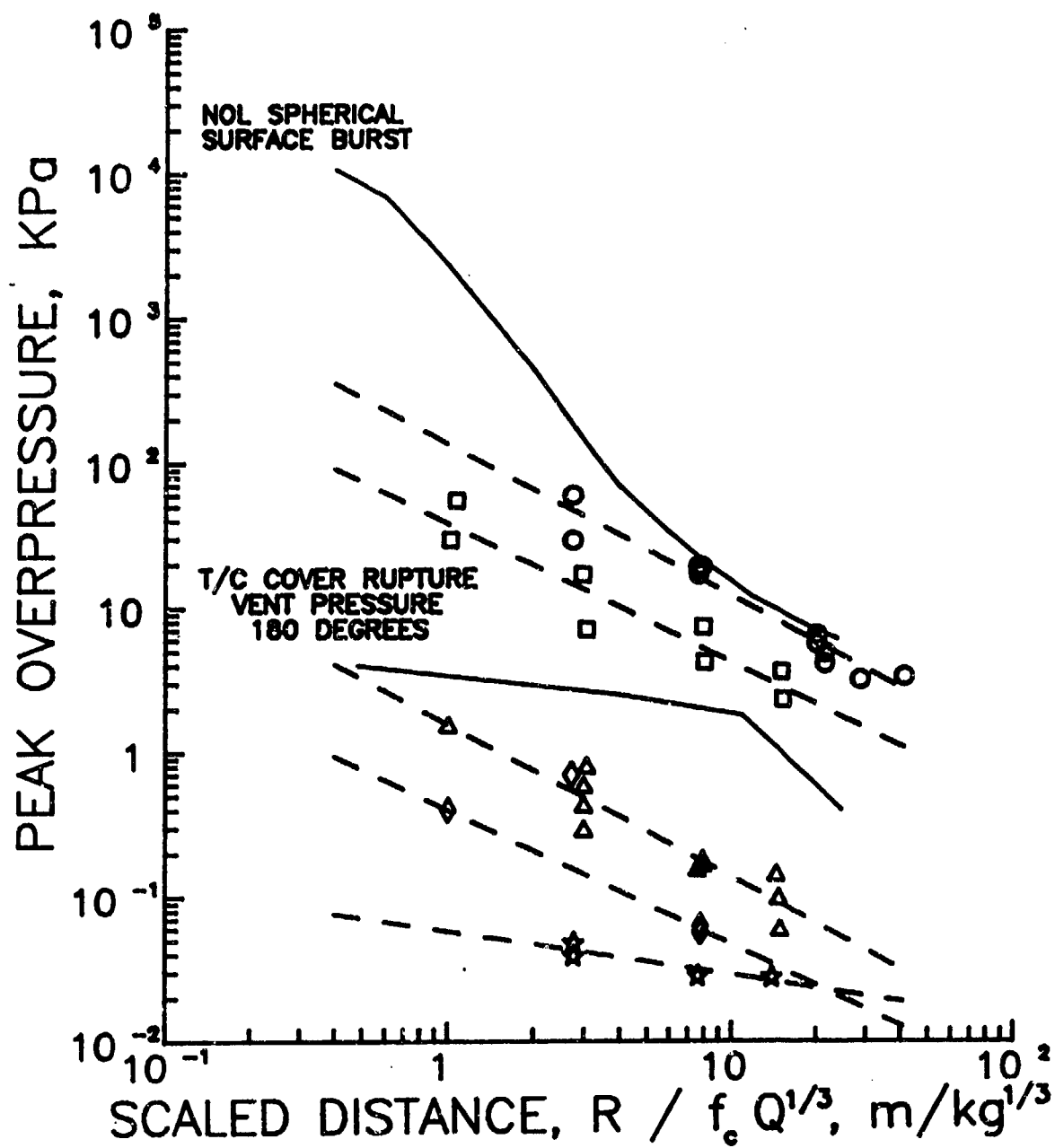


Figure 5. Comparison of vented airblast overpressure data from fully-coupled, buried small-scale detonations in sand (Jenssen, 1979) with the NOL calculated pressure for spherical surface bursts and measured vent pressures from the decoupled Tunnel/Chamber test.

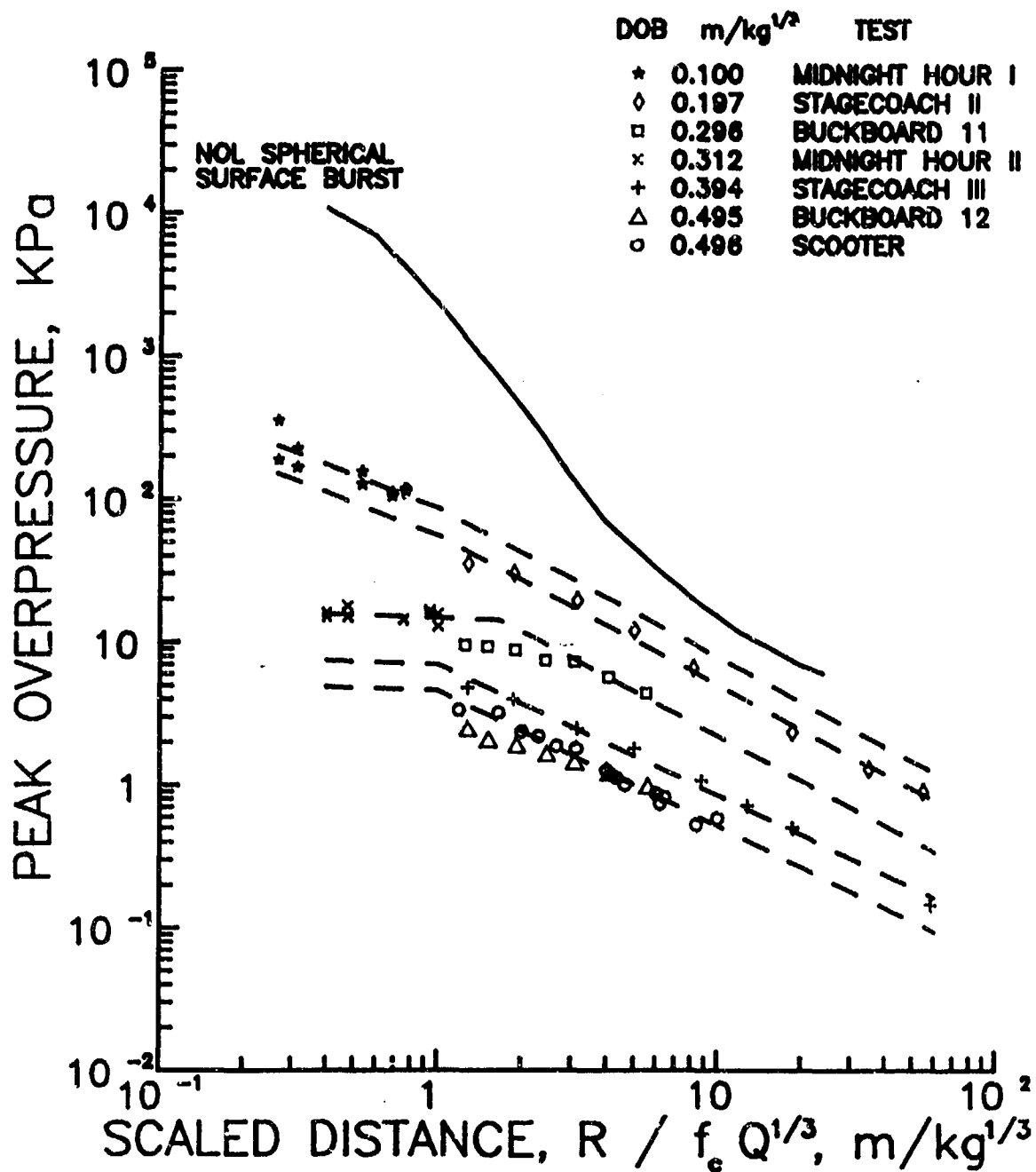


Figure 6. Peak pressure versus scaled horizontal distance for fully-coupled, buried detonations in desert alluvium, with estimated best-fit curves.

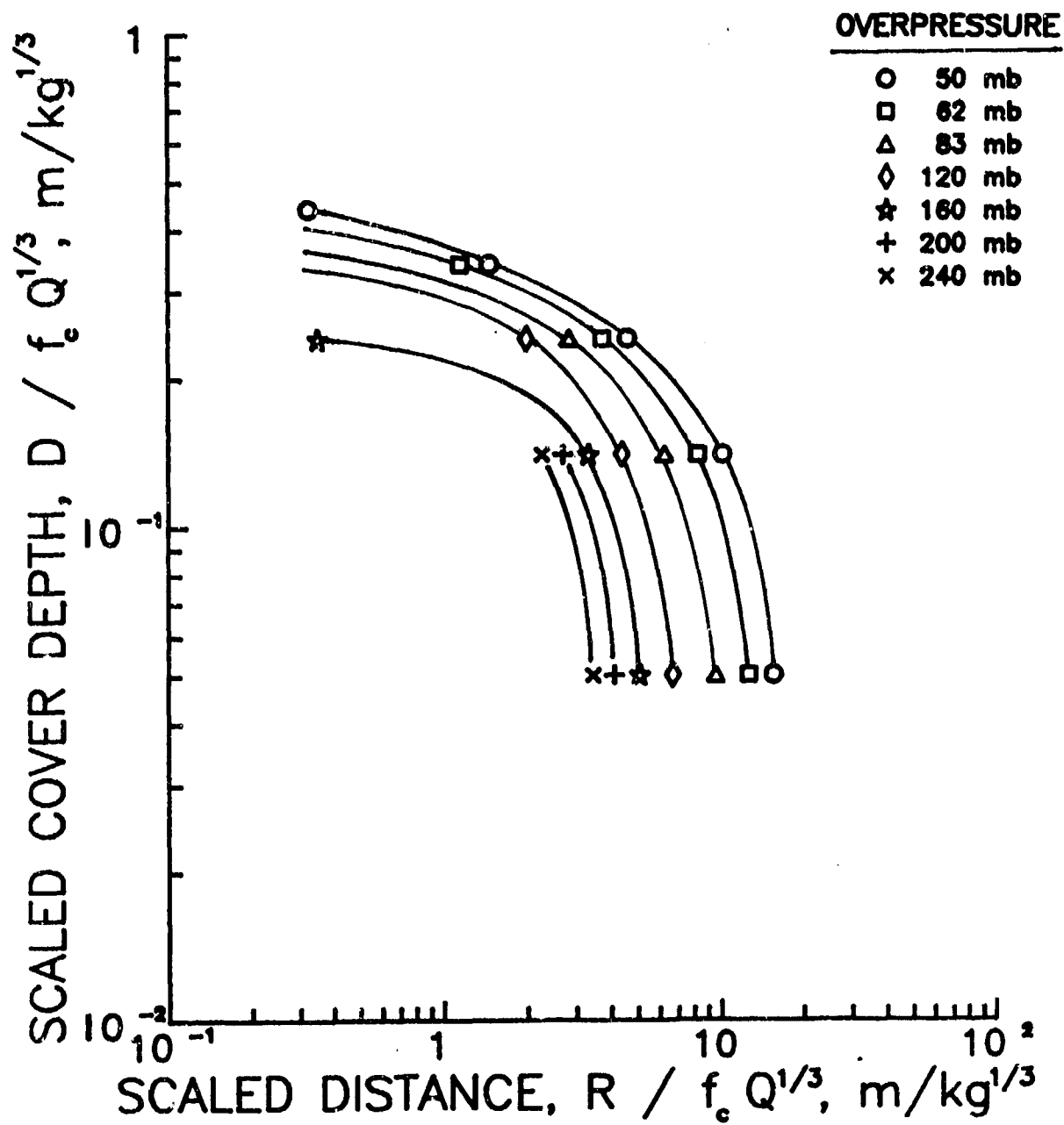


Figure 7. Airblast overpressure contours as a function of scaled cover depth and scaled horizontal distance from detonations in underground munitions storage chambers.

EJECTA HAZARD RANGES FROM UNDERGROUND MUNITIONS STORAGE MAGAZINES

Charles E. Joachim
U.S. Army Engineer Waterways Experiment Station
Vicksburg, Mississippi

INTRODUCTION

Current ejecta quantity-distance (Q-D) criteria for underground munitions storage magazines are based on a few large, high explosive tests, coupled with a limited number of model and full-scale experiments in igloos and underground magazines. The ejecta hazards from accidental detonations in underground magazines are from two sources: overburden rupture and venting (shallow storage chambers), and the breakup of the access tunnel portal or material (including unexploded ordnance) expelled through it. Over the past decade, launch velocity curves for overburden ejecta have been developed in Norway, as a function of cover depth and chamber loading density. This paper describes the analyses conducted and the relation found between the Norwegian launch velocity curves, a simple computational model, and existing ejecta data.

COVER RUPTURE

The primary variables which govern rupture (or cratering) of the overburden above an underground munitions storage chamber are the chamber loading density, cover thickness, and to a limited extent, overburden material. Because of the air volume in the underground chamber, these explosions are not fully coupled to the soil or rock in which the magazine is constructed, and therefore are less efficient in rupturing (cratering) the overburden and producing ejecta than the standard buried charges which are the source of most cratering data. The difference is mainly one of degree, however, since the mechanics of the rupture (crater) formation are essentially the same. Accordingly, the effect of overburden thickness on these effects is described here from a classical cratering context.

For a given explosive loading density, crater size will at first increase steadily as the depth of burst (DOB) is increased. At some depth called the "optimum" DOB, the crater size will reach a maximum. For further increases in DOB, the weight of the overburden tends to suppress the formation

of the crater. As the energy of the explosion becomes less able to throw ejecta beyond the edge of the crater, more material falls back within the crater boundary, thus reducing the apparent crater depth. The crater radius will decrease slightly until a DOB called the containment depth is reached, at which the crater completely disappears and is replaced by a mound of bulked soil or rock. Finally, the camouflet depth is that DOB at which little or no surface disturbance occurs, and the explosion forms only a subsurface cavity. Figures 1 (for soil) and 2 (for rock) from Reference 1 illustrate characteristic variations in crater parameters as a function of DOB.

The apparent crater radius decreases and approaches zero as the charge DOB approaches $2.0 \text{ m/kg}^{1/3}$ for soil or $1.2 \text{ m/kg}^{1/3}$ for soft rock (1.0 for hard rock). The limits are shown by the upper bound lines in Figures 1 and 2, respectively. Explosions at these DOB's are fully contained, producing only surface heaving. Therefore, munitions storage chambers with cover depths greater than 2.0 (soil), 1.2 (soft rock) or $1.0 \text{ m/kg}^{1/3}$ (hard rock) will not produce significant ejecta hazards from rupture of the overburden.

EXPLOSIVE COUPLING

If an earth-covered or underground storage chamber is completely filled with explosives, so that no empty volume remains, the explosive loading density will be approximately 1600 kg/m^3 . In most cases, however, the chamber is not completely filled, so the loading density is some fraction of this value. Explosive "coupling" refers to the intimacy of contact between a volume of explosive and the surrounding soil or rock. If a chamber is completely packed with explosives, the detonation is "fully coupled", with a coupling factor (f_{cf}) of 100%. As the explosive loading density is decreased, the coupling factor decreases proportionally.

Ground shock, cratering, and ejecta/debris throwout all decrease for lower coupling factors. The coupling factor can be estimated from Figure 3 (based on underground coupling experiments in halite and model ammunition storage chamber experiments at the U.S. Army Engineer Waterways Experiment Station). The effective charge weight (Q_e) is the product of the explosive weight (Q) and the coupling factor (f_{cf}) that applies for a given chamber loading density ($Q_e = f_{cf} Q$). The effective explosive weight can then be used

in Figure 1 or 2 to obtain predicted crater dimensions for a large detonation in an underground storage chamber.

EJECTA HAZARD CRITERIA

The debris hazard criteria given in the U.S. DOD Explosives Safety Standards (Reference 1) and the NATO AC/258 manual (Reference 2) consider two sources of hazardous debris: rock thrown by the overburden rupture and material blown through the access tunnel portal. The Explosives Safety Standards require a Inhabited Building Distance for debris of 610 m along and 15 degrees either side of the extended access tunnel centerline. The NATO AC//258 Inhabited building Distance for debris is 600 m over the same 30 degree arc.

For debris originating from rupture of the magazine cover, the Explosives Safety Standards give a hazard range of

$$D_{id} = f_d f_c Q^{0.41} \quad (1)$$

where D_{id} is the hazard range, m

f_c is a function related to the scaled overburden depth, m

Q is the explosive quantity stored in the chamber, kg

and f_d is a function of chamber loading density, given by the relation

$$f_d = 0.364 (Q / V)^{0.18} \quad (2)$$

where V is the chamber volume, m^3

The function f_c is given graphically in Figure 4 for hard rock (granite or limestone) and for soft rock (sandstone). The relation between the function f_d and the coupling factor (f_{cf}) is shown graphically in Figure 5.

The minimum overburden thickness above the chamber for the Shallow Underground Tunnel/Chamber Explosion Test was 9.4 m, giving a scaled (TNT-equivalent) overburden depth of $0.35 \text{ m/kg}^{1/3}$. The earth cover function, f_c , for this scaled overburden depth is $5.09 \text{ m/kg}^{0.41}$, from the "soft rock" curve of Figure 4. The loading density function calculates to be 0.77. Substituting these values in Equation 1, the Inhabited Building Distance for protection from debris from the Shallow Underground Tunnel/Chamber Explosion

Test is 236 m.

The NATO AC/258 debris criteria for a scaled cover depth of $0.35 \text{ m/kg}^{1/3}$ are given as

$$D4 = 5.10 Q^{0.41}, \quad \text{for hard rock} \quad (3)$$

and $D5 = 5.00 Q^{0.41}, \quad \text{for soft rock} \quad (4)$

These criteria were developed for a loading density of 270 kg/m^3 . A reduction is allowed for smaller loading densities. For the TNT-equivalent loading density of 66.4 kg/m^3 that was used for the Shallow Underground Tunnel Chamber Test, the correction factor for the NATO AC/258 "soft rock" criterion is 0.80. For hard rock, the Inhabited Building Distance for debris is 308 m before correction for loading density, and 246 m with the correction.

The current Explosives Safety Standards criterion for a debris hazard is a fragment or debris density of one hazardous particle per 56 m^2 . An analysis of the debris on the motion picture records of the Tunnel/Chamber test indicated that almost all debris seen on the film was potentially lethal (kinetic energy greater than 79 J), and thus considered hazardous. As shown in Figure 6, a debris density of one missile impact per 56 m^2 occurred at a distance of 656 m. This distance is 1.08 times the hazard range calculated by the Standards, and is 1.09 times the NATO AC/258 Inhabited Building Distance for debris range along the access tunnel axis.

The debris and ejecta collection on the Tunnel/Chamber Test was concentrated within a sector extending 45 degrees each side of the extended tunnel axis; therefore the effect of azimuth on debris range can only be based on data within this sector. These data are shown in Figure 7, where curves are drawn to approximate the debris limits at azimuths of 0, 20, and 40 degrees. As shown here, the distance to a debris density of one strike per 56 m^2 is 656 m, 447 m, and 287 m along the 0, 20, and 40-degree azimuths, respectively. For the Tunnel/Chamber Test configuration, Figure 8 compares debris hazard ranges, as a function of azimuth, based on criteria given in the Explosives Safety Standards and NATO AC/258, with ranges derived from actual debris data collected on the Tunnel/Chamber Test. As shown in the comparison,

both sources slightly underpredict the hazard ranges in front of this tunnel/chamber geometry and loading density.

EJECTA VELOCITY

The pre-and posttest locations of the artificial missiles used for the Tunnel/Chamber Test are given in Reference 4. The ejecta ranges are plotted versus their pretest locations in Figure 9. In this figure, "slant distance" is the distance from the center of the 20,000 kg charge to a missile's pretest or posttest position, as calculated from surface coordinates and elevation data. The symbols in Figure 9 identify missile pretest locations with respect to the surface ground zero (SGZ), which is a point on the overburden directly above the center of the explosive charge. FRONT denotes pretest missile locations down-slope from the SGZ. As shown in Figure 9, the test data indicates that missiles originating at locations down-slope from the SGZ (FRONT) travel the greatest distance, and those originating at up-slope locations (BACK) travel the least. All missiles were found down-slope from their original positions. The differences in displacement of missiles on the east side compared to those on the west side of the magazine is attributed to slope effects. The overburden surface dropped gradually to the east and rapidly to the west.

Launch velocities were computed for three artificial missiles using the known missile displacement and assuming a launch angle of 45 degrees. The calculated launch velocities are plotted in Figure 10, where a comparison is shown with results of previous tests Reference 5), which include data from storage wall debris tests, aircraft shelter detonations, and large-scale buried detonations, both tamped and untamped. The artificial missile launch data from the Tunnel/Chamber Test are in good agreement with the other data shown in Figure 10.

COMPUTED HAZARD RANGE

Ejecta range was computed from the launch velocity curves of Figure 10 using a trajectory algorithm obtained from Reference 6. A concrete missile mass of 454 kg, a storage chamber volume of 331 m³, and an explosive weight of 22,000 kg were assumed for these calculations (the storage volume and weight

correspond to the Tunnel/Chamber Test). The computed ejecta hazard ranges are plotted versus scaled cover depth in Figure 11. The cover depth (D) is scaled by two factors: the cube root of the charge weight ($Q^{1/3}$), and the chamber loading density to the 0.18 power ($q^{0.18}$). As shown in Figure 11, the computed ejecta hazard range for loading densities between 10 and 100 kg/m³ collapse onto a single curve when plotted versus scaled cover depth. Lighter loading densities give shorter calculated ejecta hazard ranges at shallow scaled cover depths, and approach the common upper bound curve as scaled cover depth increases.

A simple calculation was performed to estimate an upper bound of the overburden ejecta hazard range for the Tunnel/Chamber Test conditions (a loading density of 66.4 kg/m³). The WES computer code BREACHWL, which calculates the velocity of the breached section of a wall from an internal pressure-time history was used to compute ejecta velocity. The pressure-time history used was that recorded at the chamber wall (Gage C-3) on the Tunnel/Chamber Test, shown in Figure 12. Since the waveform ended prematurely due to cable failure at 40 msec the time history was arbitrarily extended to 320 msec by halving the pressure every 20 msec. The resulting velocity waveform is presented in Figure 13. A rock density of 2540 kg/m³ was assumed for these calculations. An estimated ejecta hazard range was obtained using the calculated peak missile velocity as input to the trajectory algorithm. These computations were performed for cover depths ranging from 4.2 to 56 m.

Measured and calculated ejecta hazard ranges are compared with the Explosives Safety Standard debris Inhabited Building Distance for hard and soft rock in Figure 14. The comparison includes data from the Shallow Underground Tunnel/Chamber Test (ejecta/debris collection and artificial missile recovery), the 100 kg/m³ launch velocity curve (Figure 11) and the BREACHWL calculated data. As seen in Figure 14, the experimental data is in good agreement with the ranges derived from the 100-kg/m³ launch velocity curve. The launch velocity curve crosses both Explosive Safety Standard debris Inhabited Building Distance curves at a cover depth of approximately $0.28 Q^{1/3}$ meters for a loading density of 100 kg/m³, which suggests that the Standard may not be conservative for shallower cover depths. Since the 100 kg/m³ launch velocity curve is in agreement with the measured Tunnel/Chamber

Test missile data and an upper bound to the ejecta hazard range data the Figure 14 also indicates that the Explosive Safety Standard is very conservative at cover depths much greater than $0.28 Q^{1/3}$ meters.

A similar comparison with the NATO AC/258 Inhabited Building Distance for hard and soft rock are shown in Figure 15. The NATO curves both intersect the 100 kg/m^3 launch velocity curve at a cover depth of $0.32 Q^{1/3}$ meters. This suggests that the NATO Inhabited Building criteria for debris may be unconservative at shallower cover depths, and overly conservative when the overburden thickness is greater than $0.32 Q^{1/3}$ meters.

CONCLUSIONS

The minimum cover depth given in the current NATO manual ($1.4 \text{ m/kg}^{1/3}$) for an underground magazine that is required to ensure containment of debris hazards is safety conservative and no change is recommended. The debris data from the Shallow Underground Tunnel/Chamber Test indicate that the Inhabited Building Distance for ejecta along the extended access tunnel centerline is unconservative and both the distance and the arc of coverage should be increased. Although the data are limited, the comparison of measured data and hazard ranges calculated from estimated launch velocities indicates that the Explosive Safety Standard and NATO AC/258 both are non-conservative for shallow cover depths, and overly conservative at greater cover depths. More data is needed to better define these relations.

ACKNOWLEDGEMENT

We gratefully acknowledge permission from the Chief of Engineers and the sponsors to publish this paper.

REFERENCES

1. Davis, Landon. K.; McAneny, Colin. C.; Joachim, Charles E.; 1981, "PROJECT SPERRE, Report 3, Phase II: Field Tests--Explosive Cratering Experiments in Granite and Sandstone," Technical Report SL-81-5, U.S. Army Engineer Waterways Experiment Station, Vicksburg, MS.
2. U.S. Department of Defense; "Ammunition and Explosives Safety Standards," DOD 6055.9-STD), 1984, Assistant Secretary of Defense (Manpower, Installations and Logistics), Washington, D.C.
3. North Atlantic Treaty Organization; "Manual on NATO Principle for the Storage of Ammunition and Explosives, Part III," 1977, AC/258-D/258, Group of Experts on the Safety Aspects of Transportation and Storage of Military Ammunition and Explosives (AC/258).
4. Halsey, Carl C.; Durbin, William F.; Berry, Sharon L.; 1989, "KLOTZ Underground Magazine Trial, Data Report," NWC TM-6562, Naval Weapons Center, China Lake. CA.
5. Helseth, Einar S.; "Underground Ammunition Storage, Model Test in Scale 1:100 in Sand," 1982, Fortifikatorisk Notat Nr 160/82, Progress Report to KLOTZ Club, Norfolk, VA.
6. Swizdak, Michael, M.; Private Communication, Naval Surface Weapons Center, Silver Springs, MD.

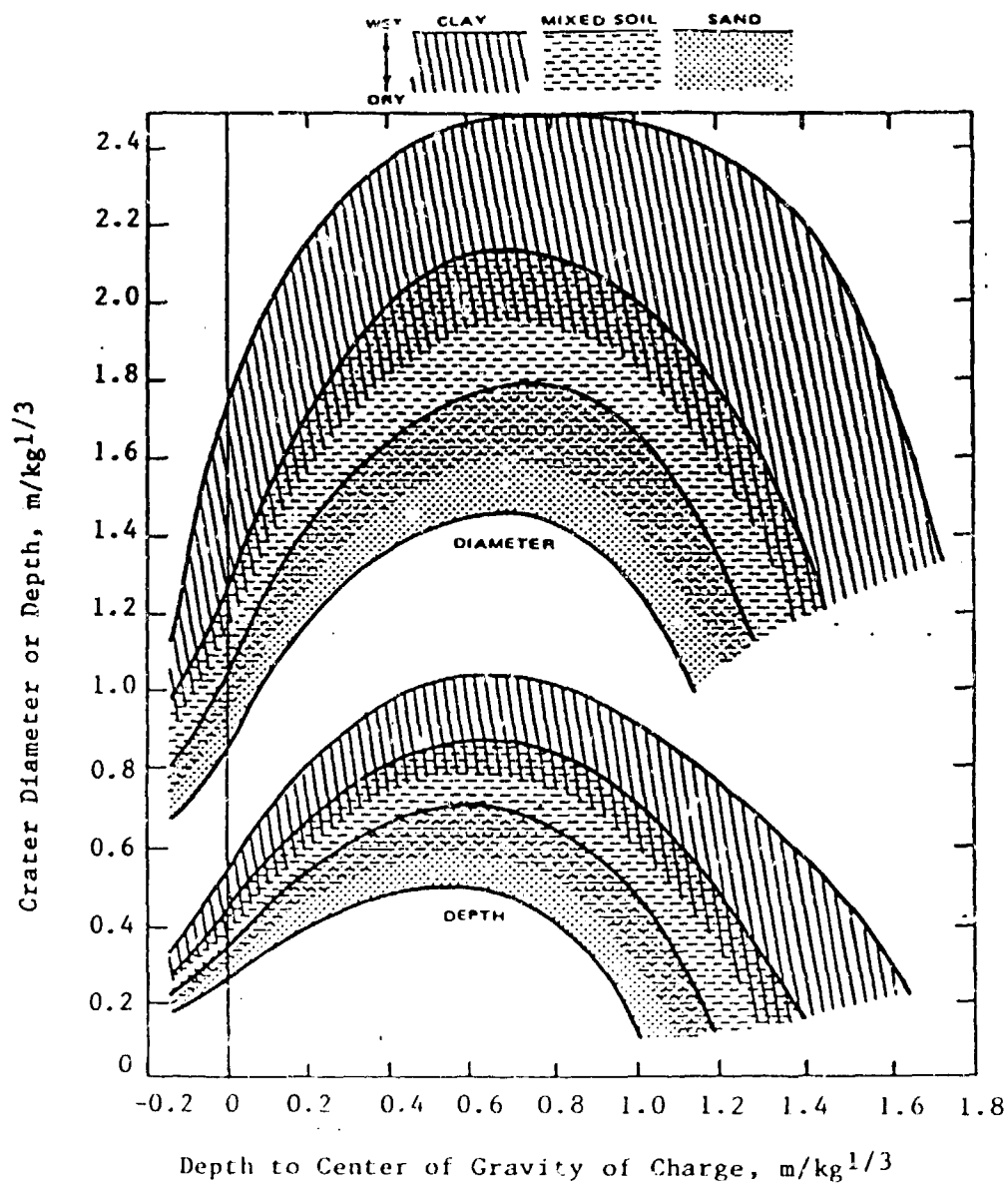


Figure 1. Apparent crater dimensions from explosions in various soils as a function of depth of burst (DOB) and general soil type.

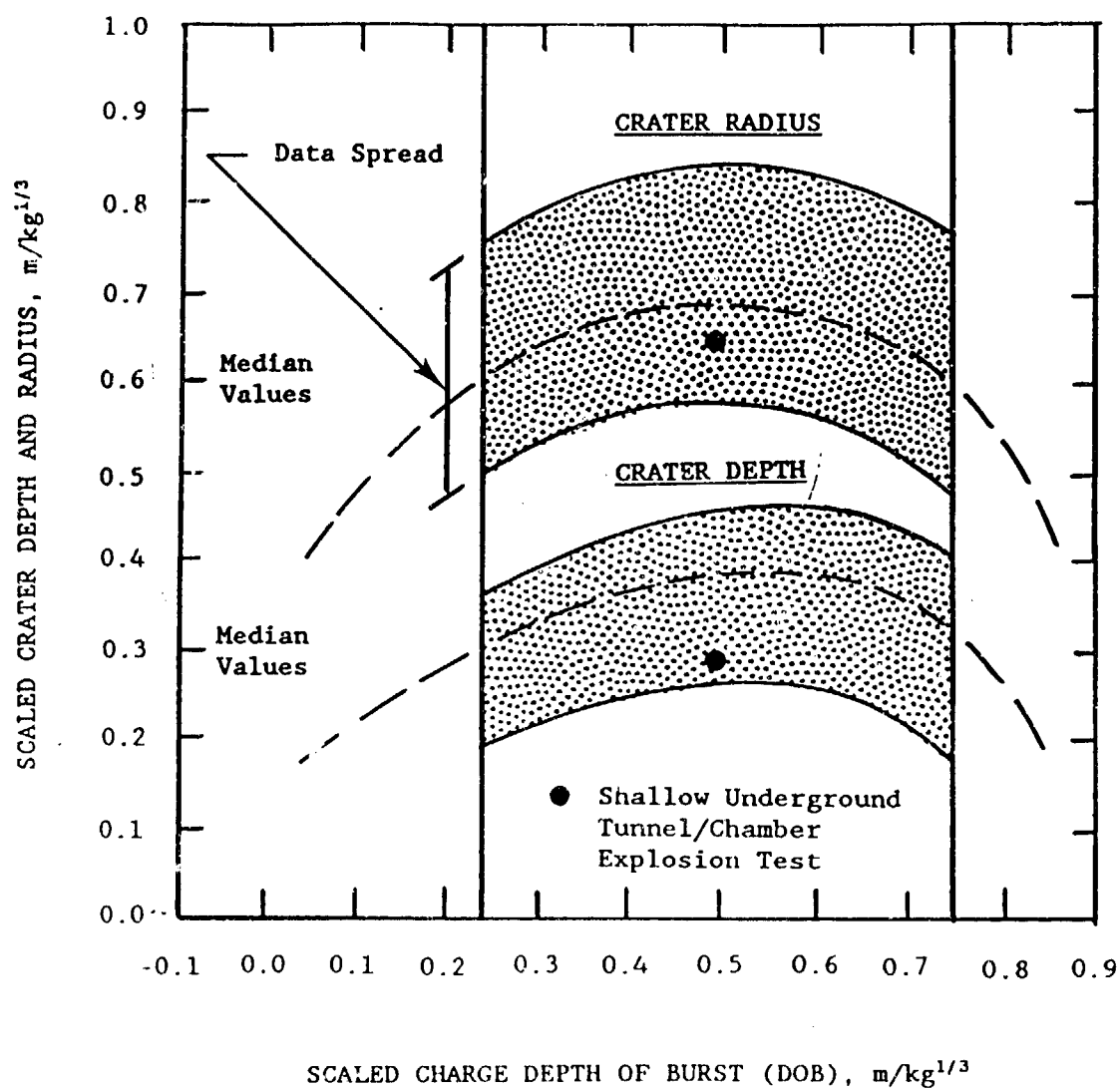


Figure 2. Apparent crater dimensions from explosions in rock as a function of depth of burst (DOB).

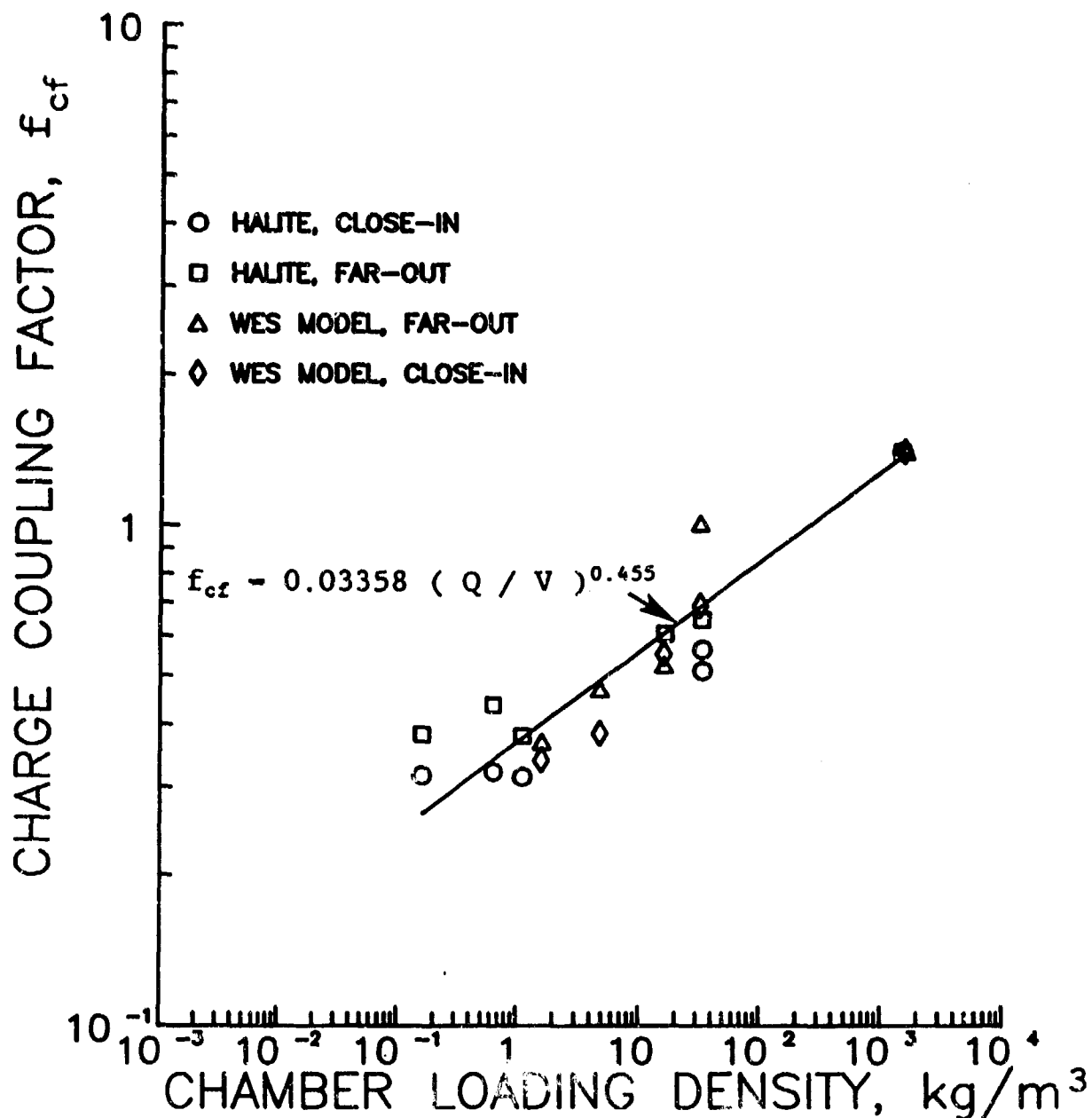


Figure 3. Charge coupling factor as a function of chamber loading density. Coupling data are derived from coupled and decoupled peak particle velocity measurements in halite and peak strain measurements from WES model tests.

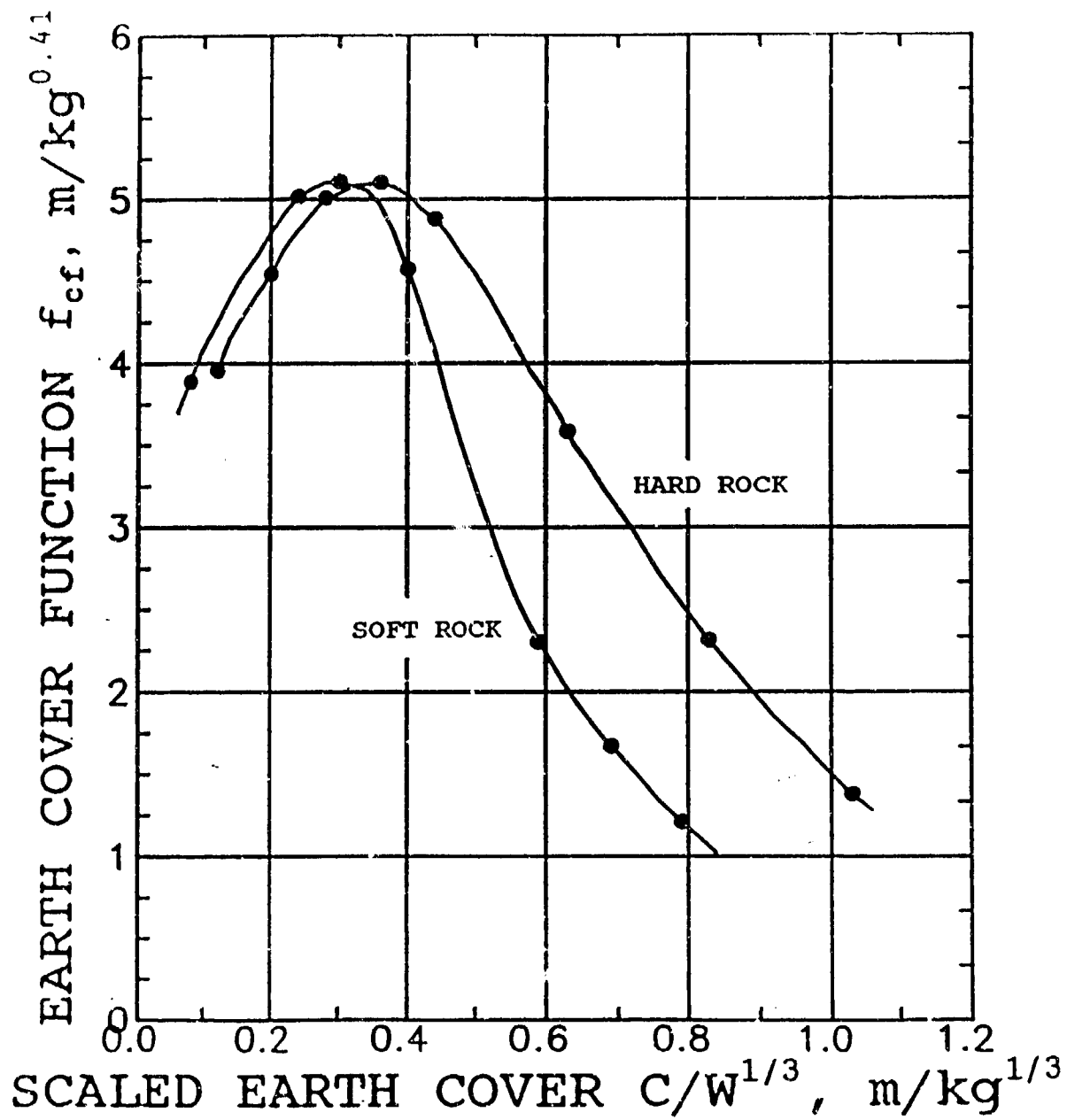


Figure 4. Earth cover function, f_c , for ejecta/debris versus scaled chamber earth cover depth; Ammunition and Explosives Safety Standards (Reference 2).

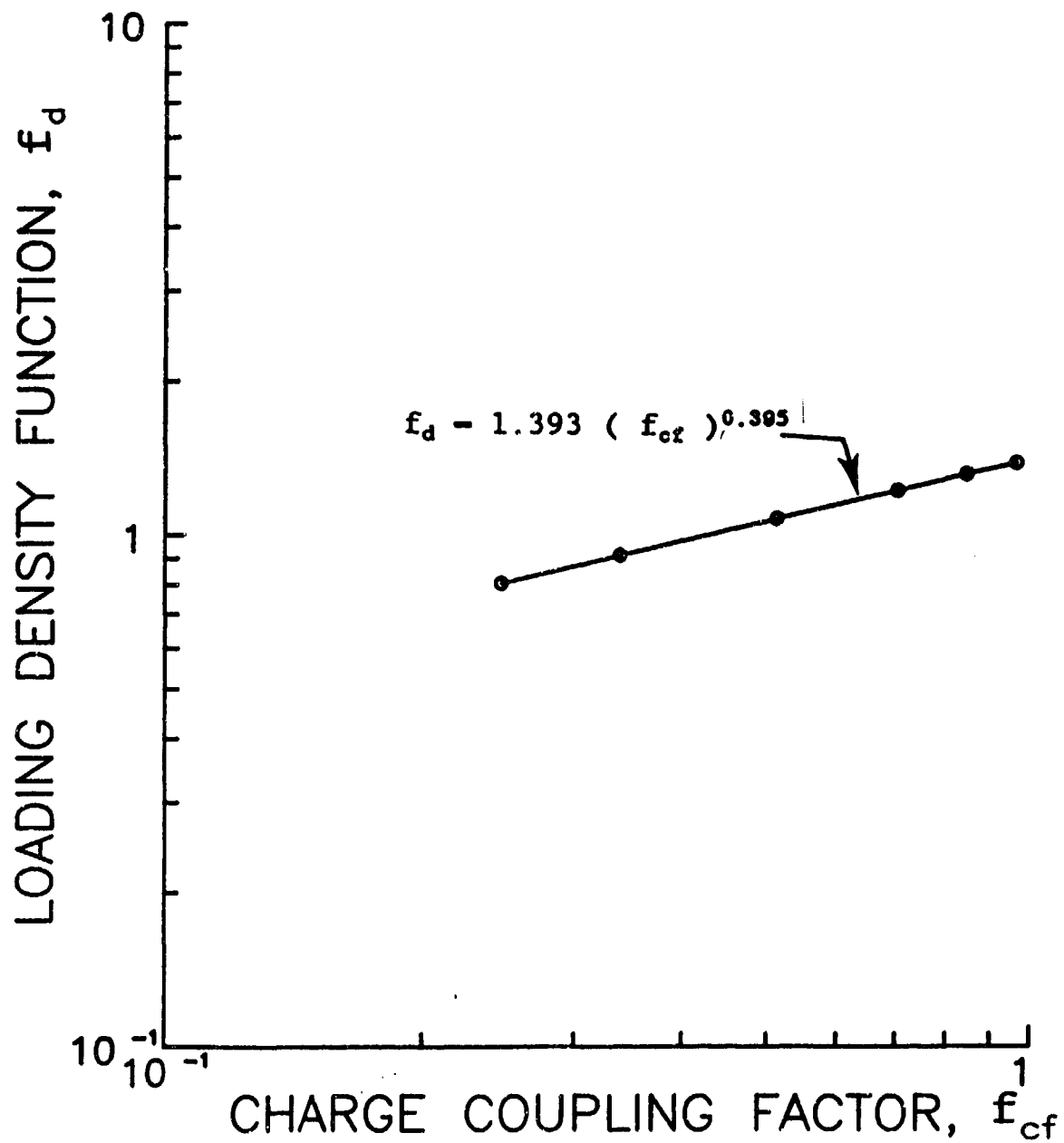


Figure 5. Charge loading function, f_d , for ejecta/debris versus charge coupling factor, f_{cf} .

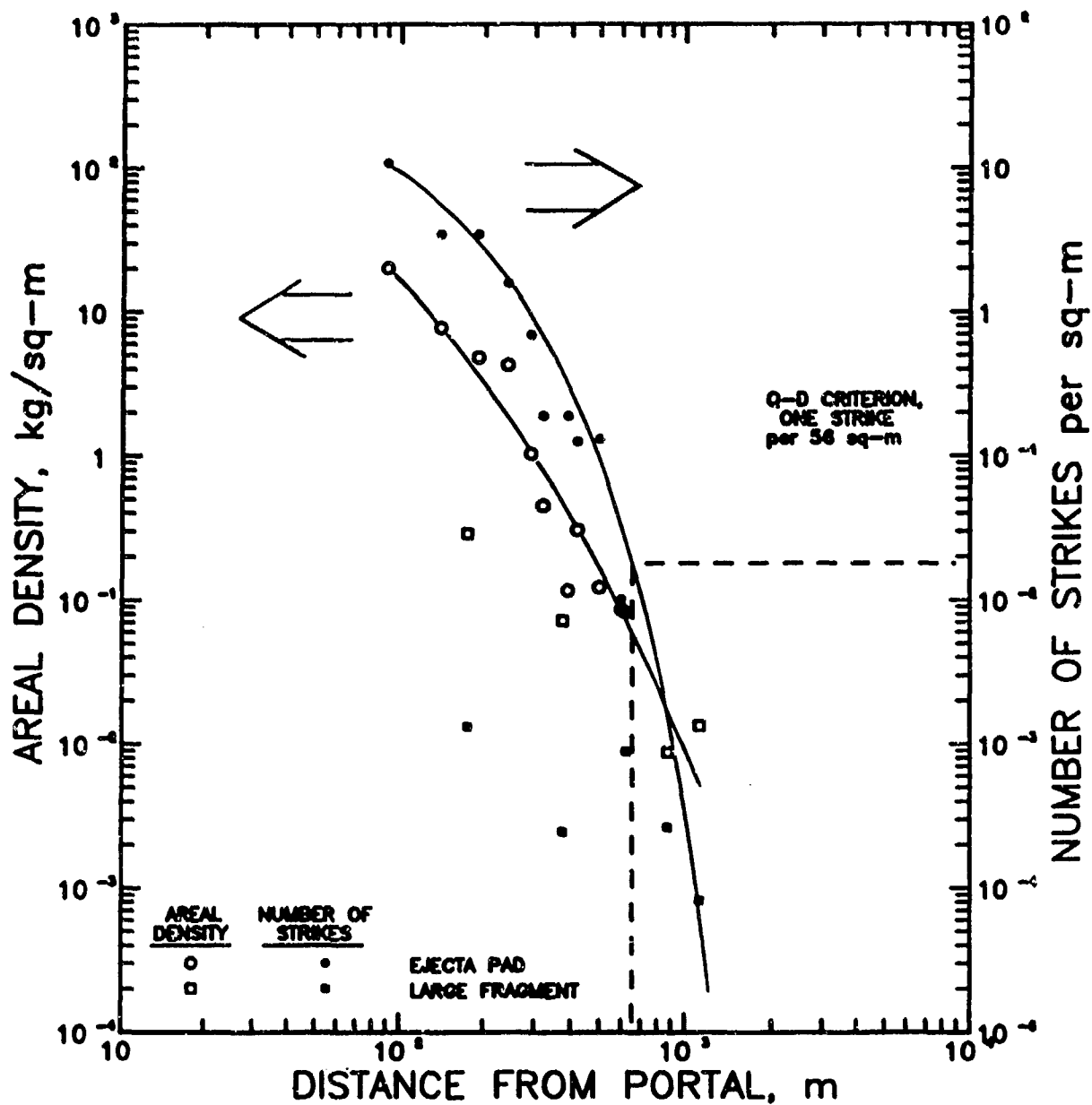


Figure 6. Areal density and number of strikes of natural missiles versus distance from tunnel portal, Shallow Underground Tunnel/Chamber Explosion Test.

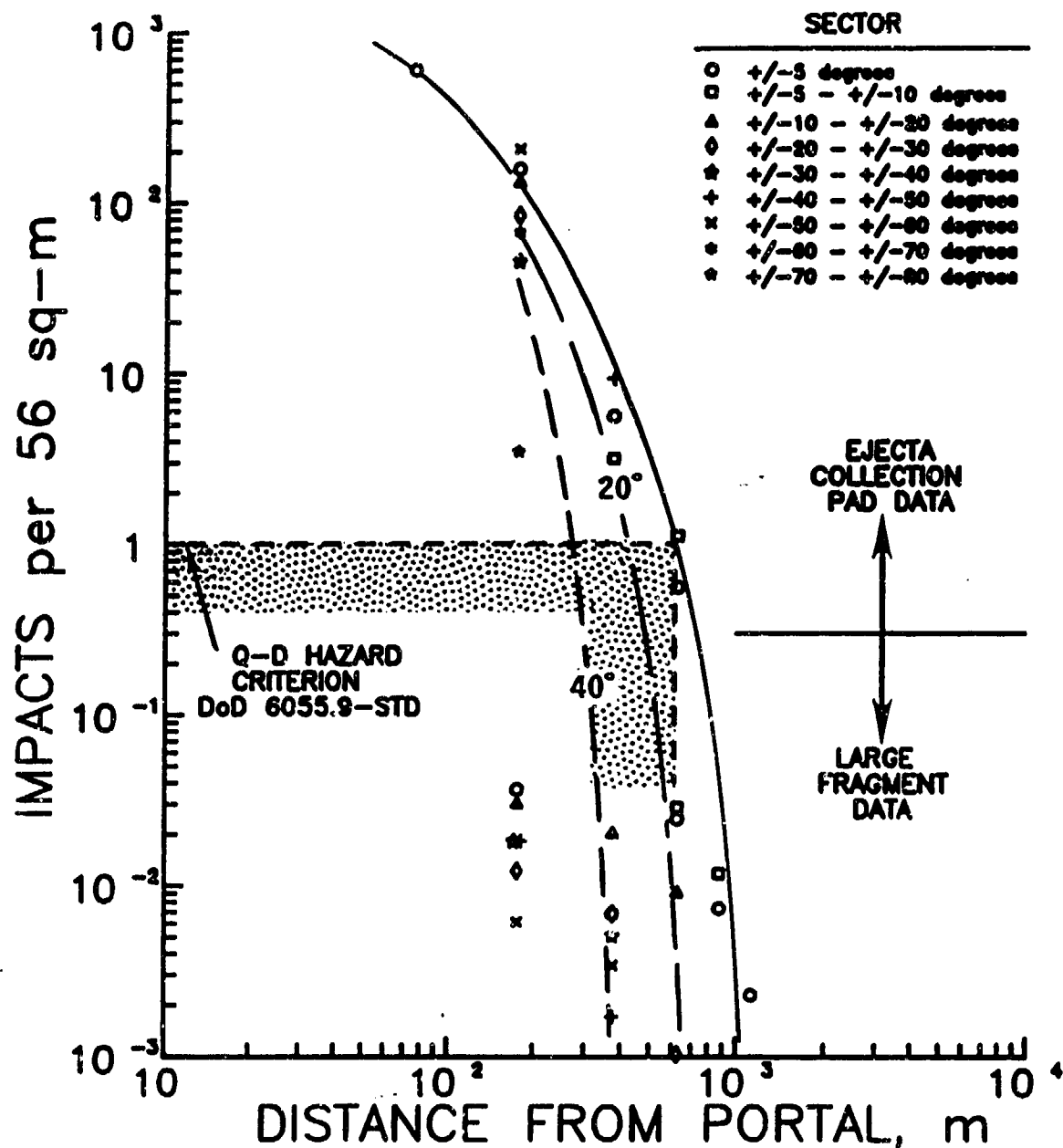


Figure 7. Ejecta/debris missile impact density versus distance from portal, Shallow Underground Tunnel/Chamber Explosion Test. Curves show general limits of missile density ranges along extended tunnel axis (0-degree azimuth) and with ± 20 degree and ± 40 degree sectors.

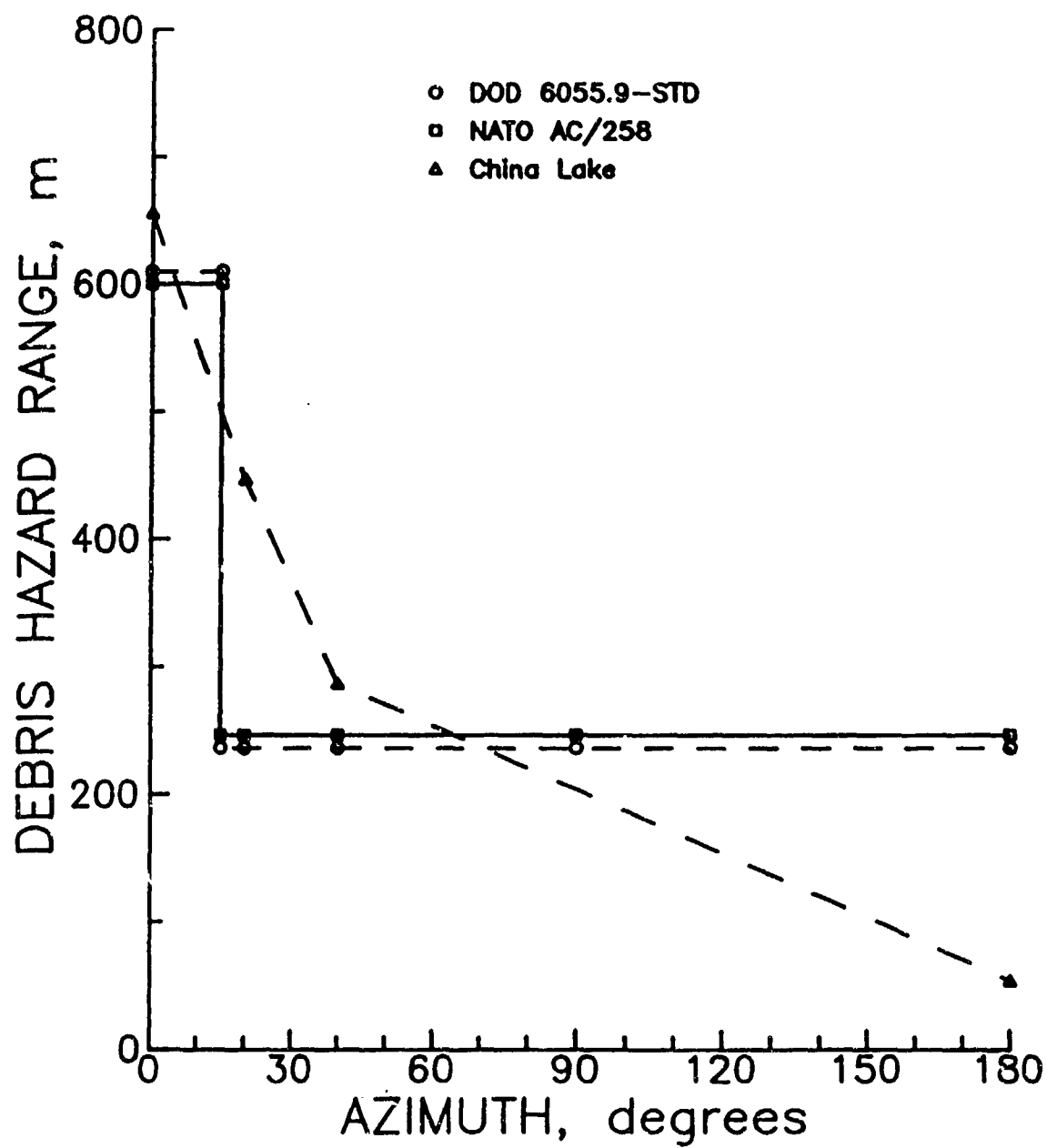


Figure 8. Inhabited Building Distances from debris hazards specified in the Explosives Safety Standards and NATO AC/258 for a 20,000-kg detonation, compared to ranges indicated by data collection on the Shallow Underground Tunnel/Chamber Explosion Test.

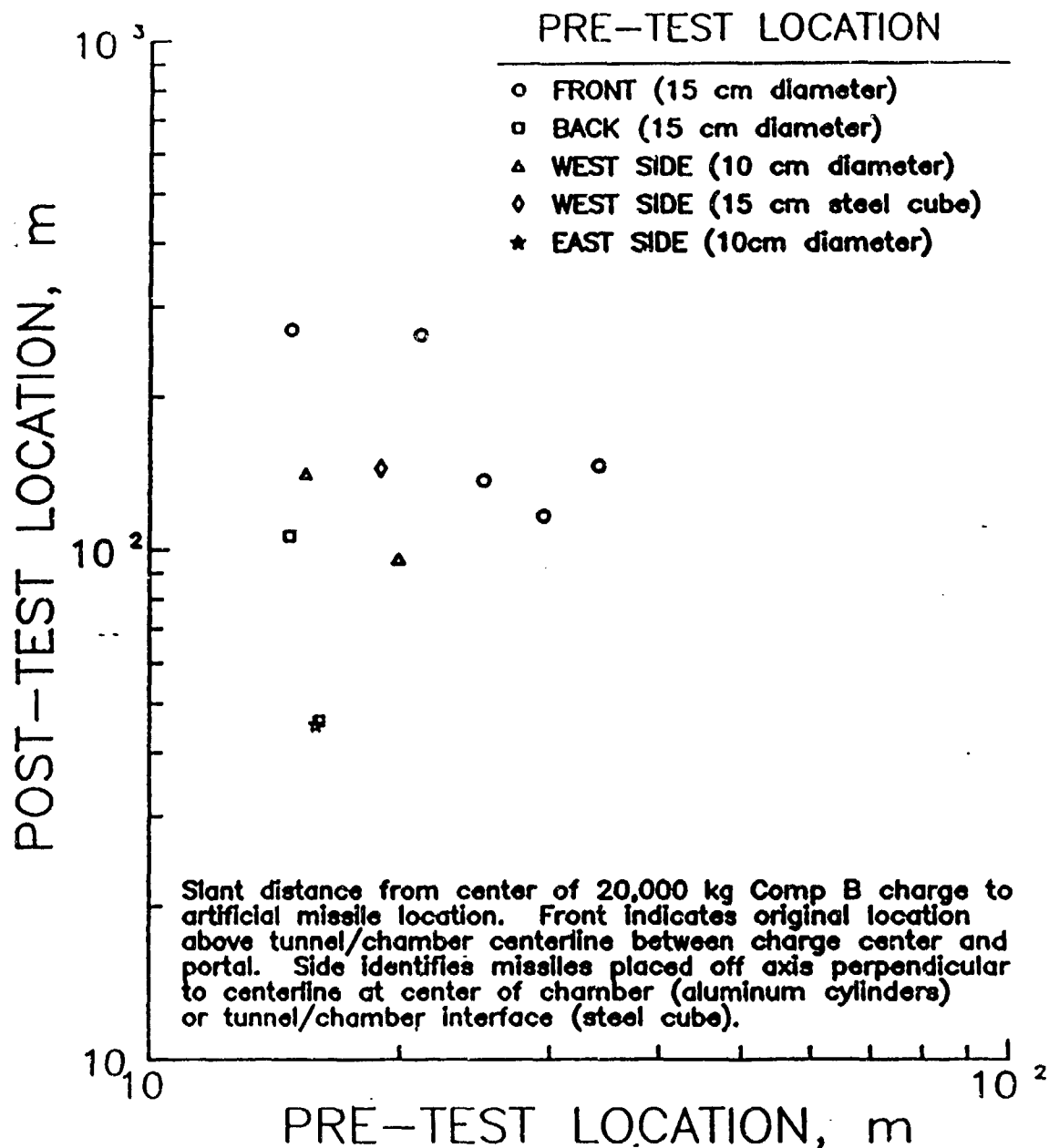


Figure 9. Artificial missile post-test versus pretest slant distance, Shallow Underground Tunnel/Chamber Explosion Test. Missiles were 10 and 15 cm diameter aluminum cylinders, 10 and 15 cm long, respectively. One 15 cm steel cube was also recovered.

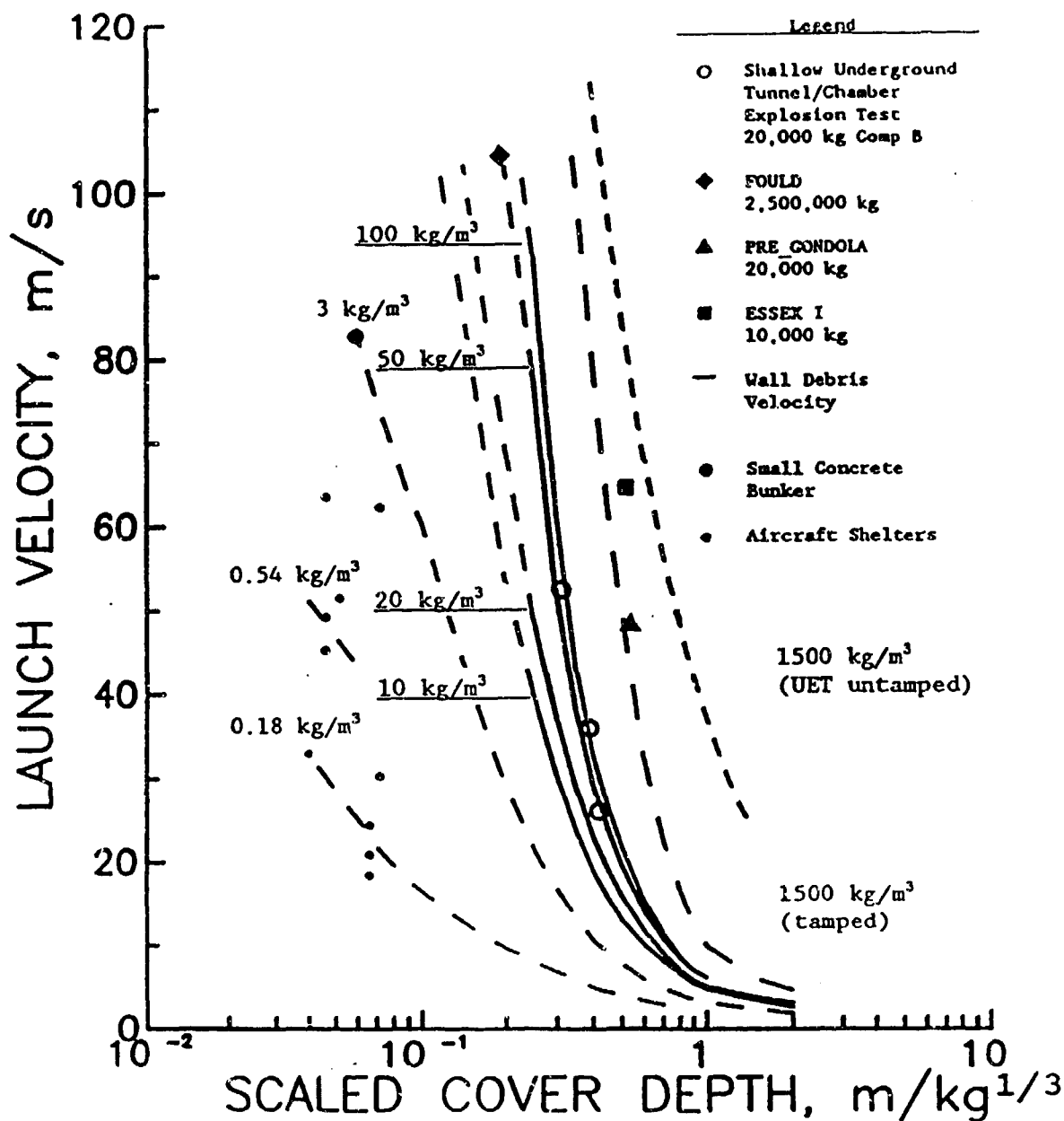


Figure 10. Launch velocity of cover rock ejecta from Shallow Underground Tunnel/Chamber Test, compared to ejecta velocities from other sources on previous explosive tests, (from Helseth, 1982). Scaled cover depth for Tunnel/Chamber Test varied from front of chamber to rear.

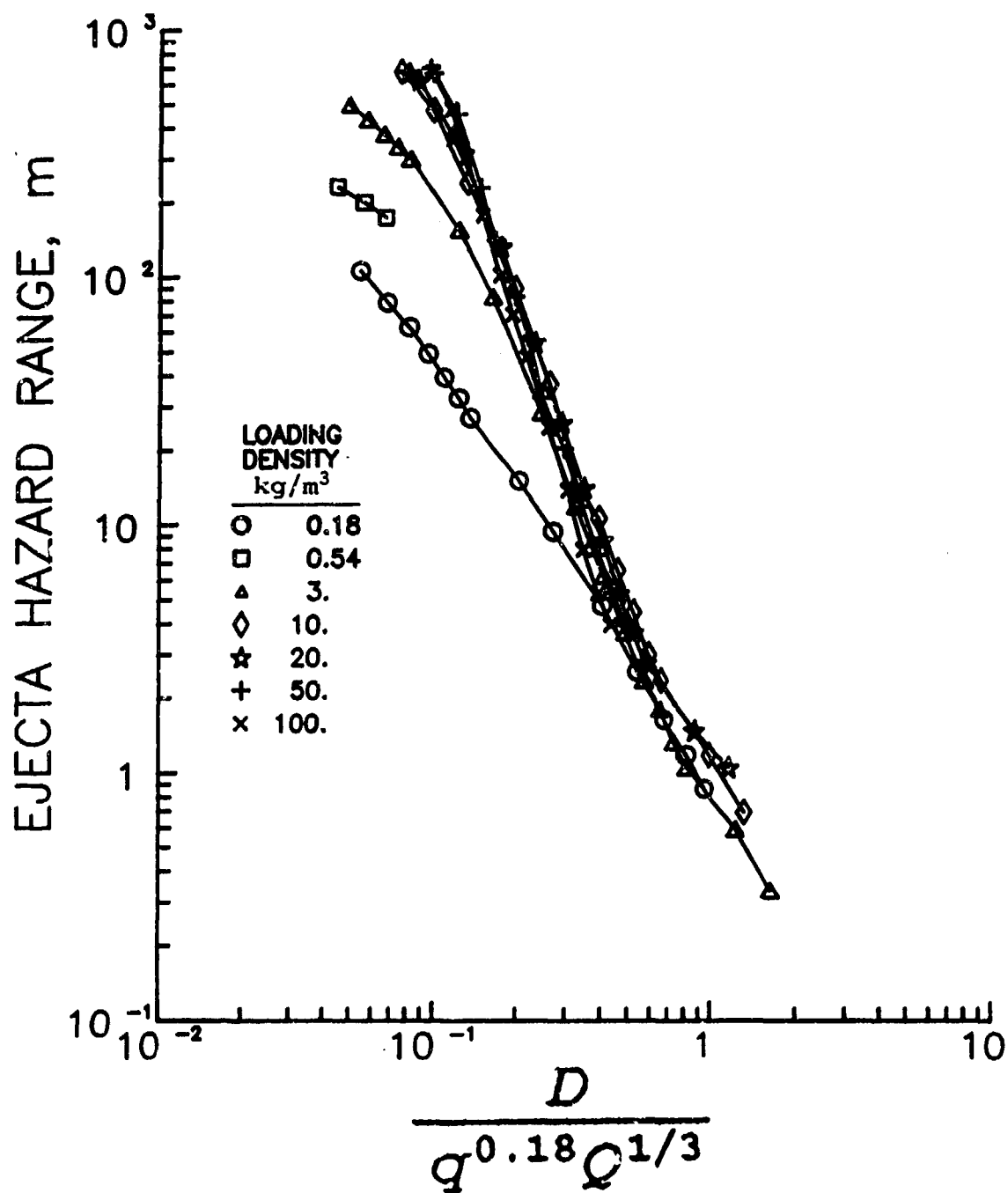


Figure 11. Ejecta hazard range, computed from launch velocity curves using trajectory algorithm with air drag, versus scaled cover depth. Cover depth (D) was scaled by product of loading density ($q^{0.18}$) times charge weight ($Q^{1/3}$). Chamber loading densities range from 0.18 to 100 kg/m³.

SIMPLIFIED WALL BREACH CALCULATIONS INPUT CHAMBER PRESSURE

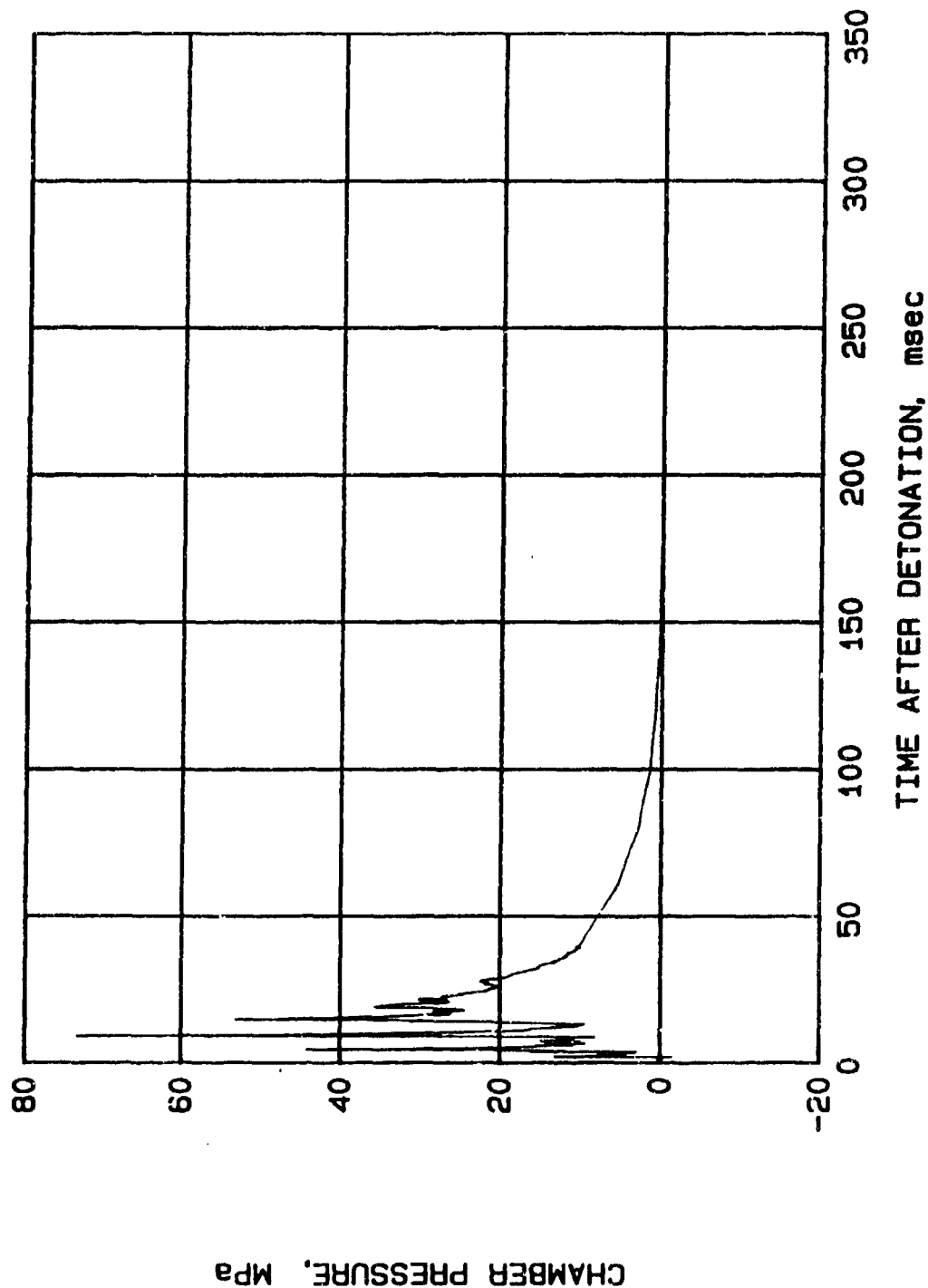


Figure 12. Shallow Underground Tunnel/Chamber Explosion Test chamber pressure-time history, Gage C-3. Instrumentation cable failed at 40 msec after detonation. Time history pressure decay has been approximated at later times by halving at 20 msec intervals.

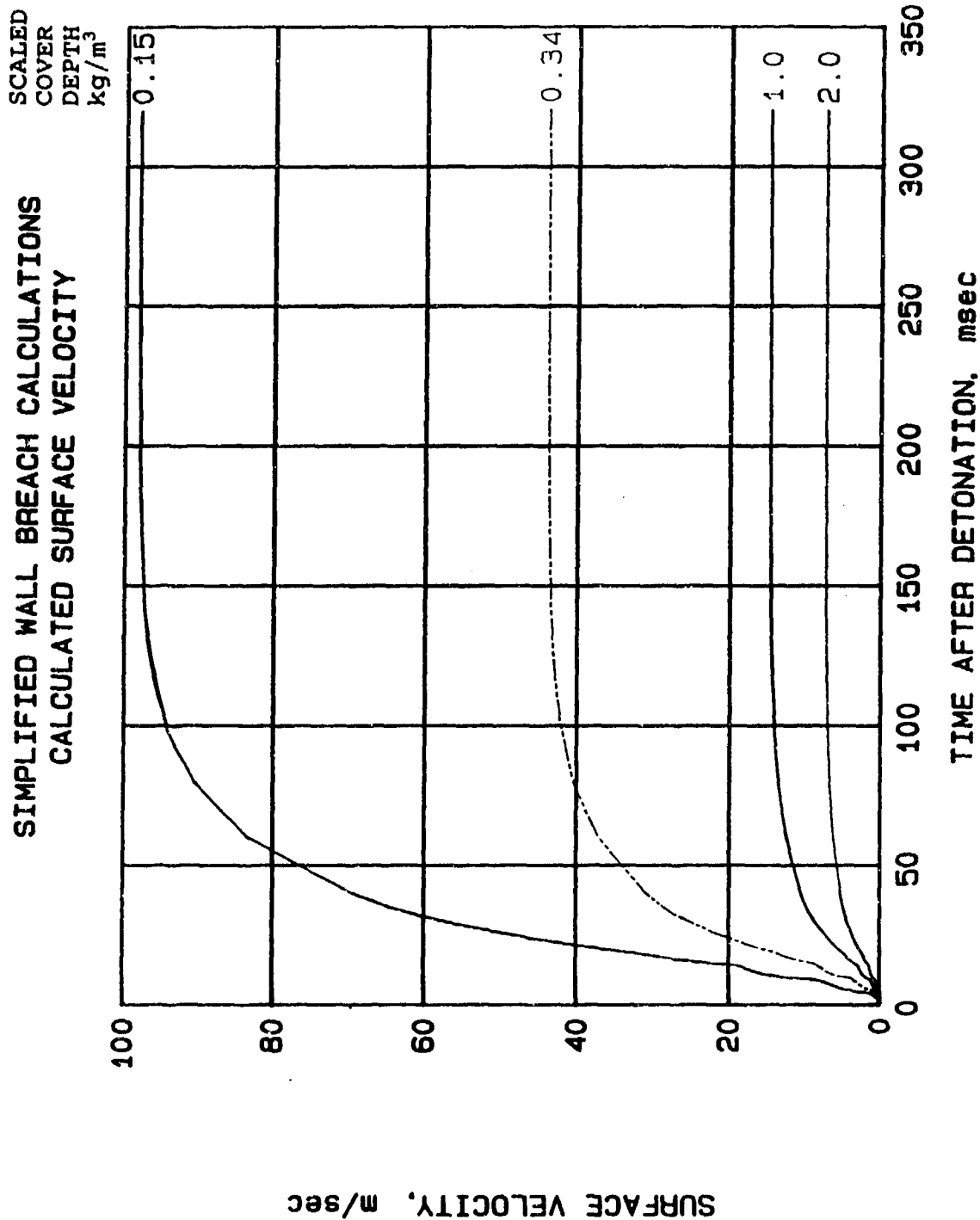


Figure 13. Surface velocity calculated with WES BREACHWL code versus time after detonation. The calculations used the measured pressure-time history given in Figure 12 for the chamber pressure function and a rock density of 2540 kg/m³ was assumed.

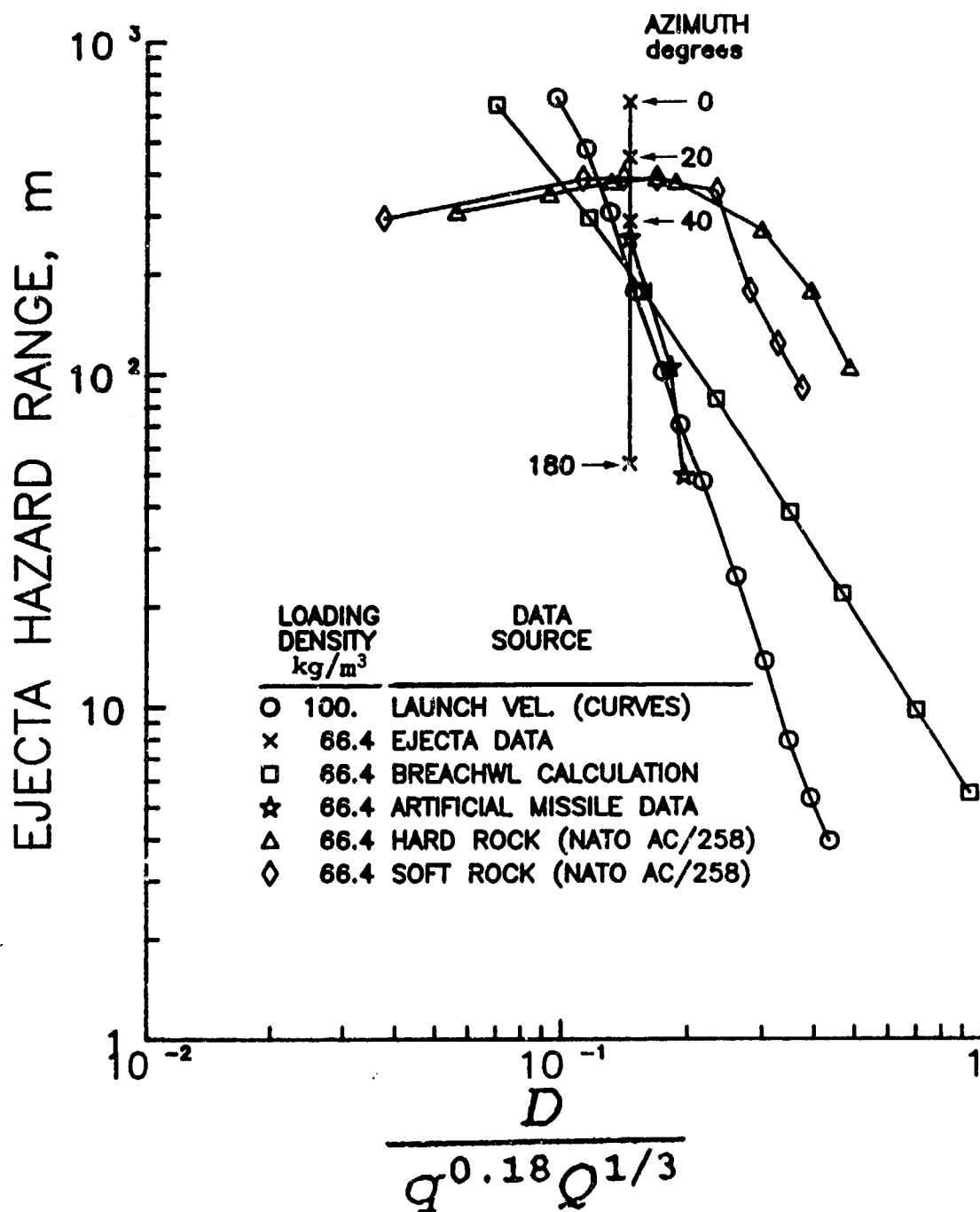


Figure 14. Ejecta hazard range versus scaled cover depth. Comparison of Inhabited Building Distance for debris from Explosives Safety Standards, measured data from Tunnel/Chamber Test, and computed distances (launch velocity curves and WES BREACHWL code).

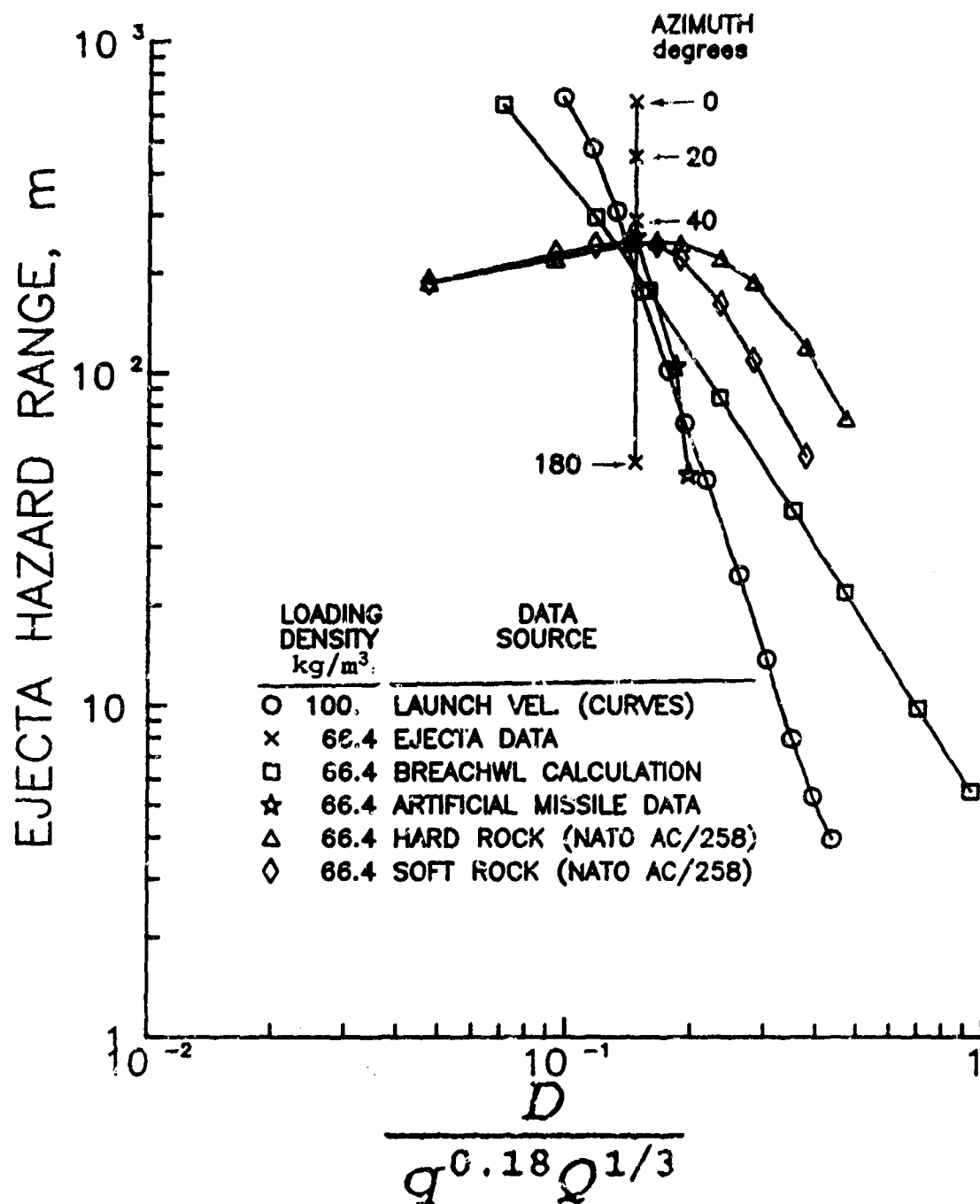


Figure 15. Ejecta hazard range versus scaled cover depth. Comparison of Inhabited Building Distance for debris from NATO AC/258, measured data from Tunnel/Chamber Test, and computed distances (launch velocity curves and WES BREACHWL code).

MIXING OF LIQUID CRYOGENS IN THE SIMULATION OF LIQUID HYDROGEN/LIQUID OXYGEN EXPLOSION HAZARDS

T.S. Luchik, K.M. Aaron, E.Y. Kwack, P. Shakkottai and L.H. Back

Jet Propulsion Laboratory
California Institute of Technology
Pasadena, California USA

ABSTRACT

Experiments simulating mixing of liquid oxygen (LO_2) and liquid hydrogen (LH_2) have been performed. The non-reactive mixtures were obtained by injecting jets of the oxidizer into a pool of the fuel simulant. Three fluid combinations were tested: LO_2 into liquid helium (LHe), liquid nitrogen (LN_2) into LHe and LN_2 into LH_2 . Experimental observations included flash X-ray and high speed video imaging, hot film anemometry, and thermocouple and diode thermometry. Results showed that the jet fluid stays coherent throughout the mixing process and that peak boiling of the pool fluid occurs shortly after jet impingement. Estimates of bulk density indicate a smaller range of variation than is currently being used for explosive yield calculations.

1. INTRODUCTION

Several of the planetary missions at the Jet Propulsion Laboratory (JPL) use Radioisotope Thermoelectric Generators (RTGs) as part of the spacecraft's power system. In carrying out the required RTG hazard definition analysis for these missions, it became evident that the potential threat to the RTGs from an explosion of liquid oxygen (LO_2) and liquid hydrogen (LH_2) as a result of a launch vehicle accident is not well defined or understood. LH_2 and LO_2 are the propellants for the National Space Transportation System (STS) (used to launch the Galileo mission and planned for the Ulysses mission) and the Centaur G upper stage booster (planned to be used with a Titan IV and used to launch the Mariner Mark II series spacecraft). The lack of understanding stems from an inadequate data base on close-in blast characteristics for LO_2/LH_2 explosions. The existing data base, obtained during the PYRO [1] tests in the 1960's, emphasized far field blast characteristics for the purpose of determining the minimum safe distance for locating ground structures. However, it is the near field blast environment which impacts RTG safety. A survey of the available literature on LO_2/LH_2 explosions reveals inadequacies in the following areas:

1. The fluid mixing dynamics of LO_2/LH_2 prior to detonation and particularly interphase mixing, are not well understood.

Approved for public release, Distribution unlimited

2. The detonation and/or deflagration behavior of a LO_2/LH_2 mixture, even with prior knowledge of the mixture composition, cannot be described accurately.
3. The effects of short-time scale unreacted propellants on the long time scale blast yield are not characterized. This is particularly important relative to predicting close-in blast-loading effects that accelerate debris as projectiles.

An Explosion Hazards Program [2] was initiated to address the aforementioned inadequacies with special reference to accidental LO_2/LH_2 explosions resulting from a launch vehicle accident. The program has been divided into three tasks, each focused on a separate aspect of the explosion hazard problem. Task 1 is focused on the study of the fluid dynamics and heat transfer associated with the mixing of LO_2 and LH_2 prior to explosion. Task 2 was designed to study the detonation characteristics of well defined, homogeneous mixtures of oxygen and hydrogen. Task 3 involves the study of LO_2/LH_2 detonation characteristics in a variety of simulated accidental mixing configurations. Task 3 is currently in the planning stage. This paper reports in detail on Task 1 and gives a brief description of one phase of Task 3 which is designed to link Task 1 experiments to the Task 3 experiments.

From an explosion hazards perspective, it is the initial mixing of the LO_2 and LH_2 which is of primary importance. It is believed that during the initial mixing that a detonable mixture of multi-phase oxygen and hydrogen is formed. Current predictive techniques assume that the initial blast yield is directly proportional to the bulk-mean density of the mixture. This property, bulk density, is somewhat ad-hoc since hydrogen and oxygen are immiscible. Nonetheless, it is clear to see that reasonable limits must be placed on this parameter if a predictive code is to be used to obtain realistic estimates of blast yield from full scale simulations.

The study of this problem, even in inert mixtures, presents several difficulties. The mixture is at cryogenic temperatures, it is multi-phase, multi-constituent and is transient in both energy and momentum. The oxidizer is cooled and eventually freezes while the fuel evaporates and is heated. The net result is a harsh environment to make any type of measurements.

Because it was desired to study the mixing of the fuel and oxidizer prior to detonation, simulants for either the fuel or oxidizer were used in all Task 1 tests. Initially tests were performed with LHe as the fuel simulant so that either LN_2 or LO_2 could be used as the oxidizer. This allowed a direct comparison of LN_2 to the real oxidizer, LO_2 . Later tests were performed using LH_2 as the fuel. However, only LN_2 could be used as the oxidizer simulant in this case. Thus, performing similar tests with these three inert combinations, allows one to draw conclusions on the mixing of the actual fuel and oxidizer prior to detonation.

Several scenarios were considered in the Task 1 investigation. Figure 1 shows schematically the three most credible scenarios and how each was modelled for laboratory study. The first of these, the deep mixing scenario, is reported on in this paper. These experiments

involve the mixing of two cryogenic fluids. A jet of one fluid is injected into a deep pool of a second fluid in a manner similar to that of the work of Bishop et al. [3]. Their tests showed that significant jet penetration occurred only when the more dense fluid (oxidizer simulant) was injected into a pool of the less dense fluid (fuel simulant). When the jet and host fluids were switched very little penetration and mixing occurred. Therefore in the present study, only the mixing of oxidizer simulants injected into pools of fuel simulants are considered.

Specifically reported herein is the current status of the Task 1 experimentation. Section 2 briefly describes the experimental facility, and also contains a summary of the instrumentation used in the experiments. Results of the deep pool mixing tests are presented in Section 3, and Section 4 gives the relevant conclusions on the current work and a brief discussion on planned future experimentation in this ongoing work.

2. APPARATUS

This section gives a brief overview of the facility, instrumentation and procedures used in the Task 1 experiments. For more detailed descriptions see Luchik et al. [4,5].

2.1 Facility

A schematic of the facility is shown in Figure 2. The facility consists of a primary enclosure, a secondary enclosure and three flow systems: 1) a liquid fuel transfer system, 2) a liquid oxidizer (jet fluid) transfer system and an inert gas purge system.

The primary enclosure is mainly an exhaust duct for the liquid fuel (or simulant fuel) that is boiled off during an experiment. This enclosure houses all plumbing to the oxidizer tank as well as instrumentation used for thermal and velocity measurements made during an experiment. The stainless steel dump tank used in the experiments is 14.6 cm in diameter and has a capacity of 10.4 liters. Flow out of the dump tank was controlled using a pneumatically operated-cryogenic ball valve. Because of the nature of the experiments, knowledge of the valve timing was critical and hence, the valve was calibrated. Results of the calibrations showed that the valve, when operated at 100 psi, responded to the operator in 60 ms and went from the fully closed position to the fully open position in 40 ms. These values were independent of the overall time that the valve was open. The valve response is shown in Figure 3. The flow rate out of the dump tank was controlled by regulating the pressure of the fluid inside the tank. An interface at the bottom of the enclosure is used to seal the Pyrex glass experimental dewar to the enclosure. The dewar has a diameter of 14.3 cm and is roughly one meter in length. Pyrex glass was used to enable visual observation of the experiments. Located at the top of the primary enclosure, was a 10.2 cm diameter exhaust stack where the fuel evaporation rate was measured. The exhaust gas then flowed into a dilution duct where the exhausted fuel was diluted below its flammability limit and was exhausted to the atmosphere. A schematic of the primary enclosure, dump tank, experimental dewar and instrumentation is shown in Figure 4.

As shown in Figure 2, the primary enclosure was located inside the secondary enclosure. This enclosure was purged free of oxygen prior to each experiment and the oxygen level was monitored throughout the experiments using a Teledyne Analytical Systems Model 8000 gas detection system. Purging served two purposes. First, removing all of the air (oxygen) excludes the possibility of an accidental explosion during an experiment. Second, removing all of the oxygen from the environment and replacing it with nitrogen greatly enhanced the visual observation of the experiment, since no water vapor was available in the environment to condense on the outside of the experimental dewar. This purging of the secondary enclosure and diluting of the fuel exhaust was accomplished using an inert gas purge system [4].

2.2 Instrumentation

Chromel-constantan thermocouples (type E) were chosen for these experiments based on arguments presented by Barron [6] and ASTM [7]. However, as noted by Barron, no commercial thermocouple is useful below 30-40K because of the lack of sensitivity at these low temperatures. Because the experiments performed are transient in nature, the temporal response of the instrumentation is quite important. The size of the thermocouples chosen for the experiments was 76 μm which had a response of about 8 ms (90%). This size was a good compromise between speed and robustness (the experiments were fairly violent and smaller thermocouples did not survive the environment with regularity).

Cryodiodes were used in locations where sub-40K temperatures were expected. The sensitivity of a cryodiode is excellent at low temperatures. However, the cryodiode does have two major disadvantages. The diodes have response times which varied with the ΔT due to the large thermal capacitance of the can housing the diode. Times as great as 2 seconds were measured for a ΔT of 200K. Although the diodes were quite robust themselves, the wiring to the diode was delicate and often broke during experimentation.

Pressures in the primary and secondary enclosures and in the dump tank were measured using Validyne pressure transducers. The transducers are fairly standard strain gage type transducers. Temperature effects at the transducer were minimized by using a length of Tygon tube from the point of measurement to the transducer, which was maintained nominally at 300K.

Hot film anemometers and a pitot-static probe were used to measure velocities of the fuel boil-off gas at the mouth of the experimental dewar while only a hot film anemometer was located in the stack of the primary enclosure. However because of difficulties when helium was used as the fuel simulant, only the stack anemometer yielded useful quantitative information.

The hot-films had better accuracy and time response than the pitot probe. However, the hot-films were far more difficult to calibrate since they had to be calibrated over a range of temperatures and velocities. A typical calibration equation is given by equations (1) and (2).

$$u = (-0.753 + 13.6 E_{\text{mod}})^{2.5} \quad (1)$$

where

$$E_{\text{mod}} = \frac{E_{\text{hf}}}{(T_w - T_g)^{0.45}} \quad (2)$$

and T_w is the hot film temperature, E_{hf} is the anemometer output in volts, T_g is the gas temperature in K, and u is velocity in m/s. From this equation it is clear to see that the accuracy of the velocity measurement is largely dependant on the voltage output of the anemometer and the measurement of gas temperature in the vicinity of the probe. Both of the values vary with time during an experiment. A partial calibration curve corresponding to the above equations is shown in Figure 5. Details of the hot film calibrations are give by Kwack et al. [8]. The pitot-static probe measures velocity using Bernoulli's equation

$$u = (2\Delta P / \rho_g)^{0.5} \quad (3)$$

and

$$\Delta P = \text{constant} * E_{\text{pitot}} \quad (4)$$

Here ΔP is the pitot-static pressure difference, ρ_g is the gas density and E_{pitot} is the pressure transducer output. Although the equation for the pitot probe looks simpler than the hot film calibration equation, note that the density of the gas is a function of temperature. Thus, the experimental measurement is not simpler than for the hot-film, only the calibration is simpler.

Measurements at the exhaust stack were simpler than those at the mouth in that the environment was less harsh than that at the mouth. The temperature of the gas at this location varied from 50 K to about 250K. Thus, a large range of calibration was necessary. At the mouth of the dewar, the temperature varied little, but the temperature at this location was seldom greater than 25K during the experiment. The cold temperatures tended to destroy hot films after repeated cycling.

A Spin Physics model SP-2000 high speed motion analyzer was used to obtain video recordings of each experiment. For these experiments, recordings were obtained in excess of 500 fps. Typically, the vertical field of view was 45 cm with a minimum spatial resolution of 2.2 mm by 2.2 mm. The experiment was back lighted with 3 quartz halogen lights which yielded good contrast between the host and jet fluids. The video images were digitized and some image processing techniques were applied to the images to help better define the mixing zone at selected times during the experiments. However, the image processing techniques did not yield any additional information that had not already been gathered from simple viewing of the video tapes.

A Hewlett-Packard 300 kV flash X-ray system was used to obtain an X-ray of the mixing process. This yielded one observation per experiment with a 50 ns exposure. Each head

has a beryllium window, rather than aluminum, to allow better transmission of the low energy X-rays, which are more sensitive to low molecular weight matter, like LN_2 , LO_2 , LH_2 and LHe . A wide variety of X-ray receivers have been used in this system including a Science Applications Incorporated RTR 300 X-ray image intensifier, DuPont medical and non-destructive testing (NDT) films, screens and cassettes, and Eastman Kodak films. A large number of tests were run using various combinations of the above products as well as varying the source to object distance and flash X-ray output voltage. The "best" receiver tested was the combination of three Dupont products: a Dupont Kevlar Cassette with Chronex Quanta Fast Detail screens and either NDT 57 or Chronex 4 film. However, even with this combination, no quantitative results have been obtained with the X-ray system to date. The reason for this is that there exists a lack of contrast between the jet and host fluids used in these experiments.

Although the X-ray images have not given quantitative information, they have yielded valuable information which has been used in developing a qualitative model of the initial mixing during the mixing of the jet and host fluid. It should be noted that the only imaging technique, other than neutron absorption, able to penetrate the mixing zone is the flash X-ray technique.

A schematic of the data acquisition system is shown in Figure 6. The host computer is an IBM PC compatible. The main function of the compatible during data acquisition is as a memory device for the high speed A/D boards. Data sampling occurred over 23 channels at a rate of 100 scans per second. As can be seen from the figure, the hot wire/film, cryodiode and pressure transducer data are fed directly into the A/D boards while the thermocouple information must be passed through an intermediate amplifier. The A/D board also signals the host computer at appropriate times to trigger the dump tank operator valve and the flash X-ray system. The host achieves the triggering process through the use of a parallel I/O board and relay board. The host computer also controls the Spin Physics motion analyzer through an RS-232 port.

3. RESULTS

The independent variables for the experiments were the jet velocity, the jet momentum, the dump duration, and the distance between the nozzle exit plane and the free surface of the pool fluid. This distance is referred to as ullage herein. For the various experiments all of the independent variables were varied.

Initially, liquid helium was used as a fuel simulant for the purpose of comparing liquid nitrogen to liquid oxygen. This would prove useful in interpreting the liquid hydrogen/liquid nitrogen experiments. Physical properties of all of the fluids used in the experiments are listed in Table 1. More information on cryogenic fluid properties can be found in Barron [6], Sychev et al. [9,10,11] and Scott [12]. From this table, to a first order approximation, LN_2 appears to be a good simulant for LO_2 in that the thermophysical properties of the fluids are similar. Helium, on the other hand, has one significant property difference from hydrogen, the latent heat of vaporization. This value for helium is approximately a factor of 20 lower for helium than that for hydrogen. Since this property

directly affects boiling, the helium evaporation rate cannot be used in any way to approximate hydrogen evaporation. Also, because of the relatively low latent heat of vaporization of liquid helium (21 kJ/kg), the parasitic boil off of helium was high, making the ullage very difficult to control with good accuracy.

Varying the nozzle diameter was one way of controlling the mass flow rate of the jet independent of the jet velocity. However the jet diameter played another important role in the experiment. From an X-ray perspective, it was preferable for the jet to be as large in diameter as possible to maximize X-ray contrast between the jet and the host fluid. Fluid dynamically, a small diameter jet is preferable to minimize wall effects. These, of course, are conflicting requirements. Nozzles with diameters of 3.17 mm, 6.34 mm and 12.7 mm were used in the experiments, but only experiments with the 12.7 mm diameter nozzle yielded useable X-radiographs.

Table 1. Some properties of helium, hydrogen, nitrogen and oxygen.

	Helium	Hydrogen	Nitrogen	Oxygen
T_{BP} (K) (1 atm)	4.2	20.26	77.35	90.18
T_{FP} (K) (1 atm)	-----	13.8	63.15	54.36
ρ_{BP} (kg/m ³)	125	70	807	1141
ρ_{BP}^l (kg/m ³)	17	1.3	4.6	4.5
h_{fg} (kJ/kg)	21	454	199	213
h_{ts} (kJ/kg)	-----	-----	25.1	13.8
$h_{\gamma-\beta}$ (kJ/kg)	-----	-----	-----	23.4
$T_{\gamma-\beta}$ (K)	-----	-----	-----	43.8
$h_{\beta-\alpha}$ (kJ/kg)	-----	-----	-8.4	2.9
$T_{\beta-\alpha}$ (K)	-----	-----	35.6	23.6
c_p (kJ/kg-K)	5.40	12.15	4.73	1.0
$c_{p,BBP}$ (kJ/kg-K)	4.98	9.66	2.13	1.67
$c_{p,IBP}$ (kJ/kg-K)	-----	-----	1.88	1.42

3.1 Helium Test Results

Over 70 separate helium experiments were performed where complete data sets were collected, roughly one-half with LO₂ as the jet fluid and one-half with LN₂ as the jet fluid. The velocity range from 3 m/s to 11 m/s was covered and ullage was varied from 20 cm to 76 cm. The purpose of performing tests with helium was to gain some experience in the mixing of two cryogenic fluids in a totally inert environment, but more importantly to determine the similarities and differences in LN₂ and LO₂ as jet fluids. Since later tests would only involve mixing of LN₂ with LH₂, a good working knowledge of this comparison would allow any extrapolation of the present results to the real situation where LO₂ and LH₂ would be involved.

Although many tests were run, not all tests were different. Several were similar by design to obtain information on the run to run variation of the experiments. The results of these

replicate tests were quite good. Not only was there qualitative agreement in the data but also the quantitative data agreed quite well. An example of this agreement is shown in Figure 7 for the measured helium gas mass flow rate at the stack, the parameter most sensitive to run to run variations. In this Figure, the jet velocity is 3.5 m/s, the nozzle diameter is 6.35 mm and the dump duration is 0.45 sec.

Temporal contours of the mixing zone are shown in Figure 8 for an LN_2/LHe experiment and an LO_2/LHe experiment. Each of these experiments was nominally at the same conditions, a jet velocity of 3.2 m/s, 6.35 mm nozzle and 22 cm ullage, with only the jet fluid being different. The solid contours are "mixing zone" contours at 20 msec time increments while the dashed contour at time $t = 0$ is the estimated liquid "jet" contour. This estimate of the actual jet fluid location is based on experiments with an LN_2 jet into cold helium gas ($T < 20\text{K}$) and from X-ray observations. From those experiments involving the LN_2 jet into cold He gas it was seen that a mixing zone formed between the relatively warm jet fluid and cold He gas. From this knowledge, we see that prior to impingement of the liquid jet on the helium free surface, a mixing zone is formed. This figure is another example of excellent agreement between the LN_2 and LO_2 jet studies.

It is sufficient to say that the results of the LN_2 tests and the LO_2 agreed well in almost every way with one exception. Information pertaining to the size of the frozen particles observed in the experiments differed. It was noted from the experiments that the solid particles become visually observable at the head of the jet initially and a short time later at the outer most extremity of the mixing zone generally near the region of the initial jet impingement. The particles are first seen about 200 to 400 msec after jet impingement for all tests, and this time does not vary systematically with any of the independent variables nor with the jet fluid. As observed from the motion of the particles in the case of the LN_2 jet, they are platelet in shape and fall through the liquid helium at a velocity of about 1 m/s. Quantitative information obtained, based on a sample of 500 particles, indicate that the average size of a particle is 38 mm^2 with sizes ranging from 4 mm^2 to 130 mm^2 , and in general the platelets are less than 1 mm thick. The particles in the case of the LO_2 jet were smaller than that of the LN_2 jet and were generally smaller than the resolution of the video system used. However, large particles could be visualized occasionally. Although no mean size data were obtained for O_2 , it was noted that the large O_2 particles were also platelet shaped. The size difference was the only significant difference noted between the nitrogen and the oxygen jets.

The solids seen in all of the experiments were much larger than is predicted from instability theory, which predicts droplet sizes of the order of microns. Thus, measurements of particle size would indicate that freezing is occurring at the jet outer extremity while the jet is still intact which agrees with the X-ray images that show that the jet is largely coherent during the mixing process. However, this hypothesis is impossible to verify experimentally since the mixing bubble cannot be penetrated with enough spatial resolution and dynamic range to visualize the actual solidification process. The smallest particles discernable, because of the pixel resolution of the video system, was 4 mm^2 for most of the tests, but as small as 1 mm^2 in some cases. Therefore, some small particles may be formed in the mix but are not discernible optically with the current instrumentation.

3.2 Hydrogen Test Results

For the hydrogen tests as in the helium tests, several tests at similar conditions were performed to determine the run-to-run variation of the tests. As was seen in the helium tests, the duplicate experiments yielded similar results.

Figure 9 shows some of the general mixing dynamics for the experimental configuration obtained from the hydrogen tests. The jet impinges on the host fluid which causes boiling of the host and cooling to the eventual freezing point of the jet. As the jet continues to penetrate, a mixing pocket forms which contains some mixture of the gas and liquid state of the host and liquid and solid state of the jet. As time progresses, the fluids within the mixing pocket transfer enough heat between each other so that some freezing of the jet occurs while the host continues to boil off. During the initial mixing of the jet and host fluid the mixing zone is optically too dense to penetrate using conventional optics. However, the radiographs have shown that the jet fluid essentially stays intact and has a diameter approximately equal to that when it leaves the nozzle. Figure 10 shows the mixing zone developed by a 12.7 mm jet of LO_2 with an impingement velocity of 3.2 m/s into LHe approximately 0.2 sec. after jet impingement (A radiograph of an LO_2 jet into liquid helium is shown in Figure 10 because the radiographs obtained from the hydrogen tests were just not publication quality, although they did contain the same information as the radiograph shown). The mixing zone contains both jet and host fluid in its liquid state as well as vaporized host. A comparison of visual images to the radiographs showed that the mixing zone is roughly 5 to 8 times the diameter of the jet. The X-radiographs show further that within the mixing zone the host is largely gas on a volume basis. Somewhat later in the mixing process (about 200 msec to 400 msec) solidification of the jet occurs at the head of the jet and near the point of initial impingement.

Mixing zone contours obtained from images taken with the Spin Physics motion analyzer are shown in Figure 11. These images were obtained for a 3.05 m/s jet of LN_2 into a pool of hydrogen. The nozzle diameter in this experiment was 12.7 mm. Each contour represents an instant in time and the contours are separated in time by 20 ms. As in Figure 8, the jet contour at impingement has been shown by a dashed line and was determined in a similar manner to that of Figure 8. Immediately after impingement, the jet velocity is significantly decreased from its initial velocity. The velocity is less for smaller diameter jets. Figure 12 shows the variation of an average of the jet penetration speed with nozzle size and time. A second surge generates a mixing zone that appears similar to the initial mixing zone. As with the helium studies, very little can be said on the radial rate of formation of the mixing zone other than it does develop more slowly radially than axially.

From the mixing zone impingement contours and from the Spin Physics video in general, several pieces of information were obtained. These include an estimate of the bulk or mean density within the mixing zone, and information on the solidification of the jet fluid.

One method of obtaining the bulk density within the mixing zone was obtained by assuming that the mixing zone volume can be described by a pseudo-body of revolution of a given time contour. Note that since the mixing zone contours are not symmetric, it is only

necessary to rotate each contour through 180° and disregard the surface discontinuity at 180°. Then if one assumes that all of the hydrogen within the mixing volume is in the gaseous state at its normal boiling point and all of the jet fluid is in its liquid state at the normal boiling point, the bulk density of the mixing zone can be calculated using

$$\bar{\rho} = \frac{\dot{m}_{\text{jet}}\Delta t + \rho_{\text{GH}_2} \left(V_{\text{mix}} - \frac{\dot{m}_{\text{jet}}\Delta t}{\rho_{\text{jet}}} \right)}{V_{\text{mix}}} \quad (5)$$

which can be manipulated to obtain

$$\bar{\rho} = \rho_{\text{GH}_2} + \frac{\dot{m}_{\text{jet}}\Delta t}{V_{\text{mix}}} \left(1 - \frac{\rho_{\text{GH}_2}}{\rho_{\text{jet}}} \right) \quad (6)$$

Here \dot{m}_{jet} is the mass flow rate of jet into the mixing zone and V_{mix} is the volume of the mixing zone at Δt seconds after impingement. This is an upper estimate since all of the jet fluid is assumed to be participating in the heat transfer involved in boiling the host fluid. Table 2 shows the average values of the upper estimate of bulk density within the mixing zone at early times after impingement obtained from the various experiments. All averages were obtained from mixing zone contours 120 msec after impingement of the jet. For comparison the density of hydrogen vapor at 20.3K is 0.0013 g/cm³. The estimated values for an oxygen jet were made simply by assuming that the volume occupied by the LN₂ had the density of LO₂ at its normal boiling point. These results are consistent with what was experimentally found in the helium tests.

This estimated bulk density does vary with the radius of the jet, a result seen in the helium tests. As is shown in Luchik et al. [5], a simple argument can show this to be the expected case which yields

$$\frac{\bar{\rho} - \rho_{\text{GH}_2}}{\rho_{\text{jet}} - \rho_{\text{GH}_2}} \propto \frac{u_{\text{jet}}\Delta t}{\ell} \frac{r_{\text{jet}}^2}{r_{\text{jet}}} \approx C_1 r_{\text{jet}} \quad (7)$$

A second method, which estimates the minimum bulk density can be made from knowledge that the jet largely remains intact in the mixing zone. This indicates that only a portion of the original jet fluid is taking part in the heat transfer required to boil the hydrogen. The analysis is identical to that in Luchik et al. [5] except that H₂ has been substituted for He. The result is the following equation:

$$\bar{\rho}_{\text{min}} = \rho_{\text{GH}_2} \left(1 + \frac{h_{\text{fg,H}_2}}{\Delta h_{\text{jet,max}}} \right) \quad (8)$$

The maximum enthalpy change in the jet fluid is achieved by cooling it to the liquid pool temperature (20.3K for liquid hydrogen). $\Delta h_{\text{jet,max}}$ has the value of 124 kJ/kg for N₂ and 136 kJ/kg for O₂. Doing this assumes that the minimum jet mass is involved in the heat

transfer required for boiling heat transfer, thus yielding the minimum bulk density. Substituting the values for the thermophysical properties gives $\bar{\rho}_{\min} = 0.0059 \text{ g/cm}^3$ for LN_2 jets and $\bar{\rho}_{\min} = 0.0055 \text{ g/cm}^3$ for LO_2 jets. These values are roughly a factor of two lower than the upper estimate values obtained for the 3.17 cm diameter nozzle indicating that even with that small nozzle size only about one-half of the jet was participating in the heat transfer to the hydrogen. These results are significant in that current predictive techniques cover a range of bulk densities with an upper limit more than one order of magnitude greater than the maximum values presented here.

Table 2. Bulk density estimates during initial jet impingement.

Jet Velocity (m/s)	Nozzle Dia. (mm)	LN_2 jet $\bar{\rho}$ (g/cm ³)	LO_2 jet $\bar{\rho}$ (estimated) (g/cm ³)
3.0-5.0	3.17	0.013	0.015
3.0-5.0	6.35	0.014 ± 0.006	0.018
3.0-5.0	12.7	0.023 ± 0.009	0.032

The size of most of the solid particles in these experiments varied from 7 mm² to 70 mm² with the largest particle seen being 350 mm². The particles in the hydrogen tests appeared platelet in shape. The size information for the N_2 particles as well as the shape is consistent with what had been seen in the helium tests with a LN_2 jet. The particle size was observed to increase as the jet diameter was increased. Particle information for N_2 was found to be independent of the pool fluid with which it was mixed. This leads to the conclusion that SO_2 particles generated in a mix of LO_2/LH_2 would be similar to those in the LO_2/LHe tests.

The instantaneous temperature of the H_2 gas at the mouth of the dewar is given in Figure 13 while the instantaneous evaporation rate of H_2 is presented in Figure 14. Results from three different experiments are shown to show the consistency from experiment-to-experiment. Nominal conditions for these experiments are a 12.7 mm diameter jet of N_2 flowing with jet velocity of 3.5 m/s for a period of 0.65 sec. In all cases the ullage was roughly 42 cm. Note that impingement of the jet occurs about 0.24 seconds after the dump valve has been energized ($t = 0$) and that the gas temperature prior to mixing is 70-100K due to heat transfer from the surroundings. As the rate of evaporation increases, the gas exits the dewar without exchanging heat because the gas residence time in the dewar has decreased. The "peak and valley" nature of the data shown in the graph are believed to be related to the surging of jet fluid in the mixing region seen in the video images. Although not shown, the time at which peak boil off occurred did not vary appreciably. The value of peak boil off was found to vary with the nozzle diameter for a given jet velocity. This result suggests that a principle parameter in the early mixing is the diameter of the jet. More work is needed to verify this trend.

Integrated values of the hydrogen boiled off from a visual displacement measurement along with some representative data taken from the hot-film at the mouth of the experimental

dewar are given in Table 3. The purpose of this is to show the accuracy of the hot-film data. Individual values of the ratio of hydrogen boiled off to jet fluid added varied from 0.16 to 0.26.

Table 3. Comparison of time integrated hot film data and hydrogen boil off displacement measurement.

Run	\dot{m}_{jet} (g/s)	Δm_{jet} (g)	Δm_{LH_2} (g)	$\Delta m_{GH_2, HF}$ (g)	$\frac{\Delta m_{GH_2, HF}}{\Delta m_{jet}}$
663	306	138	23	25.1	0.18
664	306	199	40	40.8	0.21
665	306	199	37	39.6	0.20
666	306	199	44	41.9	0.21

The values obtained are reasonable and can be shown analytically by assuming that a small amount of jet fluid is dumped into a large container of LH_2 and that the final equilibrium temperature of the nitrogen in the hydrogen bath is 20.3 K, then we can develop the relationships (see Luchik et al. [5] for derivation)

$$\frac{\Delta m_{H_2}}{\Delta m_{jet}} = \frac{\Delta h_{jet, max}}{h_{fg, H_2} + c_{p, GH_2}(T_{GH_2, Final} - T_{BP, H_2})} \quad (9)$$

where c_p is the specific heat, h_{fg} is the latent heat of vaporization, T is temperature and the subscripts H_2 and jet refer to the given constituent. $\Delta h_{jet, max}$ is as before, 124 kJ/kg for N_2 and 136 kJ/kg for O_2 and represents the energy release from the jet fluid when cooled to 20.3K. Assuming that the hydrogen boils off and leaves the control volume at it's boiling point, one can obtain the maximum ratios of hydrogen boiled to jet fluid added. These values are 0.27 and 0.30 for N_2 and O_2 respectively.

However, if the hydrogen gas leaving the control volume is allowed to exchange heat with the jet fluid, the mass ratios can be less than the maximum. Since hydrogen has a high heat of vaporization (454 kJ/kg) and a relatively low specific heat the variation of boil off with gas exit temperature is small as is shown in the following equation for LN_2/LH_2 .

$$\frac{\Delta m_{H_2}}{\Delta m_{N_2}} = \frac{124.0 \text{ kJ/kg}}{12.15 \frac{\text{kJ}}{\text{kg-K}}(\Delta T_{GH_2, Final}) + 454 \frac{\text{kJ}}{\text{kg}}} \quad (11)$$

Here $\Delta T_{GH_2, Final}$ is the amount of temperature rise, above the normal boiling point, of the gaseous hydrogen exiting the control volume. A similar equation results for LO_2 , with only numerator being changed to 136 kJ/kg. The boiling of hydrogen occurs at 20.3 K but the temperature that hydrogen leaves the control volume can be higher than that because of heat transfer from either the liquid jet fluid or the relatively warm solid particles to the gaseous hydrogen. Table 4 summarizes the results obtained from the above equation for

both LO_2 and LN_2 . Using an average boil-off ratio of 0.2 (From Table 3), Table 4 shows that the average temperature of the hydrogen gas exiting the experimental dewar was 13K warmer than its normal boiling point. However, the thermocouple at the mouth of the dewar only indicated a superheat of about 5K during active boiling. No reason is offered for this discrepancy. This implies that between 73% and 88% of the jet fluid energy went into the actual vaporization of the hydrogen liquid pool, on average.

Table 4. Equilibrium calculation of the ratio of liquid hydrogen vaporized to liquid nitrogen or liquid oxygen solidified.

$T_{\text{GH}_2, \text{Final}} - T_{\text{BP, H}_2}$	$\Delta m_{\text{GH}_2} / \Delta m_{\text{LN}_2}$	$\Delta m_{\text{GH}_2} / \Delta m_{\text{LO}_2}$
0.0	0.27	0.30
5.0	0.24	0.26
10.0	0.22	0.24
15.0	0.19	0.21
20.0	0.18	0.20
25.0	0.16	0.18

4.0 SUMMARY AND FUTURE WORK

Deep pool mixing studies of LN_2/LHe , LO_2/LHe and LN_2/LH_2 have been completed. The present mixing studies included varying jet velocities, jet dump duration times, jet diameter and ullage spaces. However, the qualitative nature of the mixing zone does not seem to be greatly affected by these variables although the rate of formation of the mixing zone occurs more rapidly when LHe is the pool fluid than when LH_2 is the pool fluid. Ullage space seems to have little effect on the liquid-liquid mixing zone. Heat exchange between the liquid jet and the colder gas in the ullage space seems to have little effect on the dynamics of the liquid-liquid interaction.

The preliminary experiments with LO_2 and LN_2 as the jet fluids showed that N_2 was an excellent simulant for O_2 in all respects except one. The one aspect where N_2 differed from O_2 was in the formation of solid particles. All of the particles observed in the experiments were similar in shape. The motion of these particles in the high-speed video recordings indicated that the particles were platelet in shape. However, in the helium studies, a large number of particles were visualized when LN_2 was the jet fluid whereas when LO_2 was the jet, far fewer particles were clearly visualized. It is believed that the O_2 particles were present, but were too small to be seen with the resolution of the camera system. The solid particles for the N_2 jet were the same size and shape regardless of the pool fluid into which the LN_2 was injected.

The axial rate of formation of the mixing zone slowed with time after impingement of the jet with the formation nearly stopping 150 to 200 ms after jet impingement. Some 50 to 150 ms passed before a second surge of jet fluid was seen. The radial rate of formation of the mixing zone was very slow. Maximum boiling of the hydrogen pool occurred 200 to 300 ms after jet impingement and the value of the maximum boil off rate scaled with the nozzle

diameter for a given jet velocity. This indicates that the maximum boil off rate was heavily dependant on the surface area of the jet (ie. the jet could be modeled as a column of fluid submerged in a pool of hydrogen). This further indicates that the amount of jet fluid sheared from the jet is small. This is further evidenced by the large discrepancies in the maximum and minimum bulk densities and the results of the flash radiographs.

Two different values were obtained for bulk density. One assumed that all of the jet fluid was involved in the heat transfer required to vaporize the hydrogen in the mixing volume. This estimate is a maximum estimate for bulk density since all other indicators show that the entire jet mass is not diffused throughout the mixing zone. The second estimate for bulk density was based on heat transfer concepts. It assumed that the minimum jet mass transferred all of the available energy to the hydrogen and that this energy was used for vaporization only. This estimate is, by definition, the minimum bulk density in the mixing zone allowed by the physics of the problem. The values determined as the upper limit on bulk density for a liquid nitrogen jet into a pool of hydrogen varied with the nozzle diameter and had values ranging from 0.013 g/cm³ for the 3.17 mm nozzle to 0.023 g/cm³ for the 12.7 mm nozzle. Values for $\bar{\rho}$ were then estimated for LO₂ jets into LH₂. These values were only slightly higher than those for LN₂. The minimum value of bulk density, as determined by analysis, for a LO₂/LH₂ mixture was $\bar{\rho}_{\min} = 0.0055$ g/cm³. This range of experimentally/analytically determined values are significantly lower than the estimates being used in predictive detonation environment techniques which use upper limit values as high as $\bar{\rho} = 0.4$ g/cm³.

The next series of experiments in Task1 of this continuing program is a study of the "Range Destruct" mode of the Titan IV/Centaur G' configuration (see Figure 1). Here a small charge located on the side of the Centaur tanks is detonated causing an axial rip in the fuel an oxidizer tanks to occur. This takes place while the payload fairing (PLF) of the launch vehicle is still in place. Liquid fuel and oxidizer pour out of the tanks and are trapped in the PLF space. A portion of each of the propellants flash vaporize since the initial pressure in the propellant tanks is significantly higher than that in the PLF. Also, as these fluids flow out of their respective tanks, they can contact the relatively hot surface of the PLF, augmenting the vaporization of each of the fluids as well as intermix, cooling some of the oxidizer while vaporizing the fuel. Because a detonable mixture of gaseous fuel and oxidizer will essentially encompass the RTGs in the payload, knowing the gas composition in this region as a function of time is of critical importance from a safety viewpoint. A simulation of such an event is planned for the laboratory with LN₂ being substituted for the oxidizer. All of the instrumentation described in this paper will be used in that experiment as well as a novel acoustic technique for determining the gas composition at several points in the flow as a function of time.

The Task 3 work planned for the future involves actual jet mixing of LO₂ and LH₂ in a manner similar to that described in this text. If the O₂/H₂ mixture does not auto-ignite after a prescribed period, a charge will be used to initiate the O₂/H₂ reaction. During these tests both near and far field detonation wave characteristics will be measured. JPL's direct interest in this problem is the near field. In the near field, over-pressures, blast loading and fragment dynamics are of importance to the RTG safety issue and will thus be the focus

of the JPL effort. Tests are also being designed so that the contribution of the air environment to the various blast characteristics can be separated from those directly due to the propellant oxidizer.

ACKNOWLEDGEMENTS

The work described in this paper was carried out in the Applied Technologies Section of the Jet Propulsion Laboratory, California Institute of Technology, under Contract with the National Aeronautics and Space Administration. The encouragement of M.J. Cork, Launch Approval Engineering, JPL Flight Project Office, and R.M. Clayton, Task Manager of the LO_2/LH_2 Explosion Hazards Program, is gratefully acknowledged. The assistance of Gracio Fabris and Dennis O'Conner during the initial stages of experimentation, and Wayne Bixler, Stan Kikkert and Ken Harstad throughout this continuing work is also acknowledged. Finally, the authors wish to thank John Fisher of DuPont for providing X-ray films, screens and cassettes as well as his technical advice and assistance.

NOMENCLATURE

c_p	specific heat
E	output voltage
h_{ig}	heat of vaporization
h_{if}	heat of fusion
ℓ	liquid penetration distance at time when bulk density was calculated
Δm	mass difference
\dot{m}	mass flow rate
T_g	gas temperature
T_{probe}	hot film substrate temperature
T_w	hot film/wire temperature
t_e	valve energize time
Δt	time increment
u	axial velocity
V_{mix}	mixing volume

Greek Symbols

ρ	density
$\bar{\rho}$	bulk density
τ	time constant

Subscripts

BP	boiling point
FP	freezing point

g
jet
l
s

gas value
jet
liquid
solid

REFERENCES

- [1] Willoughby, A.B., Wilton, C., & Mansfield, J. 1968, Liquid propellant explosive hazards. Final Report, AFRPL TR-68-92, URS Research Company.
- [2] Massier, P.F., Marshall, J.W., & Clayton, R.M. 1988, Liquid hydrogen/liquid oxygen explosion hazards program plan. JPL D-5113, Internal Document, Jet Propulsion Laboratory, Pasadena, CA.
- [3] Bishop, C. V., Benz, F. J., & Ullian, L. J. 1986, Mixing of cryogenic fluids and predicted detonation properties for multi-phase liquid oxygen and liquid hydrogen, Presented at the 1986 JANNAF Propulsion Meeting.
- [4] Luchik, T.S., Aaron, K.M., Fabris, G., Clayton, R.M., & Back, L.H. 1989, Cryogenic mixing processes in the simulation of LO_2/LH_2 explosion hazards: Experimental facility and initial results with LN_2/LHe . JPL D-6394, Internal Document, Jet Propulsion Laboratory, Pasadena, CA.
- [5] Luchik, T.S., Aaron, K.M., Kwack, E., Shakkottai, P., Clayton, R.M., & Back, L.H., 1990, Cryogenic mixing processes in the simulation of LO_2/LH_2 explosion hazards: Results with LN_2/LHe and LO_2/LHe . JPL D-6987, Internal Document, Jet Propulsion Laboratory, Pasadena, CA.
- [6] Barron, R. F. 1985, Cryogenic Systems. (Monographs on Cryogenics), pp. 13-58, Oxford University Press, New York.
- [7] Manual on the use of Thermocouples in Temperature Measurements, ASTM special publication 470A, 1974. American Society for Testing and Materials, Philadelphia.
- [8] Kwack, E., Shakkottai, P., Luchik, T.S., Aaron, K.A., Fabris, G., & Back, L.H. 1990, Hot-Film calibrations at cryogenic temperatures, Submitted to Experiments in Fluids.
- [9] Sychev, V.V., Vasserman, A.A., Kozlov, A.D., Spiridonov, G.A., & Tsymarny, V.A. 1987a, Thermodynamic Properties of Nitrogen, Hemisphere Publishing Corp., New York.
- [10] Sychev, V.V., Vasserman, A.A., Kozlov, A.D., Spiridonov, G.A., & Tsymarny, V.A. 1987b, Thermodynamic Properties of Oxygen, Hemisphere Publishing Corp., New York.

- [11] Sychev, V.V., Vasserman, A.A., Kozlov, A.D., Spiridonov, G.A., & Tsymarny, V.A. 1987c, Thermodynamic Properties of Helium, Hemisphere Publishing Corp., New York.
- [12] Scott, R.B. 1959, Cryogenic Engineering, D. Van Nostrand Co. Inc., Princeton, NJ.

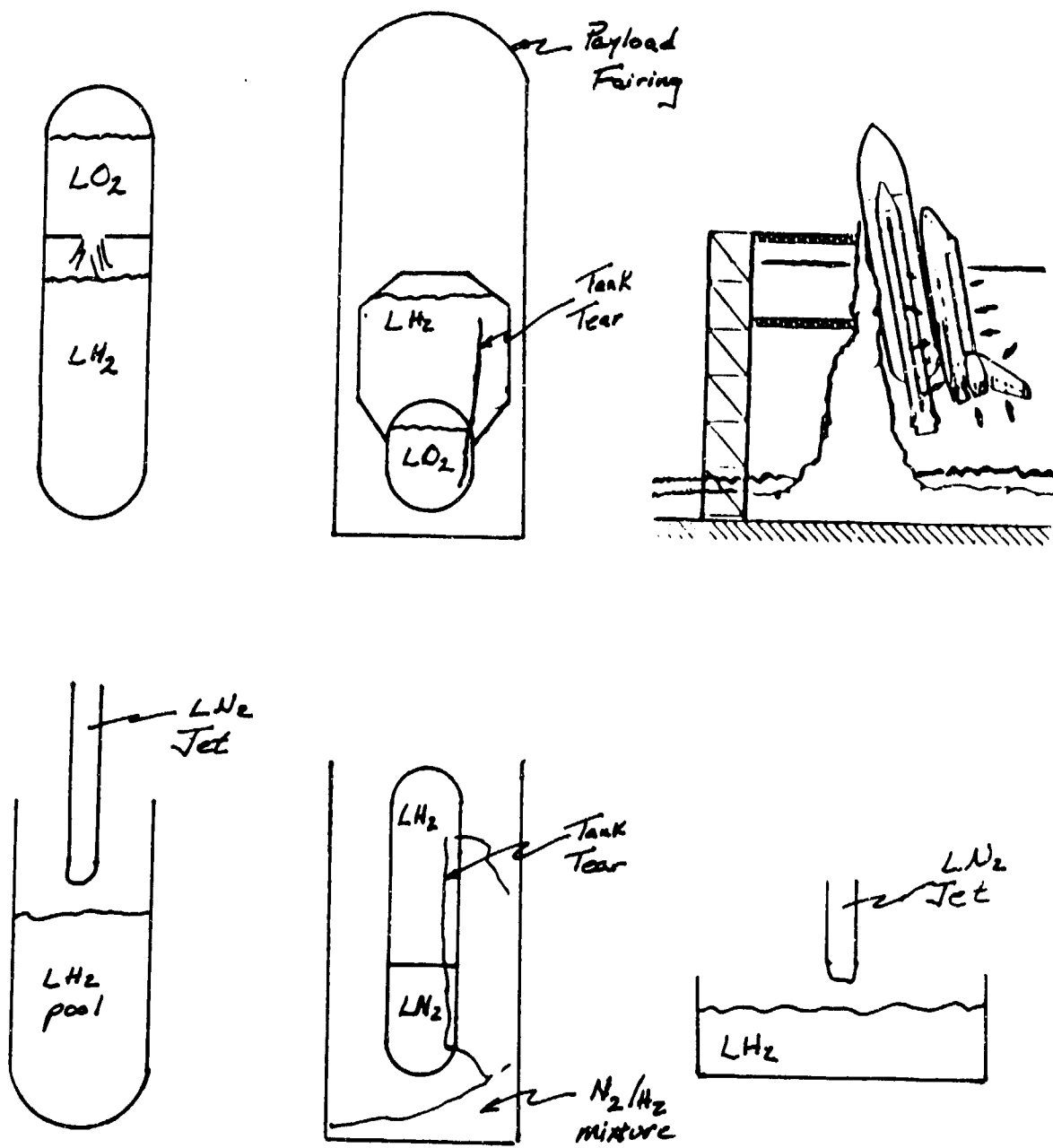


Figure 1. LO₂/LH₂ accident mixing scenarios.

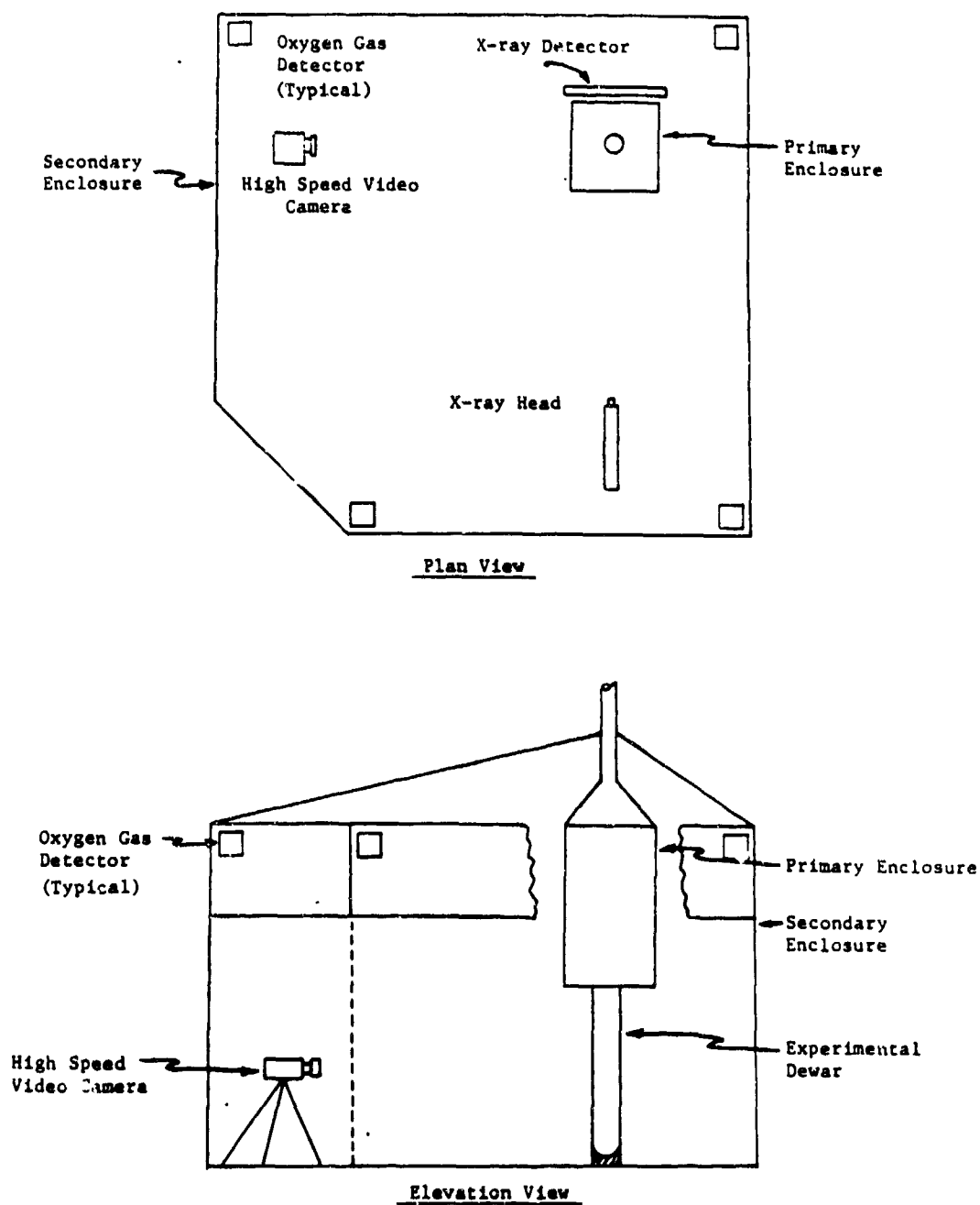


Figure 2. Facility schematic.

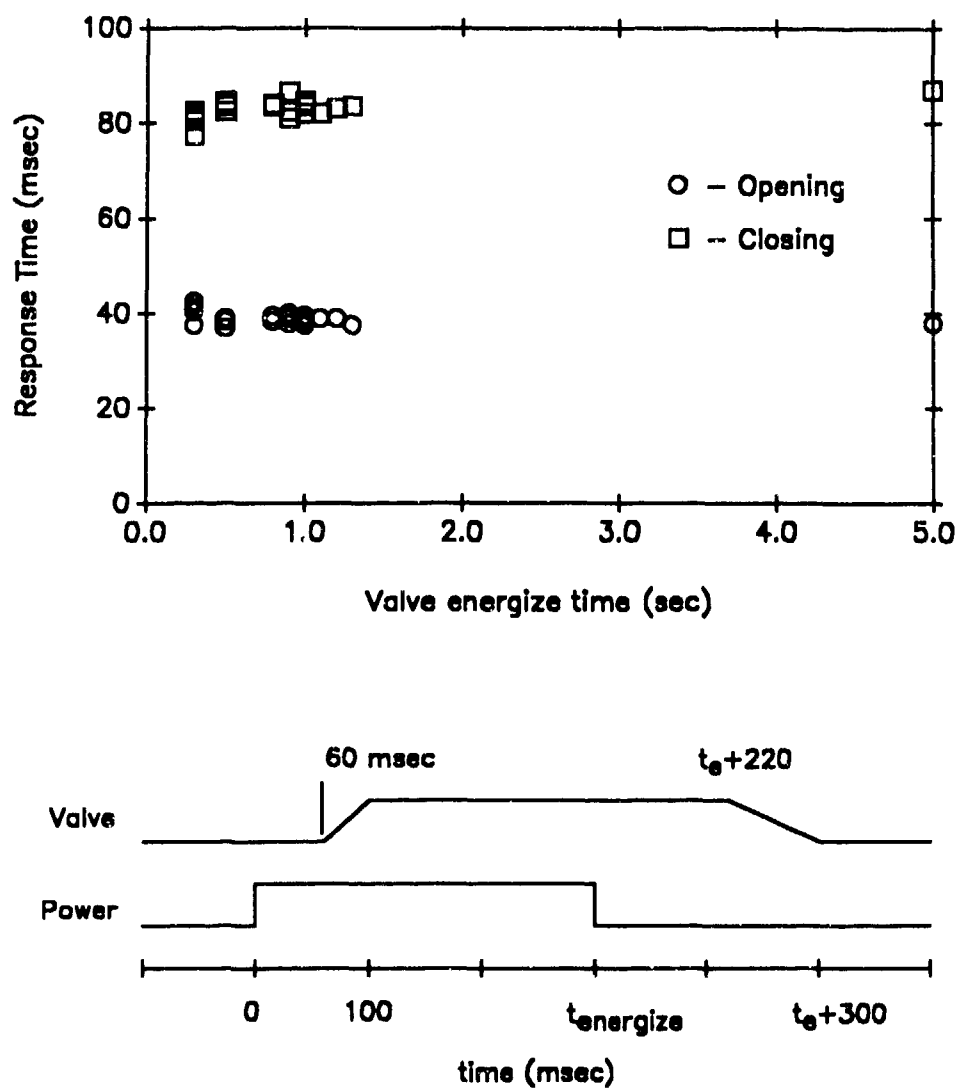


Figure 3. Dump valve response characteristics.

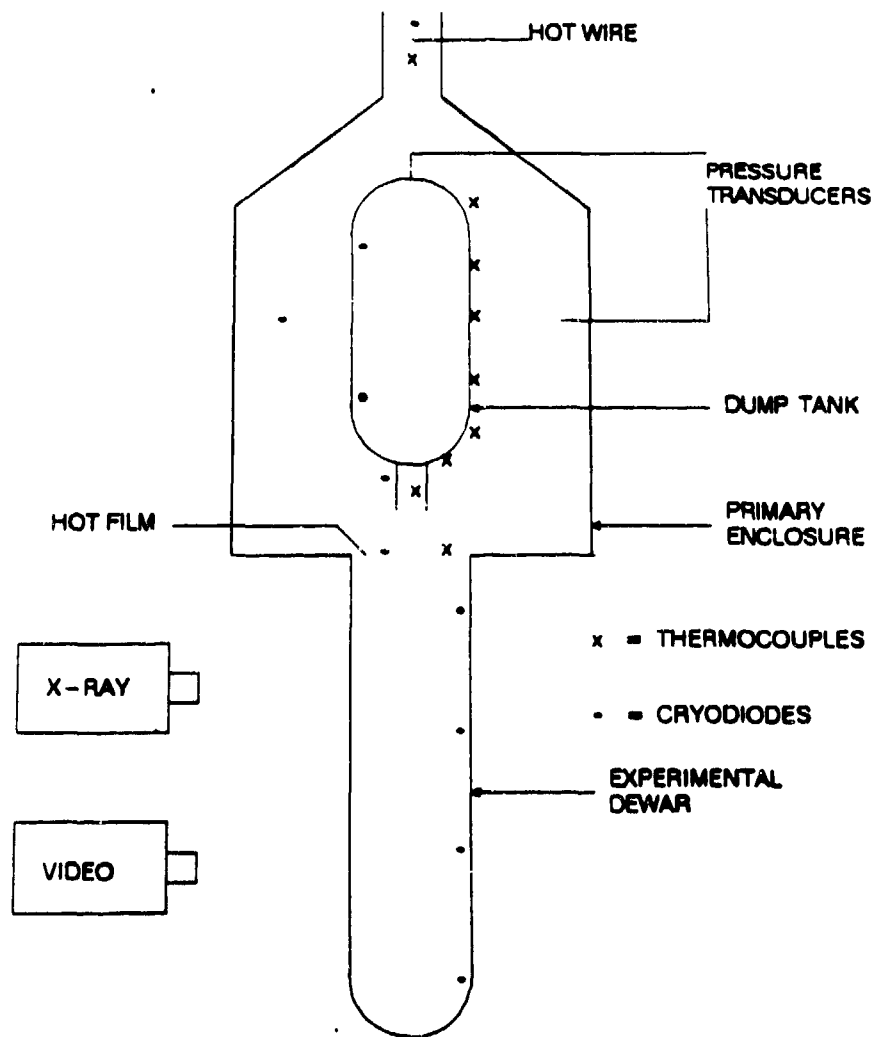


Figure 4. Schematic of primary enclosure.

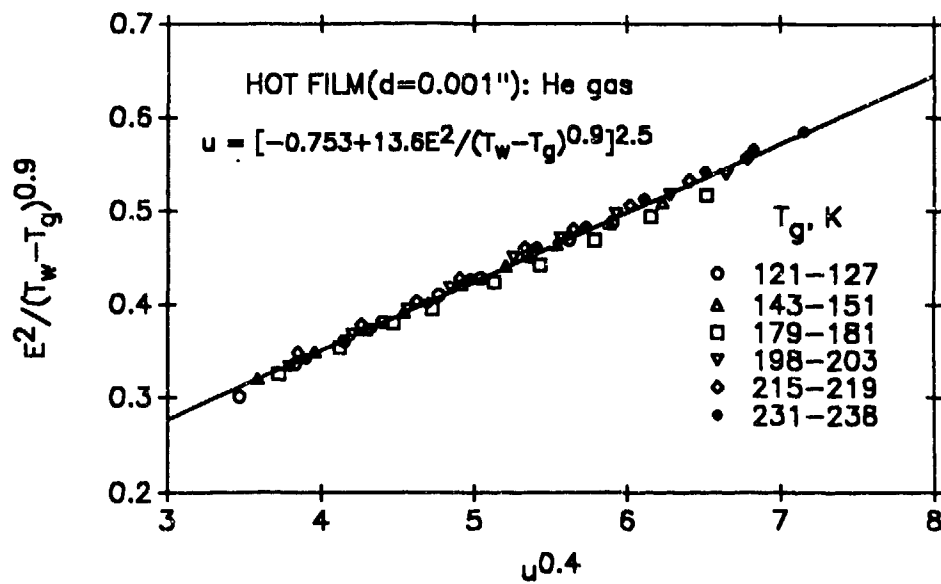


Figure 5. Hot-film anemometer calibration curve.

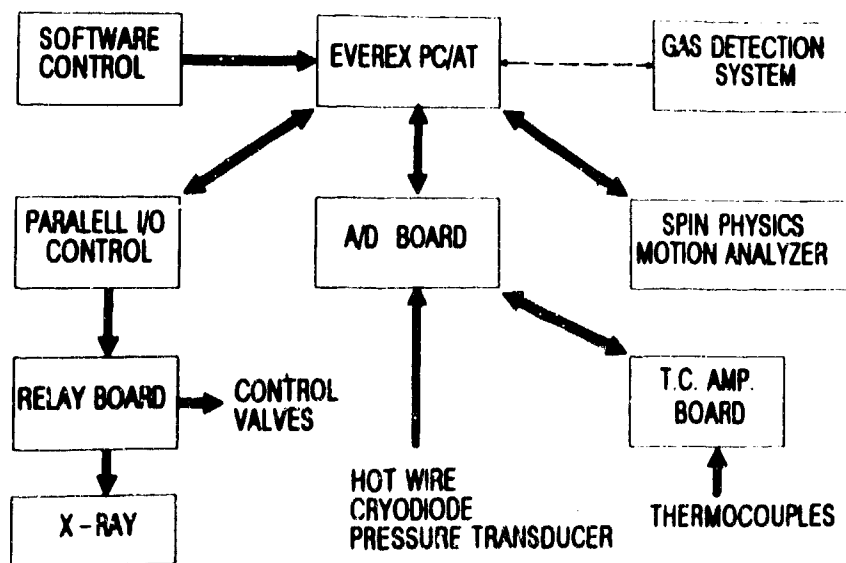


Figure 6. Data acquisition system

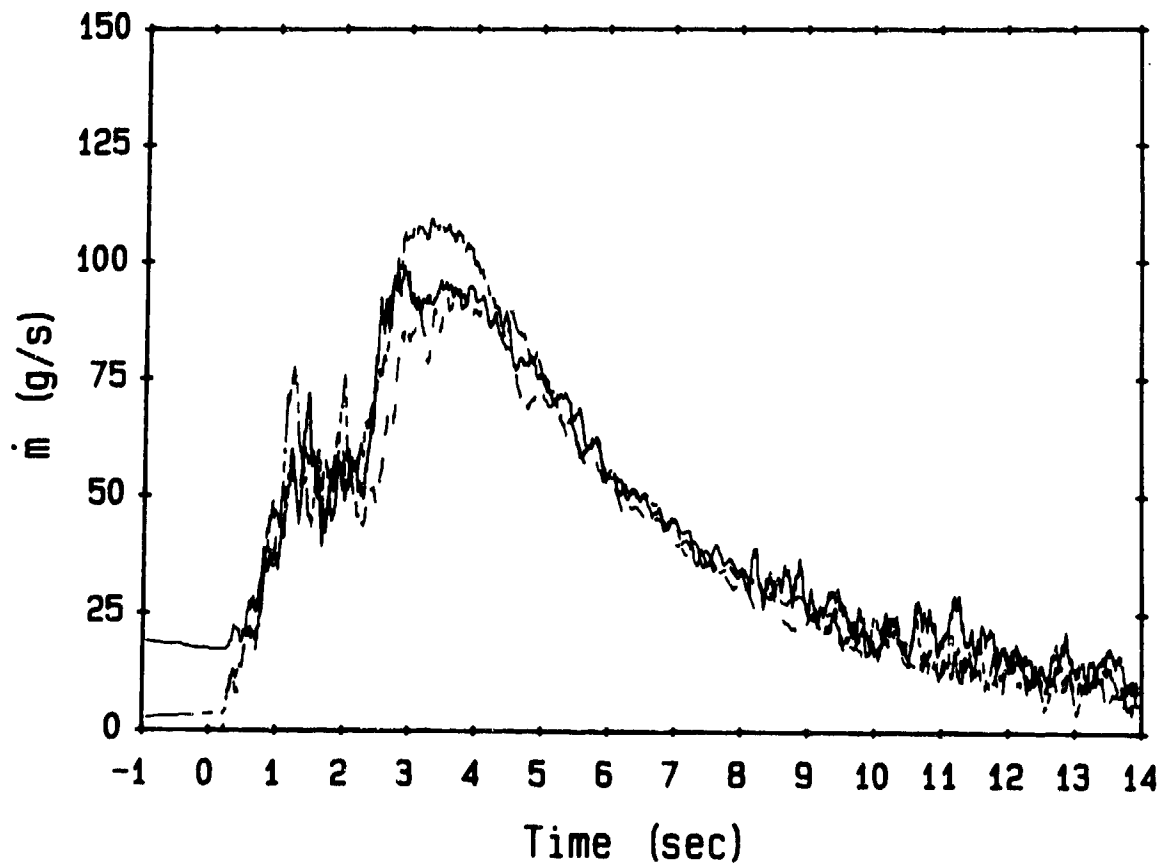


Figure 7. Helium evaporation rate for three similar tests.

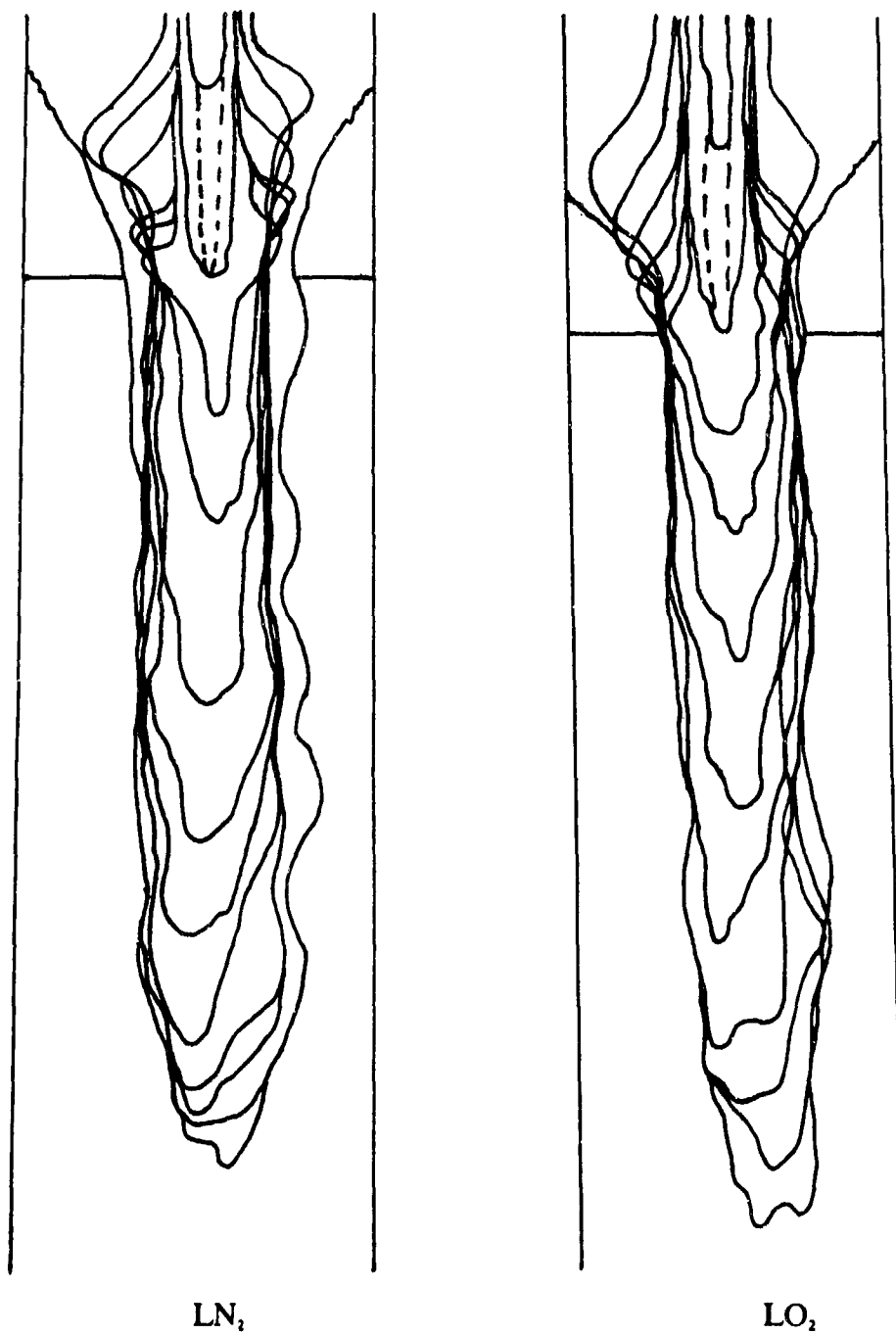


Figure 8. Mixing zone contours for LO_2 and LN_2 jets into LHe

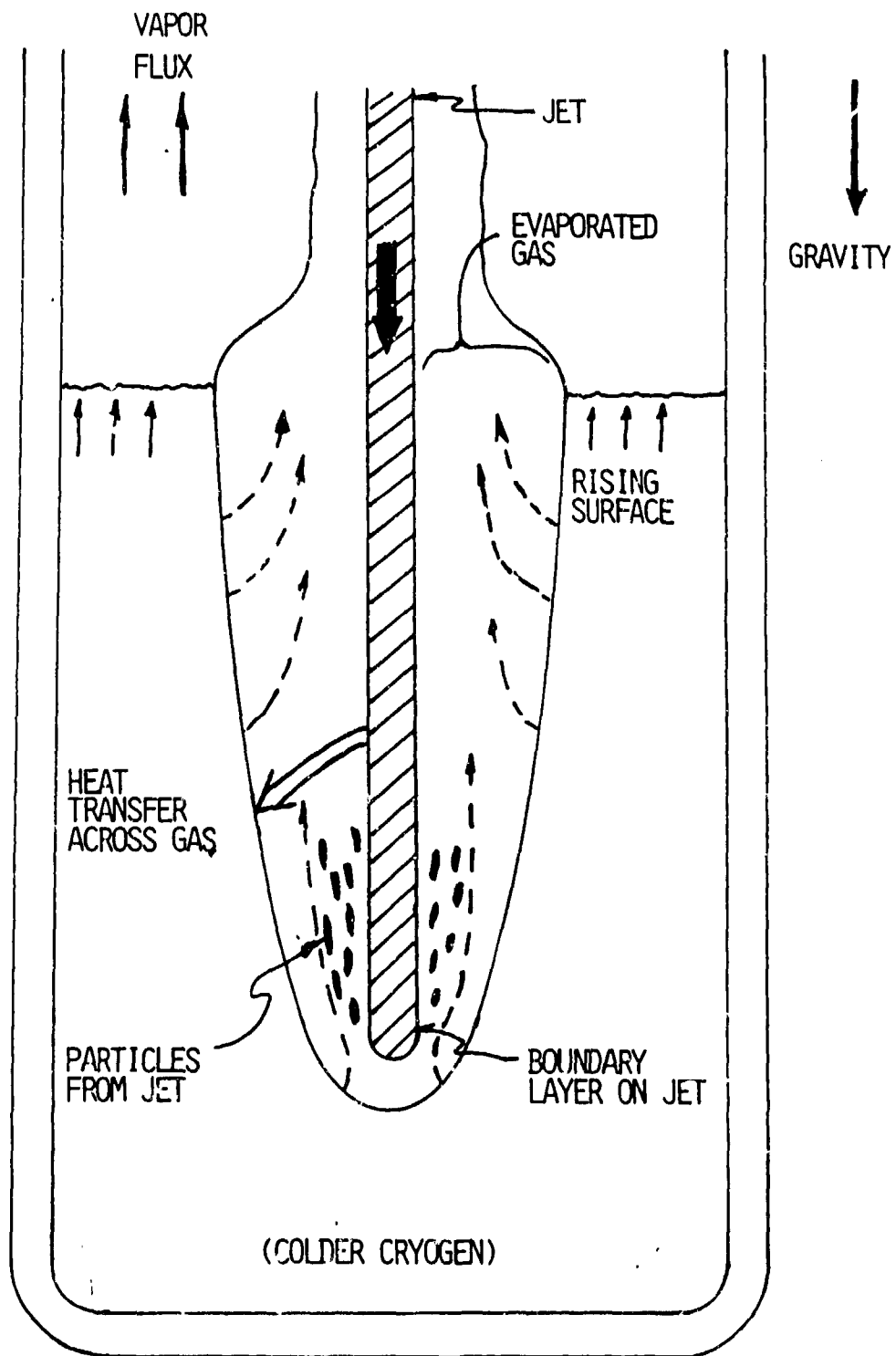


Figure 9. General mixing zone characteristics.

**HOT SPOT MECHANISM IN BUBBLE
SENSITIZED COMMERCIAL EXPLOSIVES**

**S.K. Chan, ICI Explosives
and
K.K. Feng, Canadian Explosives Research Laboratory**

HOT SPOT MECHANISM IN BUBBLE
SENSITIZED COMMERCIAL EXPLOSIVES

by

S.K. Chan
Senior Research Scientist,
ICI Explosives, Beloeil Site,
McMasterville, Quebec, Canada J3G 1T9

K.K. Feng
Head, Explosives Research,
Canadian Explosives Research Laboratory,
CANMET, Energy, Mines & Resources, Canada

ABSTRACT

Water-gels and emulsions exhibit two fundamental hot-spot mechanisms, namely shock heating of materials surrounding voids and adiabatic compression heating of bubble gases. By a comparison of the reaction kinetics derived from (a) VOD-diameter data using the recently developed computer code CPEX and (b) a reaction model proposed previously, it is shown that at the detonation regime, the dominant hot-spot mechanism is shock heating and the remaining explosive outside of the hot-spots is consumed by burning as proposed in the model. At the lower compression rates, the dominant initiation sensitization mechanism is the adiabatic compression of the gas in entrained bubbles. This is proven by the results from an experimental impact test on chemically sensitized water-gel explosive. The same mechanism operates in the DDT regime of these explosives. The time to ignition is shown to be related to the time of pressurization in both the impact test and the DDT tests.

INTRODUCTION

It is well known that explosive initiation sensitivity is significantly increased by the action of hot spots (1). However, the fundamental mechanisms of such hot spots are still a highly uncertain subject, particularly for a solid explosive. The number of possible hot spot mechanisms for the latter is extremely large involving mechanisms unique to solids (2) in addition to the commonly accepted ones for liquids, e.g. adiabatic compression of occluded gas voids (3) and shock heating (4). Water-gels and emulsions have characteristics of liquids, as far as initiation mechanisms are concerned. These much simpler mechanisms, which operate largely independently and at different ranges of initiation compression rates, allow a much easier understanding of the operation of the initiation mechanisms in these explosives, especially in the area of detonation. The latter has been successfully modelled by Chan (5,6). Recent development in detonation theory of non-ideal explosives (6,7) has produced an extremely powerful tool to deduce overall reaction rates from experimental detonation velocities at various charge diameters. This technique allows an independent check of the validity of reaction models proposed in Ref. 6. The two different reaction kinetics are compared in this paper.

At lower compression rates for water-gel and emulsion explosives, e.g. mechanical impact and pressurization due to internal ignition in confined or semi-confined medium such as in deflagration to detonation transition (DDT) events, hot spots are generated by the adiabatic compression of the gas pockets. This is related to the safety of the manufacturing and transport of such

explosives which has recently received much attention since the accidental explosion of emulsion explosive in a piston pump at the McMasterville site of C-I-L Inc. in 1988. This paper presents some previously unpublished data on the ASTM impact initiation and DDT of water-gel explosives which demonstrates the importance of adiabatic compression as a mechanism in such initiation mechanisms.

INITIATION UNDER DETONATION CONDITIONS

The experimental work of Campbell et al (8) and the theoretical work of Mader (4) have demonstrated convincingly that shock heating of materials surrounding the air bubbles is the most effective hot spot mechanism under shock initiation conditions such as those in the detonation wave. To demonstrate the shock heating effect quantitatively for liquids, shock temperatures of the materials upstream and downstream of a one-dimensional air-gap traversed by a plane shock wave (9) are shown in Fig. 1. In this Figure T_1 is the temperature of nitromethane heated by the shock wave from the initial temperature of T_0 , T_2 is the residual temperature after the material expands into the air-gap and T_3 is the temperature behind the reflected shock created in the upstream gap material after it impacts the opposite face of the air-gap. Mader's results for T_1 and T_3 are also shown in Fig.1. There is good agreement between the two sets of calculations. The results in Fig. 1 show clearly that under shock pressures of the order of 10 GPa, T_3 is almost 2700 K assuming an initial temperature of 293 K. The detonation shock causes the high temperature T_3 in the hot spot and instantaneously ignition follows.

The above shock void interaction hot spot mechanism was used

The above shock void interaction hot spot mechanism was used in the detonation models of References (5) and (6). The experimental detonation velocities were determined for a liquid explosive (EGMN/AN/EG/Water 50/25/20/5). The desired densities were obtained by mixing in glass microspheres (B15BX, 3M) (5). The recently developed I.C.I. slightly divergent flow computer code CPEX (7) is used here to re-analyze this data for the purpose of determining the reaction kinetics of the explosive. The theoretical fits to the VOD versus inverse charge diameter for three initial densities (1.1, 1.15, 1.2 kg/dm³) are shown in Figs. 2a-c. The CPEX deduced extent of reaction / time curves are shown in Fig. 3 for the three initial densities at a pressure of 5 GPa. The lower parts of these curves suggest that the extent of reaction of the hot spots, as indicated by the point of sharp change in slopes, correspond to the initial void volume fraction of 0.077, 0.115 and 0.154 for the three densities respectively. Beyond the hot spot volumes, the reaction curves resemble closely the theoretical grain burning curves of Ref. 6 as shown in Fig. 4. This can be taken as an independent confirmation of the validity of the grain burning model proposed in Ref. 6.

In the reaction model of Ref. 6, the hot spots were assumed to have an effective volume equal to $2^{3/4}$ of the initial void volume. The curves of Figs. 3 suggest that it should be equal to the void volume. Another assumption in this model was that the hot spots were to be initiated both by bulk thermal reaction and by burning instantaneously at the collapsed wall of the bubble by the hot compressed gas (see Fig. 5). However, the shape of the CPEX reaction curves in Fig. 3 in the hot spot reaction region indicates there is no grain burning reaction in this region. Otherwise, the

initial slopes of these curves should be higher than the slopes of the curves beyond these regions, instead of a gradually increasing slope. The hot spots with their higher temperature should have higher burning speed than the cooler material outside of the hot spots. In retrospect, this is not surprising. The glass microspheres are at very low pressure (typically about 0.1 atmosphere), which reduces the ability of the compressed gas to ignite the surrounding explosive. Furthermore, the glass wall material would absorb most of the gas energy. Thus the hot spot reaction in this case is reduced to one of thermal reaction in the shock heated hot spots in the explosive.

INITIATION UNDER IMPACT AND DDT CONDITIONS

When a gas bubble is present in a liquid explosive, including water gel and emulsions, the impact sensitivity is increased significantly (1). This makes the explosive more hazardous in the handling and manufacturing processes. In order to simulate the effect of gas bubbles on the impact sensitivity of such explosives, the ASTM Impact Test tool (10) shown in Fig.6 was used to test these explosives. About 30 mm³ of explosive is placed in the steel cup. An air space of 26 mm³ is formed in the centre of the O-ring under the stainless steel diaphragm. The cup assembly is positioned in the container body in direct contact with a roller bearing, which is connected to strain gauges for force measurement. The air space in the cup is precompressed to about 7 mm³. This tool was used to study the response of an EGMN based water-gel explosive. An impact weight of 5 kg was used. Positive results were obtained above a drop height of 0.36 m. The pressure record

from a positive test is shown in Fig. 7. The pressure increase following the initial impact pulse is attributed to the combustion of the explosive. There seems to be little doubt that the initiation mechanism is the ignition of the explosive by the hot compressed air.

Another hazard test carried out on the above EGMN based water-gel explosive was the DDT test. The test setup is shown schematically in Fig. 8. It consists of a heavy wall seamless steel tubing (19 mm ID/50.8 mm OD) with lengths of either 0.5 m or 0.9 m. An igniter is placed inside the closed end of the tube (11). The igniter compound used was either 2 g of RDX or RDX/black powder mixture. The outer wall of the steel tube at the igniter location was connected to strain gauges to monitor the pressure build-up history. A thin wall collapsible aluminum wave velocity probe was placed in the centre of the tube which was filled with the test explosive. Two EGMN based water-gel explosives which showed DDT behaviour were tested. These explosives (EXP-A contained 3% aluminum and EXP-B contained 7% of aluminum) had nominal density of 1.12 kg/dm^3 . These explosives were produced by chemical gassing, and contained small gas bubbles with nominal average diameter of $70 \text{ }\mu\text{m}$. The volume percent of air bubbles are 27 and 32% respectively for the two explosives. Figure 9 shows the igniter end pressure and wave velocity records for a test with EXP-A initiated with RDX/black powder igniter. The transition to detonation can be clearly seen from the wave velocity record which has a steady velocity of 0.77 km/s from the igniter to 0.58 m downstream at which it changes sharply to 4.25 km/s , corresponding to the detonation velocity of this explosive. The pressure reaches 0.45 GPa prior to a dramatic increase which seems to be the source

of the transition to detonation. If the trajectory of the detonation wave is extrapolated back to the igniter location, the time coincides with the moment of explosion in the pressure record. The initial pressurization rate was 490 GPa/s and the time from initiation of the igniter to the moment of the explosion is .640 ms (Fig. 9). A summary of other pressurization rate (normalized by the initial atmospheric pressure) and delay to explosion data is shown in Fig.10. There is a good correlation of these two parameters. The data from the impact test (Fig. 7) for EXP-A is also shown in the same figure. The impact data fits in very well with the DDT data indicating the close relationship between the two initiation events. This suggests that the DDT mechanism is the ignition of the explosive by the hot compressed bubble gas similar to that occurring in the impact test.

CONCLUSION

The results presented in this paper demonstrated the two basic hot-spot mechanisms in water-gel explosives. The shock heating of materials around voids is the dominant mechanism if shock initiation events involve a particle velocity above a few hundred meters per second. However, for more gentle pressurization, such as mechanical impact or combustion in a confined medium, the adiabatic compression of bubble gas becomes the more effective hot-spot mechanism. The presence of glass microspheres in an explosive is probably not effective for this latter mechanism since there is insufficient gas present in the microspheres and the glass would also absorb most of the gas energy to prevent transfer of heat to the explosive. This suggest that glass microsphere sensitized explosives are much safer in

compression events. However, there is always a danger of the presence of air pockets of volatile gases. Nevertheless, the hazards engineer should be aware of the potential hazards of manipulating such an apparently safe medium in rapid pressurization operations, despite the relative safety of the use of glass microspheres. For hazard quantification purposes, more work is still needed to quantify the ignition conditions.

REFERENCES

1. Bowden F.P. and Yoffe A.D., "Initiation and growth of explosion in liquids and solids", 1952, Cambridge University Press
2. Winter R.E. and Field J.E. "The role of localized plastic flow in the impact initiation of explosives", Proc. Roy. Soc. Lond. A. 343, 399-413 (1975).
3. Chaudhri M.M. and Field J.E. "The role of rapidly compressed gas pockets in the initiation of explosives", Proc. Roy. Soc., Vol. A340, 113-128 (1974).
4. Mader C.L., "Initiation of detonation by the interaction of shock with density discontinuities", Physics of Fluids, Vol. 8, 1811-1816, (1965).

5. Chan S.K., "A model for predicting the critical diameter of bubble sensitized explosives", Proceedings, Symposium H.D.P.: Behaviour of Dense Media Under High Dynamic Pressures, Paris, (1978), 233-244.
6. Chan S.K., "Theoretical prediction of the velocity-diameter relation of bubble-sensitized liquid explosives", Propellants, Explosives, Pyrotechnics, 8, 184-192 (1983).
7. Kirby I.J. and Leiper G.A., "A small divergent detonation theory for intermolecular explosives", Proceedings of the 8th Symposium (International) on Detonation, Albuquerque, p.176 (1985).
8. Campbell A.W., Davis W.C. and Travis J.R., "Shock initiation of detonation in liquid explosives", Phys. Fluids, 4 498-510, (1916).
9. Chan S.K., "A shock sensitivity model for aerated liquids", Report EL6810, (1976), Canadian Industries Limited, Montreal, Canada.
10. ASTM Standards ANSI/ASTM D 2540-70 (Reapproved 1980), "Standard Test Method for Drop Weight Sensitivity of Liquid Mono-propellants", American Society for Testing and Materials, Philadelphia, Pa., U.S.A.
11. Chan S.K. "Deflagration to detonation transition behaviour of water-gel explosives", C-I-L Inc. (now ICI Explosives, Canada), McMasterville, P.Q., Canada.

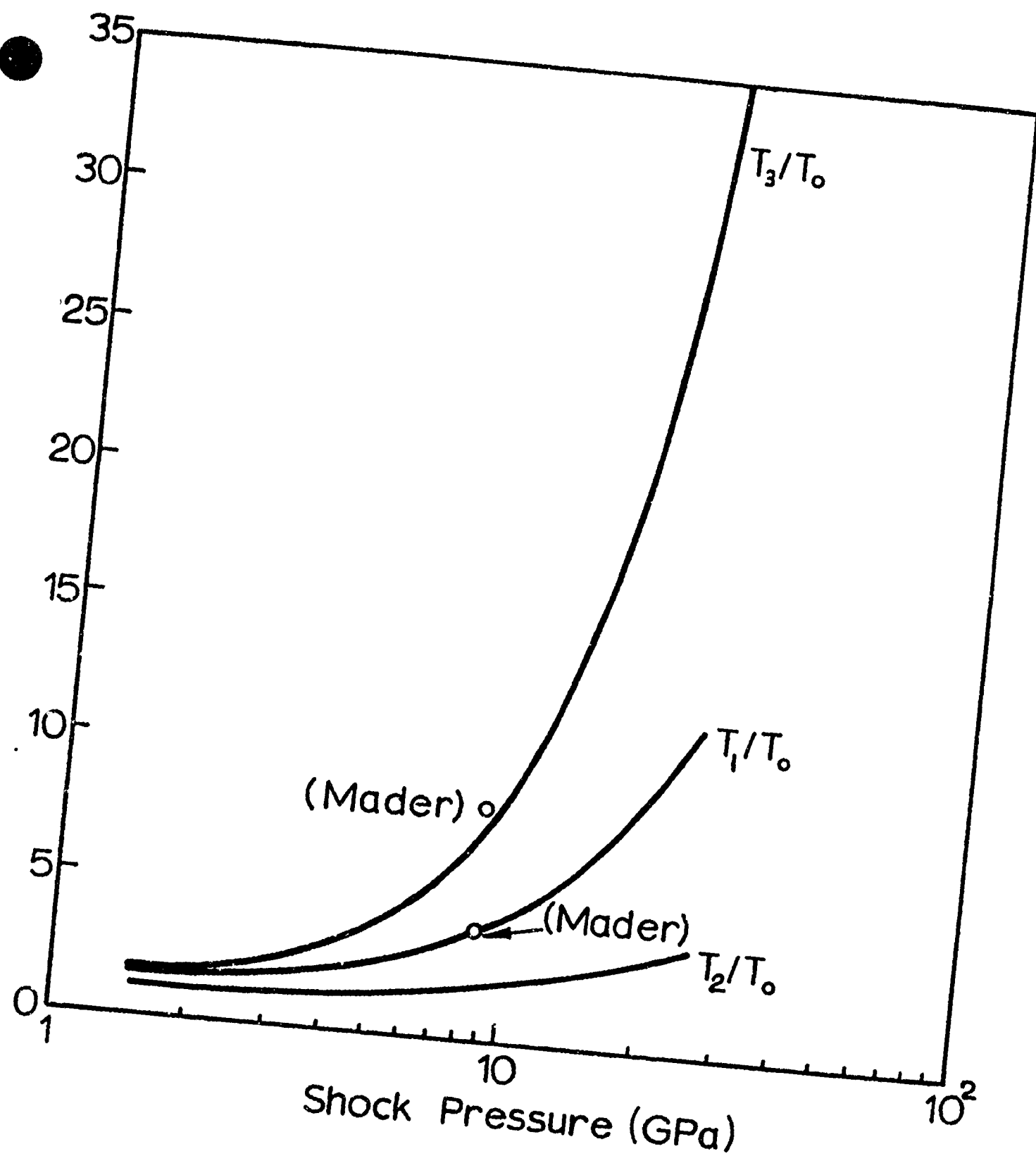


Figure 1, Shock temperature of nitromethane upstream and downstream of a one dimensional air-gap traversed by a plane shock wave.

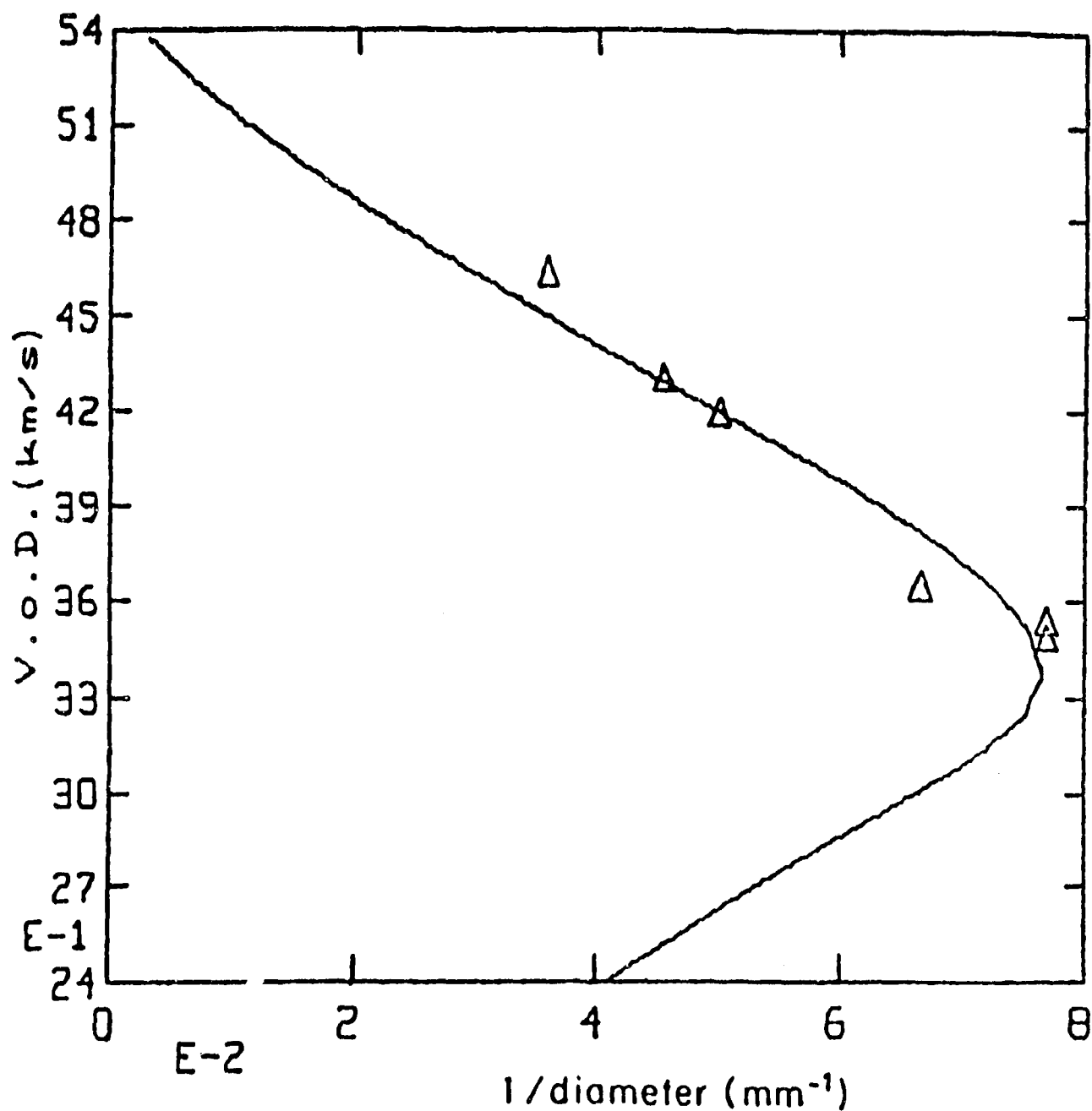


Figure 2a, Theoretical detonation velocity versus reciprocal charge diameter on 1.1 g/cm³ EGMN at unconfined condition.

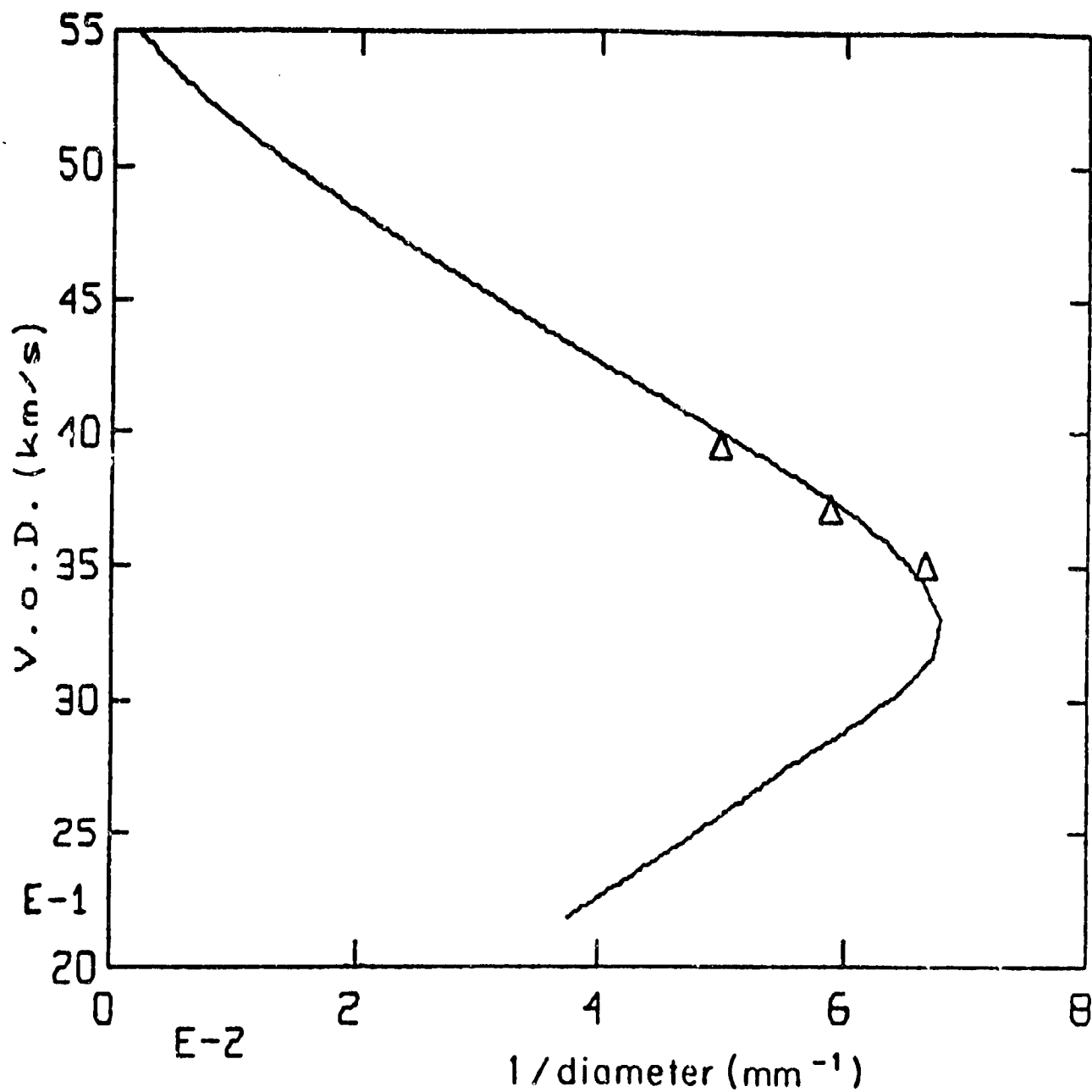


Figure 2b,

Theoretical detonation velocity versus reciprocal charge diameter for 1.15 g/cm³ EGMN at unconfined conditions.

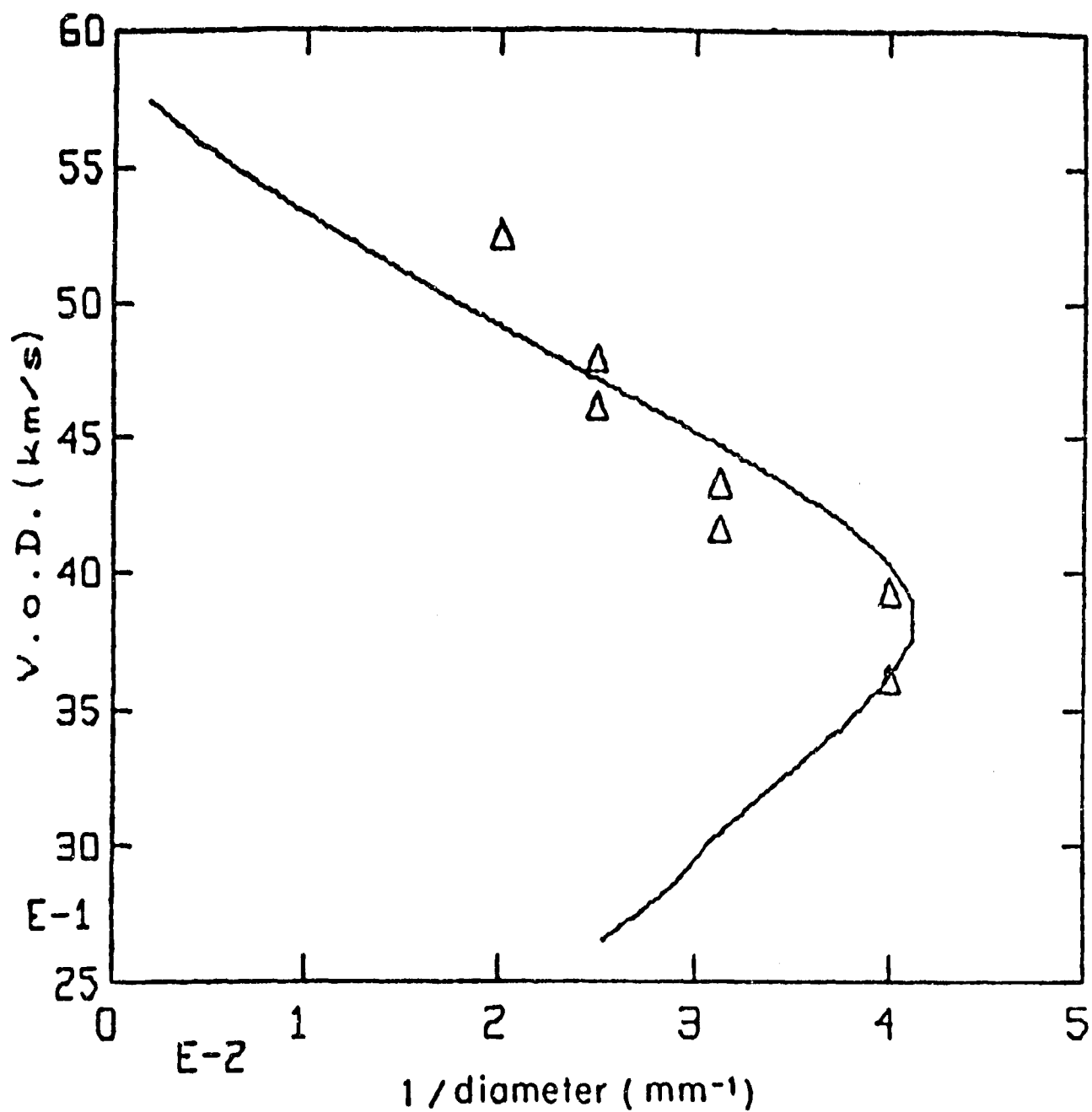


Figure 2c,

Theoretical detonation velocity versus reciprocal charge diameter for 1.2 g/cm³ EGMM at unconfined conditions.

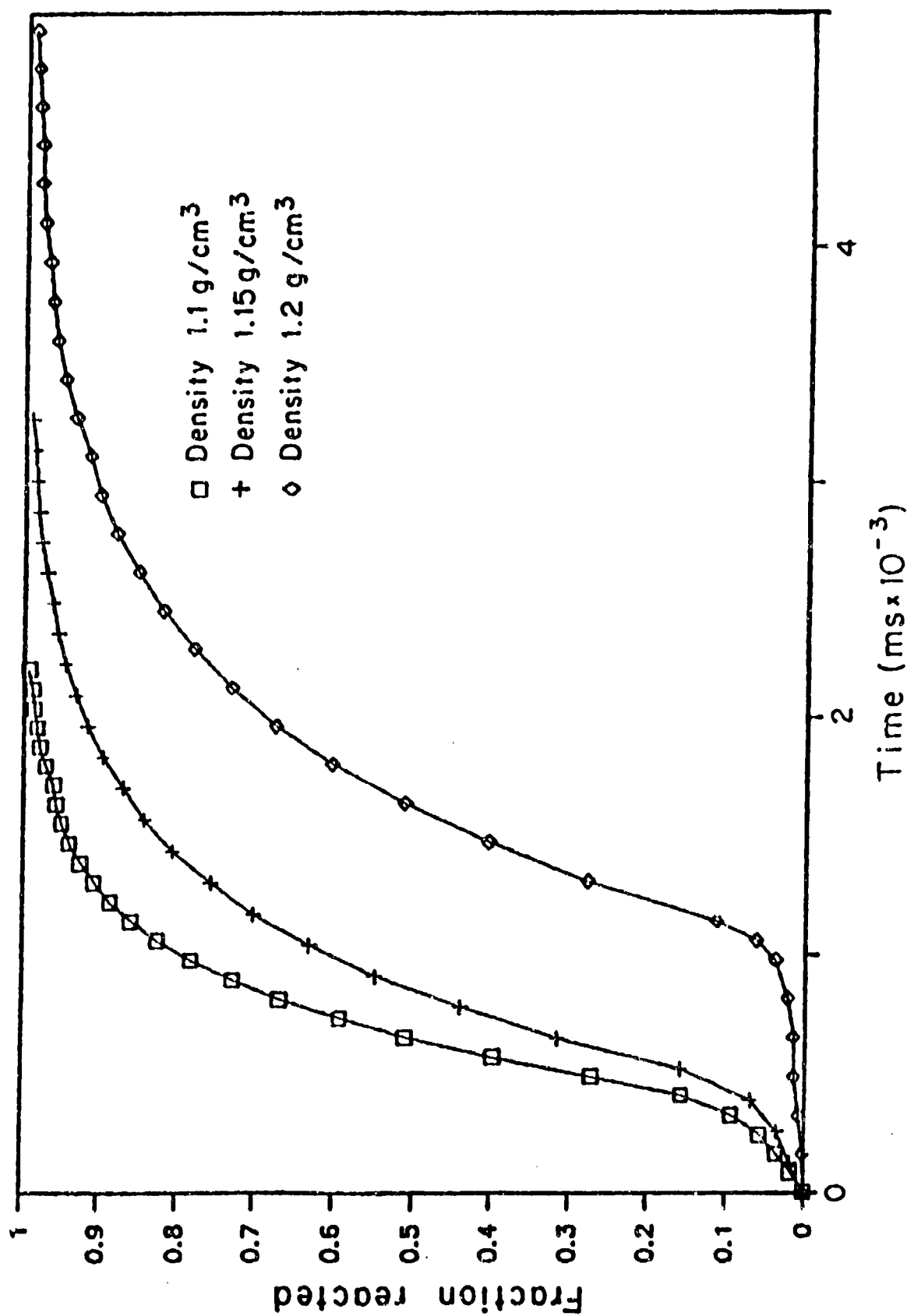


Figure 3, Fraction reacted vs. time curves for the initial densities (1.1, 1.15, 1.2 g/cm³) at a pressure of 5.0 GPa.

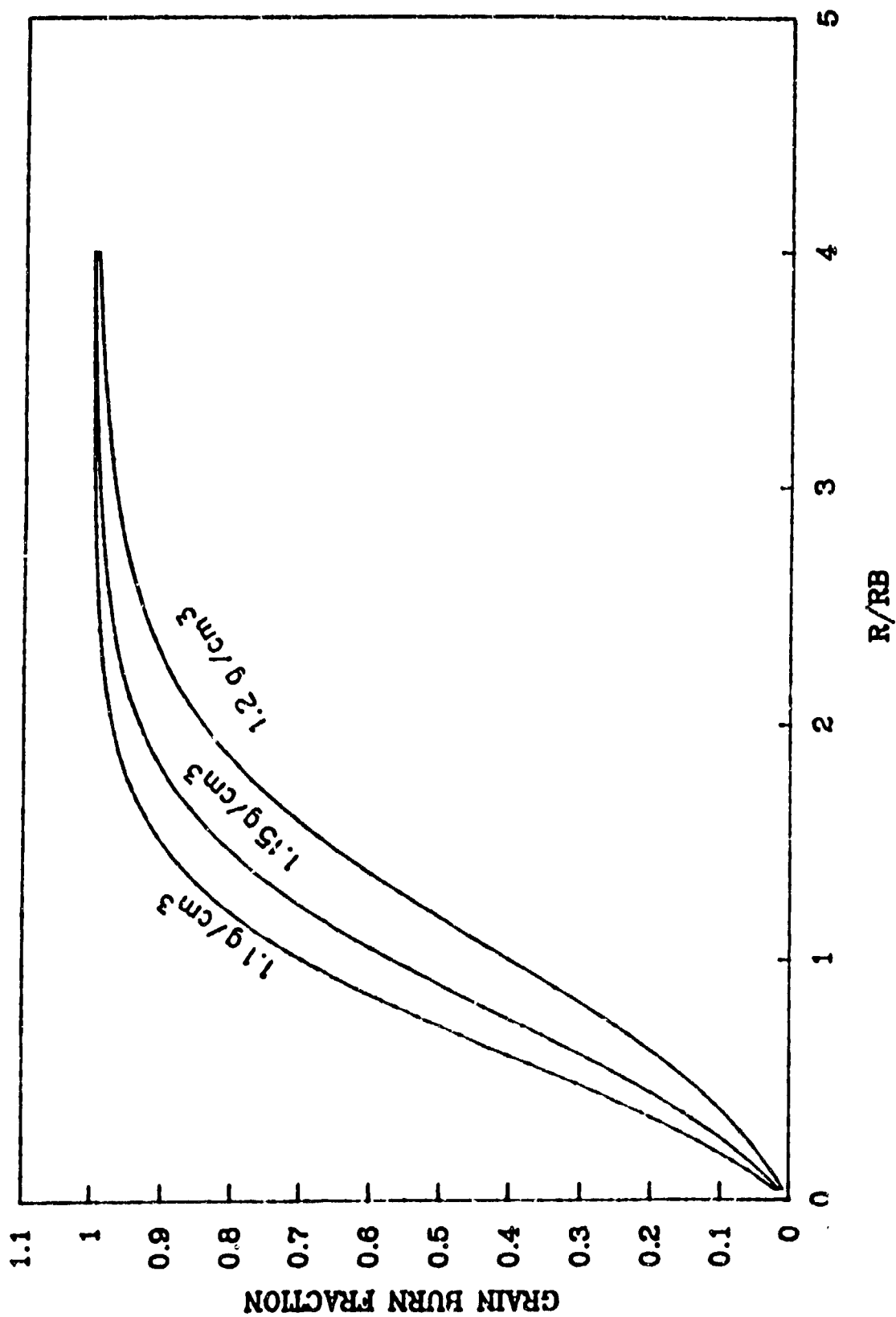


Figure 4, Comparison of the grain burn fraction versus flame propagation distance with the analytical fits for initial density of 1.1 g/cc, 1.15 g/cc and 1.2 g/cc.

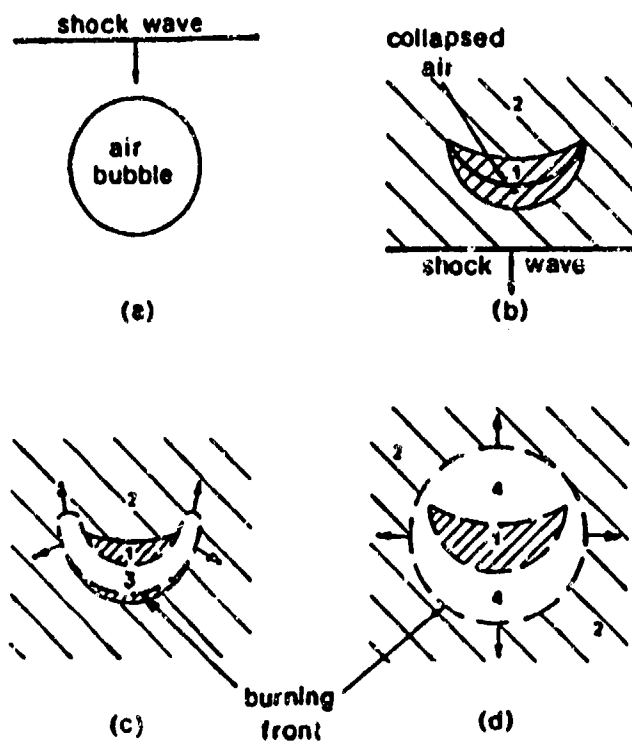


Figure 5, Schematic representation of the reaction behind the detonation shock wave.

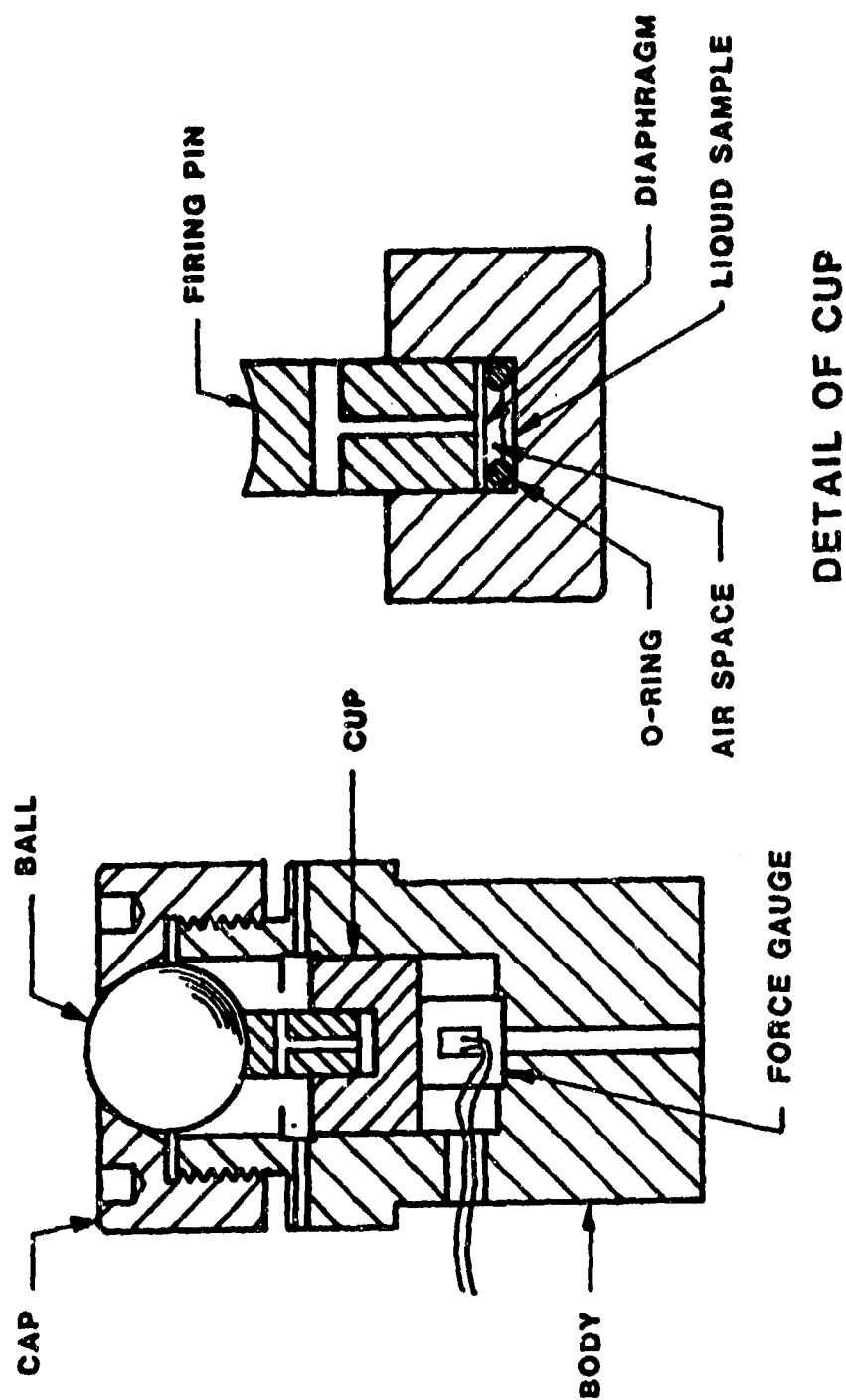


Figure 6, Experimental arrangement for ASTM impact test.

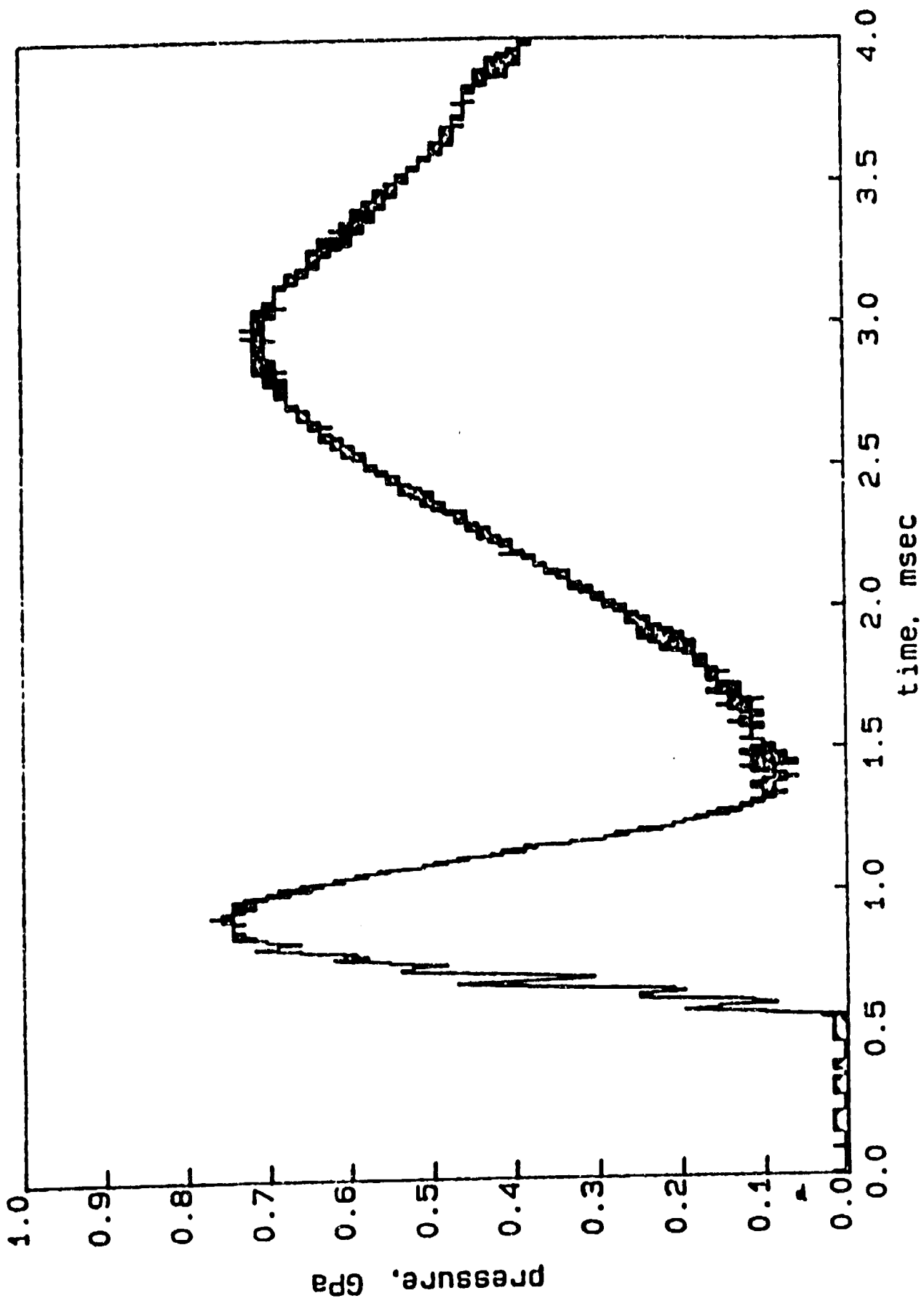


Figure 7, Pressure records from ASTM impact test on a EGMN based explosive.

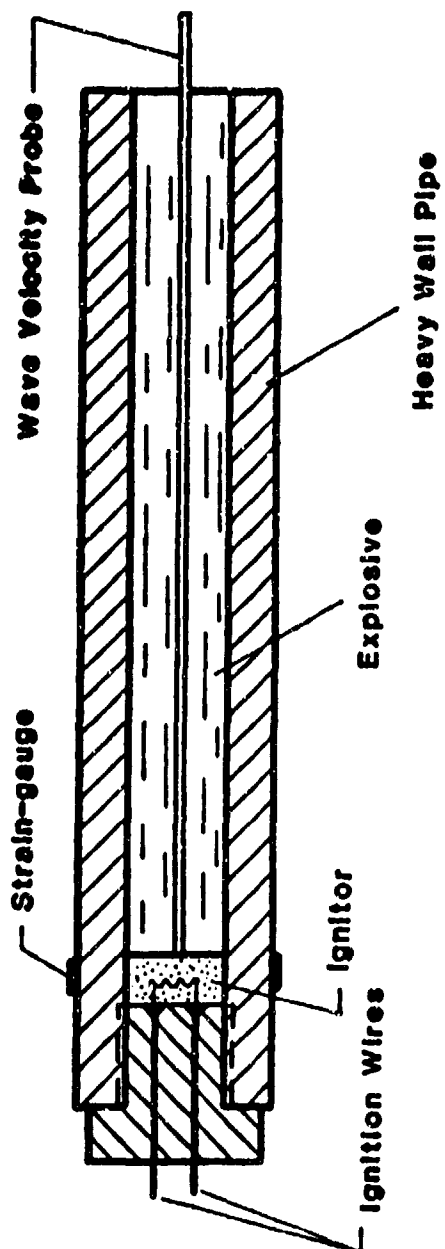


Figure 8, Schematics of experimental set up of DDT test.

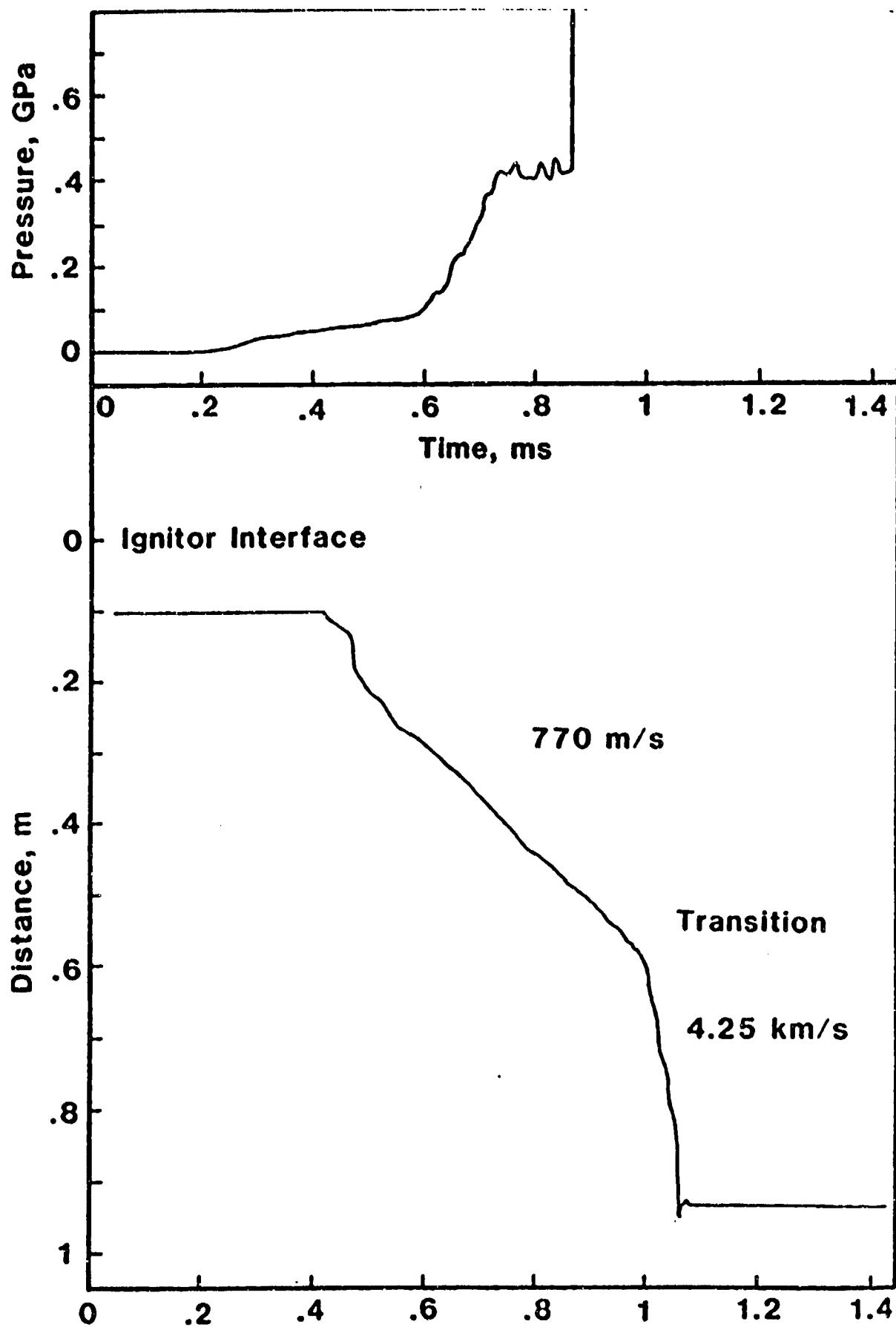


Figure 9, Ignition end pressure and wave velocity records for a test with EXP-A initiated with RDX/black powder igniter. 1311

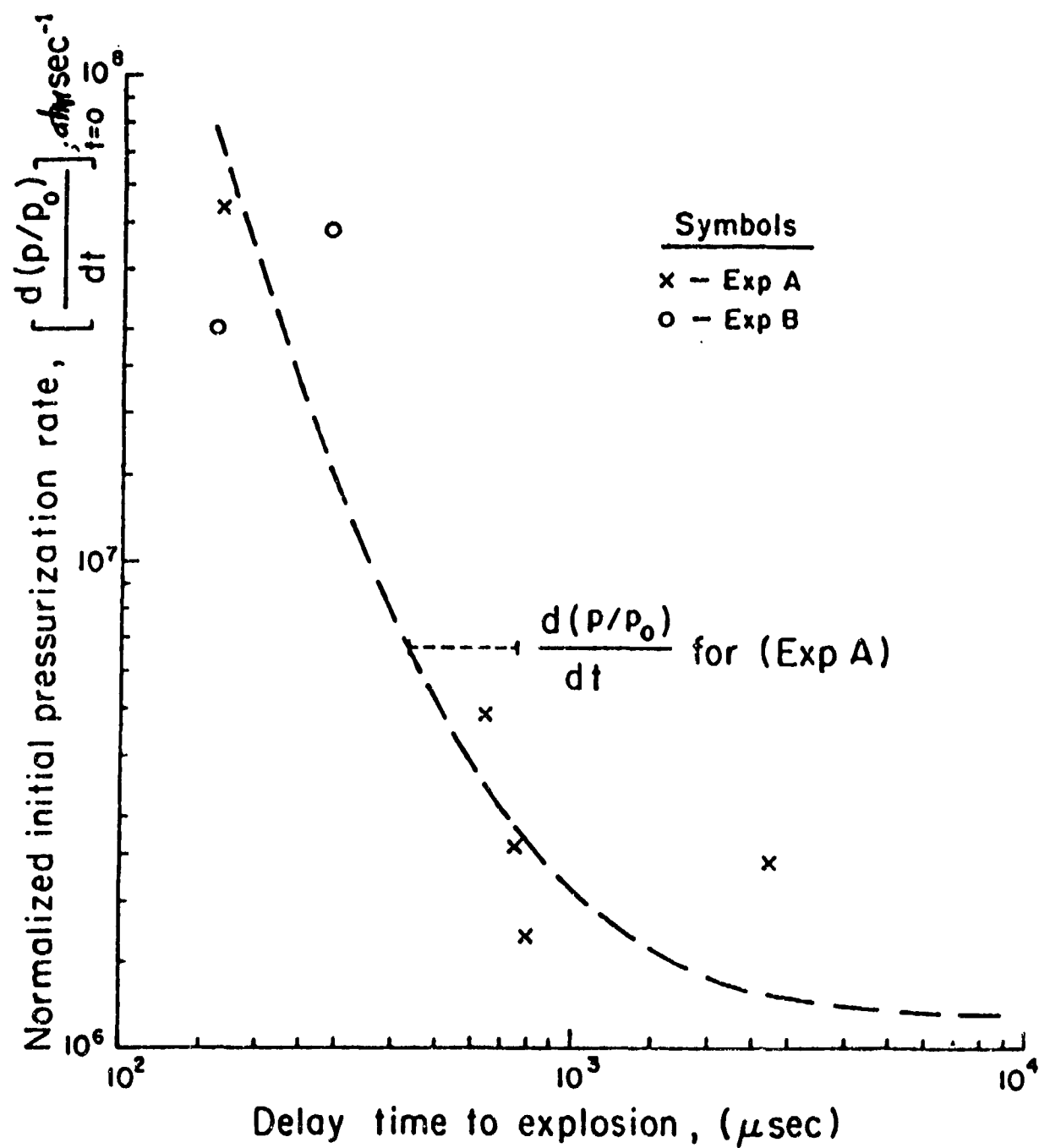


Figure 10, Correlation of the pressurization rate with the delay time to explosion.

EXPLOSIVE SAFETY TESTING AT NEW MEXICO TECH: THE BROWER ADIABATIC COMPRESSION TEST

K.R. Brower, D.B. Olson, and P.A. Persson

**Research Center for Energetic Materials
New Mexico Institute of Mining and Technology
Socorro, New Mexico 87801**

ABSTRACT

A new hazard test has been developed at the Research Center for Energetic Materials at New Mexico Tech in which bubble compression ignition of liquid or solid material is simulated under well defined conditions of temperature and pressure. Small samples of the test explosive are placed in a piston-cylinder apparatus and a drop weight, usually 1 kg, is used to initiate rapid compression ignition. A series of drop heights can be used to vary the ignition conditions. The rebound energy imparted to the drop weight from the ignition is measured. The temperature and pressure conditions, typically in the ranges 800-2000 K and 200-1200 atm, are determined from the compression ratio and nature of the gas in the chamber. Chemical analysis of the residual explosive or product gases can be performed to elucidate the reaction mechanism of the ignition.

INTRODUCTION

Adiabatic compression of gas bubbles is generally accepted as a potential ignition source of liquid explosives and propellants. Indeed, gas bubbles have been known as primary sensitizing agents of liquid energetic materials since the early days of nitroglycerin production¹. Nitromethane, for example, can be made sensitive to a No. 8 cap by the addition of 1.5% of glass bubbles². Bubble compression is relevant to hazards in such varied practical applications as hydrazine transfer to space vehicles, operation of liquid propellant guns, and pumping of commercial emulsion explosives. Initiation of solid explosives in gun projectiles by compression of voids, the so-called setback problem, has been the subject of several investigations³.

No single drop weight apparatus for measuring the sensitiveness of liquid explosives is generally used. The NATO AOP-7 manual⁴ gives a small scale test which has been discussed in terms of its use for hazard classification of liquid propellants⁵. This test is performed using an ASTM test apparatus⁶ in which a small amount of liquid is placed in an O-ring in the bottom of a cylindrical cavity and covered with a steel diaphragm. A 2 kg weight is dropped from various heights onto a steel ball in contact with a steel striker on top of the diaphragm and sample. The air trapped inside the O-ring with the sample is heated by compression to ignite the sample. A positive event is indicated by a ruptured diaphragm.

The conditions that cause ignition of samples in this apparatus are not well established, and events are only classified as go or no-go ignitions. A similar "Liquid Explosive Impact Test" is listed in Reference 7.

Several authors have analytically studied the process of ignition by compression of voids using numerical simulation techniques³. For voids contained in solids, the physical properties of the material are found to be important since heating also occurs (in addition to gas phase compression heating) as the result of viscoplastic work, inviscid plastic work, and/or condensed phase compression.

A new compression ignition test has been developed by Brower and coworkers⁸ in which small samples of liquid (or solid) are subjected to potential ignition by hot compressed gas at pressures up to about 1200 atmospheres and temperatures up to or greater than 2000 K. Conditions can be varied by the choice of gas and the drop height. The energy release from partial or complete ignitions can be measured and product samples can be taken for chemical analysis. Heating mechanisms other than by gas compression are eliminated since the sample is not significantly deformed. This test and some results are discussed below.

EXPERIMENTAL

The apparatus consists of a hardened steel O-ring sealed piston and cylinder of 1.3 cm bore with a small diameter side arm tube for filling with gases other than air and for withdrawing product samples. Figure 1 shows a schematic diagram of the apparatus. This assembly is held in an aluminum block (which can be heated) on top of a lead brick. A 1 kg drop weight from heights of up to 120 cm is used to drive the piston. The drop weight has a mechanical catch which arrests its motion at the point of maximum rebound height. A rebound of less than 4 cm is obtained from tests on inert samples. The rebound height from test sample ignitions can be used to calculate the mechanical work released by the sample. Expansion of the gas upon rebound of the piston quenches the chemical reactions and limits the duration of the event to about 500 μ s.

The experimental test conditions have been determined using a variety of diagnostics. The compression ratio is determined from the known initial volume of the system and measurements of the minimum clearance between the piston and cylinder. This has been measured by placing a small lead sphere inside the apparatus and measuring its final thickness. The compression ratio was also measured using a magnetic velocity sensor on the weight (differentiated to give acceleration). Pressures derived using the two methods agreed⁹ within 6%. Assuming all of the work done by the piston goes into heating the gas, the ratio of initial and final volumes can be related to final pressures and temperatures

using the ideal gas law. The following relationships are obtained:

$$P_f = P_i (V_i/V_f)^\gamma$$

$$T_f = T_i (V_i/V_f)^{\gamma-1}$$

where the subscripts i and f refer to initial and final (maximum compression) states and γ is the ratio of heat capacities, C_p/C_v , of the gas (mixture). It can be seen from the exponents that the temperature ratio increases less rapidly with increasing compression ratio than the pressure ratio. For argon, air, C_2H_6 , and SF_6 , γ has values of about 1.67, 1.40, 1.25, and 1.09 respectively. Figure 2 shows final pressure and temperature ratios calculated using the above equations for air compression at various V_i/V_f ratios. Figure 3 shows the difference in final temperatures obtained for compression of air at two initial temperatures, 298 and 398 K. The different temperatures obtained using three gases of different heat capacity ratios are shown in Figure 4. It can be seen that polyatomic explosive vapors with γ approaching one greatly reduce the heating by adiabatic compression, whereas a monatomic gas such as argon gives maximum heating. This effect can be used to advantage in selecting test conditions, but can be a complicating factor if test sample vapors alter the γ of the gas atmosphere in the apparatus. When necessary, the apparatus and sample are cooled to reduce the sample vapor pressure and so to achieve high final test temperatures.

In practice, the compression ratio for a given test series can be measured as a function of drop height from lead shot measurements. These data are then used to calculate maximum pressure and temperatures for given initial conditions. A compression ratio of 100, for example, gives 630 atm and 1880 K when air is used in the apparatus. Test samples consist of ≈ 10 -20 mg of liquid (or solid). The Bruceton up/down method can be used to determine the drop height for a given threshold rebound height or degree of sample decomposition.

RESULTS

This apparatus and technique were initially developed for a study of nitromethane decomposition and the effects of various additives⁸. Partial ignitions were obtained for neat nitromethane using drop heights as small as 20 cm, with complete consumption of the small sample when the drop height was about 70 cm. Some nitromethane data⁸ are shown in Figure 5 which shows that a variable response from partial ignitions is obtained. This ability to get a graded response is a distinct advantage over tests in which only a go or no-go is determined, since it makes it possible to study the early stages of the ignition process and allows a better differentiation of the sensitivity of various materials.

Figure 6 shows test results⁹ for solid and liquid TNT (melting temperature = 81°C) obtained at constant drop height. Not only does the fraction of tests that are positive ignitions increase with increased temperature, but the average rebound height also increases

(12 cm rebound at 70°C and 35 cm rebound at 90°C). This can be compared to normal drop weight impact tests on TNT as a function of temperature where the impact sensitivity greatly decreases at temperatures above 75°C because the soft or melted sample is not heated as efficiently upon mechanical impact. The data from the compression ignition test show that, in fact, TNT is more sensitive to ignition when hot (as is reasonable).

Another example application of this test procedure to solid material is illustrated in Figure 7 for mixtures of ammonium perchlorate with two different hydrocarbon fuels. The drop height, gas, and initial temperature were held constant in these tests and the composition of the samples was varied¹⁰. A stoichiometric mixture of AP with hydrocarbon will contain about 9 weight percent hydrocarbon. The data in Figure 7 indicate that fuel lean (less fuel than stoichiometric) mixtures are more sensitive to ignition by hot compressed air than the stoichiometric mixture. The maximum pressure and temperature conditions for these tests were about 2050 K and 700 atm. Figure 8 shows additional rebound data for three mixtures of AP with hydrocarbon taken at various initial drop heights. The shape of the rebound data with drop height is seen to be similar to that of the temperature obtained as a function of drop height (c.f., Figure 2 and 3).

CONCLUSIONS

A new hazard test has been developed in which ignition from hot, rapidly compressed gas, such as occurs in bubble or void collapse, of liquid or solid material is simulated under well defined conditions of high temperature and pressure. Small samples of explosive are tested in a piston-cylinder apparatus using a drop weight to initiate rapid compression ignition. A series of drop heights and compression of different gases can be used to vary the ignition conditions and to obtain a gradual increase in response with increasing drop height. The rebound energy imparted to the drop weight from the ignition can be used to measure the energy release from the sample. The apparatus is simple, inexpensive to build, and can be used in the laboratory environment without unusual safety precautions.

This test procedure and apparatus give much greater control and knowledge of the conditions to which samples are subjected than other impact tests for liquids. Having knowledge of the pressure, temperature, and duration of the exposure of the energetic material to hot gases allows better analysis of the results and possibly extension to other situations of larger scale.

REFERENCES

1. Bowden, F.P. and Yoffe, A.D., Initiation and Growth of Explosion in Liquids and Solids, (Cambridge University Press, Cambridge, 1952).
2. Minnick, J.J., "Gelled Nitromethane Explosive Containing Fluid Encapsulations," U.S. Patent 3,338,165,
3. For example, see Pasman, H.J., "Shell Prematures by Compression Ignition and Their Laboratory Simulation," DREV Report 707/75, April 1975, DREV, Quebec, Canada, and Frey, R.B., "Cavity Collapse in Energetic Materials," The Eighth Symposium on Detonation, 1985, and references contained therein.
4. NATO AOP-7, "Manual of Tests for the Qualification of Explosive Materials for Military Use."
5. Seals, W.O., Herrera, W.R., Petino, G., Jr., and Grelecki, C., "Hazard Classification of Liquid Propellants," Twenty-Third DoD Explosives Safety Seminar, Atlanta, GA, August 1988.
6. "Drop Weight Sensitivity of Liquid Monopropellants," ASTM Test Designation D2540-70.
7. "Liquid Explosive Impact Test," Explosive Research and Development Establishment, Waltham Abbey, Essex, England as listed in: Walker, G.R., Whitebread, E.G., and Hornig, D.C., Manual of Sensitiveness Tests, February 1966, Published by the Canadian Armament Research and Development Establishment on behalf of TTCP Panel O-2 (Explosives), Working Group on Sensitiveness.
8. Brower, K.R. and Liu, P., "Chemical Factors in the Sensitivity of Nitromethane to Explosion by Bubble Collapse," RCEM Report A-07-88, New Mexico Tech, October 1988.
9. Brower, K.R. and Liu, P., "Chemical Sensitizing of Explosives. Stimulation of Energetic Materials by Exposure to Hot Compressed Gas," Proceedings of the RCEM Open Seminar, Safety and Hazard Evaluation, New Mexico Tech, April 1989.
10. Brower, K.R., Hill, B., Olson, D.B., and Tsosie, B., "Sensitivity of Ammonium Perchlorate with Additives at Different Temperatures," CETR Final Report to Astronautics Laboratory, October 1989.

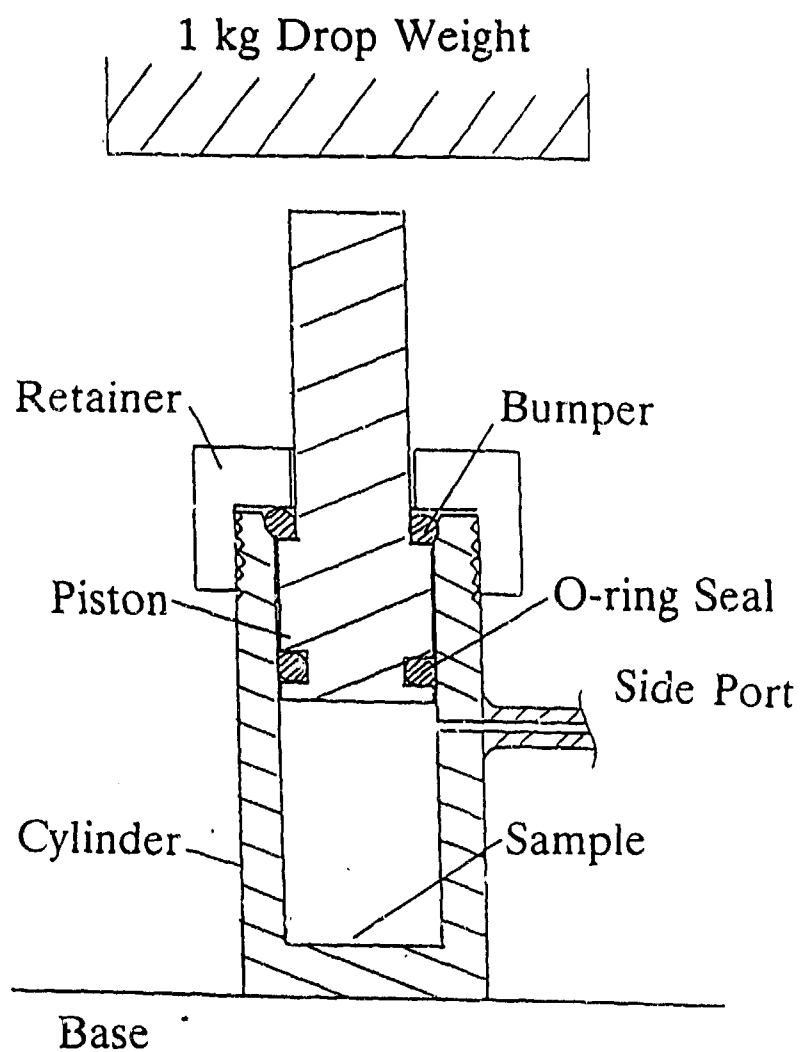


FIGURE 1. ADIABATIC COMPRESSION APPARATUS

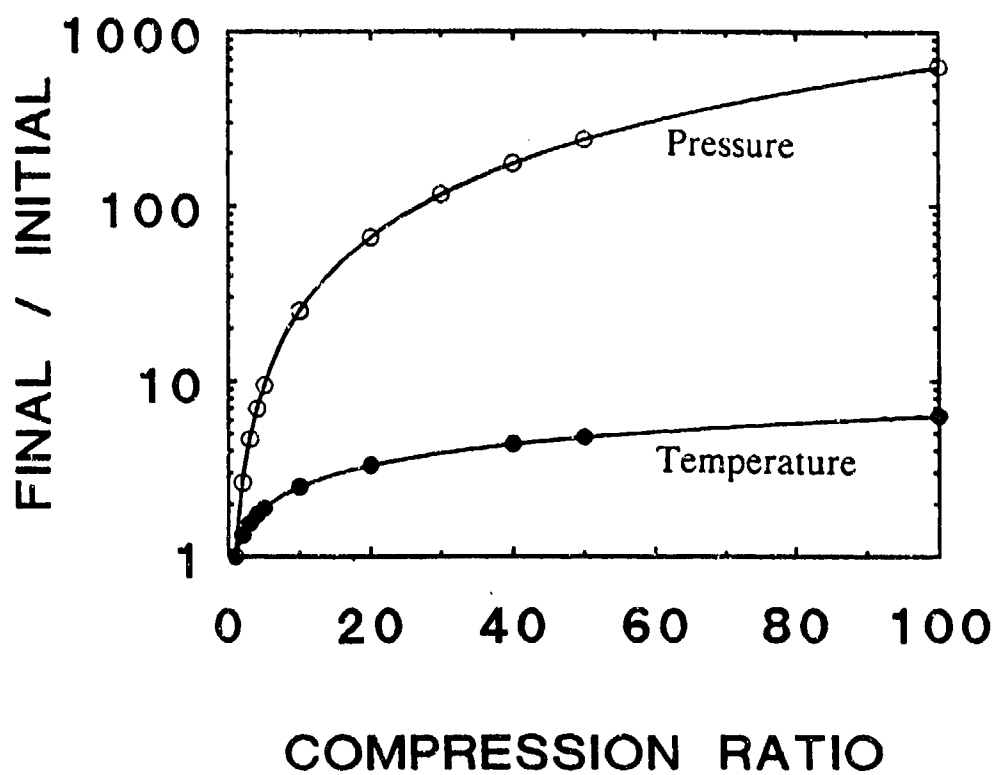


FIGURE 2. CALCULATED TEMPERATURE AND PRESSURE RATIOS FOR AIR COMPRESSION

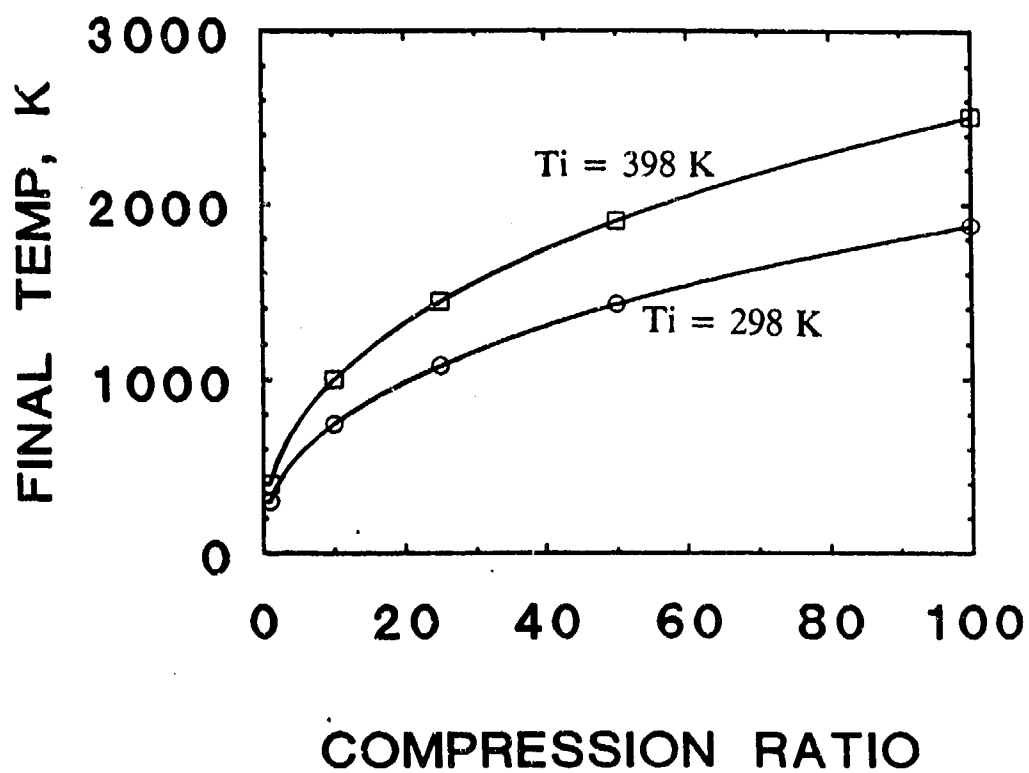


FIGURE 3. CALCULATED FINAL TEMPERATURES FOR AIR COMPRESSION

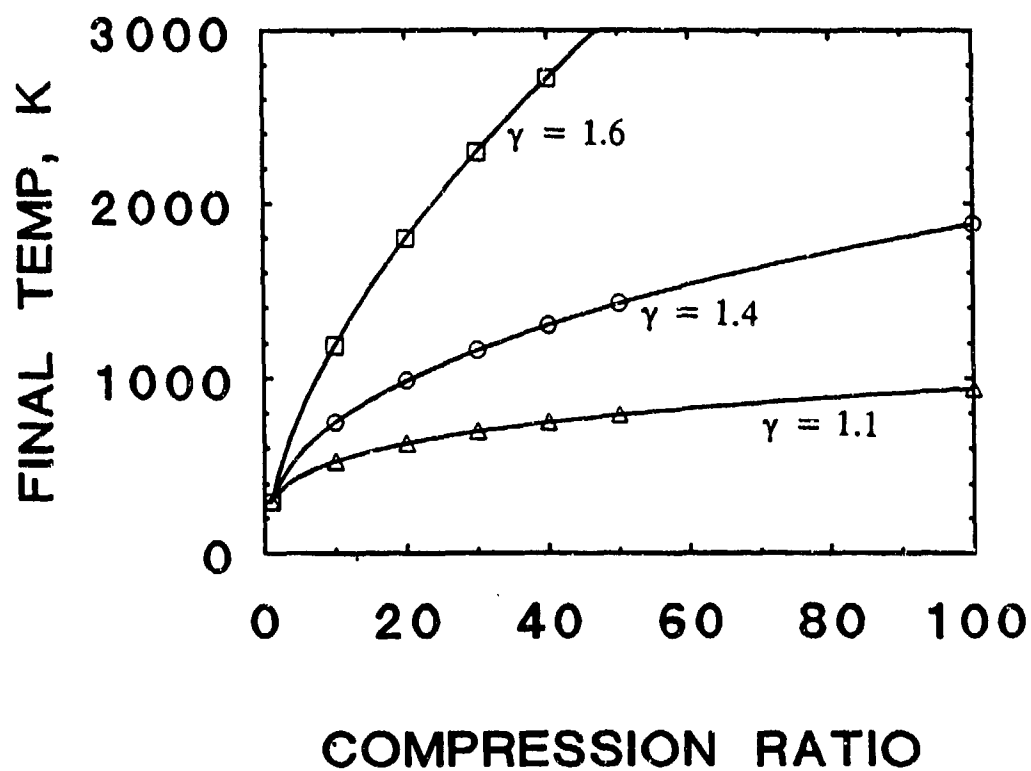


FIGURE 4. CALCULATED FINAL TEMPERATURES FOR COMPRESSION OF DIFFERENT GASES

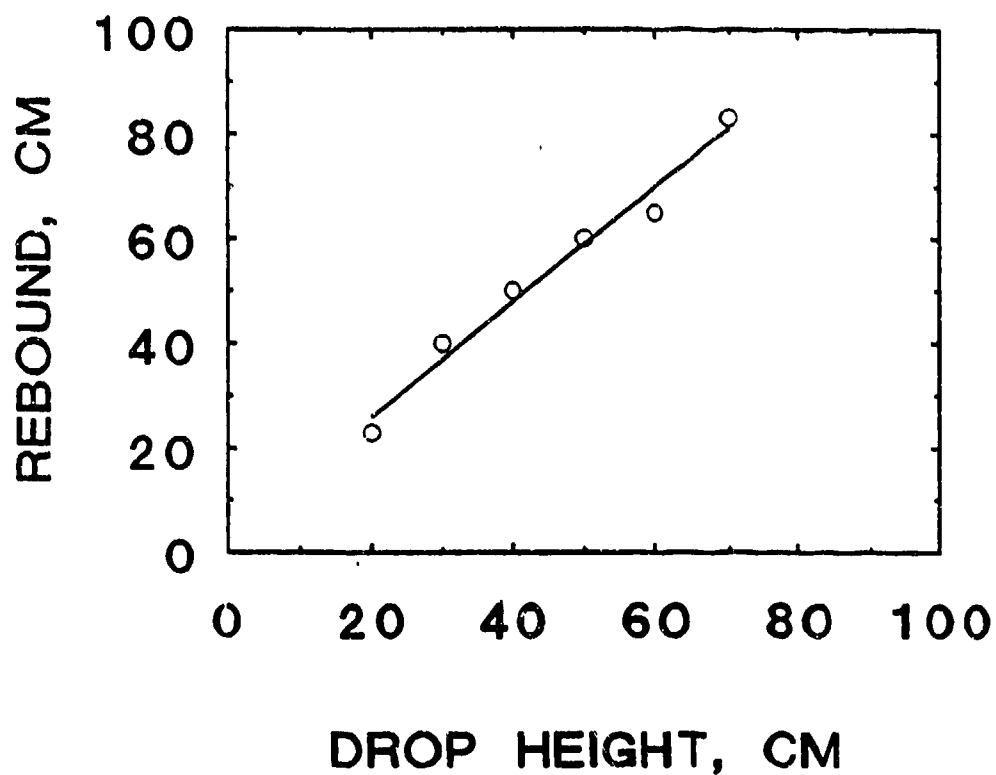


FIGURE 5. REBOUND HEIGHTS FOR NITROMETHANE IGNITION
Data adapted from Reference 8. Sample size = $12 \mu\text{l}$.
Energy release at 70 cm drop height is ca. 1500 J/g.

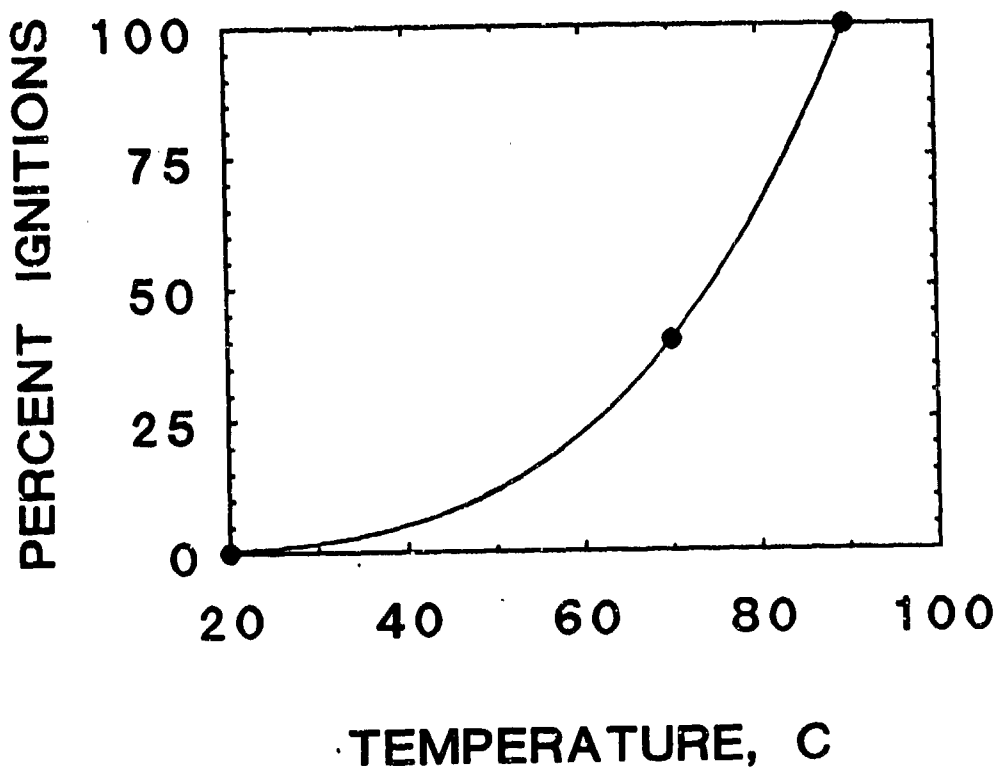


FIGURE 6. COMPARISON OF LIQUID AND SOLID TNT IGNITIONS
Drop height = 40 cm. Data from Ref 9. The average rebound
height for ignitions at 70°C was 12 cm compared to 35 cm
at 90°C.

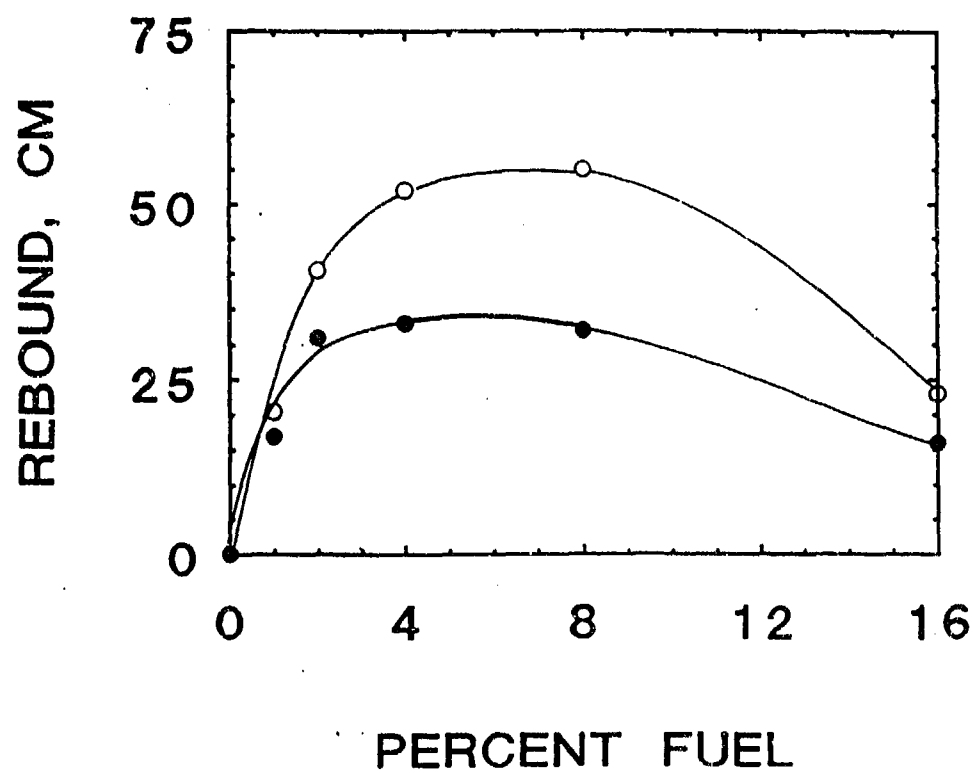


FIGURE 7. REBOUND HEIGHTS FOR AP/HYDROCARBON MIXTURES. Drop height = 90 cm; gas = air at ambient temperature and pressure.

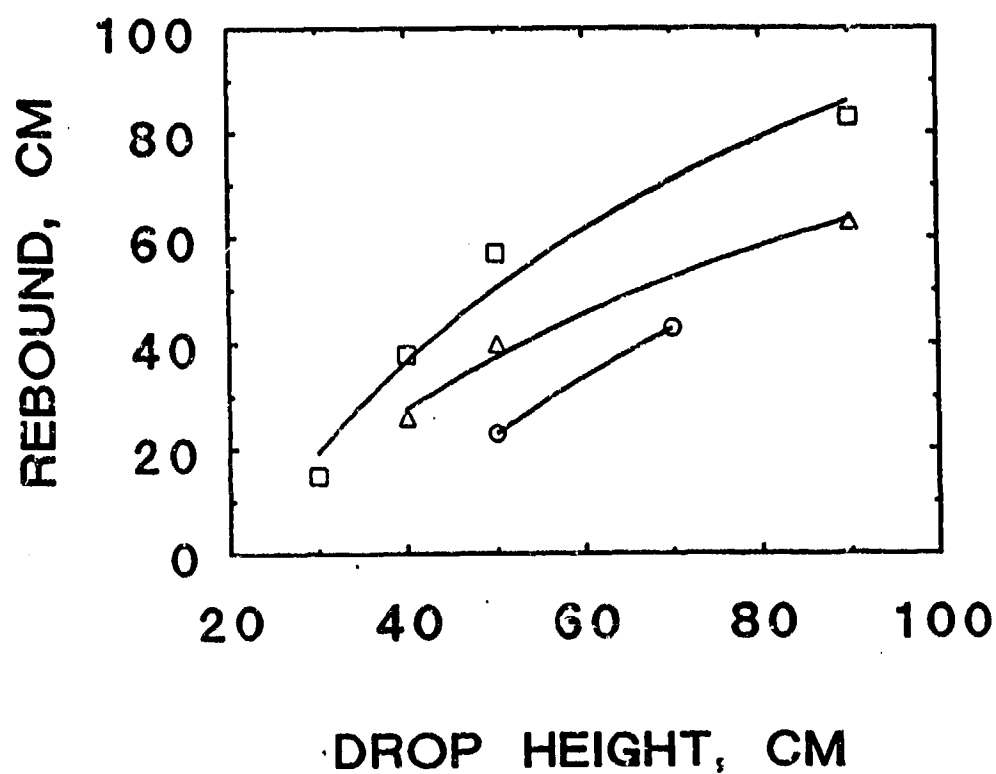
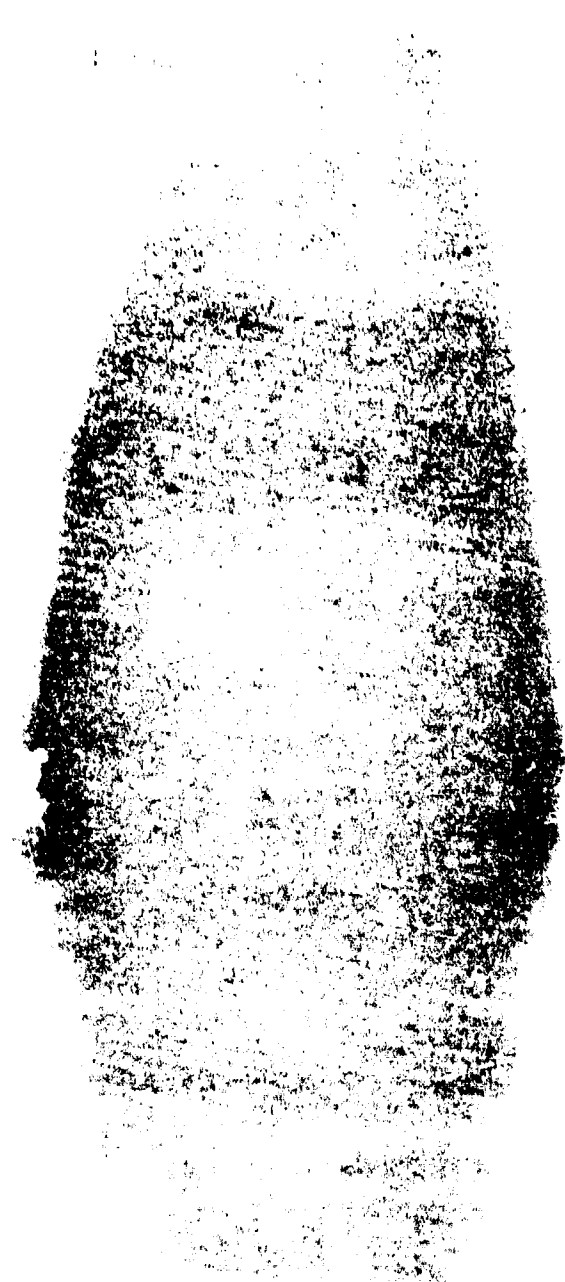


FIGURE 8. REBOUND HEIGHTS FOR AP/HYDROCARBON MIXTURES. Gas = air at 100°C and ambient pressure.
○ = 1% fuel; Δ = 2% fuel; □ = 4% fuel.



Mix
zone

Prior to jet
impingement



Initial helium
level

Photograph of LO₂ jet impingement

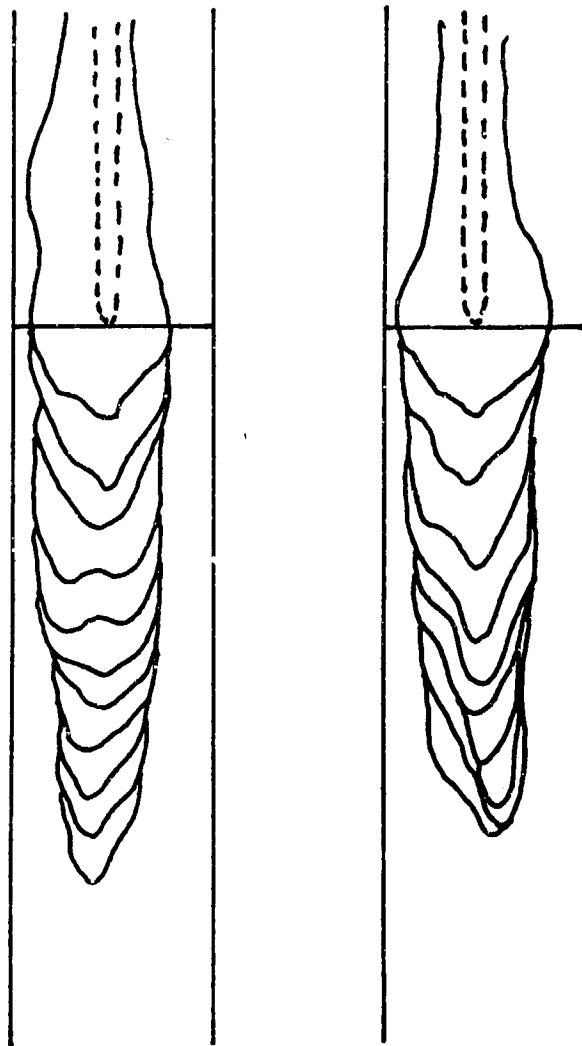


Figure 11. Mixing zone impingement contours for LN_2 into LH_2 .

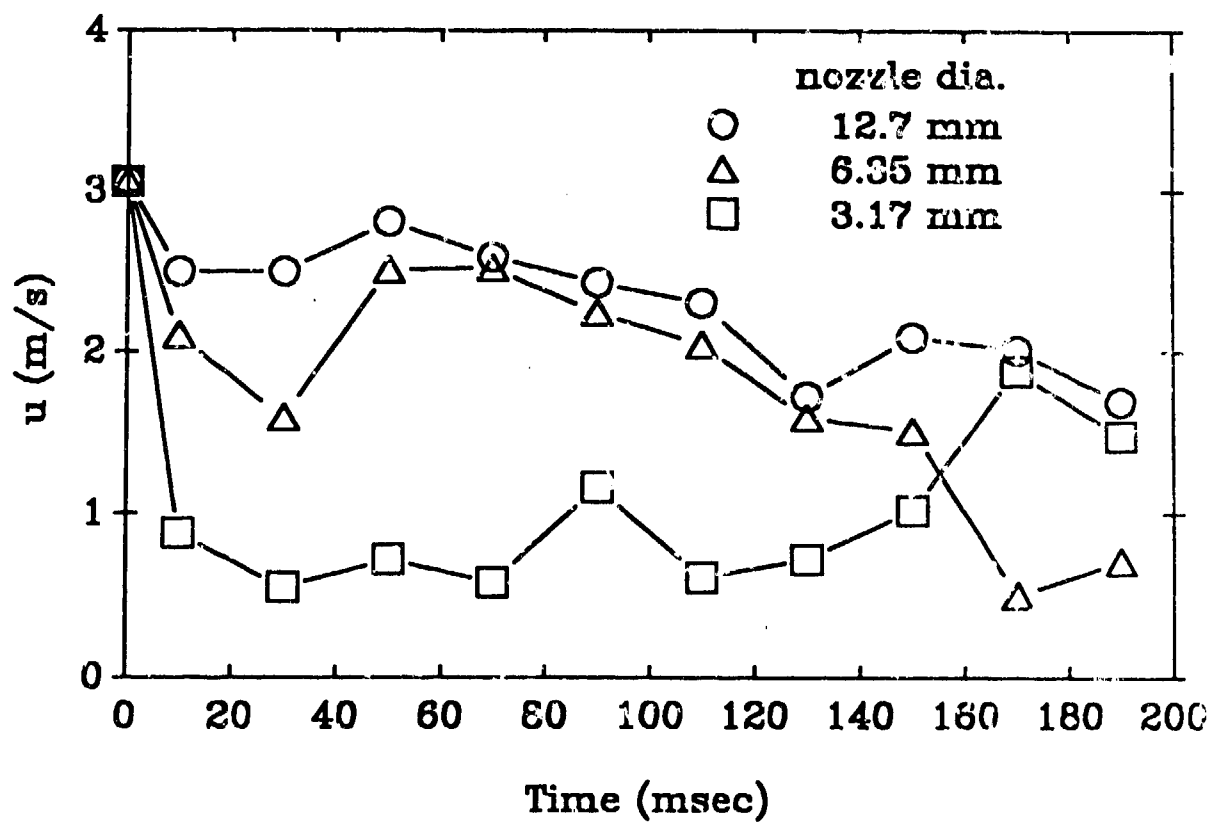


Figure 12. Jet penetration velocity after impingement.

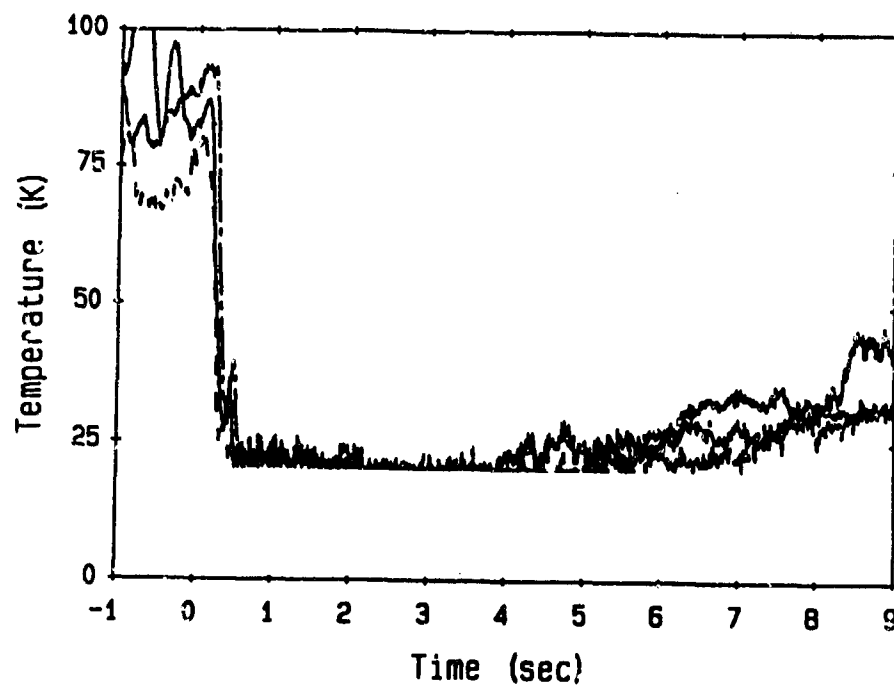


Figure 13. Mouth temperature variation for three similar tests.

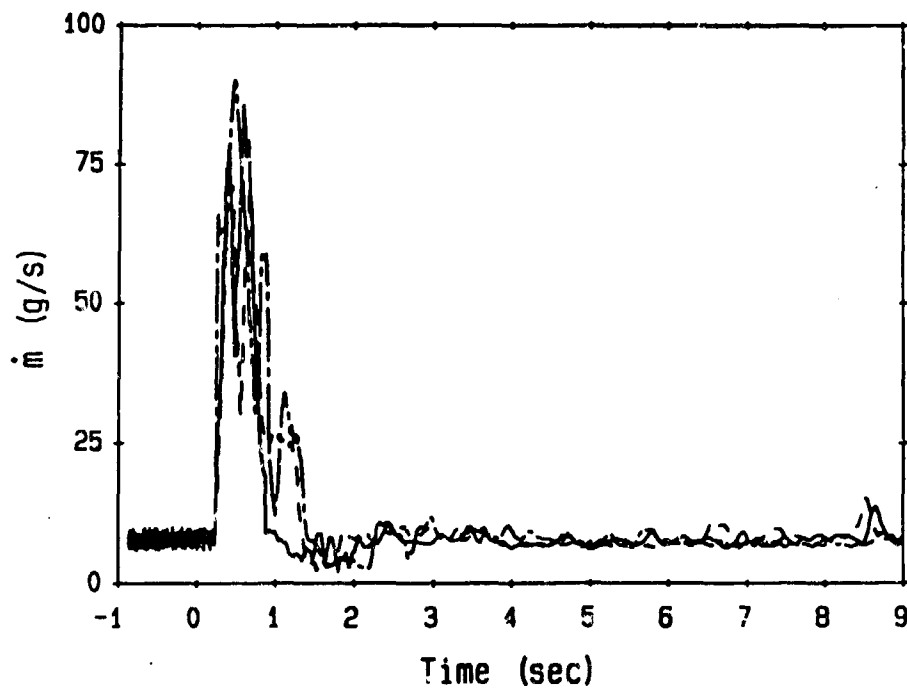


Figure 14. Mass flowrate at the mouth of the dewar for three similar tests.

**PROPAGATION AND FIRE TESTS CONDUCTED ON A
SECONDARY STEEL CONTAINER DESIGNED FOR
MOVEMENT OF CHEMICAL AGENT ARTILLERY PROJECTILES**

DANIEL B. HILL
Ammunition Equipment Directorate
Tooele Army Depot, Utah

Presented at:
TWENTY-FOURTH DOD EXPLOSIVES SAFETY SEMINAR
Dept. Of Defense Explosives Safety Board
St. Louis, Missouri
28-30 August 1990

ABSTRACT

A Secondary Steel Container (SSC) has been developed to hold two pallets of 8" projectiles or three pallets of 155mm projectiles for use in the movement of chemical agent munitions. To answer questions on the impact that the container might have on the maximum credible event from the detonation of one projectile in the pallets, propagation tests were conducted. Two fire cookoff tests were also conducted to evaluate the time that fire fighters would have to extinguish a fire involving SSCs in MIIIVANS subjected to a large fuel fire resulting from an accident.

**PROPAGATION AND FIRE TESTS CONDUCTED ON A
SECONDARY STEEL CONTAINER DESIGNED FOR
MOVEMENT OF CHEMICAL AGENT ARTILLERY PROJECTILES**

INTRODUCTION

In response to a requirement for retrograde movement of lethal chemical agent artillery projectiles from the Federal Republic of Germany, the Army developed a steel overpack container that will provide secondary containment of agent (in liquid or vapor state) that may leak from the projectiles during transport. The overpack is further designed such that several of them can be transported in a MILVAN shipping container. This paper describes two test programs conducted to evaluate: (1) the potential for propagation of detonation of projectiles within the overpack, thus affecting maximum credible event calculations; and (2) time to cookoff of projectiles, should the MILVAN be involved in an accident resulting in an engulfing fire, thus impacting fire response planning for the move.

The U.S. Army Defense Ammunition Center & School (JSADACS), located at Savanna Army Depot Activity in Savanna, Illinois, designed the steel container which is now called the Secondary Steel Container (SSC). The container is designed to provide a vapor tight containment for explosively-loaded chemical ammunition in accordance with requirements of Amendment 25 to the International Maritime Dangerous Goods (IMDG) Code. The container will hold two pallets (six projectiles each) of 8 inch artillery projectiles, or three pallets (eight projectiles each) of 155mm projectiles.

At the request of a DA-level Chemical Retrograde Task Force, the Ammunition Equipment Directorate (AED) at Tooele Army Depot, Utah conducted several tests during the period 4 October 1989 through 1 March 1990. This paper is later divided into two sections for purpose of describing each test separately. The tests are reported in AED Test Reports 17-89¹ and 04-90².

Propagation Test Summary

The projectiles are normally stored and/or transported in standard wooden pallets, burstered and without fuze. In such configuration, the palletized projectiles are U.N. Hazard

¹ Hill, Daniel B., Tests to Determine Extent of Propagation or Damage When 8" or 155mm Chemical Agent Simulant Filled Projectile Detonates Within Standard Pallet and in Pallet Overpack, 19 October 1989

² Hill, Daniel B., Secondary Steel Container Fire Tests, 30 March 1990

Class/Division 1.2 non-mass detonating munitions, indicating that in event of accidental detonation of one projectile within the pallet, propagation to adjacent projectiles will not occur. With development of the overpack container, it became necessary to determine if the containment might cause detonation of additional projectiles, thereby changing the hazard classification. The data was desired specifically for 8" M426 GB or VX projectiles and 155mm M121A1 GB or VX projectiles.

Tests were conducted on the two different sizes of projectiles during the period 4-10 October 1989 to determine if propagation would occur within the overpack container. An additional objective was to determine how many projectiles might be expected to leak their liquid agent fill. The tests were conducted using a liquid agent simulant. Three detonation tests were conducted for each size projectile:

- Single 8" projectile was detonated
- Donor in 2 std pallets of 8" projectiles was detonated
- Donor in 2 pallets of 8" projectiles within overpack was detonated

- Single 155mm projectile was detonated
- Donor in 3 std pallets of 155mm projectiles was detonated
- Donor in 3 pallets of 155mm projectiles within overpack was detonated

No propagation occurred in any of the tests. In the overpacked 8" projectile test, four projectiles incurred sufficient damage to leak their liquid fill. In the overpacked 155mm test, seven projectiles leaked.

Fire Test Summary

A movement planning scenario envisions an accident resulting in a large fuel fire that engulfs a MILVAN loaded with SSC which are filled with projectiles. Assuming that projectiles will eventually begin to cookoff in such a fire, it was desired to know how much time a fire response team may have to fight the fire before the first projectile detonates; therefore, tests were conducted on 6 February and 1 March 1990 which subjected SSCs to fuel fires. The test SSC were each loaded with three explosive filled 155mm projectiles and 21 inert projectiles. All were filled with ethylene glycol/water mix to simulate chemical agent. The SSCs were placed into CONEX containers to represent a MILVAN shipping container. Each assembly was suspended over a pan of fuel which was then ignited.

In the first test, the fire lasted approximately 44 minutes and, although no projectiles cooked off or detonated, the test appeared to demonstrate that a reasonable amount of time would be available to safely fight the fire. In the second test, one projectile burster cooked off in one hour ten minutes and a

second burster cooked off in one hour seventeen minutes. The third live projectile did not function.

DESCRIPTION OF SSC

The SSC is a front-loading, skid-mounted steel container with the following approximate overall dimensions: 33 $\frac{1}{4}$ " wide x 42 $\frac{1}{4}$ " long x 47 $\frac{1}{4}$ " high. See Figure 1. Its interior dimensions will accommodate two pallets of 8" projectiles or three pallets of 155mm projectiles, with appropriate wood blocking/bracing to prevent shifting of the pallets within the SSC.

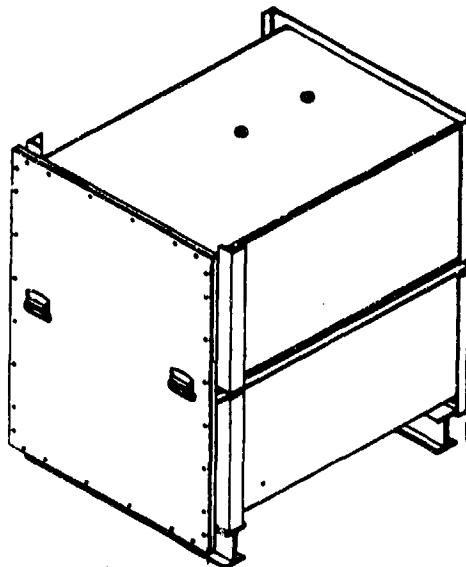


FIGURE 1. SECONDARY STEEL CONTAINER

The SSC is constructed essentially of 3/16" thick medium carbon steel plate, forming a box that is mounted on two standard 5" flange beams that provide side access for forklift. The front of the container is a 5/8" thick flange plate to which a 1/4" thick closure door is bolted with 28 3/8" socket head capscrews that thread into the flange plate. A 3/16" thick butyl rubber gasket is glued to the closure door and provides the vapor-tight seal for the container. The closure door has two handles welded to it for manual handling. Threaded fittings at the top of the container permit attachment of an air monitoring device and a valve to allow air to be drawn into the container while monitoring. The SSC weighs approximately 800 lbs.

PROPAGATION TESTS

These tests were conducted in two phases for each of the two test munitions. Phase 1 was a baseline test in which two 8" or three 155mm standard pallets were placed side by side and a donor round in one pallet was detonated to obtain baseline damage and pressure data to be used for comparison with data from Phase 2. In Phase 2, two 8" or three 155mm standard pallets were placed within the Secondary Steel Container and a donor round in one pallet was detonated to assess any propagation effect caused by the SSC.

Prior to each Phase 1 test, a single round (for each size munition) was detonated to obtain pressure baseline data for comparison with Phase 1 data.

Objectives of the tests included:

1. Obtain "baseline" data for projectiles in standard pallets, to include measurement of blast pressure (to aid in determining if explosive propagation occurred), visual assessment of damage to other rounds within the donor pallet, and visual assessment of damage to rounds within acceptor pallets; specifically to determine the number of (and which) projectiles suffered sufficient damage to release simulant.
2. Determine if Secondary Steel Container affected or altered the results achieved in Phase 1 tests.
3. Determine fragment dispersion.

Blast pressures were determined by measuring peak positive incident overpressures with low-impedance piezoelectric pressure transducers placed at ground surface along two air blast instrumentation lines at 90 degrees to each other. In all tests, the donor round was placed at the intersection of these two blast lines. A 1½" thick steel witness plate provided a base for all tests. The donor round was initiated by an Exploding Bridgewire (EBW) firing circuit from a control center approximately 700 ft. away. High-speed cameras and real-time video documented the tests.

Munitions Preparation

The chemical agent version of the 8" projectile is the M426. The high-explosive version is the M106. M106 projectiles modified to the M426 configuration were used for these tests. The modified M106 was assembled with the M83 burster, which contains 7 lbs of composition B4; the supplementary charge containing 0.30 lbs of TNT; the appropriate cardboard spacer and support; and a lifting plug. The projectile cavity was filled

with 14.5 lbs of ethylene glycol/water (50/50 wt) to simulate the density property of chemical agent GB. Assembled and filled projectile weight is approximately 195 lbs. Palletized weight (6 rds/pallet) was approximately 1253 lbs.

155mm projectiles that had been modified from the M107 HE configuration to M121A1 chemical configuration were also used for these tests. The modified M107 was assembled with the M71 burster, which contains 2.45 lbs of composition B4; the supplementary charge containing 0.30 lbs of TNT; the appropriate cardboard spacer and steel support cup; and a lifting plug. The projectile cavity was filled with 6.5 lbs of liquid simulant. Assembled and filled projectile weight was approximately 99 lbs. Palletized weight (8 rds/pallet) was approximately 831 lbs.

All components were painted to assist identification in fragment collection after the tests. The 8" projectiles and all their components were painted one color while the 155mm were painted a distinctively different color. The donor projectile for each test was configured as follows:

1. The detector-type lifting plug was removed and a 1/8" hole drilled to accept an ionization probe. The detection screw was removed so the EBW detonator could be inserted into the approximately 36 grams of composition C4 that was packed into the lifting plug cavity.
2. The cardboard spacers were packed with composition C4 (approx 66 gm in the 8", 49 gm in the 155mm). The spacer, w/C4, was then emplaced atop the supplementary charge in the projectile.

SSC Preparation

The SSC for each test were painted different colors and were painted differently from the projectiles. After installation of the pallets of projectiles into the SSC, wood blocking and bracing was installed to preclude shifting or moving of the pallets within the SSC.

Test Setup

In both single projectile tests, the projectile was elevated above the witness plate, using wooden blocks, to a height approximating the elevation of the palletized projectiles within the SSC. In both Phase 1 tests, the pallets of projectiles were also elevated above the witness plate.

In the Phase 2 tests, the SSC, with projectiles and wood bracing already installed, were positioned in location at the test site. The EBW detonator was then inserted through the inspection hole, and the ionization probe inserted through the specially-drilled hole into the composition C4 in the lifting

plug. The electrical wires were fed through the sampling hole in the top of the SSC. The SSC cover plate was then bolted in place, following specified torquing instructions.

Prior to each test, a spherical charge of approximately one lb. of composition C4 was detonated to validate the pressure transducer array. A fragment search was conducted at the conclusion of the tests. Fragments found in each 200 ft. cell within each of three 5' search sectors were reported as were major pieces of debris or unexploded components found outside the search sectors.

Results

8" Projectile Tests

Single Projectile Baseline Test-Pressure data is given in Table 1. Fragment dispersion for within and outside the search sectors was plotted and no fragments were found beyond 600 ft. from the detonation.

Standard Pallet Baseline Test-Pressure data is given in Table 1. Although no propagation occurred and all explosive components from acceptors were recovered, the damage was significantly more widespread in this test than was seen later in the overpack test. Five M83 bursters and eight supplementary charges were ejected from their projectiles; some as far away as 600 ft. One projectile was thrown 400 ft. Eight projectiles leaked their liquid fill.

Overpacked Pallet Test-Pressure data is given in Table 1. No propagation occurred and all explosive components from acceptors (two supplementary charges) were recovered. Four projectiles leaked their liquid fill. Two leaked significantly from around their burster cases; these were thrown 200 ft. Two were seepage-type leakers from around the joint between fuze adapter and projectile body. One was thrown 75 ft. and the other was thrown 50 ft. Deformation around the projectile nose caused the burster case press fit to break loose, allowing the liquid to leak. Damage to projectiles was not nearly as severe as was seen in the pallet baseline test; i.e., no projectile bodies were cracked although some were severely dented, only two projectiles lost their fuze adapters, and all others even retained their lifting plugs. The SSC split open at the rear and top joints with the top and the door being blown completely off.

TABLE 1-BLAST PRESSURE DATA FOR 8" PROJECTILE TESTS

TEST	BLAST LINE	TRANSDUCER STATION	R ft.	P _{so} psi	t _a ms	t _o ms
SINGLE ROUND	A	1	15	15.73	83.6	31.6
		2	22	11.73	131.4	34.6
		3	40	7.64	288.0	7.95
	B	4	15	13.61	81.4	32.4
		5	22	10.96	133.2	32.6
		6	40	5.73	244.0	14.6
STANDARD PALLET	A	1	15	11.92	86.08	34.4
		2	22	5.78	142.8	42.2
		3	40	3.34	297.6	52.5
	B	4	15	11.41	83.0	33.2
		5	22	7.68	137.6	39.8
		6	40	3.94	290.8	86.0
OVERPACKED PALLET	A	1	15	5.44	140.4	51.8
		2	22	3.62	198.0	46.8
		3	40	2.28	352.6	49.2
	B	4	15	4.89	141.4	59.5
		5	22	3.91	200.6	86.2
		6	40	2.00	358.4	72.4

R = Horizontal distance from center of donor round to transducer station, feet

P_{so} = Peak positive incident pressure, pounds per square inch

t_a = Time of arrival of blast wave, milliseconds

t_o = Duration of positive phase, milliseconds

155mm Projectile Tests

Single Projectile Baseline Test-Pressure data is given in Table 2. Fragment dispersion for within and outside the search sectors was plotted and no fragments were found beyond 600 ft. from the detonation. The blast pressure at transducer 5 in Blast Line B is abnormally low, however, it's likely that some ground-level obstruction (rock or dirt mound) deflected the blast wave.

Standard Pallet Baseline Test-Pressure data is given in Table 2. No propagation occurred and no explosive components were released or ejected from any acceptors. Transducer 5 recorded an abnormally high pressure which is unexplained. There was no extensive damage to any of the acceptors; i.e., none were

broken or cracked, however seven rounds leaked their liquid fill. One projectile was thrown approximately 600 ft. The leakage results from deformation of the projectile nose causing the burster case press-fit to break loose.

Overpacked Pallet Test-Pressure data is given in Table 2. No propagation occurred and no explosive components were ejected from acceptors. Blast pressure readings appear normal. Seven projectiles were leakers. Two leakers were thrown 175 ft., one 150 ft., one 100 ft., and three were thrown 50 ft. All leakers were seepage-type leakers with no significant loss of liquid; and no projectiles were severely damaged. The SSC did not blow apart as was seen in the 8" test. The door blew off, landing approximately 500 ft. away.

TABLE 2-BLAST PRESSURE DATA FOR 155mm PROJECTILE TESTS

TEST	BLAST LINE	TRANSDUCER STATION	R ft.	P _{so} psi	t _a ms	t _o ms
SINGLE ROUND	A	1	15	8.42	96.0	2.4
		2	22	4.10	153.8	1.3
		3	40	2.34	313.8	38.0
	B	4	15	8.61	94.8	25.4
		5	22	1.78	173.6	16.4
		6	40	3.04	308.3	62.8
STANDARD PALLET	A	1	15	6.36	104.8	29.5
		2	22	2.31	163.6	26.0
		3	40	1.87	322.8	77.2
	B	4	15	6.20	103.2	28.4
		5	22	8.30	157.6	39.5
		6	40	1.71	322.0	36.0
OVERPACKED PALLET	A	1	15	2.71	135.4	43.4
		2	22	1.87	195.2	41.4
		3	40	0.75	352.8	48.0
	B	4	15	1.97	123.4	65.2
		5	22	1.49	189.4	71.5
		6	40	0.75	348.6	36.7

R = Horizontal distance from center of donor round to transducer station, feet

P_{so} = Peak positive incident pressure, pounds per square inch

t_a = Time of arrival of blast wave, milliseconds

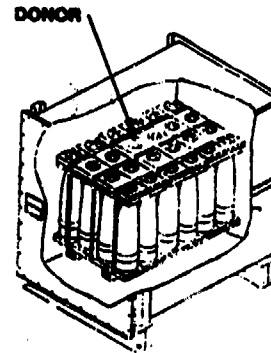
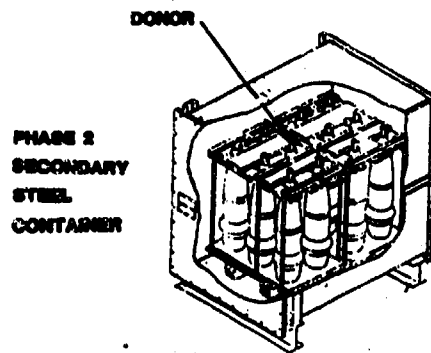
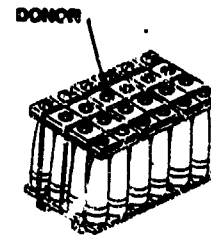
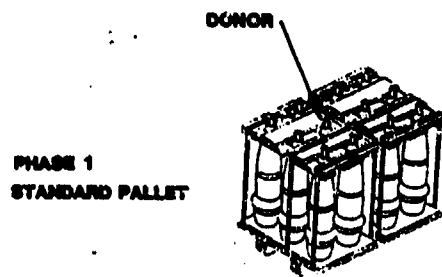
t_o = Duration of positive phase, milliseconds

Conclusions

8" Projectile Tests-No significant anomalies were seen in the pressure data; i.e., the blast pressures seemed to decay normally as the pressure wave expanded outward across the transducers. The measured pressures also decreased with each test as would be expected, given the confinement of surrounding projectiles and the container. The lesser damage to acceptor projectiles in the overpacked pallet test might be explained by the instantaneous increase in air volume in the container, caused by the donor detonation, creating an air cushion between projectiles which minimized mechanical damage to them. The SSC also contained fragments, resulting in fewer being dispersed than seen in the standard pallet test.

16mm Projectile Tests-With exception of anomalous readings at transducer 5 in the standard pallet and the overpacked pallet tests, the blast pressures appeared normal. As described above, mechanical damage to projectiles was minimal, and there was very little fragmentation.

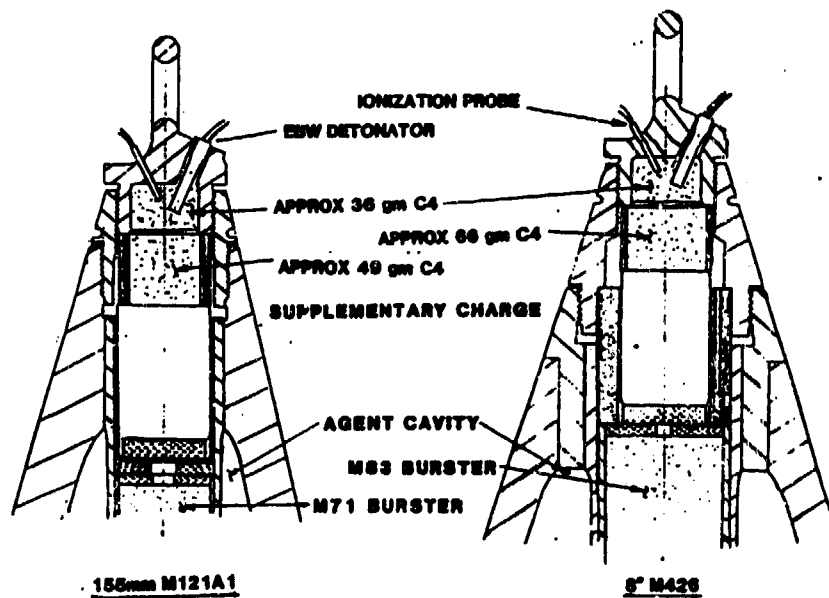
The following five pages of photos illustrate the test setups and results. Discussion of the Fire Tests continues after the photos.



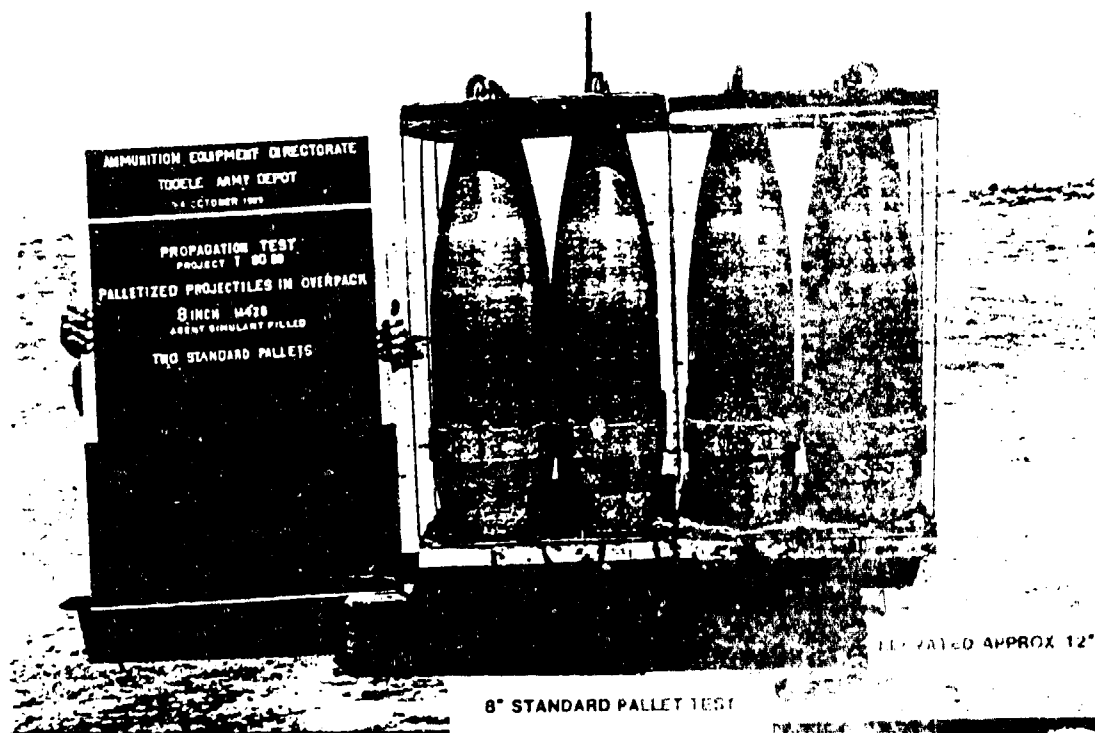
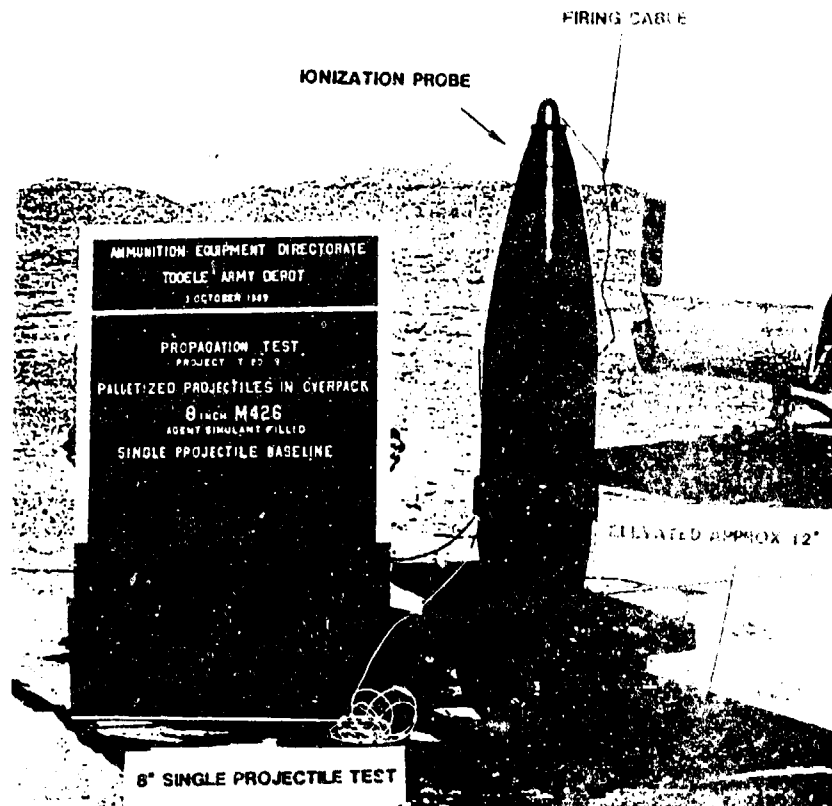
8" PROJECTILE M426

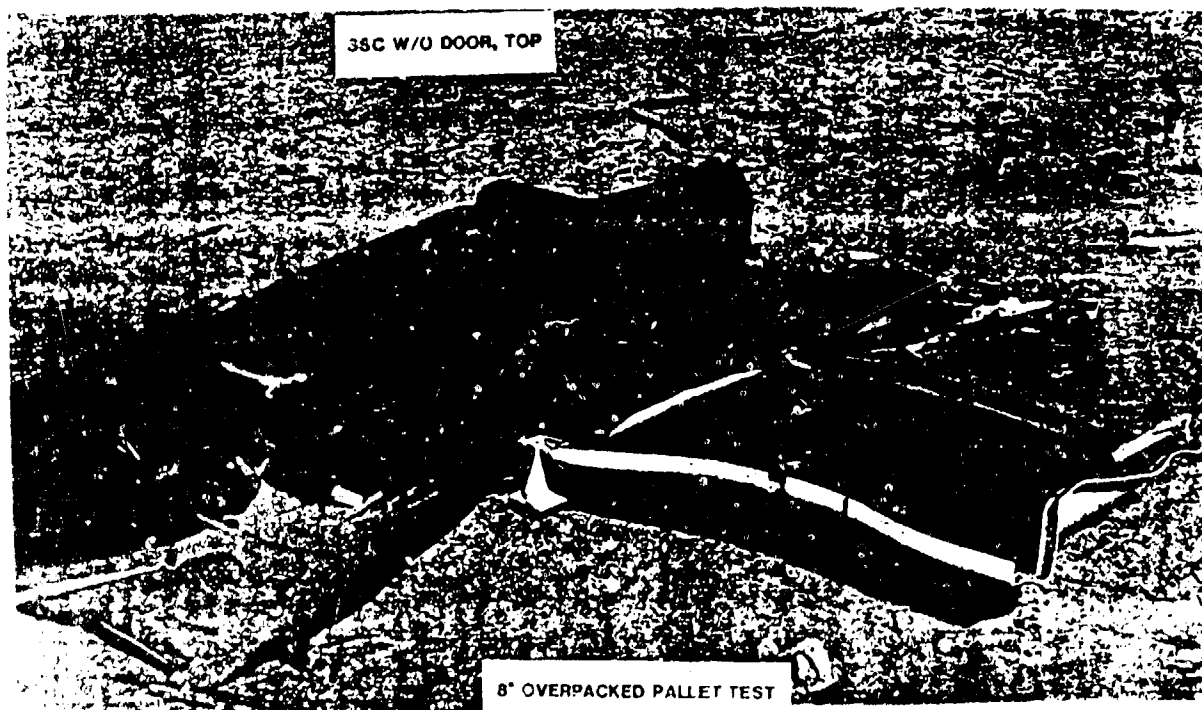
155mm PROJECTILE M121A1

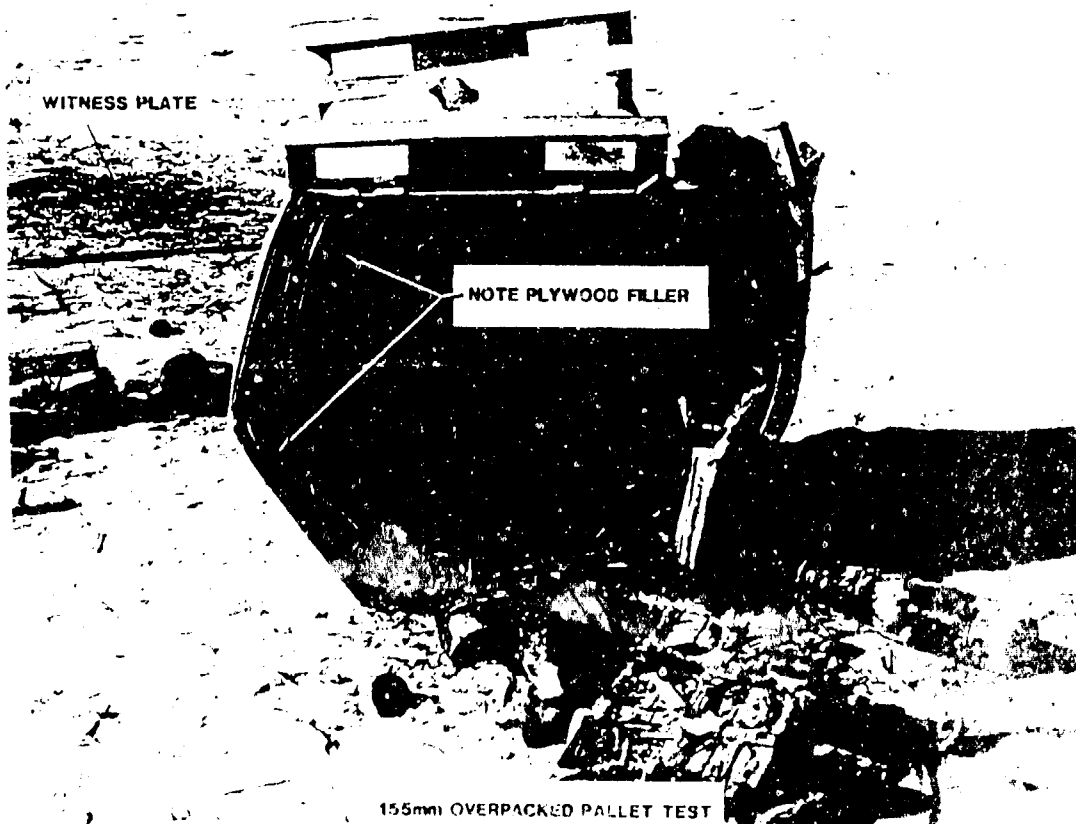
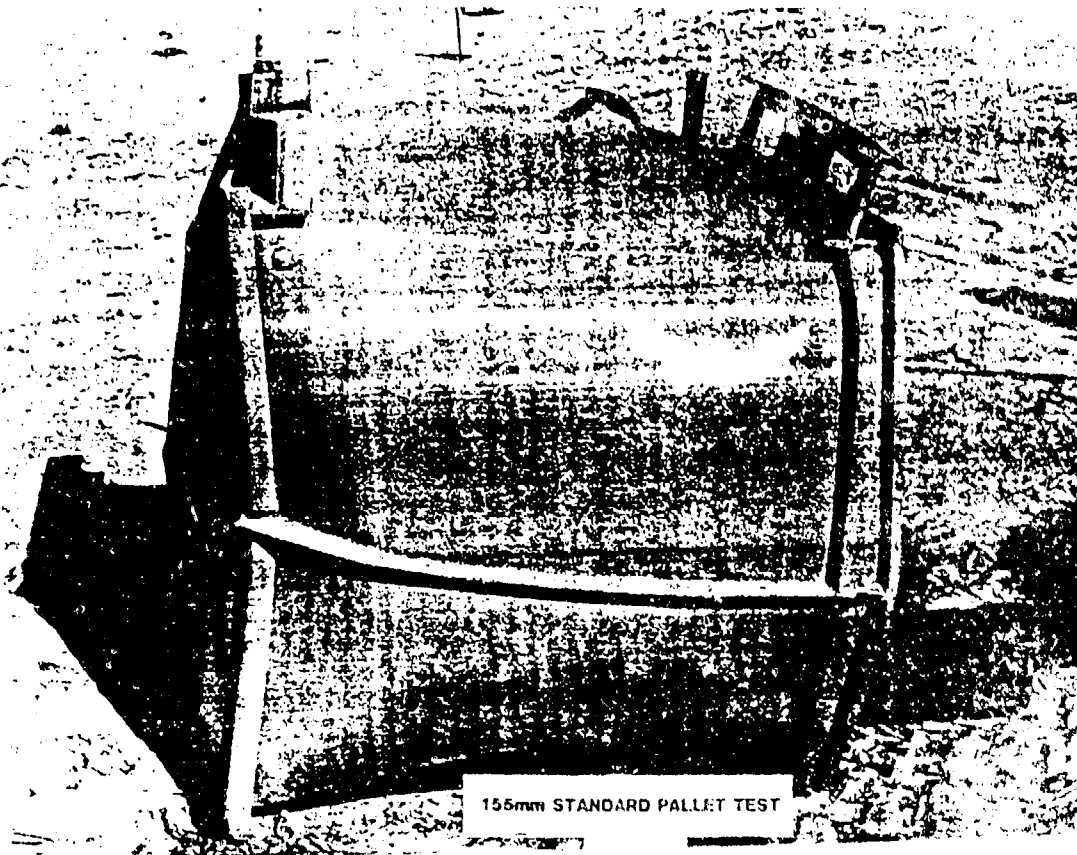
TEST CONFIGURATIONS

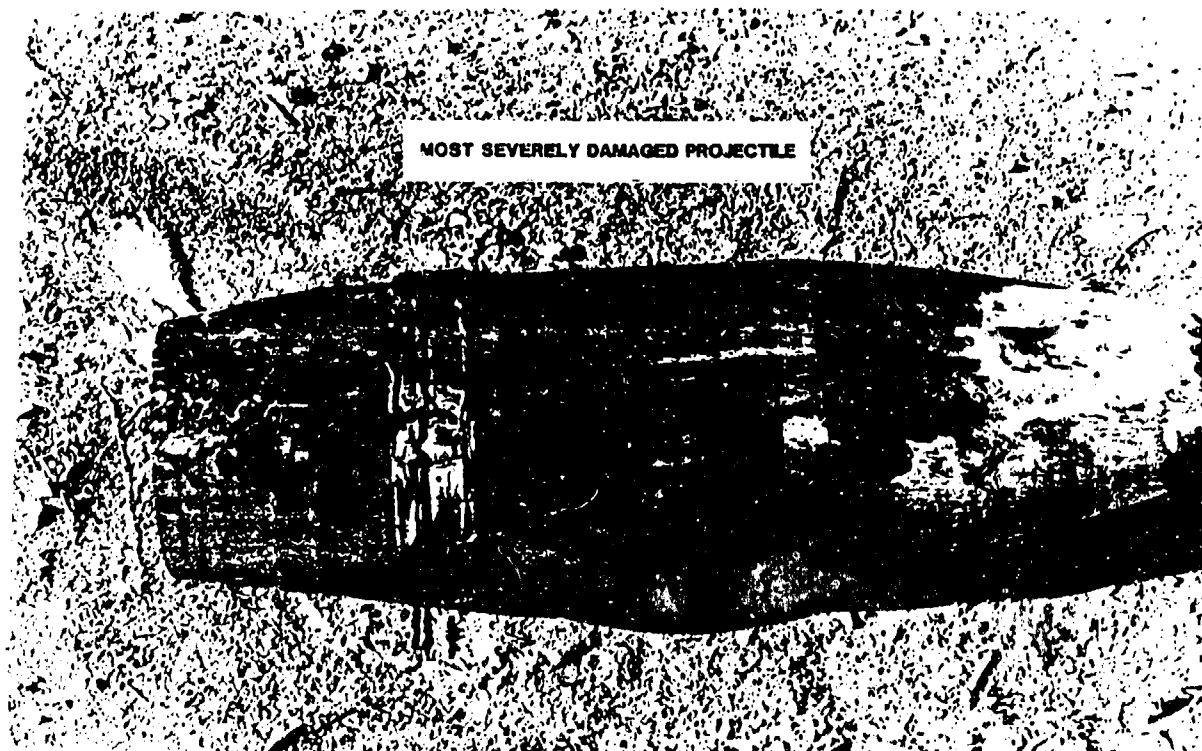
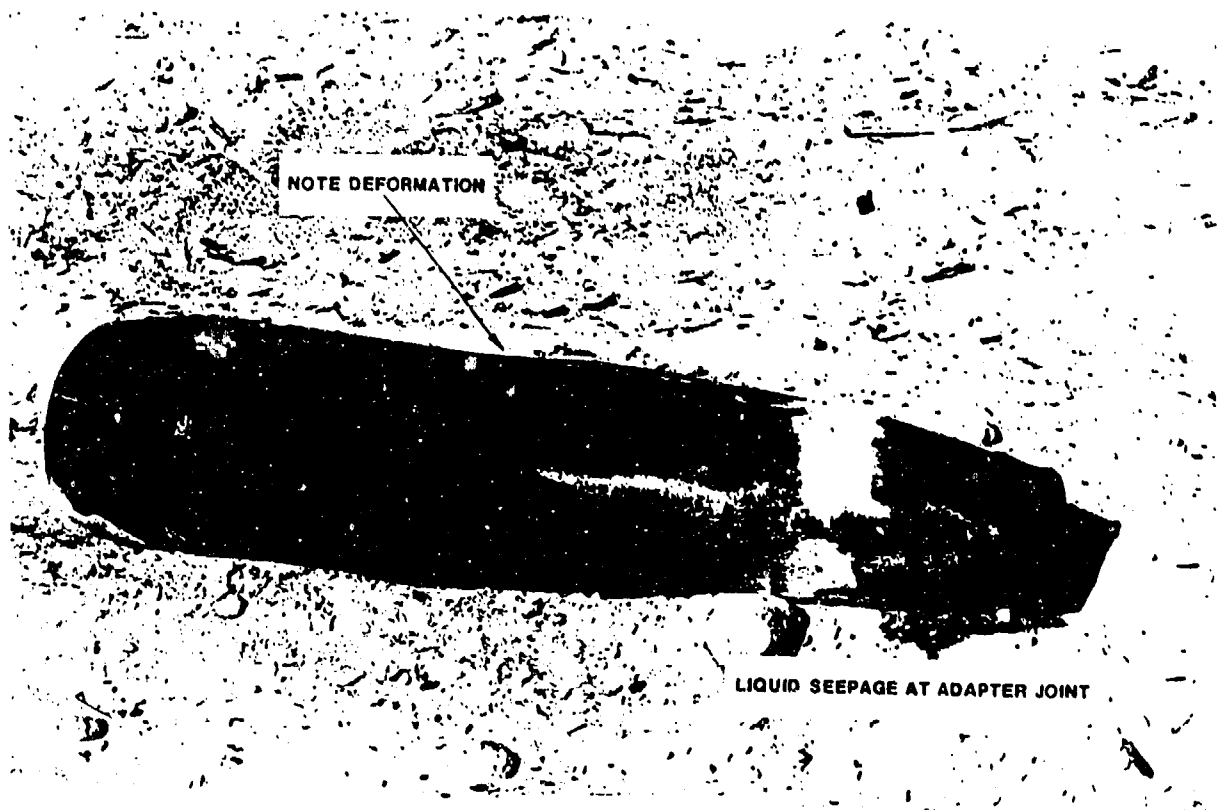


PREPARATION OF DONOR PROJECTILE









FIRE TESTS

Two tests were conducted, on 6 February and 1 March 1990, which subjected SSCs to fuel fires with the objective of determining length of time to "cookoff" of explosively loaded 155mm projectiles within the container. The test SSC were each loaded with three explosive filled 155mm projectiles and 21 inert projectiles. All were filled with ethylene glycol/water to simulate chemical agent. The SSCs were placed into CONEX containers which represented a MILVAN shipping container. Each assembly was suspended over a pan of fuel (first test JP-5, second test diesel fuel) which was then ignited. Thermocouples recorded time/temperature histories, including the temperatures at the tops of the three bursters in the live projectiles.

In actual loading, the SSC are intended to be installed in the MILVAN with the SSC door facing outward, toward the MILVAN sidewall. For each of these tests, a fixture was fabricated to closely approximate the configuration of one SSC at the rear corner of a MILVAN.

The 155mm M121A1 (with liquid agent simulant) was selected as the test munition instead of the 8" because of its' thinner wall and the fact that, within the SSC, it is slightly closer to the container wall, suggesting shorter time to cook-off. Three pallets of projectiles (24 total) were placed into the SSC. Three projectiles were explosively loaded with a composition B-filled M71 burster. Two outside projectiles were approximately 3/8" from the SSC sidewall (one was adjacent to a plywood sheet which was fill material placed between the SSC door and the pallet of projectiles). The other live projectile was placed near the center of the SSC. All wood blocking/bracing specified by the SSC loading drawing was used (plywood sheets were at the side opposite the live projectiles).

The SSC was then placed into a corner of a standard Conex shipping container (representative of a MILVAN container). The door side of the SSC was approximately 4" from one wall of the container. The positioning was determined by wooden side blocking required by the MILVAN loading drawing. One side wall of the SSC (adjacent to two of the live projectiles) was approximately 24" from the other Conex wall. The Conex corner was then partitioned with floor to ceiling panels against the back and other side walls of the SSC, creating an enclosure for the SSC with an air volume roughly equivalent to the unit volume that will exist in the MILVAN, which is approximately 69 ft³ of free air. The partition panels were insulated to prevent loss of heat from within the enclosure and to prevent entry of heat into the SSC through two walls (i.e., suggestive of surrounding SSC). The floor of the enclosure was lined with hardwood material to simulate the MILVAN flooring.

All projectiles were filled with an ethylene glycol/water mix to simulate liquid agent. Three projectiles were assembled with an explosive burster and a supplementary charge. The others had a plaster of paris-filled simulant burster and supplementary charge. The projectiles were appropriately palletized in wooden pallets and banded.

The corner of the Conex assembly was positioned above a burn tray filled with fuel. For the first test, the tray was initially filled with approximately 220 gallons of JP-5 fuel. Some literature indicated a burn rate of 0.1 in/min for JP-5 fuel. Using this rate, it was anticipated that 8.5" fuel depth should permit 85 minutes burn time. For the second test, the tray was filled with 275 gallons of diesel fuel. As a precaution against spilling fuel on the ground in event the burn tray was punctured by a detonation of the projectile(s), the burn tray was positioned within a larger, thick-walled pan.

The fuel was ignited by emplacing a small combustible container of gasoline in the fuel and igniting the gasoline with an M206 Countermeasure Flare which was ignited by electric squib.

Instrumentation for both tests consisted of several chromel/alumel thermocouples located throughout the Conex and the SSC. Thermocouples were also attached to the live projectiles. The thermocouple data was collected by a Fluke Datalogger. The tests were documented by video.

Results

Test One

At the start of the test, the ambient temperature was 42° F and the wind was blowing at 13 knots, impacting on the test fixture side adjacent to the SSC door. Subsequent readings were 7 knots, from the same direction. The temperature remained constant throughout the test, dropping only to 41° F at the end.

The fire burned approximately 44 minutes, significantly less time than expected because of the wind. Although the flames reached to the top of the Conex container, the wind generally swept the flames away from one side, affecting heat transfer through that side and through the SSC door. The measured flame temperature averaged 1300-1500° F. Note that the flame temperature was measured by a thermocouple inserted into the flame at one corner of the fuel pan and its readings fluctuated widely because the flame was affected by the wind.

No detonation occurred. Burstern 1, 2 & 3 reached maximum temperatures of 220, 180 & 200° F, respectively; but at

approximately 1 hour 9 minutes after the fire died out, having continued to absorb heat from surrounding projectile bodies and the SSC. Table 3 gives the burster temperatures at the time the fire died down and the apparent average rate of temperature climb at that time.

TABLE 3-BURSTER TEMPERATURES
(at time fire died down)

<u>BURSTER NO.</u>	<u>°F</u>	<u>°C</u>	<u>RATE OF TEMP CLIMB, °F/min</u>
1	122.9	50.5	9°/min
2	91.1	32.8	3°/min
3	132.4	55.8	3°/min

Burster 3 exhibited sign of near melting in that it was lightly stuck to the bottom of the support cup. The TNT supplementary charge atop Burster 2 experienced some melting; i.e., the light gage aluminum closure disc was completely melted away and the explosive was melted down approximately 1/8". Burster 1 wasn't examined because the projectile couldn't be disassembled. Liquid temperatures in Projectiles 1 & 3 were essentially the same as the respective bursters and exhibited the same temperature rise rates. The liquid temperature data for Projectile 2 was lost due to thermocouple malfunction. Much of the projectile body temperature data was also lost due to malfunctioning thermocouples; however, maximum temperatures, recorded well after the fire died out, were 215° F on the exterior of Projectile 3, and 187° F on the base of Projectile 1.

Unfortunately, the thermocouple measuring the air temperature inside the SSC failed and no data was obtained. The thermocouples measuring door and wall exterior temperatures recorded maximums of 493 and 921° f, respectively. These temperatures were measured just before the fire died down and were in a relatively steep rate of climb. The floor temperature (inside the SSC) was at about 225° F when the fire died but continued to climb to a peak of 665° F 33-34 minutes later. The interior sidewall temperature peaked at 637° F about halfway through the burn; and the door interior wall temperature reached 371° F. There was some charring of the wood blocking/bracing but no significant combustion. The butyl rubber gasket was largely melted away although there were segments that were relatively intact.

Air temperatures inside the Conex were measured at several locations. Air temperatures rose very quickly to 400° F, within about 4 minutes after ignition. Air Temperature 1 reached 1000° F in approximately 27 minutes and Air Temperature 2 reached 1000° F in about 41 minutes, shortly before the fire died out. The floor temperature was measured at the surface of the wood floor, beneath the SSC. The temperature curve exhibited an abrupt change in rise rate at about 12-13 minutes after ignition and the

wood floor could be seen burning at about 20 minutes. The wood floor was eventually totally consumed by fire.

Test Two

The second test was conducted in the afternoon of 1 March. The ambient temperature was 51° F and there was just a slight breeze blowing, 0-5 knots from the west. The temperature remained relatively constant throughout the test, dropping to 48° F by end of test. A light rain fell during much of the test. Although the breeze was light, the fire did not fully engulf one side of the test fixture as completely as desired. The flame temperature averaged 1100-1300° F.

At one hour ten minutes after ignition of the diesel fuel, just as the fire was starting to die down, a significant explosion occurred. Seven minutes later, at one hour seventeen minutes, a second, less devastating explosion occurred; and four minutes after that, at one hour twenty-one minutes, a flash, without sound, was seen on the TV monitors.

Upon subsequent inspection it was determined that only projectiles 2 and 3 had functioned. Projectile 3, located to the rear of the SSC, was the first to detonate. The flash seen on the TV monitor was probably caused by liquid fill venting from one of the projectiles, possibly from the unexploded projectile 1. None of the other projectiles were damaged at all. A steel burster case with empty aluminum burster tube within was found outside the earthen enclosure. It could not be determined with certainty which projectile it came from. The condition of the functioned projectiles (i.e., flared mouths, bodies not cracked or broken, nose closure missing), and the partially intact nature of the burster case suggest low-order detonation with the burster partially ejected. Video of the test reveals that the first detonation caused considerable damage to the test fixture, opening up the SSC and destroying the Conex.

A review of the video reveals that at about 25 minutes into the burn, the wood floor within the enclosure started burning and within a few minutes flame could be seen at the top corner of the Conex. The Conex floor and one air temperature curve reflect a drastic increase in temperature. SSC Temperatures show a quick rise in the SSC door temperatures (inside & outside), indicative of the fact that the flame engulfed that side of the Conex more than the other. SSC air temperature curve reflects a relatively normal rise as does the SSC exterior side wall temperature. The SSC floor and interior wall temperatures show a dramatic rise, initially corresponding to the rise in Conex floor temperature and then probably sustained by combustion of wood within the SSC. The Projectile #1 temperatures do not have a curve for the burster top, which was lost when dumping data from the datalogger to the computer; however, the liquid cavity temperature shows the same sharp rise seen in the subsequent curves for Projectiles 2 &

3. The exterior temperatures for the projectile bodies seem to follow the rise in the SSC floor temperature (resulting from combustion of wood within the SSC), which eventually catches up to the SSC air temperature. The interior temperatures, however, (liquid cavity and burster top) appear to have reached a critical temperature just prior to 2000 seconds where an exothermic degradation process begins in both the explosive and the ethylene glycol fill which drives those temperatures to 1500° F before leveling off. The reaction continues at a much slower rate until detonation.

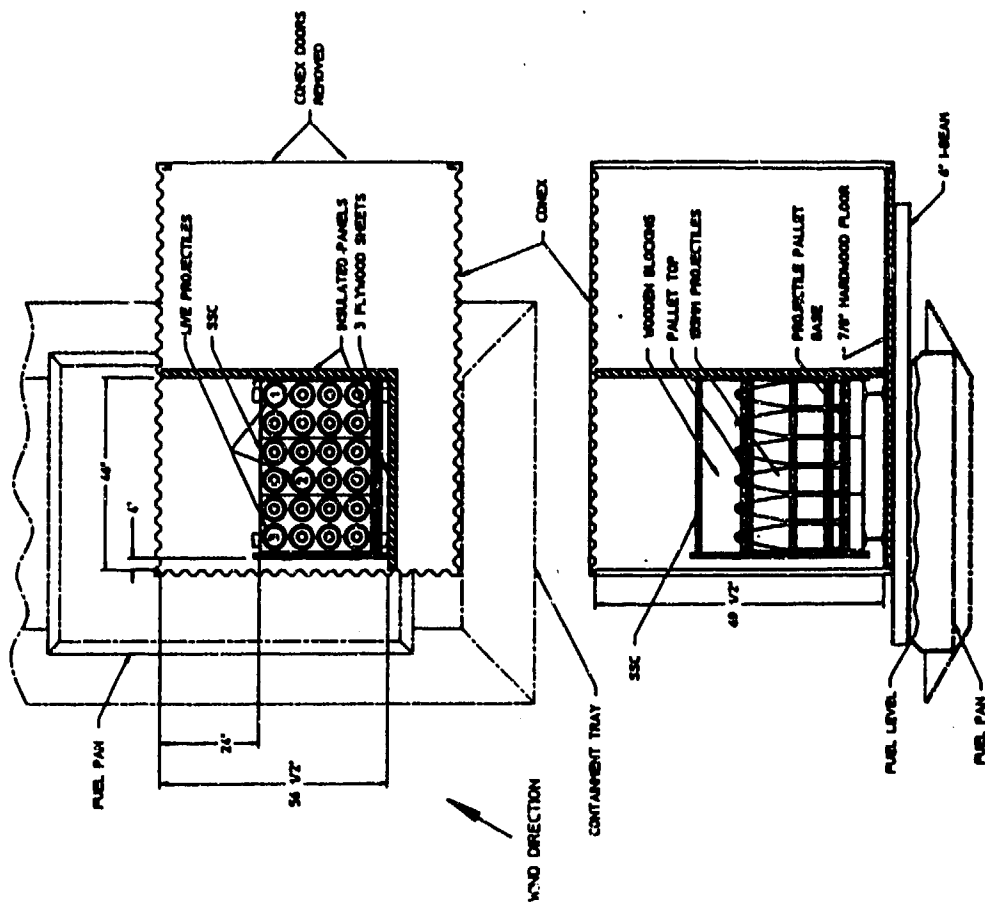
Conclusions

The two fire tests indicate that a reasonable amount of time is available to fire response personnel to fight a fire in the accident scenario described in the Introduction to this report, assuming that a response team can be on the scene within just a few minutes of ignition of such a fire. The SSC, with good structural integrity, appears to provide excellent protection for the projectiles from short-term exposure to fire, even under worst case conditions. Further, the blocking and bracing of the SSC within the MILVAN should generally ensure that the SSC will not be exposed directly to fire, providing the initial delay of heat transfer to the SSC.

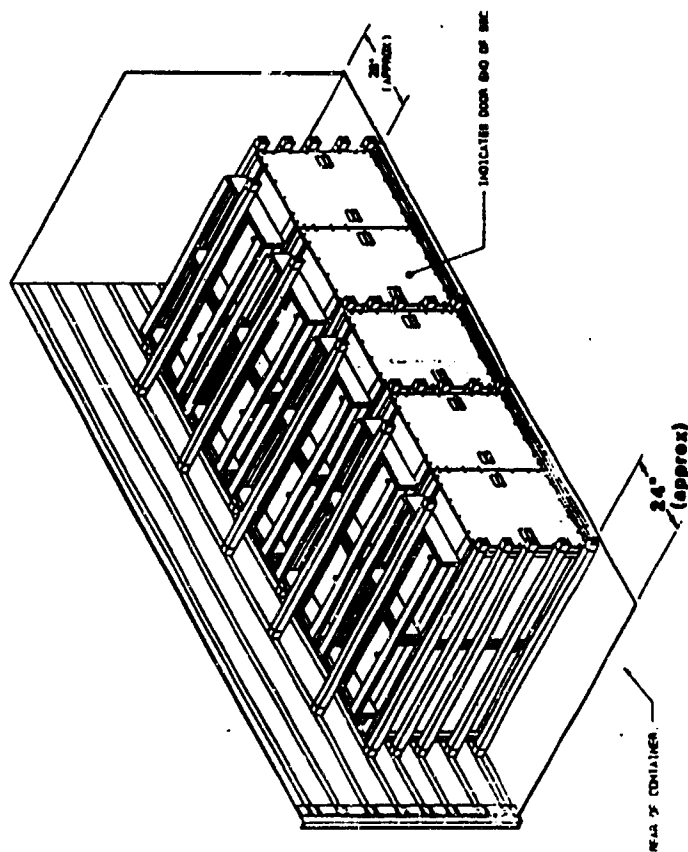
In both tests, the temperatures of the projectiles (both inside and outside) were near or below 150° F for the first 30 minutes, indicating relatively slow heat transfer through the SSC into the projectiles. Once the Conex wooden floor started burning at about 25 minutes in Test 2, however, temperatures within the SSC started to climb sharply. The Conex wooden floor in Test 1 rose to ignition temperature in about 15 minutes but did not actually begin to combust until 45-50 minutes after ignition of the fire. The conclusion here is that early combustion of the wooden floor in Test 2 was the driving mechanism that led to the detonations of the projectiles. Consideration may be given to treating the MILVAN wooden floors with fire retardant materials to gain further delay in combustion of the floor.

Thermocouple data from the two tests are not entirely consistent, largely because of the different wind conditions in each test which caused the fire to engulf the two critical sides of the Conex differently in each test. However, trends in rise rates in the two tests are reasonably consistent, especially for the first 25 minutes.

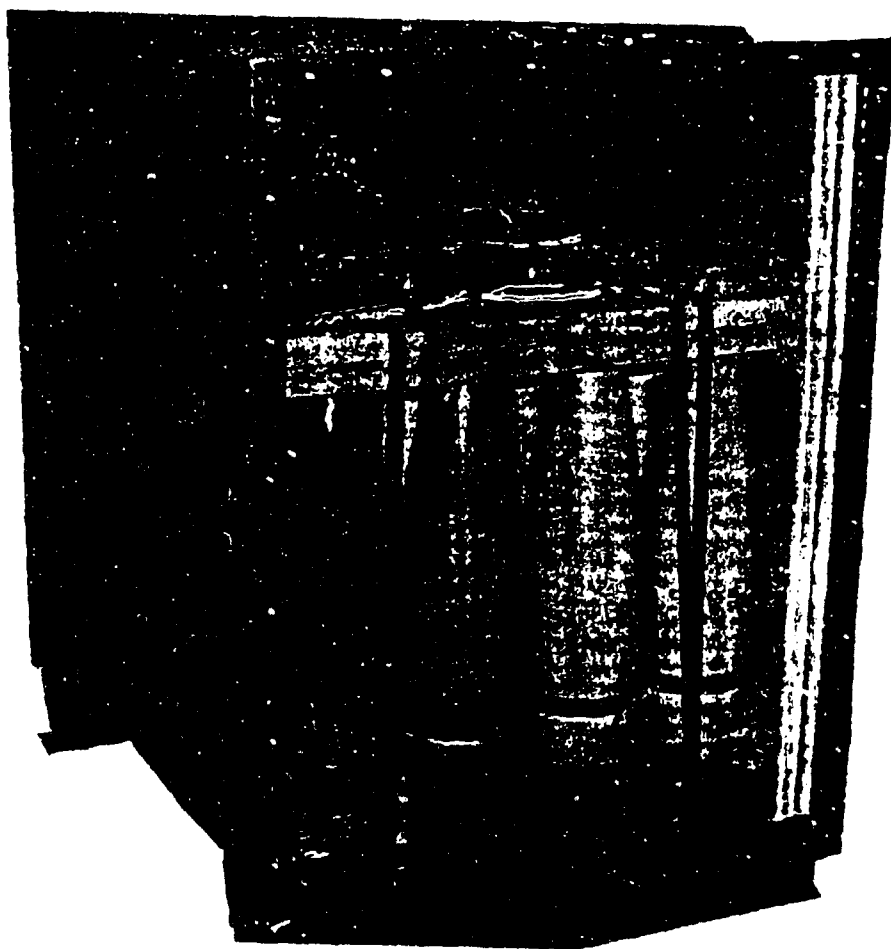
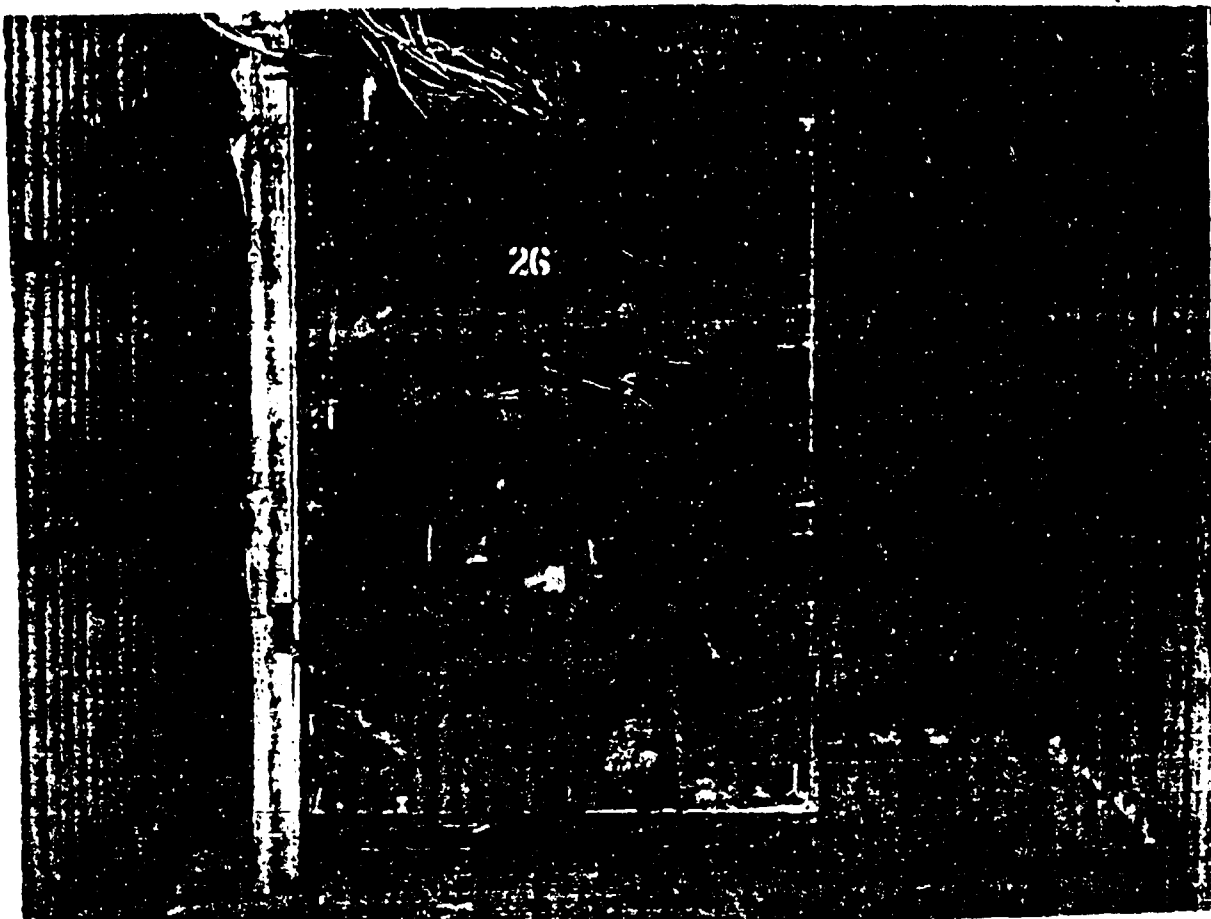
The next several pages illustrate setup and results for the two fire tests.

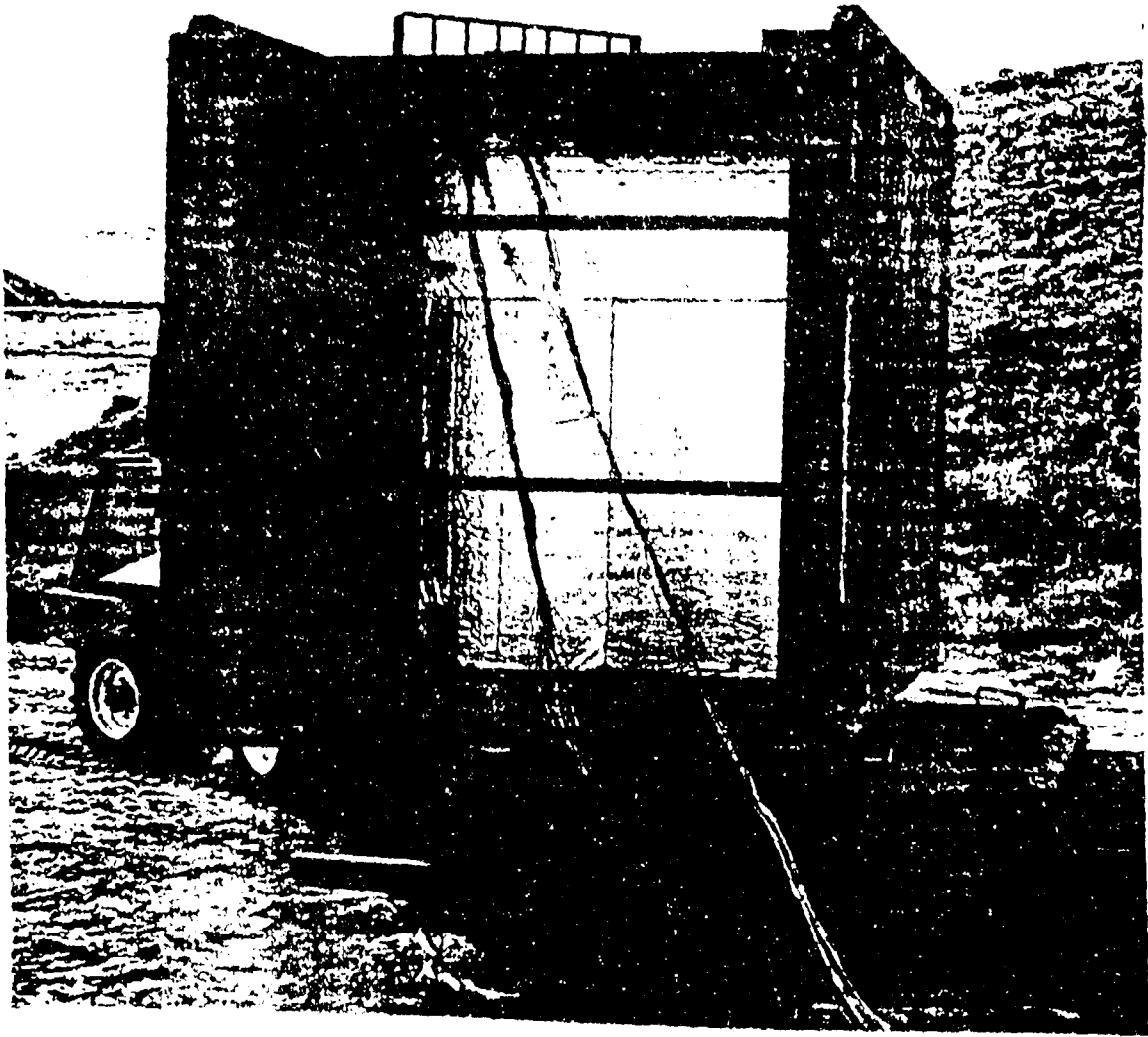


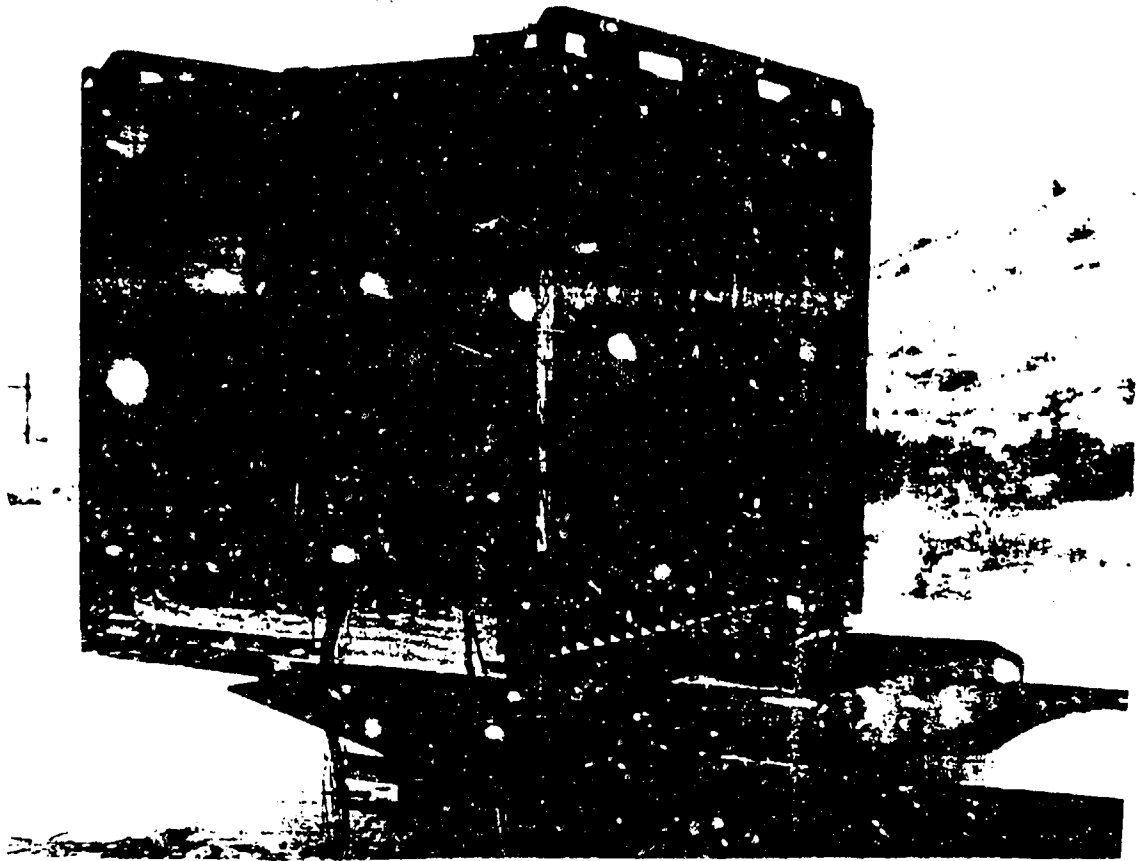
TEST SETUP

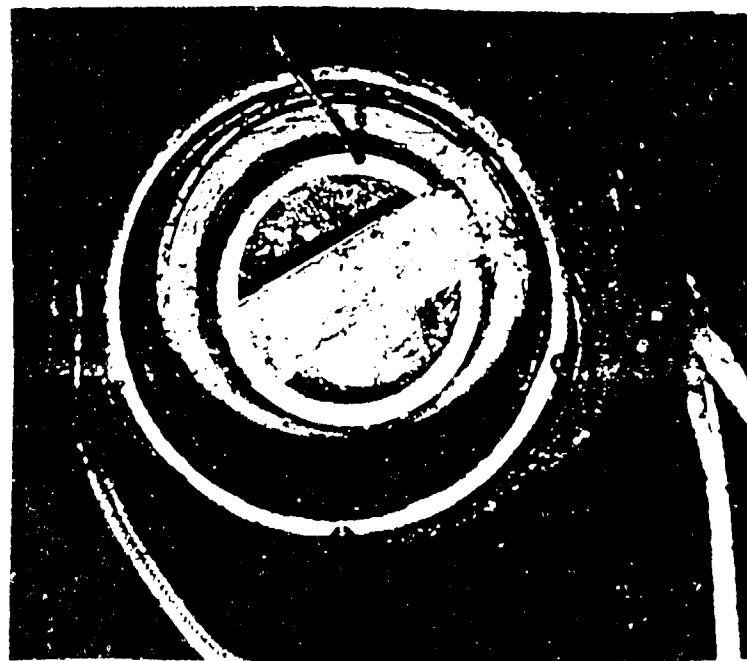
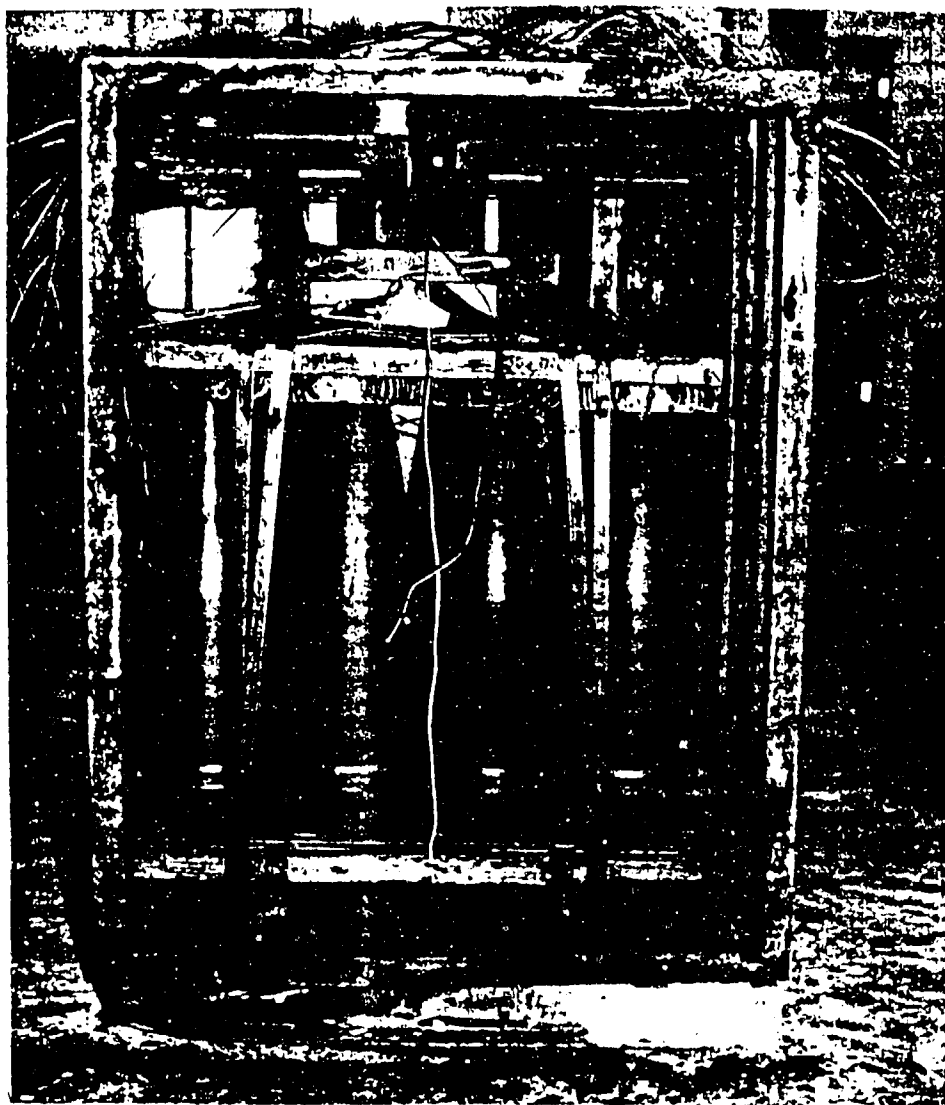


CUTAWAY-MILVAN WITH SSC

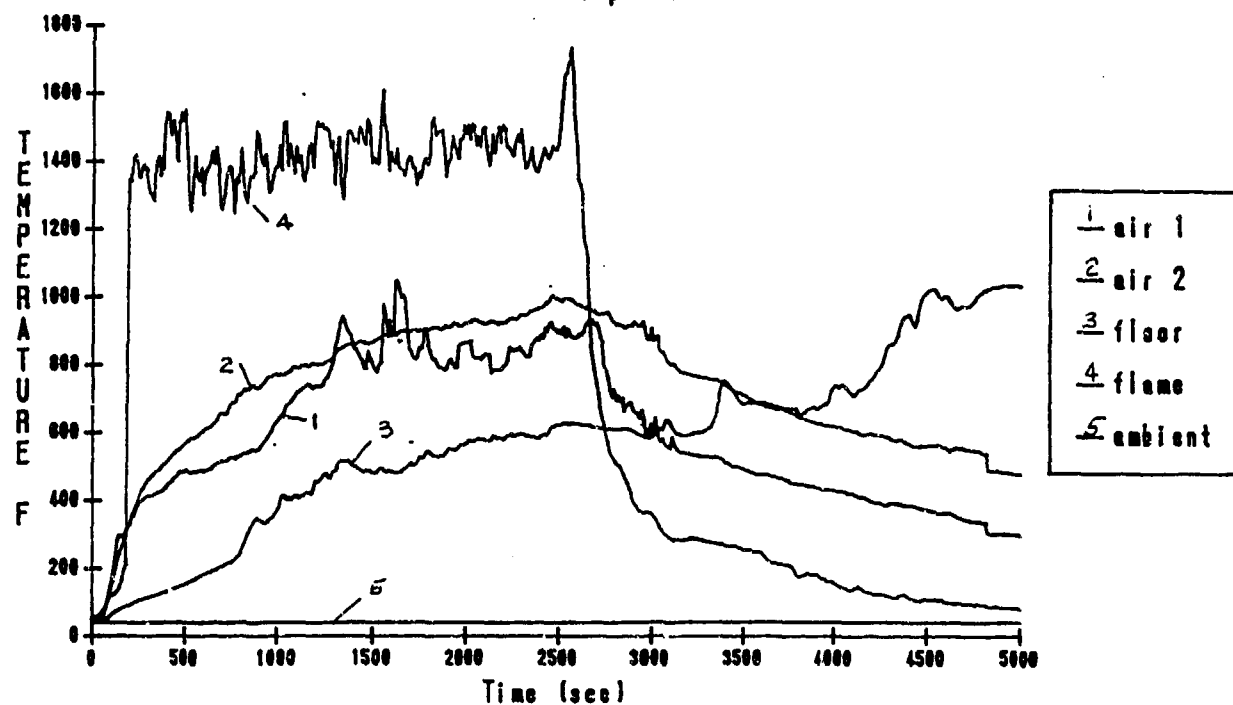




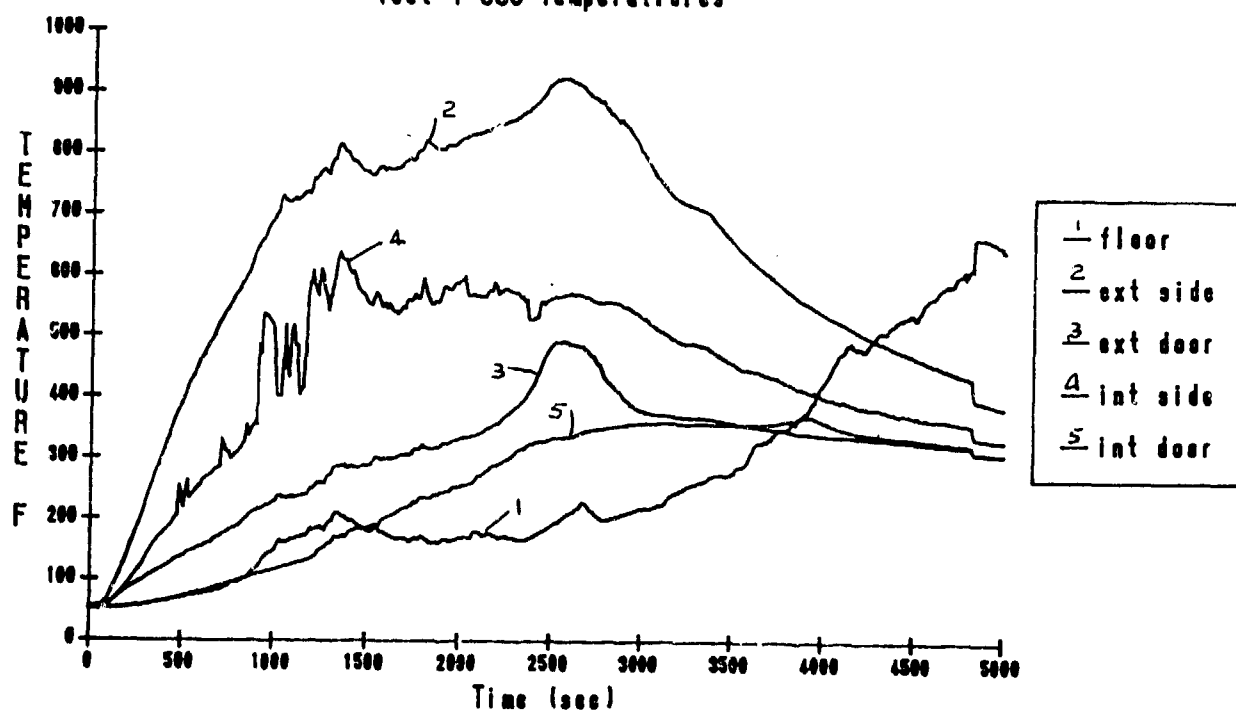


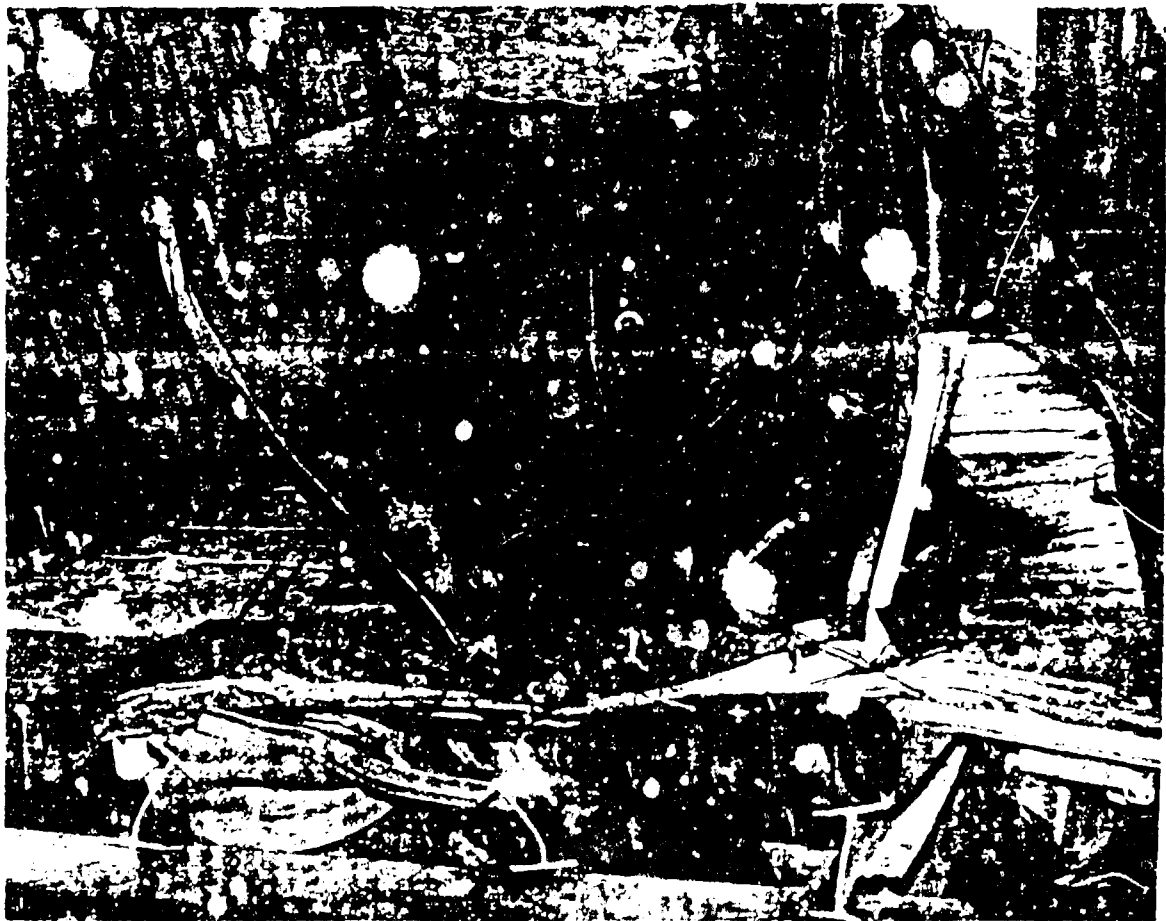
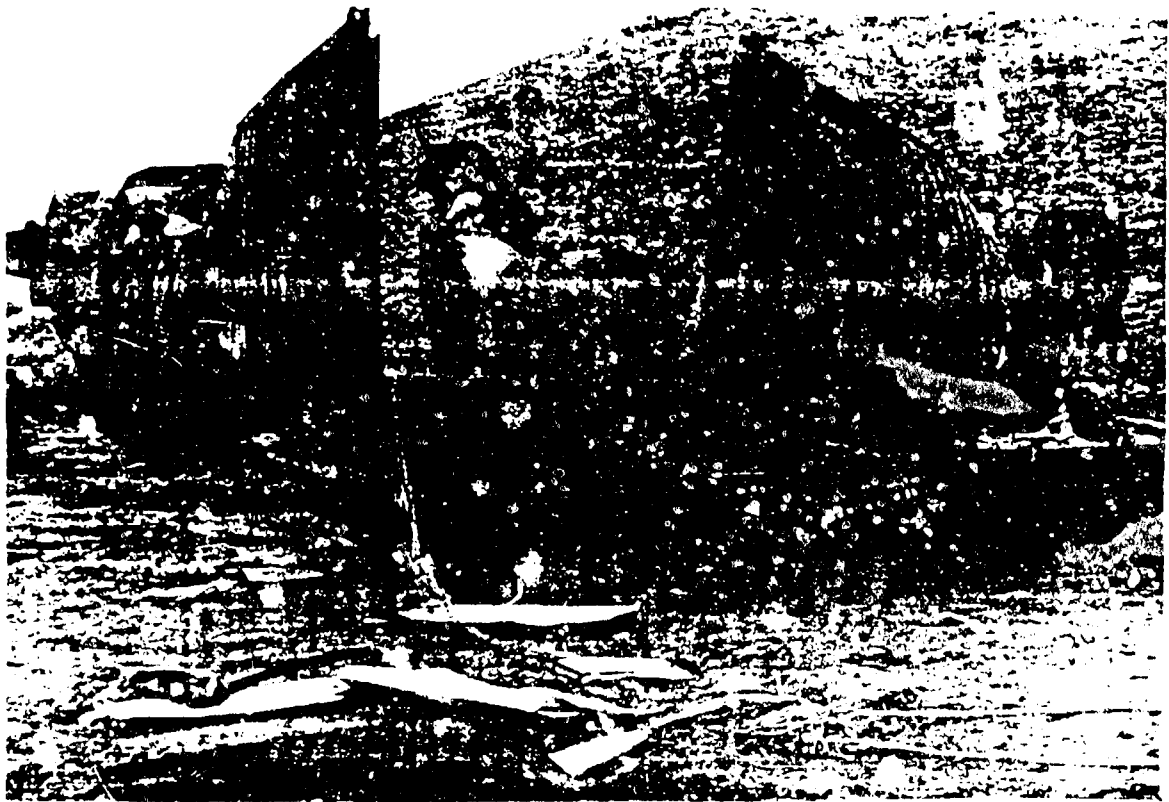


Test 1 CONEX Temperatures

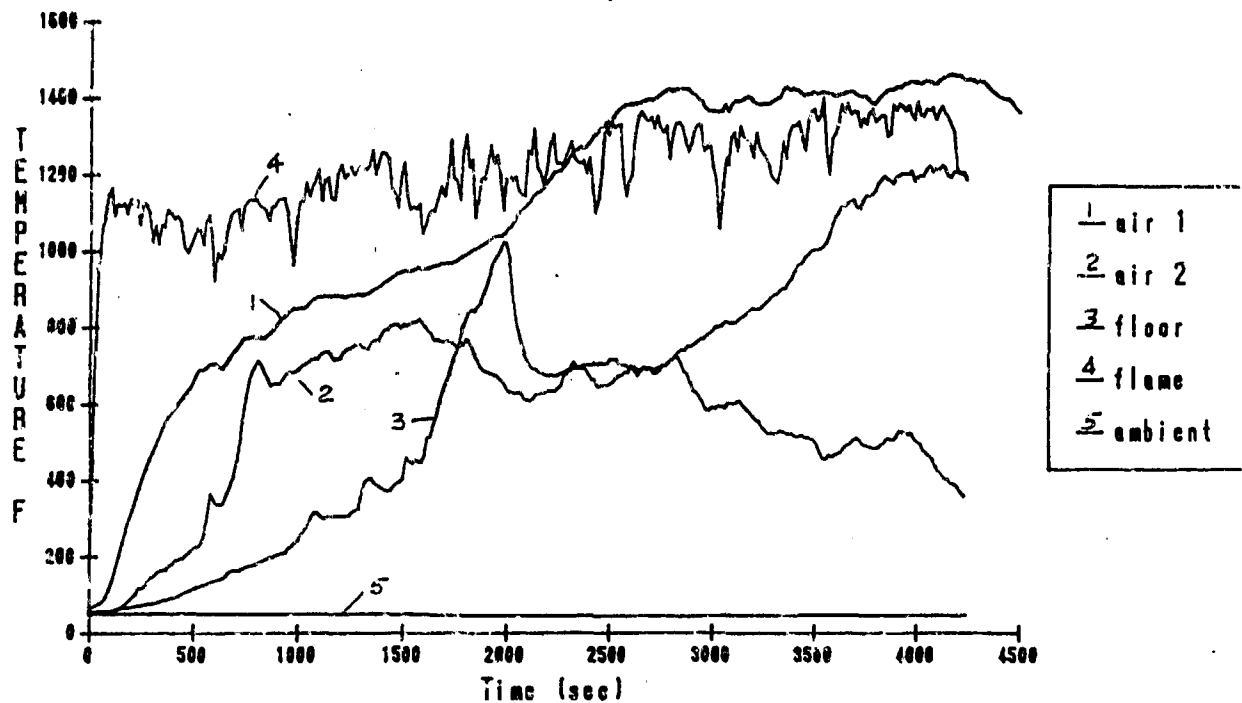


Test 1 SSC Temperatures

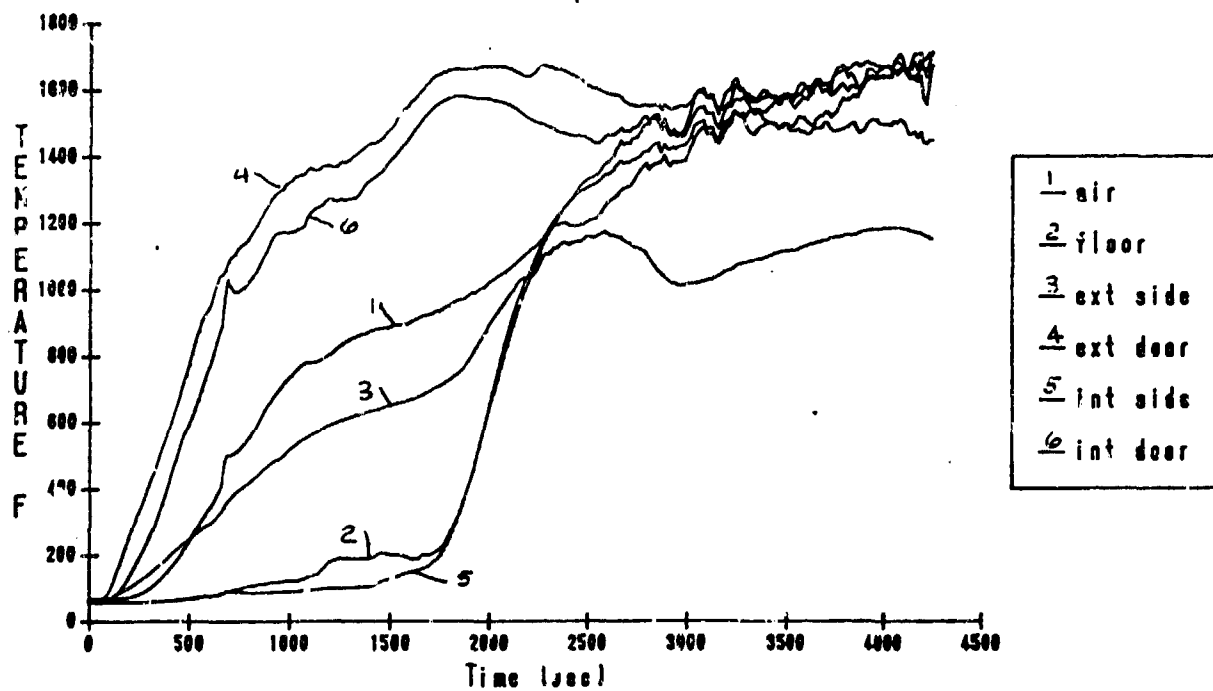




Test 2 CONEX Temperatures



Test 2 SSC Temperatures



**MASS DETONATION HAZARD ASSESSMENT
FROM VIOLENTLY DEFLAGRATING MUNITIONS**

**M. CHICK, T.J. BUSSELL AND L.McVAY
MATERIALS RESEARCH LABORATORY, DSTO
MELBOURNE, VICTORIA, AUSTRALIA**

**TWENTY FOURTH DoD EXPLOSIVES SAFETY SEMINAR
ST. LOUIS, MISSOURIS, USA
AUGUST 1990**

MASS DETONATION HAZARD ASSESSMENT FROM
VIOLENTLY DEFLAGRATING MUNITIONS

M. Chick, T.J. Bussell and L. McVay

Materials Research Laboratory
Melbourne, Victoria, Australia

ABSTRACT

We report on an investigation aimed at assessing whether the controlled, violent deflagration of Composition B loaded 105 mm shell can lead to the detonation of nearby rounds. Tests were grouped into 3 categories; single deflagrating donor - multiple acceptor arrays, projection of acceptor shell by a deflagrating donor and its impact on structural surfaces and multiple impacts causing transient interactions in acceptor shell. Trials were conducted with shell without boosters and fuzes, shell with boosters and plugs representing fuzes and recovered, damaged rounds.

Acceptors were recovered intact but with flattened faces and cracked fillings with no signs of reaction. No detonations were recorded. Separate experiments with single shell indicated that when low order reactions were deliberately stimulated in part of the filling then a deflagration to detonation transition could occur.

Consequently our results do not support the processes occurring in the deflagrating donor/acceptor tests as contributors to the mass detonation hazard of Composition B loaded 105 mm shell.

1. INTRODUCTION

Evidence presented by Frey et al [1] and Stosz [2] has shown that mass detonation can result from reactions other than the shocks generated by detonating donor rounds. Some of these events take several milliseconds [1] and are therefore not associated with shock initiation. The details of the origin and growth of these reactions are not understood. It is not surprising therefore that tracking down the causes of mass detonation in large munition arrays has proved difficult and has led to the need to design simplified tests to evaluate candidate processes. To this end we have been investigating the likely consequences emanating from a donor shell undergoing a violent deflagration while positioned in various munition arrays. The arrays were designed to reproduce conditions encountered during munition storage and transport. Our investigation utilises a recently developed technique that allows the production of a controlled deflagration of a munition without the possibility of a transition to detonation invalidating the result [3].

Our aim is to investigate a range of munition types. The first part of the program has been undertaken using Composition B loaded 105 mm shell because of its availability and widespread use. Further testing is planned using munitions with thinner cases and a higher explosive charge / case mass ratio.

This paper presents the results of our investigation using 105 mm shell.

2. TECHNIQUE FOR PRODUCING CONTROLLED DEFLAGRATING DONOR SHELL

The technique for violently deflagrating donor 105 mm shell [3] consists of firing a shaped charge jet along the axis of the round with a velocity below the threshold to produce detonation of the filling. In this way the reaction produced in and behind the bow wave set-up in front of the penetrating jet sweeps through the length of the filling leaving no bulk explosive for a deflagration to detonation transition. Detonation does not result directly from the bow wave since the pressure-time profile is subcritical. Criteria for the jet initiation of explosive fillings has been discussed in detail elsewhere [4,6].

The application of the technique to a Composition B filled 105 mm HE M1 donor shell is shown in Figure 1 and summarised below.

The MRL 38 mm diameter shaped charge was used in the tests since there is a considerable data base on its effect on munition fillings [4-6]. This shaped charge contains a conventional copper liner with a 42° apex angle. The subcritical jet velocity was produced by firing the jet at 2 charge diameters' standoff through a steel barrier of appropriate thickness placed in contact with the shell case. The minimum thickness of the steel barrier (τ) was determined from the known critical jet velocity for the detonation threshold (V_c) using the Dipersio/Simon equation [7] to calculate the total thickness of steel required and subtracting the case thickness at the jet entry position;

$$\tau = s \left[\left\{ \frac{V_t}{V_j} \right\}^{1/\gamma} - 1 \right]$$

where s the standoff from the shaped charge to the top of the steel barrier,

V_t the velocity of the jet tip, and

γ the square root of the ratio of the steel barrier and jet densities.

For the 38 mm diameter shaped charge jet V_j was adjusted downwards to take account of the effect of the 105 mm shell side confinement on the Composition B filling, determined as 4.85 km/s [8]: this was equivalent to a total steel thickness of 72.5 mm. Since the thickness of the steel case at the jet entry position was 17.5 mm, a minimum of 55 mm of extra steel was required. The side confinement also holds the explosive together thereby assisting the deflagration process.

Characteristics of a deflagrating Composition B filled 105 mm shell that may be important in a mass detonation hazard assessment have been determined and are summarised below. Recovered fragments are shown in Figure 2 and were dispersed over an area of about 350 m radius. They are considerably larger and show different fracture patterns compared to those recovered from a detonating round, see Figure 3. The witness block under the nose of the shell exhibited no indentation but had the compressed remains of the booster can stuck to it. A detonation produced a well formed dent. Peak overpressure was measured at about 25% less than for a detonating round. High speed photography showed that initial shell burst occurred in the region of the driving band after an expansion of about 30% of a shell diameter (i.e 15 mm increase in shell radius).

Initial jet penetration velocities through the filling can be varied by adjusting the thickness of the added steel barrier on the base of the shell; the value selected for the tests was 3 km/s. Since the bow wave is coupled to the jet and reaction occurs within the bow wave, it is assumed that the deflagration velocity will have a similar value. This high reaction velocity and the characteristics measured above confirm that our tests are studying the effects from a particularly violent type of deflagration.

1. SINGLE DONOR-MULTIPLE ACCEPTOR TESTS

The direct effect of the expanding case, fragment impact and blast from a deflagrating donor round on adjacent shell was determined using the set up shown in Figure 4. These tests were based on the methods used at BRL by Howe [9] for studying the effects of detonating donors. Acceptor standoff distances were 0, 10, 25 and 50 mm as measured from the driving band. In some of the tests large fibreboard packs were placed 1 m from the shell for controlled recovery, in other tests the shell were recovered after free flight and impact with the ground. Tests were

performed on shell with no boosters and fuzes (2 shots), shell with pressed flake boosters and plugs representing fuzes (PRF) (1 shot) and recovered, damaged shell (1 shot). Four shots were fired in which all acceptors were in contact with the donor.

A test was performed using the set-up in Figure 5 to assess the effect of shell jostling. The donor and row of acceptor shell were in contact and backed by a 25 mm thick steel plate and supporting sandbags.

In the tests in this and sections 4.0 and 5.0 the type of event was determined from witness block indentation, recovered fragment characteristics, impacted surface damage and in some tests, instrumentation records (overpressure, high speed photograph). Some donor rounds included probes on either side of the steel barrier as a check on the performance of the shaped charge jet. No substandard jets were detected.

All donor rounds deflagrated as planned. Recovered acceptor shell without the boosters and fuzes from the Figure 4 type firing set-up were flattened on the side adjacent to the donor, see Figure 6. Driving bands were either dislodged or distorted. Aluminium booster cans were crumpled but in position; when removed they showed that the filling was cracked without signs of reaction. The increased sensitivity of the filling to shock type stimuli was assessed by determining the critical jet velocity for the detonation threshold using the 38 mm diameter shaped charge. The critical value of 4.8 km/s compares to a value of 5.2 km/s for the undamaged material.

Recovered rounds with boosters and PRF exhibited similar damage with the addition that the plugs were bent, see Figure 7. Repeat firings using recovered shell produced cases with two flattered faces, no driving bands, dislodged or badly distorted booster cans and a filling with extensive cracking but no signs of reaction.

Acceptor shell from the shot where they were placed in a row (Figure 5) were recovered intact within 1 m of ground zero. The acceptor adjacent to the donor showed similar damage to that described above. The other acceptors showed progressively less damage as the original position moved away from the donor i.e the closer rounds appeared to act as a buffer for this type of impact.

The tests from this section suggest that the effect of case expansion, fragment impact and blast from a deflagrating Composition B loaded 105 mm shell can inflict severe damage on neighbouring rounds without being the direct cause of mass detonation.

4. ACCEPTOR SHELL PROJECTION AND IMPACT TESTS

These tests were undertaken to assess the hazard from the impact of projected shell on hard structural surfaces. A potential source for this type of event would be from a deflagrating donor shell ejecting neighbouring rounds when located in a munition stack during storage (temporary or permanent) and transport. Important structural surfaces would include concrete and steel.

The velocity of a projected acceptor from a deflagrating donor shell was measured at 40 m/s using multiple glass break screens [11]. This value is considerably lower than the critical fragment impact velocities of several hundred metres per second and upward reported by Howe et al [10] using a range of fragment sizes and Composition B with a steel cover thickness of 10 mm. The 105 mm shell case has a similar thickness along its central section. In our tests and for the type of event under study however the filling in the shell prior to impact would be damaged as a result of the deflagration projection process. This was shown in the examination of the fillings from the soft recovery tests described in Section 3.0 and critical jet velocity tests confirmed the accompanying increased sensitivity. A further feature of our tests is that the shell/target impact represents a fragment size beyond that reported in Reference 10.

The test set-up is shown in Figure 8 with the concrete target positioned 2 m from ground zero. Firings were undertaken with shell without boosters and fuzes, recovered damaged shell and shell fitted with boosters and a PRF. Separate tests were conducted with unboosted shell in which the concrete block was used to support a 10 mm thick steel plate.

All donors deflagrated as planned and projected rounds were recovered damaged but intact. Both the steel and concrete targets produced similar effects. The acceptor rounds had a flattened area on one corner with surface marks continuing along the length of the case. This type of corner-side slap on the target was compatible with the shape of the impression formed by the shell impact on the fibreboard packs in the soft recovery experiments reported in Section 3.0. Visual inspection showed the filling cracked but there was no signs of reaction. Rounds with a booster and PRF were likewise damaged plus the plug was bent. The experiment with damaged acceptors produced a second flattened face but the round remained intact; this retesting of damaged shell may be considered a worse case situation.

It is concluded that the projection of Composition B loaded 105 mm shell at velocities likely to be encountered from a neighbouring round undergoing a violent deflagration is unlikely to be the direct cause of a mass detonation. Our study has not addressed the impact of a shell projected by a detonating donor where higher flight velocities may be achieved.

5. TRANSIENT INTERACTIONS IN SHELL FILLINGS

Tests in this category were designed to assess whether transient interactions within the explosive filling would promote a deflagration to detonation transition (DDT). Such interaction may arise as a result of two rounds deflagrating either simultaneously or within a limited time frame of one another.

In the test shown in Figure 9 the central acceptor was subjected to the simultaneous impact from two adjacent deflagrating donors. For the set-up in Figure 10 two shells were deflagrated within a predetermined time interval. Thus the expanding case from the first shell deflagrated

impacted on the second shell. The time delay was to allow the compression wave from the case impact to pass through the explosive filling and interact with the deflagrating front sweeping through the second shell. The concept is illustrated by the sketch in Figure 11. Experiments were conducted with time intervals of 16, 19 and 100 μ s. For the shorter time intervals the deflagration fronts were calculated to be about 50 mm apart. Thus the effect of case interaction was expected to occur after both deflagrations were well established. Jet penetration equations and measurements [4,6,7] gave an estimated time for the jet to traverse the Composition B filling in the 105 mm shell of 92 μ s. Consequently the 100 μ s time interval set between the deflagration of the two shell was designed to allow the compression wave resulting from case expansion and impact of the first shell to form a wide front prior to its interaction with the deflagration in the filling of the second shell.

The baffle in Figure 10 was designed to avoid the blast and fragmentation from the first shaped charge detonated moving the second shaped charge. Examination of the blast and fragment patterns on the walls of the baffle (they were symmetrical with respect to one another) and the jet penetration holes in the recovered steel barriers (central alignment and no key holing) indicated there was no interference between the shaped charges. This conclusion was supported by the Hycam photography records taken at between 35,000 and 40,000 pictures per second.

The central shell from the double, simultaneous impact experiment was recovered intact with two flattened faces, no driving bands and a cracked filling. Again visual inspection showed no signs of reaction. In the delayed interaction experiments all shell deflagrated without detonation occurring. Consequently these tests failed to provide any evidence that this type of transient interaction within the filling may be a contributing process to a mass detonation hazard of Composition B loaded 105 mm shell.

6. DEFLAGRATION TO DETONATION IN SINGLE SHELL TESTS

Other experiments investigating the response of Composition B loaded 105 mm shell to shaped charge jets have produced DDT. In these tests, jets with subcritical velocities (for detonation) in the range 2.8 to 5.0 km/s, were fired across the diameter of the shell towards the nose end of the filling, but not close to the booster cavity. Four shots out of 12 produced a DDT at the base end of the shell - this was clearly evident from the changing indentation pattern along the steel witness plate. Penetration holes in the case from these jets are 10 mm diameter and less and hence the reaction stimulated by the jet cannot effectively vent. Consequently the pressure build-up promotes a DDT in the large unconsumed mass of explosive towards the shell base. These results demonstrate that once a low order reaction has been stimulated in Composition B loaded 105 mm shell the potential exists for a mass detonation hazard. They further suggest that the impact and interaction processes in our tests did not produce the initial low order reaction.

7. CONCLUSIONS

Deflagrating donor, Composition B loaded 105 mm shell without boosters and fuzes did not cause the detonation of adjacent rounds in the following types of test;

- (a) single donor - multiple acceptor array
- (b) acceptor projection (at 40 m/s) and impact on concrete and steel targets,
- (c) simultaneous double impact on an acceptor,
- (d) interaction between two deflagrating rounds.

Trials using tests (a) and (b) with recovered, damaged shell and with shell containing boosters and plugs representing fuzes also did not produce detonations.

Consequently the processes in these tests are not supported as contributors to the mass detonation hazard of Composition B loaded 105 mm shell. Separate DDT experiments on single shell suggest this is because the impact and interaction processes did not produce the initial low order reaction.

8. ACKNOWLEDGEMENTS

We should like to record our gratitude to the Commanding Officer and support personnel of the Army Proof and Experimental Establishment (P&EE) Graytown, Victoria, for assistance with the field firings and ensuring the ready availability of support resources.

9. REFERENCES

1. Frey R.B., Watson J., Gibbons G., Boyle V. and Lyman O., "The Response of Compartmentized Ammunition", Proceedings of the Joint Government Industry Symposium on Insensitive Munitions Technology, NSWG, White Oak, Maryland, US, March 1990.
2. Stosz M. Private Communication 1987.
3. Chick M. and Bussell T.J. Paper in course of publication.
4. Chick M. and Hatt D.J., "The Mechanism of the Initiation of Composition B, by a Metal Jet", Proceedings of the Seventh Symposium (International) on Detonation, NSWG MP 82-334, 1981.
5. Chick M., MacIntyre I.B. and Frey R.B., "The Jet Initiation of Solid Explosives", Proceedings of the Eighth Symposium (International) on Detonation, NSWG MP 86-194, 1985.
6. Chick M., Bussell T.J., Frey R.B. and Bines A., "Jet Initiation mechanisms and Sensitivities of Covered Explosives", Preprints of Ninth Symposium (International) on Detonation, 1989.
7. DiPersio R. and Simon J., "The Penetration Standoff Relationship for Idealised Shaped Charge Jets", BRL Report BRL 1542, 1964.

7

8. Chick M., Bussell T.J. and McVay L., "Terminal Effects of Shaped Charge Jets on Thick Cased Munitions", Proceedings of 11th International Symposium on Ballistics, 1989.
9. Howe P., "The Phenomenology of Interround Communication and Techniques for Prevention", BRL Report ARBRL-TR-02048, 1978.
10. Howe P., Watson J.L. and Frey, R.B., "The Response of Confined Explosives Charges to Fragment Attack", Proceedings of Seventh Symposium (International) in Detonation, NSWC MP 82-334, 1981.
11. Bussell T.J., Box P. and Marian F., Paper in course of publication.

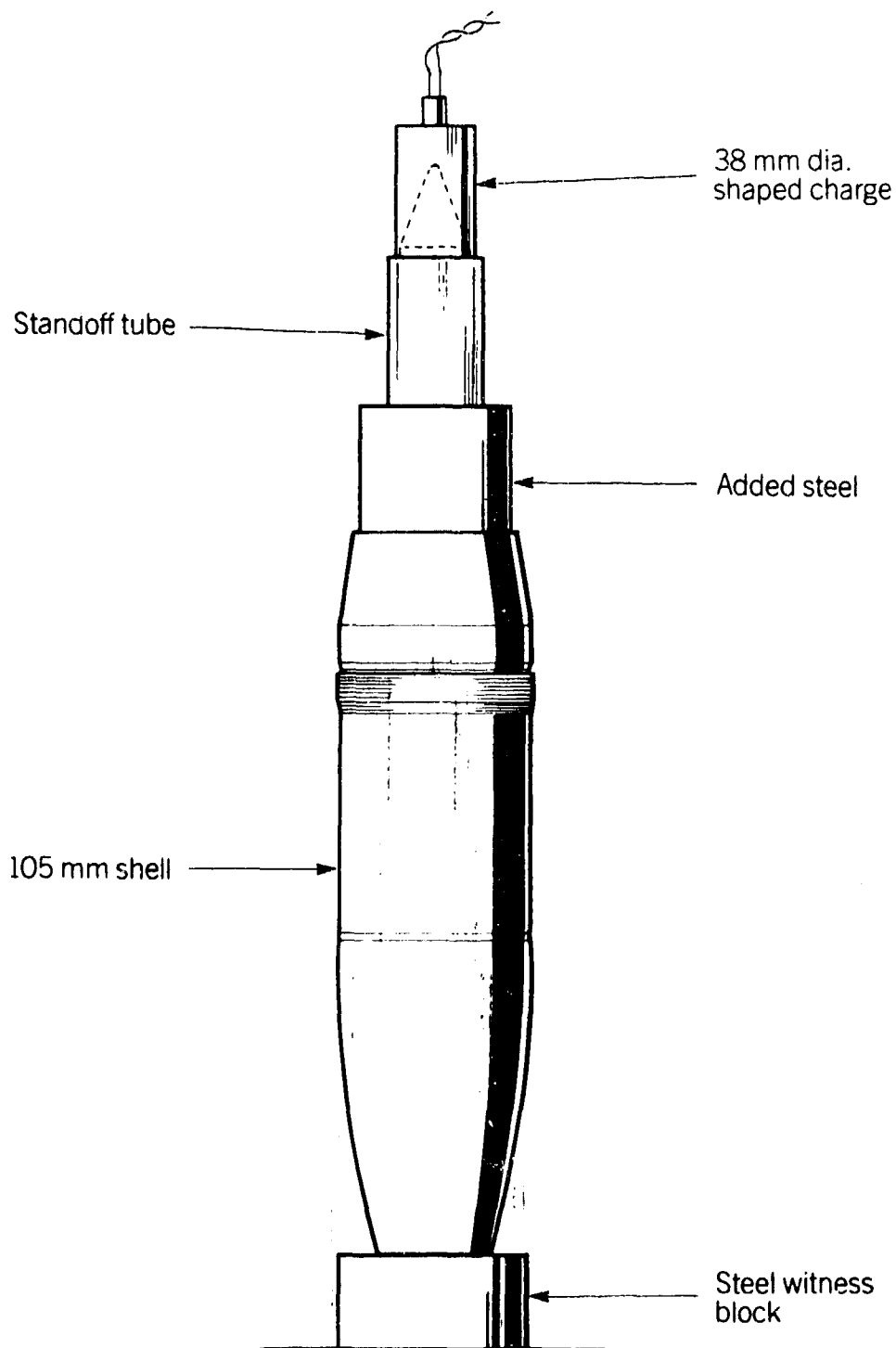


FIGURE 1.

SET-UP FOR USING A SUBCRITICAL SHAPED CHARGE JET
TO VIOLENTLY DEFLAGRATE A 105 mm SHELL FILLING



SC(FT105) 29

FIGURE 2

RECOVERED FRAGMENTS AND WITNESS PLATE
FROM VIOLENT DEFLAGRATION OF 105 mm COMPOSITION B
FILLED SHELL



SC(FT105) 30

FIGURE 2
RECOVERED FRAGMENTS AND WITNESS PLATE FROM DETONATION
OF 105 mm COMPOSITION B FILLED SHELL

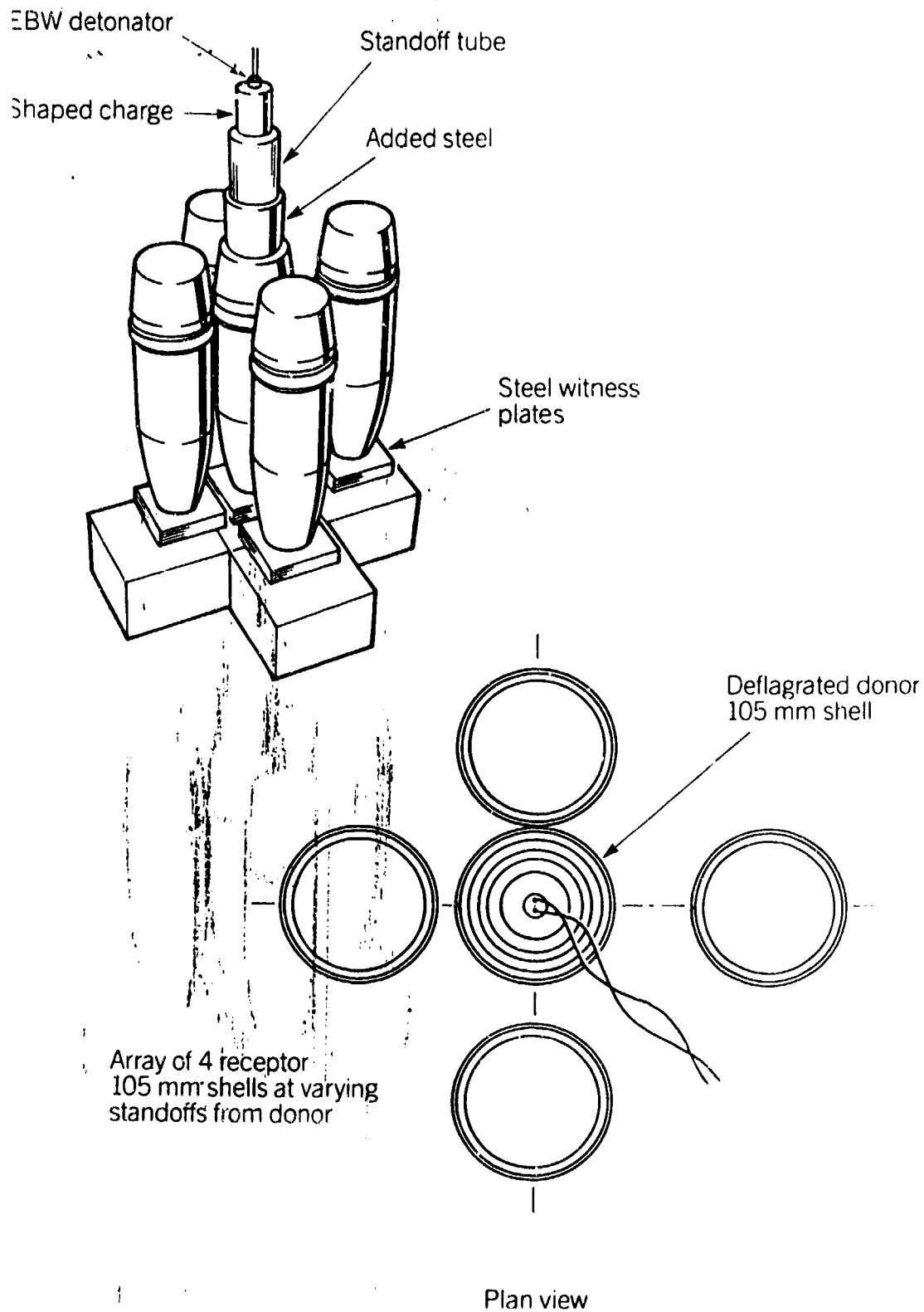


FIGURE 4.

SET-UP FOR SINGLE DEFLAGRATING DONOR - MULTIPLE
ACCEPTOR TESTS

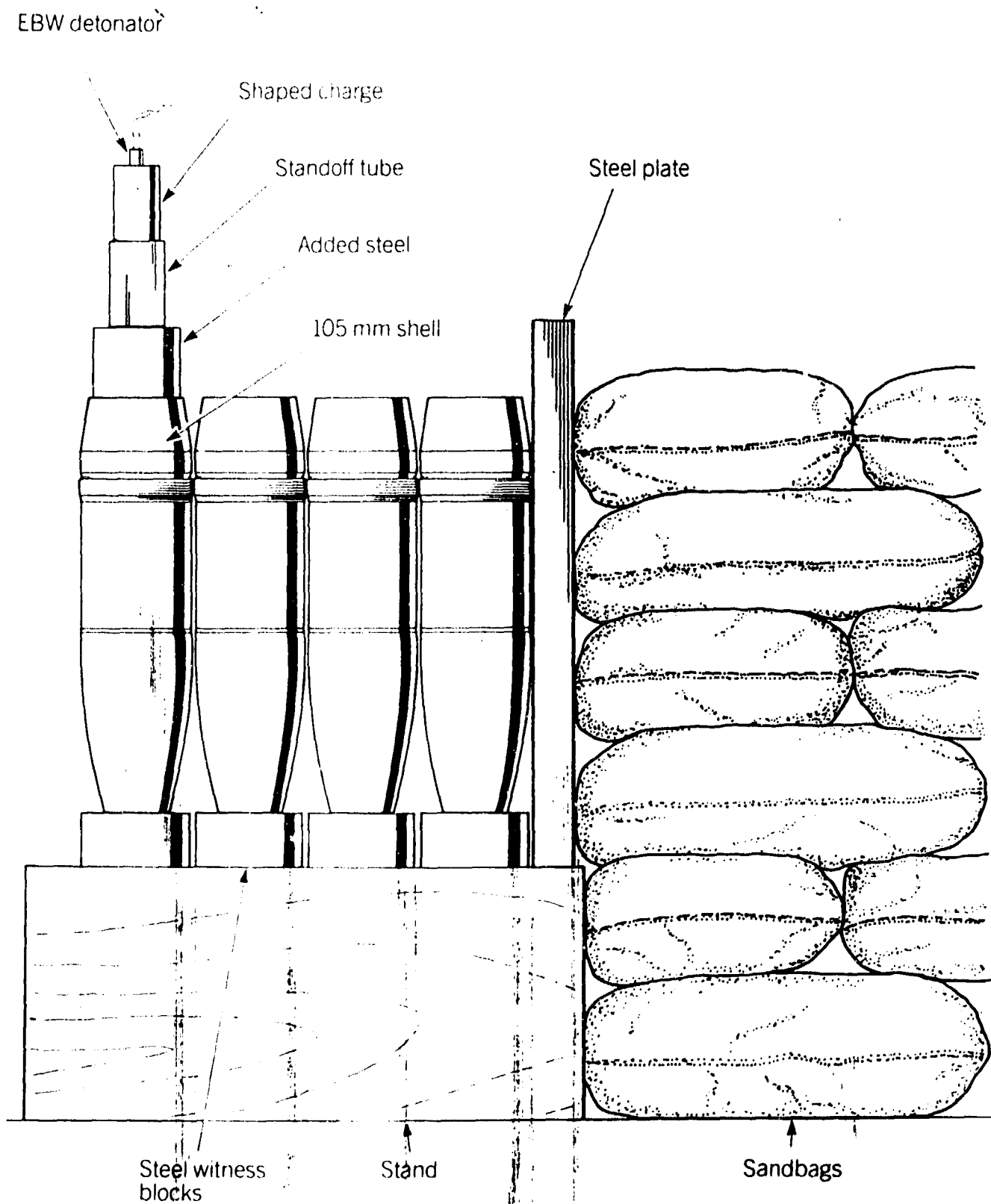


FIGURE 5

SET-UP FOR SINGLE DEFLAGRATING DONOR - ROW OF ACCEPTOR TEST



FIGURE 6
SHELL RECOVERED FROM A SINGLE DEFLAGRATING DONOR
MULTIPLE ACCEPTOR TEST

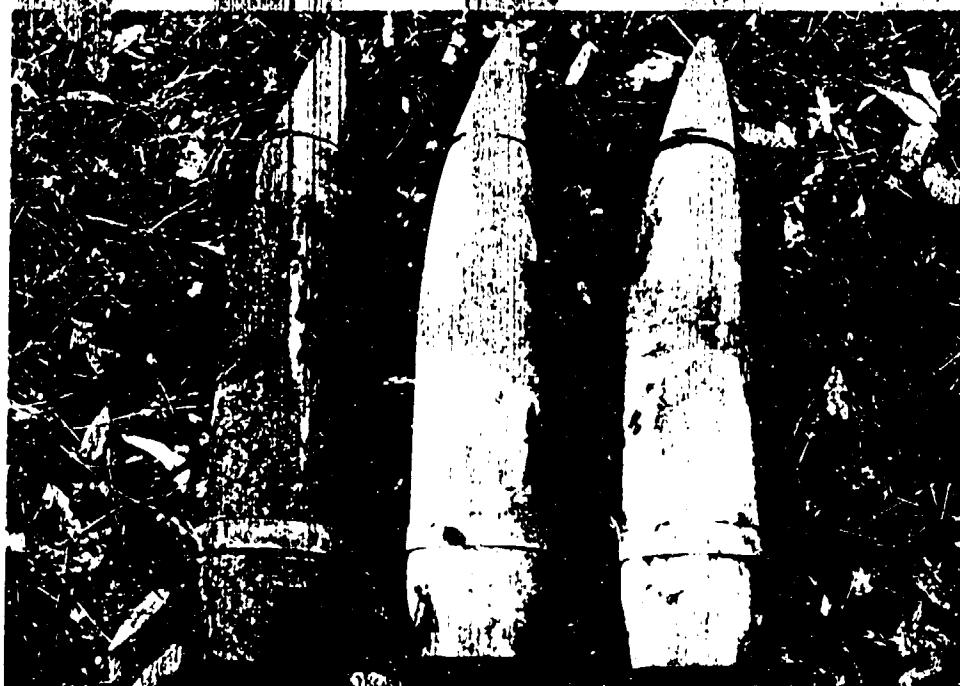


FIGURE 7
SHELL RECOVERED FROM TESTS USING ROUNDS WITH BOOSTERS
AND PLUGS REPRESENTING FUZES

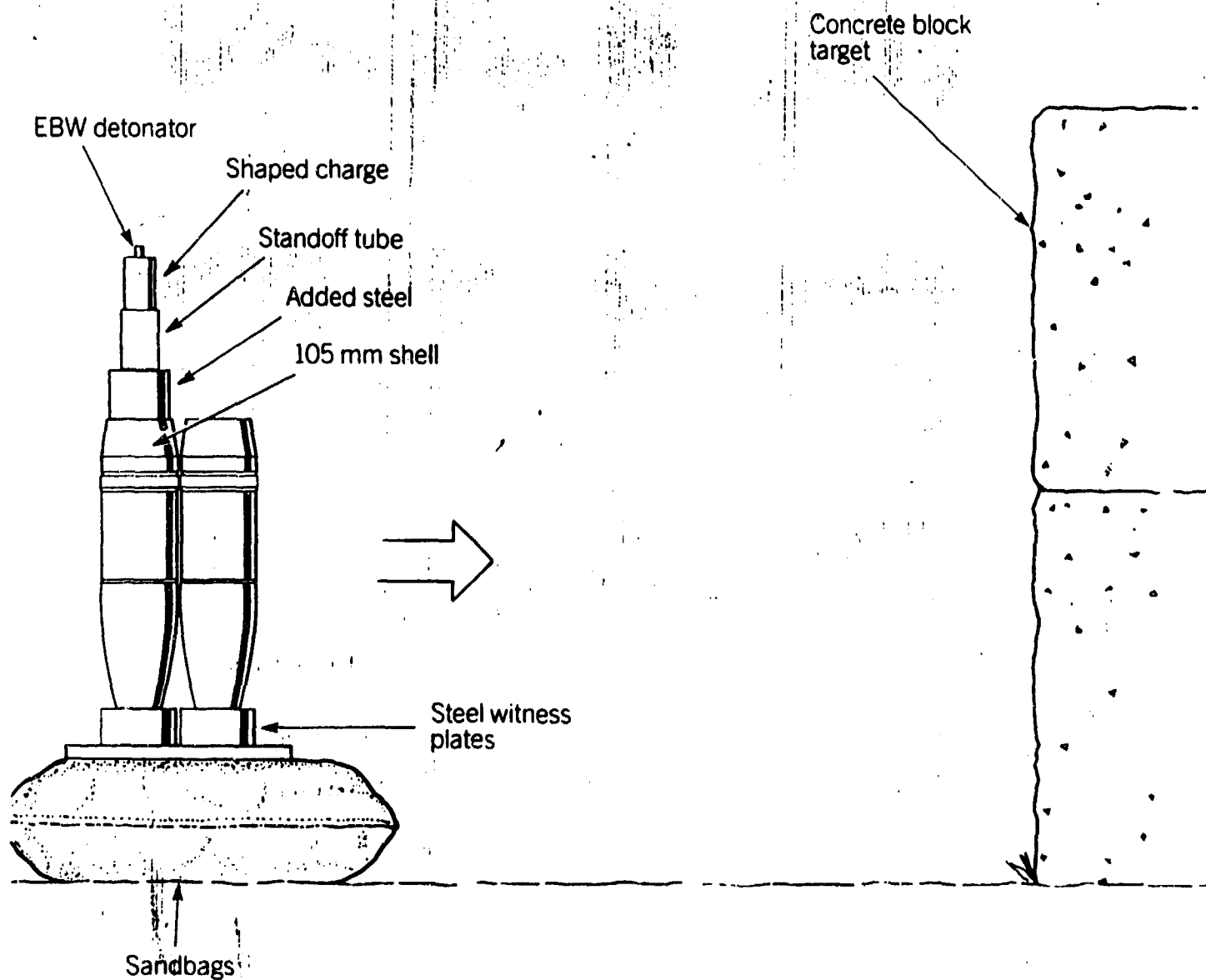


FIGURE 8.
SET-UP FOR ACCEPTOR SHELL PROJECTION AND IMPACT
ON A HARD SURFACE

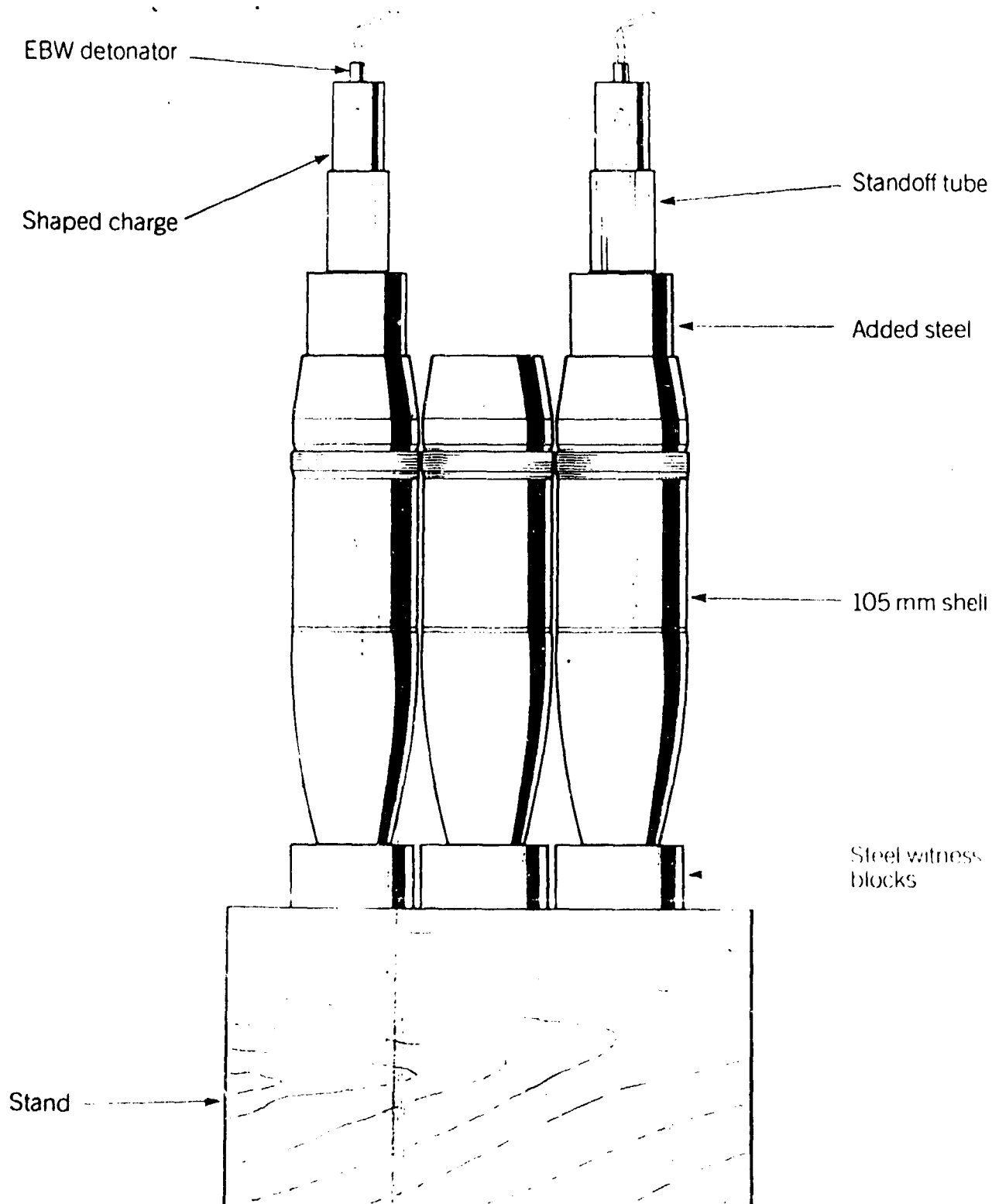


FIGURE 9.
SET-UP FOR SINGLE ACCEPTOR SIMULTANEOUSLY
IMPACTED BY TWO DEFLAGRATING DONOR ROUNDS

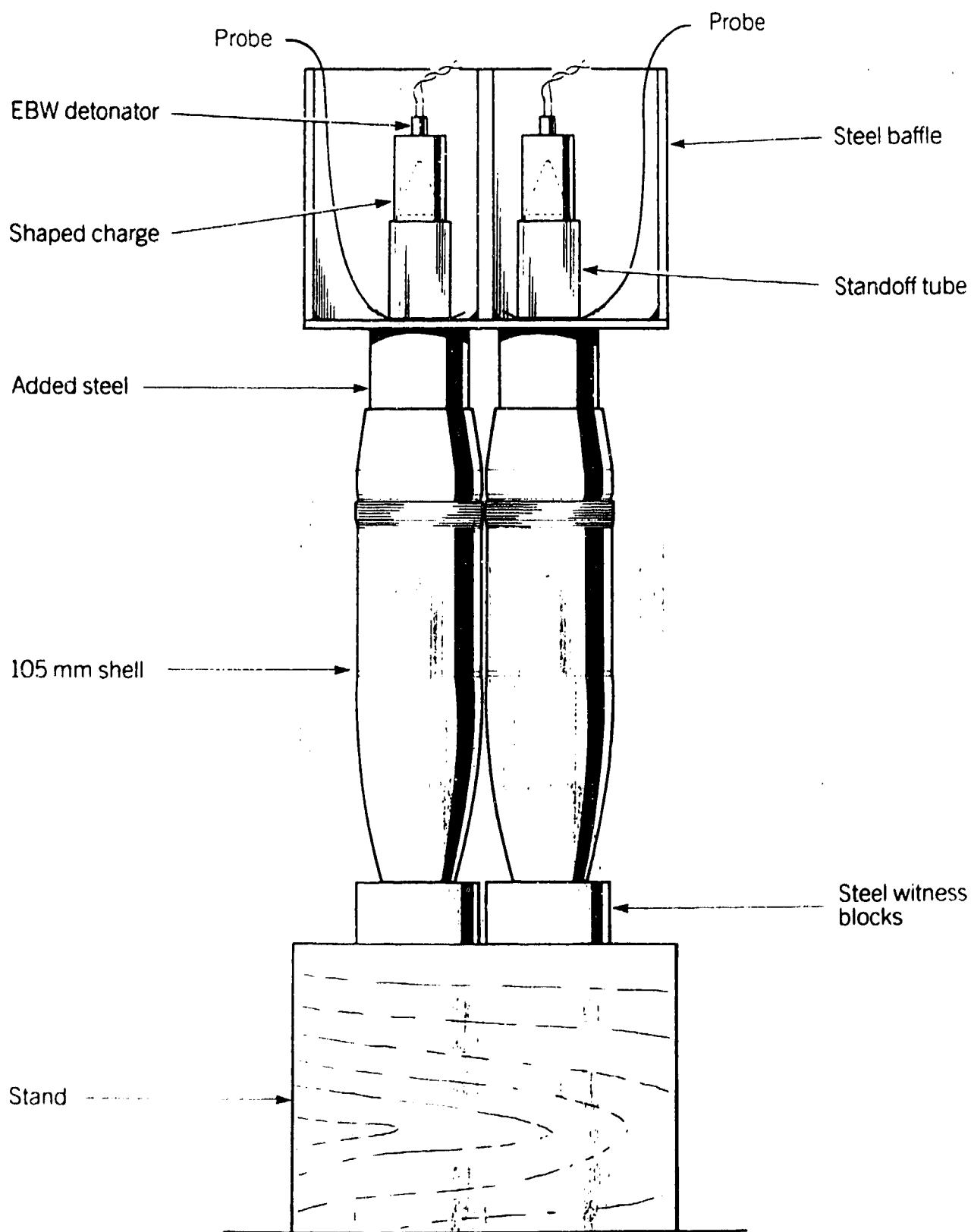


FIGURE 10.

SET-UP FOR THE DEFLAGRATION OF TWO SHELL AT
A PREDETERMINED TIME INTERVAL

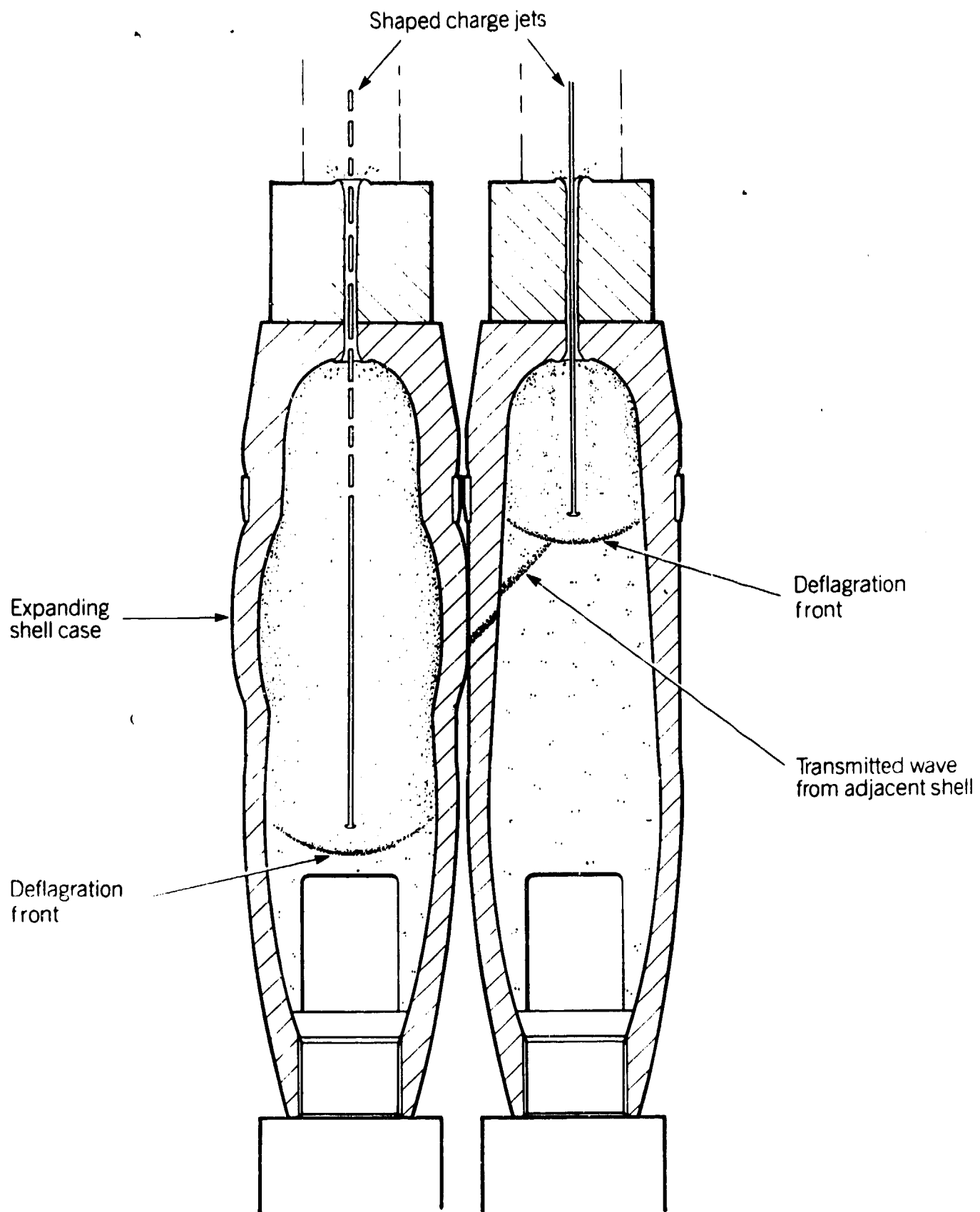


FIGURE 11.
ILLUSTRATION OF DEFLAGRATING
SHELL INTERACTION
1381

CONTINUED KLOTZ CLUB TESTS

by

Bengt E Vretblad

**FortF - Royal Swedish Fortifications Administration
Eskilstuna, Sweden**

**The opinions expressed in this paper are not necessarily those
of the Klotz Club.**

ABSTRACT

The Klotz Club has been performing tests in Sweden to get more data in particular on fragments thrown from detonations in rock storages. In 1989 two tests were made to illustrate the effectiveness of a berm in front of the storage entrance to reduce the hazardous zone.

INTRODUCTION

At the 22nd DDESB meeting, in Anaheim, California, 1986, the Klotz-Club and parts of the work within it were described and some results from an initial test series with detonations in an installation in rock were given, /1/. At the 23rd DDESB meeting, in Atlanta, Georgia, 1988, a further analysis of data from this test series was presented together with data from additional tests with higher loading densities, /2/. In 1989 a berm was built in front of the entrance, the purpose of which was to permit studies of its effectiveness to reduce fragment velocities and fragment throw and thus reduce the hazardous zone in front of a munition storage.

TEST OBJECTIVES

The test series was designed to give data on

- * fragment dispersion and

- * blast propagation

and how these were influenced by a berm in front of the tunnel.

THE INSTALLATION

The installation, when originally built, was designed to meet with the requirements

- * Chamber volume 200-300 m³
- * Smooth walls of access tunnels
- * Fragment-trap geometry
- * Fragment collecting area in a sector in front of the installation.

As the main objective with the installation was to make multiple tests with debris a site had to be selected where large amounts of explosives could be detonated without impairing the community, where competent rock with adequate rock cover could be found and at the outside of which a surface suitable for collecting fragments could be arranged. This led to the shooting range at ArtSS, Älvdalen, Sweden.

Outside the entrance cutting a sector -5° - $+10^{\circ}$ from the tunnel axis from which fragments could be collected was made. The area was close to flat up to 150 m from the entrance and then steeper to form a target area in total more than 300 m from the tunnel. A road leads across the tunnel axis about 175 m from the entrance.

Figure 1 depicts the geometry outside the installation.

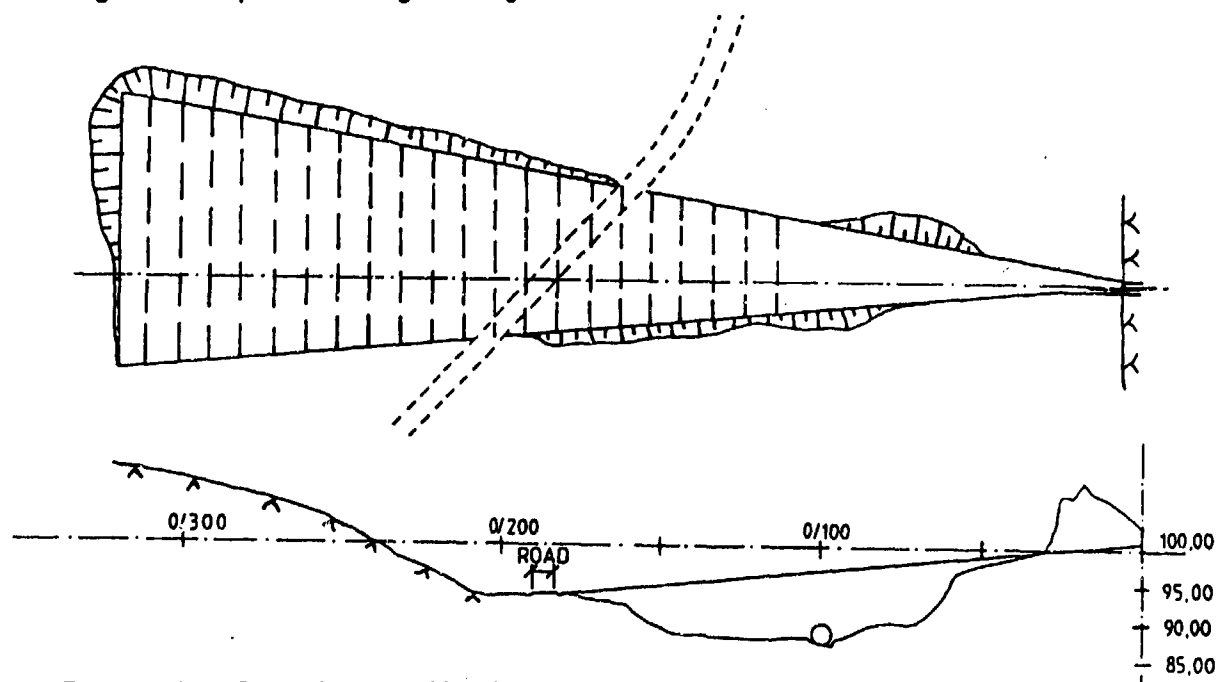


Figure 1. Geometry at the test site

The tunnel cross-section is 6.3 m^2 . The walls are shotcreted. In the end of the tunnel is a chamber with a cross-section of 12 m^2 and a volume of 300 m^3 e.g. a length of about 25 m designed. In 45° to the tunnel is another tunnel with the same cross-section. At the end of one end of that tunnel is a 17 m long chamber with a volume of 200 m^3 . At the other end of it there is a 10 m long tunnel with the purpose of collecting debris and fragments coming out of the 200 m^3 chamber.

The entrance part of the tunnel is made of reinforced concrete to ascertain that the geometry would not change during the test series. Also to facilitate a comparison with other test data a well defined geometry is needed.

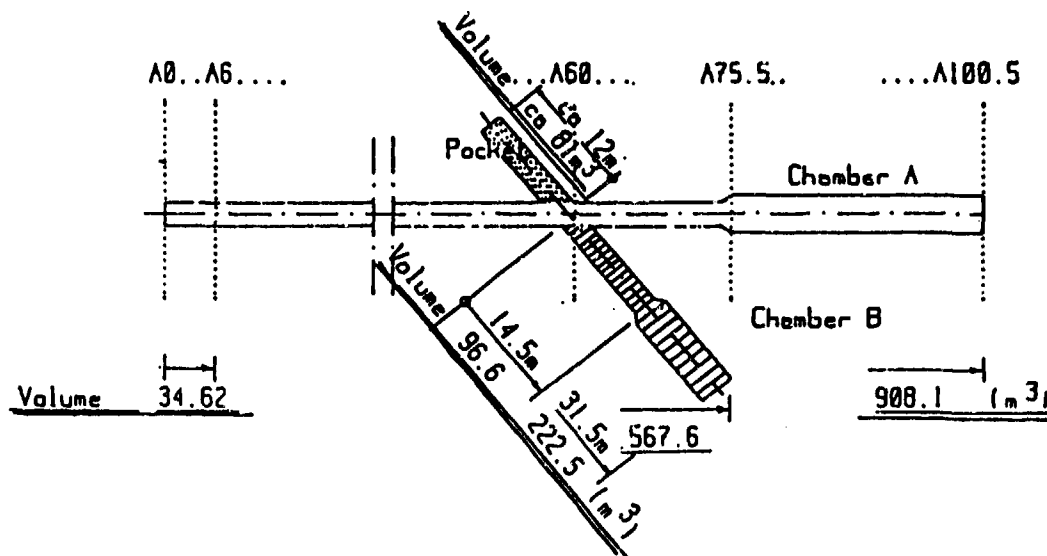


Figure 2. The installation

According to different manuals for storage of munition in rock a berm in front of the entrance to the installation may be used to decrease the risk of fragments reaching far.

Different designs of berms have been discussed. Relevant to such designs are:

1. To prevent exiting fragments from the installation to rebound the angle between the barricade and the tunnel axis should be large.

2. As the fragments, e.g. due to impacts on the tunnel walls, can not all be considered to have trajectories parallel to the tunnel axis the berm must have a larger crosssection than the tunnel. From earlier Klotz Club tests, /1,2/, the angle sidewise from the tunnel axis in which most fragments were recovered was found to be very small, however.
3. The mass of the berm should be large enough not to be displaced by the blast and the fragments, nor should it be penetrated nor eroded by these.

The considerations led to a design according to figure 3 for the berm.

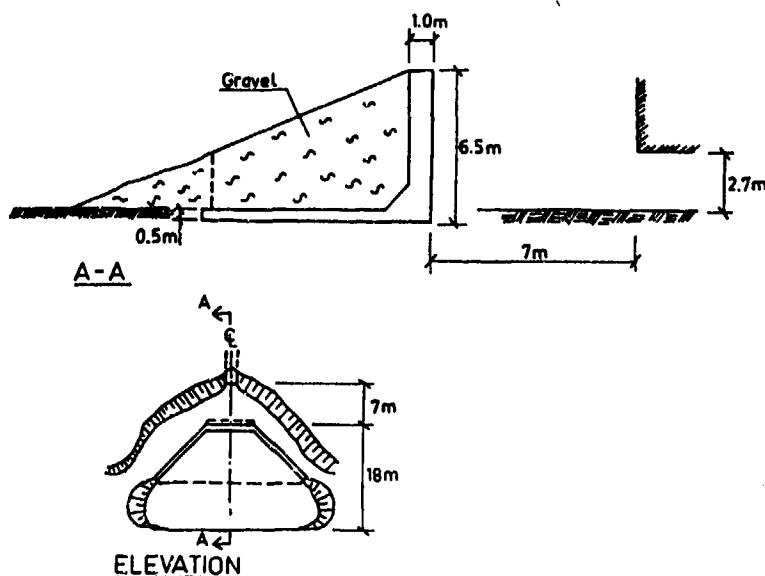
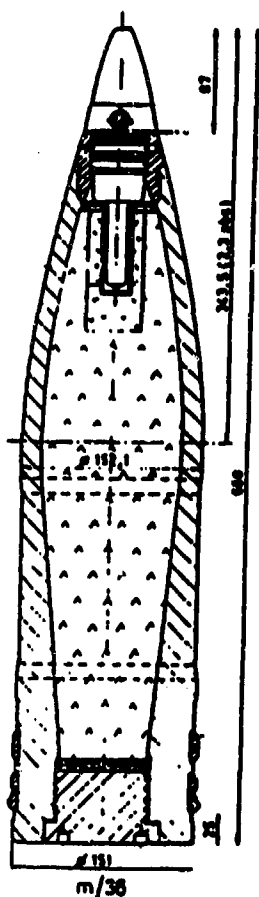


Figure 3. Measures of the berm.

The berm was made of reinforced concrete. The front wall was made 1.0 m thick and the sidewalls as well as the bottom slab were made 0.5 m thick. The barricade was after concreting backfilled with gravel material.

The tests were designed to be identical to the earlier performed tests #5 and #8, see /2,3/. Conclusively, for the first test with a berm (test #10) the charge comprised 180 projectiles m/36 in chamber A, see figure 4, and for the second test (#11) a stack of ANFO-bags totalling 5 tons were placed also in chamber A.



Masses

Projectile empty	39.190 kg
TNT	5.450 kg
In total	<u>44.640 kg</u>

Figure 4. Projectile m/36.

MEASUREMENTS

Measurements were made of blast and fragments.

Blast measurements

The transducers for blast pressure measurements were placed according to figure 5.

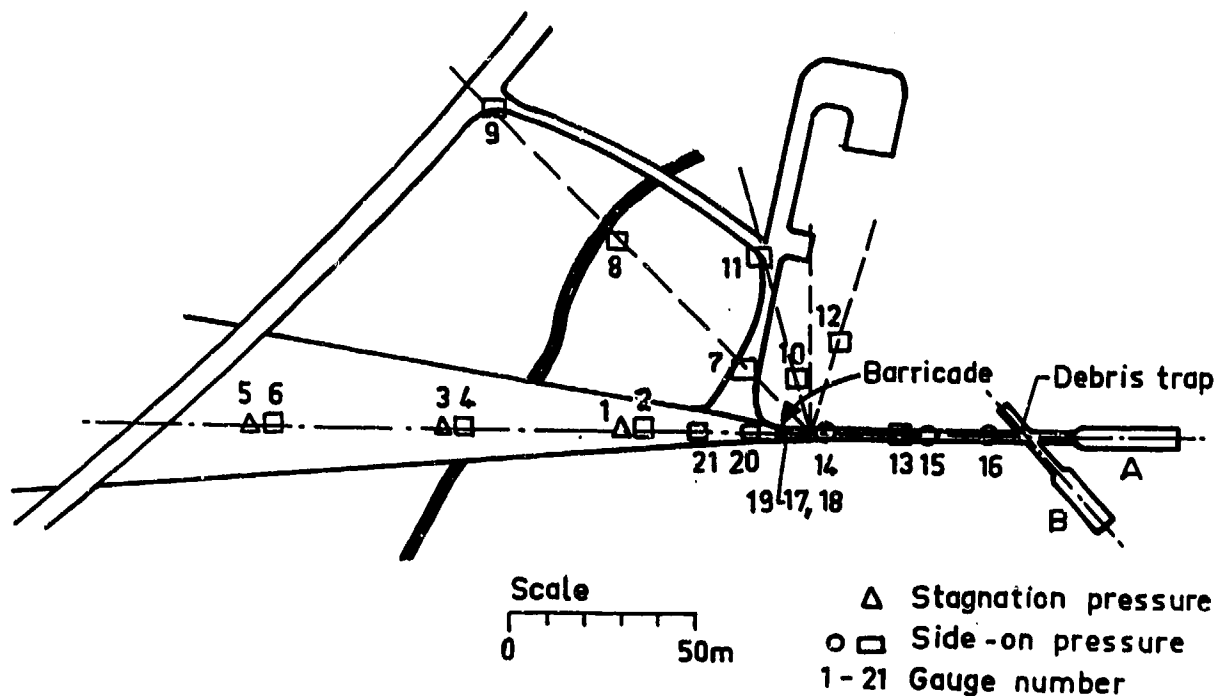


Figure 5. Positions for the airblast gauges.

The side-on pressure gauges outside the installation were PCB 113A51. For stagnation pressure Kistler 412 transducers were used. In the tunnel system PCB 113A24 gauges were placed.

The gauges outside the tunnel were placed about 0.5 m above the ground surface.

Additionally, passive gauges consisting of nails were placed in the side-walls of the berm to give indication of the direction of the drag pressure.

Smoke puffs

The fragments and their trajectories will be influenced more by the dynamic pressure than the static pressure. For the analysis of fragment data, therefore, the static pressure only is of limited value.

12.

The blast wave from a detonation leaves the air in a state of spatially varying entropy. From this follows, that there is no functional relationship giving one distinct relation between various thermodynamic properties of the air. This means e.g. that it is not possible by measuring the time variation of the side-on pressure to have the time variation of the dynamic pressure at the same location.

The dynamic pressure on the other hand is often difficult to measure. In particular, the difficulties increase when fragments are present as these might destroy the types of gauges usually used.

However, a technique with smokepuffs has been developed and used with very satisfactory results at the University of Victoria by Professor John Dewey and his coworkers /4/.

By placing smoke puffs in the air just before the blast arrives it is possible to identify different points and study the movements of these points as the blast arrives. The directions and velocities of the displacements can then be used to characterize the flow at the different points.

The analysis of the smoke puff tracers can provide the flow at different heights and at different distances.

References on the technique can be found in /4/.

The design of a smoke launcher is shown in figure 6.

The base of the launcher is a 50 mm diameter steel pipe cap with a short steel nipple attached. A 0.6 m long, 50 mm diameter, plastic tube is threaded to the steel pipe. In the pipe gunpowder and a detonator are placed. Cotton wadding is used to contain the propellant. A wooden block fitting into the tube is placed on top of the cloth to act as a driver of the tracer material placed in an inner plastic pipe, with 38 mm diameter, on top of the block.

Both black and white smoke powder were used. The white powder was an approximately 20:1 mixture of fumed silica and titanium dioxide while the black powder was carbon black.

The launchers were triggered to ignite after the high-speed cameras had started and before the blast arrived.

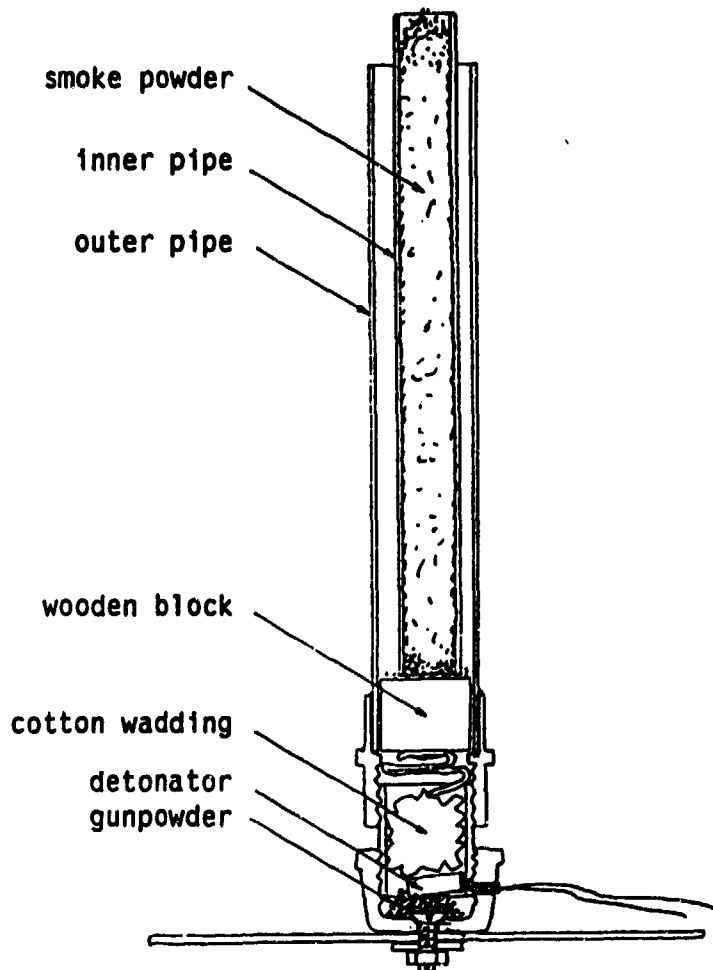


Figure 6. Smoke launcher (from /4/)

The smoke trails were established in a vertical plane above the berm in front of the tunnel exit and along the tunnel axis. Figure 7 and figure 8 show the positions of the launchers.

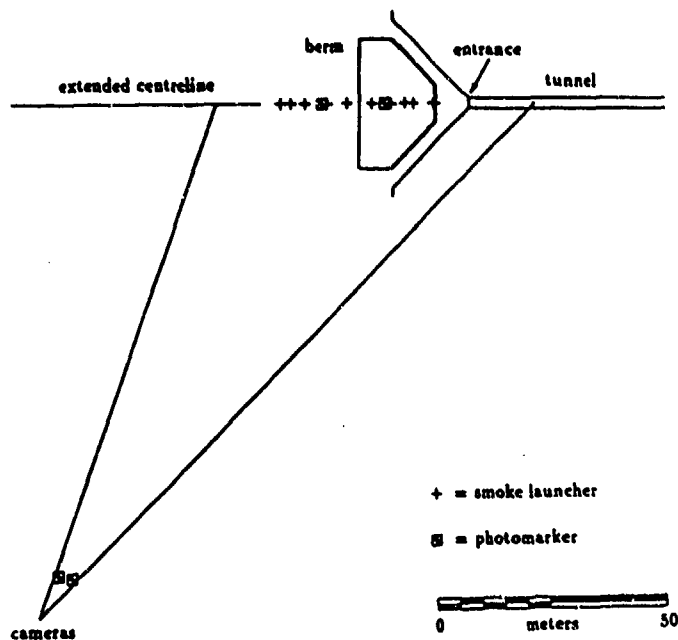


Figure 7. Plan layout of smoke launchers, photomarkers and cameras, cfr /5/

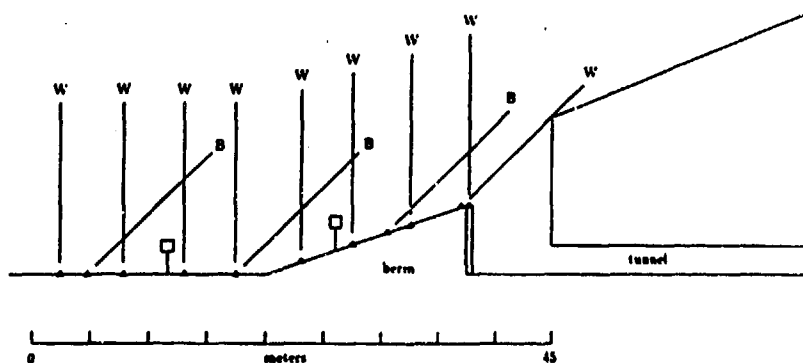


Figure 8. Elevation view of launchers and photomarkers, cfr /5/
W = white smoke, B = black smoke.

The figures also show the positions of the photomarkers and the 16 mm high-speed cameras. Two LOCAM cameras at nominally 500 pps and one HYCAM camera at nominally 1000 pps were used. Two of the cameras were operated by the Norwegian Geotechnical Institute. The same Institute also made a survey over the site to determine the relative positions of cameras, markers, launchers and the tunnel system. These positions were needed for the smoke puff analysis.

Recording and data reduction systems

A Sangamo Sabre tape recording system with a 14 tracks 1" tape FM IRIG WBI was used. Together with it was also used a digital recording system John & Reilhofer 8K13 with 8 channels.

The data reduction was made with MEDUSA software.

Fragments

In shot #10 the fragments were from the artillery projectiles, while in shot #11 artificial fragments were sawn out of steel plates and put into wooden boxes. The boxes were placed close to the charge.

The steel fragments were in three sizes weighing 50 g, 100 g and 500 g. Each box contained 250, 125 and 41 kg of each, respectively. The total weight of the steel fragments in each box was therefor 416 kg. 12 boxes were used giving a total of 5000 kg. The boxes were placed around the outmost half of the charge as earlier tests have verified that the fragments at the inner end remain in the chamber and do not cause hazards at the outside.

Additionally, artificial debris in the shape of and with the mass approximately like the artillery rounds for the test #10 were used. These debris were 680 mm long 160 mm diameter steel pipes filled with concrete. The mass was 47 kg.

Pairs of cylinders were placed on the floor of the tunnel at four locations.

To make a detailed study of the trajectories of the ejecta easier the area outside the tunnel was prepared with timber logs laid down perpendicular to the tunnel axis at 10 m interval. Highspeed cameras and videocameras were placed perpendicular to and along the tunnel axis. Some areas were cleaned and other covered with plastic to facilitate the recovery of fragments.

TEST EXECUTION

The explosives were put in the center of the chamber. The 180 artillery projectiles were charged individually. The 5 ton ANFO charge was initiated at six different locations in the explosive.

The first shot was executed on August 30 and the second shot was fired on September 20. At both events the weather conditions were excellent for testing.

Just before the detonation of the charge the highspeed cameras and the video cameras were started and the smoke puffs launched. The execution of the test was followed from an observation post.

After each shot the entrance to the tunnel had to be secured and the toxic gases must be ventilated. For this purpose a plastic hose was put into the tunnel and connected to a ventilating equipment. The day after the shot the air in the tunnel was good enough to permit people to go into the installation.

After the tests the fragments were collected carefully in the tunnel system and outside the installation.

TEST RESULTS

Blast pressure

As the geometry outside the installation is very specific to the site selected a detailed comparison of blast measurements around the installation can only be made between the different shots and not with e.g. design code values based on more ideal geometries.

In figure 9 such a comparison is made for shots #7-11. Shot #7 was with 1

ton HE while #8 and #9 were with 5 tons HE (shot #9 was executed in chamber B the other four in chamber A.

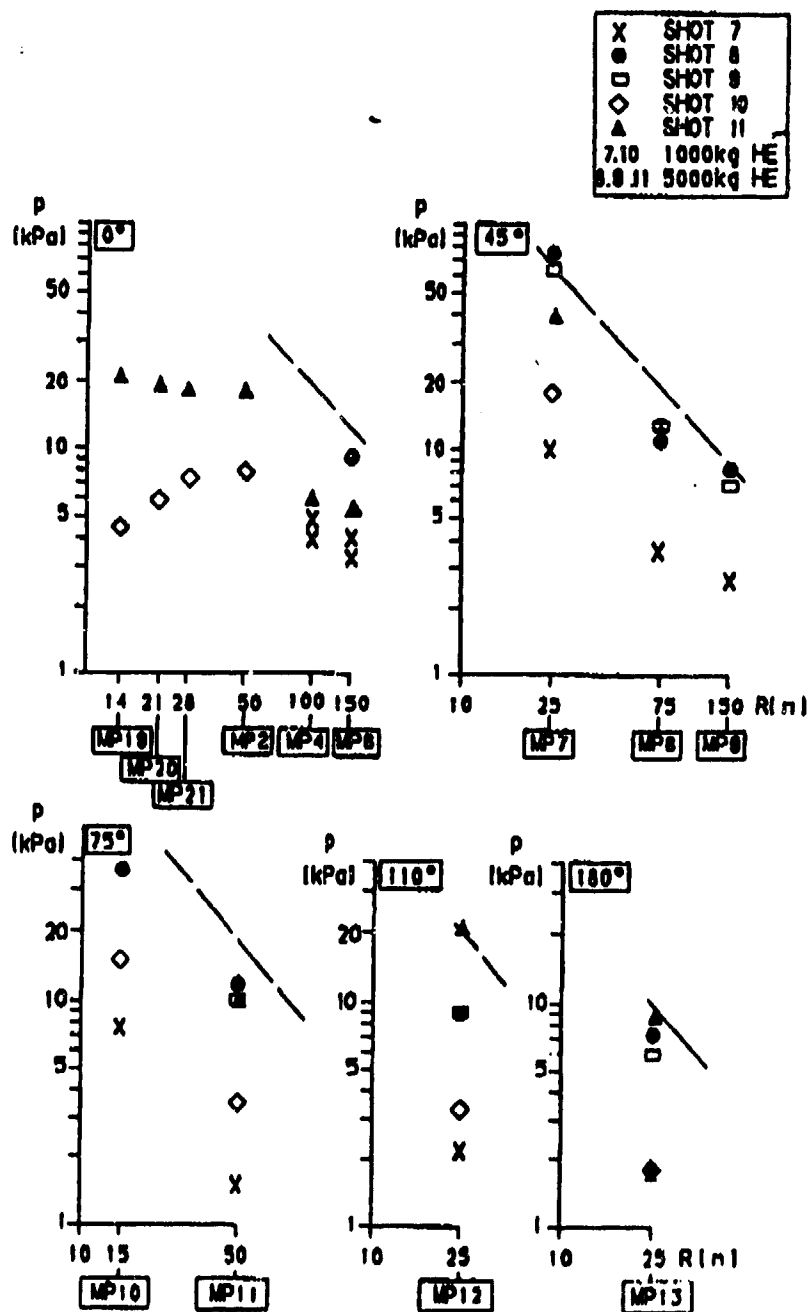


Figure 9. Pressure outside the tunnel compared with corresponding results from earlier tests. The line gives maximum pressure according to the Swiss doce TLM75.

Smoke puff measurements

Only the smoke puff registrations from the 5 ton shot were analyzed in detail, /5/. All the launchers worked successfully. However, the black smoke puffs were difficult to observe in the highspeed films why certain features in the white puffs were used in the analysis instead of the crossings between white and black smoke. The high-speed film from one LOCAM camera could be used while the event was not successfully recorded on the other two cameras at the 5 ton event.

The analysis is given in detail in /5/ and compared with precalculations from /6/ and measured pressures.

Figure 10 shows pressures according to the measurements and the smoke puff analysis along the tunnel axis.

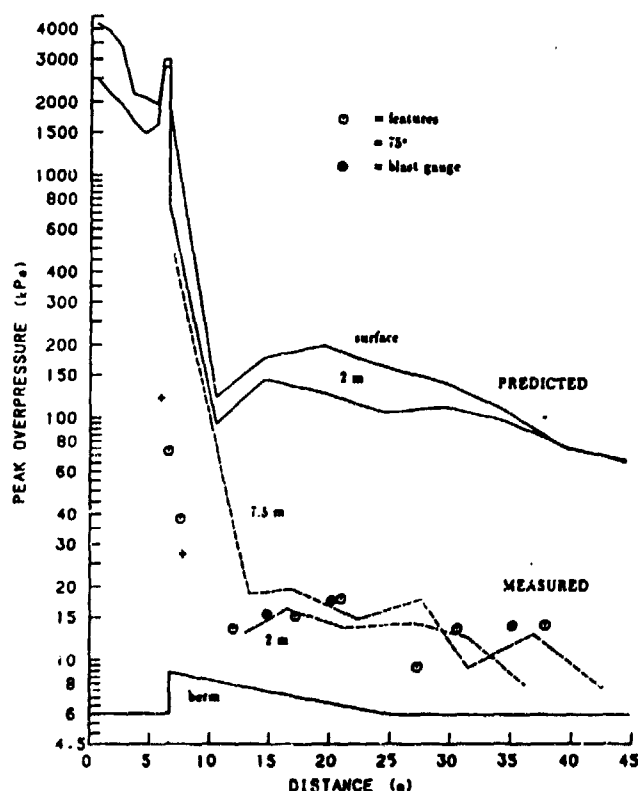


Figure 10. Pressures along the tunnel axis. (From /5/.)

The pressure calculated from the smokepuff analysis is in good agreement with the pressure measurements. The comparison between the S-CUBED calculations and measurements is presented in /7/.

The direction of the drag could be studied from the inclination of the passive nail gauges, see figure 11.



Figure 11. Nail gauge on the sidewall of the berm showing the direction of the drag pressure.

4.2.2. Fragments

The fragments were produced by the ammunition upon detonation and were found along the berm in shot #11. The fragments found along the berm were identified, weighed, and measured.

There was a distinct difference in the fragment dispersion pattern between the two shots.

At the first shot (#10) the loading density was low, about 3 kg/m³. At this shot about half of the fragments remained in the inner part of the chamber as could be expected. The other half of the fragments were spread out in the tunnel and outside it. In total more than 95 % of the initial fragment mass was found within the chamber and the tunnel. The fragments outside were found in the close in area just in front of the berm and near it. No fragments were found more than ten meters from the entrance to the tunnel. Obviously, the berm was very efficient in stopping fragments at this test.

At the second shot the loading density was higher, about 16 kg/m³. This time, there were less fragments in the tunnel than at the first shot. Also, the dispersion pattern outside the entrance was considerably changed from the first shot. Many fragments remained in front of the berm, cfr figure 11, but at this event also a substantial amount of fragments were spread out around the installation. Fragments were found above the tunnel and, in particular, along the entrance- and exit ways to and from the tunnel. These were in about 45 degrees from the tunnel axis. Fragments were collected at distances up to about 200 m from the tunnel.

Note in figure 12, that the shape of the tunnel can be identified at the berm by the hits of fragments on the wooden scaffolding. The figure clearly illustrates how the fragments follow trajectories close to parallel with the tunnel axis.



Figure 12. Fragments in front of the berm outside the tunnel.

Some, but few, fragments were found behind the berm. The fragment density was calculated and compared with the fragment density at shot #8, where the conditions were identical but for the berm in front of the tunnel entrance. The results are shown in figure 13. Behind the berm the fragment density is orders of magnitude lower than if no berm was present. Close to the tunnel in about 45 degrees the fragment density is similar to the fragment density without a berm.

Also, as can be seen in the figure the fragment density at far distances, where the berm is not a direct obstacle is almost the same as along the tunnel axis with no berm. Obviously, with the higher loading density the berm redirects the fragments. This means that it could be possible by using a berm to decrease the amount of fragments in certain directions.

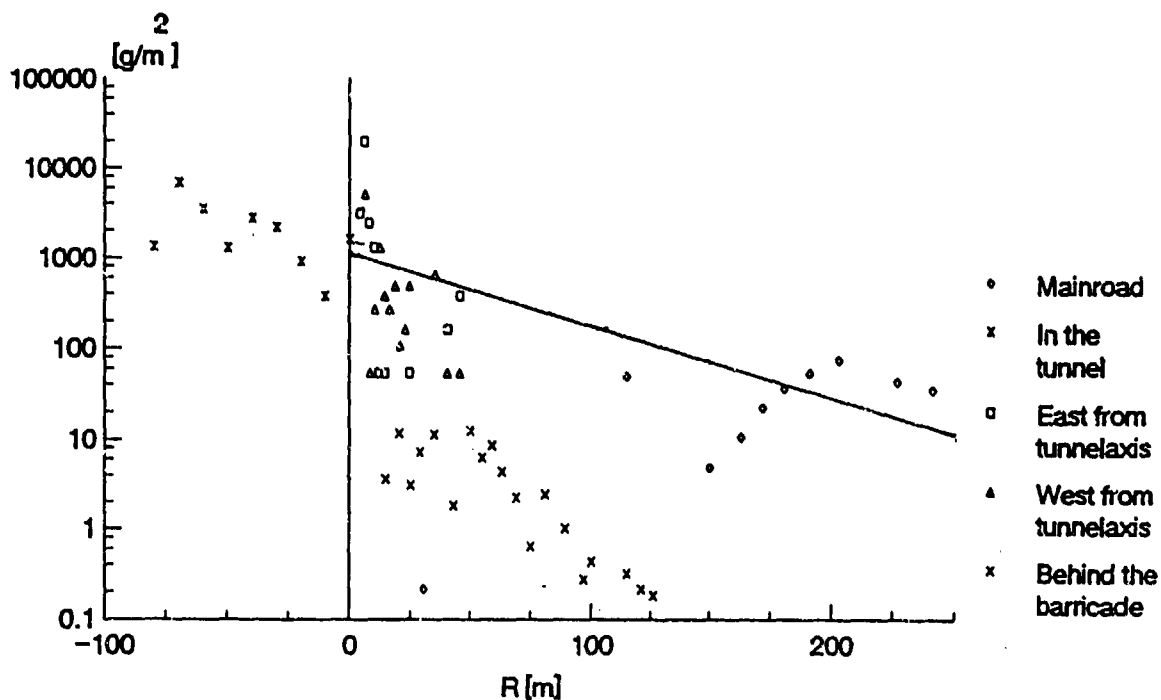


Figure 13. Fragment density vs distance from tunnel entrance.

CONCLUSIONS

The tests performed show that a berm in front of the entrance to a munition storage in rock can be highly efficient in decreasing the flow of fragments outside the storage at low loading density and thereby reduce the risks outside it.

At higher loading densities the berm can redirect fragments.

The design of the berm used in the tests did not prevent fragments from going far from the tunnel entrance. It remains to be studied how effective a design can be worked out.

ACKNOWLEDGEMENTS

In the planning and during the execution of the tests many valuable suggestions have been made by members of the Klotz Club and of the Steering Committee. Excellent efforts have also been made by a lot of individuals among these and at ArtSS and FortF.

Professor John Dewey has made a dedicated work with the smokepuff measurements and Mr Jan Kristiansen of the Norwegian Geotechnical Institute has made on site survey measurements and operated the highspeed cameras. This has been made under a contract from the Norwegian Defence Construction Service on the initiative of Mr Arnfinn Jenssen. Precalculations of the blast has been made at S-CUBED by Mr Charles Needham and Dr Lynn Kennedy and coworkers.

The author is most grateful for all dedication and excellent achievements during all stages of the project.

REFERENCES

- /1/ Vretblad, B, Klotz-Club Tests in Sweden. Minutes 22nd Explosives Safety Seminar. Anaheim, California, 1986.
- /2/ Vretblad, B, Klotz-Club Tests in Sweden. Paper presented at Department of Defense Explosives Safety Seminar, Atlanta, 9-11 August, 1988 and FortF Report C6:88.
- /3/ Vretblad, B, Data from the 1987 Klotz Club tests in Sweden. FortF Report C3:88.
- /4/ Dewey, J M & McMillin, D J, Smoke Puff Photogrammetry China Lake Tunnel Test. NDCS October, 1989.

- /5/ Dewey, J M & McMillin, D J, 1989 Älvdalen tunnel test. Smoke puff photogrammetry. NDCS, July, 1990.
- /6/ Kennedy, L W, Schneider, Kenneth D and Crepeau, Joseph E, Prediction Calculations for Klotz Club Tests in Sweden. S-CUBED (A Division of Maxwell Laboratories, Inc.) Report SSS-TR-89-11049, 1989.
- /7/ Kennedy, L W, Pre- and Post- Test Calculations for the Alvdalen 5000 kg Tests. Department of Defense 24th Explosives Safety Seminar, St Louis, Aug 27-30, 1990.

Pre- and Post-Test Calculations for the Älvdalen 5000-kg Tests

**Lynn W. Kennedy, Kenneth D. Schneider, Joseph E. Crepeau,
and Charles E. Needham
S-CUBED, A Division of Maxwell Laboratories, Inc.**

Abstract

In support of the 5000-kg test performed by the KLOTZ Club in the summer of 1989 at Älvdalen, Sweden, S-CUBED undertook a series of calculational simulations using our second-order hydrocode, SHARC. These simulations included a two-dimensional, rigid-wall calculation of the interior and two three-dimensional calculations of the exterior. Drag-sensitive particles were included in the interior calculation to simulate the steel-plate fragments and 155-mm shells used in the test as artificial debris. Cross-sectional area measurements from the tunnel interior were used to incorporate wall irregularities in the calculation corresponding to actual measurements.

Two versions of the exterior calculation were completed. One included the 7-m high berm in front of the tunnel exit; the other was done without the berm. Both of these included a representation of exterior terrain features. The exterior calculations were continued until the shock had traveled to a range of more than 100 m from the tunnel opening. Because the results of the pre-test calculations did not agree as well as had been expected with the experimental data, the interior calculation and a portion of the exterior calculation with berm were repeated after the test.

Results from these calculations are shown, and comparisons with experimental data are made where they are available. Suggestions are made which may improve calculational/experimental correspondence in the future.

1. Interior Calculations

The interior layout for the test simulated by the calculations reported here is shown in Figure 1. The tunnel complex consisted of an explosion chamber, Chamber A; an entrance tunnel; a "debris catcher"; and a side chamber, Chamber B. The tunnel was about 6 m wide; length dimensions

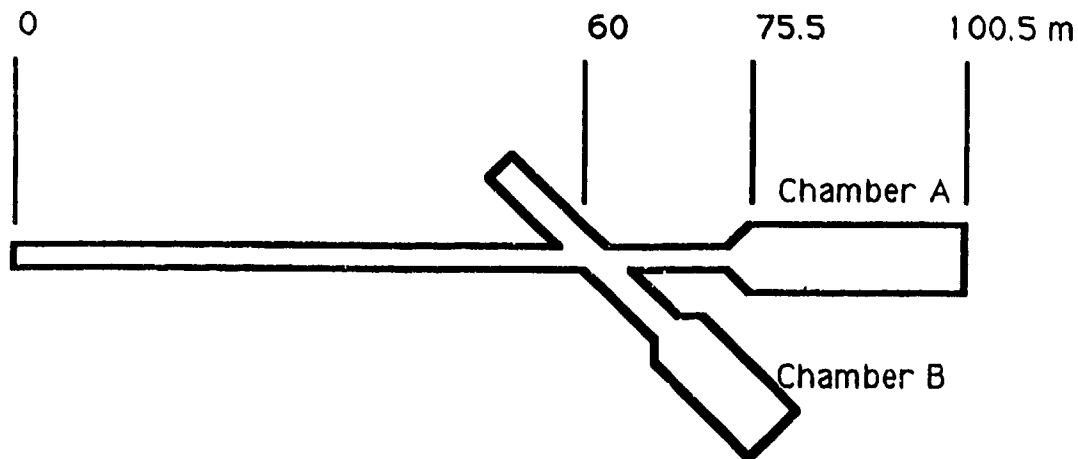


Figure 1. Internal Tunnel/Chamber Complex Layout

are shown in the figure. The test explosive consisted of 5000 kg of ammonium-nitrate/fuel-oil (AN/FO) in bags, stacked twelve high on a wooden pallet in Chamber A.

The interior calculation was set up to model the actual test configuration as closely as possible. From cross-sectional measurements of the chamber, a pattern of irregularities in the walls was defined to simulate the actual wall roughness. Because area measurements were available for only the back 5 m of Chamber A, this pattern was reflected end-for-end and across the centerline to provide a somewhat random distribution of wall roughness elements along the length of the chamber. The result for Chamber A is shown in Figure 2. This is a plan view; the calculation was two-dimensional, so a unit height for the entire internal configuration was taken at 2.3 m. The dotted lines in the figure indicate the locations of stations, at which calculated values of hydrodynamic parameters were saved as functions of time.

Figure 3 illustrates the calculational setup for the explosive charge and boxes of debris particles stacked in front of it. Because of the two-dimensional simulation, charge dimensions had to be altered somewhat in order to retain the appropriate total yield. The eight detonation points are shown, as are the initial locations of the debris particles, which were modeled as drag-sensitive massive spheres.

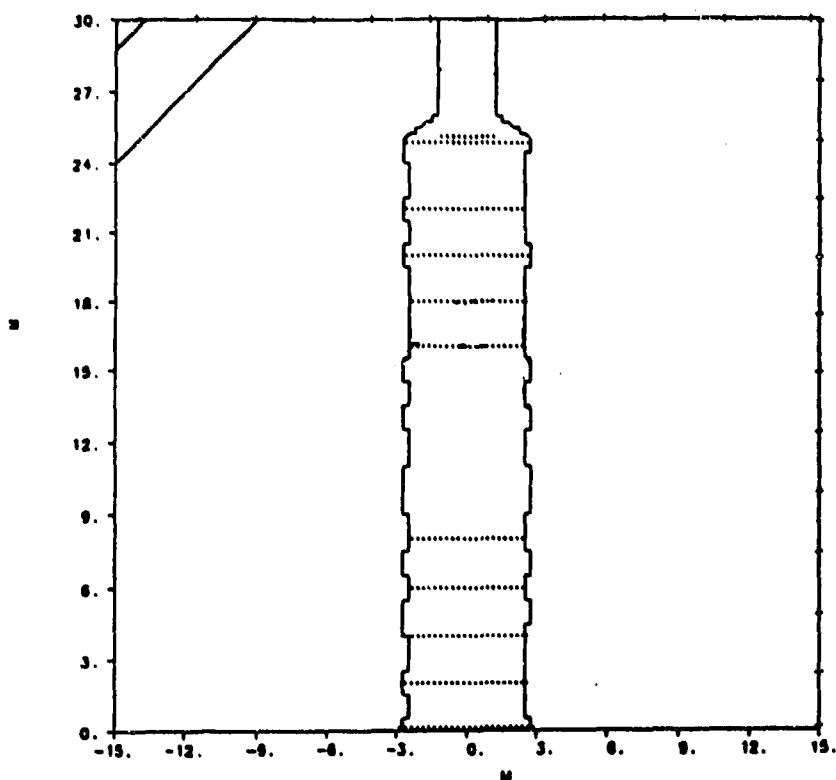


Figure 2. Outline of Chamber A in Calculation

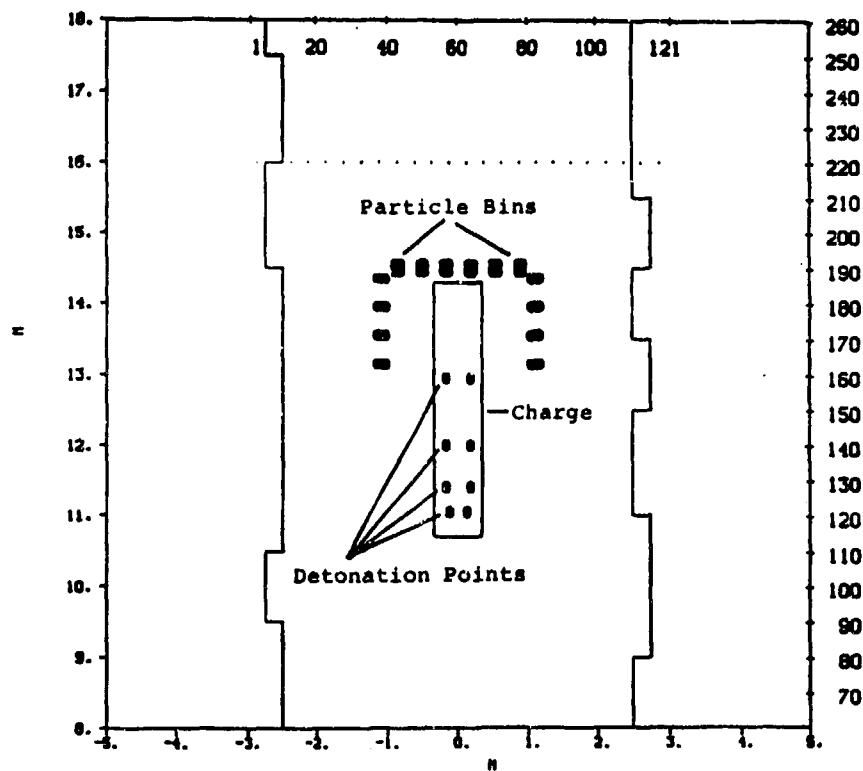


Figure 3. Detail Showing Charge as Simulated in Calculation

2. Exterior Calculations

For the exterior portion, the calculation was transferred to a three-dimensional mesh. Boundary conditions from the interior portion were fed in at a plane within the tunnel, 25 m back from the opening. The plan view and elevation sketch of Figure 4 illustrate the general configuration as it was defined for us. A long, triangular apron slopes downward from the mouth of the tunnel. Beyond the road, the slope is upward. On each side of the tunnel mouth, there are embankments formed by cutting away the mountain to build the portal. In Figure 5, details of the berm, which was placed in front of the mouth as a blast deflector and debris catcher for the 1989 shot, are shown. The berm was 7 m high, and consisted of a concrete facing wall filled in with dirt on the downslope side. As shown, the berm was 7 m from the tunnel opening.

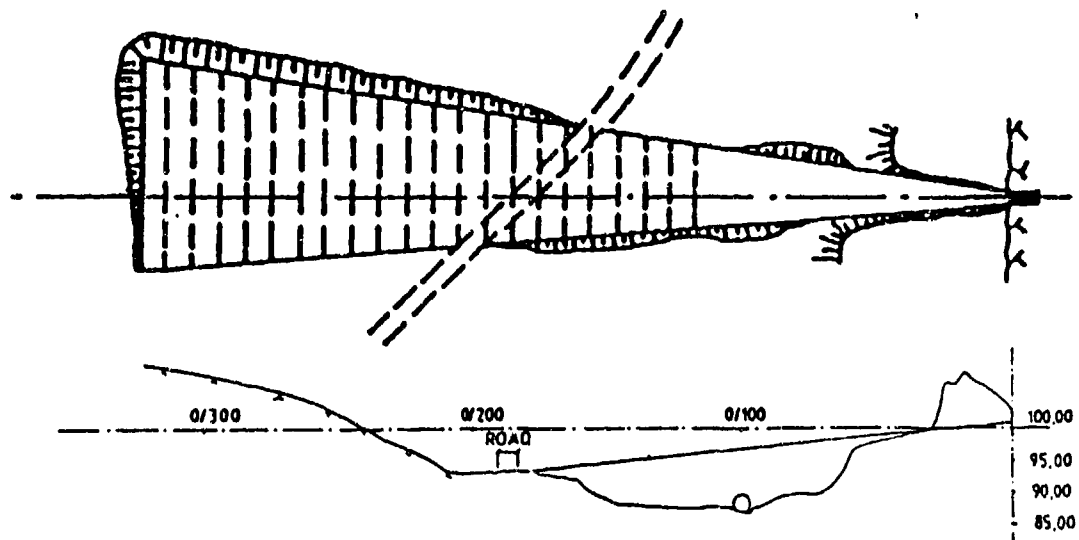


Figure 4. Exterior Plan View and Elevation Sketch

An earlier test event, in 1987, used essentially the same configuration without the berm. The embankments at the sides were carved away slightly to allow for placement of the berm. Figure 6 shows the configuration as modeled in the calculations. To save calculation time, only half of the test bed was modeled. A mirror image was assumed, reflected at the tunnel centerline. Figure 6 is the configuration without the berm. The tunnel opening (actually, half of the tunnel opening) can be seen at the back on the right. The berm configuration is identical except for placement of the berm in front of the tunnel opening.

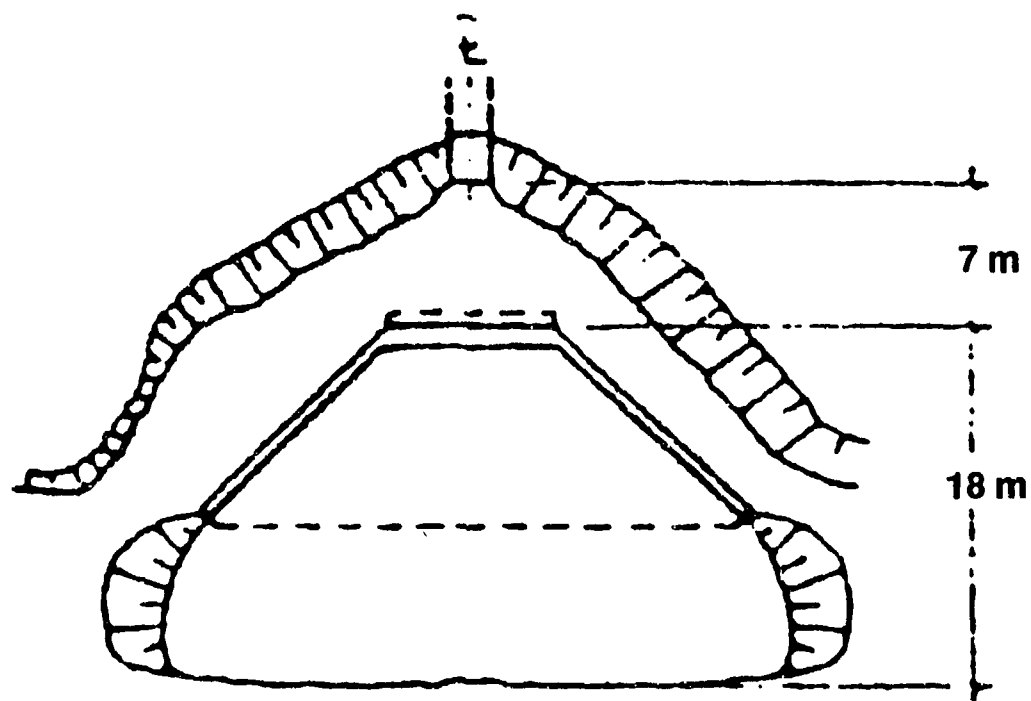


Figure 5. Exterior Detail and Berm

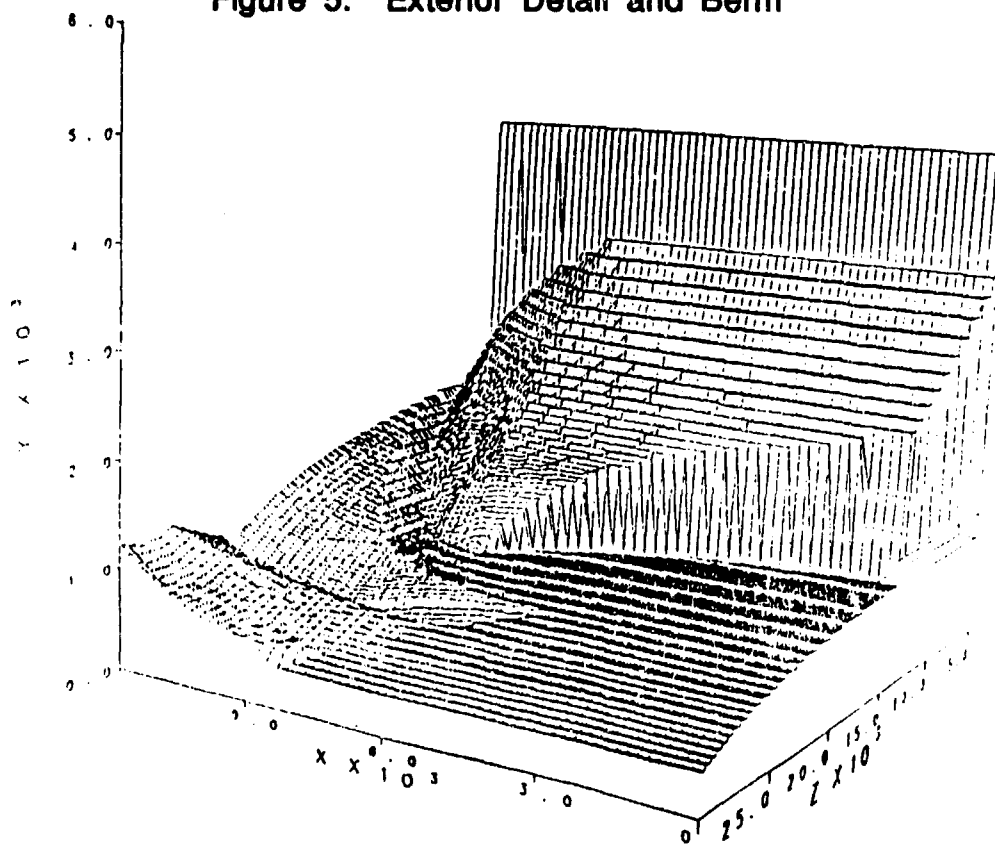


Figure 6. Terrain Plot Without Berm

3. Results

The results of the pre-test calculations were not in good agreement with the experimental data, so they are not presented here. They are documented in our report on the subject*. Figure 7, which was prepared by Dr. John Dewey for his report on the smoke-puff photography for the test, illustrates these results. Maximum overpressure amplitudes predicted by the calculations were in some cases as much as an order of magnitude above those observed. Because of this, we looked very carefully at the calculations in order to determine the cause of the discrepancy. Previous

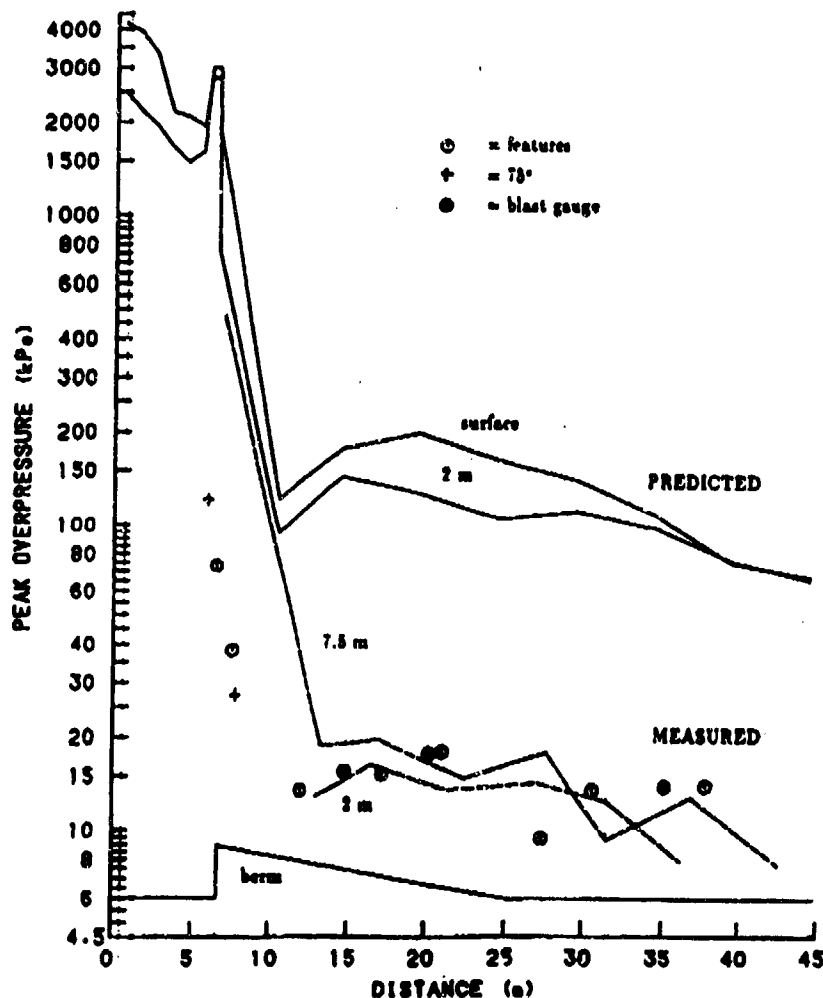


Figure 7. Comparison of Pre-Test Calculational Results with Experimental Peak Overpressures, as Functions of Range

* L.W. Kennedy, K.D. Schneider, and J.E. Crepeau, "Prediction Calculations for KLOTZ Club Tests in Sweden," S-CUBED Report SSS-TR-89-11049, December 1989.

experience with our hydrocode made us certain that the basic calculational method was sound, but there were possibilities about the modeling assumptions that could be reviewed.

No serious mistakes were found in the way the calculations had been set up. We did find two areas where we had misinterpreted the information that was provided. First, we had understood that the volume of Chamber B, the side tunnel expansion chamber, was 126 m³. In actuality, it was 223 m³. Also, the total mass of the steel debris particles was 4992 kg, not 546 kg as we had thought. This latter misunderstanding occurred because the provided figures referred to numbers of kg of particles, rather than to numbers of particles.

Neither of these changes had large effects on the calculational results. What did make a difference was a revision we incorporated after talking with John Dewey and Charles Needham, experts who have been involved in high-explosive testing, and specifically in testing with AN/FO, for many years. They pointed out that, because AN/FO is a non-ideal explosive, it is difficult to get it to detonate completely in an unconfined configuration. The shock front in an AN/FO detonation may run 10 to 15 cm ahead of complete energy release, so that when this shock wave reaches the outer surface, it reflects as a tensile wave, causing the outer portion of the AN/FO to separate from the rest of the charge without detonating. Additional degradation can occur in non-spherical explosives if the shock reaches one free surface earlier than it reaches other free surfaces, as would occur with the rectangular shape and multiple detonation points for this test.

Based on this information, we deleted 8 cm of explosive from all free surfaces of the charge except the bottom (which was confined by the wooden pallet). The undetonated explosive could burn later, when exposed to the hot gases of the detonation products, but its energy would not contribute to the shock wave. The net result of this was that only 68%, or 3400 kg, of the AN/FO was retained for the post-test calculations. This change, as might be expected, had a significant effect on the results.

4. Results of Post-Test Calculation

Results of the post-test calculation are shown in the following figures. Figure 8 is a calculated overpressure waveform compared with an experimental record from inside the tunnel. It is from a point on the floor 25 m back from the portal. As can be seen, the correspondence is reasonable although not exact. Peak values at the wavefront are about the same, as are levels behind the front. Individual spikes can be attributed to differences in placement or sizes of irregularities on the tunnel walls. This leads to the conclusion that the interior and the AN /FO yield are being treated approximately as tested.

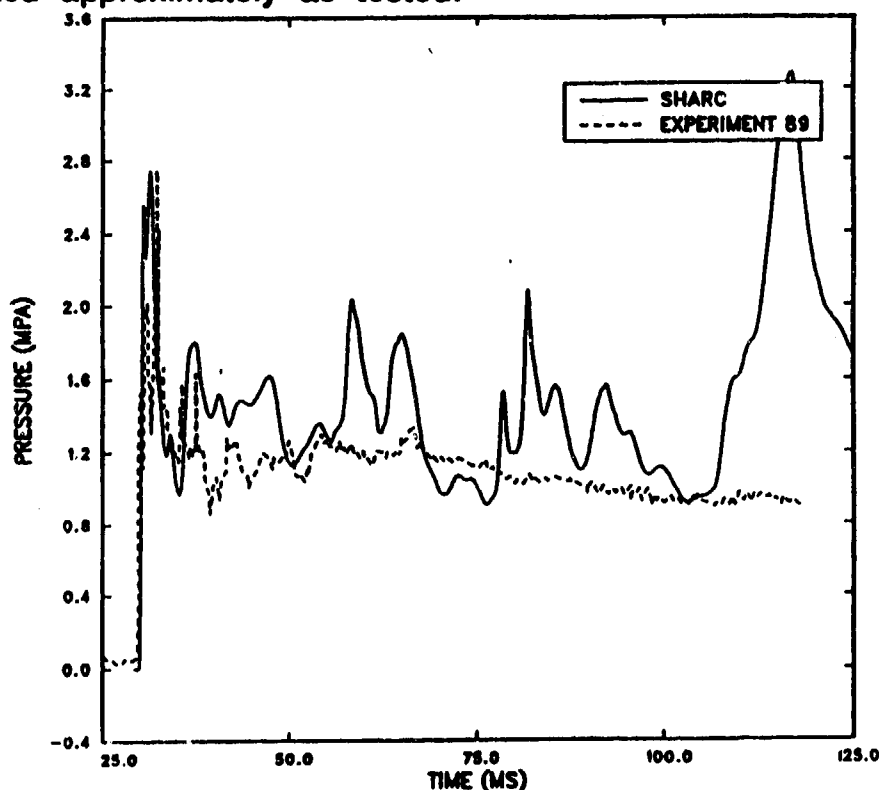


Figure 8. Comparison of Post-Test Calculation with Experimental Overpressure Record, 25 m Inside Entrance Tunnel

A different story emerges for the exterior. At the base of the berm (Figure 9), the calculated waveform appears to be high, both near the wavefront and behind it. At the top of the berm (Figure 10), there are similarities in the waveforms, but the calculated peak value is still high by a factor or two. A more definitive comparison appears in Figure 11, in which smoke puff displacement/time data is compared with a massless

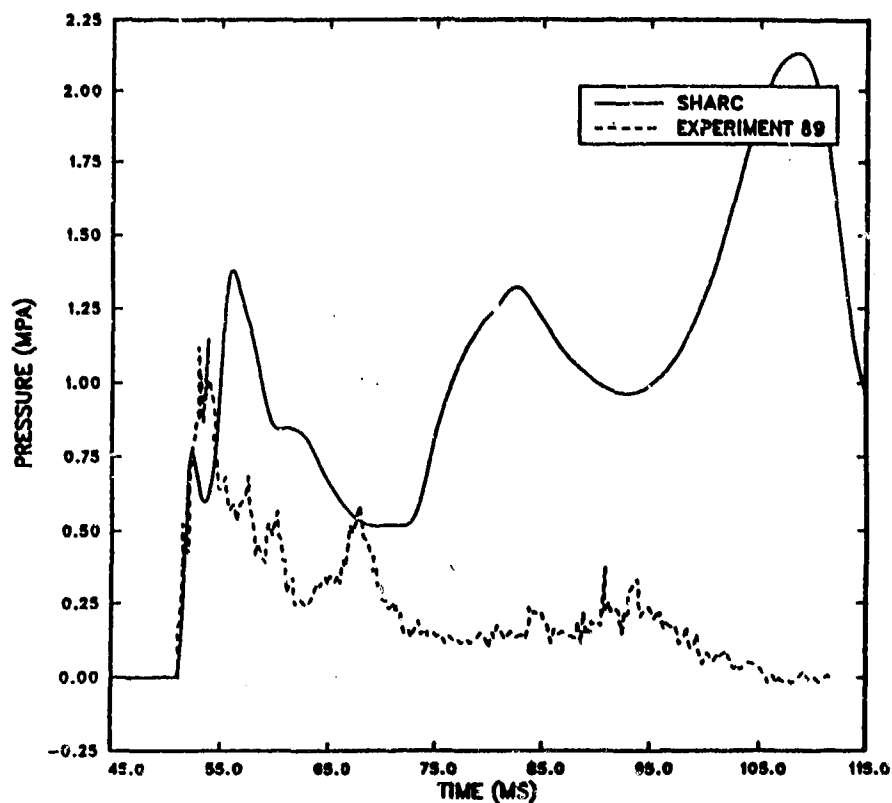


Figure 9. Comparison of Post-Test Calculation with Experimental Overpressure Record, at Base of Berm

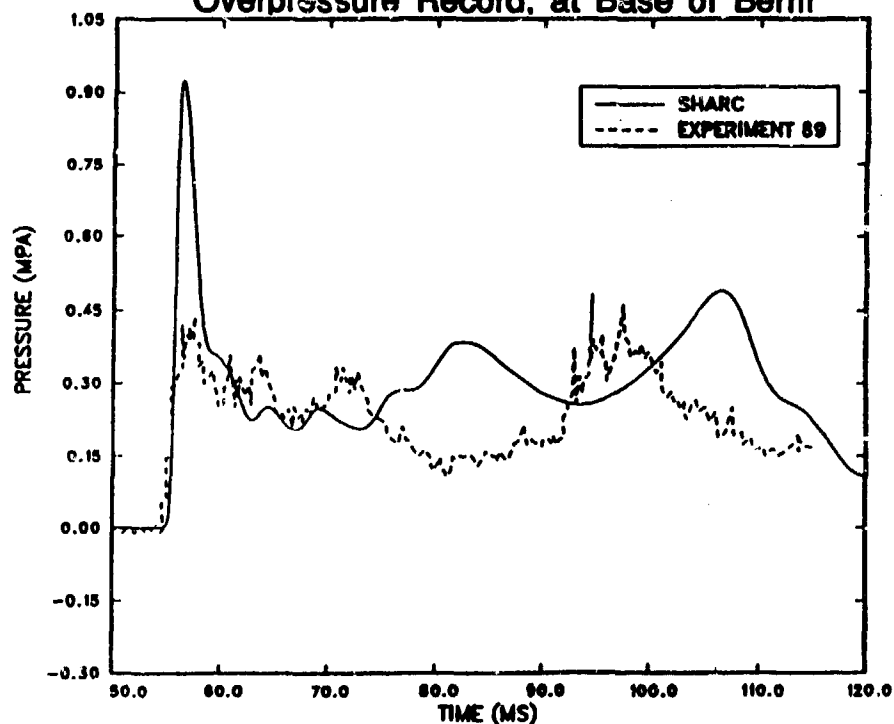


Figure 10. Comparison of Post-Test Calculation with Experimental Overpressure Record, at Top of Berm

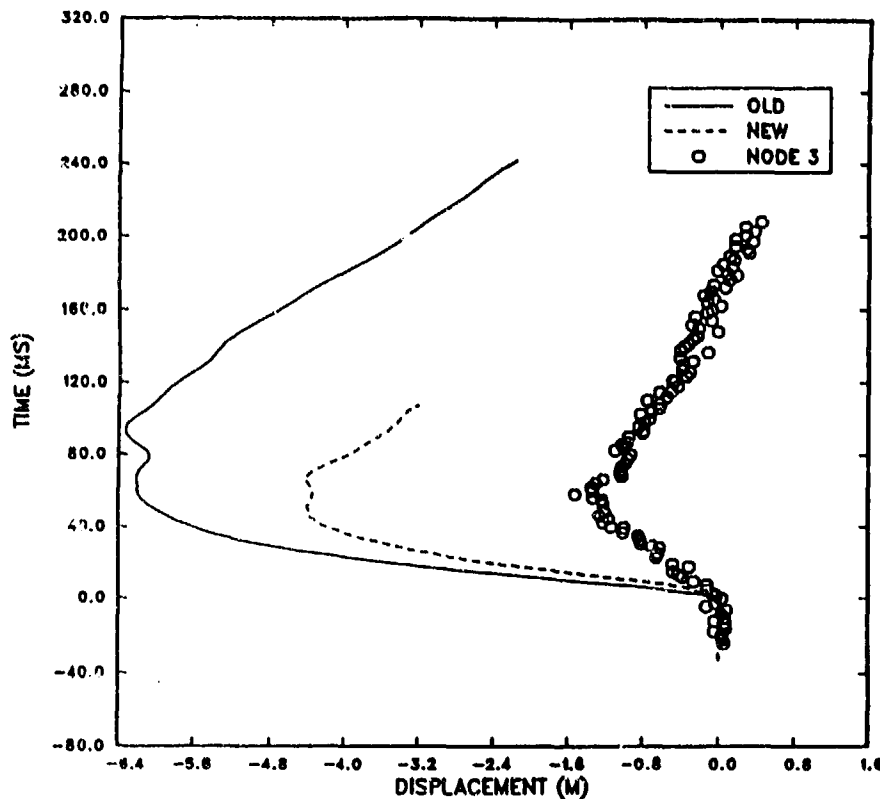


Figure 11. Comparison of Tracer Particle Record with Trajectory of Smoke Puff Node, 17 m from Portal over Berm

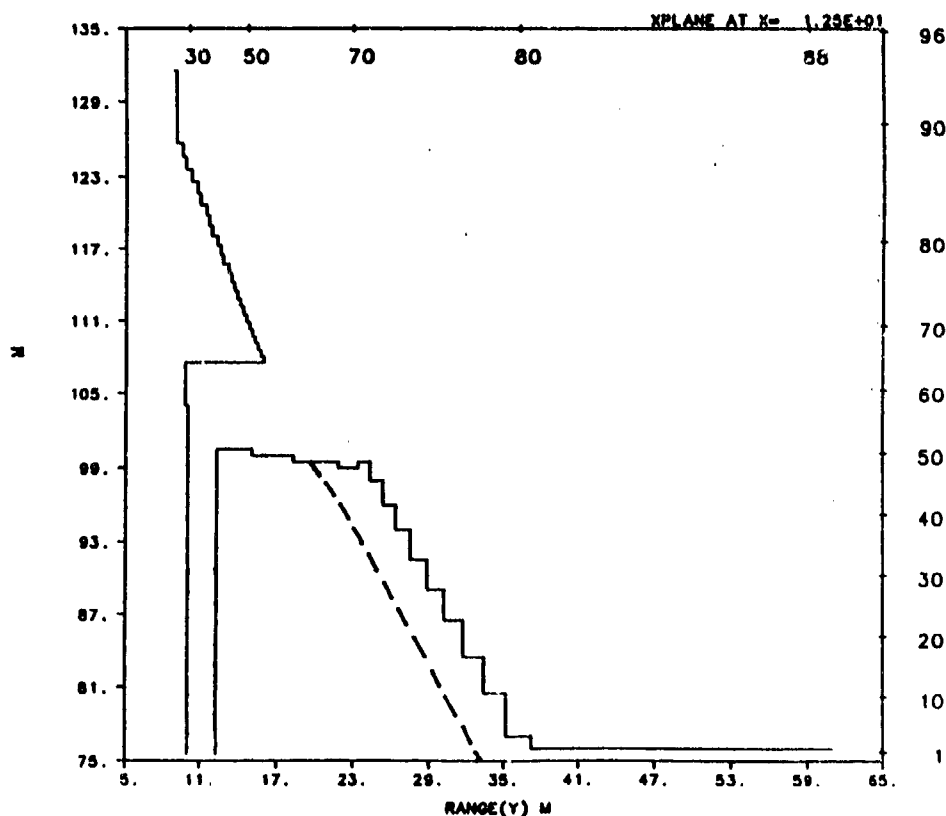
tracer particle trajectory from the calculation. The tracer particles were originally placed at locations corresponding to those for smoke-puff deployment. In the figure, which is an example from a node at 17 m from the portal over the berm, the circles are the experimental data, the solid line is the pre-test calculation, and the dotted line is the post-test calculation.

5. Possible Reasons for the Discrepancy

There are several possible reasons that can be cited as to why these differences between calculations and experiment occurred. First, it is possible that the detonation was even less complete than the 68% assumed, so that the effective yield of the explosive charge was less than 3000 kg. Second, the rigid walls and two-dimensional configuration of the calculation may not adequately model the physical response of the tunnel interior. We did find that in the larger China Lake test, in which the tunnel complex was destroyed, some energy was absorbed in the walls and overburden, so that these materials needed to be treated with a real

equation-of-state. Both of these reasons, however, would be expected to affect the interior results as well as the exterior, whereas our interior results were in fairly good agreement with the data.

A third possibility involves modeling of the terrain in the immediate vicinity of the portal. If the space available for expansion of the shock into the exterior is not modeled correctly, it could influence the channeling of that shockwave and hence its magnitude at important measuring points. The last two figures, Figures 12 and 13, illustrate what this means. The first, Figure 12, is an x-plane plot of the tunnel, berm, and overburden. This plane is vertical and runs along the centerline of the tunnel. The overburden is shown to be high and massive. But the actual profile of the ground over the portal was more like that shown by the dashed line, so that more space was available into which the emerging shock could expand. Figure 13 is a z-plane plot, again vertical but this time perpendicular to the tunnel centerline. At 8 meters from the portal,



SHARC ALVDALEN TEST EXTERIOR WITH BERM JUN 90 (KEN)

Figure 12. X-Plane Plot of Berm and Overburden, Showing Uncertainty of Configuration Profile

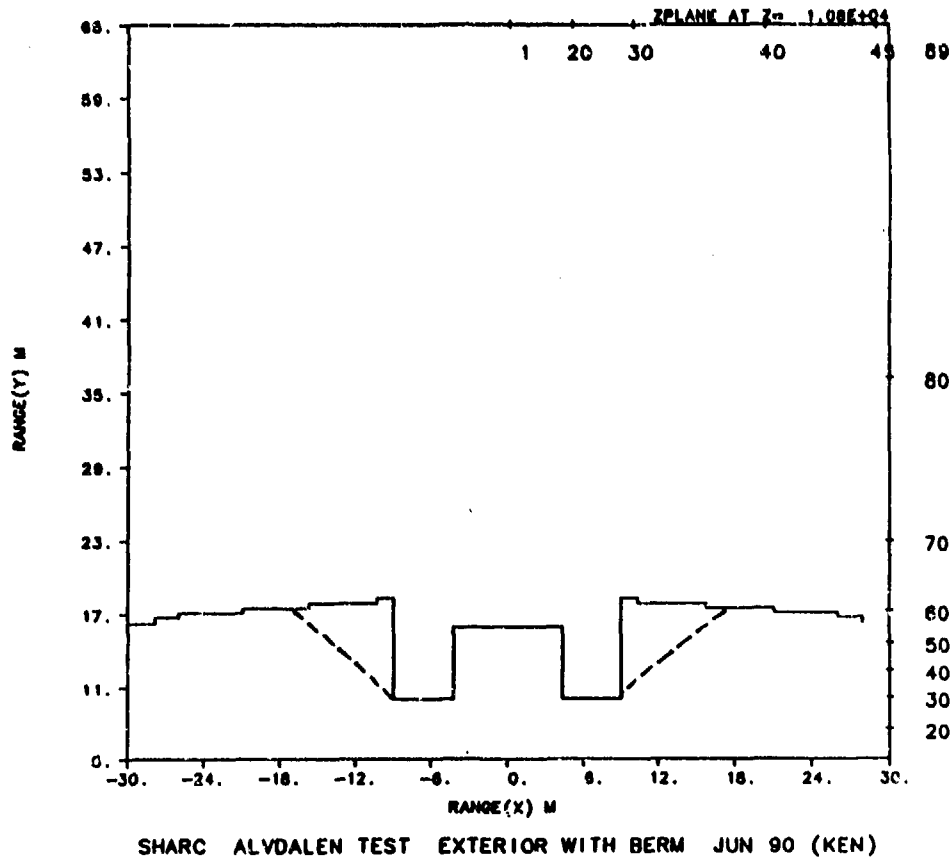


Figure 13. Z-Plane Plot Through Berm and Side Embankments, Showing Uncertainty of Slope

this plane passes through the front part of the berm and through the embankments on each side. These banks were more sloped than was modeled by the calculation, as shown by the dashed lines, and thus there was a significant difference in the space available for the expanding shock wave. We did not model the contours of these features carefully because we did not recognize their importance at the time the calculations were set up. Improvements could be made in this area which would enhance the ability of calculations to produce accurate predictions for test configurations.

LOADS PREDICTION PROGRAM FOR ACCIDENTAL EXPLOSIONS IN UNDERGROUND MUNITIONS STORAGE FACILITIES

Arnfinn Jenssen, Norwegian Defence Construction Service
Chester Canada, DOD Explosives Safety Board
Charles Needham, Maxwell Laboratories, S-Cubed Division
Lynn Kennedy, Maxwell Laboratories, S-Cubed Division

ABSTRACT

The KLOTZ Club is a multi-national group of explosives safety specialists concerned with the safe storage of military ammunition and munitions. One topic of present interest to the KLOTZ Club is the effects of the hazardous environment that would result from an accidental explosion in an underground military munitions storage facility. The necessary placement and/or design of nearby above-ground structures, to provide the required degree of safety for their occupants, is of concern. A knowledge of the predicted hazardous environments, and the resulting loads on the structures (blast, impulse, debris, ground shock, and thermal flux), is required if the prescribed degree of safety is to be provided.

For an above-ground storage facility, only a few parameters are needed to characterize the effects. An underground facility, however, requires the consideration of a number of variables if safety hazards are to be adequately predicted and mitigated. In order to properly account for this multitude of parameters, the KLOTZ Club decided, at its 1990 working group meeting, to sponsor development of a "Loads Prediction Computer Program for Underground Storage of Military Munitions". As presently conceived, the program is to run on an AT or 386-class personal computer. It is to be able to predict the details of the hazards expected from accidental detonation of the stored explosives within the facility with sufficient accuracy to permit revision of storage plans for existing facilities and design of planned facilities, as well as siting and design of occupied structures to be built near to or contiguous with the facilities. Loads prediction capabilities for a wide range of site-specific underground storage facility designs are planned. All parameters that significantly influence hazardous loading environments will be considered. These will include such factors as facility geometry and size, composition and competency of the earth cover, the explosive material and its storage and packaging configuration, effective loading density, and geology. The pro-

gram will be based on available experimental results (both large- and small-scale), on computational analyses, and on an understanding of the physics of the detonation and its interaction with the facility and the structures. The undertaking is as large as well as significant one, and may take several years to complete. However, the predictions should prove extremely useful for both the proper siting and design of planned underground storage facilities and for assessing risks related to various storage configurations in existing facilities.

1. Introduction.

A topic of current and continuing interest to the KLOTZ Club membership and other explosives safety specialists, both military and civilian, is the effects of the hazardous environment that would result from an accidental explosion in an underground munitions storage facility. The KLOTZ Club, at its 1990 working group meeting, decided, as part of its work toward quantifying these effects, to undertake development of a PC-based program aimed at predicting these hazardous environments and the loads resulting from them. This paper presents a brief summary of the authors' thoughts over the past year on why such a program is needed, what it should be expected to do, and how development of such a program should be approached.

Underground storage, for purposes of this discussion, is taken to include both deeply-buried facilities, whose covers do not rupture as a result of explosion of their prescribed load of explosives and propellants, and shallow-buried facilities, whose covers will rupture. In the former case, the major hazard is from directional blastwaves, debris, and burning gases emerging from portals or vent openings. In the latter case, the rupturing overburden may contribute to the debris hazard, and the blast, debris, and thermal hazards are not directionally contained.

For an above-ground storage facility, only a few parameters are generally needed to characterize the hazardous effects. An underground facility, however, requires the consideration of a number of variables if the safety hazards are to be adequately predicted and mitigated. These variables include the type, amount, and configuration of the explosive/propellant load, the facility geometry and size, the composition, competency, geology, and geometry of the earth cover, and features of the terrain exterior to the facility. Because of the large number of parameters, an engineering table

or simple algorithm is not adequate to provide the desired results. This has been shown on numerous occasions, when attempts have been made to provide "quick" predictions for experimental tests. The predictions have sometimes proved to be "off" by as much as an order of magnitude. As an illustration, Figure 1 shows the range of predictions that were provided for a test in 1988 at the US Naval Weapons Center, China Lake.

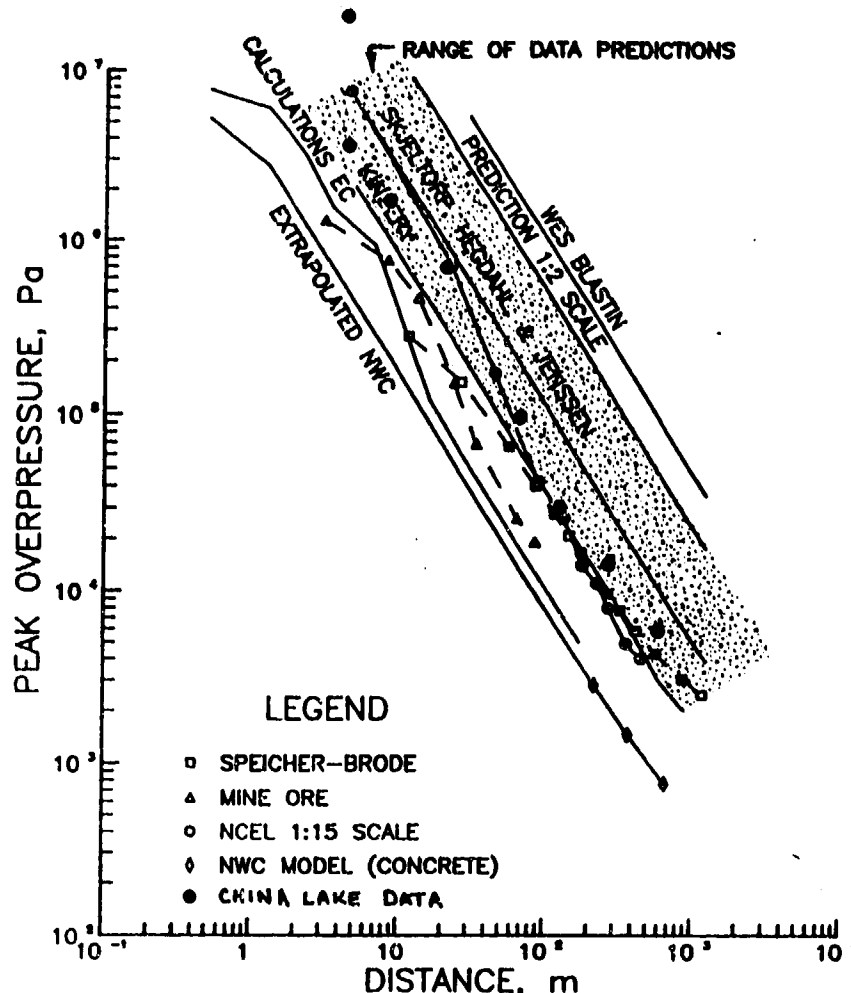


Figure 1: Airblast Predictions for Shallow-Buried Underground Tunnel/ Chamber Test at China Lake.

For this reason, an easy-to-use PC or workstation-based program is needed to generate the environments of interest. Such a program should be sufficiently rugged that it could be used to investigate the effect of proposed changes of size, geometry, etc. It should also be well-documented, so that it could be used by test engineers as well as by facility

designers (to address safety issues in planned facilities) and site managers (to assess risks related to various storage configurations in existing facilities). Finally, its ranges of applicability and its degree of accuracy in various regions needs to be carefully defined and documented.

2. Need for Program.

a. Design of New Facilities.

One major area in which the planned program is needed is for the design of new facilities. Underground storage of munitions is becoming more attractive, both because it is perceived to be safer than above-ground storage, and because of increasing scarcity and cost of real estate to provide an adequate cushion of space around above-ground facilities. Although many governments and industries need to stockpile explosives and propellants, both for defense and for peacetime uses, many of them may not have the resources or the space available to provide this cushion. In planning for storage, it is necessary to plan precisely, using highly accurate planning tools, in order to maximize storage capabilities and minimize costs. The use of berms, debris catchers, blast traps, blast doors and other devices, plus the use of terrain features to protect nearby structures and personnel, are all possible design features that might be incorporated in new facilities to increase their safety or to reduce the real estate required for safety zones.

b. Maximization of Loading in Existing Facilities.

Because of increased environmental awareness and increasingly stringent regulations regarding the storage of explosive and propellant materials, coupled with the need for additional storage capabilities, many organizations are seeking to expand, or at least to justify the safety of, the loads allowed in currently-existing facilities. In order to do this, a highly accurate and thoroughly validated hazardous environment prediction capability is needed. The site manager may wish to assess a number of different storage configurations, and thus to evaluate how he might best arrange his particular mix of explosives and propellants to provide complete compliance with all safety regulations, and hence maintain the highest degree of safety for on-site employees and adjacent areas where people may live or work.

c. Inadequacy of Existing Programs.

Although some algorithms and models currently exist for the prediction of environments from explosions in underground storage facilities, these are generally specialized to apply to a particular type of facility or a particular configuration. They may also predict only a single type of hazardous environment. For a given planned test configuration, predictions, as previously mentioned, may vary by an order of magnitude. Such variations in predictions make it difficult for experimenters even to set a range for gauge responses. For facility designers, the uncertainty is frustrating.

A start has been made, and several factors now make it practical to attempt a comprehensive program for prediction of environments from underground munitions storage facilities:

- 1) A data base of high explosive and propellant information is being compiled which directly relates to this problem.

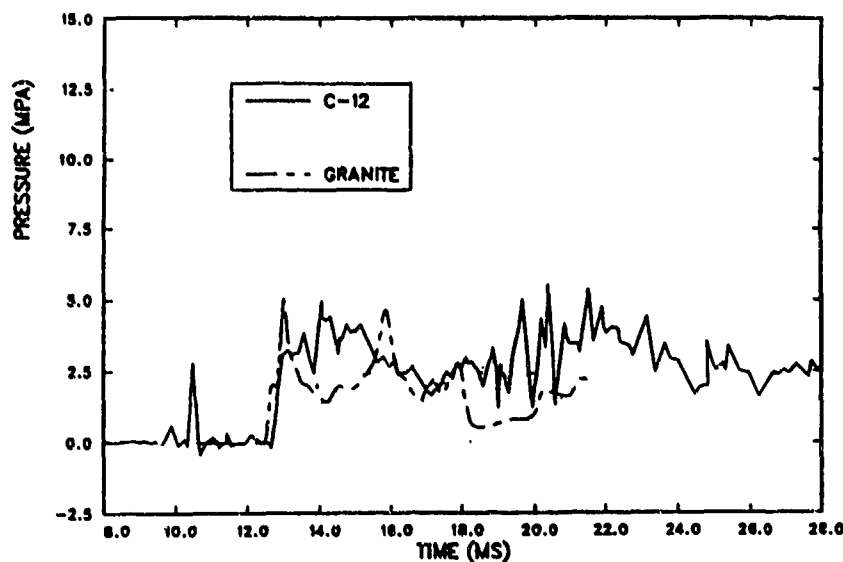
- 2) Hydrodynamic code capabilities are sufficiently advanced that they can deal with these configurations, and preliminary validation runs show excellent correlation with experimental data. An example of the correspondence between experimental and calculated results is shown in Figure 2. The test was the one at China Lake, and the calculation was run with the S-CUBED hydrocode SHARC.

- 3) New personal computers are extremely powerful and can run relatively complex programs in an interactive mode. In addition, the use of these personal computers is becoming widespread.

3. Requirements for Program.

In deciding how to proceed in constructing a PC program to provide the desired information, two lists need to be made. The first is a list of the environments we want to predict. These are the environments which we believe will prove to be the most hazardous to buildings and personnel in the area of the storage facility and those environments inside the facility which may lead to the spread of fires as well as to prompt or delayed detonation of other munitions stored there. The second is a list of variables which will describe the detonation and the facility, and hence will affect the hazardous environments. These variables will be used as inputs to the PC program. A preliminary version of both of these lists, with discussion of each item, is given in the following two subsections.

CHINA LAKE
CALCULATION, EXPERIMENTAL COMPARISONS
OVERPRESSURE VS. TIME



CHINA LAKE C-12 COORD: -2.2 M

ACCESS TUNNEL PRESSURE

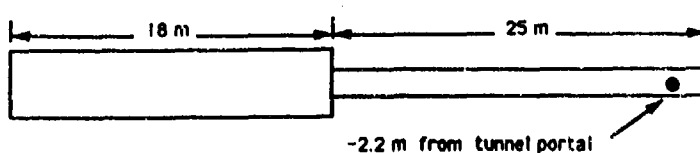


Figure 2: Comparison of Experimental and Calculated Overpressure Records from the China Lake Test.

a. Prediction of Environments and Loads.

There are four types of environments/loads currently being considered for inclusion in the PC program. The first, and the first to be addressed, will be airblast, because a great deal of work has already been done in this area and the tools to define it, the hydrodynamic codes, are in place. Within the airblast investigation, not only overpressure will be considered, but also impulse, dynamic pressure, and dynamic pressure impulse. Dynamic pressure is one of the primary parameters significant in structure and vehicle damage, and it is also active in the pickup and acceleration of debris. Impulse is the parameter usually provided as input to structural response calculations.

A second environment/load of interest will be the debris hazard. Debris can come from shell casings, packaging materials, and equipment contained with the explosive/propellant in the facility, or it can come from the geologic materials and concrete structures which form the overburden. The size distribution and directional acceleration of these debris materials by the airblast or ground shock environment can make them a significant hazard, both within the facility and outside. Once accelerated, heavy pieces of debris can travel for long distances, because they are slowed only by air drag forces.

Ground motion is thought at this point to be less significant than the two environments/loads mentioned above, because it is generally not so severe at close-in ranges. Depending on the size of the explosive charge, the range of interest, the geological configuration, and the strength of the affected structures, it could be important in some cases. Hydrodynamic and elastic-plastic codes are available to investigate the ground motion environment, and there is some data.

Thermal environments are included for consideration because, in cases of incomplete detonation or of ignition of propellants, gases may be produced which are burning as they are swept out of the facility. Temperatures inside the facility are also a consideration for sympathetic detonation. For a large, shallow-buried facility, a fireball will be formed which could ignite nearby structures if they are not provided with some protection. The possibility also exists that unprotected personnel may be working in the area. The flow fields governing the movement of these gases, the ignition of auxiliary fuels with which they may come in contact, and the resulting thermal radiations are subjects which need to be addressed.

b. Variables.

The list of input variables which will need to be included for the PC program is necessarily incomplete at this time. We expect that the list will be revised as new factors are found to be needed, old factors are dropped because they are determined to be unimportant, and new ways are discovered to describe or define significant factors. The discussion in this section describes three comprehensive areas which will need to be included. The best way to describe the various input parameters in these areas has yet to be determined.

The first group includes descriptors of the explosive charge itself: the amounts and kinds of explosives and/or propellants, the packaging or casings containing and separating the various components, and the storage or stacking arrangements. Amounts/kinds will determine the total energy release as a result of the contemplated incident. Packaging/casings will determine the amount and timing of sympathetic detonations, and will contribute to the debris available to be accelerated. Stacking arrangements will also possibly be significant in this regard.

A second group of descriptors involves the internal configuration of the facility: the sizes of the storage chambers and the cross sectional areas, lengths, and curvatures of associated access tunnels. Internal separating walls and blast doors or debris traps may also be included in this category. The amount, materials, and properties of the overburden, which determine when or if it ruptures and how much energy it absorbs, should also be considered.

Finally, the external configuration will affect the hazardous environments. Terrain features, the existence and placement of berms and debris catchers, and the geology of the earth in the vicinity will be factors. In addition, the distance of structures from the storage facility, their placement relative to openings, and their strength and integrity should be considered. Proposed uses of these structures or equipment will be factors in determining the allowable environments at various locations.

4. Approach.

It is anticipated that the first environment to be investigated will be airblast. This is because a fair amount of work has already been done in this area: data is available and some preliminary correlations have previously been made. This should lead to the generation of a workable PC model for airblast within about a year. The steps to be accomplished in developing the airblast model are outlined below. Development and subsequent improvement of models for the other environments should proceed in a similar manner. It is expected that the models for each individual environment will be combined into an integrated program in which all possible hazardous effects can be investigated.

a. Review of Available Data.

The first step in the process of preparing an environments prediction model should be a review of currently available airblast data from tests and theoretical calculations. The data should be examined and sorted according to its applicability to configurations of interest and according to the completeness of information about the yield and configuration of the explosion which generated the data. Cause-and-effect correlations should be identified. It is emphasized that review of the data must be accomplished with the physical principles that govern airblast generation and propagation kept firmly in mind. This will allow the reviewers to identify inconsistencies in the data and to discard any data that seems to be incorrectly recorded or identified.

b. Review of Current Models and Definition of Regions of Inadequacy.

At this stage, the correlations and normalizations of the data provided by all researchers should be examined. Two such correlations are those by Skjeltnor, Hegdahl & Jenssen and by Kingery. Some of the current models have been developed by entering peak pressure data on a pressure vs. range logarithmic grid. The data is then fit by a straight line which defines an inverse power for decay of peak pressure with range. Although this is a powerful technique, we now know that a single value of the decay exponent is not appropriate for all ranges. By using a more comprehensive algorithm, a better fit to the data can be obtained which will provide good results over a broad range of pressure values. In addition, an estimate of the accuracy of the fits, both within the range of the data and beyond it, can be obtained.

c. Validation of Computational Tools.

It is anticipated that the experimental data will be found to be insufficient for generation of a complete model. This is because the nature and cost of experiments require that data be collected at only a few points and for only a few selected configurations. In order to provide for a complete understanding of blast wave propagation, data at a large number of locations, and information about the variation of other hydrodynamic parameters (for example, density and gas flow velocity) as functions of time and space are needed. For this reason, we expect to include the results of numerical hydrodynamic calculations in the data base. A few calculations

have previously been accomplished, and these have been used to validate the procedures. In particular, three-dimensional calculations have been completed simulating recent tests at China Lake (California) and Älvödal (Sweden). The results of these calculations are to be reported at this Seminar by representatives from S-Cubed, Albuquerque, New Mexico.

d. Performance of Selected Parameter Studies with Calculations.

Once we are satisfied that the calculational techniques are valid, calculations can be performed to fill in gaps in the experimental data base and to perform parameter studies. The results of these calculations will help us to understand how the parameters listed above affect the airblast environments in regions of interest. The suite of calculational configurations should be carefully chosen to minimize both the number and complexity of calculations to be performed. Calculations, like large-scale tests, can be expensive, and it is important that they be carefully designed to maximize useful output. It is expected that the calculations will concentrate initially on high explosive sources. Techniques also exist, however, for calculating the results from propellant burning. Both types of sources, and mixtures of the two, are of interest for the final model.

e. Analysis of Calculations.

A thorough analysis of completed calculations is necessary to obtain a full understanding of the physics applicable to each situation. Not only overpressure peak values, but complete waveforms should be studied to determine origins of the various features which affect the blast environment. All basic and derived hydrodynamic parameters (pressure, impulse, density, flow velocity, energy, temperature, gas composition, and dynamic pressure) should be considered.

f. Development of Models.

Once a relatively complete data base is assembled, consisting of experimental data and calculations and including an understanding of the physical principles which give rise to the observed results, mathematical algorithms can be developed which, as functions of the various parameters identified as significant, can reproduce the observed environments. These algorithms can be mathematical expressions, tables from which numerical

answers are interpolated, and rules for combinations of results from several sources. An important part of model development is the assurance of physical consistency. If care is not taken, "glitches" can occur which produce unreasonable results for some combinations of variables.

g. Model Testing.

As the models are developed, they can be tested against the available data, both calculational and experimental, to ascertain whether or not they are providing reasonable answers which agree in all respects with the data. At this point, it will be appropriate to conduct some new experiments, either at large- or small-scale, so that the models can be tested against data which was not used in building the models. The experiments should be designed to exercise as many aspects of the models as possible. Comparison of results will provide a basis for judging the accuracy of the models in a real prediction situation.

h. Incorporation of Models into PC Program.

The validated models will then be incorporated into a personal computer or work station program. This is a straight-forward activity, but must be accomplished with care if the results are going to be useful to a variety of users. The most important part of this step is development of the user-interface menus so that they are understandable and logically organized. Another important part is development of documentation, either on-line or as separate documents. All aspects of the code and how it works must be carefully explained if misuse by inexperienced workers is to be avoided.

i. Refinement and Improvement of Models.

Finally, further refinement of the models should be undertaken to incorporate the other environments of interest and to accommodate new data or new configurations which were not covered in the first round of development. The cycle of data review, calculations and analysis, preliminary development of models, testing, and incorporation into the PC program can be followed through for debris, using much of the same experimental and calculational data used for the airblast investigation. Our experience has been that models of this type are never fully completed, because a completed capability always leads to the desire to apply the model to new situations. These new situations point up deficiencies, which in turn re-

quire new development, new analysis, and new testing. The product then, which is the PC program, can continue to be improved even while it is being used and providing useful results.

UNDERSTANDING THE RISK OF AMMUNITION KICKOUT
FROM EXPLOSION-SUPPRESSIVE STRUCTURES

Presented By:

Richard B. Shipe
US Army Combat Systems Test Activity
Aberdeen Proving Ground, Maryland 21005
Telephone: 301-278-3607

ABSTRACT

ABSTRACT

**UNDERSTANDING THE RISK OF AMMUNITION KICKOUT
FROM EXPLOSION SUPPRESSIVE STRUCTURES**

Richard B. Shipe
USACSTA ATTN: STECS-SO
Aberdeen Proving Ground, Maryland 21005

This paper presents a system safety model that justifies relaxing operating restrictions at weapons and ammunition test facilities.

The mission of the U.S. Army Combat Systems Test Activity (USACSTA or CSTA), Aberdeen Proving Ground (APG), MD, includes the evaluation of large caliber weapons. As these weapons increase in size, so does the danger associated with testing them. The availability of land for large caliber firing ranges is decreasing. Because of that unavailability, incompatible operations are often conducted contiguously. In such cases, personnel and facilities are exposed to the dangers associated with weapons testing.

There is no guarantee an explosive accident will never happen in a test structure, but it is a very unlikely occurrence. For an accident to occur, a complex sequence of events must happen. If that sequence is explicitly identified, then it can be controlled. By controlling selected hazards, the risk (risk is the expected value of an event or accident) can be reduced. If it has been reduced to an acceptable degree, the requirements applied to the design and subsequent operation of any facility can be relaxed.

Because of the high cost of constructing weapons test facilities, alternatives must be designed in the context of the risks associated with such testing. Using System Safety techniques, those risks can be identified and modeled. This paper suggests a model from which can be derived safe and cost-effective construction, design and operating alternatives for weapons testing facilities.

DIGEST

TITLE Understanding the Risk of Ammunition Kickout from Explosion Suppressive Structures

PURPOSE To inform a reader of the risk of ammunition being thrown from a containment structure (e.g. a magazine or explosive operating building), and whether that risk varies with the design style of the structure.

CENTRAL IDEA Understanding the circumstances that could lead to an unsuppressed detonation of a munition in an industrial, depot, or testing environment will make such an event more predictable, hence more preventable. An explicit model defining those circumstances demonstrates the low risk associated with a kickout, and it allows the risk to be compared between construction styles.

CONCLUSION Whatever the risk of ammunition kickout, it is not markedly different for any suppressive structure, regardless of construction style, if that structure has a frangible wall that will be lost in a detonation or an entrance way that allows direct access from the outside. This is explicitly defined by the fault tree contained herein.

ACKNOWLEDGMENT

This paper synthesizes a study conducted at the U.S. Army Combat Systems Test Activity (USACSTA or CSTA) by Mr. Thomas A. Lucas and I from January 1986 through October 1988. That study was recently published by the AMC Action Committee for System Safety as Technical Report 90-4. The quality and thoroughness of that original study are creditable to Mr. Lucas.

I also acknowledge Mr. William Watson who generated the cut sets in this paper using the software: Fault Tree Analysis using Personal Computers version 6, August 1987, developed by Mr. Jack Copeland. A special appreciation is extended to Misters Martin Mossa and Rodolfo Gil, from the USACSTA Safety Office, whose insights and criticisms helped focus and guide the technical considerations of this paper.

Historical Background

The mission of the U.S. Army Combat Systems Test Activity (USACSTA or CSTA), Aberdeen Proving Ground, MD, includes the evaluation of ammunition and weapons. As these systems increase in effectiveness, so does the risk associated with storing, handling, and testing them. That increase in risk is a result of encroachment, since the availability of land area for storing and testing those high-risk systems is decreasing. Because of that decrease, incompatible operations are often conducted contiguously. In such cases, personnel are subject to high risk exposure. The danger inherent in weapon testing, then, is an unexpected, unconfined detonation - an ammunition explosion. This is so because high-value facilities and equipment are necessarily exposed to the effects of such an event, and more important, people are exposed as well.

Weapons testing is not confined to weapon firing. It is a range of tests that demonstrate the reliability of a weapon and its ammunition. In addition to weapon firing, the testing includes regimes to demonstrate the hardness of ammunition. Rough handling and environmental tests are conducted to prove that hardness. The tests are conducted in sophisticated facilities which must meet the operational requirements of the testing and still embody explosion-suppressive qualities. That those operational and protective requirements are contradictory has resulted in facilities being designed and built that are adequately suppressive, but operationally restrictive.

To mitigate the real and political costs that would result from an explosive accident has necessitated expensive and conservative construction. This has been true at USACSTA, especially where test areas abut densely populated, public areas. At Aberdeen Proving Ground, there are two recent examples: a 14M \$ welded steel containment facility and a 10M \$ MCA project for laced, reinforced concrete firing barricades, both at USACSTA. Facilities so designed and constructed meet the dogmatic requirements of design codes, but may exaggerate or understate real dangers and may, then, be more costly than necessary. Because of the high cost of constructing test facilities, alternatives designed in the context of a risk profile (risk is the expected value of an accident) are desirable. Using analytic techniques, like the fault tree analysis described in this paper, such a profile can be developed. This report suggests a profile from which can be derived safe and cost-effective construction, design and operating alternatives. This paper defines the risk of an unconfined explosion.

Defining Kickout

The purpose of an explosion-suppressive structure is to mitigate the effects of a detonation; an explosion occurring outside the confinement provided by such a structure defeats its purpose. An unconfined detonation creates concern only in the case where personnel, facilities, or assets are exposed and incur some chance of injury or damage. Kickout is one such exposure. It is the escape from a containment structure (such as a storage, operating, or test facility) of an unexploded round of ammunition following an explosion in the structure. Although there is no guarantee an explosion will never happen in a suppressive structure, nor is there a guarantee a round of ammunition will never be ejected, a kickout is a very unlikely occurrence. For a kickout to occur, a complex sequence of events must happen. If that sequence is explicitly identified, then it can be controlled. If negligible, then it can be accepted.

This paper models the problem of kickout, which affects the design of magazines, barricades, and other suppressive structures. The model defines the mechanisms which cause an unconfined, unsuppressed explosion, and logically describe the order of their occurrence. The solution provided in this report is an identification of the events and hazards associated with the kickout phenomenon so its risk can be understood.

Describing the Fault Tree

The problem, then, is to create a model from which can be deduced the causes of an unsuppressed, unconfined explosion at an operating, test or storage facility. From that generic model, the case of kickout can be deduced as well. The logical choice for a model is a fault tree.

The tree defining the conditions necessary for an uncontained, unsuppressed detonation is a logic diagram consisting of three branches, each representing one variable of a mathematical statement. Logically, the top event can occur only if the underlying conditions in each branch have been satisfied. Each of the three branches defines one of the general conditions leading to the undesired outcome. That outcome is defined as "injury to personnel or facility damage caused by an unconfined detonation". The tree flows downward from the top event to the specific root causes. General outcomes at the head of the tree are connected to intermediate and root causes by logic gates. The gates depict the logical conditions of union and intersection that are analogous to addition and multiplication. Where describing a fault tree gate in the text, an additive or union condition is represented by an underlined, italic *or*, a multiplicative or intersection condition by an underlined, italic *and*.

The Head Event

Although kickout and a detonation that might result from a kickout are the principal interests of the fault tree, the tree is more general. In it are addressed many cases other than kickout. The conditions necessary for the top event are these: a round of ammunition is unconfined (it is outside the suppressive structure), and a person or facility is exposed, and the unconfined round of ammunition transmits energy. Further, it is probable that in a densely populated area, given an unconfined detonation, some damage or injury will occur.

There are three ways a munition might cause damage. If it is intact, the round can impart energy only if it is thrown or propelled and directly strikes a receiver. Alternatively, it can detonate. Given a detonation, energy might be transmitted via propelled fragments, or heat flux, or blast overpressure. Where the detonation occurs is significant. An exploding bomb can cause damage within some limited radius. If no exposed asset is within that radius, no damage or injury can be imparted. At military installations, undesirable exposures often exist; people and facilities are usually within the radius at which a munition, detonating unsuppressed, can cause damage or injury. Explosives are stored in a way that limits this exposure. They are isolated from populated areas and stored in bunkers designed to contain or direct missiles and the shock wave that result from an explosion.

Exposure of Assets

Exposure of personnel and facilities to the hazards of kickout is briefly detailed in the central branch of the tree. The branch is separated into two sections. One is the blast hazard - overpressure and heat flux - and the other a missile or fragment hazard. Neither of these conditions have been developed because of their complexity, although both normally exist.

Energy Released by Munition

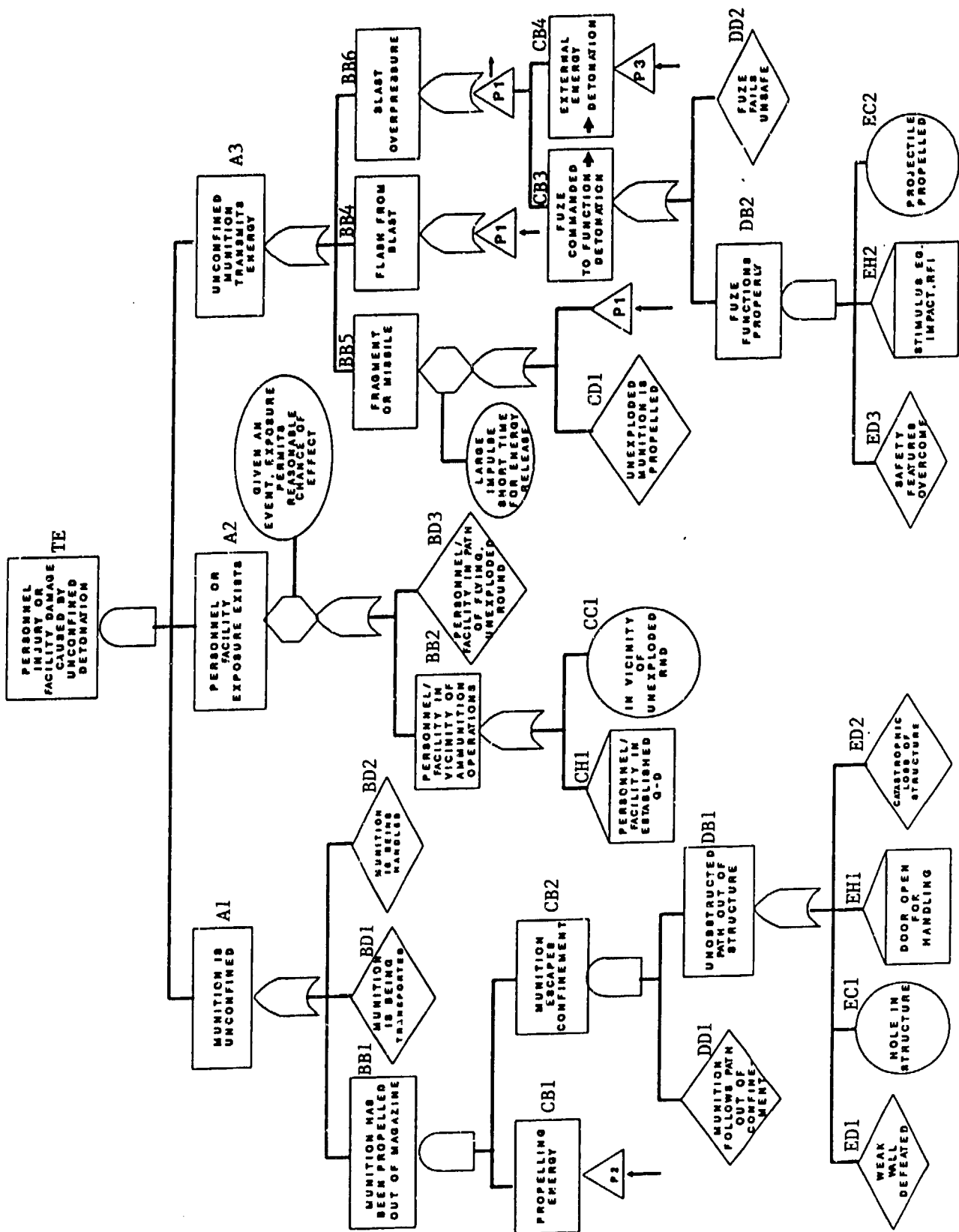
The third condition that must be met for the top event to occur is defined in the right branch of the tree. For exposed assets to incur damage, the unconfined munition must transfer energy. The transfer might result from the blast shock of the detonation, or from missiles and fragments, or the heat flux of the fireball. A fragment can only cause damage if it directly strikes a receiving asset and transfers sufficient energy (the accepted lower limit for that energy transfer is 79 Joules). Another way for a munition to cause injury or damage is by its detonation. This could be caused by the proper functioning of internal mechanical or electrical mechanisms, or by the application of heat from an external energy source.

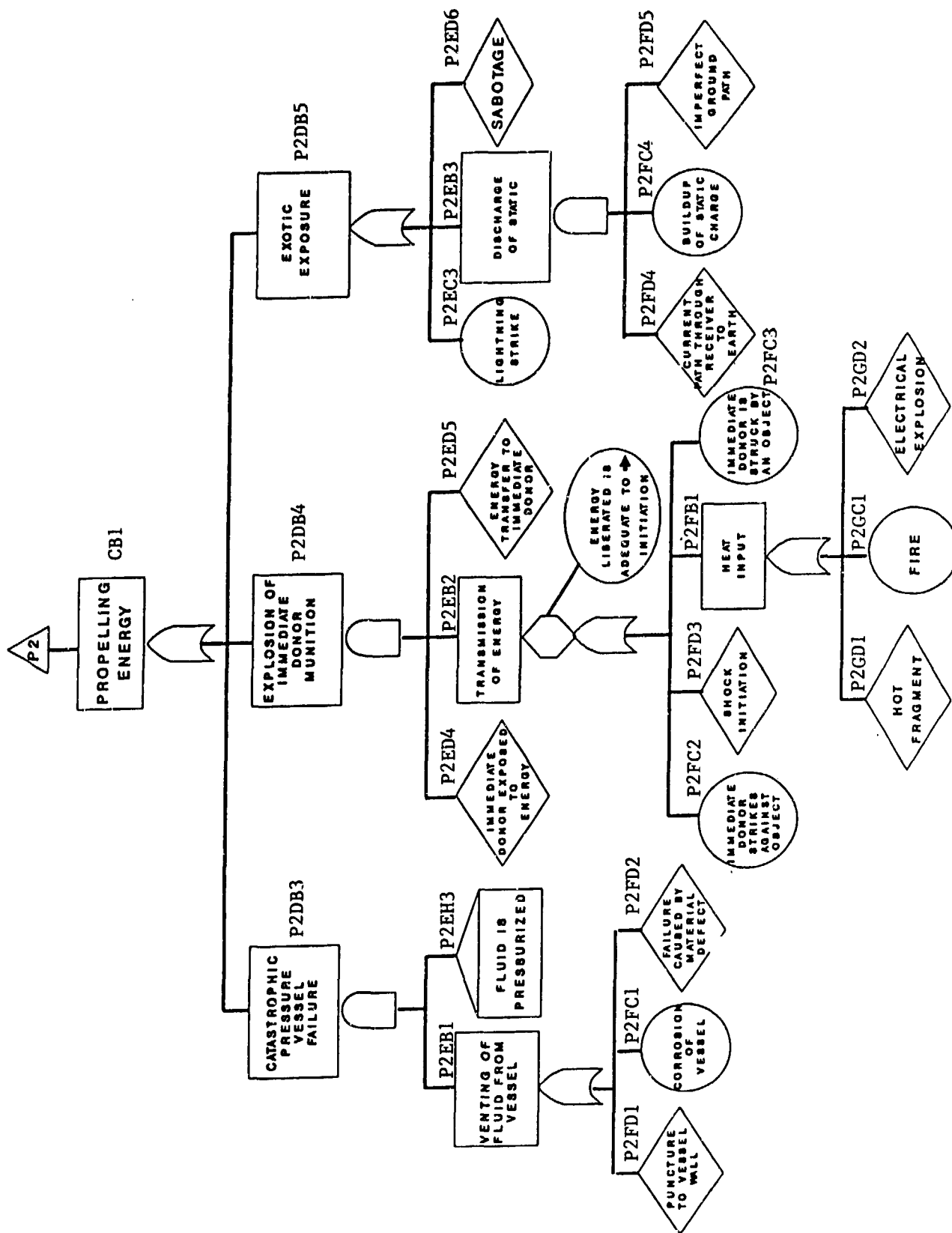
Munition is Unconfined

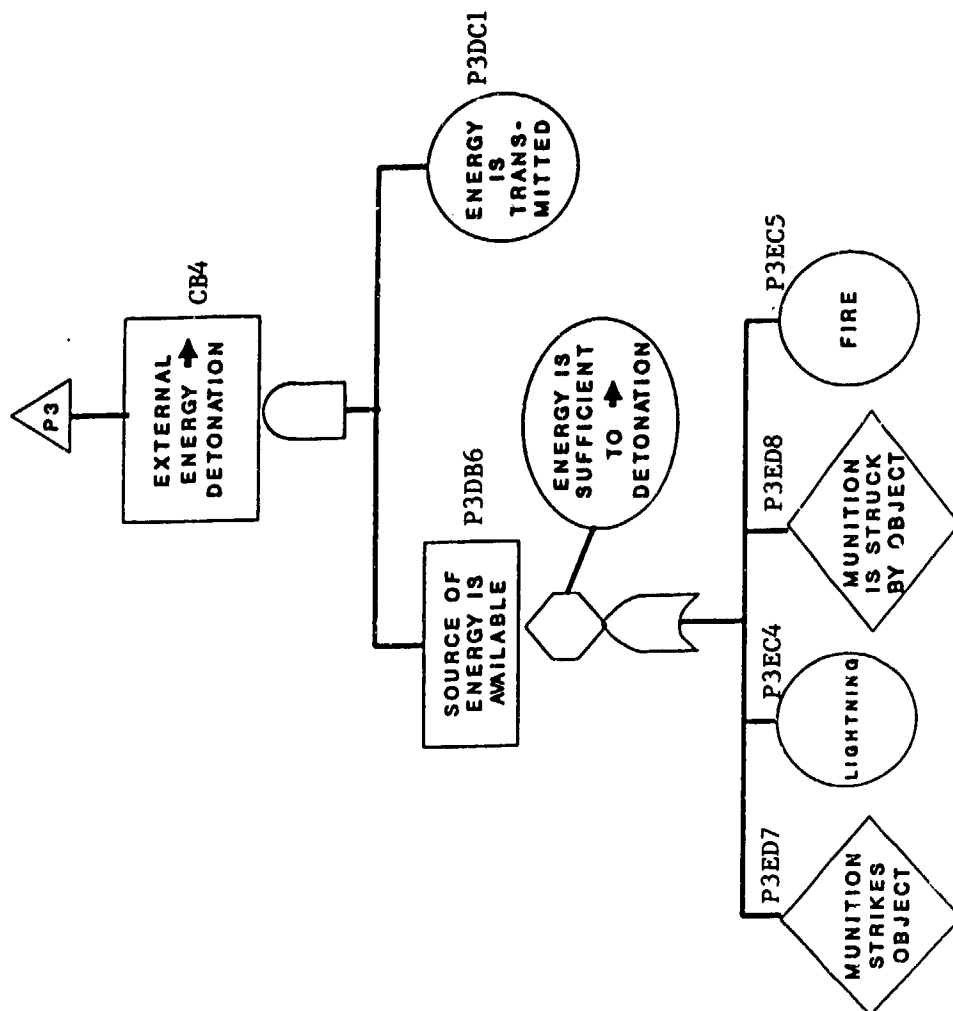
The left branch of the tree details the way blast and fragmentation mitigation features of a protective structure can be defeated. This branch defines the circumstances that must exist for a receiver to be directly exposed to an unexpected energy transfer.

Most often, direct exposure occurs when ammunition is being packed or unpacked, transported, or handled during testing. While exposure clearly exists in these cases, the risk of an accident is controlled through the use of training and special procedures which minimize the likelihood of an event.

For a kickout to occur, a relatively intact round of ammunition must be thrown outside a suppressive structure. An impulsive energy source and a path out of the structure must be present, and the round, when thrown, must travel along that path. An impulsive release of energy is necessary for a kickout to occur. That release might result from a detonation, or a pressure vessel failure, or an electrical explosion. A path out of the containment structure might exist because of a structural failure, or an inherent weakness, or because a natural opening exists (e.g. doors, windows, or frangible surfaces). It is important to recognize that all suppressive structures with frangible walls or surfaces or with access doors can permit a kickout. This weakness is an inherent characteristic of the suppressive qualities of those structures, and is irrespective of the construction medium, whether concrete, steel, earth, or sheet metal and sand.







FAULT TREE DATA

INPUT DATA LIST

TOP EVENT: PERSONNEL INJURY/FACILITY DAMAGE

GATE DATA

1	TE	A	3	0	A1	A2	A3
2	A1	O	1	2	BB1	BD1	BD2
3	A2	O	1	1	BB2	BD3	
4	A3	O	3	0	BB3	BB4	BB5
5	BB1	A	2	0	CB1	CB2	
6	BB2	O	0	2	CH1	CC1	
7	BB3	O	2	1	CB3	CB4	CD1
8	BB4	O	2	0	CB3	CB4	
9	BB5	O	2	0	CB3	CB4	
10	CB1	O	3	0	P2DB3	P2DB4	P2DB5
11	CB2	A	1	1	DB1	DD1	
12	CB3	O	1	1	DB2	DD2	
13	CB4	A	1	1	P3DB6	P3DC1	
14	DB1	O	0	4	ED1	EC1	EH1 ED2
15	DB2	A	0	3	ED3	EH2	EC2
16	P2DB3	A	1	1	P2EB1	P2EH3	
17	P2DB4	A	1	2	P2EB2	P2ED4	P2ED5
18	P2DB5	O	1	2	P2EB3	P2EC3	P2ED6
19	P2EB1	O	0	3	P2FD1	P2FC1	F2FD2
20	P2EB2	C	1	3	P2FB1	P2FC2	P2FD3 P2FC3
21	P2EB3	A	0	3	P2FD4	P2FC4	P2FD5
22	P2FB1	O	0	3	P2GD1	P2GC1	P2GD2
23	P3DB6	O	0	4	P3ED7	P3EC4	P3ED8 P3EC5

FAULT TREE DATA

FAULT EVENT DATA

1	BD1 D MUNITION IS BEING TRANSPORTED
2	BD2 D MUNITION IS BEING HANDLED
3	BD3 D PERSONNEL/FACILITY IN PATH
4	CH1 H PERSONNEL/FACILITY IN QD
5	CC1 F IN VICINITY OF UNEXPLODED RND
6	CD1 D UNEXPLODED IS MUNITION IS PROPELLED
7	DD1 D MUNITION FOLLOWS PATH OUT
8	DD2 D FUZE FAILS UNSAFE
9	ED1 D WEAK WALL DEFEATED
10	EC1 F HOLE IN STRUCTURE
11	EH1 H DOOR OPERD FOR HANDLING
12	ED2 D CATASTROPHIC LOSS OF STRUCTURE
13	ED3 D SAFETY FEATURES OVERCOME
14	EH2 H STIMULUS e.g. IMPACT
15	EC2 F PROJECTILE PROPELLED
16	P2EH3 H FLUID IS PRESSURIZED
17	P2ED4 D IMMEDIATE DONOR EXPOSED TO ENERGY
18	P2ED5 D ENERGY TRANSFER TO IMMEDIATE DONOR
19	P2EC3 F LIGHTNING STRIKE
20	P2ED6 D SABOTAGE
21	P2FD1 D PUNCTURE TO VESSEL WALL
22	P2FC1 F CORROSION OF VESSEL
23	P2FD2 D FAILURE CAUSED BY MATERIAL DEFECT
24	P2FC2 F IMMEDIATE DONOR STRIKES AGAINST OBJECT
25	P2FD3 F SHOCK INITIATION
26	P2FC3 F IMMEDIATE DONOR IS STRUCK BY AN OBJECT
27	P2FD4 D CURRENT PATH THROUGH RECEIVER TO EARTH
28	P2FC4 F BUILDUP OF STATIC CHARGE
29	P2FD5 D IMPERFECT GROUND PATH
30	P2GD1 D HOT FRAGMENT
31	P2GC1 F FIRE
32	P2GD2 D ELECTRICAL EXPLOSIVE
33	P3DC1 F ENERGY IS TRANSMITTED
34	P3ED7 D MUNITION STRIKES OBJECT
35	P3EC4 F LIGHTNING
36	P3ED8 D MUNITION IS STRUCK BY OBJECT
37	P3EC5 F FIRE

FAULT TREE DATA

GATE TE WAS NOT USED

(GATE MAY BE 'TOP EVENT' GATE)

FAULT TREE ANALYSIS PROGRAM

EXAMPLE CUT SETS FOR PERSONNEL INJURY/FACILITY DAMAGE

CUT SET # 37

BD1	MUNITION IS BEING TRANSPORTED
CH1	PERSONNEL/FACILITY IN QD
ED3	SAFETY FEATURES OVERCOME
EH2	STIMULUS e.g. IMPACT
EC2	PROJECTILE PROPELLED

CUT SET # 42

CH1	PERSONNEL/FACILITY IN QD
CD1	UNEXPLODED IS MUNITION IS PROPELLED
DD1	MUNITION FOLLOWS PATH OUT
ED1	WEAK WALL DEFEATED
P2ED6	SABOTAGE

CUT SET # 51

CC1	IN VICINITY OF UNEXPLODED RND
CD1	UNEXPLODED IS MUNITION IS PROPELLED
DD1	MUNITION FOLLOWS PATH OUT
ED1	WEAK WALL DEFEATED
P2EC3	LIGHTNING STRIKE

CUT SET # 93

CH1	PERSONNEL/FACILITY IN QD
DD1	MUNITION FOLLOWS PATH OUT
DD2	FUZE FAILS UNSAFE
ED1	WEAK WALL DEFEATED
P2FD4	CURRENT PATH THROUGH RECEIVER TO EARTH
P2FC4	BUILDUP OF STATIC CHARGE
P2FD5	IMPERFECT GROUND PATH

CUT SET # 101

BD3	PERSONNEL/FACILITY IN PATH
CD1	UNEXPLODED IS MUNITION IS PROPELLED
DD1	MUNITION FOLLOWS PATH OUT
EH1	DOOR OPENED FOR HANDLING
P2FD4	CURRENT PATH THROUGH RECEIVER TO EARTH
P2FC4	BUILDUP OF STATIC CHARGE
P2FD5	IMPERFECT GROUND PATH

CUT SET # 102

BD3	PERSONNEL/FACILITY IN PATH
CD1	UNEXPLODED IS MUNITION IS PROPELLED
DD1	MUNITION FOLLOWS PATH OUT
ED2	CATASTROPHIC LOSS OF STRUCTURE
P2FD4	CURRENT PATH THROUGH RECEIVER TO EARTH
P2FC4	BUILDUP OF STATIC CHARGE
P2FD5	IMPERFECT GROUND PATH

CUT SET # 107

BD3	PERSONNEL/FACILITY IN PATH
DD1	MUNITION FOLLOWS PATH OUT
DD2	FUZE FAILS UNSAFE
EH1	DOOR OPERD FOR HANDLING
P2FD4	CURRENT PATH THROUGH RECEIVER TO EARTH
P2FC4	BUILDUP OF STATIC CHARGE
P2FD5	IMPERFECT GROUND PATH

Logic Model of the Top Event

The figure is a depiction of the fault tree described in the text. It has 59 basic events connected through 33 gates to intermediate events leading to the head or top event. At least some of the fault events at the bottom of the tree must exist before the top event can occur. This can be shown using the Laws of Boolean Algebra. The following symbols are directly taken from the figure:

$$P_{\text{Top Event}} = P_{A1} \times P_{A2} \times P_{A3}$$

where: $P_{\text{Top Event}}$ = the probability of occurrence of the Top Event.

P_{A1} = the probability a round of ammunition is outside the structure, left branch of the tree.

P_{A2} = the probability a person or facility is exposed, center branch of the tree.

P_{A3} = the probability a round of ammunition transmits energy, right branch of the tree.

If the probability of occurrence of the undesired event, $P_{\text{Top Event}}$, were to be calculated, it would be the product of probabilities of the three directly contributing branches.

The tree depicted in this paper has been condensed from one contained in AMC Action Committee for System Safety Technical Report 90-4. It has roughly an eighth the resolution of that tree.

Logic Model of the Kickout Branch

Kickout is the only event in the third rank of the left-hand branch that is a rare event. Both BD1 and BD2 are regularly occurring events. Discount the cases where a munition is outside a containment structure while being manipulated - as in BD1 and BD2, and consider the case of the undesired outcome occurring as a result of a kickout. What contribution does a kickout play in the probability of occurrence of the Top Event?

Kickout is very unlikely. This is obvious because of the circumstances necessary to cause it. For a kickout to occur, there must be an impulsive event. That event must create an opening in the structure or magazine containing the munitions, and given an event has occurred, there must be munitions remaining that are then propelled through the opening in the structure.

$$BB1 = CB1 * CB2$$

$$CB1 = DB3 + DB4 + DB5$$

$$CB2 = DD1 * (ED1 + EC1 + EH1 + ED2)$$

$$DB3 = EH3 * (FD1 + FC1 + FD2)$$

$$DB4 = ED4 * EB2 * ED5$$

$$= ED4 * ED5 * (FC2 + FD3 + FC3 + GD1 + GC1 + GD2)$$

$$DB5 = EC3 + ED6 + FD4 * FC4 * FD5$$

So That: $CB1 = EH3 * (FD1 + FC1 + FD2) + EC3 + ED6 + FD4 * FC4 * FD5 + ED4 * ED5 * (FC2 + FD3 + FC3 + GD1 + GC1 + GD2)$

And: $CB2 = DD1 * ED1 + DD1 * EC1 + DD1 * EH1 + DD1 * ED2$

Therefore: $BB1 = \{EH3 * (FD1 + FC1 + FD2) + EC3 + ED6 + FD4 * FC4 * FD5 + ED4 * ED5 * (FC2 + FD3 + FC3 + GD1 + GC1 + GD2)\} * \{DD1 * ED1 + DD1 * EC1 + DD1 * EH1 + DD1 * ED2\}$

By examining the Boolean statement for kickout (Event BB1), 48 cut sets can be identified. The cut sets are three, four, or five point failures. This implies that the Top Event occurring as a result of a kickout requires the contribution of at least five basic events. For this case, TE seems to have a remote probability of occurrence - at least qualitatively - since it depends on the sum of five, six, and seven point failures. The probability of the top event's occurring is the sum of the products of the probabilities of the minimal cut sets.

Conclusion

Because the developed Fault Tree model was more extensive than was anticipated, it was impractical, given the scope of this study, to quantify. Even so, it is clear the possibility of the Top Event occurring does exist, but only if the complex set of conditions defined by the tree have been satisfied. The fault tree confirms a number of scenarios whereby an injury or damage resulting from a kickout could occur. There are many event combinations that could cause this. Equally obvious is that there is no way to reduce $P_{(TOP\ EVENT)}$ to zero. This implies there will always be a risk of kickout.

Elimination of the possibility of the head Event is impossible. However, a long string of events, which is diagramed in each branch of the tree, is required to satisfy that condition. What makes the chance of a kickout that causes injury or damage seem so remote is each of the events that can cause that outcome is an accident. Further, these accidental events must occur in combinations of five, six, or seven; since they must occur serially, the combination of events is very unlikely.

Whatever the risk of ammunition kickout, it is not markedly different for any suppressive structure, regardless of construction style, if that structure has a frangible wall that will be lost in a detonation or an entrance way that allows direct access from the outside. This is explicitly defined by the fault tree contained herein.

GLOSSARY

Cut Set - a combination of fault events whose occurrence as a set will cause the top event.

Donor - a round of ammunition which functions in the vicinity of other rounds of ammunition thus imparting energy to them.

Event

a. When regarding ammunition, a detonation or explosion.

b. An occurrence in the tree.

Head or Top Event - the main event of the fault tree, the undesired outcome.

Immediate Donor - The donor munition that initiates an unconfined munition.

Kickout - when a round of ammunition which does not detonate from an initial event in a structure is thrown from the structure.

Receiver - a round of ammunition which receives energy when another round of ammunition in the vicinity functions.

Risk - the expected value associated with a given hazard; it is the product of the severity of a hazard and the likelihood of its occurrence. Probabilities have not been calculated or assigned to individual events because it is beyond the scope of this report to do so. In this report, risk has several contexts: when pertaining to kickout, it is the consequence caused by a round detonating or escaping a containment structure after an event has occurred; when pertaining to a fault tree, it is the head event.

Unrelated - People or facilities which are not directly involved in a testing scenario but could be injured or damaged because of their proximity to a test when a kickout occurs.

REFERENCES

REFERENCES

Hammer, Willie. Product Safety Management and Engineering, Prentice - Hall Inc., Englewood Cliffs, New Jersey.

Moriarity, Brian and Harold Roland. System Safety Engineering and Management, John Wiley and Sons, NY, 1983.

Price, Paul, "Design of Steel Structures to Resist the Effects of HE Explosions", Picatinny Arsenal, Dover, New Jersey, Report No. 4837, August 1975.

Shipe, Richard B., and Thomas A. Lucas. "Assessment, Fault Tree Analysis and Solution To Ammunition Kickout Problem", Aberdeen Proving Ground, Maryland, USACSTA Report 6813, February 1989, and AMC Action Committee for System Safety Technical Report 90-4, April 1990.

Vesely, W. E., et. al., Fault Tree Handbook, U. S. Nuclear Regulatory Commission, Washington, D. C., January 1981.

TEST DATA ON THE STORAGE OF MIXED MUNITIONS IN CONEX CONTAINERS

WILLIAM LAWRENCE
US Army Ballistic Research Laboratory
Aberdeen Proving Ground, Maryland 21005

ABSTRACT

A series of 10 tests was conducted to identify debris, fragments, and airblast hazards associated with the detonation of the explosives in Conex containers. Eight of these tests were conducted at Socorro, NM, and the last two tests were conducted at China Lake, CA. The first three and last two tests were conducted without any kind of confinement around the Conex containers. The fourth, fifth, and sixth tests were conducted by sandbagging the Conex containers on three sides. In tests 7 and 8, the containers were sandbagged on three sides, and a 12-foot sandbag wall (20-foot wall in test 8) wall was erected at a distance of 15 feet from the front side of the container.

A lot of fragments were found beyond 300 feet in Tests 1, 2, 3, 6, 9, and 10. Only a few fragments were found beyond 300 feet in Tests 4, 5, 7, and 8. Some fragments were found beyond 600 feet in Tests 6, 9, and 10. A few metal fragments of Conex container were also found between 900 and 1,155 feet in Tests 9 and 10.

The fragment density at any distance was computed on the basis of a worst-case assumption. It was assumed that any fragment found in a sector at a distance greater than x feet from the origin could hit a standing person in that sector. The fragment density was computed as the number of fragments divided by the vertical area and multiplied by 600. That gave the fragment density per 600 square feet.

The fragment density, at different locations, is calculated by using 30-degree sectors. When the mean fragment density was computed, the sectors in which no fragments were found were excluded. The fragment density and distance were plotted for 25, 75, 160, and 500 lbs of explosive. For 500 lbs of explosive, the fragment density of less than one fragment per 600 square feet is at about 800 feet. For 160 lbs of explosive (sandbagged test), the fragment density of less than one fragment per 600 square feet is at about 600 feet. On the other hand, the fragment density of less than one fragment per 600 foot, for 75 lbs of explosive, is between 700 to 800 feet.

Comparison of sandbagged and unsandbagged test data clearly shows that sandbagging the containers does decrease the fragment density at larger distances. It also suggests that more tests may be needed, for explosive weights between 75 and 500 lbs and for explosive weights more than 500 lbs. The test data approximately supports the existing explosive weight and distance curve.

INTRODUCTION

A large quantity of different types of munitions are stored in a Conex container. Small caliber ammunition, fragmentation grenades, smoke grenades, signal flares, M42 submunitions, mines, file destroyer, and rockets are stored in the containers. Table I shows a typical basic load of ammunition stored in a container. The study had three objectives. The first objective was to determine the type of debris and fragment hazard distance from point of reaction when the munitions in a single Conex container are detonated. The second objective was to prevent propagation of reaction from one

TABLE I

A Typical Basic Load of Ammunition Stored in a Conex Container

CTG Cal .45 Ball	1360 Rds
CTG .50 Cal	1800 Rds
CTG 5.5mm Ball M16	23600 Rds
CTG 5.56mm Tracer M16	4930 Rds
CTG 7.62mm Ball & Tracer Lined	9370 Rds
CTG 40mm M433	144 Rds
Grenade Fragmentation M67	195 EA
Grenade Smoke Green	8 EA
Grenade Incendiary	130 EA
Grenade Smoke Red	8 EA
Grenade Smoke HC	8 EA
Grenade Smoke Violet	10 EA
Grenade Smoke Yellow	8 EA
Fire Starter	8 EA
Grenade Launcher Smoke Screening	8 EA
Signal Illum Grenade	36 EA
RKT 66mm M72A2	15 EA
Mines M18A1	12 EA
File Destroyer M4	1 EA
Signal Illum Ground Red Star	72 EA
Illum Star Ground White	72 EA
Signal Illum Ground Green Star	72 EA

container to an adjacent container, and the third objective was to minimize the physical damage to the adjacent Conex by the addition of sandbag walls along the three sides of containers.

The project was funded and supported by the Department of Defense Explosives Safety Board and the Project Manager for Ammunition logistics. The task of designing and conducting the tests and providing the technical data package was undertaken by the Ballistic Research Laboratory, Aberdeen Proving Ground, MD.

TESTING AND RESULTS

A series of 10 tests was performed to identify debris, fragments, and airblast hazards associated with the detonation of the explosives (inside a container) and to check whether the mass detonation of explosives in one container would propagate to the adjacent container. A detailed description of the first six tests are given in reference (3). Only a brief summary of the first six tests will be given here. The tests 7 through 10 will be described in more detail.

TEST NO 1

The goal of this test was to identify the external debris, fragments, and to determine the quantity-distance arcs when the explosive (in the Conex container) was detonated. Table II lists the ammunition placed inside the container. The mines were detonated inside the container. The fragments and other debris were located within 100 feet from the point of detonation. Some of the fragments were found beyond 350 feet from the test location. Three metal fragments from the Conex were located between 320 feet and 375 feet from the point of reaction. Five fragmentation grenades were located at 375 feet. Figure 1 shows the after-test photographs.

TEST NO 2

The goal of this test was to assess the damage to the acceptor container and its contents when the explosive, in the donor Conex, is detonated. The acceptor container was placed at a distance of 15 feet (arbitrarily chosen) from the donor container. The same amount and type of munitions as in Test 1 was placed in the donor. The wooden ammunition boxes and other debris burned for more than one hour near the acceptor container. The acceptor container was turned over and sustained some physical damage. The donor container was broken up into many fragments. Many of these fragments were thrown to a distance greater than 300 feet. Some fragments and other rounds were found beyond 375 feet from the test location, but most of the fragments were located within a radius of 100 feet. After-test photographs are shown in Figure 2.

TEST NO 3

The goal of this test was to assess the damage to the live munitions, inside the acceptor Conex, by decreasing the separation distance (distance between the containers) from 15 feet to 8 feet. The wooden boxes and other fragments burned in the space between the two containers for one to two hours. Some of the signal flares and grenades were cooked off because of the fire. The acceptor container was flipped over and caved in. The munitions inside the acceptor Conex did not detonate. Some of the munition boxes were broken, but no damage was done to the munitions inside the acceptor container. The fragments and other debris were thrown out at a distance greater than 300 feet

TABLE II

Ammunition in a Conex Container

CTG, Cal .45 Ball and .50 Cal	3160 Rds
CTG, 5.56mm Ball/Tracer M16	28530 Rds
CTG, 7.62mm Ball & Tracer Lined	9370 Rds
Grenade, Fragmentation M67	195 EA
Grenade, Smoke	175 EA
RKT, 66mm M72A2 (unfuzed)	15 EA
Mines, M18A1	12 EA
File Destroyer, M4	1 EA
Signal, Illum Ground	260 EA
Rifle Grenade, M42	216 EA



Figure 1. Test No. 1. (a) File Dest, Conex part, and Smoke grnd; (b) Conex part and Smoke Grnd; (c) Frag Grnd; and (d) Smoke grnd, M42 grandes (grnd), and 66mm Rockets (Rkt).

from the point of reaction. Ten metal fragments were found between 300 feet and 335 feet from the test location. Thirty-five M42, two smoke grenades, and one fragmentation grenade were found between 300 feet and 350 feet. Figure 3 shows after-test photographs.

TEST NO 4

The aim of this test was to check whether some kind of sandbag wall/shield will prevent the acceptor container from overturning and sustaining physical damage. The sandbag walls, about one foot taller than the height of the container, were built along three sides of the containers. The wooden boxes and other debris burned for more than two hours. Some munitions (grenades, flares, etc.) were cooked off. The middle sandbag wall was partially collapsed. The acceptor Conex did not move or flip over and no damage was done to munitions inside the acceptor Conex. Much of the blast was absorbed by the sandbag wall, thus preventing the acceptor Conex from sustaining much damage. The donor container and other munition boxes were broken into many fragments. Two fragments (3 x 6 feet) from the door of the Conex container were located at 369 and 561 feet from the test location. One fragment from the Conex was found at 450 feet. One 66-mm rocket (warhead) was found at 305 feet. After-test results are shown in Figure 4.

TEST NO 5

The aim of this test was to learn about the extent of the fragments/debris hazards by detonating the same amount of the explosives in the donor Conex when sandbags were placed on top of the donor container. The same type of sandbag walls were built along three sides of the containers as in Test 4. The door of the donor Conex was found between 50 and 60 feet from the container. The roof of the donor container flew up but fell right back in the container. The debris and fragments did not go very far from the point of detonation. A few parts of the signal flares were located beyond 300 feet from the test location. Most of the munitions and other fragments burned inside the donor container and continued burning for more than three hours. The sandbag wall between the acceptor and the donor containers was partially collapsed. The walls of the acceptor container suffered some damage, but the container itself remained intact. The acceptor container did not flip or turn over.

TEST NO 6

Double sandbag walls, along the three sides of the containers, were built for this test. Munition placement, inside the donor Conex, was changed without changing the total amount of explosive. This time, 60 lbs of explosive (rockets, M42, and fragmentation grenades) were placed close to 100 lbs of C-4 bare charge. The 160 lbs of explosive was placed against the inside wall of the donor Conex (the wall close to the acceptor Conex) and on the lower shelf of the wooden rack. The 100 lbs of explosive was detonated. A big fire ball was seen, and a tremendous explosion was heard. A few flares and grenades burned for a few minutes. No other fire was observed in this test. No explosive (rockets, mines, etc.) was recovered. This means that all 160 lbs of explosive was consumed during the explosion process. The detonation did not propagate to the live munitions, inside the acceptor Conex. One side (the side towards the donor Conex) of the acceptor Conex was caved in, but it did not flip over. The donor container and some of the munition boxes were broken into many fragments. These fragments were found at different locations. Twenty-six metal fragments (8 inches to 5 feet long) were found at a distance between 440 feet and 673 feet from ground zero. After-test pictures are shown in Figure 5.

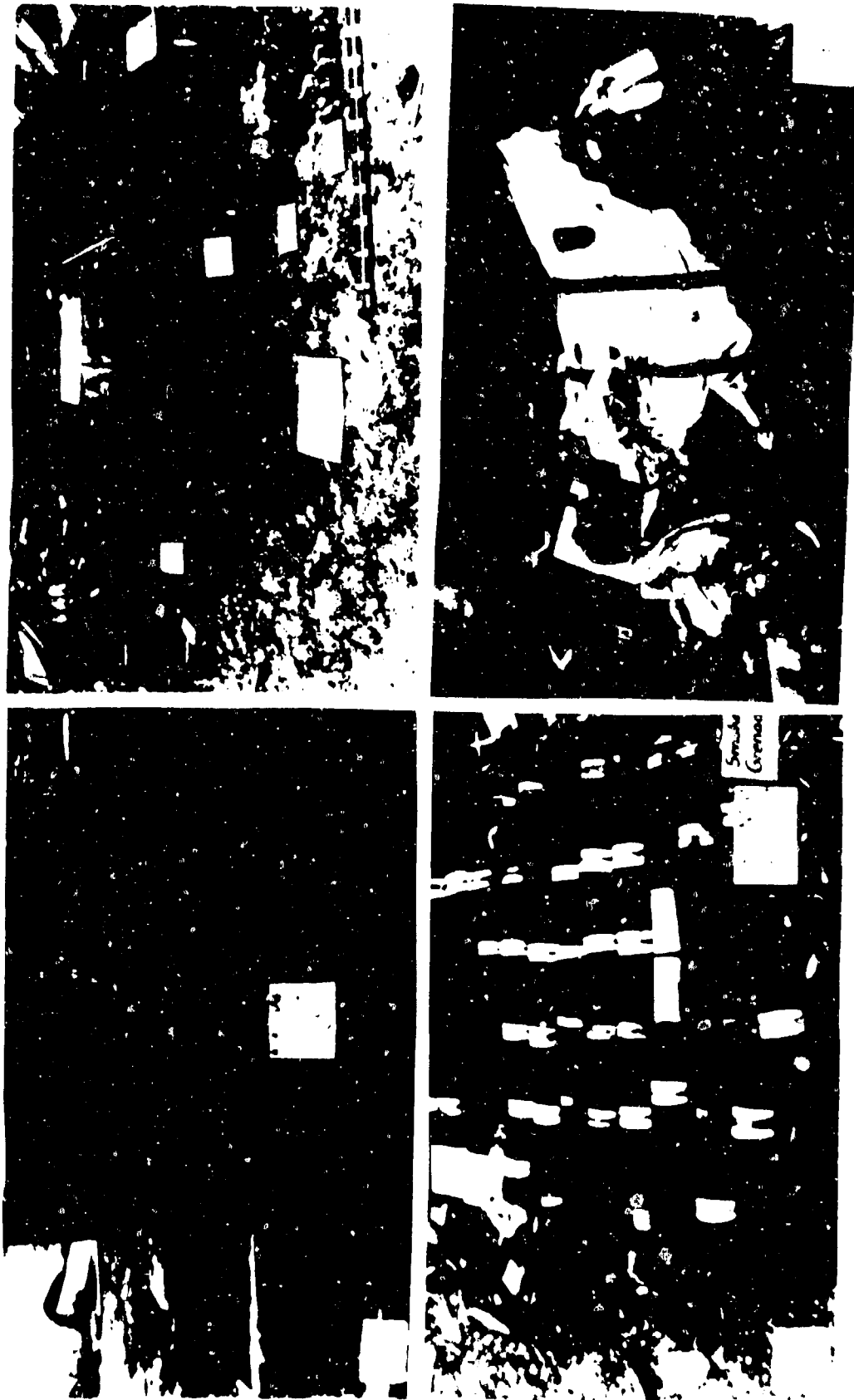


Figure 2 Test No. 2. (a) Acceptor Conex; (b) 7.62mm, 50 Cal. and Frag grnd; (c) Smoke grnd; and (d) 66mm Rocket.



Figure 3. Test No. 3. (a) Part of Donor Conex; (b) Signal flares;
 (c) Mixed munitions; and (d) M42 grnd.



Figure 4.1. Test No. 4. (a) Overall View after the Test; (b) Acceptor Cone; and (c) Bottom part of Donor Cone.



Figure 4.2. Test no. 4. (a) 66mm Rockets; (b) Flares; (c) Rocket parts, 50 Cal, and 7.62mm; and (d) 50 Cal and M42 grnd



Figure 5. Test No. 6. (a) 5.56mm, 50 Cal, and 7.62mm; (b) Conex part; (c) Ammo Box; and (d) Smoke grd.

TEST NO 7

No sandbag wall was built in front of the Conex in any of the tests conducted previously. In this test, a 12-foot-long and 7-foot-high sandbag wall was built at a distance of 15 feet from the front wall of the Conex container. The sandbag walls were also built around three sides of the container. Two layers of sandbags were also placed on top of the container. The same type and amount of munitions as in Test 2 was placed in the donor container. Three pressure transducers were placed at a distance of 30 feet, 60 feet, and 75 feet from the front door of the container. Twelve mines were placed at the center of the container. The stacking details of the munitions inside the container are shown in Figure 6, and the sandbag wall configuration is shown in Figure 7.

The mines were remotely detonated. About 70% of the fragments were located within a 60-foot radius. A very few fragments were also found beyond 300 feet from the container. A few grenades and flares cooked off. The wooden boxes and other debris burned for many hours. The pressures of 3.8 psi at 30 feet, 2.2 psi at 60 feet, and 1.0 psi at 75 feet were registered by the pressure transducers. Figure 8 shows after-test photographs.

TEST NO 8

This test was conducted to check whether increasing the length of the front sandbag wall would have any effect in reducing the number of fragments. So, a 20-foot-long and 7-foot-high wall was constructed in front of the Conex container at a distance of 15 feet. Three sides of the Conex container were also confined by the sandbag walls and two layers of sandbags were placed on the top of the container as in Test 7.

The same type and amount of the munitions as in Test 7 was placed in the container. Three pressure transducers were placed at the same location as in Test 7. Twelve mines were placed at the center of the container.

The mines were detonated. Not very many fragments were found beyond 300 feet from the container. A lot of grenades, flares, and other small arms cooked off. It was estimated that about 90 to 95% of the fragments were in a 60-foot radius. A lot of fragments burned for many hours. The pressures of 2.2 psi at 30 feet, 2.5 psi at 60 feet, and 0.9 psi at 75 feet were registered by the transducers.

TESTS AT CHINA LAKE, CALIFORNIA

The Department of Defense Explosives Safety Board requested that we conduct a few tests detonating 75 lbs (inside the Conex) or more bare charge without any kind of sandbag confinement around the Conex container. These tests could not be conducted at Socorro, NM, because of safety and nonavailability of a large, flat area for the collection of debris/fragments after the test. So, an alternate test site was selected to conduct these tests.

A site in excess of 2,500 feet by 2,500 feet was de-bushed on a generally flat lakebed surface at Cactus Flats, China Lake, CA. The radial lines and circular arcs were staked and marked on the ground with chalk. Radial lines were marked every 30 degrees. Circular arcs were chalked at 60 feet, 30-foot intervals from 60 to 300 feet, and 600 feet. Distances from ground zero were marked at 100-foot intervals along each of the radial lines from 600 to 1,200 feet.

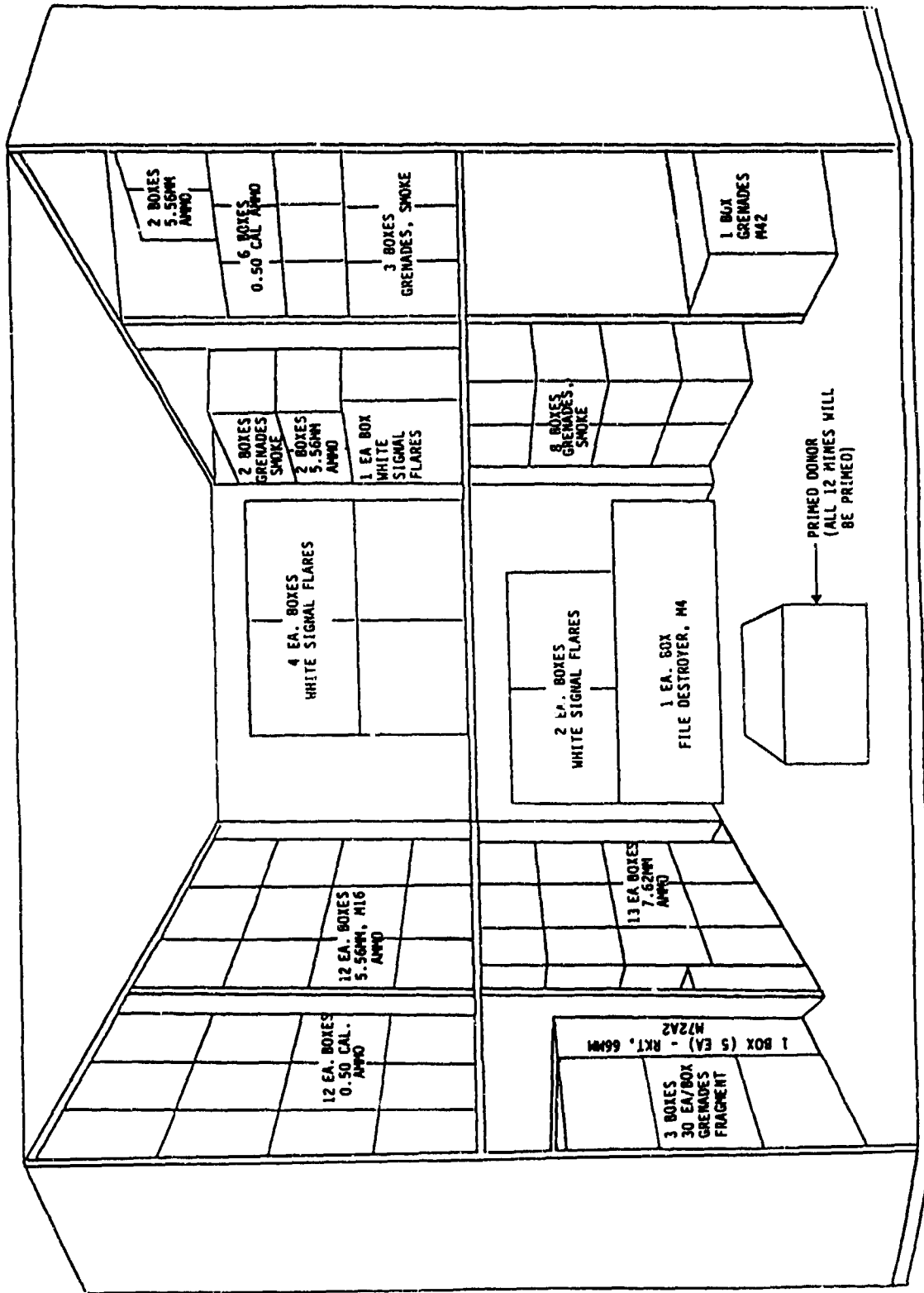


Figure 6. The Ammunition in the Container, Test Nos. 7 and 8.

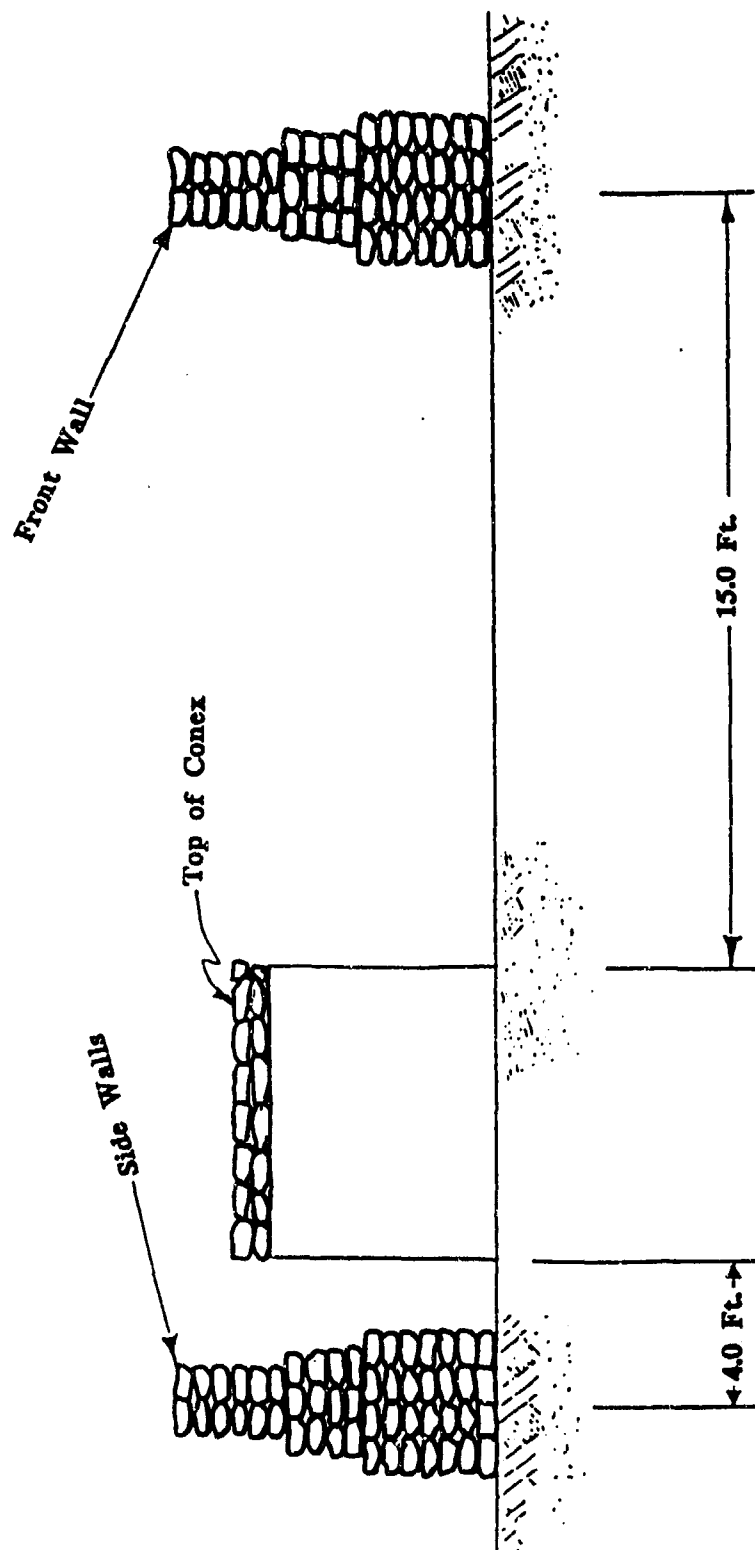


Figure 7. The Sandbag Wall Configuration for Test Nos. 7 and 8.

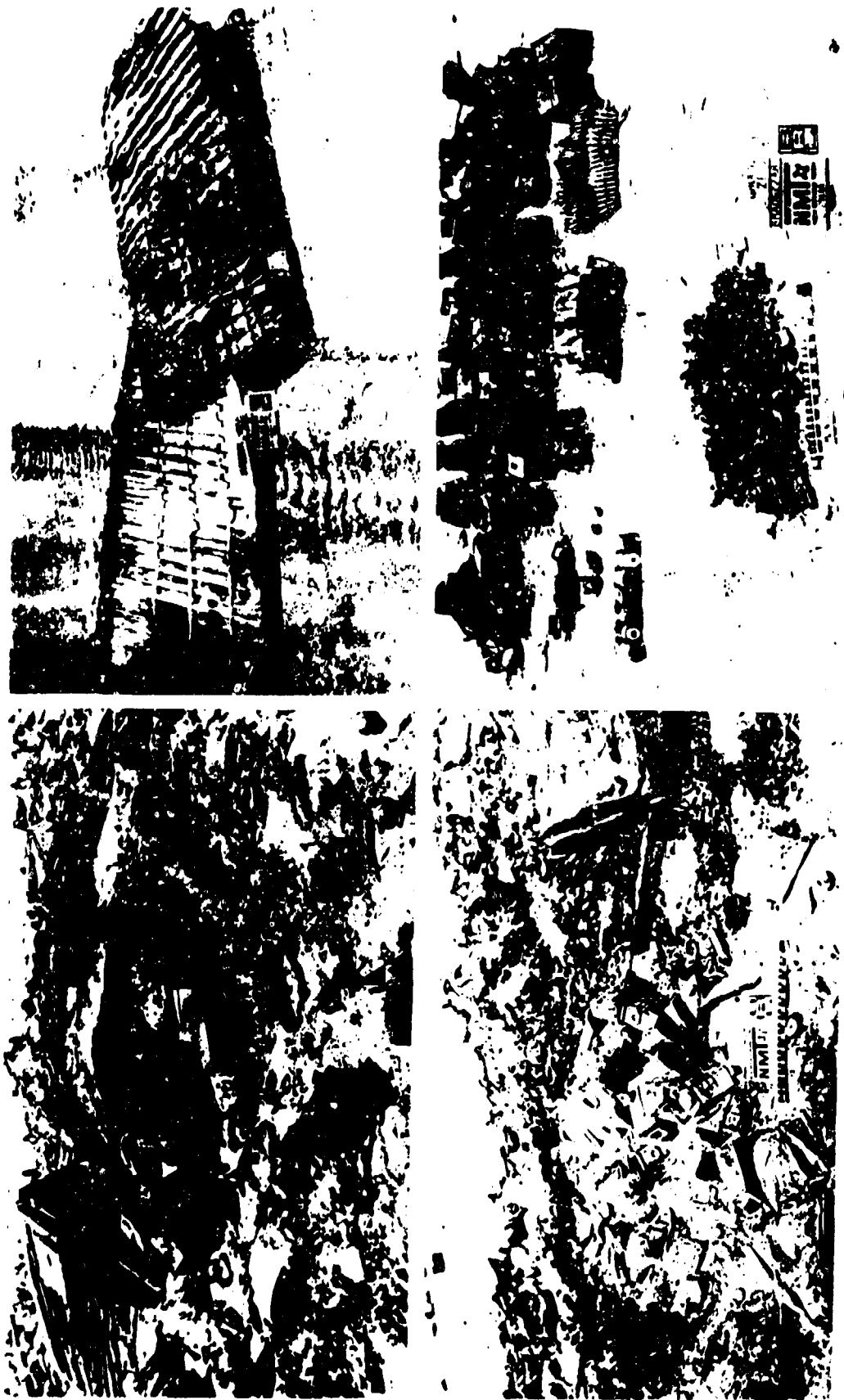


Figure 8.1. (a), (b), (c), and (d) Conex part, Ammo boxes, Mixed munition, and Conex part at Ground zero, Test No. 7.



Figure 8.2. (a), (b), (c) and (d) Overall view of the post-test site, Test No. 7.

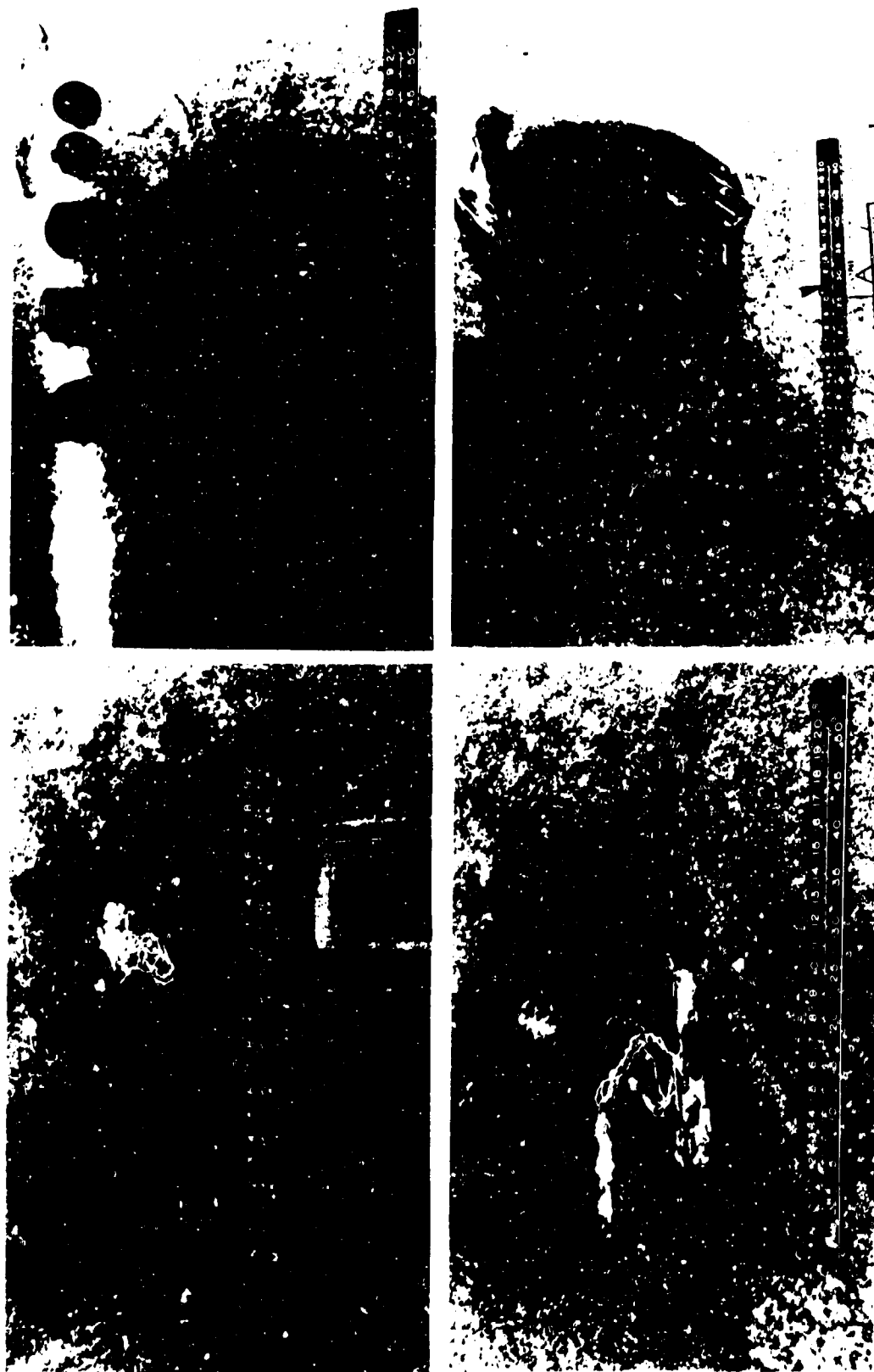


Figure 8.3. Test No. 7. (a) Grnd and Flare between 180 and 210 feet;
 (b) Grnd and 50 Cal between 210 and 240 feet; (c) and
 (d) Grnd, Flare and Conex part between 240 and 270 feet.

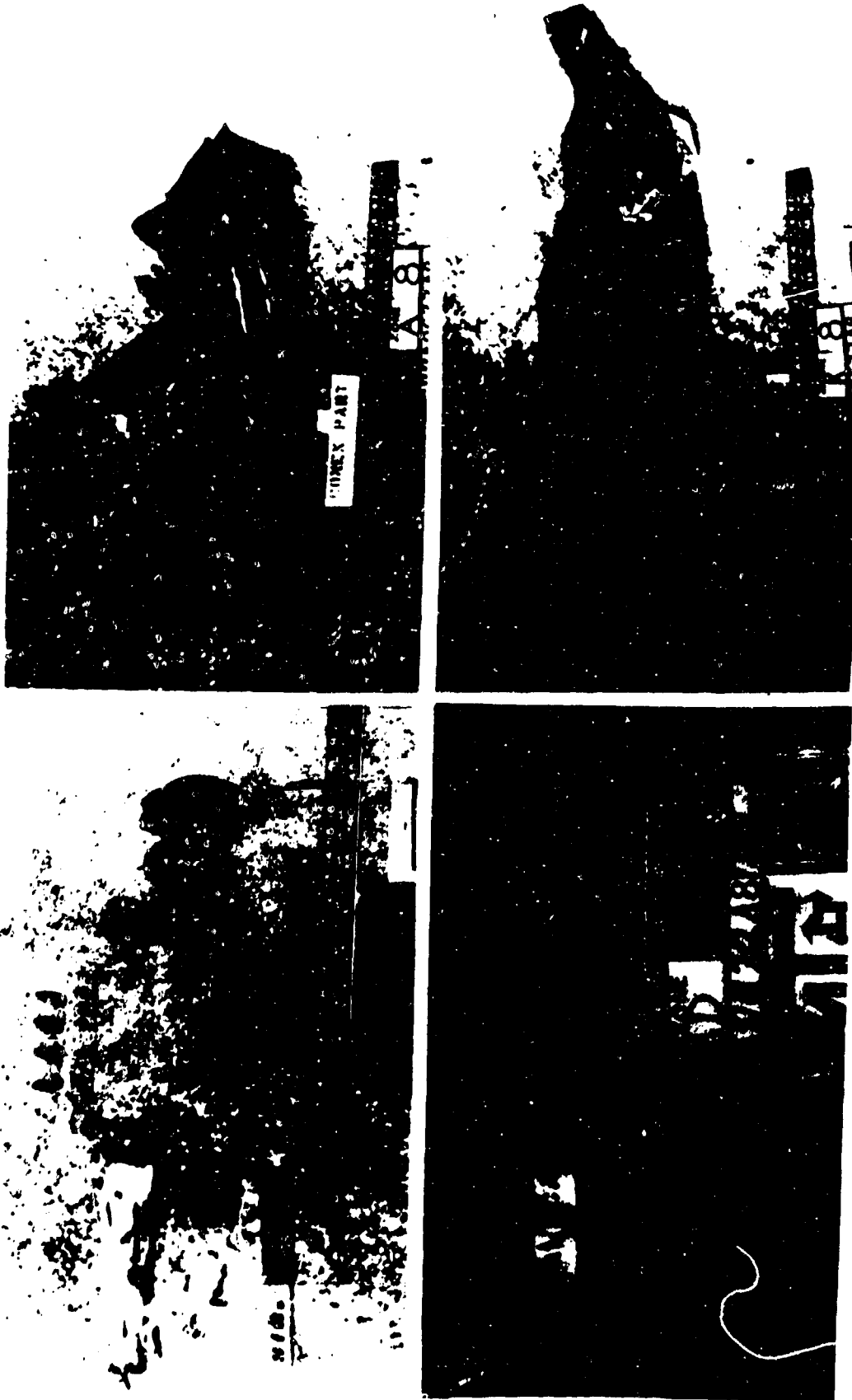


Figure 8.4. Test No. 7. (a) Flare, 50 Cal and Grnd; (b) and (d) Conex parts; (c) 50 Cal between 270 an 300 feet.

TEST NO 9

The same amount of munitions (as in the tests conducted at Socorro, NM) were placed in the container. Three Bikini blast pressure gauges were placed outside of the door of the container at 30, 60, and 90 feet from ground zero. A 75-lb bare charge (70 lbs Comp B and 5 lbs C-4) was placed at the center of the container. The remaining munitions were placed in the container the same way as in other tests. A packing arrangement of the munition in the container is shown in Figure 9.

The charge was initiated using the explosive bridge wire detonator. The Conex container was broken into many fragments. Some of the fragments were thrown to large distances. One fragment was found at a distance of 906 feet, and the second fragment was located at a distance of 824 feet from ground zero. The majority of the munitions and other debris or fragments were found within the 60-foot radius. Many smoke grenades were initiated by the detonation of the bare charge. The M72A2 rockets were broken apart by the detonation but did not appear to have functioned. The mines were expelled and survived with minimal damage. The wooden shelves and other wooden ammunition storage boxes were set afire by the detonation, but the fire lasted for less than one hour. Some of the ammunition cooked off. After-test pictures are shown in Figure 10.

TEST NO 10

Two Conex containers (acceptor and donor) were employed in this test. The same amount of munitions (as in the last test) was placed in the donor container. The acceptor container was placed at a distance of eight feet from the donor container. A few grenades, rockets, mines, and other ammunition were placed in the acceptor container. Again, three Bikini blast pressure gauges were placed at 30, 60, and 90 feet from ground zero. A 500-lb bare charge (495 lbs of Comp B and 5 lbs of C-4) was placed at the center of the acceptor container. Ammunition placement in the containers is shown in Figures 11 and 12.

Again an explosive wire detonator was used to initiate the 500-lb charge. Both containers were destroyed. A shallow crater was formed under the donor container, but no crater was formed under the acceptor container. Fragments of the Conex containers were found at the greatest distances from ground zero. One 6-inch by 14-inch fragment of container was found at 1,156 feet from ground zero. A 1-inch by 3-foot-long rod from the door latch mechanism of the container was found at 1,138 feet. Some of the file destroyer material was burned by the fire, but no ammunition inside the acceptor container detonated.

Ammunition boxes were scattered within the area. Most of the boxes were damaged and broken open. Some of the ammunition cooked off. Four linked 0.50-caliber rounds were located at a distance of 689 feet. One box of 7.62-mm ammunition was found at 1,100 feet. The rockets were broken apart but did not seem to function. The inert mines were expelled and survived with minimum damage. The signal flares and smoke grenades were scattered in different sectors. The majority of the debris and other fragments were found within a 90-foot radius of ground zero. After-test photographs are shown in Figure 13.

OVERALL RESULTS

The locations where the debris/fragments were found varied from test to test. In some tests, the debris/fragments did not go beyond 300 feet from the point of detonation, but in other tests some

TOP	12 Boxes 0.50 Cal 3 Boxes 7.62 Ammo 2 Box 5.56 Ammo	TOP	1 Box (15 ea) RKT-66mm-M72A2
BOTTOM	8 Boxes 0.50 Cal	BOTTOM	20 Boxes Smoke Grenades
COMP B: BARE CHARGE ON THE FLOOR 70 POUNDS C-4 5 POUNDS		BOTTOM 1 Box File Destruct 12 Inert Mines	
TOP	8 Boxes 5.56 Ammo	TOP	1 Box Signal Flares 10 Boxes Smoke Grenades 11 Boxes 5.56 Ammo
BOTTOM	12 Boxes 7.62 Ammo	BOTTOM	1 Box Signal Flares 14 Boxes Smoke Grenades

Figure 9. Ammunition in the Container, Test No. 9.



Figure 10.1. Test No. 9. (a) Mixed munition at ground zero;
(b) Grnd, and ammo boxes between 60 and 90 feet.

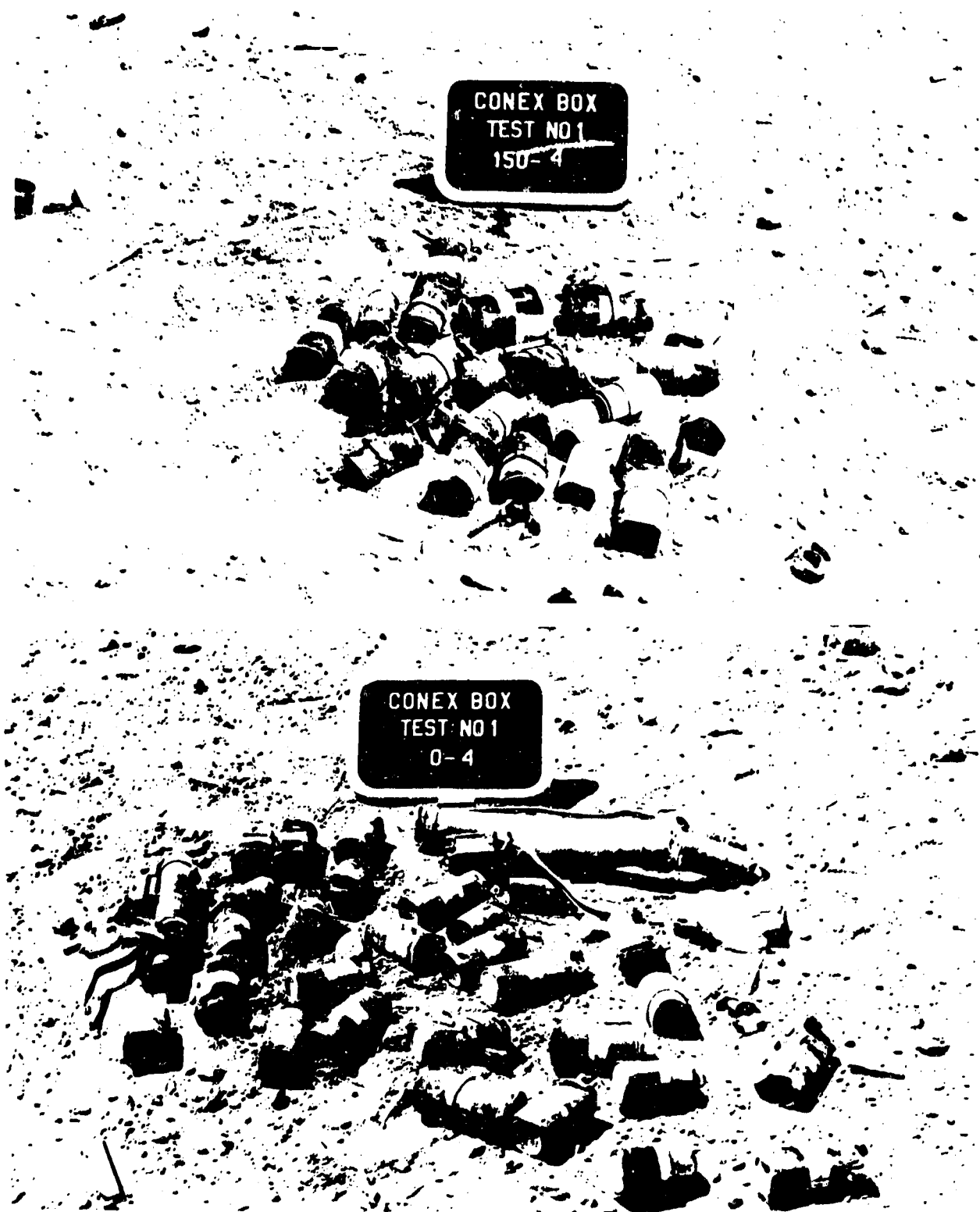


Figure 10.2. Test No. 9. (a) and (b) Grnd and 66mm Rkt between 120 and 150 feet.

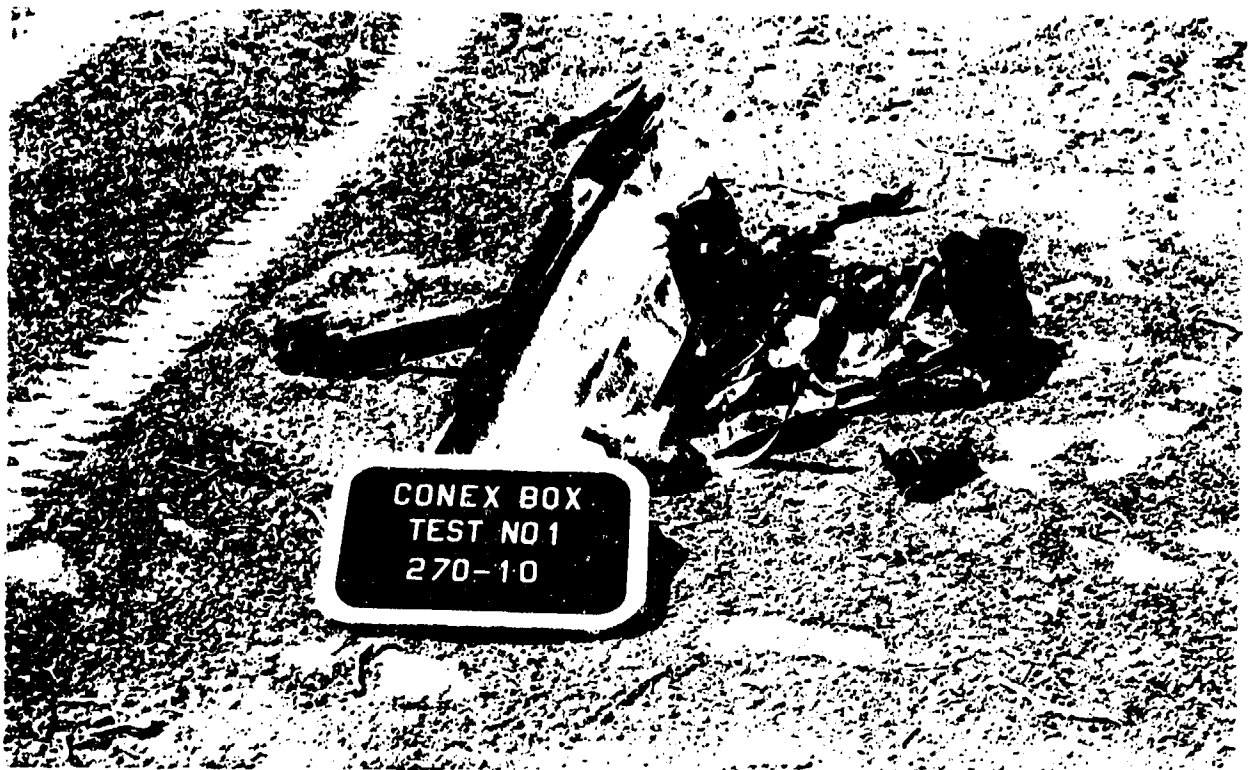


Figure 10.3. Test No. 9. (a) Part of Conex between 300 and 400 feet
(b) Conex part and Grnd between 500 and 600 feet.

TOP	12 Boxes 0.50 Cal 3 Boxes 7.62 Ammo 2 Box 5.56 Ammo	TOP	1 Box (15 ea) RKT-66mm-M72A2
BOTTOM	8 Boxes 0.50 Cal	BOTTOM	20 Boxes Smoke Grenades
COMP B: BARE CHARGE ON THE FLOOR 495 POUNDS C-4 5 POUNDS		BOTTOM 1 Box File Destruct 12 Inert Mines	
TOP	8 Boxes 5.56 Ammo	TOP	1 Box Signal Flares 10 Boxes Smoke Grenades 11 Boxes 5.56 Ammo
BOTTOM	12 Boxes 7.62 Ammo	BOTTOM	1 Box Signal Flares 14 Boxes Smoke Grenades

Figure 11. Ammunition in the Donor Container, Test No. 10.

TOP 6 Boxes 7.62 Ammo	TOP 1 Box (15 ea) RKT 66-mm M72A2
BOTTOM 5 Boxes 0.50 Cal	BOTTOM 11 Boxes Smoke Grenades
BOTTOM 1 Box File Destruct	
TOP 25 Inert Mines	
TOP 5 Boxes 5.56 Ammo	BOTTOM 1 Box Signal Fiars
BOTTOM 9 Boxes 7.62 Ammo	BOTTOM 8 Boxes Smoke Grenades

Figure 12. Ammunition in the Acceptor Container, Test No. 10.



Figure 13.1. Test No. 10. (a) Conex part between 300 and 400 feet;
(b) Conex part between 400 and 500 feet.

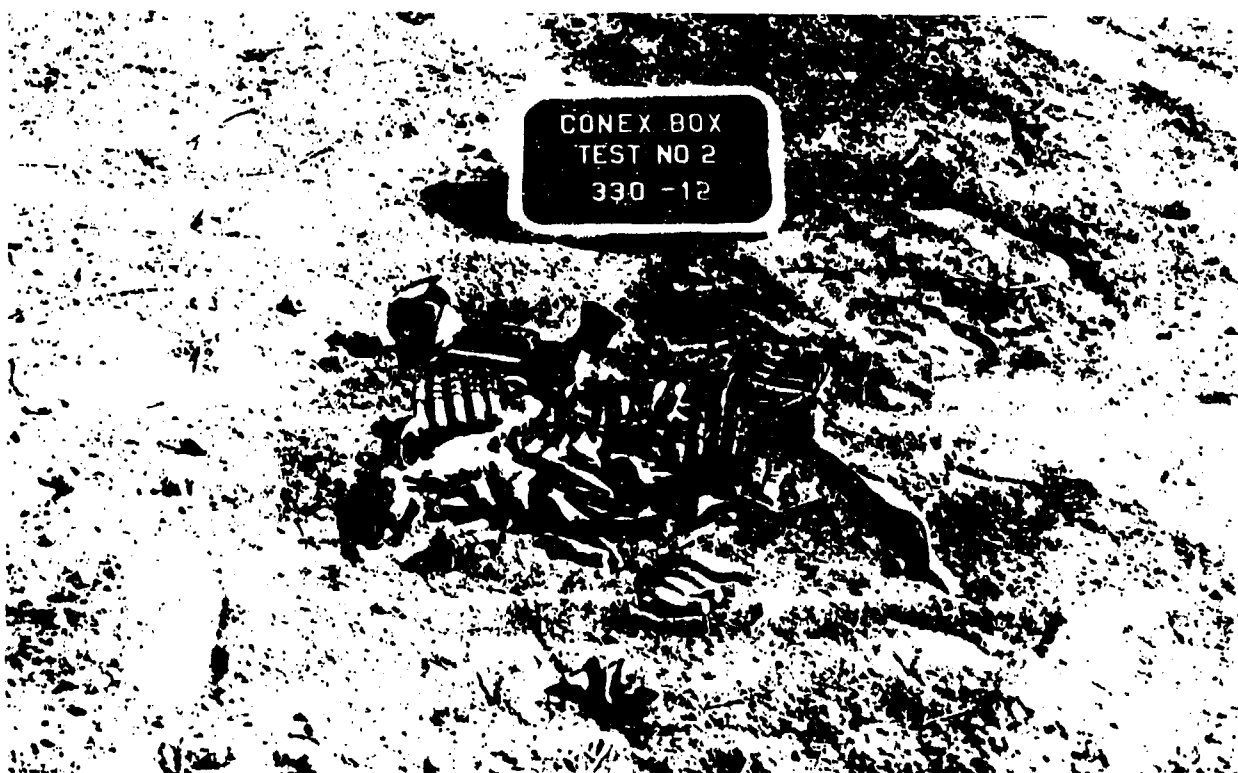


Figure 13.2. Test No. 10. (a) Conex part; and (b) small arm between 500 and 600 feet.

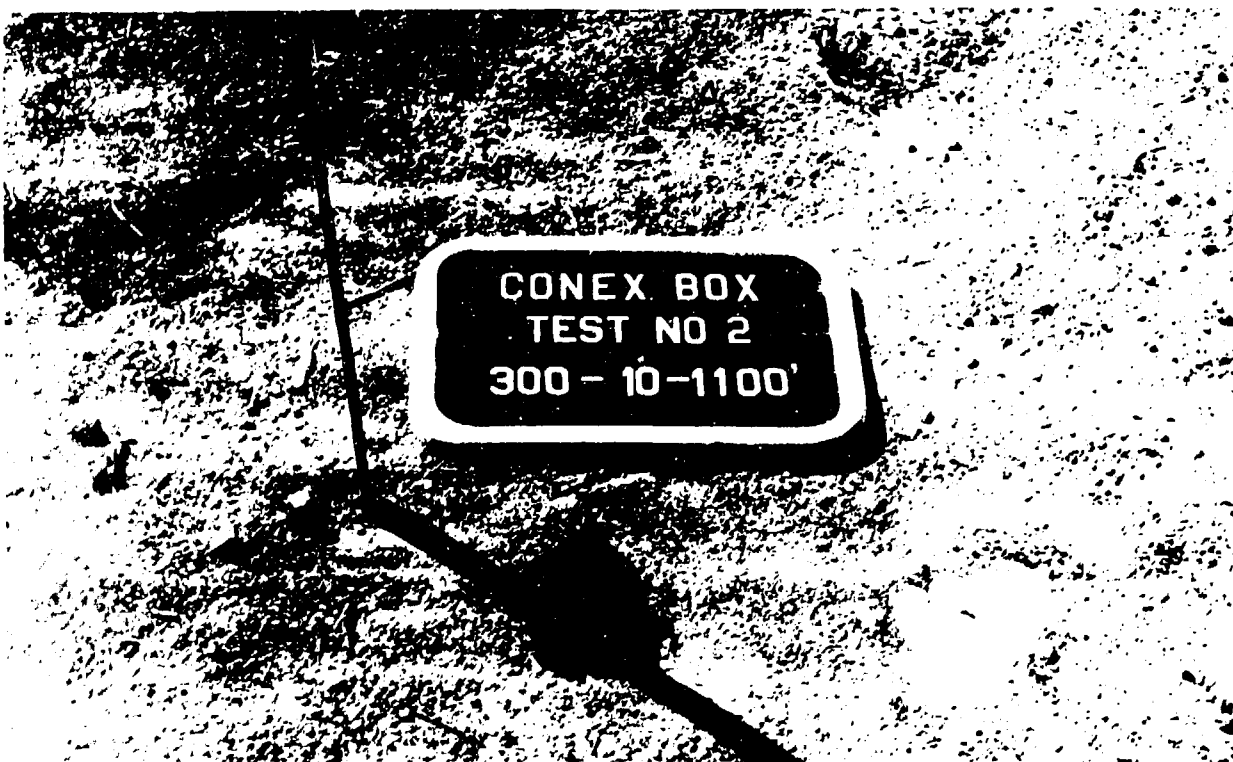
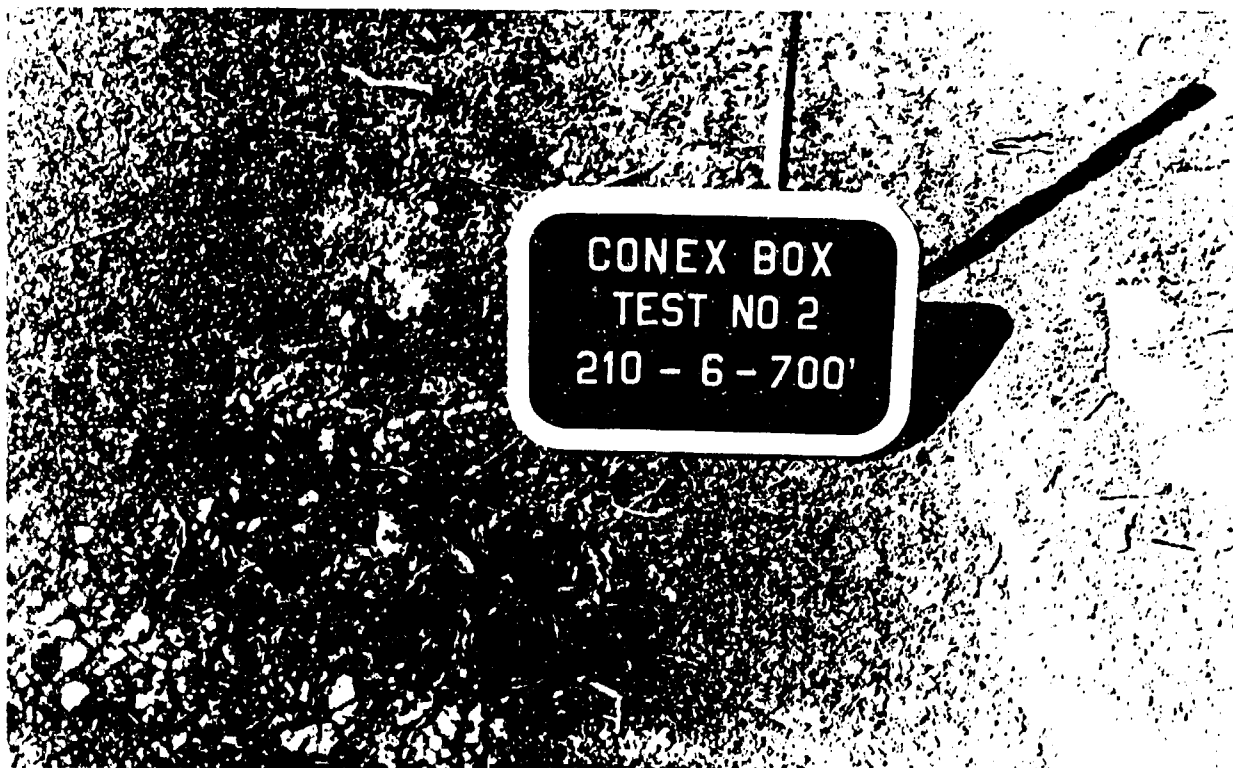


Figure 13.3. Test No. 10. (a) Ammo box at 700 feet; and (b) Part of Grenade at 1100 feet.

debris/fragments were found beyond 600 feet. The kick-out data from the last four tests are given in Tables III - V.

The fragment density at any distance was computed on the basis of a worst-case assumption. It was assumed that any fragment found in a sector at a distance greater than x feet from the origin could hit a standing person in that sector. The fragment density was computed as the number of fragments divided by the vertical area and multiplied by 600. That gave the fragment density per 600 square feet.

The fragment density, at different locations, is calculated by using 30-degree sectors. When the mean density was computed, the sectors in which no fragments were found were excluded. The fragment density and distance were plotted for 25, 75, 160, and 500 lbs of explosive. These plots are shown in Figures 14 and 15. For 500 lbs of explosive, the fragment density of less than one fragment per 600 square feet is at about 800 feet. On the other hand, the fragment density of less than one fragment per 600 feet, for 75 lbs of explosive, is between 700 to 800 feet.

In some tests, the fire started a few minutes after the detonation and lasted for a few minutes, but in other tests the fire started and lasted for some time and restarted and kept on burning for a long time (many hours). In Tests 2 and 3, the fragments and/or debris burned for one to two hours in the space between the containers. In Test 4, the fire lasted for more than two hours. In Tests 5, 7, and 8, the fragments and other munitions burned many hours. No appreciable fire was observed in Test 6. In Tests 9 and 10, the fire lasted for less than one hour.

Several rounds (7.62 mm, 5.56 mm, .50 cal, flares, grenades, etc.) were cooked off as a result of fire or heat. Some of the live munitions were recovered in each test. From the recovered munitions, it was estimated that about 25 to 35 lbs of explosive were consumed during the detonation process in each of the first four tests. It is estimated that all 160 lbs of the explosive was expended in Test 6 because no explosive was recovered in this test.

In Tests 2 and 3, the acceptor Conex was turned/flipped over and caved in, thus sustaining some physical damage. No appreciable damage was done to the contents of the acceptor container. The acceptor Conex did not move or flip over in Tests 4, 5, and 6. Much of the blast was absorbed by the sandbag wall (between the containers), thus preventing the acceptor container from sustaining much damage. The blast inside the donor Conex was so high that it created a two- to three-foot-deep crater underneath the donor Conex.

SUMMARY

A series of tests was conducted to determine the fragments hazard distance when the explosive, inside the donor Conex, is deliberately or accidentally detonated. First, three tests were conducted to determine the external debris and hazard distance and to check whether the detonation of explosives in one container would detonate the explosive in the adjacent container. The next three tests were conducted by sandbagging the containers on three sides. The next two tests were conducted by sandbagging the containers on three sides and sandbagging the walls at the front, 15 feet from the containers. Last, two tests were conducted by detonating 75 and 500 lbs of bare charge in donor containers without sandbags.

A lot of fragments and debris were found beyond 300 feet in Tests 1, 2, 3, 6, 9, and 10. Fewer fragments and other debris were found beyond 300 feet in Tests 4, 5, 7, and 8. Some fragments were

TABLE III
CONEX TEST NO. 7

Zone	A	B	C	D	E	F
9	2-50P	3-FG				
8	10-FG 2-WPFB 4-50P 1-MF			2-50P 2-50C		
7	1-MF 4-FG 1-WPFB			2-50P 1-50C 1-M42	3-50P	
6	5-FG 12-50P 5-50C		4-50P	1-50C	7-50P 1-50C	
5	1-FG 1-WPFB	4-50C 1-556P 4-50P	3-50C 4-50P	3-50C 1-50P	3-50C	5-50P 1-50C 2-WPFB
4	1-FG 7-50P,C 2-MF 1-WPF	2-50C 3-50P 1-762C	3-50P 1-762C	3-50C 4-50P	3-50P 1-50C	1-50C 2-50P
3	6-FG 8-50C 3-50P	1-762C 4-50C 4-50P	13-50C 1-50P 1-762C	5-50C 2-50P	5-50C 2-50P	4-50C 1-WPF
2	4-FG 9-50P,C 2-762P	13-50P,C 1-WPFB 1-762P	5-50C 2-762C 7-50P	8-50C 3-50P 1-WPF	3-50C 5-50P 1-WPFB	6-50C 1-50P
1	5-FG 6-50P,C 1-762P	19-50P,C 2-762P,C 1-FG	11-50C 5-50P 1-WPFB	5-50C 6-50P	5-50C 3-50P	1-556C 3-50C 2-50P
0	8 BOXES-50, 439-50, 20 BOXES-5.56, 41 BOXES-7.62, 47-SG, 3-M42, 41-FG, 154-WPF, 2-66 W/H, 4-66 MTR					

TABLE III (continued)

CONEX TEST NO. 7

ZONE	G	H	I	J	K	L
9					1-FG	
8				2-50P	8-50P 1-MF	
7				1-50P 1-50C	1-FG 1-50P	
6	1-WF			2-MF 2-50P 1-762P	1-WPF 2-50P 2-MF	9-50P,C 5-762P,C 1-WPF
5	2-WPF			3-50C 1-WPF	4-50C 2-50P 1-762C	2-50C 3-50P 1-WPFB
4	3-50C 1-WPF		5-50P,C 1-M42 1-WPF 2-MF	2-50C 1-MF	2-50P 1-762C 2-762P 4-50C	1-50C 1-50P 1-MF
3	3-50C 1-WPF	1-WPF 2-50C	4-50P,C 5-WPF 1-556C	6-50P,C 4-762P,C 1-WPF	5-50C 1-762P 3-50P	3-5-P,C 1-762P 1-762C
2	1-50P 1-WPFB	4-50C 2-WPFB 8-WPF	6-50P,C 4-WPFB	1-50P 1-50C 1-WPF	4-50P,C 1-762C 1-M42	13-50P,C 3-WPFB 1-M42
1	6-50C 4-50P	3-WPFB 4-50C 3-50P	1-50C 1-WPF	5-50P,C 1-WPF 1-M42	17-50P,C 4-762P,C 2-WPF	12-50P,C 2-762P,C 2-WPF
0	3 BOXES-7.62B, 2 BOXES-5.56B, 5 BOXES-50B, 75-SG/SGB 1-FG, 38-M42, 32-WPFB/WPF					

TABLE IV
CONEX TEST NO. 9

ITEM NO	BEARING DEG/MIN/SEC	DISTANCE FEET (M)	DESCRIPTION/SIZE
1	351/37/03	530.6 (161.7)	BUILDING FRAGMENT - 4' BY 5'
2	349/50/25	636.6 (194.0)	BUILDING FRAGMENT - 1' BY 7'
3	351/14/33	663.8 (202.3)	SMOKE GRENADE
4	358/44/50	663.3 (202.2)	SMOKE GRENADE
5	0/25/46	657.7 (200.5)	SMOKE GRENADE
6	1/3/16	625 (190.5)	BUILDING FRAGMENT - 8" BY 8"
7	1/11/09	698.2 (212.8)	SMOKE GRENADE
8	5/52/06	689.6 (210.2)	SMOKE GRENADE
9	7/54/26	701.3 (213.8)	SMOKE GRENADE
10	8/25/05	618.5 (188.5)	SMOKE GRENADE
11	83/31/34	625.4 (625.4)	CHAIN LINK DIVIDER MATERIAL FOR FILE DESTRUCT
12	163/20/55	605.7 (184.6)	SMOKE GRENADE
13	185/10/21	619.8 (188.9)	SMOKE GRENADE
14	183/34/58	604.7 (184.3)	SMOKE GRENADE
15	265/30/20	739 (225.2)	BUILDING FRAGMENT - 2' BY 2.5'
16	273/27/55	637.5 (194.3)	BUILDING FRAGMENT - 5' BY 8"
17	278/03/45	623.5 (190.0)	BUILDING FRAGMENT - 3' BY 3'
18	277/33/47	678.3 (206.8)	BLDG FRAG - 6" BY 18" AND DOOR HANDLE 18" APART
19	272/36/02	650 (198.1)	HASP FROM DOOR LATCH
20	272/07/32	767.8 (234.0)	DOOR LATCH ROD - 1" BY 2'
21	272/57/59	784.8 (239.2)	BUILDING FRAGMENT - 2' BY 2'
22	278/21/57	823.9 (251.1)	BUILDING FRAGMENT - 4" BY 18"
23	284/18/79	775.7 (236.4)	BUILDING FRAGMENT - 6" BY 3'
24	286/37/49	652.8 (199.0)	BUILDING FRAGMENT - 2' BY 3'
25	296/13/05	905.8 (276.1)	SECTION OF DOOR LATCH MECHANISM
26	304/52/52	605.8 (184.6)	BUILDING FRAGMENT - 1.5" BY 6"
27	328/54/41	603.4 (183.9)	BUILDING FRAGMENT - 2' BY 3'
28	343/14/34	632 (192.6)	SMOKE GRENADES (2) - 5' APART ON ROADWAY
29	341/44/48	631.2 (192.4)	SMOKE GRENADE - ON ROAD
30	345/00/48	608.4 (185.4)	SMOKE GRENADE
31	336/05/31	340.7 (103.8)	BUILDING FRAGMENT - 1.5" BY 2.5', SM BLDG FRAG SHARDS
32	335/04/16	446.2 (136.0)	BUILDING FRAGMENT - 8" BY 1'
33	352/58/38	370 (112.8)	BUILDING FRAGMENT - 3' BY 2'
34	352/29/44	442.2 (134.8)	BLDG FRAGS (3) - 2 @ 2' BY 7', 1 @ 6" BY 8"
35	9/10/46	372.7 (113.6)	BUILDING FRAGMENT - 3' BY 5'
36	1/42/29	295.2 (90.0)	BUILDING FRAGMENT - 2.5' BY 4'
37	33/21/55	346.5 (105.6)	BUILDING FRAGMENT - 2' BY 2'
38	39/21/55	311.2 (94.9)	BUILDING FRAGMENT - 1' BY 5'
39	37/30/22	296.5 (90.4)	BUILDING FRAGMENT - 1' BY 2' (JUST INSIDE 300' ARC)
40	44/20/47	293.5 (89.5)	BUILDING FRAGMENT - 1' BY 2' (JUST INSIDE 300' ARC)
41	54/46/11	360 (109.7)	BUILDING FRAGMENT - 2' BY 2'
42	71/27/15	315.8 (96.3)	BUILDING FRAGMENT - 2' BY 7'
43	86/41/54	323.4 (98.6)	BLDG FRAGS (3) - 6" BY 18", 2' BY 5.5', 1" BY 6"
45	75/31/41	568.1 (173.2)	CHAIN LINK DIVIDER MAT'L, BLDG FRAG @ 4' BY 1'
46	142/58/10	417.8 (127.3)	SMOKE GRENADE
47	159/14/01	448.5 (136.7)	BUILDING FRAGMENT - 1" BY 6"
48	166/40/08	378.5 (115.4)	BUILDING FRAGMENT - 2' BY 2.5'
49	172/34/11	342.7 (104.5)	BUILDING FRAGMENT - TWISTED - 8" BY 8"
50	190/35/25	313.9 (95.7)	BLDG FRAG - 1" BY 6", 2 BOXES 7.62 AMMO
51	241/14/08	463.3 (141.2)	BLDG FRAGS - 1 @ 2' BY 4', MANY SMALL FRAGMENTS
52	255/16/18	427 (130.1)	BUILDING FRAGMENT - 3' BY 5.5', PART OF DOOR LATCH
53	256/36/33	566 (172.5)	BUILDING FRAGMENT - 3' BY 3'
54	275/29/31	546.1 (166.5)	BLDG FRAGS (4) - AVERAGE 4" BY 4"
55	283/57/50	360.8 (110.0)	DOOR FRAME - 1.5' BY 6' WITH SECTION OF WALL

TABLE V
CONEX TEST NO. 10

ITEM NO.	BEARING DEG-MIN-SEC	DISTANCE FEET (M)	DESCRIPTION / SIZE
1	97/12/33	625.7 (190.7)	BUILDING FRAGMENT - 1' BY 8'
2	346/28/42	658.6 (200.7)	BOX 50 CAL AMMO - BROKEN, SCATTERED
3	350/04/27	748.3 (228.1)	BUILDING FRAGMENT - TWISTED - 2' BY 3.5'
4	348/45/33	798.2 (243.3)	BUILDING FRAGMENT - STRIP - 1.5' BY 8'
5	335/04/38	687.4 (209.5)	BUILDING FRAGMENT - 13' BY 27"
6	332/12/50	1043.9 (318.2)	BUILDING FRAGMENT - TWISTED - 6' BY 12"
7	319/37/49	940.3 (286.6)	BUILDING FRAGMENT - 2.5' BY 2.5'
8	328/10/37	696.4 (212.3)	BUILDING FRAGMENT - 2' BY 3'
9	326/35/26	622.6 (189.8)	BUILDING FRAGMENT - STRIP - 1.5' BY 3'
10	316/41/38	783.8 (238.9)	BUILDING FRAGMENT - 1' BY 1'
11	299/41/23	599.2 (182.6)	DOOR FRAME WITH HINGE (GREEN-COLORED DONOR)
12	294/15/39	617.1 (188.1)	BUILDING FRAGMENT - TWISTED - 2' BY 3'
13	297/18/37	723.0 (220.4)	BUILDING FRAGMENT - 4' BY 8"
14	291/32/39	786.4 (239.7)	BUILDING FRAGMENT - 3' BY 18"
15	298/22/50	869.6 (265.1)	BUILDING FRAGMENT - 1.5' BY 2'
16	286/45/43	919.8 (280.4)	BUILDING FRAGMENT - 1' BY 16"
17	278/01/32	623.8 (190.1)	BUILDING FRAG - 4" BY 3' / DOOR LATCH ROD 1" BY 3'
18	281/32/02	661.7 (201.7)	BUILDING FRAGMENT - 6' BY 6"
19	277/31/17	679.8 (207.2)	BUILDING FRAG - 6" BY 1.5' / DOOR HANDLE (GREEN)
20	280/26/43	746.6 (227.6)	BUILDING FRAGMENT - 3" BY 2'
21	281/55/24	815.6 (248.6)	BUILDING FRAGMENT - 4" BY 6"
22	275/44/54	827 (252.1)	BUILDING FRAGMENT - 6" BY 1.5'
23	274/04/18	751.7 (229.1)	BUILDING FRAGMENT - 8" BY 1'
24	269/26/26	695.4 (212.0)	BUILDING FRAGMENT - 3" BY 8"
25	268/50/32	675.5 (205.9)	BUILDING FRAGMENT - 4" BY 6"
26	265/29/24	738.4 (225.1)	BLDG FRAGS (2) 1- 3" BY 3.5'; 1 - 2" BY 6"
27	261/30/42	763.3 (232.7)	BUILDING FRAGMENT - 3" BY 3'
28	272/37/24	649.5 (198.0)	CLUSTER 3 SMALL BLDG FRAGS AND NWC LOCK HASP
29	272/58/16	1138.3 (347.0)	DOOR LATCH ROD - 1" BY 3'
30	259/15/33	940.9 (286.8)	BUILDING FRAGMENT - TWISTED - 8" BY 1'
31	244/38/52	692.7 (211.1)	BUILDING FRAGMENT - 1' BY 2'
32	234/43/12	604.2 (184.2)	DOOR HINGE
33	243/20/57	1155.7 (352.3)	BUILDING FRAGMENT - TWISTED - 5" BY 14"
34	232/48/10	688.6 (209.9)	FOUR LINKED 50 CAL ROUNDS
35	225/19/46	589.5 (179.7)	DOOR FRAME (GREEN)
36	225/20/12	676.3 (206.3)	1 BOX 7.62 AMMUNITION
37	223/02/38	665.9 (203.0)	9 ROUNDS 7.62 AMMUNITION
38	215/25/44	612.9 (186.8)	1 BOX 7.62 AMMO AND SCATTERED ROUNDS
39	214/34/48	707.9 (215.8)	BUILDING FRAGMENT - 8" BY 1'
40	212/17/43	764.3 (233.0)	1 BOX 7.62 AMMUNITION
41	218/37/39	754.5 (230.0)	1 BOX 7.62 AMMUNITION
42	225/54/56	1120.5 (341.5)	BUILDING FRAGMENT - 1.5" BY 1'
43	214/52/33	930 (283.5)	1 BOX 7.62 AMMUNITION
44	203/32/52	675.4 (206.0)	BUILDING FRAGMENT - TWISTED - 1' BY 2'
45	204/00/54	712.6 (220.4)	BUILDING FRAGMENT - TWISTED - 8" BY 8"
46	209/59/37	1100 (335.3)	1 BOX 7.62 AMMO - 6" FROM 1100' HUB ON 210 DEG RADIAL
47	180/07/08	900 (374.3)	1 SMOKE GRENADE AND 2 FLARES
48	162/56/14	735.8 (224.3)	BUILDING FRAGMENT - 8" BY 2'
49	166/42/52	693.6 (211.4)	BUILDING FRAGMENT - 2" BY 5'
50	169/39/52	678.8 (206.9)	BUILDING FRAGMENT - 6" BY 6"
51	156/12/44	733.1 (223.4)	BUILDING FRAGMENT - TWISTED - 8" BY 1.5'
52	131/07/45	663.7 (202.3)	BUILDING FRAGMENT - 4" BY 8"
53	120/38/35	602.1 (183.5)	BUILDING FRAGMENT - 6" BY 8"
54	115/23/11	619.9 (188.9)	BUILDING FRAGMENT - 8" BY 5'

TABLE V (continued)

CONEX TEST NO. 10

ITEM NO.	BEARING DEG-MIN-SEC	DISTANCE FEET (M)	DESCRIPTION / SIZE
55	99/57/39	668 (203.6)	BUILDING FRAGMENT - 3" BY 1'
56	85/05/26	836 (254.8)	BUILDING FRAGMENT - 15" BY 18"
57	88/27/25	727.3 (221.7)	BUILDING FRAGMENT - 3" BY 1'
58	88/43/20	619.4 (188.8)	BUILDING FRAGMENT - 3" BY 1'
59	83/35/41	626.4 (190.9)	CHAIN LINK DIVIDER MATERIAL FOR FILE DESTRUCT
60	83/16/56	653.8 (199.3)	BUILDING FRAGMENT - 4" BY 1'
61	81/14/27	667.4 (203.4)	BUILDING FRAGMENT - 4" BY 18"
62	82/10/15	698 (212.8)	BUILDING FRAGMENT - 3" BY 18"
63	81/15/13	838.8 (255.7)	BUILDING FRAGMENT - 2" BY 15"
64	70/25/24	701.6 (213.9)	CHAIN LINK DIVIDER MATERIAL FOR FILE DESTRUCT
65	45/55/39	726 (221.3)	BUILDING FRAGMENT - 3" BY 1'
66	29/10/51	723.5 (220.5)	BUILDING FRAGMENT - 6" BY 1'
67	12/2/11	927.6 (282.7)	BUILDING FRAGMENT - 1" BY 3'
68	10/26/34	739.1 (225.3)	BUILDING FRAGMENT - 1" BY 2'
69	9/48/21	606.4 (184.8)	1 BOX 50 CALIBER AMMUNITION
70	6/51/50	605.7 (184.6)	BUILDING FRAGMENT - 6" BY 1'
71	12/2/11	927.6 (282.7)	REPEAT OF #67
72	3/55/51	1084 (330.4)	BUILDING FRAGMENT - 9" BY 9"
73	0/57/29	646.4 (197.0)	DOOR HINGE
74	359/46/47	695.6 (212.0)	1 BOX 50 CALIBER AMMO, BROKEN OPEN
75	351/25/49	558.1 (170.1)	BUILDING FRAGMENT - 1" BY 2'
76	346/19/51	460.9 (140.5)	BUILDING FRAGMENT - 2" BY 3'
77	291/26/19	532 (162.2)	BUILDING FRAGMENT - 2" BY 2'
78	263/44/11	320.7 (97.7)	BUILDING FRAGMENT - 6" BY 18"
79	269/35/41	304.1 (92.7)	1 BOX 7.62 AMMUNITION
80	250/09/41	433.7 (132.2)	BLDG FRAGS (2) - 1-6" BY 6"; 1-2" BY 4"
81	237/25/25	551.5 (168.1)	ACCEPTOR DOOR (WHITE)
82	231/36/08	527 (160.6)	ACCEPTOR DOOR (WHITE)
83	228/26/17	523.2 (159.5)	ACCEPTOR DOOR LATCH MECHANISM
84	224/53/43	436.7 (133.1)	ACCEPTOR DOOR FRAME
85	224/22/32	343.4 (104.7)	BUILDING FRAGMENT - 6" BY 6"
86	225/24/56	302.4 (92.9)	2 BOXES 7.62 AMMUNITION
87	186/07/54	389.1 (118.6)	ACCEPTOR WALL SECTION - 6" BY 6"
88	186/04/49	451.7 (137.7)	ACCEPTOR WALL SECTION - TWISTED - 3" BY 6"
89	195/27/46	425.3 (129.6)	BUILDING FRAGMENT - 2" BY 3'
90	195/36/00	318 (96.9)	ACCEPTOR DOOR FRAME WITH HINGES 1" BY 6"
91	186/42/49	355.6 (108.4)	ACCEPTOR DOOR FRAME - 1" BY 6"
92	181/55/41	358.5 (109.3)	1 BOX 5.56 AMMUNITION
93	160/59/12	457.3 (139.4)	BUILDING FRAGMENT - 1" BY 8"
94	152/47/22	465.7 (141.9)	BUILDING FRAGMENT 2" BY 4"
95	145/47/22	449.9 (137.1)	BUILDING FRAGMENT - 1.5" BY 3'
96	115/09/10	425.5 (129.7)	ACCEPTOR SIDE WALL - 6" BY 6"
97	48/06/30	597.5 (182.1)	BUILDING FRAGMENT - TWISTED - 1.5" BY 6"
98	50/23/17	474.5 (144.6)	ROCKET - BROKEN
99	40/42/09	480.2 (146.4)	2 ROCKETS (BROKEN), 1 SMOKE GRENADE WITHIN 15' RADIUS
100	22/18/09	345.8 (105.4)	1 ROCKET, BROKEN
101	5/48/18	346.1 (105.5)	1 BOX 7.62 AMMUNITION
102	346/26/02	309.2 (94.2)	1 BOX 5.56 AMMUNITION
103	246/57/10	258.8 (78.9)	BLDG FRAGS (2) - 1 - 2" BY 6"; 1 - 6" BY 5"
104	243/45/00	158.8 (48.4)	BUILDING FRAGMENT - 2" BY 6"
105	264/19/12	163.8 (49.9)	BUILDING FRAGMENT - 3" BY 6"
106	201/48/19	135.9 (41.4)	BUILDING FRAGMENT - 3" BY 6"
107	184/04/33	66 (20.1)	ACCEPTOR FLOOR AND SECTION OF WALL (WHITE)
108	201/01/31	291.2 (88.8)	BUILDING FRAGMENT - 3" BY 4"
109	121/03/01	274.3 (83.6)	BUILDING FRAGMENT - 1" BY 6"
110	49/41/11	58 (17.7)	BUILDING FRAGMENT - 1" BY 6"

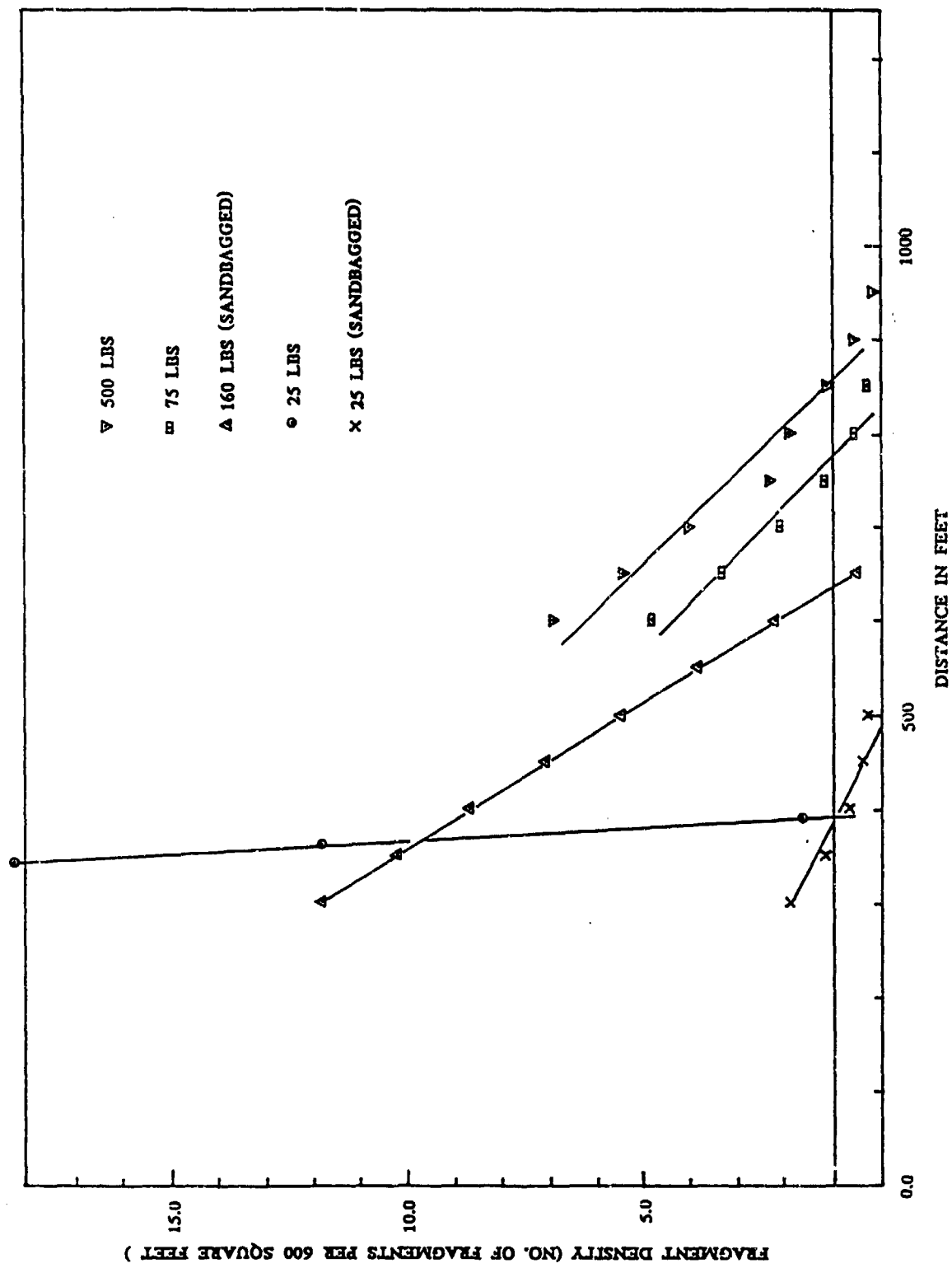


Figure 14. Fragment Density and Distance Plot.

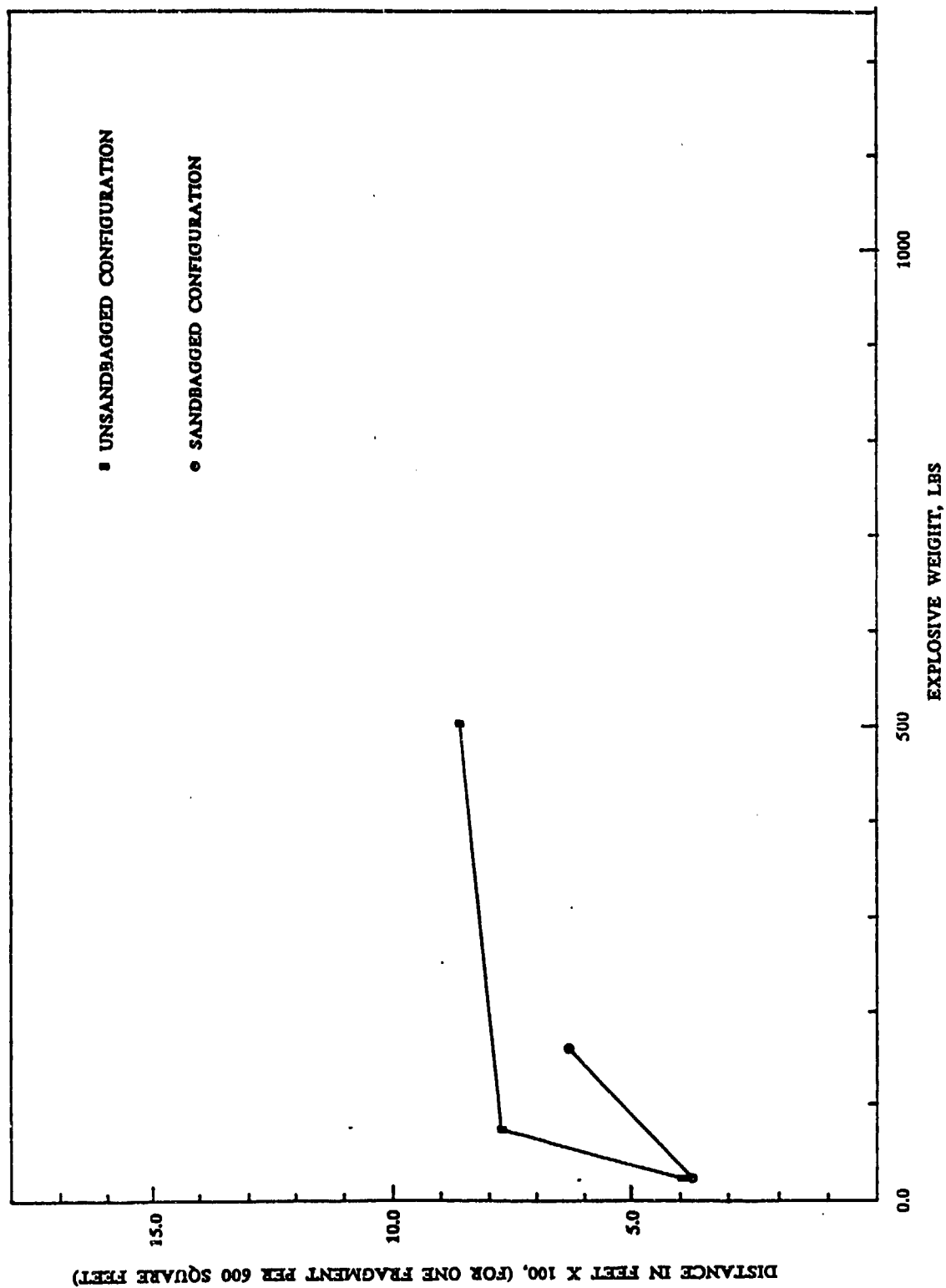


Figure 15. Distance and Explosive Weight Plot.

found beyond 600 feet in Tests 6, 9, and 10. A few metal fragments were also found between 900 and 1,155 feet in Tests 9 and 10.

Detonation did not propagate to the adjacent container in any test even when the distance between the containers was decreased to eight feet. An eight-foot separation distance was selected because at overseas bases the containers were separated by a distance of greater than six feet.

Ammunition cook-off occurred in all the tests. Sandbagging the containers decreased the fragment density at larger distances, but it increased the cook-off and burning rate of the munitions and other debris near the location of the test. So, the probability of cook-off or burning of the munitions and other fragments/debris is greater when the containers are sandbagged.

REFERENCES

1. DoD 6055.9 STD, DoD Ammunition and Explosive Safety Standards, July 1984.
2. AR 385-64, Ammunition and Explosive Safety Standards.
3. William Lawrence, "STORAGE OF MIXED MUNITIONS IN THE CONEX CONTAINERS," TWENTY-THIRD DOD EXPLOSIVE SAFETY SEMINAR, Atlanta, GA, August 1988.

ACKNOWLEDGEMENTS

The author would like to thank Mr. David Collis and his staff, TERA Group, New Mexico Institute of Technology, and Mr. Carl Halsey and his staff, China Lake, CA, for conducting the tests.

TAFI- TRADE AND FINANCE ESTABLISHMENT
5 AEULESTRASSE P.O.B 83 FL. 9490 VADUZ

**THE BLAST AND FRAGMENT RESISTANT
CONSTRUCTION SYSTEM (BFR)
for
AMMUNITION QUICKLOAD PROGRAM**

The DOD
EXPLOSIVE SAFETY BOARD SYMPOSIUM
St. Louis Missouri
August 1990

Prepared by
Yaakov Yerushalmi P.E.

April 1990

TECHNICAL AGENTS Y.Y. LTD

3 HAPARTIZANIM ST.
PETACH-TIQA
49551

TEL: 972-3-344235
FAX: 972-3-349935
TLX: 361291

THE ASP CONSTRUCTION SYSTEM for AMMUNITION QUICKLOAD PROGRAM

Yaakov Yerushalmi

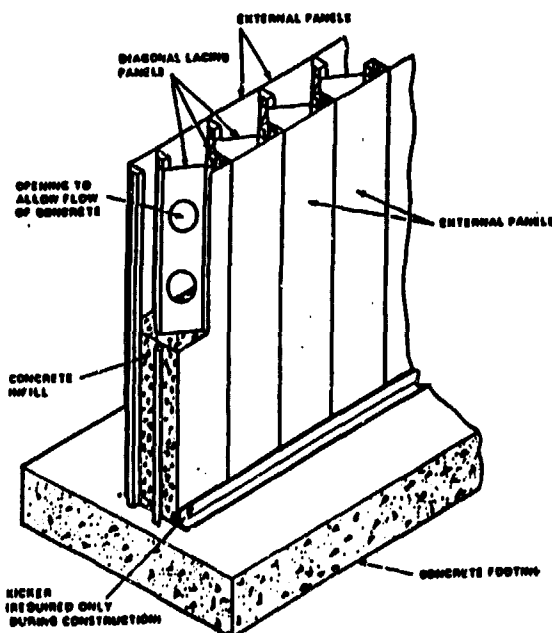
1.0 INTRODUCTION

The patented blast and Fragment Resistant construction system (BFR), known as the ASP, was developed for use in structures to resist the effects of accidental explosions, protective structures for the military and against acts of terror. The system has been tested extensively, and these tests show a significant price and cost performance advantages of the BFR system, as compared to reinforced concrete alternatives, in a wide range of accident and malevolent threat scenarios. This paper will briefly describe the system, its applications, main tests performed and recent tests, performed by the Ballistics Research Laboratory (BRL) for Ammunition Quickload Program. The purpose in the BRL test was to assess whether BFR movable panels can prevent chain detonation of trucks loaded with ammunition at a distance of 15 ft.

2.0 SYSTEM DESCRIPTION

The wall element of the BFR system, is a composite structure of interior and exterior steel panels and diagonal internal steel lacing panels, filled with a special concrete mix. (See figure 1). The BFR wall is erected on conventional concrete foundations, Roof slabs are constructed using a bottom BFR exterior panel in a similar manner to floor decking.

Reinforcement bars are used to tie the walls to the foundation, to the roof, or to intermediate slabs. BFR beams and columns can be utilized to strengthen structures. Almost any exterior or interior finish can be applied to BFR walls and buildings. Standard BFR walls are 8", 10", or 12" thick. When a single BFR wall cannot supply the required protection, a layered or "sandwich" design is utilized. A representative BFR sandwich wall consists of two separate 8" thick BFR walls, separated by 16" void. The 16" void is filled with 2" diameter stones. (See Figure 1).



BFR Panel Assembly (ASP)
1488

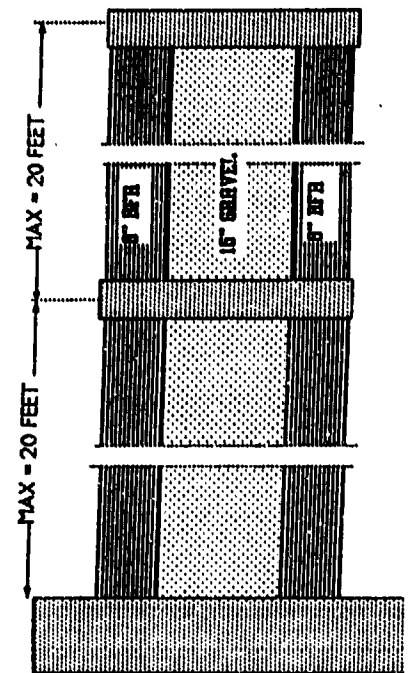
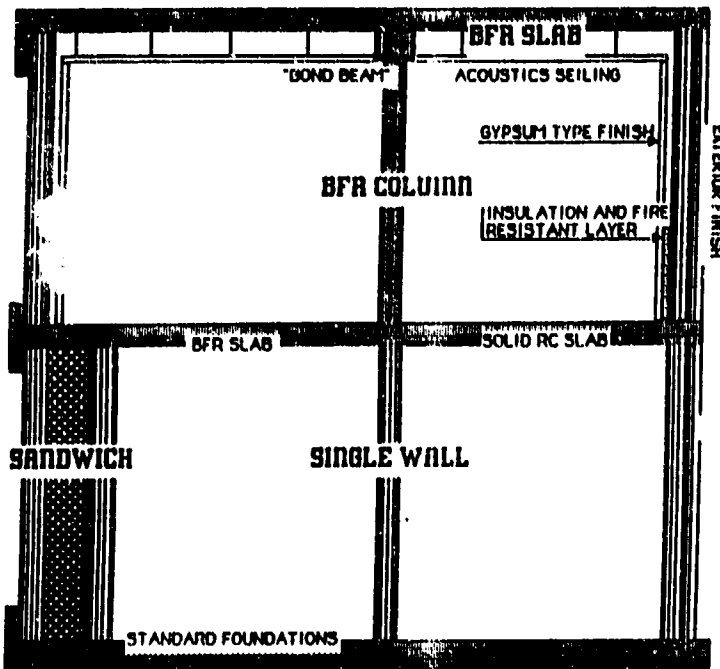


Figure 1

The system is in use for the following applications.

- (a) **SAFETY** - Ammunition and explosives magazines. Separation walls for upgrading the protection levels in existing explosive facilities, utilizing minimal space, enabling quick and clean construction. Production and testing chambers for confined or semi-vented explosions. Protected control rooms and bare cubicles.
- (b) **MILITARY** - Structures and separation walls designed to withstand near miss of air bombs.
- (c) **ANTI-TERROR** - Structures, such as computer centers or embassy buildings, designed to withstand terrorist and demolition attacks using car bombs, direct hit of shaped charges, and heavy placed charges. Upgrading protection levels of existing buildings.
- (d) **SHIELDING** - Protective structures with requirements for RF or EMP shielding.
- (e) **BARRIERS-US** standard for protection of sensitive facilities (Reference 1).

3.0 GENERAL TESTS PERFORMED ON THE BFR SYSTEM

Four different tests of buried and above ground BFR box structures (wall thickness 10") subjected to near miss of MK-82, MK-83 and MK-84 aerial bombs. Tests established that for a near miss criteria a 10" BFR wall section is equivalent to 20" RC. The high resistance to fragmentation is achieved due to the well anchored back and front plates eliminating back spalling, front cratering and edge effects. The back and front plate together with the diagonal panels confines the concrete, having a higher strength compared to standard RC.

The Naval Surface Weapons Center test (Reference 2) was intended to assess the resistant capabilities of the BFR sandwich construction against repeated direct hits of RPG-7 warheads. Five rockets were detonated on a circumscribed target area of wall (1.65 sf). The sample tested was a sandwich section consisting of 8" BFR wall, a 16" gap filled with 2" size granite stones, and a rear wall of 8" BFR. Maximum penetration was 19"; average penetration of the five rockets was 16". Penetration in the BFR section is about half of the penetration of the RPG-7 warhead in solid RC section. The measured results of this test are similar to the result of two different tests performed outside the USA. The conclusion is that the 32" thick layered BFR sandwich section is equivalent to a 50" solid RC section.

The purpose of the French Corps of Engineers test (Reference 3) was to apply reflected pressures with relatively long duration on BFR gable wall, simulating scenarios of accidental explosion of ammunition magazines. (See Figure 2).

A BFR wall panel 11.5 feet long, by 10 feet wide, was constructed on a heavy steel frame. The steel frame was bolted to an existing heavy concrete structure. The BFR wall was bolted to the top and the bottom of a steel frame. Sliding or movement of the BFR wall was precluded. The blast loads were generated by detonation of 1750 lbs of TNT at various distances. Free field and reflected blast parameters were measured, as well as strains, accelerations, and displacements. Four detonations were done starting with a peak reflected pressure of 7 psi up to peak reflected pressures of about 200 psi with positive duration of about 15 msec.

The conclusion from this test is that 10" thick BFR wall can serve for the construction of front gable wall of ammunition magazines.

4.0 THE AMMUNITION QUICKLOAD PROGRAM

The "Quickload" tests used large quantities of ammunition on flat-bed trailers. Ammunition for USA military units are stored on flat-bed trailers in compounds near inhabited buildings. Most of the ammunition consists of mass-detonating munitions. If one trailer load detonates there is currently no fully satisfactory method to prevent detonation propagation of munitions on other trailers.

The purpose of the test was to assess whether BFR movable panels can prevent chain detonation of ammunition trucks. Five movable BFR panels 12" thick and 8' high were placed between two trucks loaded with ammunition. Distance between the side line of the ammunition stored on the trucks was 15'. The Donor trailer contained 160 M107 projectiles (155mm) and 160 staggered M3A1 propellant charge cans. The Acceptor trailer contained 96 projectiles and 96 M3A1 propellant charges.

The test took place in March 1988 (Reference 4). Accidental detonation was simulated by simultaneous detonation of four rounds on the Donor truck. All the projectiles of the Donor truck were detonated. A crater of 58" deep x 25 feet x 24 feet was left by the explosion.

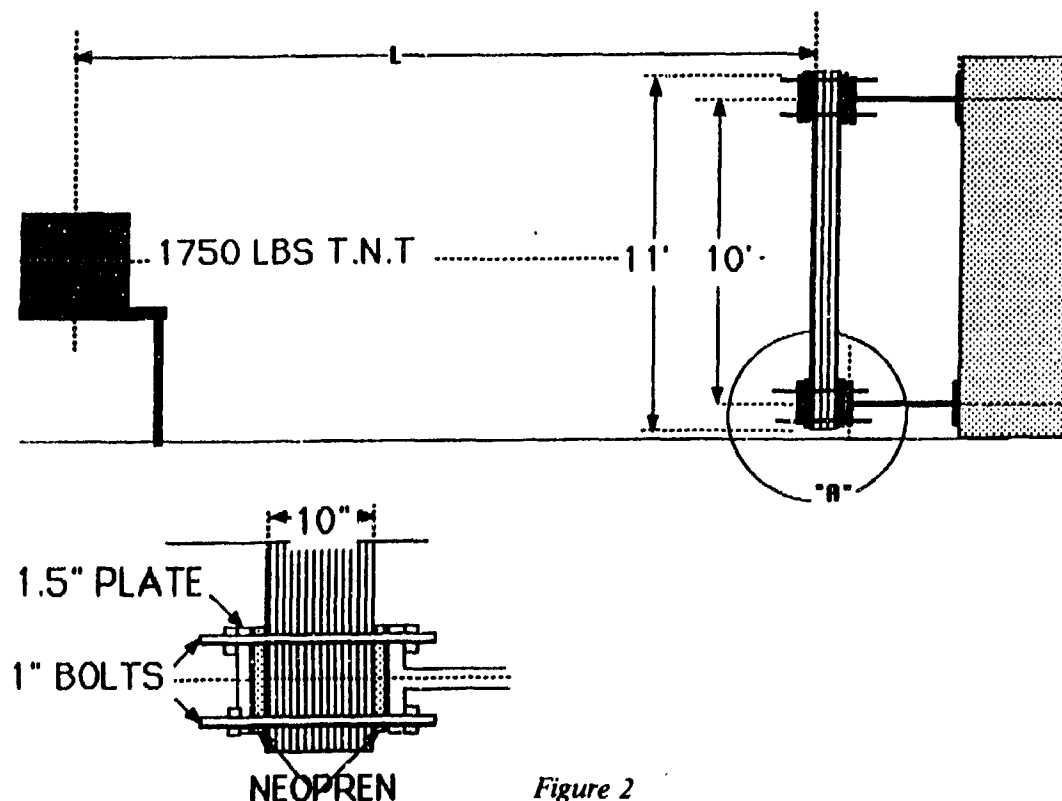


Figure 2

The test has revealed success since a chain detonation was prevented (Figure 3). The overpressure at a distance of 450 feet was 1.72 psi at 550 feet, 0.89 psi and at 650ft 0.74 psi. Two additional tests (Reference 5) which had identical setups to the test described above, were carried out in FEB 1989. Both tests were successful, with similar results.

Based on three successful tests the recommendation of BRL is that the specific BFR movable wall can be used to separate truckloads of ammunition which have a Net Equivalent Weight of 2500 lbs with a minimum separation distances of 15 feet. For Basic load Ammunition Holding Areas (BLAHA), shielded with the BFR system, the Q-D requirement for public traffic routes is 600 feet and unhabited building distance is 900 ft regardless of the number of loaded trucks.

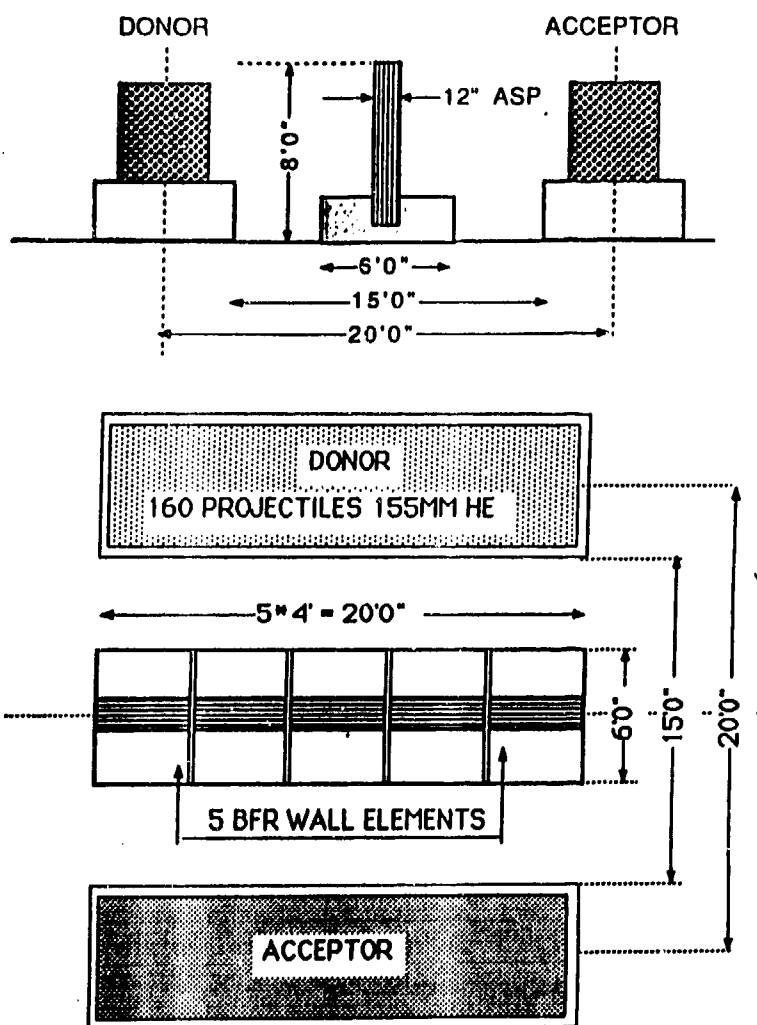


Figure 3

5.0 LIST OF REFERENCES

5.1 Reference 1

Baricades-DEF 149-30-1 US Army Engineers Division, Huntsville. Dec 12, 1988.

5.2 Reference 2

Testing of the ASP sandwich barrier with shaped-charges (RPF-7) warheads by H.M. DeJarnette Research and Technology Department. 19 February 1986. Naval Surface Weapons Centers, White Oak, Silver Spring, Maryland 20903-5000.

5.3 Reference 3

Protection against blast and splinters of strong walls, Part I: ASP Wall Direction centrale de Genie (French Chief of Engineers Office), Captien, November 1987.

5.4 Reference 4 & 5.

ASP walling system concrete barrier, (ASP) test results, ammunition quickload test series, prepared for U.S. Army Armament Research and Development Command, Ballistic Research Laboratory, Aberdeen Proving Ground, Maryland 2005. Contract No. DAAA15-87-D-0006, Task No. 4, New Mexico Institute of Mining and Technology/Tera Group, Socorro, New Mexico 87801, 3 June 1988. Additional report from 19 April 1989.

A MICROPHYSICAL MODEL FOR THE ELECTROSTATIC DISCHARGE SUSCEPTIBILITY OF SOLID ROCKET PROPELLANTS*

By

**Ronal W. Larson
Rodney A. Perala
Mark F. Gyure
Paul Beale**

**ELECTRO MAGNETIC APPLICATIONS, INC
12567 West Cedar Drive, Suite 250
Lakewood, CO 80228
303/980-0070**

ABSTRACT

Since the occurrence of the ESD related accident involving a Pershing II solid rocket motor segment in January of 1985, there has been much interest in the effects of static electric fields on solid rocket propellants. It has been found that these propellants can undergo dielectric breakdown under moderate electric fields, from as low as about 80 kV/M to a few hundred kV/M. This dielectric breakdown can also lead to propellant ignition under certain conditions involving temperature, confinement, sample size, and other variables.

The objective of this paper is to present some of the results of a basic research effort in which a microphysical model of propellant susceptibility has been developed. Much of the modeling has been based on a branch of physics called Percolation Theory, which is used to describe the properties of a random disordered system. In this case, the system is the propellant mixture consisting of conducting aluminum particles, ammonium perchlorate particles, and the nonconducting HTPB matrix. Primarily, the criteria for ESD ignition are described and discussed in this paper.

1.0 INTRODUCTION

In January 1985, a serious accident involving the Pershing II missile occurred in Germany that has since been attributed to Electrostatic Discharge (ESD). In the intervening five and one-half years, it has become clear that there are both macroscopic and microscopic reasons for ESD to be a serious hazard for solid propellants. Based on both static and transient macroscopic simulations (both theoretical and experimental), it is now well appreciated that the propellant fields from realistic charge densities can exceed those known to cause breakdown. Unlike most dielectrics,

* Work Supported by the U.S. Army Research Office (ARO) under Contract # DAAL03-87-C-0021

Presented at Twenty-Fourth DoD Explosives Safety Seminar, Adams Mark Hotel, St. Louis, Missouri, 28-30 August 1990

propellants often have breakdown field strengths that are lower than air breakdown. The reason for this enhanced breakdown is that in many solid propellants, small metallic particles (about 20 % by weight of the mixture) serve as the primary fuel. These particles are primarily responsible for the enhanced propellant breakdown sensitivity, since they serve to enhance any electric field applied to the propellant.

From a modeling standpoint, the macroscopic analysis of the field distribution is not simple, but good accuracy is possible, and there are few doubts that hazardous electrical field strengths can occur. From a microscopic viewpoint, modeling is able to explain, primarily through the statistical details of the proximity of the aluminum particles, many of the experimental breakdown variations. However, the details of the behavior of propellant breakdown fields, conductivity and permittivity as a function of time (or frequency) and temperature are not yet completely understood.

In this paper, it is not possible to give a full introduction into the ESD breakdown phenomenon in solid propellants. However, a review was given of the four major parts of the breakdown phenomenon in a Lightning/ESD symposium paper [1]. Those areas and a review of the ESD accidents are given in a longer report [2] from which much of this paper is taken.

We can summarize the four major ESD areas of Reference 1 by noting:

Charge Generation occurs triboelectrically during separation of dissimilar (usually dielectric) parts. It can occur either by movement of the entire motor or core, by "flapping" of fin formers (metal parts used during casting to create internal cavities that give improved combustion properties), or by some similar means. Although yet little studied, charge associated with lightning strikes is also of sufficient magnitude to cause an internal breakdown.

Macroscopic geometric field enhancement can be caused by sharp metal corners or close spacings after flux line "flipping" into the propellant caused by movement of parts. Lightning hazards would not require movement of parts in order to reach breakdown field levels.

Microscopic field enhancement occurs because of the physical makeup of solid propellants, especially the close proximity of aluminum particles. Low temperatures substantially enhance the probability of breakdown, for reasons still not understood.

Ignition following an initial breakdown is determined by pressure confinement and the details of the "circuit", which determine the time duration and energy released during the discharge. Minima in each must be exceeded that are functions of the pressure. Both experimentally and analytically, we are getting closer to understanding how to obtain these minima. However, many experiments clearly do not achieve the minimum energy configurations.

Because this conference has not yet had papers on ESD safety hazards, this paper begins with a summary of the historical evidence for an ESD hazard. The paper then focuses on a microscopic view of the ignition problem and on identifying the basic physical relationships in ESD-induced ignition. These relationships are shown in nomogram form for easy visualization.

The authors acknowledge the work of Dr. Fred Eriksen, Mr. John Curry and Mr. Mike Frisoni in performing parts of the work described in this paper.

2. HISTORICAL REVIEW

2.1 The Pershing II Accident Investigation

Interest in the subject of ESD and solid propellants was greatly changed in January, 1985 following a Pershing II incident in Germany that killed several U. S. soldiers. Among many other alternatives, ESD triboelectric charging was postulated; both measured charge transfer and interpreted electric field readings were in support of that hypothesis. At that time, EMA was under contract to the U.S. Army Missile Command (MICOM) to assist in their work involving electromagnetic effects (EME) associated with Army missiles. After the accident, MICOM was placed in charge of the investigations, and EMA was assigned responsibility for the ESD analysis portion of the investigation.

It was shown through EMA's detailed modeling and analysis of the PII system that internal predicted fields were consistent with fields that measurements at the MICOM and Martin-Marietta (Orlando) showed could initiate a propellant ignition. A full scale replication test, in large part designed by EMA, confirmed the probability that ESD could have caused the accident. No other possible explanation of the accident fit the facts developed during the accident investigation. A decision was made to conductively paint the dielectric case of the Pershing II in order to prevent a voltage build-up occurs on this surface. This work has been largely reported through MICOM reports on the accident [4, 5].

Other investigators active following the Pershing accident were working at MICOM, Martin-Orlando, Hercules, and Thiokol, primarily in the experimental areas of breakdown fields and electrical parameter determination. This work, as well as EMA's analytical investigation, are also reported in the Accident Investigation reports [4, 5] as well as at meetings of JANNAF (the Joint Army, Navy, NASA, Air Force organization that coordinates technical interchange activities of the government laboratories and agencies and the manufacturing organizations they support [6-8]). The EMA contribution to the Pershing accident investigation did summarize early thoughts about microstructural fields and the capabilities of percolation theory to contribute to this area. However, the majority of the EMA efforts related to the Pershing investigation were related to macroscopic analysis and to assisting in various testing efforts.

Interest at MICOM has recently shifted to the possible susceptibility of the Pershing II system to lightning. Work has also progressed on the Pershing I system, an older solid propulsion system with a metal casing. The 1988 (Oklahoma City) and 1989 (Bath, England) International Lightning Conferences have several papers on the subject of lightning protection of motors.

2.2 Subsequent Safety Modifications to Handling Procedures

As one result of concern in the industry about similar ESD hazards for other missile systems, Martin Marietta/Denver (on behalf of the U.S. Air Force's Ballistic Missile Office) began an extensive ESD analysis of the Peacekeeper system. They conducted empty motor tests and placed ESD instrumentation on launches from Vandenberg AFB, as well as sponsored propellant characterization and breakdown tests by other groups. EMA was responsible for all of the analytical studies and assisted in much of the experimental work taking place at Thiokol and Vandenberg. This work also eventually culminated in the decision to conductively paint the Peacekeeper motor to prevent a recurrence of the Pershing II incident.

Again, a significant amount of electrical propellant breakdown and ignition data was obtained during this period of study - mostly from the suppliers of the three Peacekeeper stages -

Hercules, Morton-Thiokol, and Aerojet. Martin-Orlando again performed testing in response to Martin-Denver requests for assistance. The Air Force Rocket Propulsion Laboratory at Edwards Air Force Base was also especially active during this period. The EMA responsibilities during this period were concentrated on the analysis of the internal fields for various charge configurations encountered during handling and launch. Most of these results were communicated among the propellant research community through Air Force sponsored safety meetings known by the acronym PESDWG (Peacekeeper ESD Working Group), with some appearing again at JANNAF symposia [9-15].

The task of similarly investigating the ESD susceptibility of the U. S. Navy solid propellant motors fell to Lockheed as the general systems contractor for the Fleet Ballistic Missiles. After several years of study, with EMA as its principal support contractor for analysis, Lockheed reached the conclusion that conductive painting need not be done for the FBMs, because of a much higher conductivity of these propellants. This decision was based on an extensive comparison of experimental tests and the analytical results. Microstructural analysis was not a part of this FBM work, although there were several experimental studies that have been used in comparisons with other microstructural research described below.

The Naval Surface Weapons Center at China Lake had been active earlier, but took a lead role in this Navy portion of U.S. ESD research. Again, the major motor manufacturers were involved, with information from this phase of the investigation has also appearing through the JANNAF conferences [13-16], as well as several EMA reports to Lockheed [17, 18].

2.3 The Peacekeeper, Stage I Accident Investigation

On December 29, 1987 a second tragic accident took the lives of five workers at the Air Force motor manufacturing facility in Wasatch, Utah operated by the Thiokol Corporation. The accident occurred as the core used for casting a central void in the rocket motor was being withdrawn from the rocket motor some weeks after casting. Unlike the previous ESD investigations, the electrostatic charge was here everywhere internal to the outer case of the motor, so that having a conductive case is of no real consequence. The fields internal to the propellant, however, could be of similar magnitude to that found when similar modest charge levels (10 microcoulombs per square meter) were assumed. After several months, Thiokol concluded that ESD was the most probable cause of the accident. An Air Force report has been released on this accident investigation. EMA reports, concentrating on macroscopic analyses, on the internal field strengths were an important contributor to the conclusion that ESD was a most probable cause of the accident [19]. Subsequent experimental research at MTI has indicated that a combination of electrical fields and mechanical pressures were critical in this accident. Microstructural phenomena were probably critical as well.

2.4 Subsequent Safety Modifications to Core Removal Operations

Morton Thiokol has successfully made a number of changes in their core removal processes. As the high probability of an ESD-caused ignition of the MTI first stage Peacekeeper became more obvious, the Air Force Ballistic Missile Office also asked Aerojet Solid Propulsion Company (ASPC) to perform a similar analysis for their second stage of the same missile. The EMA report on their core stripping operations has indicated significant differences from those of MTI, but especially in the character of the propellant, which has an appreciably shorter electrical time constant [20]. These have indicated a safer situation for the second stage motor.

The similarity in tooling and core popping operations between MTT's Peace-keeper and Space Shuttle solid rocket motors also suggested to MTT the appropriateness of an ESD analysis for the shuttle motors. The Shuttle motor's propellant turned out to be even more conductive than that used in the Peacekeeper, so large fields were virtually impossible to obtain at any core removal speed, but certainly not at the modest core-removal speeds used [21].

2.5 Other Historical Aspects of ESD Hazards

An important U.S. mechanism for the dissemination of information are the annual (sometimes semiannual) meetings of an ESD panel operating as a part of a Hazards Subcommittee of JANNAF. Usually a dozen or more talks are presented on all facets of ESD hazards by almost as many organizations. Most of these talks are preserved in conference proceedings.

ESD testing of small samples of propellants was a regular practice of all U.S. solid propellant manufacturers in the years before 1985. Except for a few highly active propellants, these tests "showed" that ESD was not a major hazard; although they broke down, ignition rarely occurred. In retrospect, we now see that the testing was not adequate to determine true safety margins (for instance, all such tests were - and most still are - performed at room temperature).

During an EMA literature review on ESD in 1985, little prior theoretical or experimental material was uncovered on ESD and solid propellants. The primary prior evidence that ESD could be a significant safety hazard was a paper by Kent and Rat [3a, 3b], reporting on accidents in France attributable to ESD. They briefly referenced percolation theory, and called for testing on larger samples, which they felt strongly indicated cause for greater worldwide concern about the ESD hazard with solid propellants. The French also identified a number of serious accidents at their solid rocket facilities that they felt were attributable to ESD. The French warnings do not seem to have become known within the U.S. propellant industry at that time. Immediately after the accident, the French were quickly sought out as the main experts in the field. It now appears that their development of a percolation coefficient was not based on analytical work, but rather was based on heuristic reasoning.

The French also discussed the measurement of electrical parameters (especially volume resistivity) as being important in identifying propellant formulations that would be especially hazardous. As a result of this observation, but also to provide input for system modeling, a great deal of recent U.S. effort has gone into the gathering of this experimental data as a function especially of temperature and time (or frequency).

One additional valuable study was found that preceded the Pershing II accident. This was by Dalton Cantey of Lockheed Missile Company, who was interested in electrical parameters as a surrogate for measuring mechanical parameters [3c]. His hope was to study mechanical property degradation due to aging in the field by measuring electrical characteristics instead. As a result, he provided a significant early broad-band contribution on the unusual long-time electrical behavior of the propellant.

Additional ESD research at EMA and elsewhere is reported in References [22-27].

3. PHYSICS OF THE IGNITION PROCESS

The steps in a solid propellant ESD breakdown and ignition process occur approximately as follows:

1. A positive charge density (of approximately 10 microcoulombs per square meter) is deposited on a dielectric (often Kevlar) surface as it separates from or slides against another stationary dielectric (often Teflon) which carries an equal negative charge density.
2. As the two dielectrics separate, the flux lines from the positive charge predominantly turn inward, thereby creating a potentially high field in the propellant or at the propellant surface (especially if the propellant is conductive and isolated from ground).
3. With an insulative propellant, an E-field can be established in the propellant, especially near small metallic regions where flux density concentration can occur. With a conductive propellant, the entire grain can be established at a lower potential.
4. A discharge is initiated either through the propellant or to it. The energy deposited can be determined with knowledge of the arc resistive characteristics - assumed to be on the order of 100-1000 Ohms.
5. The arc vaporizes some of the propellant; subsequent chemical reactions are exothermic and substantially more energy is now available to further raise the propellant surface temperature.
6. The probability of full ignition is greatly enhanced by maintenance of pressure. In a large motor, this probably occurs naturally. In the laboratory, it is more difficult to obtain since cracking prevents the required increase in surface temperature. In Section 4, we will discuss ignition more quantitatively.

In the above picture of the ESD ignition process, we shall refer to steps 1, 2 and 3 as system level or macroscopic processes: e.g., the charging process or the propellant polarization in the source fields. They all take place at the system level. Steps 4, 5 and 6 take place at a local or microscopic level. Step 4 can be described primarily by dynamic parameters, for example currents and discharge times, and we refer to it as the micro-discharge. Ignition occurs in steps 5 and 6 and involves thermodynamic considerations and reactive chemistry.

4. MICROSCOPIC OVERVIEW

4.1 Introduction

Analyses of ESD-caused ignition (as opposed to breakdown) of solid propellants include investigation of:

1. Electrical energy available to start ignition in typical system level geometries,
2. Electrical energy deposition in typical arcs as a function of sample size and characteristics such as resistance,
3. Electrical energy, power, and time requirements for arcs to cause ignition,
4. Resistive loss mechanisms in arcs, and,
5. Physical properties of solid propellants (e.g., heat capacity) that relate to ignition.

The above considerations can be broken up into two levels of investigation: a system or macroscopic level, and a local or microscopic level. In Section 3 we discussed the electrostatics of

system level ESD charging. Our discussion of the local or microscopic level is contained in Sections 4.3 and 4.4, and will be broken up into the arc electrodynamics and the ignition physics. Section 4.3 addresses the relationship between energy and properties of the arc, and Section 4.4 discusses the basic laws relating to propellant ignition, and the extrapolation of current ignition threshold data to the short time scale of micro discharges.

We note that the ESD community often uses the words vulnerability and susceptibility to describe aspects of the breakdown and ignition problem. In our terminology, the available energy on a system level is related to vulnerability, and the energy in the micro discharge (between particles in metal loaded propellants, for example) is related to susceptibility.

One of the objectives of this paper is to provide a set of nomograms to quantify the relationships between the various important ignition parameters. There are many parameters including power, power density, energy, energy density, voltage, charge, current, resistance, capacitance, time, and charge density, for example. There is generally a physical property of an object that is a parameter for curves on the nomogram. Examples of such parameters are arc length, capacitance, spark gap distance, source charge density, and resistance. It is hoped that these nomograms will help the reader to appreciate quantitatively the many relationships that exist at the system and local levels. Additional information that may be helpful in understanding the concepts in this paper are contained in Reference 2, although most of this work has followed that publication.

4.2 System Level Electromagnetic Principles

At the system level we will show the relation between the internal voltages and fields, and the external sources which are charge densities. The physical properties of the system that relate these quantities are capacitance and system level gap dimension. The mathematical relations between the variables are:

$$Q = Q_s A \quad (1a)$$

$$V = Q/C \quad (1b)$$

$$V = E d \quad (1c)$$

$$U_a = 1/2 C V^2 \quad (\text{or } 1/2 Q V) \quad (1d)$$

where

Q	=	total charge (coulombs)
Q_s	=	charge density per area (coulombs per square meter)
A	=	area (square meters)
V	=	voltage across the system (volts)
C	=	capacitance of the system holding the source charges (farads)
E	=	magnitude of electric field (volts /m)
d	=	system level gap (distance over which E is developed) (meters), and
U_a	=	available energy (joules)

Figure 1 shows these equations in graphical form (nomograms), using log-log scales for each nomogram. For example, Figure 1a (the right-hand figure) shows Eq. 1a, where we can enter a known area A (abscissa) and an assumed charge density Q_s , to obtain a specified charge. These nomograms allow one to more clearly visualize the relationship of the many system level electromagnetic parameters.

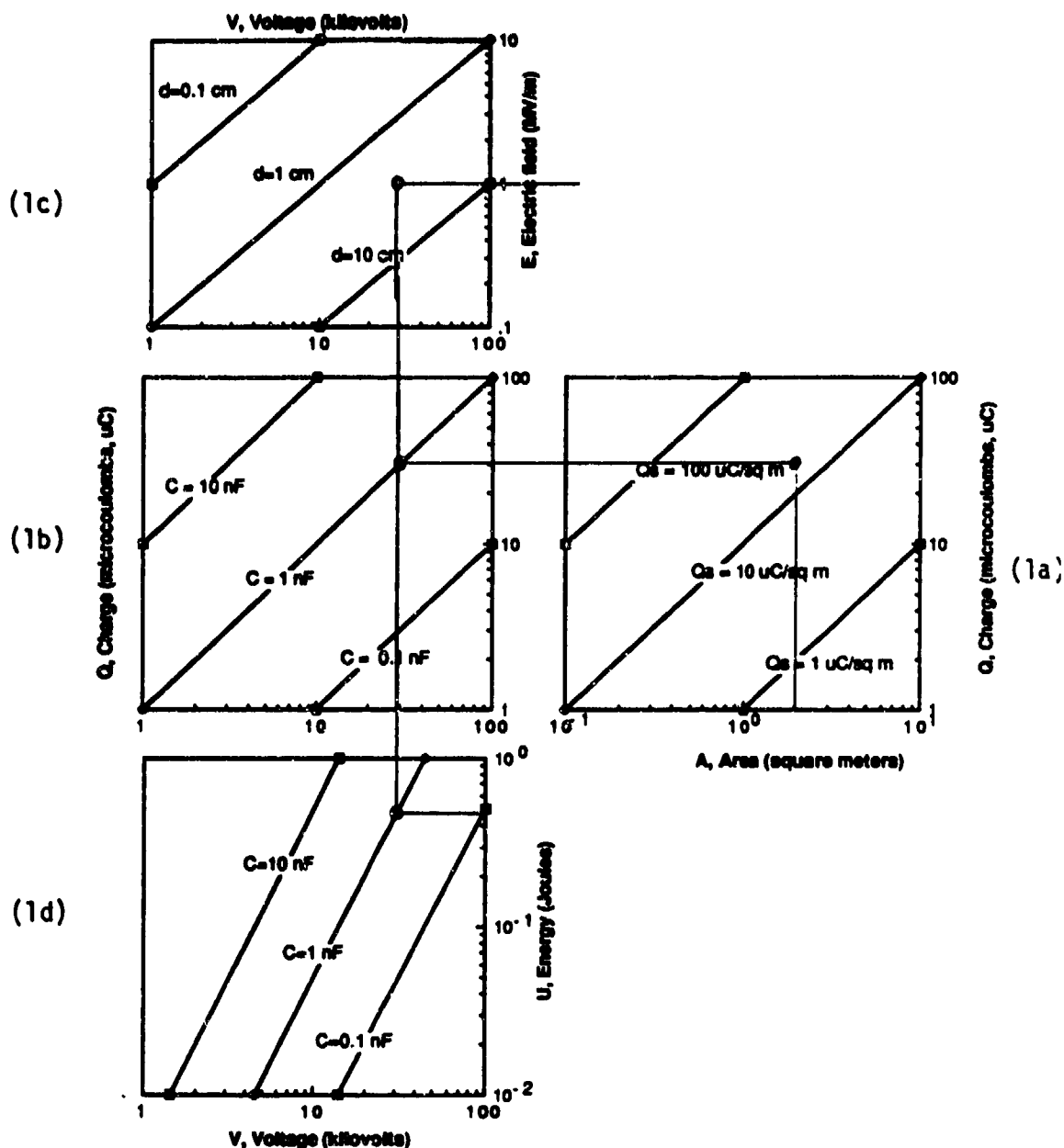


Figure 1 System Level Relationships Between Available Charge, Voltage, Field and Energy
(See text for defining relationships and explanation of example)

In the example, we assume an area of two square meters and a charge density of $Q_s = 15$ $\mu\text{coulombs per square meter}$. This gives a total charge Q of 30 $\mu\text{coulombs}$. Traveling left from Figure 1a to Figure 1b gives a voltage if the total equivalent capacitance is known. In our example case, an assumed value of 1 nanofarad would lead to a voltage of 30 kilovolts. With this voltage, average fields (Figure 1c) and energies (Figure 1d) can also be established. In the example, a field of 1 MV with a gap of 3 cm as shown in Figure 1c gives an energy of 0.45 joules with 1 nF.

All equations here were linear except the quadratic dependence of the available energy, U_a , on voltage, as seen in the steeper slope for Figure 1d. Figure 1 can be used to establish upper limits for the various quantities that may later be dictating an arc and possible ignition.

4.3 Microstructural Electro Magnetic Principles

We now look more closely at the possible values for discharge energy, to assure ourselves that they are not in fact greater than the available energy. Figure 2 shows four interconnected nomograms. Although each nomogram can be used to find any variable as a function of the other two, we underline below the most likely variable to be solved for. The four nomograms respectively are:

- | | |
|-----------------|---|
| a. Lower left: | Resistance vs voltage with <u>current</u> as a parameter |
| b. Upper left: | <u>Power</u> vs voltage with current as a parameter |
| c. Lower right: | Resistance vs <u>Time</u> with capacitance as a parameter |
| d. Upper right: | Power vs time with <u>power density</u> as a parameter |

The equations for these nomograms are:

$$I = V / R \quad (2a)$$

$$P = I V \quad (2b)$$

$$t = R C \quad (2c)$$

$$U = P t \quad (2d)$$

By entering a voltage in Figure 2a (which can be obtained from later graphs, with knowledge of breakdown field and separation), and an assumed resistance (obtained from independent studies of breakdown physics), we can determine the likely current between the discharging spheres, using Eq. 2a. In the example shown, we assume 10 volts and 1000 amperes, giving a current of 10 milliamperes (ma). In fact, we know that both the voltage and the resistance are time-varying, so the current certainly is also. The graph should only be used to get an average value.

Traveling upward with the same voltage to Figure 2b, and using the currents just obtained (alternatively, we could have used the resistance with the formula $P = V^2/R$), we can obtain the power (time rate of change of energy deposited), using Eq. 2b. A possible error can creep in here, since the currents are reversed from their order in Figure 2a. In the example, we obtain a power level of 0.1 Watts.

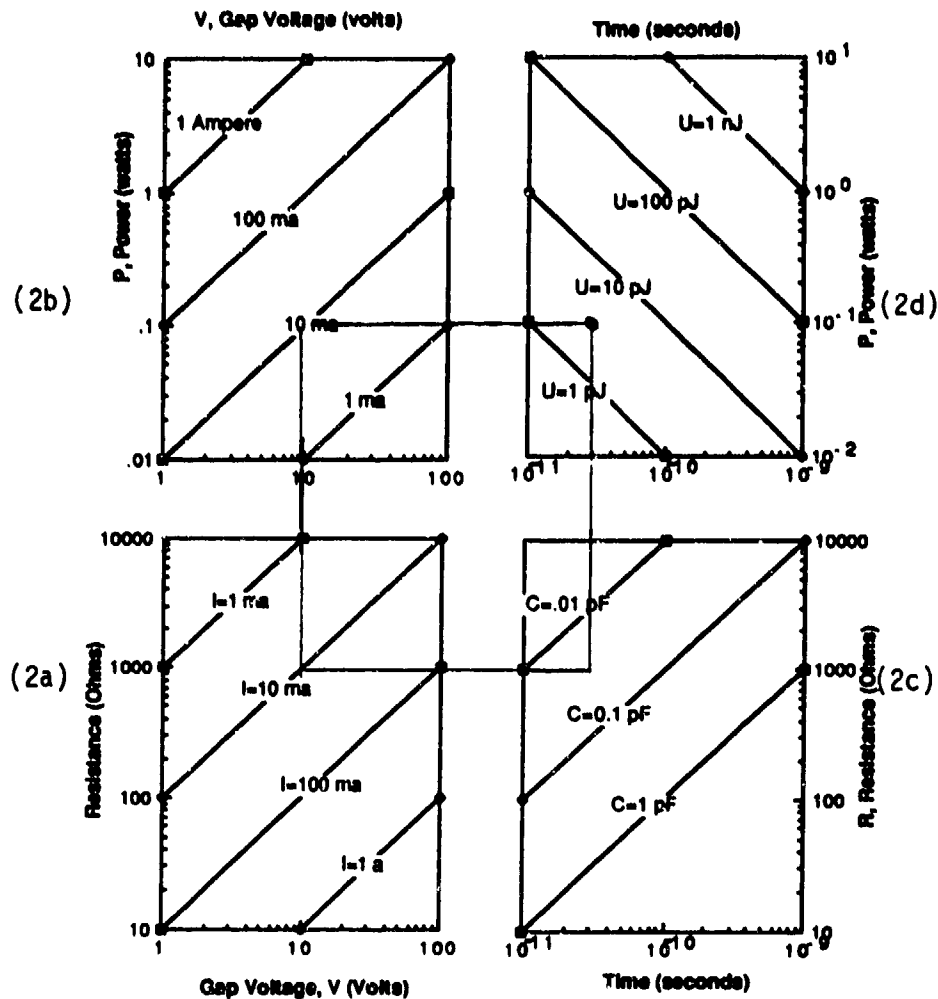


Figure 2 Discharge Parameters (Volts, Current, Resistance, Power, Capacitance, Time, Energy)

In the lower right quadrant, we have a means of determining the time scale of the discharge, using Eq. 2c. The time, t , is read off of the abscissa, with the discharge resistance, R entered on the ordinate, using an assumed intersphere capacitance, C . In the example, we take $C = 0.03$ picofarads, so the assumed R of 1000 ohms gives a discharge time of 3×10^{-11} , or 30 picoseconds.

In the upper right quadrant, the results obtained from Figure 2b and 2c are combined to allow an independent determination of the energy deposited by the arc, using Eq. 2d. In the example, we find about 3 picojoules. The energy so obtained should not be larger than the available energy obtained from the charge transfer

$$U_d = \int I V dt = V \int I dt = 0.5 Q V = 0.5 C V^2 \quad (2e)$$

To this point, we have established a system level vulnerability energy and a discharge level susceptibility energy (this section). Although a breakdown is assumed to have occurred, it is not

obvious that an ignition will ensue. This is the subject of the next section, where we first concentrate on those physical changes (other than ignition) that will first result from the breakdown.

4.4 Ignition

Our available experimental information on the power or energy density required for ignition comes from laser and ESD experiments. A major difference in the form of energy application is that the vast majority of the laser energy can be applied right at the surface which must be heated up to attain an ignition. Only reflection of the laser beam causes inefficiency; this is sometimes controlled through darkening additives. Electric sparks, on the other hand, typically demand a large voltage drop within the propellant or along its surface, which is only peripherally useful in heating the surface. This large energy may possibly be minimized by using low resistances, but this in turn leads to shorter arcs and a higher power density (but not energy density) requirement. Current breakdown experimental research will eventually lead to a good understanding of this trade-off with different resistances. In an operational (not laboratory) situation, there is a selection process which will lead to those being the most sensitive naturally occurring first.

Another difference is that the arc diameter can be much less than the several millimeters used in laser experiments. For small currents and higher pressures, diameters are estimated to be no more than a few microns (hence appreciably less than a millimeter). However, with an arc to a surface, the arc also is known to move around, so we might first start with a 1 square millimeter as a possible area. In laboratory simulations, the length of the arc may only be about 1 mm, so the area of the majority of the energy deposition may be even less than 1 sq mm.

One other large difference for electric spark-caused ignition is that the entire arc is at high temperature -- not only the surface. As the binder and ammonium perchlorate decomposes, the reaction products will be ionized and (it is believed) can thereby more readily react in or near the arc. Since these reactions are exothermic (they release energy), it seems possible that the electric arc may be more efficient than the lasers in causing ignition. Future research will possibly confirm this, when the full energy balance is understood.

Breakdown conditions are sometimes cited as being equivalent to ignition in terms of defining a serious safety hazard. Indeed, serious concerns have been raised by the observation that ignition seems to have been well underway (before stopped by propellant cracking) without a full discharge across test samples [Ref. 28]. There is little experimental data on the amount of energy that is associated with these anomalous conditions, but the required external energy would appear to be on the order of picojoules. However, experimental testing also shows that there are substantial differences - certainly in most experiments, few breakdowns do lead to ignition. However, we should note that in high pressure test configurations, other investigators do find that most discharges will lead to ignition.

4.5 Microdischarge Damage

Here, we explore obtaining a hazardous situation with microdischarges (tiny arcs that occur between small spheres) of very small energy content. Although the energy content is low, the power density can be very high, given the small dimensions of an arc between spheres. We will explore this question with the set of nomograms in Figure 3. The primary quantities of interest are the breakdown field and discharge energy. The required equations are:

$$E = V/h \quad (3a)$$

$$U = .5 C V^2 \quad (3b)$$

$$U = C_v dT v_c \quad (3c)$$

$$v_c = \pi r^2 h \quad (3d)$$

$$A = 2 \pi r h \quad (3e)$$

$$U_d = U / A \quad (3f)$$

where,

E	=	electric field
V	=	voltage
h	=	height of discharge
U	=	discharge energy
U _d	=	discharge energy density
C	=	capacitance
C _v	=	constant volume specific heat
dT	=	temperature change
v _c	=	arc cylinder volume.
A	=	arc cylinder lateral area

Each equation is plotted in the six parts of Figure 3. Our principal interest is in determining the radius of the arc, assuming that the breakdown occurs. Solving the set of equations 3, we find:

$$r = E (C h)^{.5} / (6.28 C_v dT)^{.5} \quad (3g)$$

However, the effects of the four separate parameters (E, C, h, C_vdT) are hard to visualize, and the nomogram gives a more compact visualization of the relationships. Figure 3a (lower left diagram) allows us to specify an assumed cylinder height and breakdown field. In our first example, we assume that an average field of about 10 MV/m might be sufficient (this is possibly low), giving a sphere to sphere voltage of about 50 volts. This is an appreciably larger voltage than required for breakdown across say 100 microns of aluminum oxide with a breakdown field strength of perhaps 1 GV/m, where only about 10 volts would be required.

Traveling upwards to Figure 3b, we can intersect with capacitive lines near 0.01 picofarads, appropriate to a 20 micron sphere size (using $C=4\pi\epsilon a$ for a single sphere). Even with the closer spacing of the 100 angstrom example of case 2 (and consequent higher capacitance), we deduce that the case 1 energy is higher by almost a factor of 10, with an energy of 12.5 picojoules.

We assume a thermal capacity of 10^6 joules per cubic meter per degree Kelvin and a desired temperature rise of 1000 degrees, so the C_vdT product is 10^9 . This value of thermal capacity needs more research (that is currently under way), but the use of nomograms allows a rapid determination of the sensitivity of this parameter. To keep the units manageable, we convert to picojoules and cubic microns (with a cubic micron denoted as cu in the figure and $1 \text{ cu} = 10^{-18}$

cubic meters, making the appropriate diagonal labeled 1000 pJ/cu). We thus predict approximately .012 and .0015 cubic microns (cu) respectively for the two cases.

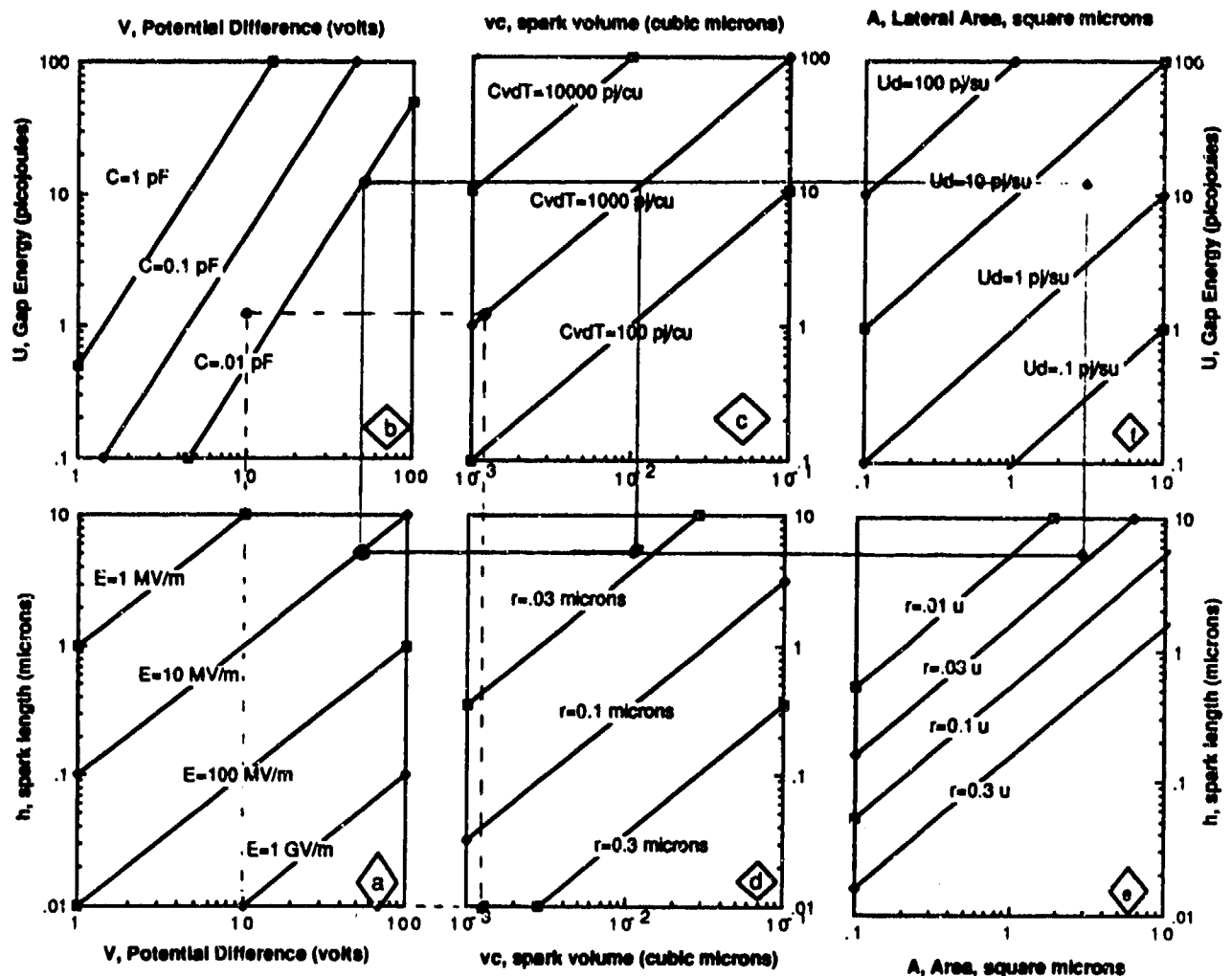


Figure 3 Characteristics of the Discharge Arc: Voltage, Field, Height, Capacitance, Volume, Radius, Area, Energy and Energy Density (Surface and Volume)

Traveling downwards to part d of Figure 3 to find a cylinder radius (using Eq. 3d), we find about 0.03 and 0.5 microns respectively. The aspect ratios (h/r) for the two cases are very different - about 167 and 0.02, the former a long thin cylinder and the latter a disk-shaped object. The temperatures predicted here would not be achieved, since we are violating the assumption of a relatively homogeneous material, with the large aluminum spheres so nearby in case 2.

Part e of this figure (lower right) carries the computation of the radius (obtained in part d) an additional step to obtain the lateral surface area of the cylindrical discharge path, using Eq. 2e. The lower part of this figure is not valid for estimating energy transfer, since the height of the

cylinder is there smaller than the radius. However, the nomogram still accurately gives the lateral surface area. With this qualification, the "total" area for dissipation of energy in the discharge is read along the abscissa of Figure 3e. Note the closer spacing of the diagonal lines, since the lateral area is only dependent on the first power of the radius (Eq. 3e), whereas the volume of Figure 3d is dependent on the second power. In the example shown, a lateral area of 3 square microns (abbreviated su) is shown.

Traveling upward to Figure 3f, we can bring the energy obtained in Figure 3c over horizontally, and find at the intersection the energy density, using Eq. 3f. In this example the energy density is about 3 picojoules per square micron. This value of energy density can then be used to determine the likelihood of ignition using the ignition characteristics of the next section.

4.6 Ignition Characteristics

Figure 4 introduces the subject of ignition characteristics. Here the interest is in the magnitude of the power and energy densities that are required to cause ignition as a function of the length of time of application of the power or energy. The new aspect of this is the continuation of familiar arguments into the regime of sub nanosecond pulses. Here the anchor value is taken as 1 watt per square mm at 100 milliseconds (based on data in Hermance [Ref. 29], showing approximately 25 calories per cm²-sec, and private communications with workers in the field, giving about the same value). We see that at the lowest time scale on the graph (10^{-11} seconds), approximately 100 kW/sq mm is required for ignition - five orders of magnitude greater than for a time of 0.1 seconds. However, note that this power level seems more manageable when considered at a micron level - it is only 0.1 watts per square micron. Figure 4a also shows a cross-hatched region of departure from the -2 slope, due to insufficient pressure. In this region, an increase in pressure is required to return to the original slope.

Figure 4b shows the same plot as it is displayed by individuals interested in ESD damage of electronic parts. Now the slope is seen to have a value of -0.5. Although the electronics damage specialist also talks of a slope of negative .5, that person is talking only of melting, and of course not of ignition as we are doing here. However, the similarity in slopes and presentation is of course because both are explained as thermal phenomena. The change in slope due to pressure appears different in Figure 4b, but is of course due to the same phenomenon. This phenomenon is not noted in the electronic parts literature, where they are normally looking at damage deep inside a high resistivity portion of a multilayered chip, and the thermal melting is unaffected by external pressures.

The presentation reversal of Figure 4b is especially useful in going to Figure 4c, which shows the energy in the same ignition event. Most importantly, the energy required for ignition actually decreases with decreasing time (or increases with increasing time). As the product of power and time, the log energy vs log time plot is found to have a slope of $-.5 + 1 = +.5$. This is relatively easily perceived in Figure 4c, with a simple increase in the slope by the power of 1, due to the multiplication of power by time to obtain energy. The reduction of the GO area due to insufficient pressure is now seen as a horizontal line defining a region in which reduction of time is no longer able to cause ignition, as it is above and to the right of that line.

The main advantage of this presentation is seen in Figure 4d, which is the companion to Figure 4a, but with a slope of +2. This exponent is not immediately obvious, nor is the behavior with insufficient pressure. The most important feature of the graph are the very low values of energy seen with short time depositions. If one could get all the way to point 2 on this plot, then a deposition of only 1 microjoule per square mm in 10^{-11} seconds is predicted to be adequate. Expressed in terms of picojoules and square microns, this is the same number: 1 picojoule per square micron.

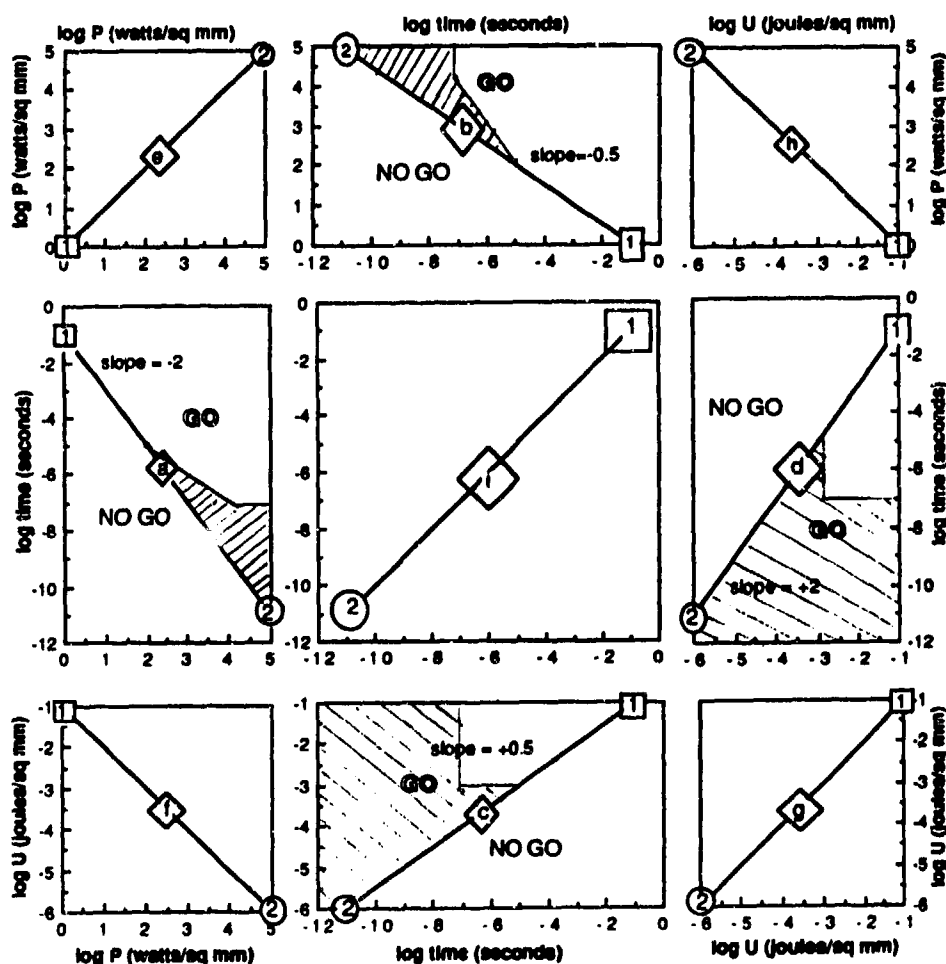


Figure 4 Hypothetical Propellant Ignition Characteristics.

These energy and temperature values seem reasonable in terms of what we know about the problem, although they are much smaller than experimentally reported values known to have caused an ignition. The lowest ignition energy we know of is on the order of millijoules for a 1 inch sample. Microjoules are reported for one case when extreme pressure was also present. We

think that a lot of the remaining difference can be made up as the energy contained in multiple breakdowns involving large strings of particles.

The remaining variable to worry about is the energy and temperature increase required for the Ammonium Perchlorate particles to participate in a chemical reaction. This will depend greatly on the size of the AP particle, which generally is much larger than the volume calculated above for the discharge volume. This is presumably why sufficient energy is available to melt (perhaps vaporize) the alumina (and a small amount of aluminum), but not enough to cause ignition.

5. SAFETY OVERVIEW

The previous material has summarized some of the analytical work at EMA dealing with ESD breakdown. This has primarily dealt with the "generic" microscopic analyses that we have performed under ARO sponsorship. However, there is another large body of work, both at EMA and elsewhere that has dealt with specific motor configurations that could not be covered in this paper. Although much can be learned from the general, non-specific analyses, the specific analyses are necessary to ensure safety for specific systems.

From these more specific system analyses we can draw general truths, summarized in terms of the four main ESD areas described in Section 1:

Charge Generation Safety

a. Materials should be selected which minimize the initial electrostatic generation. Although this rule is often contradictory with other requirements (for minimum friction for example), the motor manufacturing community has been able to find replacement materials that are proving satisfactory.

b. Conductive materials are generally less likely to generate charge.

c. Proper grounding can rapidly remove charge and/or minimize potential differences.

Geometric Field Enhancement Safety

a. Design of solid propellant motors must take account of the ESD hazard in the future, but it is almost impossible to introduce a modification into an existing design. Proper design will ensure adequate spacing of metal parts and will avoid sharp corners that can augment the interior fields.

b. Metal shielding can prevent large fields through the "Faraday" shielding phenomenon. This is especially important for lightning safety. Enclosing propellants in a metallic enclosure is the best means of ensuring safety. The use of carbon fibers in composite cases is an excellent alternative.

c. Applying conductive paint to nonmetallic enclosures is of high importance. This approach has been used retroactively with several motor systems and has been under consideration with other fielded systems. Inspection programs should be in place to ensure that these paints are adequately connecting the metallic parts of the motor to the non-metallic.

d. Grounds must be in place to tie all parts of the motor together. Personnel must understand the function of the grounding systems through training programs. In some circumstances, personnel should use personal wrist straps during handling operations.

Microscopic Field Enhancement Safety

a. The size of the aluminum and other particles are primarily dictated by specific energy requirements and considerations other than ESD. However, the wide range in breakdown fields among different propellant formulations suggests that a great deal of ESD safety improvement can be obtained if more attention is given to the formulation. The primary task will be to keep the aluminum particles separated. The use of smaller ammonium perchlorate particles is an important first step in this direction.

b. The conductivity of the binder is especially important in establishing safety, with additives being helpful to increase conductivity.

Ignition Safety

a. Pressure and confinement are extremely important in going from a relatively insignificant breakdown to the more catastrophic ignition. Steps must be taken, especially during the manufacturing process, to ensure that friction is low and that mechanical pressures are minimized, whenever electric charges may be present.

b. Since discharge time is so important, with the shorter discharges being more hazardous, sufficient resistance must be in the grounding paths as to avoid a very rapid discharge. Slow discharge (microseconds or milliseconds) is better than rapid (picosecond) discharge.

6. CONCLUSIONS

This paper has attempted to provide a brief introduction into present understanding about the ESD hazard with solid propellants. Although the understanding is still imperfect, much has been learned since the 1985 Pershing II accident. It is clear that the hazard can be primarily attributed to the close proximity of aluminum particles, which can preferentially cause a breakdown through a propellant rather than around it.

We have attempted to develop a graphical mechanism for demonstrating the inter-relationships between all of the many ESD variables - both for ESD and for ignition. It is believed that these nomograms show all the various major trends more clearly than would tabulations or multiple graphs with parametric variations. The primary critical variables are the diameters and spacing of particles.

Secondly, we have explored quantitatively the possibility that the amount of energy available in a microdischarge might be sufficient to cause an ignition, using an extrapolation of experimental results obtained for longer times of power application. It seems likely that the energy is available to cause material melting and vaporization over a radius of about one thousand angstroms (0.1 micron), when the gap length is large. More work is required to determine the likelihood of the large spacings required to see the larger energies. We do not believe that we have proved the possibility that internal micro-discharges are adequate to cause an ignition, but we do believe that we have shown it is possible.

Primary among the areas requiring more research are more accurate measures of the arc resistance. More accurate determination of parameters such as the duration of the microdischarges will enable the resistance to be determined. The analysis of the micro-discharge is found to be much more complicated than the corresponding macro-analysis. Significant additional research is required.

Safety has been improved and repetitions of the two major accident scenarios are unlikely. However, the ESD hazard largely is continuing and cannot be removed for many existing propellant formulations. Future formulations can be improved, but the propellant ESD hazard will never be completely eliminated.

ESD hazards have largely been analyzed from the standpoint of the two accidents (one handling, one during manufacture) attributed to triboelectric electrostatic charge generation. Hazards due to lightning have not been subject to significant study - either theoretical or experimental. It seems likely to the authors that the safety record is due more to the low likelihood of a strike than to the safety precautions in place following a strike.

The possible use of high power microwave (HPM) energy to intentionally cause an internal discharge in a solid propellant motor has apparently not yet been analyzed. Our belief is that an HPM safety hazard is likely to exist with some fielded solid propellant systems.

REFERENCES

1. Larson, Ronal W., "An Overview of the Ignition of Solid Propellants by ESD and Transient Phenomena", 1988 International Aerospace and Ground Conference on Lightning and Static Electricity, April 19-22, 1988, Oklahoma City.
2. Larson, Ronal W., P. D. Beale, M. F. Gyure, J. E. Lindsay, Jr., J. D. Curry, "Microstructural Modeling of Electrical Breakdown in Solid Fuel Propellants", EMA Report 89-R-37, April 5, 1989
- 3a. "Etude Des Phenomenes D'Electricite Statique dans la Fabrication et La Manipulation des Propergol Solides," Note Technique No. 94/80/CRB/DR, SNPE, 7 November 1980, R. Kent, and R. Rat, (Diffusion Restreinte).
- 3b. Kent, R., and R. Rat, "Static Electricity Phenomena in the Manufacture and Handling of Solid Propellants," J. of Electrostatics, 17, pp. 299-312, (1985).
- 3c. Cantey, Dalton, "Solid Propellant Structural Integrity Investigations," Rocket Propulsion Laboratory, Edwards, CA, RPL-TDR 64-32, Vol. I, 17 April 1964.
4. Knaur, J.A., "Technical Investigation of 11 January 1985 Pershing II Motor Fire, U.S. Army Missile Command, Technical Report RK-85-9, Vol. III A, 31 December 1986.
- 5a. Perala, R., et al., "PII ESD Hazards Analysis Summary," EMA-85-R-33, August 1985.
- 5b. Easterbrook, C.C. et al., "Analysis and Interpretation of Electrostatic Discharge Testing of Pershing II Empty and Live Stage Motors," EMA-86-R-11, December 1985.

6. Berger, M.A., L.A. Losee, and T.C. Speed, "Effect of Measuring Parameters on the Volume Resistivity and Dielectric Constant of Solid Rocket Propellants," 1987 JANNAF Propulsion Systems Hazards Subcommittee Meeting, CPIA Publication 464, Vol. 1, p. 287, March 1987.
7. Knaur, J.A., R.E. Betts, and J.F. Crawford, "History of QBJ-29 Propellant Testing at MICOM," Technical Report RK-85-9, U.S. Army Missile Command, Redstone Arsenal, AL, December 1985.
8. Crawford, J.F., J.A. Knaur, R.E. Betts, "Electrostatic Sensitivity of QBJ-29 Propellant, JANNAF Propulsion Systems Hazards Subcommittee Meeting, CPIA Publication 446, Vol. 1, p. 407, 1986.
9. Gibson, P.W., and Benedict, R.E., "Electrostatic Sensitivity Testing at the Air Force Rocket Propulsion Laboratory," in Proceedings of the 1986 JANNAF Propulsion Systems Hazards Subcommittee Meeting, Vol. 1, CPIA Publication 446, 1986, pp. 337-353.
10. Gibson, P.W., "Small Scale Electrostatic Discharge Test Development," presentation to Electrostatic Hazards Panel, 1986 JANNAF Joint Propulsion Meeting, New Orleans, LA, August 1986.
11. Gibson, P.W., and R.E. Benedict, "Effects of Formulation on the Electrostatic Sensitivity of Solid Rocket Propellants," the 1987 JANNAF Propulsion Systems Hazards Meeting, NASA-Marshall Space Flight Center, Huntsville, AL, March 1987. CPIA Publication 464, p. 371.
12. Crawford, J.F., "Electrostatic Discharge (ESD) Hazard Evaluation of an Air Force Rocket Propulsion Laboratory (AFRPL) Composite Propellant," Abstract presented at the 1987 JANNAF Propulsion Systems Hazards Meeting, NASA-Marshall Space Flight Center, Huntsville, AL, March 1987.
13. Covino, J., and F.E. Hudson, III, "Electrostatic Discharge (ESD, Sensitivity of a Selected Number of Solid Rocket Propellants," JANNAF Propulsion Systems Hazards Subcommittee Meeting, pp. 335-352, 1987. CPIA Publication 446, Vol. I.
14. Covino, J. and F.E. Hudson, III, "The Measurement of Dielectric Constants for Propellants and Propellant Ingredients," the 1987 JANNAF Propulsion Systems Hazards Meeting, Redstone Arsenal, AL, March 1987. CPIA Publication 464, p. 277.
15. Kraeutle, K.J., J. Covino, and K.J. Graham, "The Measurement of the Surface and Volume Resistivity of Nonaluminized and Aluminized Binders," Proc. of the 1986 JANNAF Propulsion Systems Hazards Subcommittee Meeting, CPIA Publication No. 446, Vol. I, p. 299, March 1986.
16. Kraeutle, Karl J., "The Effect of Temperature and of Particulates on the Electrical Resistivity of Solid Propellant Binder," presented at JANNAF Hazards Conference, Los Angeles, CA, March 1988.

17. Larson, R. W. et al, "Electric Fields in the Lockheed C³ First Stage Following the External Discharge of Electrostatic Charge on the Case," EMA-87-R-4, October 1986.
18. Larson, R. W. et al, "Electric Field Modeling of External ESD During Macrotesting of an FBM Stage," EMA-88-R-67, September 1988, with John D. Curry, Poh H. Ng and Henry S. Weigel.
19. Larson, R.W. "ESD and the PK 322 Incident," EMA-88-R-19, January 1988, with R. A. Perala, P.M. McKenna, T. Rudolph, J.D. Curry, V.R.D. SunderRaj, E.L. Thompson, H.S. Weigel, C.C. Easterbrook, J.S. Bowers and M.D. Goldberg. (for Morton-Thiokol)
20. Larson, R. W. "ESD Simulation Modeling of the Peacekeeper Stage II Core Stripping Operations," EMA-88-R-66, December 7, 1988 with J.D. Curry, M.A. Frisoni, V.D. SunderRaj, and H.S. Weigel. (For Aerojet Solid Propulsion Company).
21. Larson, R. W. "ESD Simulation Modeling of the Space Shuttle Core Stripping Operations," EMA-88-R-66, December , 1988 with J.D. Curry, M.A. Frisoni, V.D. SunderRaj, and H.S. Weigel. (For Morton-Thiokol)
22. Larson, R.W. with Paul D. Beale, "Microstructural Modeling of Electrical Breakdown in Solid Fuel Propellants," presented at the Workshop on ESD Ignition of Composite Solid Propellants, April 18 - 19, 1989, Nashville, Tennessee.
23. Vivek SunderRaj, John D. Curry, and R. W. Larson, "Modeling of Electrostatic Fields in Solid Propellants Using Finite Element Techniques," presented at the Denver EMC conference, May 24, 1989.
24. Larson, R.W. and Gyure, Mark, "The Electrical Breakdown of Solid Rocket Propellants by Electrostatic Fields," Presented at the 1989 Int. Conf. on Lightning and Static Electricity, held in Bath, U.K., September 26-28, 1989. (Based on ARO work)
25. "ESD Modeling and Instrumentation Relative to C4 Anomalies", EMA-89-R-66, with John Curry, Cal Easterbrook, Fred Eriksen, and Mike Frisoni, September 1989. (Report to Lockheed)
26. Larson, R.W., "Analytical Considerations in the ESD-Caused Ignition of Solid Propellants", presentation at JANNAF Conference, Laurel, MD, April 4, 1990 (Based on ARO work).
27. D.M Mann, et al., "Workshop Summary: ESD Ignition of Composite Solid Propellants", April 4, 1990, presented at the JANNAF Propulsion Systems Hazards Subcommittee Meeting.
28. Private communication with Dr. Bruce Isom, Hercules, September, 1989.
29. Hermance, Clark, "Solid Propellant Ignition Theories and Experiments," Chapter 5 in Fundamentals of Solid-Propellant Combustion, edited by K.K. Kuo and Martin Summerfield, Progress in Astronautics and Aeronautics, Vol. 90, 1984.

LIGHTNING WARNING STATION

OPERATIONAL SYSTEM FOR ADVANCED LIGHTNING WARNING

P. Richard, DIMENSIONS,
91194 Saint Aubin Cedex, France

I INTRODUCTION

Efficiency and Safety are determinant factors in many different activity domains such as industry, military or aerospace. Among all dangerous or perturbing factors, lightning has been until recently often considered as an unavoidable and unpredictable phenomena though it can be the cause of important hazards and damages in human activities. Operational systems however exist for the monitoring of severe weather: radars can locate heavy precipitation and convective areas, but they are unable to distinguish electrified and non electrified clouds; lightning location systems can be used either to locate cloud-to-ground flashes, but in this case they are limited to mapping functions without possibility of early detection of thunderstorms, or they can be used to locate the total lightning activity (SAFIR system) and thus give early warning informations before cloud-to-ground flashes. All these systems have their own interest and applications, but they can often reveal to be either too performant or costly for applications limited to a single site.

Simpler and less expensive solutions for lightning warning on a single site do exist, however this simplicity must not be gained to the detriment of efficiency and safety. For these reasons Dimensions has developped, on the basis of a know-how developped at the French National Agency for Aerospace Research (ONERA), a local "lightning warning station" performing the monitoring of the electrical activity of nearby thunderclouds and giving early warning informations in case of lightning hazards on the site. This equipment is based on a simple principle: the analysis of the electric field produced by thunderstorms. It represents however a new generation of product in the domain of lightning warning since it integrates state of the art measurement techniques and original know-how for the analysis of the electric field and the elaboration of lightning warning informations, thus giving to the user the most reliable and efficient informations for applications to the safety and efficiency of its sensitive operations.

This paper presents the principles and techniques used in the "lightning warning station", its operation and performances are discussed and illustrated through an example of thunderstorm situation.

II SYSTEM PRINCIPLES

1 Lightning Warning Principles

Before discussing the principles used for the elaboration of warning informations, we will first describe the typical behavior of thunderstorm clouds during their development.

1.1 Typical development of a thunderstorm cell

Thunderstorms are convective clouds created by the thermal instability of a humid air mass. They are made of convective cells. These cells develop very rapidly, they last a few tens of minutes, grow up to altitudes of 10 to 15 km and have a diameter of about 10 km. Thunderstorms are frequently multicellular, and can extend over tens or hundreds of kilometers and last several hours.

During its development a thunderstorm cell presents very strong updrafts (up to 50 m/s) carrying up precipitation particles. The electrification of the thundercloud is due to the charging of graupels and ice crystals by collisions and to their separation by differential vertical motions. These processes result in a tripole electrical structure with a main negative charge around 6 km, a positive charge in the upper part of the cloud and a small positive charge at the cloud base. Winter thunderstorms have a similar structure, but over a smaller vertical extent.

The electrification of the thundercloud creates a strong electric field (Figure 1 [A]). It can exceed 10 kilovolts per meter on the ground in the vicinity of the thunderstorm, and reaches several hundred kilovolts per meter within the cloud. This initial electrification phase last 5 to 20 mn. The active phase starts with the first intra-cloud discharges (figure 1 [B]). During the first part of the active stage, the activity is made uniquely of intra-cloud discharges occurring between the main negative and the upper positive charge regions. Their rate increases until the cell reaches its maximum vertical development (Figure 1 [C]). They induce very rapid changes in the electrostatic field, which can be observed at a distance of several tens of kilometers; they also radiate electromagnetic waves which can be detected and used for lightning location at long range (SAFIR system). Intra-cloud discharges are much more frequent than cloud to ground lightnings, they typically represent 70 to 90% of the total activity of a thunderstorm.

The first Cloud to ground lightning is usually observed 5 to 30 minutes after the first intra-cloud lightnings. The peak cloud to ground lightning activity occurs subsequently typically 5 to 10 min after the maximum of Intra-cloud activity, it is usually associated to the subsequent descent of precipitation particles below the main negative charge layer and can be accompanied in severe thunderstorms by strong downdrafts and intense precipitations at ground level.

1.2 Lightning warning principles and advantages

A thunderstorm is a rapidly evolving phenomena which can be monitored through the analysis of the electric field that it generates in its vicinity. Until now, the most frequently used techniques were based on the measurement of the static value of the electric field and a warning was issued when the field was increasing over a predetermined threshold. This type of principle does not take into account the dynamic behavior of phenomena and usually only provides a rough information about the situation; the warning is subject to fluctuations and depends on the value of the threshold and on the local conditions which can disturb the measurement (such as local space charge layer).

The principle of the warning processing used in the "lightning warning station" is to take into account the dynamic behavior of thunderstorms in order to better characterize the phenomena and to forecast its short term evolutions. This analysis is performed in real-time, it is a real "intelligent processing" of the electric signal generated by the thundercloud.

This intelligent processing relies on 3 main levels of analysis:

- the standard measurement of the static value of the electric field; it characterizes the electrification level over the site.
- The analysis of the variations in the electric field; it characterizes the intensity of electrification processes within the thundercloud, as well as the movements of electrified clouds in the vicinity of the sensitive site.
- The detection and analysis of lightning flashes (intra-cloud and cloud-to-ground) which enables the early detection of active thunderclouds up to 30 minutes before the first cloud-to-ground flashes, the characterization of thundercloud severity, and the long range detection of approaching active thunderstorms (~30 km).

On a practical stand-point this processing gives four different warning levels:

Level 0 (green)

- no thunderstorm activity.

Level 1 (blue)

- Early detection of electrical activity. Tendency towards thunderstorms in the nearby area;
- Typical delay: 15-45 min.;
- No confirmed short-term risk for the site.

Level 2 (orange)

- Distant thunderstorm activity (>10km), short term thunderstorm hazard on the site
- Typical delay: 5 - 20 min.;
- Possible disturbances on the site.

Level 3 (red)

- High-risk situation. On-site thunderstorm, lightning stroke hazard;
- Typical delay: less than 10 min.;
- Lightning-stroke hazard on this site;
- Possible disturbances on the site.

The same principles are used for lightning warning clearing.

2 sensor principles:

The automatic lightning warning station hardware comprises a measurement system (electric field sensor) and a warning terminal (figure 2).

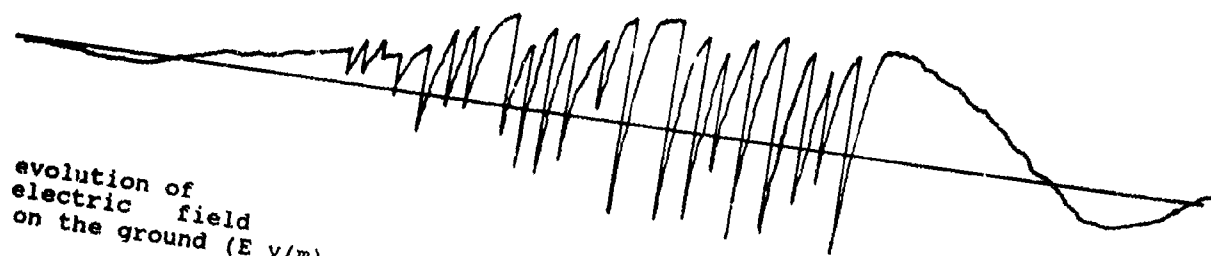
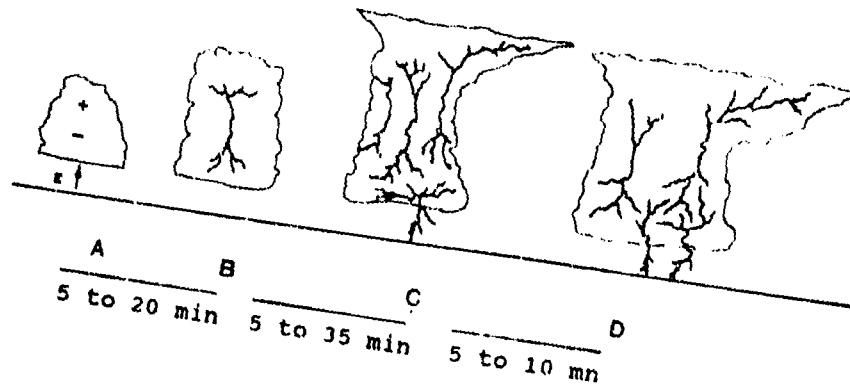
2.1 The Sensor

The electric field sensor includes:

- An atmospheric electric field measurement system based on the field mill principle;
- A micro-processor central processing unit;
- A backed-up power supply.
- A modem for transmitting data to the warning terminal either through the standard telephone network or dedicated transmission lines.

The sensor has auto-test and functional test capabilities. The sensor condition is periodically transmitted to the terminal,

evolution of
electrical activity



evolution of
electric field
on the ground (E v/m)

Fig 1 Typical development of a thunderstorm cell

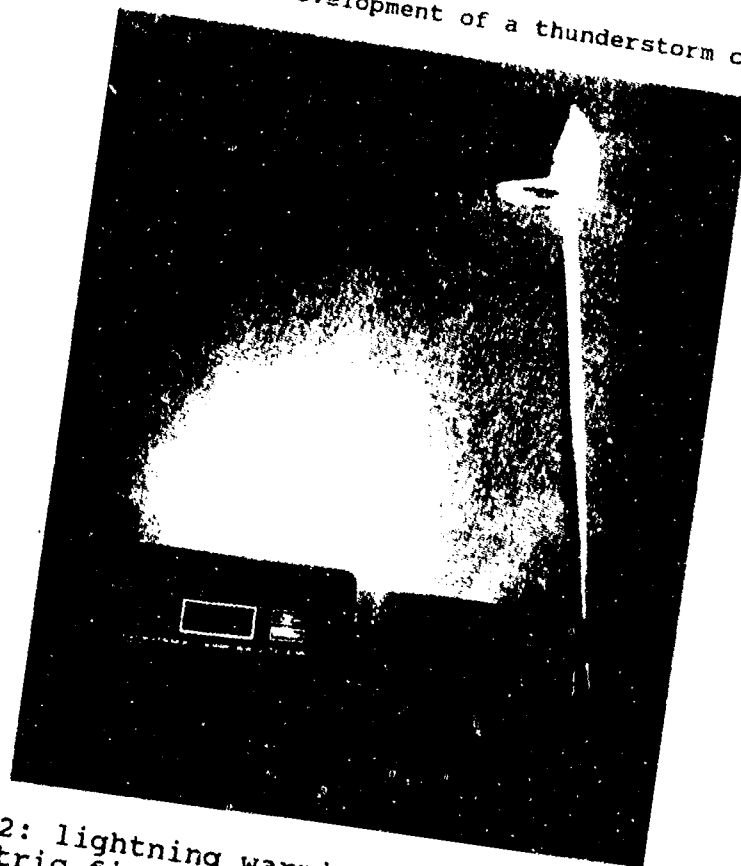


Fig 2: lightning warning station hardware
Electric field sensor and display terminal

it can confirm to the user the quality of system operation and the validity of lightning warning messages. System installation is simple. It only requires a free area with a radius of about ten meters, a power supply and a transmission line (RS-232 or telephone network). The sensor may be installed on a building terrace or in a courtyard; it can take the influence of the site it is installed on into account for the computation of warning data.

2.2 The Terminal

The warning terminal can be either a stand-alone warning display unit or a PC-type micro-computer. It is connected to the sensor through a telephone or a RS-232 line.

The stand alone display unit is adapted to most decision facilities (whether automatic or not) and to applications that do not require later data archiving or processing. It displays warning level as a three-color code and a status of system

operating conditions, shown by means of indicator lights. Included are control lines for remote-controlling of external devices (generators, isolator switches, sirens, etc).

The PC terminal (figure 3) has all of the display unit's functions, but it provides a more user-friendly interface, continuous storage of measurements and a post-processing software package for processing stored data (statistics, afterward justification of an alarm decision, ...). Moreover, it may receive and manage information from several sensors when a wide area is to be covered.

When used through the telephone network, in order to reduce communication costs, the sensor is operated in an automatic call mode, and connects automatically to the terminal (display unit or PC) in case of lightning warning.

III APPLICATIONS

1 Example of thunderstorm situation

Lightning warning stations are already in use on different military and aerospace centers. We present here a typical situation observed at the "Centre Spatial Guyanais" in French Guiana where these sensors are installed in complement to a SAFIR thunderstorm monitoring and lightning warning system (figure 4). We are thus able in this particular case to analyse the behavior of the lightning warning station in comparison with location of lightning flashes.

The thunderstorm cell develops (figure 4) on the ocean about 30km North-East to the launch pads. Thunderstorm lifetime is about 1 hour and it propagates in direction of the space

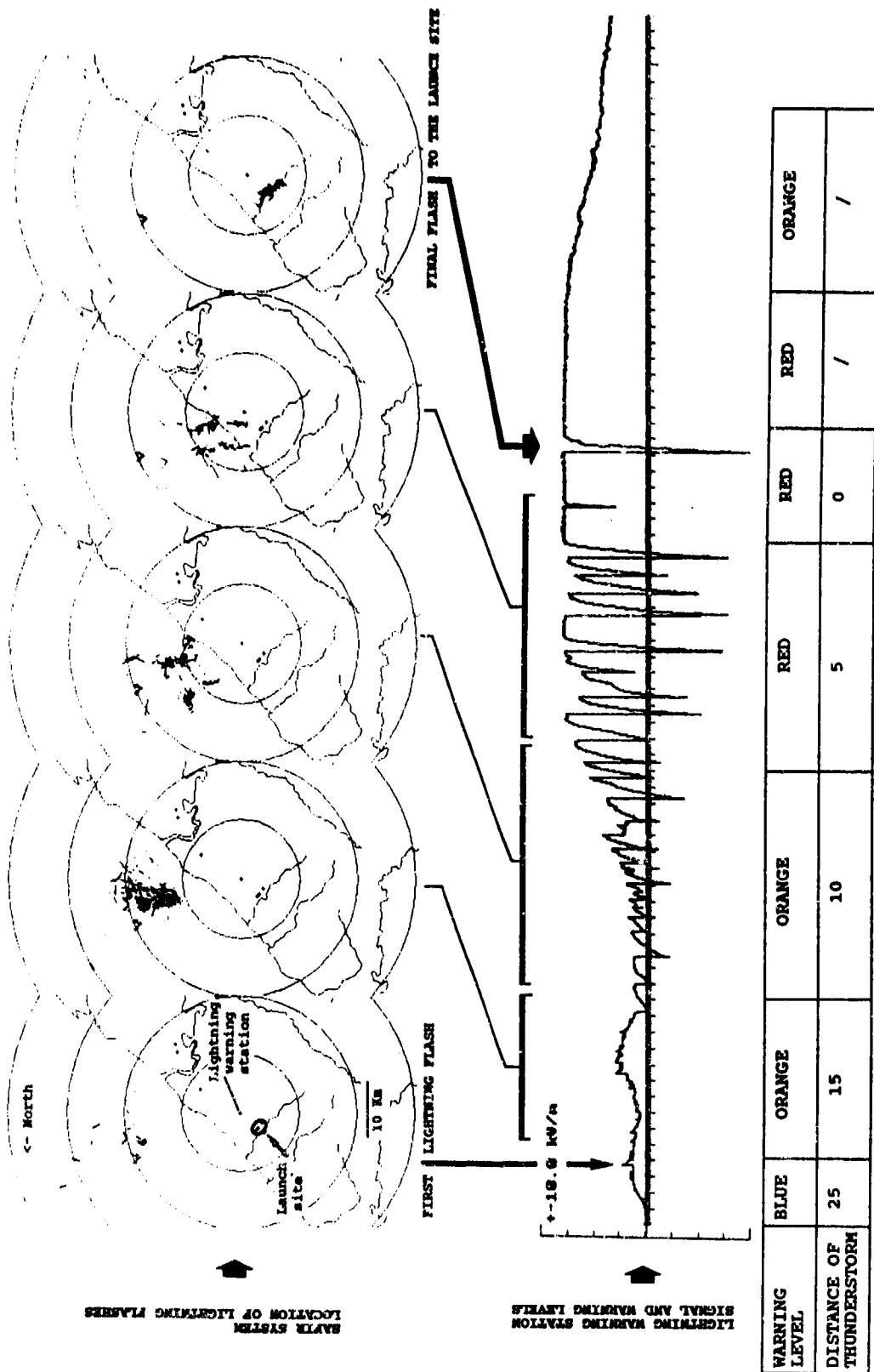


Fig 4 time evolution of warning information, comparisons with the location of the thunderstorm

center. The last flash, among a total of 48 lightning flashes, strikes the launch area.

The lightning warning station is located a few kilometers away from the launch pads; at the beginning of this situation warning level is 1 (blue) due to earlier detection of fluctuations in the electric field value which reveal unstable conditions.

The station detects its first lightning flashes 43 minutes before the lightning strike on the launch site, at this moment the thundercloud is 25 km away, warning level is set to 2 (orange).

Warning level is then set to 3 (red) more than 20 minutes before flash to the launch site, the thundercloud is still 10 km away. Warning is then maintained to red until final flash and still for ten more minutes.

This situation is a typical example of early warning capability and long range detection of the lightning warning station, a thunderstorm warning is given here more than 40 minutes before lightning strike to the sensitive site when the thunderstorm is still 25 km away, lightning hazard is then confirmed to the user with a 20 min advanced delay.

2 applications

The intelligent processing performed by the lightning warning station enables a fully automatic operation of the equipment, it can provide early warning informations up to several tens of minutes in advanced and can be applied to the manual or automatic implementation of safety procedures and protection systems.

System reliability and warning efficiency will find their main applications and justification for sensitive activities which mainly involve: computer systems, automated production systems, volatile chemicals, explosives, telecommunication equipments, power systems, electronic and radio-systems; it also increases the safety of personnel working under exposed conditions.

**DEVELOPMENT OF A DOD HANDBOOK ON
INSPECTION AND TESTING OF LIGHTNING PROTECTION
AND GROUNDING SYSTEMS**

presented by

**Mitchell A. Guthrie
Kilkeary, Scott & Associates, Inc.
2301 S. Jefferson Davis Hwy., Suite 1328
Arlington, VA 22202**

presented at

**24th DoD Explosives Safety Seminar
St. Louis, MO**

29 August 1990

TABLE OF CONTENTS

Abstract	ii
Acknowledgements	iii
1.0 Introduction	1
2.0 Background	2
3.0 Grounding Systems Test Plan	3
4.0 Visual Inspection Procedures	4
5.0 Electrical Testing	10
6.0 Summary	15
Bibliography	17

LIST OF FIGURES

Figure

1	Typical Integral Lightning Protection System Installation	3
2	Typical Navy Mast-Type Lightning Protection and Grounding System	4
3	Sketch of a Navy Ordnance Facility showing Electrical Test Points	8
4	Proposed Data Sheet for Example Structure	9
5	Electrode Locations for Air Force Fall-of-Potential Ground Resistance Test	12
6	Biddle Instruments Recommended Electrode Configuration For Fall-Of-Potential Ground Resistance Test	13
7	Earth Resistance Test Data for DoD Magazine	14

ABSTRACT

There is currently little standardization in the instrumentation of ground system testing and visual inspection requirements in the Department of Defense. As result, the Department of Defense Explosives Safety Board (DDESB) has tasked the Naval Surface Warfare Center to develop a handbook that will provide recommendations on the development of a grounding system quality control program and provide general discussions on conducting visual inspections and electrical testing. This paper provides a general discussion on the proposed content of the handbook with emphasis on the development of a grounding system quality control program and on the results of a survey on the implementation of current grounding system test requirements in the field. The paper will forward any preliminary recommendations proposed for inclusion on the handbook.

ACKNOWLEDGEMENTS

A special thanks is given to John L. (Jack) McGinnis of the Naval Surface Warfare Center for his support in the discussion of the material presented in the paper. Thanks is also given to Mr. Ignacio Cruz of the Naval Weapons Station Yorktown, Virginia, (formerly of DDESD) for the inspiration for the paper and to Dr. Jerry Ward of DDESD for support in the generation of a handbook on ground system testing.

I would also like to thank Kristin Leaptrot and Kelley Floberg for their support in the production of this paper.

DEVELOPMENT OF A DOD HANDBOOK ON INSPECTION AND TESTING OF LIGHTNING PROTECTION AND GROUNDING SYSTEMS

1.0 Introduction

There is currently little standardization in the grounding system test and inspection procedures used at Department of Defense (DOD) ordnance facilities. As a result, the Department of Defense Explosives Safety Board (DDESB) has tasked the Naval Surface Warfare Center (NAVSWC) to develop a handbook which will provide recommendations on the development of a grounding system quality control program and provide discussions on conducting visual inspections and electrical testing of grounding systems for ordnance facilities. The Defense Nuclear Agency (DNA) suggested that the goal should also be to produce a publication that will permit those personnel responsible for inspection and maintenance of these systems to readily understand both the how and why of pertinent requirements [1]. It was suggested that the document contain guidance that will be easy to understand with clear definitions of what is satisfactory and what is unsatisfactory. Check sheets and general test procedures should be provided.

It is agreed that the general opinion of personnel in the field responsible for the design, installation, maintenance, and inspection of grounding systems for ordnance facilities is that specific visual inspection and electrical test procedures should be used for all DOD ordnance facilities. However, the existing service requirements for grounding systems testing [2][3][4][5] are very general as to the specific items that are to be tested and the test procedures to be used. Implementing documents for the services could be interpreted to be in conflict as to specific details of implementation. For example, Air Force Pamphlet 91-38 [6] allows that the reference electrodes for a three-point fall-of-potential earth resistance test be installed in such a way that the potential electrode is one-half of the diagonal distance of the building, but not less than 25 feet. The current electrode is to be placed 90 degrees from the potential electrode and the "item under test", at the same distance as the potential electrode. NAVSEA OP-5 [3], Chapter 4-9.2.5 requires that these tests be conducted "in accordance with the appropriate instrument manufacturer's instructions". It also references James G. Biddle Company's Manual 25T [7] on earth resistance testing which requires that the current and potential electrodes be in a straight line and that the spacing of the electrodes must be determined by some baseline testing of the installed grounding systems. In order to establish a specific test procedure, the services must agree on the resolution of those areas where there can be perceived to be conflicts between the

implementing documents of the services. DOD 6055.9-STD [2] only provides general guidance in those areas where potential conflicts exist. In addition, there is a very broad spectrum of age, construction, and end use of facilities currently being utilized by DOD agencies.

Kilkeary, Scott and Associates, Inc. (KSAi) has been tasked to support NAVSWC in the production of this handbook. As a part of this task, KSAi has reviewed several DOD documents dealing with grounding systems installation and testing requirements for ordnance facilities [2][3][4][5][6][8][9][10] and other literature on the subject [11][12][13][14]. This paper reports on the recommendations of KSAi on inspection and testing techniques proposed for the handbook.

2.0 BACKGROUND

DOD 6055.9-STD [2], NAVSEA OP-5 [3], AFR 127-100 [4], and AMCR 385-100 [5] provide requirements for the installation of lightning protection and grounding systems for DOD ordnance facilities. DOD 6055.9-STD [2] does not require a counterpoise for a lightning protection system if the resistance-to-ground is less than 10 ohms. Army [5] and Air Force [4] regulations are identical to the DOD [2] requirement. However, NAVSEA OP-5 [3], 4-9.2.3 requires that 1/0 AWG cable form a closed loop around the area to be protected to electrically interconnect lightning protection system down conductors, regardless of resistance-to-earth. In addition, Navy requirements do not allow the use of an integral lightning protection system for ordnance facilities even though all other services [2][4][5] will accept mast-type, overhead wire, and "Faraday-type" lightning protection systems. Figure (1), taken from AMCR 385-100 [5], provides a detail of a typical integral lightning protection system installation for an Army or Air Force application. Figure (2), taken from NAVSEA OP-5 [3], provides a detail of a typical Navy mast-type lightning protection and grounding system installation.

A primary difference between the internal grounding requirements of the various services is the Navy use of an "ordnance grounding system". NAVSEA OP-5 [3], 4-7.1.5 requires that the ordnance grounding system be installed as a single-point grounding system, isolated from all other grounding systems except through direct attachment to a buried (secondary) ground girdle (see Figure (2)). All of the DOD requirements reviewed required the bonding of metallic bodies in the facilities as part of the lightning protection system. Surge suppression for all incoming metallic conductors is also required by all of the requirements documents. They all also require that fences have bonds across

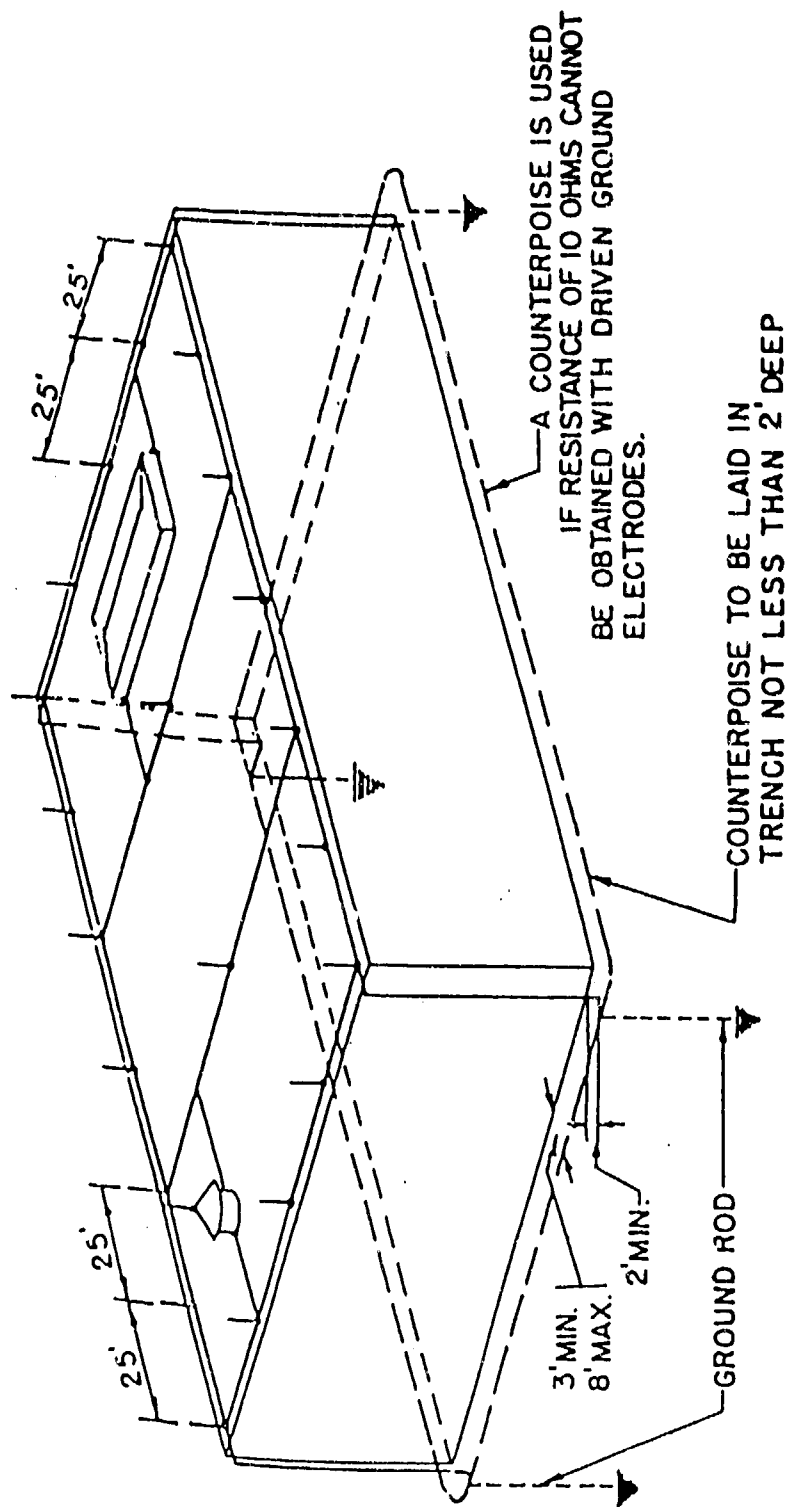


Figure 1. Typical Integral Lightning Protection System Installation

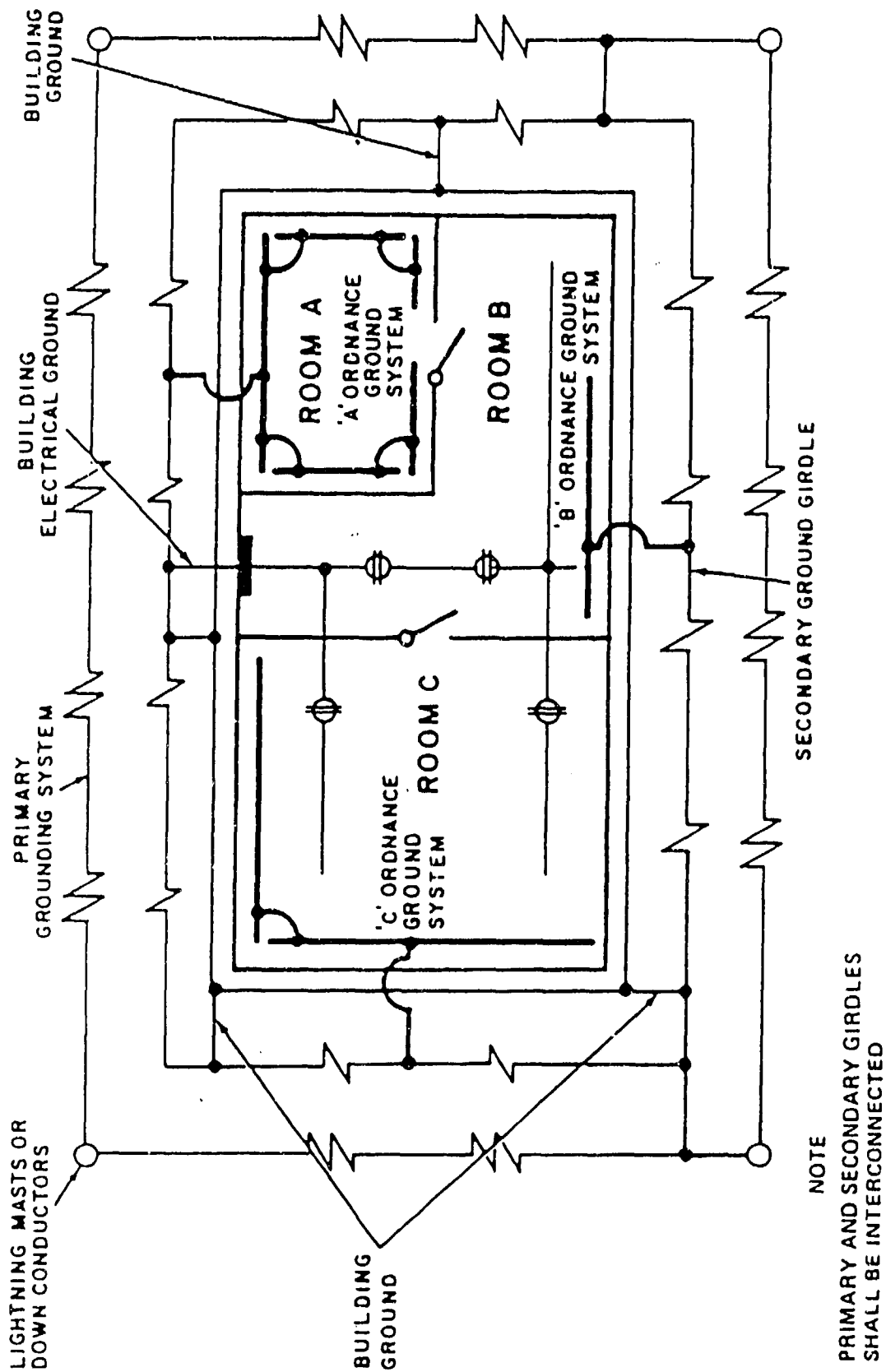


Figure 2. Typical Navy Mast-Type Lightning Protection and Grounding System

gates. DOD 6055.9-STD [2] requires that fences and railroad tracks be bonded to the lightning protection grounding system if they come within six (6) feet of the structure. DOD 6055.9-STD also requires that wires and connectors on lightning protection systems not be painted.

DOD requirements [2] specify that the lightning protection systems shall be inspected visually every seven (7) months and tested electrically every fourteen (14) months. DOD [2] and Navy [3] requirements specify that the testing be conducted in accordance with the appropriate instrument manufacturer's instructions by personnel familiar with lightning protection systems. NAVSEA OP-5 [3], 4-9.2.5 requires that the resistance of each mast and overhead lightning conductor to earth shall be measured every 14 months. It also requires that the resistance-to-ground of all metal objects that require interconnection with the lightning protection system be measured and recorded. The resistance between these components and the lightning protection system shall be less than one (1) ohm.

Army [5] and Air Force [6] documents provide specific lightning protection and grounding systems test procedures. AFP 91-38 [6], 2-3 states that the electrical test procedures forwarded in the document is the "correct procedure for testing typical" Air Force systems. The resistance-to-ground test method discussed in AFP 91-38 [6] utilizes reference electrodes spaced at 90 degrees to the edge of the building. The distance between electrodes is to be one-half of the diagonal distance of the building, but not less than 25 feet. The inference from the Navy requirements [3] would require that the reference electrodes be in a straight line at a distance determined by some baseline testing. AFR 127-100 [4] and AMCR 385-100 [5] also requires a continuity test for masts or overhead wire lightning protection systems from the top of the mast or overhead wire to the ground point connection. No such test requirements are included in NAVSEA OP-5 [3]. Both the Army [5] and the Air Force [4] requires continuity measurements between air terminals and ground electrodes for integral lightning protection systems. Navy documents [3] do not address the testing of integral lightning protection systems.

All of the DOD documents reviewed [2][3][4][5][6] require that the test instruments used in the testing of DOD lightning protection systems be capable of ten (10) percent accuracy at one (1) ohm for bonding measurements and ten (10) ohms for resistance-to-ground measurements. Only instruments designed for the testing of earth resistance may be used in resistance-to-ground testing.

NFPA 78 [12], Appendix M-4 recommends an annual visual inspection and a thorough inspection every five (5) years. The inspection requirements in NFPA 78 [12] Appendix L-7 are identical to those in DOD 6055.9-STD [2], paragraph F. NFPA 78 [12],

Appendix B recommends the use of checklists for routine maintenance to enhance the repeatability of the procedures used in the inspections. The Appendix recommends that the maintenance program should contain provisions for: (1) the inspection of all conductors and systems components, (2) tightening of all clamps and splicers, (3) measurement of system resistance, (4) measurement of the earth resistance of the ground terminals, (5) inspection and/or testing of surge suppression devices, and (6) inspection and testing to ensure that the effectiveness of the lightning protection system has not been altered as a result of additions to or changes in the structure.

3.0 GROUNDING SYSTEMS TEST PLAN

KSAI recommends that the proposed DOD handbook encourage each facility to establish a grounding systems test plan for the facility. This grounding systems test plan should detail the responsibility for the overall implementation of the plan and should also detail the responsibilities delegated to other offices. Specifically, the grounding system test plan should identify the procedure by which grounding systems test points will be selected, the procedure to be used in the visual inspection of lightning protection and grounding systems, the responsibility for the development of specific electrical test procedures, the responsibility for the review of electrical test data and the initiation of corrective action, the procedure by which priorities for corrective action are to be established, and the responsibility for ensuring that any necessary modification are made. It is also recommended that the grounding system test plan identify specific procedures by which it will be ensured that the test procedures for a facility is upgraded any time the operations or structural configuration of the facility is changed. Finally, training requirements and personnel qualifications for each level of responsibility should be included in the grounding system test plan.

None of the services require such a grounding system test plan for a facility. However, all of the services require that the electrical testing and visual inspections be conducted and that records of the electrical testing be maintained for a minimum of five (5) years. The grounding system test plan is suggested as a technique to ensure that the maintenance and inspection requirements of the Department of Defense are met and the procedures used to implement the plan are clearly documented and can be easily inspected to ensure maximum grounding system effectiveness.

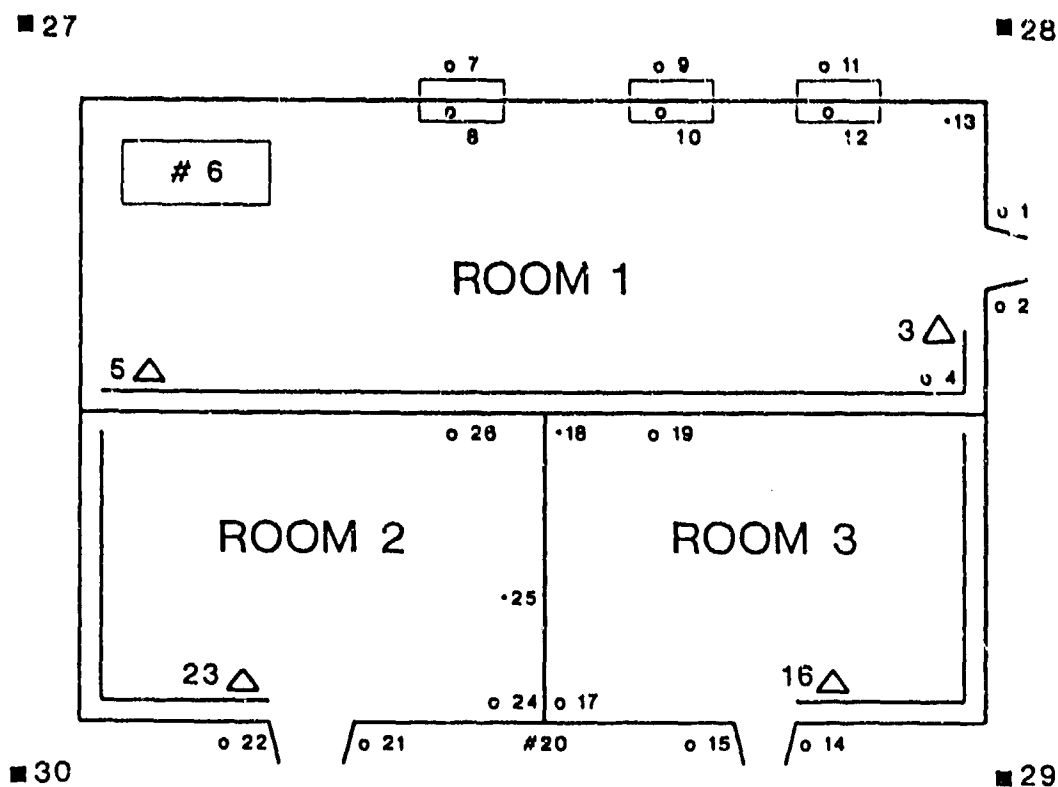
It is recommended that a visual inspection checklist be provided in the grounding system test plan. None of the requirements documents reviewed [2][3][4][5] specifically address a visual inspection checklist. However, each of the documents provide suggestions on the items to be reviewed during visual inspections. Section 4.0 of this report provides recommendations on visual inspection checklists.

It is recommended that the grounding system test plan discussed in the proposed handbook encourage the use of a sketch of the grounding system for a structure to identify the test point location and type of measurement required for each test point. An example of such a sketch for a Navy structure is provided in Figure (3). In the example provided, the types of grounding systems are identified by symbol on the sketch and are listed below the sketch to ensure no confusion. A proposed electrical test record form indicating the type of test required is provided as Figure (4). It is recommended that the electrical test results recorded in the field be transferred to a computer data file where they can be reviewed and maintained for the life of the structure. The effectiveness of a trend analysis is enhanced when several seasons of test data is available.

If the resistance-to-ground of individual ground rods for lightning protection and grounding systems is to be measured in order to compute the earth resistance of a buried ground ring, it is necessary that the grounding system test plan identify that the ground rods (and perhaps grounding girdles) be provided with test pockets to allow their disconnection from the ground girdle. Subsequent designs of grounding systems at the facility should include such test pockets. For Navy installations, ordnance grounding systems should be installed in such a manner to allow that it be disconnected (to test for isolation) and then reconnected (to ensure proper bonding to the secondary grounding system). Such a design should be implemented at Navy and Marine Corp installations whenever isolation testing of the ordnance grounding systems is included in the grounding systems test plan.

4.0 VISUAL INSPECTION PROCEDURES

NFPA 78 [12], Appendix B-1.2 recommends that the visual inspections include checks to ensure the system is in good repair, there are no loose connections (or paint on the joints) that might result in high resistance connections, the system has not been weakened by corrosion or vibration, all conductors are securely fastened, there has been no additions or alterations to the structure that would require additional protection, and that there has been no visual indication of damage to surge suppression devices. KSAi also suggests that ground fault interrupters (GFI)



- | | |
|-------------------------|--------------------------|
| 1 = Door | 16 = Ordnance ground bus |
| 2 = Door | 17 = Structure |
| 3 = Ordnance ground bus | 18 = Conduit |
| 4 = Structure | 19 = Missile stand |
| 5 = Ordnance ground bus | 20 = Ground grab bar |
| 6 = Metal table top | 21 = Door |
| 7 = Window guard | 22 = Door |
| 8 = Window | 23 = Ordnance ground bus |
| 9 = Window guard | 24 = Structure |
| 10 = Window | 25 = Conduit |
| 11 = Window guard | 26 = Structure |
| 12 = Window | 27 = Mast |
| 13 = Conduit | 28 = Mast |
| 14 = Door | 29 = Mast |
| 15 = Door | 30 = Mast |

Figure 3. Sketch of a Navy Ordnance Facility showing Electrical Test Points

BUILDING KSAI

3-Point Fall-of-Potential (10 ohms maximum)

Test Point	Resistance (ohms)	Test Point	Resistance (ohms)
1		30	
20		28	

Bonding Measurements (1 ohm maximum)

Test Point	To	Test Point	Resistance (ohms)	Comments
1		28		
20		30		
30		29		
30		27		
1		20		
1		2		
1		5		
1		4		
1		6		
1		7		
1		8		
1		9		
1		10		
1		11		
1		12		
1		13		
20		14		
20		15		
20		16		
20		17		
20		18		
20		19		
20		21		
20		22		
20		23		
20		24		
20		25		
20		26		

Figure 4. Proposed Data Sheet for Example Structure

also be checked (where practical) as a part of the visual inspection. KSAi suggests that Navy inspections also include a check of all ordnance grounding systems to ensure that they are independently bonded to the secondary ground girdle. It is also recommended that a copy of the previous electrical test data be reviewed prior to the visual inspection and that any unusual test points be examined in detail during the inspection.

The use of checklists in visual inspections is recommended. Lt. Colonel (USAF) Mercer, Defense Nuclear Agency representative to the DOD Lightning Protection and Equipment Grounding Requirements Working Group (LPEGRWG), presented a Lightning Protection System Inspection Guide [15] for review by the LPEGRWG. The guide was developed by DNA Field Command for use by their inspection teams. The guide was arranged along the lines of a checklist, asking questions and providing references of applicable requirements documents. KSAi supports the use of such a checklist for conducting visual inspections to aid the inspection personnel in assuring that all of the critical items have been tested and to ensure repeatability of the visual inspections. KSAi is aware of some Navy facilities that are currently in the process of developing their own checklist for visual inspections of grounding and lightning protection systems. The checklists proposed are similar in design to the DNA checklist, although only Navy documents are referenced. It is recommended that the handbook provide an outline for a suggested checklist, but each individual facility should have the freedom to tailor their checklist to best meet the applications specific to the station.

5.0 ELECTRICAL TESTING

KSAi is aware of a large variation in ground system test techniques used at DOD facilities. Some activities have reported that they conduct point-to-point resistance testing between the item under test and a reference point, some conduct 3-point fall-of-potential testing (with different electrode location requirements between services), and some use a combination of the tests.

The Navy [3] requires that 3-point fall-of-potential resistance-to-ground testing be conducted for all lightning protection masts or overhead wires and for all metallic objects requiring bonding to the secondary grounding system. However, in areas of constant soil resistivity it is possible that independently grounded objects could yield a very similar resistance-to-ground. KSAi feels that it is most important that the bonding resistance between the metallic components be measured to ensure there are no independently grounded objects.

As discussed in Section 2.0, there is a good deal of difference in the resistance-to-earth measurement techniques used by the services. AFP 91-38 [6] requires the test procedure summarized in Figure (5) while NAVSEA OP-5 [3] can be interpreted to require that the electrodes be installed in a straight line, as shown in Figure (6) (taken from Biddle Instruments "Getting Down to Earth"[7]). Biddle Instruments [7] suggests that the electrode spacing "D" be such that the electrodes are located outside of the "sphere of influence" of the electrode under test. Biddle suggests a series of tests to determine which electrode configurations will be required for a particular installation.

Metallic items in the ground or inconsistencies in soil resistivities can influence the validity of resistance-to-earth measurements. The principle of a 3-point fall-of-potential grounding resistance test is to inject a constant current into the ground via the C2 electrode and measure the potential between the P2 electrode and the item-under-test (see Figure (6)). Any conductor in the ground such as metal water pipe or conduit can influence the current path in the ground and therefore cause errors in the values measured.

In addition, the Navy [3] specifies that a resistance-to-ground of 10 ohms or less is acceptable. However, Figure (7) provides an example of typical resistance-to-ground test data for a DOD magazine. A review of the data shows that the air terminal and the vent consistently exhibit a higher earth resistance than the other test points, even though none of the values recorded are greater than 10 ohms. However, the large difference in resistance-to-ground values is an indication that the air terminal and vent are not bonded to the other grounds in the structure. It is recommended that the handbook provide recommendations on the review of electrical test data. Some discussion should be provided on the development of ground system test procedures that will provide the data required for proper analysis.

It is recommended that the handbook propose the use of both resistance-to-ground and point-to-point bonding resistance measurements. The handbook should stress the importance of bonding measurements and should provide guidance on the selection of test points. It is recommended that the handbook stress the use of electrical test data sheets with test point locations clearly labeled on the data sheet or a supporting sketch of the facility. It is recommended that the DOD Lightning Protection and Equipment Grounding Requirements Working Group address the specific 3-point fall-of-potential test methods that should be included in the handbook.

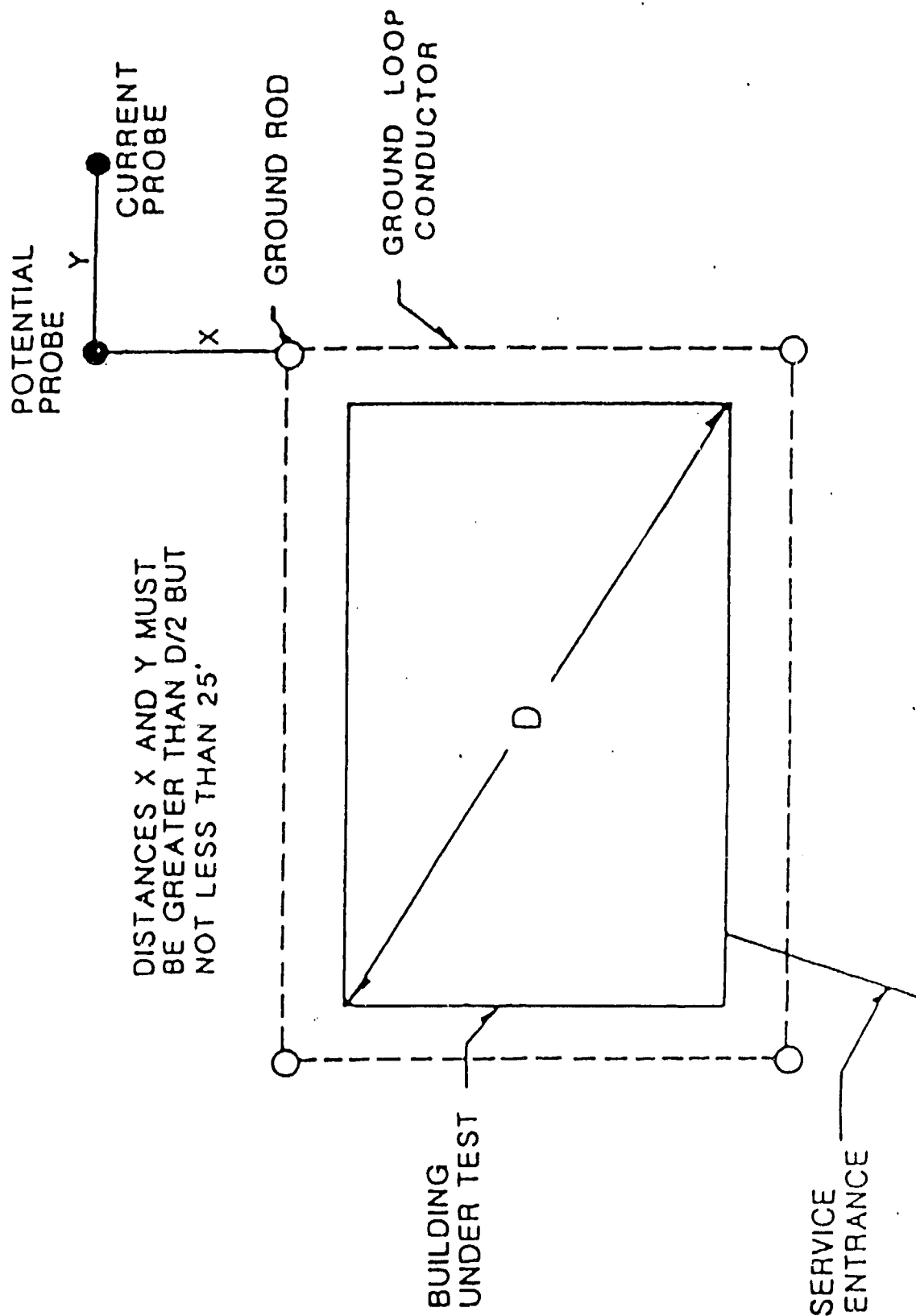


Figure 5. Electrode Locations for Air Force Fall-of-Potential Ground Resistance Test

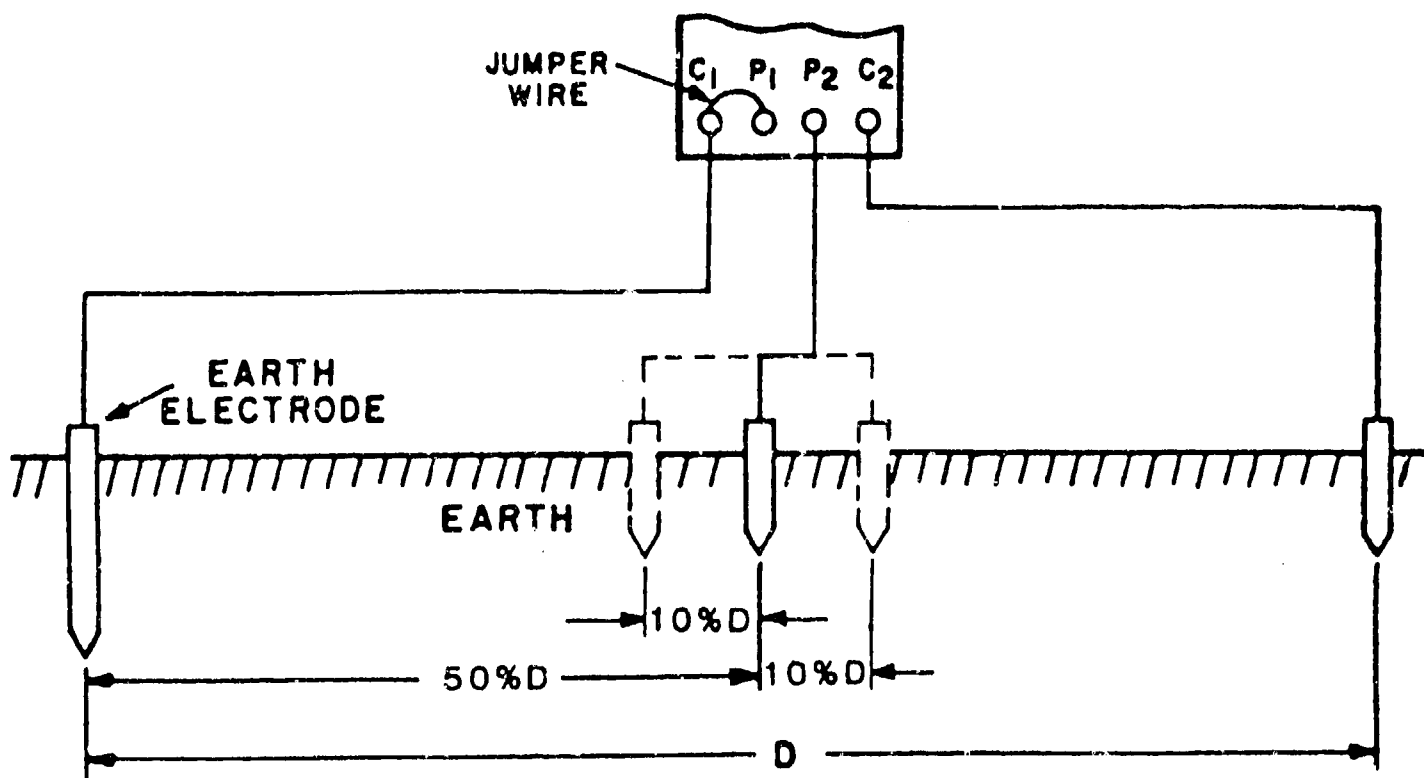


Figure 6. Biddle Instruments Recommended Electrode Configuration for Fall-of-Potential Ground Resistance Test

BUILDING 9AX3

Test Point:	Location	Date	5/9/86	4/7/87	7/18/88	10/27/89
1	Door	3.0	2.6	3.6	3.0	
2	Inside Gnd	3.0	2.6	3.2	3.1	
3	Inside Gnd	2.8	2.6	3.4	3.1	
4	Inside Gnd	2.8	2.6	3.2	3.1	
5	Inside Gnd	2.8	2.6	3.2	3.0	
6	Door	3.0	2.6	3.2	3.0	
7	Air Terminal	6.5	6.0	7.0	6.5	
8	Vent	6.3	6.2	6.9	6.5	

Figure 7. Earth Resistance Test Data for DoD Magazine

6.0 SUMMARY

In summary, the Department of Defense Explosives Safety Board has tasked the Naval Surface Warfare Center to develop a handbook on conducting visual inspections and electrical testing of DOD ordnance facility grounding systems. It is the intent of this action to promote some standardization in the implementation of grounding system inspection and testing requirements. It has been recommended that the handbook provide clear guidance as to correct and incorrect installations and that specific electrical test procedures and checklists be provided. However, the requirements being implemented in the field are very general and sometimes one service's implementation of a requirement is very different from another service. In order to provide specific guidance for conducting visual inspections and provide specific electrical test procedures, the services must first agree to a single test procedure. It is recommended that the DOD Lightning Protection and Equipment Requirements Grounding Working Group provide the forum for the resolution of such issues.

It is recommended that the handbook encourage the development of grounding systems test plans for DOD ordnance facilities. The grounding system test plan should detail the responsibilities for each phase of the implementation of the plan, should identify the key items to be checked during visual inspections, should provide guidance for the selection of test points in electrical testing, should identify personnel responsible for conducting visual inspections and electrical testing, should provide specific grounding system test procedures, should identify personnel responsible for the review of the test data, identify how work requests are to be processed should any repairs be required, and detail the procedure to be used in assigning priorities to the work requests. Electrical testing Standard Operating Procedures (SOPs) should be developed and included in the test plan, along with any visual inspection checklists. If specific sketches of the ordnance facilities are developed (see Figure (3)), these too should be included in the grounding system test plan. In summary, the grounding system test plan should contain a complete summary of all elements of grounding systems inspection and testing at a DOD facility.

It is recommended that a visual inspection checklist be established for inclusion in the handbook. It may be necessary to develop a different checklist for each service. The checklist should list all items to be inspected and provide some pass/fail criteria for the inspection. It should also provide references for each requirement.

It is recommended that both point-to-point bonding resistance and three-point fall-of-potential earth resistance testing is discussed in the handbook. Specific details for the procedures used in conducting both types of tests should be included in the handbook. It is recommended that the handbook stress the importance of bonding resistance testing and provide some discussion on the limitations of earth resistance testing.

In conclusion, the handbook must be written so that it is easily understood and contain guidance that is directive in nature. Detailed test procedures and inspection guidelines should be provided for maximum usefulness of the document. In practice, such a combination may not be practical without each of the services agreeing on specific procedures that are to be included in the handbook.

BIBLIOGRAPHY

- [1] Defense Nuclear Agency letter LEEE of 8 May 1989.
- [2] DOD 6055.9-STD, "Ammunition and Explosives Safety Standards", Department of Defense Explosives Safety Board, Washington, DC, July 1984.
- [3] NAVSEA OP-5, "Ammunition and Explosives Ashore", Volume 1, Fourth Revision, Change 15, Naval Sea Systems Command, Washington, DC, 15 February 1988.
- [4] AFR 127-100, "Explosives Safety Standards", Headquarters US Air Force, Washington, DC, May 1983.
- [5] AMCR 385-100, "Safety Manual", Army Material Command, Alexandria, VA, 1985.
- [6] AFP 91-38, "Maintenance of Electrical Grounding Systems", Headquarters US Air Force, Washington, DC, 2 October 1989.
- [7] Getting Down to Earth, Fourth Revision, Biddle Instruments, Blue Bell, PA, April 1981.
- [8] MIL-HDBK-1004/6, "Military Handbook, Lightning Protection", Naval Facilities Engineering Command, Washington, DC, 30 May 1988.
- [9] Army TM 5-811-3, Air Force AFM 88-9, Chapter 3, "Electrical Design, Lightning and Static Electricity Protection", Departments of the Army and the Air Force, Washington, DC, 28 August 1988.
- [10] MIL-HDBK-419, "Grounding, Bonding, and Shielding for Electronic Equipments and Facilities", Volumes I and II, Department of Defense, Washington, DC, 21 January 1982.
- [11] NFPA 70, "National Electrical Code", National Fire Protection Association, Quincy, MA, 1989.
- [12] NFPA 78, "Lightning Protection Code", National Fire Protection Association, Quincy, MA, 1989.
- [13] Sarajoa, E. K., "18. Lightning Earths", Lightning, Volume 2, edited by Dr. R. H. Golde, Academic Press, London, 1977.
- [14] Moore, C. B., M. Brook, and E. P. Krider, A Study of Lightning Protection Systems, prepared for Atmospheric Science Program of The Office of Naval Research, Arlington, VA, October 1981.
- [15] Defense Nuclear Agency Field Command, "Lightning Protection System (LPS) Inspection Guide", Kirtland Air Force Base, NM, presented to DOD Lightning Protection and Equipment Grounding Requirements Working Group.

SAFETY MANAGEMENT IN THE EXPLOSIVES INDUSTRY

By

G E WILLIAMSON, HM CHIEF INSPECTOR OF EXPLOSIVES

**HEALTH AND SAFETY EXECUTIVE
H M EXPLOSIVES INSPECTORATE
MAGDALEN HOUSE
STANLEY PRECINCT, BOOTLE
MERSEYSIDE L20 3QZ**

SUMMARY

1. Studies show that generally across industry human error is the cause in some 90% of incidents and that 70% of incidents could have been prevented by management action. They point to the crucial significance of a systematic approach to the management of health and safety, the need to be aware of the human factor as a distinct element in that framework.
2. Reference is made to the fundamental causes of the explosion at Peterborough UK in March 1989 to illustrate the way those pointers could equally well apply in the explosives industry, the way management failings may leave individual action or inaction as the last link in a chain leading to disaster.
3. Explosives incidents are relatively infrequent. There is the need for greater pooling of information. A new data-base 'EIDAS' offers one way forward.

SAFETY MANAGEMENT

4. A principle embodied in UK safety legislation is that the primary responsibility for doing something about accidents lies with those who create the risks and those who work with them. The first purpose of HM Explosives

Inspectorate is to ensure that systems exist that are likely to lead to the identification and prevention by management of significant faults, and that the attitude of management is conducive to this. One problem, by no means unique to the explosives industry, is that although the hazards may be appreciated, the low probability of an event and a history then of nothing appearing to go seriously wrong may engender complacency. An important goal is to secure much fuller recognition and understanding of effective safety management.

5. There is nothing new in the idea that safety requires to be managed. It is clearly demonstrable that close attention to the management of safety is effective in preventing accidents and that it is compatible with and indeed promotes first rate commercial performance.
6. There is a considerable body of literature on the subject, good guidance, even rules. But success in managing safety can only be achieved by having a clear corporate commitment, the establishment by positive action of a 'safety culture' which permeates the whole of an organisation. It is a matter for leadership, the acceptance of responsibility at the top and exercised through a clear chain of command, seen to be real and felt throughout the organisation. It is a matter for conviction that high standards are achievable, that set objectives and targets can be met, that hazards can be identified and preventative measures devised then audited and reviewed. It is an approach that does not allow error to go by default but that requires investigation and the immediate rectification of deficiencies. It is then an approach that requires all rules and standards to be observed by all staff. Effective communication is vital.
7. Brief mention might be made of some of the key elements in the safety management framework:

EFFECTIVE SAFETY POLICY

8. A legal duty in the UK but a matter of good practice if not a requirement elsewhere is the written statement - the 'safety policy' - which is the reference document for the management of health and safety within the concern. This specifies objectives, the organisation required to achieve them and the arrangements made for carrying out the policy. It covers the monitoring of the effectiveness of the organisation and arrangements and the results they achieve, and the revision of the policy as and when appropriate.

9. The policy statement should ensure there is no confusion about responsibility within the organisation, say between line managers and safety specialists, and should specify lines of communication.

SET OBJECTIVES

10. The setting and monitoring of relevant objectives and targets need to be based on satisfactory internal information systems. Line managers should be held accountable and there should be a systematic evaluation of their performance in this aspect of their job.

EXPERTISE

11. Training is an essential ingredient of any successful safety policy. Lack of training is a major contributory cause if not the main source of human error. Managers need to have knowledge of the health and safety legislation applicable to their area of responsibility, of the general principles of occupational health and safety and of the elements of safety management.
12. There is the need to learn from past mistakes and accidents and in particular to learn from experience at other places where the same hazard may exist.

SET STANDARDS

13. Having established the nature and extent of the hazards, they should be eliminated where possible. Where they cannot be eliminated, measures need to be taken and standards set to control them. Standards are the prerequisite for monitoring and review. Parallels can be drawn with the standards and procedures which control quality; demands imposed by documented systems subject to audit produce a climate where similar systems concerned with health and safety can be more easily introduced.
14. A realistic approach is required, one which takes account of the way that people actually work. Procedures must be clear, unambiguous and capable of being understood by everyone concerned. But they should not be overwhelmed by paperwork.

MONITOR

15. Monitoring by the organisation is an essential function which covers not only hazards and risks but compliance with procedures, systems of work, the adequacy of information, instructions, training and supervision.
16. In the control of high hazard, low probability situations particular attention should be paid to the identification and analysis of near misses rather than to statistics of accidents. It has been established that in industry generally for every serious injury incident there were 10 minor injury incidents, 30 property damage only incidents and 600 near miss accidents.
17. Audits play a vital part but care is required to ensure they do not dominate policy. It is recognised that management systems can come to structure themselves to gain high scores and to overcome the value of the audit as a tool towards effective control.

COMMITMENT

18. It is important to promote commitment by individual responsibility and accountability, by proper recognition of success, by promotion and reward of enthusiasm and good results. This again underlines the need for proactive monitoring based on success not failure.

HUMAN FACTORS

19. The term embraces a range of issues but resolves into the question as to how to harness the individuals capacity to operate skillfully and make correct judgements in unprecedented situations without being vulnerable to the same persons possible mistakes and errors. It is now widely accepted that the majority of accidents in chemical and other high hazard industries have their primary cause in human failings rather than in purely technical failures. People will make mistakes but by thought, pre-design and proper motivation this tendency can be reduced and consequences mitigated.
20. To take that last point further, it is rarely, if ever, sufficient to ascribe an accident merely to individual human error. Most accidents have multiple causes and in looking beyond the most immediate it will invariably be found that the incident was but the culmination of a

number of failures in management control - say lack of pre-consideration, lack of adequate monitoring or supervision or _ _ _ _ _.

THE PETERBOROUGH INCIDENT

21. This incident and in particular the blast damage and injuries are more fully described in the paper to be presented by Dr R Merrifield. The purpose now is to look at some of the more fundamental causes. They involve human error but relate more particularly to basic management failings - a view later endorsed by the Courts in setting a record fine. At the root was the consignment of an explosive in unauthorised and unsafe packaging.
22. The relevant law in the UK as elsewhere is quite specific. Before any explosive is consigned it must be authorised and classified by the National Competent Authority. Classification as in accord with the UN scheme relates to the packaging method, but there is also a longer standing requirement in the UK that the packaging of the explosive concerned, a type of cerium fusehead comb, must be specially authorised by a Government Inspector.
23. There is no doubt that the law was understood by the company. Systems were in place to ensure compliance at least with respect to the mainstream output of its factories. The company had developed and proved safe a packaging method for the cerium fuseheads as supplied cut from the comb. The packaging had been authorised and the whole item classified as 1.4G by the Competent Authority; any ignition was confined to one tin of 500 fuseheads, further effects limited to slight displacement of the lid of the wooden outer transport case holding up to 50 tins in all.
24. But around 1980, a fireworks company required cerium fuseheads on the comb. These were too big to pack according to the authorised method but the order appears to have by-passed the normal controls. Deliveries were initially packed in wooden boxes, and those replaced by tinned boxes in October 1985. The people responsible on the plant cannot have understood the basic requirements of any packaging methods for such fuseheads. The boxes, made outside, were of very poor quality with rust and weld spatter on inner surfaces, holes at corners. The packing of combs then ad hoc leaving too much freedom of movement for an excessive number, equivalent to 8000 as opposed to 500 fuseheads. Two such boxes were placed in a more normal wooden transit case, then handled as if 1.4G also incorrectly assumed.

25. The company organisation and systems of work were examined in an attempt to discover how the failures described above had come about. The joint Managing Directors and members of senior and middle management were interviewed. There had been several changes in systems of control and personnel since October 1985 when the fuseheads combs were first packaged and transported in tinned boxes. The management structure was a complex matrix system in which managers had both functional and business responsibilities covering separate areas of work.
26. A Design Representative and Packaging Adviser were responsible for packaging requirements. However, they checked new products and amendments to existing ones when they occurred, but did not review those introduced in previous years such as fusehead combs. No clear explanation was given for the use of unapproved packages for fusehead combs, the method appeared to have bypassed any assessment for compliance with requirements.
27. The safety department was primarily concerned with manufacture, ie plant and processes, and had little involvement in product development and design including correctness for transport. There was no clear managerial responsibility for safety in either of these functions.
28. No written specification for fusehead comb packages existed, nor were there any written operating instructions on the method of packing. No inspection of containers for suitability for use in transport, against laid down rules, was carried out.
29. It is necessary to add however that after the incident, a complete review of all products and packagings made within the company found nothing else untoward. Considerable work has been done to establish good working practices, many initiatives taken in the organisation to improve overall safety performance, not least in obtaining commitment to and conviction in a new safety culture. Sticking to the rules is a must and in every possible respect.
30. From a technical viewpoint, vibration of cerium combs in the unauthorised tin box as might be experienced during transport, could lead to damage of the fuseheads and accumulation of loose composition. Mixing with even a small quantity of rust would further enhance the extreme sensitiveness of fusehead composition to friction and impact. A relatively small jolt could cause ignition and, because of the excessive numbers in each tin, a fire ball well able to set any other packagings on a vehicle alight. An accident which could have been avoided just waiting to happen.

31. But can we be certain that all explosives are always transported in the packagings for which their classification is valid? And what of other departures from the rules? It is important to learn from such mistakes but vital to ensure that systems exist that lead to the identification and prevention by management of such faults.

EIDAS

32. A new Explosives Incidents Database Service (EIDAS) has been set up in the UK to promote the greater pooling and promulgation of information on explosives incidents. Modelled on the internationally recognised MHIDAS system covering the more general major hazard incidents, also developed by the Safety and Reliability Directorate on behalf of the Health and Safety Executive, the goal is to achieve an equivalent status and standing.
33. The aims of EIDAS are:
- a. To establish a management and control system for collecting and analysing explosives incident data.
 - b. To provide an efficient system for storing and distributing the data.
 - c. To provide a "follow up" service to obtain more detailed information on occurrences as requested by the customer.
 - d. To make the system readily available to a world-wide network to gain maximum utilisation.

INVESTIGATION OF AN EXPLOSIVE
ACCIDENT USING SIMULATION AS A TOOL

by

J.F. DROLET, G. COUTURE AND R. FARINACCIO

DEFENCE RESEARCH ESTABLISHMENT VALCARTIER
P.O. Box 8860, COURCELETTE
QUEBEC, CANADA, G0A 1R0

ABSTRACT

A new energetic polymer (EXP) under development at the pilot plant scale was currently produced in 5-kg batches. Solvent extraction to purify EXP was required and an equipment called Rotary Film Evaporator (RFE) was available and selected for use. The RFE was last operated some 15 years ago with inert polymer. Prior to further use it was cleaned and operated with inert polymer after consultation with the previous users in order for the new users to develop their expertise in operating it. On 12 Oct 89 after 24 hours of preheating of the RFE, the EXP polymer was introduced in the piping. Approximately 30 to 60 seconds later an explosion occurred in the piping followed by a small fire. One employee was slightly injured and the fire was quickly put out by the other one present. A board of inquiry was immediately formed and interviewed the employees as the first step in the investigation. After examination of the evidence, the temperature recordings and the deposition of the witnesses, a few hypothesis were retained to explain the explosion of EXP. An extensive laboratory study was conducted on samples of EXP left over from the same batch but did not reveal any clear explanation for what happened. Overheating of the equipment or of the piping was still the favored hypothesis despite the fact that temperature recorded at the time of the explosion (between 90 and 135°C) were appreciably lower than the auto-ignition temperature of EXP (215°C). It was only after a detailed and exact simulation of the conditions that prevailed at the moment of the explosion that proof of the existence of a much higher temperature (350°C) in one section of the piping allowed us to explain without any doubt ignition of EXP.

INTRODUCTION

A new energetic polymer (EXP) had been synthesized at the laboratory scale and its auto-ignition temperature, thermal stability, impact and friction sensitivity determined. EXP was now produced at the pilot plant scale in 5kg batches and the production process was viewed as a breakthrough. Every one in the division was enthusiastic about its potential military applications and confidence was building-up. Solvent extraction to purify EXP was required and an equipment in one of the pilot plant buildings was identified as potentially suitable for this purpose. This equipment called Rotary Film Evaporator (RFE) had not been used for about 15 years. After consultation with the engineers who had operated the RFE previously with inert polymers, a young engineer responsible for the development of EXP decided to use it for the purification of EXP. After cleaning of the equipment and a test run with an inert polymer, the operating conditions were established and a run with EXP was planned. During this first run, an explosion occurred in the feeding pipes of the equipment and the engineer suffered minor injuries.

An investigation team was immediately formed to find the cause of the ignition of EXP. This report describes how this investigation team conducted their study. It covers the different hypothesis that were examined by the investigation team and establishes that a detailed experimental simulation of the accident conditions allowed them to find the cause of the accident.

THE EQUIPMENT

A schematic of the equipment used is shown in Fig. 1. The polymer is fed by gravity from a reservoir to valve #1 through a flexible plastic tube (section A) and flows in the equipment pipes. From section B to C, the stainless steel pipes are heated with electric heating tape and covered with insulation. The purpose of heating is to lower the viscosity of the polymer and allow easy flow through the system. In that same section a gear pump is used to move the polymer to the evaporator. Valve #2 and a by-pass is used to prime the system. The stainless steel piping from section C to D had just been equiped with new heating tape, the old one being faulty, and the insulation was not replaced since it was judged unnecessary. Two thermocouples (T2 and T4) gave readings of the temperature at the locations indicated in Fig 1. The Rotary Film Evaporator (RFE) is equiped with heating mantles at both ends and temperatures recorded with thermocouples T1 and T3 at these locations. A spring valve in section CD is adjusted to open only at 35 psi to maintain a good vacuum in the RFE.

THE ACCIDENT

On the day prior to the accident, the heating of the equipment for the purification process was started to ensure equilibrium and readiness to proceed on the next day. In the morning of the accident, the temperatures were read on the multi point recorder as follows: T1 and T3 showed 135°C, and T2 and T4 showed between 85 and 95°C. The technician and the engineer responsible for the production of EXP at the pilot plant scale were then ready to proceed and introduced their last batch of EXP (#39) in the reservoir of the purification process equipment. Valve V1 and V2 were opened and the gear pump started to prime it. Valve V3 was then opened and V2 closed. When EXP started to flow at the exit of Valve V3, the gear pump was stopped and the evaporator motor started to adjust the rotation speed of the equipment. At this moment the two operators noted some bubbling in the EXP reservoir. Realising that something was wrong, the motor of the RFE was stopped. An explosion then occurred in the piping at the elbow (point C in the schematic) almost at the same moment. The engineer was hit on the head by a fragment but managed to exit the building. The plastic pipe in Section A was projected away and a flame was emanating from the piping at this point. The technician, who was not injured, extinguished the fire, phoned for help and exited the building.

A picture of the equipment is shown in Fig. 2 after the accident. Polymer residues was seen on the walls, the ceiling, the floor and the equipment. Figure 3 shows the polymer reservoir attached to the ceiling and the gear pump in the back with the different valves and piping. Figure 4 shows the remaining part of the pipe that was burst open and the heating tape that was wound around. Finally, Fig. 5 shows the stainless steel elbow where the explosion occurred and some plastic parts that connected the EXP reservoir to the equipment.

THE INVESTIGATION

An investigation team was formed immediately to find the cause for the ignition of EXP. After inspection of the site of the accident and taking several photos of the equipment, the operators were interviewed.

Several hypothesis were made to explain the ignition of EXP.

- a) the presence of an unstable by-product in EXP
- b) a malfunction of the gear pump
- c) a high temperature at some point in the system.

The first hypothesis was based on the fact that in batch #39, the chemical reaction that lead to the formation of EXP had been altered to facilitate its production at the pilot plant scale. More specifically, the

order of addition of the reactants had been changed. This procedure was used previously for batch #37 and the chemical analysis had not shown any difference compared to the original process, but further verification was warranted here due to the experimental nature of this process. Fortunately, about 1kg of batch #39 was left on the site of the accident. Several tests, namely Carbon 13 NMR, DTA, TGA, DSC and GPC, were conducted at the Chemistry laboratory to detect the suspected presence of an unstable by-product that could have been formed during the production of EXP.

Unfortunately, nothing out of the ordinary was found by the analyses. The auto-ignition temperature of EXP had been established previously as 214°C, way above the temperatures recorded by the thermocouples on the equipment. It was decided to run an auto-ignition temperature tests on a sample from batch #39 to confirm that nothing was wrong with the polymer. These tests gave an average auto-ignition temperature of 216°C.

The second hypothesis was quickly checked by disassembling the gear pump. Examination of the parts showed no sign of abnormal friction.

In the mean time, the investigation team was performing a simulation of the piping being heated with the same heating tape and the very same rheostat that was used at the accident site. The objective was to see the effect of the number of layers of heating tape on the temperature of the wall of the pipe.

A schematic of the simulation test is shown in Fig. 6 and the results appear in Fig. 7. It can be concluded from the results that the number of layers has a strong effect on the temperature of the pipe but in this case, it does not seem to bring it high enough (170°C) to explain the ignition of EXP.

A closer examination of the conditions that prevailed at the moment of the accident revealed that a short section of the pipe that was heated with heating tape was also insulated.

A second simulation similar to the one just described above but with the addition of insulation over the heating tape (see Fig. 8) was prepared. As shown in Fig. 9, this simulation revealed that the temperature inside the piping could have reached, after equilibrium, a temperature as high as 370°C, a temperature more than sufficient to cause the auto-ignition of EXP (auto-ignition of EXP is $214 \pm 2^\circ\text{C}$).

The result of this simulation concluded the investigation of the accident and was a great relief to the scientists working on the development of EXP. It was now clear that the stability of EXP was not at fault.

The investigation team made a number of recommendations to prevent another similar accident and prevent injuries to personnel. These are:

- 1) installation of a safety valve in the equipment;
- 2) not using heating tape as a source of heat in the presence of energetic materials;
- 3) formation of a team of experts to study the risks associated with new processes or new equipment and make the proper recommendations.
- 4) writing of SOPs even for a one time operation when the level of risk is high.
- 5) operation of equipment by remote control whenever possible.

CONCLUSION

The objective of any accident investigation is to find the cause of the accident in order to take the appropriate measures to prevent it from happening again. It has been demonstrated here that a detailed simulation of the conditions of the accident gave the information that allowed the investigation team to understand what caused the ignition of EXP and make proper recommendation to correct the situation. It is not implied that simulation is the only tool that will reveal the cause of an accident, but whenever practical or feasible, it will put the investigators on the right track to find the absolute cause of an accident.

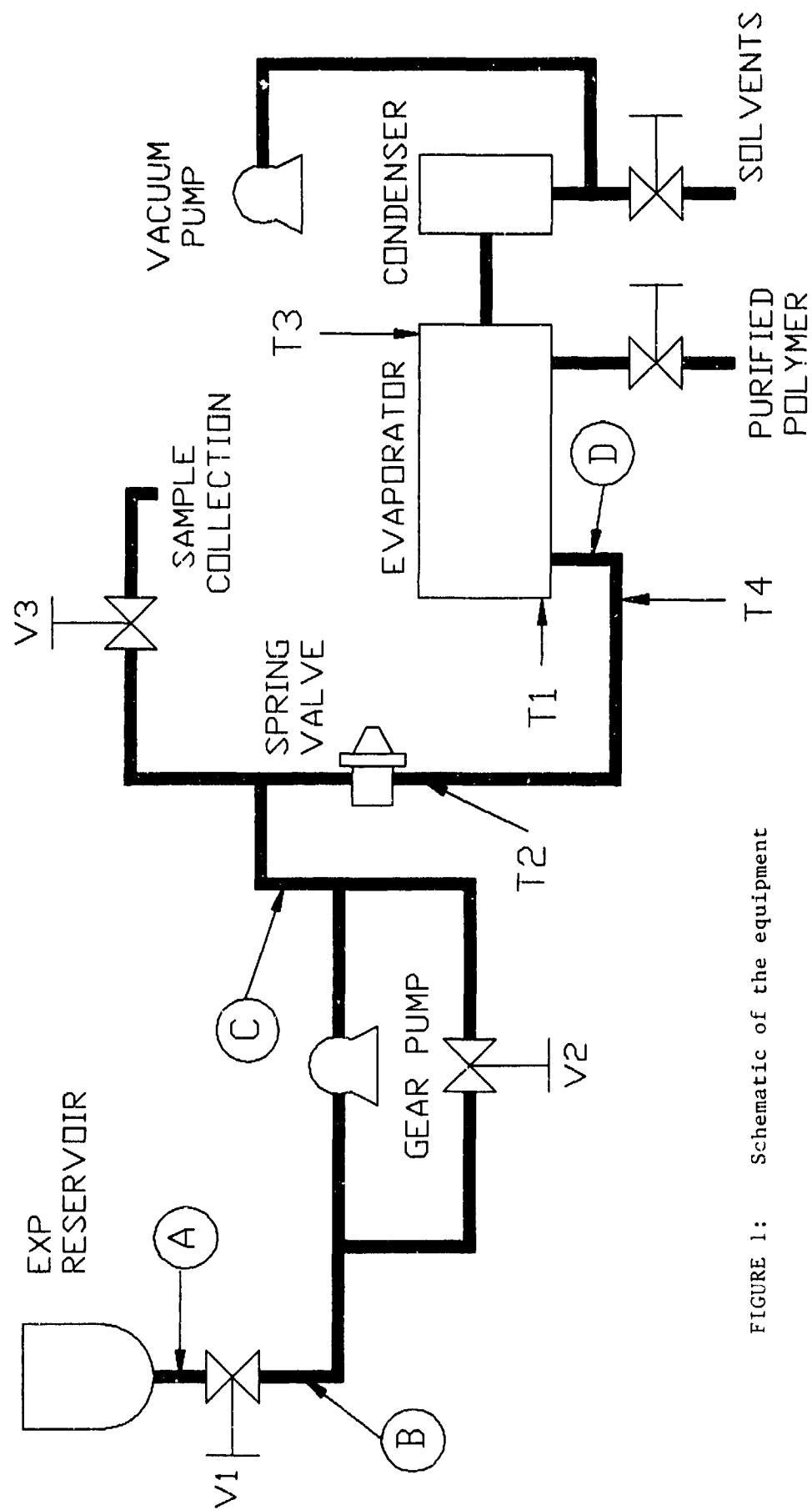


FIGURE 1: Schematic of the equipment

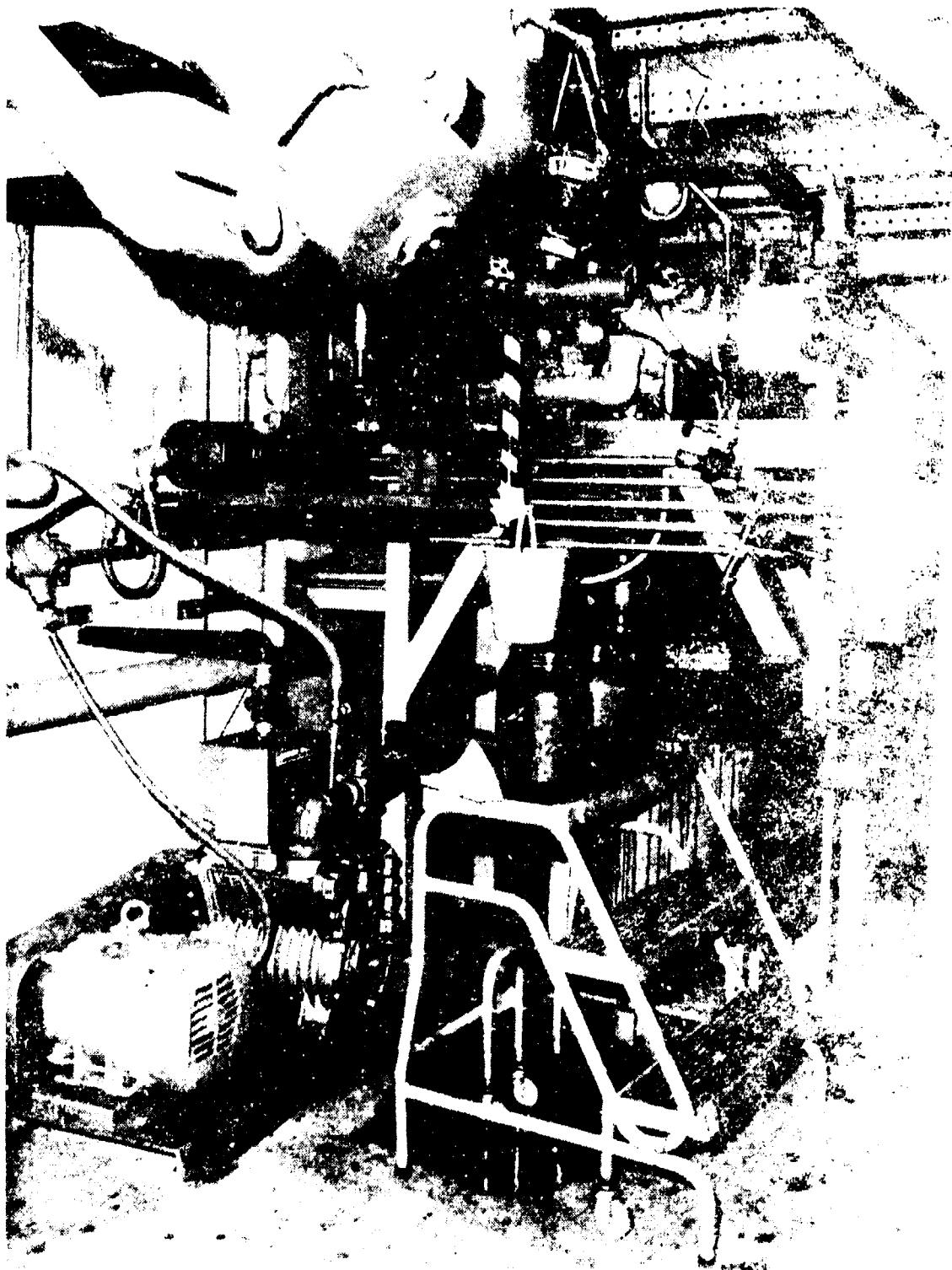


FIGURE 11 - Overall view of pump



FIGURE 3: EXP container after accident

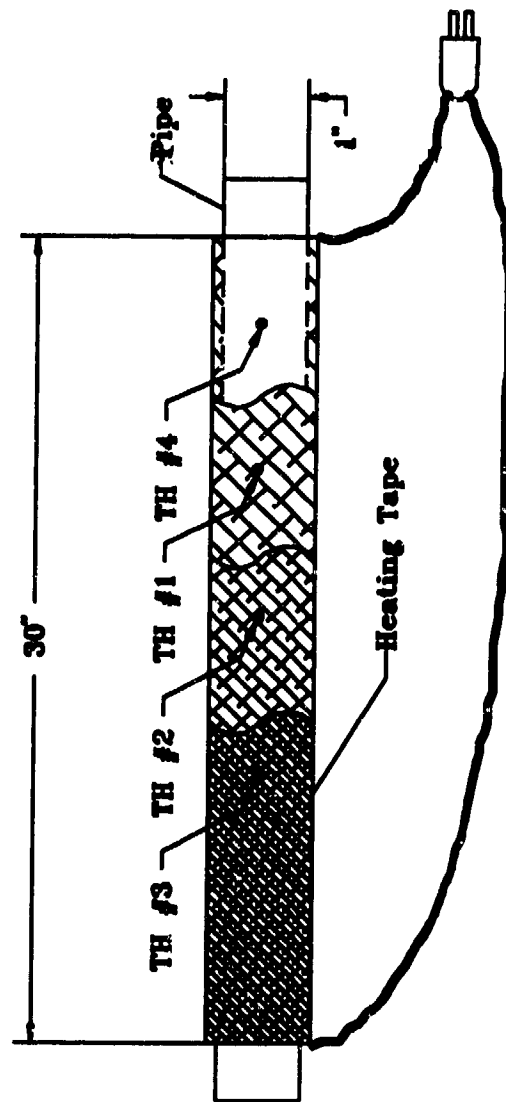


2. Location of the boat.



FIGURE 6: First simulation test

SIMULATION OF PIPE HEATED WITH ELECTRIC TAPE



Thermocouple #1 - under one layer of heating tape
 Thermocouple #2 - under two layers of heating tape
 Thermocouple #3 - under four layers of heating tape
 Thermocouple #4 - inside closed pipe

Note: Pipe was filled with air and closed at both ends.

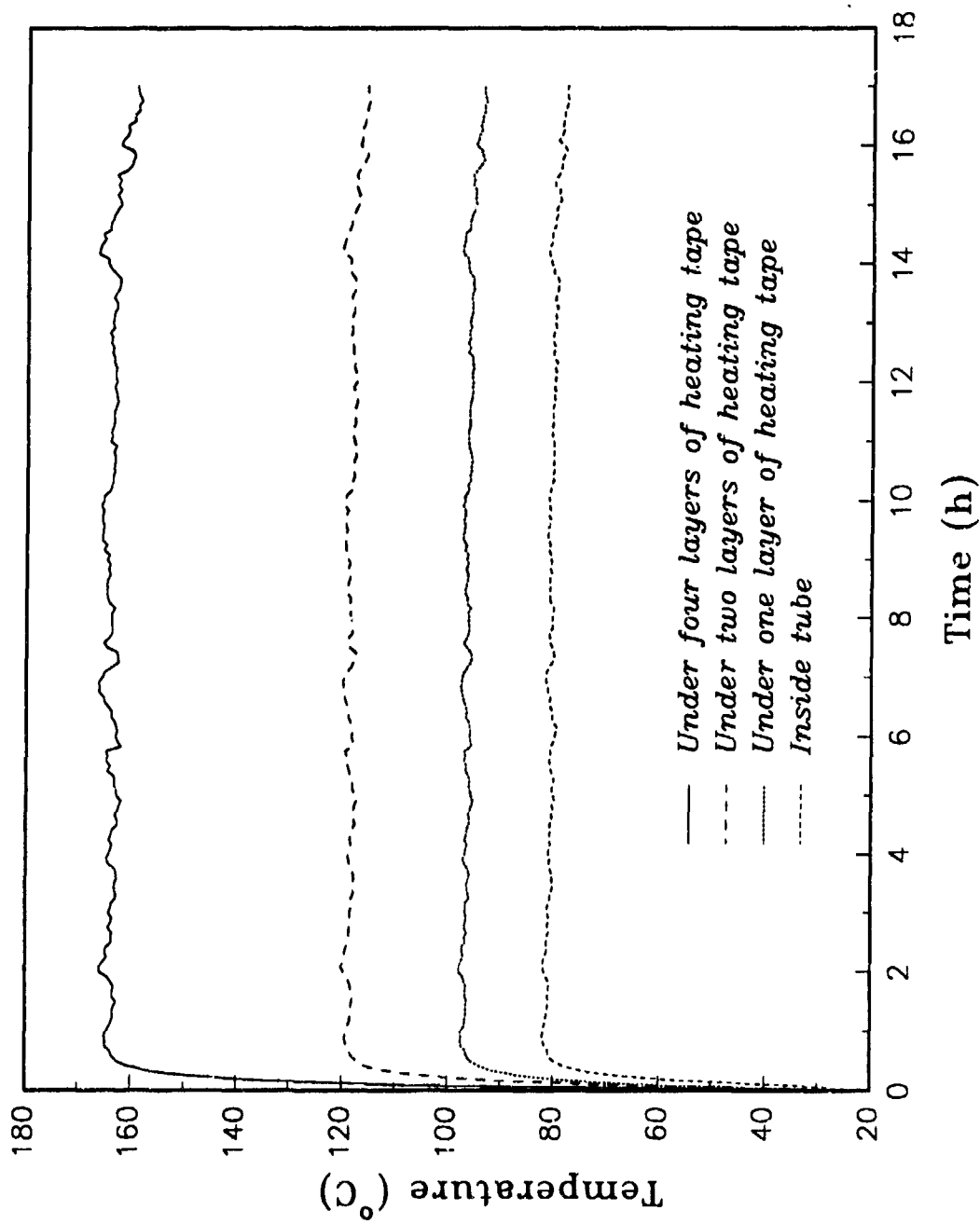


FIGURE 7: Test results from first simulation

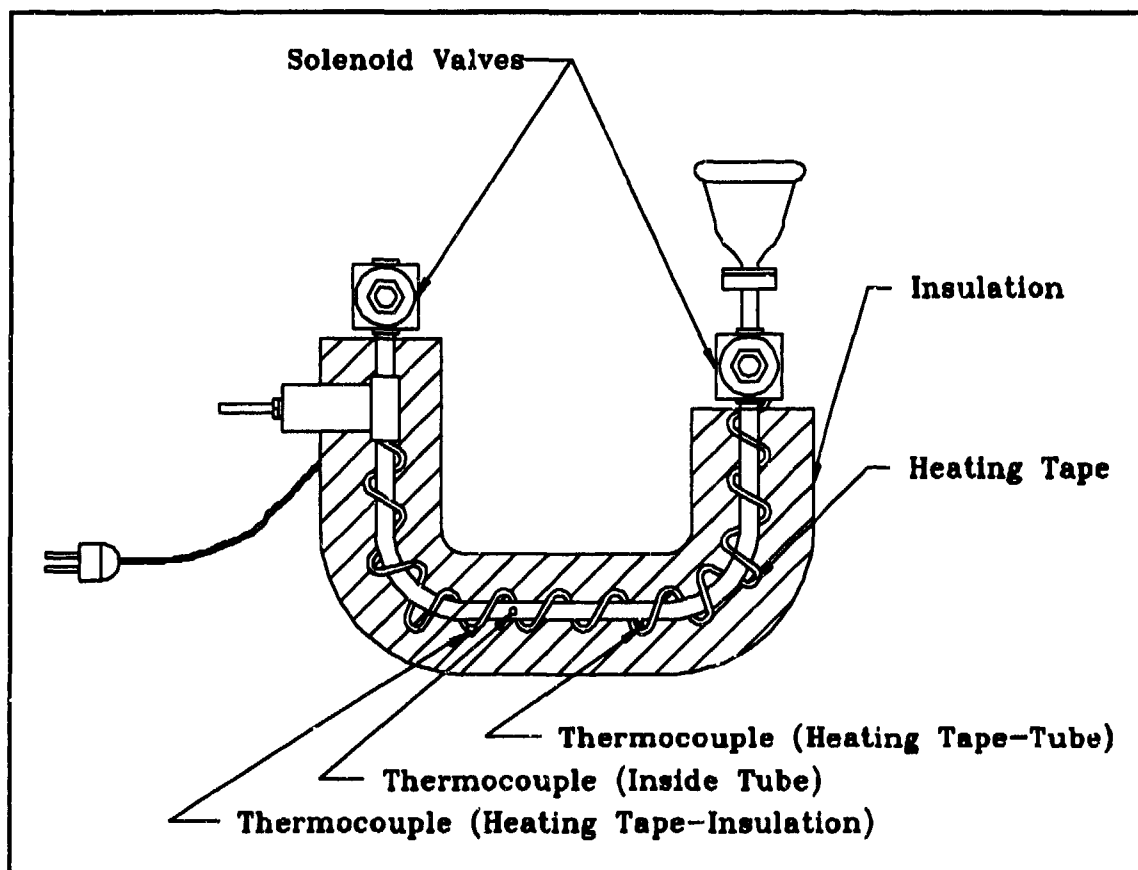


Figure 8: Second simulation of heated pipe.

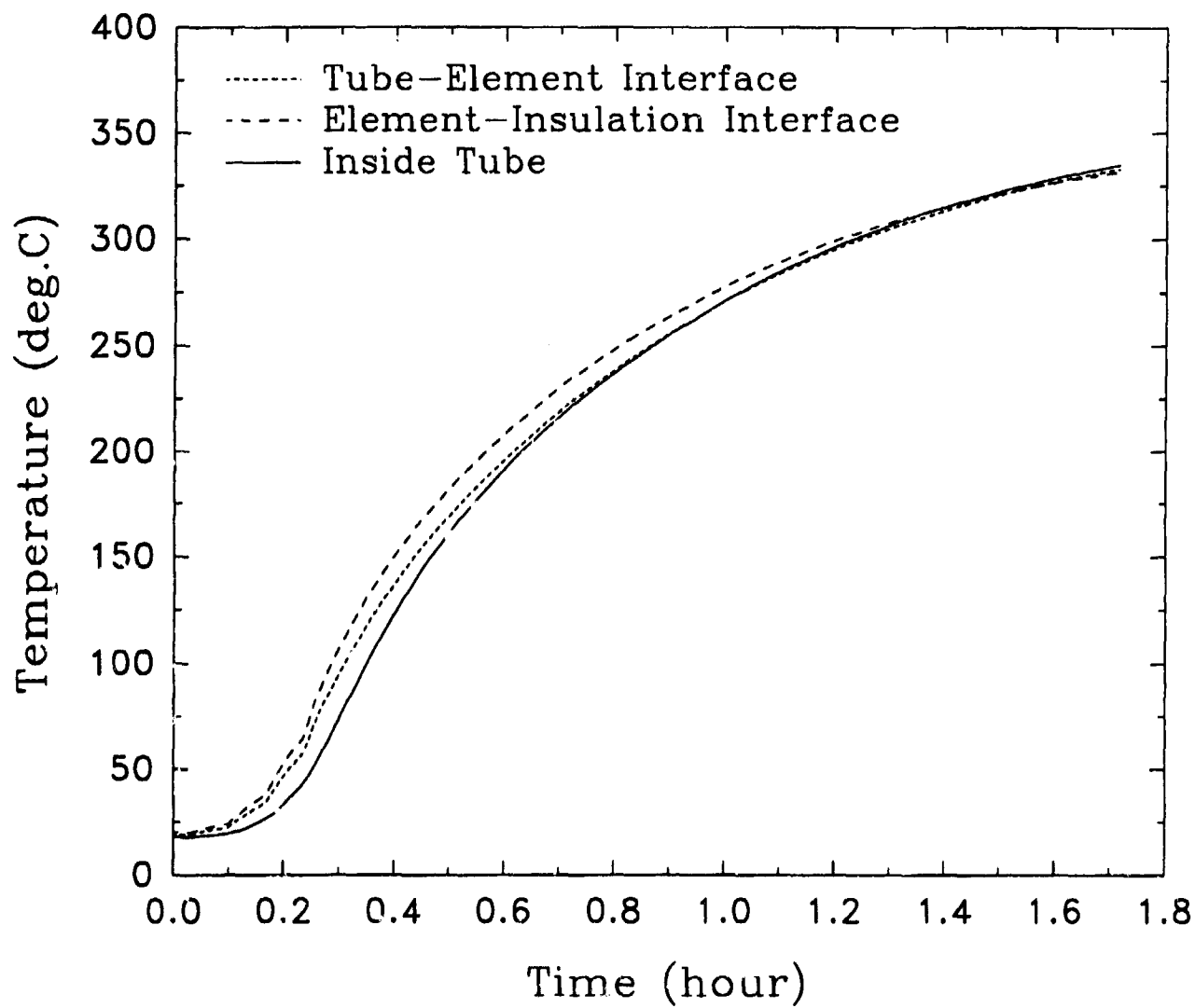


Figure 9: Experimental results of second simulation test.

24TH DOD EXPLOSIVES SAFETY SEMINAR
ADAM'S MARK HOTEL, ST LOUIS, MISSOURI
28-30 AUGUST 1990

AMMUNITION ACCIDENTS - THEIR CAUSES, INVESTIGATION AND PREVENTION

Presenter: Lt Col A J Morley BSc MSc RAOC

Authors: Lt Col A J Morley BSc MSc RAOC/Maj D C Hewitt RAOC

ABSTRACT

The Presentation covers a brief description of the role of the Directorate including the involvement with ammunition accidents. Several examples are used to show how accidents have occurred worldwide and address Design Faults, Poor Storage Control, Movement of Ammunition, Equipment Failures, Production Faults, In-Service Deterioration, Handling, Tampering and Errors of Drill. Investigation techniques are described using an accident that occurred in the UK involving 81mm Mortar ammunition resulting in three fatalities, as an example. The Presentation concludes with the measures taken in the British Army to prevent the re-occurrence of accidents. A video entitled "The Stupidity Factor" (14 mins) which illustrates the causes of typical ammunition accidents, is also available.

AMMUNITION ACCIDENTS - THEIR CAUSES, INVESTIGATION AND PREVENTION
PRESENTATION BY LIEUTENANT COLONEL A J MORLEY BSc MSc RAOC
DIRECTORATE OF LAND SERVICE AMMUNITION

INTRODUCTION

Thank you for the opportunity to speak at the 24th Department of Defence Explosives Safety seminar.

Before I start talking about the subject of ammunition accidents I would like first of all, to take a few minutes to explain the role of the Director for whom I work.

As Director of Land Service Ammunition he is responsible to the Director General of Ordnance Services for:

Equipment and Supply Management including global stock control and deployment, provision calculations, requisition, monitoring contract processes and progressing orders through production to receipt.

Long Term Equipment Planning for ammunition and explosives.

Sponsoring Ammunition and Explosive Regulations. His staff write and update all ammunition technical regulations.

Training of all ammunition technical personnel, including Explosives Ordnance Disposal Operators.

Explosives Engineering including surveillance, repair, modification, quality assurance, reliability analysis and disposal of munitions.

As Chief Inspector of Explosives for the British Army he is responsible for:

Setting Army Policy and Monitoring Safety Standards for storage, handling, transportation and inspection of ammunition and explosives giving technical advice on the interpretation of current regulations and implementing additional regulations resulting from new legislation. This work is monitored and verified by the Defence Explosives Safety Authority, who in turn liaise closely with the Health and Safety Executive, from whom we heard earlier today.

Proof of Ammunition. Members of his staff carry out Complete Round Proof *ie the proving of ammunition in conditions as close to the service environment as possible. For example the proving of 105mm Howitzer ammunition will be done using a unit of the Royal Artillery firing preselected and conditioned ammunition through their own guns but with monitoring equipment provided by DLSA. The results so obtained allow us to advise on the condition of the stock holdings

Approving New Ammunition Storage and inspecting existing ammunition storage including Royal Army Ordnance Corps ammunition units, and what is more pertinent to the subject of my presentation today:

Ensuring Safe User Drills, methods of repair and proof.

The Technical Investigation of all ammunition incidents including accidents.

Let me now give my credentials. My task within the Directorate is the munition manager for all Land Service Guided Weapons and I am also Head of the UK delegation to the ammunition working party one of whose tasks is the sponsorship of STANAG 2940 the Reporting of Major ammunition malfunctions.

AIM

This brings me nicely on to the subject of ammunition accidents that I wish to talk to you about today. I will spend a little time outlining the causes of accidents; go on to describe how we investigate accidents and finally address the problems of how to prevent accidents - a problem faced by us all.

ACCIDENTS GENERALLY

Accidents are a feature of every day life. We have all, unless we are very lucky, been involved in a road accident, for example. More people are injured in the "Safety" of their own homes each year than in any other location.

Being a Soldier is a hazardous profession! For training to be realistic soldiers are, necessarily, placed in situations which are potentially hazardous. The use of ammunition and explosives, munitions of war designed to kill or maim, places the men at risk. Of course, design features, robust construction and procedures make the use of ammunition at training safe and I shall be discussing that further, but the potential for an individual to be involved in an accident are manifold.

Before I go any further let me stress the point that ammunition is inherently safe but accidents do occur. The first I was involved in was as an Army Cadet at the age of 14 or 15. At the end of an exercise we were left with two of these - a thunderflash - a simulator for making loud bangs to represent grenades, gunfire etc. The instructors with us said "We'll show you how to get rid of these", so they cut them open, poured the contents on a road and put a match into the pile of gun powder. The resultant explosion removed all the skin from the back of his hand. That may I say is not the correct way to dispose of misfired Thunderflashes.

As you can imagine therefore I am a great believer in soldiers not tampering with ammunition.

But now let me give you an idea of the frequency of ammunition accidents, this slide shows the number of ammunition accidents which have occurred in the last seven years. The total column refers to the total number of accidents for a particular year. An accident is an ammunition incident which causes injury, death or damage to equipment or property, hence the apparent disparity between the number of accidents and the numbers injured and killed. There is no discernible trend, although last year was particularly bad in terms of the number of casualties. To put these figures into perspective, the British Army is approximately 300,000 strong, including reservists or part time soldiers. So what are the causes?

CAUSES

Design Faults. If we are to reduce ammunition accidents to a minimum we must design safety into the ammunition our soldiers use. Fortunately, over a long period of time, ammunition design has achieved a very high standard. However, design faults do still come to light after ammunition is brought into service. An example of this is oversize washers on L2 HE Grenades causing partial detonations.

Storage. In a disciplined organisation, the application of stringent procedures and regulations, should ensure that ammunition storage accidents do not happen. However, accidents in storage do occur.

Faisalabad, Pakistan. As recently as 10 Apr 88 a complete ammunition depot was destroyed. No firm details are available but it is believed to have started with a HD 1.1 event followed by other major explosions and fires. There were an estimated 100 casualties including many fatalities.

Brazil. 12 tons of PETN in store caught fire. Fortunately most of it burnt away before the residue detonated. Traversing restricted propagation.

Inkomo, Zimbabwe - Aug 81. A fire led to a series of HD 1.1 events via propagation. The complete depot was lost, but, as it happened on a rest day there were no casualties.

Severomorsk, Russia - May 83. During a seven month period in 1983-84 six ammunition storage locations in Russia suffered explosive events. The most serious of these was at Severomorsk Naval base on the Kola Peninsula. Three separate storage areas were involved and the result severely affected the operational readiness of the most powerful Russian fleet.

What were the causes of these accidents - or what caused some of them to reach such dramatic scales? Almost certainly inadequate safety distances between buildings and sites was one factor. This may have been the result of inadequate regulations or the incorrect application of regulations.

Movement. Transporting ammunition and explosives is potentially more hazardous than storing it as there is more opportunity for things to go wrong. Trucks may crash, set on fire, trains may be de-railed, ammunition can be dropped during intermodal transfers:

USSR - 1988. A freight train carrying commercial explosives exploded near a station causing heavy casualties and severe damage.

Ambazac, France - May 86. A lorry carrying 19 tons of Dynamite exploded. A fire took hold and spread to the load causing mass detonation. Fortunately the driver took the vehicle off the main road and evacuated the area. There were no casualties, but over 100 houses were damaged.

Equipment Failures. A 76 mm gun on a tracked recce vehicle (Scorpion) had a faulty safety system which caused accidental firing. Our 9 mm sub-machine gun breach mechanism wore so badly that the sears, which held the breach block to the rear enabling single round firing, failed causing the full discharge of the magazine.

Production Faults. Shell 175mm Gun HE - at high angles of elevation loaded shell were falling back onto the propelling charges - resulting in a breech explosion which destroyed the M107 Gun. This was due to the driving band being incorrectly profiled. These examples necessitated 100% rework of affected stocks.

In-Service Deterioration. Round 84mm Inf HEAT, Carl Gustav - level of stabiliser in the igniter had degraded with age - similar propellant stored in bulk by civilian industry had ignited spontaneously.

Handling. I have spoken about how faults can be built into ammunition but we can all accept that this is a fairly rare occurrence. I have illustrated how accidents, some of great magnitude, can occur during storage and transportation. But these are rare events because both storage, and to a lesser extent transportation, can be carefully controlled. The real potential for accidents is realised when ammunition is brought into use by the soldier at training. In this case the ammunition is exposed, used for the purpose for which it was designed (generally to kill) and often used in a hostile environment where the user is under stress.

Tampering. There is also another effect caused by the soldier handling "real" ammunition that of arousing curiosity - and that is what I would like to talk to you about next. Soldiers are blessed (or cursed) with great curiosity. They like to know how things work. For most this thirst for knowledge is satisfied by instruction and reading books and manuals. For a few, however, that is not enough. They need to look for themselves and try to take things to pieces. This leads to one of the causes of accidents caused during handling - Tampering!

Tampering is the cause of relatively few accidents. In an average 12 month period, of, say, 200 reportable ammunition accidents - 5 can be expected to result from tampering. However, it is likely that at least one person will have been injured on each occasion.

Errors of Drill. Errors of Drill account for between 10-20% of all ammunition accidents and cause a significant number of casualties - 20 in an average year. Examples of errors of drill are firing ball small arms ammunition through a rifle fitted with a blank firing attachment, firing the 84mm recoilless weapon system with someone in the rearward danger area, and double feeding an 81mm Mortar tube after a misfire. All these accidents have happened and I shall be telling you more about the lattermost in a moment. What leads to errors of drill? Inadequate training, working under stress and difficult conditions, tiredness during long exercises. Sometimes it can be the result of incorrect procedures and drills in training pamphlets but this is rarely the case.

Negligent Discharge (ND). It is surprising how many people fire weapons, particularly personal weapons, accidentally. More ammunition accidents are caused by soldiers negligently discharging their weapons than by any other single cause. Something like 30-40% of reportable ammunition accidents are caused by negligent discharges and contribute significantly to the annual casualty list, an average of 17 in any year. Again, what are the causes? Negligent discharges usually occur because people do not unload their weapons properly and at the correct place. This may be because of tiredness, stress or poor procedures.

But there is one underlying trend in most ammunition accidents which occur because of handling errors - a lack of supervision.

INVESTIGATION

Having discussed the causes of ammunition accidents, and I am not saying that my list is exhaustive, I am now going to consider their investigation. To do this I am going to use a real case history, an accident involving a mortar section firing under field conditions at Otterburn Training Area, UK on 18 Mar 82.

Otterburn is one of our main training areas; it is bleak, rough, undulating, moorland terrain. The unit was on a one week mortar live firing practice and had already had three days successful training. During that time they had had three misfires but had not reported them through the ammunition incident reporting chain as required by regulations. This was a significant error as you will see.

At 1102 hrs on the fourth day - Thursday - an explosion occurred at No 2 Mortar position causing serious casualties. Three soldiers were killed and two others seriously injured.

Immediate action included tasking the Civil Police (because death had occurred), the Special Investigations Branch of the Military Police and the Ammunition Technical Officer (ATO) one of DLSA's technical staff deployed throughout the UK. A Sergeant Ammunition Technician was immediately tasked by Range Control to attend. He arrived at 1127 hrs, asked that nothing be touched or removed, including the bodies, and checked the area for any ammunition which could be in a dangerous state. Having satisfied himself that the area was safe he sought assistance from his Company Headquarters and then organised a meticulous search of the area. Every fragment found was marked with white tape but was not moved. A grid search pattern was established and the location of each fragment accurately plotted. Witnesses were identified and held ready for questioning.

By the time the ATO Company Commander arrived at 1315 hrs police photographers had recorded the scene and witnesses were being questioned by both civil and military police.

The ammunition on site which had been prepared for firing was inspected by the ATOs, repackaged and the technical details recorded. These details were passed to DLSA and a worldwide ban imposed pending the outcome of the investigation. Witnesses were interviewed by the ATO to provide background information to the incident. The light was failing by this time so the area was left under guard, and in depth questioning of witnesses was carried out by the ATO off-site. At this stage everything indicated that correct procedures had been followed.

Further interviews were carried out and included all personnel involved in the accident. The Otterburn Range Armourer stated that the weapons had been correctly maintained and that they were serviceable. The weapon's log books confirmed that they had been subjected to a recent inspection and found to be serviceable.

The following day a more intensive search was carried out, every fragment was plotted and labelled before collection and removal to the ATOs HQ for further investigation. But ammunition damaged in the explosion was destroyed at a nearby site.

As a result of an initial inspection of the fragments the suspicion was that, a second bomb had been involved, so an extended search of the area was carried out to 600 m from the explosion site but no further mortar bomb fragments were found, however two pieces of the mortar barrel were. The remains of the weapon were inspected by the District Armourer who could not attribute the accident to the weapon.

This led the team into a more detailed inspection of the fragments which showed that the lower section of the mortar barrel had been reduced to very small fragments consistent with a detonation in that area. The upper part of the barrel was bulged which would be consistent with an obstruction (2nd - bomb) in the barrel deflecting the effects of an explosion outwards. This was confirmed by the discovery of fragments of a second tail unit at the scene. There was now significant evidence to support a two bomb theory and it was concluded that:

Bomb 1 Misfired.

A double feed occurred.

Bomb 2 functioned normally when the primary cartridge hit the forward contours of the bomb 1 fuze.

Hot propellant gases/pressure caused bomb 1 fuze magazine/gain to function.

The accident was the result of an error of drill.

The investigation of any accident includes, as a standard procedure:

Inspection of site.

Questioning of witnesses.

Inspection of weapons and equipment.

Taking account of the environment.

Investigation of procedures used and if necessary:

The use of experts/scientists.

Manufacturers input.

A report giving details of the accident and where possible giving the cause of the accident.

Every accident is the subject of a Board of Inquiry at which the cause is, if possible, identified and recommendations are made to prevent future accidents.

PREVENTION

This brings me to the final part of my presentation and that is how do we prevent accidents?

Design. The first task is to ensure that ammunition is designed and manufactured correctly. This should be possible because it is carried out in slow time under controlled conditions.

We must respond rapidly to ammunition accidents, investigate thoroughly and implement resultant recommendations.

Ammunition involved in an accident must be suspended from use. Our system of imposing ammunition bans must be comprehensive and rapid. This is both a national and NATO requirement STANAG 2940 requires that any major ammunition malfunction which occurs involving ammunition listed in the interoperability catalogue must be reported to all member nations as quickly as possible and follow up reports published as appropriate.

Movement and Storage Regulations must be correct, and must be enforced.

User drills and procedures must be carefully developed and tested to reduce risks to a minimum).

Allied to this, training must be thorough, realistic and properly supervised. It is the lack of proper supervision that is the common thread running through most ammunition accidents.

Finally, publicity is one way in which we try to bring peoples attention to accidents and their consequences. DLSA issues periodic accident reports and we have recently produced an updated training film called "The Stupidity Factor" which is shown to soldiers during training. There is something of the stupidity factor in us all; we do things without thinking, sometimes we become distracted when we should be concentrating. But we hope it does not result in an ammunition accident which can cause this.

CONCLUSION

Gentlemen, that concludes my presentation. Accidents involving ammunition will continue to happen because of its very nature, and because of human nature. Our task is to ensure that accidents are kept to a minimum so that our soldiers can work and train in safety.

QUESTIONS

**REPORT ON THE
PETERBOROUGH EXPLOSION**

Peterborough, UK; 22 March 1989

BLAST DAMAGE AND INJURIES

by

R. MERRIFIELD

**Health and Safety Executive
H M Explosives Inspectorate**

**Magdalen House
Stanley Precinct, Bootle
Merseyside L20 3QZ**

SUMMARY

- 1** At 09.45 on 22 March 1989 a vehicle carrying approximately 800 kg of mixed explosives exploded at the premises of Vibroplant Ltd on an industrial estate in Peterborough. The main bulk of the load was blasting explosives. The explosion caused the death of a fireman and injured well in excess of 100 people, 87 of whom received hospital treatment. Two of the injured were admitted to intensive care.
- 2** The vehicle was specially modified to carry explosives and operated by Nobels Explosives Company (NEC), a subsidiary of ICI. Shortly after it entered the Vibroplant yard a minor explosion occurred inside the load carrying compartment, causing a fire. The fire continued for some 12 minutes, during which time the fire brigade was called and took up position. After the 12 minutes the entire load, apart from a small number of detonators, detonated en masse.

- 3 The investigations have concluded that the source of the fire and hence the cause of the ensuing explosion was a box of cerium fusehead combs which were destined for a fireworks manufacturer. The combs were in an unauthorised and unsafe packaging. NEC were subsequently fined £250,000 for breaching Section 3 of the Health and Safety at Work Act 1974.

DESCRIPTION OF SITE

- 4 The Vibroplant yard where the explosion occurred is on the edge of an industrial estate mainly comprising small to medium size commercial and industrial properties, consisting principally of large steel and pre-cast concrete framed buildings. These were clad with metal sheeting or, for the offices parts of the buildings, cavity brickwork. The estate is situated on the south side of Peterborough, see Figure 1.
- 5 The entrance to the yard of Vibroplant is set back and separated from the road by a pavement and grass verge some 24m wide: the yard is about 90 by 60 m, bounded on the south side by a 2 m high, 9" brick wall, and on the other sides by a chain link fence. The surface of the yard was asphalt over hard core. There was a 'sleeping policeman' speed ramp just inside the main gate.

DESCRIPTION OF VEHICLE

- 6 The vehicle was a Ford D series 11.5 tonne box van, specially modified to carry up to 5 tonnes of explosives. The sheet aluminium box load compartment was fitted with a roller shutter door at the rear, and was separated from the cab of the vehicle by a fire resistant screen.

EXPLOSIVES CONTENTS

- 7 At the time of the incident the vehicle contained:

High Explosives	- Powergel 800,	150 kg (6 by 25 kg cases)
	- Powergel E800,	500 kg (20 by 25 kg cases)
	- Magna Primers	56 kg
	- Ammon Gelit	75 kg
Detonators	- No 8 Star,	500 in number
	- Magnadet,	250 in number
Fuseheads	- Vulcan,	10,000 in 1 box
	- Cerium,	2,400 in 3 boxes
	(uncut combs)	

EVENTS LEADING TO THE EXPLOSION

- 8** The high explosives and detonators were typical of those used in quarrying and other blasting work. Powergels are relatively insensitive and are initiated by detonator and booster such as Magna Primer or other more sensitive explosives such as Ammon Gelit. The fuseheads were to be used at a fireworks factory as electrical igniters in pyrotechnic devices. The Cerium fuseheads were supplied uncut on combs with 20 fuseheads per comb - see Figure 2. The Vulcan fuseheads were supplied already cut into single devices.
- 9** It was a matter of chance that the explosives vehicle missed its way while heading for a nearby explosives factory, and used the yard belonging to Vibroplant as a turning place.
- 10** As the vehicle entered the yard of Vibroplant it passed over the concrete speed ramp whereupon there was a minor explosion inside the load compartment which blew the rear roller shutter door outwards. As the driver continued in a clockwise circle around the yard he noticed in his rear mirror, blue smoke behind the lorry. He stopped the vehicle near the middle of the yard facing the exit. Both the driver and mate went to the rear of the vehicle to investigate and subsequently to arrange contact with the emergency services.
- 11** The roller shutter door was hanging out of its guides on the passenger side and only partially in the guides on the drivers side. The door was secure both top and bottom. Through the gaps at the sides of the door could be seen smoke and flames inside the compartment. Initially the fire produced only a small amount of black smoke. As it progressed however, minor "pops" and bangs were heard with increasing frequency. As the fire progressed further, thick yellow smoke was observed and immediately before the explosion the sides of the vehicle were seen to bulge. The vehicle exploded at approximately 09.45, 12 minutes after the start of the fire.
- 12** At the time of the explosion 2 fire tenders and a fire rescue vehicle were in attendance. Two firemen took a branch (nozzle) just beyond the edge of the wall on the south side and at the entrance to the yard and stood ready to receive water. This was some 15 metres away from the burning vehicle. When the vehicle exploded one of these two firemen was killed.

INVESTIGATION

Examination of High Explosives and Detonators

- 13** Subsequent tests on samples of both high explosives and detonators involved in this incident showed normal behaviour. Their packagings

fully met the requirements laid down. Examination of production records revealed no anomalies. All were found to be safe to transport.

Examination of Fuseheads

- 14 The Vulcan fuseheads were found to be in a satisfactory condition and properly packed. The Cerium fusehead combs however were found to be packed in unauthorised and unsafe packagings. The type of packaging used was both illegal and dangerous in that there were excessive numbers of fuseheads per box, the packaging was loose resulting in presence of loose composition inside metal boxes, and presence of rust. Fusehead composition was examined and found to be extremely sensitive both to impact and friction. Mixtures with rust (1%) had a 10 fold increase in impact sensitivity. Boxes of combs dropped from a height of 1.2 metres exploded in some tests but not others. Ignition trials on one box of cerium combs produced a fireball approximately 2.5 m in diameter, and lasting 0.3 seconds.

CAUSE OF THE EXPLOSION

- 15 The sequence of events that led to the explosion began when a minor explosion inside the vehicle started a fire. After about 12 minutes the main bulk of the cargo, blasting explosives, detonated.
- 16 The initial minor explosion was probably caused by ignition of the Cerium fusehead combs when the vehicle jolted over the speed ramp control. The likely mechanism for ignition being impact or friction of the fusehead debris or loose composition against the metal box packaging. The fusehead composition was probably sensitised by the presence of rust. The fireball which followed threw burning debris around the load compartment, starting a number of fires.
- 17 The mechanism for detonation of the whole cargo cannot be firmly established. One possibility is the presence of detonators which were scattered about during the fire and landing on or near heated and perhaps sensitised explosives. Another possible mechanism is the burning to detonation of the Pentolite boosters or the Ammon-Gelit.

BLAST DAMAGE AND INJURIES

Damage Caused by Explosion

- 18 Appended are aerial photographs both of the Vibroplant yard some time before the explosion, and the general area after the explosion (Figures 3 and 4).
- 19 The epicentre of the explosion is marked by a depression (dimensions 46 cm deep, 3.5 m radius) in the tarmac surface of the yard. The floor of the explosives vehicle was approx. 1 meter off the floor.

- 20 Approximately 130 cars were damaged to varying degrees, i.e approx. 60 beyond viable repair, 13 badly damaged, 51 slightly damaged, and the remainder superficially damaged.
- 21 Blast damage to the two buildings on either side of the explosion, i.e to Vibroplant and City Electrical Factors, was considerable -see Figures 5 and 6. Damage to the Vibroplant building was such that it had to be demolished at the earliest opportunity. Damage to buildings further afield consists of large doors blown in, metal cladding removed, asbestos roofs collapsed, metal cladding damaged, window frames blown in,extensive window damage etc. The number of buildings significantly damaged was of the order of 150.
- 22 Window damage was extensive reaching as far out as an archaeological site (Flag Fen) some 1260m away.

Discussion on Blast Damage

- 23 Historically there have been relatively few explosives incidents not associated with the immediate act of explosives manufacturing, i.e few incidents off-site. This incident has presented a unique opportunity to study the explosion effects of a relatively small quantity of commercial blasting explosive, upon a modern industrial estate. Additionally, by comparing actual damage with what we would have predicted for this situation allows us to confirm or refine as appropriate,damage/injury predictive techniques.
- 24 It is common to relate structural damage simply to blast overpressure,as shown in Table 1 (reference 1), when attempting either to predict the damage which is likely to be caused by an accidental explosion, or, in any post accident investigation of an explosion to estimate the equivalent quantity of TNT involved in the same. This, however, ignores the considerable effects of impulse, i.e the duration of the positive phase of the blast wave. With the relatively small quantity of explosive involved in this incident this is an important factor. A compilation of blast overpressure / damage criteria which includes a consideration of impulse is given at Table 2 (reference 2). This procedure has developed over many years, with much useful information gathered largely from World War II bomb attacks, the A bomb attacks on Japan, and American trials with nuclear weapons. From Tables 1 and 2 it can be seen that many of the blast damage 'markers' are construction elements of traditional British brick/tiled roof houses. In this incident the types and quantities of explosives are known with certainty. The premises, however,both surrounding the explosion and affected by it are principally not houses, but steel clad and/or brick fronted,steel and concrete framed industrial buildings. In view of the limited amount of published information on the blast

overpressure effects from approx. 800 kg of known explosive to these industrial buildings, it is worthwhile therefore, to record here, the main explosion effects in terms of 'new' industrial type markers.

- 25 A summary of damage versus distance 'contours' are given in Table 3. In column [4] (of Table 3) are listed the distances at which the various levels of damage occurred. Column [6] gives the corresponding overpressures predicted from 800 kg of TNT. Column [5] lists the distances (using information from Table 2 and other sources) at which these levels of damage are expected to occur.
- 26 Window damage in this incident was very variable and generally in excess of what might have been predicted. The extremity of window damage at the Flag Fen archaeological site some 1260m away was due to flexing of the flimsy wooden structure. Other reasons for much reported damage was the fact that in some buildings, long sections of windows have been blown out from the sides of steel framed/metal clad buildings without many of the panes breaking, even when the frames landed on the ground. Other reasons for variability include that the windows range from small to very large, thin to thick, single and double glazed, glazing held by putty/ beading/ rubber, frames of wood/plastic/metal, frames retained weakly/strongly etc. Another fundamental problem in assessing window damage with the large buildings here was that distances to that building, for the purposes of damage assessment, are normally taken from the rear of the same to the blast source. When using a simple Table 2 type approach this will clearly introduce increasing inaccuracy with increasing length of building. On the same line, a particular record of percentage window damage for a long face of a building which is in line with the direction of travel of the blast wave is again subject to much error due to the considerable variation in overpressure along its length.
- 27 Fragments were thrown over a wide area - see Figure 7. The prime requirement in the immediate post accident situation was to collect all live pyrotechnic items from the surrounding area. Recognisable pieces of vehicle (except the many small pieces of aluminium from the body) were also collected. The extremity of fragment throw was not accurately determined, but within a licensed fireworks site some 380-400 m away, a number of small items in the weight range 100-3000 gramme were found. Also at approx 470 m a number of cars were allegedly damaged by falling gravel.
- 28 In general, the steel and concrete framed building withstood the effects of the blast very well. The steel framed buildings, being able to flex, performed better than the concrete framed buildings. A few concrete purlins failed and collapsed, but these resulted in no injuries.

- 29 Overall, the blast damage appears to be consistent with a high order detonation of a quantity of explosives equivalent to 800kg of TNT.

INJURIES

- 30 The number of persons injured in this explosion was well in excess of 100. Of these, 80 were admitted to hospital; i.e 2 in intensive care (1 punctured lung, 1 burns), 12 as in-patients with other blast related injuries (head, spine, eardrums), and the remainder with superficial injuries (cuts, shock).
- 31 The fireman killed in the incident was approximately 15 or so metres away from the centre of the explosion and was killed by a fragment (see Figure 8). One of the badly injured persons (burned) was a fireman who had been standing close to the fatality. The other badly injured person was outdoors approx. 40 metres away, and was hit by a fragment. The injury 'contours' are summarised in Table 4.
- 32 Persons outdoors and close to the explosion sustained perforated eardrums (see Figure 9), cuts and bruises from flying debris, and were thrown to the ground (see Figure 10). Persons indoors sustained the greatest numbers of injuries from flying glass. Other injuries indoors were due to collapsed ceilings.

Discussion of Injuries

- 33 During World War II the V1 bomb attacks on London caused the greatest number of injuries and fatalities to persons indoors by partial or complete demolition of the houses. i.e people were crushed and asphyxiated respectively by falling debris and dust. In this incident there were no instances of complete building collapse and consequently no related serious crushing injuries. Any housing at the sorts of distances from the explosion that both Vibroplant and City Electrical Factors were, would have been expected to have suffered considerable damage with corresponding numbers of serious injuries /fatalities (for 800 kg TNT, radii of A and B damages respectively are 22.1 and 32.2 metre). Against this background these two closest 'industrial' type buildings survived well.
- 34 In the 12 minute period between the onset of fire and the final explosion, numbers of people congregated both outdoors in close proximity to the van, and against windows which overlooked the Vibroplant yard (see Figure 8). This had the effects of causing persons outdoors to be blown off their feet, sustain hearing damage, and for some to be injured by fragments. Persons indoors sustained serious cuts from flying glass, translational injuries, and injuries from falling

ceilings/debris. Cuts injuries accounted for the majority of hospitalised persons. Previous expectations for an incident such as this might have been that the delay between the onset of the fire and the final explosion would have caused persons in the vicinity to move well away. This of course did not happen.

CONCLUSIONS

- (i) Overall, the the blast damage appears to be consistent with a high order detonation of approximately 800 kg of high explosives.
- (ii) A pre warning of the fire before the explosion, coupled with inadequate evacuation of the area, caused persons to congregate both in the open, close to the vehicle, and inside buildings adjacent to glazing. This resulted in many injuries from flying glass, fragments, and damaged eardrums.
- (iii) In general, the steel and concrete framed building withstood the effects of the explosion very well. The steelframed buildings being able to flex, performed better than the concrete- framed buildings. A few concrete purlins failed and collapsed, but these resulted in no injuries. The same explosion in the centre of an housing estate would have produced more serious injuries.
- (iv) Information gathered in this tragic incident, on the explosion effects of a fairly small quantity of commercial blasting explosive upon a modern industrial estate is very valuable and can be used for refinement, if necessary, of damage assessments techniques.

REFERENCES

- 1 CLANCEY V J S, Diagnostic features of explosion damage. Sixth Int. Mtg of Forensic Sciences, Edinburgh (1972).
- 2 SCILLYN F and HIGH W G, The Blast Effects of Explosions, 5th Int. Symp. Loss Prevention in the Process Industries, Cannes 15-19 September 1986, vol. 1, paper 39.

TABLE 1: DAMAGE PRODUCED BY BLAST OVERPRESSURE

Pressure (psig)	Damage
0.02	Annoying noise (137 dB), if of low frequency
0.03	Occasional breakage of large glass windows already under strain.
0.04	Loud Noise (143 dB). Sonic boom glass failure.
0.1	Breakage of small windows under strain.
0.15	Typical pressure for glass failure.
0.3	Some damage to ceilings, limit of missiles.
0.4	Limited minor structural damage.
0.5-1.0	Large and small windows usually shattered, occasional damage to window frames.
0.75	Minor damage to house structures 20-50% tiles displaced.
0.9	Roof damage to oil storage tanks
1.0	Partial demolition of houses, made uninhabitable
1.0-2.0	Asbestos cladding shattered Fastenings of corrugated steel and aluminium panels fail and panels distort Tiled roof lifted and replaced
1.3	Steel frame of clad buildings slightly distorted
1.5	Slight damage to window frames and doors
2.0	Partial collapse of walls and roofs of houses Loadbearing brickwork unaffected 30% trees blown down
2.0-2.5	Some frame distortion of steel framed buildings
2.0-3.0	Concrete or cinder brick walls 8-12", not reinforced shattered
3.0	90% trees blown down Steel framed buildings distorted and pulled away from foundations. Frameless, self-framing, steel panel buildings demolished
3.0-4.0	Rupture of oil storage tanks
3.5	Oil storage tanks distorted
4.0	Cladding of light industrial buildings ruptured
4.0-5.0	Severe displacement of motor vehicles
4.5	Severe distortion to frames of steel girder framed buildings
5.0	Wooden utility poles snapped
7.0	Rail cars overturned
7.0-8.0	Brick panels (8-12"), not reinforced, fail by flexure
7-9	Collapse of steel girder framed buildings
7-10	Cars severely crushed
8-10	Brick walls completely demolished
9	Collapse of steel truss type bridges Loaded train wagons completely demolished
>10	Complete destruction of all unreinforced buildings
13	18" brick walls completely destroyed
70	Collapse of heavy masonry or concrete bridges
280	Lip of crater

TABLE 2: DAMAGE PRODUCED BY BLAST OVERPRESSURE.

Structural Element	Failure Mode	Approximate Peak Side on overpressure (psig) from different quantities of TNT		
		1 Te	10 Te	100Te
Window Panes	5% broken	0.15	0.10	0.10
	50% broken	0.36	0.24	0.21
	90% broken	0.90	0.60	0.54
Primary missiles	Limit of travel	0.20	0.14	0.12
Houses	Tiles displaced	0.64	0.42	0.38
	Doors / window frames blown in	1.30	0.86	0.77
see notes at end of Table	Category D damage	0.71	0.44	0.42
	Category Ca damage	1.8	1.15	1.10
	Category Cb damage	4.0	2.4	2.3
	Category B damage	11.5	5.2	5.0
	Category A damage	26.5	11.5	11.0
Rail wagons	Superficial damage	4.6	2.6	2.5
	Damaged but repairable	11.5	5.7	5.5
	Bodywork crushed	20	8.7	8.4
	Limit of derailment	26.5	1.5	11.0
Telegraph poles	Snapped	52	26	24
Large trees	Destroyed	57	26	24
Railway line	Limit of destruction	205	97	93

Note:

B Damage:

relates to a category of house damage caused by bomb damage in World War II viz, houses so badly damaged that they are beyond repair and must be demolished when opportunity arises. Property is included in this category if 50-75% of the external brickwork is destroyed, or in the case of less severe destruction the remaining walls have gaping cracks rendering them unsafe.

A Damage:

Houses completely demolished, i.e, with over 75% of the external brickwork demolished.

Ca Damage:

Houses that are rendered uninhabitable, but can be repaired reasonably quickly under war time conditions, the damage sustained not exceeding minor structural damage, and partitions and joinery wrenched from fixings.

Cb Damage:

Houses which are rendered uninhabitable by serious damage, and need repairs so extensive that they must be postponed until after the war. Examples of damage resulting in such conditions include partial or total collapse of roof structure, partial demolition of one or two external walls up to 25% of the whole, and severe damage to load bearing partitions necessitating demolition and replacement.

D Damage:

Houses requiring repairs to remedy serious inconveniences, but remaining inhabitable. Houses in this category may have sustained damage to ceilings and tilings, battens and roof coverings and minor fragmentation effects on walls and window glazing. Cases in which the only damage amounts to broken glass in less than 10% of the windows are not included.

TABLE 3:DAMAGE DISTANCE CONTOURS

1)	[2]	Damage/Other [3]	Distance (m)		O.P (psi) [6]
			Obs. [4]	Expect. [5]	
a.	Clean Area:	Area of yard near to explosion cleared of cars etc.	14	n.a	78
b.	Fireball:	Vehicles set on fire, and fireman was engulfed in flames.	18	17.5	44
c.	Frames:	Serious damage to concrete frames of building	110		1.7
		Steel frame moved.	120		1.5
d.	Walls:	Cavity brick/block walls of steel framed building belonging to Vibroplant and City Electrical Factors, totally destroyed.	30	< 35	14
		-next nearest facing wall damaged only along top edge where meets with steel roof beams.	70	n.a	3.2
		Metal cladding; fastenings fail, and followed by buckling.	115	68-113	1.6
e.	Roofs:	Metal roof cladding on steel frames removed.	30	n.a	14
		Asbestos cement type roof panels badly damaged /removed.	90	70-110	2.2
		GRP roof lights all destroyed.	140	n.a	1.25
f.	Windows:	Windows were broken as far out as the Flag Fen archeological site. The flimsy wooden structure there (at ca. 1260 m.) flexed considerably causing the distant damage.	1260	n.a	0.06
		90% window damage (small,single-glazed ca. and well retained units)	225	182	0.69
		50% window damage	ca.360	360	0.37
		5% window damage	ca.580	695	0.19
		Damage to window frames.	160	110-195	1.06
continued					

TABLE 3 continued: DAMAGE DISTANCE CONTOURS

1)	{2}	Damage/Other [3]	Distance [m]		O.P (psi) [6]
			Obs. [4]	Expect. [5]	
g.	Missiles:	<p>Fragments were thrown over a very large area - see Figure 7 appended.</p> <p>The prime requirement in this instance was to collect all pyrotechnic items from the surrounding area and dispose them. Recognisable pieces of the vehicle (except for the manysmall pieces of aluminium from the body of the vehicle) were also collected. The extremity of fragment throw has not been persued rigorously, but certainly within an HSE licensed fireworks site, some 380-400 m away were found a number of small items in the weight range 100 - 3,000 gramme. Also, further out still at approx 470 m a number of cars were allegedly damaged by falling gravel.</p>	400	-	0.32
			470	560	0.26

TABLE 4: INJURY CONTOURS

1)	{2}	Injuries. [3]	Distance [m]		O.P (psi) [6]
			Obs. [4]	Expect. [5]	
a.	Burns:	<p>Fireman 'engulfed in flames at.....</p> <p>Fireman slight burns at.....</p>	18 25	17.5 na	44 21
b.	Perforated eardrums:	<p>100% within a distance of.....</p> <p>50% at a distance of.....</p> <p>Furthest reported instance.....</p>	28 30 45	na 29 54	17 15 6.6
c.	Fragments:	<p>Serious injuries experienced up to this distance (excluding flying glass injuries).</p> <p>* - clearly there was potential for more injuries much further out-see Figure 7.</p>	40	*	
d.	Blown off feet:	<p>Persons outdoors blown over up to....</p> <p>50% " " " " " " ...</p>	70 55	93 45	3.2 4.7
e.	Cuts from glass.	<p>Cuts to all persons indoors.</p> <p>Cuts to many</p> <p>Cuts to few.....</p> <p>Furthest instance of cuts...</p>	0-50 70-100 100-150 ca. 200	n.a " " "	>5.5 3.2-1.9 1.9-1.15 0.80

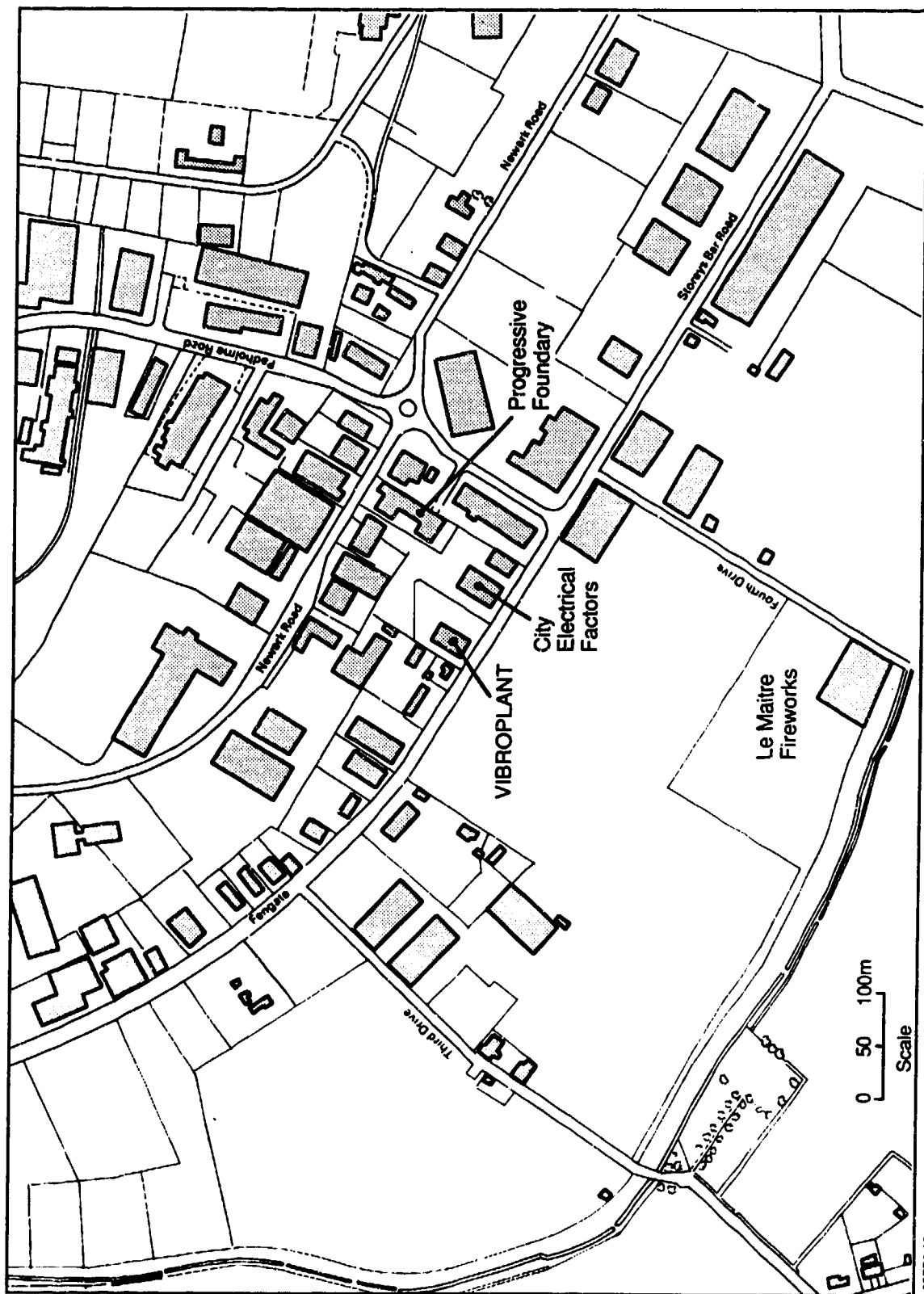


Fig 1 Plan of area around Vibroplant, Peterborough.



cms

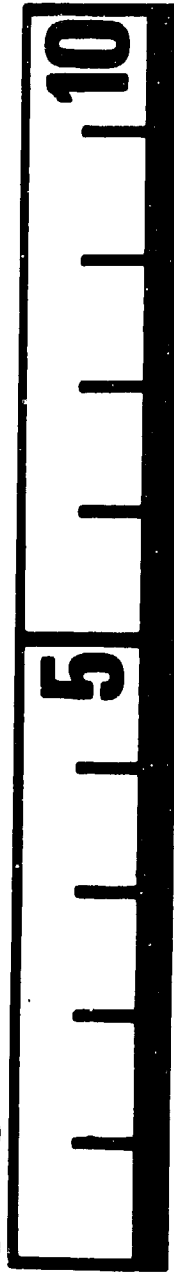


Fig 2 A - Cerium Fusehead Comb. B - Cut Fuseheads.



Fig 3 Scene of explosion - before

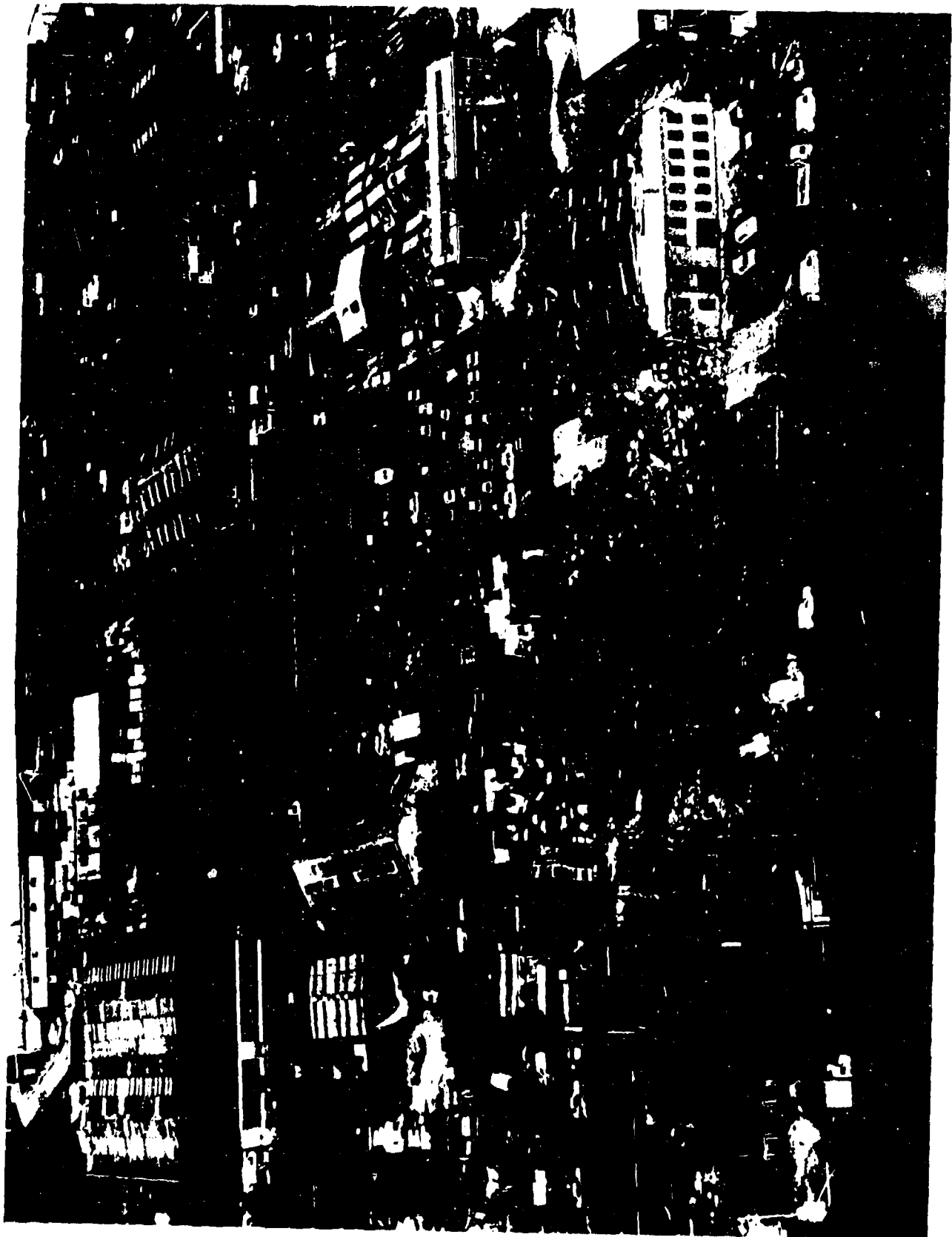


Fig 4 Scene of explosion - after



Fig 5 Damage to City Electrical Factors



Fig 6 Damage to Vibroplant Ltd.

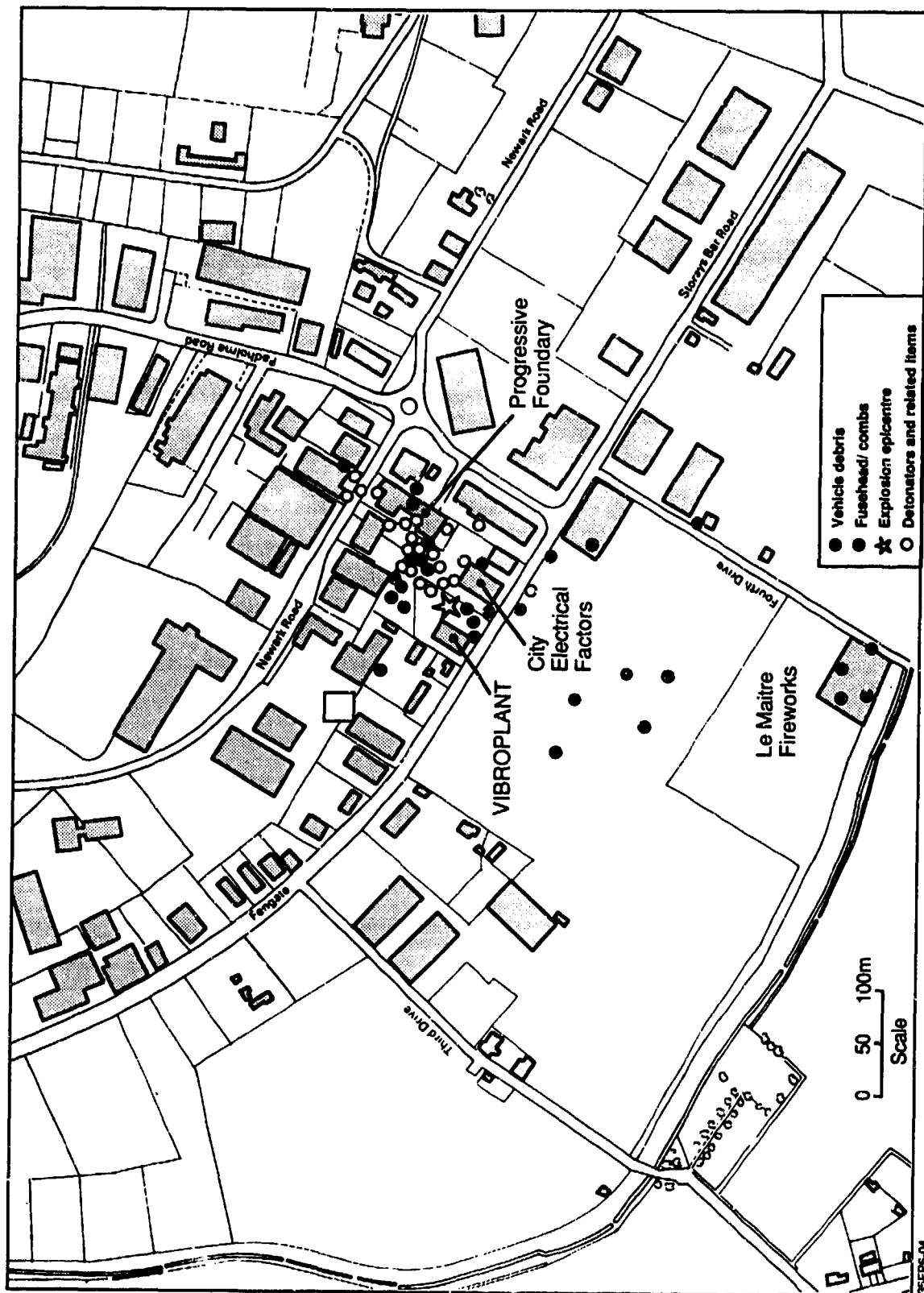
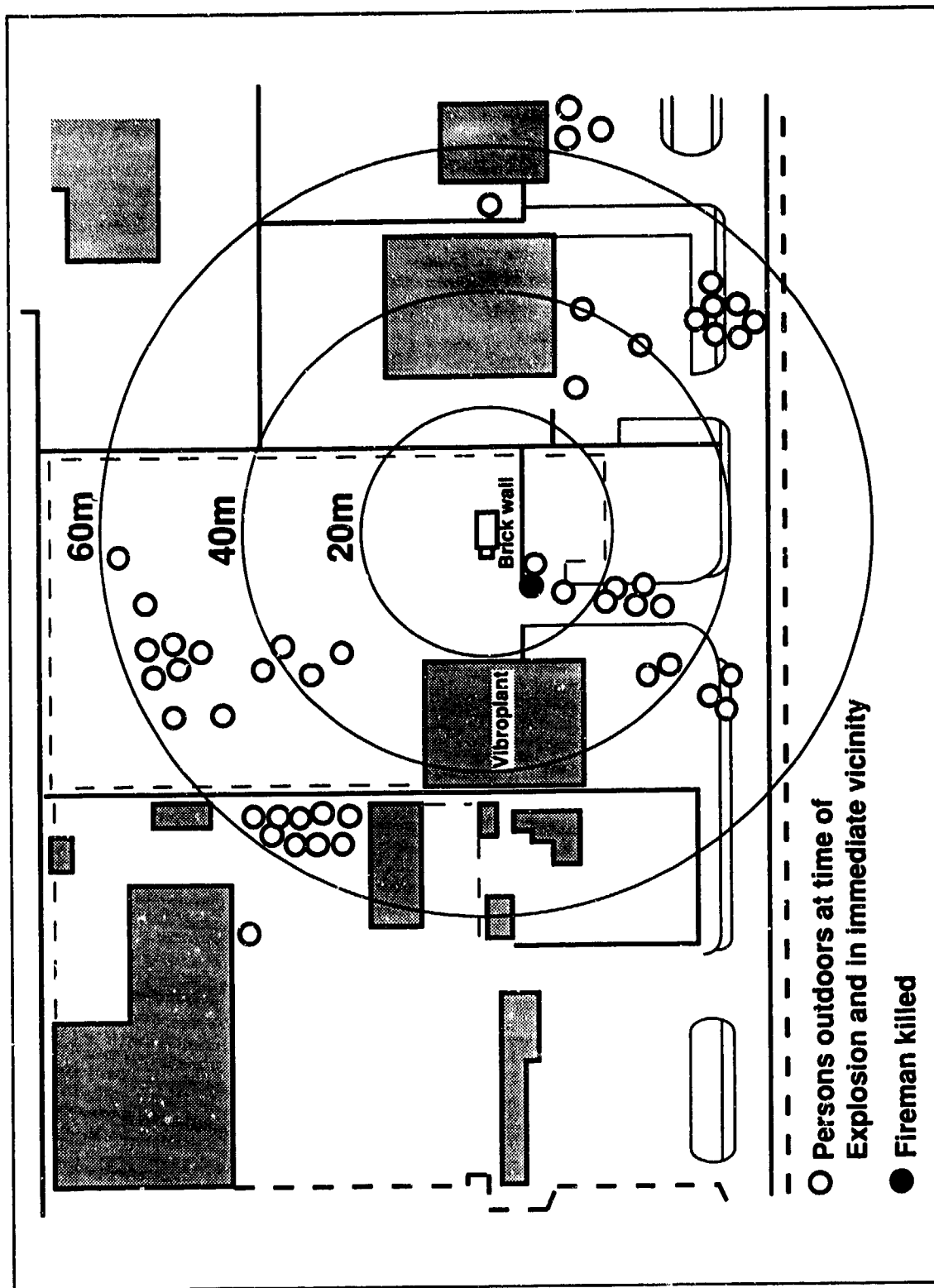


Fig 7 Explosion at premises of Vibroplant, Peterborough. Debris plan



35FR8-01

Fig 8

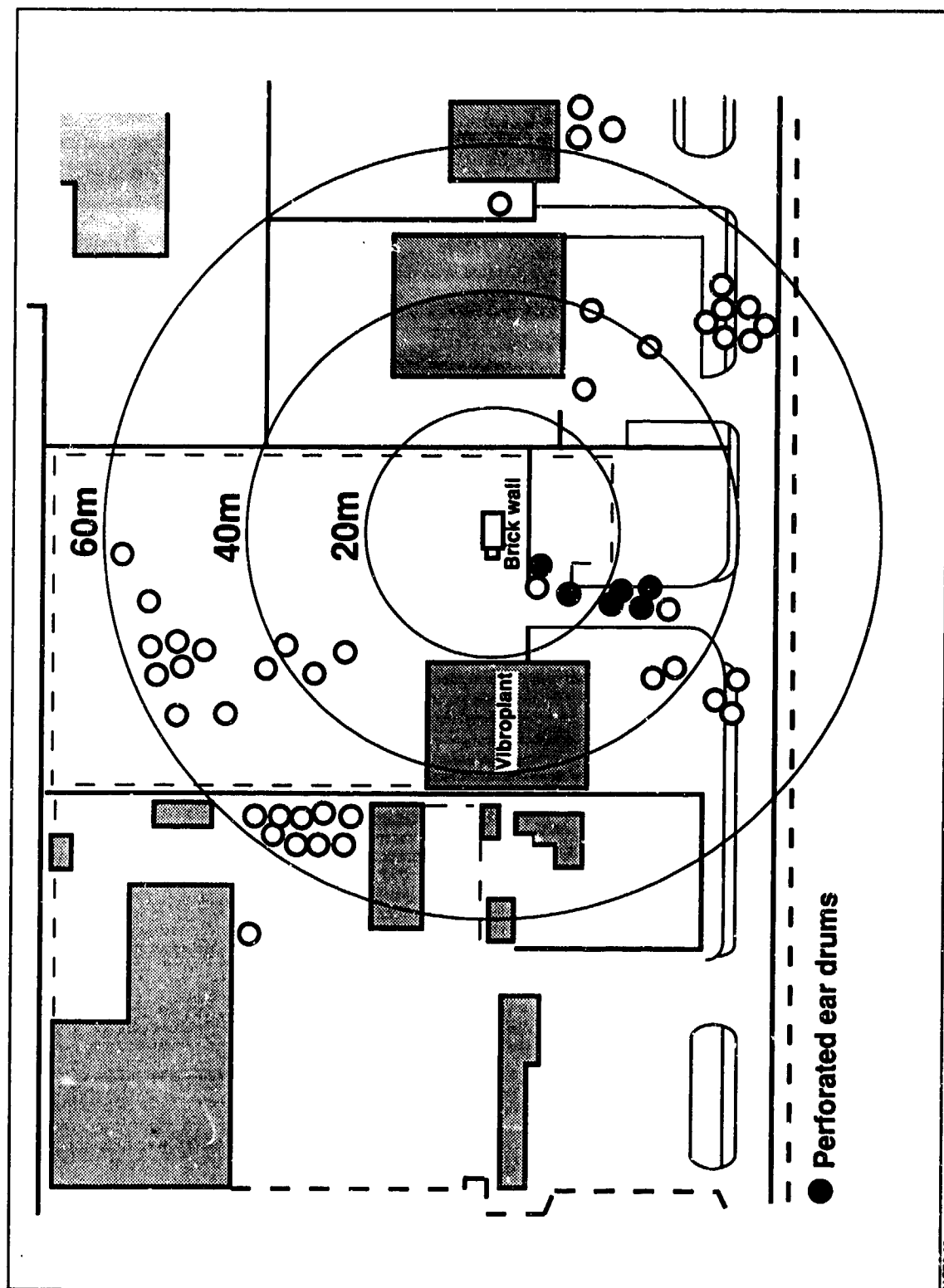


Fig 9 Injuries sustained to persons outdoors

33FP6-02

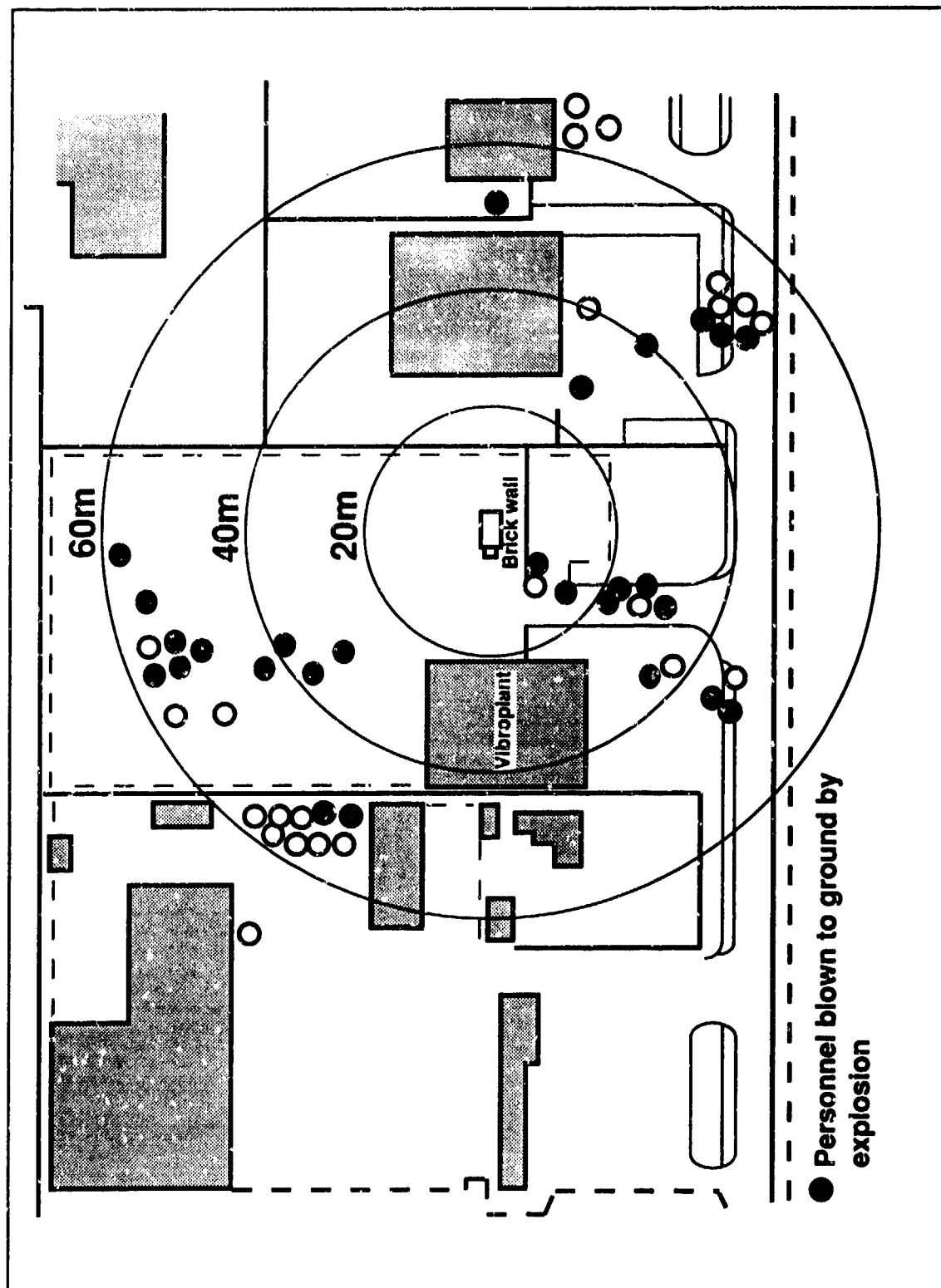


Fig 10 Blown to ground

357 P4-03

Site-300 Contained Firing Facility



Totally Contained High Explosive Test Facility Site 300

Lawrence Livermore National Laboratory

Presentation to

**24th DOD/ESB Meeting
Saint Louis, Missouri**

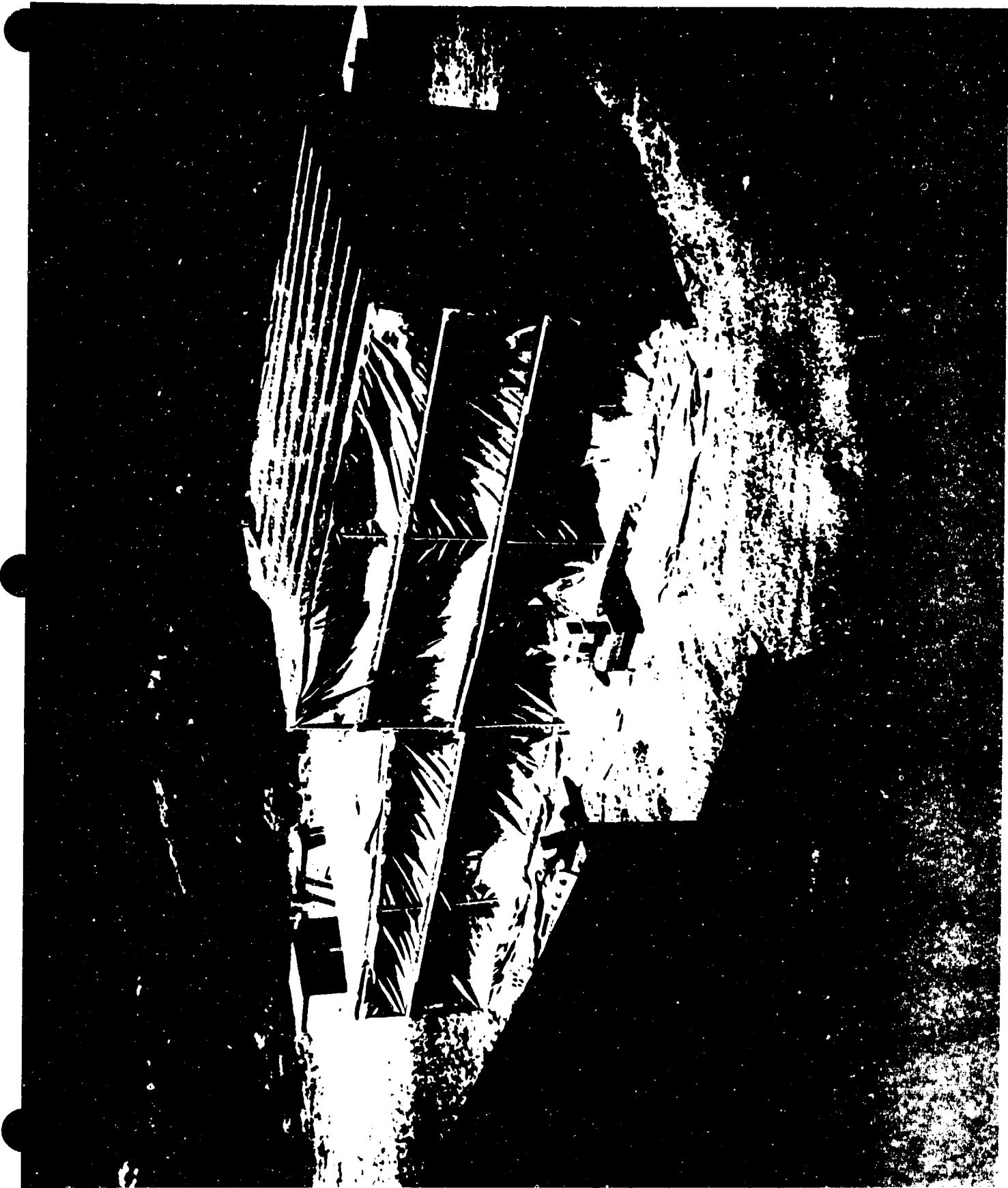


LLN 300





Site 300 Bunker 801

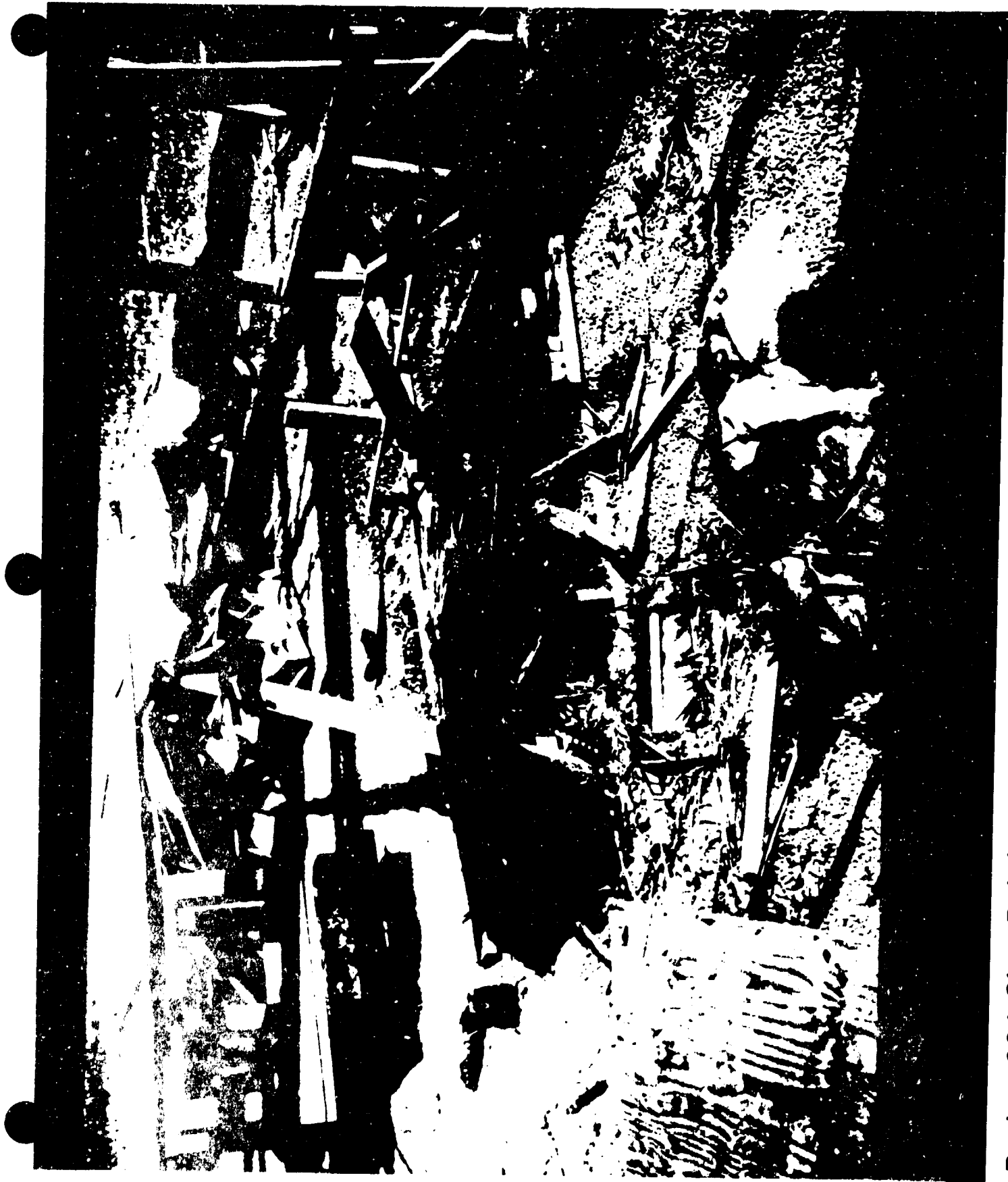


Bunker 801 Shot Tent



1602

Site 300 Typical HE Test



Bunker 801 Shot Debris

JUSTIFICATION: The rationale for this project includes four areas



- ENVIRONMENTAL CONSIDERATIONS
- OPERATIONAL ADVANTAGES
- FLEXIBILITY IN DIAGNOSTIC TECHNOLOGY
- PUBLIC PERCEPTION

JUSTIFICATION: Selection of Bunker 801



Bunker 801 contains a combination of diagnostic capabilities that exist nowhere else.

- Digital Electronic Pin Capability

Approximately 600 space-time resolution elements

- High Speed Optics
Streaking, framing cameras

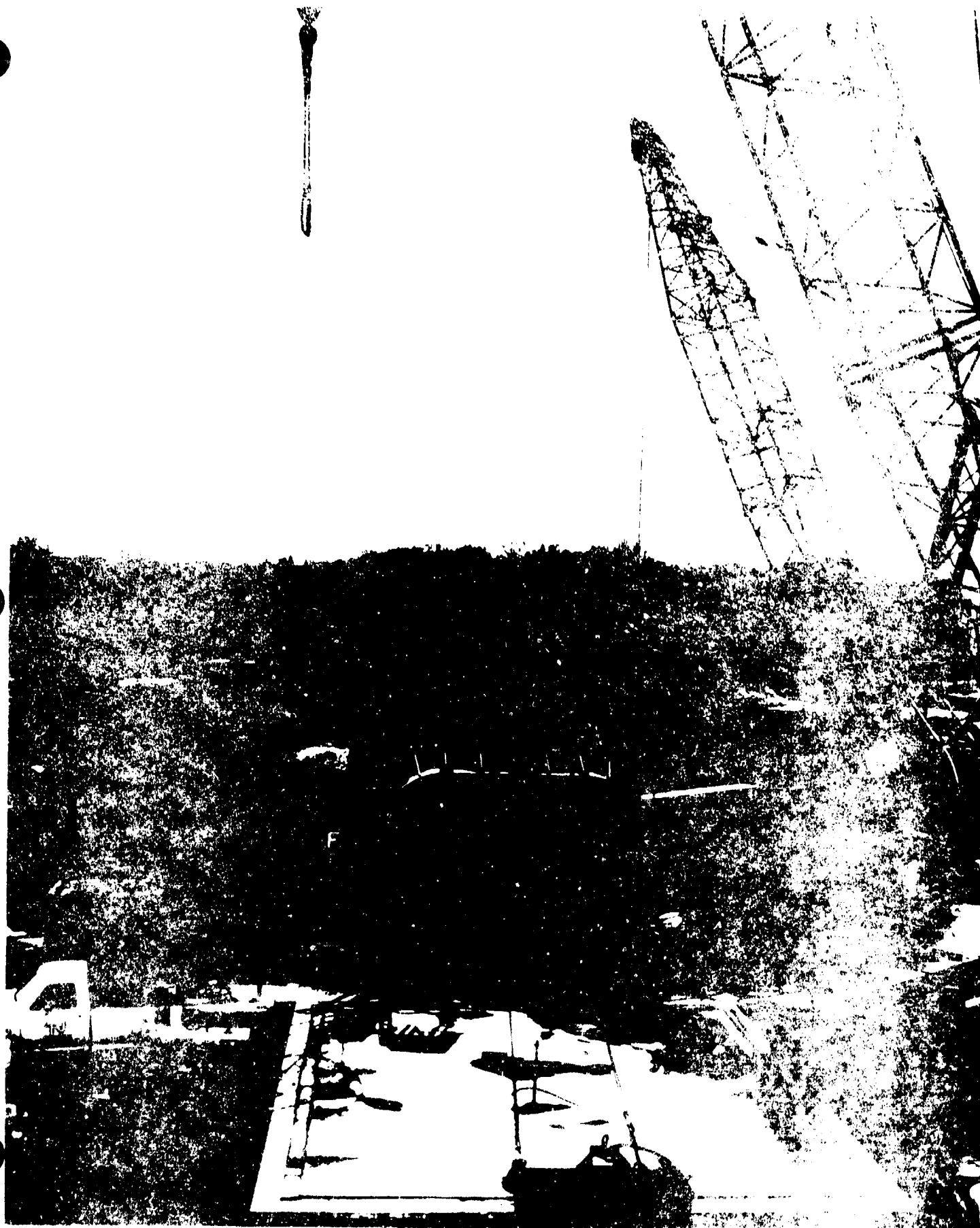
- Flash X-Ray

High resolution, high penetration capability

Our designers rely on this complete suite of data to achieve design objectives



Aberdeen Proving Ground Superbox Facility

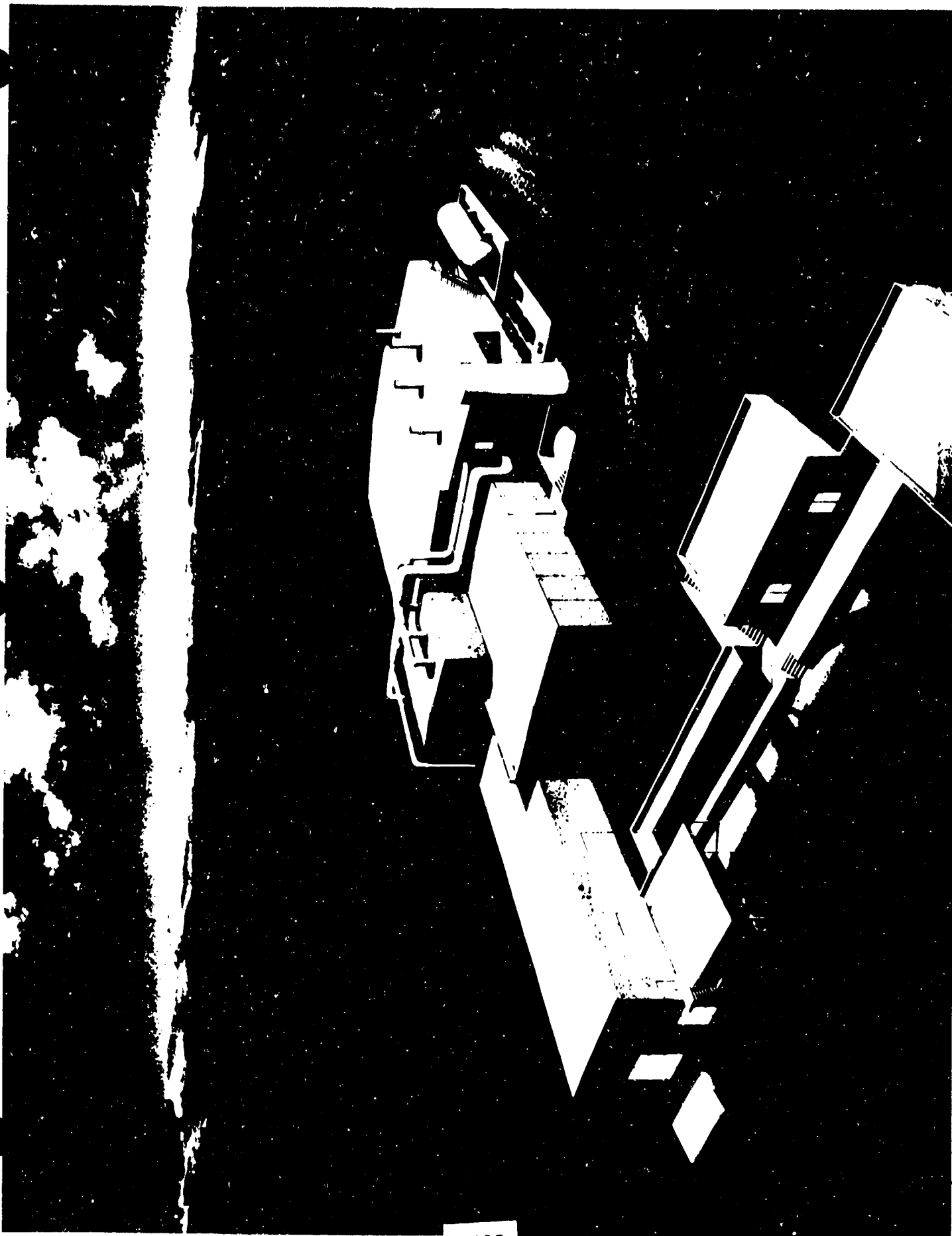


Proving Ground Superbox Facility

Proposed FY92 Contained Firing Facility – Bunker 801 Site 300

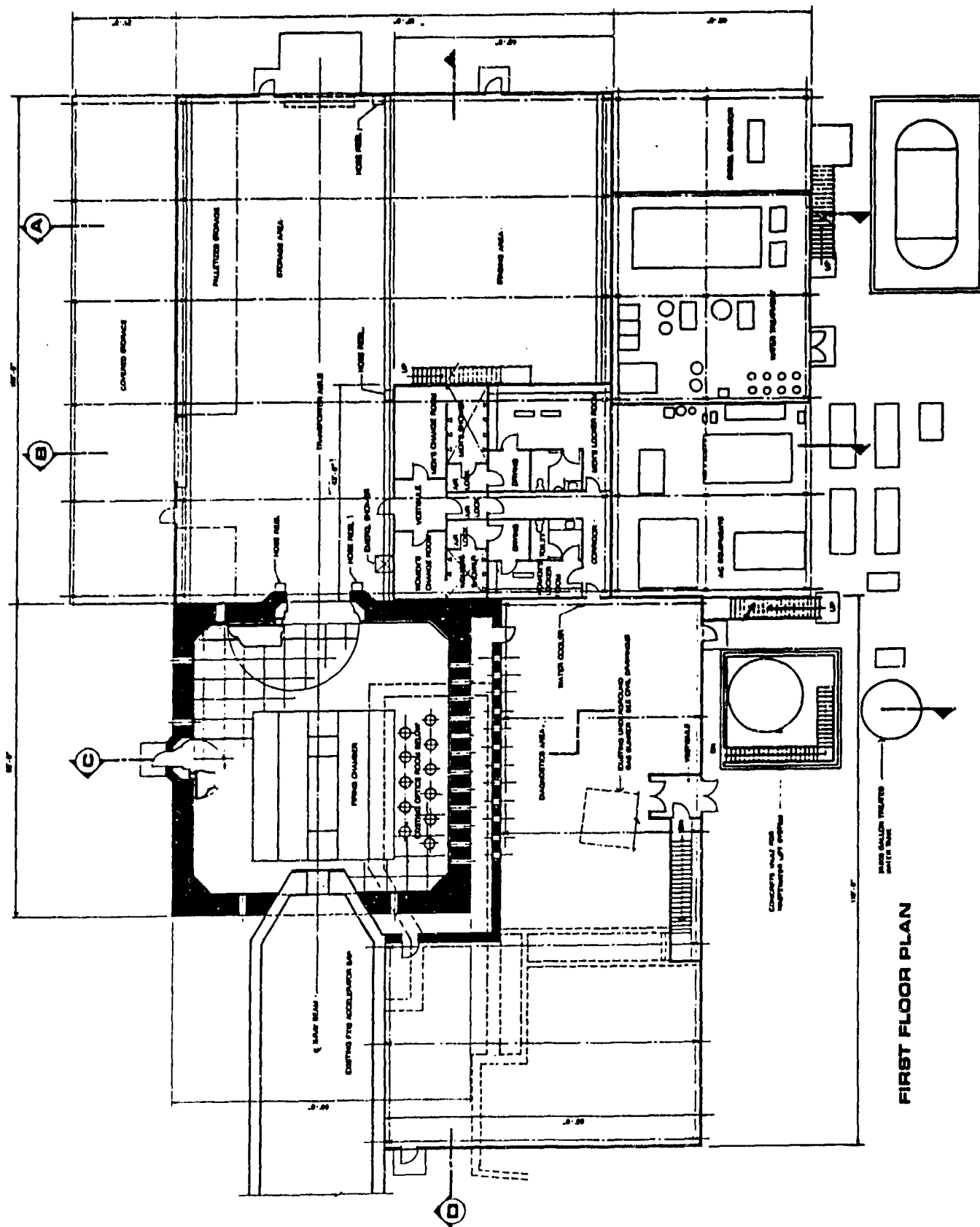


1608



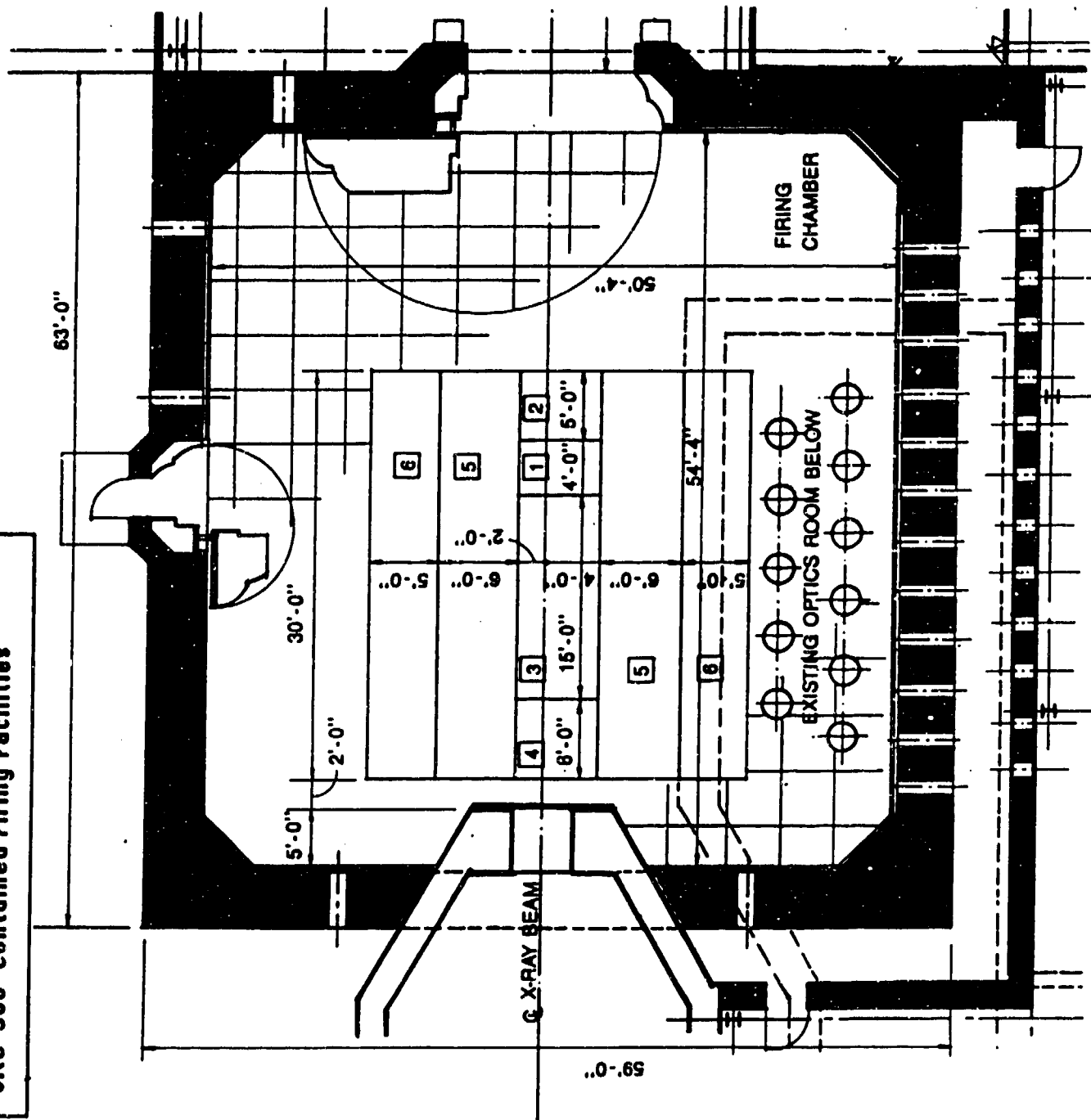
Site 300 Bunker 801 Proposed Contained Firing Facility

Site-300 Contained Firing Facilities



FIRST FLOOR PLAN

Site-300 Contained Firing Facilities



FIRING TABLE ZONES		
NO.	EXPLOSIVE WEIGHTS	
	Kg	EQUIV. TNT
1	60	206.3
2	45	154.7
3	40	137.5
4	35	120.3
5	15	51.6
6	5	17.2



Project Description:

The firing chamber is designed for 206 # TNT equivalent explosive

- **55' x 51' x 30' high (3,700 s.f. gross)**
- **5' floor, 4' walls, 4.5' roof (reinforced concrete)**
- **1" steel pressure liner on walls and roof - 2" on floor, 6" armor plate firing anvil**
- **4" mild steel plate for fragment protection, walls and roof**
- **12' x 14' equipment door: 3' x 8' personnel door**
- **Permanent lighting: ~ 10 foot candles**
- **TV cameras with blast protectors**
- **Utilities include: He, Ne, A, N₂, C.A., Vacuum, water and chilled water, power**

CF3d firing chamber 4/2/90

Project Description:

The chamber ventilation systems include a HVAC system as well as a firing chamber exhaust system

EXHAUST SYSTEM

1. 36 air changes per hour
2. Blast dampers rated for 100 PSI
3. Pre-Filters similar to HEAF
4. HEPA filters - 99.97% efficiency
5. Regenerative carbon system for noxious gases
6. Bag-out house for HEPA filter

HEATING AND AIR CONDITIONING SYSTEM

1. Maintain 78° F for cooling, 72° F for heating, 60% RH
2. 100% fresh air
3. 95% efficient industrial type final filters
4. Electrical resistance heaters
5. Electrical steam humidifier
6. Blast dampers - in chamber

CF3a/project description 4/2/90

Project Description:

The chamber washdown system has the dual function of environmental washdown system and fire suppression system

- Automatic & manual system controls
- Spray nozzle (Stang "Shadertip") at center of ceiling
1" round, 300 gpm, 42 ft. spray distance, 100 psig.
30 minute capacity in holding tank
- Wash water to be filtered and re-used
- Holding tank - 10,000 gallon
- Water filter (clarifier) system - 40 s.f. (26 gpm max.)
- Recovery tank (15,000 gallon)

CF3bWashdown 4/2/90



Project Description:

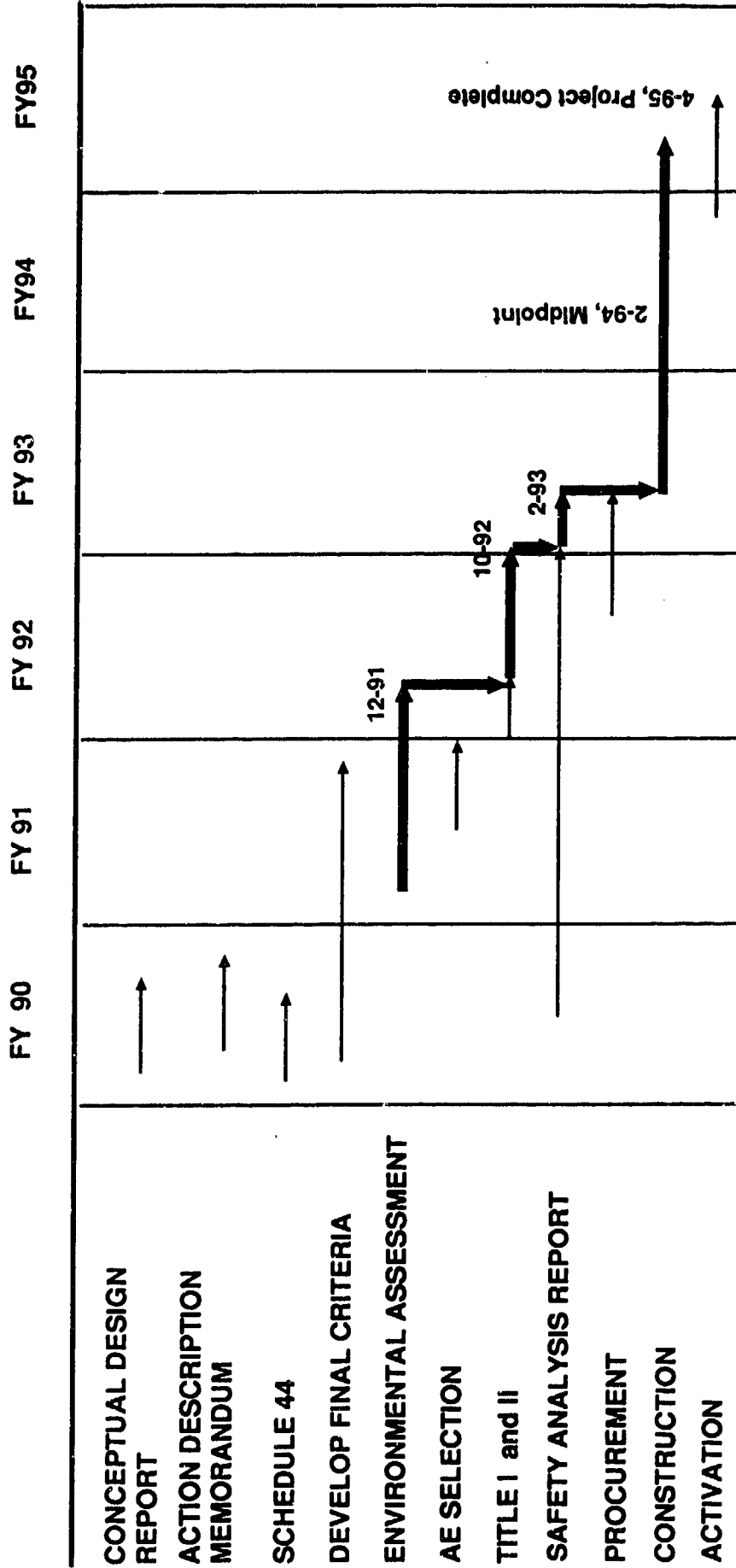
The support structures - including a staging area and a "clean" diagnostics area

- **STAGING AREA (grey area)**
16,600 s.f. total floor area including 6,000 s.f. of mezzanine
- **"CLEAN" DIAGNOSTICS EQUIPMENT AREA**
6,200 s.f. floor area
- **Rigid steel framing**
- **Tilt-up reinforced concrete walls**
- **Metal roof deck with concrete slab floors w/drains**
- **HVAC systems, fire sprinkler system, normal lighting**
- **Stairway from existing camera area to diagnostic area**
- **Manual wash down (grey area)**
- **2' Concrete personnel shielding wall (diagnostic area)**
- **Shower/toilet areas (men and women)**
- **Outside covered storage areas (approx. 4,500 s.f.)**

CF3c/support structures 4/290

Site-300 Contained Firing Facilities

PROJECT SCHEDULE:



CRITICAL PATH:

Site-300 Contained Firing Facilities

CONSTRUCTION COSTS MAJOR ELEMENTS

Improvement to Land (incl'd. soil disposal)		\$2,910
Utilities		430
Support Facility (16,600 SF)	\$ 210/ft. ²	3,490
Diagnostic Facility (6,200 SF)	\$ 209/ft. ²	1,300
Firing Chamber (3,700 SF)	\$4,437/ft. ²	<u>16,420</u>
including approximately:		\$24,550
Armor Plate	\$3,230	
Washdown System	4,400	
HEPA/Filter/Ventilation	2,700	
F/C Structure	4,050	

cf/Const. Cost/7/12/90

PROJECT COST ESTIMATE SUMMARY



	Estimated Cost (K\$)
Item	Total
a. Engineering, Design, & Inspection at Approx. 21.2%	
1) Title I & II	\$ 4,000
2) Title III:	1,000
3) Proj. Mgmt. (Title I & II)	200
	\$ 5,200
b. Construction Costs	
1) Improvements to Land	\$ 2,910
2) Buildings	21,210
3) Utilities	<u>430</u>
Subtotal	\$24,550
4) Activation	4,200
5) PM/CM (Title III)	<u>1,350</u>
Total Construction Costs	\$30,100
c. Standard Equipment	4,000
d. Removal Cost, Less Salvage	<u>0</u>
Subtotal	\$39,300
e. Contingency at Approx. 17.5%	<u>6,900</u>
TOTAL PROJECT COST	\$46,200

EQUIVALENCY CALCULATIONS



- 60 Kg. PBX 9404 Equates to 206 Lbs. TNT
- 1.3 (HE → TNT) DOE 6430.1A Pages 13-69
For Shock Pressure and Impulse
- 1.2 Safety Factor - TM 5-1300 - Page 11
Materials, Construction Methods,
Unknown Factors
- $(60) (2.2) (1.3) (1.2) = 206$

BLAST DESIGN BASIS



- 206 Lbs. TNT Equivalent - for Gas and Impulse
- Concrete Only Used in Calculation for Blast Resistance
- Yield Design - $F_y = 60,000 \text{ PSI}$
 $F_c' = 6,000 \text{ PSI (28 days)}$
- Floor Slab - 2/3 Load in Flexure and Shear Resisted By Slab, 1/3 by Earth
- Shrapnel - (2)2 " Mild Steel Tiles
- Steel Pressure Liner

CF/Blast Design Basis/5-22-90

BLAST DESIGN TECHNIQUE



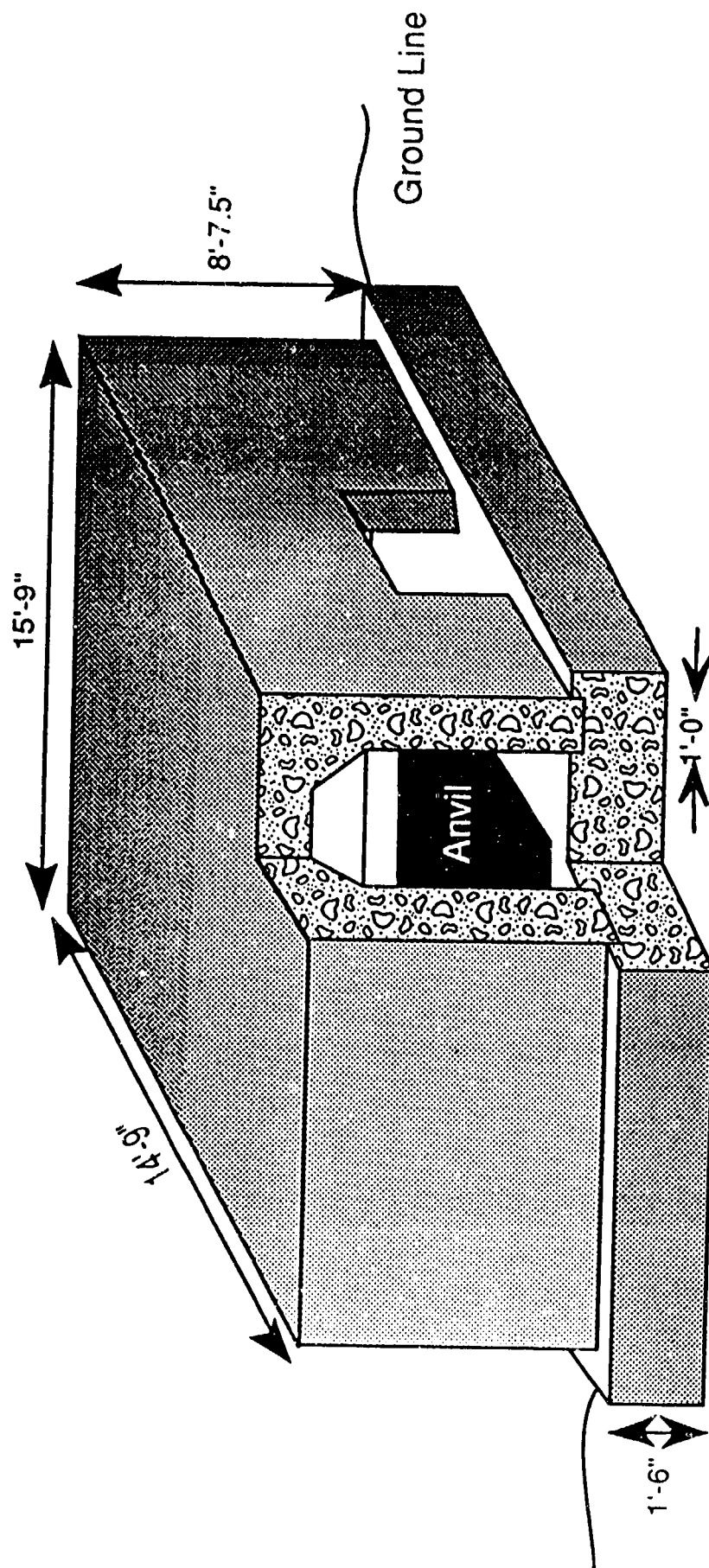
- TM5-1300, TM5-855-1 And NCEL Shock Program
- Ductility Factor $\mu = 1$ (Elastic)
- TNT Used for Gas Calculation
 - TNT Heat of Combustion = 3.62 K Cal/Gram
 - PBX 9404 Heat of Combustion = 2.28 K Cal/Gram
- Gas and Impulse Loading Effects Combined to Produce Equivalent Resistance Required
- Gas and Dynamic Effects Produce Fairly Equivalent Results

CONSERVATISM OF DESIGN



- 1.2 Materials Deficiencies, Construction Methods, Unknown Factors, Workmanship 20%
- 1.3 Worst Case Conversion of Energetic Explosives to TNT (PBX 9404 \approx 1.15) 15%
- Neglect 1.25 Increase for Concrete Compression 10%
1.10 Increase for Reinforcing Steel Doors
- Combination of Shock and Gas Effects - 100%
These are not Additive
- 1" and 2" Steel Pressure Liners not used in Calculation 20%
- TNT Used for Gas Calculation 30%
Compounds to 4.7

CF/Conservatism of Design/5-22-90



1/4" Replica Scale Model of Proposed Firing Chamber

Test and Evaluation of a 1-kg Storage Magazine

Summary

The High Explosives Applications Facility (HEAF) at Lawrence Livermore National Laboratory (LLNL) has an explosives magazine capable of storing a large number of 1-kg charges. In this paper we describe the testing and analysis carried out to ensure that this storage facility satisfies all requirements for safety and for nonpropagation of an explosion.

The design of the storage magazine was based primarily on the satisfactory results of a field test. The design embodies conservative estimates of reflected internal shock waves and empirical knowledge of similar designs. The field test was configured to represent adjacent sections of an actual magazine. The supporting analysis of the test configuration showed that high-gradient shock amplitudes delivered to the adjacent cubicle were negligible. Lower-gradient (long-wave) stress amplitudes were not analyzed at that time. The test observations showed very mild stresses in the target chamber. The test displaced the adjacent cubicle about 10 ft to the west, virtually undamaged. After the test the door and tray mechanism operated normally. The foam box containing the target charge exhibited a small amount of soot on the outside but very little deformation. The other adjacent cubicle, from which rotating-mirror cameras viewed the test through cutouts, also showed no significant distortion. It was displaced about 5 ft. The top plate of the explosion chamber showed significant distortion but no puncture, and remained attached at the end welds.

We have subsequently carried out a more detailed analysis to ensure that the installed magazine will perform as indicated by the test result. The additional analysis also examined the question of adjacent cubicles above and below the donor cubicle as well as to the side. In the course of this study we reviewed both the test and earlier analysis. We recomputed both shock and residual pressure with 1-D spherical calculations. We also analyzed the relief of pressure when the front door of a cubicle is expelled. Finally, we carried out a 3-D analysis of the installed magazine on the basis of the above results. To assess the margin of safety, we included in the 3-D analysis an increased charge weight of 1.25 kg of PBX-9404. The assumptions of the calculation, which applied the 1.25 factor to a cubicle adjacent to and above the explosion, are somewhat more severe than the test conditions. Nevertheless, the calculations show that an explosive charge encased in foam in an adjacent cubicle, whether above or alongside (as in our test), would be subjected to stresses far below ($\ll 1/10$) the levels that could detonate the acceptor charge.

As the pictures of our test indicate, the cubicle was moved only a few feet from its initial location, and the acceptor cubicle is nearly intact. The target explosive charge was merely displaced from its initial location in its foam container and showed no damage whatsoever.

We believe that our analysis, our test design, test results, and the final design of the storage magazine ensure conservative, safe, nonpropagating storage for 1-kg charges of PBX-9404, which represents the highest energy content of explosives currently in use.

A. Test Description

The test configuration comprised three magazine compartments arranged in a horizontal array. The assembly was held together by a system of brackets, bolts, and strips. Safe file drawers were installed in two of the compartments. Drawer latches engaged notches in the compartment steel plate.

[Section E of this report lists layout drawings (and numbers) for both the test configuration and the HEAF magazine. Section F contains several photos of the test assembly before and after the test and also photos of the HEAF magazine.]

The test configuration can be described in a right-handed XYZ coordinate system centered at the centroid of the middle test compartment (Fig. 1). The +Z vector is horizontal and passes through the

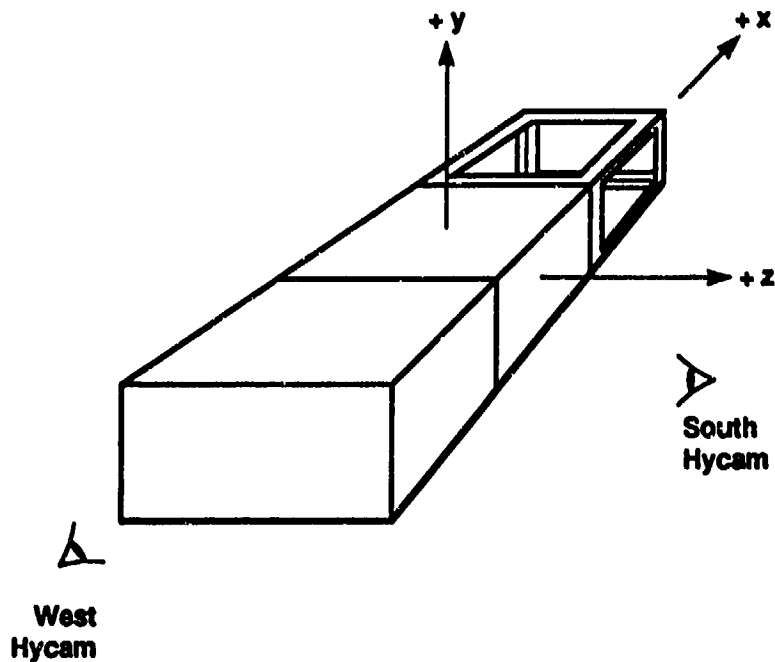


Fig. 1. Schematic illustration of test set-up showing XYZ coordinate system.

center of the light (about 10 lb) "door." The door was viewed by the "south" HYCAM high-speed framing camera. The +X vector is horizontal, running west to east through the sidewall centers. The +Y vector is vertical, passing through the topwall center. The "west" HYCAM looked at the west compartment mostly in the +X direction.

There were large cutouts in the east compartment topwall and sidewall, and the door was omitted, leaving the front (viewed by the south HYCAM) open. Mod-6 and #152 rotating-mirror cameras viewed the inner sidewall of the east compartment. Both the backwall and sidewall of the east compartment were painted white with red grids so that the rotating-mirror cameras could observe early-time sidewall motion. Xenon photo flood lamps (#623) provided the lighting. These lamps require 25 to 50 μ s to achieve full brightness. The lamps and the cameras were turned on shortly before detonation. The Mod 6 rotating-mirror camera, with enough film for 1.4 ms, was oriented perpendicular to the sidewall. The #152 rotating-mirror camera, with enough film for 1 ms, looked in at the edge at a slight grazing angle.

The cylindrical ($L/D = 2$) high-explosive charge, 1 kg of PBX-9404, was placed inside a foam box (0.2 g/cm^3) with its cylindrical axis paralleling the horizontal X coordinate. An 800-g PBX-9404 acceptor high-explosive charge was similarly oriented inside a foam box in the west compartment. The mass of the latter was 200 g less than that of the donor, a difference not considered significant.

The three adjacent compartments were mounted on a heavy pallet with a 2-by-6 floor. Three-in.-thick redwood provided shock isolation between the compartments. A preliminary DYNA2D cylindrical hydrodynamic calculation showed that only 1 in. of redwood was sufficient to unload the initial spike pulse across the 3/4-in. steel plate used in fabricating the compartment walls.

The walls of the test compartment were skip-welded on the inside with 1/4-in. fillets and were also continuous-welded to the flanges about the door opening. This arrangement differs from the HEAF magazine array, in which the individual compartments have both internal and external 1/4-in. fillet skip welds along all wall edges. The HEAF magazine welding is estimated to be equivalent to 22% of the wall thickness, while the test magazine welding was estimated to be about 10%.

B. Test Results

Results showed that the rotating-mirror camera records resolved no sidewall deformation. No grid distortion was observed. These results are consistent with the observed test results described below.

The south HYCAM (4130 frames/s) shows a luminous shock on the top wall at the start. Leakage about the middle compartment door is visible one frame after detonation. The smoke cloud reached the edge of the adjacent west compartment at 10 frames. This corresponds to a mean velocity of 847 fps. The door (directed at the camera) was visible through smoke after 41 frames. The door appeared to ride at the front of the smoke cloud at 50 frames. The blowdown study gave the door a terminal velocity of about 650 fps. The door struck earth in the vicinity of 70 frames, as evidenced by dust.

The west HYCAM (4370 frames/s) shows the entire center compartment rising (+Y) and rotating (XY, +Z). It can be seen through the smoke well enough after 76 frames to measure its motion. Measurements of its vertical motion at 76, 344, and 403 frames lead to an estimated vertical velocity of 15 fps. The velocity of the door could not be evaluated, since the smoke cloud expanded to the right and reached the boundary of the picture before the door became visible.

After the shot the top plate of the center compartment is clearly bowed; the internal fillet welding is broken. The internal fillet welding of the bottom plate is ruptured and has pivoted about its unbroken flange welding. We observed a large bulge in the middle of the bottom plate. The side plates show virtually no deformation. The west side compartment has been displaced about 10 ft to the west. It was virtually undamaged. The door and tray mechanism operated in normal fashion. The door cover had been blown off. The target charge inside showed no damage whatever: no scabs, cracks, or scratches. The foam-box container exhibited a small amount of soot on the outside but very little deformation. The east side compartment, which contained the cutouts for the rotating-mirror cameras, also showed no significant distortion. It appeared to be displaced about 5 ft.

C. Analysis

We have carried out more recent studies of the HEAF magazine array to estimate blowdown behavior, the effect of the foam charge container, and the levels of distortion and motion in the cavity walls, including the acceleration and velocity of the target charge. The blowdown study indicated that the magazine evacuation time is about 1 ms. A thermochemical code (TIGER) provided the initial equilibrium gas conditions. We ran 1-D spherical calculations using KOVEC to confirm the earlier DYNA2D pre-test calculation and to estimate the effect of the foam box inside the explosion chamber on the impulse delivered to the cavity walls. These KOVEC calculations showed that foam inside the explosion chamber increased the impulse by about 50%.

While the foam box increases the impulse in the explosion chamber, it contains and protects the high-explosive charges in adjacent chambers. Since neither the test results nor our calculation results indicate any possibility of a reaction propagating through the magazine, we did not perform an optimization study of the foam box.

We used this information in the DYNA3D finite-element model that we created to evaluate the response of the high-explosive magazine to charge detonation. For the 3-D analysis, we used the procedure developed by W. E. Baker¹ to create an array of reflection impulse pressure vs time signatures acting on the inside surfaces of the rectangular cavity filled with air.

To assess the effect of increased explosive loading in the safety margin, we performed blowdown and KOVEC calculations for both 1.00-kg and 1.25-kg charges of PBX-9404. DYNA3D calculations were performed for charge weights of 1.00 kg and 1.28 kg. To produce pressure impulses increased by 25%, the DYNA3D results show that the charge weight would have to be increased by 28%. For a charge weight of 1.00 kg, the DYNA3D study produced a deformation of the top plate similar to that observed in the test. (Details of the 1-kg analysis are in Section C.3.) The same analysis for a charge weight of 1.28 kg produced a peak acceleration on the top target charge of 11150 g's, leading to a maximum long-wave pressure loading on the charge of 2450 psi (0.166 kb). The peak acceleration on the side charge was much smaller at 4600 g's.

In the test the target charge was in a compartment alongside the explosion; in the DYNA3D model it was on top. Since the top impulse is roughly double the side impulse, the DYNA3D calculation modeled the most severe case to be encountered in the HEAF magazine.

Comparable tests in which PBX-9404 was detonated require pressures five times larger and pulse durations that are two to three times longer (see HAZARD ESTIMATE, Section C.3).

C.1 Blowdown Study

We judged that a proper analysis of the test and the installed magazine should include consideration of the pressure relief afforded by the ejection of the light-weight, lightly constrained, front "door" of the cubicle.

Blowdown pressure vs time is required input to the DYNA3D analysis (described in Section C.3). Our blowdown calculations were for an explosion chamber filled with ambient air and without a foam box, as assumed by the DYNA3D model. In Section C.3 we add the impulse enhancement produced by the foam box (described in Section C.2), by multiplying all DYNA3D model pressure input vectors by 1.5.

We modeled a single magazine compartment; a charge of PBX-9404 was "volume-burned" within, and the products were assumed to reach equilibrium conditions with the enclosed ambient air. We used the thermochemical code TIGER to calculate the initial conditions of the hot gas. For a 1.00-kg charge the results were 156 atm and 3819 K. For a 1.25-kg charge, the results were 193 atm and 3848 K.

The rectangular compartment is confined by four heavy sidewalls (431 lb total), a heavy backwall (50 lb), and one light grout door (10 lb). A compartment surrounded by adjacent cubicles is assumed to have a much increased side-wall effective mass of 2394 lb, a value that includes the mass of the adjacent compartments. The walls and the door are not connected along the edges and are free to move in response to cavity pressure. After the door has opened 1/2 in., hot gas is allowed to flow out of the system through the opening rectangular annulus. The initial cavity volume equals the compartment volume. The equilibrium cavity volume increases as the walls and door move. Gas flow is not permitted through the edge spaces that open when the compartment side walls move out. The enclosed gaseous internal energy, pressure, and temperature are reduced by the outflow of mass and enthalpy and by the work of moving the walls and door. Blowdown time is defined as that required for the cavity pressure to decline to 2 atm. Figure 2 is a sketch of the blowdown model.

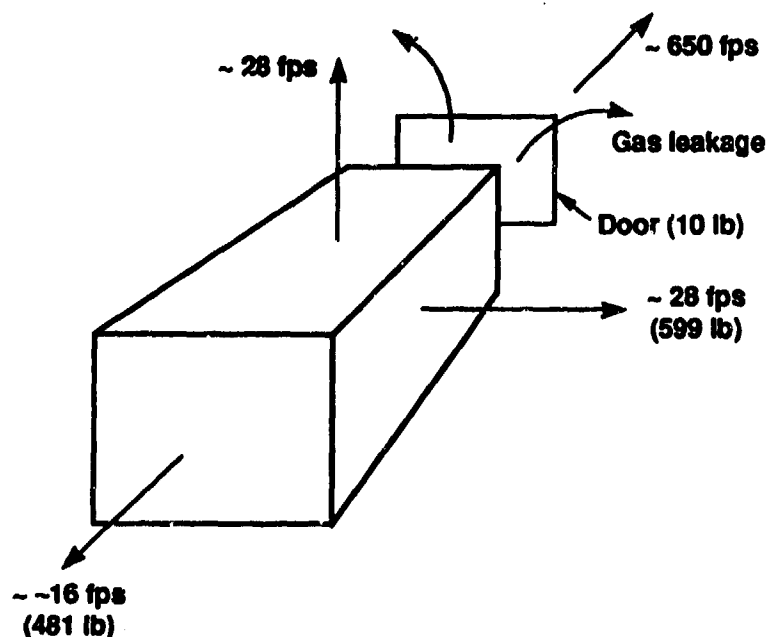


Fig. 2. Schematic of blowdown model.

We first performed a parametric study with a 1.00-kg charge of PBX-9404 in which we varied effective sidewall mass and flow coefficient to evaluate the effect upon blowdown time, door velocity, and sidewall velocity. Then we performed a comparative calculation with a 1.25-kg charge, a flow coefficient of 0.5, and a sidewall mass of 2394 lb. Figure 3 plots cubicle pressure vs time for both a 1.0-kg charge and a 1.25-kg charge. The corresponding terminal door velocities were 649 fps and 789 fps. The terminal sidewall velocities were 28 fps and 33 fps. The blowdown time remained approximately the same at about 1 ms. In the preliminary parametric study, the blowdown time increased to about 2 ms when the flow coefficient was reduced by a factor of eight, from 0.5 to 0.0625. This range of blowdown time is shorter than that computed with the chamber venting formula of Baker¹ et al. at a mean time flow area. These formulae were fitted to data for fixed-volume chambers with negligible wall kinetic energy.

When the door opens, its driving pressure changes from cavity pressure to "drag" pressure. Drag pressure is estimated from cavity gas density, outflow velocity, and a drag coefficient of 1.0, acting on the cross-sectional area of the door. Ambient air drag is allowed to oppose door motion. A function, F , generates a value that varies from 1.0 to 0 to accomplish the change in door driving pressure. The value is 0.5 when the open perimeter area between the door and the magazine equals the cross-sectional area of the door. In general the effective door driving pressure = (cavity pressure $\times F$) + [drag pressure $\times (1 - F)$].

We wrote a PC BASIC program to make the blowdown estimates and calculated three motions: the door, the sidewalls, and a reaction mass with a weight equalling the four sidewalls plus the backwall. Gas parameters and the outflow rate were calculated. The input was transformed into English units to make ready use of the gas-flow information in *Mark's Mechanical Engineer's Handbook*.⁵ The calculations and the code output are in English units.

C.2 Detonation Calculations

Calculations using the LLNL's KOVEC 1-D hydrodynamic code showed that initial shock pressure transmitted into the acceptor cubicle is attenuated to an insignificant level. This confirms the pre-test

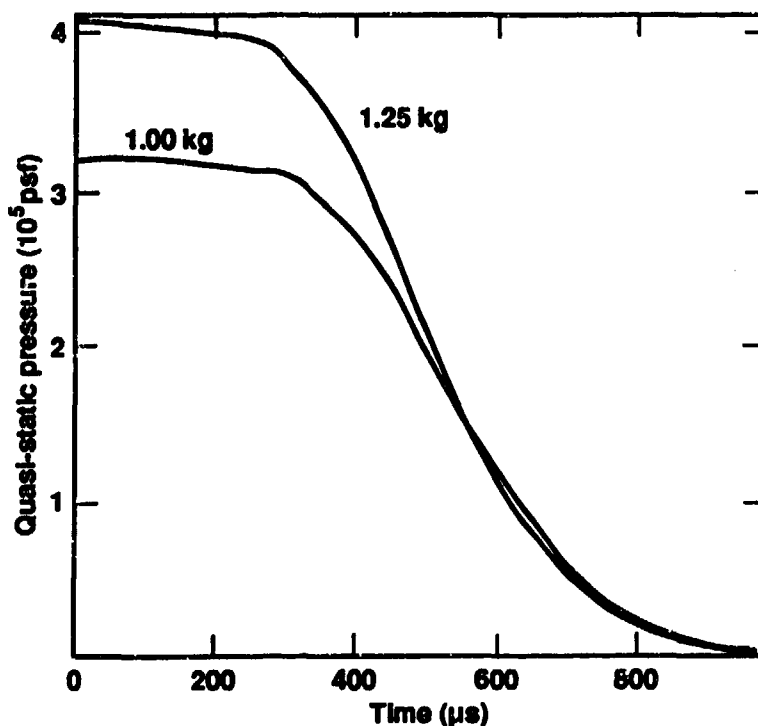


Fig. 3. Blowdown pressure vs time for 1.00-kg and 1.25-kg charges of PBX-9404.

analysis, which also indicated negligible sharp shock amplitudes. Figure 4 illustrates the comparative pressure levels in the redwood buffer, the steel wall of the acceptor cubicle (outer steel shell), and the foam in the acceptor cubicle. The redwood buffer pressure is ~ 0.2 kb, the steel-wall pressure is less than 0.05 kb, and the pressure in the acceptor-cubicle foam is less than 0.005 kb (73 psi).

We originally intended to detonate the high-explosive charge within the DYNA3D model of the cubicle. This proved to be impractical for two reasons. First, zone entanglement occurred early, and frequent rezoning was necessary to continue. Second, the relatively coarse zone dimensions required to keep the cost and time tractable were insufficient to obtain good resolution of the transmitted pressure in the structural plate and the reflected pressures in the foam and air so as to make a valid evaluation of the influence of the foam within the explosion chamber. We therefore simulated detonation with 1-D KOVEC Lagrange hydrodynamic models for spherical cavities containing air only and air plus foam.

Figure 5 shows the dimensions of the spherical models. The radius of the inside steel plate encloses the volume of the rectangular cavity. When foam is to be included, the outer radius of the foam ring encloses the volume bounded by the external surface of the foam box. The inner radius of the foam ring encloses the volume of the cavity inside the foam box. Of course the charge radius encloses the charge volume. Both the inside and outside steel plates are $3/4$ in. thick. They are separated by 3 in. of redwood. Zone resolution for the charge is 17/cm; for air, 9/cm; for foam, 7/cm; for steel, 25/cm; and for redwood, 10/cm.

We used the JWL equation of state (EOS) for the detonating PBX-9404 high explosive and the constitutive properties of 304 stainless steel in the steel plate. Actually, the magazine is fabricated of A36 mild steel. The density, yield strength, and shear-modulus values for both materials are similar, as shown in Table 1. The purpose of the KOVEC calculations was not compromised by using these parameters for 304 stainless steel.

Air was represented with a gamma-law EOS with gamma equal to 1.4 and the ambient initial energy. A Gruneisen EOS for polyurethane foam with a density of 0.32 g/cm^3 was used to represent the isotropic pressure component of loading for both the polystyrene foam with a density of 0.2 g/cm^3 and the

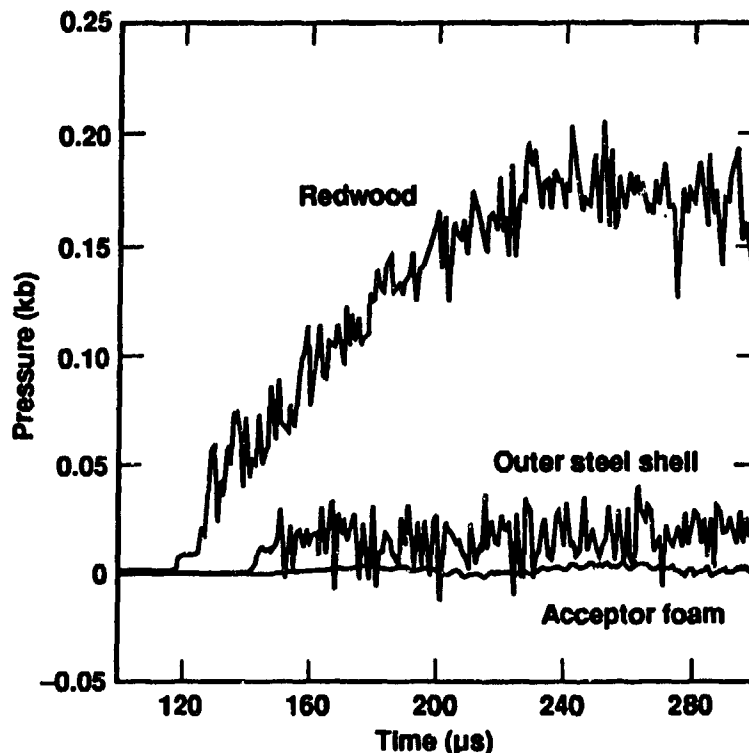
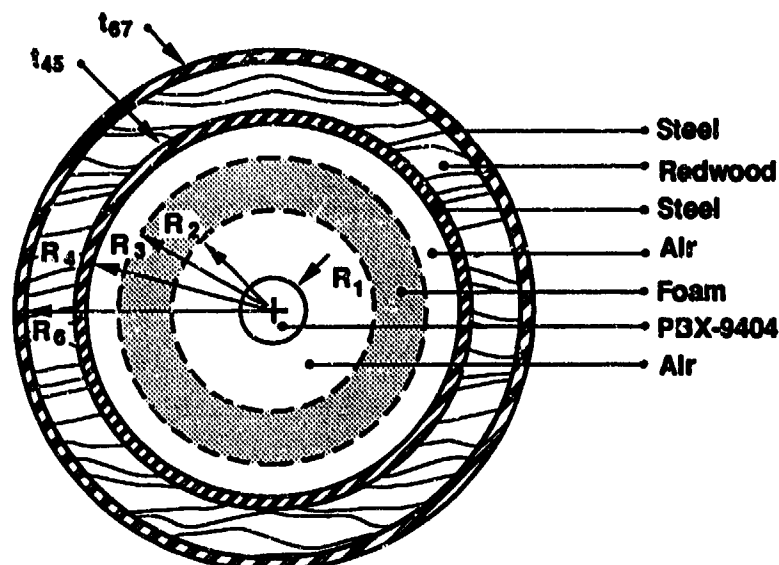


Fig. 4. Radial pressure in redwood, outer shell, and acceptor foam, 1.25-kg charge of PBX-9404.



$R_1 = 5.062$ (1.00 kg), 5.453 (1.25 kg)
 $R_2 = 15.162$
 $R_3 = 23.477$ $t_{45} = 1.905$
 $R_4 = 28.059$ $t_{67} = 1.905$
 $R_6 = 37.584$

All dimensions are in centimeters

Fig. 5. Schematic of the 1-D KOVEC models.

Table 1. Properties of magazine materials.

Material	Density (pcf)	Yield strength (psi)	Shear modulus (psi)
Foam	12.47	191.0	1.91E+05
Redwood	28.00	860.0	4.47E+05
304 SS	492.70	49314.0	1.17E+07
A36	488.30	43512.0	1.16E+07

redwood with a density of 0.449 g/cm^3 . This assumption means that these materials will exhibit the same shock Hugoniot behavior. The computed isotropic pressure will then vary directly with the density. To represent the shock heating, we selected a Gruneisen parameter of 1.1. We also assigned elastic-plastic constitutive properties to all structural materials. The KOVEC code operates in the Mb-cm- μs unit system. Table 1 lists the density and constitutive properties in the English unit system.

C.2.1 Structural Response

Figures 6 through 10 all illustrate radial air pressure vs time acting on the inside surface of the inner steel shell. Figure 6 is for the detonation of a 1-kg PBX-9404 charge when there is no foam inside the explosion cubicle. It shows comparisons with the theoretical rigid-wall reflected impulse and with the TIGER code equilibrium volume burn pressure used as the initial value for the 1-kg-charge blowdown calculation. Figure 7 compares responses to the detonations of 1.25-kg and 1.00-kg charges when there is no foam present. Figures 8 and 9 show the same information for two time scales when foam is present. In Fig. 9 the truncated peak for the response to the 1.00-kg charge reflects the 1.0- μs choice of output time

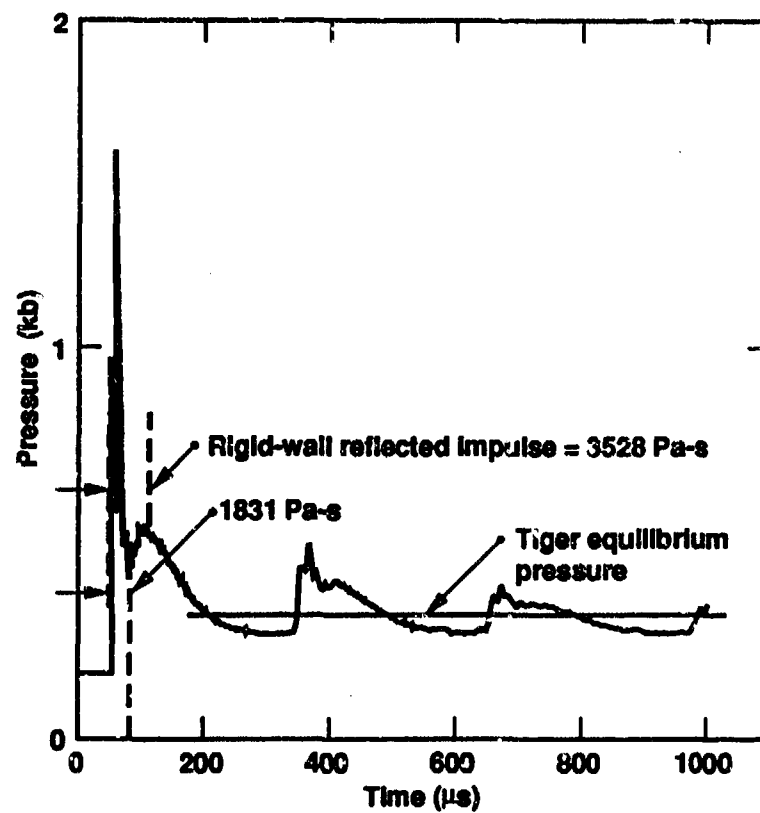


Fig. 6. Pressure due to the detonation of a 1.00-kg charge inside a yielding cubicle compared with that in a rigid-wall cubicle, both air-filled.

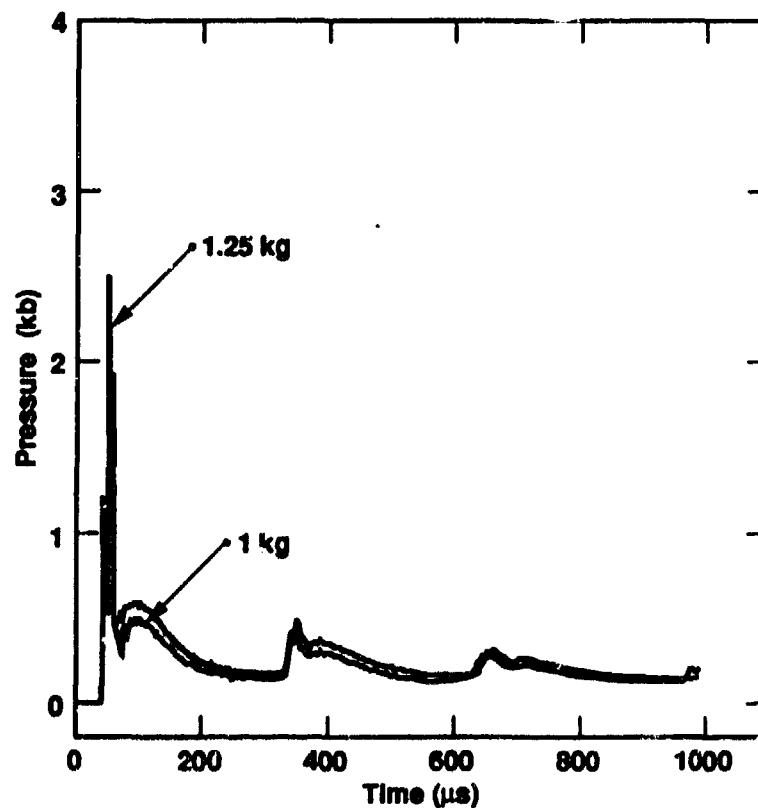


Fig. 7. Pressure due to the detonation of 1.00-kg and 1.25-kg charges inside an air-filled cubicle.

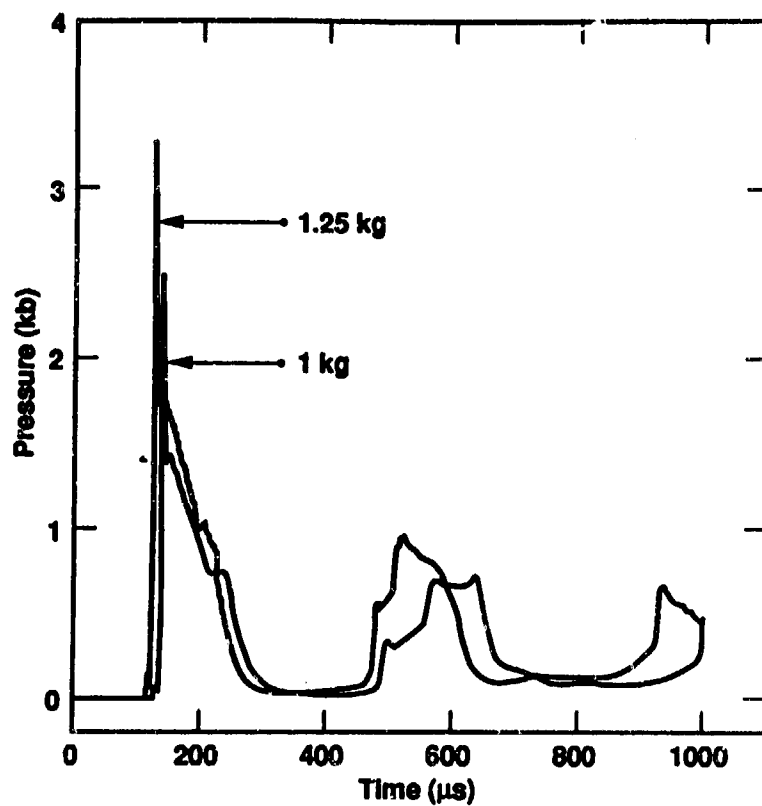


Fig. 8. Pressure due to the detonation of 1.00-kg and 1.25-kg charges inside a cubicle with foam.

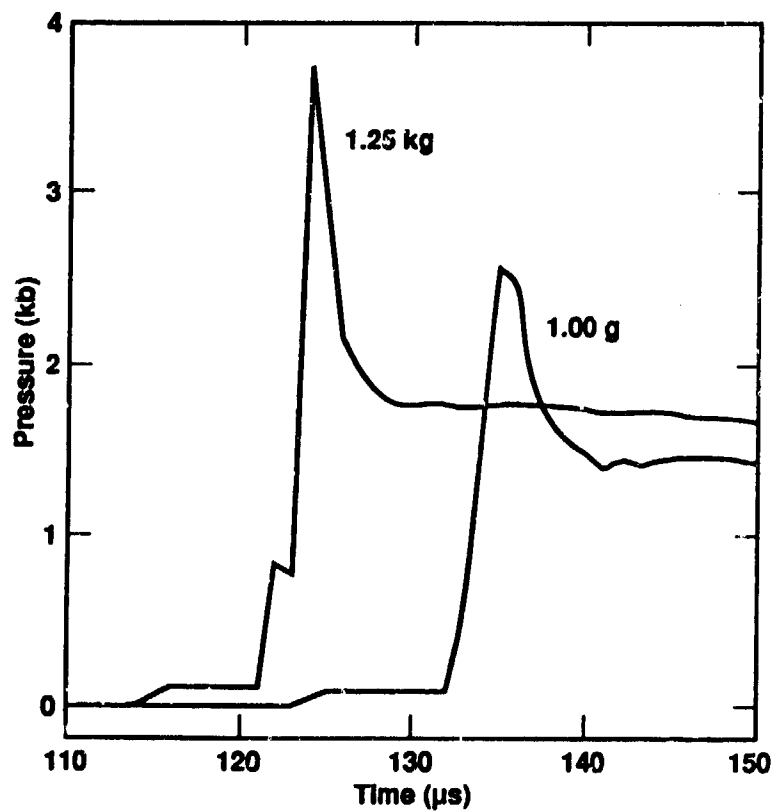


Fig. 9. Pressure due to the detonation of 1.00-kg and 1.25-kg charges inside a cubicle with foam.

increment. The calculation time increment is much shorter, on the order of $0.001 \mu\text{s}$. Figure 10 compares the response inside a foam-filled cubicle with that inside an air-filled cubicle.

Figures 11 and 12 give the radial pressure and hoop tensile stress vs time in the first calculation zone of the inner steel shell, which is adjacent to the air-pressure responses just discussed, with foam and a 1.25-kg charge. The response in Fig. 11 following the initial pulse shows wave reflections inside the steel shell. The initial negative hoop tension in Fig. 12 reflects the pressurization of the steel shell before significant radial displacement has taken place. The radial pressure in Fig. 12 can be compared with the air-pressure response for the 1.25-kg charge in Fig. 9; it is virtually identical until after $130 \mu\text{s}$, when the steel-shell wave reflections appear.

The regions with no hoop tension between the reflective pulses result from preventing the structural shells from sustaining hydrostatic tension. This assumption allows the spherical structural system to displace radially as an approximation to the kinematic response of the "real-world" rectangular box. While precluding hydrostatic tension is not a true fracture criterion, in this instance it performs a service somewhat similar to that in the calculation.

Figures 13 and 14 show middle-zone velocities and displacements vs time following the detonation of 1.25-kg and 1.00-kg charges inside an air-filled cubicle with no foam. Figures 15 and 16 show the same information for a cubicle with foam. From these figures, as well as from the pressure-time signatures just discussed, it is clear that the foam inside the explosion cubicle increases the impulse that is applied to the structural elements of the cubicle.

C.2.2 Effect of Foam on Impulse Results

We estimated the impulse "enhancement" due to the foam from the displacements plotted in Figs. 14 and 16, the inner-shell velocity peaks plotted in Figs. 13 and 15, and the final outer-shell velocities plotted in Figs. 13 and 15. The enhancement values (described below in more detail) ranged between 30 and

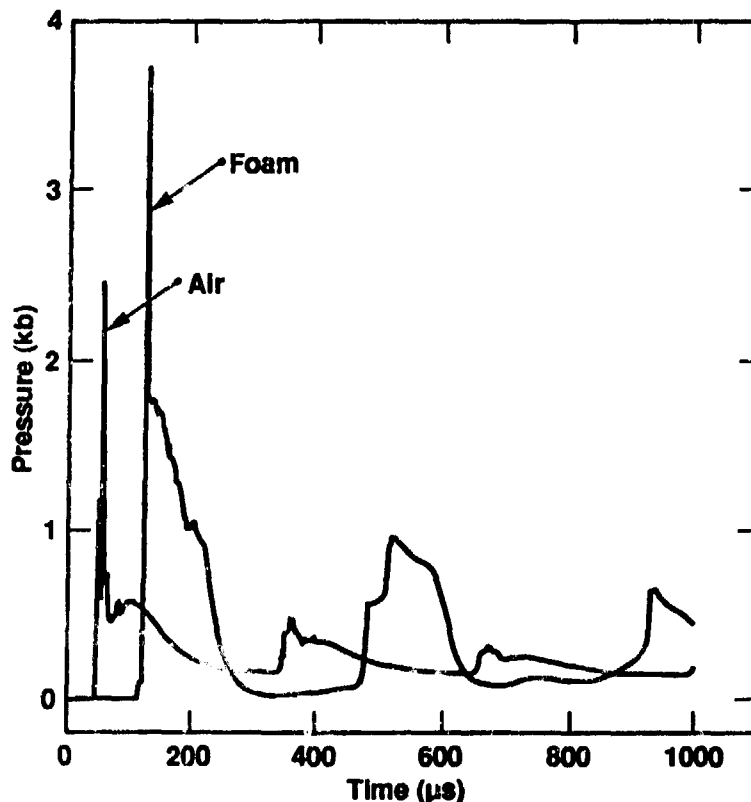


Fig. 10. Pressure due to the detonation of a 1.25-kg charge inside cubicles with foam and with air only.

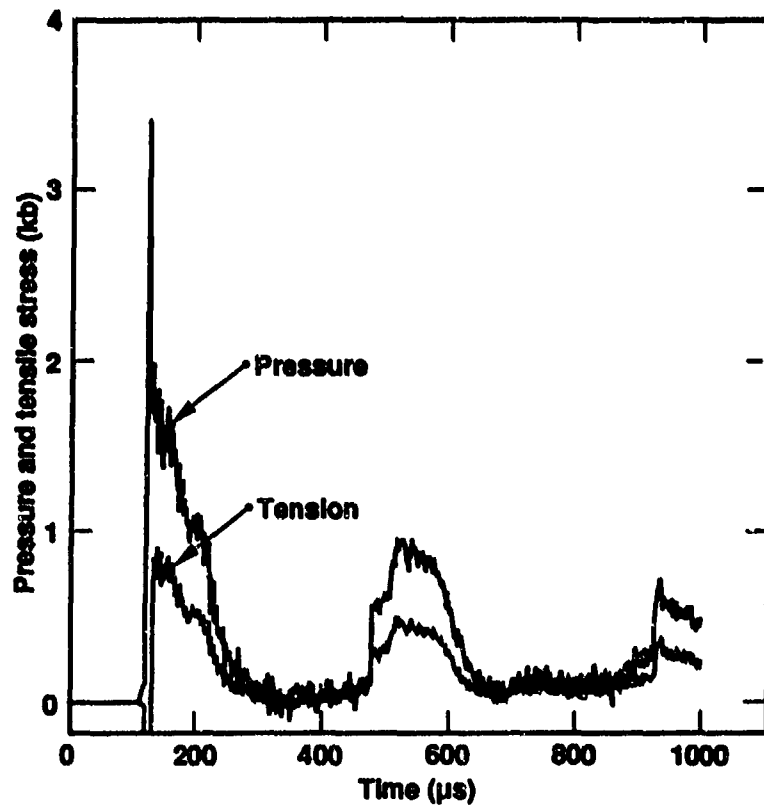


Fig. 11. Inner-shell radial pressure and hoop tension due to the detonation of a 1.25-kg charge inside a cubicle with foam.

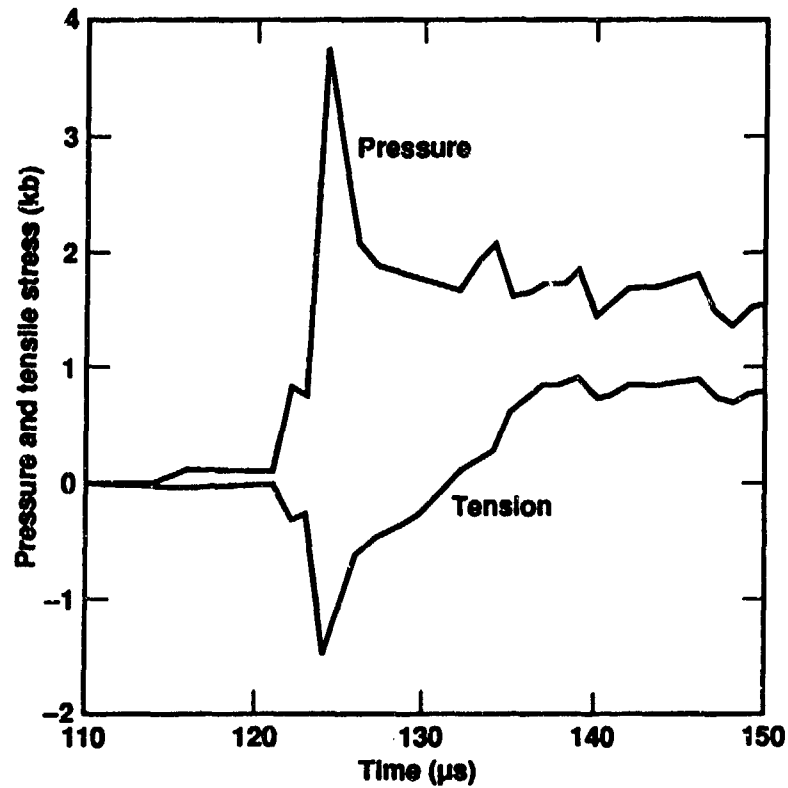


Fig. 12. Inner-shell radial pressure and hoop tension due to the detonation of a 1.25-kg charge inside a cubicle with foam.

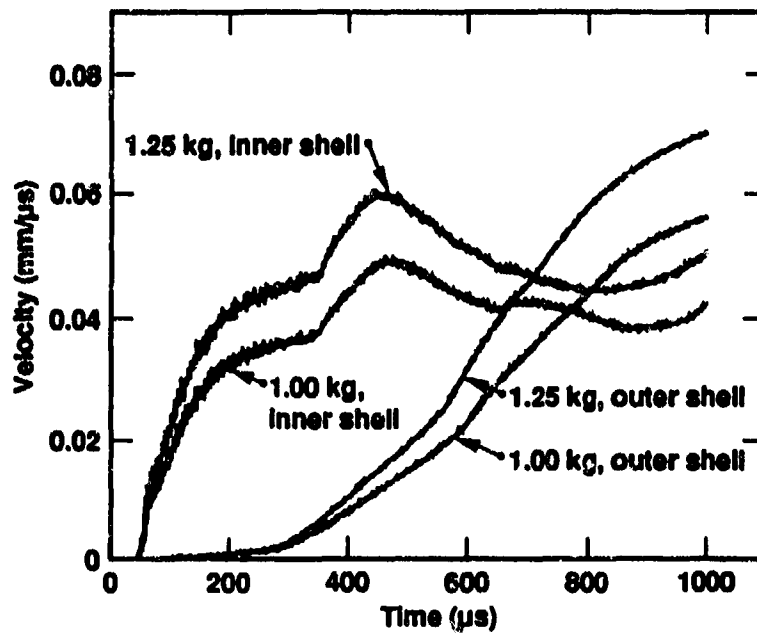


Fig. 13. Velocity of inner and outer shells following the detonation of 1.00-kg and 1.25-kg charges inside an air-filled cubicle.

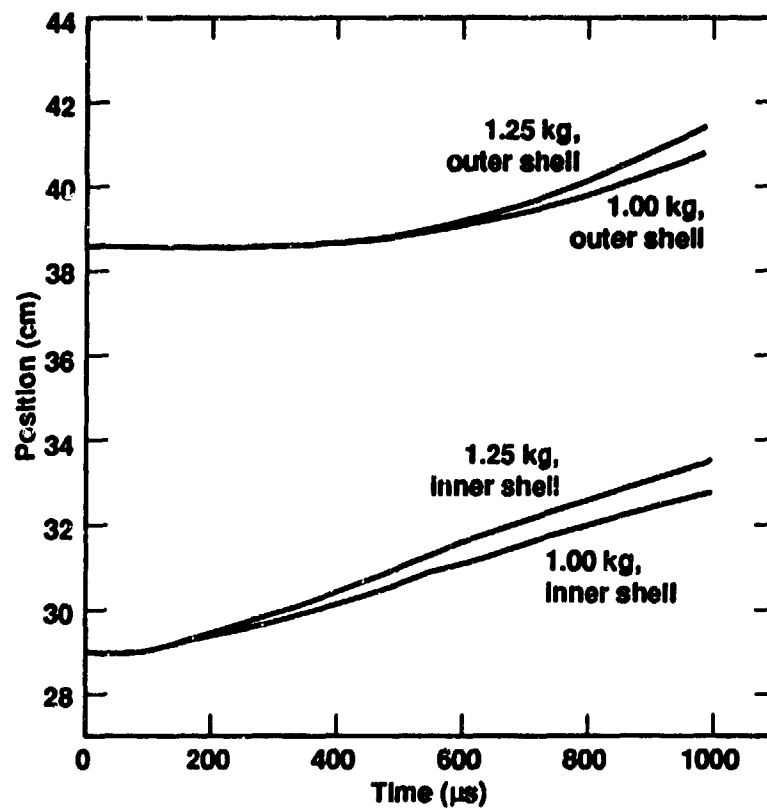


Fig. 14. Inner and outer shell displacement following the detonation of 1.00-kg and 1.25-kg charges inside an air-filled cubicle.

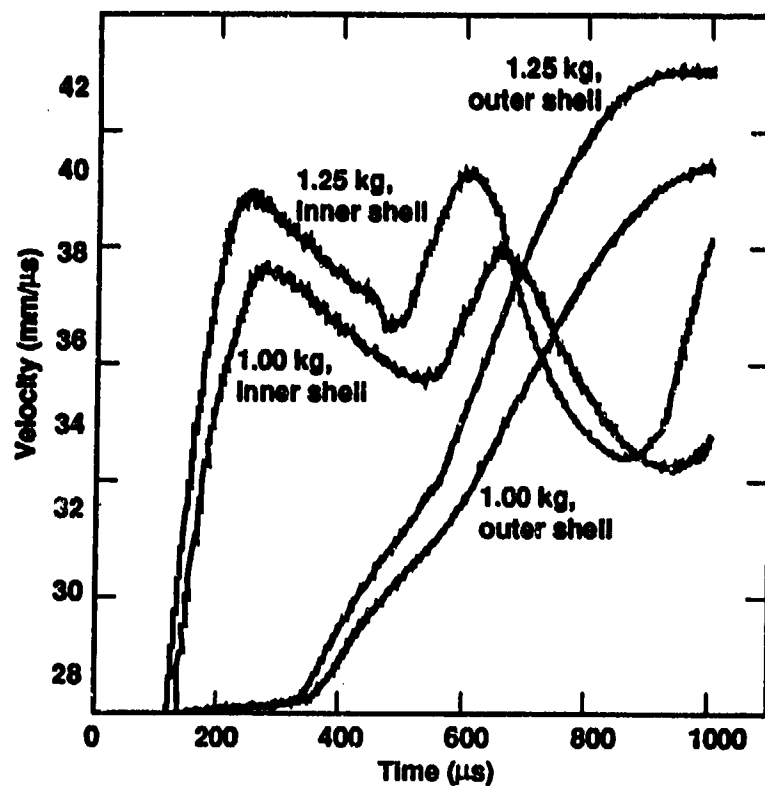


Fig. 15. Velocity of inner and outer shells following detonation of 1.00-kg and 1.25-kg charges inside a cubicle containing foam.

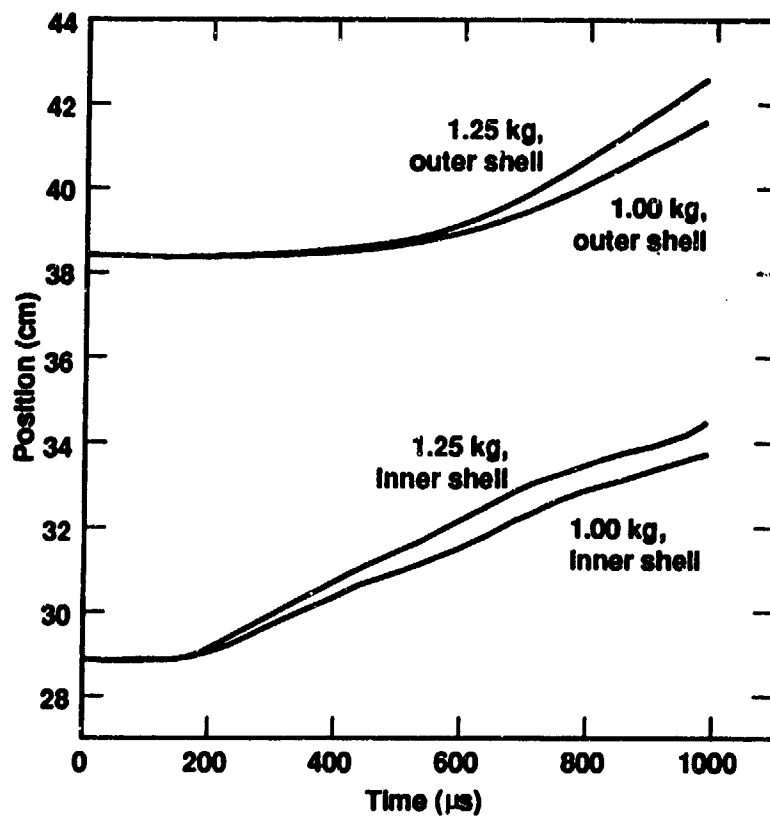


Fig. 16. Displacement of inner and outer shells following detonation of 1.00-kg and 1.25-kg charges inside a cubicle containing foam.

76%, with an average of 48.5%. In the DYNA3D modelling described in Section C.3, we used a foam enhancement factor of 50%.

These KOVEC calculations extended for only 1000 μs , a duration too short for final spherical model equilibrium to occur. However, they extended long enough for gaps to open between the inner and outer steel shells and the redwood buffer material. Using the displacements plotted in Figs. 14 and 16, we can estimate the maximum redwood buffer compressions for cubicles with and without foam. If we choose this as the measure of impulse enhancement by the foam, then the initial 3-in. redwood is compressed by 0.822 in. at 635.0 μs by the 1.00-kg charge inside the cubicle with no foam and by 1.069 in. at 670 μs by the 1.25-kg charge inside the cubicle with foam, a 30% increase.

Alternatively, we can choose inner-shell velocity peaks from Figs. 13 and 15, with and without foam, with the 1.25-kg charge. The first peak comparison is a foam enhancement of 76%: 0.046 mm/ μs at 320 μs vs 0.081 mm/ μs at 260 μs . The second peak comparison is a foam enhancement of 43%: 0.06 mm/ μs at 430 μs vs 0.086 mm/ μs at 610 μs . For the air-filled case we note that very little shell yielding took place between the first and second radial pressure pulses, since there is no falloff in velocity. For the case with foam, substantial inner-shell yielding occurred, as evidenced by the velocity falloff.

Finally, our primary interest is in motion of the outer shell. Here we compare final calculated velocities from Figs. 13 and 15 at 1000 μs ; the foam enhancement is 44%: 0.07 mm/ μs vs 1.01 mm/ μs .

Structural response increases when foam is present because the initial foam density is about 166 times that of ambient air, and thus provides much better impedance with the steel.

C.3 3-D DYNA3D Finite-Element Analysis

The units used in this study were SI: kg, m, and s. An attempt was made to calculate an upper bound for the acceleration and the terminal velocity a stored high-explosive charge would experience if the charge in an adjacent cubicle detonated. Two cases with a 1-kg donor charge were calculated, one for an air-filled cavity and another for the foam-filled cavity, in which the pressure vectors were multiplied by 1.5 to account for the increase in impulse estimated in the KOVEC study. For the foam case, the results we obtained gave a maximum acceleration of 11,500 g's and a terminal velocity of 83 m/s. Figure 17 illustrates the vectors of acceptor charge acceleration and velocity for this increased-impulse case. Figure 18 illustrates comparative information for the case with no foam enhancement.

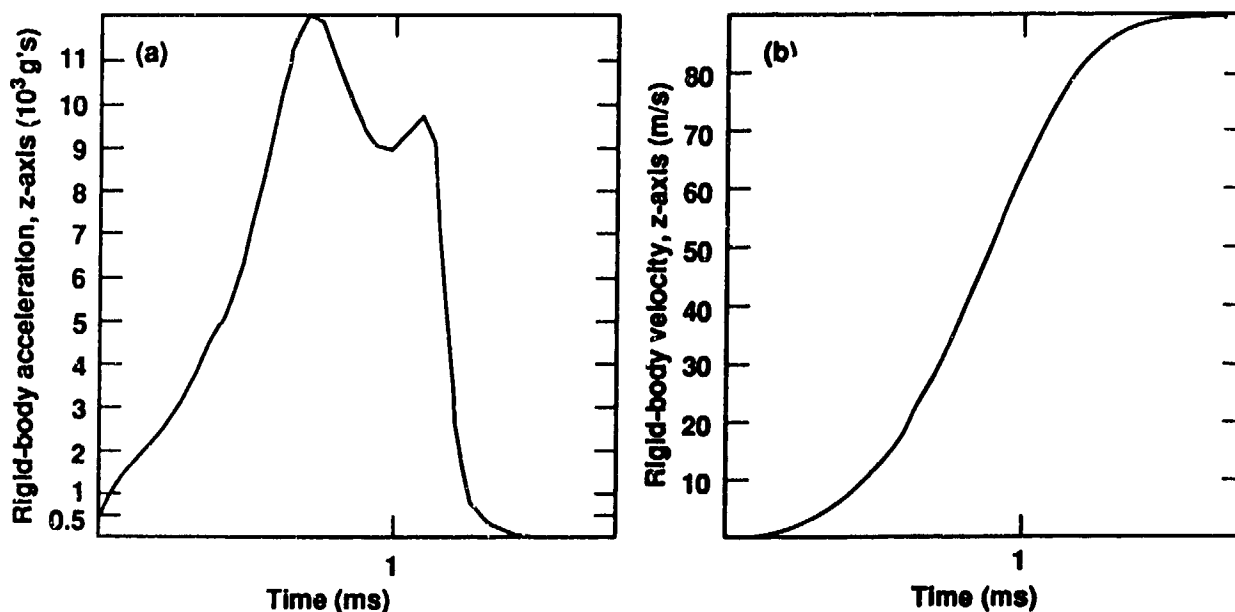


Fig. 17. (a) Acceleration and (b) velocity of the charge closest to the explosion of a 1-kg donor charge in a foam box inside a chamber. The foam increased the pressure impulse by 50%.

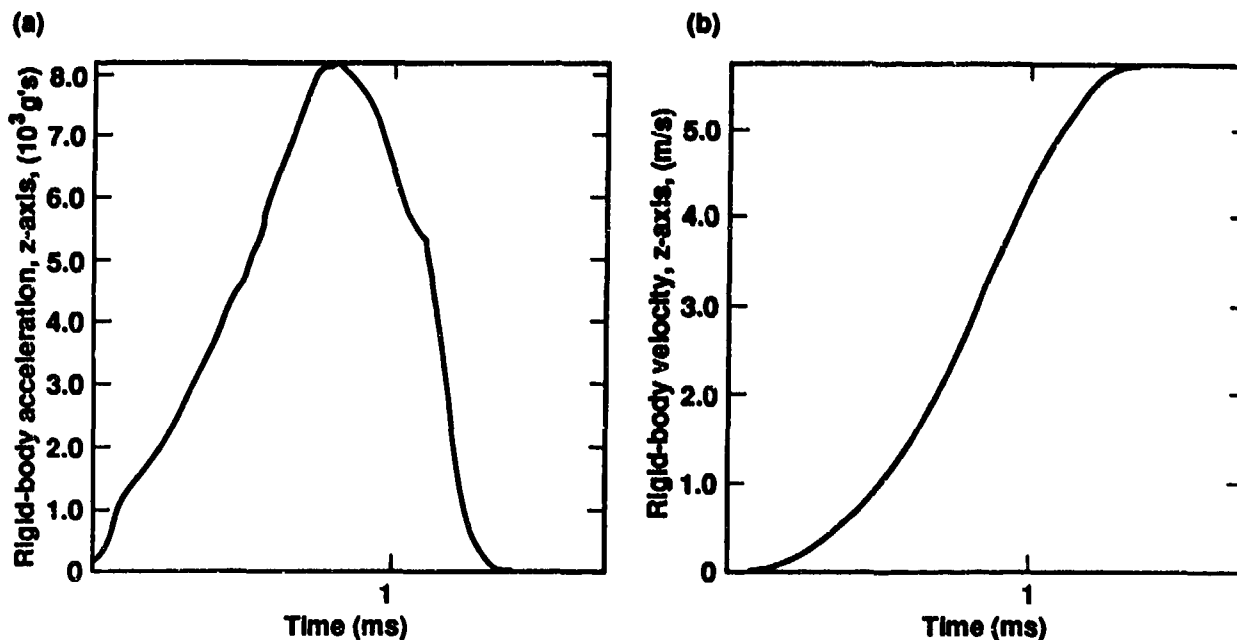


Fig. 18. (a) Acceleration and (b) velocity of the charge closest to the explosion of a 1-kg donor charge in an air-filled explosion chamber.

We calculated a third case with the foam-enhanced pressure vectors scaled up an additional 25% to establish that additional material safety margins are incorporated into the design. A factor of 1.2 or 1.25 is commonly referenced in DOE safety standards. In our calculation procedure, this is equivalent to increasing the donor charge mass from 1.00 kg to 1.28 kg. There was also a minor change in geometry to give a 3-cm clearance between the side-mounted receptor charge and its bracketing foam pads and between the top-mounted receptor charge and its bracketing foam pad on top. Figures 19 and 20 show both frontal and isometric views of the calculation model. Figure 21 illustrates model deformation at six times for a total calculation time of 3 ms (3000 μ s).

Figure 22 illustrates the acceleration and velocity vectors for both the overhead receptor charge and the side receptor charge. Peak acceleration for the overhead charge was 11,150 g's. The corresponding peak pressure was 2405 psi (0.166 kb). The width of the acceleration pulse was about 600 μ s. The initial pulse is approximately a sinusoid with a root-mean-square (rms) value for the accumulation of $P^2 \tau$ on the order of 8.27 kb²- μ s. Acceleration of the side charge reached only 41% of that of the charge in the chamber above. At 3 ms, the calculation indicates the velocity of the overhead charge had decreased to 1 m/s. The charge, located in the chamber to the side, was moving outward at 11 m/s but decelerating.

Figures 23 to 26 are for an air-filled cubicle with a 1.00-kg donor charge without driving pressure enhancement to account for the presence of foam. Their purpose is to illustrate the basic calculation procedure.¹

C.3.1 Hazard Estimate

Our hazard estimate is based on the results of the DYNA3D model calculations. It assumes that a 1.28-kg PBX-9404 charge is detonated. To account for the 50% impulse enhancement resulting from the foam box in the explosion chamber, we multiplied by 1.5 the pressure values in the ambient air-filled cavity calculations, as estimated in Section C.2. Pressures and accelerations were evaluated for an acceptor charge located in a foam box in the chamber above the explosion chamber.

We use the commonly applied $P^2 \tau$ criterion (Ref. 3) to estimate whether a PBX-9404 acceptor charge will detonate. The skid test and other data give a threshold value for PBX-9404 (Ref. 4) (1.842 g/cm³, 2.5 mm/s) of 297 kb²- μ s, a value corresponding to a "critical" energy of 644 kJ/m². The rms pressure value for $P^2 \tau$ obtained in the 3-D analysis for the approximate sinusoidal-shaped pulse that acts on the charge (see summary above) is $(0.166)^2 \times 600/2 = 8.27$ kb²- μ s, or 1/36 of the threshold value.

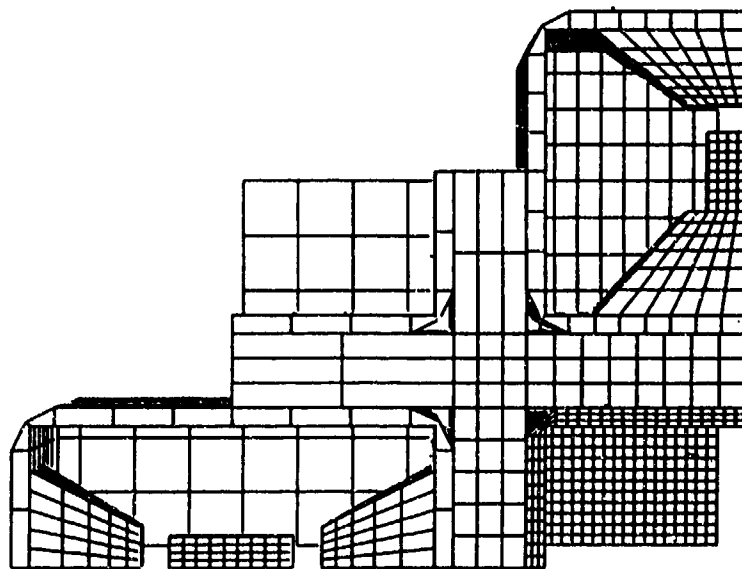


Fig. 19. Frontal view of final DYNA3D model.

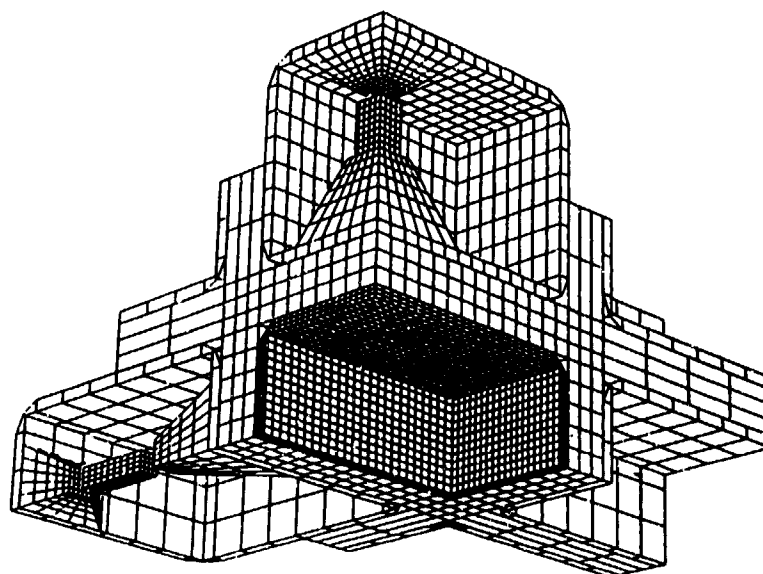


Fig. 20. Isometric view of final DYNA3D model.

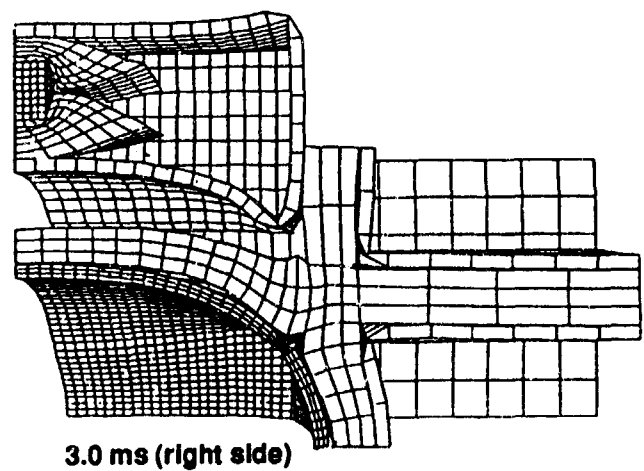
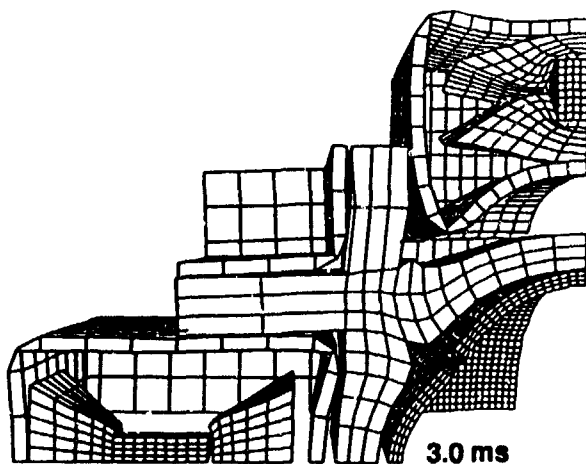
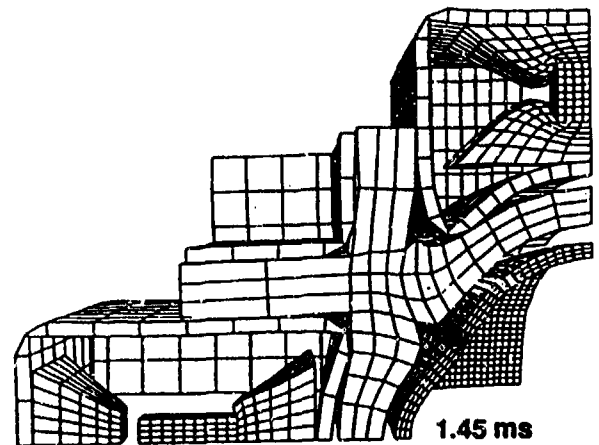
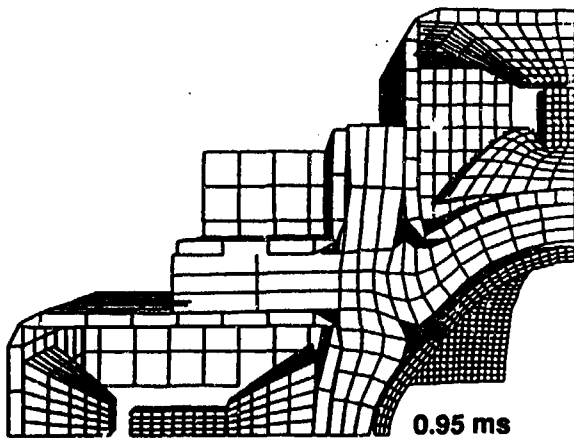
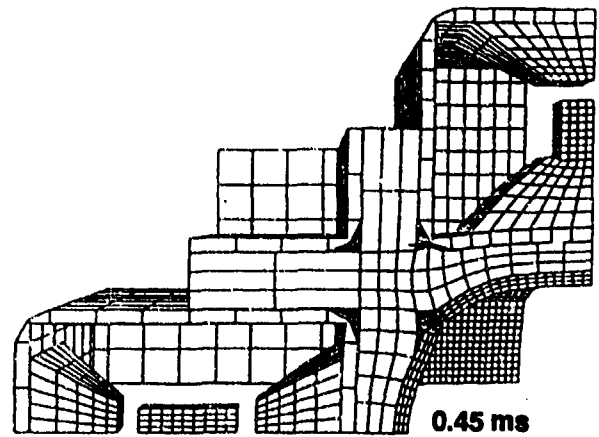
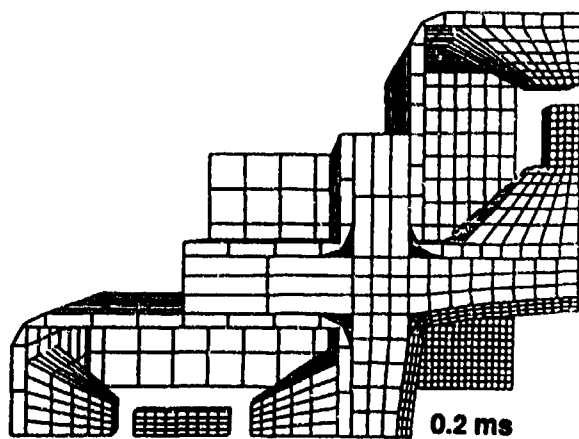


Fig. 21. Magazine deformation following detonation of 1.28-kg of PBX-9404 (detonation energy 6.77 MJ) in lower right chamber.

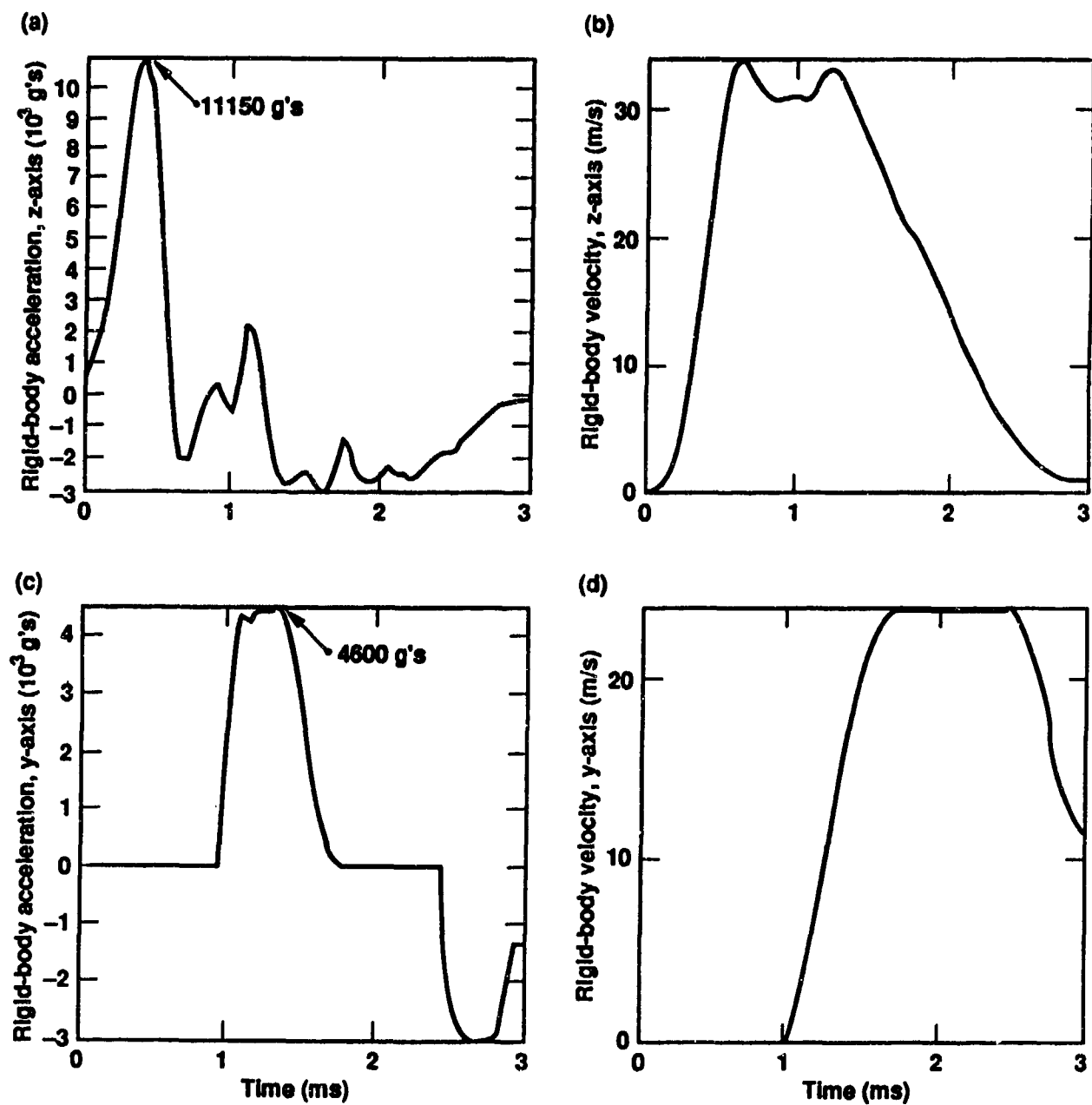


Fig. 22. Acceptor charge responses to detonation of 1.28-kg donor charge. (a) Acceleration of overhead charge. (b) Velocity of overhead charge. (c) Acceleration of side charge. (d) Velocity of side charge.

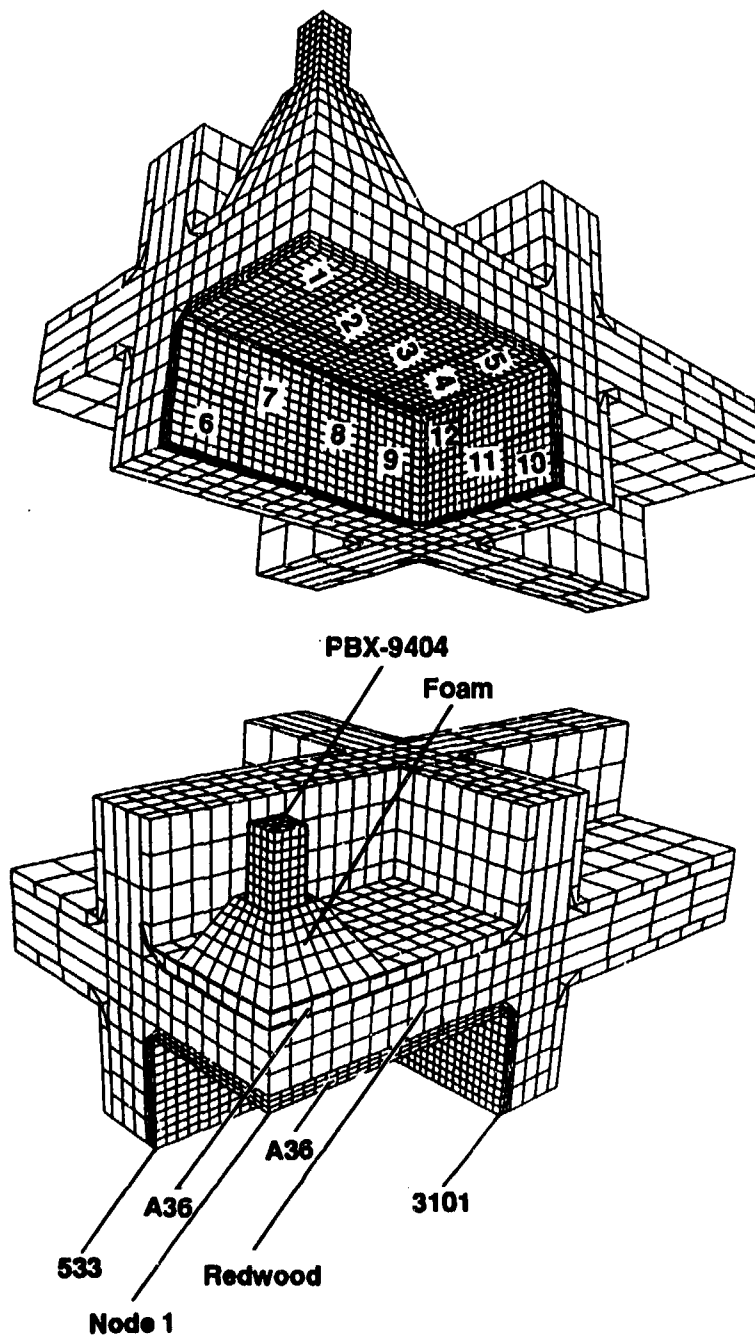
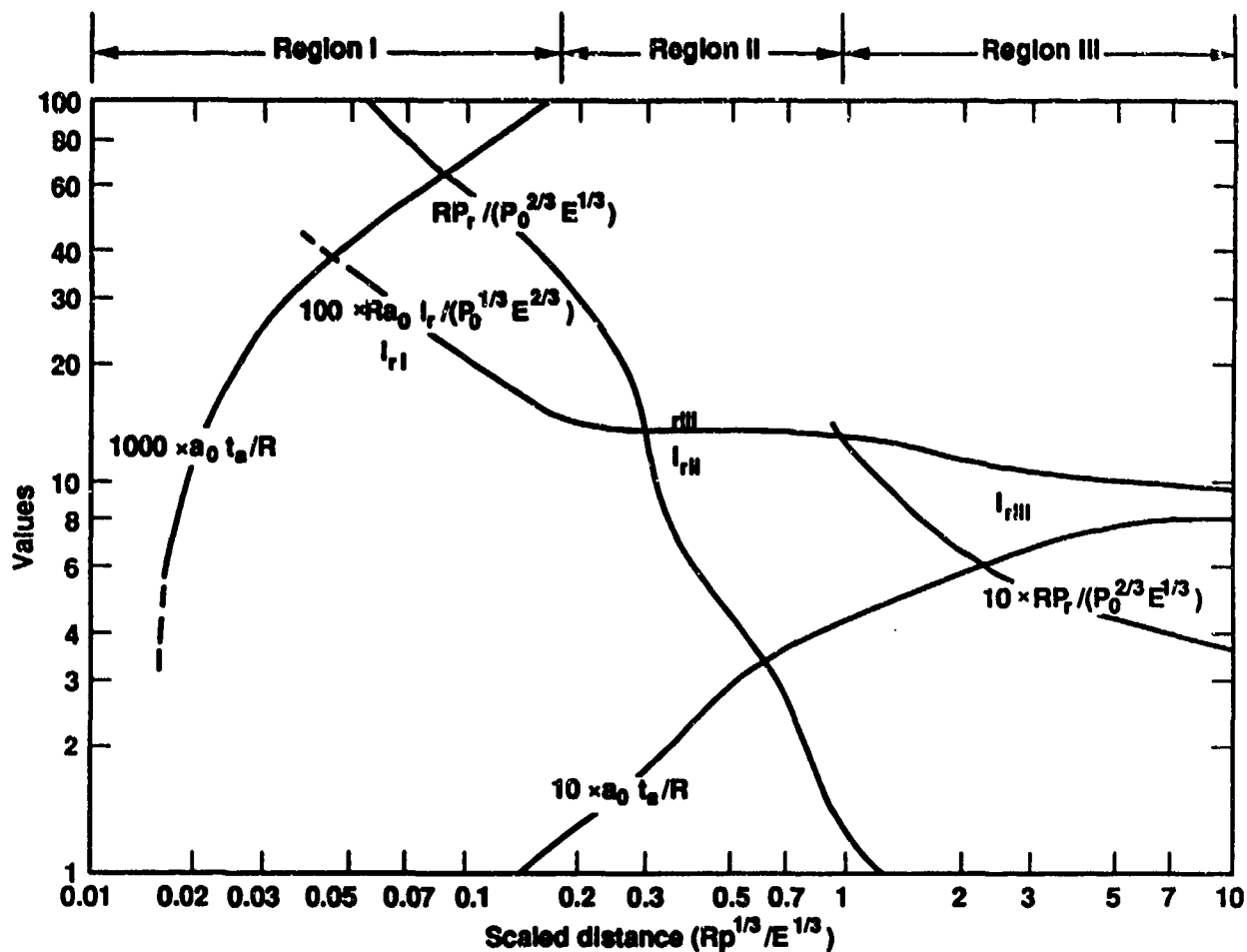


Fig. 23. Loading zones, materials, and corner code numbers.



$$I_{rI} \approx 1.038 P_0^{0.087} E^{0.913} / (a_0 R^{1.74})$$

$$I_{rII} \approx 0.145 P_0^{1/3} E^{2/3} / (a_0 R)$$

$$I_{rIII} \approx 0.113 P_0^{0.225} E^{0.715} / (a_0 R^{1.146})$$

$$I_r \text{ [N s/m}^2\text{]}$$

$$P_0 \text{ [N/m}^2\text{]}$$

$$E \text{ [N m]}$$

$$a_0 \text{ [m/s]}$$

$$R \text{ [m]}$$

R , distance from charge centroid

P_r , normally reflected over pressure

E , detonation energy

I_r , normally reflected impulse per unit area

P_0 , initial pressure

t_a , shock arrival time at R

a_0 , sound velocity

I_{rI} , impulse at close range

I_{rII} , impulse at medium range

I_{rIII} , impulse at far range

Fig. 24. Nondimensional parameters of air shocks.

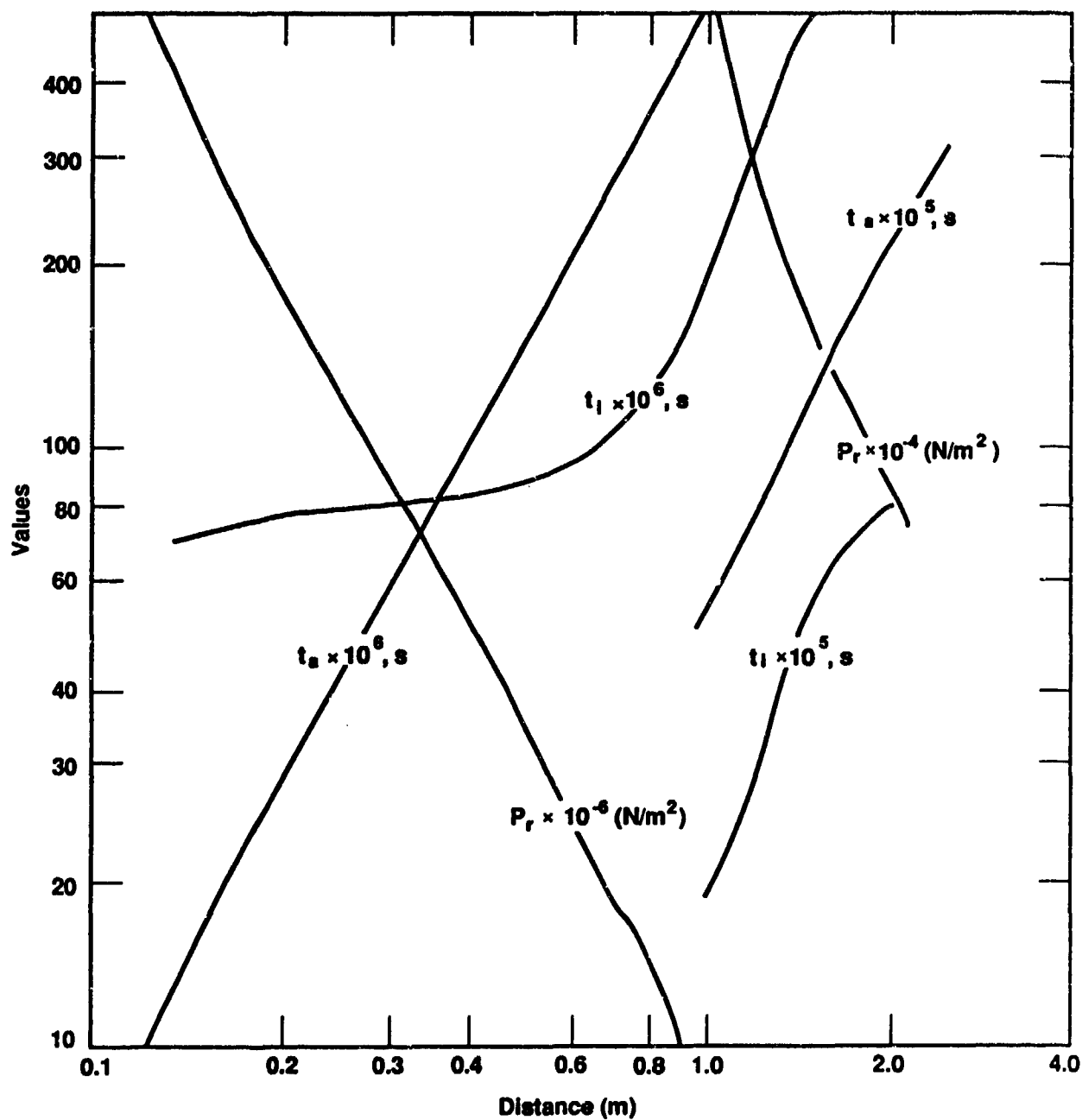


Fig. 25. Peak reflected overpressure P_r , transit time t_a , and triangular pulse baseline t_i for detonation energy of 5.36 MJ.

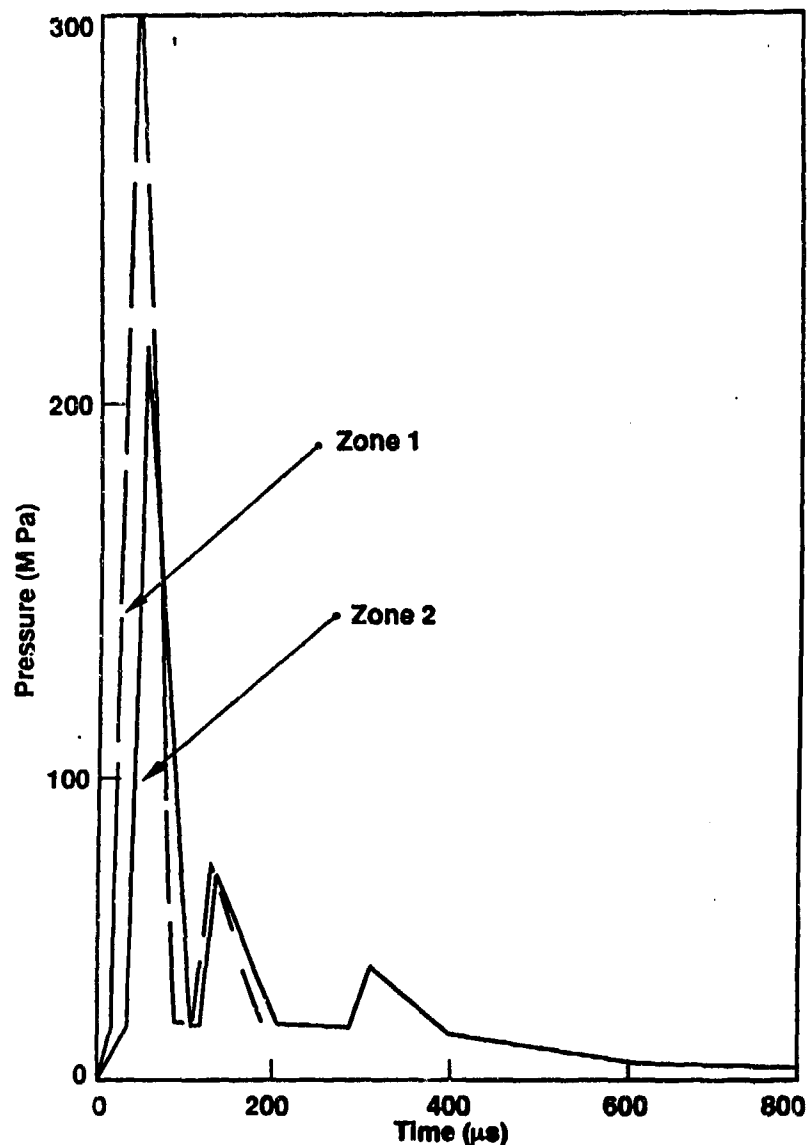


Fig. 26. Pressure-time loading functions for zones 1 and 2.

C.3.2 Programs

We used the DYNA3D analysis code⁶ with mesh generation and input file supplied by means of INGRID. Graphics were obtained from TAURUS.

C.3.3 Loading Functions

Figure 23 illustrates an earlier version of the model showing the 12 loading zones inside the explosion cavity used to specify the pressure history after a detonation.

We used a value of 5.36 MJ for the energy of detonation of the 1-kg charge of PBX-9404. The charge was suspended in the center of the cubicle, surrounded by air at standard conditions. Using the average distance to each of the loading zones, we calculated a nondimensional scaled distance for the zones and the indicated peak reflected overpressure, normally reflected specific impulse, and arrival time. For this purpose we used correlations of experimental data summarized in Fig. 24. Figure 25 illustrates the reflected overpressures and pulse lengths for an energy of 5.36 MJ. In a strong enclosure, reflected shocks and the quasi-static pressure can be significant as well. We estimated the strength and arrival time of two

reflected shocks and combined the three shock pulses with a blowdown quasi-static pressure decay controlled by the blowoff cubicle door. Figure 25 illustrates the loading function for zones 1 and 2 nearest to the explosion.

C.3.4 Materials

The materials of the magazine are structural steel, redwood, and polystyrene foam. The following constitutive parameters were used for the structural materials:

Steel, type A36:

Density	7830 kg/m ³
Shear modulus	80 GPa
Yield strength	0.30 GPa
Hardening modulus	2.7 GPa
Failure strain	23%
Bulk modulus	162 GPa

Redwood:

Density	448 kg/m ³
Shear modulus	3.1 GPa
Yield strength	5.9 MPa
Hardening modulus	10 MPa

Foam:

Density	200 kg/m ³
Shear modulus	1.0 GPa
Yield strength	2.0 MPa
Hardening modulus	10 MPa

For both redwood and foam, we imposed the same Gruneisen equation of state as in the 1-D KOVEC study. It had the following parameters:

Sound speed	350 m/s
Gamma	1.1
Coefficients ¹	1.29

D. References

1. W. E. Baker, P. A. Cox, P. S. Westine, J. J. Kulesz, and R. A. Strehlow, *Explosion Hazards and Evaluation* (Elsevier Scientific Publishing Company, 1983), pp. 238-252.
2. B. M. Dobratz, and P. C. Crawford, *LLNL Explosives Handbook*, Lawrence Livermore National Laboratory, Livermore, CA, UCRL-52997 Change 2 (January 31, 1985), Table 8-7, pp. 8-21 to 8-23.
3. A. M. Weston, J. F. Kincaid, E. James, E. L. Lee, L. G. Green, and J. R. Walton, "Correlation of the Results of Shock Initiation Tests," *Proceedings of the Seventh Symposium (International) on Detonation*, NSWC MP 82-334, (June 16-19, 1981), pp. 887-897.
4. L. G. Green, E. J. Nidick, Jr., and F. E. Walker, *Critical Shock Initiation Energy of PBX-9404, A New Approach*, Lawrence Livermore National Laboratory, Livermore, CA, UCRL-51522 (January 25, 1974).
5. T. Raumeister and L. S. Marks, *Marks' Mechanical Engineers' Handbook*, 6th ed. (McGraw-Hill, 1958), Chapter 4.
6. J. O. Hallquist and R. G. Whirley, *DYNA3D User's Manual (Nonlinear Dynamic Analysis of Structures in Three Dimensions)*, Lawrence Livermore National Laboratory, Livermore, CA, UCID-19592 (May 1989).

E. List of Attachments

PLS 88-191-005DB, HEAF magazine layout drawing
PLS 88-191-006D, Sheet 2, HEAF magazine layout drawing
M. Hisaoka, layout, HE storage test, 8 Mar. 88, 0.25 scale

F. List of Photographs

HEAF magazine (2)

Pre-shot test setup (2)

Drawers installed

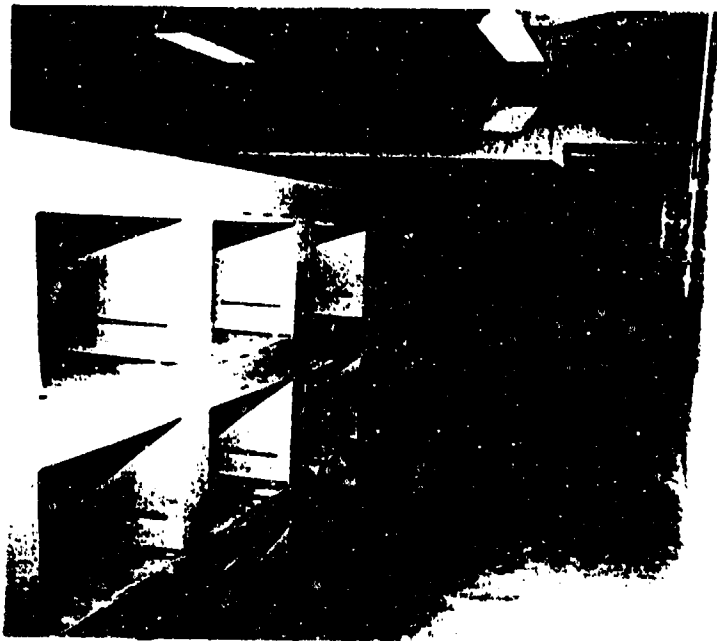
Open drawer, center

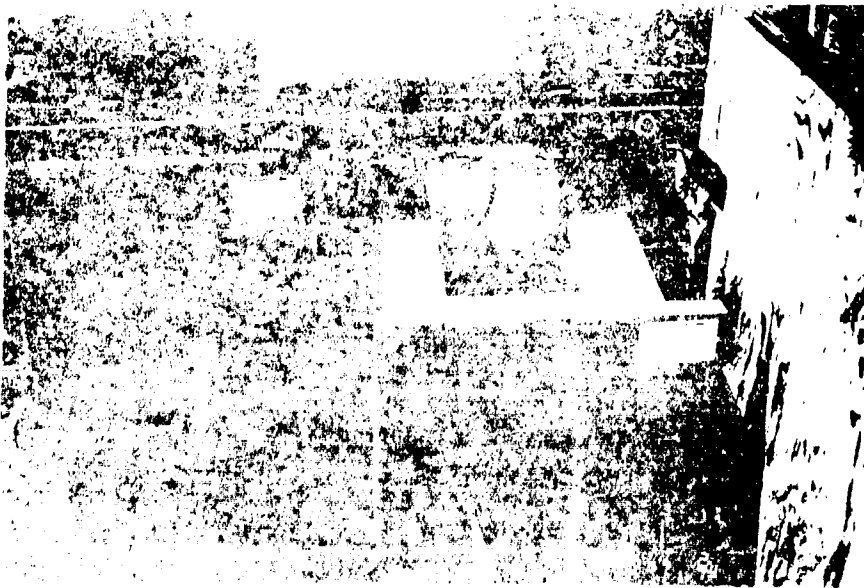
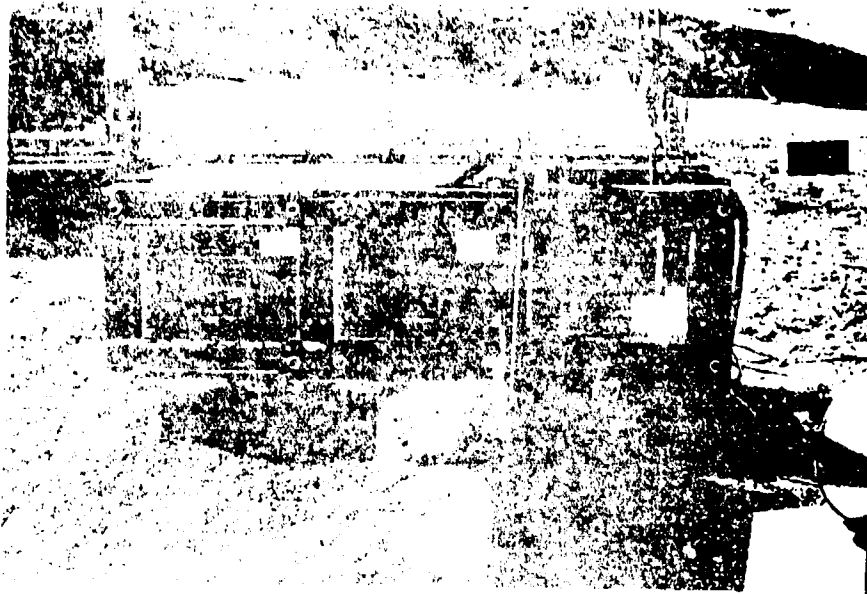
Post-shot test rescrub (3)

Explosion chamber

Acceptor chamber

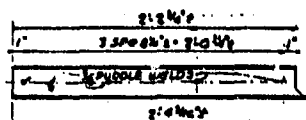
Overall view







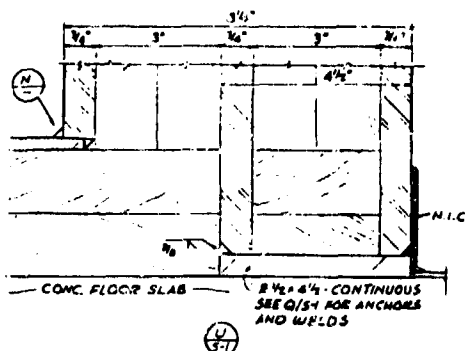
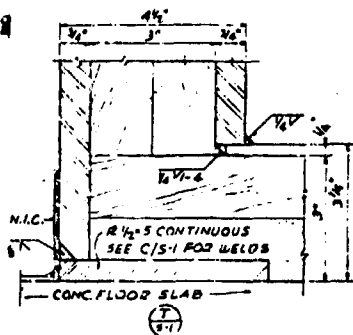
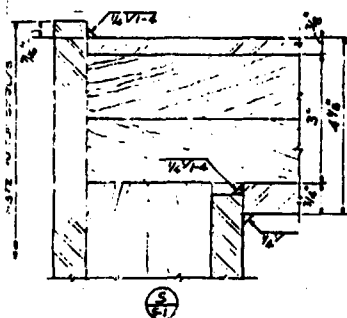
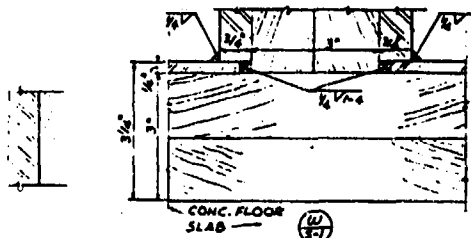




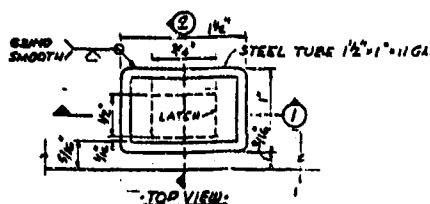
1/2\"/>

DRAWER CHANNEL GUIDES

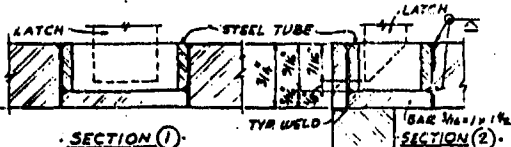
SCALE: 1/2\"/>



* USED MILD STEEL PLATE ASTM A36 IS ACCEPTABLE. PLATE THICKNESS SHALL BE 3/16\"/>

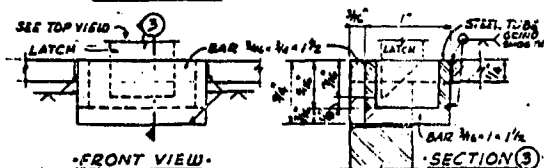


TOP VIEW



SECTION 1

LATCH SLOT DETAIL
SCALE: FULL SIZE



FRONT VIEW

LATCH SLOT DETAIL
SCALE: FULL SIZE

DRAWER NOTE:

THE UNIVERSITY FURNISHED DRAWER UNITS EACH CONSIST OF ONE DRAWER FRONT, ONE DRAWER BODY, ONE DRAWER CARRIAGE AND TWO DRAWER CHANNEL GUIDES. THE SUBCONTRACTOR SHALL ASSEMBLE AND INSTALL EACH DRAWER PER THE FOLLOWING SEQUENCE.

1. SLIDE THE DRAWER BODY ONTO THE INSIDE FACE OF THE DRAWER FRONT AND ANCHOR WITH 6 SHEET METAL SCREWS.
2. SLIDE THE DRAWER BODY WITH THE ATTACHED DRAWER FRONT ONTO THE DRAWER CARRIAGE.
3. SLIDE THE DRAWER CARRIAGE WITH THE DRAWER IN IT ONTO THE DRAWER CHANNEL GUIDES. THE DRAWER CHANNEL GUIDES SHALL BE INSTALLED BY THE SUBCONTRACTOR PER DETAIL V ON THIS SHEET.

GENERAL NOTES

A. GENERAL

1. ALL WORK AND MATERIALS SHALL CONFORM TO 1988 U.S.C.
2. USE NEW MATERIAL FOR ALL CONSTRUCTION. (EXCEPTION: STEEL MAY BE USED STEEL.)
3. FIELD VERIFY ALL DIMENSIONS PRIOR TO FABRICATION.
4. DESIGN CRITERIA FOR STORAGE FACILITY:
SEISMIC LOADS: 0.33 W (STATIC), VERT. & HORIZ.
5. N.I.C. NOT INCLUDED IN SUBCONTRACT.

B. MATERIALS

1. STRUCTURAL STEEL SHALL CONFORM TO ASTM A-36. *
2. WELDING SHALL BE IN ACCORDANCE WITH AWS D1.1. USE E70XX ELECTRODES.
3. CONCRETE ANCHORS SHALL BE EITHER WEDGE TYPE 'PHILLIPS' RED HEAD, OR SELF DRILL, OR APPROVED EQUAL. SUBCONTRACTOR SHALL SUBMIT TO THE UNIVERSITY CERTIFICATION OF PULLOUT AND SHEAR VALUES WHICH SHALL COMPLY WITH I.C.B.O. REQUIREMENTS FOR 1/2\"/>
4. ALL WOOD SHALL FIT TIGHTLY BETWEEN PLATES AND BETW. SLAB AND PLATES. PLANE THE BOARDS IN RE 1655 T IN THE 3\"/>

HALF SIZE

RELEASE FOR CONSTRUCTION			
NAME	DATE	FEVA	DATE
I.O.			
H.C.			
P.M.			
S			

SECTIONS & DETAILS

Lawrence Livermore
National Laboratory
Livermore, CA 94550
PLANT ENGINEER

BUILDING 191
H.E. STORAGE
CUBICLES

DESIGN: HARRY WOLF & PARR DATE 9-16-82
DRAWN: R.H. KUECHLE DATE 9-16-82
CHECK: G.S. SHARP DATE 9-16-82
PE/A: GARY SLIGO DATE 9-16-82
S/L/P/L: Madhu Ramani DATE 9/22/82
SECURITY: JEFF DATE 9-26-82
W/P: R.J. GANNON DATE 9-28-82
H.C.: J. P. HARRIS DATE 9/29/82

SHEET S-2 OF 2
SET OF 2

PPN 191-AB-007
DWN NO. PLS88-191-00GD

AUTOCLAVE EXPLOSION AND PROTECTION ANALYSIS

**Kathy H. Spivey
Wilfred Baker Engineering, Inc.**

**Dr. Wilfred E. Baker
Wilfred Baker Engineering, Inc.**

ABSTRACT

An industrial firm has been using small autoclaves in a process involving the chemical reaction of high-pressure, high-temperature oxygen with hydrocarbon solids. A runaway chemical reaction could occur and develop pressures and temperatures within the autoclave, leading to explosive failure.

Our firm, Wilfred Baker Engineering, Inc. (WBE), was contracted to analyze and design a containment vessel to completely contain effects of postulated worst-case autoclave explosive failures. This paper describes the analysis and resulting containment vessel design. A design based on readily available components resulted, giving complete containment of shock and quasi-static pressures, and worst-case fragment impacts from autoclave explosive failures.

INTRODUCTION

Recently, an industrial firm experienced an accident involving an explosion in a small autoclave. The autoclave had an internal volume of 1 liter and was rated at 3,000 psi gauge pressure. Literature from the manufacturer stated that the autoclave was hydrostatically proof tested at 1.5 times the rated pressure. The manufacturer believed the vessel was capable of containing 2 to 3 times the rated pressure without failing.

From an examination of recovered parts, it is evident that failure of the autoclave was induced by leakage of high-temperature gas from the vessel through or past the sealing head gasket. The head-clamping ring was completely burned through near a gap between the split head rings and almost burned through near the gap on the opposite side of the split ring. There was local melting of the vessel adjacent to the top seal, as well as other evidence of the presence of quite high temperature. The vessel was pressurized to 2,500 psi with oxygen and had been heated to about 150°C for many hours before the accident. It appears that some exothermic reaction between the oxygen and hydrocarbon solids had occurred to raise pressure and temperature to failure level within the vessel. Best estimate of conditions at failure was a pressure of about 7,000 psig and a temperature of about 3,000°C. Estimated gas volume was about 30 cubic inches.

WBE's sponsor planned to continue the high-pressure, high-temperature processing using not only the 1-liter autoclaves, but also larger autoclaves of 7-liter (2-gal.) capacity. Immediate safety protection was needed for the 1-liter vessel. Within several months, protection was also needed for several 7-liter vessels. Within the next five years, the company anticipated the need to operate 20 to 40 7-liter vessels. WBE was contracted to design and analyze a containment structure for the autoclaves to ensure personnel safety in the case of a similar accident.

To satisfy the short-term safety needs, internal blast loads from the worst-case explosion noted above were predicted, as well as fragment hazards and dynamic response of containments for the vessels. Suitable containments were designed, using readily available components to contain the explosion effects with adequate safety margins. Components readily available to the sponsor included steel pipes, plates, flanges, and bolts. Recommended geometry for immediate containment design was a short cylinder with welded-in flanges and blind-flange plates closing each end.

TECHNICAL APPROACH

A. Containment Design and Analysis

1. Shock Loads

Blast loading of the cylindrical wall and end blind flanges of the containments consists of initial reflected air shock waves, followed by a longer-term, quasi-static pressure. The free-field air shock wave properties were calculated using equations and curves in Chapter 2 of Reference 1. To calculate starting shock strength, an in-house program, PBURST, was used to solve the shock tube equation:

$$\frac{P_1}{P_o} = \frac{P_{so}}{P_o} \left\{ 1 - \frac{(\gamma_1 - 1) \left(\frac{a_o}{a_1} \right) \left(\frac{P_{so}}{P_o} - 1 \right)}{\sqrt{(2\gamma_o) [2\gamma_o + (\gamma_o + 1) \left(\frac{P_{so}}{P_o} - 1 \right)]}} \right\}^{\left(\frac{-2\gamma_1}{\gamma_1 - 1} \right)} \quad (1)$$

(Ref. 1)

In this equation, P_{so}/P_o is the dimensionless air shock pressure at the instant of burst. P_1/P_o is the dimensionless sphere pressure, and a_o/a_1 is the ratio of the velocity of sound. The sphere dimensionless shock overpressure is:

$$\bar{P}_{so} = \frac{P_{so}}{P_o} - 1 \quad (2)$$

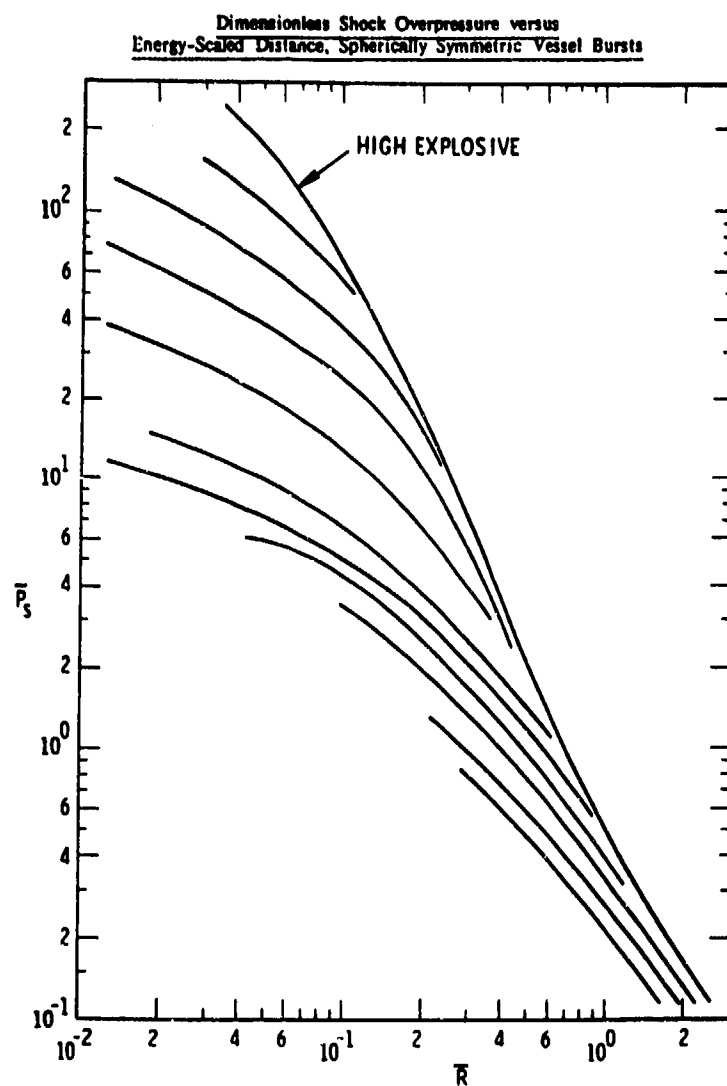
(Ref. 1)

PBURST solves the equation iteratively for P_{so}/P_o , from which P_{so} can be calculated from Eq. (2). Scaled shock radius is calculated using:

$$\bar{R}_1 = \left[\frac{3(\gamma_1 - 1)}{4\pi \left(\frac{P_1}{P_o} - 1 \right)} \right]^{\frac{1}{3}} \quad (3)$$

(Ref. 1)

The values of \bar{P}_{so} and \bar{R}_1 are the starting points on Figure 1. Once this pair is plotted, a curve is sketched through this point that follows the general trend of the other curves. From this curve, side-on blast pressure and impulse loads on the containment side walls were found. These values were then increased by a known factor to account for normal reflection from the loaded surfaces. The increase factor was calculated using the ratio of peak reflected overpressure to side-on overpressure from the WBE in-house basic program entitled PRPS. This program automates a Brode equation, which calculates shock reflection in a real gas.



Baker, W. E.; Kulesz, J. J.; Ricker, R. E.; Bessey, R. L.; Westine, P. S.; Parr, V. B.; Oldham, G. A. *Workbook for Predicting Pressure Wave and Fragment Effects of Exploding Propellant Tanks and Gas Storage Vessels*; NASA Lewis Research Center. November 1975; NASA CR-134906, p. 2-27. (Reprinted September 1977).

Figure 1. Dimensionless Shock Overpressure Versus Energy-Scaled Distance, Spherically Symmetric Vessel Burst (Ref. 1)

2. Quasi-Static Pressures

After the initial free-field blast loading, quasi-static gas pressures occur as the high-pressure gas from the vessel expands nearly isentropically into the containment. This quasi-static pressure was found by calculating the pressure rise caused by isentropic expansion of gas from the autoclave and corresponding isentropic compression of air in the containment. For this calculation, the containment was assumed to be gas tight. Schematically, the initial and final states for the process are shown in Figure 2. Equations governing these processes can be found in any standard thermodynamics textbook and are shown below:

$$pV^\gamma = \text{constant} \quad (4)$$

$$p_i V_i^\gamma = p_f V_f^\gamma \quad (5)$$

$$p_o (V_2 - V_1)^{\gamma_o} = p_f (V_2 - V_f)^{\gamma_o} \quad (6)$$

where

- p = pressure
- V = volume
- γ = ratio of specific heats
- o = ambient conditions
- f = final phase
- i = initial phase

To obtain final pressure, p_f , and final volume, V_f , the equations above must be solved iteratively. The quasi-static pressure is then found using the following equation:

$$P_{QS} = p_f - p_o \quad (7)$$

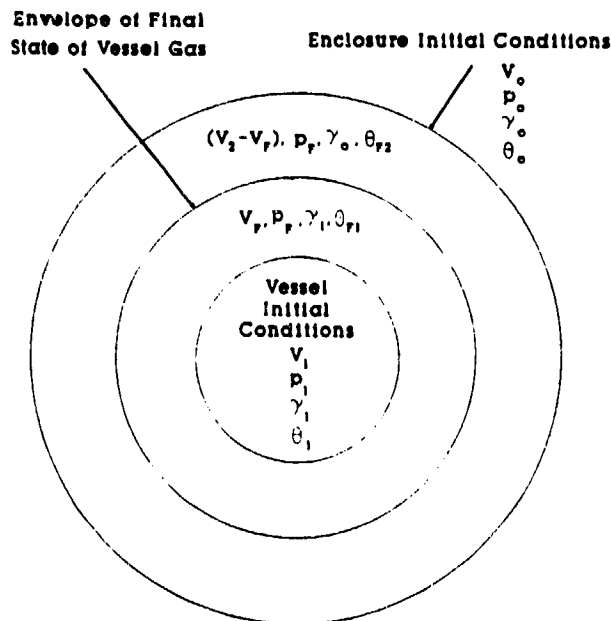


Figure 2. Schematic of Vessel in Enclosure, and Final States

Along with the quasi-static pressure rise due to gas expansion, some quasi-static increase could occur with the burning of combustible gas vented into the chamber. The total energy which could be released by chemical reaction between the polymer and the high-pressure pure oxygen for both 1-liter and 7-liter autoclaves was calculated. The calculation showed that the chemical reaction for the 7-liter autoclave (worst case) can release at most $3.80 \times 10^5 \text{ Cal} = 1.494 \times 10^9 \text{ in-lb} = E_T$. However, it was shown that the energy required to raise temperature and pressure in this autoclave to the bursting pressure of 7,000 psig is $E_B = 4.851 \times 10^6 \text{ in-lb}$. Because the energy for vessel failure is less than the total energy which could be released with combustion, combustion must be incomplete when the vessel fails.

Combustion may or may not continue after burst due to the fact that the sudden expansion would drastically lower the temperature and may quench the combustion. Continuing combustion would cause at most a slow pressure rise within the containment vessel surrounding the autoclave. Because the containment vessel need not be pressure tight, some venting can occur to limit pressure rise. To calculate the maximum for the slow pressure rise within the containment for combustion following autoclave failure, we simply inverted the equation for burst energy from Reference 1 to find P_{QS} :

$$P_{QS} = \frac{(\gamma_1 - 1)E_1}{V_c} \quad (8)$$

Here

γ_1 = ratio of specific heat for combustion products = 1.2

E_1 = available combustion energy

V_c = chamber volume

The available energy is

$$E_1 = E_T = E_B = 9.189 \times 10^6 \text{ in-lb}$$

3. Vessel Response

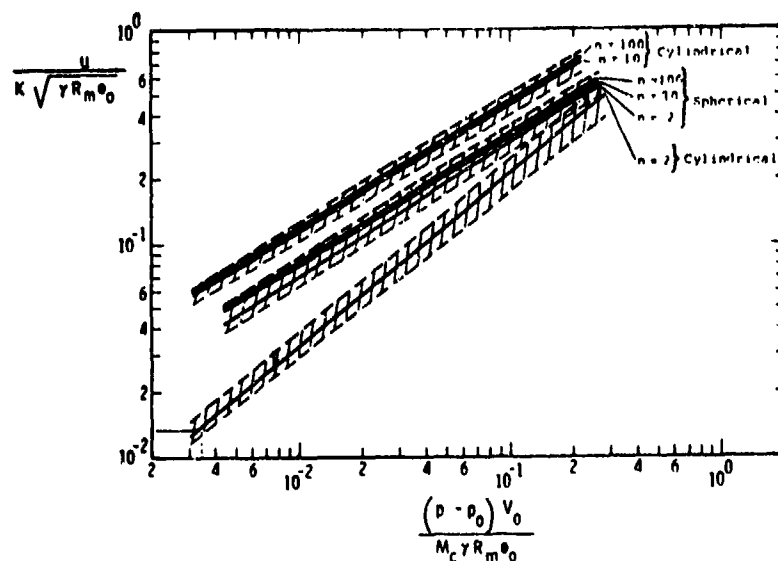
All sections of the containment vessel, the cylinder, end plates, and bolts, were designed and the structural response analyzed for safety. Each section was converted into a single-degree-of-freedom (SDOF) spring-mass system in order to perform a dynamic analysis using methods given in Reference 2 and our in-house computer program, BIGGS.

For the cylindrical section, a hoop section was analyzed for the dynamic analysis. Pressure was assumed to be applied uniformly to the interior of the hoop. For the end plates, Reference 3 equations for a clamped, elastic, circular plate were used. Unlike the cylinder, which is naturally a one degree-of-freedom system, the end plates have many degrees of freedom. Thus, the end plates had to be converted into an SDOF system using constants given in Reference 4.

The bolts were analyzed dynamically as a series of elastic-plastic springs resisting the motion of the cover as an attached mass which is loaded by the internal explosion loads within the containment vessel. The bolts chosen had to be readily available to our sponsor. The number and diameter of bolts were chosen based on dynamic analysis to give a ductility ratio of μ less than 6 (ductility ratio is the maximum deflection divided by the elastic yield deflection). It was noted that the bolts should not be torqued to normal tension for a bolted joint. Because this is not designed as a pressure type vessel, gapping or opening of the joint is perfectly acceptable under the dynamic loading.

B. Fragments

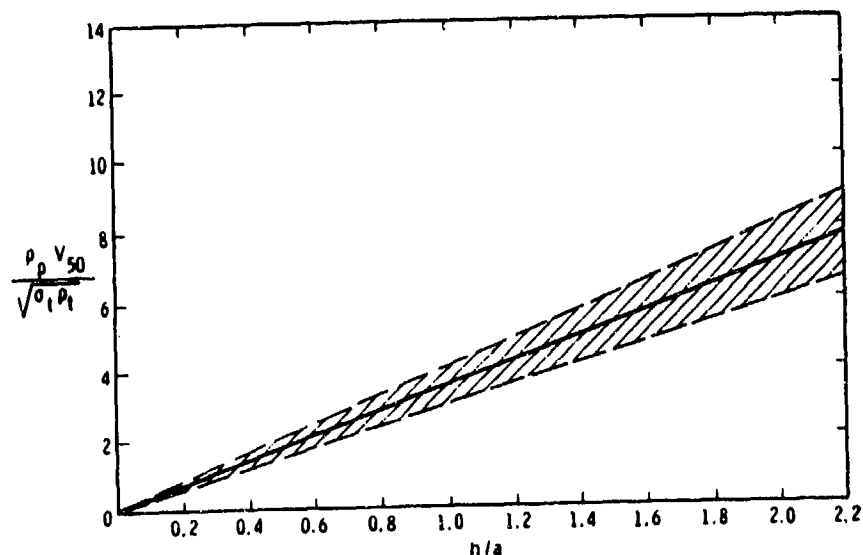
The containment vessel was analyzed for missile impact by pieces of the autoclave heads and the effect of that impact in the event of autoclave failure. To predict missile velocity, curves and equations were used from Reference 1. It was assumed that all parts but the ring would be projected along the axis of the autoclave if the ring fails. Velocity of the worst-case fragment was found using Figure 3 from Reference 1.



- u = velocity of fragment
- K = constant related to relative masses of vessel fragments
- γ = ratio of specific heats
- R_m = ideal gas constant
- θ_0 = absolute temperature
- p = internal pressure
- p_0 = atmospheric pressure
- V_0 = internal volume
- M_c = mass of the container

Figure 3. Scaled Fragment Velocity Versus Scaled Pressure
(Ref. 1)

Figures from Reference 1 were also used to determine if the containment vessel wall would stop a worst-case fragment (see Fig. 4).



- ρ_p = projectile material density
 V_{50} = threshold impact velocity for perforation
 σ_t = yield stress of target material
 ρ_t = target density
 h = thickness of target material
 a = fragment radius

Figure 4. Nondimensional Limit Velocity Versus Nondimensional Thickness for "Chunky," Nondeforming Fragments (Ref. 1)

RESULTS

For the cylinder response, it was decided initially to analyze several readily available vessel sizes. Before completion of the analysis, WBE was directed to use one specific size which had already been analyzed for the 1-liter and 7-liter autoclaves. Results appear for all containment vessels in which analyses were completed at the time of this decision (Table 1).

Table 1. Structural Response to Pressure Loads

Case No.	Component	Elastic Yield (in.)	Maximum Yield (in.)	Ductility Ratio
1	One-liter autoclave, containment vessel 15" I.D., 24" long, 3/8" thick	0.011	0.027	2.40
	End plate, 1" thick bolt circle diameter = 18"	0.028	0.008	0.29
2	Seven-liter autoclave, containment vessel 23" I.D., 24" long, 1/2" thick	0.022	0.060	2.75
	End plate, 1" thick bolt circle diameter = 27"	0.078	0.089	1.13
3	Seven-liter autoclave, containment vessel 36" I.D., 36" long, 1/2" thick	0.027	0.033	1.22
	End plate, 1" thick bolt circle diameter = 41"	0.143	0.099	0.69
4	One-liter autoclave, containment vessel 36" I.D., 36" long, 1/2" thick	0.027	0.007	0.28
	End plate, 1" thick bolt circle diameter = 41"	0.143	0.023	0.16

All components were well under the safety margin of $\mu = 6$. Thirty 6-in. internal diameter, 36-in.-long containment vessels were chosen for both the 1-liter and 7-liter autoclaves. In both case 3 and case 4 analyses, a shell thickness of 1/2 in. was used. The chosen containment has a thickness of 3/8-in. steel. Although this specific size containment was not analyzed, ductility ratios for the 1/2-in.-thick vessel are so low that reducing the thickness of the wall will not increase the ductility ratio past the safety margin. One-in.-thick end plates were chosen for the containment vessels.

Structural response to the quasi-static pressure due to combustion was examined by comparing the stress due to pressure rise to the static yield stress of the chosen containment. For the cylinder, hoop stress due to the quasi-static pressure rise was found to be 3,611 psi, while the static yield stress is approximately 40,000 psi. Thus, the cylinder is not affected by this pressure. The maximum bending stress under pressure for the end plates was found to be 12,190 psi, which is also well below the static yield stress. Thus, neither the cylinder nor the end plates are damaged by the combustion pressure. The maximum possible

combustion pressures following an autoclave failure cannot harm the 36-in. internal diameter, 36-in.-long containment vessel which was designed to withstand dynamic and quasi-static pressures caused by the failure of a 7-liter autoclave.

Bolt analysis was performed on the chosen containment by varying the number of bolts until a sufficient number was found to provide a ductility ratio of less than 6. Thirty 3/4-in. bolts were chosen to hold the end plates in place.

For fragment impact analysis, the largest possible fragment was selected as a worst-case fragment. Both the fragment velocity and the required fragment velocity for a 50% chance of penetrating the containment wall, V_{50} , were calculated. The velocity of the worst-case fragment was found to be 149 in./sec, and V_{50} was found to be 10,000 in./sec. This perforation velocity limit is more than 67 times the impact velocity of the fragment. Thus, the impact cannot damage the cylinder or the end plate, which is more than twice as thick as the cylinder wall.

CONCLUSIONS

Based on our design analyses, we concluded that a 36-in.-diameter, 36-in.-long steel containment cylinder fabricated from available steel cylinders, flanges, and plates would contain worst-case 7-liter autoclave failures with excellent safety margins. Some minor hoop stretch could occur in the cylinder. Some minor head bolt stretch could also occur. All other parts would remain elastic. Impacts of missiles from failed autoclave parts are completely contained with no damage to the container.

REFERENCES

1. Baker, W. E., et al., Explosion Hazards and Evaluation, Elsevier Publishing Co., 1983.
2. Biggs, J. M., Introduction to Structural Dynamics, McGraw-Hill Co., 1964.
3. Timoshenko, S., Theory of Plates and Shells, McGraw-Hill Co., 1940.
4. "Suppressive Shields, Structural Design, and Analysis Handbook," U. S. Army Corps of Engineers, HNDM-1110-1-2, November 1977.

"Designing for Explosive Safety"
The Explosive Components Facility at Sandia National Laboratories

William A. Couch

Abstract

The Explosive Components Facility (ECF) is to be a new major facility in the Sandia National Laboratories (SNL) Weapons Program. The ECF is a self-contained, secure site on SNL property and is surrounded by Kirtland Air Force Base which is located 6-1/2 miles east of downtown Albuquerque, New Mexico. The ECF will be dedicated to research, development, and testing of detonators, neutron generators, batteries, explosives, and other weapon components. It will have capabilities for conducting explosive test fires, gas gun testing, physical analyses, chemical analyses, electrical testing and ancillary explosive storage in magazines.

The ECF complex is composed of a building covering an area of approximately 91,000 square feet, six exterior explosive service magazines and a remote test cell. Approximately 50% of the building space will be devoted to highly specialized laboratory and test areas, the other 50% of the building is considered nonhazardous (i.e. no energetic material). Critical to the laboratory and test areas are the blast-structural design consideration and operational considerations, particularly those concerning personnel access control, safety and environmental protection. This area will be decoupled from the rest of the building to the extent that routine tests will not be heard or felt in the administrative area of the building.

While the ECF is designed in accordance with the DOE Explosives Safety Manual to mitigate any off-site blast effects, potential injuries or death to the ECF staff may result from an accidental detonation of explosive material within the facility. Therefore, reducing the risk of exposing operation personnel to hazardous and energetic material is paramount in the design of the ECF.

Introduction

The Explosive Components Facility (ECF), will be a new major facility in the Sandia National Laboratories (SNL) Weapons Program. The concept of the ECF is to consolidate the activities of four departments dispersed among a number of SNL facilities into one building, thus providing a more efficient capability for the weaponization of vital components in the federal arsenal. The consolidation of the Explosive Components Department, Neutronic Components Department, Power Sources Department and Weapons Evaluation Department will enhance and streamline the operation of each.

Hazards addressed in the design of the facility include explosives, pyrotechnics, propellants, lasers, microwaves, radioactive materials, neutrons, x-rays, toxic chemicals, reactive chemicals, hazardous waste and conventional industrial safety hazards. Explosives offer the potential for the highest severity accident occurring within the ECF and, therefore, will receive substantial attention in the design of the ECF.

The Explosive Components Facility Building will be a single story office/laboratory building occupying approximately 91,000 square feet (8,450 square meters) of area. The building is divided into two distinct functional areas; explosive and non-explosive. The explosive area will contain 47,000 square feet (4,370 square meters) of explosive laboratories and work areas. The explosive test area (containing more than 500 grams of TNT equivalent) will consist of approximately 12,000 square feet (1,110 square meters) and will contain firing bays, associated assembly rooms and mazes; an explosive aging area; a propellant area; a lithium cell battery abuse area; and an explosive staging area. The remaining 35,000 square feet (3,250 square meters) of the explosive area will consist of wet chemistry type labs, pyrotechnic labs, physical testing labs, and supporting operations areas for the firing bays.

The non-explosive area will contain approximately 44,000 square feet (4,090 square meters) of: office and light laboratory area; mechanical room and mechanical penthouse areas; and, support areas including computer room, storage rooms, conference rooms, multipurpose (vending and eating) room, and restrooms. The non-explosive laboratory areas include software and electronic laboratories, optic laboratories, and experimental assembly space. The service areas include the mechanical and electrical equipment room, shops, and raw stock storage, shipping and receiving room, and short-term storage space. A penthouse will be constructed and will contain the HVAC air handling equipment and utilities equipment. Since these are non-explosive spaces, standard construction techniques and operational considerations will be followed.

Codes and Standards

The Explosive Components Facility will meet the 1988 Uniform Building Code (UBC) requirements for Seismic Risk Zone 2B and the 1982 edition of the American National Standards Institute (ANSI) Standard A58.1 for minimum design loads, excluding seismic loads. Wind loading is based on an 81 mile per hour wind speed, an Exposure C, and an importance factor of 1.07. The entire roofing system will meet the Factory Mutual Class I system acceptance and I-90 wind uplift resistance requirements, as well as the Underwriter's Laboratory (UL) Class A membrane requirements. The requirements of the Department of Energy document, "Design and Evaluation Guidelines for Department of Energy Facilities Subjected to Natural Phenomena Hazards," UCRL-15910, will be used where they are more stringent than the UBC and ANSI requirements.

In addition to these structural requirements, the portion of the ECF to be used for explosive laboratories and work areas is being designed to meet the requirements of: the "DOE Explosives Safety Manual" (DOE/EV/06194, Rev 4); the Department of the Army publication entitled, "Structures to Resist the Effects of Accidental Explosives" (TM5-1300); the Tri-Services Manual entitled, "Seismic Design for Buildings" (TM5-809-10); and the Department of Energy Order 6430.1A entitled "General Design Criteria." Building egress will conform to the applicable requirements of the National Fire Protection Association "Life Safety Code" (NFPA 101) and the DOE Explosives Safety Manual (DOE/EV/06194). Ladders, stairways and other working or walkway areas will be designed according to the requirements of the Code of Federal Regulations, Title 29, Part 1910, "Occupational Safety and Health Standards."

Operational Considerations and Activities

To develop an understanding of the operations conducted in the ECF, it is important to note that it is a research and development facility which functions differently than a production facility. As a research and development facility, the descriptions of activities are generically grouped in terms of "like" operations rather than a specific well defined industrial process even though, in practice, there are individual differences in equipment, hazards, and personnel. Each activity conducted is, however, required by Sandia policy and practice to be conducted in accordance with the guidelines of a Safe Operating Procedures (SOP) which outlines the required parameters for each operation as well as the mandatory safety precautions.

Specific activities to be conducted in the explosive area of the facility are grouped into the following categories:

1. Shipping, Receiving, and Storage of Explosives, Pyrotechnics and Propellants;
2. Physical and Chemical Testing of Explosives, Pyrotechnics and Propellants;
3. Neutron Device Research, Development and Testing;

4. Battery Research, Development and Testing; and
5. Stockpile Surveillance of Explosives, Pyrotechnics and Propellants.

Design Considerations

Functionally, the ECF has been designed to support and enhance the safety of the above listed activities through optimization of the use of space and structural materials. The design of the facility has made use of the grouping of "like" activities into functional areas which share the similar needs for blast mitigation and environmental protection. Such a design facilitates effective management controls regarding the overall safety of any given activity. The design concept of the ECF and the small quantities of explosives which will be present in the facility eliminate missile and blast pressure concerns for other buildings near the ECF. Firing pads are completely enclosed by blast walls which will contain all debris and missile hazards.

The non-explosive area of the building will be separated from the explosive area to minimize any adverse effects which would result from an accidental detonation within the explosive area. The design of the north wall of the explosive area will stop the primary design fragment and contain the overpressure resulting from an accidental detonation of 10 grams within an explosive laboratory area.

Explosive Laboratory Area

The roof and floor of the explosive laboratory areas will be of reinforced concrete which will be designed to withstand the effects of an accidental detonation equal to the maximum credible event that may occur in the particular laboratory area. Doors from all rooms opening into the corridor of the explosives area are oriented perpendicular to the corridor walls. In the event of an accidental detonation within the room, this arrangement will reduce the amount of debris entering the corridor to that allowed by the DOE Explosives Safety Manual.

The corridor of the explosive area will not be designed to withstand an accidental detonation. Up to 500 grams of explosives may be transported through this corridor only when packaged in Department of Transportation (DOT) approved or equivalent containers. The roof and floor of the corridor will be of reinforced concrete construction. Walls will be of the construction type dictated by adjacent room use. This corridor is considered to be an occupied area. A maximum credible event in an adjacent room will result in allowable overpressure and less than allowable levels of debris in this corridor.

Doors will be installed at the two area separation walls (fire walls) located in the corridor. The two area separation walls within the explosive area are required per the National Fire

Protection Association "Life Safety Code" (NFPA 101). Doors will also be installed in the area separation wall between the explosive and non-explosive area (per NFPA 101). The latter wall is located at the south end of the two connecting corridors. To comply with the Uniform Building Code (UBC) requirements, these doors will be of three hour fire resistive construction. Due to the pressure anticipated in the corridor from an accidental detonation in a laboratory, all area separation doors (as well as the exterior doors) will be low pressure resistant doors in lieu of labeled fire doors. Although not UL tested fire doors, the pressure resistant (blast) doors will be of more substantial construction than the standard labeled fire door. Standard panic hardware will be used to facilitate exiting. Magnetic devices will be used to hold open the doors located in the corridor. Upon actuation of the alarm system, the magnets will release and the doors will close. These doors will then be sprayed with water to prevent overheating. Initial overpressure from an accidental detonation will travel through the corridor prior to the doors closing.

The doors located between the explosive and non-explosive area will be normally closed to control access to the explosive area and to control an allowable level of overpressure that would result from an accidental detonation in a laboratory or corridor. The exterior doors will be equipped with standard panic hardware for egress, and will be equipped with an access control device to control ingress. The rooms within the explosive area will be designed to control the effects of an accidental explosion and to protect personnel that may be located in adjacent rooms or in the corridors.

Explosive Test Area

Nine test firing bays are located at the rear of the explosives test area. Each firing pad cubicle will be designed to fully protect the operating personnel from the overpressure, hazardous fragments, and thermal effects of planned detonations within the firing pads. The walls, roof, and slabs-on-grade will be designed to accommodate repeated detonations without damage to the structure. Two door openings, equipped with blast doors, will be used to provide access control and full containment. The door opening in the rear (south) wall of each firing pad cubicle will be equipped with a pair of blast doors which will be designed to withstand the effects of the maximum credible event weight of 1000 grams. These blast doors provide ingress and egress for test equipment too large to be transported through the mazes.

The door opening located in the wall between each firing bay and its adjacent maze will be equipped with a single blast door. For economy now, eight of these doors will be designed to withstand the effects of charge weights that are less than 1000 grams. If future explosive testing requirements dictate a need for the firing pads to be used with charge weights in excess of the existing door design limit, the door openings may then be refitted with blast doors having a designed resistance of up to 1000 grams. In order to retain the ability to test 1000 gram components, the ninth single blast door is designed to withstand the effects of a charge weight of 1000 grams. Each firing bay will contain the fragments

and pressure of a planned detonation. Immediately following the detonation, the valve used to close off the exhaust system will be opened to exhaust the space of products of combustion. The exhaust stack will discharge at a height of seven feet above the roof.

During "set-up" activities associated with a test on a firing pad, the pair of blast doors at the rear of the firing bay will be secured. However, the blast door between the maze and the firing bay may be open to facilitate transporting the experiment from the assembly room to the firing bay. If an accidental detonation occurs while transporting the experiment, the DOE overpressure and fragment criteria will not be met at the maze opening. Preliminary calculations show that the criteria will be met at a distance of 9.2 feet (2.8 meters) from the maze into the support area.

Adjacent to the firing pads are two rooms which will each contain a test firing chamber. Each chamber will be designed and proof tested to contain the effects of repeated test involving up to 1000 grams of TNT equivalent explosives. Two concrete pedestal foundations will be constructed in a pit below grade for each test firing chamber. The floor of the test firing chambers will be at the same elevation as the finished floor of the ECF. The walls, roof, and slab-on-grade for these two rooms will be of the same level of design as the firing pads. The doors between these rooms and adjacent mazes will be of hollow metal construction in lieu of blast doors since the firing chambers are designed to fully contain the effects of the blast. Experiments will be transported from the assembly room to the test firing chambers in Department of Transportation (DOT) approved, or equivalent, containers.

Since planned detonations will occur within either an enclosed test firing pad or inside of a test firing chamber, there will be no blast overpressure wraparound produced. This test firing pad arrangement will permit set-up activities to continue at other firing pads while testing in a nearby pad is in progress. However, set-up and testing will not occur simultaneously on firing pads that use the same assembly room.

The assembly rooms are explosive assembly areas where the floor, roof, and three walls are constructed of reinforced concrete. The concrete will be designed to withstand the effects of a 1000 gram detonation. A drywall partition will serve as the rear (south) wall of the assembly room and will contain an access door. This door and the exterior door located in the south wall of the building will be of hollow metal construction. Overpressure due to an accidental detonation in the assembly room will cause the room door (if closed) to blow-out into the adjacent maze, and will also cause damage to the drywall partition. The overpressure will then be vented through the mazes and may blow-out the exterior door. A concrete fragment wall and roof located outside the exterior door will contain the exterior door and other fragments produced by the accidental explosion and overpressure.

The walls, floor and roof of each maze will be constructed of reinforced concrete which will be designed to withstand the effects of a 1000 gram detonation. Mazes will be used in lieu of installing blast doors in the wall between the assembly areas and their support areas. These mazes will have a configuration which will cause a loss of the energy released by a detonation; thus, causing pressure decay. At the openings between the mazes and the support areas, the overpressure caused by an accidental detonation within the assembly room will be reduced to no more than 15 psi (103 KPa) as required by Chapter VI of the DOE Explosives Safety Manual. It will also limit the missiles (hazardous fragments), that may be present at the maze opening, to those that will impart no more than 58 ft-lbs (79 J) of impact energy as required by the DOE Explosives Safety Manual.

A sidewalk and service drive will be located at the rear (south side) of the ECF Building. Access to this drive will be through vehicle gates in the security fencing which encloses that portion of the rear of the building. Access will be administratively controlled by the ECF Safety Officer and will be permitted only during scheduled periods.

Ancillary Test Area

A Remote Test Cell (RTC) will also be located south of the building. The RTC will be used by the Neutronic Components Department for their work with neutron generators, and for a once-a-year Stockpile Integrated Laboratory Test (SILT) which will involve a kilogram quantity of a beryllium/depleted uranium system. Testing will be performed remotely with controls located inside the ECF. The structure will totally contain the fragments and overpressure of a planned 250 gram TNT equivalent detonation.

On-Site Explosive Storage

On-site storage of explosives for testing will be provided in six earth covered service magazines. Each magazine will contain approximately 480 square feet (44.6 square meters) of interior floor area and will be of reinforced concrete construction. An aproned slab-on-grade will serve as the floor and foundation for the one foot thick walls and roof. An interior height of 12 feet (3.7 meters) will accommodate the access door which will have dimensions of seven feet high and three feet wide. The door will open into a maze that will have an opening into an exterior sidewalk and service drive. The maze is utilized to attenuate the blast effects in the event of an accidental detonation within the magazine. The maze will also be utilized to "catch" the magazine door and prevent it from becoming a missile. In the front wall of the maze (face of the structure), will be a 3/4 inch (19 mm) thick steel access panel covering an opening that is five feet wide and seven feet high. This access opening will allow installation and removal of the non-propagating cabinets which will be used in each magazine. The magazines are spaced seven feet apart with three magazines on each side of the service drive. The exterior openings of opposite magazines will be offset to allow the reinforced concrete retaining wall (which includes

the front wall of the maze) to contain fragments or debris from an accidental detonation within the magazine. The front maze wall will serve as the first line of containment for the access door and any fragments or debris.

Each magazine will contain two rows of non-propagating cabinets (ten to a row) which will be installed back-to-back. The fronts, sides and tops of the cabinets will be at least two feet clear ("stand-off" distance) of the magazine walls and roof. The bottom of the lowest cabinet will be located one foot clear of the floor. A cabinet will contain up to a 2,268 gram (5.0 lbs.) TNT equivalent charge. Each magazine will be designed for a maximum credible event of 2,268 grams.

The magazines will be accessed by way of the service drive at the west end of the ECF Building. Access through the ECF perimeter fence will be by way of a motorized gate located north and west of the front entrance to the building. An interior manual gate will be located at the southwest corner of the ECF Building and will be opened by operating personnel for final access to the service magazine area. Access to the magazines will be administratively controlled by the ECF Safety Officer.

Safety Systems and Access Control

The SNL Lightning Early Warning (LEW) System warns personnel that an electrical storm (high potential gradient) is approaching. The LEW stations, which are located throughout the SNL facilities, measure and indicate the potential for electrical discharge. Remote local stations are also supported by the system. A LEW station will be established at the ECF, as will a number of local stations. The LEW station will be located in the control room of the ECF. Sensing probes and antennas will be located around the perimeter of the ECF property.

Indicator lights and digital readouts of the potential gradient will be displayed at locations throughout the interior of the building. These lights will receive signals from a control panel located adjacent to the terminal cabinet. When the potential for lightning is less than 1,500 volts/meter, a green light will be displayed. When the potential for lightning is between 1,500 and 2,000 volts/meter, an amber light will be displayed. A red light will turn on when the potential exceeds 2,000 volts/meter. Personnel will consult this system prior to conducting planned detonations in the firing pads.

The Fire Control System (FCS) will safely protect personnel during hazardous operations. The FCS will ensure that the hazardous area (firing pads, gas gun, etc.) has been cleared and will provide a visual/audible warning system to prevent personnel from entering the hazardous area. The FCS master control station will be located in the control room. Access to the general area will be controlled from this station. The station panel will contain alarm point status lights for each of the hazardous operation areas located throughout the ECF.

Local control stations will be established at hazardous operation areas throughout the ECF. Each station will control access to its area. If a person enters the hazardous area, the controls will turn off the operation. System controls include electric dead bolts and locks, rotating red flashing lights, audible alarms, panic switches, limit switches, master and local control panels, and a programmable controller.

A permit signal will be sent from the master control to the local control station after the general area has been cleared and all controls activated. At that time, the local control station will ensure that all controls are activated and will then give a permit signal to the local firing control, gas gun or laser control circuit. Panic switches will be located at key points throughout the explosive test area. The panic switches will terminate the firing sequence in the event of an emergency. Indicator lights and audible alarms will be installed near the interior and exterior doors of each firing pad, gas gun and test firing chamber. The lights and audible alarm will indicate that the firing pad, gas gun or test firing chamber is in use and ready to fire.

Provisions will be made in the FCS to allow the future installation of closed circuit television as another system control.

In addition to the FCS, the movement of personnel within the ECF will be controlled to mitigate the exposure of casuals to the hazardous operations within the building. Personnel Access Control (PAC) will be provided by a key pad and magnetic card reader located adjacent to the entrance of the controlled doors throughout the hazardous areas of the ECF. The key pads and magnetic card readers will be wired to the PAC host computer located in the computer room. Access to the hazardous areas will be permitted by using a numeric code or the magnetic strip on the Sandia badge. Emergency access to the controlled areas will be provided by special badges placed in strategic locations throughout the ECF or a special key pad code made available to all ECF personnel. The use of a special badge or key pad code will alarm the PAC.

All explosives and flammable material laboratories will contain a static ground bus to which static free benches, metal shelving, and personnel grounding wrist bands will be connected. This grounding system will help prevent the accumulation of static electricity on equipment, on materials being handled, or on operating personnel. The static ground bus will be connected to the building grounding system and the lightning protection system in accordance with requirements of the DOE Explosives Safety Manual and the DoD Ammunition and Explosives Safety Standards manual.

Environmental Impact

Because of the structural integrity of the facility and the relatively small amounts of explosives, toxic materials and radioactive materials present in the ECF, there is little

opportunity for impact to the environment or to the general public. Therefore, normal operations will present negligible impact because of the small amount of hazardous materials present in the facility, the presence of engineering and administrative controls preventing their release, and the distance to other facilities or persons outside of the ECF. However, annual soil sampling and analysis will be performed at various sites surrounding the ECF to assure the continued protection of the public and the environment.

Conclusion

By both intent and design, the ECF will comply with all existing and applicable DOE, Air Force, industry consensus, state, federal, and local codes, standards, criteria, statutes and regulations. Compliance is assured through multiple layers of design and procedure reviews by both Sandia and DOE. Once the facility is constructed and operating, additional periodic reviews of ECF activities will be conducted to assure continued compliance with current criteria. The risk of exposing operating personnel to hazardous materials and high energy components has been addressed in the design of the facility as has the risk of off-site impact to the environment and to the public. Based on the types of hazards, quantities of hazardous materials, facility design, engineering controls, and administrative controls employed in the design and use of the ECF, the risk to members of the public and to the environment from this facility will be negligible. Overall risk of operating the Explosive Components Facility has been reduced to a level that is as low as reasonably achievable for an energetic materials facility.

References

DOE/EV/06194, Revision-4, "DOE Explosives Safety Manual," U.S.Department of Energy, December, 1988.

"Final Environmental Assessment," Explosive Components Facility, Sandia National Laboratories, Albuquerque, New Mexico, July, 1990.

"Safety Assessment of the Explosive Components Facility," Sandia National Laboratories, Albuquerque, New Mexico, May, 1990.

Title I Floor Plans by Frankfurt-Short-Bruza Associates, P.C., for Explosive Components Facility, Sandia National Laboratories, dated February 9, 1990.

VENTED SUPPRESSIVE SHIELDING (VSS) IN EXPLOSIVE OPERATIONS

Dr. David J. Katsanis
Shielding Technologies, Inc.
1003 Old Philadelphia Road
Aberdeen, Maryland 21001

ABSTRACT

Vented Suppressive Shielding (VSS) was developed by the U. S. Army during the 1970s for use in ammunition production plants to protect personnel and equipment from the hazards of accidental explosives. At that time a variety of VSS types were designed and tested, and constraints for approved use were defined. Recently requirements have surfaced for VSS for explosives finishing operations in ammunition production and for explosive ordnance disposal. The specifications for the applications have resulted in advanced VSS designs. The new applications and designs are described. Test results are presented.

INTRODUCTION

Foundations for VSS technology were laid in a 5-year Army program during the mid-seventies and were based on extensive engineering analysis, design, and testing by Army, Navy and contractor research laboratories and facilities. Results of that early testing were reported at DDESB Explosive Safety Seminars prior to 1980. Recent work on VSS for deflagrating and pyrotechnic materials supported by NOS, Indian Head, Maryland was reported in 1986 at Anaheim.

In the Army 5-year program, seven general classes or groups of VSS were designed, fabricated, tested, and approved by DDESB for use in hazardous operations with detonating and deflagrating materials. Table I (on the following page) is a summary of the VSS groups with a brief indication of representative applications and level of protection offered. Table II (shown below) is a list of charge parameters for approved shields. Figure 1 (following Table 1) illustrates schematically the general configurations of VSS groups.

Table II. Charge Parameters for Approved VSS

<u>Shield Group</u>	<u>Minimum Sealed Distance (ft/lb 1/3)</u>		<u>Maximum M/V (lb/ft³)</u>
	<u>Wall</u>	<u>Roof</u>	
3	1.63	1.45	0.04157
4	2.23	2.19	0.00762
5	4.14	6.79	0.00215
6A	1.01	N/A	0.2297
6B	1.22	N/A	0.132
Prototype 81mm	3.62	3.21	0.0034
Milan 81mm	4.23	3.75	0.0028

Since the early work on VSS, Shielding Technologies, Inc. (STI) and T&E International (the predecessor of STI) have advanced VSS technology by developing VSS designs and patented improvements in blast suppression and flame resistance. New designs for pyrotechnic operations were developed and reported at the Twenty-Second Explosives Safety Seminar in cooperation with the Naval Ordnance Station at Indian Head, Maryland.

This report concerns new and improved VSS designs for use with detonating materials and explosive devices. The high over pressure and moderately severe fragments hazards of such devices usually require a VSS Group 3 type of design. The original Group 3 VSS has been altered by changes in size and improvements in the design of the roof, liner and method of attaching the ends. The changes are explained in the following section and the report concludes with a summary of key test results.

2. NEW VSS DESIGNS

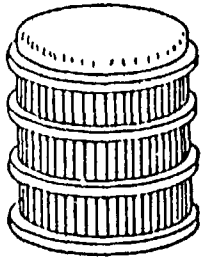
The VSS group 3, as originally designed and tested, was a vertical cylinder of interlocking I-Beams with reinforced concrete roof and foundation bolted to the ends of the vertical cylinder. The test fixture was

Table I: Summary of Suppressive Shield Groups

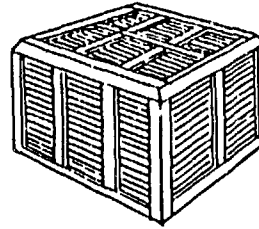
Shield Group	Hazard Parameter Blast	Fragment	Representative Application	Level of Protection*
1	High	Severe	Explosive Melter 2000 lbs plus 2 pour units 250 lbs each.	50% Reduction in blast pressure at intraline distance
2	High	Severe	Explosive bulk, 750 lbs Minute Melter	50% Reduction in blast pressure at at intraline distance.
3	High	Moderate	Explosive bulk, (37 lbs) Detonators, Fuzes	Category I at 6.2 feet from shield**
4	Medium	Severe	Explosive bulk, (9 lbs) Processing ammunition	Category I at 19 feet from shield**
5	Low	Light	30 lbs pyrotechnic, igniter material,	Category I at 3.7 feet from shield**
6	Very high	Light	Laboratory handling and transportation	Category I at 1 foot from shield**
7	Medium	Moderate	Flame/fireball attenuation	Category I at 5 feet from shield**
81 mm	High	Moderate	81 mm Mortar drill/ face and/or cast finishing.	Category I at 3 feet from shield**

* All shield groups contain all fragments.

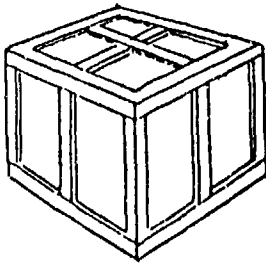
** Category I level of protection refers to blast pressure below the threshold for ear injury and thermal hazard below the threshold for burns on unprotected skin.



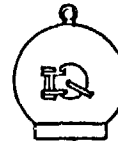
A. Suppressive Shield Groups
1, 2 and 3



B. Suppressive Shield Group
4



C. Suppressive Shield Group
5



D. Suppressive Shield Groups
6A and 6B



E. Suppressive Shield Groups
Prototype 81mm and Milan 81mm

Figure 1: General Configuration of Suppressive Shield Groups

approximately ten feet internal diameter and ten feet internal height. It was tested with a proof charge of 45.7 pounds of 50-50 pentolite (TNT equivalent 51.6 pounds).

STI has designed, fabricated and tested models in approximately 1/8 and 1/64 scale. The 1/8 scale version, designated Model P8605.0, is a horizontal cylinder body about five feet internal diameter and five feet long inside. The 1/64 scale version, Model P8801.0, is 30 inches in diameter and 30 inches long. The ends of these scale model VSS are improved by substituting a double layer of nested steel dished heads for the concrete ends. Each end now consists of two dished heads with resilient epoxy in the space between the two heads. Instead of the bolted connection between the old concrete ends and the cylindrical body, the improved STI design uses a welded connection. The heads are welded to a ring which is welded to the body. The advanced liner design consists of corrugated and flat perforated steel plate layers with copper wire mesh between the steel plates.

A third new design is a scaled up version of the new models except it is a vertical cylinder with double dished head roof and a concrete foundation.

Two proposed applications of the Group 3 VSS include one version about 22 feet in diameter and 22 feet high for explosive processing operations. This unit is for use with quantities of explosive material as large as 310 pounds of TNT equivalent. The other version is a magazine 36 feet in diameter and 36 feet high for 1320 pounds of TNT equivalent.

Table III compares size and operating charge for the six different models:

Table III: Comparison of Group 3 VSS Designs

<u>Model</u>	<u>Application</u>	<u>Normal Size</u>	<u>Operating Charge</u>
P8801.0	EOD	2-1/2 feet	4*
P8605.0	EOD	5	14*
Prototype	Bulk Explosives	10	40
P8934.0	Charge Finishing	14	75
P90140.0	Explosives Processing	22	310 (Proposed)
P90600.0	Magazine	36	1320 (Proposed)

SUMMARY OF KEY TEST RESULTS

VSS Model P8801.0 and Model P8605.0 were tested to verify structural integrity and suppression capability.

1. Results of Testing the Model P8605.0

Table IV on the following page is a summary of the tests and internal overpressure measured with the Model P8605.0.

TABLE IV: SUMMARY OF TESTS AND INTERNAL PRESSURE FOR MODEL P8605.0

Test Number	Charge		Peak Pressure psi*	Duration microsec	Remarks
	Sticks	Kilograms			
I	1	0.24	58.7	250	First Peak
			62.5	250	Second Peak
			53.7	250	Third Peak
II	11	2.62	562.5	300	First Peak
			482.5	250	Second Peak
			425.0	250	Third Peak
III	44	10.50			Chamber blew open, Data invalid.
IV	1	0.24	24.2	350	First Peak
			52.0	500	Second Peak
			34.7	350	Third Peak
V	11	2.62	--	--	Tape saturated No Data
VI	16	3.85	2810	75	
VII	22	5.24	3650	75	
VIII	27	6.52	2990	75	
IX	36	8.79	3870	18.7	Charge orientation changed from trans- verse to axial.

Test number III indicated the assumed TNT equivalency of 50% for the dynamite was in error. Equivalency should be closer to 100%. The unexpectedly high pressure revealed a design deficiency in the door that caused the head to fail. The door was redesigned, the head strengthened, and testing was continued.

Pressure Suppression:

Effectiveness of the Model P8605.0 in suppressing blast overpressure was determined by piezoelectric measurement of transient over-pressure outside the prototype shield with a pencil gage. Paper blast meters were used to obtain an independent rough check on the piezoelectric pencil gage and also the paper blast meters provided data on pressure gradients outside the VSS. The pencil gage was located two meters from the center of the side of the VSS and three

paper blast meters were located at 2, 4, and 6 meters from the center of the side. Two additional paper blast meters were in front of the door at two meters and four meters distance.

Peak overpressure measured from the pencil gage data is tabulated in Table V.

Table V: PEAK SIDE-ON OVERPRESSURE FROM THE PENCIL GAGE, MODEL P8605.0

<u>Test</u> <u>Number</u>	<u>Charge</u> <u>Stick</u>	<u>Kgms</u>	<u>Peak Side-on</u> <u>Overpressure psi</u>
I	1	0.24	0.25
II	11	2.62	3.25*
III	44	10.50	3.56**
IV	1	0.24	0.21
V	11	2.62	0.83
VI	16	3.85	1.01
VII	22	5.24	1.45
VIII	27	6.52	1.66
XI	36	8.79	1.22***

* Interior blast suppression panels opened. The openings were closed with steel plates welded over the openings.

** This is the first peak. Later peaks were as high as 4.5 psi but the container door blew open and these may be unusually high from blast out of the open end.

*** On the last shot, the door frame was cleaned up and the door was jacked into a fully closed position. The charge orientation was changed from tranverse to longitudinal (3 packs of 12 sticks each, end-to-end along the axis of the VSS).

Except for tests numbered II and III, all of the above measured pressures are below 2.3 psi, the threshold for eardrum rupture. On test number II the interior blast panels sprang open and allowed gaseous products of combustion to escape between the gaps in the blast suppression liners. On subsequent tests the gaps were closed by steel plates welded between the blast suppression liners. The design of the blast suppression liners has been changed to allow sufficient flexibility so that the panel numbers can move to respond to the blast, but not open.

Fragment and Flame Suppression:

Fragment and flame suppression is complete as verified by closed circuit TV observation during test and by close examination of high speed motion pictures taken from the front and side of the VSS prototype during the tests. No sign of flame or fragments was detected. Additional verification of fragment suppression was obtained by use of a 8 x 16 foot witness panel placed four meters to the side of the VSS. The witness panels were examined after each test for fragment impact. None were detected on any test.

Structural Response:

Visual inspection, strain data, and measurement of fiducial marks before and after each test indicate no permanent deformation of structural members of the prototype VSS. Structural integrity was maintained.

Conclusions from testing of the Model P8605.0 VSS are as follows:

1. Test data demonstrate that the redesigned prototype Model P8605.0 VSS, with round door and double heads, will:
 - a. Maintain structural integrity and experience no permanent deformation with a proof charge of 36 sticks (19.3 pounds) of 40% super gel dynamite (1x8 inch sticks). (This is the theoretical equivalent of 8.8 kgm of TNT.)
 - b. Reduce hazardous effects of fragments, flame and gas pressure to a safe level by:
 - (1) Reducing an internal shield pressure of 3870 psi to a peak side-on blast overpressure below 2.3 psi at a distance of 2m.
 - (2) Suppressing all flame effects and fragments.
 - (3) Containing all fragments.
2. TNT equivalency of 40% supergel dynamite is a function of charge weight and configuration. It can range from 40% to more than 100% and possibly as great as 250%. Additional testing to make a direct comparison is required for precise values. Future tests should be planned using a TNT equivalency of dynamite at 100%.

2. Results of Testing the Model P8801.0

Objectives of the Model P8801.0 tests were to:

1. Verify by actual test that the Model P8801.0 will maintain structural integrity when subjected to the overpressure, thermal, and fragment impact loads from detonation of:
 - a. A maximum of 10 sticks of dynamite.
 - b. A 5-pound pipe bomb with 1.25 pounds of black powder.
2. Explore the reaction characteristics of contaminated diethyl ether in a 1-gallon can ignited by a primer cord wrapped around the can.
3. Demonstrate empirically that the Model P8801.0 VSS reduces the hazardous effects of fragments, flame and gas pressure to a personnel-safe level.

4. Obtain and record technical data on physical strength, suppression and containment capabilities of VSS with an interlocking I-beam structure with laminated dished heads.
5. Demonstrate performance with 1-1/2 and 3 pounds C-4.

To meet Objective 1, a series of tests shots was planned with increasing quantities of dynamite, followed by a pipe bomb test. Testing was conducted with IRECO 40% "extra gel" dynamite. This type dynamite is in the form of sticks about 1-1/8 inch in diameter and 8 inches long. Each stick weighs about 1/2 pound (slightly less than 1/4 kilogram). The dynamite was selected as a commonly used and readily available explosive material. Previous testing indicated this type of material is roughly equivalent to TNT.

To meet Objective 2, a 1-gallon can of contaminated diethyl ether was double wrapped with a primer cord, placed in the VSS, and the primer cord was detonated. Visual and video coverages were used to determine whether the ether would ignite and burn within the VSS.

Objective 3 was met by recording internal and external blast overpressure data, by temperature data, by video recording of the explosive events, by post test visual examination of the VSS and environment, and by measurement of the fiducial strain references on the outside of the VSS.

A summary of the six tests is tabulated below in Table VI:

TABLE VI: SUMMARY OF TESTS

<u>Test Number</u>	<u>Charge Description</u>
1	3 sticks, dynamite
2	5 sticks, dynamite
3	7 sticks, dynamite
4	10 sticks, dynamite
5	4.5 lb. pipe bomb, 1.25 lb. black powder
6	1 gallon ether, double wrap primer cord
7	1-1/2 pounds C-4
8	3 pounds C-4

Internal Pressure:

Pressure inside the VSS was measured using T-18 crusher gages with a 1/10 square inch piston and aluminum spheres. The T-18 gages were borrowed from the Wright Malta Test Facility, Ballston Spa New York and the aluminum spheres were purchased from the US Army Test and Evaluation Command, Aberdeen Proving Ground, Maryland. Gage number 5845 was placed on the bottom of the VSS approximately 7 inches from the door and gage number 6163 was suspended at center left (9 o'clock position) about 6 inches from the interior wall. Pressure determined from the final height of the spheres is tabulated below in Table VII:

TABLE VII: INTERNAL PRESSURE DATA

Gage 5845 Door		Gage 6163 Center	
<u>Test Number</u>	<u>Pressure</u>	<u>Pressure</u>	<u>Charge</u>
1	830 psi	810 psi	3 sticks
2	1190	1200	5 sticks
3	2320	990	7 sticks
4	2710	1570	10 sticks
5	420	Not used	1.25 lb. b.p.
6,7,8	Pressure not measured		

Internal pressures measured at the door location increase with charge weight in a normal manner. Pressure measured at the center location also increased as expected except for Test Number 3 with seven sticks of dynamite. The pressure of 990 psi seemed low. Differences between pressure at the door and at the center of the VSS are indicative of a charge shape focusing effect.

Pressure Suppression:

Pressure suppression was determined by measurement of the peak reflected overpressure external to the VSS by use of paper blastmeters. Anderson Blasgages were used for this purpose. Data from this series of tests indicated peak reflected overpressure below 1.3 psi at the center side of the VSS at a distance of two meters from the external wall of the VSS. Paper blastmeters at a distance of two meters from the door of the VSS indicated a peak reflected overpressure less than 2.6 psi on the first test shot, less than 1.9 psi on the second test shot, and less than 1.3 psi on all of the other test shots.

Since a peak reflected overpressure of 5 psi is the accepted threshold for ear damage, the pressure suppression for all test shots is considered adequate. This is approximately comparable to the 2.3 psi peak side-on pressure previously measured with piezoelectric pencil gages.

The external pressure measured in the first two test shots indicates gas leakage at the door of the VSS. The measured pressure decreases as the door seats on the rim of the head. Internal pressure forces the door against the ring and indents the steel slightly. After the first two shots, the small indentation in the door appear to act as a seal and block gas leakage to improve pressure suppression and decrease external pressure measured.

Fragment and Flame Suppression:

Fragment and flame suppression was determined by examination of video tapes of the event and by examination of the VSS after the event. Video tapes indicated no fragments or flame. Examination of the VSS after the event indicated no fragments had escaped from the VSS on any of the tests, but residual of sand blasting material used to clean the VSS before painting was blasted out of the interstices of the VSS. The sand blasting material is a corundum type composition which can injure the eyes or exposed skin of personnel near the VSS. Future VSS will not be sand blasted.

It is recommended that personnel who may have to work near a loaded VSS wear protective clothing, face shields, and ear protection.

Structural Response:

After each test, the VSS was examined to determine whether any part of the structure was deformed. Fiduciary marks were measured to determine whether the bands or head were stretched beyond their elastic limit. No signs of loading above the elastic limit or permanent deformation were detected. From the results of the test it is clear that the VSS can be used with a larger charge than that used in these tests. Considering the ten sticks of dynamite as a proof charge for this VSS design, an operational charge of eight sticks or four pounds of 40% supergel dynamite is recommended.

Test data reported herein indicate that the Model P8801.0 VSS will:

1. Maintain structural integrity and experience no permanent deformation with a proof charge of 10 sticks (five pounds) of 40% super gel dynamite (1x8 inch sticks with nominal weight of 1/2 pound each stick). Previous testing indicates this is approximately the equivalent of five pounds of TNT.
2. Reduce hazardous effects of fragments, flame, and gas pressure to safe level by:
 - a. Reducing an internal shield pressure of 2710 psi to a peak reflected blast overpressure below 1.3 psi at a distance of 2m.
 - b. Suppressing all fragment and flame effects.
 - c. Containing all fragments.

A method has to be found to clean the VSS prior to painting without using a material that can be blown out of the interstitial spaces in the VSS and which does not offer a potential for injury of personnel near the VSS.

The Model P8801.0 VSS, as designed, can probably be used with charges significantly larger than those used in these tests. Testing should be planned for some time in the future with quantities of dynamite larger than ten sticks.

The suppressive capability of the VSS is so good that inexperienced observers are not aware of the potential for damage of unsuppressed explosions. Future testing should include provisions for comparative shots of unsuppressed explosions.

A subsequent test with 7 sticks of high energy dynamite revealed cracks in the head welds caused by the C-4 testing. This indicates the need for careful weld inspection after the VSS is subjected to a high blast pressure.

CONCLUSION

VSS is a unique protective barrier that protects against overpressure, fragmentation and fire ball. The STI improvements to the Group 3 design enhance performance of the VSS by increasing the strength of the ends, and improving the suppression capabilities. Scaling laws for VSS technology are verified by successful performance of scale models in testing.

Other applications of VSS technology are viable, and they demonstrate a cost effective safety alternative to other forms of blast protection.

VSS can be used in a variety of new areas to improve personnel safety and facility protection. These include:

- 0 U.S. Embassy Security Program - perimeter and internal walls, VSS rooms, and VSS protection of air ventilation ducts.
- 0 Airport Security - VSS containers for suspected explosives in luggage and in unattended packages.
- 0 Protection of Weapon System Components - a protective container around large rocket sections.
- 0 SDI - protection of critical ground facilities such as free-electron laser structures.
- 0 Storage of Explosives - walls and magazine storage VSS units for reduction of quantity-distance requirements.
- 0 Manufacture of Propellants - barriers to protect personnel and equipment and reduction of quantity-distance requirements.
- 0 Explosive Ordnance Disposal (EOD) - VSS enclosures for the safe disposal of pipe bombs, bulk explosives, dynamite, explosive devices, and fireworks within demolition areas requiring the reduction of blast overpressure fireball and dB levels, specified by municipal regulations.
- 0 Oil Platforms to protect personnel and equipment from flame, blast and fragments in a blow-out or fire.

Application of Risk Assessment Techniques To Evaluate Public Risk and Establish Priorities for Cleanup of Ordnance at Formerly Used Defense Site

Prepared For

**Department of Defense Explosives Safety Board
Twenty-Fourth DoD Explosives Safety Seminar**

28-30 August 1990

By

C. David Douthat, P.E., CSP

**U.S. Army Corps of Engineers
Huntsville Division
Huntsville, Alabama**

BACKGROUND

The Defense Environmental Restoration Program (DERP) is congressionally mandated (Public Law 99-190 and 99-499) and directs the Secretary of Defense to carry out a program of environmental restoration. This mission of environmental restoration has been assigned to the U.S. Army Corps of Engineers (USACE).

The DERP Program allows for the restoration of both active Department of Defense (DOD) sites as well as sites that was formerly used by a DOD component. The program for restoration of active installations is commonly referred to as the Installation Restoration Program (IPR) while the program for restoration of former installations is known as Formerly Used Defense Sites (FUDS).

The DERP goals are (1) to provide for the identification, investigation and cleanup of contamination of hazardous and toxic wastes, (2) to correct other environmental damage which create an imminent and substantial endangerment to the public or the environment, and (3) to dispose of unsafe buildings and structures. The purpose of this paper is to discuss item 2 above with regard to unexploded ordnance on formerly used defense sites.

The Corps of Engineers has been actively establishing a data base of sites meeting the criteria of the DERP-FUDS. That inventory currently stands at over 7,050 sites that fall into the previously mentioned categories of contamination. Of these 7,050 sites, there have been identified 900 formerly used sites that have a high potential for ordnance contamination. With this magnitude of ordnance contaminated sites, it became evident to the USACE, that some mechanisms for evaluating the degree of risk and prioritizing any investigation and remediation effort would be necessary. On 5 April 1990, an execution policy and criteria for evaluating explosive ordnance (EXO) was established. As a part of this policy, a procedure for evaluating public risks was implemented. This paper will discuss the development of this risk assessment procedure, its application to specific projects and application of this procedure to ordnance contamination on other candidate programs.

RISK ASSESSMENT PROCEDURE DEVELOPMENT

In the initial stages of development of a procedure to evaluate levels of ordnance contamination and prioritize remediation, it became evident that real issue was public exposure to EXO. Ordnance, unlike Hazardous and Toxic Wastes (HTW), was generally not mobile, in effect it had no medium such as groundwater for transport (the exceptions being erosion or ocean transport). The public generally had control of their exposure to EXO, in effect if you did not touch or disturb the EXO the risk was minimal.

The AR 385-10 and MIL-STD 882B establish policy and procedures for evaluating the risks associated with the operation of Army and DOD facilities and equipment. This procedure

evaluates the probability of occurrence, as well as the severity of an occurrence. The combination of the two criteria in the form of a risk matrix provide management with a qualitative tool to evaluate the relative risk associated with operation of the particular facility or equipment.

In considering methods for evaluating EXO sites a similarity emerged in that the severity of a mishap was directly related to type of UXO and the probability of a mishap was relevant to the potential for accessibility of the EXO to the public. Applying existing Army and DOD criteria and method to evaluate public risks to EXO would greatly simplify the acceptance of the method plus the method was a proven technique for evaluating risks. The primary differences were (1) that the risks being evaluated were not worker related, they were the general public and (2) the evaluation was not of facilities or equipment but of a piece of land.

HAZARD SEVERITY

In the development of the hazard severity, five general categories of EXO were identified. These categories included (1) conventional ordnance and ammunition (small arms ammunition to bombs), (2) pyrotechniques (incendiary, flares, etc.), (3) bulk high explosives (TNT, HMR, RDX, etc.), (4) propellants (solid and liquid), and (5) chemical agents/weapons (GB, VX, HD, BZ, etc.). Within these 5 categories values were assigned from 0 to 25 based upon the expected hazard associated with public exposure to particular ordnance item. These values were subjective and based upon engineering experience and judgment of the USACE ordnance engineering and explosive safety staff. The Hazard Severity Table is provided by Table A.

TABLE A
HAZARD SEVERITY

Description Value	Category	
	Level	Value
CATASTROPHIC	I	21
CRITICAL	II	13
MARGINAL	III	5
NEGLIGIBLE	IV	5

HAZARD PROBABILITY

The hazard probability addresses area, extent and accessibility of the EXO to the general public. The areas evaluated include (1) location of contamination (surface, subsurface, within pipes or vessels) (2) proximity to inhabited buildings or structures to the EXO site, (3) the number and type of structure (military, child care, hospital etc.), (4) accessibility of site to the

public (i.e., barriers provided), (5) site dynamics that could expose ordnance in the future such as erosion. Within these five categories and subcategories, values were assigned from 0 to 5 based on the potential exposure of the exposure to the EXO. Again these values were based upon sound engineering, experience, and judgment of an ordnance engineering and explosive safety staff. The hazard probability table is provided by Table B.

TABLE B
HAZARD PROBABILITY

Description	Level	Value
FREQUENT	A	≥ 27
PROBABLE	B	$\geq 21 < 27$
OCCASIONAL	C	$\geq 15 < 21$
REMOTE	D	$\geq 8 < 15$
IMPROBABLE	E	< 8

RISK MATRIX

While the probability of occurrence and hazard severity assess the risk to the public, a risk matrix must provide guidance to management on actions or mitigative measures that should be implemented. The risk matrix for EXO was developed to provide environmental managers with environmental remediation recommendation. This Risk Assessment Code (RAC) matrix is shown in Table C. During the initial phases of development of the RAC, 76 EXO sites with good historical information were selected to use as a verification phase for the overall procedure. These 76 sites were independently evaluated using the RAC. Upon completion of this initial assessment, adjustments and refinements were made to better reflect the actual risks of EXO contamination. There was nothing scientific or statistical concerning the verification only practical application of the RAC procedure that has provided a significant level of confidence to the users of the RAC in actual field applications. A summary of RACs for the 76 sites is shown in Table D.

TABLE C

Probability Level		FREQUENT A	PROBABLE B	OCCASIONAL C	REMOTE D	IMPROBABLE E
Severity Category:						
CATASTROPHIC I		1	1	2	3	4
CRITICAL II		1	2	3	4	5
MARGINAL III		2	3	4	4	5
NEGLIGIBLE IV		3	4	4	5	5

RISK ASSESSMENT CODE (RAC)

- RAC 1 Imminent Hazard - Emergency action required to mitigate the hazard or protect personnel (i.e., fencing, physical barrier, guards, etc.).
- RAC 2 Action required to mitigate hazard or protect personnel. Feasibility study is appropriate.
- RAC 3 Action required to evaluate potential threat to personnel. High priority confirmation study is appropriate.
- RAC 4 Action required to evaluate potential threat to personnel. Confirmation study is appropriate.
- RAC 5 No action required.

TABLE D

Risk Assessment for 76 Selected Sites

<u>RAC</u>	<u># SITES</u>
1	1
2	15
3	4
4	43
5	13
	<hr/> 76

APPLICATION OF THE RISK ASSESSMENT PROCEDURE

To assist the reader in understanding the RAC procedure, a project was selected to illustrate the procedure. The reader should understand that an EXO site risk assessment must be based upon documented evidence consisting of record searches, reports of Explosive Ordnance Disposal (EOD) detachment actions, field observations, interviews, and measurements. Any field activities should be made with the assistance of qualified EOD personnel.

The site selected for application of the RAC procedure is Mission Trails Park (MTP) San Diego, California, a portion of the former Camp Elliott Marine Corps Base. The following site description has been extracted from the Inventory Project Report (INPR). Additional information necessary to complete RAC were obtained through site visits.

SITE DESCRIPTION

The former Camp Elliott was operated from 1940 until 1960. In 1960 approximately 13,277 acres of the original 32,000 acres were declared excess. As a result, ownership of the property was transferred to the General Services Administration (GSA). The property was disposed of through land swaps, grants, and sales between 1960 and 1963. A portion of the 13,277 acres, (approximately 2,100 acres), is the subject of this report. The City of San Diego has acquired most of this property and is in the process of acquiring the rest of the property for the Mission Trails Regional Park for a park and recreational area.

Following an initial background review and site visit, the western slopes of Fortuna Mountain were identified as the area of highest contamination. The information for the project area is limited, however, there was a clearance sweep of this area in 1973. The 1973 Explosive Ordnance Clearance Sweep was conducted from 16 October to 30 November 1973. This was a visual surface sweep, a total of 933 ordnance-related items were found.

Additional information was collected from the Feasibility Study of Remedial Action Alternatives for Conventional Explosive Ordnance items on the Former Camp Elliott, San Diego, California Final Draft Engineering Report and Environmental Impact Statement 16 October 1987. The Feasibility Study deals with another area of the former Camp Elliott namely Tierrasanta. Tierrasanta is adjacent to the Mission Trails Regional Park and has had several surface and subsurface sweeps conducted to remove ordnance related items. The most recent sweeps were a direct result of the 1983 accident that killed 2 youths and critically injured one more when a 37mm high explosive projectile that they had found exploded. Both areas, Tierrasanta and Mission Trails Regional Park, were part of a special training center on Camp Elliott. It was in these areas that the Marines conducted artillery and anti-tank training. Information on firing sites was not available. The locations of the actual firing sites are not known but they have been approximated by DeYoung Johnson Group, Inc. (DJG) as shown in Figure 2-16. Using these firing site locations, target areas can be projected to show the areas most likely to have contamination. The western slopes of Fortuna Mountain are within the area most likely to be contaminated.

The San Diego Fire Department in 1984 and 1985 responded to 3 reports of possible ordnance near Fortuna Mountain. A total of 8 military rounds (7 each/75mm armour piercing rounds, 1 each/105mm high explosive) were found. In the Tierrasanta area they responded approximately 81 times and found 393 ordnance related items. This is not a complete list of all the items that have been found. This is merely an example of what was found between 1 January 1984 to 26 April 1984 and 15 July 1985 to 25 September 1985 by the San Diego Fire Department. A completed Risk Assessment for this site is provided by Appendix A.

OTHER CANDIDATE PROGRAMS

The development of this RAC procedure for EXO contamination has been for the formerly used defense sites. The RAC was tailored to evaluate public risks. This RAC procedure has potential for evaluating EXO contamination at other than formerly used sites. These include the active installation programs, the base closure programs, the range modernization program, the overseas base closures as well as the superfund program. Modification to the RAC would have to be done to accommodate the risks to be evaluated. For example on the IRP or range program, public exposure would not generally be of concern where worker safety would. For base closures, public safety is obviously of concern particularly with regard to potential land uses through remediation and returning the property back to functional public use. Superfund generally would not deal with military ordnance but there is always the potential for commercial explosives. All of these programs have the need for some type of procedure to address the risk associated with ordnance contamination and the RAC for FUDS offers great potential.

SUMMARY

The Huntsville Division has been designated as the U.S. Army Corps of Engineers Mandatory Center of Expertise (MCX) and Design Center for Explosive Ordnance Engineering for the Army. With this designation, the Huntsville Division has demonstrated an element of technical capability and experience that is necessary to evaluate and remediate sites contaminated with EXO.

This paper has discussed the history of the DERP-FUDS for unexploded ordnance, the development of the RAC procedure for EXO contamination and application of the RAC to an actual project.

EXO is a safety and environmental hazard that has resulted in unreasonable risks to the general public, contractors, and Army personnel. It is felt that this RAC procedure provides our environmental program managers with the necessary tools to evaluate public risks and make the appropriate decision concerning remediation of EXO contaminated sites. The program manager for EXO at the Huntsville Division is Mr. Robert Wilcox at 205-895-5802. The technical manager is Mr. C. David Douthat at 205-895-5785.

APPENDIX A

RISK ASSESSMENT PROCEDURES FOR EXPLOSIVE ORDNANCE (EXO)

Site Name : Camp Elliott
 Site Location : San Diego, CA
 DERP Project #: JA09CA006702

Rater's Name: Douthat
 Organization: CEHND
 RAC : II-A RAC 2

EXO RISK ASSESSMENT:

This risk assessment procedure was developed in accordance with MIL-STD 882B and AR 385-10.

The EXO risk assessment is based upon documented evidence consisting of records searches, reports of Explosive Ordnance Disposal (EOD) detachment actions, and field observations, interviews, and measurements. These data are used to assess the risk involved based upon the hazards identified at the site. The risk assessment is composed of two factors, hazard severity and hazard probability.

Any field activities should be made with the assistance of qualified EOD personnel.

Part I. Hazard Severity. Hazard severity categories are defined to provide a qualitative measure of the worst credible mishap resulting from personnel exposure to various types and quantities of unexploded ordnance items.

TYPE OF ORDNANCE

A. Conventional Ordnance and Ammunition

	YES VALUE	NO VALUE	VALUE
Small Arms (.22 cal - .50 cal)	2	0	2
Medium/Large Caliber (20 mm and larger)	10	0	10
Bombs, Explosive	10	0	0
Bombs, Practice (w/spotting charges)	6	0	0
Grenades, Hand and Rifle, Explosive	10	0	10
Grenades, Practice (w/spotting charges)	6	0	6

Landmines, Explosive	10	0	0
Landmines, Practice (w/spotting charges)	6	0	0
Rockets, Guided Missiles, Explosive	10	0	10
Detonators, Blasting Caps	10	0	0
Demolition Charges	10	0	0
Conventional Ordnance and Ammunition ORS Value (Maximum of 10).			10

B. Pyrotechnics

	<u>YES</u> VALUE	<u>NO</u> VALUE	VALUE
Any Munition Containing White Phosphorus or other Pyrophoric Material (i.e., Spontaneously Flammable)	10	0	0
Any Munition Containing A Flame or Incendiary Material (i.e., Napalm, Triethylaluminum Metal Incendiaries)	6	0	0
Military Flares	4	0	0
Pyrotechnics Value (Maximum of 10).			0

C. Bulk High Explosives (Bulk explosives not an integral part of conventional ordnance).

	<u>YES</u> VALUE	<u>NO</u> VALUE	VALUE
Primary or Initiating Explosives (Lead Styphnate, Lead Azide, Nitroglycerin, Mercury Azide, Mercury Fulminate, etc.)	10	0	0
Booster, Bursting or Fuse Explosives (PETN, Compositions A, B, C, Tetryl, TNT, RDX, HMX, HBX, Black Powder, etc.)	10	0	0
Military Dynamite	10	0	0
Less Sensitive Explosives (Ammonium Nitrate, Favier	3	0	0

Explosives, etc.)

High Explosives Value
(Maximum value of 10).

0

D. Propellants

	YES VALUE	NO VALUE	VALUE
Solid or Liquid Propellants	6	0	0

E. Chemical Agent/Weapons

	YES VALUE	NO VALUE	VALUE
Radiological	25	0	0
Toxic Chemical Agents (Choking, Nerve, Blood, Blister)	25	0	0
Incapacitating Agent (BZ)	10	0	0
Riot Control and Miscellaneous (Vomiting, Tear, Chlorine, Mustard Simulant)	5	0	0
Any Munition Containing Smoke, Illumination, Signal Charge	4	0	0

Chemical Agent/Weapons Value (Maximum 25). 0

Total Ordnance and Explosive Waste Characteristics Value (Total = 10
A + B + C + D + E with a Maximum value of 61).

TABLE 1
HAZARD SEVERITY

Description	Category	Value
CATASTROPHIC	I	≥21
CRITICAL	II	≥13 <21
MARGINAL	III	≥ <13
NEGLIGIBLE	IV	< 5

* Apply Hazard Severity to Table 3.

Part II. Hazard Probability. The probability that a hazard has been or will be created due to the presence and other rated factors of unexploded ordnance or explosive materials on a formerly used DoD site.

AREA, EXTENT, ACCESSIBILITY OF CONTAMINATION

A. Locations of Contamination

	YES VALUE	NO VALUE	VALUE
Within Tanks, Pipes, Vessels or Other confined locations.	5	0	0
On the surface or within 3 feet.	5	0	5
Inside walls, ceilings, or other parts of Buildings or Structures.	4	0	0
Subsurface, greater than 3 feet in depth.	3	0	3

Value for location of UXO. (Maximum
Value of 5).

5

B. Distance to nearest inhabited locations or structures likely to be at risk from EXO site (roads, parks, playgrounds, and buildings).

Distance to Nearest Target

	VALUE	
Less than 1250 feet	5	
1250 feet to 0.5 miles	4	
0.5 miles to 1.0 mile	3	
1.0 mile to 2.0 miles	2	
2.0 miles to 5.0 miles	1	
Over 5.0 miles	0	
Distance to Persons Value (Maximum Value of 5).		5

C. Numbers and types of Buildings within a 2 mile radius measured from the hazardous area, not the installation boundary.

Number of Buildings	VALUE	
0	0	
1 to 10	1	
11 to 50	2	
51 to 100	3	
101 to 250	4	
251 or Over	5	
Number of Buildings Value (Maximum Value of 5).		5

D. Types of Buildings

	VALUE
Educational, Child Care, etc.	5
Residential, Hospitals, Hotels, etc.	5
Commercial, Shopping Centers, etc.	5
Industrial Warehouse, etc.	4

Agricultural, Forestry, etc.	3	
Detention, Correctional	2	
Military	1	
No Buildings	0	
Types of Buildings Value (Maximum Value of 5).		5

E. Accessibility to site refers to the measures taken to limit access by humans or animals to ordnance and explosive wastes. Use the following guidance:

Barrier	Assigned Value
A 24-hour surveillance system (e.g., television monitoring or surveillance by guards or facility personnel) which continuously monitors and controls entry onto the facility;	0

or

Barrier	Assigned Value
An artificial or natural barrier (e.g., a fence combined with a cliff), which completely surrounds the facility; and a means to control entry, at all times, through the gates or other entrances to the facility (e.g., an attendant, television monitors, locked entrances, or controlled roadway access to the facility).	0
Security guard, but no barrier	1
A barrier, (any kind of fence) but no separate means to control entry	2
Barriers do not completely surround the facility	3
No barrier or security system	5
Accessibility Value (Maximum Value of 5).	

F. Site Dynamics - This deals with site conditions that are subject to change in the future, but may be stable at the present. Examples would be excessive soil erosion by beaches or streams, increasing land development that could reduce distances from the site to inhabited areas or otherwise increase accessibility.

	VALUE	
None Anticipated	0	
Expected	5	
(Maximum Value of 5)		5
Total value for hazard probability.		
Sum of Values A through F.		30
(Not to exceed 30). Apply this value to Hazard Probability Table 2 to determine Hazard Level.		

TABLE 2
HAZARD PROBABILITY

Description	Level	Value
FREQUENT	A	≥27
PROBABLE	B	≥21 <27
OCCASIONAL	C	≥15 <21
REMOTE	D	≥ 8 <15
IMPROBABLE	E	<8

* Apply Hazard Probability to Table 3.

Part III. Risk Assessment. The risk assessment value for this site is determined using the following Table 3. Enter with the results of the hazard probability and hazard severity values.

TABLES 1 AND 2

HAZARD SEVERITY - III
(from Table 1)

HAZARD PROBABILITY- A
(from Table 2)

TABLE 3

Probability Level		FREQUENT A	PROBABLE B	OCCASIONAL C	REMOTE D	IMPROBABLE E
Severity Category:						
CATASTROPHIC	I	1	1	2	3	4
CRITICAL	II	1	2	3	4	5
MARGINAL	III	2	3	4	4	5
NEGLIGIBLE	IV	3	4	4	5	5

RISK ASSESSMENT CODE (RAC)

- RAC 1 Imminent Hazard - Emergency action required to mitigate the hazard or protect personnel (i.e., Fencing, physical barrier, guards, etc.).
- RAC 2 Action required to mitigate hazard or protect personnel. Feasibility study is appropriate.
- RAC 3 Action required to evaluate potential threat to personnel. High priority confirmation study is appropriate.
- RAC 4 Action required to evaluate potential threat to personnel. Confirmation study is appropriate.
- RAC 5 No action required.

Justification. In narrative form, summarize the documented evidence that supports this risk assessment.

**Remediation of Ordnance Contamination
Tierrasanta Community
San Diego, California**

Prepared For

**Department of Defense Explosives Safety Board
Twenty-Fourth DoD Explosives Safety Seminar**

28-30 August 1990

by

William A. Chaffin, P.E.

**U.S. Army Corps of Engineers
Huntsville Division
Huntsville, Alabama**

BACKGROUND

The decontamination of formerly used military-related training sites which still contain unexploded ordnance is becoming a matter of increasing concern to the public, such as the site of Tierrasanta Community, San Diego, California.

As previously presented, the Huntsville Division, Corps of Engineers (CEHND), has been given responsibility for remediation of Formerly Used Defense Sites contaminated with explosive ordnance. This presentation describes the development of our first remediation project under this program. The Tierrasanta site is typical of a former military training site which has developed into an ordnance remediation project. (See Figure 1)

During the first World War some of the Tierrasanta site was used by the U.S. Army as artillery and machinegun ranges. No structures remained after demobilization and real estate records do not document land use. In the 1930's the Marine Corps leased over 19,000 acres for training. After World War II broke out in Europe, it was expanded into a Marine Corps Training Center and designated Camp Elliott. Weapons training by the Marines ranged from .22 caliber rifles to 155mm field artillery. Figure 2 is a list of items found during the Feasibility Study. Figure 3 shows the range of U.S. Ordnance and why such a large area is contaminated.

In 1944, the Marines relocated to Camp Pendleton and control of Camp Elliott was turned over to the Navy. Various military units used Camp Elliott but no weapons training was conducted. In 1960, Camp Elliott was closed and annexed by the City of San Diego. In 1962, the General Services Administration (GSA) began selling portions of the former Camp Elliott for civilian uses. Parcels of land were sold over a several year period.

Several surface clearance operations were conducted to remove unexploded ordnance items. One was accomplished by the Navy in 1964, a second in 1965 by the Marine Corps and a third by the U.S. Army in 1973.

In 1970, the subdivision of Tierrasanta was formally opened and approximately 1200 single family homes were sold in a few months. Over 6000 homes have been build on the site since then. In December 1983, two young boys of the Tierrasanta Community were killed and a third was seriously injured when a 37mm shell they had found exploded.

PROJECT ASSIGNMENT

The sequence of events from a tragedy to an ordnance clearance project was as follows:

10 Dec 83 Two boys killed by exploding 37mm shell.

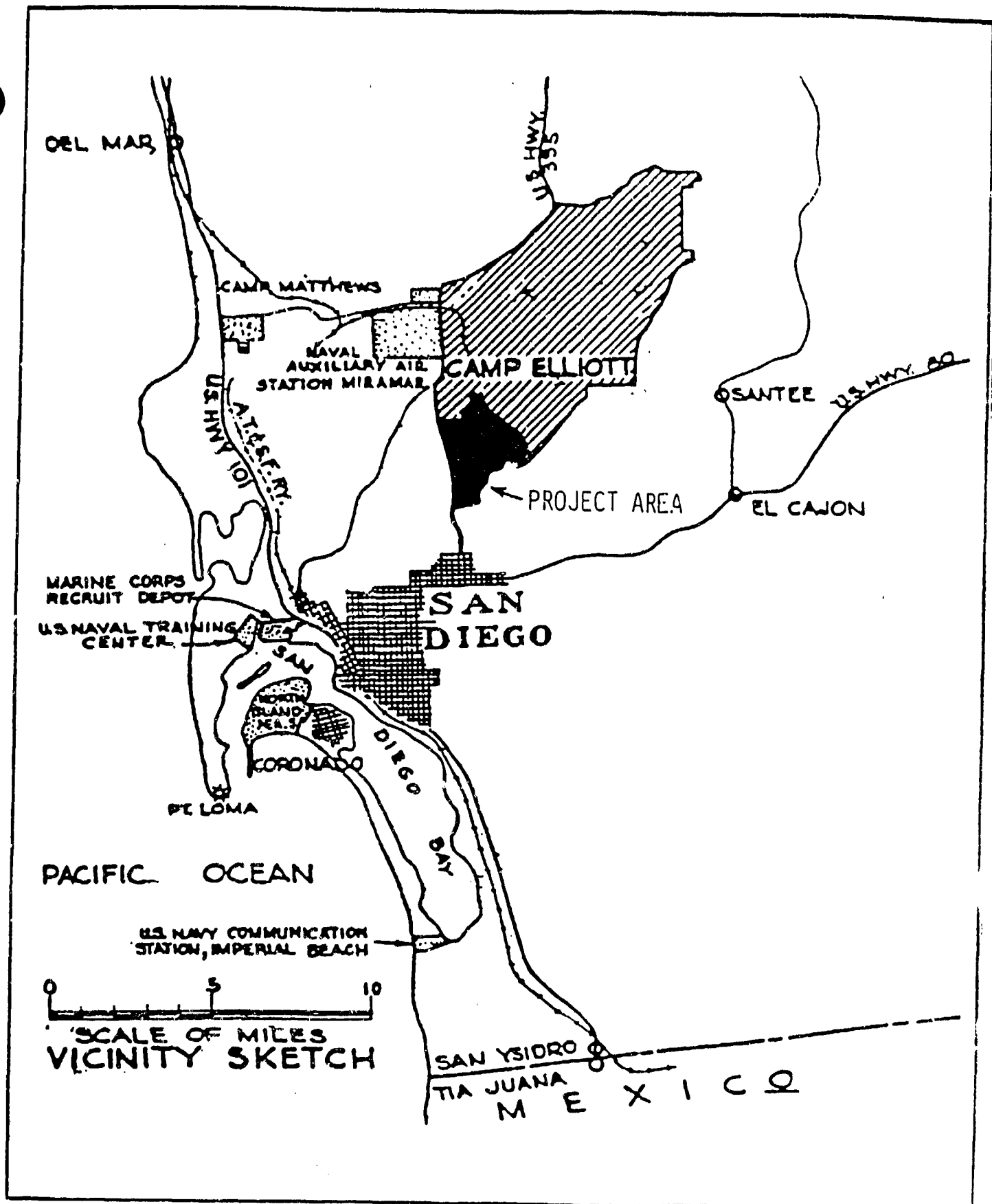


Figure 1
Project Location

ITEM TYPE	TOT	SUBAREAS				
		A	B	C	E	F
Fragments	954	94	30	585	77	168
Ordnance Clips	231	41	10	131	6	43
Associated Belt Links (7.62, 30, 50)	147		10	137		
Shotgun Shells	116	22		28	40	26
5.56-Cal Cartridges	110	33		44	9	24
22-Cal Cartridges	100			1	95	4
Assorted Slugs (2.23, 5.56, 30, 45, 50, 308, lead)	51	6		8	8	29
7.62 Cartridges	42			42		
M48 Fuzes	16			8		8
81-MM Mortars	13					13
75-MM Projectiles	12	1		4	4	3
Nose Caps	11			3	2	6
3" Projectiles	8	1		4	2	1
M1907 Fuzes	6			6		
Lead Balls	5				5	
30-Cal Cartridges	5					5
Fuzes (Unknown types + stems)	5	4		1		
60-MM Mortars	5					5
Tracers	3					3
Grenade Spoons	3			3		
Base Plugs	3	1		1		1
3" Base Plates	2			2		
Mk 11 Mod 9 (37-MM)	2			2		
6" Projectiles	2				2	
M-2 Antipersonnel	2				2	
45-Cal Cartridges	2			1		1
105-MM Projectiles	2				2	
Mk 23 Practice Bombs	1				1	
Primer	1	1				
M38 Fuze	1	1				
50-Cal Cartridge	1					1
TOTAL	1864	205	50	1013	255	341

Figure 2

- A. U.S. 81 MM MORTAR
- B. U.S. 37 MM ANTI TANK GUN
- C. U.S. 105 MM HOWITZER
- D. U.S. 155 MM HOWITZER

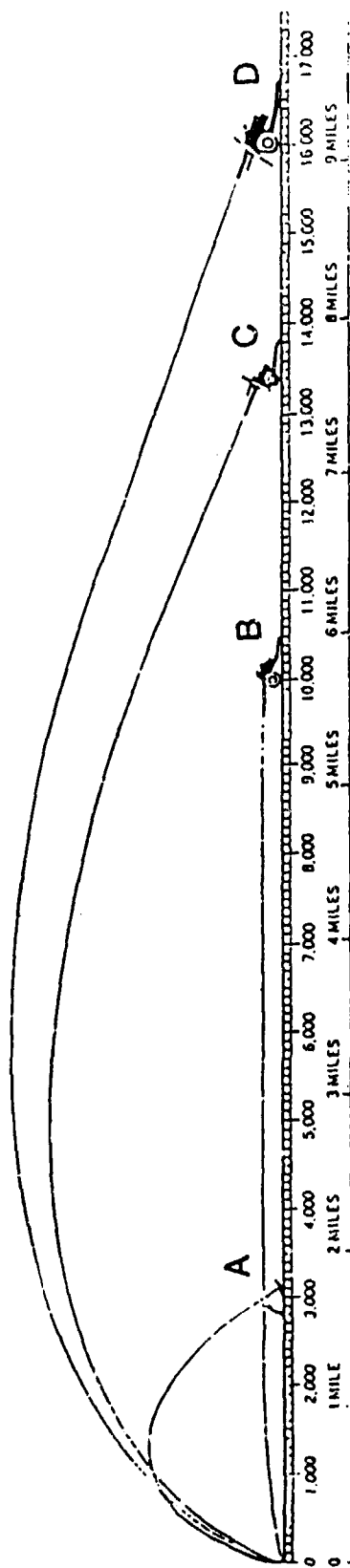


Figure 3

26 Feb 85	HQUSACE directs CEHND to conduct site survey of Former Camp Elliott.
Apr 85	Site survey by CEHND and Los Angeles District.
17 Sep 85	Former Camp Elliott determined to be eligible for remediation under Defense Environmental Restoration Program - Formerly Used Defense Sites (DERP-FUDS).
26 Oct 85	HQUSACE directs CEHND to prepare feasibility study to remediate ordnance problem.
28 Feb 86	Approval of project plan.
Apr-Jun 86	Site visits and public meetings.
Jun-Jul 86	Scope of Work completed and selection of A-E.
25 Sep 86	Proposal of A-E completed and contract awarded.
14 Nov-19 Dec 86	Surface and subsurface ordnance sweeps by A-E and subcontractors.
29 Apr 87	Public workshop in Tierrasanta Community. Presented alternatives and received comments.
6 Nov 87	Draft FS and EIS to EPA.
3 Dec 87	Public hearing on FS/EIS.
6 Jun 88	Final FS/EIS to EPA.
5 Aug 88	Draft Scope of Work and Acquisition Plan drafted.
19 Aug 88	Record of Decision signed by Deputy Assistant Secretary of Defense (Environment).
15 Sep 88	CBD announcement published.
21 Oct 88	Selection Board - A-E selected.
20 Jan 89	A-E Design and Price Proposal received (3 times the Government Estimate).

9 Mar 89	Revised proposal received.
3-24 Mar 89	Negotiated with A-E to impasse.
5 Apr 89	Began design inhouse. Los Angeles District to provide aerial survey and photogrammetry. Navy property added to project.
Feb-Mar 90	Design completed. Environmental Assessment for Navy property received
28 Mar 90	Advertised in CBD.
10 Apr 90	Pre-Bid Conference in San Diego.
8 May 90	Bids opened at CEHND.
9 May 90	Protest received from unsuccessful bidder.
Present	Awaiting decision on protest. Low bidder attempts to adjust bid due to error.

DEVELOPMENT OF DESIGN

The design of the ordnance removal project became more complicated as it progressed. The decision had been made early in the design phase to have a construction contract. So the design had to be in sufficient detail that a contractor could submit a fixed-price bid. Drawings were developed to describe the terrain, brush types, and types of brush clearing requirements in great detail (See Table 1). Estimates were also made on quantities of ordnance, ordnance-related debris and nonordnance-related debris were contained in each area. All metal debris had to be removed to reduce interference with the ordnance locator.

Environmental constraints were a big consideration in the design. The six subareas required brush clearing with exception of one (See Table 2). Some brush clearing could be done by controlled burning, but only at certain times of the year. Some areas had vernal pools where the mesa mint grows. The mesa mint is on the Federal Endangered Species List. The habitat of the black-tailed gnatcatcher had to be treated as a seasonal project. Labor categories included not only laborers and ordnance specialists, but a biologist and archaeologist as well.

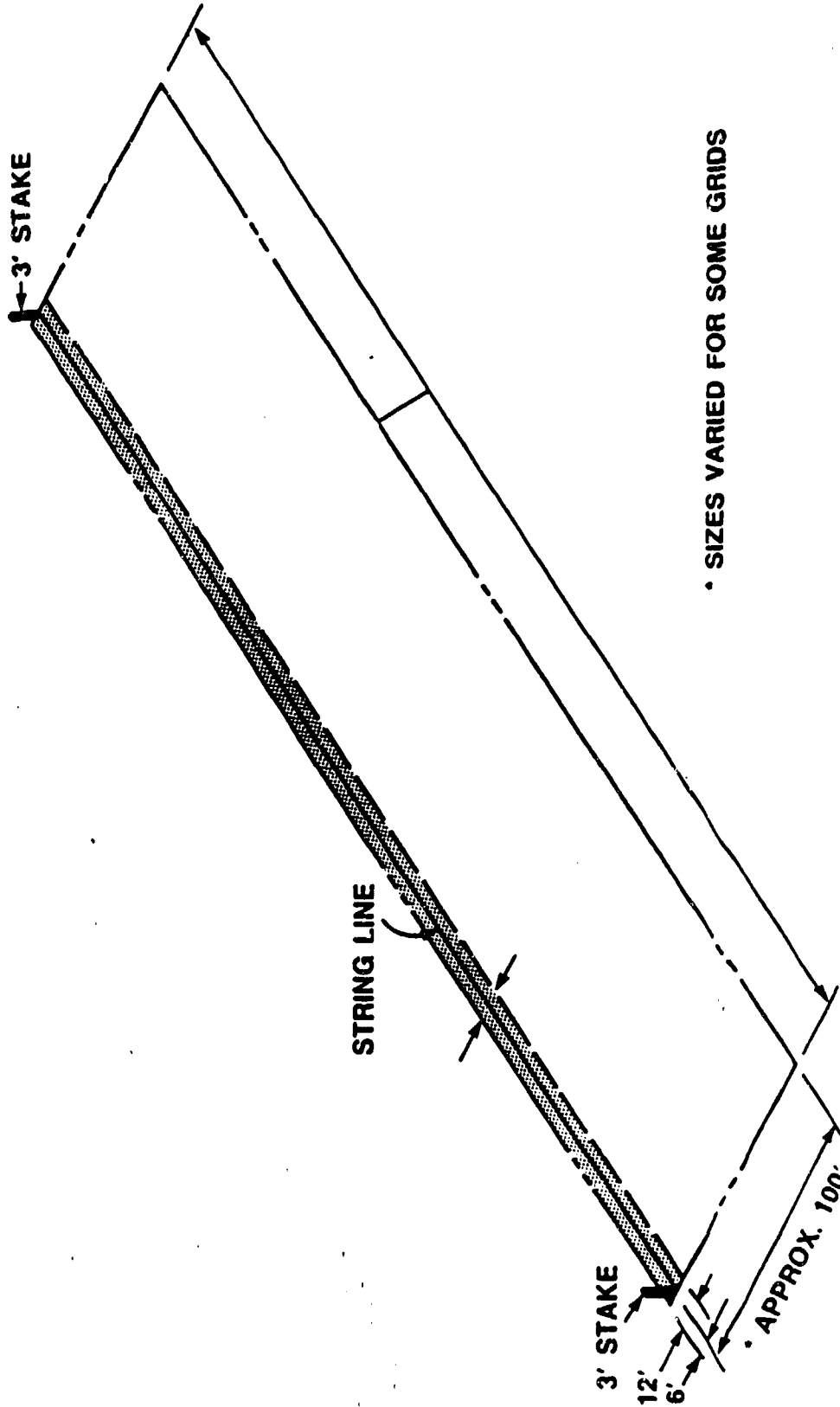
The ordnance clearance operation was almost as difficult to define. Parameters for searching, excavation, live ordnance versus scrap and staging of live ordnance had to be described in enough detail to obtain a fixed-price bid. Figure 4 shows a sample grid designed to ensure coverage of the entire area with ordnance locators.

TABLE 1

<u>Terrain Type</u>	<u>Vegetation</u>	<u>Slope</u>
1	Clear	Level - 0 -10 degrees
2	Grassy/Brushy	Level - 0- 10 degrees
3	Brushy/Trees	Level - 0 -10 degrees
4	Clear	Moderately Sloped 10-30 degrees
5	Grassy/Brushy	Moderately Sloped 10-30 degrees
6	Brushy/Trees	Moderately Sloped 10-30 degrees
7	Clear	Steep-Greater than 30 degrees
8	Grassy/Brushy	Steep-Greater than 30 degrees
9	Brushy/Trees	Steep-Greater than 30 degrees

TABLE 2

<u>Subarea</u>	<u>Size(Acres)</u>	<u>Options</u>
A	167	1. Reacquire by Government 2. Manual Brush Clearing 3. Fence
B	85	1. Manual Brush Clearing 2. Fence - Hwy Right-of-Way
C	358	1. Manual Brush Clearing 2. Ordnance Sweep
D	58	1. No Action-Portion being Developed 2. Ordnance Removal in Remainder
E	454	1. Control Burning 2. Manual Brush Clearing 3. Ordnance Sweep
F	774	1. Manual Brush Removal 2. Ordnance Sweep



SAMPLE GRID LAYOUT

EXPLOSIVE ORDNANCE SURVEY

TERRASANTA COMMUNITY

SAN DIEGO CALIFORNIA

Figure 4

LESSONS LEARNED

a. Construction contract is probably not the best type of contract for this activity. There are too many variables to define with the necessary detail to support a fixed-price bid. A contract for Time Materials or Costs plus fee would be more appropriate.

b. Quality Control is very difficult to define on a project where 100% accuracy can never be guaranteed. CEHND will have an ordnance removal team for quality assurance. Acceptance will be based on a resurvey of some work areas and a field judgment of the contractor's diligence.

c. Future projects do not require a Remedial Investigation/Feasibility Study (RI/FS). When a project is assigned, an Engineering Evaluation and Cost Analysis (EE/CA) will be performed and go to contract. Must comply with the Comprehensive Environmental Response, Compensation, and Liability Act (CERCLA) but do not require EPA approval prior to a project.

CONTRACT STATUS

The design was completed in March 1990 and was advertised in the Chicago Business Daily (CBD). A pre-bid conference was held in San Diego to allow potential bidders to ask questions and have them answered in a group setting. Bids were opened at Huntsville Division on 8 May 1990. There was a wide disparity in the bids received. The bids ranged from approximately one-half the government estimate to four times the government estimate. One bidder lodged two protests. The apparent low bidder was subjected to a qualification audit due to concerns about their ability to perform the contract. The apparent low bidder also alleged an error in the bid and requested an adjustment. We are awaiting decisions on these issues from Headquarters, Corps of Engineers. CEHND has recommended all the allegations be rejected.

I had hoped to be able to present a successful conclusion to this project development. I had planned to have slides showing personnel searching with ordnance locators and digging with excavating tools. Hopefully this will be a short delay and we can begin to remediate this ordnance hazard soon.

**Overview of the
Mandatory Center of Expertise
and
Design Center for Explosive Ordnance
Engineering**

**Prepared For
Department of Defense Explosives Safety Board
Twenty-Fourth DoD Explosives Safety Seminar
28-30 August 1990**

**by
Robert G. Wilcox, MCX Manager
U.S. Army Corps of Engineers
Huntsville Division
Huntsville, Alabama**

ABSTRACT

Overview of the Mandatory Center of Expertise

and

Design Center for Explosive Ordnance Engineering

On 5 April 1990, HQUSACE established Huntsville Division Corps of Engineers as the Mandatory Center of Expertise (MCX) and Design Center for Explosive Ordnance Engineering to respond to formerly used and active Defense sites which are contaminated with explosive ordnance. This paper provides descriptive overview of the mission including: What is explosive ordnance? - What is explosive ordnance engineering? - What is the MCX? - What is the Design Center and how will it function? - How big is the mission?

WHAT IS EXPLOSIVE ORDNANCE?

The use of explosive shells in warfare predates the Revolutionary War. Occasionally dangerous pieces of ordnance are still found on old Civil War battlegrounds. These shells are as potentially lethal as the day they were manufactured.

As technology progressed since that time, the human race has sought better ordnance to gain advantages over adversaries. This required facilities for research, development, manufacture, testing, storage, transportation, and disposal of new weapons, and areas for training with new and improved weaponry. All of these activities resulted in lands being contaminated with unexploded ordnance, military chemicals, and explosive waste (explosive ordnance per AR75-14).

In 1986 Congress decided that explosive ordnance is a form of contamination that should be regulated under the Comprehensive Environmental Restoration and Compensation Liability Act (CERCLA). Chapter 160 of the Superfund Amendments and Reauthorization Act amended CERCLA and established the Defense Environmental Restoration Program (DERP). The program goals for DERP are:

- a. The identification, investigation, research and development, and cleanup of contamination from hazardous substances, pollutants, and contaminants.
- b. Correction of environmental damage (such as detection and disposal of unexploded ordnance) which creates an imminent and substantial endangerment to the public health or welfare or to the environment.
- c. Demolition and removal of unsafe buildings and structures, including buildings and structures of the Department of Defense at sites formerly used by or under the jurisdiction of the Secretary.

These goals gave rise to three Corps of Engineers Missions: Hazardous and Toxic Waste (HTW), The Explosive Ordnance Engineering, and the Unsafe Debris.

The Secretary of Defense has the responsibility to carry out CERCLA response actions for releases of hazardous substances at:

- a. Each facility or site owned by, leased to, or otherwise possessed by the United States and under the jurisdiction of the Secretary.
- b. Each facility or site which was under the jurisdiction of the Secretary and owned by, leased to, or otherwise possessed by the United States at the time of actions leading to contamination by hazardous substances.
- c. Each vessel owned or operated by the Department of Defense.

DoD's response to a., above, is embodied in the Installation Restoration Program. The Formerly Used Defense Sites Program corresponds to b., above. CERCLA response action is required at any site currently or formerly used by the Department of Defense that is contaminated by hazardous or toxic waste, explosive ordnance, or unsafe debris.

Explosive ordnance is anything designed to damage personnel or materiel through explosive force, incendiary action, toxic effects. A policy letter dated 5 April 1990 from HQUSACE defines explosive ordnance as: bombs and warheads; guided and ballistic missiles, artillery, mortar, and rocket ammunition, small arms ammunition, antipersonnel and antitank land mines, demolition charges, pyrotechnics, grenades, torpedoes and depth charges, containerized or uncontainerized high explosives and propellants, nuclear materials, chemical, and radiological agents, and all similar or related items or components explosive in nature or otherwise designed to cause damage to personnel or materiel. Soils with explosive constituents will be considered explosive ordnance if the concentration is sufficient to present an imminent safety hazard.

Explosive ordnance, given exposure to people, usually provides an imminent or substantial endangerment to the public or to the environment. Congress has decided that the DoD should clean it up.

There is a tendency to associate CERCLA response actions with hazardous and toxic waste. However, there are three separate and distinct goals under DERP. They are not equivalent. They are not hierarchical in that explosive ordnance and unsafe debris are not subsets of HTW. Each type of contamination has negative impacts, but they are very different. There is a tendency to think of explosive ordnance as a type of very reactive hazardous waste. This notion is misleading and results in programmatic waste and inefficiencies. No one appears to lump unsafe debris with HTW. Why then, would one assume explosive ordnance is a form of HTW just because it is regulated under CERCLA?

The fundamental differences between HTW and explosive ordnance are discussed below:

Mobility

Hazardous and toxic waste is generally mobile, moving through the environment via many pathways: ground water, surface water, air paths and direct contact. Some forms of HTW will bioaccumulate and attack human welfare through food chain routes.

Explosive ordnance is basically non-mobile. Only the direct contact route is pertinent to explosive ordnance.

Targets

HTW attacks the welfare of anyone who: drinks, swims, bathes, or eats meat or vegetables irrigated with contaminated water. HTW can effect people who breathe air in the vicinity of

a contaminated site and HTW can effect people who use the site through dermal contact. In general, HTW casts a broad net for far ranging target populations.

Explosive ordnance on the other hand, requires nearly direct personal contact on the site to produce harm.

Negative Effects

In general, HTW produces long term health effects which are population significant. The dynamics of exposure pathways, dose/response characteristics of individuals, interactions of exposures with carcinogenic, and other necrotic stimuli from industrial and domestic origins make it difficult to establish clear cause/effect relationships for the individual. However, the pervasive nature of this contamination and statistical assessments make it very clear that the effects of HTW are a serious national concern.

Explosive ordnance leaves no doubt about cause/effect in the case of an accident. It really doesn't matter if you're over weight or a heavy smoker. A mishap involving explosive ordnance can cause immediate death or injury.

Control

An individual's control over HTW exposure is nonexistent. Even a trained professional does not carry out normal day-to-day activities on guard against inadvertent exposures. The paths of exposure are too related to survival needs of the individuals to control potential exposures.

Explosive ordnance on the other hand, does not relate itself to survival needs such as eating, drinking, and breathing. It does however, arouse curiosity. In children this can be lethal, but it is controllable in adults. Explosive-ordnance- contaminated land, if properly managed, can be productive and provide no threat to human welfare without extensive remediation.

Administrative

The USEPA is unquestionably the lead agency regulating an HTW site. They have promulgated regulations, delegated authority to the states and retained certain authorities.

DOD is the recognized national expert in matters relating to the safe handling and disposition of military munitions and ordnance. DOD and Army regulations governing transportation, storage, maintenance, inspections, safety, and security in handling of military munitions and ordnance are very stringent and provide maximum protection for personnel and the environment. Furthermore, Section 300.120(C) of the Final National Contingency

Plan states that DoD is the removal response authority for incidents involving military weapons and munitions. The USEPA has concurred in the preparation of AR200-1 which requires that clearance of conventional ordnance from private lands be conducted under Ammunition and Explosives Safety Standards (AR385-64).

Overlapping Areas of Concern

Soil that is contaminated with explosives provides the most significant area of overlapping concern. Explosives are dangerous at high concentrations in soil. Figure 1 provides a theoretical way to differentiate an HTW project from an explosive ordnance project. Nitro Aromatics will usually fail the Bureau of Mines Gap Test at approximately 10% by weight in soil. This would correspond to providing an imminent and substantial endangerment as referenced under the second Goal of DERP. Safety concerns would extend to approximately .1% by weight because sampling techniques cannot assure a representative sample. At concentrations below that the explosives are typical HTW compounds that produce long term health effects. Primary explosives (ie. lead azide) are extremely dangerous and may propagate in soil at almost any detectable concentration. The problem with this approach is that the type of study will not be determined until the study is underway. The initiating problems will be the determining factor i.e., if the study is in response to a contaminated well or regulatory pressure under RCRA or CERCLA it will be an HTW study. If it is in response to neighborhood children playing with the little red rocks that just happen to be flammable, it will be an explosive ordnance project. Under either scenario, the other component of the contamination must not be ignored.

WHAT IS EXPLOSIVE ORDNANCE ENGINEERING?

The Explosive Ordnance Mission has two major objectives:

- a. To reduce risk to the general public through CERCLA response actions for sites contaminated with explosive ordnance.
- b. To execute response actions for sites contaminated with explosive ordnance with minimum risk to government personnel and contractors.

Explosive Ordnance Engineering is interdisciplinary planning, study, design, and remedial action involving explosive ordnance contamination in accordance with CERCLA and the National Contingency Plan. Various reports which facilitate programmatic planning require engineering and other professional disciplines. These reports are - Site inspections, engineering reports (remedial investigations), feasibility studies, engineering evaluations, and cost analysis, miscellaneous route surveys, and others.

Explosive ordnance engineering is not explosive ordnance disposal. The MCX is not an alternate national bomb squad. Required disposal activities will be carried out with FORSCOM Explosive Ordnance Disposal resources or contract services.

WHAT IS A DESIGN CENTER?

As Design Center, Huntsville Division will centrally manage the Explosive Ordnance Engineering Mission for the Formerly Used Defense Sites Program. Initially, projects will be executed at Huntsville Division. As the mission grows, proposals will be considered from the geographic Divisions to nominate explosive ordnance design districts. Decentralization of the execution is envisioned in the long term.

WHAT IS AN MCX?

An MCX is an element within the Corps of Engineers with demonstrated technical capability in a specialized area which must be utilized by other Corps field offices. It is inefficient to develop capabilities at all Field Operating Activities (FOA) therefore, a center of expertise was established to focus the existing expertise within the Corps of Engineers. The MCX was established by HQUSACE to respond to the Department of the Army's responsibilities in executing projects at sites contaminated with explosive ordnance. Huntsville was selected because of experience with remedial response at several sites contaminated with explosive ordnance. Although Huntsville Division is the only MCX, other agencies will have major roles in this program. If agreements can be reached Missouri River Division, the Toxic and Hazardous Materials Agency and the Navy Technical Center for Explosive Ordnance Disposal will be other major players. Huntsville Division will provide the focal point for the existing expertise and serve to disseminate expertise to the FOAs supporting the DERP.

HOW LARGE IS THIS PROGRAM?

A key word search was conducted on the DERP - FUDS data base (Currently, 7,050 suspected former military sites are in that data base) to locate former DoD sites that are potentially contaminated with explosive ordnance. The key words used were "range", "bomb", "artillery" and others. Huntsville Division identified 941 potential sites. It must be mentioned that many sites that are potentially contaminated give no clues to that effect in the site name. Many sites have not been identified to the original data base. Contamination has been discovered on some sites that have been evaluated and determined that the site was ineligible for DERP funding based on field studies and record searches. All of these situations have occurred after the search was conducted. It serves to provide little confidence that the total program scope is before us at this time.

These sites have a very high probability that some remedial action will be necessary. Although most sites were swept and disposed of with restricted use provisions in the deeds, many sites of former military activity have been developed into subdivisions, parks, and colleges. This type of development provides a higher risk of fatal exposures to explosive ordnance. Remedial actions at these sites could easily cost several BILLION dollars.

Other programs will need the services of the the MCX and Design Center for Explosive Ordnance Engineering. Among them are the Installation Restoration Program and Base Closures. At this time there is no estimate of the scope of those programs. It is sufficient to say that we have a very large task ahead of us and we will need a lot of help from the safety professionals of the Department of Defense.

EXO AND HTW CONTAMINATION IN SOIL

*OTHER EXPLOSIVES WILL FAIL GAP TEST AT DIFFERENT CONCENTRATIONS. HOWEVER, THE CONCEPT REMAINS VALID.

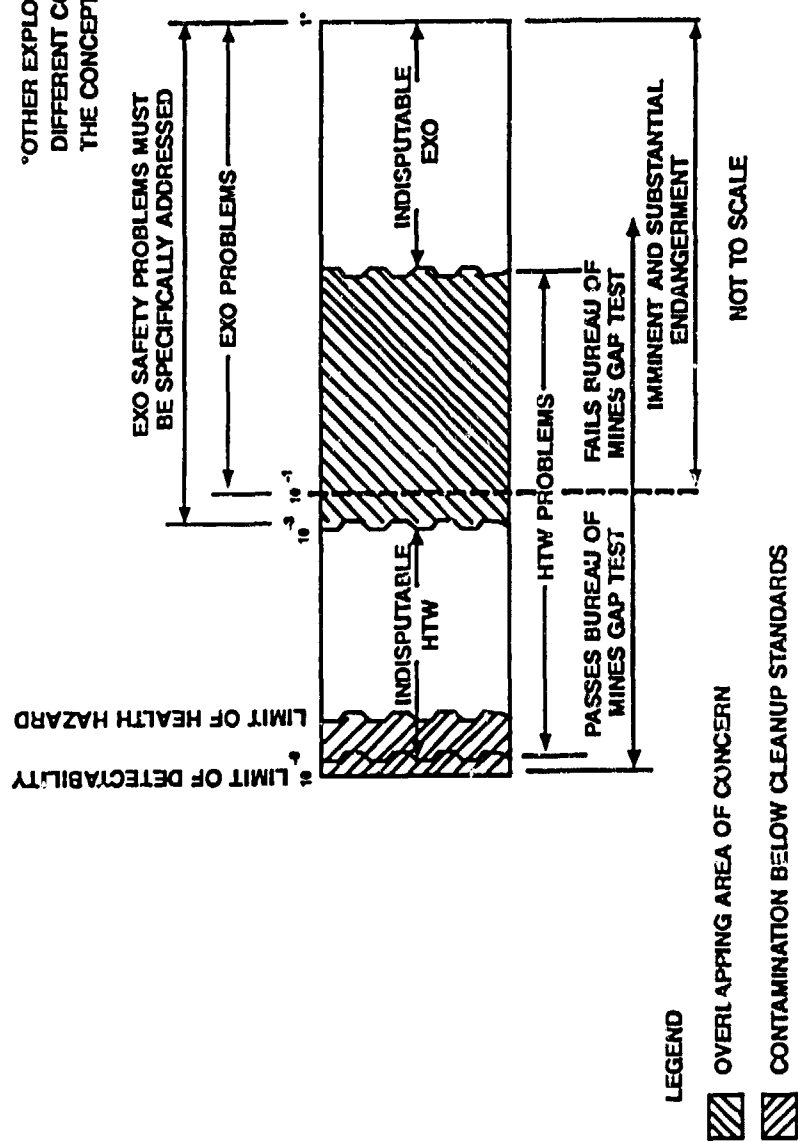


FIGURE 1

EXPLOSIVE ORDNANCE ENGINEERING

GEOGRAPHIC DISTRIBUTION

DERP - FUDS

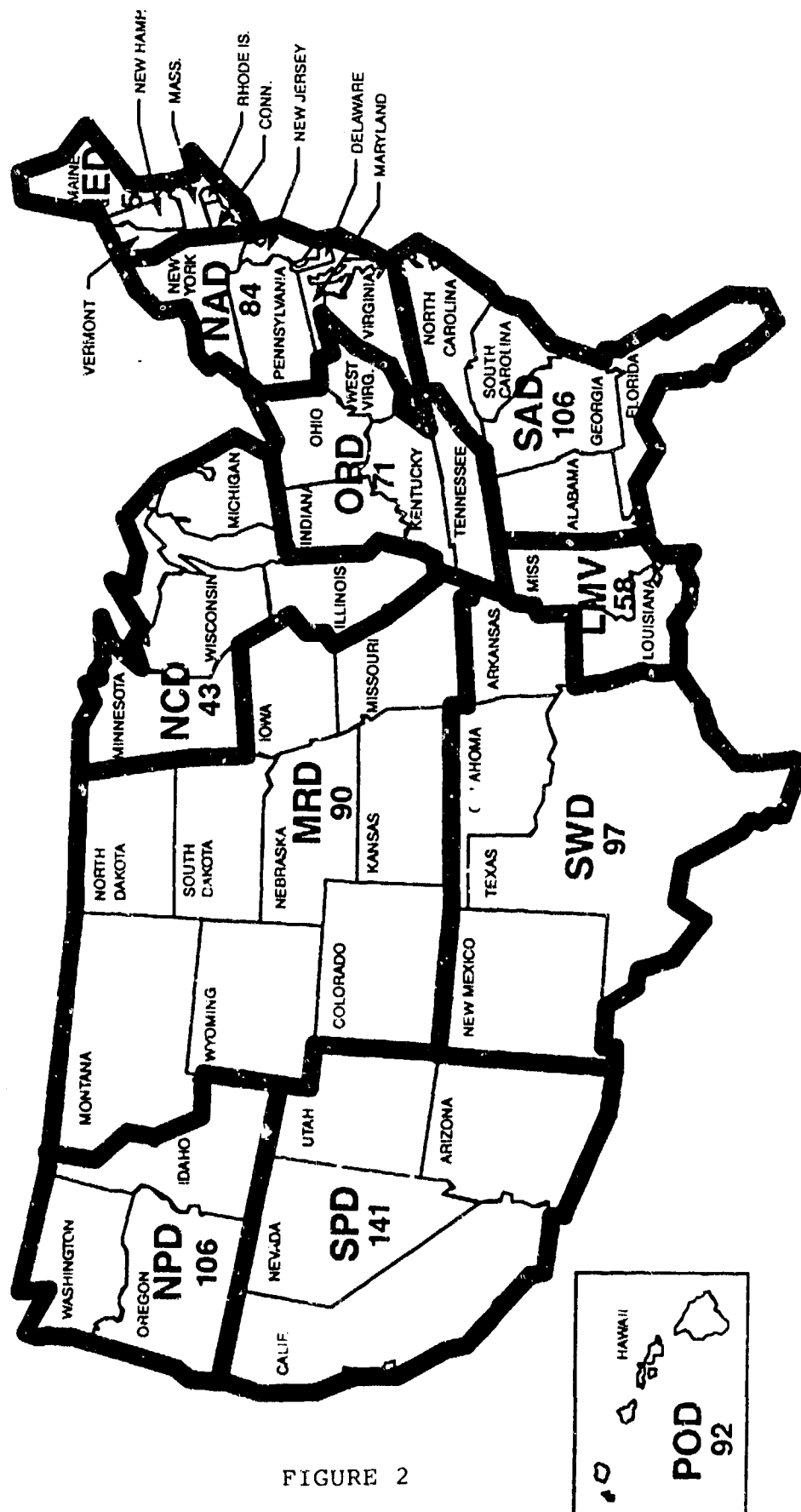


FIGURE 2

RESULTS OF AN ACCIDENTAL
EXPLOSION IN A PROPELLANT
PROCESS BUILDING

A. BOIMEL M.sc. Civil Engineer

Israel Military Industries
P.O.Box 1044 , Ramat-Hasharon, Israel

TWENTY-FOURTH DOD EXPLOSIVES SAFETY SEMINAR
ADAM'S MARK HOTEL, ST LOUIS, MISSOURI
28-30 AUGUST 1990

A B S T R A C T

In January 1990, an accidental explosion occurred in a propellant process building in one of Israel Military Industries' plants.

The building collapsed and debris was found beyond the surrounding barricades.

The paper describes the building and its vicinity before and after the explosion.

Simple calculations according to the manual "Structures to resist the effects of accidental explosions", were made in order to determine the amount of T.N.T equivalent that would have caused the same effects to the structure and its surrounding.

INTRODUCTION

On January, 2nd 1990 , at 3:00 P.M. , an explosion occurred in a building containing about 1500 Kg. of propellant in process, in one of I.M.I's plants.

Fortunately, no one was hurt and only minor damage occurred to adjacent structures

The building collapsed, and debris was thrown beyond the surrounding barricades, while most of the structural elements were found within the area enclosed by the barricades.

Since we knew the exact location of the center of the explosion, we made some simple calculations according to the manual "Structures to resist the effects of accidental explosions" (last edition) (1) , in order to determine what amount of T.N.T equivalent would have caused the same effects to the structure and its surrounding.

This is in spite of the fact that no real detonation occurred. We need this information for future consideration regarding that propellant material.

From now on, we shall assume that the material which exploded in this building was T.N.T .

THE BUILDING DESCRIPTION

The building (shown in pic. no' 1) was made of a reinforced concrete skeleton and the walls - of concrete blocks.

The building had two wings :

- 1) The production hall, measuring 12.1 x 9.6 x 8.0 m.
- 2) The utility room, measuring 7.0 x 7.1 x 5.0 m.

The northern wall - partly attached to the utility room, was made of reinforced concrete beams and columns, filled with concrete blocks.

The western wall - (shown in fig. no' 1) was made of reinforced concrete beams and columns filled with concrete blocks.

The eastern wall - (shown in fig. no' 2) was made of reinforced concrete beams and columns filled with concrete blocks. A double winged steel door measuring 4.0 x 6.5 m. was made of R.H.S steel profiles, covered on both sides with 2 mm. steel plates.

The door was encased with a reinforced concrete frame supporting the main concrete beam on the roof.

The wall above the top level of the door to the ceiling, was made of reinforced concrete.

The southern wall - (shown in fig. no' 3) This was a light- weight wall, about 1/4 of its area was made of concrete blocks and 3/4 was made of reinforced concrete beams and columns filled with thin plastic panes.

A steel bridge connected an escape doorway with the nearby barricade.

The roof - was a reinforced concrete solid slab partly supported by a huge concrete beam. This beam supported a monorail in the production hall as well.

The roof of the utility room was a two-way ribbed floor slab.

The exact point of the center of the explosion is seen in the longitudinal section of the building (fig. no' 4).

THE SURROUNDING AREA

Fig. no' 5 is a map of the area. The two nearby buildings to the north-east (B) and to the south-east (C) resemble the damaged building (A). Those were surrounded by barricades and suffered only minor damage, especially the light weight walls and the glass windows.

115 m. to the south, a one story office building (D) was slightly damaged. All the glass panes were shattered. Some wooden doors were torn from the hinges.

160 m. to the east, a reinforced concrete control building (E) suffered only minor damage while 3 out of 4 glass windows were shattered.

Other buildings in the area were not damaged at all except for a few plastic panes which were sucked out.

From several sources dealing with glass breakage due to explosions, we could estimate the amount of T.N.T equivalent to be between a 100 to 500 kg. and later on we shall limit our search to these values.

DAMAGE TO THE BUILDING

As a result of the explosion, the entire structure collapsed. All the reinforced concrete elements and most of the wall blocks, however, were found within the surrounding barricades.

The reinforced concrete columns were torn out of the pile caps and were ruined. The beams and the columns were blown in the direction of the barricades.

The roof was heavily cracked, the huge concrete beam was broken and all the roof, as a unit, landed on the wreckage below.

There was debris found beyond the surrounding barricades.

From the northern wall , concrete blocks were thrown to a maximum distance of 50 m.

From the southern wall , concrete blocks were found 60 m. away from the building.

From the eastern wall , the two wings of the steel door were thrown. One wing landed on the road 102 m. away and the other wing was found 70 m. from the building on top of the barricade of the adjacent building.

The road leading to the building was covered with broken concrete blocks. The steel door of the utility room was found 30 m. from its frame.

At a distance of 10 m. , on the retaining wall of the barricade edge, there landed - as a unit - the reinforced concrete wall that was above the steel door.

The pictures no' 2 to 10, describe the damage to the structure.

THE CALCULATIONS

The reason for the simple calculations made, was to estimate the amount of T.N.T equivalent that, if detonated in the center of the explosion, might have caused the same effects to the structure.

This information is essential for future consideration of safety distances and hardened structures involved, dealing with this type of propellant materials.

From the way the debris was scattered it was obvious that it was thrown perpendicular to the walls. This implies that the explosion effect was the same as an explosion confined within a cubical structure.

In case of a partially confined explosion, the manual (1) distinguishes between two kinds of impulses acting on the walls. The first is induced by the shock wave which is amplified due to the reflections by the other surfaces of the confining structure.

The other impulse is created by the accumulation of gaseous products and is characterized by pressures whose magnitude is generally much less than those of the shock pressure, but with a significantly longer duration.

As we shall see later from the calculated initial velocity of the secondary fragments, gas pressure from a T.N.T explosion acting on the walls is irrelevant, since there were no walls left to enable gas pressure to develop.

For the calculations, we chose representative fragments.

From the maximum flight distance of the fragment and from other data regarding their mass and shape we were able to find their initial velocity.

The impulse, which caused the flight, was calculated by equating it to the momentum.

Based on the manual (1) for a confined explosion in a cubicle-type structure, we found the impulses acting on the walls for different values of T.N.T charge.

With that data, we easily found out by interpolation the amount of T.N.T that if detonated in the known center of explosion, would have caused the fragment to reach the same maximum distances.

To arrange such a table, we needed to substitute for each different wall the T.N.T quantity versus the impulses it caused.

Since the charts in the manual present data only for distinct values of the scaled distance, we followed the procedure below:

- 1) For the relevant logarithmic chart (according to the configuration and geometry) we marked the corresponding value of the L/R_a for the wall we were dealing with.
- 2) We changed the axis of L/R_a so that it would represent the scaled distance axis Z .
- 3) We projected the intersections of the distinct value of Z_a with the value of L/R_a on the suitable Z_a values along the new Z axis.
- 4) We joined the projected points with a fitting curve.
- 5) We drew, by the same method, curves for different values of L/H , l/L , h/H .
- 6) For every curve we got, we prepared a table describing the changing explosive quantity W , the scaled distance, the scaled impulse obtained by multiplying the scaled unit impulse with $W^{1/3}$.
- 7) We interpolated between the different values obtained from the different curves and got the impulse values acting on the wall versus different values of T.N.T charge (between a 100 to 500kg. T.N.T equivalent in our case).

After obtaining this table, we calculated the initial velocity of representative secondary fragments and this according to the following steps:

- 1) We determined the maximum flight distance of the fragment.
- 2) We calculated the weight and the mass of the fragment.
- 3) Out of table 2-8 of the manual, we determined the drag coefficient C_d .
- 4) We calculated the non-dimensional distance.
- 5) Out of figure 2.252 of the manual we got the non-dimensional initial velocity and from it we obtained the initial velocity of the fragment.
- 6) By multiplying the mass with the initial velocity we got the initial momentum of the element we were dealing with.
- 7) By equating the impulse with the momentum we obtained the impulse that made the element fly, and out of the table we had made earlier, we obtained the T.N.T quantity that if exploded, would have created that impulse.

IMPULSES ON THE WALLS

The impulses acting on the walls versus varying values of T.N.T quantities were calculated for the eastern and northern walls.

Because the center of the explosion was relatively close to the western wall, very high impulses are anticipated for points on that wall near the center of the explosion, and low impulses will act on far points.

Since the values obtained from the charts of the manual, are average values of the distributed impulses on the wall, we believe that the values representing the average impulse on the western wall will not give us a true picture regarding the secondary fragments' initial velocity, and therefore, we considered only the eastern and western walls.

The eastern wall - according to fig. 2.51 of (1) for side wall of a three wall cubicle with a roof, we reached the following parameters :

$$\begin{aligned} N &= 3 & 1/L &= 2.5/8.0 = 0.31 \\ Ra &= 9.6 \text{ m} = 31.5 \text{ feet} & L/Ra &= 8.0/9.6 = 0.83 \\ h/H &= 6.1/9.6 = 0.64 & L/H &= 8.0/9.6 = 0.83 \end{aligned}$$

According to table 2-3 of (1) the illustrations for a scaled average unit impulse for the above parameters are as follows:

h/H	1/L	figure
0.5	0.25	2.136
0.5	0.5	2.137
0.75	0.25	2.139
0.75	0.5	2.140

Fig. 6 to fig. 9 represent the scaled unit impulse versus the scaled distance Z, and this for the value of $L/Ra = 0.83$

Tables 1 and 2 present the values of the unit reflected impulse obtained from these diagrams including the interpolated values for $L/H = 0.83$

Table no. 5 is a summarized table containing the interpolated values where the middle column presents the interpolated values for our case (the eastern wall).

The northern wall - Back wall of three wall cubicle with roof.

$$\begin{aligned} N &= 4 & 1/L &= 2.5/12.1 = 0.21 \\ Ra &= 6.1 \text{ m} = 20 \text{ feet} & L/H &= 12.1/8.0 = 1.51 \\ h/H &= 2.5/8 = 0.31 & L/Ra &= 12.1/6.1 = 1.98 \end{aligned}$$

The illustrations in the manual for the above parameters are as follows:

h/H	1/H	figure
0.25	0.1	2.144
0.25	0.25	2.145
0.50	0.1	2.146
0.50	0.25	2.148

Fig. 10 to fig. 13 represent the scaled unit impulse versus the scaled distance Z, and this for the value of $L/Ra = 1.98$

Tables 3 and 4 present the values of the unit reflected impulse obtained from these diagrams including the interpolated values for $L/H = 1.51$

Table no. 6 is a summarized table containing the interpolated values where the middle column presents the interpolated values for our case (the northern wall).

Fig. no'14 is a summarized graph which describes the impulse on the northern and the eastern walls versus T.N.T charge.

STEEL DOOR IN THE EASTERN WALL

Each wing was constructed of R.H.S steel grid covered with 2 mm. steel plates on both faces. The space in between was filled with an insulation material and it weighed :

$$W = 846 \text{ kg.} = 1863 \text{ lb.}$$

The mass of that element was :

$$M = \frac{1863}{32.2 \times 12 \times 10^{-6}} = 4,821,428 \frac{\text{lb-msec}^2}{\text{in}}$$

One wing landed on the access road 102 m. away while the other one was found on top of the barricade of the adjacent building about 70 m. away.

Since we could not be sure about the true flight distance of that wing, without the interruption of the trees on the barricade and since the calculation procedures in the manual refer only to a maximum flight distance, we considered only the 102 m. distance in our calculations.

According to table 2-8 of (1) the drag coefficient C_d for a long rectangular member face-on is :

$$C_d = 2.05$$

For such a huge fragment like the door wing, we believe that this maximum value represents our case.

The non-dimensional range is :

$$\frac{12 P_o C_d A_d R}{M} = \frac{12 \times 0.115 \times 2.05 \times (78.7 \times 260) \times 102}{4,821,428 \times 0.3048} = 4.02$$

Where :

A_d = drag area of the object [in²]

P_o = air density $\left[\frac{\text{lb-msec}^2}{\text{in}^4} \right]$

R = range of the object flight [feet]

With this calculated term we entered fig. 2-252 and obtained the value:

$$\frac{12 P_o C_d A_d V_o^2}{Mg} = 30$$

from which the initial velocity was calculated :

$$V_o = \left[\frac{30 \times 4,821,428 \times 32.2}{12 \times 0.115 \times 2.05 \times 78.7 \times 260} \right]^{\frac{1}{2}} = 283.6 \text{ feet/sec.}$$

By equating the impulse with the momentum :

$$I = M V_o$$

$$I = \frac{4,821,428 \times 283.6 \times 12}{1,000} = 16,408,284 \text{ lb-msec.}$$

and the unit impulse was obtained by dividing it by the door wing area:

$$i = \frac{16,408,284}{78.7 \times 260} = 802 \text{ psi-msec.}$$

Out of fig. 14 that we had made ,we see that this is the unit impulse created by an explosion of about 215 kg. T.N.T

CONCRETE BLOCKS FROM THE NORTHERN WALL

The blocks from the northern wall were thrown to a maximum distance of $R = 50 \text{ m.} = 164 \text{ feet.}$ True, there were blocks scattered at shorter distances but since the manual relates only to a maximum range prediction, we chose the maximum range for our calculations.

The weight of a block including the mortar is :

$$W = 25 \text{ kg.} = 55 \text{ lb.}$$

The mass of the block is :

$$M = \frac{W}{g} = \frac{55}{32.2 \times 12 \times 10^{-6}} = 142,340 \frac{\text{lb-msec}^2}{\text{in}}$$

The presented area of a block is :

$$A_d = 124 \text{ in}^2$$

According to table 2-8 of the manual, the drag coefficient for a cube element, face-on is $C_d = 1.05$ and for an edge-on cube $C_d = 0.8$. We averaged those values and assumed :

$$C_d = 0.925$$

The non-dimensional range is :

$$\frac{12 P_o C_d A_d R}{M} = \frac{12 \times 0.115 \times 0.925 \times 124 \times 164}{142,340} = 0.18$$

Out of fig. 2-252 we get the non-dimensional velocity :

$$\frac{12 P_o C_d A_d V_o^2}{Mg} = 0.2$$

from which the initial velocity was calculated :

$$V_o = \left[\frac{0.2 \times 142,340 \times 32.2}{12 \times 0.115 \times 0.925 \times 124} \right]^{\frac{1}{2}} = 76.1 \text{ feet/sec.}$$

$$i = \frac{142,340}{124} \times \frac{76.1 \times 12}{1,000} = 1048 \text{ psi-msec}$$

Out of fig. 14 we see that this is the impulse created by an explosion of 255 kg. T.N.T .

CONCRETE WALL ABOVE THE STEEL DOOR

This huge reinforced concrete element above the top level of the steel door in the eastern wall, was found near the building, where the center of gravity was 10 m. away from the wall, and 6.7 m. below its initial position.

Because of the huge mass of this element, which assures low velocities, and since the distance of the flight was relatively short, we may ignore drag forces, and consider the motion as a free fall with initial velocity.

The fall duration was :

$$T = \left[\frac{2h}{g} \right]^{\frac{1}{2}}$$

$$S = 10 \text{ m.}$$

$$S = V_o T$$

$$h = 6.7 \text{ m.}$$

$$V_o = S \left[\frac{g}{2h} \right]^{\frac{1}{2}}$$

and by substituting the above values we obtained the initial velocity :

$$V_o = 10 \times \left[\frac{9.8}{2 \times 6.7} \right]^{\frac{1}{2}} = 8.55 \text{ m./sec.}$$

The weight of the element was :

$$W = 11 \text{ ton} = 24,200 \text{ lb.}$$

and the mass was :

$$M = \frac{24,200}{32.2 \times 12 \times 10} = 62,629,400 \frac{\text{lb-msec}^2}{\text{in}}$$

By equating the impulse with the momentum :

$$I = M V_o = 62,629,400 \times \frac{8.55 \times 39.37}{1000} = 21,086,490 \text{ lb-sec.}$$

and the unit impulse was :

$$i = \frac{21,086,490}{1.45 \times 9.6 \times 39.37^2} = 977 \text{ psi-msec.}$$

According to fig. 14 we can see that to create such an impulse on the eastern wall, we need to explode 280 kg. of T.N.T .

CONCLUSION AND RECOMMENDATION

I.M.I adopted the regulations of the D.O.D standards. (Ammunition and Explosives Safety Standards - DoD 6055.9-STD)

This accident proved that the separation distances that had been taken from the D.O.D quantity - distance tables were adequate.

The acceptor buildings suffered only minor damage due to overpressure and although some fragments were found beyond the donor buildings barricades, they didn't reach other buildings.

By calculating the fragments' initial velocity according to the manual, we were able to find the impulse which propelled those fragments, and from that data we found the T.N.T equivalent and we can see that the values we got for different fragments were reasonably accurate.

However, if the building is rebuilt, we have the following recommendations to minimize debris hazard in case of accident reoccurrence :

- 1) To add to the height of the existing barricades.
- 2) To reinforce the double winged door by attaching it to the concrete roof or the frame, with a spring like cable which will reduce the flight distance in case of another explosion.
- 3) To build the upper part of the walls with reinforced concrete rather than the regular blocks used in the original building.
- 4) The entire southern wall should be built of completely light weight materials instead of what existed in the past. This would give more relief to the pressure and would eliminate debris hazard in the southern direction.

BIOGRAPHY

- (1) "STRUCTURE TO RESIST THE EFFECT OF ACCIDENTAL EXPLOSIONS."

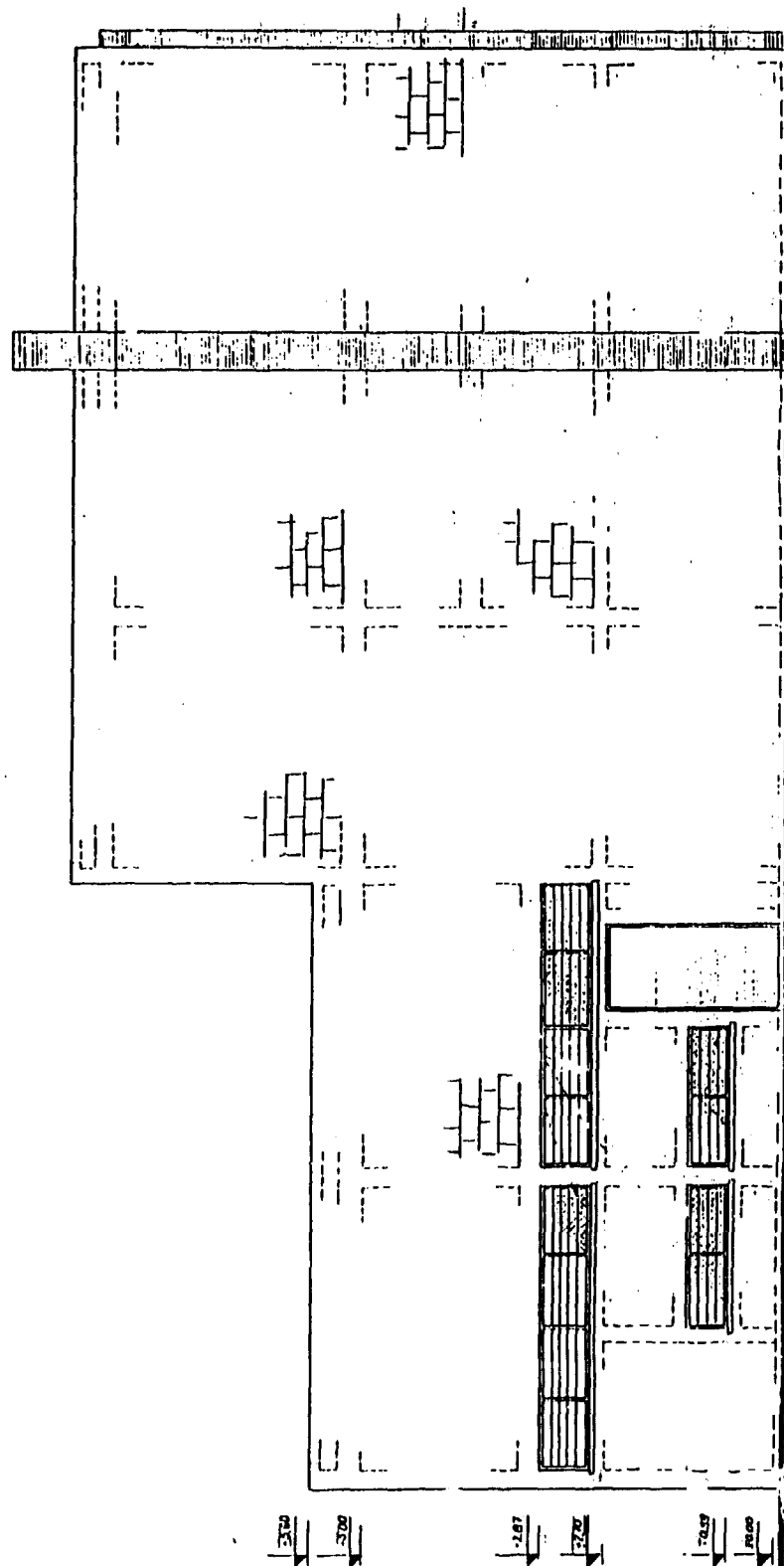


Fig. no' 1 - The western wall

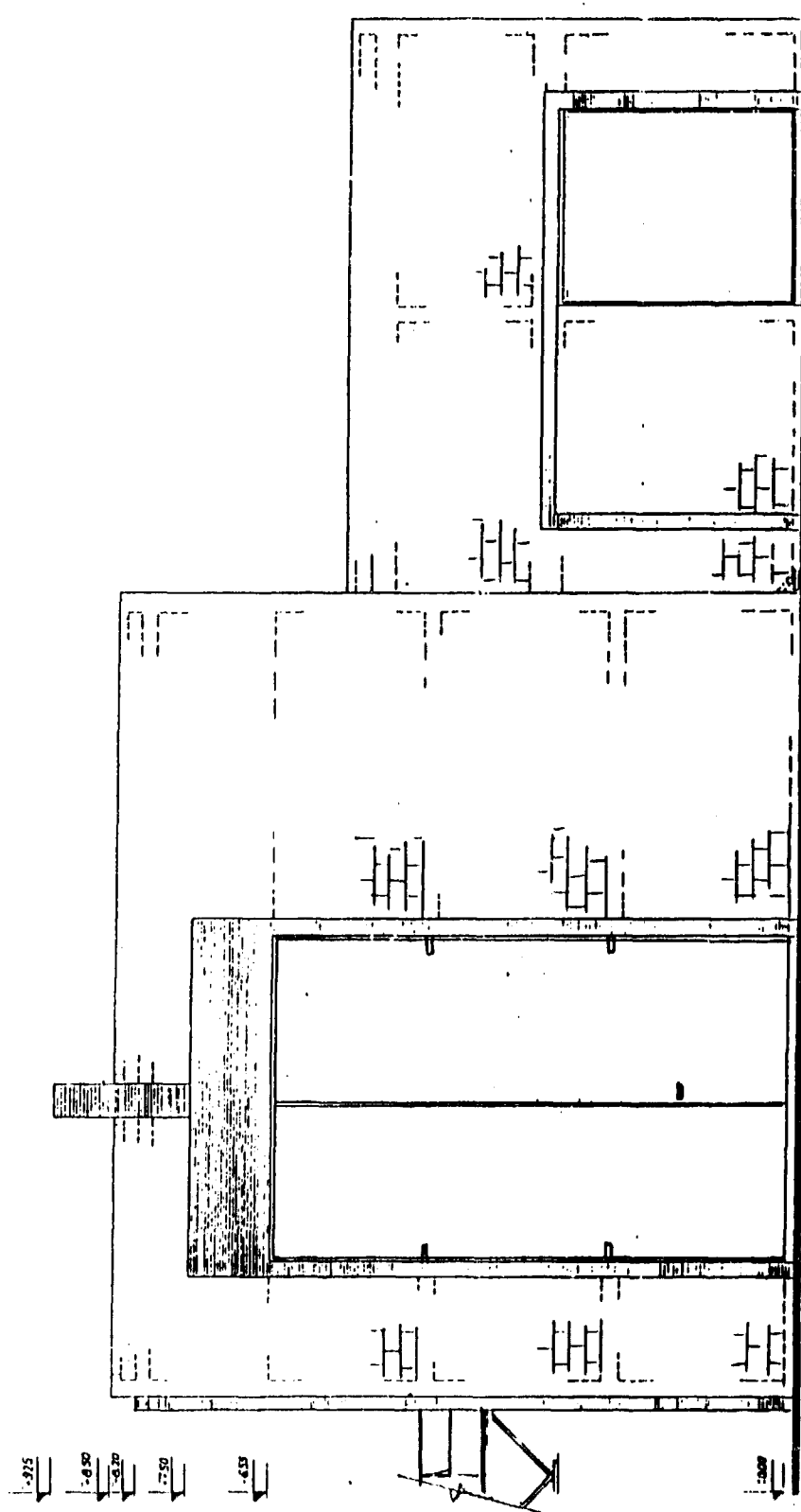


Fig. no' 2 - The eastern wall

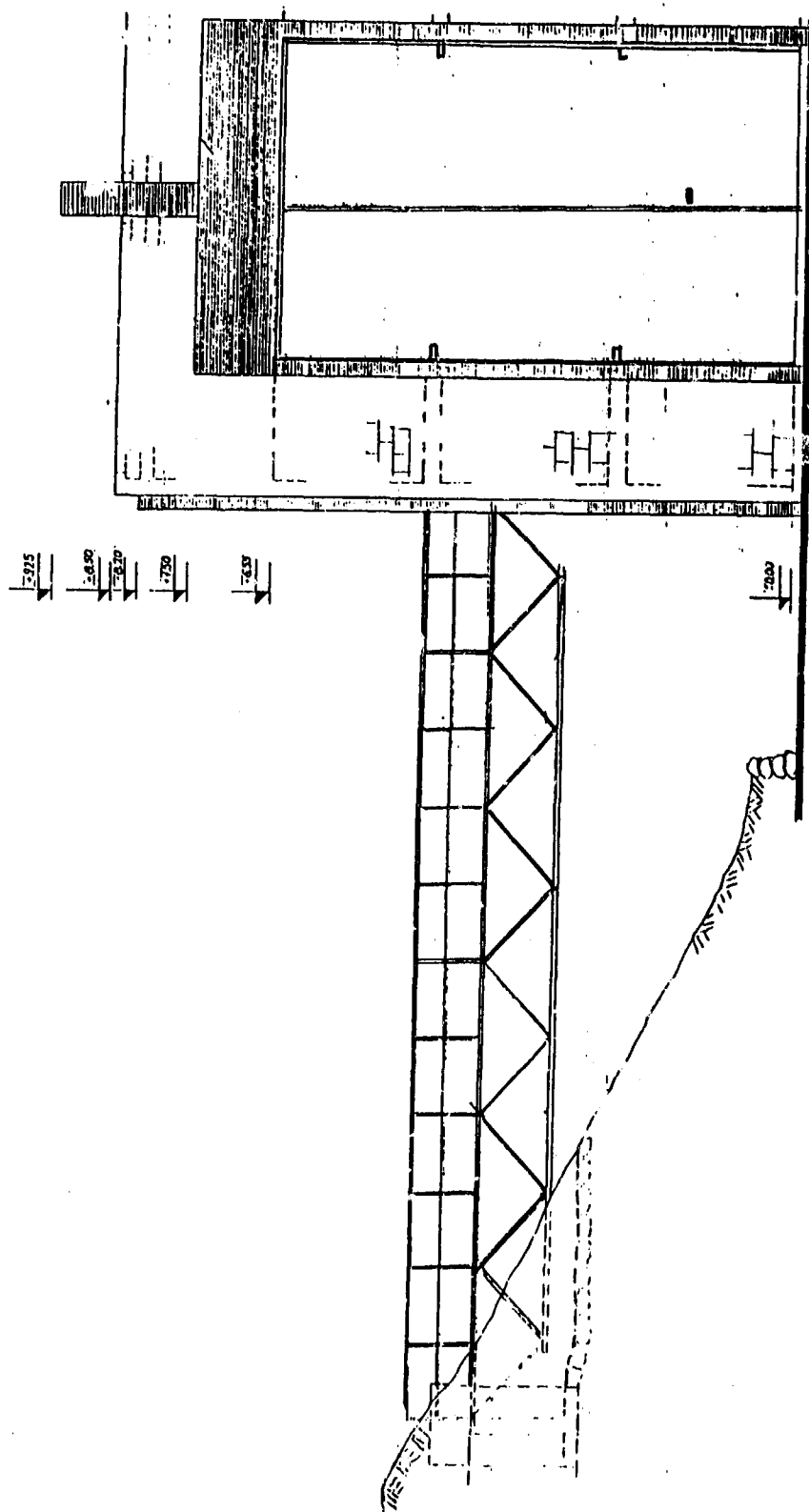


Fig. no' 2 - The eastern wall (continued)

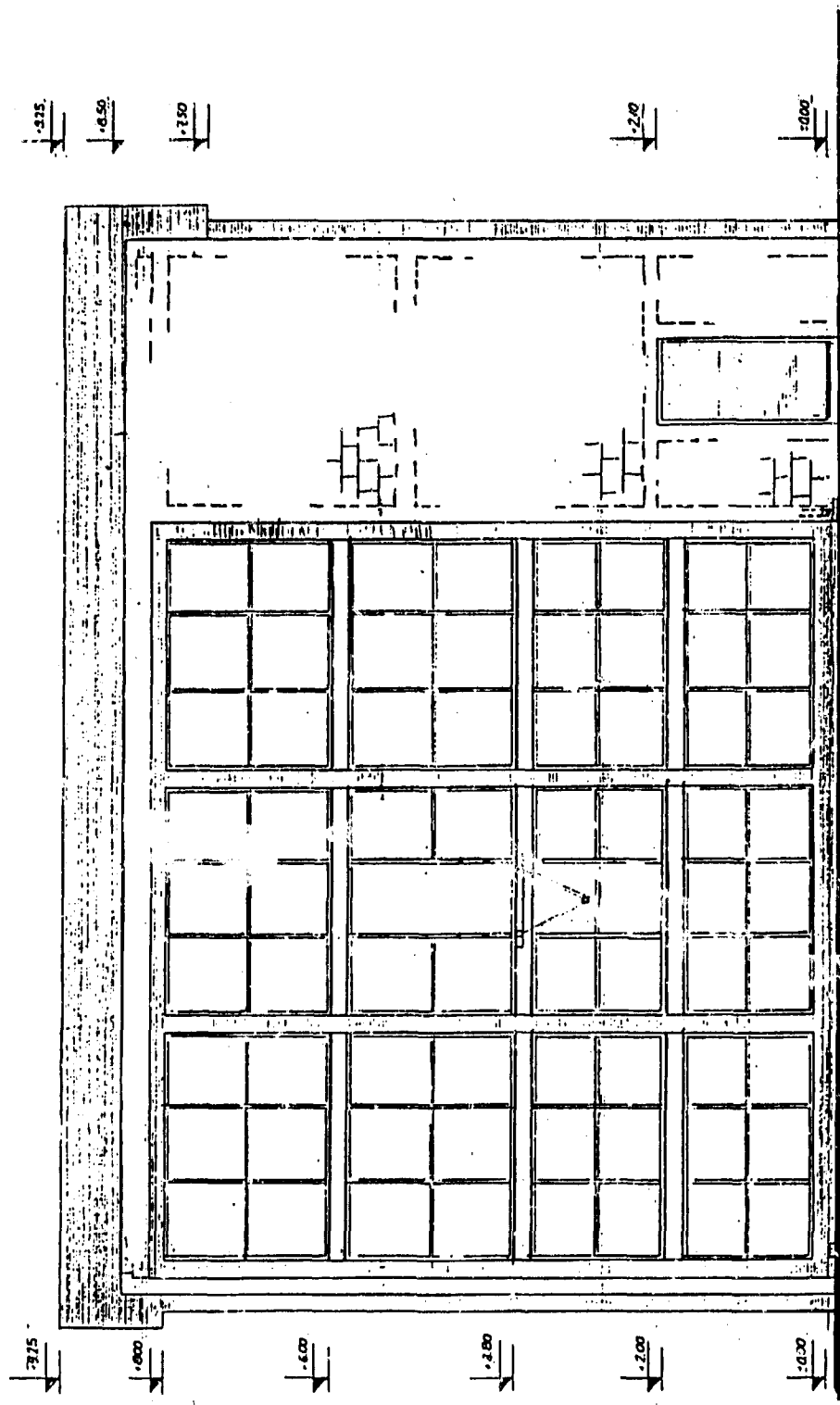


Fig. no' 3 - The southern wall (The light weight wall)

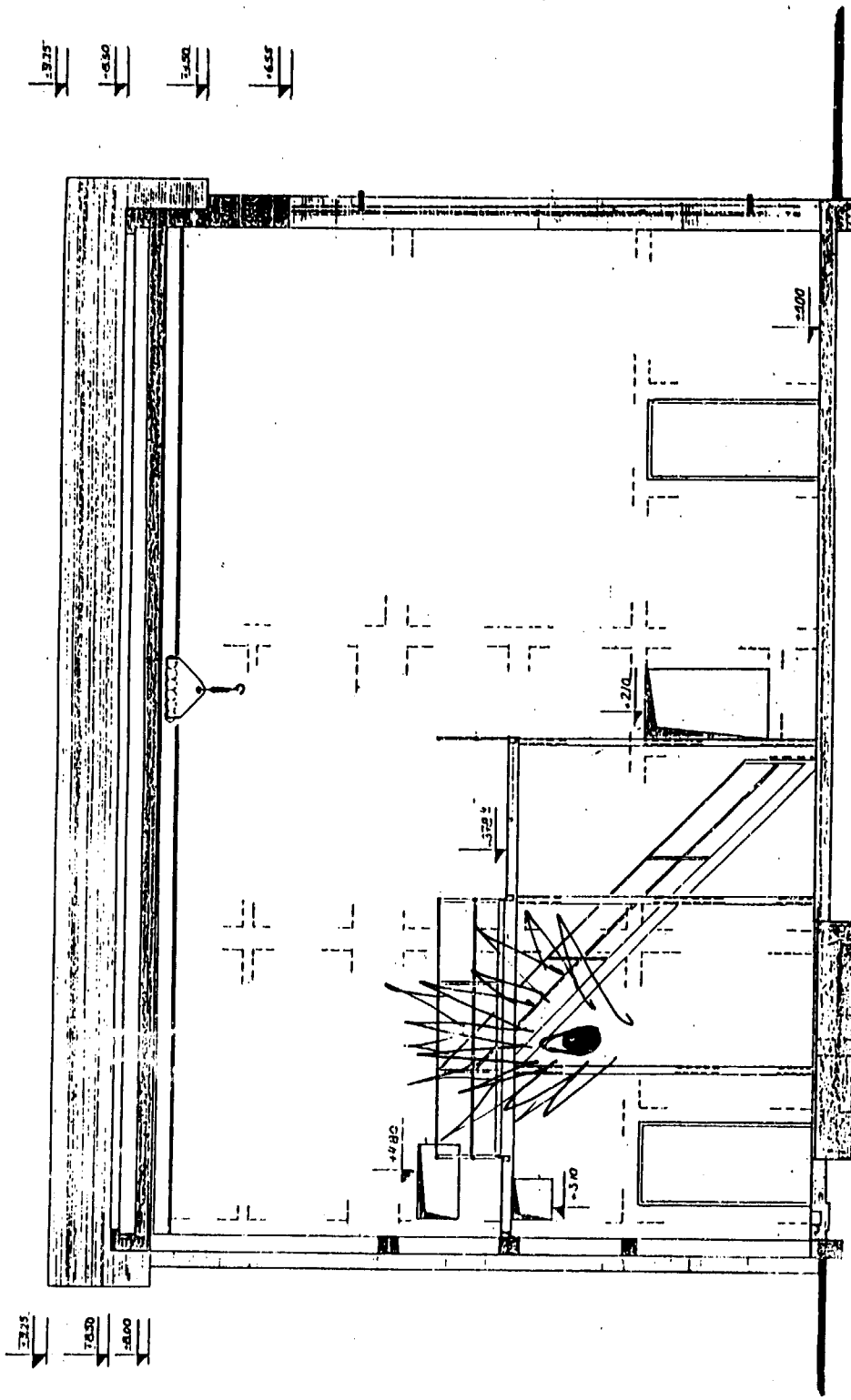


Fig. no' 4 - Longitudinal section of the production hall

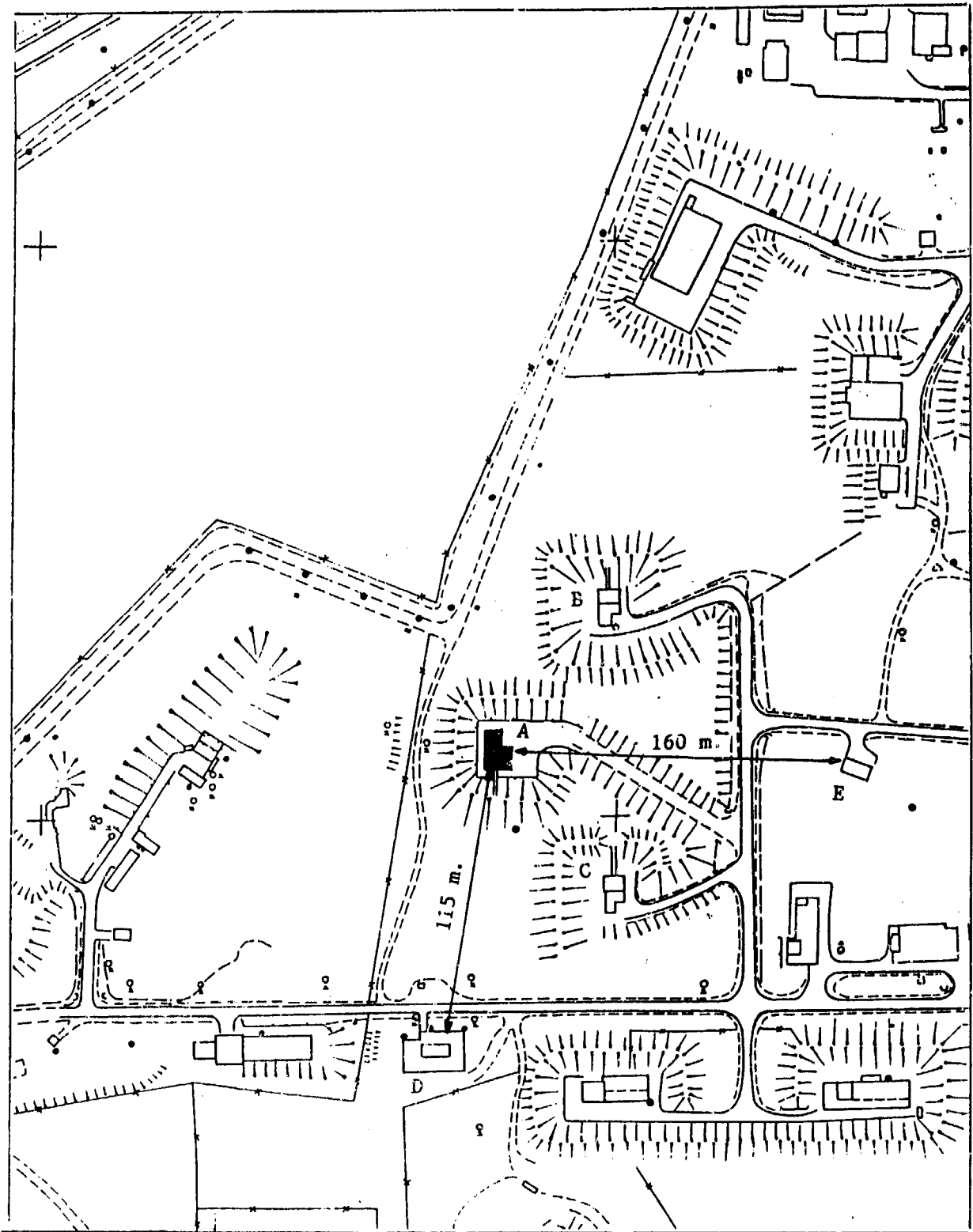


Fig. no' 5 - Map of the area

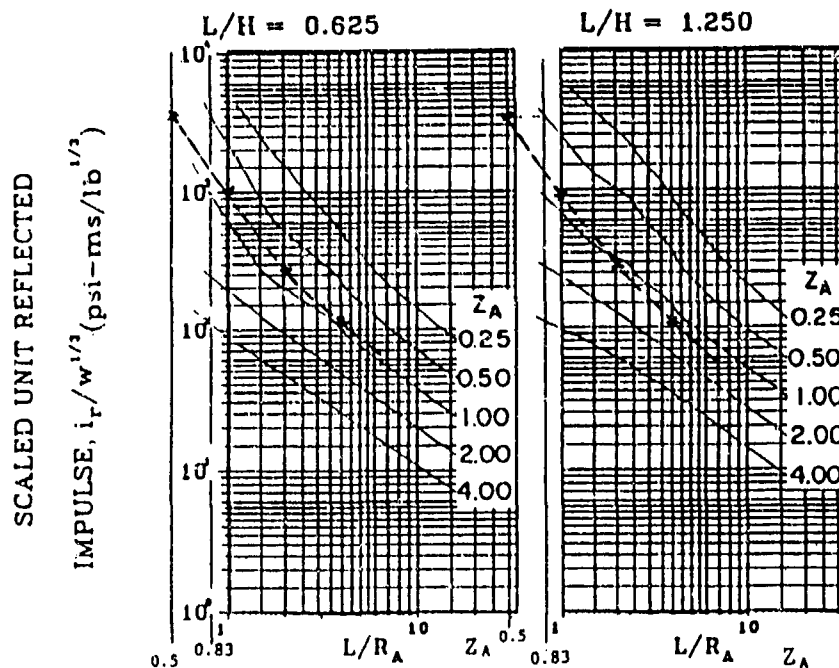


Figure 2-136 Scaled average unit reflected impulse
(6) ($N = 3$, $\ell/L = 0.25$ and 0.75 , $h/H = 0.50$)

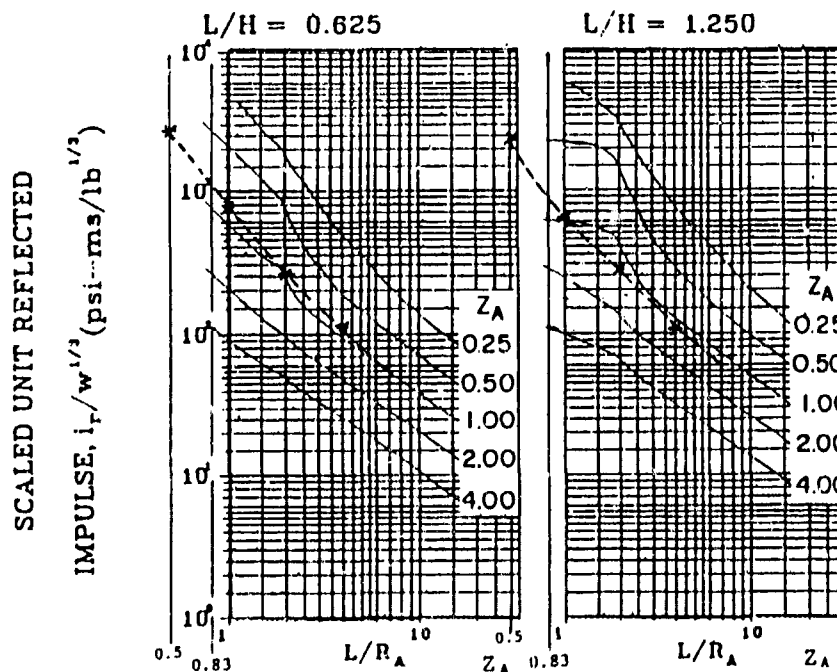


Figure 2-137 Scaled average unit reflected impulse
(7) ($N = 3$, $\ell/L = 0.50$, $h/H = 0.50$)

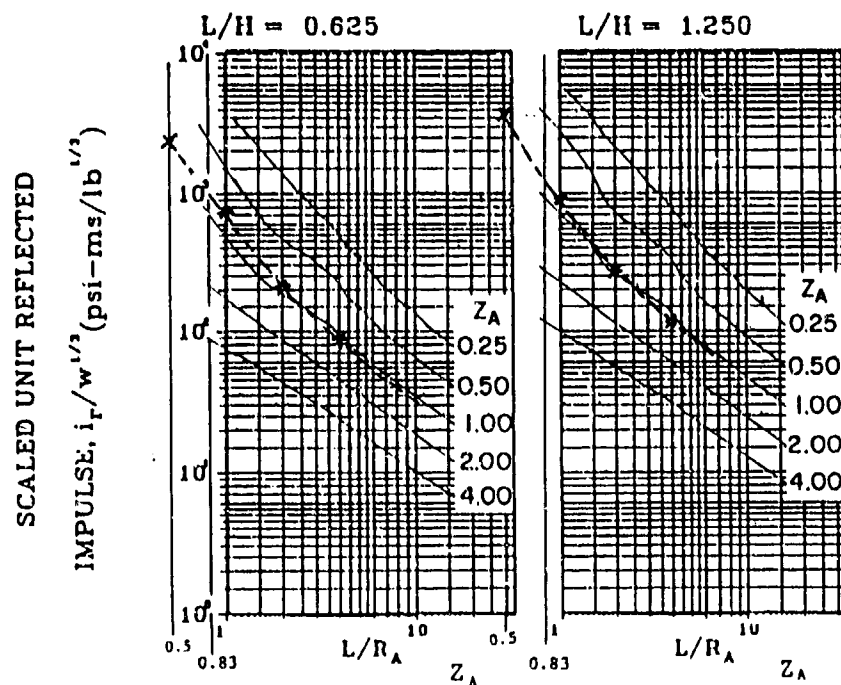


Figure 2-139 Scaled average unit reflected impulse
(8) ($N = 3$, $\ell/L = 0.25$ and 0.75 , $h/H = 0.75$)

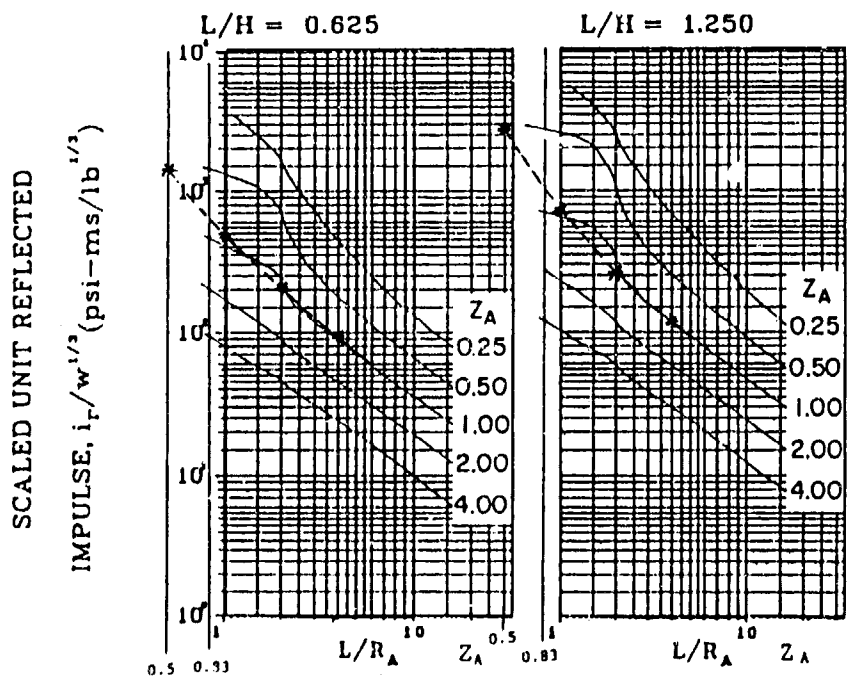


Figure 2-140 Scaled average unit reflected impulse
(9) ($N = 3$, $\ell/L = 0.50$, $h/H = 0.75$)

W kg	W lb	W ^{1/3}	Z	fig. 2.136			fig. 2.137		
				L/H=0.625	L/H=1.25	L/H=0.83	L/H=0.625	L/H=1.25	L/H=0.83
100	220	6.04	5.22	573	483	543	422	483	442
150	330	6.91	4.56	691	691	691	622	622	622
200	440	7.61	4.14	912	837	887	760	760	760
250	550	8.19	3.84	1064	982	1036	900	900	900
300	660	8.71	3.62	1219	1132	1190	1045	1132	1073
250	770	9.17	3.44	1375	1375	1375	1192	1283	1222
400	880	9.58	3.29	1437	1437	1437	1341	1389	1356
450	990	9.97	3.16	1595	1595	1595	1395	1495	1428
500	1100	10.32	3.05	1754	1754	1754	1551	1651	1584

Table no' 1 - Unit reflected impulse [psi-msec]

W kg	W lb	W ^{1/3}	Z	fig. 2.139			fig. 2.140		
				L/H=0.625	L/H=1.25	L/H=0.83	L/H=0.625	L/H=1.25	L/H=0.83
100	220	6.04	5.22	422	543	461	404	543	449
150	330	6.91	4.56	552	691	597	453	691	531
200	440	7.61	4.14	646	837	700	608	875	696
250	550	8.19	3.84	737	982	817	737	1064	844
300	660	8.71	3.62	827	1088	913	836	1219	962
350	770	9.17	3.44	962	1192	1037	962	1329	1083
400	880	9.58	3.29	1053	1389	1163	1025	1437	1160
450	990	9.92	3.16	1196	1488	1292	1096	1437	1208
500	1100	10.32	3.05	1341	1599	1426	1240	1651	1343

Table no' 2 - Unit reflected impulse [psi-msec]

SCALED UNIT REFLECTED

IMPULSE, $i_r/w^{1/2}$ (psi-ms/lb^{1/2})

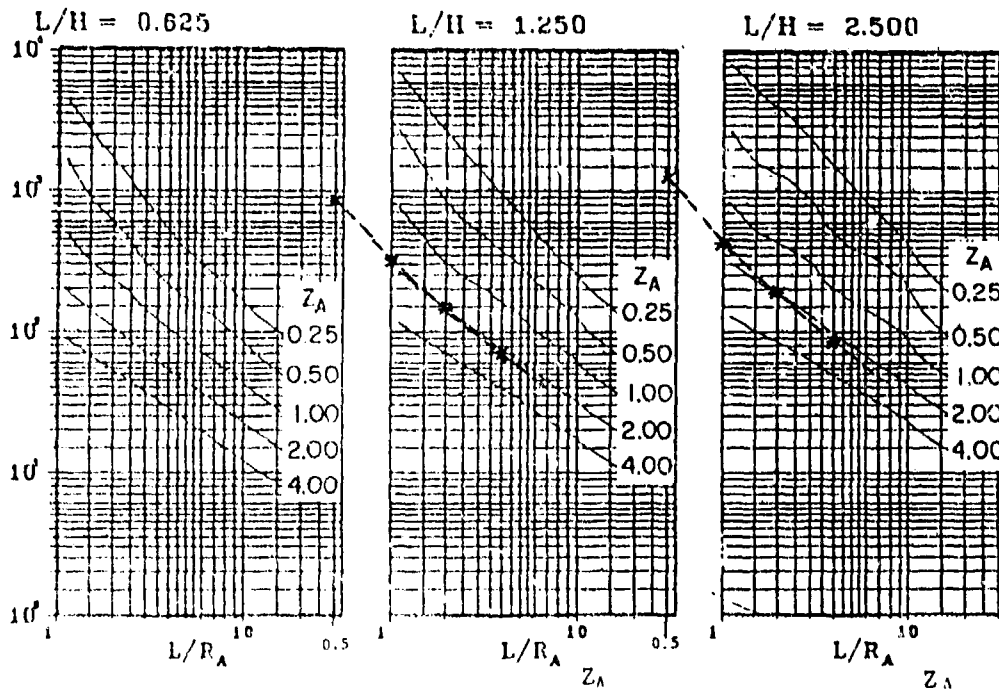


Figure 2-144 Scaled average unit reflected impulse
(10) ($N = 4$, $l/L = 0.10$, $h/H = 0.25$ and 0.75)

SCALED UNIT REFLECTED

IMPULSE, $i_r/w^{1/2}$ (psi-ms/lb^{1/2})

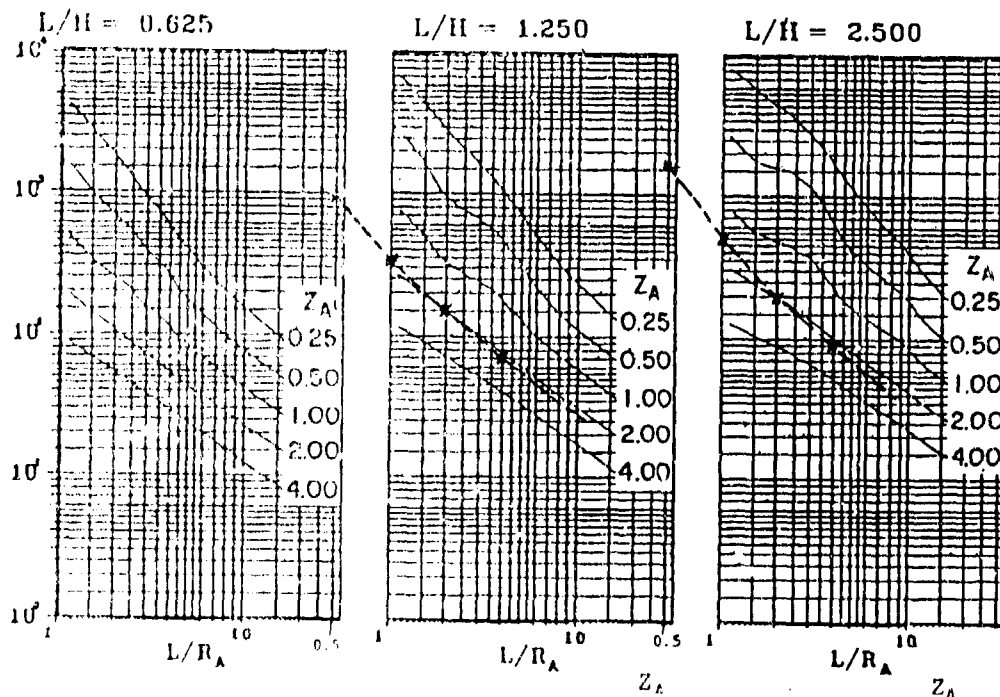


Figure 2-145 Scaled average unit reflected impulse
(11) ($N = 4$, $l/L = 0.25$ and 0.75 , $h/H = 0.25$ and 0.75)

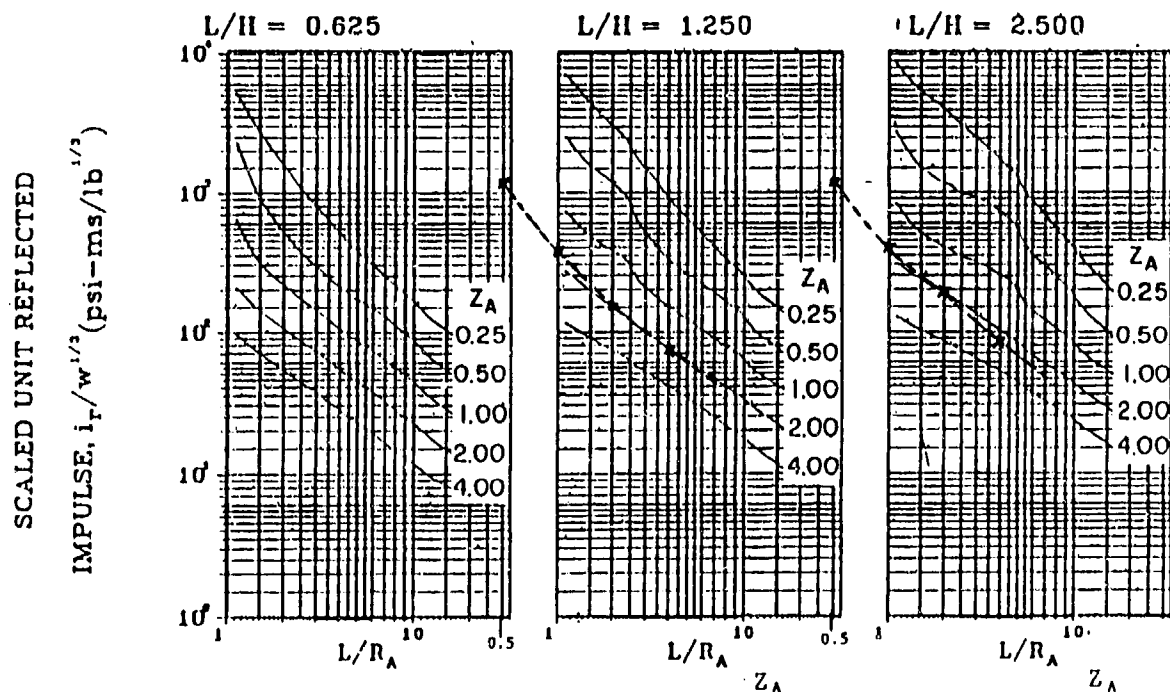


Figure 2-147 Scaled average unit reflected impulse
(12) ($N = 4$, $\ell/L = 0.10$, $h/H = 0.50$)

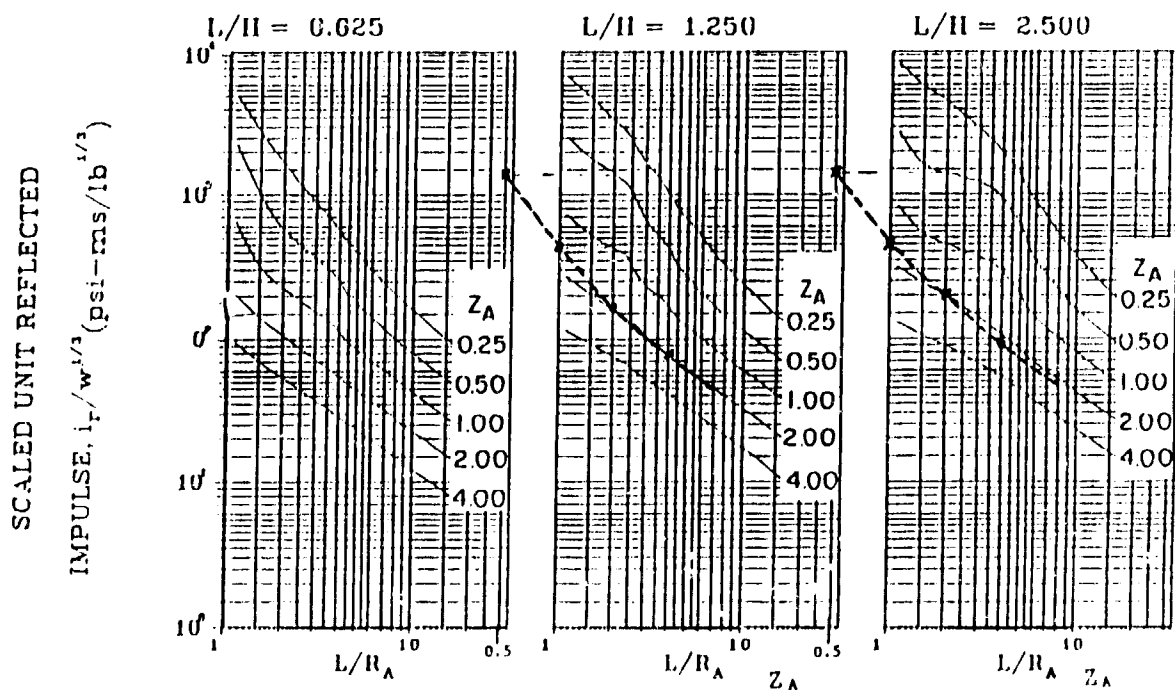


Figure 2-148 Scaled average unit reflected impulse
(13) ($N = 4$, $\ell/L = 0.25$ and 0.75 , $h/H = 0.50$)

				fig. 2.144			fig. 2.145		
W kg	W lb	W ^{1/3}	Z	L/H=1.25	L/H=2.5	L/H=1.51	L/H=1.25	L/H=2.5	L/H=1.51
100	220	6.04	3.31	513	604	531	513	604	531
150	330	6.91	2.89	691	829	719	691	829	719
200	440	7.61	2.63	837	1065	884	837	1065	884
250	550	8.19	2.44	982	1269	1041	982	1269	1041
300	660	8.71	2.30	1132	1437	1195	1132	1437	1195
350	770	9.17	2.18	1237	1604	1313	1237	1604	1313
400	880	9.58	2.09	1341	1724	1420	1341	1724	1420
450	990	9.97	2.01	1445	1894	1538	1445	1894	1538
500	1100	10.32	1.94	1548	2064	1655	1548	2064	1655

Table no' 3 - Unit reflected impulse [psi-msec]

				fig. 2.147			fig. 2.148		
W kg	W lb	W ^{1/3}	Z	L/H=1.25	L/H=2.5	L/H=1.51	L/H=1.25	L/H=2.5	L/H=1.51
100	220	6.04	3.31	543	634	561	513	664	544
150	330	6.91	2.89	725	829	746	691	829	719
200	440	7.61	2.63	875	1065	915	800	1027	847
250	550	8.19	2.44	1023	1228	1065	941	1228	1000
300	660	8.71	2.30	1132	1437	1195	1088	1393	1151
350	770	9.17	2.18	1283	1558	1340	1237	1513	1294
400	880	9.58	2.09	1437	1724	1496	1437	1820	1516
450	990	4.97	2.01	1545	1894	1617	1645	2043	1728
500	1100	10.32	1.94	1651	2064	1737	1754	2218	1850

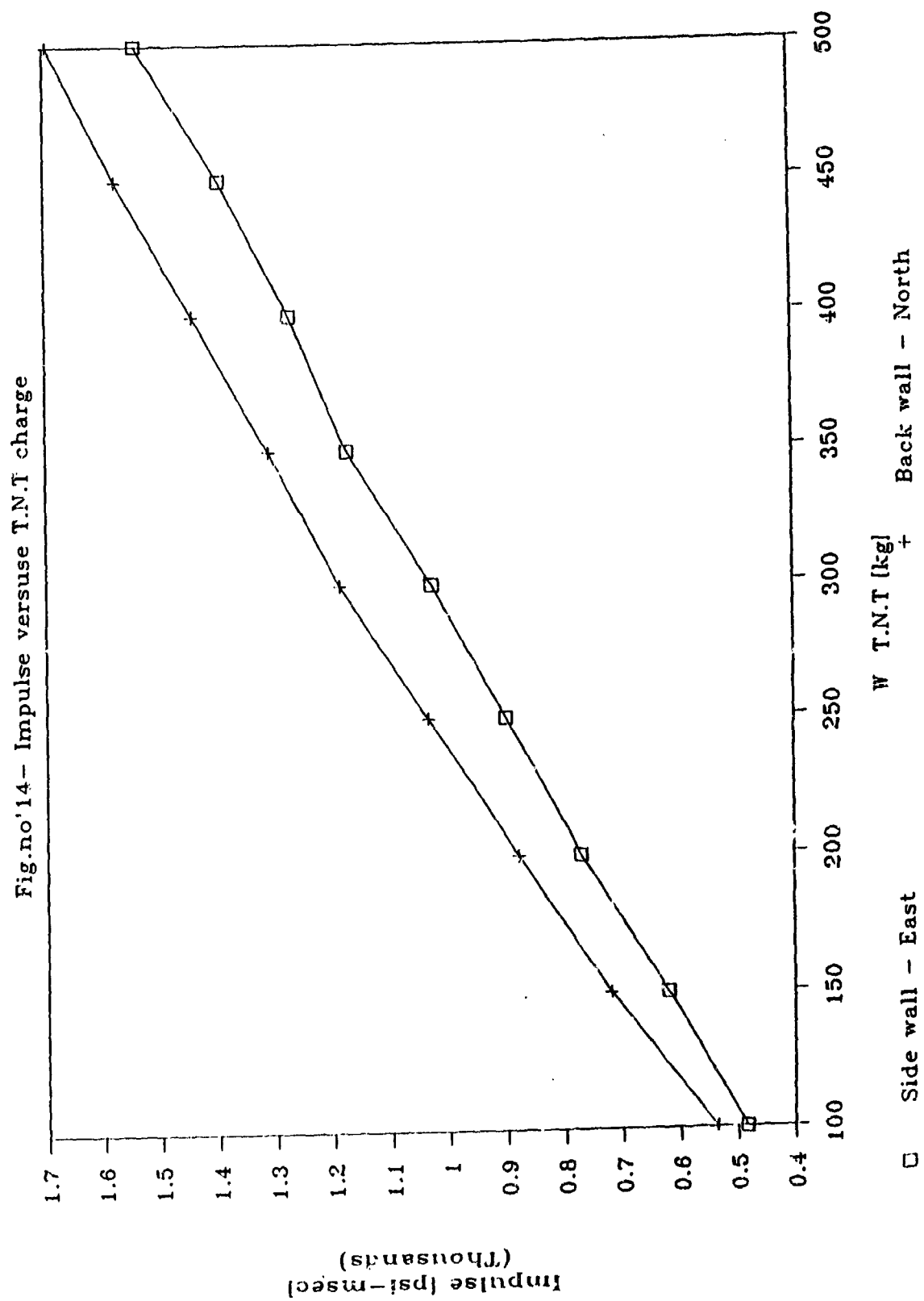
Table no' 4 - Unit reflected impulse [psi-msec]

W kg	W lb	fig 2.136	fig 2.137	interpolated values			fig 2.139	fig 2.140
		h/H=0.5 1/L=0.25	h/H=0.5 1/L=0.5	h/H=0.5 1/L=0.31	h/H=0.64 1/L=0.31	h/H=0.75 1/L=0.31	h/H=0.75 1/L=0.25	h/H=0.75 1/L=0.5
100	220	543	442	517	<u>483</u>	458	461	449
150	330	691	622	673	<u>620</u>	580	597	531
200	440	887	760	855	<u>771</u>	705	700	696
250	550	1036	900	1002	<u>901</u>	823	817	844
300	660	1190	1073	1160	<u>1028</u>	925	913	962
350	770	1375	1222	1336	<u>1174</u>	1048	1037	1083
400	880	1437	1356	1416	<u>1273</u>	1162	1163	1160
450	990	1595	1428	1553	<u>1395</u>	1271	1292	1208
500	1100	1754	1584	1711	<u>1539</u>	1405	1426	1343

Table no' 5 - Interpolated values of the impulses
on the eastern wall [psi-nsec]

W kg	W lb	fig 2.144	fig 2.145	interpolated values			fig 2.147	fig 2.148
		h/H=0.25 1/L=0.10	h/H=0.25 1/L=0.25	h/H=0.25 1/L=0.21	h/H=0.31 1/L=0.21	h/H=0.50 1/L=0.21	h/H=0.50 1/L=0.10	h/H=0.50 1/L=0.25
100	220	531	531	531	<u>535</u>	548	561	544
150	330	719	719	719	<u>720</u>	726	746	719
200	440	884	884	884	<u>879</u>	866	915	847
250	550	1041	1041	1041	<u>1035</u>	1018	1065	1000
300	660	1195	1195	1195	<u>1187</u>	1163	1195	1151
350	770	1313	1313	1313	<u>1311</u>	1307	1340	1294
400	880	1420	1420	1420	<u>1442</u>	1510	1496	1516
450	990	1538	1538	1538	<u>1575</u>	1695	1617	1728
500	1100	1655	1655	1655	<u>1695</u>	1817	1737	1850

Table no' 6 - Interpolated values of the impulses
on the northern wall [psi-nsec]



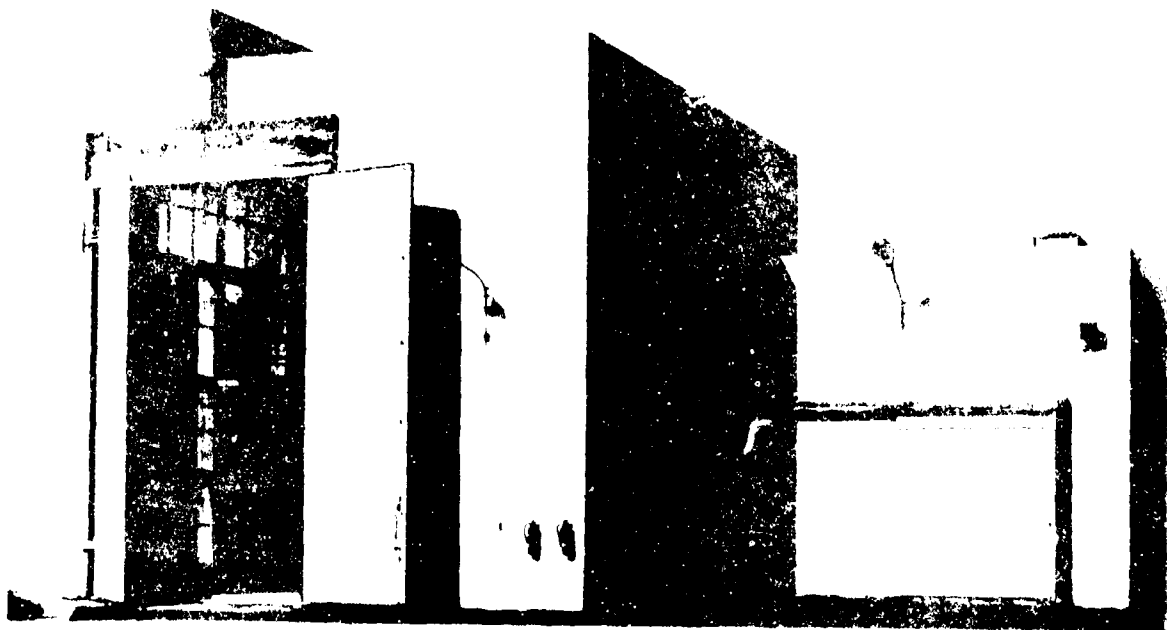
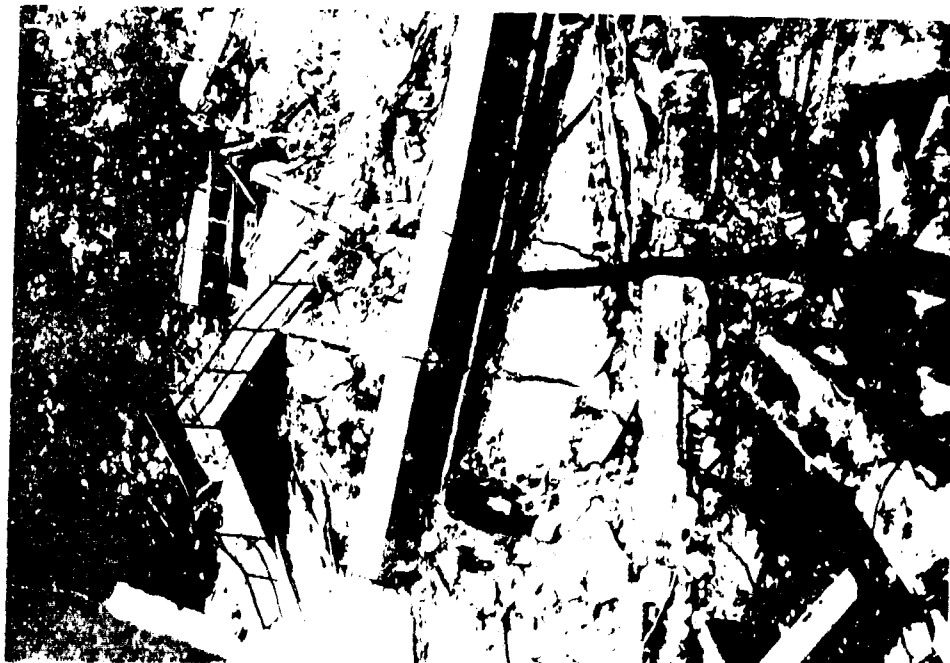


Fig. no' 1 - The building before the accident



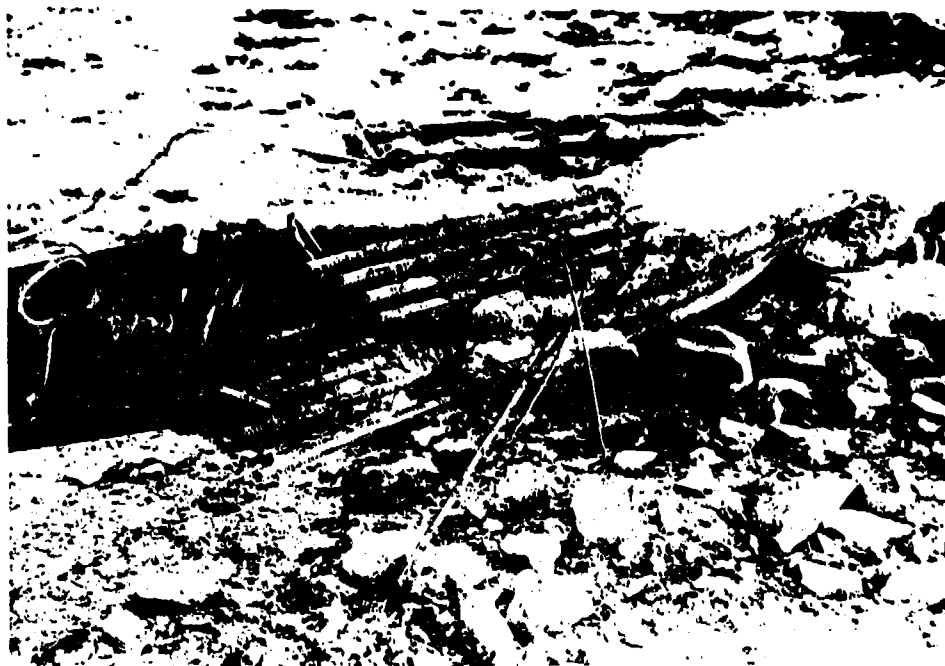
Fig. no' 2 - A view from the ground level



Pic. no' 3 - A view from the
southern barricade



Pic. no' 4 - The light weight wall
of the nearby building



Pic. no' 5 - A broken reinforced concrete column



Pic. no' 6 - A reinforced concrete wall element on the retaining wall of the barricade edge



Pic. no¹ 7 - The steel door wing 102 m. from its frame



Pic. no¹ 8 - The steel door 30 m. from its frame

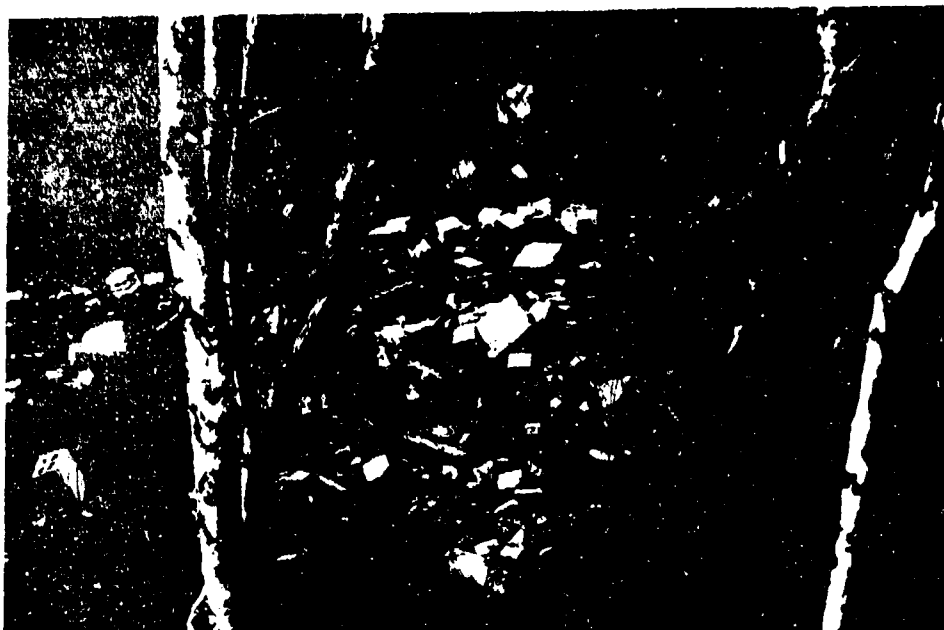


Fig. no' 9 - Wall blocks beyond the barricade



Fig. no' 10 - The steel door lying on top of the barricade 20 m. away

**INVESTIGATION OF
HAWTHORNE ARMY AMMUNITION PLANT
MAGAZINE FIRE - 9 AUGUST 1989**

ROBERT A. LOYD

**U.S. ARMY ARMAMENT
MUNITIONS AND CHEMICAL COMMAND**

**24th DEPARTMENT OF DEFENSE
EXPLOSIVES SAFETY SEMINAR
27-30 AUGUST 1990**

Investigation of the Hawthorne Army Ammunition Plant (AAP) Magazine Fire
9 August 1989

1. Executive Summary: A magazine fire involving 30,715 pounds of Navy propelling charges (hazard class 1.3/mass fire) occurred at Hawthorne AAP. The material was stored in Magazine 116-14-E. The propellant was unservicable (condition code H), awaiting disposal instructions. At 0930, 9 August 1989, a nearby work crew heard a "bang" followed by smoke and sparks coming from the magazine door vents and smoke from the rear ventilator. The doors were then forced open by the pressure of the burning propellant followed by a large jet of flame. The magazine was allowed to cool overnight. An explosive ordnance disposal (EOD) team entered the magazine the next morning and determined there was no unburned propellant in the magazine. The most probable cause was spontaneous ignition due to low stabilizer of 8-inch, 55-caliber bagged propelling charges (national stock number (NSN) 1320-00-089-4275; Department of Defense identification code (DODIC) D605 located in the left front portion of the magazine. This was based on: the known low stabilizer content (0.04 to .13 percent) of seven 8-inch propelling charges lots located in this area (lot numbers DG-2-CO-68, DGR-1-ILAW-55, DGR-11-CO-68, DGR-13-CO-68, DGR-14-CO-68, DGR-5-CO-69, and DGR-8-C-51); heavy fire damage occurring in the left front portion of the magazine; and analysis of observations made by several witnesses.

2. Description of facility: The fire occurred in a Navy triple-arch magazine (encs 1-4). It was built in the 1943 to 1945 timeframe, based on Navy Bureau of Yards and Docks Drawing Number 217869. The facility consists of three separate earth-covered igloos/magazines with a common headwall and loading dock. Each magazine is concrete and arched along its long axis. Each has 4-foot wide double doors that open to a 6-foot wide concrete loading dock. The doors are wood, covered with 22-gauge metal. Each door has a hooded vent approximately 12 inches by 18 inches in the lower portion of the door. There is also a rear stack ventilator 15 inches in diameter and extending 30 inches above the earth cover. The ventilator stack is covered with a vent cap made of glazed ceramic, metal, and screening. It sets on top of the stack, but is not fastened to the stack. It weighs 195 pounds. The magazine is 80 feet long, 25 feet wide, and 12 feet high at the top of the arch. The magazines are separated by 13 feet of earth to a height of 6 feet above floor level. It then decreases to not less than 2 feet of earth cover which continues over the magazine roof. The headwall is 8 inches thick and is constructed of reinforced concrete. There are two sets of railroad tracks in front of the loading dock. The metal portions of the magazine are bonded and grounded. The railroad tracks are also bonded and grounded. There is no lightning protection system.

3. Events surrounding the fire:

a. Prior to fire:

(1) The magazine was entered on 15, 17, 25, and 27 July 1989 during the performance of a location survey by the Day and Zimmermann - Basil (DZB) Inventory Division. Nothing unusual or out of the ordinary was noted.

(2) The bonding and grounding system of the magazine was checked on 16 March 1989. The readings were 5.9 ohms for the building ground and 0.1 ohms for bonding of metal bodies. This is within the values permitted by

AMCR 385-100, Safety Manual, 1 August 1985, and DOD 6055.9-STD, Department of Defense Ammunition and Explosives Safety Standards, July 1984. There is no lightning protection system, and none is required where all metallic parts are bonded and grounded.

(3) A thunderstorm passed through the area at approximately 2300 the night prior to the fire (approximately 10 hours prior to the fire).

(4) A work crew drew keys for Magazines 116-10 through 116-20 on the morning of the fire. They were performing maintenance on magazine doors. The crew was on the loading dock of an adjacent magazine (116-12) at the time of the fire. They were scheduled to start work on Magazine 116-14 within an hour.

(5) There were no outstanding safety-related work orders or known safety deficiencies for Magazine 116-14-E.

b. During the fire:

(1) The fire was initially observed by a work crew on an adjacent magazine dock (Magazine 116-12) and two DZB safety personnel near Magazine 116-40 while returning from the Western Area Demil Facility (WADF). Magazine 116-40 is located approximately 1,300 feet from Magazine 116-14. They first observed sparks, fire, and smoke coming from the door ventilators and smoke coming from the rear ventilator. The volume of fire and smoke coming from the ventilator then increased significantly. This was followed by a "rush of air", with the doors being pushed open and the rear ventilator cap being "blown off". The very intense burning continued for approximately 3 minutes and then decreased significantly. During this period of decreased burning, several loud "bangs" were heard.

(2) The fire was reported by the work crew and the DZB safety engineers. The fire department, security, and other personnel responded. Road blocks were established around the edge of the magazine area. No attempt was made to enter the area or fight the fire. It was permitted to burn itself out.

c. Events following the fire:

(1) The area was secured, and a fire watch was posted. An Army EOD team from Sierra Army Depot entered the magazine the next morning. They determined that all the propellant had been consumed by the fire and that the magazine could be safely entered. This was the first entry made following the fire.

(2) The Government Safety Manager and DZB plant photographer then entered the magazine to make an initial assessment and take photographs.

(3) A local investigation was initiated with technical assistance provided by Mr. Robert Loyd, U.S. Army Armament, Munitions and Chemical Command (AMCCOM) Safety Office.

4. Description of magazine contents: The magazine contained 30,715 pounds of energetic material. All items were hazard class 1.3 (mass fire), and were awaiting disposal instructions. All items were in storage compatibility group Most items were stored on Navy metal pallets with the remaining few items store on wooden pallets. There was also a small quantity of wood used for blocking and bracing. The following items were stored in Magazine 116-14-E:

a. 81mm mortar increment bags; NSN 1315-00-425-0725; DODIC C020; quantity 237,084; net explosive weight (NEW) per item - 0.03 pounds; total explosive weight - 7,113 pounds; and stored in wooden boxes similar to those shown in enclosure 5. The increment bags were from a Marine Corps renovation job. The following lots were involved:

HEP-66803
CIL-68549
CIL-68550
CIL-68553
HEP-68247
HEP-63962
HEP-68963
RAD-67251
RAD-67572
RAD-67610
RAD-67611
Mixed Lot (derived from lots RAD-67610 and RAD-67611)

b. 5-inch, 54-caliber propelling charge (cased with plug); NSN 1320-00-039-3353; DODIC D305; quantity - 5; NEW per item - 18.6 pounds; total explosive weight - 93 pounds; and stored in metal shipping containers similar to those shown in enclosure 6. The propelling charge lot number, with the corresponding index number and propellant lot number is listed below.

BV-25X-C-60 APDF-10395 IHBF-19

c. 5-inch, 54-caliber propelling charge (cased with plug)
NSN 1320-00-879-3925; DODIC - D324; quantity - 125; NEW per item - 21.0 pounds; total explosive weight - 2,625 pounds; and stored in metal shipping containers similar to those shown in enclosure 6. The propelling charge lot number, with the corresponding index number and propellant lot number, is listed below:

BV-13-SB-69 SPDF-10980 unknown

d. 6-inch, 47-caliber propelling charge (cased with plug); NSN 1320-00-009-0352; DODIC D370; quantity - 4; NEW per item - 33.882 pounds; total explosives weight - 136 pounds; and stored in metal shipping containers. The propelling charge lot numbers, with the corresponding index numbers and propellant lot numbers, are listed below:

CH-114-Y-72	SPDN-7288	NHCDCD-83
CH-115-Y-72	SPDN-7288	NHCDCD-83
CH-116-Y-72	SPDN-7288	NHCDCD-83
CH-118-Y-72	SPDN-7288	NHCDCD-83

e. 8-inch, 55-caliber propelling charge (bagged); NSN 1320-00-089-4275; DODIC D605; quantity - 433; NEW per item - 45.4 pounds; total explosive weight - 19,658 pounds; and stored in metal shipping containers. The propelling charge lot numbers, with the corresponding index numbers and propellant lot numbers, are listed below:

DG-1-HA-52	SPDW-10113	IHDD-104
DG-1-HA-53	SPDW-10109	IHDD-109
DGR-1-CO-69	SPD-9070	IHDD-86
DGR-10-CO-67	SPD-8862	IHDD-?
DGR-6-C-51	SPDN-8521	IHDD-75
DGR-6-CO-67	SPD-8311	IHDD-73
DGO-6-CO-69	SPD-8520	IHDD-74
DGR-6-YO-67	SPD-9711	IHDD-94
DGR-8-CO-68	SPD-8664	IHDD-77
DGR-1-HAW-55	SPDN-6359	IHDD-47
DGR-11-CO-68	SPD-7843	IHDD-64
DGR-13-CO-68	SPD-6990	IHDD-51
DGR-14-CO-68	SPD-8521	IHDD-75
DGR-3-YO-67	SPDN-7499	IHDD-60
DGR-5-CO-67	SPDN-6082	IHDD-44
DGR-8-C-51	SPD-3288	IHDD-34
DGR-8-CO-69	SPD-5409	IHDD-41
DGR-5-CO-69	---	---

f. 8-inch, 55-caliber propelling charge (bagged); NSN 1320-00-039-3814; DODIC D607; quantity - 15; NEW per item - 45.4 pounds; total explosive weight - 681 pounds; and stored in metal shipping containers. The propelling charge lot numbers, with the corresponding index numbers and propellant lot numbers, are listed below:

DG-1-SJ-68	SPD-9069	IHDD-35
DGR-6-C-51	SPD-8521	IHDD-75
DGR-8-CO-68	SPD-8664	IHDD-77
DG-2-CO-68	SPD-8664	IHDD-77

g. 8-inch, 55-caliber propelling charge (bagged); NSN 1320-00-089-3803; DODIC D608; quantity - 9; NEW per item - 45.4 pounds; total explosive weight - 409 pounds; and stored in metal shipping containers. The propelling charge lot numbers, with the corresponding index numbers and propellant lot numbers, are listed below:

DG-4-MCA-51	SPDG-9440	NCDD-100
DG-5-CD-68	SPDG-10905	unknown

5. Description of damage:

a. Propellant: The propellant in the magazine was totally consumed by the fire. Numerous unburned propellant grains were thrown out the door (encls 7 and 8).

(1) Bagged propelling charges: The 8-inch, 55-caliber bagged propelling charges were stored in metal shipping containers. The walls of the containers are made of light-gauge aluminum. The ends and lids are constructed of heavier gauge aluminum. Containers located near the rear of the magazine had substantial portions of the walls remaining, and most of the ends/lids remained intact (encl 9). The containers located in the center of the magazine had most of the wall missing, but most of the ends remained intact (encls 10-12). The containers located in the front left portion of the magazine (when facing to the rear) were almost totally destroyed (encl 13). Virtually none of the walls remained, and major portions of the ends/lids were destroyed. Aluminum slag was found on the floor. This indicates the aluminum was exposed to temperatures of more than 1,200 degrees Fahrenheit for a period of time sufficiently long to have become molten (encl 14). This was the only area this occurred in within the magazine. Small droplets of aluminum slag were also found outside of the magazine, directly in front of the doors (encl 15).

(2) Cased propelling charges: There were 134 cased propelling charges (5- and 6-inch). They were stored in metal shipping containers. Approximately 10 percent of them suffered a violent rupture of the metal casing. Most were located in the front left portion of the magazine (encls 16-19).

(3) Mortar increments: 81mm mortar increments were stored in wooden boxes. The boxes were totally consumed with only ash remaining (encl 20).

b. Structure:

(1) The doors were heavily damaged. The metal cladding of the doors remained attached to the hinges but was deformed by the heat. There was fracturing of the concrete around the hinges where they are attached to the headwall. The wood was ignited by the fire and continued to smolder until the next morning and was completely consumed. There was no damage to other magazines in the 116-14 facility (encls 21-24).

(2) There was moderate spalling of the concrete and very heavy smoke damage in the rear third of the magazine (encls 25, 9, and 26). There was heavy spalling of the concrete in the center to the front portion of the magazine on the right side. The 81mm mortar increments were stored in this area (encl 20). There was light to moderate smoke damage to the left front corner of the magazine (encls 18 and 19). There was localized spalling and smoke damage in other areas of the magazine, especially along the lower portions of the walls where propellant containers were close to the walls (encl 17). There was an indentation approximately 1-inch deep in the front wall near the side wall, which was caused by the impact of a 6-inch 47-caliber cased propelling charge. There was severe spalling on the exterior front wall opposite the impact. An area approximately 2 feet by 2 feet, several inches deep was damaged. The steel mesh (reinforcing bar) was exposed, and fragments were thrown across the entire width of the 6-foot loading dock (encls 23, 27, and 28).

(3) Railroad tracks: The two railroad tracks directly in front of the magazine were damaged. The track farthest from the dock received the heaviest

damage. Expansion of the rails from the heat, and later cooling, displaced the ties up to 4 inches on the long axis, 2 inches on the short axis, and 2-3 inches on the vertical axis. Numerous ties were severely charred (encls 29-32).

6. Discussion:

a. Deflagration versus detonation: A review of the fire scene and witness statements indicated a deflagration (or rapid burning) occurred rather than a detonation.

(1) There were 134 cased propelling charges (5- and 6-inch). Approximately 10 percent of them suffered a violent rupture of the metal casing (encls 17-19). A large quantity of the remaining cased propelling charges were scattered about the magazine. Some traveled more than 40 feet. Several 5-inch, 54-caliber case propelling charges exited the door and were found in front of the magazine near the railroad tracks (encls 29-34). One 5-inch, 54-caliber propelling charge (that had a violent rupture) was found approximately 295 feet from the headwall (near the next magazine row) (encl 33).

(2) A number of closing plugs for the cased charges were found inside and outside of the magazine. Several almost intact closing plugs were found in front of the magazine beyond the railroad tracks (encls 31, 35, and 36). This indicated they had been pushed out of the case as pressure built up in the case.

(3) Numerous unburned propellant grains were found outside the magazine (encls 7 and 8).

(4) There was an absence of cratering or significant damage to the floor and foundation of the magazine.

(5) There was no rupture of the magazine or displacement of the earth cover.

(6) All items stored in the magazine had a hazard class of 1.3 (mass fire).

(7) The rear ventilator cap weighting 195 pounds was found approximately 30 feet behind the magazine in soft sand. It was undamaged (encls 37-39).

b. Fire sequence: Based on the physical evidence and witness statements, the fire appears to have started in the front left portion of the magazine in 8-inch, 55-caliber bagged propelling charges. This caused smoke and sparks to come out of the door vents and smoke out of the rear ventilator. The fire then spread to the 81mm mortar increments and remaining 8-inch, 55-caliber bag charges. As the propellant burned, the pressure increased causing the rear ventilator cap to pop off and the doors to open. This produced the large tongue of flame that came out of the doors and rear ventilator. The sage brush in front of the magazine was burned for a distance of approximately 135 feet with a burn pattern of approximately 45-degree radiating from the door (encls 1, 2, 35, and 40).

The 5-inch, 54-caliber and 6-inch, 47-caliber cased propelling charges started to deflagrate during the initial fire ball and continued after the fireball had subsided. They were stored in aluminum shipping containers with tight fitting lids.

c. Fire department: The fire department and other emergency personnel responded, but no attempt was made to fight the fire. It was permitted to burn itself out and cool overnight. A fire watch was posted.

d. Navy propellant - general:

(1) Smokeless powder is the propellant used in propelling charges of Navy gun ammunition. The 8-inch propelling charges use a single-base propellant with nitrocellulose (NC) as the main ingredient. It is colloided with ether and alcohol. A small quantity of diphenylamine stabilizer is added to assist in preserving the stability of the propellant. The proportion of diphenylamine is usually 0.5 to 1.0 percent. It is referred to as SPD propellant with the "SP" indicating single-base smokeless powder and "D" indicating diphenylamine stabilizer. Lots which have been reworked are indicated by a "W", and lots with material added to reduce the absorption of moisture are indicated by an "N".

(2) Decomposition: There are many factors which affect the decomposition of propellant during storage - high temperature, moisture, and age being the most important. The internal oxidation gives rise to the evolution of nitrogen dioxide (NO_2) which, in turn, oxidizes and denitrates the propellant, producing more NO_2 and heat, causing further oxidation and denitration, etc. Thus, the reaction is self-perpetuating or autocatalytic. If the NO_2 produced could somehow be removed, then the decomposition would continue at a slow, even rate. If, however, it is not removed, the propellant can rapidly reach its ignition temperature. This results in either a violent burning or deflagration results depending on the degree of confinement of the resulting gases.

(3) Stabilizer: To minimize these effects and thereby reduce the safety hazard of propellant and increase their shelf life, stabilizer is added to the propellant. Diphenylamine is used as a stabilizer primarily for single-base propellant. The diphenylamine combines with the NO_2 , effectively removing it and drastically reducing the rate of decomposition. This permits the decomposition to continue at a slow, even rate. There are only a limited number of reaction locations on each of the stabilizer molecules to absorb the oxides of nitrogen. Therefore, stabilization is only effective until the material is saturated. Afterward, the decomposition of NC can proceed essentially as with unstabilized material, to the point of risk of autoignition.

(4) 1988 Navy Gun Propellant Safety Surveillance Annual Report: The report is prepared by the Naval Ordnance Station, Indian Head, Propellant Group. The report contains the following two statements:

(a) "Pyro (SPD, SPDF, SPDW, and SPDB) propellants have a safe shelf age between 30 and 40 years, decreasing with age. Many of these propellant lots have passed their predicted safe shelf life which means there is a greater than 5-percent chance that they will be condemned." (Note: The actual

recommendation to dispose of a propellant lot is only made after a lot fails the oven test. The sample of propellant is stored at 65.5 degrees Celsius. When it fumes in 30 days or less, the lot is considered to have failed the test.)

(b) "We have not yet established a definite relationship between the quantity of stabilizer remaining in a sample of propellant and the length of safe shelf life expectancy, between days to fume and remaining stabilizer content."

(5) Lot number: Smokeless powder index numbers are assigned serially to smokeless powder (propellant) that has been manufactured and proofed. The numbers aid in the identification of each index and also give an approximate indication as to the age of the propellant. A propellant lot number is also assigned to identify the manufacturing facility. When the propellant is used in the assembly of propelling charges, a separate propellant lot number is also assigned. One propellant index number can be used in several propelling charge lots.

e. Navy Propellant - Magazine 116-14-E:

(1) Propelling charge lots DG-2-CO-68, DGR-1-HAW-55, DGR-11-CO-68, DGR-13-CO-68, DGR-14-CO-68, DGR-5-CO-69, and DGR-8-C-51 were identified as having low stabilizer content. It ranged from 0.04 to 0.13 percent stabilizer content. Disposal was directed by Navy Notices of Ammunition Reclassification (NARs) 645-87, 1020-87, 597-88, and 598-88 and Army ammunition information notice (AIN) 12-88. When stabilizer content reaches 0.20 percent, disposal of the propellant is normally recommended.

(2) Information provided by Naval Ordnance Station, Indian Head, MD, Propellant Group, to Naval Weapons Support Center Crane, Code PM4, and to the AMCCOM Safety Office (10 August 1989) indicated the following data on "Last Fume Date/Days to Fume" for the following propelling charge lots: DGR-8-CO-68 - no data; DGR-1-HAW-55 - day 221 of 1989/255 days; DGR-11-CO-68 - day 89 of 1989/252 days; DGR-13-CO-68 - day 114 of 1989/172 days; DGR-14-CO-68 - day 34 of 1989/239 days; DGR-3-YO-67 - 173 of 1986/23 days; DGR-5-CO-69 - day 94 of 1989/229 days; and DGR-8-CO-69 - day 192 of 1984/14 days. Disposal of lots DGR-3-YO-67 and DGR-8-CO-69 was directed by NARs 645-87 and 597-88, respectively.

(3) At least two of the propelling charge lots have propellant that was used in several lots. This is indicated by a common index number. For example, propelling charge lot DGR-8-CO-68 has the same index number (8664) as lots DGR-8-CO-68 and DG-2-CO-68, and propelling charge lot DGR-14-CO-68 has the same index number (8521) as lot DGR-6-C-51.

f. Disposal actions: Hawthorne AAP submitted a request to the State of Nevada for permission to open burn/open detonate a quantity of propellant identified as having low stabilizer content. Part of the material stored in Magazine 116-14E was included in the request. The request was denied. The denial was based, in part, on the fact that the stabilizer tests were conducted on material not stored at Hawthorne AAP; these tests did not correctly reflect the condition of material stored under ideal conditions at Hawthorne AAP.

g. Potential causes: At the beginning of the investigation, a variety of fire causes was considered. They included electrical malfunction; mechanical malfunction; sabotage/arson; lightning; careless smoking; flammable liquids or gases; friction; high ambient temperature in the magazine; and spontaneous combustion. Other causes were not considered due to the absence of any evidence which would support such a determination.

h. Discounted causes: The following causes were considered, but were discounted, based on the available evidence:

(1) Electrical malfunction: There was no electrical service to the magazine.

(2) Mechanical malfunction: There was no permanent or temporary mechanical equipment in the magazine, including material handling equipment.

(3) Sabotage/Arson: The Hawthorne AAP Government security staff determined there was no sabotage/arson. Additionally, the latch was found to still be through the hasp and secured with a Navy padlock (encl 41).

(4) Lightning: A thunderstorm moved through the Hawthorne AAP area at approximately 2100, 8 August 1989. There was more than a 10-hour gap between the storm and the fire. There was no evidence of lightning strikes in and around Magazine 116-14 and adjacent magazines. The bonding and grounding system of the magazine and adjacent railroad tracks was checked on 16 March 1989. The readings were 5.9 ohms for the building ground and 0.1 ohms for bonding of metal bodies. This is within the values permitted by AMCR 385-100 and DOD 6055.9-STD. There is no lightning protection system. A check of the system after the fire revealed no problems or abnormal readings. The readings were 3.6 ohms for the building ground and 0.1 ohms for bonding of metal bodies. The rear vent cap showed no signs of a lightning strike, fire damage, or smoke damage.

(5) Careless smoking: There was no evidence of discarded smoking materials or matches. The entire area is a "no smoking" area.

(6) Flammable liquids and gases: There was no evidence of flammable liquids or gases being used or stored in or around the magazine.

(7) Friction: There was no mechanism present to cause friction.

(8) High ambient magazine temperature: There is no indication of high temperatures in the magazine prior to the fire. A recording thermometer was located in Magazine 116-14-A. It indicated a high temperature of 78 degrees Fahrenheit when checked after the fire.

(9) Spontaneous ignition of 81mm mortar increments: The 81mm mortar lots had stabilizer contents ranging from 0.40 to 0.80 percent based on information provided by the AMCCOM Product Assurance Directorate.

(10) Spontaneous ignition of 5- and 6-inch propelling charges: There was no indication of low stabilizer in the 5-inch, 54-caliber and 6-inch, 47-caliber cased propelling charges.

1. Most probable cause: Spontaneous ignition of 8-inch, 55-caliber bagged propelling charges located in the front left portion of the magazine is the most probable cause. This was due to the loss of stabilizer and subsequent increase in rate of decomposition. This is based on the physical evidence and witness statements.

(1) Propelling charge lots DG-2-CO-68, DGK-1-HAW-55, DGR-11-CO-68, DGR-13-CO-68, DGR-14-CO-68, DGR-5-CO-69, and DGR-8-C-51 were identified as having low stabilizer content. They were located in the left front portion of the of the magazine. It ranged from 0.04 to 0.13 percent stabilizer content. Disposal was directed by Navy NARs 645-87, 1020-87, 597-88, and 598-88 and Army AIN 12-88. When stabilizer content reaches 0.20 percent, disposal of the propellant is normally recommended.

(2) The heaviest fire damage was located in the front left corner of the magazine where the 8-inch, 55-caliber propelling charges were located. The 8-inch, 55-caliber bagged propelling charge containers were stored in aluminum shipping containers. The walls are made of light-gauge aluminum. The lids and ends are constructed of heavier gauge aluminum. The containers located near the front, to the left of the door, were almost totally destroyed. Virtually none of the walls remained, and major portions of the ends/lids were destroyed. Aluminum slag was found on the floor. This indicates the aluminum was exposed to temperatures of more than 1,200 degrees Fahrenheit for a period of time sufficiently long to have become molten. This was the only area this occurred in.

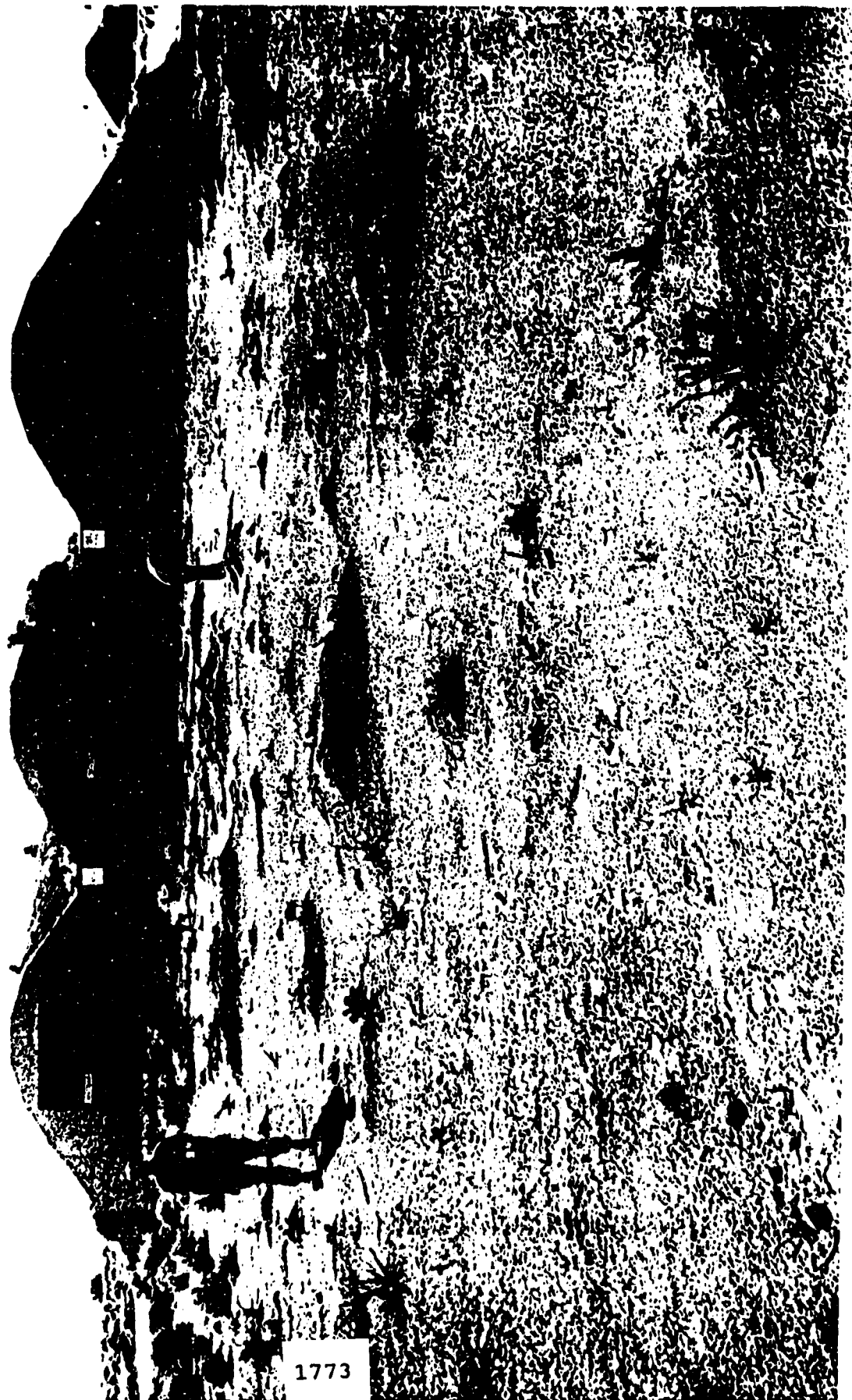
(3) Containers of 8-inch, 55-caliber bagged propelling charges located near the rear of the magazine had substantial portions of their walls remaining. Most of the ends/lids remained intact, as they were constructed of heavier gauge metal. The containers located in the center of the magazine had most of the wall missing, but most of the ends remained intact.

(4) Witnesses indicated they first observed sparks/fire and smoke coming from the door ventilators and smoke coming from the rear ventilator. This was followed by a "rush of air", the doors being pushed open, and the rear ventilator cap being blown off. A jet of flame came from the doors burning the sage brush. A smaller jet of flame came from the rear ventilator and was described as looking like "a rocket taking off". The very intense burning continued for approximately 3 minutes and then decreased significantly. During this period of decreased burning, several loud "bangs" were heard. These were apparently 5-and 6-inch cased propelling charges deflagrating. This delayed deflagration can be attributed to the fact that the cased charges had a closing plug and were stored in metal shipping containers. This provided some insulation from the heat generated by the initial fireball.

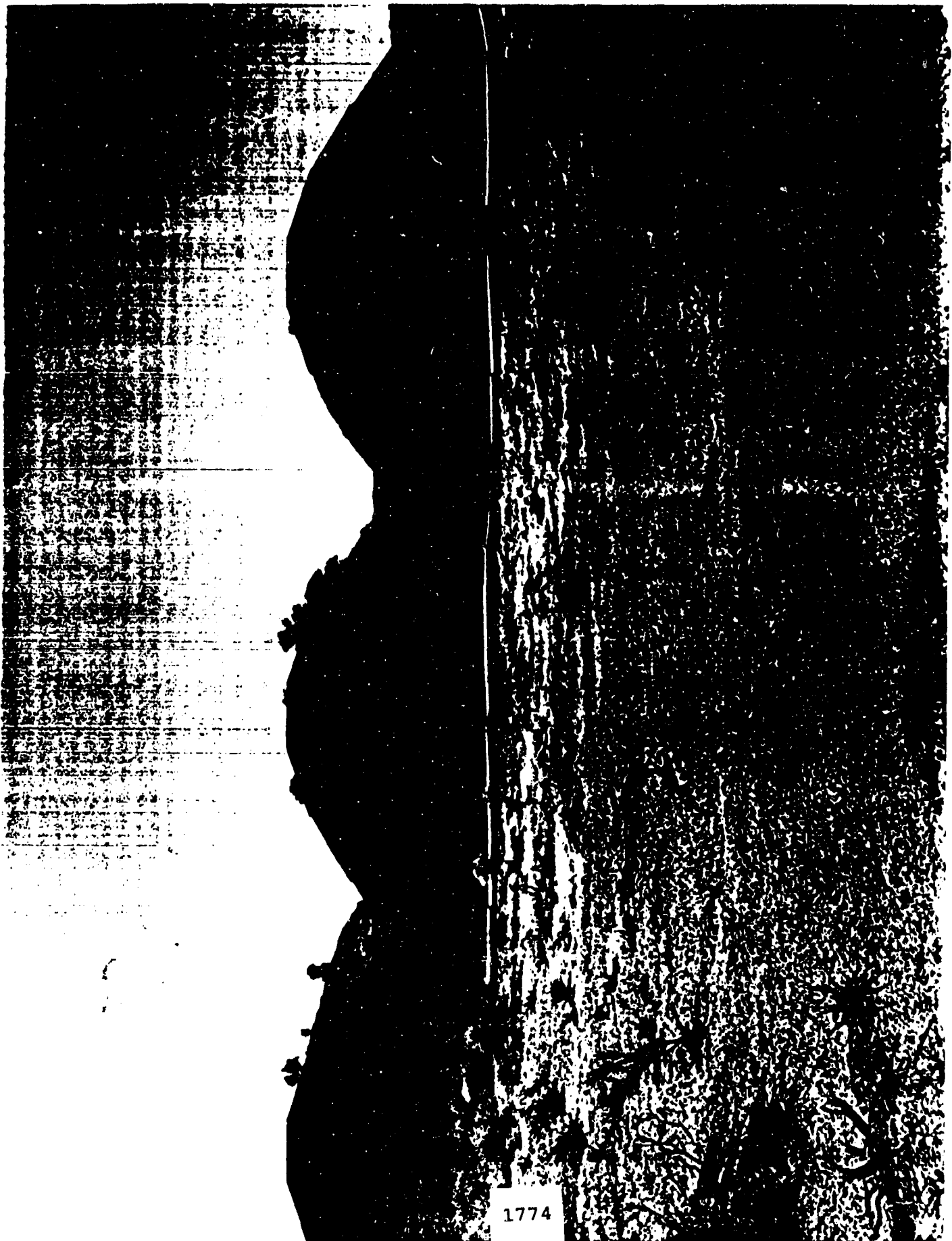
7. Conclusions:

a. When the heat generated by the decomposition was added to the system and combined with the increased pressure within a sealed shipping container, the stabilizing capacity of the remaining diphenylamine was overwhelmed, and the autoignition temperature of the propellant was reached. The result was a violent reputure and deflagration of the propellant stored in Magazine 116-14E.

b. Based on the available evidence, the most probable cause of the fire was the spontaneous ignition of 8-inch, 55-caliber bagged propelling charges due to the loss of stabilizer and subsequent increase in rate of decomposition occurring in one of the lots located in the left front portion of the magazine. They were propelling charge lots DGR-2-C-68, DGR-1-HAW-55, DGR-11-CO-68, DGR-13-CO-68, DGR-14-CO-68, DGR-5-CO-69, and DGR-8-C-51.



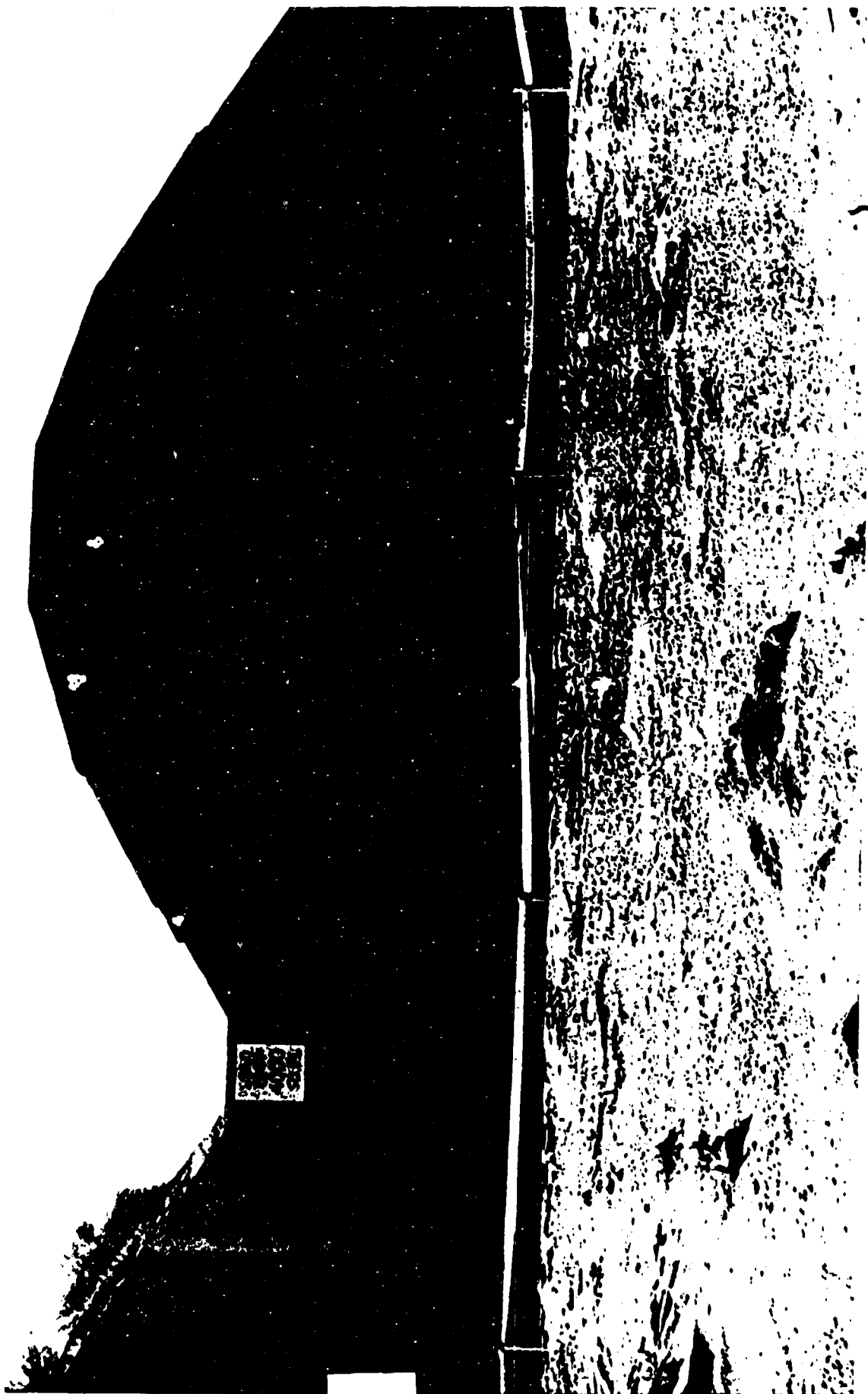
1773



1774

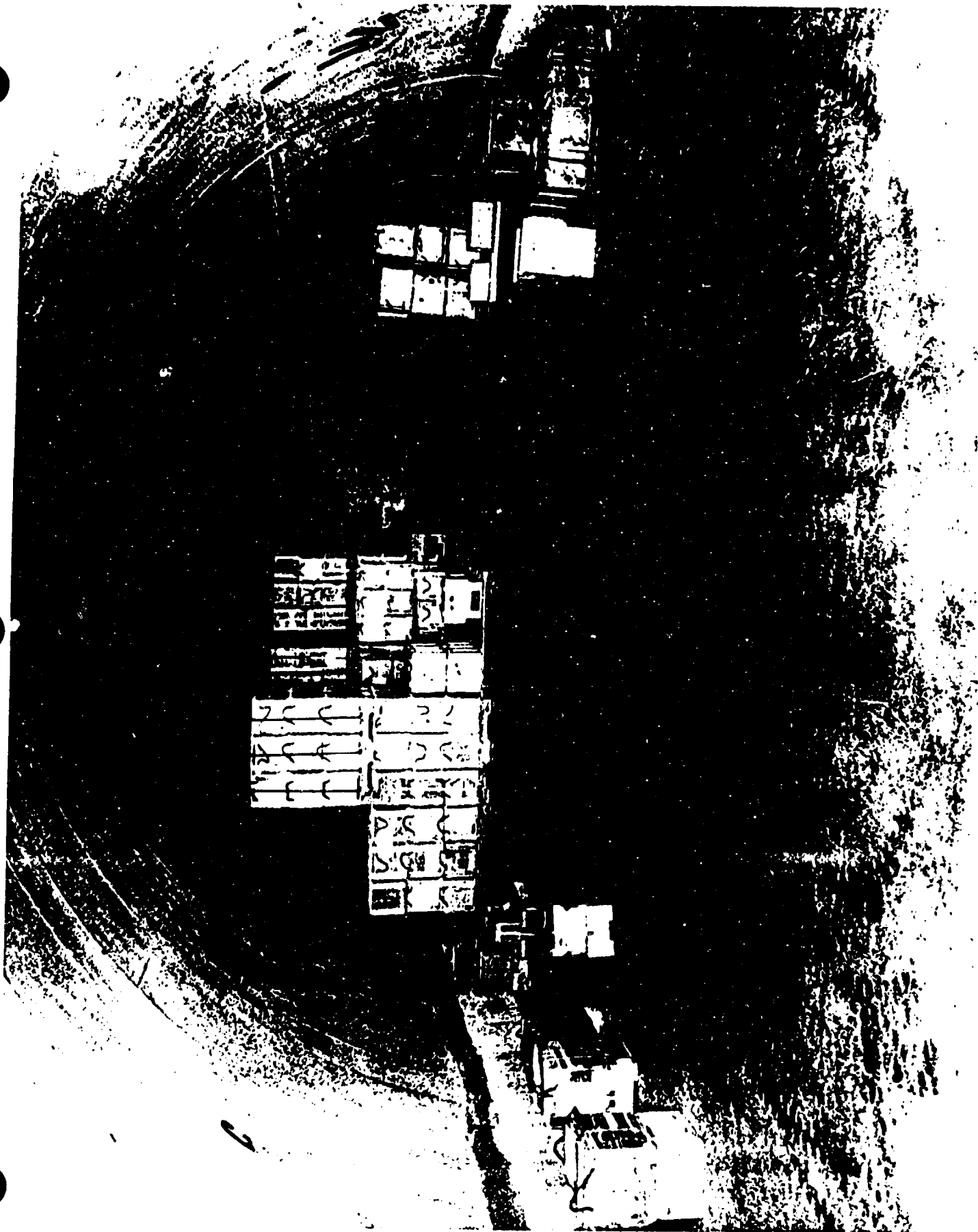


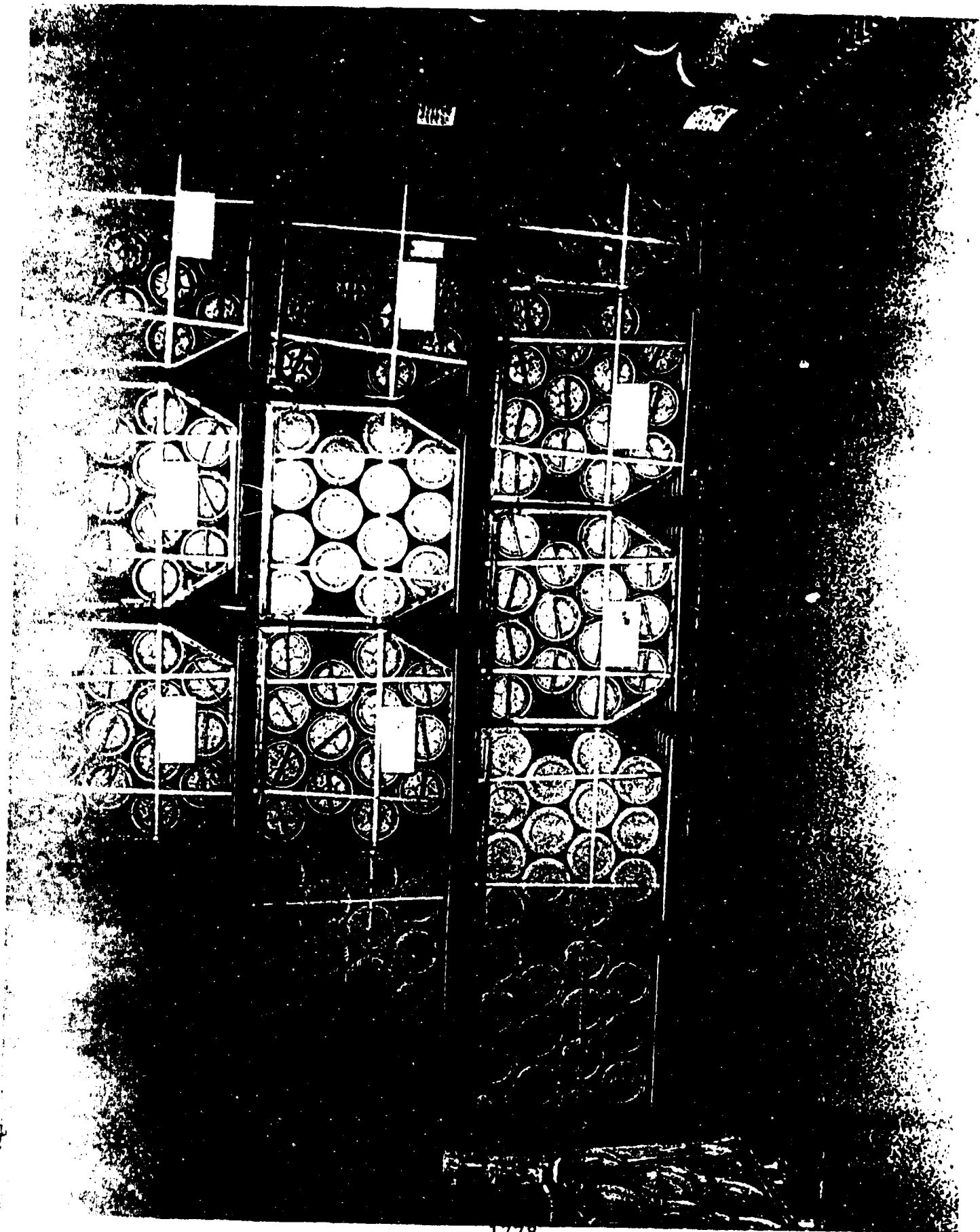
1775



1776

4



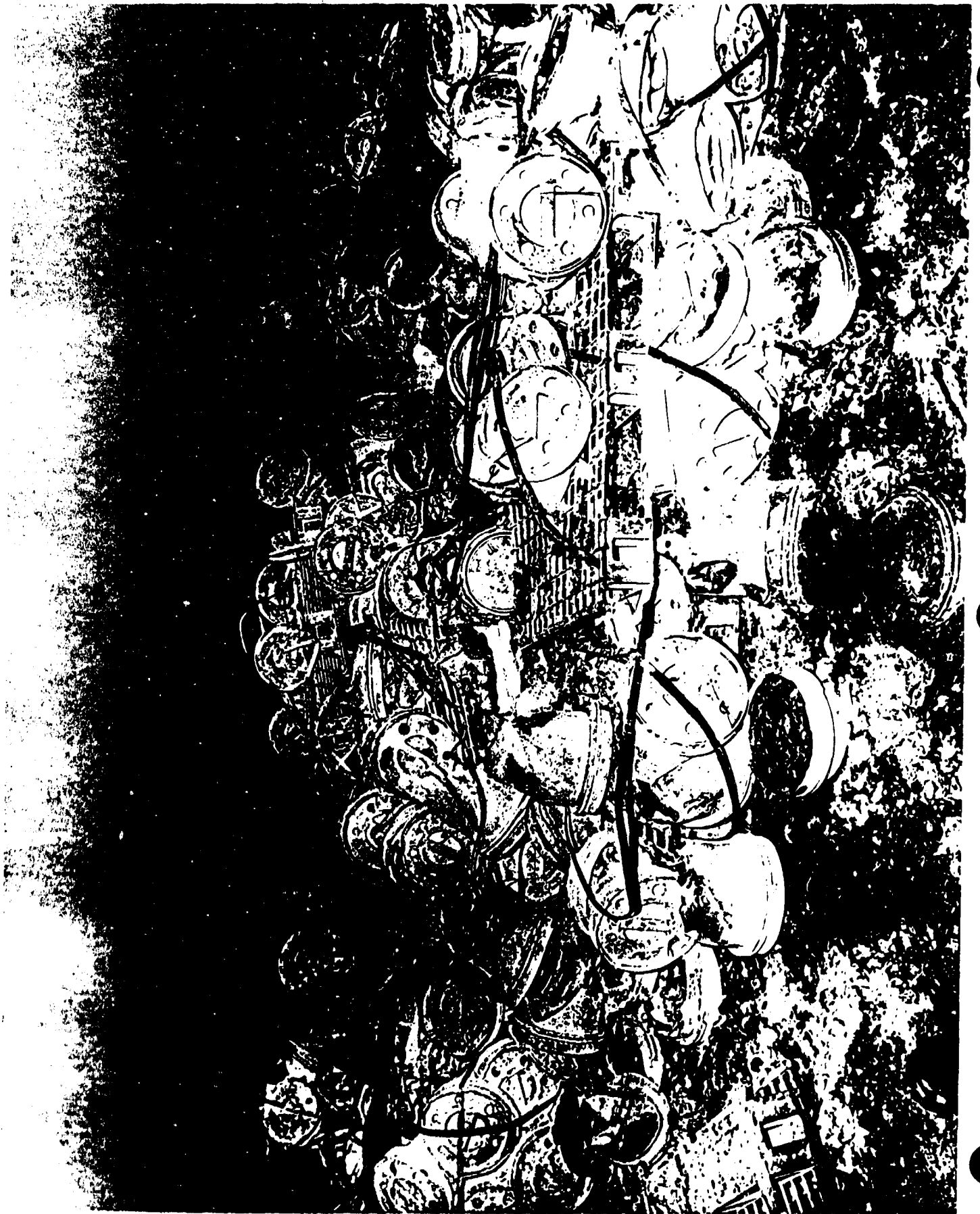




1779









1783

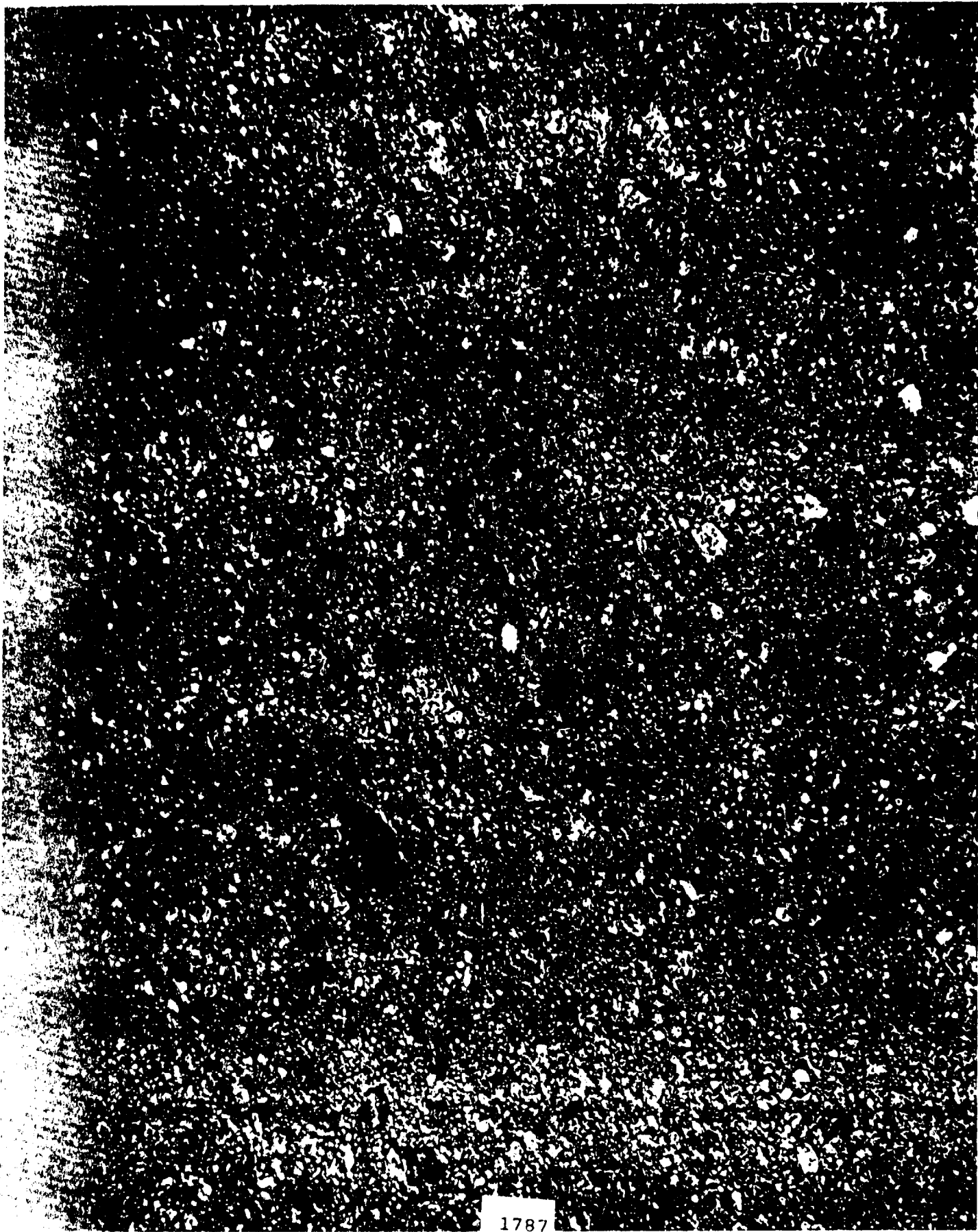
11





1785





1787

15





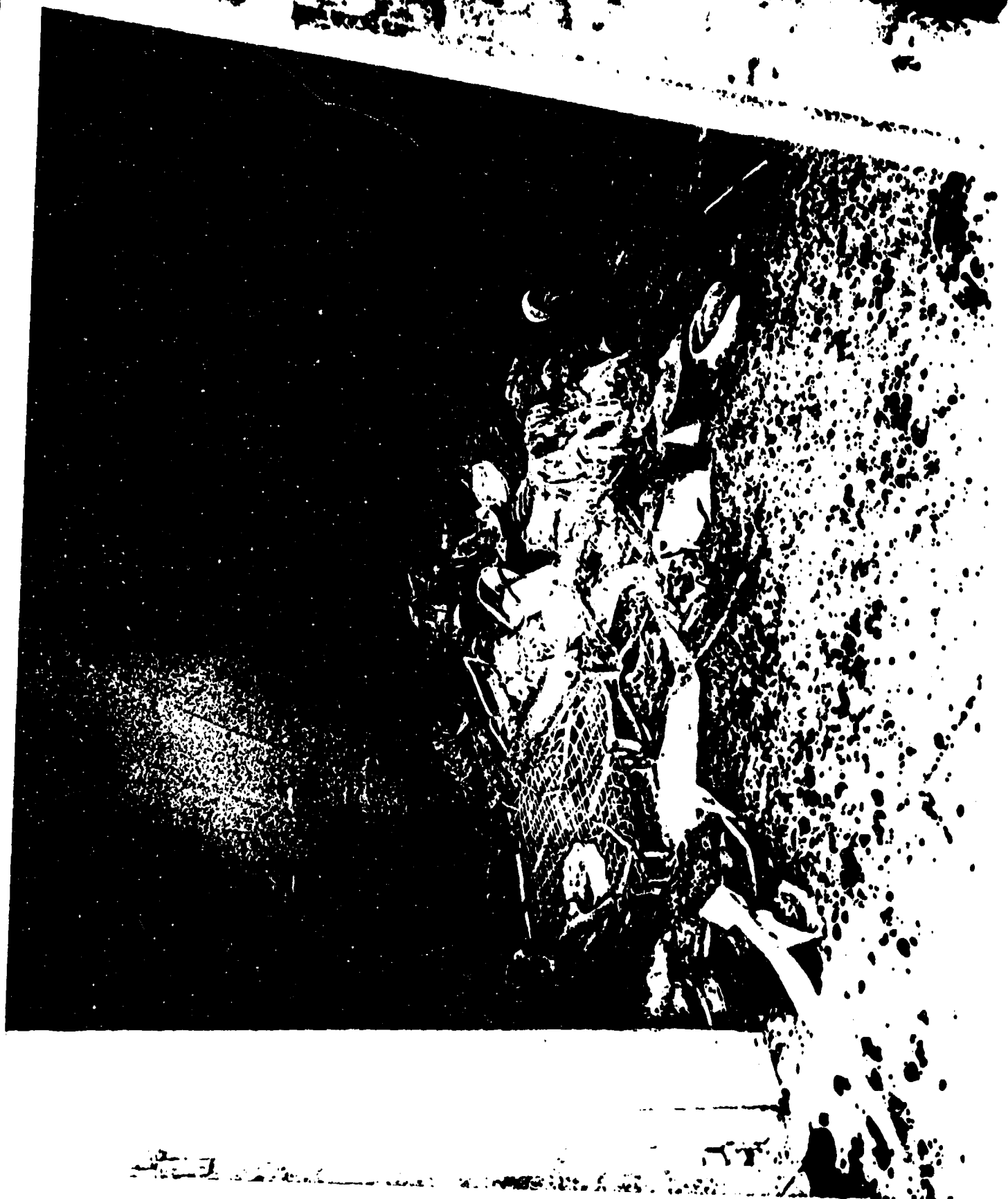
1789

17



1790

18



1791





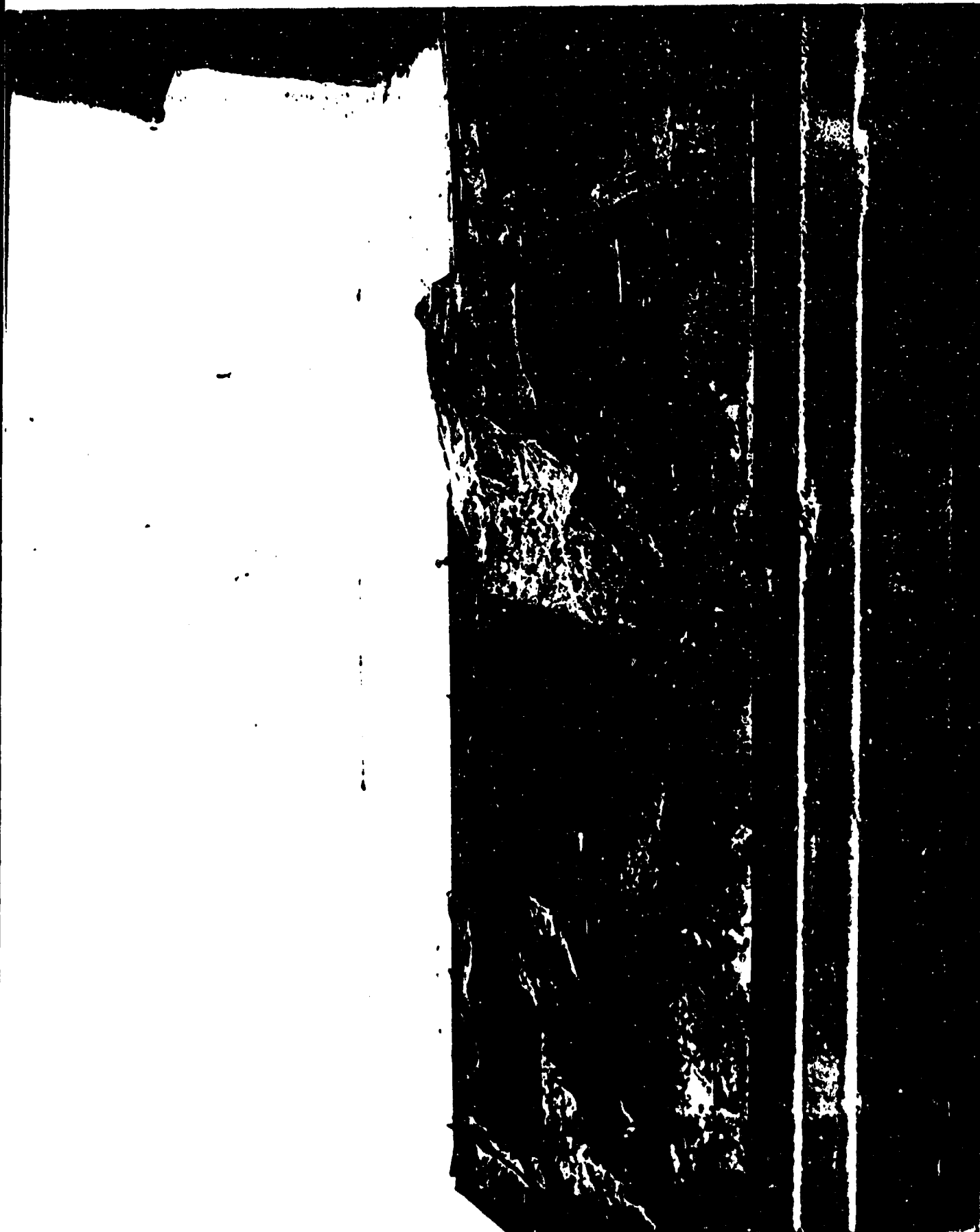
1791





1793

21



1794

22



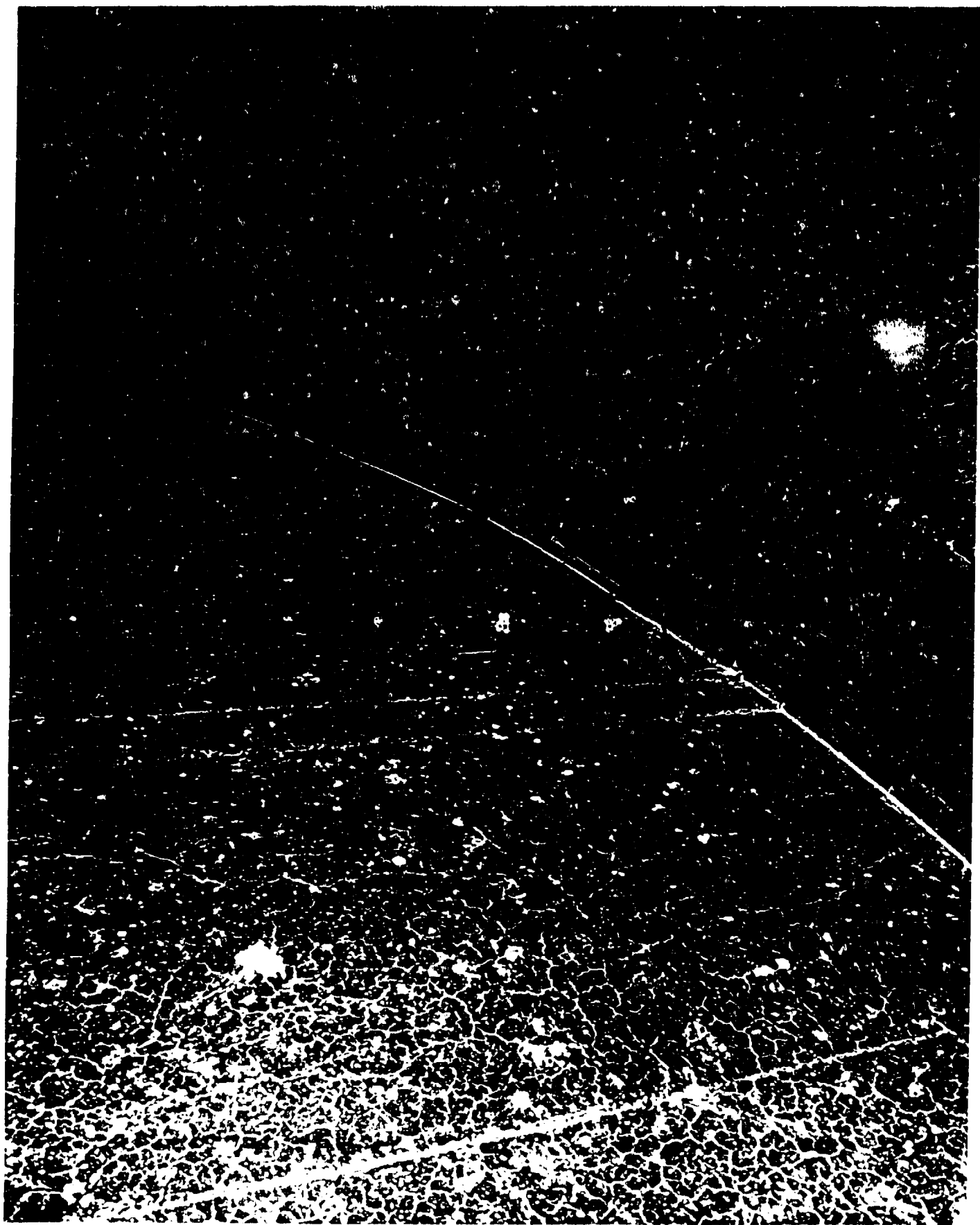
1795

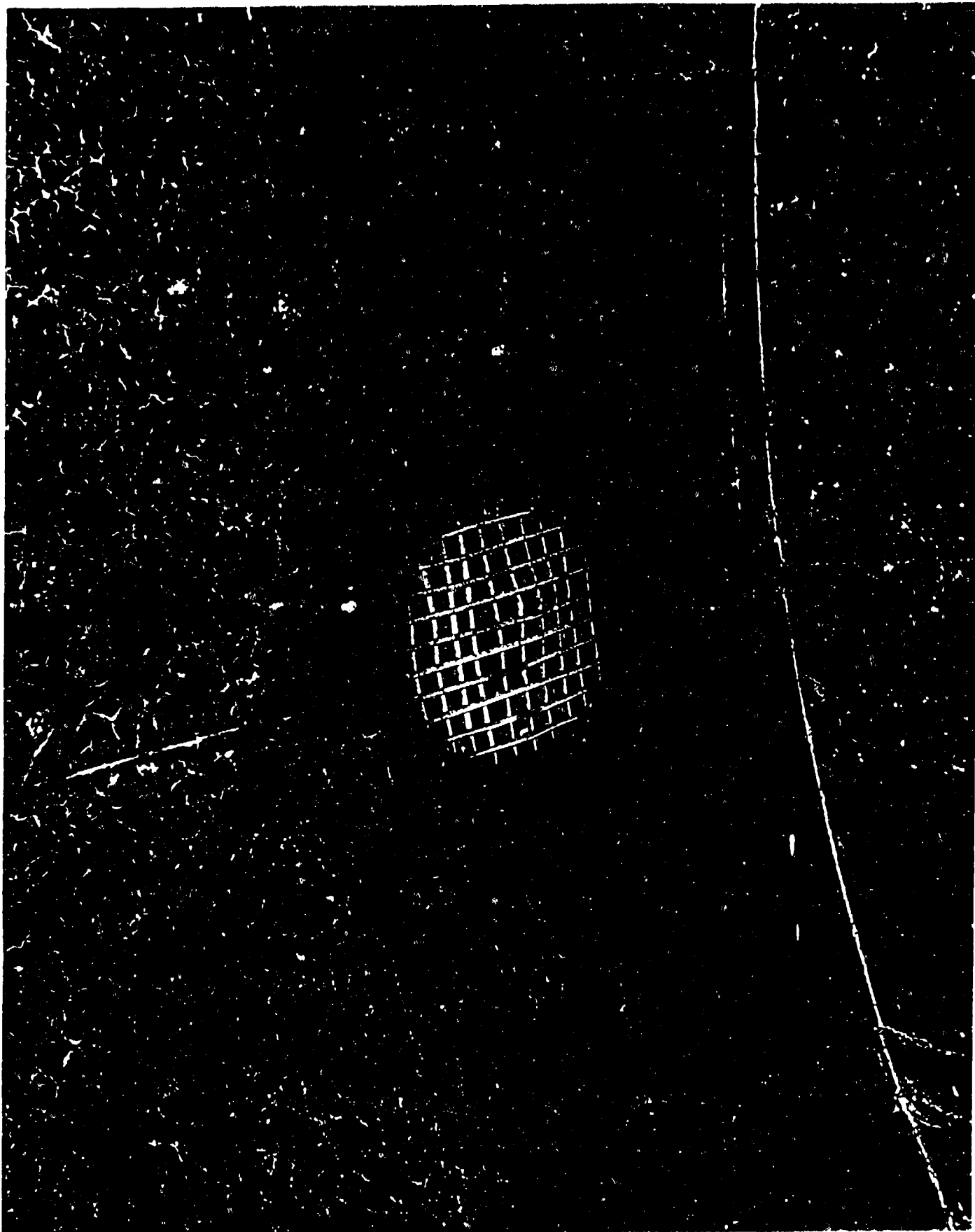
23



1796

24



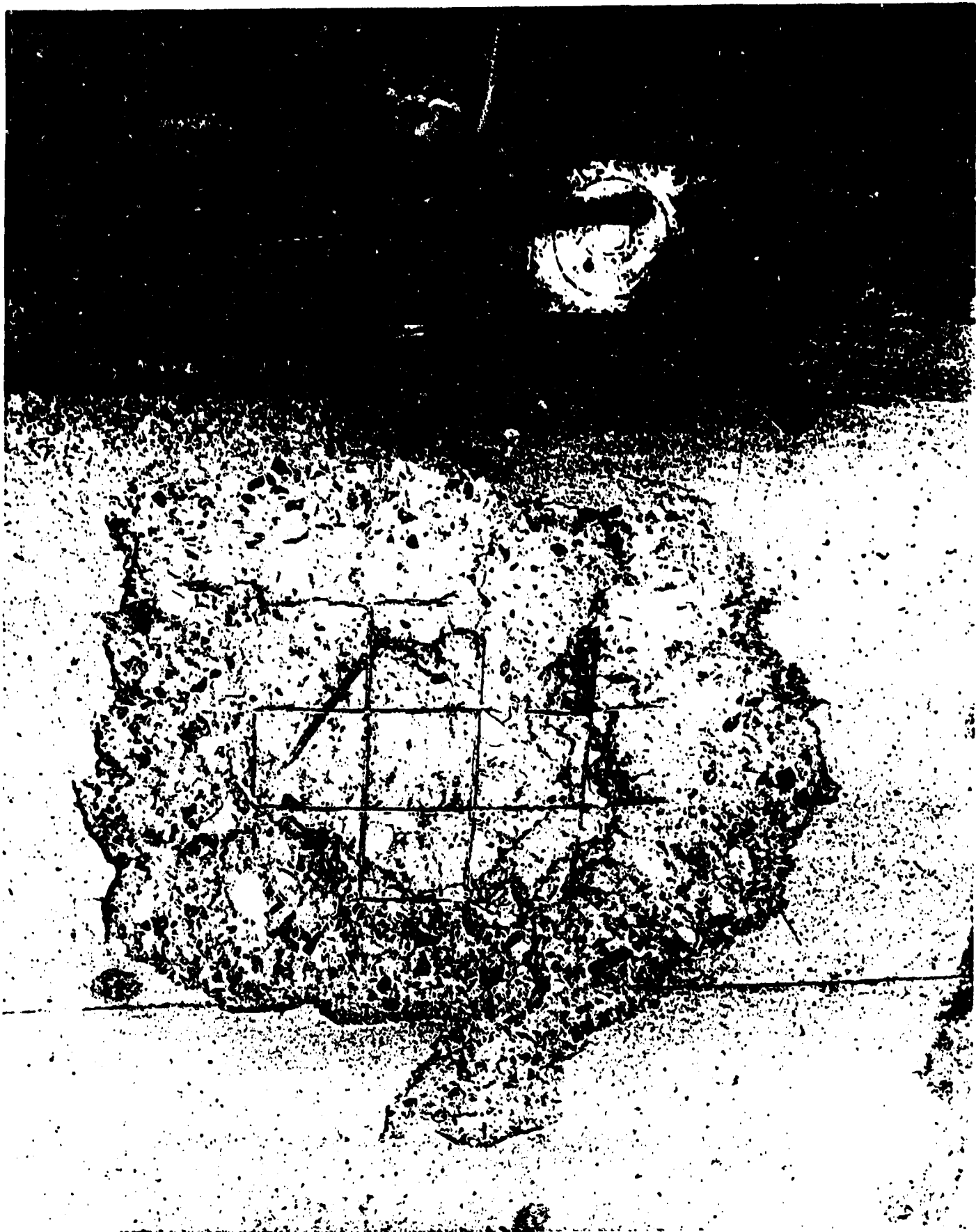


1798

6



1799



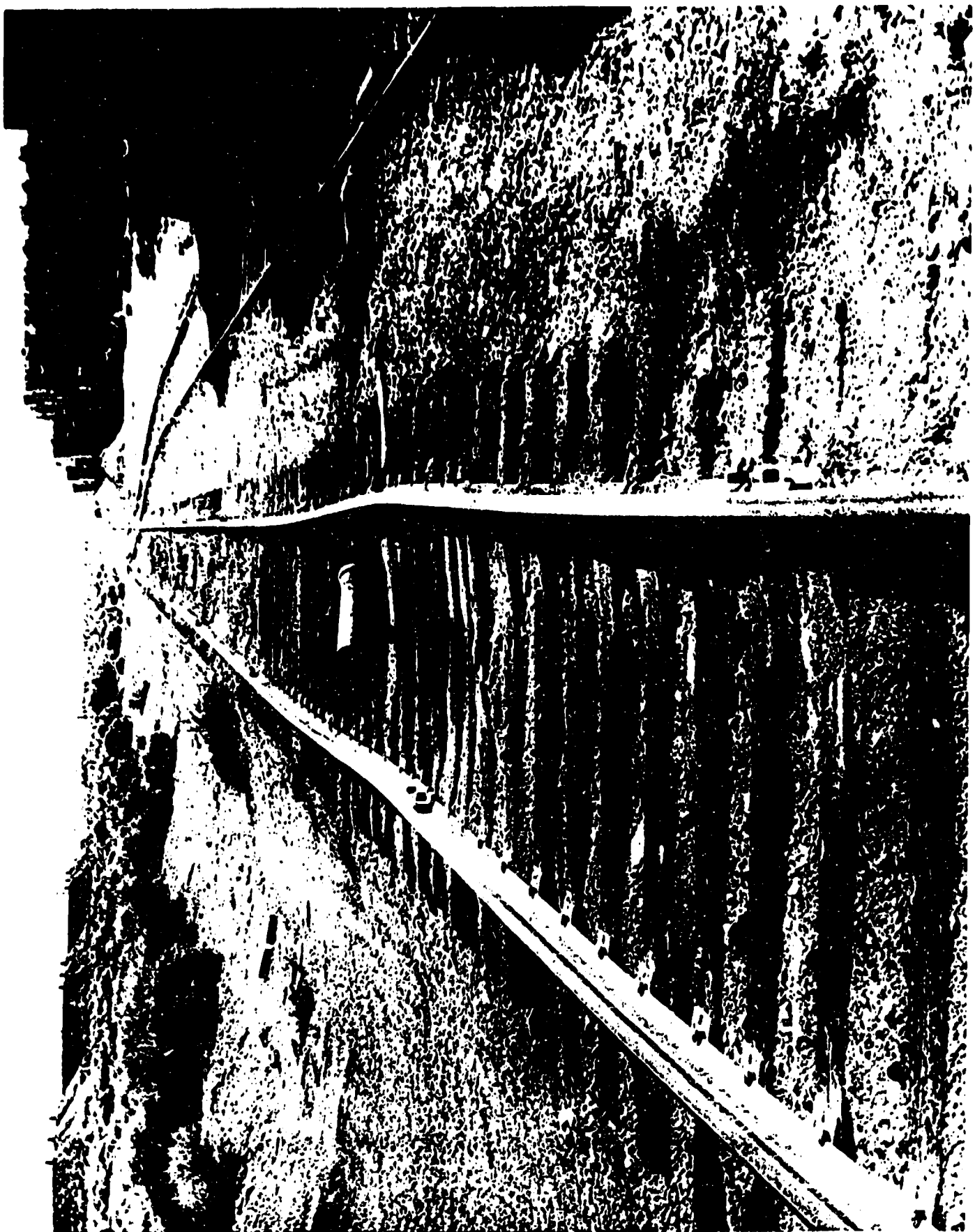
1800

28



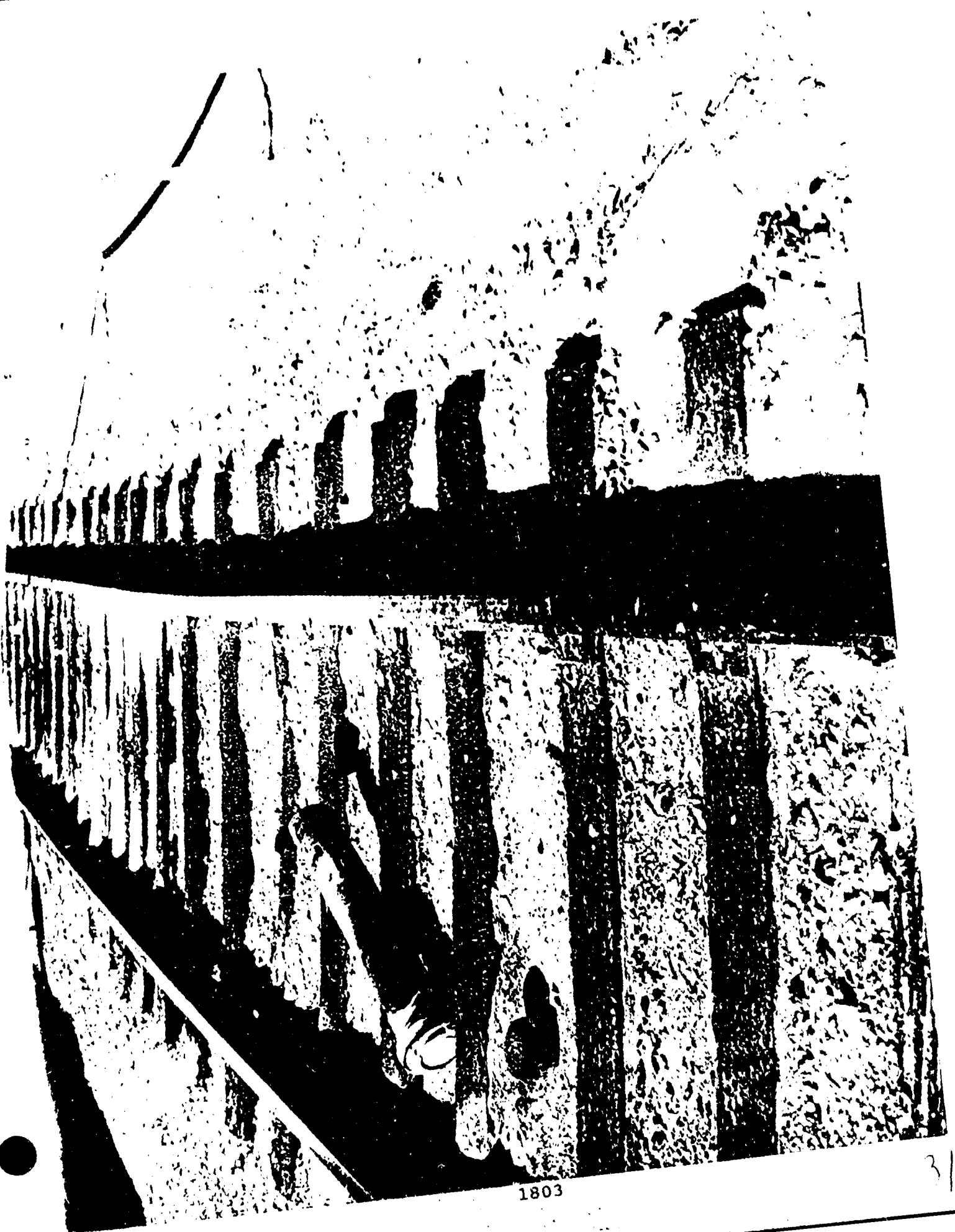
1801

29

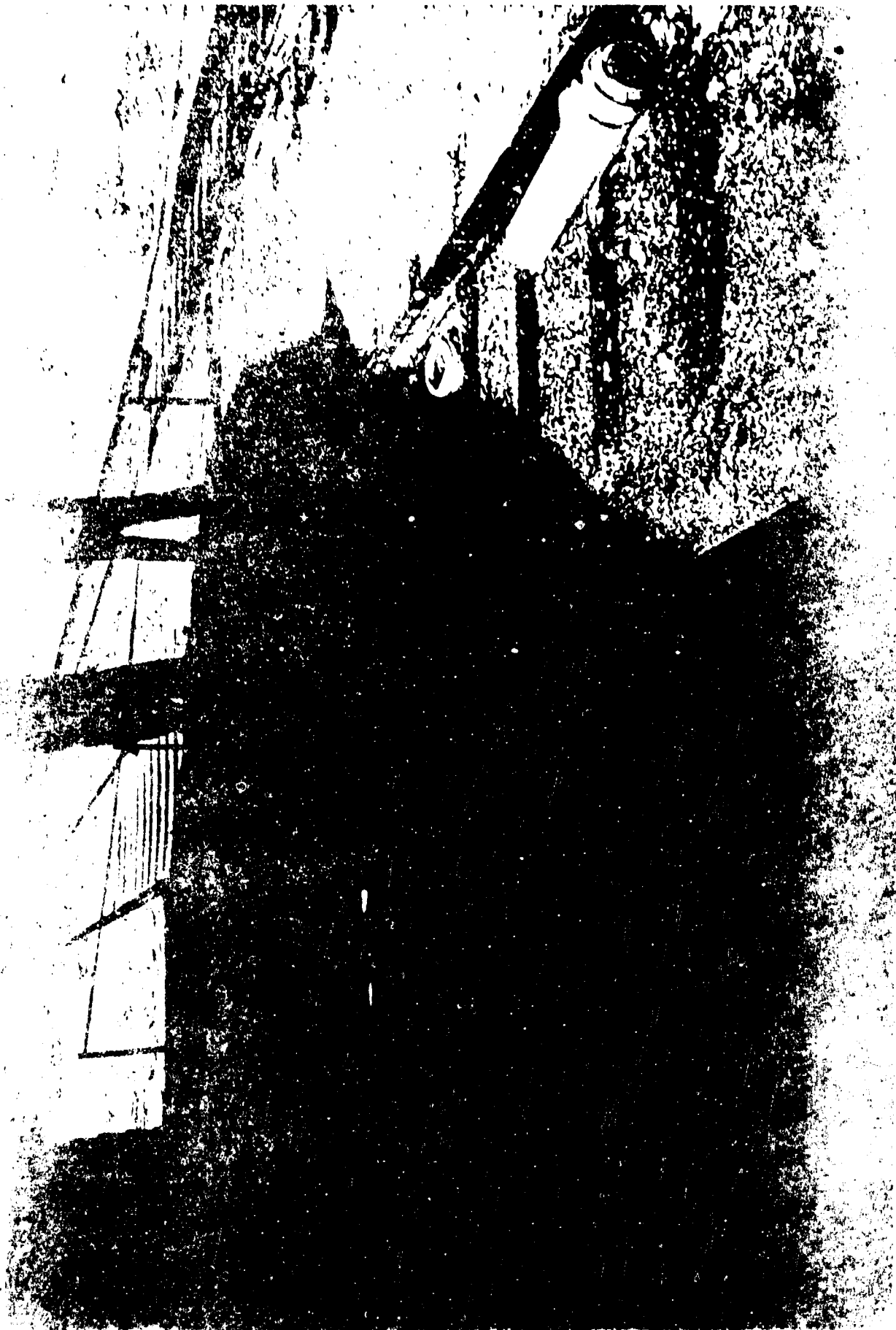


1802

30



1803



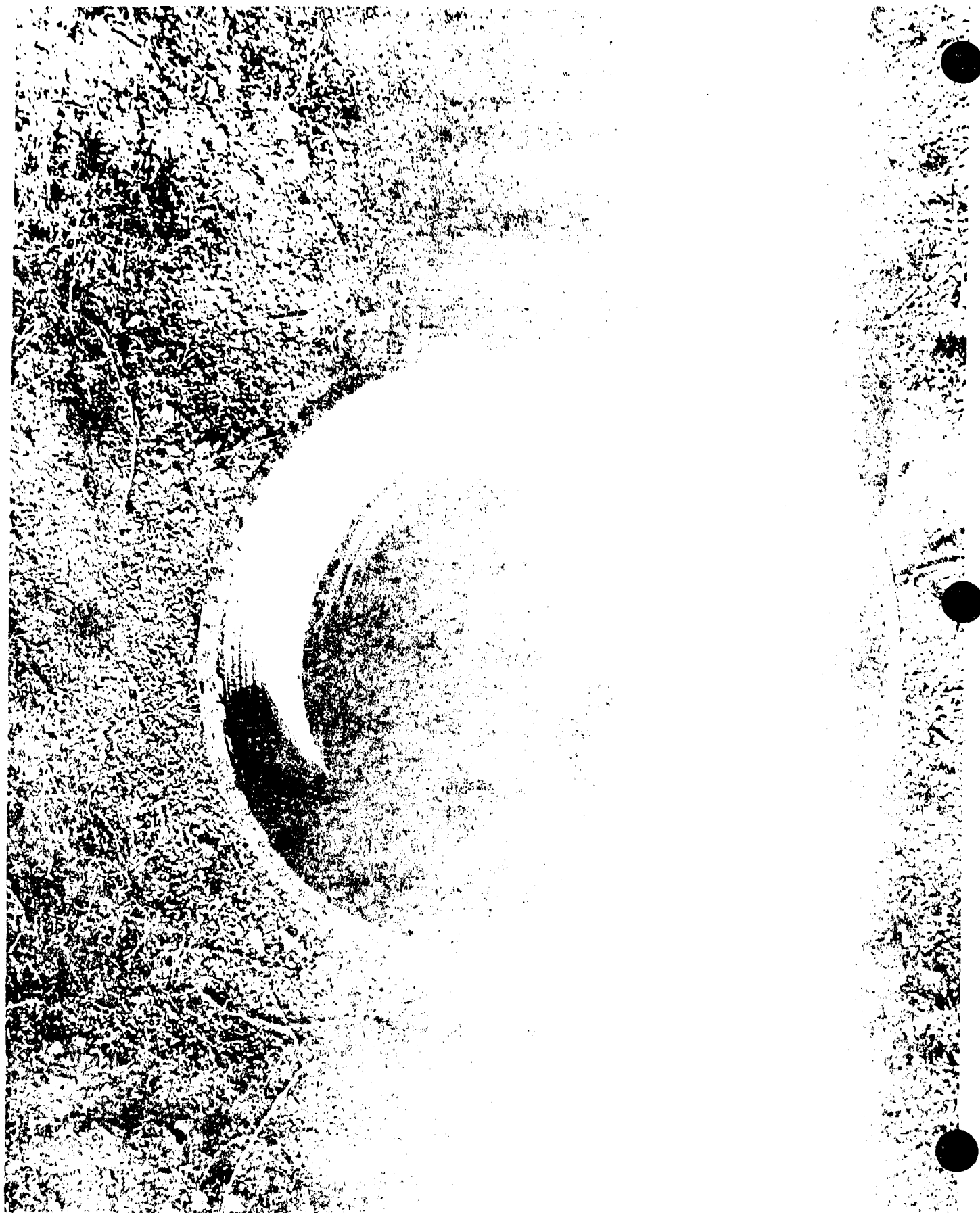
















Scaled Debris Throw of Third Generation Norwegian/US Aircraft Shelters

By

Patricia M. Bowles
Kirk A. Marchand
John W. Strybos

ABSTRACT

A new aircraft shelter design is to be used in the construction of shelters throughout Norway. The new shelter is called the third generation Norwegian/US shelter due to structural characteristics common to both the third generation Norwegian shelter and the third generation US shelter. Since test data for debris and blast hazards do not exist for this new shelter configuration, NATO has recommended using current aircraft shelter siting criteria to establish safe locations for the newly constructed shelters. The current criteria are based on test results and conclusions from the DISTANT RUNNER program, which was a series of full scale explosion tests including both external and internal detonations of munitions stored in third generation US aircraft shelters. Although there are structural similarities between the third generation US shelters and the third generation Norwegian/US shelters, major differences between the front door systems and the lack of any rock rubble berm on the DISTANT RUNNER tested shelters raised some concern about applying the current criteria to siting of the new shelters. An initial 1/15 scale test series recently completed documents the effect of a rock rubble berm on the initial velocities and angles at which concrete debris leave a shelter following an internal detonation. Three different shelter designs and three explosive yields were tested in the series, which included tests with and without a rock rubble berm for all configurations. The tests provide meaningful data on the effect of placing berms on existing and new shelters and on the response differences between the three aircraft shelter designs.

1.0 Introduction

A new aircraft shelter design proposed by Norway is being used in the construction of shelters throughout Norway. The new shelter is called the third generation Norwegian/US aircraft shelter due to structural characteristics common to both the third generation US shelter and the third generation Norwegian shelter. Since test data for debris and blast hazards do not exist for this new shelter configuration, NATO (North Atlantic Treaty Organization) has recommended using current aircraft shelter siting criteria to establish safe locations for the newly constructed shelters. The current criteria are based on test results and conclusions from the DISTANT RUNNER program (References 1-3), which was a series of full scale explosion tests including both external and internal detonations of munitions stored in third generation US aircraft shelters. Although there are structural similarities between the third generation US shelter and the third generation Norwegian/US aircraft shelter, some concern about applying the current criteria for siting the third generation Norwegian/US aircraft shelter has been raised.

An initial design comparison study conducted by Southwest Research Institute (SwRI) noted structural differences which would affect shelter breakup under internal loads (Reference 4). The study concluded that the major differences between the front door systems of the two shelters and the lack of any rock rubble berm on the shelters tested in DISTANT RUNNER should preclude utilization of current criteria in siting the new shelters. Since the comparisons made in this study could not form an adequate basis of information for establishing quantity-distance (Q-D) criteria for the new shelters, a number of recommendations were made. The recommendations were presented to develop a level of confidence necessary to establish new Q-D criteria.

The first recommendation was a series of small scale tests to determine the effect of the proposed rock rubble berm on the response of the shelter arch when subjected to internal explosive loading. Tests to be performed on models of the new shelter design and the DISTANT RUNNER type shelters were suggested. The Norwegian Defence Construction Service (NDCS) funded SwRI to conduct 1/15 scale tests of three different charge quantities in the two aforementioned shelters and in a Federal Republic of Germany (FRG) shelter, all in both a bermed (with rock rubble) and an unbermed (without rock rubble) configuration. That test series is the subject of this paper.

2.0 Objectives

The objective of the subject program was to document the effect of a rock rubble berm on the initial velocities and angles at which concrete debris leave a shelter following an internal detonation. To quantify this effect, the program included 1/15 scale model tests of three different shelter designs: the third generation Norwegian/US, the DISTANT RUNNER, and the FRG shelters. Three explosive yields were included to observe differences in breakup due to internal loading. All combinations of shelter and charge amount were to be tested with and without the rock rubble berm.

The models used were replica structures in diameter and crown height with limited section length. The doors were not replica panels, but were designed to have a mass and attachment which would provide a scaled quasistatic impulse replicating that expected in full scale. The door mass/unit area was designed to provide the correct scaled gas impulse for the limited section length and corresponding limited volume. This technique was chosen since a consistent two dimensional debris pattern was expected. The rear wall of each model was non-responding and rigid. The arches were simulated with modeled concrete and reinforcement.

The TNT equivalent 1/15 scale charges used were 0.09 Kg (0.2 lb), 0.27 Kg (0.6 lb), and 0.82 Kg (1.8 lb), corresponding in full scale to 307 Kg (675 lb), 909 Kg (2000 lb), and 2727 Kg (6000 lb) respectively. The original test plan included a larger 1/15 scale charge weight of 1.4 Kg (3 lb) instead of the 0.09 Kg (0.2 lb) charge; however, early tests indicated the shelters were so overpowered by this load that velocity and angle data would be not only difficult to obtain from the high speed film, but also may not be very useful in defining quantity-distance.

High speed cameras provided most of the data needed to meet the program objectives. In order to obtain quality velocity and angle data from the high speed films, three explosive sources were investigated. The use of high explosives as the source clearly limited the amount of data which could be extracted from film analysis. As a means to minimize the detonation flash and smoke which obscure the observance of debris movement, a hydrogen/oxygen mixture was tried as the source. Although good results were obtained from initial tests, the mixture proved to be too sensitive to early ignition and had to be discarded. The majority of the tests were conducted using a more stable propane/oxygen mixture as the source.

Although the objectives of this test program were simple in scope, the tests provided meaningful data on the effect of placing berms on existing and new shelters and on response differences between the three aircraft shelter designs. A secondary objective of the program was to add to the database of debris launch velocities from internal detonations in concrete structures. There may indeed be a way to relate all these data to enable prediction of launch velocity for a variety of structures without the need to test each time a new structural design is introduced. Further analysis toward this goal is recommended.

3.0 Modeling of Structures

The aircraft shelters were modeled in 1/15 scale. Table 1 summarizes a structural comparison of the three shelters tested. Tables 2, 3, and 4 list predicted loads on the full scale structures. The corrugations on the shelters were not modelled since commercially available corrugated steel did not have the correct corrugations and thickness. Also, the corrugated steel, while providing form work for full scale construction, is only 3 mm in thickness, or 0.3% of the total cross section. The tensile capacity of the liner was included in the steel area which was scaled to design the model reinforcement. The reinforcement spacing and number of layers were modeled as these are critical to the failure pattern. The vent panel weight was selected by calculating the venting and volume requirements necessary to produce the same scaled gas impulse for the particular load using methods

Table 1. Structural Comparison

Building Dimensions	Norwegian/US	DISTANT RUNNER	FRG
inside plan width	23.5 m	21.6 m	24.0
inside plan length	37.2 m	36.6 m	30.0
inside height at crown	7.04 m	8.43 m	7.75
volume	5079 m ³	5221 m ³	4338 m ³
Arch			
corrugation depth	360 mm	360 mm	none
arch thicknesses at base (including corrugation)	1360 mm	810 mm	1200 mm
arch thickness at crown (including corrugation)	810 mm	810 mm	1200 mm
total circumferential reinforcement (area/unit spacing)	3.8 mm ² /mm	1.31 mm ² /mm	1.59 mm ² /mm
total horizontal reinforcement (area/unit spacing)	2.5 mm ² /mm	1.31 mm ² /mm	1.59 mm ² /mm
typical circumferential reinforcement spacing	100 mm o.c.	150 mm o.c.	300 mm o.c.
typical horizontal reinforcement spacing	100 mm o.c.	150 mm o.c.	300 mm o.c.
corrugation material (connections detailing the same for both)	3 mm min. thickness	3 mm min. thickness	
arch base connection to footing	double legs at 100 mm o.c.	single #4 leg at 150 mm o.c.	double legs @ 300 mm o.c.
floor slab connection at arch base	slab overlaps footing	no slab overlap	no slab overlap
personnel door	near front door	at one side with protection wall	

Table 1. Structural Comparison (Cont'd)

Front Door	Norwegian/US	DISTANT RUNNER	FRG
panels	hollow-core steel plates with internal stiffeners: interior plate-10 mm exterior plate-20 mm stiffeners-10 mm thickness-250 mm	composite steel/concrete supported by exterior trusses: steel plate-3.2 mm concrete-300 mm	composite steel/concrete: 20 mm steel outer plate and inner plate, 500 mm concrete in between
support against internal load	simple support top and bottom	track mechanism only	simple support bottom, sides and top free
weight/sca	280 kg/m ²	770 kg/m ²	1520 kg/m ²

Table 2. Predicted Loads (307 Kg TNT)

	Norwegian/US	DISTANT RUNNER	FRG
* P_r (KPa)	400	407	737
i_r (KPa-sec)	1.633	1.647	2.115
t_d (sec)	.0082	.0081	.0057
** P_{qs} (KPa)	276	276	317
i_{qs} (KPa-sec)	31.49	39.07	43.75
t_{qs} (sec)	.229	.283	.276

Table 3. Predicted Loads (909 Kg TNT)

	Norwegian/US	DISTANT RUNNER	FRG
* P_r (KPa)	1138	1158	2198
i_r (KPa-sec)	3.627	3.654	4.747
t_d (sec)	.00638	.00631	.00432
** P_{qs} (KPa)	676	662	772
i_{qs} (KPa-sec)	58.6	69.6	79.37
t_{qs} (sec)	.173	.210	.206

Table 4. Predicted Loads (2727 Kg TNT)

	Norwegian/US	DISTANT RUNNER	FRG
* P_r (KPa)	3441	3509	6435
i_r (KPa-sec)	8.27	8.34	11.01
t_d (sec)	.00481	.00475	.00342
** P_{qs} (KPa)	1503	1503	1598
i_{qs} (KPa-sec)	91.0	108.3	120.99
t_{qs} (sec)	.121	.144	.151

* based on point source to door for hemispherical surface burst

** Reference 5

in Reference 5. The aggregate in the concrete was modeled and selected such that it could fit in between the spacing of the model reinforcing steel. The reinforcing steel was modeled using wire mesh and wire. The details of the reinforcing are discussed in Reference 6.

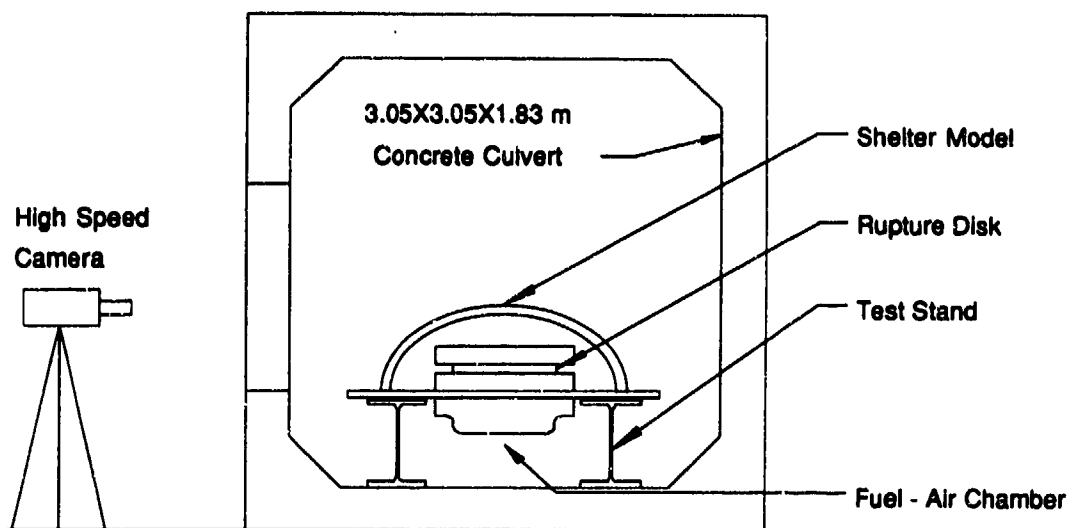
4.0 Testing

4.1 Test Setup

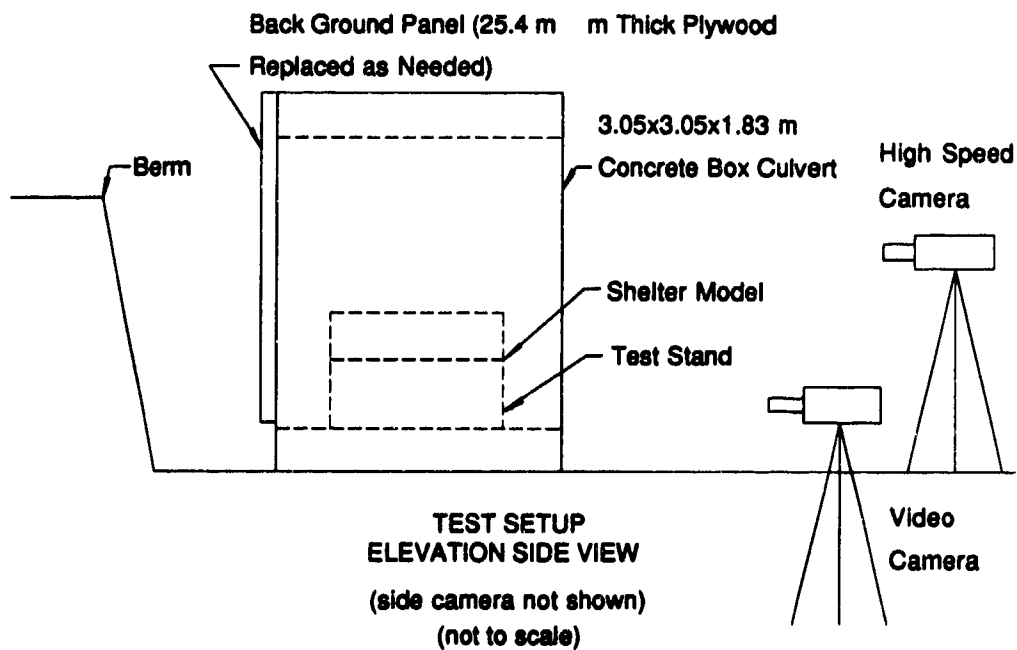
The test setup is shown in Figure 1. The test stand was used to support the shelter model and contained a chamber for the fuel/air mixture. The front of the test stand consisted of a rigid steel panel which formed the "rear wall" of each shelter tested. The vent panel of each shelter faced the rear end of the test stand. The test stand and shelter were placed inside a 3.0 meter tall by 3.0 meter wide by 1.8 meter deep reinforced concrete box culvert. Viewing ports were cut into the side and roof of the culvert for cameras and lights. Background panels, fabricated from 25 mm thick plywood, were painted and attached to the culvert. The background panels were painted blue with a 150 mm by 150 mm white grid pattern. The grid pattern was used for the data analysis. Two high speed cameras and a videotape camera were used to record each test. One high speed camera was focused on the side of the model and the other camera and the video camera were focused on the front of the test frame. The high speed cameras operated at between 1000 to 3000 frames per second depending on the available light conditions for the test. The high speed films were analyzed to determine the velocity and the trajectory of the debris. Blast gages were mounted in the test stand to record the blast pressure/impulse. Still camera coverage was used to provide before and after documentary pictures.

4.2 Data Analysis

The principal source of data consisted of 16mm high speed films recorded during each test. The films were obtained from two perpendicular cross-sectional views, one being a frontal orientation, the other a side view. The films from all tests were analyzed using an NAC brand Film Motion Analyzer. This machine projects the film image over a digital tablet which allows a local reference Cartesian coordinate system to be established for an individual frame. The position of objects within a frame can be represented by Cartesian coordinates. The coordinates from a number of frames can then be used to establish velocities for each visible piece of debris. Angles at which the debris leave the shelter were also measured from the high speed films.



TEST SETUP
FRONT ELEVATION
(not to scale)



TEST SETUP
ELEVATION SIDE VIEW
(side camera not shown)
(not to scale)

Figure 1. Test Setup

5.0 Summary of Results

5.1 Test Summary

Table 5 presents a summary of data for the test series. It should be noted that while trajectory was not quantified based on film analysis, observed trajectories were observed to be essentially perpendicular to shelter surfaces in all tests. Therefore, initial debris trajectory becomes simply a function of shelter geometry.

Table 5. Summary of Results

Test No.	Shelter Type***	Berm	Expl* Yield (Kg)	Pred I _Q (Pa-S)	Max Meas I _Q (Pa-S)	Max Meas Debris Velocity (m/s)	Remarks
1	S	No	.27	4509	4137	42.3	3 pieces
2	U	No	.82	6068	6206	51.8	2 pieces
3	U	No	1.36	7378	7240	-	-
4	None	N/A	.27	-	-	-	-
5	S	No	.27	4509	4344		3 major pieces
6	U	No	.27	3930	4137	43.3	2 piece breakup
7	U	No	.82	6068	-	-	Pre-ignition
8	D	No	.27	4620	2758	42.0	2 piece breakup
9	G	No	.27	5309	4654	39.7	3 pieces
10	D	No	.82	7240	7240	78.7	2 pieces
11	G	No	.82	8067	7585	38.0	2 piece breakup
12	U	Yes	.27	3930	3792	37.1	2 pieces
13	U	Yes	.82	6068	6895	19.7**	2 pieces
14	D	Yes	.27	4620	2992	25.9	2 pieces
15	D	Yes	.82	7240	6854	77.1	2 pieces
16	G	Yes	.27	5309	4150	55.4	3 pieces
17	G	Yes	.82	8067	6998	43.6	2 pieces
18	U	Yes	.09	2101	1738	8.2	1 piece
19	D	Yes	.09	2606	1227	8.2	1 piece
20	D	No	.09	2606	1793	-	(No Data) 1 piece
21	G	No	.09	2919	1331	8.2	1 piece
22	G	Yes	.09	2919	1682	9.2	1 piece

* Note that tests 1-3 were C4 charges, all others were fuel/air.

** Early time measurements only

*** U=Third Generation Norwegian/US, D=DISTANT RUNNER, G=FRG, S=Source

It also should be noted that only tests 1-3 were conducted with C4 high explosive charges. While these charges better replicate the actual load-time functions expected in a full scale event, as described previously, they generated obscuring light and smoke such that their use was discarded in favor of the fuel/air detonations. Table 6 presents a comparison of the HE (C4) and fuel/air (propane/oxygen) tests.

As Table 6 shows, impulse measurements varied 5% from HE to fuel/air on the 0.27 Kg test and 11% on the 0.82 Kg test. Velocities on the 0.27 Kg test were only within 15%. These are reasonable values, and validate the use of the fuel/air substitute, even though the fuel/air time histories were typically 10-15 ms in duration, while the HE durations were about one-half of that value.

Table 6
Comparison of Fuel/Air and HE Tests

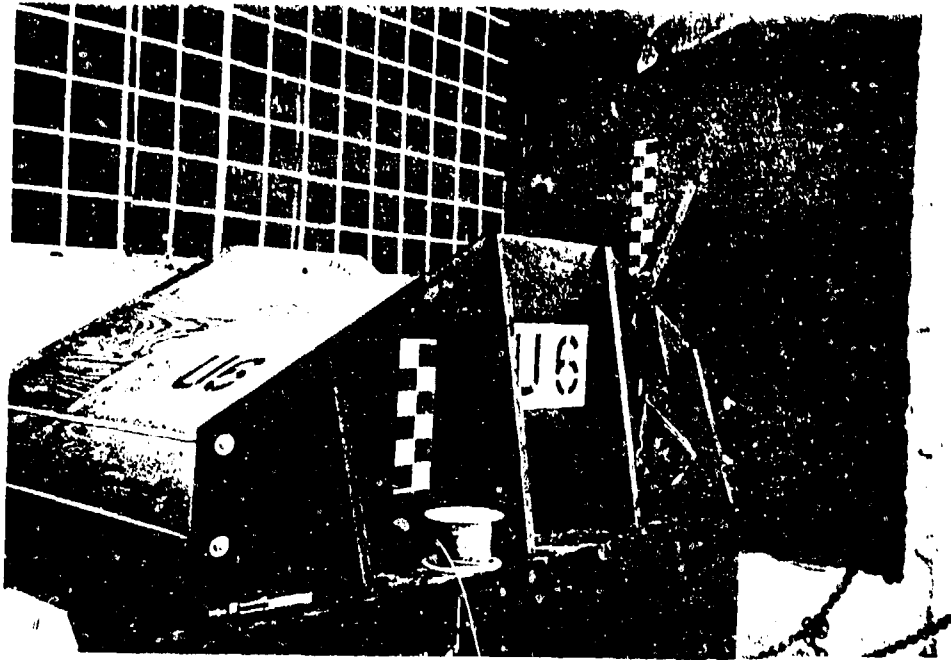
TNT Eq. Charge Weight (Kg)	Test No.	HE Impulse (I_0) (Pa-s)	Fuel Air Impulse (I_p) (Pa-s)	Max. Meas. Velocity (m/s)
.27	S1	4137	4344	42.3
	S5			57.4
.82	U2	6206	6895	51.8
	U13*			-

* Bermed test

5.2 Observed Failure Patterns

The pattern of shelter breakup can be generalized in three distinct groupings. The groups are defined by the size and amount of significant debris objects resulting from a shelter test. The debris generated during a test are directly related to the shelter breakup pattern. Factors which affect the breakup pattern for a test include shelter type and geometry, explosive weight, and the degree of fixity at the base. The largest contiguous pieces of debris were considered in the pattern groupings. Some shelters broke into three major pieces, two flanking segments and a crest segment (Group 1). Other shelters only broke into two pieces with the separation occurring at the crest (Group 2). The third type of breakup pattern occurred at the lowest charge weight only (Group 3). The shelter was driven upward as a single piece after rupturing at the basal support on both sides.

The third generation Norwegian/US shelter breakup pattern was identical to the DISTANT RUNNER shelter and falls into the category of two major debris segments. This is true for both 0.27 Kg and 0.82 Kg charge weights. Before and after pictures of Test 6, a 0.27 Kg charge in a third generation Norwegian/US shelter model, demonstrate this type of breakup in Figure 2. The FRG shelters behaved somewhat differently than the third generation Norwegian/US and



Test Setup



Resultant Debris

Figure 2. Results of Test 6 Using 6.25mm caliber

DISTANT RUNNER shelters. At the 0.82 Kg charge weight, the FRG shelters were noted to break up into two major segments (as with the third generation Norwegian/US and DISTANT RUNNER). However, at the 0.27 Kg charge weight the FRG shelter typically broke into three major segments. At the lowest charge weight (0.09 Kg) all three types of shelters broke at the base as mentioned above and remained in one major piece. Figure 3 illustrates this type of breakup for a bermed third generation Norwegian/US shelter model.

Since the model shelters were originally designed to replicate response due to combined blast and quasistatic load, the breakup pattern observed for the lowest charge weight (principally quasistatic load) may not be valid. It is unlikely that the basal separation would be observed in full scale shelters. It is presumed that the failure at the connections occurred as a late time response, where inertial effects would not be important and where the static arch strength at the base is important. These observations, however, may be interpreted to represent the actual structural response of the shelter without regard for the basal separation. In effect, the shelter would not be expected to break up under these loading conditions.

5.3 Observed Differences Between Bermed and Unbermed Shelters

Table 7 presents a comparison of the bermed and unbermed tests. There appears to be no noticeable trend towards higher impulses or velocities when the berm is added. Additional film analysis is recommended to both confirm velocities and examine trajectories.

Table 7
Comparison of Bermed and Unbermed Impulses and Debris Velocities

Charge Wt. (Kg)	Test No.	Berm	Impulse (Pa-s)	Debris Velocity (m/s)
.09	U18	Yes	1738	8.2
	D20	No	1793	-
	D19	Yes	1227	8.2
	G21	No	1331	8.2
	G22	Yes	1682	9.2
.27	U6	No	4137	43.3
	U12	Yes	3792	37.1
	D8	No	2758	42.0
	D14	Yes	2972	25.9
	G9	No	4654	39.7
	G16	Yes	4150	55.4
.82	U7	No	-	-
	U13	Yes	6895	19.7*
	D10	No	7240	78.7
	D15	Yes	6854	77.1
	G11	No	7585	38.0*
	G17	Yes	6998	43.6

* Early time measurements only

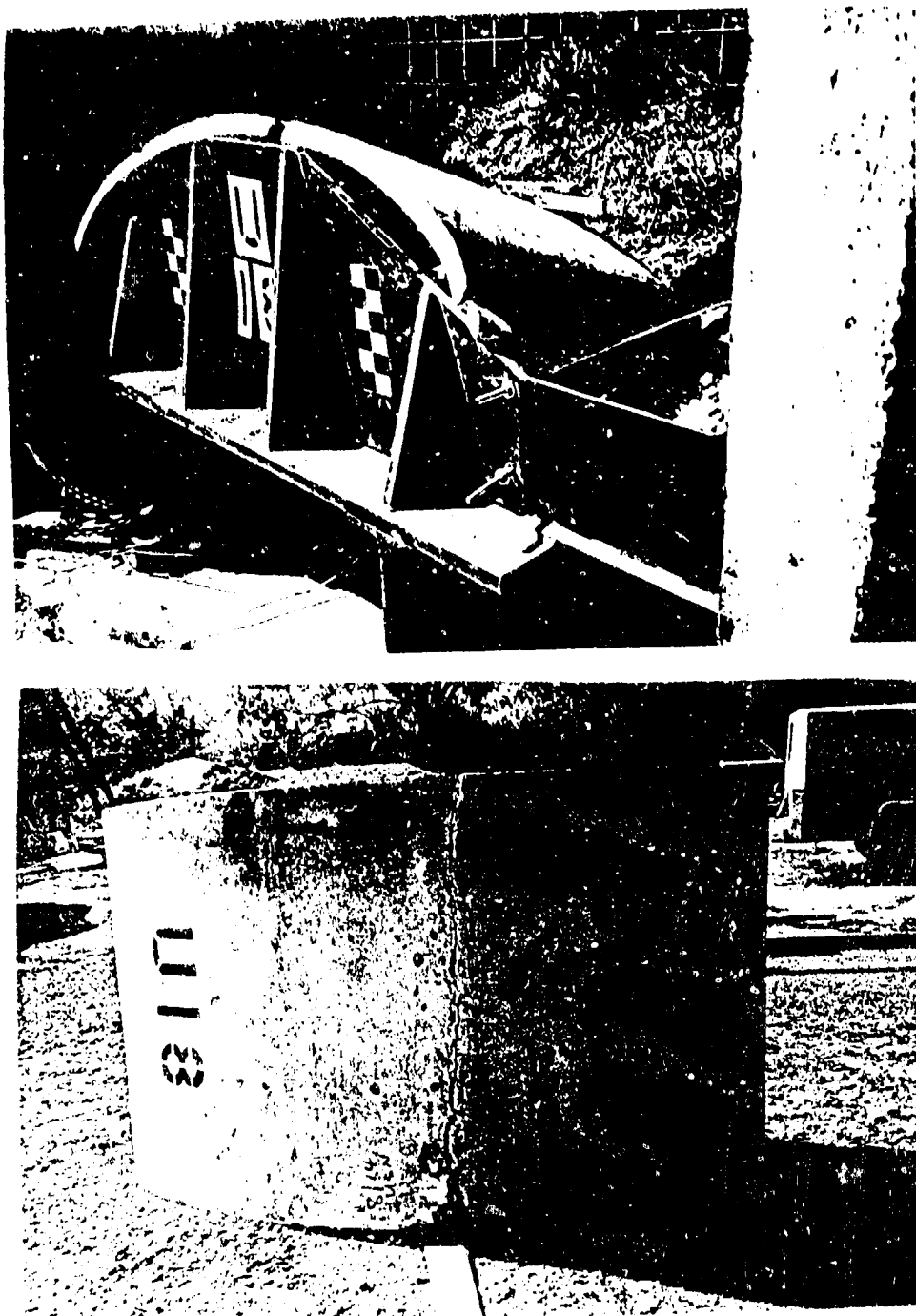


Figure 3. Typical Breakup for 0.09 Kg Charge Weight
(Test 18)

6.0 Recommendations

Qualitative observations on angles and failure patterns, along with measured velocities, indicate the response of the shelters is not greatly affected by the presence of the rock rubble berm against the shelter sides. There were some slight offsets of initial failure lines when the berm was in place, but the debris velocities did not change significantly. Based on a cursory analysis of the test results, several key refinements should be made. These items are presented in this section.

A pivotal parameter for this study was the quasistatic impulse. Since the debris velocities following an internal detonation are largely defined by this impulse, that was what needed to be scaled properly in the tests. One must remember the 1/15 scale shelters were models of a section of each shelter. The length was not 1/15 of the full scale shelter arch length. Thus, to obtain the correct load, the vent panel used in place of the door was designed in each case to remain in place long enough to attain the proper scaled quasistatic impulse. The quasistatic impulse prediction to be matched for each test was calculated using methods in Reference 5, allowing the covered vent areas (doors) to vent according to their mass/unit area. Calculations in Reference 3 for the DISTANT RUNNER shelter were made assuming immediate venting through the doors and the vent openings at the top of the arch and, thus, are lower than the predictions used for these tests. Velocities calculated using these impulses are lower than those expected and measured from the SwRI tests. Since the large database of DISTANT RUNNER debris characteristics indicates many impact distances which would agree with higher velocities than the one reported Event 4 arch velocity (measured from film), further investigation of the load prediction method is highly recommended. The actual gas load duration (and, thus, immediate venting or delayed venting) in the DISTANT RUNNER tests and in the 1/15 scale SwRI tests needs to be resolved.

The next step recommended in the original design comparison study (Reference 4) was to perform larger scale tests (1/4 or 1/3) of the third generation Norwegian/US shelter with models of the whole shelter, including the front door and frame. The larger scale models would be tested, again with and without the rock rubble berm, using properly scaled amounts of the same three full scale charge weights examined in this study. These tests would include debris mapping as well as measurement of velocities and documentation of failure patterns. This test series should then be followed by a detailed analysis before establishing quantity-distance for the new shelter design.

A number of recent tests have provided velocity data for debris resulting from internal detonations in reinforced concrete structures, both aboveground (or unbermed) and buried (or bermed). It is most desirable to determine a relationship between the amount of cover on a structure (i.e. concrete plus berm thickness), charge amount, and debris launch velocity. One attempt to relate the launch velocity to the scaled cover is documented in Reference 7. After more detailed analysis of the 1/15 scale test results and performance of the larger scale tests, these data should be added to the data summarized in Reference 7, and a rigorous effort to refine this velocity relationship needs to be undertaken. If such a relationship can be established, it would eliminate the need to fund specific testing and analysis every time a new aircraft shelter design is introduced. This is indeed a worthwhile goal for all involved in the safe siting of structures.

References

1. Flory, Robert A., "DISTANT RUNNER Results: A 5 Event High Explosive Test Series Involving U.S. Air Force 3rd Generation Aircraft Shelters," Minutes of the Twentieth Explosives Safety Seminar, Volume II, pp. 1817-1835.
2. Ward, Dr. Jerry M., "DISTANT RUNNER - Debris Recovery and Analysis Program for Events 4 and 5," Minutes of the Twentieth Explosives Safety Seminar, Volume II, pp. 1837-1881.
3. Ward, Dr. Jerry M., "DISTANT RUNNER - Debris Recovery and Analysis Program for Events 4 and 5," Naval Surface Weapons Center, White Oak Laboratory, Silver Spring, MD, April 1982.
4. Whitney, M., Bowles, P. and Polcyn, M., "Aircraft Shelter Design Comparison," Final Report for SwRI Project 06-2061, prepared for Norwegian Defence Construction Service, Oslo, Norway, March 1988.
5. Ayvazyan, H., Dede, M., Dobbs, N. (Amman & Whitney), Whitney, M., Bowles, P. and Baker, W. (Southwest Research Institute), "Structures to Resist the Effects of Accidental Explosions, Volume II: Blast, Fragment, and Shock Loads," Special Publication ARLCD-SP-84001, December 1986.
6. Strybos, J.W., Bowles, P.M., Lewis, M.J., and Marchand, K.A., "Scaled Debris Throw of Third Generation Norwegian/US Aircraft Shelters: Data Summary Report," SwRI Project 06-2673, prepared for The Norwegian Defence Construction Service, Oslo, Norway, December 1989.
7. Helseth, Einar S., "Underground Ammunition Storage: Model Test in Scale 1:100 in Sand," Norwegian Defence Construction Service, Fortifikatorisk Notat Nr. 160/82, August 1982.

JOINT AUSTRALIAN/UK STACK FRAGMENTATION TRIALS
PHASE 4 PRELIMINARY REPORT

Presented to the 24th Explosives Safety Seminar

by

J Henderson

Technical Adviser (Explosives), ESTC
Ministry of Defence, United Kingdom

August 1990

SUMMARY

This is a Report of Phase 4 of the Joint Australian/UK Stack Fragmentation Trials. This particular trial was designed to quantify the explosion effects, i.e. blast and debris, that would be expected to arise as a result of an accidental explosion in a UK designed NATO Standard Igloo explosives storehouse. The report describes the specification of the trial, the support work required and examines the results of the debris collection and the blast measurement records. Additional work was also carried out to attempt to ascertain the initial velocity of the structural debris from the donor and this is described in outline detail only.

The trial was coalesced with the Australian Explosive Store-House Design Trial in which three Australian designed "Spantech" arch earth-covered magazines were constructed at appropriate inter-magazine distance at side to side, front to rear and rear to front orientations, relative to the donor igloo. These were instrumented internally to ascertain their structural response to the blast from the donor igloo and externally to ascertain the typical blast loadings that would be expected on adjacent igloos in the event of the donor accidentally exploding. The aim was to demonstrate that the Spantech structures would behave in a similar fashion to a NATO standard igloo.

Preliminary conclusions are drawn from the trials and recommendations for incorporation of the results in the UK's ESTC explosive storage leaflets are given.

A full account of the trials and all the results will be given in the final Phase 4 Report to be published later in 1990.

ACKNOWLEDGEMENTS

The UK acknowledges the major contribution made by the Australian Department of Defence to the work reported here. The work was made possible by the use of the Woomera range and the support provided by and through the Directorate of Trials. In addition Waterways Experiment Station (WES) contributed significantly to the instrumentation task.

The trials were arranged through British Defence Research Scientific Staff Canberra (Mr G Burrows) with Director of Trials (Group Captain W Hall). The main contributors to the trials were the Australian Army (Project Officer, Major D Stuart and Project Officer Field, Major C Brereton with EOD Staff and detachments from 21 Construction Squadron), RMB Salisbury (under Mr G Appleby), OSD Salisbury (under Dr A Rye and Mr J Leach) and DSCW Personnel at Woomera (under Mr D Fail). The WES support staff were Mr J Ingram and Dr R Franco. Staff were also supplied from Australian Ordnance Factories to carry out weighing and sorting of fragments.

The trials would not have been possible without the additional aid of the Australian Department of Defence in supplying surplus anti-tank mines for use in the trials.

The trials proposals were discussed in detail and approved by the UK Explosives Storage and Transport Committee (ESTC), and its Explosion Effects Sub-committee.

1. BACKGROUND TO PHASE 4

1.1 The Explosion Effects Sub-Committee (EESC) of ESTC recommended, in the early 80's a programme of investigation of the effects of fragment and debris arising from stacks of ammunition inside typical UK traversed store-houses. This programme formed the basis of Phases 1-3 of the Joint Australian/UK Stack Fragmentation Trials conducted at Woomera between 1982 and 1988 and reported in References 1-4.

1.2 The work carried out in Phase 1-3 consolidated the information required by UK to verify and revise, where possible, existing distances for fragment and debris throw from limited (< 6000 kg) quantities of explosives in a variety of explosive storehouse structures. Although firm conclusions were offered the series of trials showed that it was not possible to take for granted the existing, often very subjective standards, for minimum fragment and debris hazards for explosives storage buildings. However there was, and still is, no intention to gather any more data for this part of the Quantity-Distance tables even although there were obviously still some unanswered questions regarding the protection required from fragmentation effects of concrete magazines.

1.3 Much work has been commissioned by the US DDESB to investigate the problems of open, untraversed stacks of fragmenting ammunition, in particular with respect to maximum and safe fragment distances. Similar work has been conducted for a variety of individual weapons by the UK Ordnance Board. However very little information exists for the situation when these same weapons and fragmenting ammunition are stored inside a structure which does more than simply provide weather protection. This was the primary reason for the UK conducting the initial series of Stack Fragmentation Trials.

1.4 However the question still remained whether the existing blast generated Quantity-Distances provide a sufficient degree of protection against fragment and debris effects for more typical storage quantities of several tens of tonnes NEQ of ammunition and explosives. Normally such quantities would be stored in igloos according to present day standards and the EESC considered that some work was needed to verify the existing Quantity-Distances for larger igloos in terms of debris and blast hazards. This becomes especially important when it is realised that AC 258 reduced the outside Quantity-Distances from the rear and side of igloos with NEQs of less than 45,000 kg, and it is not apparent that any consideration was given to the debris hazard posed by igloos. In addition, in

the light of the UK's journey down the route of potential application of Risk Analysis techniques to the storage and handling of explosives it is even more essential to obtain some picture of the hazards posed by igloos, as well as other types of storage, at distances intermediate between ground zero and inhabited building distances, and beyond.

1.5 Consequently the author, as Technical Adviser (Explosives) to ESTC, opened negotiations in late 1988 with the Australian Department of Defence with a view to conducting a trial with a NATO Standard Igloo, loaded to some 75,000 kg NEQ, to investigate the effects from an accidental explosion of the contents of such a structure.

2. AIM OF PHASE 4

2.1 The objectives of the Phase 4 programme were to investigate the following aspects:

2.1.1 Break up of a UK designed NATO standard double bay igloo structure when exposed to the detonation of high explosives and the subsequent weight distribution, direction, distance and density of projections.

2.1.2 Validation of the blast pressure attenuation recommended by NATO AC 258 for the rear and side orientation of Igloo structures, particularly for Igloos containing in excess of 45,000 kg Net Explosives Quantity.

2.1.3 Validation of the pressure parameters used for the design of NATO Standard Igloos.

2.1.4 Comparison of free-field blast pressures produced by an explosion in an Igloo structure with those from an equivalent quantity detonated in free-air.

2.1.5 Measurement of initial Igloo structural and cover debris velocities resulting from an internal explosion.

3. PHASE 4 TRIAL SPECIFICATION

3.1 After extensive discussions in UK and Australia Phase 4 was finalised at a total of two tests. The first would be in a NATO standard double bay igloo and the second would be a detonation of an equal amount of explosives in the open. The details of the trial specification are as noted below.

Building Construction

3.2 Test 1 Donor : Standard UK reinforced concrete box, double bay, igloo structure to design as given at Annex A, with concrete floor slab.

3.3 Test 2 Donor : Concrete floor slab to simulate igloo floor used in Test 1.

3.4 After detailed discussion with the Australian department of Defence it was agreed to coalesce the Stack Fragmentation Trials Phase 4 with the Australian Explosive Store-house (ESH) Design Trial. The objectives of the ESH Design Trial were to :

3.4.1 Investigate, analyse and report upon the physical damage sustained by the ESH trial buildings as a result of the Stack Frag 4 explosion.

3.4.2 Assess and recommend any resultant design changes to the ESH trial buildings considered essential for the satisfactory performance of their design function.

3.4.3 Investigate, analyse and report upon the blast overpressures recorded at selected positions adjacent to and upon the receptor buildings.

3.4.4 Investigate, analyse and report upon building displacement and acceleration records measured at selected positions within the receptor buildings.

3.5 As a result of this decision to coalesce the two trials, which produced significant savings to both the Australian Department of Defence and the UK Ministry of Defence, the receptor structure layout was finalised as follows:

3.5.1 Receptor 1 : Spantech structure, with standard 7 bar igloo head-wall and doors, constructed at $0.8 Q^{1/3}$ front-to-rear wall separation from Donor structure to represent a NATO Standard Igloo in outline shape, situated at standard separation from an adjacent igloo structure.

3.5.2 Receptor 2 : Spantech structure, with standard 7 bar igloo head-wall and doors, constructed at $0.5 Q^{1/3}$ side-to-side wall separation from Donor structure to represent a NATO Standard Igloo in outline shape, situated at standard separation from an adjacent igloo structure.

3.5.3 Receptor 3 : Spantech structure, with standard 7 bar igloo head-wall and doors, constructed at $0.8 Q^{1/3}$ rear-to-front wall separation from Donor structure to represent a NATO Standard Igloo in outline shape, situated at standard separation from an adjacent igloo structure.

3.6 The basic Spantech structures used were as shown diagrammatically at Annex B.

Charges

3.7 Test 1 : Detonation of 75,000 kg TNT equivalent in Proposed Donor structure. Obsolete anti-tank mines, TNT filled, were used for the donor charge. The charge was primed at some 600 points because of concerns that the mines might not all detonate simultaneously.

3.8 Test 2 : Detonation of 75,000 kg TNT equivalent in the open, with charge placed in as close proximity as possible to the position for Test 1 in order that the instrumentation layout used for Test 1 could be re-utilised as far as possible.

Measurement of Far Field Blast Pressures

3.9 Three lines of four gauges to measure the side-on overpressure in directions 40, 130 and 220 degrees with respect to ground zero, being to the front, side and rear respectively of the structure. The structure to be orientated so that the centre line of the structure lies in the NE/SW direction with the door pointing due NE. Details of the actual gauge layout are given schematically at Annex C.

Measurement of Blast Pressures on the receptor structures

3.10 The receptor structures were instrumented for blast measurement as per Ordnance Systems Division (OSD) Instrumentation Plan dated 5 Jan 90 (Ref 6). Annex D shows schematically the approximate positions of these gauges.

Internal Blast Pressure Measurements

3.11 Four (4) internal airblast gauges were located within the structure to measure internal blast pressures.

Accelerometer Measurements

3.12 In addition to the airblast pressure gauges, four (4) single axis accelerometers were installed on the top of the donor Igloo overburden to measure the acceleration of the cover breakup and initial debris velocities. Two (2) accelerometer packages were positioned near the top centre of the overburden, and

the remaining two (2) packages were placed near the centre top edge of the overburden.

Photographic Coverage

3.13 Photographic coverage was provided as follows (Ref 7) :

3.13.1 High speed cine coverage with a field of view extending to 50 metres in front and to the rear of the structure. The intention being to attempt to ascertain the extent of initial venting from the front of the structure and through the earth cover.

3.13.2 High speed cine coverage with a field of view extending to 50 metres either side of the structure. Viewing to be from the rear of the structure to attempt to ascertain the extent of venting through the earth cover.

3.13.3 Wide angle coverage of the event out to 500 metres on both sides of the structure. This was intended to provide documentary coverage of the event but might show the trajectories of large debris.

3.13.4 Aerial photography of each test to document the spread of debris and dust cloud during the course of the explosion.

Debris Search Areas

3.14 The following search areas were established for collection of building debris as shown schematically at Annex E.

3.14.1 Four main fan searches in NE, SE, SW and NW directions. Sectors were 5 degrees either side of the main compass direction from 100 to 500 metres and a constant width (87.3 metres being the width of the 10 degree arc at 500 metres) from 500 to 1000 metres. All search areas were marked at 20 metre intervals from 100 to 1000 metres.

3.14.2 Four subsidiary radial search areas divided into 10 degree widths from 260 to 280, 400 to 420, 600 to 620 and 900 to 920 metres.

3.15 At a late stage in the planning of Phase 4 a suggestion was received from A Jenssen of the Norwegian Defence Construction Service to place marked objects on the roof and walls of the donor structure to allow observations to be made on the launch angle and velocity of the donor structure (Ref 10). To this end 24 steel cylinders, each 6 ins in diameter, length 6 ins and filled with concrete were prepared and placed on the walls and roof of the igloo on the earth overburden. In addition three plastic buckets filled with concrete were actually buried in the roof overburden.

4. IMPLEMENTATION OF PROPOSALS

4.1 The author opened negotiations with the Australian Department of Defence in late 1988 as a result of the initial recommendations for future work arising out of the preliminary report from the Stack Frag Phase 3 trials.

4.2 In early 1989 proposals were submitted to D Trials (Ref 5), as a direct result of a planning visit to Australia made by the author in Feb 89. These proposals were accepted in Nov 89 by D Trials, who had appointed a Trials Manager, initially Major R Baguley who had coordinated the Stack Frag Phase 3 trials but he was posted to other duties and replaced at a late stage in the trials planning by Major D Stuart, and a Project Officer Field, Major C Brereton, who had conducted Stack Frag Phase 3 in early 1988. At this time UK reached agreement with Waterways Experiment Station (WES) of Vicksburgh, USA, for the provision of additional instrumentation with particular reference to measurements inside and on top of the donor structure. This allowed the instrumentation plan to be extended significantly.

4.3 A further planning visit by the author in December 1989 resulted in a revised instrumentation plan which utilised effectively the support available from OSD and WES (Ref 6). During this planning visit the idea of coalescing Stack Frag 4 with the Explosive Store-house Design trial was agreed in principle.

4.4 Range Measurements Branch issued a trial instrumentation plan (Ref 7) as a result of the UK trials proposal and further discussions held during the planning visits by the author.

4.5 In Mar 90 D Trials issued a Defence Trial Directive which effectively combined the two trials (Ref 8). This was followed by the Trial Technical Instruction in early 1990 (Ref 9).

4.6 In the meantime a site for the trial was established some 25 km N of Woomera village, as shown at Annex I. Construction work commenced at Woomera in late 1989. The donor igloo was built by a local construction contractor at Woomera and the three Spantech structures were built under contract by Spantech to the Australian Services DOD Facilities and Property Division. All construction work was completed on schedule by late April 1990. The construction was supervised by representatives of the Australian Construction Services. (Ref 11)

4.7 All major trials support agencies were on site at DSC Woomera in late May 1990 and the donor charge was successfully detonated on 31 May 1990.

5. DEBRIS COLLECTION

5.1 Prior to the detonation the search areas shown in Annex E were marked out. It was then a relatively straightforward but nevertheless lengthy task to comb each marked area for debris which was collected into sandbags. These were then conveyed back to the site administration area, some 6 km distant, to be weighed and collated.

5.2 It was very quickly realised that there was an excessive amount of debris in the search areas close to ground zero, ie within 200-300 metres. In some cases it amounted to several hundred fragments with the minimum being around 100. In order to simplify the collation process it was decided to record only a total of the number of lethal fragments without recording each weight individually for these for these close-in high density areas. However in order to get an estimate of the weight distribution several of these search areas (c. 20% of the total were collated completely by weight).

5.3 It did not prove possible to collect all fragments from the search areas. Some were excessively large and heavy, typically 0.5m x 0.5m x 0.3m and some had impacted with such force that they were buried deep in the ground. All such fragments were recorded by dimension and listed as fragments in excess of 5kg weight.

5.4 The only fragments which were collected or identified were from the concrete structure itself. These included concrete, reinforcing bar and door elements. There was also a large amount of crater ejecta projected out to 200-300 metres from Ground Zero. This was not analysed directly by collection but is recognised as forming an important part of the overall debris density.

5.5 One other factor which proved to be of importance in the actual debris collection was the break-up of fragments on impact. Although this had been seen to a very limited degree in previous trials the degree of break-up and its widespread occurrence was not anticipated. The breakup complicated the collection in two major ways, viz:

5.5.1 Relatively small fragments (5-50kg in weight) which broke into several pieces on impact or when actually recovered. (Either at the time of recovery or during transport to weighing point). This led to a significant over-estimation of debris density at all ranges and its significance is discussed more fully in Section 6.

5.5.2 Very large (in excess of 0.5m x 0.5m x 0.3m) reinforced concrete sections which impacted and partially broke up spreading the resultant debris over large areas (typically 20m x 5m). In about 5-10% of the cases this was further complicated by the "fragment" bouncing after initial impact, finally coming to rest up to 25m from the original position. In a few instances there were several impact points as the fragment skipped or rolled to its final resting place.

6. DEBRIS ANALYSIS AND DISCUSSION

6.1 The debris was weighed and collated manually and then analysed by weight interval using a LOTUS 123 spreadsheet, in common with previous phases of the Stack Frag Trials.

6.2 As for previous phases it has been assumed that debris would be at or around its terminal velocity when it strikes the ground. Even given the situation of an untraversed igloo it is felt that this is not completely unrealistic since, on the three sides, the receptors provided some degree of traversing for the donor. Therefore it has been assumed that only metal debris over 75g or masonry debris over 150g would be potentially lethal and anything under these weights would be of little significance. As the collection progressed it transpired that there was very little debris under these particular weights, except where larger fragments had broken up on impact.

6.3 However there was left the overall problem of coping with the additional debris produced at all ranges, because of break-up either at impact or as a result of handling and transporting the collected debris. Although difficult to quantify the author estimated, by carrying out several sample surveys during the actual collection phase, that the total number of fragments were over-estimated in any particular sector by a factor of at least two. In some instances the over-estimation was probably significantly more than double and it is likely that there were some instances where it was less than double, although the occurrence of this latter category was not considered significant.

6.4 As a result it was decided to introduce the somewhat arbitrary reduction factor of 2 to produce the adjusted results. It must be stressed that this still gives a conservative estimate for the actual fragment density.

6.5 A further complication which has not been taken into account was the influence of crater ejecta at relatively close-in ranges, which is variable in size with a significant proportion being potentially lethal. The crater ejecta did, in some extreme cases, get projected to 700-800 metres. In most instances however the occurrence of crater ejecta was relatively evenly distributed out to 200-250 metres decreasing rapidly in density out to approximately 400 metres. It is estimated that up to 250 metres there was as much crater ejecta, which could be considered lethal since it was large lumps of baked clay, as there was building debris. Over the next 100 metres the significance of the crater ejecta reduced to about 25% of the building debris. As the range further increased it reduced rapidly and became non-existent, except for isolated instances, beyond 400 metres. Since the critical value for lethal fragment density was found to be in excess of this distance in the four principal search directions no account has been taken of the crater ejecta in the calculated fragment densities.

6.6 Like the building debris the crater ejecta was more pronounced in the directions normal to the original faces of the donor building. Outside the main 10 degree search angles there was very little crater ejecta beyond the 300 metre mark. At ranges intermediate between 100 and 300 metres in these areas there was a much greater concentration of crater ejecta than building debris but there was a lower absolute level than in the main search angles.

6.7 For ease of comparison the results of the four main directional (searches, ie 45, 135, 225 and 315°) are shown in Figure 6.1. The figure demonstrates emphatically the effect of orientation with respect to the donor as well as

demonstrating the ranges at which the critical value of Lethal Fragment Density (LFD) is reached.

6.8 Figure 6.2 shows the variation of LFD with direction at a distance of 400-420m. Once again it shows the dramatic effect of orientation with the peaks occurring in a direction normal to any face of the building. Although the peaks are obvious at 45°, 225° and 315° the peak at 135° has been hidden by debris which has been projected between 55° and 125°. It is noticeable that this effect is not symmetrical, although the test layout was essentially so, and no explanation is offered for the phenomenon. Certainly beyond 400m there was no evidence of significant debris except in the sectors immediately adjacent, ie in the 55° and 125° directions. Perhaps there may have been a slight preferential propagation or venting effect in this direction but there is no other evidence to suggest this.

6.9 Note also the LFD does not immediately drop off outside the main directional search areas, although the effect is generally limited to the sector immediately adjacent to the main directions searched. In all directions, with the exception of the 55-125° sector, the LFD reduces rapidly to the critical value, although only in a few instances does it reduce to zero. It should be appreciated that 400m is less than half the Inhabited Building Distance for a 75,000 kg charge.

6.10 Figure 6.3 shows the variation with direction at a range of 600-620m. Note that the search was limited to the sector from 225° to 315° because of the large areas which had to be searched. Note also that the 235° and 305° areas are slightly larger than the nominal 10° because of the arrangement for searching in the main directional areas. This effect has been taken account of in the calculation of LFD.

6.11 No fragments were found from 245° through to 295°, validating further the directional cross effect seen in all the Stack Trials to-date. In no direction is the debris density of concern.

6.12 Figure 6.4 shows the variation of LFD with direction at a range of 900-920m. The search was limited to the sector from 315° through to 45° because of the large area to be searched. Again note that the 325° and 35° areas are larger than the others, being taken account of in the calculations.

6.13 In no direction is the density of concern although fragments were found in almost every area in comparison with the results given in para 6.10. This is probably the influence of the "unprotected" headwall generating more energetic fragments than those walls which were earth covered. There was no evidence to suggest that there were any fragments beyond this range in any direction other than that to the front of the donor igloo. However one concrete filled cylinder from the side wall of the igloo was found just beyond the searched areas.

6.14 As was originally anticipated the building doors were projected directly out to the front of the igloo. However they were very effectively fragmented by the explosion. Large pieces (over 0.5x0.5m in plan) were identified as part of the large fragment survey. This located some 28 pieces of door and door supports, accounting for about 50% of the total door material.

6.15 The ventilators from the rear part of the igloo roof were located in the 225° search fan at 200 and 440m. Additionally a further large metal plate was found at 230m in the 310° direction. This was probably one of the ventilator covers from the front headwall.

6.16 There is one final point which is worthy of mention. At 1200m distance, direction 50°, an impact point was discovered. A fan of debris was identified from here to approximately 1580m, the fan widening to c. 20m at its furthest extent. It appeared that all the debris in this fan originated from the initial impact and in summary there were some 17 large pieces of concrete (of mass over 1kg), 10 pieces of reinforcing bar and probably 2-3 dozen smaller pieces of concrete (less than the potentially lethal mass limit). It is suggested that all

of this could have come from a section of concrete of approximate size 1.5x1x0.25m, its maximum size being estimated from the lengths of r/bars identified. Obviously this would have been a significant fragment of great interest and would be worthy of some further investigation. The fragments of interest are shown in Table 6.8 page 2 by the fragments marked with an asterisk.

6.17 As the size (and thus approximate mass) and final position are known for all these large pieces it should be possible to estimate the initial velocities and angles of projection for each fragment. Apart from the piece described at para 6.41 there was also another large piece of concrete, size 2x2x0.3m, which had obviously landed end on and then fallen over at distance 450m, direction 330°. It created an impact crater 0.5m deep. Again it is considered that the possible trajectory of this piece could be estimated with some potentially interesting results.

Adjusted Lethal Fragment Density

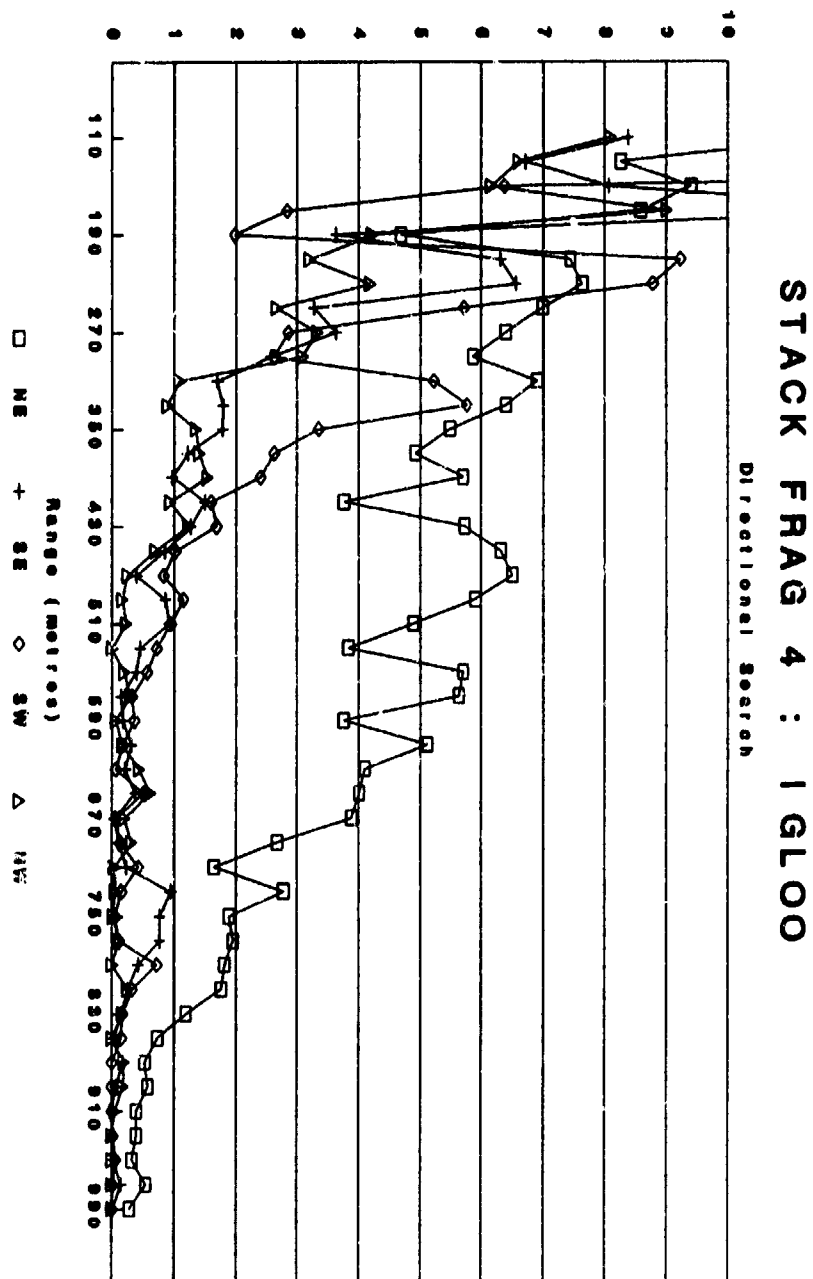


Figure 6.1

Adjusted Lethal Fragment Density

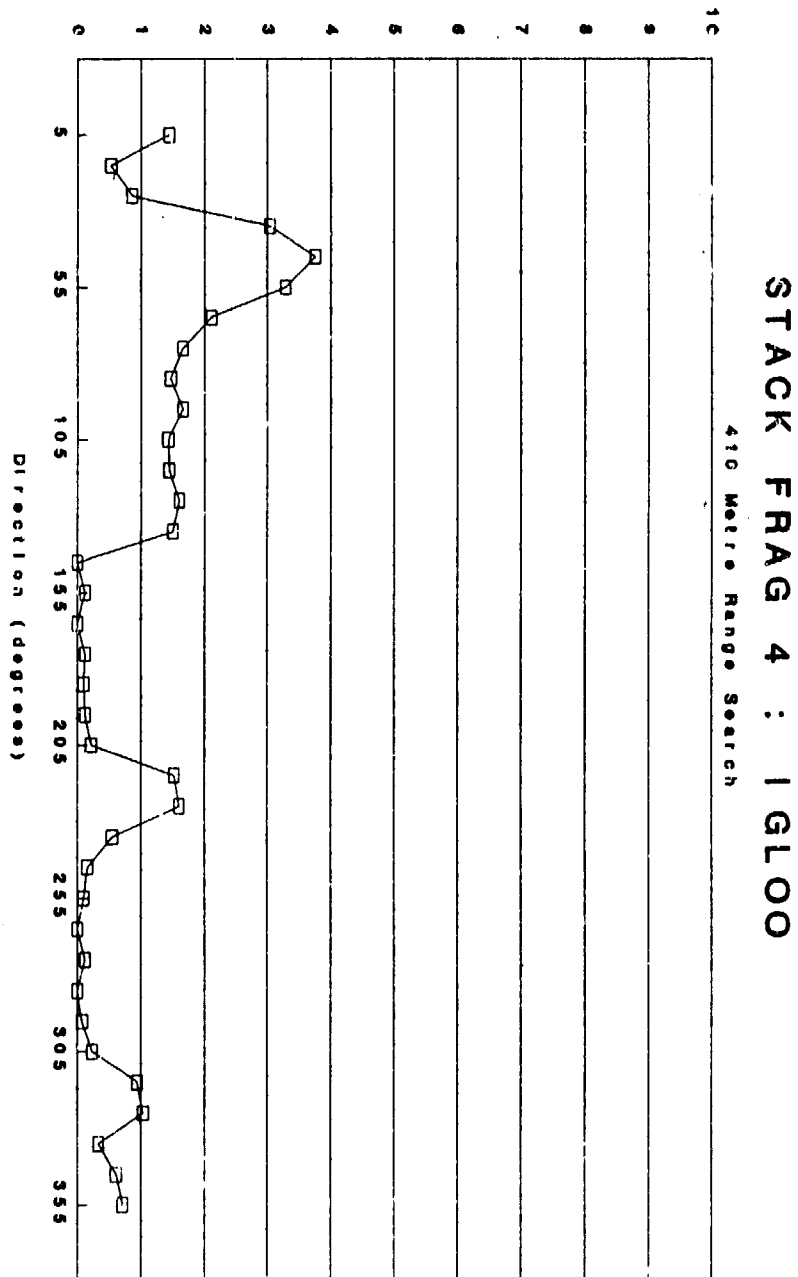


Figure 6.2

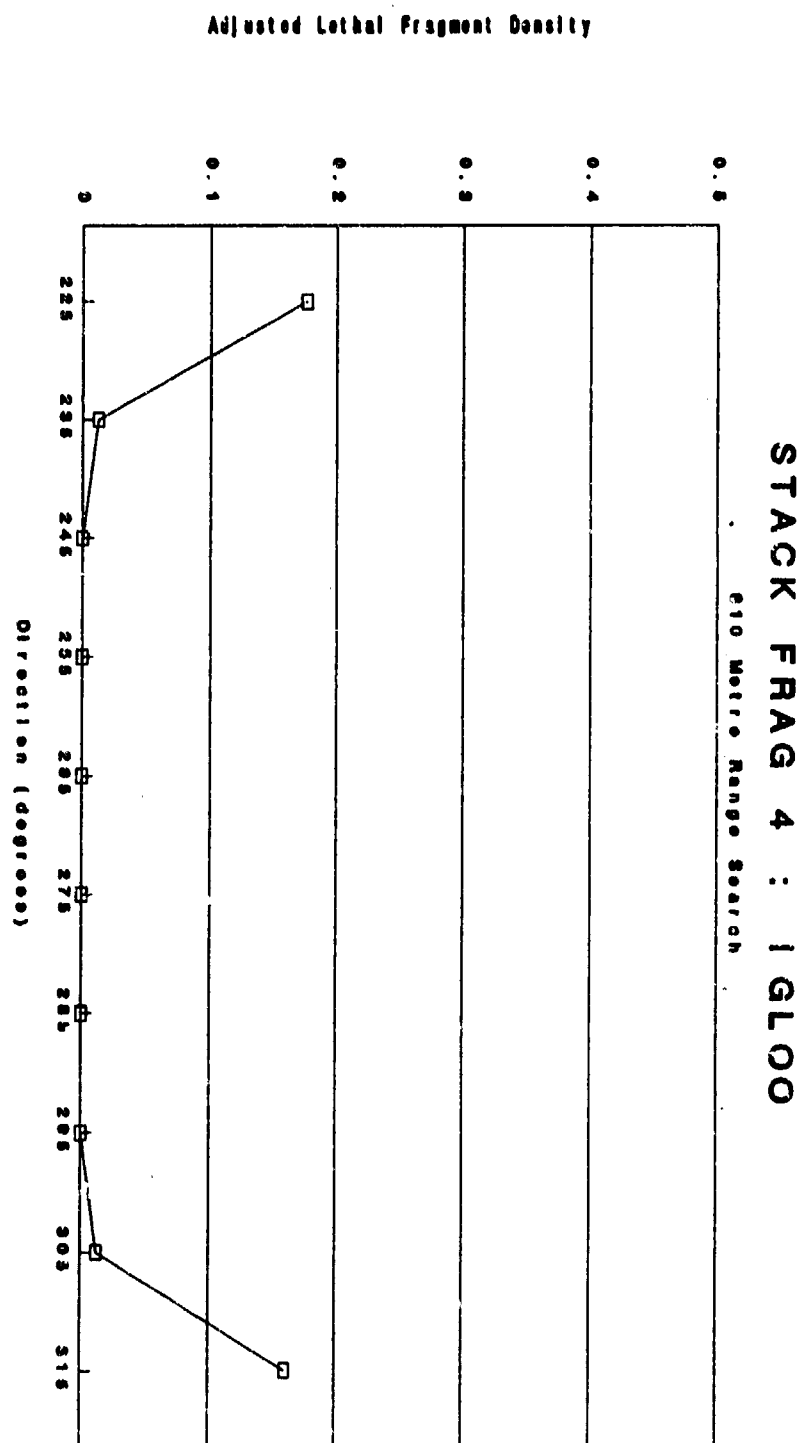


Figure 6.3

Adjusted Lethal Fragment Density

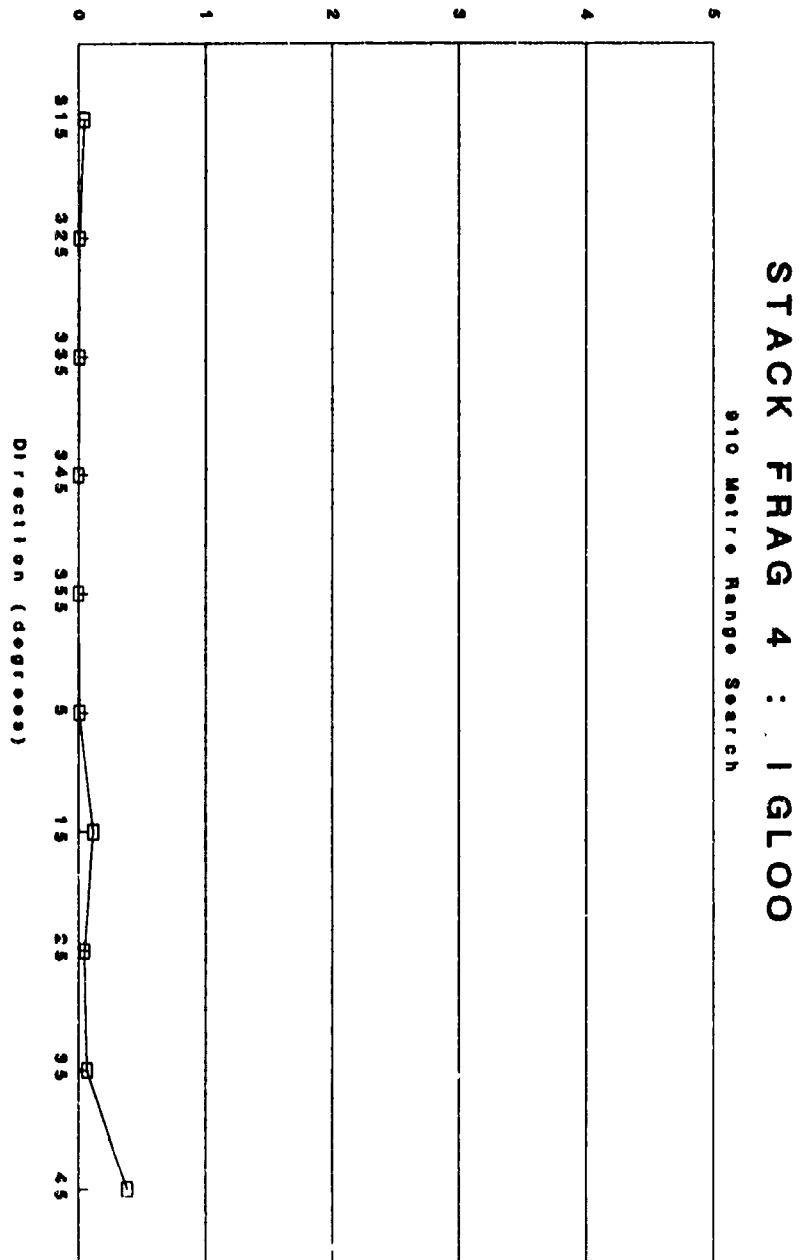


Figure 6.4

7. CRATER

7.1 There was apparently a double crater created as a result of the explosion in the donor igloo. The position of each of the constituent craters agreed well with the positions of the two original stacks of mines in the igloo. There had been some upheaval of the portion of the floor in between the two stacks.

7.2 There was a very large lip around the crater which extended vertically up to 3 metres above the original ground level and horizontally out to 5 metres beyond the edge of the crater proper. As noted in the discussions on debris the debris from the crater extended into the far field as far out as 400 metres with the bulk being inside 250 metres.

7.3 The crater is estimated as being some 36 metres long by 28 metres wide at its maximum. This compares favourably with a calculated crater diameter of 42 metres. However the depth does not exceed 2 metres at any point and is more typically 1 to 1.5 metres below the original ground level. However each of the two individual craters is approximately 20m long by 7m wide by 2m deep. As each stack was 37,500 kg NEQ the theoretical size of each of these individual craters would have been 33m in diameter

7.4 It is difficult to make informed comment on the appearance of the crater. The instrumentation deployed indicated that there was a full yield of the 75,000 kg TNT charge. There was a considerable amount of concrete in the floor and foundations of the igloo, estimated to be several hundred tonnes. A lot of this concrete was still apparent in the crater after the explosion. Undoubtedly a significant proportion of the energy normally available for excavating the crater was used in moving the concrete in the floor and foundations. Hence a much smaller or shallower crater would be expected as was found in this trial.

7.5 The total volume of the crater is estimated conservatively at only some 600-1000 m³. Theoretically it would have been expected to be roughly hemispherical with a maximum volume of about 19,000 m³.

8. BLAST INSTRUMENTATION

Far Field Pressure Measurement

8.1 WES Results : The results are given in the table below where the orientation front, side or rear refers to the orientation with respect to the donor igloo with front meaning the gauge line running away from the front side of the igloo. The full results with descriptions of the techniques used and copies of the individual gauge pressure-time histories are given in Reference 13.

Orientation	Distance (m)	Pressure (psi)	
		Measured	Estimated
Front	940	0.65	0.75
Front	620	1.1	1.5
Front	340	2.5	3
Front	90	17	30
Side	490	1.45	1.5
Side	270	3	3
Side	80	12	30
Rear	390	1.45	1.5
Rear	215	3.5	3

Note that it had been intended to measure the pressure at four points on all three radials. Because of the limited time available to the WES team some of the more distant positions were not instrumented.

8.2 OSD Results : The results are given in the table below where the orientation front, side or rear refers to the orientation with respect to the donor igloo with front meaning the gauge line running away from the front side of the igloo. The full results with descriptions of the techniques used and copies of the

individual gauge pressure-time histories are given in Reference 14.

Orientation	Distance (m)	Pressure (psi)	
		Measured	Estimated
Front	940	0.95	0.75
Front	620	1.22	1.5
Front	340	2.74	3
Front	100	n/r	30
Side	750	0.98	0.75
Side	500	1.56	1.5
Side	270	3.07	3
Side	80	12.85	30
Rear	590	0.9	0.75
Rear	390	1.75	1.5
Rear	215	3.46	3
Rear	65	18.21	30

8.3 As can be seen fairly readily from the results in paras 8.1 and 8.2 the measured results compare very favourably with the estimated results. For the closest gauges on all the radials the measured pressure was about half that originally estimated. At the two intermediate positions on each radial, corresponding to Explosives Workshop and Public Traffic Route distances, the measured results match almost exactly the predictions.

8.4 At the Inhabited Building Distance (IBD) however there is somewhat of a conflict. The only WES result which is applicable matches the prediction but the three OSD results on the three radials all exceed the predictions by a factor of between 27% and 31%. This is well outside what could be regarded as experimental error or variation. However they do not appear to be consistent with the other pressure measurements since taken at face value they appear to indicate some general pressure increase at IBD, even on the open, unattenuated side. Had these been matched with an equivalent increase at the closer in gauges then some store should be put by them. Since this is not the case it is suggested that their absolute values should be effectively put to one side until some satisfactory explanation can be put forward for the apparent variation. However since the measured pressure at the IBD on the open side is identical to that measured at the suggested IBDs on the other two sides, this can still be used to verify that the IBD on each of the radials should be at the suggested positions. It is considered that this is further justified by the fact that the WES gauge on the open side matched the predicted pressure very closely, being some 13% low which is considered to be within the experimental error for such a measurement.

8.5 This effectively means that there is a significant pressure attenuation to the side and rear of a UK standard double-bay box igloo containing 75,000 kg NEQ which is equivalent to that given by AC 258 for standard NATO igloos containing less than 45,000 kg NEQ. It should be noted that the attenuation is significant at all ranges, being greatest close in.

8.6 However further testing, preferably at model scales of not less than 1/5 should be conducted to provide statistically more meaningful results particularly at the Inhabited Building Distances. This should give some indication that the results obtained by OSD at this distance, in particular, can be considered spurious.

Donor Structure Instrumentation

8.7 A total of four internal blast gauges were fitted to the donor igloo in an attempt to measure the internal blast loadings. The three gauge packages were recovered that had originally been installed in the rear and side walls. However as noted earlier the instrument packages were recovered separated from their protective steel cylinders. As a result only the sidewall centre gauge produced a recording which could be interpreted. This indicated a peak pressure of some 10,000 psi with a duration of some 20-25 msec.

8.8 The gauge mounted in the roof of the donor was never recovered but a second instrument package had been connected externally to a second gauge in the same package. The recorder was actually located outside the igloo and was subsequently recovered and interrogated. Although the signal was abruptly cut at some 16.6 msec after detonation, when the connection was broken because of projection of the instrument package, a useful recording was obtained. This indicated that a peak pressure in excess of 18,000 psi was achieved. The pressure was still rising when the connection was broken so there is no clear indication what the final pressure would have been.

8.9 Although the results will not be directly applicable because of their limited nature the exercise of measuring the internal blast loads was well worth while. In particular it has given WES the opportunity to test their gauges in a harsh debris environment and will lead to a redesign of the actual packages to ensure that they remain intact in future tests.

8.10 The problem of gauge location remains difficult. In total five gauges were unaccounted for during this test, the roof mounted internal blast gauge and the four external mounted accelerometers. It is considered that these along with most of the unrecovered cylinders which were also placed on the roof are most probably buried in the debris which was in and around the crater.

9. DETERMINATION OF LAUNCH ANGLES AND VELOCITIES OF DONOR BUILDING DEBRIS

9.1 As advised in Ref 10 some 24 steel cylinders, each 6ins diameter by 6ins in length, were filled with concrete and made identifiable by painting with Scotchlite and embossing a reference number on the outer surface. Eleven were placed on top of the roof cover of the donor igloo, and the remaining thirteen of the side and rear earth cover.

9.2 At the date of writing (June 90) only seven of the twenty four cylinders had been recovered, despite a relatively intensive search of the area within 1000 metres of ground zero. As the cylinders found were at ranges between 580 and 1000 metres and appeared to form a reasonably distinct pattern of distribution the search was intensified in the areas where the remaining cylinders could be expected to have landed. However no more cylinders were recovered.

10. CONCLUSIONS

10.1 Undoubtedly the test was an unqualified success. It achieved virtually all the original aims of the trial with the exception of the measurement of the cover debris velocities by means of externally mounted accelerometers. As these were never recovered obviously no results were obtained (para 8.10)

10.2 Also only a limited amount of information was obtained from the internally mounted blast gauges. However these were still adjudged to have been successful in that some measurements were obtained but more importantly the gauges can be redesigned to cope better with similar conditions in the future. (paras 8.7-8.8)

10.3 The measurement of the far field pressures was very successful and has confirmed that the UK double bay box igloo provides a similar level of attenuation for the blast originating from a 75,000 kg NEQ charge as that already invoked by AC 258 for standard igloos with less than 45,000 kg NEQ. Further that such attenuations can be extended to include reductions in the quantity-distances for process building distances and public traffic route distances as well as IBD. (para 8.3-8.5)

10.4 However further testing should be carried out at model scales to provide better statistical information on which to assess the results, particularly those obtained at Inhabited Building Distance. (para 8.6)

10.5 The results of the extensive debris search, collection and analysis has demonstrated that the debris hazard from a UK double-bay box igloo reaches tolerable levels (defined as 1 potentially lethal fragment per 56 m²) well inside

the IBDs which would be proposed as a result of the pressure measurements given in Section 8. The equivalent pressure and debris IBDs are given in the table below for ease of comparison:

Orientation	Pressure IBD m	$Q^{1/3}$ Factor	Debris IBD
Front	940	22.2	850 (para 6.12)
Side	750	18	450 (paras 6.15, 6.24)
Rear	590	14	510 (para 6.20)

10.6 The crater generated as a result of the explosion was significantly shallower than expected and overall generally smaller in dimensions than the theoretically calculated size. This was considered to be not unusual because of the very large amounts of concrete in the floor and foundations of the donor igloo. (paras 7.4-7.5)

11. RECOMMENDATIONS

11.1 The quantity distances currently used by UK to the side and rear of the UK standard box igloo should be reduced as follows for UK standard igloos which contain up to 75,000 kg NEQ :

Orientation	Q-D Purpose	Current	Proposed
Side	Process Building	$8.0Q^{1/3}$	$6.5Q^{1/3}$
Side	Public Traffic Route	$14.7Q^{1/3}$	$11.9Q^{1/3}$
Side	Inhabited Building	$22.2Q^{1/3}$	$18.0Q^{1/3}$
Rear	Process Building	$8.0Q^{1/3}$	$5.0Q^{1/3}$
Rear	Public Traffic Route	$14.7Q^{1/3}$	$9.3Q^{1/3}$
Rear	Inhabited Building	$22.2Q^{1/3}$	$14.0Q^{1/3}$
Front	Process Building	$8.0Q^{1/3}$	$8.0Q^{1/3}$
Front	Public Traffic Route	$14.7Q^{1/3}$	$14.7Q^{1/3}$
Front	Inhabited Building	$22.2Q^{1/3}$	$22.2Q^{1/3}$

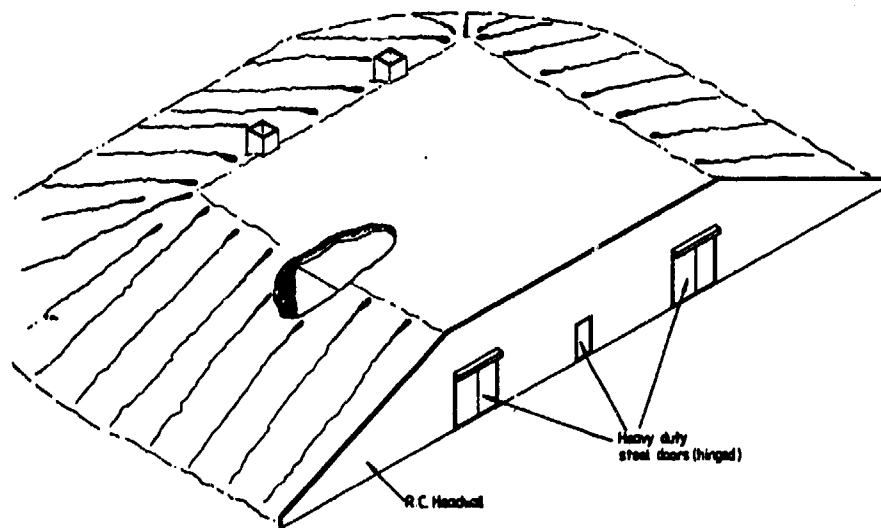
Note that as at present all igloo Q-Ds are subject to a minimum 400m distance for debris throw, unless tests have demonstrated that a lesser distance may be used for such purposes.

11.2 It is recommended that further model testing should be carried out to ascertain that the pressure levels measured in the test are correct particularly in view of the conflict of the pressures measured at the Inhabited Building Distances on all three orientations.

REFERENCES

1. Joint Australian/UK Stack Fragmentation Trials Phase 1 Report
- F Bowman, J Henderson et al - D/Safety/11/55/22 undated
2. Joint Australian/UK Stack Fragmentation Trials Phase 1B Preliminary Report
- J Henderson - ESTC/162/EE/7, WP7
3. Joint Australian/UK Stack Fragmentation Trials Phase 2 Report
- J Henderson et al - D/Safety/11/55/22 dated August 1985
4. Joint Australian/UK Stack Fragmentation Trials Phase 3 Report
- J Henderson - D/ESTC/14/1/8/2 dated May 1990
5. Joint Australian/UK Stack Fragmentation Trials Phase 4 Proposal
- D/Safety/11/55/22 dated 14 Feb 1989
6. OSD Instrumentation Plan dated 5 January 1990.
7. Range Measurements Branch Trial Instrumentation Plan RMB-IPLAN-OI-029 Issue 1 dated 15 Feb 1990.
8. Defence Trial Directive for Coalesced Defence Trials 6/445 and 6/447
- DST 88/4398/6 dated 23 Mar 90.
9. D Trials Technical Instruction DST 88/4398/7 dated 6 Apr 90.
10. Letter Jenssen/Rees dated 28 Mar 90.
11. ACS Construction Report.
12. ESH Design Trial Report.
13. WES INstrumentation Report.
14. OSD Instrumentation Report.

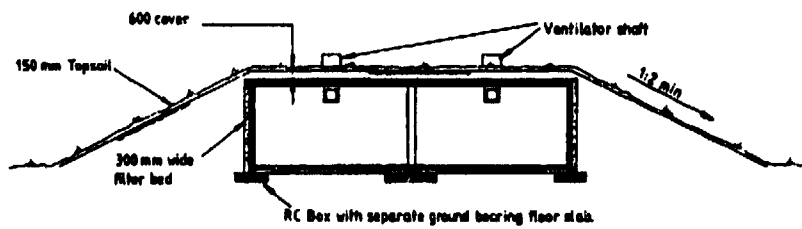
ANNEX A : NATO STANDARD DOUBLE BAY IGLOO



INTERNAL DIMENSIONS :- Length 16.00 m, Width 10.00 m, Height 4.60 m.

STORAGE CAPACITY :- $2 \times (4 \times 10 \times 3) = 240$ standard NATO pallets.

EXPLOSIVE LIMIT :- 75,000 kg. TNT Equivalent



NOTE :- For details see D.O.E layout Drg

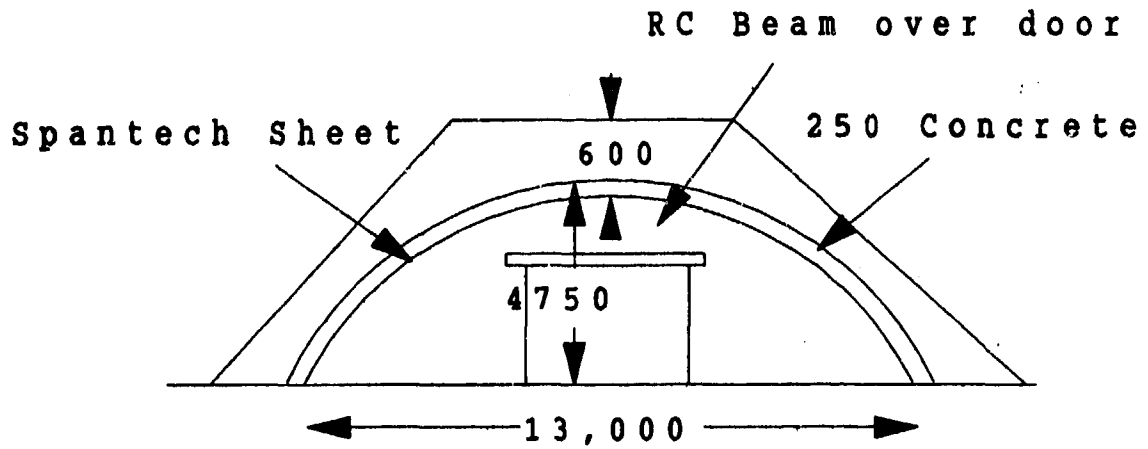
APPROVED IGLOOS - U.K. BOX (DOUBLE BAY)

ANNEX B : SPANTECH STRUCTURE

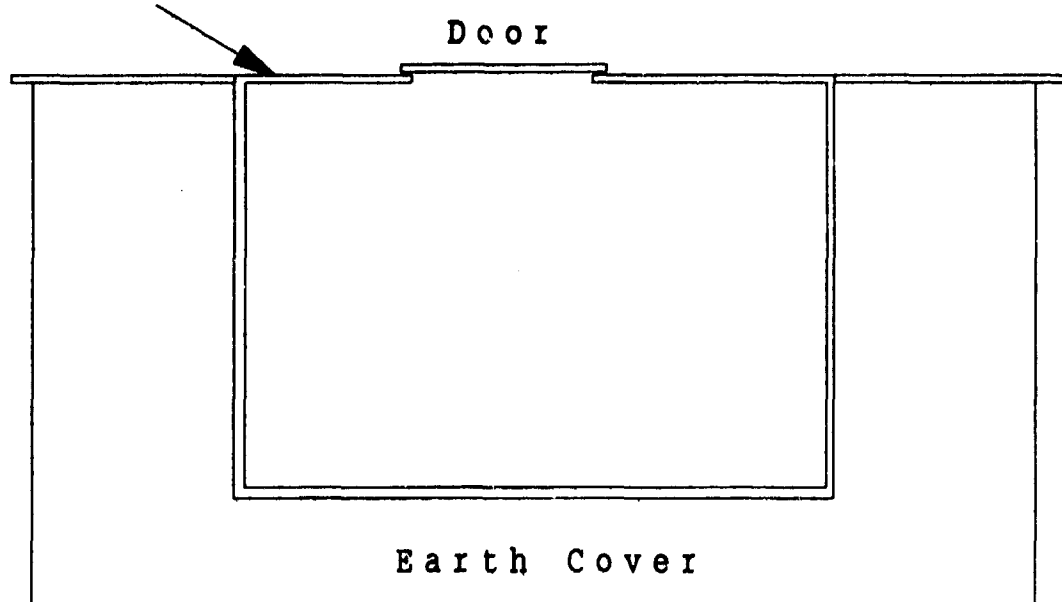
Schematic Spantech Design

Not to scale

SECTION



7 Bar Headwall PART PLAN

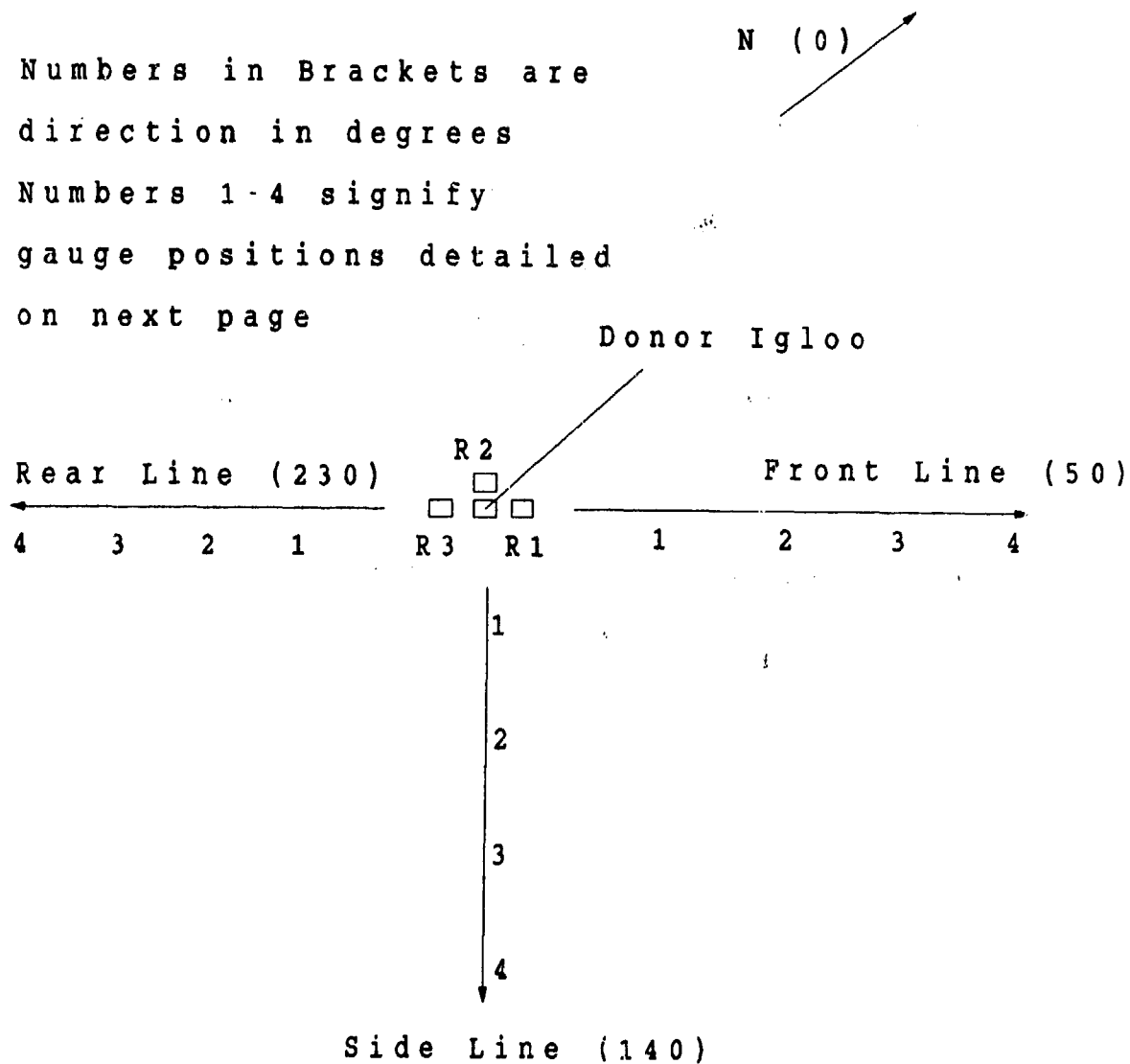


ANNEX C : SCHEMATIC GAUGE LAYOUT FOR FAR FIELD

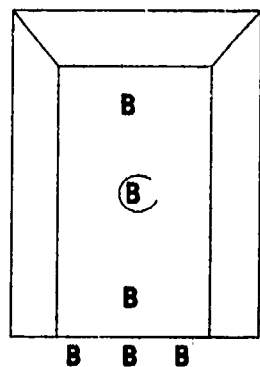
Diagrammatic Only

Not to scale

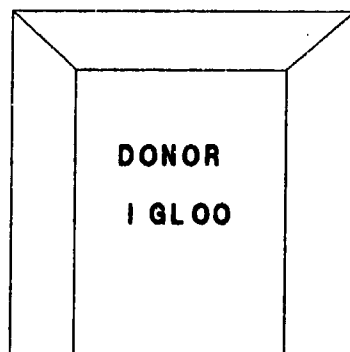
Numbers in Brackets are
direction in degrees
Numbers 1-4 signify
gauge positions detailed
on next page



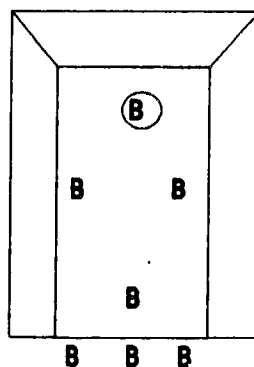
ANNEX D : SCHEMATIC GAUGE LAYOUT ON RECEPTOR STRUCTURES



RECEPTOR 3

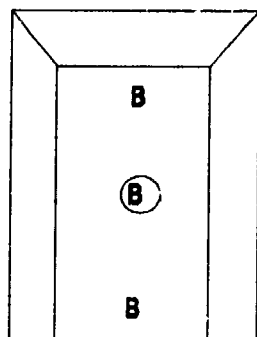


RECEPTOR 2



(B)

(B)



RECEPTOR 1

LEGEND

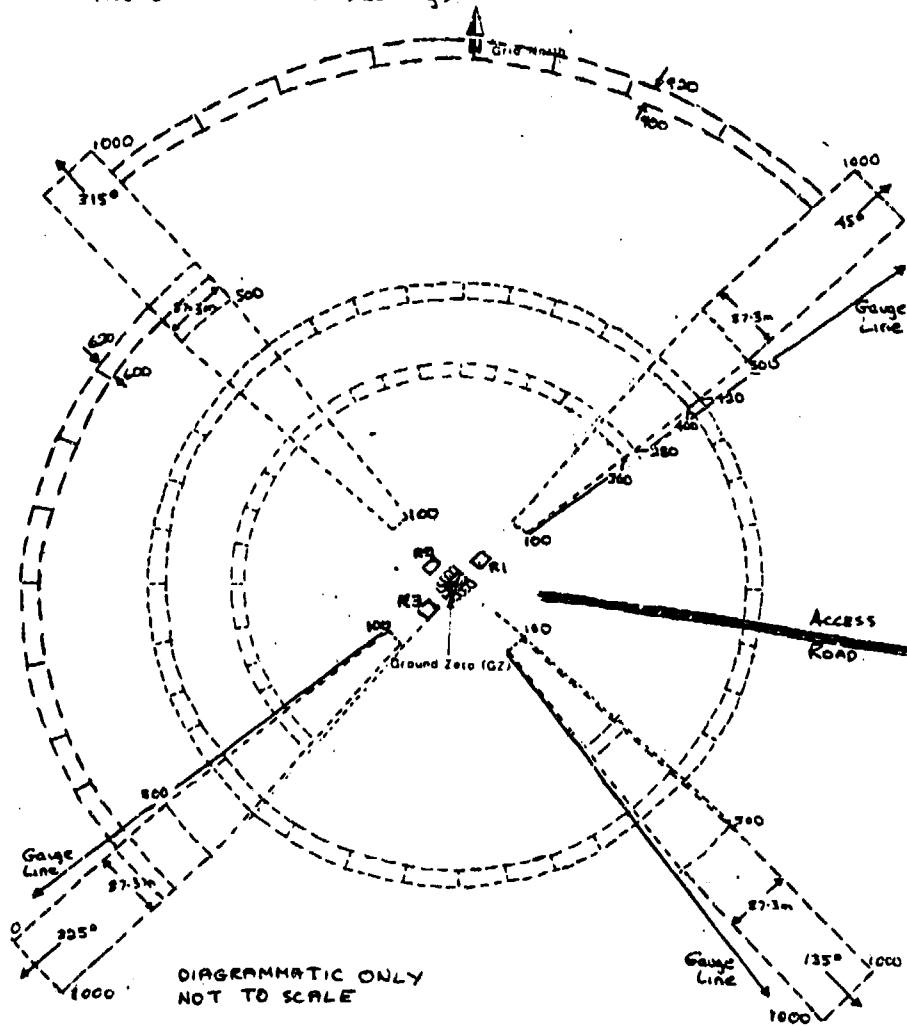
(B) WES Gauge

B WSRL Gauge



ANNEX E : DEBRIS SEARCH PATTERN

PHASE 4 PROPOSAL
 SITE LAYOUT AND SEARCH AREAS
 All distances in metres
 All directions true bearings



TRAJ--A Two Dimensional Trajectory Program For Personal Computers*

prepared by

Paul E. Montanaro
Naval Surface Warfare Center
10901 New Hampshire Avenue
Silver Spring, MD 20903-5000

ABSTRACT

The computer code TRAJ was developed to allow relatively complex trajectory calculations to be performed on a desk top personal computer. The code includes the effects of projectile mass, shape, density, launch velocity, and launch angle, as well as multiple ricochets from the ground. Terrain effects, barricades, buildings, etc can also be defined and included in the calculations. The code is briefly described and sample problems and outputs are presented.

BACKGROUND

The computer program TRAJ was originally developed at the Naval Surface Warfare Center (NAVSWC) by Porzel as part of the Naval Explosives Safety Improvement Program (NESIP)¹. It is based on an analytic solution to the classical " v^2 drag" trajectory problem. Reference 1 provides the basic assumptions and equations around which the program is written. Over the past ten years (since the publication of Reference 1), developments and improvements have continued in the program. This paper presents the latest version of the program and discusses some of the changes which have been made to the program.

These developments include (but are not limited to): (1) terrain effects--sloping terrain, hills, valleys, etc., (2) the ability to "build" structures (barricades, buildings, etc) into the trajectory path, and (3) fragment ricochets from the ground or from structures. They also include various plotting and presentation options. The ricochet and structural interaction portions of the program were developed by the Boeing Military Airplane Company (Mr. Richard A. Lorenz), under contract to NAVSWC.

The ricochet methodology is based on work originally performed by the Army and incorporated into the computer program FRAGHAZ^{2,3}. When a fragment impacts the ground or a structure, its impact angle is compared with a critical ricochet angle to determine whether the fragment will ricochet. The critical ricochet angle is dependent on the type of soil. Once it is determined that the fragment will ricochet, the ricochet angle and velocity are determined from the incident angle and velocity as well as the soil type. When ricochet occurs, the trajectory calculation continues until no further ricochets occur and the fragment has come to rest.

*This work was partially sponsored by the Department of Defense Explosives Safety Board under Military Interdepartmental Purchase Requests E8789L036 and E8790L215.

HARDWARE REQUIREMENTS

The program is written in BASIC and is designed to run on any IBM-compatible machine using DOS 3.1 operating system (or higher) with 640 kilobytes of memory and a hard disk. The program supports CGA, EGA, and VGA graphics. An IBM-AT (or faster) machine with math co-processor is highly recommended.

GENERAL

The input to the program is prepared interactively through a series of screens which question the user. At any time, the user may change his mind and replace information which has already been entered. The program is set up to operate in a modified English system of units. All lengths are in feet, areas in ft^2 , and velocities in ft/s . All weights are in pounds. Fragment densities are in g/cm^3 . Impact energies are calculated in ft-lbs .

Several kinds of information are required to perform the calculations. The most important is a description of the fragment and the initial conditions. The fragment description includes mass, shape, and density. Mass and density are straightforward. The shape is not. The shape of an object is described by its shape factor, length in direction of motion, and cross sectional area. The shape factor is a required input, and is described below. Length in direction of motion, or cross sectional area can be entered as an option; but not both.

Shape Factor. The shape factor can be thought of as the ratio of the volume of the fragment to the volume of a rectangular box with the minimum dimensions required to hold the fragment. Typical explosively-formed fragments have shape factors around 0.333. Pre-formed fragments have a shape factor of 1.000. A sphere has a shape factor of $\pi/6$ (0.524). Experimentally-determined shape factors for concrete debris have ranged from 0.33 to 0.44.

Length in Direction of Motion. This is directly what it seems. If, for instance, it is known or postulated that a fragment flies like a spear, then the total length of the fragment would be the length in the direction of motion. In the program, this is referred to as Characteristic Fragment Length.

DESCRIPTION OF INPUT SCREENS

MAIN MENU

See Figure 1. Upon entering the program, you will see the Main Menu. It defines the six possible decision paths which are allowed within the program.

The first time a particular problem is run, Item 1 should be selected. This will lead to further screens which will be discussed later.

After Item 1 is completed, the trajectories are automatically calculated and stored on the hard disk. At this point, the Main Menu reappears. Here, a screen plot of the trajectories can be displayed through the use of Item 3. Item 4 presents a summary table of the final conditions for each of the trajectories computed. Item 5 presents details of the complete trajectory for each case. Item 2 is used to preview barrier or structure data before trajectory calculations are done (see THIRD INPUT SCREEN). It simply plots the terrain and any associated structures or barriers--but no trajectories. Item 6 causes the program to exit back to DOS.

Let us assume that Item 1 was initially selected.

FIRST INPUT SCREEN

See Figure 2. The program first reads an input data file "TRAJ.IN" from the hard disk. This file contains all of the trajectory input conditions that were used on the last Traj run. If you copy this file in DOS to another name, you can preserve these input conditions for future use, and copy them back to "TRAJ.IN" when needed. If the information on the screen is correct, answer Y to the question "Is this screen O.K. (Y/N)?" If the information requires modification, answer N.

The program is setup to do many trajectory calculations at one time using different initial velocities, angles, and masses. If you have answered N, the first information requested is the initial velocity: beginning, ending, and increment. The beginning and ending initial velocities are obvious. The increment may be either positive or negative. The beginning initial velocity is incremented by the amount chosen until the ending initial velocity is obtained (or exceeded). Thus a series of initial velocities can easily be chosen. The pointer is moved by use of the "Enter" key. If an item does not need to be changed, pressing "Enter" will accept the default value shown.

The second set of required data is the initial angle. This works in exactly the same way as the initial velocity. It must be remembered that each angle selected will be run with all initial velocities selected.

The third item required is the mass (or masses) of the fragments. This is simply a list of all the masses of interest (separated by an "Enter"). Up to 20 masses may be chosen. It should be noted that if the user chooses 10 initial velocities, 10 initial angles, and 10 masses, the program will calculate 1000 trajectories, which will take quite a long time (> 60 minutes). Also a screen plot of these would be far too crowded to allow interpretation.

The final item on this screen is the density of the fragments. If the material is one of the default materials, simply enter the corresponding number and press "Enter". Otherwise, choose "other" and enter the appropriate density.

When this is completed the prompt "Is this screen O.K. (Y/N)?" will appear. If all the information showing on the screen is correct, type Y. Then type space bar to continue to the next screen or M to return to the main menu (use this also if you want to return to a previous screen). If any of the information is still not correct, type N. This will allow you to cycle through the information on that screen again, changing anything needed.

SECOND INPUT SCREEN

See Figure 3. Again, the first thing encountered will be the dialog: "Is this screen O.K. (Y/N)?". To make changes on this screen, type N.

Select a shape factor from one of the options listed or choose other and enter the value.

If desired enter either the cross sectional area or the characteristic length (but not both), and enter zero for the other. If both are entered, the cross sectional area entered will be ignored.

If the trajectory is to be calculated for conditions other than at sea level, then the value of the atmospheric density and sound speed for that altitude will be required.

The fragment starting height allows the trajectory to start somewhere other than at ground level.

A drag coefficient table versus Mach number table is built into the program and is presented on this screen. The table is in terms of Drag Coefficient vs. Mach Number. Two choices are available with this table. The first asks whether interpolation between table entries is requested. If No is selected, the drag coefficient remains constant between Mach number entries. For example, the drag coefficient is assumed to be 0.8 for Mach numbers between 0.0 and 0.75, and 0.88 for 0.75 to 0.9, etc. If Yes is selected, the drag coefficient varies linearly from 0.8 to 0.88 for Mach numbers between 0.0 and 0.75, etc. The second choice allows direct change or modification to the table itself.

Again, when this is completed the prompts "Is this screen O.K. (Y/N)?" and "Type space bar to continue or M to return to main menu" will appear. If all the information showing on the screen is correct, type Y. Then type space bar to continue to the next screen. If any of the information is still not correct, type N. This will allow you to cycle through the information on that screen again, changing anything needed.

THIRD INPUT SCREEN

See Figure 4. This screen defines the terrain and any structures or barriers.

The first item is the minimum altitude. This defines a "lower limit altitude", below which calculations will not be carried out. This can be used for flat ground, but ricochet will not occur.

Next, you are asked if you would like to view the table of soil constants. These are required for the ricochet calculations. This table simply presents descriptions of the soil and their associated constants. It is shown in Figure 5. This is helpful in selecting the proper values.

Finally you are asked to define the terrain and barriers/structures. These are defined

by the coordinates (x,y) of points on the terrain or structure. The terrain is built up in segments—three pairs of points per segment. If only two points are given for a segment, a straight line is fitted between them. If three points are given for a segment, a quadratic is fitted. A soil constant is also required for each segment. If a value of 0 is put in for the soil constant, no ricochets will be allowed over that segment. Up to 10 segments are allowed.

Again, when this is completed the prompts "Is this screen O.K. (Y/N)?" and "Type space bar to continue or M to return to main menu" will appear. If any of the information is still not correct, type N. This will allow you to cycle through the information again, changing anything needed. If all the information showing on the screen is correct, type Y. Then type space bar. The program counts as each trajectory calculation is completed. When all of the calculations are completed, the input data file "TRAJ.IN" is written to disk.

Suppose that you have put in the coordinates of a terrain/barrier system and you wish to preview them before performing the calculations. In that case, instead of typing space bar to continue, type M and return to the Main Menu. On the main menu, select option 2 ("Plot Working Barrier Data"). This will produce a screen plot of the information provided. If it is correct, Enter option 1, and then choose Y on each screen. If the terrain/barrier is not correct, when Screen 3 appears, make the appropriate changes.

When the trajectory computations are completed, you are returned to the Main Menu.

GETTING A PRINTOUT OF SCREEN PLOTS

To obtain a printout of working barrier or fragment trajectory plots, type the DOS command "graphics" before running TRAJ. Then when a plot is displayed on the screen, press the "print screen" key and a copy of the screen will be sent to the printer. Some versions of DOS do not support "print screen" for VGA graphics, so in this case select EGA graphics when doing screen plots.

SAMPLE CALCULATIONS

Let us consider two problems. Each will be described. Then samples of the input screens and the outputs will be presented.

PROBLEM 1 (Figures 2 - 8)

Trajectories are calculated for a 20 pound concrete fragment. Initial velocities are 200 and 300 ft/s at angles of 30, 40, and 50 degrees above the horizontal. The terrain slopes downward from the source 50 feet in 800 feet to the base of a hill. The rounded hill peaks at 150 feet above the source at a distance of 1300 feet. The hill descends to level terrain 55 feet below the source at a distance of 1750 feet. The soil type is dry sand. Ricochet is enabled, but does not occur.

This problem illustrates: (1) the reversal of fragment range after maximum range is achieved; (2) trajectory termination on a downward slope, or linear barrier; (3) trajectory termination on a curved contour, or quadratic barrier; and (4) construction of a complex ground contour by connecting linear and/or quadratic segments.

PROBLEM 2 (Figures 9 - 15)

Trajectories are calculated for a 20 pound concrete fragment. Initial velocities are 200 and 300 ft/s at angles of 5, 7.5, and 10 degrees above the horizontal. The terrain slopes upward from the source 35 feet in 500 feet to a level plateau 200 feet in length. The terrain then returns to source level at a distance of 890 feet from the surface. A 4.4 foot vertical barrier is located about three-quarters of the way up the initial slope. The soil type is dry sand. Ricochet is enabled.

This problem illustrates: (1) ricochet on both ascending and descending slopes; (2) multiple ricochets for a single trajectory; (3) trajectory termination on a vertical barrier.

SUMMARY

The above examples illustrate the versatility of TRAJ, with its ability to handle uneven terrain with multiple barriers, its incorporation of ricochet, and its ability to calculate multiple trajectories with a range of input conditions in one run.

REFERENCES

1. Porzel, F. B., "Technology Base of the Navy Explosives Safety Improvement Program," Minutes of the Nineteenth Explosives Safety Seminar, Los Angeles, CA, 9-11 September 1980.
2. McCleskey, F., "Fragmentation Hazard Computer Model," Minutes of the Twenty-First Explosives Safety Seminar, Houston, TX, 28-30 Aug 1984.
3. McCleskey, F., "Quantity-Distance Fragment Hazard Computer Program (FRAGHAZ)," NSWC TR 87-59, February 1988.

Figure 1: MAIN MENU

MAIN MENU

1. CHANGE INPUT CONDITIONS, CALCULATE NEW TRAJECTORIES
2. PLOT WORKING BARRIER DATA
3. PLOT FRAGMENT TRAJECTORIES
4. DISPLAY FINAL CONDITIONS FOR FRAGMENTS
5. DISPLAY COMPLETE TRAJECTORY CONDITIONS FOR FRAGMENTS
6. EXIT PROGRAM

ENTER SELECTION NUMBER AND PRESS ENTER

Figure 2: FIRST INPUT SCREEN - PROBLEM 1

FRAGMENT TRAJECTORY DATA INPUT

	BEGINNING	ENDING	INCREMENT
INITIAL VELOCITY (FT/SEC)	200	300	100
INITIAL ANGLE (DEG)	30	60	10

LIST OF MASSES (LB)	SELECT FRAGMENT DENSITY (gm/cm ³)
20	1. STEEL 7.8
	2. ALUMINUM 2.7
	3. CONCRETE > 2.4 <
	4. CAST IRON 7.1
	5. OTHER —

IS THIS SCREEN O.K. (Y/N) ?

Figure 3: SECOND INPUT SCREEN - PROBLEM 1

SELECT FRAGMENT SHAPE FACTOR

1. TYPICAL FRAGMENTS 0.333
2. PREFORMED FRAGMENTS 1.0
3. OTHER > .46 <

FRAGMENT AREA (SQFT)

(Enter Zero when Area is Unknown) 0

CHARACTERISTIC FRAGMENT LENGTH (FT)

(Enter Zero when Length is Unknown) 0

AMBIENT DENSITY (LBS/CUFT) .07647

AMBIENT SOUND SPEED (FT/SEC) 1116.45

FRAGMENT STARTING HEIGHT (FT) 0

IS THIS SCREEN O.K. (Y/N) ?

INTERPOLATE THE DRAG
COEFFICIENT TABLE (Y/N)

Y

DO YOU WANT TO CHANGE THE
DRAG COEFFICIENT

MACH NUMBER TABLE (Y/N)

N

1.08	4
1.14	2
1.26	1.15
1.09	.9
.88	.75
.8	0

Figure 4: THIRD INPUT SCREEN - PROBLEM 1

GROUND/TERRAIN AND BARRIER DATA INPUT

MINIMUM ALTITUDE (FT) -60 VIEW TABLE OF SOIL CONSTANTS (Y/N) N

NO.	1ST POINT	2ND POINT	3RD POINT	SOIL	...	Y = A*X ² + B*X + C	...
I	PTS X(FT) Y(FT)	X(FT) Y(FT)	X(FT) Y(FT)	CONST	A	B	C
1	2 0 0	800 -50		0-4			
2	3 800 -50	900 -45	1000 0	2.00	+.000D+00-	.625D-01+	.000D+00
3	3 1000 0	1300 150	1600 0	2.00	+.200D-02-	.335D+01+	.135D+04
4	3 1600 0	1700 -45	1750 -55	2.00	-.167D-02+	.433D+01-	.267D+04
					+.167D-02-	.595D+01+	.525D+04

IS THIS SCREEN O.K. (Y/N) ?

Figure 5: TABLE OF SOIL CONSTANTS

SOIL CONSTANTS

HARD GREY CLAY	0.07, 0.47
WET EARTHWORK	0.11
EARTHWORK	0.13
WET CLAY	0.16
SOFT YELLOW CLAY	0.24 - 0.27, 0.66, 1.09
DAMP CLAY	0.39
CLAY SOIL, SAND CLAY EARTHWORK	0.53
CLAY-SAND GRAVEL	0.70
GRASSY EARTHWORK	0.81
SAND GRAVEL	1.67
DRY SAND	1.71 - 2.07
EARTH-SAND GRAVEL	2.24
SAND	2.91 - 4.0

PRESS ANY KEY TO CONTINUE

Figure 6: FINAL CONDITIONS DISPLAY - PROBLEM 1

TRAJ ANGLE (DEG)	PATH LENGTH (FT)	HORIZ. RANGE (FT)	HEIGHT (FT)	ENERGY (FT-LBS)	VELOCITY (FT/SEC)	TIME (SEC)
INITIAL VEL. = 200 MASS = 20 INITIAL ANGLE = 30.000 # RICOCHETS = 0						
-44.797	857.394	784.364	-49.023	0.576D+04	136.094	6.10608
INITIAL VEL. = 200 MASS = 20 INITIAL ANGLE = 40.000 # RICOCHETS = 0						
-54.947	966.240	820.719	-52.249	0.594D+04	138.215	7.48030
INITIAL VEL. = 200 MASS = 20 INITIAL ANGLE = 50.000 # RICOCHETS = 0						
-63.146	1024.297	780.609	-48.788	0.625D+04	141.850	8.61986
INITIAL VEL. = 300 MASS = 20 INITIAL ANGLE = 30.000 # RICOCHETS = 0						
-36.976	1187.870	1110.118	89.908	0.645D+04	144.107	6.60515
INITIAL VEL. = 300 MASS = 20 INITIAL ANGLE = 40.000 # RICOCHETS = 0						
-50.089	1346.817	1170.052	121.856	0.633D+04	142.693	8.34218
INITIAL VEL. = 300 MASS = 20 INITIAL ANGLE = 50.000 # RICOCHETS = 0						
-62.415	1486.509	1142.034	108.411	0.708D+04	150.916	10.14341

DO YOU WISH TO SEE THE OUTPUT AGAIN (Y/N) ?

Figure 7: PLOT OF WORKING BARRIER DATA - PROBLEM 1

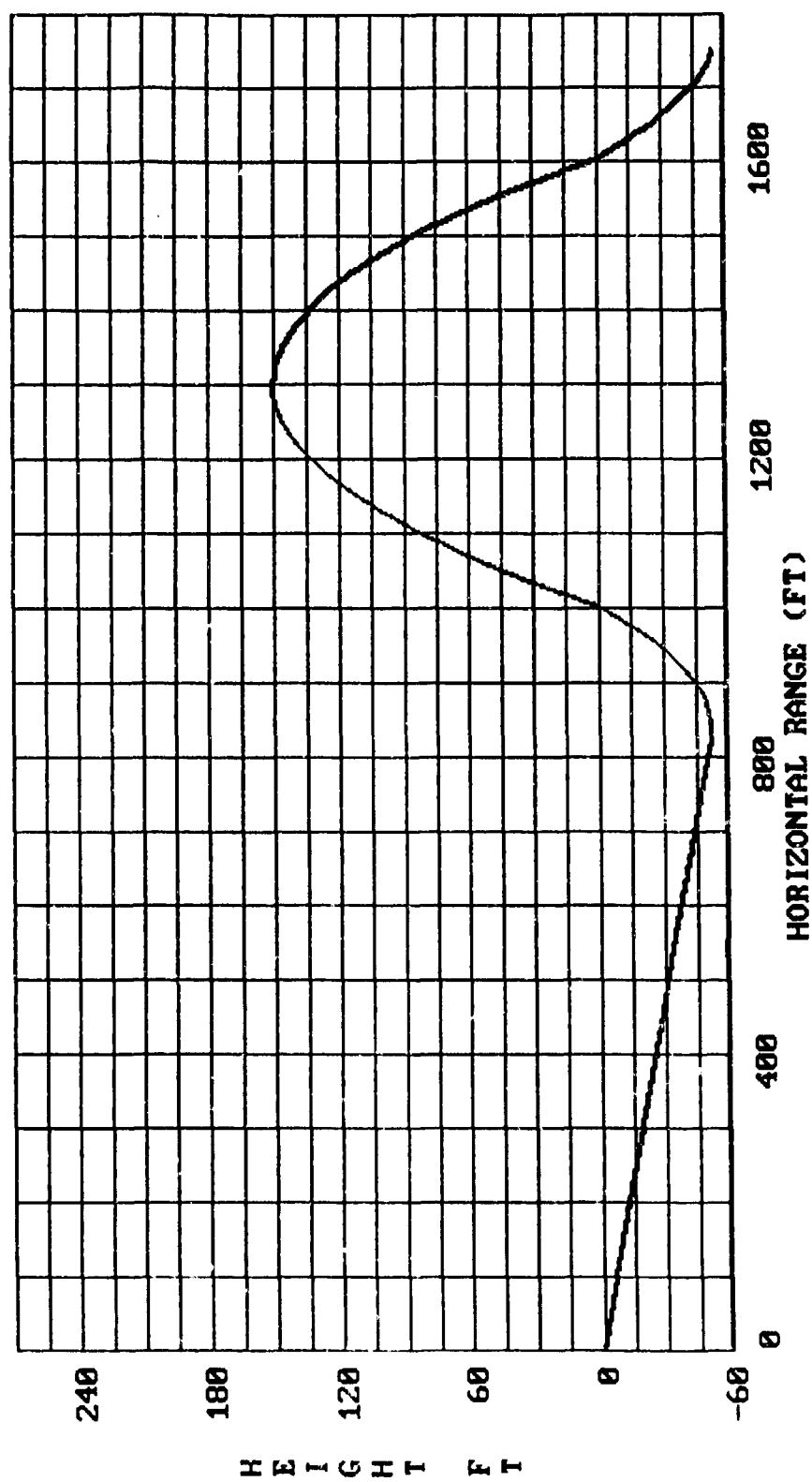


Figure 8: PLOT OF FRAGMENT TRAJECTORIES - PROBLEM 1

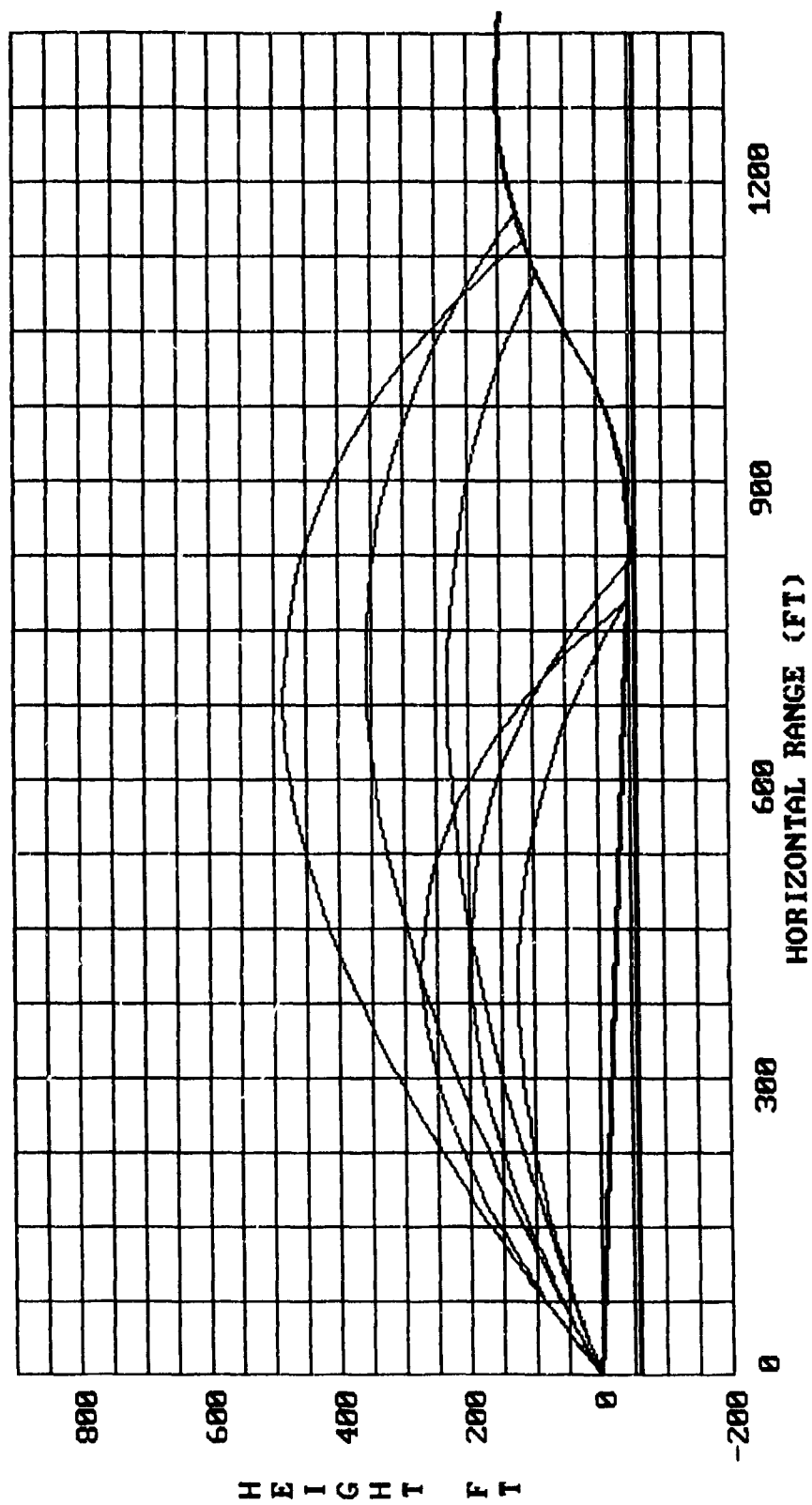


Figure 9: FIRST INPUT SCREEN - PROBLEM 2

```

                                FRAGMENT TRAJECTORY DATA INPUT

                                BEGINNING      ENDING      INCREMENT
INITIAL VELOCITY (FT/SEC)      200           300          100
INITIAL ANGLE (DEG)            5            10           2.5

LIST OF MASSES (LB)           SELECT FRAGMENT DENSITY (gm/cm^3)
20                             1.  STEEL              7.8
                              2.  ALUMINUM             2.7
                              3.  CONCRETE             > 2.4 <
                              4.  CAST IRON            7.1
                              5.  OTHER              _____

```

IS THIS SCREEN O.K. (Y/N) ?

Figure 10: SECOND INPUT SCREEN - PROBLEM 2

```

SELECT FRAGMENT SHAPE FACTOR                                INTERPOLATE THE DRAG
1.  TYPICAL FRAGMENTS      0.333                                COEFFICIENT TABLE (Y/N)      Y
2.  PREFORMED FRAGMENTS    1.0
3.  OTHER                   > .46 <

FRAGMENT AREA (SQFT)                                           DO YOU WANT TO CHANGE THE
(Enter Zero when Area is Unknown)  0                                DRAG COEFFICIENT
                                                                MACH NUMBER TABLE (Y/N)      N
                                                                1.08              4
                                                                1.14              2
                                                                1.26              1.15
                                                                1.09              .9
                                                                .88              .75
                                                                .8              0

AMBIENT DENSITY (LBS/CUFT)      .07647

AMBIENT SOUND SPEED (FT/SEC)    1116.45

FRAGMENT STARTING HEIGHT (FT)   0

                                IS THIS SCREEN O.K. (Y/N) ?

```

Figure 11: THIRD INPUT SCREEN - PROBLEM 2

GROUND/TERRAIN AND BARRIER DATA INPUT

MINIMUM ALTITUDE (FT) 0 VIEW TABLE OF SOIL CONSTANTS (Y/N) N

NO.	1ST POINT	2ND POINT	3RD POINT	SOIL	...	Y = A*X^2 + B*X + C	...
I	PTS	X(FT)	Y(FT)	X(FT)	Y(FT)	X(FT)	Y(FT)
1	2	0	0	500	35		
2	2	500	35	700	35		
3	2	700	35	890	0		
4	2	380	26.6	380	31		

SOIL CONST 0-4

CONST	A	B	C
2.00	+.000D+00	+.700D-01	+.000D+00
2.00	+.000D+00	+.000D+00	+.350D+02
2.00	+.000D+00	-.184D+00	+.164D+03
2.00	+.000D+00	+.100D+31	+.000D+00

IS THIS SCREEN O.K. (Y/N) ?

Figure 12: FINAL CONDITIONS DISPLAY - PROBLEM 2

TRAJ ANGLE (DEG)	PATH LENGTH (FT)	HORIZ. RANGE (FT)	HEIGHT (FT)	ENERGY (FT-LBS)	VELOCITY (FT/SEC)	TIME (SEC)
INITIAL VEL. = 200 6.054	381.766	MASS = 20 380.000	28.890	INITIAL ANGLE = 5.000 0.654D+04	# RICOCHETS = 4 73.822	2.79901
INITIAL VEL. = 200 -0.871	381.813	MASS = 20 380.000	29.354	INITIAL ANGLE = 7.500 0.672D+04	# RICOCHETS = 2 100.686	2.58409
INITIAL VEL. = 200 11.934	382.173	MASS = 20 380.000	27.909	INITIAL ANGLE = 10.000 0.675D+04	# RICOCHETS = 2 74.400	2.54044
INITIAL VEL. = 300 -12.045	902.083	MASS = 20 894.088	0.000	INITIAL ANGLE = 5.000 0.113D+05	# RICOCHETS = 6 31.880	6.20394
INITIAL VEL. = 300 -22.674	908.656	MASS = 20 899.766	0.000	INITIAL ANGLE = 7.500 0.102D+05	# RICOCHETS = 3 32.758	5.68059
INITIAL VEL. = 300 -15.074	906.747	MASS = 20 896.732	0.000	INITIAL ANGLE = 10.000 0.106D+05	# RICOCHETS = 3 30.970	5.80167

DO YOU WISH TO SEE THE OUTPUT AGAIN (Y/N) ?

Figure 13: PLOT OF WORKING BARRIER DATA - PROBLEM 2

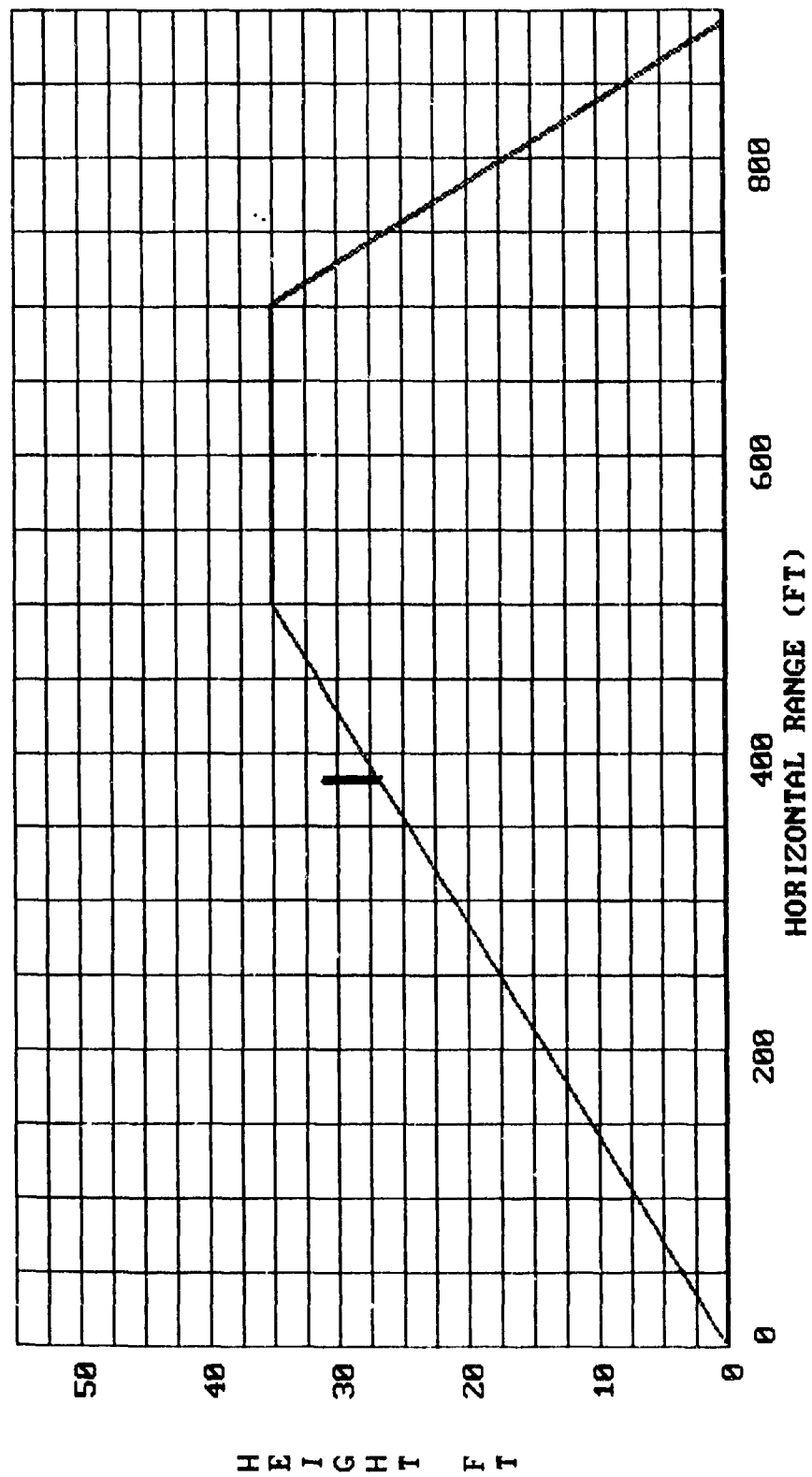


Figure 14: PLOT OF FRAGMENT TRAJECTORIES - PROBLEM 2

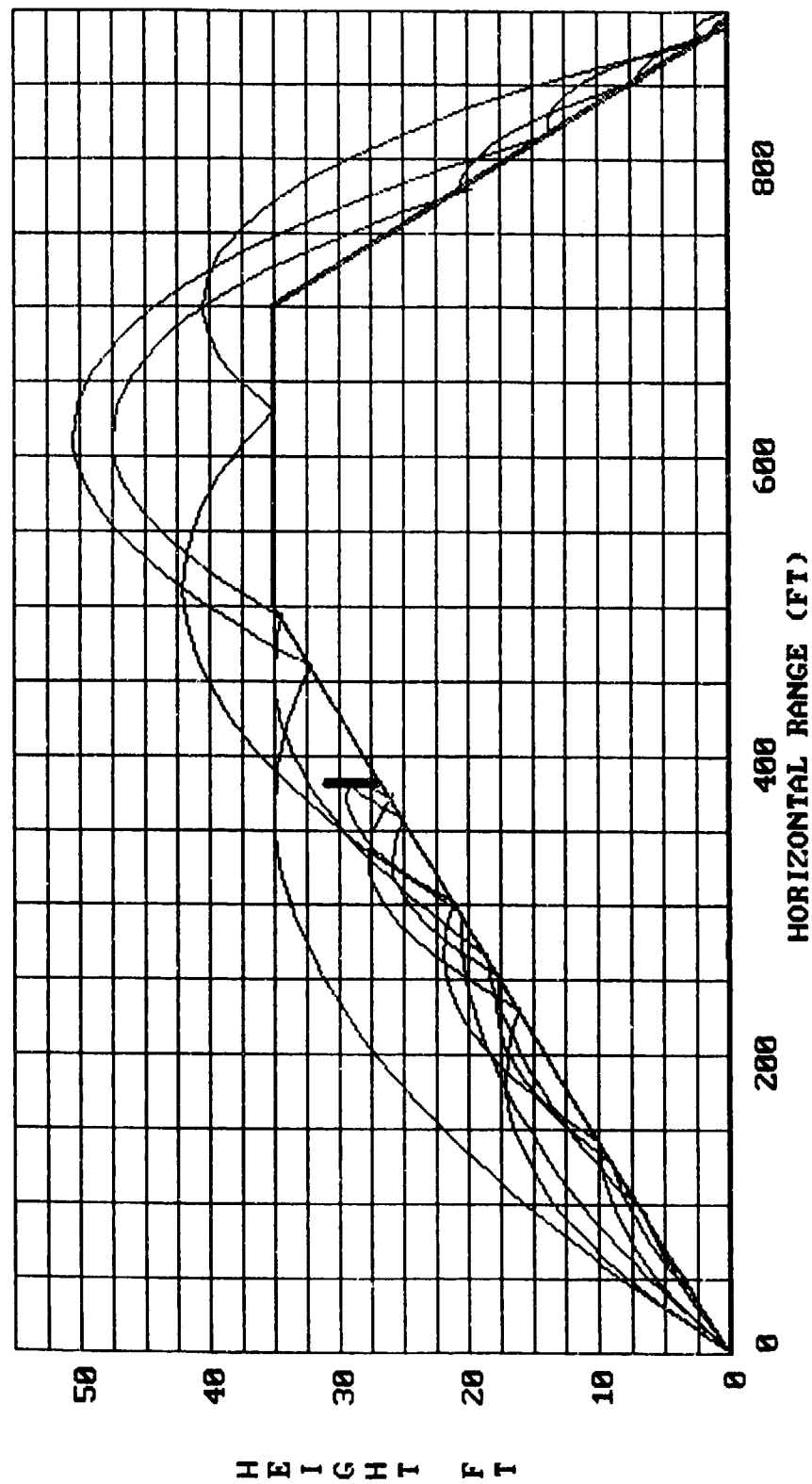


Figure 15: COMPLETE TRAJECTORY CONDITIONS DISPLAY - PROBLEM 2

ANALYTICAL SOLUTION FOR TRAJECTORY WITH VARIABLE DRAG 06-30-1990

SAMPLE RUN

TRIM= 0

NUMBER OF BARRIERS= 4

1	NUMBER OF POINTS= 2	SOIL CONST= 2	A= 0
	X1= 0 X2= 500 X3= 0	B= .07	
	Y1= 0 Y2= 35 Y3= 0	C= 0	
2	NUMBER OF POINTS= 2	SOIL CONST= 2	A= 0
	X1= 500 X2= 700 X3= 0	B= 0	
	Y1= 35 Y2= 35 Y3= 0	C= 35	
3	NUMBER OF POINTS= 2	SOIL CONST= 2	A= 0
	X1= 700 X2= 890 X3= 0	B= -.1842105	
	Y1= 35 Y2= 0 Y3= 0	C= 163.9474	
4	NUMBER OF POINTS= 2	SOIL CONST= 2	A= 0
	X1= 380 X2= 380 X3= 0	B= 1E+30	
	Y1= 27 Y2= 31 Y3= 0	C= 0	

200 VELOCITY # 1
20 MASS # 1
5 ANGLE # 1

LENGTH UNIT-FT MASS UNIT-LBS TIME UNIT-SEC ENERGY UNIT-FT-LBS

NUMBER OF (C,U) PAIRS IN THE DRAG COEFFICIENT TABLE = 6

1.00	4	1.14	2	1.26	1.15	1.09	.9	.88	.75	.8	0
------	---	------	---	------	------	------	----	-----	-----	----	---

FRAGMENT STARTS AT (FT)	X= 0	Y= 0
TRAJECTORY LIMITS (FT)	X9= 0	Y9= 0
RADIUS OF CURVATURE (FT)	R= 1	
INITIAL ANGLE (DEG)	A0= 5	AMB. DENSITY (LBS/CUFT) D0= 7.647D-02
INITIAL VELOCITY (FT/SEC)	U0= 200	AMB. SOUND SPEED (FT/SEC) C0= 1116.45

FRAGMENT MASS (LBS)	M= 20	GRAVITY (FT/SEC/SEC)	G= 32.174
SHAPE FACTOR	B= 0.4600	DRAG DECAY CONSTANT	C= 0.44330D-03
FRAGMENT AREA (SQFT)	A6= 0.437980	DRAG COEFFICIENT	C1= .8
CHARACTERISTIC LENGTH (FT)	L= 0.661800	(DRAG IS INTERPOLATED)	
FRAG. DENSITY (LBS/CUFT)	D= 150	STEP SIZE UP (DEG)	I= .5
ENERGY UNIT (FT-LBS)	E5= 32.174	STEP SIZE DOWN (DEG)	I2= .5

TRAJ ANGLE (DEG)	PATH LENGTH (FT)	HORIZ. RANGE (FT)	HEIGHT (FT)	ENERGY (FT-LBS)	VELOCITY (FT/SEC)	TIME (SEC)
5.000	0.000	0.000	0.000	0.124D+05	200.000	0.00000
4.500	10.798	10.761	0.894	0.122D+05	198.380	0.05421
4.000	21.417	21.351	1.682	0.120D+05	196.813	0.10795
3.500	31.865	31.776	2.365	0.119D+05	195.297	0.16124
3.000	42.149	42.043	2.948	0.117D+05	193.829	0.21410
2.981	42.539	42.433	2.969	0.117D+05	193.774	0.21611
2.986	42.439	42.333	2.963	0.117D+05	193.788	0.21559
6.476	42.439	42.334	2.963	0.117D+05	181.456	0.21559
5.828	53.967	53.795	4.159	0.115D+05	179.811	0.27942
5.181	65.277	65.053	5.284	0.113D+05	178.231	0.34259
4.533	76.381	76.117	6.225	0.111D+05	176.712	0.40516
3.886	87.290	86.996	7.026	0.109D+05	175.253	0.46715
3.238	98.014	97.699	7.692	0.107D+05	173.850	0.52859
2.590	108.563	108.234	8.229	0.105D+05	172.501	0.58950
1.943	118.945	118.608	8.640	0.104D+05	171.204	0.64992
1.295	129.171	128.830	8.929	0.102D+05	169.958	0.70986
1.432	127.023	126.682	8.877	0.103D+05	170.217	0.69723
1.419	127.234	126.893	8.883	0.103D+05	170.191	0.69847

1.418	127.239	126.898	8.883	0.103D+05	170.191	0.69850
9.078	127.239	126.898	8.883	0.103D+05	155.814	0.69850
8.170	139.203	138.727	10.677	0.103D+05	154.176	0.77569
7.262	150.896	150.313	12.248	0.985D+04	152.623	0.85192
6.354	162.336	161.672	13.604	0.966D+04	151.151	0.92724
5.447	173.541	172.818	14.756	0.948D+04	149.755	1.00171
4.539	184.529	183.763	15.713	0.932D+04	148.431	1.07541
3.631	195.313	194.520	16.482	0.916D+04	147.177	1.14837
2.723	205.909	205.099	17.069	0.901D+04	145.990	1.22066
1.816	216.332	215.513	17.482	0.888D+04	144.866	1.29233
0.908	226.592	225.771	17.726	0.875D+04	143.802	1.36342
0.000	236.704	235.882	17.807	0.862D+04	142.797	1.43398
-1.256	250.475	249.651	17.656	0.847D+04	141.497	1.53086
-1.462	252.708	251.883	17.603	0.844D+04	141.294	1.54665
-1.434	252.405	251.581	17.611	0.845D+04	141.322	1.54451
-1.435	252.410	251.586	17.611	0.845D+04	141.321	1.54454
11.540	252.410	251.586	17.611	0.845D+04	117.926	1.54454
10.386	261.190	260.204	19.281	0.828D+04	116.769	1.61936
9.232	269.771	268.660	20.743	0.813D+04	115.686	1.69319
8.078	278.171	276.963	22.007	0.799D+04	114.676	1.76612
6.924	286.405	285.127	23.083	0.786D+04	113.735	1.83822
5.770	294.489	293.161	23.977	0.774D+04	112.859	1.90957
4.616	302.437	301.076	24.696	0.763D+04	112.047	1.98025
3.462	310.262	308.881	25.247	0.752D+04	111.295	2.05032
2.308	317.977	316.586	25.636	0.743D+04	110.601	2.11986
1.154	325.593	324.198	25.866	0.734D+04	109.964	2.18892
0.000	333.123	331.727	25.942	0.727D+04	109.381	2.25757
-1.958	345.732	344.332	25.728	0.715D+04	108.513	2.37331
-3.917	358.172	356.754	25.091	0.706D+04	107.789	2.48834
-4.071	359.148	357.728	25.023	0.705D+04	107.738	2.49740
-4.051	359.019	357.599	25.032	0.705D+04	107.745	2.49620
-4.051	359.020	357.600	25.032	0.705D+04	107.745	2.49621
13.374	359.020	357.600	25.032	0.705D+04	76.625	2.49621
12.037	363.351	361.825	25.985	0.694D+04	76.000	2.55296
10.700	367.593	365.983	26.821	0.683D+04	75.428	2.60899
9.362	371.756	370.082	27.546	0.674D+04	74.906	2.66436
8.025	375.848	374.127	28.165	0.665D+04	74.433	2.71916
6.687	379.877	378.123	28.681	0.658D+04	74.007	2.77345
6.055	381.761	379.995	28.890	0.654D+04	73.822	2.79895
6.054	381.766	380.000	28.890	0.654D+04	73.822	2.79901

NO. OF RICOCHETS = 4
 AVE. DRAG COEFF. = 3.123498 AVE. DRAG DECAY CONST. = 1.730826E-03
 X(APPROX.) = 91.1522 Q= .6876818
 X(CORCTD.) = 107.9432 Q= 6.383077E-12
 FINAL VALUES.....X = 380 Y = 28.89038

200 VELOCITY # 1
 20 MASS # 1
 7.5 ANGLE # 2

LENGTH UNIT=FT MASS UNIT=LBS TIME UNIT=SEC ENERGY UNIT=FT-LBS

NUMBER OF (C,U) PAIRS IN THE DRAG COEFFICIENT TABLE = 6
 1.08 4 1.14 2 1.26 1.15 1.09 .9 .88 .75 .8 0

FRAGMENT STARTS AT (FT) X= 0 Y= 0
 TRAJECTORY LIMITS (FT) X9= 0 Y9= 0
 RADIUS OF CURVATURE (FT) R= 1
 INITIAL ANGLE (DEG) A0= 7.5 AMB. DENSITY (LBS/CUFT) D0= 7.647D-02
 INITIAL VELOCITY (FT/SEC) U0= 200 AMB. SOUND SPEED (FT/SEC) C0= 1116.45

FRAGMENT MASS (LBS) M= 20 GRAVITY (FT/SEC/SEC) G= 32.174
 SHAPE FACTOR B=0.4600 DRAG DECAY CONSTANT C=0.44330D-03
 FRAGMENT AREA (SQFT) A6= 0.437980 DRAG COEFFICIENT C1= .8
 CHARACTERISTIC LENGTH (FT) L= 0.661800 (DRAG IS INTERPOLATED)
 FRAG. DENSITY (LBS/CUFT) D= 150 STEP SIZE UP (DEG) I= .625

ENERGY UNIT (FT-LBS)

E5= 32.174

STEP SIZE DOWN (DEG) I2= .75

WRLJ I	PATH LENGTH (FT)	HORIZ. RANGE (FT)	HEIGHT (FT)	ENERGY (FT-LBS)	VELOCITY (FT/SEC)	TIME (SEC)
1.500	0.000	0.000	0.000	0.124D+05	200.000	0.00000
6.875	13.524	13.417	1.692	0.122D+05	197.881	0.06798
6.416	23.260	23.088	2.819	0.120D+05	196.381	0.11737
5.950	33.000	32.771	3.869	0.118D+05	194.902	0.16715
5.476	42.742	42.465	4.838	0.116D+05	193.445	0.21733
4.994	52.486	52.168	5.728	0.115D+05	192.010	0.26788
4.505	62.231	61.880	6.535	0.113D+05	190.596	0.31883
4.008	71.979	71.600	7.258	0.111D+05	189.206	0.37015
3.504	81.728	81.328	7.897	0.110D+05	187.838	0.42187
2.991	91.479	91.064	8.450	0.108D+05	186.493	0.47397
2.471	101.233	100.806	8.915	0.107D+05	185.171	0.52645
1.943	110.988	110.554	9.290	0.105D+05	183.873	0.57932
1.408	120.746	120.308	9.576	0.104D+05	182.599	0.63258
0.865	130.507	130.066	9.770	0.102D+05	181.349	0.68621
0.314	140.270	139.829	9.870	0.101D+05	180.124	0.74023
0.235	141.644	141.203	9.877	0.101D+05	179.953	0.74786
0.242	141.529	141.088	9.876	0.101D+05	179.968	0.74723
0.242	141.530	141.089	9.876	0.101D+05	179.968	0.74723
10.332	141.530	141.089	9.876	0.101D+05	159.963	0.74723
9.471	153.532	152.912	11.940	0.985D+04	158.242	0.82266
8.760	163.236	162.493	13.478	0.968D+04	156.884	0.88425
8.034	172.947	172.100	14.896	0.952D+04	155.557	0.94642
7.294	182.662	181.728	16.192	0.936D+04	154.261	1.00913
6.541	192.381	191.376	17.363	0.921D+04	152.997	1.07239
5.773	202.105	201.043	18.406	0.906D+04	151.767	1.13620
4.992	211.832	210.728	19.319	0.892D+04	150.569	1.20055
4.197	221.565	220.429	20.099	0.878D+04	149.407	1.26544
3.388	231.303	230.145	20.743	0.865D+04	148.279	1.33087
2.567	241.046	239.875	21.250	0.852D+04	147.188	1.39682
1.732	250.795	249.616	21.615	0.840D+04	146.133	1.46329
0.884	260.550	259.368	21.838	0.828D+04	145.116	1.53028
0.024	270.311	269.129	21.916	0.817D+04	144.137	1.59777
0.000	270.576	269.394	21.916	0.817D+04	144.110	1.59961
-1.364	285.790	284.606	21.736	0.801D+04	142.665	1.70571
-2.728	300.720	299.526	21.204	0.786D+04	141.341	1.81085
-2.935	302.960	301.763	21.093	0.784D+04	141.151	1.82671
-2.911	302.704	301.507	21.106	0.784D+04	141.173	1.82490
-2.912	302.708	301.511	21.106	0.784D+04	141.172	1.82492
12.469	302.708	301.511	21.106	0.784D+04	108.790	1.82492
11.430	309.469	308.125	22.506	0.771D+04	107.877	1.88733
9.916	319.085	317.574	24.287	0.753D+04	106.643	1.97699
8.357	328.718	327.084	25.817	0.737D+04	105.486	2.06781
6.755	338.368	336.649	27.087	0.722D+04	104.409	2.15976
5.113	348.039	346.268	28.087	0.709D+04	103.418	2.25283
3.432	357.732	355.933	28.810	0.696D+04	102.516	2.34697
1.716	367.449	365.638	29.247	0.685D+04	101.705	2.44213
0.000	377.010	375.197	29.391	0.676D+04	101.003	2.53646
-0.868	381.798	379.985	29.354	0.672D+04	100.687	2.58394
-0.871	381.813	380.000	29.354	0.672D+04	100.686	2.58409

NO. OF RICOCHETS = 2

AVE. DRAG COEFF. = 2.120243

AVE. DRAG DECAY CONST. = 1.174891E-03

X(APPROX.) = 135.421 Q= .6913177

X(CORCTD.) = 160.8871 Q= 1.777936E-08

FINAL VALUES.....X = 380 Y = 29.35426

200

VELOCITY # 1

20

MASS # 1

10

ANGLE # 3

LENGTH UNIT=FT MASS UNIT=LBS TIME UNIT=SEC ENERGY UNIT=FT-LBS

NUMBER OF (C,U) PAIRS IN THE DRAG COEFFICIENT TABLE = 6

1.08 4 1.14 2 1.26 1.15 1.09 .9 .88 .75 .8 0

FRAGMENT STARTS AT (FT) X= 0 Y= 0
 TRAJECTORY LIMITS (FT) X9= 0 Y9= 0
 RADIUS OF CURVATURE (FT) R= 1
 INITIAL ANGLE (DEG) A0= 10 AMB. DENSITY (LBS/CUFT) D0= 7.647D-02
 INITIAL VELOCITY (FT/SEC) U0= 200 AMB. SOUND SPEED (FT/SEC) C0= 1116.45

FRAGMENT MASS (LBS) M= 20 GRAVITY (FT/SEC/SEC) G= 32.174
 SHAPE FACTOR B=0.4600 DRAG DECAY CONSTANT C=0.44330D-03
 FRAGMENT AREA (SQFT) A6= 0.437980 DRAG COEFFICIENT C1= .8
 CHARACTERISTIC LENGTH (FT) L= 0.661800 (DRAG IS INTERPOLATED)
 FRAG. DENSITY (LBS/CUFT) D= 150 STEP SIZE UP (DEG) I= .625
 ENERGY UNIT (FT-LBS) E5= 32.174 STEP SIZE DOWN (DEG) I2= 1

TRAJ ANGLE (DEG)	PATH LENGTH (FT)	HORIZ. RANGE (FT)	HEIGHT (FT)	ENERGY (FT-LBS)	VELOCITY (FT/SEC)	TIME (SEC)
10.000	0.000	0.000	0.000	0.124D+05	200.000	0.00000
9.375	13.604	13.410	2.290	0.122D+05	197.774	0.06840
8.919	23.328	23.010	3.836	0.120D+05	196.208	0.11776
8.455	33.058	32.629	5.305	0.118D+05	194.663	0.16755
7.982	42.790	42.260	6.697	0.116D+05	193.138	0.21774
7.502	52.523	51.904	8.008	0.114D+05	191.636	0.26833
7.014	62.257	61.561	9.238	0.112D+05	190.155	0.31932
6.517	71.994	71.229	10.385	0.111D+05	188.697	0.37072
6.012	81.732	80.909	11.448	0.109D+05	187.261	0.42253
5.499	91.471	90.599	12.424	0.107D+05	185.849	0.47474
4.977	101.213	100.300	13.314	0.106D+05	184.459	0.52735
4.447	110.957	110.011	14.115	0.104D+05	183.093	0.58037
3.908	120.703	119.731	14.825	0.103D+05	181.751	0.63380
3.361	130.451	129.460	15.443	0.101D+05	180.433	0.68763
2.806	140.202	139.196	15.968	0.997D+04	179.139	0.74186
2.242	149.955	148.940	16.397	0.983D+04	177.871	0.79650
1.670	159.711	158.690	16.730	0.970D+04	176.627	0.85154
1.090	169.470	168.446	16.966	0.956D+04	175.410	0.90698
0.501	179.232	178.206	17.101	0.943D+04	174.218	0.96282
0.000	187.434	186.408	17.137	0.933D+04	173.237	1.01004
-1.000	203.538	202.511	16.998	0.913D+04	171.366	1.10350
-2.000	219.309	218.276	16.585	0.894D+04	169.606	1.19601
-2.871	232.790	231.745	16.013	0.879D+04	168.159	1.27583
-2.749	230.927	229.884	16.104	0.881D+04	168.356	1.26476
-2.756	231.032	229.989	16.099	0.881D+04	168.345	1.26538
12.364	231.032	229.990	16.099	0.881D+04	130.978	1.26538
11.591	238.326	237.125	17.613	0.867D+04	129.957	1.32129
10.546	247.984	246.602	19.468	0.850D+04	128.647	1.39598
9.475	257.652	256.123	21.149	0.833D+04	127.382	1.47150
8.378	267.328	265.681	22.650	0.817D+04	126.167	1.54783
7.257	277.013	275.276	23.968	0.802D+04	125.003	1.62495
6.111	286.708	284.904	25.097	0.788D+04	123.891	1.70285
4.940	296.413	294.564	26.032	0.775D+04	122.833	1.78153
3.747	306.129	304.251	26.768	0.762D+04	121.832	1.86095
2.531	315.857	313.964	27.301	0.750D+04	120.888	1.94111
1.294	325.598	323.699	27.627	0.739D+04	120.004	2.02198
0.037	335.352	333.451	27.740	0.729D+04	119.181	2.10354
0.000	335.635	333.734	27.740	0.729D+04	119.158	2.10591
-1.845	349.719	347.815	27.515	0.716D+04	118.084	2.22465
-3.691	363.582	361.660	26.846	0.705D+04	117.160	2.34250
-5.428	376.473	374.509	25.822	0.696D+04	116.420	2.45289
-5.070	373.830	371.877	26.064	0.698D+04	116.562	2.43020
-5.097	374.032	372.078	26.046	0.697D+04	116.551	2.43193
-5.098	374.035	372.082	26.046	0.697D+04	116.551	2.43196
14.530	374.035	372.082	26.046	0.697D+04	75.611	2.43196

13.622	376.922	374.881	26.748	0.689D+04	75.165	2.47025
10.581	386.283	384.031	28.712	0.665D+04	73.845	2.59589
11.944	382.142	379.970	27.903	0.675D+04	74.404	2.54003
11.934	382.173	380.000	27.909	0.675D+04	74.400	2.54044

NO. OF RICOCHETS = 2
 AVE. DRAG COEFF. = 3.11069 AVE. DRAG DECAY CONST. = 1.723728E-03
 X(APPROX.) = 157.1988 Q= .6930333
 X(CORCTD.) = 212.6061 Q= 3.415425E-06
 FINAL VALUES.....X = 380 Y = 27.9093

300 VELOCITY # 2
 20 MASS # 1
 5 ANGLE # 1

LENGTH UNIT-FT MASS UNIT-LBS TIME UNIT-SEC ENERGY UNIT-FT-LBS

NUMBER OF (C,U) PAIRS IN THE DRAG COEFFICIENT TABLE = 6
 1.08 4 1.14 2 1.26 1.15 1.09 .9 .88 .75 .8 0

FRAGMENT STARTS AT (FT) X= 0 Y= 0
 TRAJECTORY LIMITS (FT) X9= 0 Y9= 0
 RADIUS OF CURVATURE (FT) R= 1
 INITIAL ANGLE (DEG) A0= 5 AMB. DENSITY (LBS/CUFT) D0= 7.647D-02
 INITIAL VELOCITY (FT/SEC) U0= 300 AMB. SOUND SPEED (FT/SEC) C0= 1116.45

FRAGMENT MASS (LBS) M= 20 GRAVITY (FT/SEC/SEC) G= 32.174
 SHAPE FACTOR B=0.4600 DRAG DECAY CONSTANT C=0.44330D-03
 FRAGMENT AREA (SQFT) A6= 0.437980 DRAG COEFFICIENT C1= .8
 CHARACTERISTIC LENGTH (FT) L= 0.661600 (DRAG IS INTERPOLATED)
 FRAG. DENSITY (LBS/CUFT) D= 150 STEP SIZE UP (DEG) I= .4166667
 ENERGY UNIT (FT-LBS) E5= 32.174 STEP SIZE DOWN (DEG) I2= .5

TRAJ ANGLE (DEG)	PATH LENGTH (FT)	HORIZ. RANGE (FT)	HEIGHT (FT)	ENERGY (FT-LBS)	VELOCITY (FT/SEC)	TIME (SEC)
5.000	0.000	0.000	0.000	0.280D+05	300.000	0.00000
4.583	20.118	20.047	1.681	0.272D+05	295.661	0.06755
4.377	29.852	29.751	2.441	0.268D+05	293.589	0.10059
4.168	39.609	39.482	3.168	0.264D+05	291.530	0.13394
3.955	49.367	49.215	3.860	0.260D+05	289.489	0.16753
3.739	59.125	58.951	4.514	0.257D+05	287.465	0.20135
3.521	68.883	68.689	5.132	0.253D+05	285.459	0.23542
3.299	78.642	78.431	5.713	0.250D+05	283.470	0.26972
3.074	88.401	88.175	6.255	0.246D+05	281.499	0.30427
2.939	94.175	93.941	6.558	0.244D+05	280.342	0.32482
2.963	93.152	92.920	6.505	0.245D+05	280.546	0.32118
2.962	93.207	92.974	6.508	0.245D+05	280.535	0.32137
6.526	93.207	92.975	6.508	0.245D+05	262.629	0.32137
5.983	113.373	113.021	8.706	0.237D+05	258.726	0.39873
5.714	123.099	122.696	9.697	0.234D+05	256.871	0.43646
5.441	132.851	132.402	10.645	0.231D+05	255.029	0.47456
5.164	142.603	142.113	11.546	0.227D+05	253.204	0.51294
4.882	152.357	151.828	12.400	0.224D+05	251.397	0.55160
4.597	162.111	161.549	13.206	0.221D+05	249.608	0.59053
4.307	171.865	171.274	13.964	0.218D+05	247.836	0.62975
4.013	181.620	181.003	14.671	0.215D+05	246.082	0.66925
3.715	191.376	190.736	15.329	0.212D+05	244.347	0.70904
3.412	201.132	200.474	15.935	0.209D+05	242.629	0.74910
3.105	210.889	210.215	16.490	0.206D+05	240.929	0.78946
2.793	220.647	219.960	16.992	0.203D+05	239.247	0.83010
2.477	230.405	229.708	17.441	0.200D+05	237.584	0.87103
2.156	240.164	239.459	17.835	0.197D+05	235.939	0.91225
1.831	249.925	249.213	18.175	0.195D+05	234.312	0.95376

1.501	259.686	258.970	18.459	0.192D+05	232.703	0.99556
1.226	267.732	267.014	18.650	0.190D+05	231.391	1.03024
1.256	266.851	266.133	18.631	0.190D+05	231.534	1.02643
1.255	266.891	266.173	18.632	0.190D+05	231.528	1.02661
9.282	266.891	266.173	18.632	0.190D+05	211.240	1.02661
8.508	285.560	284.618	21.520	0.185D+05	208.109	1.11565
8.096	295.269	294.225	22.922	0.182D+05	206.510	1.16248
7.676	305.006	303.869	24.258	0.179D+05	204.926	1.20981
7.249	314.743	313.524	25.523	0.176D+05	203.363	1.25751
6.815	324.482	323.190	26.715	0.174D+05	201.820	1.30558
6.374	334.223	332.866	27.834	0.171D+05	200.297	1.35403
5.925	343.964	342.551	28.878	0.168D+05	198.796	1.40285
5.470	353.707	352.246	29.845	0.166D+05	197.315	1.45204
5.007	363.452	361.950	30.735	0.163D+05	195.856	1.50161
4.537	373.198	371.662	31.546	0.161D+05	194.419	1.55155
4.059	382.946	381.383	32.276	0.159D+05	193.003	1.60187
3.574	392.696	391.110	32.925	0.156D+05	191.610	1.65257
3.082	402.447	400.845	33.492	0.154D+05	190.239	1.70365
2.579	412.260	410.646	33.976	0.152D+05	188.882	1.75541
2.056	422.312	420.690	34.383	0.150D+05	187.517	1.80883
1.513	432.611	430.984	34.704	0.148D+05	186.144	1.86395
0.947	443.162	441.533	34.931	0.145D+05	184.765	1.92085
0.359	453.973	452.342	35.054	0.143D+05	183.381	1.97957
0.000	460.492	458.861	35.074	0.142D+05	182.561	2.01520
-1.312	483.836	482.202	34.809	0.138D+05	179.714	2.14408
-2.052	496.702	495.063	34.432	0.135D+05	178.207	2.21597
-1.922	494.460	492.822	34.510	0.136D+05	178.466	2.20340
-1.929	494.578	492.940	34.506	0.136D+05	178.452	2.20406
-1.929	494.579	492.941	34.506	0.136D+05	178.452	2.20407
11.842	494.579	492.941	34.506	0.136D+05	145.395	2.20407
10.855	505.992	504.130	36.752	0.133D+05	143.770	2.28300
9.771	518.204	516.144	38.939	0.130D+05	142.089	2.36845
8.630	530.713	528.492	40.940	0.127D+05	140.429	2.45700
7.429	543.531	541.183	42.731	0.124D+05	138.798	2.54881
6.167	556.668	554.226	44.286	0.121D+05	137.201	2.64400
4.839	570.133	567.628	45.579	0.118D+05	135.646	2.74270
3.444	583.937	581.396	46.576	0.115D+05	134.140	2.84504
1.979	598.094	595.536	47.247	0.113D+05	132.693	2.95115
0.443	612.616	610.053	47.555	0.111D+05	131.314	3.06116
0.000	616.749	614.186	47.571	0.110D+05	130.942	3.09268
-2.140	636.403	633.834	47.206	0.107D+05	129.293	3.24373
-4.280	655.626	653.022	46.132	0.105D+05	127.881	3.39322
-6.421	674.514	671.825	44.373	0.103D+05	126.691	3.54161
-8.561	693.160	690.309	41.944	0.101D+05	125.711	3.68936
-10.701	711.650	708.536	38.852	0.100D+05	124.930	3.83691
-12.841	730.069	726.564	35.096	0.992D+04	124.340	3.98469
-14.981	748.497	744.449	30.667	0.986D+04	123.933	4.13314
-17.122	767.015	762.242	25.547	0.982D+04	123.705	4.28270
-19.262	785.706	779.995	19.713	0.981D+04	123.653	4.43382
-18.802	781.671	776.181	21.029	0.981D+04	123.649	4.40119
-18.849	782.081	776.569	20.897	0.981D+04	123.649	4.40450
-18.850	782.091	776.579	20.893	0.981D+04	123.649	4.40459
-0.715	782.091	776.579	20.893	0.981D+04	85.405	4.40459
-2.968	790.967	785.448	20.609	0.972D+04	85.001	4.50875
-5.221	799.790	794.247	19.979	0.966D+04	84.733	4.61272
-7.474	808.603	803.005	19.005	0.963D+04	84.599	4.71682
-9.727	817.448	811.748	17.682	0.963D+04	84.596	4.82137
-11.980	826.366	820.505	16.003	0.966D+04	84.723	4.92670
-14.233	835.399	829.301	13.955	0.972D+04	84.982	5.03316
-16.486	844.593	838.165	11.520	0.980D+04	85.372	5.14110
-18.740	853.995	847.124	8.675	0.993D+04	85.896	5.25089
-20.195	860.202	852.975	6.606	0.100D+05	86.308	5.32298
-19.882	858.857	851.712	7.067	0.100D+05	86.215	5.30739
-19.901	858.939	851.789	7.039	0.100D+05	86.220	5.30834
-19.901	858.941	851.791	7.039	0.100D+05	86.220	5.30836
0.589	858.941	851.791	7.039	0.100D+05	53.923	5.30836
0.540	859.018	851.868	7.039	0.100D+05	53.920	5.30980
0.000	859.869	852.718	7.043	0.999D+04	53.886	5.32557
-2.155	863.257	856.106	6.980	0.996D+04	53.802	5.38850

-4.309	866.644	859.487	6.789	0.995D+04	53.793	5.45147
-6.464	870.045	862.872	6.470	0.998D+04	53.860	5.51465
-8.618	873.474	866.271	6.020	0.100D+05	54.004	5.57822
-10.773	876.945	869.692	5.435	0.101D+05	54.225	5.64237
-12.927	880.476	873.146	4.710	0.102D+05	54.525	5.70730
-15.082	884.081	876.644	3.837	0.104D+05	54.905	5.77319
-17.236	887.780	880.196	2.808	0.105D+05	55.369	5.84027
-19.391	891.591	883.813	1.610	0.108D+05	55.918	5.90877
-21.280	895.041	887.048	0.411	0.110D+05	56.474	5.97016
-20.868	894.280	886.338	0.685	0.109D+05	56.347	5.95667
-20.897	894.334	886.388	0.666	0.109D+05	56.356	5.95763
2.299	894.334	886.389	0.665	0.109D+05	31.366	5.95763
2.108	894.436	886.491	0.669	0.109D+05	31.360	5.96089
0.000	895.539	887.614	0.690	0.109D+05	31.315	5.99672
-1.200	896.197	888.252	0.683	0.109D+05	31.308	6.01710
-2.400	896.836	888.890	0.663	0.109D+05	31.316	6.03750
-3.600	897.476	889.529	0.630	0.109D+05	31.337	6.05792
-4.800	898.117	890.169	0.583	0.109D+05	31.371	6.07838
-6.001	898.762	890.810	0.522	0.110D+05	31.420	6.09891
-7.201	899.410	891.454	0.447	0.110D+05	31.482	6.11952
-8.401	900.063	892.101	0.359	0.111D+05	31.559	6.14023
-9.601	900.721	892.751	0.256	0.111D+05	31.650	6.16106
-10.801	901.386	893.405	0.138	0.112D+05	31.755	6.18203
-12.001	902.058	894.064	0.005	0.113D+05	31.875	6.20316
-12.045	902.083	894.088	-0.000	0.113D+05	31.880	6.20394

NO. OF RICOCHETS = 6
 AVE. DRAG COEFF. = 2.992448 AVE. DRAG DECAY CONST. = 1.658206E-03
 X(APPROX.) = 283.3488 Q = .6987873
 X(CORCTD.) = 485.7435 Q = 1.306406E-06
 FINAL VALUES.....X = 894.0885 Y = 0
 INITIAL ANGLE SENSITIVITY: dx/da = 95.53631
 INITIAL VELOCITY SENSITIVITY: dx/dU = 3.238276
 INITIAL HEIGHT SENSITIVITY: dx/dY = 11.42999
 CYLINDRICAL AREA INCREASE RATIO = 5473.827
 SPHERICAL AREA INCREASE RATIO = 4912781

300 VELOCITY # 2
 20 MASS # 1
 7.5 ANGLE # 2

LENGTH UNIT-FT MASS UNIT-LBS TIME UNIT-SEC ENERGY UNIT-FT-LBS

NUMBER OF (C,U) PAIRS IN THE DRAG COEFFICIENT TABLE = 6
 1.08 4 1.14 2 1.26 1.15 1.09 .9 .88 .75 .8 0

FRAGMENT STARTS AT (FT) X= 0 Y= 0
 TRAJECTORY LIMITS (FT) X9= 0 Y9= 0
 RADIUS OF CURVATURE (FT) R= 1
 INITIAL ANGLE (DEG) A0= 7.5 AMB. DENSITY (LBS/CUFT) D0= 7.647D-02
 INITIAL VELOCITY (FT/SEC) U0= 300 AMB. SOUND SPEED (FT/SEC) C0= 1116.45

FRAGMENT MASS (LBS) M= 20 GRAVITY (FT/SEC/SEC) G= 32.174
 SHAPE FACTOR B=0.4600 DRAG DECAY CONSTANT C=0.44330D-03
 FRAGMENT AREA (SQFT) A6= 0.437980 DRAG COEFFICIENT C1= .8
 CHARACTERISTIC LENGTH (FT) L= 0.661800 (DRAG IS INTERPOLATED)
 FRAG. DENSITY (LBS/CUFT) D= 150 STEP SIZE UP (DEG) I= .4166667
 ENERGY UNIT (FT-LBS) E5= 32.174 STEP SIZE DOWN (DEG) I2= .75

TRAJ ANGLE (DEG)	PATH LENGTH (FT)	HORIZ. RANGE (FT)	HEIGHT (FT)	ENERGY (FT-LBS)	VELOCITY (FT/SEC)	TIME (SEC)
7.500	0.000	0.000	0.000	0.280D+05	300.000	0.00000
7.083	20.203	20.040	2.565	0.271D+05	295.549	0.06785

6.878	29.930	29.694	3.747	0.268D+05	293.433	0.10088
6.669	39.683	39.379	4.897	0.264D+05	291.330	0.13423
6.457	49.436	49.068	6.012	0.260D+05	289.244	0.16783
6.242	59.189	58.761	7.091	0.256D+05	287.175	0.20167
6.024	68.942	68.459	8.133	0.253D+05	285.125	0.23576
5.802	78.696	78.161	9.138	0.249D+05	283.091	0.27009
5.577	88.450	87.867	10.105	0.246D+05	281.076	0.30467
5.349	98.205	97.577	11.034	0.242D+05	279.078	0.33949
5.118	107.959	107.291	11.924	0.239D+05	277.097	0.37457
4.883	117.714	117.009	12.774	0.235D+05	275.134	0.40990
4.644	127.470	126.730	13.584	0.232D+05	273.188	0.44548
4.402	137.226	136.456	14.354	0.229D+05	271.261	0.48132
4.157	146.982	146.185	15.082	0.225D+05	269.350	0.51742
3.908	156.739	155.917	15.768	0.222D+05	267.457	0.55377
3.655	166.496	165.653	16.411	0.219D+05	265.582	0.59038
3.399	176.253	175.392	17.012	0.216D+05	263.724	0.62725
3.139	186.012	185.135	17.568	0.213D+05	261.884	0.66438
2.875	195.770	194.880	18.080	0.210D+05	260.062	0.70177
2.607	205.529	204.628	18.547	0.207D+05	258.257	0.73943
2.336	215.289	214.379	18.968	0.204D+05	256.470	0.77735
2.061	225.050	224.132	19.342	0.202D+05	254.701	0.81554
1.782	234.811	233.887	19.670	0.199D+05	252.949	0.85399
1.499	244.572	243.645	19.949	0.196D+05	251.216	0.89272
1.212	254.335	253.404	20.180	0.193D+05	249.500	0.93171
0.920	264.098	263.166	20.362	0.191D+05	247.802	0.97097
0.625	273.861	272.929	20.494	0.188D+05	246.122	1.01051
0.326	283.626	282.693	20.575	0.186D+05	244.459	1.05032
0.023	293.391	292.458	20.605	0.183D+05	242.815	1.09040
0.000	294.125	293.191	20.605	0.183D+05	242.692	1.09342
-0.037	295.290	294.357	20.604	0.183D+05	242.498	1.09822
-0.036	295.282	294.349	20.604	0.183D+05	242.499	1.09819
10.568	295.282	294.349	20.604	0.183D+05	213.678	1.09819
9.981	309.885	308.718	23.209	0.178D+05	211.152	1.16694
9.581	319.608	318.299	24.861	0.176D+05	209.495	1.21317
9.175	329.341	327.901	26.447	0.173D+05	207.856	1.25981
8.761	339.074	337.515	27.965	0.170D+05	206.237	1.30682
8.341	348.808	347.141	29.412	0.168D+05	204.638	1.35420
7.913	358.543	356.779	30.789	0.165D+05	203.059	1.40196
7.479	368.279	366.427	32.093	0.163D+05	201.500	1.45009
7.037	378.017	376.087	33.323	0.160D+05	199.962	1.49860
6.588	387.756	385.757	34.478	0.158D+05	198.445	1.54749
6.131	397.496	395.437	35.557	0.155D+05	196.949	1.59676
5.667	407.238	405.127	36.559	0.153D+05	195.475	1.64641
5.187	417.156	415.001	37.497	0.151D+05	193.996	1.69734
4.687	427.316	425.123	38.371	0.148D+05	192.504	1.74991
4.167	437.724	435.500	39.175	0.146D+05	191.002	1.80419
3.625	448.386	446.137	39.900	0.144D+05	189.490	1.86023
3.061	459.309	457.041	40.537	0.141D+05	187.969	1.91811
2.473	470.498	468.217	41.077	0.139D+05	186.442	1.97788
1.860	481.961	479.672	41.511	0.137D+05	184.909	2.03962
1.222	493.706	491.412	41.827	0.135D+05	183.373	2.10339
0.557	505.738	503.442	42.014	0.132D+05	181.836	2.16929
0.000	515.660	513.364	42.062	0.131D+05	180.597	2.22404
-1.429	540.519	538.219	41.755	0.126D+05	177.606	2.36284
-2.858	564.604	562.286	40.857	0.122D+05	174.867	2.49950
-4.286	588.007	585.641	39.401	0.119D+05	172.359	2.63430
-5.715	610.809	608.355	37.415	0.116D+05	170.064	2.76748
-7.144	633.086	630.491	34.923	0.113D+05	167.966	2.89929
-7.099	632.394	629.804	35.008	0.113D+05	168.029	2.89517
-7.103	632.463	629.872	35.000	0.113D+05	168.022	2.89558
8.596	632.463	629.872	35.000	0.113D+05	127.939	2.89558
8.119	636.731	634.095	35.620	0.112D+05	127.412	2.92901
6.378	651.960	649.200	37.543	0.109D+05	125.613	3.04938
4.528	667.651	664.818	39.036	0.106D+05	123.898	3.17515
2.572	683.755	680.889	40.035	0.103D+05	122.290	3.30598
0.509	700.293	697.418	40.481	0.101D+05	120.806	3.44205
0.000	704.310	701.435	40.499	0.100D+05	120.472	3.47534
-2.202	721.459	718.578	40.171	0.980D+04	119.164	3.61847
-4.404	738.291	735.379	39.203	0.963D+04	118.071	3.76037

-6.606	754.892	751.900	37.612	0.948D+04	117.180	3.90150
-8.809	771.343	768.200	35.407	0.937D+04	116.483	4.04231
-11.011	787.721	784.331	32.590	0.929D+04	115.970	4.18323
-13.213	804.103	800.345	29.153	0.923D+04	115.637	4.32469
-15.415	820.563	816.291	25.085	0.921D+04	115.479	4.46713
-17.617	837.178	832.217	20.362	0.921D+04	115.492	4.61100
-19.819	854.025	848.171	14.956	0.924D+04	115.675	4.75676
-22.021	871.187	864.198	8.829	0.929D+04	116.027	4.90490
-24.224	888.750	880.347	1.933	0.938D+04	116.549	5.05593
-24.310	889.449	880.984	1.646	0.938D+04	116.573	5.06192
-24.302	889.386	880.927	1.671	0.938D+04	116.571	5.06139
13.388	889.386	880.927	1.671	0.938D+04	31.476	5.06139
12.644	889.795	881.326	1.763	0.932D+04	31.373	5.07440
0.000	896.355	887.804	2.492	0.880D+04	30.478	5.28650
-2.249	897.488	888.937	2.469	0.880D+04	30.478	5.32368
-4.497	898.624	890.072	2.403	0.882D+04	30.525	5.36094
-6.746	899.770	891.211	2.290	0.888D+04	30.620	5.39841
-8.995	900.930	892.360	2.132	0.896D+04	30.762	5.43620
-11.243	902.109	893.521	1.924	0.907D+04	30.954	5.47443
-13.492	903.315	894.698	1.666	0.922D+04	31.196	5.51322
-15.741	904.553	895.896	1.353	0.939D+04	31.491	5.55273
-17.989	905.831	897.119	0.983	0.960D+04	31.841	5.59308
-20.238	907.156	898.371	0.549	0.985D+04	32.248	5.63445
-22.487	908.538	899.657	0.045	0.101D+05	32.717	5.67698
-22.674	908.656	899.766	-0.000	0.102D+05	32.758	5.68059

NO. OF RICOCHETS = 3
 AVE. DRAG COEFF. = 3.005248 AVE. DRAG DECAY CONST. = 1.665299E-03
 X(APPROX.) = 357.5755 Q = .7034488
 X(CORCTD.) = 722.2651 Q = 1.30211E-03
 FINAL VALUES....X = 899.7661 Y = 0
 INITIAL ANGLE SENSITIVITY: $dx/da = 93.3437$
 INITIAL VELOCITY SENSITIVITY: $dx/dv = 4.797993$
 INITIAL HEIGHT SENSITIVITY: $dx/dy = 7.550715$
 CYLINDRICAL AREA INCREASE RATIO = 5348.2
 SPHERICAL AREA INCREASE RATIO = 4853653

300 VELOCITY # 2
 20 MASS # 1
 10 ANGLE # 3

LENGTH UNIT=FT MASS UNIT=LBS TIME UNIT=SEC ENERGY UNIT=FT-LBS

NUMBER OF (C,U) PAIRS IN THE DRAG COEFFICIENT TABLE = 6
 1.08 4 1.14 2 1.26 1.15 1.09 .9 .88 .75 .8 0

FRAGMENT STARTS AT (FT) X= 0 Y= 0
 TRAJECTORY LIMITS (FT) X9= 0 Y9= 0
 RADIUS OF CURVATURE (FT) R= 1
 INITIAL ANGLE (DEG) A0= 10 AMB. DENSITY (LBS/CUFT) D0= 7.647D-02
 INITIAL VELOCITY (FT/SEC) U0= 300 AMB. SOUND SPEED (FT/SEC) C0= 1116 45

FRAGMENT MASS (LBS) M= 20 GRAVITY (FT/SEC/SEC) G= 32.174
 SHAPE FACTOR B=0.4600 DRAG DECAY CONSTANT C=0.44330D-03
 FRAGMENT AREA (SQFT) A6= 0.437980 DRAG COEFFICIENT C1= .8
 CHARACTERISTIC LENGTH (FT) L= 0.661800 (DRAG IS INTERPOLATED)
 FRAG. DENSITY (LBS/CUFT) D= 150 STEP SIZE UP (DEG) I= .4166667
 ENERGY UNIT (FT-LBS) E5= 32.174 STEP SIZE DOWN (DEG) I2= 1

TRAJ ANGLE (DEG)	PATH LENGTH (FT)	HORIZ. RANGE (FT)	HEIGHT (FT)	ENERGY (FT-LBS)	VELOCITY (FT/SEC)	TIME (SEC)
10.000	0.000	0.000	0.000	0.280D+05	300.000	0.00000
9.583	20.328	20.031	3.458	0.271D+05	295.427	0.06828

9.379	30.047	29.618	5.059	0.267D+05	293.269	0.10130
9.172	39.238	39.238	6.630	0.263D+05	291.121	0.13466
8.961	49.543	48.865	8.166	0.260D+05	289.990	0.16827
8.747	59.292	58.497	9.667	0.256D+05	286.878	0.20213
8.529	69.040	68.135	11.131	0.252D+05	284.782	0.23623
8.308	78.789	77.779	12.558	0.248D+05	282.705	0.27059
8.084	88.538	87.428	13.948	0.245D+05	280.644	0.30520
7.856	98.288	97.084	15.300	0.241D+05	278.602	0.34007
7.625	108.037	106.744	16.613	0.238D+05	276.576	0.37519
7.391	117.787	116.411	17.887	0.234D+05	274.568	0.41057
7.152	127.537	126.082	19.121	0.231D+05	272.578	0.44621
6.911	137.288	135.759	20.315	0.228D+05	270.605	0.48211
6.665	147.039	145.442	21.468	0.224D+05	268.649	0.51828
6.416	156.790	155.129	22.578	0.221D+05	266.711	0.55470
6.163	166.541	164.822	23.647	0.218D+05	264.791	0.59140
5.906	176.293	174.520	24.672	0.215D+05	262.888	0.62836
5.645	186.045	184.223	25.653	0.212D+05	261.002	0.66559
5.381	195.798	193.931	26.590	0.209D+05	259.135	0.70309
5.112	205.551	203.643	27.482	0.206D+05	257.284	0.74086
4.840	215.305	213.360	28.328	0.203D+05	255.452	0.77891
4.563	225.059	223.081	29.128	0.200D+05	253.637	0.81723
4.282	234.814	232.807	29.880	0.197D+05	251.840	0.85583
3.997	244.570	242.537	30.584	0.194D+05	250.060	0.89470
3.708	254.325	252.271	31.240	0.192D+05	248.298	0.93385
3.415	264.082	262.008	31.846	0.189D+05	246.555	0.97328
3.118	273.839	271.750	32.402	0.186D+05	244.829	1.01300
2.816	283.597	281.494	32.908	0.184D+05	243.121	1.05299
2.510	293.356	291.242	33.361	0.181D+05	241.431	1.09327
2.199	303.115	300.993	33.762	0.179D+05	239.759	1.13383
1.884	312.875	310.747	34.110	0.176D+05	238.105	1.17468
1.565	322.636	320.504	34.404	0.174D+05	236.470	1.21582
1.241	332.398	330.263	34.643	0.171D+05	234.853	1.25724
0.912	342.161	340.024	34.826	0.169D+05	233.254	1.29895
0.579	351.925	349.787	34.954	0.167D+05	231.674	1.34096
0.242	361.689	359.551	35.024	0.165D+05	230.112	1.38325
0.000	368.599	366.461	35.038	0.163D+05	229.018	1.41335
-1.000	396.513	394.372	34.797	0.157D+05	224.695	1.53639
-2.000	423.417	421.267	34.095	0.151D+05	220.676	1.65721
-3.000	449.409	447.233	32.963	0.146D+05	216.933	1.77600
-3.571	463.882	461.682	32.134	0.144D+05	214.909	1.84303
-3.514	462.435	460.237	32.223	0.144D+05	215.110	1.83630
-3.516	462.486	460.288	32.220	0.144D+05	215.103	1.83653
12.914	462.486	460.288	32.220	0.144D+05	159.220	1.83653
12.376	470.015	467.634	33.868	0.142D+05	158.071	1.88399
11.547	481.373	478.746	36.223	0.136D+05	156.370	1.95624
10.677	493.011	490.165	38.466	0.136D+05	154.671	2.03107
9.763	504.931	501.896	40.582	0.133D+05	152.978	2.10856
8.803	517.142	513.946	42.552	0.130D+05	151.294	2.18882
7.795	529.651	526.323	44.358	0.127D+05	149.624	2.27196
6.736	542.467	539.036	45.980	0.124D+05	147.974	2.35809
5.625	555.599	552.092	47.394	0.121D+05	146.347	2.44733
4.458	569.058	565.497	48.578	0.119D+05	144.751	2.53980
3.234	582.852	579.260	49.504	0.116D+05	143.191	2.63561
1.950	596.994	593.386	50.144	0.114D+05	141.674	2.73490
0.605	611.494	607.881	50.468	0.112D+05	140.208	2.83778
0.000	617.915	614.303	50.502	0.111D+05	139.588	2.88368
-2.042	639.205	635.586	50.125	0.108D+05	137.666	3.03725
-4.085	659.973	656.320	49.018	0.105D+05	135.993	3.18903
-6.127	680.322	676.586	47.209	0.103D+05	134.550	3.33947
-8.169	700.349	696.454	44.719	0.101D+05	133.323	3.48899
-10.212	720.142	715.990	41.560	0.993D+04	132.300	3.63802
-12.254	739.785	735.254	37.735	0.981D+04	131.471	3.78696
-14.297	759.361	754.305	33.241	0.971D+04	130.828	3.93623
-16.339	778.950	773.194	28.068	0.964D+04	130.363	4.08622
-18.381	798.629	791.975	22.197	0.960D+04	130.071	4.23735
-20.424	818.480	810.695	15.604	0.958D+04	129.947	4.39004
-21.070	824.812	816.617	13.360	0.958D+04	129.943	4.43877
-20.982	823.945	815.807	13.672	0.958D+04	129.943	4.43210
-20.984	823.970	815.830	13.663	0.958D+04	129.943	4.43228

2.475	823.970	815.830	13.663	0.958D+04	71.500	4.43228
2.372	824.256	816.116	13.675	0.957D+04	71.481	4.43629
0.000	830.794	822.652	13.811	0.947D+04	71.105	4.52800
-2.265	836.986	828.841	13.689	0.941D+04	70.863	4.61523
-4.530	843.155	834.998	13.323	0.937D+04	70.735	4.70236
-6.796	849.331	841.142	12.714	0.937D+04	70.717	4.78968
-9.061	855.542	847.293	11.857	0.939D+04	70.810	4.87746
-11.326	861.819	853.469	10.746	0.945D+04	71.013	4.96597
-13.591	868.192	859.691	9.371	0.953D+04	71.328	5.05552
-15.857	874.694	865.978	7.719	0.965D+04	71.758	5.14640
-18.122	881.359	872.351	5.771	0.979D+04	72.303	5.23894
-20.387	888.225	878.832	3.507	0.998D+04	72.970	5.33347
-22.652	895.334	885.443	0.899	0.102D+05	73.761	5.43036
-22.748	895.642	885.728	0.780	0.102D+05	73.798	5.43453
-22.739	895.610	885.699	0.792	0.102D+05	73.794	5.43410
7.114	895.610	885.699	0.792	0.102D+05	30.363	5.43410
6.817	895.760	885.847	0.810	0.102D+05	30.341	5.43902
0.000	899.132	889.207	1.012	0.100D+05	30.058	5.55070
-1.499	899.867	889.942	1.002	0.100D+05	30.054	5.57515
-2.999	900.603	890.677	0.973	0.100D+05	30.070	5.59962
-4.498	901.341	891.413	0.925	0.100D+05	30.106	5.62414
-5.998	902.082	892.152	0.857	0.101D+05	30.164	5.64875
-7.497	902.829	892.894	0.769	0.101D+05	30.242	5.67349
-8.997	903.583	893.640	0.661	0.102D+05	30.342	5.69838
-10.496	904.346	894.392	0.532	0.103D+05	30.463	5.72347
-11.995	905.119	895.150	0.381	0.104D+05	30.606	5.74879
-13.495	905.905	895.916	0.208	0.105D+05	30.771	5.77438
-14.994	906.704	896.690	0.011	0.106D+05	30.960	5.80028
-15.074	906.747	896.732	-0.000	0.106D+05	30.970	5.80167

NO. OF RICOCHETS = 3

AVE. DRAG COEFF. = 3.016831

AVE. DRAG DECAY CONST. = 1.671718E-03

X(APPROX.) = 413.1463 Q= .705964

X(CORCTD.) = 875.3461 Q= 3.902553E-02

FINAL VALUES.....X = 896.7319 Y = 0

INITIAL ANGLE SENSITIVITY: $dx/da = 76.37755$

INITIAL VELOCITY SENSITIVITY: $dx/dv = 5.330046$

INITIAL HEIGHT SENSITIVITY: $dx/dy = 4.739301$

CYLINDRICAL AREA INCREASE RATIO = 4376.111

SPHERICAL AREA INCREASE RATIO = 3984736

DATA MANAGEMENT

JOHN THOMPSON

28-30 August 1990

Presented to:

**Department of Defense
Explosive Safety Board Seminar
St. Louis, MO**

Good Morning ladies and gentleman, my name is John Thompson and this is Don Fraga we are representing RJO Enterprises based in Lanham, Maryland with offices throughout the United States and in England. RJO has a staff of more than 650 engineers, technicians and other professionals providing life cycle services in the areas of logistics, communications, information systems, command and control, and security. We are here today to discuss Data Management throughout the life cycle of material in the stockpile. Equipment and uses presented here will be primarily directed at ammunition/explosive/hazardous waste but would be equally effective in management of tanks or clothing, or any other commodity.

We will touch on possible approaches to data management and communication, and explain the operating characteristics of some equipment. We are confident that there is equipment available which satisfies current safety and security requirements for use in the various logistics and administrative areas involved, from manufacture to use or disposal.

CHART 1

The subjects shown on this chart will be presented during this session.

CHART 2

This chart is a listing of off-the-shelf, non-developmental items (NDI) of equipment presently available. The manufacturer of each item is shown in parenthesis. This list is representational only, there is a wide variety of manufacturers and components. There is equipment which is totally safe, secure, and compatible with hardware/software currently in use. Technical data for items proposed for use would be researched to insure compliance with all applicable regulations or codes, as well as compatibility with existing equipment and capability to perform all desired functions.

Portable Transceiver Work Stations (PTWS) and Intelligent Traveler (IT) (PROXIM)

Time and Attendance System (ACCU-SORT SYSTEMS)

Radio Frequency Tags (RFT) and Transponders (LOCKHEED)

Laser-Wand RF/Micro-Wand (HAND HELD PRODUCTS)

Smart Cards (Schlumberger, GEC, GPT Canada, OKIDATA)

Super Smart Cards (OKIDATA)

Bar Tag and Readers, fixed or hand held (AMSKAN)

Gridpad (Grid Systems)

Bar Code Labels - Can be printed on or off site using a variety of printers, can be of active or passive types, and can be scanned with contact or non-contact wands.

As an additional matter of interest, Microchips are on the market with physical measurements of 2 1/4" x 4 1/4" x 3/4", weighing from 1 to 3 oz. and operating on 5 - 7.5 volts with 100mw to 1w output, in the 902 - 928 MHZ range with battery life up to 1 year and a range of 10 ft. to 1/4 mile. These chips have a capacity to 32k RAM.

We have some technical data on Bar Tag system and Hand Held Products wands which we will furnish as handouts to anyone interested.

CHART 4

This chart illustrates typical communication links which can be established using equipment currently available.

Speaking clockwise, starting with "Field Input", "Field" could be a soldier in training, in-transit, or on the battlefield, or civilian personnel performing duties in support of the military. "Technicians" can be military or civilian, and located at a plant, in a depot, ASP, or ATP performing routine or special functions. "Managers" at all levels can be provided with real time data on a routine or special basis. The "Master Data File" for our purposes in this discussion represents a national inventory control point/national maintenance point, which can be accessed from any point in the system, can perform functions as programmed, and provide any station with output based on data provided. In this illustration "Host Computer" represents equipment at a depot or other major installation in the United States, or in a Communications Zone, or at a major headquarters in an overseas theater. For our purposes a "Remote Work Station" might be established at a location away from normal operations to accomplish a specific function while maintaining communication with one or more stations, to receive/transmit/relay technical or administrative data or instructions.

CHART 6

On the previous chart we looked at some communication links which can be established - on a worldwide basis if desired. On this chart we address briefly a few points in material life cycle. Using various communication techniques real time data can be transmitted from any point in the process to any desired "address".

Using tools on this chart data can be initiated by a person in the field or in a plant environment. It is even possible to enter hand written information which can be converted to computer language, and transmitted to any point in the world. A system can use LAN, hard wire, modems, antennae, various other equipment, or even satellites to move data efficiently and quickly between any desired addresses.

The following charts will provide information on equipment which can be used to perform various functions.

CHART 7

This chart presents some phases in the life cycle of material in the stockpile. Data Management can commence with the manufacture of material and be valid, real-time, until use, sale to a customer (and beyond if desired), or disposal (and beyond if desired, e.g.; hazardous waste). The next several charts will identify and explain typical equipment which may be used to accomplish real-time data management. This equipment is immediately available and compatible with most current hardware and software in service today. The components shown may not satisfy your requirements. In that case when specific needs are determined there is NDI that will accomplish the task.

CHART 9

At point of manufacture of closely managed items, a "Tool" could be affixed to each item. For instance an intelligent traveler which is a full featured RF tag with 32Kb memory (expandable), programmable in the field, with a read/write range up to 100 ft., could be programmed with the appropriate information. Through software linkage data could be transmitted to any desired terminal. This "Tool" could provide inventory information, provide security control measures, or satisfy other management requirements. If appropriate, basic log book information could be initiated at this time. The Portable Transceiver Work Station (PTWS), used with Intelligent Travelers is mobile, handheld, wireless, and has PC and transmission capabilities. PTWS operates on frequency of 915 MHZ, powered by six "C" cell NI-CAD batteries with an operative life of eight hours between charges. IT also operates on 915 MHZ and is powered by three AA alkaline cells and one "C" cell lithium battery.

Control of less expensive/less complex items can be accomplished by use of smart cards. Smart and Super-Smart cards are of plastic, with a microchip embedded. They are available in a wide variety of models, with different levels of sophistication. These cards can generally be programmed, and some models re-programmed in the field. The microchips allow for more versatility and are more powerful than barcodes. Storage capacity ranges from 256 bits to many thousands of bits. Smart cards are generally passive and do not generate any power output. However, a new generation contains a complete computer on the microchip, these operate at ranges from less than 5 MHZ to 12 MHZ. Super-Smart cards can perform full function data input/output and processing without requiring connection to a host computer. This card operates on a 1.5 VDC solar cell. Terminals used with these cards are portable, battery operated. These cards could be affixed to individual items, to individual boxes, pallets, or vehicle loads depending on the item and the shipping destination. Data loaded on tags or cards can serve as an inventory tool, as log book information, for security purposes, or other applications as desired.

CHART 10

Material in storage may have one of the indicated tools attached to individual items, crates, pallets or other containers of hazardous or non-hazardous material. Use of an automated system will make cyclic inventory easier, quicker, less manpower intensive and more accurate. Currently used inventory tags or magazine data cards can be replaced with microchip technology. Periodic or transfer inventories can be accomplished using a Gridpad or PTWS to perform field functions with a PC link to the host computer. Gridpad is a lightweight computer for use in the field, while standing or walking, is the size of a clipboard and accepts hand printed data/diagrams or written entry such as signatures. This hand written information is converted to computer language for download to PC's or host computers. Gridpad can operate with an internal rechargeable NI-CAD battery pack of 10 AA batteries with operating life of five hours between charges, or an external power source of 110/240 Vac can be used. Security features can be programmed into these systems to control both entry and communication. Networking of a combination of this equipment with any compatible hardware/software is completely feasible.

CHART 11

At time of assembly or maintenance individual components may lose their separate identity and become part of an end item. At some future point re-identification as a separate item (maint/upgrade) may occur. Equipment shown can initiate/maintain log book data, recording component information, maintenance performed, equipment use, ownership transfers and any other required data.

Inventory features can be programmed into the equipment to meet current requirements, and secure communications can be established by using appropriate compatible hardware/software. Quality assurance has not been specifically addressed, but could be readily incorporated throughout the life cycle, from manufacture to sale/use/disposal. PTWS and IT have been used to provide a paperless QA program at Red River Army Depot, Texas. That system is used to track maintenance/assembly. Condition and status of component/finished product can be monitored continuously.

CHART 12

There are several methods of disposal, we show three options on this chart for discussion purposes. Option 1 is disposal of a product as a complete item: excess, scrap, etc. Option 2, is disposal by disassembly into component parts with retention of some components, or separate item disposal through sale, re-use, etc. Option 3 is disposal by demolition or total destruction.

Disposal by options 1 or 3 can end the life cycle and all records may be closed. If option 2 is used, and selected components are retained, the inventory/ security/QA data can be re-established and perpetuated by down loading from the major item record, using equipment previously discussed.

CHART 13

During transportation any of the items on this chart can be affixed to a vehicle, or rail car or container. These items can be programmed to show movement information including: manifest/bill of lading; date and time of movement; special characteristics of the load; operators name; expected time of arrival; security information; special information for commodity oriented or management purposes; and any other detailed requirements.

CHART 14

To develop the transportation phase briefly, these are some of the actions put in motion when a depot or plant receives a requisition to ship ammunition or explosives. Non-hazardous items require similar actions, generally not as extensive but with the same management principles involved. And in all instances rapid communication with the national inventory control point is critical.

Chart 14.1

The actions listed on the previous chart "trigger" some or all of the forms listed on this chart, and probably some not shown. These forms relate to actions accomplished by the shipper; in-transit, or those forms which accompany a shipment; and receiver. Some of these forms are currently automated, and all could be generated/updated by data processing equipment now in the field. From planners, to material handlers, to the transport vehicle, to the receiver, all actions and resulting changes to data can be transmitted real-time to any manager involved in the procedure.

Chart 14.2

Maintaining real-time data on material issued to using units has, historically, been difficult. We show on this chart a very much simplified system of data collection for ammunition/explosives at Ammunition Transfer Points (ATP) and at unit level following pickup from an ATP.

Shipments from Corps Support Area (CSA) to Division Ammunition storage sites could be tracked using equipment we previously discussed for transportation application. While in storage at Division Ammunition Supply Points (ASP) inventory/condition status can be maintained using equipment similar to that used at storage depots. One of the items shown on this chart can be placed on transport vehicles used from ASP to ATP. Appropriate "readers" can be used at ATP site to adjust quantities as issues are made to using units, or as turn-ins are received. In all probability an ATP will remain in one location for only a short period of time so data can be transmitted to Division Rear or Corps Rear areas using a laptop, or other small, Standard Army Ammunition System (SAAS) compatible computer, via a modem to a tactical radio. The radio can be used for two-way secure communication assuring that rear area records are current, and that ATP personnel can be aware of developments immediately. Information received at Division or Corps areas can then be integrated into SAAS via the level of the system in use at the receiving point. Equipment used in this application is rugged, user friendly, secure, safe, and can be operated by the soldier who may lack "computer literacy" with minimal orientation.

CHART 15

Some data management applications are shown on the following charts. These seven representative areas will be briefly addressed.

All hardware we have discussed has auxiliary equipment to accomplish "Reading" or "Tracking", and can be networked from any point in the system to any other desired site or sites, regardless of the basic application.

CHART 16

Inventory data can be Real-Time from entry into the stockpile, through all phases and operations, and can be maintained in an up-to-date status throughout the life cycle.

CHART 17

Total Quality Management can be enhanced in all quality assurance/surveillance functions. This will provide for greater flexibility and assure more rapid action/reaction in all areas of responsibility.

CHART 18

In the area of Security/Safety, individuals can be furnished credit card sized identification which can be read by either indirect or direct contact with a Reader. Information on these cards can be transmitted to any designated security control point for immediate processing. A photograph can be included if visual verification of the individual possessing the identification card is required. This will provide constant real time knowledge of individuals in a given area. In the event of any emergency management would immediately know not only the number and location of personnel involved, but would also be aware of expertise on site to participate in response/rescue efforts. This function can be expanded to include recording time spent in a controlled area, for use in computing salary/wages where premiums are paid for work in these areas. Entry time - movement within - and departure, can be recorded for those areas where limitations/controls have been established. This improves safety of workers, and the data can be used as evidence in event of litigation.

Some applications in the area of Record Maintenance are as shown on this chart.

Additional applications are practically without limit, systems can be designed to meet customer stated needs. Some specifics in the production planning and budget estimating field will be discussed in the summary of this briefing.

CHART 19

Hazardous waste is constantly receiving increased attention. An economical, efficient system for tracking this material from point of generation through the packaging and transportation phase, to final storage destination, or final disposal site would assure better management of such waste, as well as compliance with government regulations. RJO recently presented a conceptual briefing in this area to DOE representatives at Oak Ridge, Tennessee. This briefing included management techniques to be applied in the field of hazardous material management from source through shipping, in-transit, receiving, and storage phases.

CHART 20

As discussed earlier it is possible to initiate log book data at the point of manufacture of component parts, or at assembly of a major item.

If desirable bar code labels can be incorporated in the system to meet specific needs. Labels can be printed at time of log book initiation or at any point in the cycle. There are many bar code readers on the market, some of the most modern are produced by Hand Held Products. Their hand-held wands are small; rugged; easy to program; IBM or similar compatible; with 128K storage, expandable to 512K; have a built-in intelligent RF modem with 32K RAM buffer; transmit at a rate of 3200 bps at a range of up to one mile line-of-sight; and address up to 255 units. Hand Held produces two primary types, micro-wand which is a contact reader, and laser-wand which is non-contact.

Log book pages containing location/owner data can be initiated at assembly and updated/changed at time of shipment or receipt, or inspection/maintenance/modernization, to assure information is current. Any recording of use, e.g. miles or hours, or repair costs, can be accomplished with the operator or other designated individual making the entry direct, using computer related equipment. An alternative would be for the operator to complete a hard copy form, and at a central point all data could be entered for specified equipment, using either key punch or scanner entry.

CHART 21

Some advantages to be realized from the use of equipment/systems discussed are listed on the next two charts. One big advantage is that training in the use of equipment is not extensive. Training provided by RJO would begin as early as necessary and continue until operators reach a satisfactory level.

Through use of currently available NDI National Inventory Control Points, National Maintenance Points, or headquarters can be linked to any desired site for transmission of any specified communication. This will allow for greater flexibility, provide real time data, and result in more effective management with a reduction in manhours, which will produce quick payback on any investment.

CHART 23/24

Various NDI and applications have been discussed throughout this briefing. With reference to real-time recording we would like to reiterate that all managers can have instantaneous access to all data. Properly used, this will allow for more effective: budgeting; predicting manufacturing cycles for both component material and finished products; and planning and programming of future cycles in the processes. An additional benefit might be reduction in inventories. There are exceptions to the reduced inventory, when certain levels of spare/repair parts, or basic load of certain military stocks must be retained. However as experience is gained through data generation and collection, it is reasonable to conclude that these levels could be realistically reduced, or more appropriately redistributed, resulting in savings not only in inventory but in transportation costs. The Navy has initiated a Rapid Acquisition of Manufactured Parts (RAMP) program as a more cost-effective solution to a need for guaranteed availability of spare parts. Developers of RAMP are to build flexible manufacturing systems with commercially available off-the-shelf products (NDI) to the extent possible. One objective of RAMP is to reduce the current 300 day spare part lead time to 30 days.

CHART 25

In summary, there is non-developmental equipment available to automate data generated throughout the total life cycle of any commodity. This can extend to the battle field where equipment or material can be traced and managed to the point of use/destruction/return to a non-combat area. As a result of rapidly increasing efficiencies in the industry costs are declining steadily, providing quicker payback on any investment. RJO does not sell hardware but has extensive experience and expertise in the data management/communication field. We will design, integrate, install, train, maintain and provide follow-on services to assure customer satisfaction and fulfillment, using safe and secure equipment which is compatible with any currently installed hardware/software. RJO personnel will work with customer representatives to analyze requirements, and existing hardware/software; develop, test and evaluate a prototype; refine and install a production system; train personnel; and provide support as required. Various sales/lease options are available to satisfy customer requirements.

That concludes this briefing. Thank you for your attention and interest. Are there any questions or points you would like to address?

CHART 26

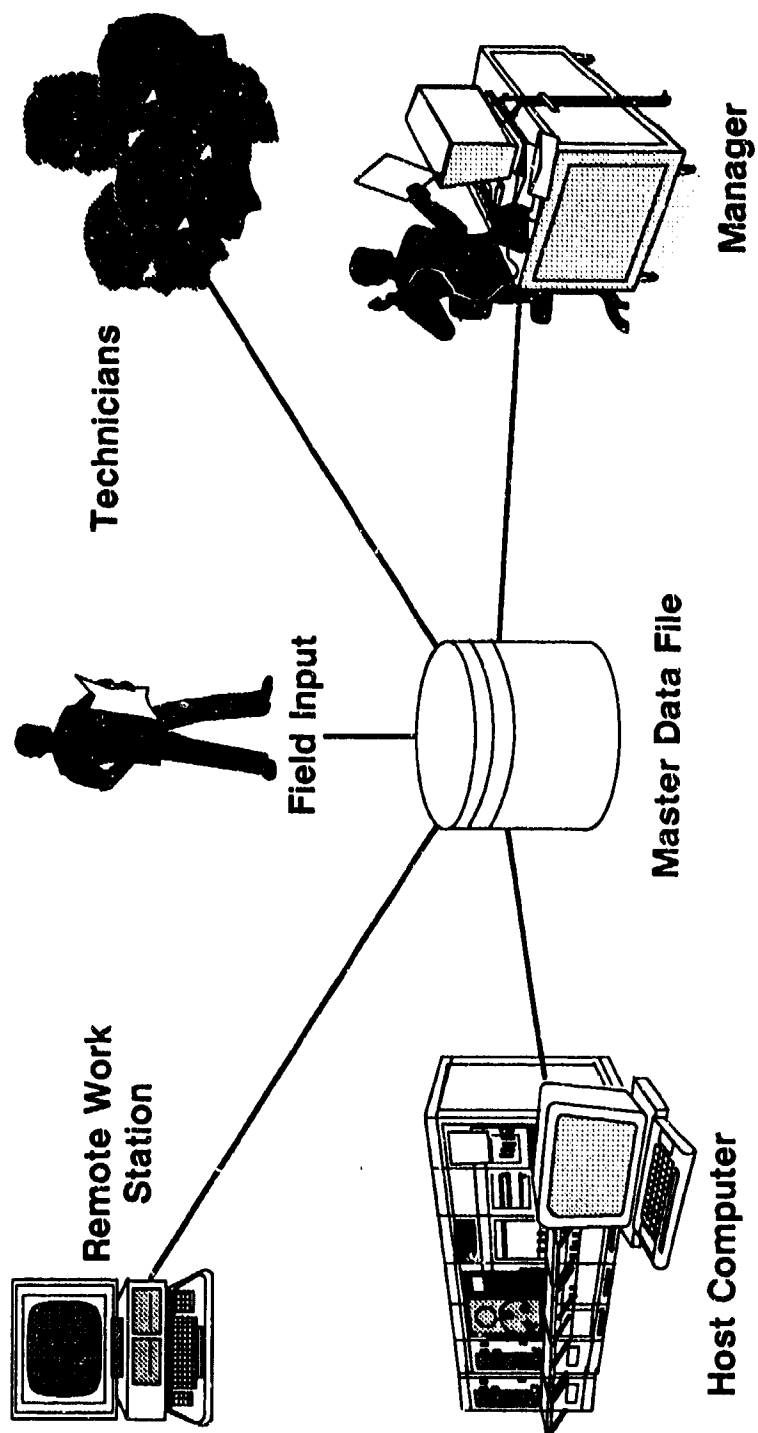
BRIEFING OVERVIEW

- 
- ★ **Typical NDI Equipment**
 - ★ **Data Management/Communication**
 - ★ **Data Collection/Management Life Cycle**
 - ★ **Applications**
 - ★ **Advantages**
 - ★ **Summary**

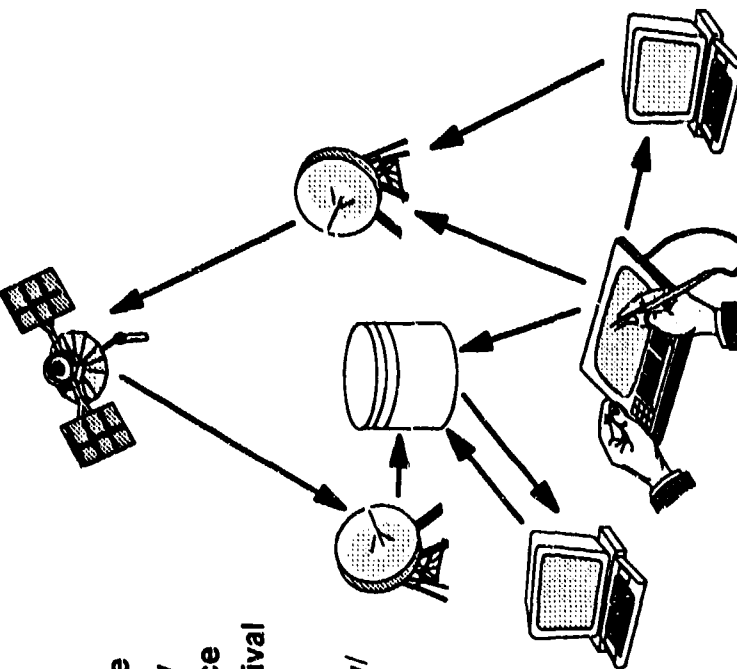
TYPICAL NDI EQUIPMENT

- ★ Portable Transceiver Work Station (Proxim)
- ★ Intelligent Traveller (Proxim)
- ★ Time and Attendance System (Accu-Sort Systems)
- ★ Radio Frequency Tag (Lockheed)
- ★ Laser-Wand RF/Micro-Wand (Hand Held Products)
- ★ SMART Cards (Several Manufacturers)
- ★ Super-SMART Card (Okidata)
- ★ Bartag and Readers (Amskan)
- ★ Gridpad (Grid Systems)
- ★ Barcode Labels (Various Manufacturers)

DATA COLLECTION/MANAGEMENT OVERVIEW



OVERVIEW

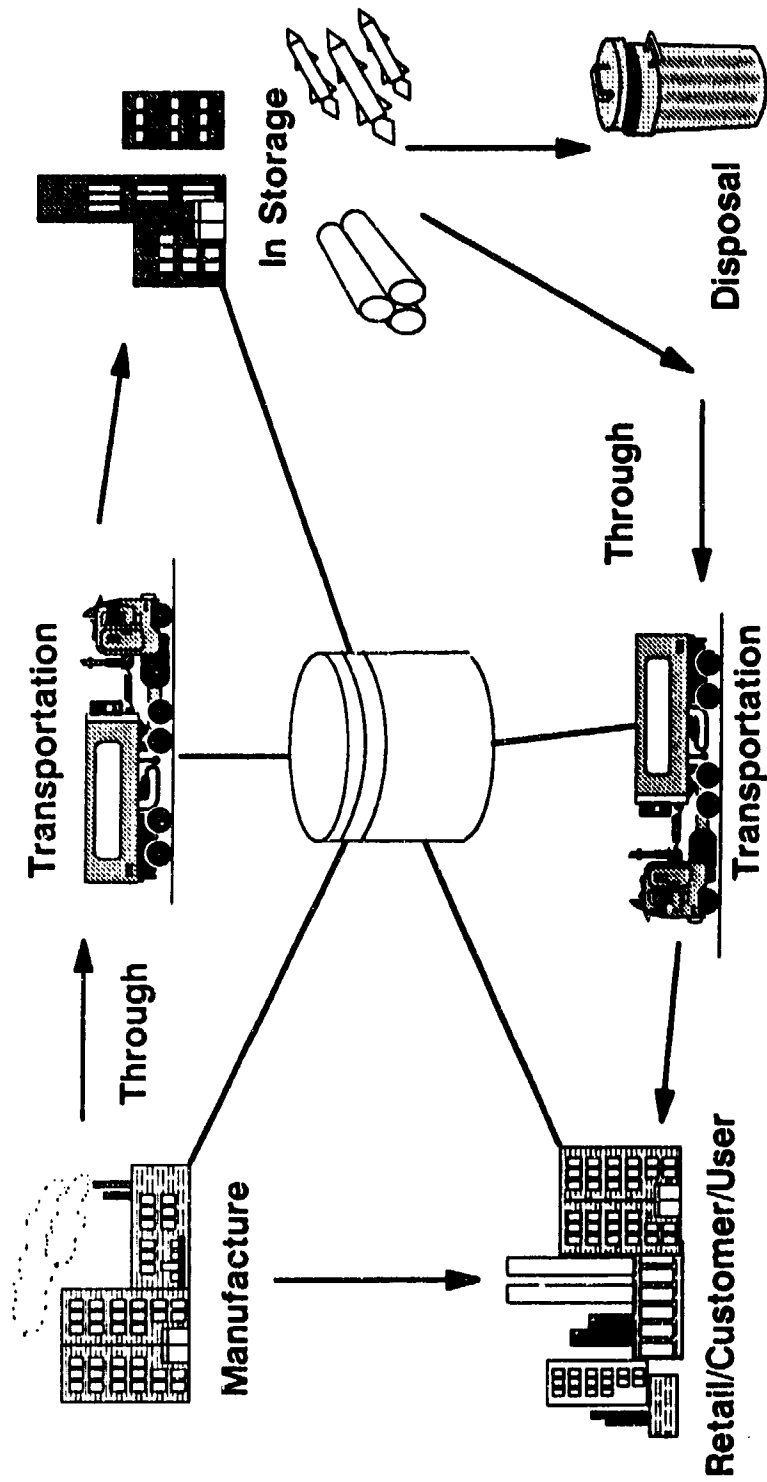


- ★ **Origin**
 - Classification
 - Inspection
 - Packaging
 - Catalog/ID Data
 - Inventory/Shipping
- ★ **Storage**
 - Location Records
 - Surveillance/Monitoring
 - Maintenance
 - Security
- ★ **Shipping/Receiving**
 - Manifest Validation
 - Quantity/Condition/Package Inspection
 - Carrier/Destination/Route
 - Storage Plan
 - Source
- ★ **In Transit**
 - Checkpoints
 - Zone Clearance
 - Safety/Security
 - Route Clearance
 - Destination Arrival
- ★ **Final Disposition**
 - Security/Safety/Monitoring
 - Inventory/Surveillance
 - Maintenance/Packaging

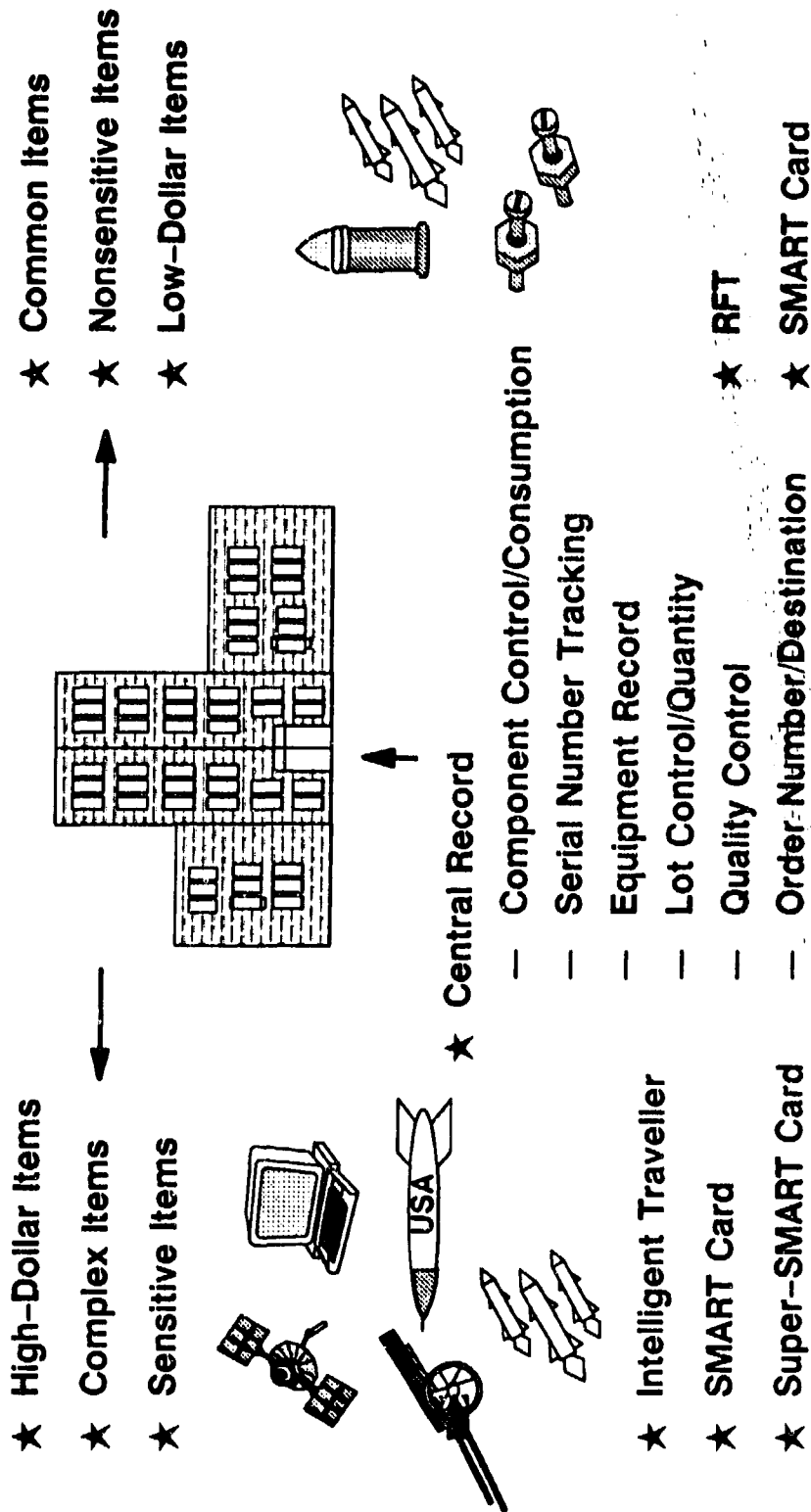
DATA COLLECTION/MANAGEMENT LIFE--CYCLE

- ★ Overview
- ★ Manufacturing
- ★ Storage
- ★ Assembly/Maintenance
- ★ Disposal
- ★ Transportation
- ★ Using Unit (Customer)

DATA COLLECTION OVERVIEW

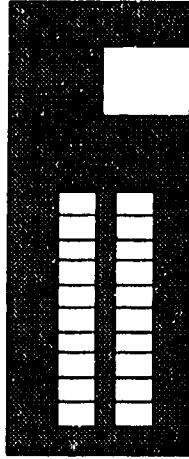


MANUFACTURING

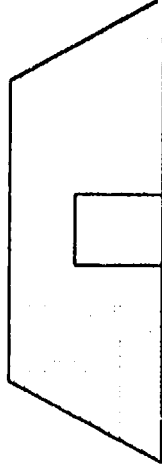


STORAGE

★ Representative Storage Sites



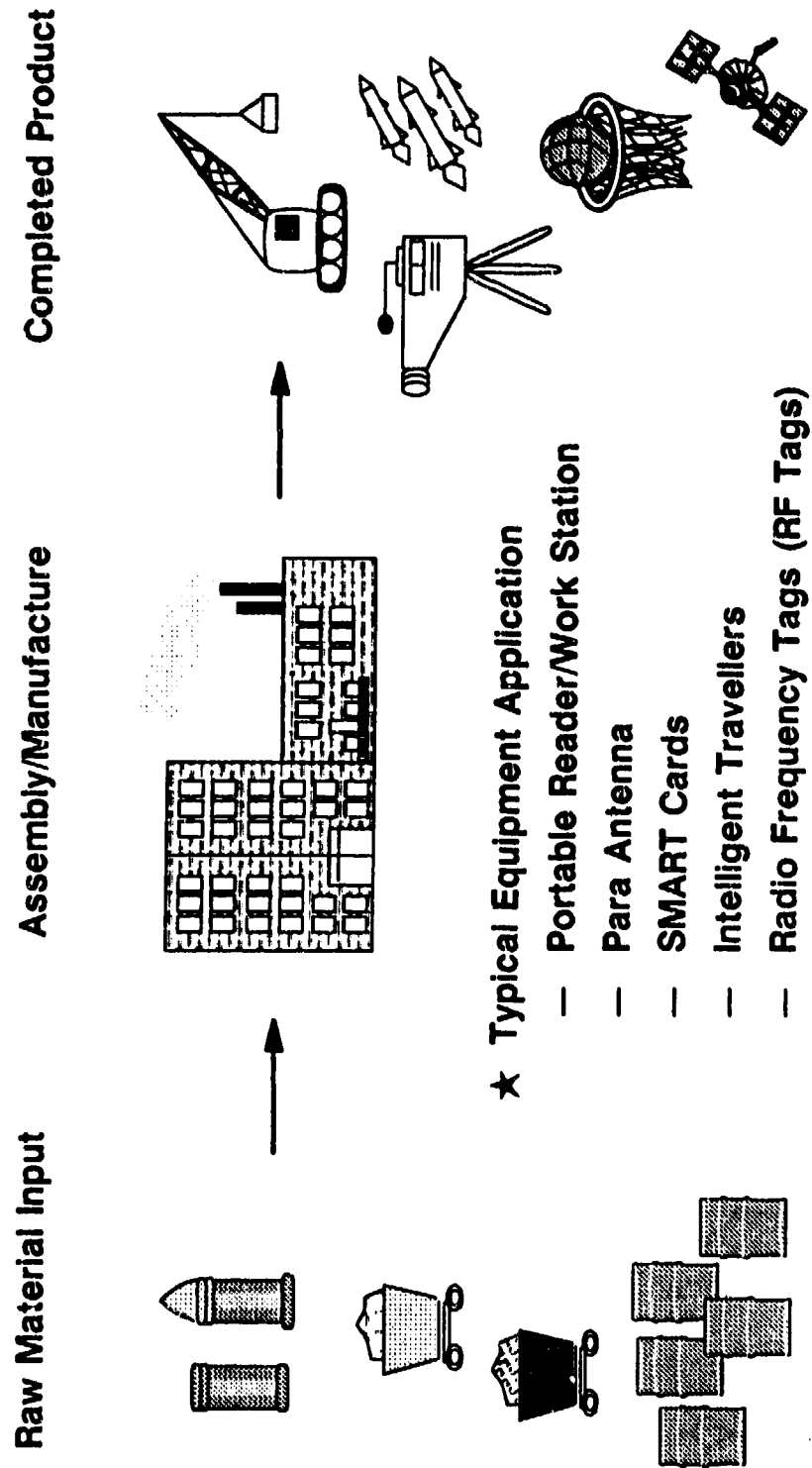
Warehouse



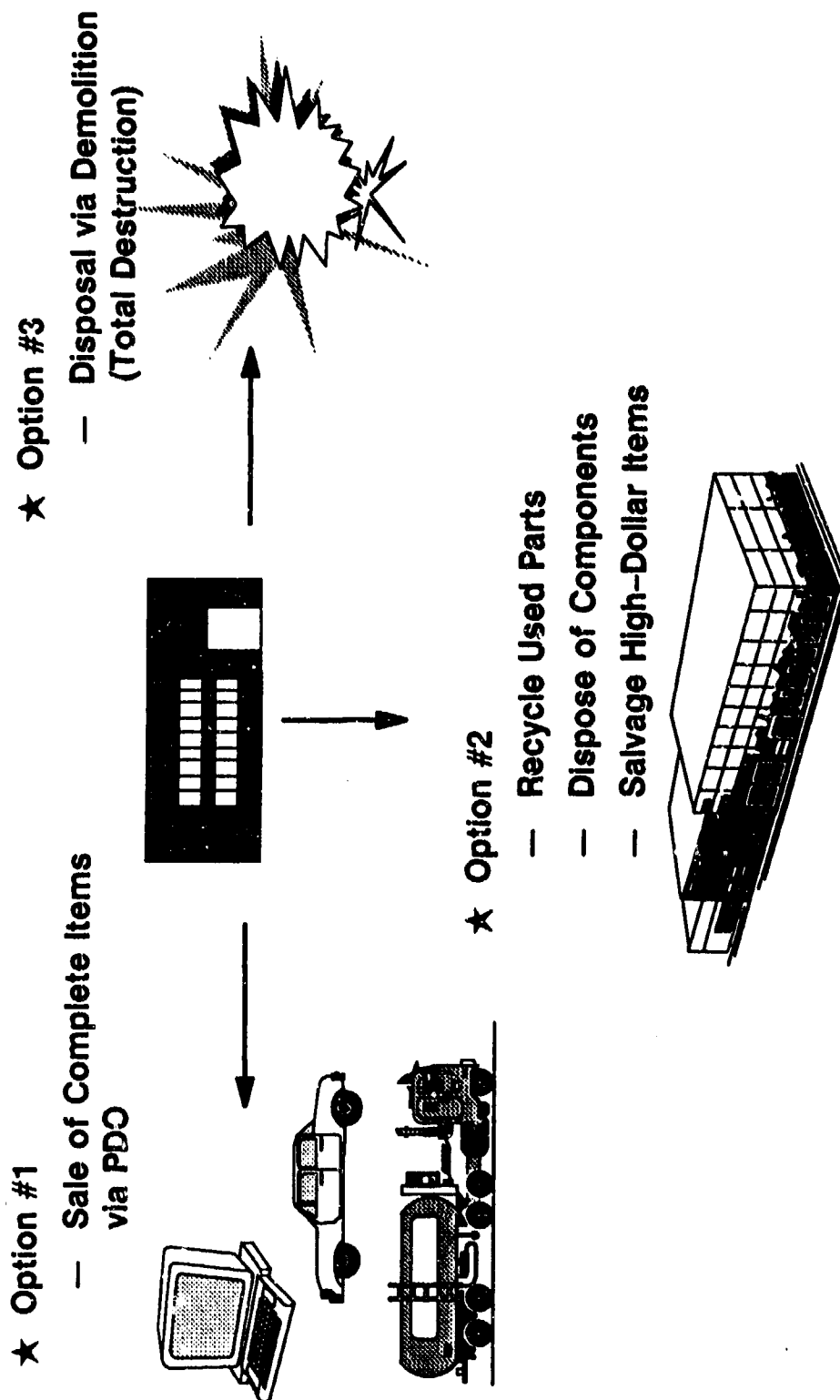
Ammo Magazine

- ★ Typical Equipment Applications
 - Intelligent Traveller
 - SMART Cards/Super-SMART Cards
 - Radio Frequency Tags

ASSEMBLY/MAINTENANCE

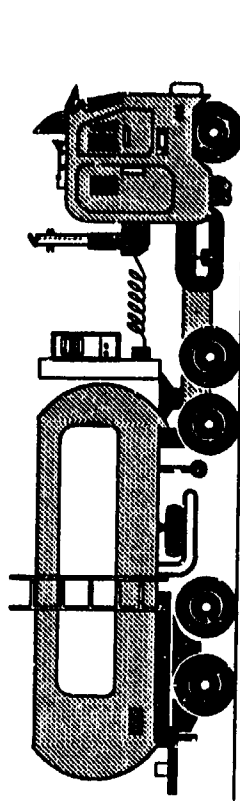


DISPOSAL



TRANSPORTATION

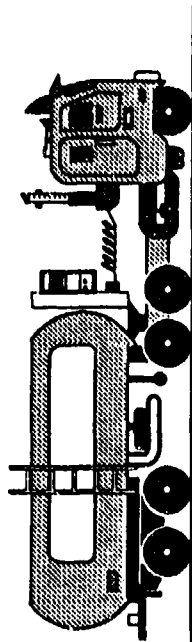
- ★ In-Transit Visibility
 - Super-SMART Card
 - Intelligent Traveller
 - Bar Tag
 - Transponder



TRANSPORTATION ACTIONS

★ Shipper

- Actions
 - Location Records
 - Surveillance/Classification
 - Packaging
 - Inventory
 - Document Preparation
 - Carrier Selection/Route/Destination
 - Loading Plan
 - Security
 - Safety



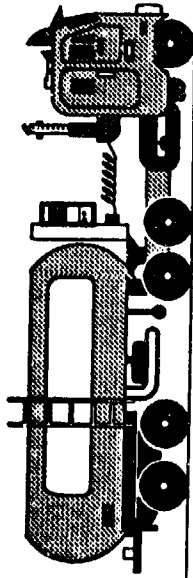
★ In Transit

- Actions
 - Check Points
 - Zone Clearance
 - Safety
 - Security
 - Accident/Incident Response
 - Route Clearance
 - Schedule

★ Receiver

- Actions
 - Destination Arrival
 - Surveillance
 - Monitoring
 - Safety
 - Security
 - Inventory
 - Storage
 - Records/Reports

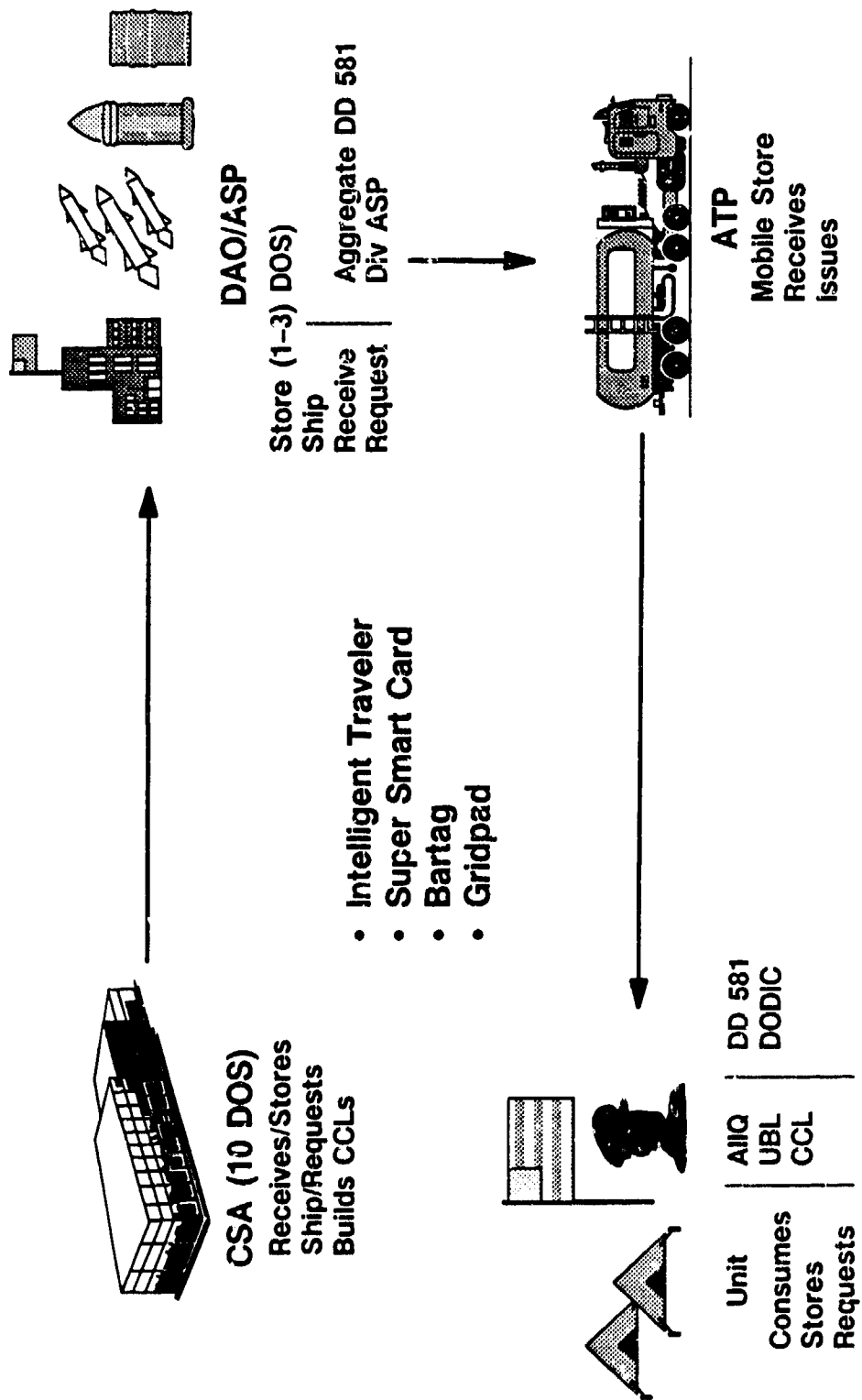
TRANSPORTATION ADMINISTRATIVE FORMS REQUIRED



★ Forms	★ Forms	★ Forms
— DD 626	— DD 626	— DD 626
— DD 836	— DD 836	— DD 1348-1
— DD 1348-1	— DD 1348-1	— Planograph
— Shipment Planning Work Sheet	— Bill of Lading	— Inspection Request/ Report
— Planograph	— DD 250	— Bill of Lading
— Bill of Lading		— DD 250
— DD 250		

Paperwork Required

SAAS/ATP



APPLICATION OVERVIEW

- ★ Inventory
- ★ Quality Assurance
- ★ Security/Safety
- ★ Records Maintenance
- ★ Additional Applications
- ★ Hazardous Waste
- ★ Log Books

SAMPLE APPLICATIONS

- ★ inventory
 - Real-Time Accurate Status
 - Shipping and Receiving
 - Storage/Location Audit/Condition/Quantity Verification
 - In-Transit Visibility
 - Maintenance Operations
 - Ownership Transfers/Control
 - Disposal Processing and Certification

SAMPLE APPLICATIONS

(Continued)

★ Quality Assurance

- Real-Time Inventory Catalog Data**
- Administrative Reporting/Tracking of Inspection Requirements**
- Testing Functions/Reporting**
- Cyclic Inspection Reporting/Condition Changes**
- Quality Deficiency Reporting**

SAMPLE APPLICATIONS

(Continued)

★ Security/Safety

- Personnel Tracking – Identification**
- Performance Monitoring**
- Controlled Area Exposure Time**
- Personnel Reliability Program**
- Area Entry/Control – Pinpoint Personnel Locations/Expertise**
- Disaster Response Contingency Planning**

★ Record Maintenance

- Log Books/Equipment History**
- Individual Item Record**
- Serial Number Tracking**

★ Additional

- Unlimited to Meet Customer Needs**
- PPBES Planning Input, Consumption/Maintenance**

SPECIFIC EXAMPLES

★ Hazardous Waste

- Tracking**
- Monitoring**
- Inspection**
- Reporting**
- In Transit**

LOG BOOKS

- ★ **Totally Automated**
- ★ **Initiated at Time of Manufacture/Assembly**
- ★ **Contain Component Data**
- ★ **Track Ownership/Location**
- ★ **Record Use/Inspection/Maintenance**

ADVANTAGES OF NDI

- ★ **Availability – No R&D Period**
- ★ **Lightweight Equipment for Field Use**
- ★ **Ruggedized Equipment for Use in Storage/Combat Environments**
- ★ **Equipment is User Friendly, Not Complex**
- ★ **Economical; Multiple Sources**
- ★ **Compatibility With Existing Hardware/Software; Flexible Selection to Need**
- ★ **Redundancy Without Add-On Costs; I/O From Any Point in the System**

ADVANTAGES TO THE CUSTOMER

- ★ **Macom Service Organization Can Be Linked to Any I/O for Selected/Desired Data**
- ★ **Reduced Manpower Requirements**
- ★ **Maximal Flexibility is Provided**
- ★ **Equipment Will Transmit Technical or Less Complex Data, i.e., E-Mail**
- ★ **Rapid Amortization**

BRIEFING SUMMARY

- ★ **NDI Items are Now Available to Automate the Entire Commodity Life Cycle**
- ★ **NDI Cost Continues to Decline**
- ★ **RJO Has the Systems Integration Expertise and Functional Process Knowledge to Implement a Cost-Effective, Efficient System**
- ★ **RJO Has a Detailed Methodology to Successfully Integrate Dissimilar NDI Components**

EXPLOSIVE SAFETY SITING OF CORPS OF ENGINEERS

STANDARD IGLOO DESIGNS

by

Earl Williams
Adib Farsoun
Wallace Watanabe

U. S. Army Engineer Division, Huntsville
Huntsville, Alabama

Twenty-Fourth DOD Explosives Safety Seminar
28-30 August 1990

ABSTRACT

The U.S. Army Corps of Engineers maintains a family of "Standard Design" storage magazines. These designs are used throughout the Department of Defense (DOD) to store explosives and munitions. The DOD 6055.9-STD defines the approved safety siting and quantity limits for "standard" and "nonstandard" magazines. Several of the Corps "Standard Designs" are directly referenced by the DOD 6055.9-STD. There is a serious lack of understanding of the limitation on the use of Corps "Standard Design" magazines as "Standard" or "Nonstandard" storage as defined by DOD 6055.9-STD. This paper provides guidance in understanding the proper use of the Corps Standard Igloo Designs to comply with the explosive safety requirements of the DOD standard.

BACKGROUND

General. The Corps of Engineers magazine standard designs have been developed in coordination with the Department of Defense Explosive Safety Board (DDESB) so that the designs would be considered preapproved when called for in construction. The DDESB's approved Army earth-covered magazines include 33-15-65, 33-15-74, 421-80-01, and 422-15-01. These standard designs are, for the most part, a complete set of construction drawings. The magazines must, however, be tailored (site-adapted) for local conditions which mainly involve the foundation. The later magazine 422-15-01 has been developed for storage and segregation of small quantities of ammo or explosives.

Siting. The above magazines, when sited to requirements of DOD 6055.9-STD, (Reference 1), will prevent communication of explosion from one magazine to another. Siting requirements as described in DDESB criteria documents are greatly influenced by the classification of the magazine, that is, whether the magazine is "Standard" or "Nonstandard". Siting requirements for those magazines labeled "Standard" are:

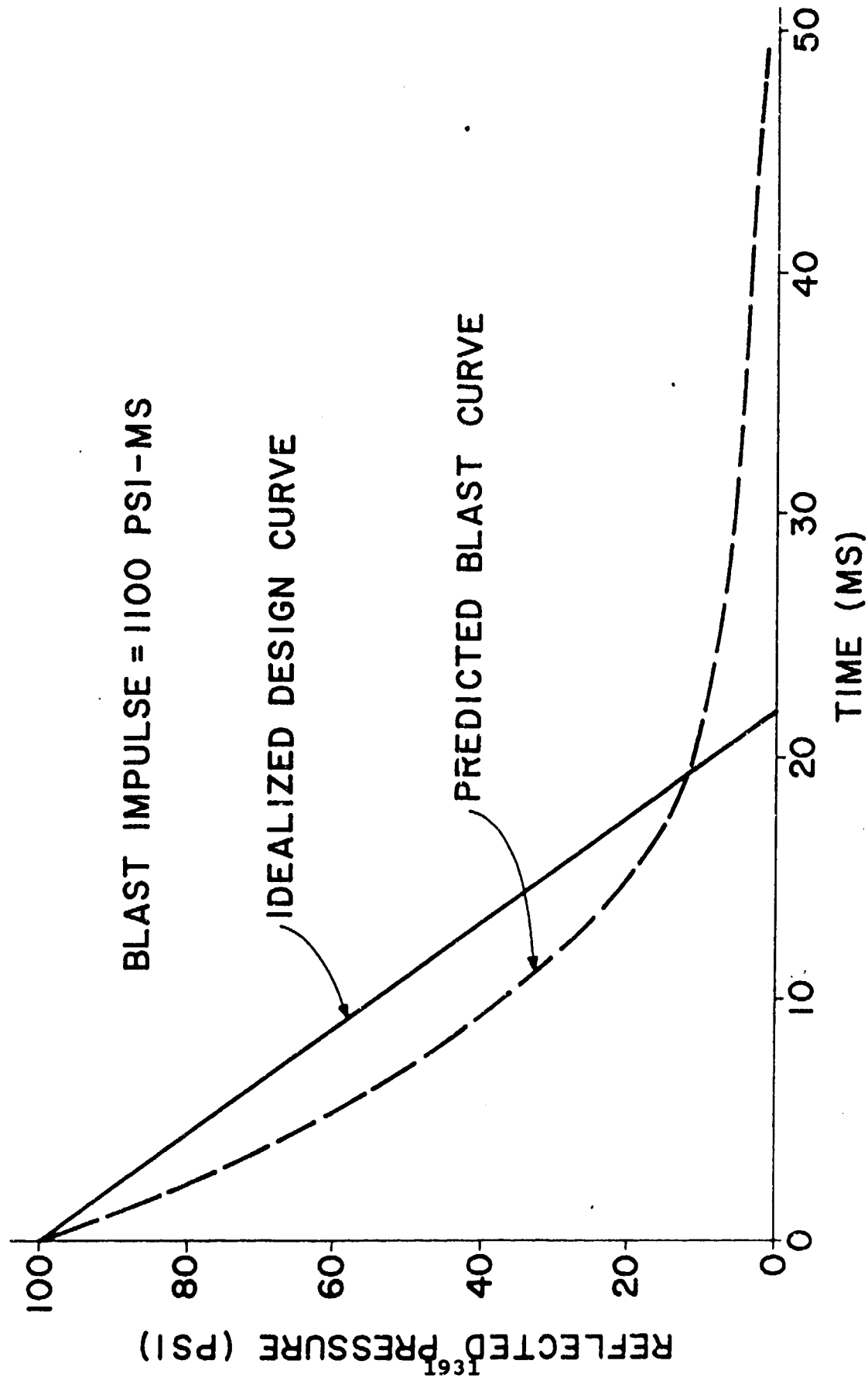
<u>Orientation</u>	<u>Intermagazine Separation</u>
Side-to-Side	1.25 $W^{1/3}$
Rear-to-Front	2.00 $W^{1/3}$
Side-to-Front	2.75 $W^{1/3}$

Design Requirements for Standard Magazines

- a. Minimum earth cover shall be 2 feet.
- b. Slope of earth fill shall be 2 horizontal to 1 vertical
- c. Headwall including door shall be designed for 1100 psi-ms shown in Figure 1.
- d. Stones larger than 10 pounds shall not be used as part of back-fill to cover arch above spring lines.

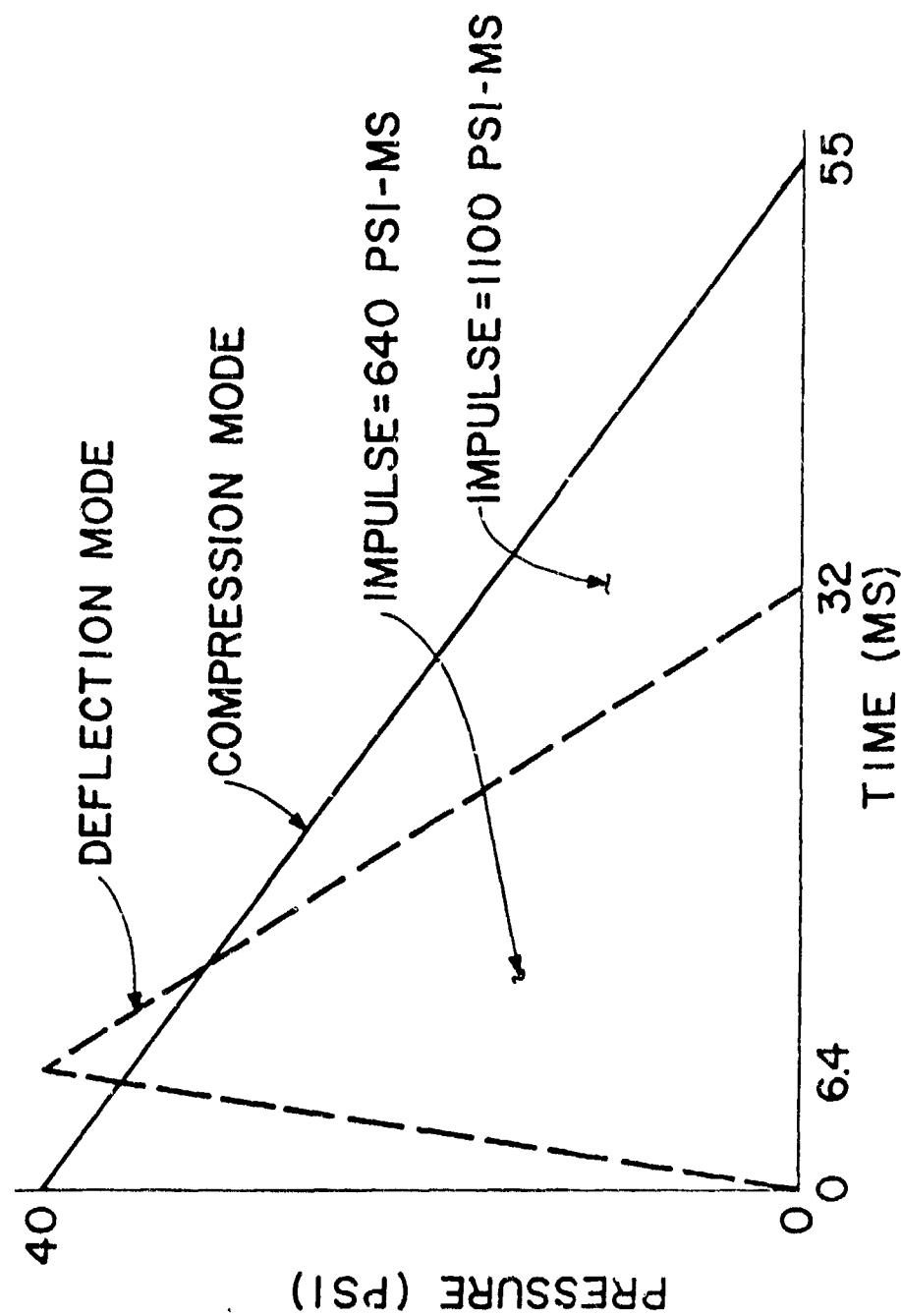
DEFINITIONS

- a. Standard Earth-Covered Magazine. A magazine of the designation listed above and listed in DOD 6055.9-STD. It is a magazine approved for the storage of 500,000 pounds net explosive weight (NEW).



IDEALIZATION OF PRESSURE-TIME FUNCTIONS (REF. 8)

FIGURE 1



COMPRESSION AND DEFLECTION MODE LOADINGS (REF. 8)

FIGURE 2

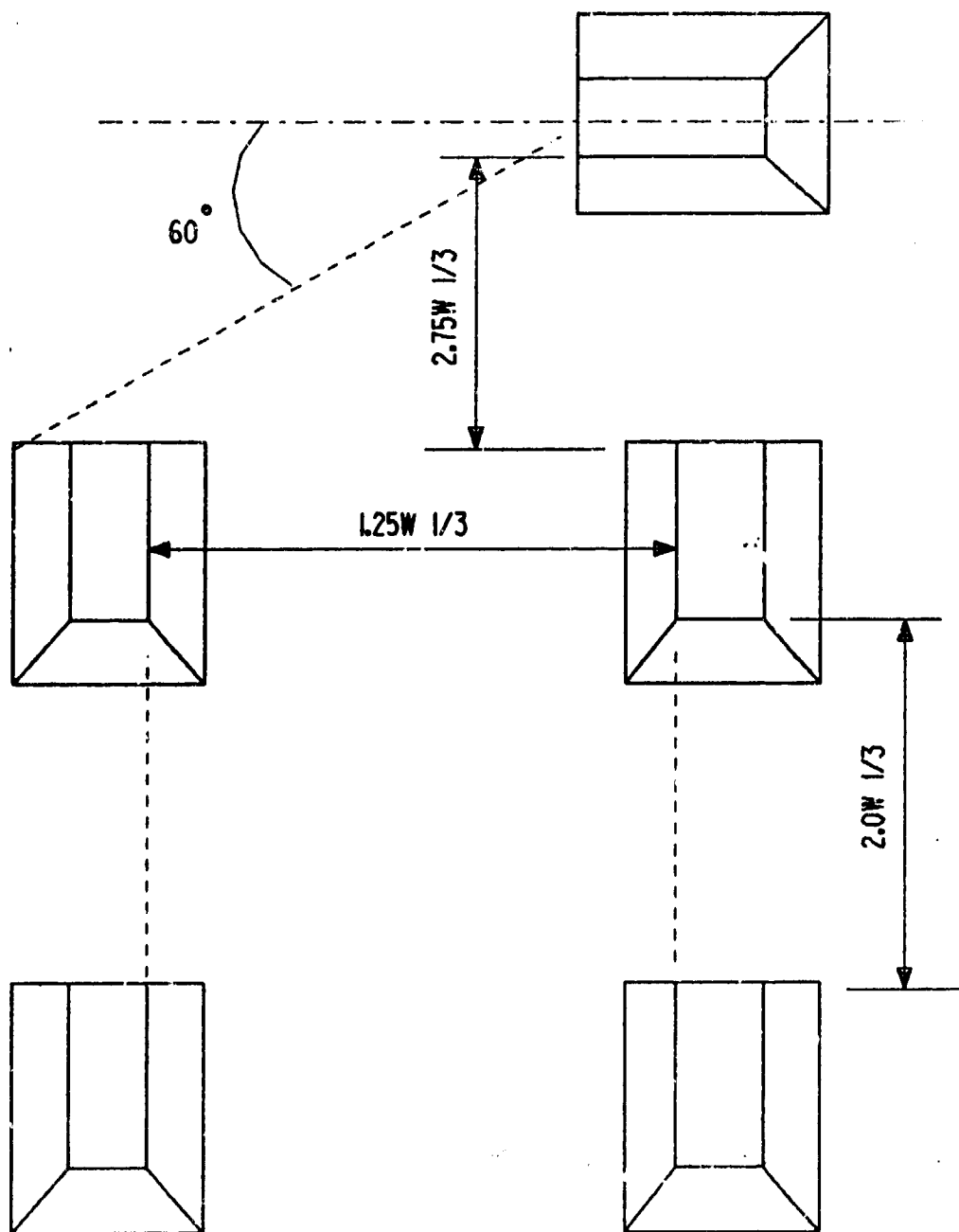


FIGURE 4 (REF.9)

b. Nonstandard Earth-Covered Magazine. A magazine that is not equivalent in strength to the standard magazine (weaker structurally) and is limited in storage to 250,000 pounds of NEW.

c. Hybrid Earth-Covered Magazine. A magazine that uses components from standard magazines, and/or modifications therefrom. These magazines cannot be considered preapproved, therefore, they require submission to the DDESB for approval prior to construction.

REQUIREMENTS TO QUALIFY AS STANDARD IGLOO MAGAZINE

Critical Structural Elements

The performance of an earth covered igloo storage magazine is dependent on four primary structural elements:

- Earth Covered Arch
- Rear wall (Bermed)
- Headwall
- blast Doors

Each of these elements must be demonstrated by test (or in some cases by analysis) to be capable of preventing simultaneous propagation by resisting the blast force that can occur for the maximum storage quantity at the minimum standard siting distance. (See Figures 1 and 2 for loading.) A standard magazine is intended to provide a desired degree of asset protection. Criteria in DOD 6055.9-STD is intended to be consistent with this requirement.

Test Verification Programs

After World War II, there remained on hand in the United States and overseas a tremendous stockpile of munitions. Available space at depots was limited based on the quantity distance limits being applied at that time. To provide for an orderly and economical disposition of these huge stocks of ammunitions, it was necessary to determine whether existing igloo storage capacities could be safely expanded without requiring large expenditures for additional land, roads and properties. A full scale test program was conducted by the Army-Navy Safety Board (a predecessor to the DDESB) at the Naval Proving Ground at Arco, Idaho (Reference 2). The purpose of this test was to determine the ability of the existing igloo structures to safely accommodate larger storage limits at the same or closer inter-magazine distances. The results of this test program showed that the storage limits for the igloo configuration tested could be safely increased to 500,000 lbs. at a separation distance of $5W^{1/3}$. In fact, the test indicated that siting at separations of $2.5W^{1/3}$ was feasible. Igloos

in this test were the two Army and two Navy standard concrete, arch type, earth-covered igloo magazines, approximate size of 26'-6" wide by 81'-0" long.

In the 1970's the DDESB undertook an extensive test program to attempt again to reduce the required separation distance for igloo storage. This test program was called the Explosive Safety Knowledge Improvement Operation (ESKIMO). These tests were conducted at the Naval Weapons Center, China Lake, California. The results of these tests are documented in References 3 through 7. The Eskimo I test in 1971 demonstrated that the most critical element in the performance of an igloo magazine was the door. It was determined that increased storage potential could be obtained through an improved door design. ESKIMO I testing was based on igloo configurations similar to the 33-15-64. The ESKIMO II tests conducted in 1973 considered a stronger door design and highlighted the need for a balanced design for the strength of the headwall and door. Changes in the door and headwall for this test consisted of a large single leaf sliding door and a strengthened headwall.

The following is a summary of the ESKIMO tests:

ESKIMO I (Reference 3), the first test, was conducted in December 1971 to determine a safe, practicable minimum separation distance for face-on exposures of the U.S. Army steel arch magazines. Explosion communication occurred to an acceptor igloo of this design at a distance in feet equal to $1.25W^{1/3}$, in which W is the weight in pounds of the high explosive in storage, but failed to occur at a distance of $2.0W^{1/3}$ to the rear of the donor. Further, the test revealed that safety and economy might be increased through improved design for closer balance in strength between the doors and headwall of the magazine.

ESKIMO II (Reference 4) was conducted in May 1973 to appraise magazine door and headwall designs. A large, single-leaf sliding door withstood the blast with minor distortion although the accompanying headwall sustained severe damage. A Stradley-type headwall, on the other hand, incurred only minor damage. In addition, the noncircular (oval) steel arch with concrete thrust beams was tested with the Stradley headwall and withstood the blast without breakup or severe distortion.

ESKIMO III (Reference 5) conducted in June 1974 further extended the study of explosives-storage magazines using information derived from ESKIMO I and II. During a further test of the oval arch and Stradley-type headwall, ESKIMO III used structures remaining from ESKIMO II, rebuilt as necessary, as well as new construction of a light-gauge, deeply corrugated, steel-arch magazine. The oval-arch magazine tested in ESKIMO II was fitted with a newly designed Stradley-type headwall with a single-leaf door. ESKIMO II proved that the Stradley-type headwall could withstand a face-on impulse of 1,750 psi-ms and that the steel oval-arch could

withstand the face-on impulses generated by that charge. ESKIMO III tested the ability of the new headwall to withstand the side-on blast imposed by the explosion of the adjacent magazine.

ESKIMO IV (Reference 6) conducted in September 1975 continued the study of explosive storage magazines, using information from the prior tests in the ESKIMO series. The door and headwall combination used on the oval-arch magazine was tested again in ESKIMO IV but with face-on blast loading as compared with the side-on loading experienced with ESKIMO III. The door that had fallen off its supports in ESKIMO III was rehung in position. ESKIMO IV provided the initial test of the combination of a newly designed headwall and single-leaf sliding door under face-on loading. ESKIMO IV also included a rebuilt standard headwall and door (OCE standard drawing 33-15-64) as a control structure and a single-leaf sliding door remaining from ESKIMO III in combination with a rebuilt standard headwall. The response of the magazines was essentially as expected with only minor damage occurring.

ESKIMO V (Reference 7) was a continuation of the study of explosive-storage magazines using information from the prior ESKIMO tests. The oval steel-arch igloo used in ESKIMO III (side on loading) and ESKIMO IV (headwall loading) was again tested. The earth cover and the concrete thrust beams were removed, and the fill was replaced. ESKIMO V also included a newly constructed magazine of the FRELOC concrete arch type. Since door response was not a concern in this test, nonpermanent steel doors were spot welded or bolted to the door openings of the igloos. The structural response of the magazines in this test was essentially as predicted and well within acceptable limits.

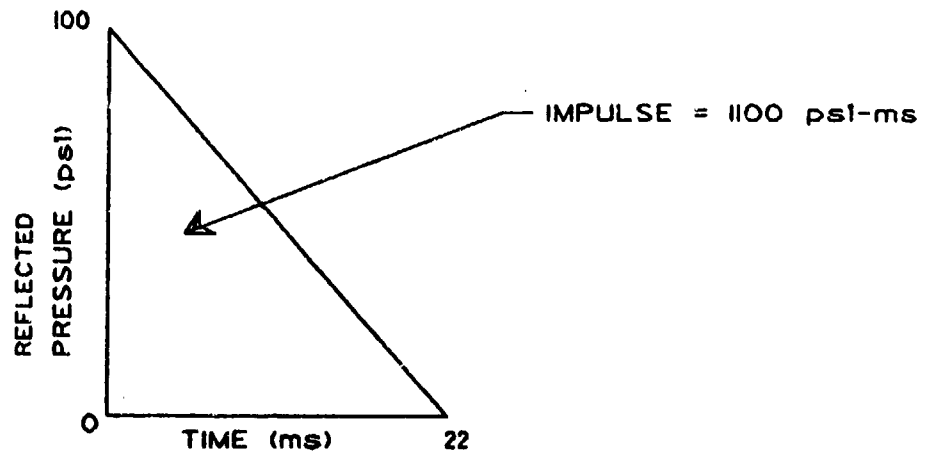
ESKIMO VI and VII tested the Navy box-type magazines which are not covered in this paper.

Limitation on Stones in Earth Cover

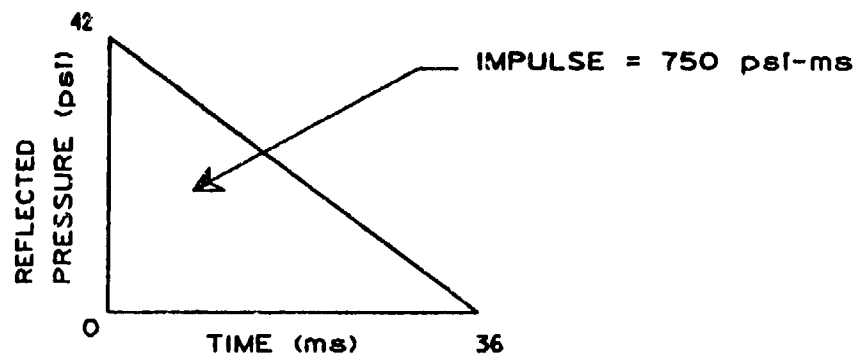
In the event of the accidental detonation of a storage magazine, the earth cover will be ejected at high velocities. The presence of large stones or debris would create an undesirable secondary fragmentation risk (Reference 1). To minimize this problem, the standard igloo magazines have clearly specified limits on material allowed over the crown of the arch.

EFFECT OF MAGAZINE SEPARATION ON HEADWALL/DOOR LOADING.

As the separation between igloos increase, the loading on the headwall/door decreases. For a comparison of loading for a side-to-side spacing of $1.25W^{1/3}$ and $5.0W^{1/3}$, see Figure 3. For any igloo sited between these two spacing of igloos, a new loading can be developed.



a. FOR 1.25 W $1/3$, REFERENCE 8



b. FOR 5.0 W $1/3$, REFERENCE 9

FIGURE 3 BLAST LOADING FOR SIDE TO SIDE IGLOOS

REVIEW OF EXISTING ARMY STANDARD DESIGNS

The large standard magazines now in use are the steel circular arch 33-15-65, concrete circular arch 33-15-74, and semicircular steel arch 421-80-01. The present safety criteria document (DOD 6055.9-STD) dictates the use of these magazines for new construction. In 1987 a small box-type concrete magazine 422-15-01 was developed by the Corps of Engineers for storing 425 pounds of explosives. This magazine was developed to allow segregation of incompatible explosives and for separating material belonging to other organizations. This magazine also received DDESB's approval. Features of each magazine are presented below.

Steel Arch 33-15-65. This magazine, developed in 1963, is an earth-covered steel arch and is available in widths of approximately 8'-0", 10'-0", 12'-0" and 14'-0" feet. The length is variable from 11'-0" minimum with 2'-0" increments. The headwall as well as the rear wall of this magazine is of reinforced concrete construction. A double-leaf steel door 6'-0" wide by 6'-4" high and located in the headwall provides access to the magazine. This magazine does not have the stiffened headwall and door as shown on the later developed magazines. This therefore raises some doubt as to the adequacy of this type of magazine to prevent explosion communication since the headwall was proven by ESKIMO series test to be the weakest element of the magazine. It is important to point out a typographical error in the current version of DOD 6055.9-STD regarding this design. First, Chapter 5, Paragraph B.1.d. incorrectly refers to this standard as a 33-15-64. Secondly, all of Paragraph B is intended to identify standard designs capable of storing 500,000 lbs. The small size of this igloo would preclude it from containing such an amount.

Concrete Oval Arch, 33-15-74. The design of this magazine was originally developed by the U.S. Army Engineering Command in Europe and earlier referred to as the FRELOC magazine. In 1973 the magazine headwall and door were strengthened as a result of full scale ESKIMO tests. This magazine is 25 feet wide and 14 feet in height. The length varies but is normally constructed in 60 feet or 80 feet lengths. The standard design provides two door size options: an 8'-0 X 8'-0 and a 10'-0 X 10'-0 sliding stiffened door. The headwall of this magazine is 12 inches in thickness with thickened wall jambs and header beam.

Semicircular Steel Arch, 421-80-01. This magazine is an assemblage of components from various sources. Those components that are structurally critical from an explosives safety standpoint are traceable to DDESB blast tests and/or approved magazines. The magazine is a steel arch, 1 gage in thickness. In general, the magazine is very similar to the 33-15-74 magazine with the exception of the arch material. The headwall and the rear wall are of similar construction, including the exhaust

stack and the louver openings in the front wall. The standard magazine drawings provide an option for a 10'-0" X 10'-0" and an 8'-0" X 8'-0" door.

Concrete Cubicle Magazine, 422-15-01. This magazine developed in 1987 is an earth-covered concrete cubicle 10'-0" X 10'-0" X 10'-0" in dimensions. It has a single leaf door approximately 4'-0" wide by 7'-0" high. As indicated above, the magazine storage capacity is 425 pounds of class 1.1 high explosives.

Availability of Standard Magazines Drawings. The Huntsville Division, U. S. Army Corps of Engineers, maintains and updates the standard drawings for all approved Army magazines. The EP 1110-345-2, "Index of Design Drawings for Military Construction," lists Army standard magazines. Copies of the standard drawings can be obtained from the Huntsville Division upon request. See Reference 11 for the ordering address.

NONCONFORMING HYBRID DESIGNS

Using Nonapproved Headwalls or Doors on Standard Arch Magazines.

Safety investigations have revealed construction of standard magazines that have been modified to suit cost and operational requirements. A non-approved headwall/door on a standard magazine would render the magazine nonstandard. If the hybrid magazine is sited at minimum distance for standard magazine, an analysis must be performed to determine the storage quantity which would prevent propagation to another magazine or vice-versa.

Mixing Headwalls and Doors From One Standard With Another.

Another problem encountered is the mixing of headwalls/doors between standard magazines. If sited at minimum distances per DOD 6055.9-STD, an analysis must be performed to determine if the headwall/door is adequate in strength to prevent propagation.

Improper Siting of Standard

Any magazine, sited less than minimum distances shown in DOD 6055-9-STD, will have to be evaluated to determine the maximum amount of explosives that could be stored in these magazines.

EVALUATION PROCEDURES FOR NON-CONFORMING DESIGNS/SITINGS

a. Analysis of Nonconforming Elements. The headwall, door, and cover must be evaluated against the requirements to prevent propagation. Any deviation from the standards elements must be analyzed to determine the capacity of these elements. If the headwall/door cannot provide Category III protection for the stored material from the loading shown in Figure 1, then these elements must be analyzed to determine what loading they can withstand and this load converted into an amount of explosives that can be stored in an adjacent igloo. In addition to the analysis, the evaluation should be compared to the ESKIMO test data.

b. Example of Deviation. In recent months, we have evaluated magazines developed from components of standard designs. The majority of these magazines did not reflect the strengthened headwall/doors as was proven by ESKIMO tests to conform to safety criteria. These magazines were classified nonstandard requiring siting per DCD 6055.9-STD criteria. There appears to be a lack of understanding at the installation level in developing new magazines for standard siting. Nonconforming magazines submitted for consideration as a standard magazine must include a detailed analysis to show the headwall/door to be sufficiently adequate in strength to prevent simultaneous detonations. This adequacy is determined at the time of design and final safety approval by comparing the design to the design criteria of the day.

c. Vintage Igloos Versus Standard Igloos. It is not appropriate to compare the structural capacity of vintage hybrid designs with that of current designs. Hybrid designs which received safety approval based on the regulations in use at the time represent a risk which was determined to be acceptable at that time. The user must understand the difference between a safety approval and the structural design limitations. A safety approval of this type allows for storage limits equal to the standard of the day. However, it may not in fact provide the protection of assets that is expected because of the reduced structural resistance. Safety approval is often interpreted to insure a level of asset protection, however, such protection is dependent on minimum structural performance which is not necessarily defined by the standard.

d. Magazines Controlled by the Grandfather Clause. Existing magazines, conforming to the safety manual current at the time of design or approved for a designated explosive limit, shall retain their classification, i.e. (standard or nonstandard). Any accepted deviation from these standards must be documented in the permanent records of the installation. The documentation must show the applicable safety criteria requirements in effect at the time the design was accepted by the approving agency (DDESB). The installation's file copy of DDESB's site submission should serve as sufficient documentation that the installation has complied with the safety criteria.

CONCLUSIONS

The following conclusions represents our interpretation of the proper applications of DOD 6055.9-STD:

a. The Standard is intended to provide criteria such that simultaneous propagations of explosions from magazine to magazine are prevented.

b. The Standard identifies several magazines approved for the storage of up to 500,000 pounds NEW. The 33-15-64 is one of those magazines.

c. However, Eskimo tests have clearly indicated that the doors and headwall of 33-15-64 were inadequate to provide the desired degree of assets protection.

d. New construction using 33-15-64 is therefore not consistent with requirements imposed by items a and c listed above. Any interpretation of item b that assumes use of this magazine for new construction is therefore faulty.

e. We interpret item b above as a safety decision by DDESB that an existing magazine may contain a certain NEW and the associated risk is acceptable. We do not interpret item b above as either permitting or encouraging new construction using designs known to be inadequate.

f. Hybrid magazines can be sited at standard magazine distances if all components and specifically the headwall/door are equivalent in strength to standard magazines specified in DOD 6055.9-STD manual. Approval by DDESB prior to construction should be mandatory.

g. Hybrid magazines not equivalent in strength to the standard approved magazines must be evaluated on a case-by-case basis and approved by DDESB prior to construction. Existing hybrid magazines should be reviewed to determine their strength and should be sited according to their strength.

h. Modifications to any of the standard magazines listed in DOD 6055.9-STD manual will render these magazines nonstandard unless verified to be sufficient in strength to prevent simultaneous propagation.

i. Users should not be misled by the presence of older standard drawings in DDESB 6055.9-STD. All new construction should be based on current technical knowledge. At this time only two Army magazines are designed based on the latest technical data and test results for 500,000 lbs. These magazines' drawings were listed earlier in this paper in paragraph titled "Review of Existing Army Standard Designs".

ACKNOWLEDGMENTS

The writers would like to acknowledge those who provided valuable input used in preparation of this paper: Dr. Chester Canada, DDESB-KT, Cliff Doyle, USATCES, Dick Wight, Headquarters, Corps of Engineers, and Mr. Paul Lahoud, Corps of Engineers, Huntsville Division.

REFERENCES

11. DOD 6055.9-STD., "DOD Ammunition and Explosives Safety Standard," October 1988, Change 2 Revision.
2. Igloo Tests, Naval Proving Ground, Arco, Idaho, August 1946.
3. ESKIMO I, Magazine Separation Test, Report Number NWC TP 5430, February 1973.
4. ESKIMO II, Magazine Separation Test, Report Number NWC TP 5557, September 1974.
5. ESKIMO III, Magazine Separation Test, Report Number NWC TP 5771, February 1976.
6. ESKIMO IV, Magazine Separation Test, Report Number NWC TP 5873, March 1977.
7. ESKIMO V, Magazine Separation Test, Report Number NWC TP 6076, February 1979.
8. Development, Design and Test of a New Door and Magazine Arch, by Black and Veatch, January 1975.
9. HNDED-CS-89-6, "Blast Door Concepts for Corbetta-Type Magazines," November 1989.
10. Department of the Army Technical Manual TM5-1300 (Revised), "Structures to Resist the Effects of Accidental Explosions," December 1986.
11. Department of the Army, Huntsville Division, Corps of Engineers, ATTN: CEHND-ED-ES, Mr. Ron Taylor, Telephone Number 205-895-5560, P.O. Box 1600, Huntsville, Alabama 35807-4301.

30 AUGUST 1990

**TWENTY-FOURTH DOD EXPLOSIVES
SAFETY SEMINAR**

SESSION: SITE PLAN AND SURVEY

**TITLE OF PRESENTATION
HEADQUARTERS, DEPARTMENT OF ARMY
WORLDWIDE PORT STUDY**

**PRESENTED BY: GARY W. ABRISZ, CHIEF
LOGISTICS EXPLOSIVES SAFETY DIVISION
U.S. ARMY TECHNICAL CENTER
FOR EXPLOSIVES SAFETY**

PRESENTATION

Slide #1

Good afternoon, I'm Gary Abrisz, the Chief of the Logistics Explosives Safety Division at the U.S. Army Technical Center for Explosives Safety, located in Savanna, Illinois.

The U.S. Army's Director of the Army Staff has directed a Worldwide Survey of commercial seaports being used to handle Department of Defense munitions. The U.S. Army Technical Center for Explosives Safety is the lead agency for the Army. We, of course, require direct participation by the Department of the Army Deputy Chief of Staff for Logistics and the Military Traffic Management Command, as well as many other organizations throughout the Department of Defense and the U.S. Coast Guard.

Slide #2

This is the outline of my presentation. I'll define the purpose, discuss briefly the historical concerns, and provide an overview of our established action plan. We have been involved in several onsite surveys including the download of ammunition from prepositioned ships afloat (which I'll refer to as PREPO throughout this presentation). This was in the Pacific area for the required maintenance cycle. I'll discuss that involvement.

Slide #3

The use of commercial seaports, as well as military ports, worldwide for movement of Department of Defense munitions raises many concerns due to the exposures to people and property in the port areas. In many instances, as you'll see, the populations are directly adjacent to operations involving millions of pounds of high explosives ammunition.

Slide #4

Historically, our largest and most destructive explosives accidents have occurred in port areas. Most everyone has heard of the 1917 Halifax Harbor, Nova Scotia, accident shown here.

The Port Chicago, California, disaster in 1944 involved ammunition ships supplying the Pacific theater and is the accident principally responsible for our present day Department of Defense standards concerning separation requirements for piers and wharves. In many ways we do things differently now with the advent of modern ships, improved handling procedures, and packaging, but the potential and concerns do remain.

Slide #5

The Army leadership recognized, based on various Army commands requesting exemptions to the Department of Defense standards and the many DDESB surveys, that we currently do not know the full extent of our capabilities to handle ammunition at ports around the world in compliance with the explosives safety standards. The extent of violations and exposures must be defined and then result in plans being developed for violation resolution.

Slide #6

In November 1988, the Director of the Army Staff directed the Port Study. The Deputy Chief of Staff for Logistics action was related to the Assistant Secretary of the Army (Installations, Logistics, and Environment) approval of an exemption for the Port of Nordenham, Germany. This was to operate in violation of the Department of Defense standards. Alternatives to Nordenham were to be pursued.

Slide #7

To accomplish the Director of Army Staff directive, a working group was established and has proceeded to accomplish the study. In March 1989, Lieutenant General Kicklighter, then the Director of Army Staff, was provided a briefing on the methodology and plan. He approved the proposed action plan. Working in parallel with this study of peacetime port capabilities, the Army Deputy Chief of Staff for Logistics was directed to identify wartime contingency port capabilities.

Slide #8

This slide shows the list of commercial ports that the Military Traffic Management Command has identified as being used for peacetime movements of ammunition over the past five years. Those with check marks we have either visited or have detailed exemption request information on. This list continues to be refined and enlarged.

Slide #9

In addition to the commercial ports, we have been directed to do special studies of the military facilities shown here. This, except for Chinhae, is in relationship to PREPO activities, which I'll discuss in more detail as we proceed.

Slide #10

This slide and the following slide show our action plan and the milestones established. We have had several onsite visits and two in-process-review meetings to adjust and revise the plan as necessary. It could, and probably will, change again.

Slide #11

We are currently in the process of collecting site-specific information concerning tonnages, frequency of use, vessels used, the vessels' load configurations, port area property, and population statistics. As I stated previously, we must define capabilities and exposures and then have plans to resolve the problem areas.

Using the information gathered, a technical assessment of each port is conducted. This identifies port capabilities, the net explosive weights being introduced, and the resulting exposures. Once defined, we will be looking at feasible alternatives to control the maximum credible event or, possibly, mitigate the effects of an explosion within a ship or at the immediate area dockside. This approach was accomplished by a special interservice working group for the Port of Hachinohe, Japan, and I'll discuss that action in more detail in a few moments.

Slide #12

First, I'll run through specific onsite surveys to give you a clear perception of the broad scope of our problems. We have exposures and situations at our military terminals in the U.S. which we address using military waivers and exemptions.

Slide #13

The Port of Valdez, Alaska, shown here, is a commercial port and the only one having an approved DDESB site plan. It is limited to the small quantity of 190,000 pounds net explosive weight. It is used by the Army's Western Command to service installations in Alaska.

Slide #14

Even our Military Ocean Terminal at Sunny Point does not meet all requirements. The main ship channel is at less than the required distance and contingency loading of the wharves would result in exposures across the Cape Fear River.

Slide #15

This is an aerial view of the three 2,000-foot wharves at Military Ocean Terminal, Sunny Point, south to north, each with a peacetime limit of six million pounds net explosive weight.

Slide #16

This slide shows, in orange, the expansion across the Cape Fear River of the quantity distance zone when the loads go up to the 19 million pounds range during contingency. An Army exemption is under review at Military Traffic Management Command and Headquarters, Department of the Army to address these exposures.

Slide #17

I mentioned earlier the Army exemption for Nordenham Port, Germany.

Slide #18

Nordenham is currently the only port used to move ammunition in and out of north central Europe. It operates under an Assistant Secretary of the Army (Installations, Logistics, and Environment) 1988 exemption. This is due to the close proximity of the Village of Nordenham and 30,000 inhabitants.

Slide #19

You can see the village in this slide. Ammunition is downloaded onto railcars and moved down-country. The use of MILVANS and ISO containers expedites the process and reduces the exposure time. The original Director of the Army Staff directive and the exemption approval relates to the Army Deputy Chief of Staff for Logistics and U.S. Army, Europe continuing to pursue alternative ports.

Slide #20

Ports, such as Eemshaven in the Netherlands, have accommodated past test shipments of ammunition into Europe and have limited exposures. We visited this port in April 1989.

Slide #21

This is a picture of the ship-berthing area at Eemshaven.

Slide #22

We have visited Central America where, in Panama, the Army uses Mindi Pier on the Panama Canal.

Slide #23

Exposures result to ship traffic, as well as the canal railroad. The pier is operated under waiver due to the limited capability.

Slide #24

This picture shows the close proximity of the shipping to the pier area. Alternatives to Mindi Pier are being reviewed and, in the interim, U.S. Army South is considering an exemption request.

Slide #25

We have traveled to Japan on several occasions to survey ports there. I'll first discuss Hachinohe Port, which I mentioned earlier received a special interservice working group evaluation based on a DDESB survey in 1987.

Slide #26

Hachinohe Port is in northern Japan and has only a capability from an explosives safety standpoint, due to exposures to the surrounding area, of handling 40,000 pounds net explosive weight. The DDESB survey in 1987 resulted in an effort to define a plan to handle three shiploads of mark 80 series high explosive bombs, cluster bomb units, and 20mm in the safest manner possible. The S.S. Dawn was to be used for all three shipments from Okinawa to Japan. An Interservice (Army, Navy and Air Force) working group prepared a specific pre-stow and port discharge plan to be used. Military Traffic Management Command engineers and stowage planners assisted explosives effects researchers and explosives safety specialists in the preparation.

Slide #27

The result was a stowage plan for the S.S. Dawn, as shown on this slide. Using the test data from the U.S. Air Force buffered storage tests for Mark 80 Series bombs, the group provided a technical concept that, in the opinion of the group, should provide for a reduction in and the control of the maximum credible event should a detonation occur onboard the vessel or at dockside. Of course, strict implementation of the plan was required to assure maximum credible event control could be realized.

Slide #28

The buffered configuration was considered to relate to a maximum credible event of 80,000 pounds net explosive weight (considering the worst case of 40,000 pounds bomb stack and 40,000 pounds cluster bomb units). This slide depicts, in yellow, the quantity distance zone reduction relative to the orange 890,000 pounds zone. This plan was used for the three ships. It is an approach we'll be looking at in other areas based on our study findings. One must, however, remember it was specific to one ship, a limited number of munition items, and testing of bombs.

Slide #29

I mentioned earlier we were tasked to review military facilities used to download and handle ammunition from the Army's PREPO during maintenance cycles. Specifically, Hiro and Akizuki, Japan, facilities. Hiro and Akizuki facilities are geographically located approximately 450 miles southwest of Tokyo, Japan, near the city of Hiroshima. The facilities are the responsibility of 83d Ordnance Battalion, headquartered at Kure, Japan. We are dealing with net explosive weights (worst case) of close to 10 million pounds onboard one vessel. The concern, of course, is doing it safely with the least possible exposures.

Slides #30 & 31

These slides show the ship with individual barges both below and above deck. The ships have tugs onboard which are lower and used to move the barges from the ship to shore. (Slide) In the past, operations were conducted at Subic Bay, Philippines, and resulted in minimal exposures. Political realities in that part of the world have resulted in the Army looking for alternative locations. (Slide) The first operations outside Subic were conducted in Japan and resulted in much greater exposures raising concerns by the DDESB and requiring thorough evaluations by the Army.

In March 1989, a Headquarters, Department of the Army Task Force Team was organized and directed by the Director of the Army Staff to make PREPO operations a priority in the worldwide ammunition port study. In part, to review the U.S. Army, Japan, request for an Assistant Secretary of the Army (Installations, Logistics, and Environment) letter of certification to allow construction at Hiro facility, Japan, in violation of the Department of Defense explosives safety standards.

Slide #32

This is an aerial view of Hiro facility in red.

Slide #33

Hiro was developed during World War II as a Japanese underground manufacturing and test complex for seaplane engines. The configuration currently used by U.S. Army, Japan for ammunition operations at Hiro includes two concrete piers, large hardstand areas, and three caves. Included also at Hiro is a surveillance workshop and inert warehouses. Hiro is surrounded by villages totaling in population of approximately 25,000. In addition, the Toyo pulp plant is located in close proximity and operates with 450 employees. From an explosives safety standpoint, there is no capability to handle 1.1 munitions at Hiro facility. It operates under major Army command waiver.

Slides #34, 35, & 36

This is a view overlooking the main cave, used for storage, and the hardstand, which is directly in front and which was used to lay down PREPO ammunition. The pulp plant and other industries are directly across the water. (Slides 35 & 36) These slides show the front of the cave and inside the cave complex.

Slide #37

This is an aerial view of the Akizuki Depot Complex in red. Akizuki Depot was a World War II Japanese Naval ammunition storage area designed to store torpedoes. Akizuki Depot is on the small island of Eta Jima, with population concentrations on each end of the installation. At the north, or top, of the red area is Koyo, a village of 2,481 people. At the south end is Akizuki, a village of 916 people. The configuration for storage includes 19 caves, 14 aboveground magazines, 3 inert warehouses, 2 open storage sites, 2 barge loading piers (3 and 4), and a wharf at each end of the area capable of barge handling. The caves vary in size, but basically average 200 feet in length, 40 feet in width, with chamber height varying from 20 to 25 feet.

Slide #38

Under normal U.S. Army, Japan operations, no Department of Defense Hazard Class/Division 1.1 ammunition is stored at Akizuki Depot. Based on the U.S. Army, Japan operational requirements, a comprehensive plan was defined by the Army task force to prescribe the safest conduct of PREPO operations consistent with mission requirements. Serious violations remained.

Slide #39

The search for alternative locations for PREPO continues. At the request of the Commanding General of the Army's Western Command in January of this year, the Headquarters, Department of the Army Worldwide Ammunition Port Study Team visited Tengan Pier; White Beach, Okinawa; Fleet Activity, Sasebo, Japan; and Apra Harbor in Guam. This was accomplished and a report prepared. I'll briefly discuss each location surveyed.

Slide #40

Okinawa is an island prefecture of the nation of Japan, located in the Ryukyu group, approximately 1,000 miles south of Tokyo. It is densely populated with over one million inhabitants residing primarily in its south and central regions. The island comprises approximately 454 square miles. The U.S. installations of all services occupy more than 20 percent of the island's area.

Tengan Pier, shown on this slide, operated by the Fleet Activity, Okinawa, is located on Kin Bay on the east side of the island. It is the primary ammunition pier for the island and routinely services U.S. Navy combatant and supply ships, as well as commercial breakbulk vessels. It is not now equipped to accommodate lighters, however Military Traffic Management Command, Okinawa, is interested in acquiring a fendering system which would allow use by barges/lighters. It operates under a Chief of Naval Operations waiver for 2.25 million pounds net explosive weight and event waivers for larger loads. It can handle around 70,000 pounds net explosive weight while meeting Department of Defense standards. The study team concluded that Tengan Pier, in combination with Kadena Munitions Storage Area, provides a potential for PREPO ammunition ship download with minimal exposures to property and people. The location has the potential to meet the Department of Defense/Army ammunition and explosives safety standards in all aspects except pier operations, which could be limited and controlled by operational considerations.

Slide #41

White Beach Naval Facility, located on Buckner Bay south of Tengan Pier and 10 miles from Kadena Ammunition Storage Area, consists of 2 piers. One, the U.S. Navy pier, is sited for 25,000 pounds net explosive weight. The other, the Army pier rebuilt in 1989, is designated as a petroleum, oils, and lubricants storage area. This and the congested traffic situation between the pier and the laydown area at Kadena Ammunition Storage Area precludes consideration of White Beach as a site for PREPO. The Navy indicated they could not accept an ammunition ship at White Beach. All such activities are sent to Tengan Pier.

Slide #42

Sasebo was visited also. It is operated by the Commander, Fleet Activities, Japan. It offers a definite laydown capability for PREPO. The ship anchorage operates under Chief of Naval Operations waiver. Using a well-defined operational plan, the anchorage could be the only area at Sasebo that a PREPO operation would create exposures beyond the maximum allowed by the Department of Defense/Army ammunition and explosives safety standards. Exposure would be limited to the time the ship is downloading and uploading barges. The Navy provides event waivers for such violations and has handled ships with heavier loads than Army PREPO. Beyond the ship anchorage, explosives safety considerations could be met in most all aspects of the operation.

Slide #43

Hario-Shima Ordnance Facility offers very calm waters in the adjacent bay with an area large enough to accommodate the necessary barge holding areas.

Slide #44

The Ordnance Facility operates under Chief of Naval Operations waiver due to the 1.2 million pounds net explosive weight required for Navy operations at this wharf. The PREPO barge operational requirements could limit this to much less net explosive weight and meet the explosives safety requirements. The potential for ammunition laydown in the Hario-Shima Ordnance Facility would exceed a total PREPO ship laydown and still meet the intent of the Department of Defense/Army ammunition and explosives safety standards.

Slide #45

The next area to discuss is Guam. The island of Guam is a U.S. territory located at the southern tip of the Marianas chain. It is approximately 212 square miles in size. It is the site of the westernmost ammunition supply point on U.S. soil lying 1,200 miles east of Manila and 1,250 miles southeast of Okinawa. The island receives nearly all of its commercial goods through this Apra Harbor that you see here via container ships. These arrive on the average of once per day. Other routine ship traffic in the harbor consists of fishing craft and those bring the ship count to approximately nine per day. Guam is a viable alternative for PREPO ammunition operations. There would be violations to the Department of Defense/Army ammunition and explosives safety standards when a ship entered the Apra Harbor and when barges are anchored in the harbor area. Looking north, shown here, is a Navy maritime prepositioned ship anchored. The Army PREPO vessels, upon anchoring there, would expose in varying degrees personnel associated with the Naval Station, the commercial port facilities, and the shipping channel.

The initial exposure caused by the arrival of the ship at anchorage would rapidly decrease as the barges are downloaded and tugged to holding areas along the Glass Breakwater on the northwest end of the harbor. Three to four days should suffice for ship offloading and again at the end of the operation for uploading. Exposures from the anchorages, for both the mother ship and for nested barges, would require identification and acceptance under current DOD criteria. Anchorages cannot be established outside the harbor due to extremely deep water and rough sea conditions. Consideration can also be given to the Naval Station "typhoon-proof" housing techniques in applying standard quantity distance principles of blast overpressure protection from the PREPO operations in Apra Harbor. The U.S. Navy, U.S. Air Force, and U.S. Coast Guard operate facilities on Guam, which also serves as the site of Headquarters, U.S. Naval Forces, Marianas.

Slide #46

Looking south on Apra Harbor here, the team identified that an operational plan could limit the exposure to the time the ship is downloading or uploading barges. Operations with barges at Kilo wharf would be subject to variable sea swells and wind conditions. Swells of 6-8 feet are common 20 percent of the year. Once offloaded, ammunition laydown areas and maintenance and inspection facilities could be provided at Orote Point and Andersen Air Force Base, in compliance with explosives safety requirements.

Slide #47

The Army did conduct PREPO download operations in May and June of this year using facilities at both Fleet Activity, Sasebo, and Akizuki/Hiro Facilities in Japan under strict operational controls. The review and search for alternative locations to improve PREPO explosives safety will continue.

Slide #48

The last port I'll discuss is Chinhae, Korea. It is the sole peacetime port for the import and export of U.S.-titled ammunition arriving in or departing from Korea.

Slide #49

The Headquarters, Department of the Army Task Force Survey Team went to Korea in October 1989. Operations reviewed included the ammunition pier at Chinhae, its support facilities, and the Ducksan Rail Switching Yard. The pier at Chinhae Port operates under an Eighth U.S. Army three million pound waiver. This quantity is based on operational considerations and does not relate to explosives safety limitations required by the DOD standards. The pier is used for five to seven ammunition ships each year.

Slide #50

An on-the-ground survey at the pier, interviews with operating and planning personnel in Korea, and a preliminary map reconnaissance of the area adjacent to the pier determined that exposures were beyond the maximum allowed by the Department of Defense ammunition and explosives safety standards to protect surrounding civilian populations. Exposures exist for quantities of ammunition above 440,000 pounds net explosive weight. Based upon a maximum credible event of three million pounds net explosive weight, Eighth U.S. Army estimates that approximately 1,300 civilian personnel and property valued at over twenty-four million dollars is hazarded in varying degrees. Ammunition is discharged from a breakbulk vessel alongside the pier and placed on the pier for arrangement into carloads.

Slide #51

It is then loaded into open-top gondola cars, blocked and braced, tarped, and moved off the pier to the Ducksan Switching Yard. There, trains are assembled for movement north to storage sites. Container handling capability is not available at Chinhae. A Military Traffic Management Command port analysis indicates that the operating space available at the pier would not accommodate container handling equipment. An Army exemption is currently under review at Headquarters, Department of the Army to acknowledge operations at Chinhae in violation of the DOD standards. There is currently being worked by USFK, a plan to modernize this pier - lengthen, widen, and provide for container handling.

Slide #52

In conclusion, the inability to move munitions through commercial and military ports worldwide and meet the Department of Defense explosives safety standards is recognized. Eventual correction or resolution of all violations

is a long-term goal. This study is to establish the port capabilities and limitations, to identify alternate ports for possible use, and establish the maximum credible event for a typical shipload to identify the potential explosives effects on the individual port and surrounding area should a detonation occur. Also, ways to control or limit the maximum credible event aboard an ammunition ship are to be defined. Ways may include:

- (a) Improved containerization/packaging.
- (b) Ammunition load configuration aboard ship (spacing, buffering/shielding).
- (c) Application of insensitive high explosives.

Slide #53

That concludes my presentation. Thank you for your attention. Should you like more information or have information or activities ongoing in your organizations that relate to this effort, please contact us at the address/phone numbers shown on this slide.

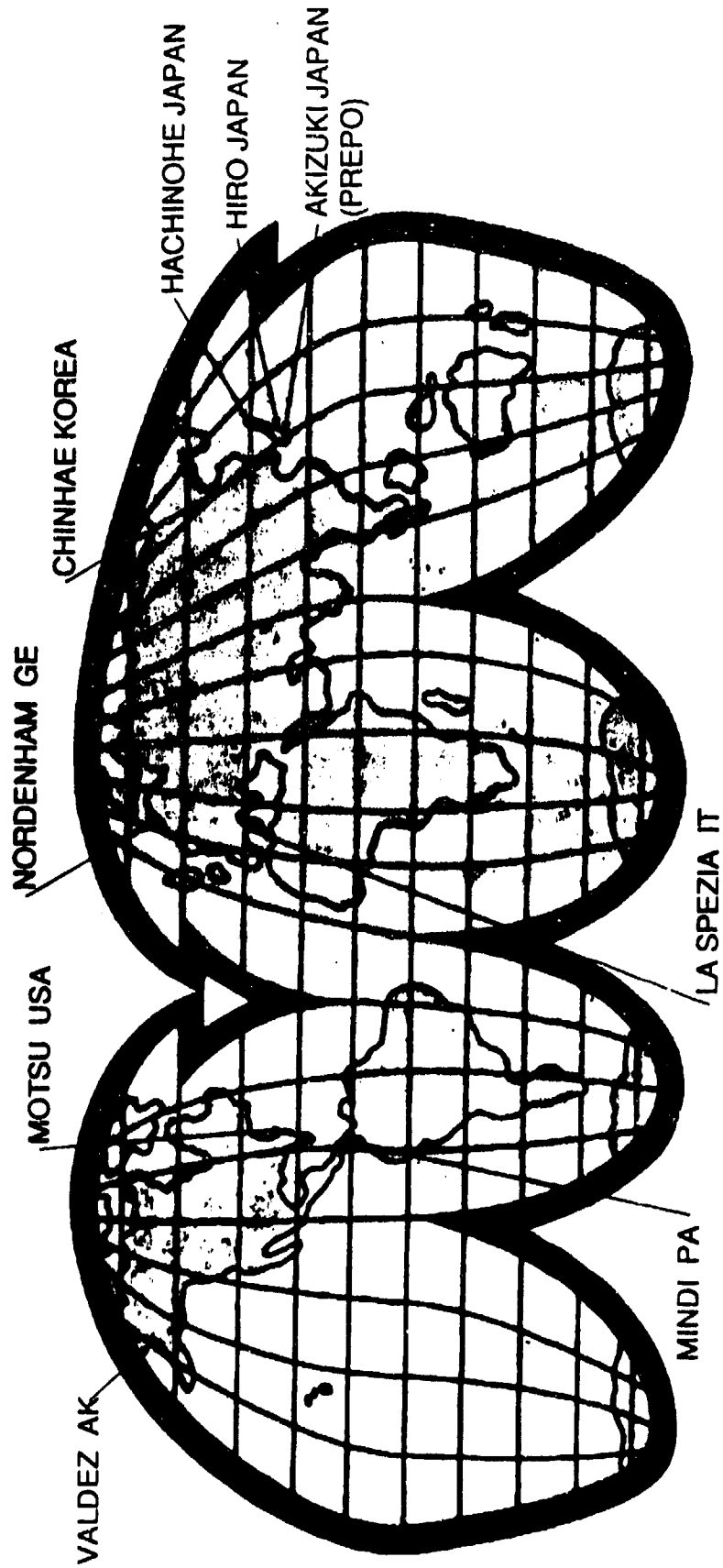
Thank you.

WORLDWIDE PORT STUDY

OUTLINE

- **INTRODUCTION**
- **HISTORICAL CONCERNS**
- **PURPOSE**
- **METHODOLOGY**
- **ACTION PLAN**
- **SURVEYS**
- **CONCLUSION**

WORLDWIDE PORTS OF INTEREST



1957

WORLDWIDE PORT STUDY

- HISTORICAL CONCERNS

- 1917 - HALIFAX, NOVA SCOTIA

- SHIP WITH 5 MILLION POUNDS TNT, GUN COTTON, AND PICRIC ACID
 - 1800 KILLED, 8000 INJURED, SEVERE DAMAGE

- 1944 - PORT CHICAGO, CALIFORNIA

- AMMO SHIP AND RAILCARS EXPLODED (3.5 MILLION POUNDS) RESULTED IN 320 DEATHS AND EXTENSIVE DAMAGE

(THIS DISASTER IS PRINCIPALLY RESPONSIBLE FOR PRESENT DAY DOD STANDARDS FOR PIERS AND WHARVES)

- 1947 - TEXAS CITY, TEXAS

- SHIP INVOLVING 7 MILLION POUNDS OF AMMONIUM NITRATE EXPLODED, 561 DEATHS, 3000 INJURIES AND MAJOR DAMAGE OUT 7000 FEET

WORLDWIDE PORT STUDY

- **PURPOSE**

- **TO IDENTIFY CAPABILITIES TO HANDLE MUNITION SHIPMENTS AND THE EXTENT OF VIOLATIONS/EXPOSURES AT ALL PORTS USED BY THE DEPARTMENT OF DEFENSE**
- **TO DETERMINE WAYS OF EVENTUAL CORRECTION OR RESOLUTION OF THE IDENTIFIED VIOLATIONS**

WORLDWIDE PORT STUDY

- **DIRECTOR OF THE ARMY STAFF DIRECTED THE STUDY - NOV 88**
- **ARMY DEPUTY CHIEF OF STAFF FOR LOGISTICS INITIATE ACTION TO STUDY ALTERNATE PORTS FOR SHIPPING AMMUNITION TO EUROPE**
- **ARMY EXECUTIVE DIRECTOR FOR EXPLOSIVES SAFETY ASSESS AMMUNITION PORTS WORLDWIDE TO ESTABLISH MAXIMUM CREDIBLE EVENTS (MCE) FOR TYPICAL SHIPLOADS AND IDENTIFY EXPLOSION EFFECTS**

WORLDWIDE PORT STUDY

- **METHODOLOGY**
 - **WORKING GROUP ESTABLISHED (HQDA, MTMC, EDES)**
 - **STUDY CONCEPT**
 - **ACTION PLAN**
- **RELATED ACTION**
 - **ARMY DEPUTY CHIEF OF STAFF LOGISTICS TASKED THE VARIOUS COMMANDERS IN CHIEF TO IDENTIFY CONTINGENCY PORTS**

WORLDWIDE LIST OF COMMERCIAL PORTS

ZEEBRUGGE BE	ROOSEVELT ROADS PR
GUANTANAMO BAY	ROTO SP
ACAJUTLA ES	BANGKOK TH
NORDENHAM GE	SATTAHIP TH
BREMERHAVEN GE	TUNIS TU
WILHELMSHAVEN GE	DERINE TK
THESSALONIKI GR	IZMIR TK
GUAM ISLAND	ISKENDERUN PORT TK
TOMBOLO DOCK IT	ISKENDERUN ANCH TK
LA SPEZIA IT	GLEN DOUGLAS UK
AUGUSTA IT	NEWPORT UK
HIRO JA	BARRY UK
HACHINOHE JA	ROYAL PORTBURY UK
YOKOSUKA JA	FELIXSTOWE DK UK
KURE JA	FELIXSTOWE UK
SASEBO JA	SOUTHAMPTON UK
CHINHAE ROK	✓ VALDEZ US
EEMSHAVEN NE	✓ WHITTIER US
TRONDHEIM NE	PEARL HARBOR US
HAMMERNESODDEN NO	✓ SUNNY POINT US
STEINVIC NO	CONCORD US
✓ VALNESETT NO	
NAHA OK	
MINDI PIER PA	
SUBIC BAY PI	
LISBON PO	

WORLDWIDE PORT STUDY

MILITARY PORTS/FACILITIES SURVEYED

- **HIRO, JAPAN (ARMY)**
- **AKIZUKI, JAPAN (ARMY)**
- **SASEBO, JAPAN (NAVY)**
- **WHITE BEACH AND
TENGAN PIER, OKINAWA, JAPAN (MTMC/NAVY)**
- **CHINHAE PORT, KOREA (REPUBLIC OF KOREA ARMY)**

WORLDWIDE PORT STUDY

ACTION PLAN

<u>ACTION</u>	<u>ACTION AGENCY</u>	<u>MILESTONE</u>	<u>STATUS</u>
MINDI/RODMAN (PANAMA) SURVEY	#USATCES	FEB 89	.
EEMSHAVEN (NETHERLANDS) SURVEY	#USATCES	APR 89	.
IDENTIFY ALL PORTS USED FOR CLASS V SHIPPING (PEACETIME)	#MTMC	29 MAR 89	.
IDENTIFY AMMUNITION PORTS USED IN LAST TWO YEARS	#MTMC/USATCES	29 MAR 89	.
HIRO TASK FORCE	#USATCES/MTMC/DALO	24-30 JUN 89	.
JCS MESSAGE TO CINCS	#DALO	26 JUL 89	.
FIRST IPR	#USATCES/ALL	5 SEP 89	.
DETAILED QUESTIONNAIRE SENT TO CINCS	#DALO	9 JAN 90	.
CHINHAIE TASK FORCE	#USATCES/MTMC/DALO	23 OCT - 1 NOV 89	.
DA/WESTCOM TASK FORCE	#USATCES/DALO	20 JAN - 2 FEB 90	.
SECOND IPR	#USATCES/ALL	17 APR 90	.

(# LEAD AGENCY)

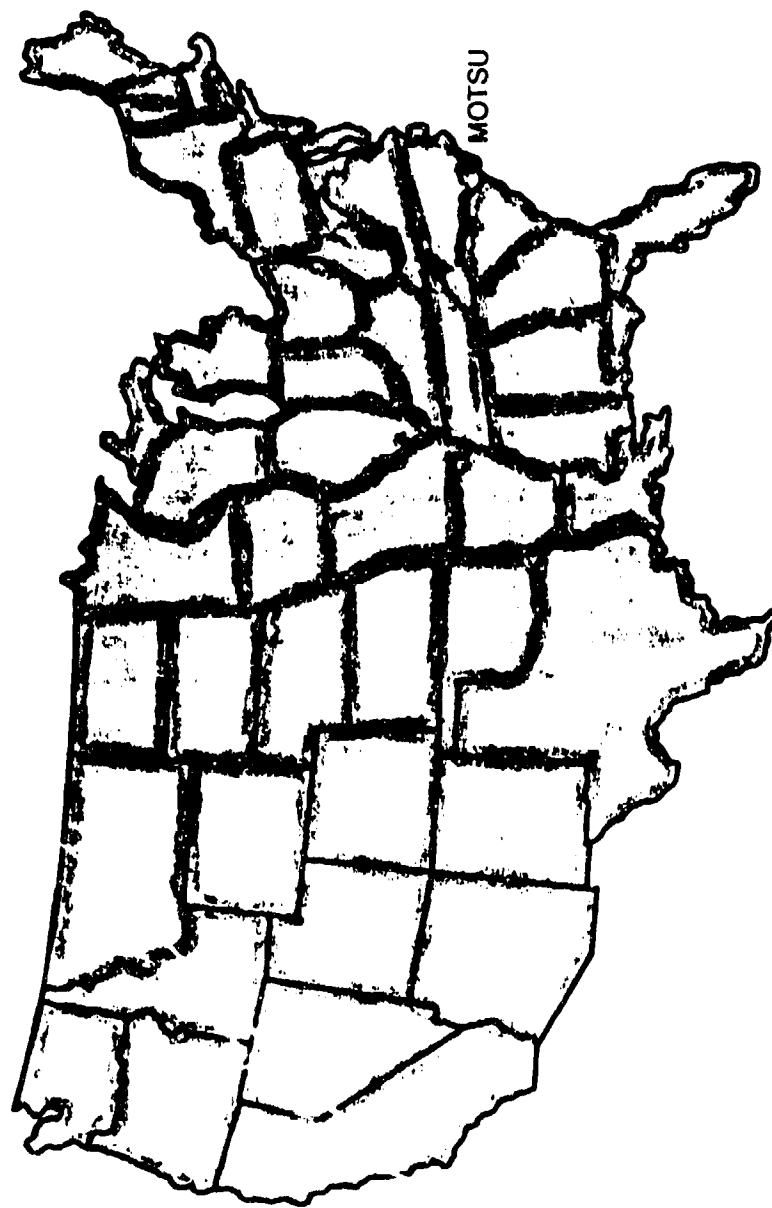
(. ACTION COMPLETE)

WORLDWIDE PORT STUDY

ACTION PLAN CONT.

<u>ACTION</u>	<u>ACTION AGENCY</u>	<u>MILESTONE</u>	<u>STATUS</u>
DALO FOLLOWUP W/CINCS	#DALO	10 MAY 90	
COLLECT SITE SPECIFIC PORT DATA			
--TONNAGES, FREQUENCY OF USE, VESSELS, LOAD CONFIGURATION	#MTMC/USATCES	30 MAY 90	
1--COLLECT SITE SPECIFIC DATA 2--DATA SET INFORMATION	#DALO	15 JUN 90	
DATA ANALYSIS	#USATCES	30 SEP 90	
PREPO CONSIDERATIONS	#USATCES/DALO	JUL - SEP 90	
THIRD IPR	#USATCES/ALL	OCT 90	
IDENTIFICATION OF MITIGATING/CORRECTIVE MEASURES/VISITS	#USATCES/ALL	OCT - DEC 90	
LAST IPR	#USATCES/ALL	FEB 91	
GENERATE/COORDINATE RESULTS	#USATCES/ALL	MAR 91	
PUBLISH REPORT/BRIEF DAS	#USATCES	APR 91	
(# LEAD AGENCY)			11

UNITED STATES



1966



1967

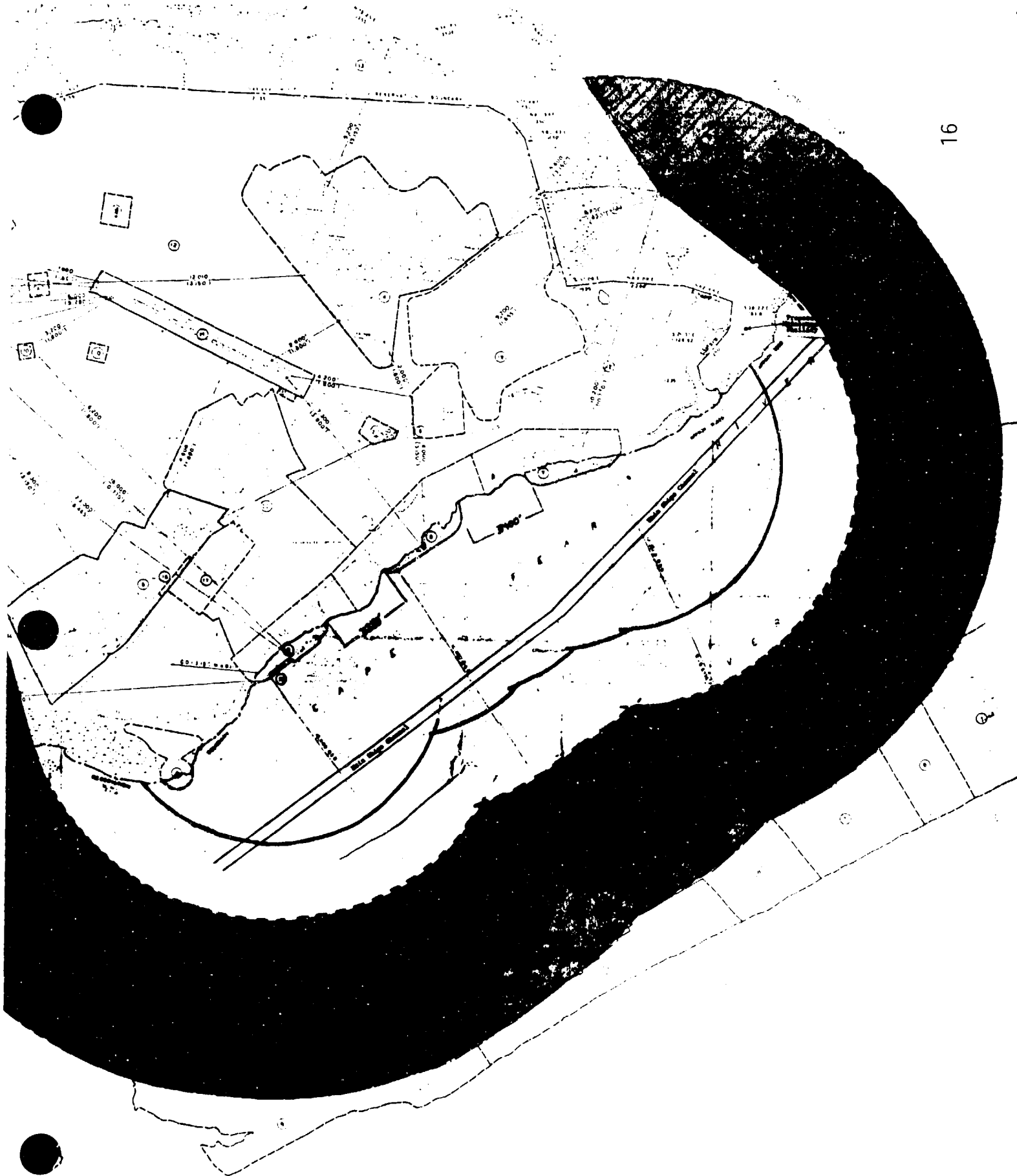
WORLDWIDE PORT STUDY

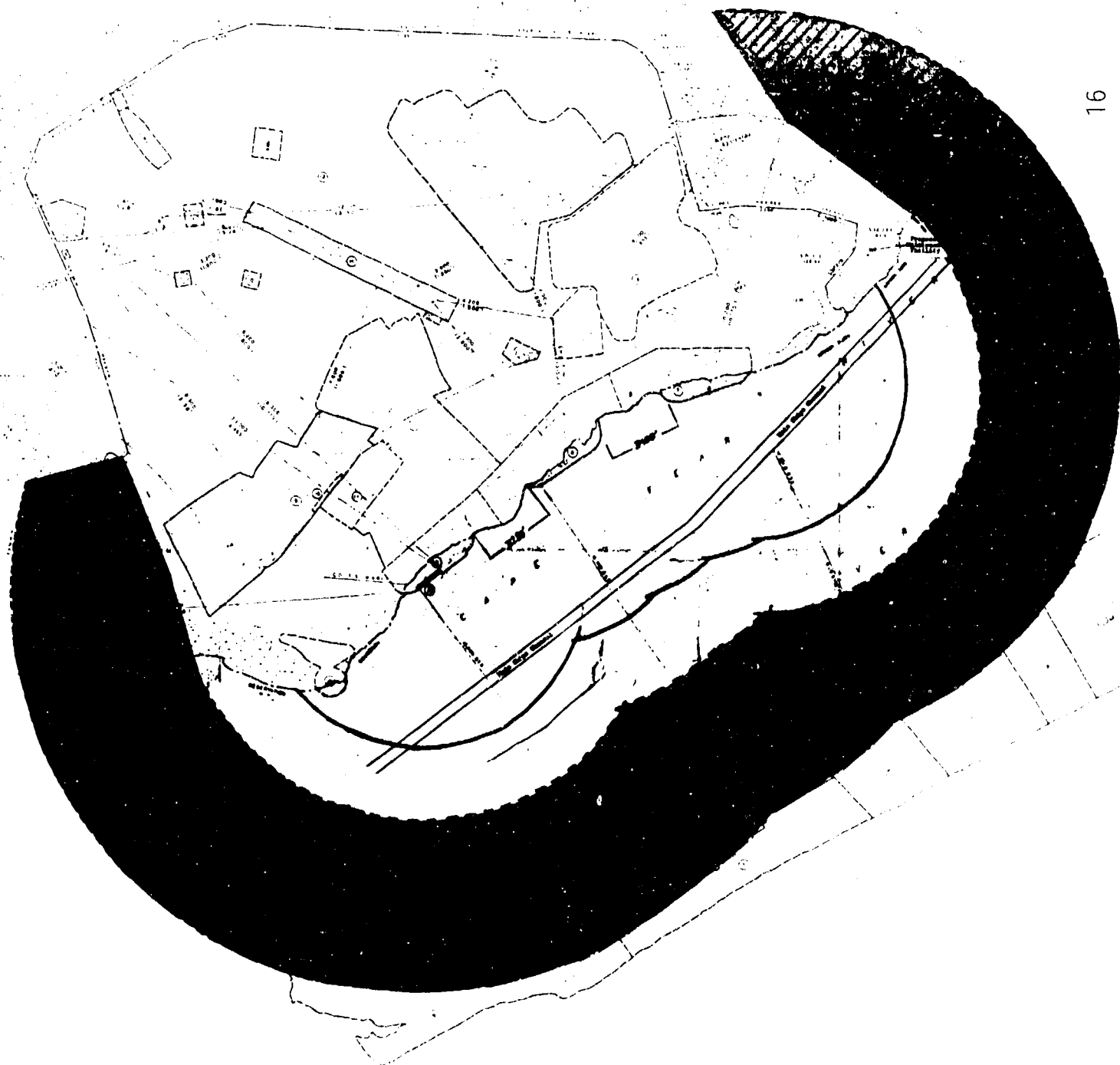
- MILITARY OCEAN TERMINAL SUNNY POINT (MOTSU)
 - MTMC TERMINAL ON THE CAPE FEAR RIVER, SOUTH PORT, NC
 - THREE 2000 FOOT WHARVES
 - PEACETIME LIMITATION APPROX 6,000,000 LBS NEW EACH WHARF
 - EXPOSES THE MAIN SHIP CHANNEL AT LESS THAN DISTANCE REQUIRED BY DOD STDS
 - CONTINGENCY NEW INCREASE TO 15,000,000 LBS NORTH TO 19,000,000 LBS SOUTH
 - EXPOSURE RESULTS TO FT FISHER, NC STATE FACILITIES AND HISTORICAL SITE
 - MTMC HAS REQUESTED AN ASA(IL&E) EXEMPTION TO OPERATE IN VIOLATION
 - IN PROCESS AT HQDA



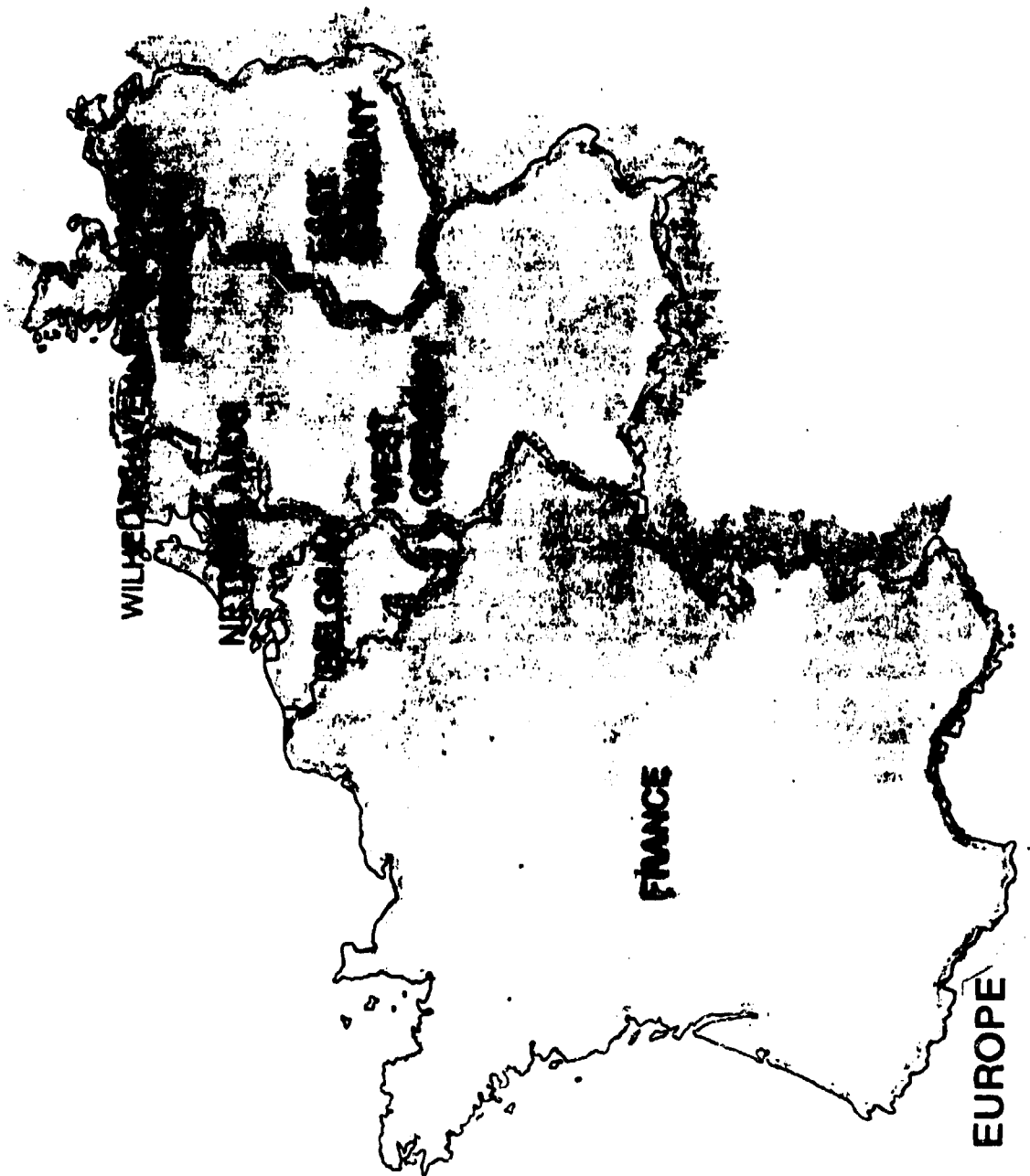
MILITARY OCEAN TERMINAL, SUNNY POINT







NORTH EUROPE

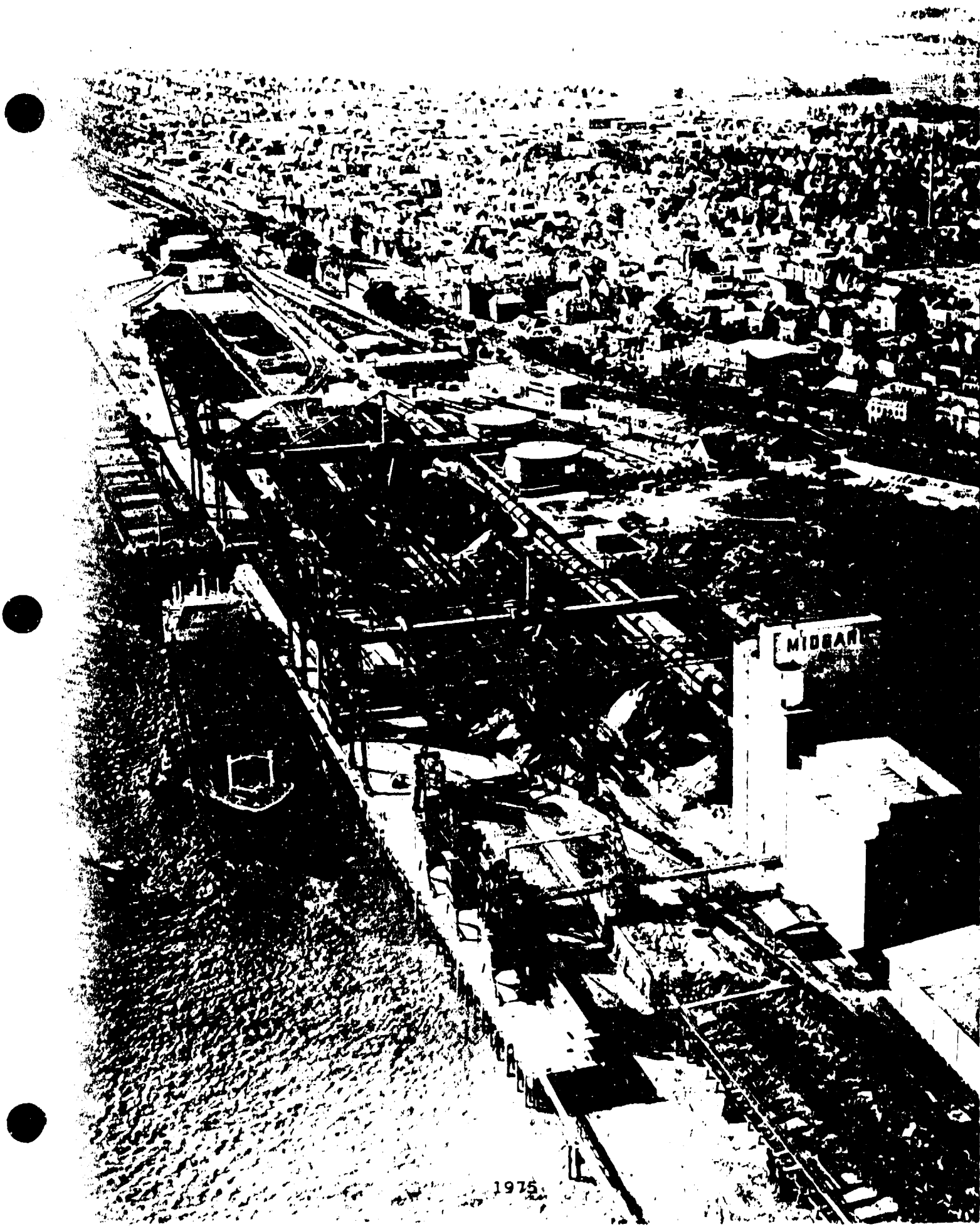


U.S. ARMY EUROPE

1973

WORLDWIDE PORT STUDY

- NORDENHAM, GE
 - COMMERCIAL PORT
 - ONLY PORT CURRENTLY USED FOR AMMUNITION INTO NORTHERN EUROPE
 - OPERATED UNDER AN ANNUAL WAIVER IN PAST
 - 3,000,000 LBS MAXIMUM NEW
 - ENDANGERS APPROXIMATELY 30,000 PEOPLE AND THEIR PROPERTY
 - ASA(IL&E) EXEMPTION PROVIDED IN SEP 66 (3 YEARS)



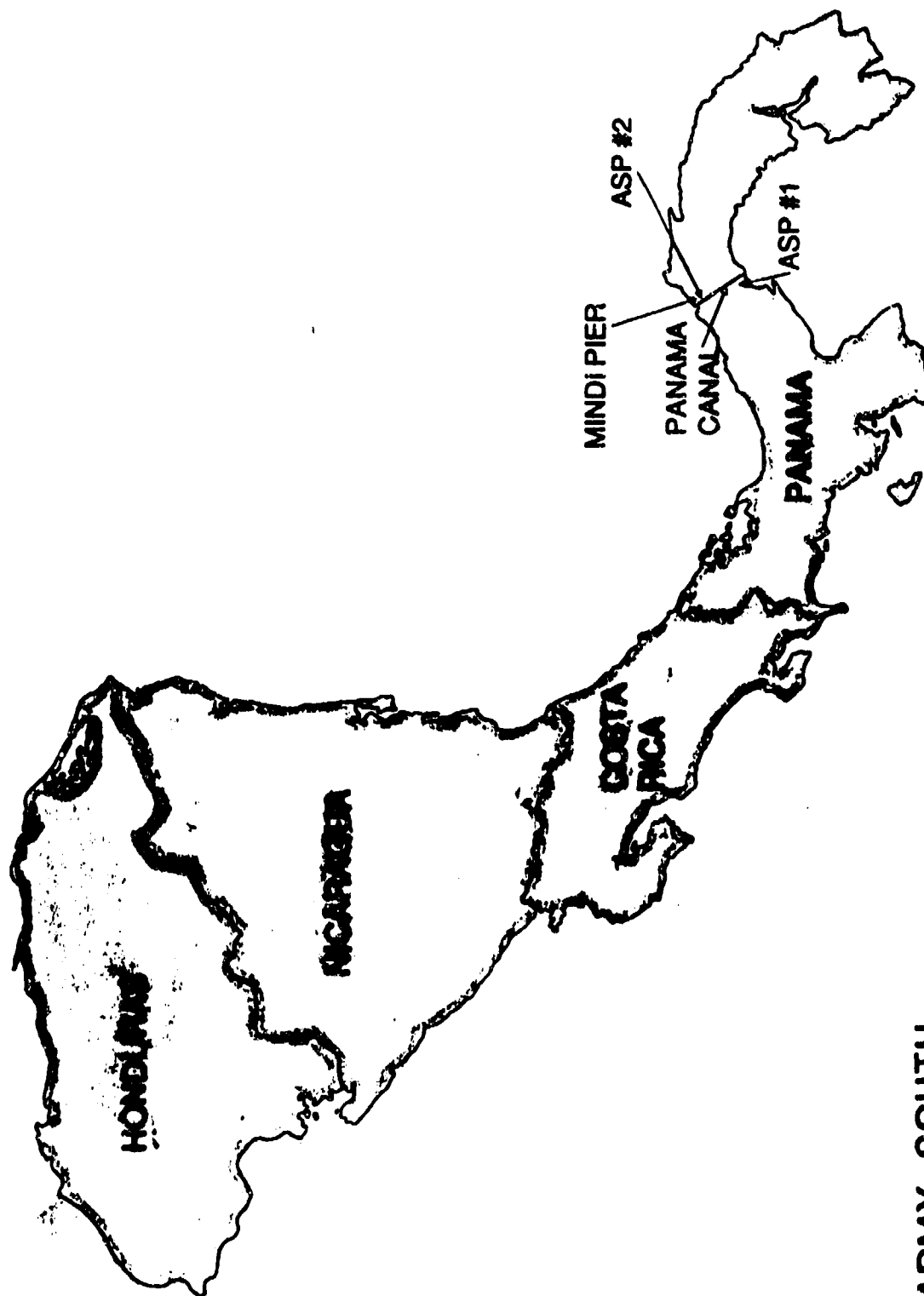
1975

WORLDWIDE PORT STUDY

- **EEMSHAVEN, NE**
 - **COMMERCIAL PORT**
 - **ACCOMMODATED TEST SHIPMENT OF AMMUNITION**
 - **LIMITED EXPOSURES**
 - **USAREUR ACTIONS TO DETERMINE FEASIBILITY**



CENTRAL AMERICA



U.S. ARMY SOUTH

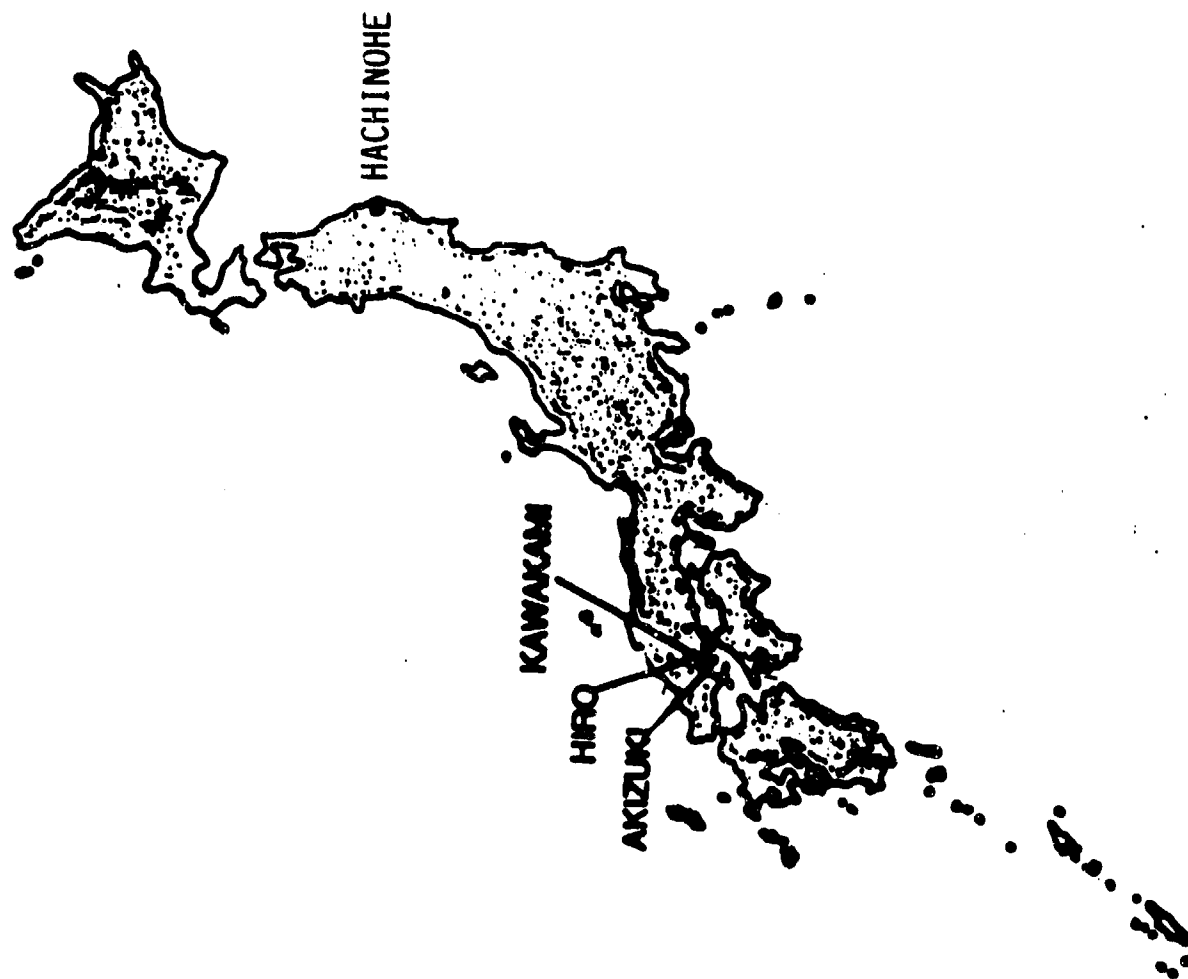
WORLDWIDE PORT STUDY

- **MINDI PIER, PANAMA**
 - **COMMERCIAL PORT**
 - **LOCATED ON THE PANAMA CANAL (ATLANTIC SIDE)**
 - **OPERATES UNDER A WAIVER**
 - **60,000 LBS NEW CAPABILITY**
 - **EXPOSURES ARE MAIN SHIP CHANNEL AND PANAMA CANAL RAILROAD**
 - **U.S. ARMY SOUTH IS CONSIDERING AN EXEMPTION REQUEST**



MINDI PIER, PANAMA

JAPAN



1981

U.S. ARMY JAPAN

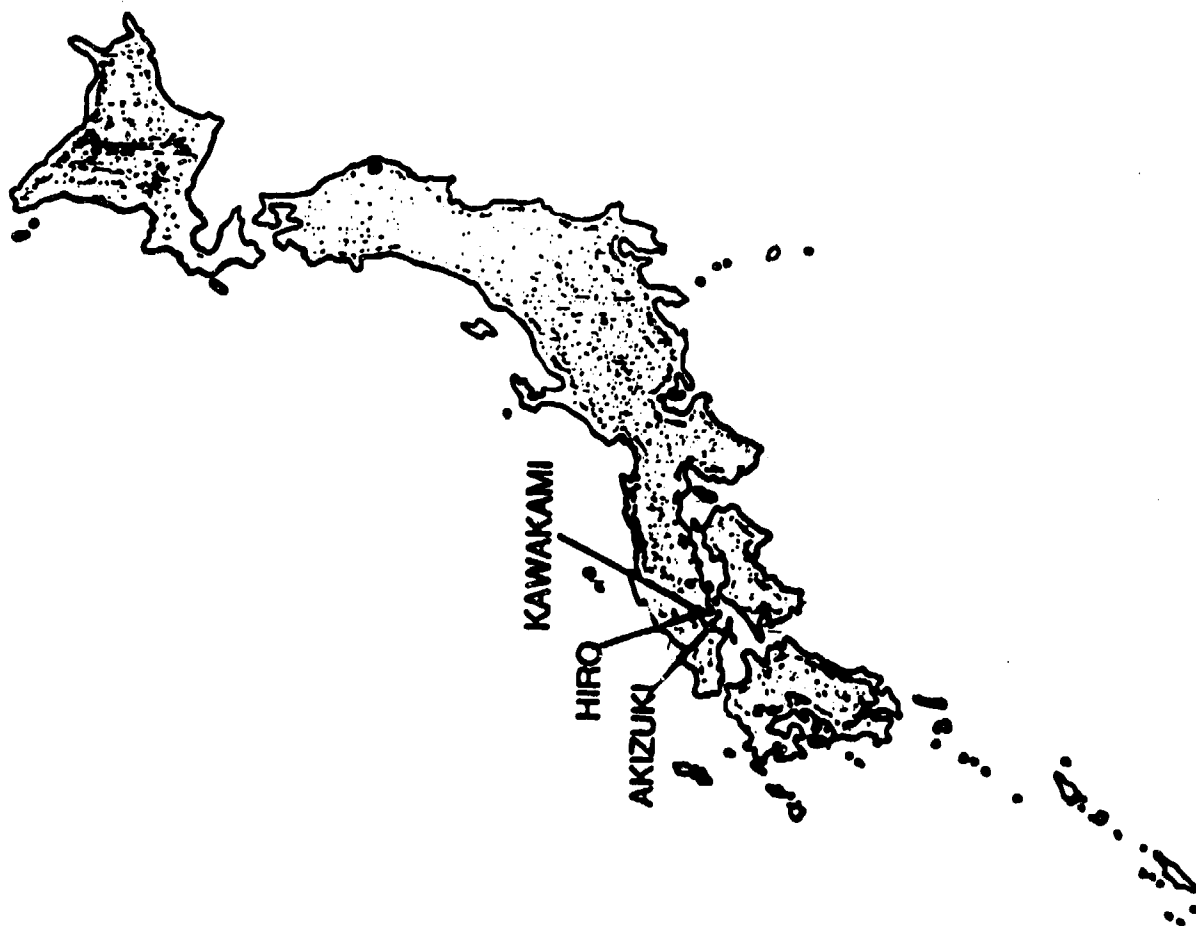
WORLDWIDE PORT STUDY

- **HACHINOHE PORT, JAPAN**
 - **COMMERCIAL PORT**
 - **DOD SURVEY 1987. 40,000 LBS NEW CAPABILITY (WHARF E)**
 - **COMMANDING GENERAL USARJ WAIVER 890,000 LBS NEW**
 - **3 SHIPLOADS, AIR FORCE BOMBS (SUPPLY MISAWA AIR FORCE BASE)**
 - **EXPOSURE TO HOST NATION POPULATION/FACILITIES**
 - **INTERSERVICE WORKING GROUP**
 - **BUFFERED CONFIGURATION**
 - **REDUCED MCE TO 80,000 LBS**

27

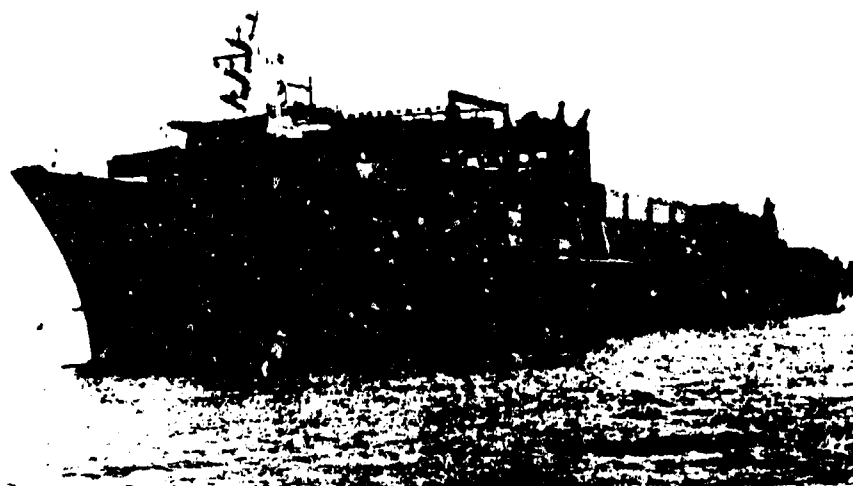
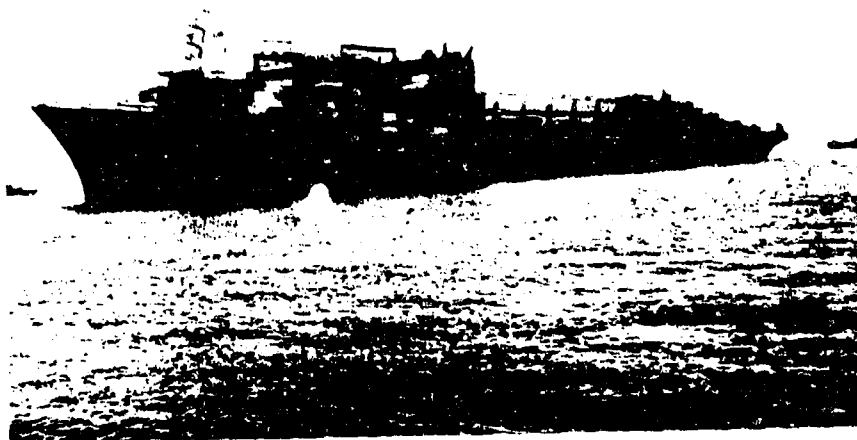


JAPAN



U.S. ARMY JAPAN

1985



1986

GREEN HARBOR



1987



HIRO STORAGE AREA

WORLDWIDE PORT STUDY

- **HIRO PIER, JAPAN**
 - **U.S. ARMY FACILITY**
 - **LOCATED APPROX 400 MILES SW OF TOKYO**
 - **AMMUNITION STORAGE LIMITED**
 - **LACK OF REAL ESTATE**
 - **PIER UNDER MACOM WAIVER**
 - **HQDA TASK FORCE TEAM EVALUATION OF PREPO OPERATIONS/ANCHORAGE**
 - **COMMANDER USARJ REQUEST FOR AN ASA(IL&E) CERTIFICATION FOR COMPELLING REASONS APPROVED AUG 89**



FROIT OF CAVE
HIRO



CAVE FRONT
HIRO



INSIDE OF CAVE
HIRO



WORLDWIDE PORT STUDY

- **AKIZUKI DEPOT COMPLEX, JAPAN**
 - **U.S. ARMY FACILITY ACROSS KURE BAY**
 - **LIMITED CAPABILITIES BASED ON EXPOSURES**
 - **VILLAGES, KOYO 2481 PEOPLE AND AKIZUKI 916 PEOPLE**
 - **WATER TRAFFIC IN KURE BAY**
 - **OPERATES UNDER MACOM WAIVERS**
 - **PREPO OPERATIONS**

WORLDWIDE PORT STUDY

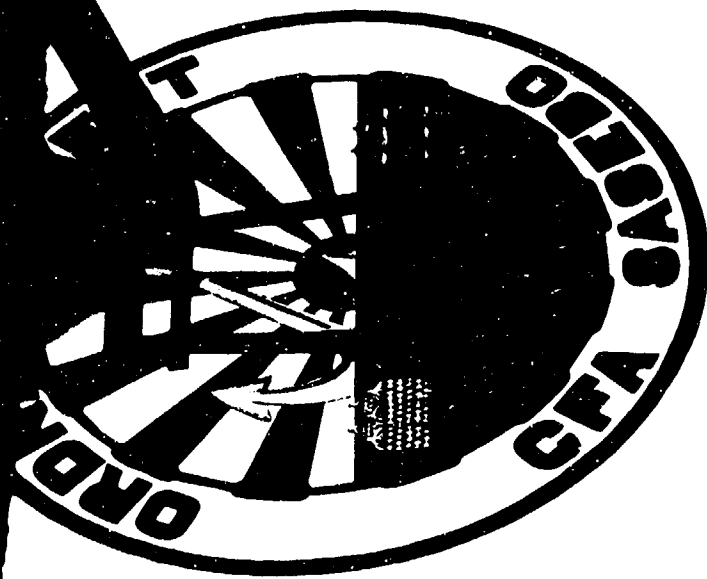
- **SEARCH FOR ALTERNATIVES FOR PREPO CONTINUED**
- **JAN 90 - CG WESTCOM REQUESTED HQDA SURVEY PORT FACILITIES ON:**
 - **OKINAWA**
 - **JAPAN**
 - **GUAM**

TENGAN PIER



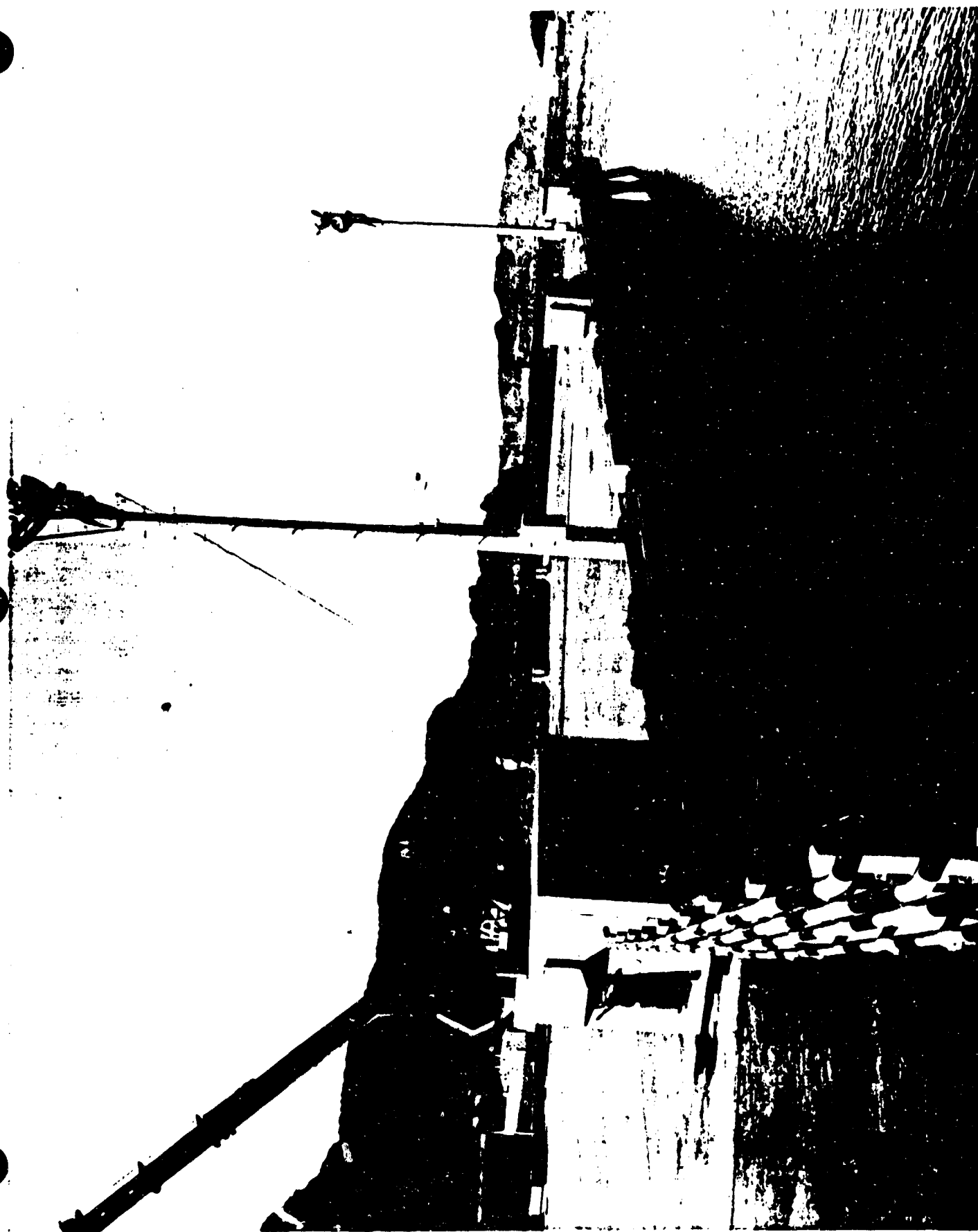
WHITE BEACH



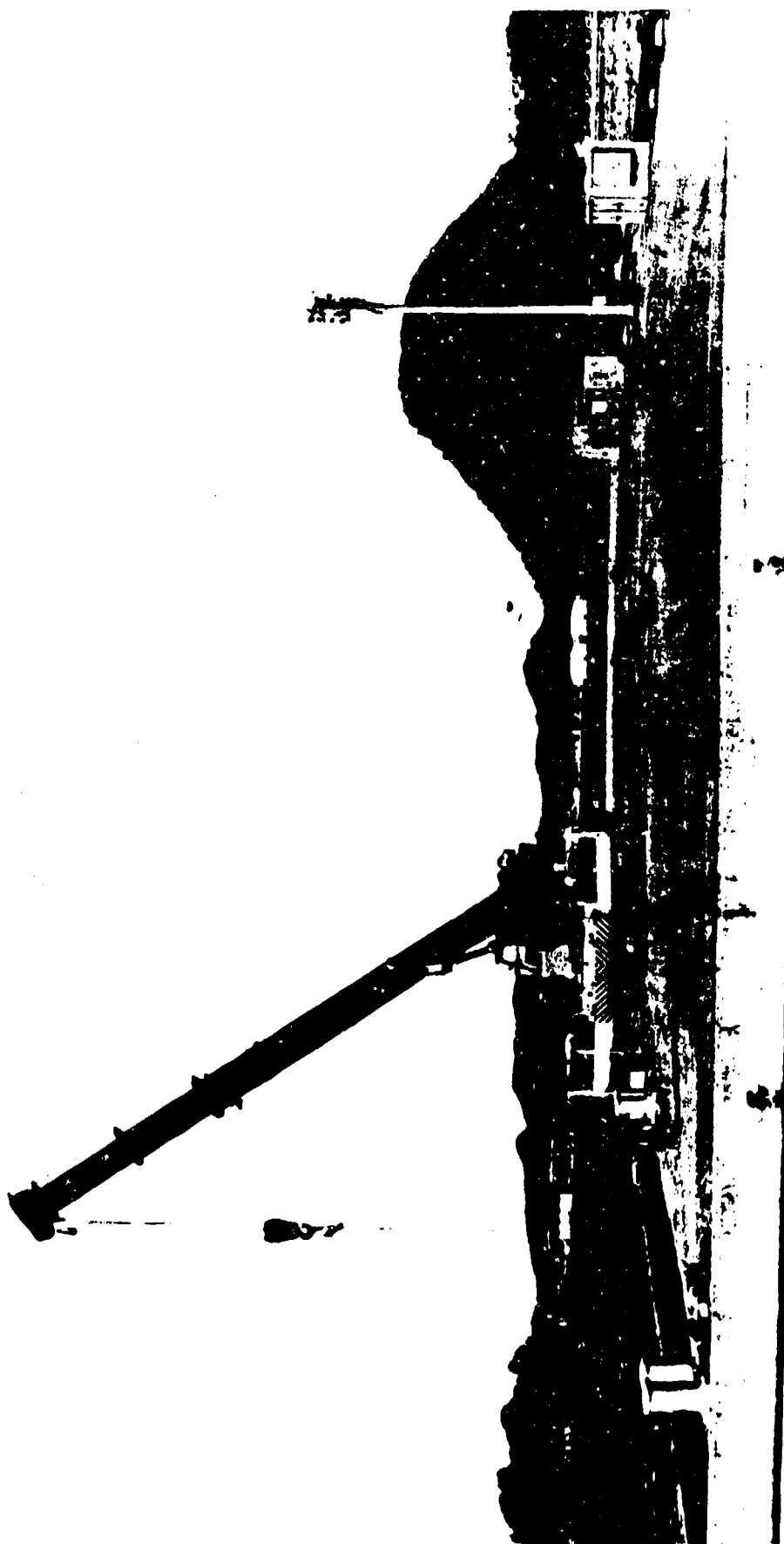


HARIO-SHIMA

IN CASE OF FIRE
火災通報は
CALL 117
FIRE STATION



1999

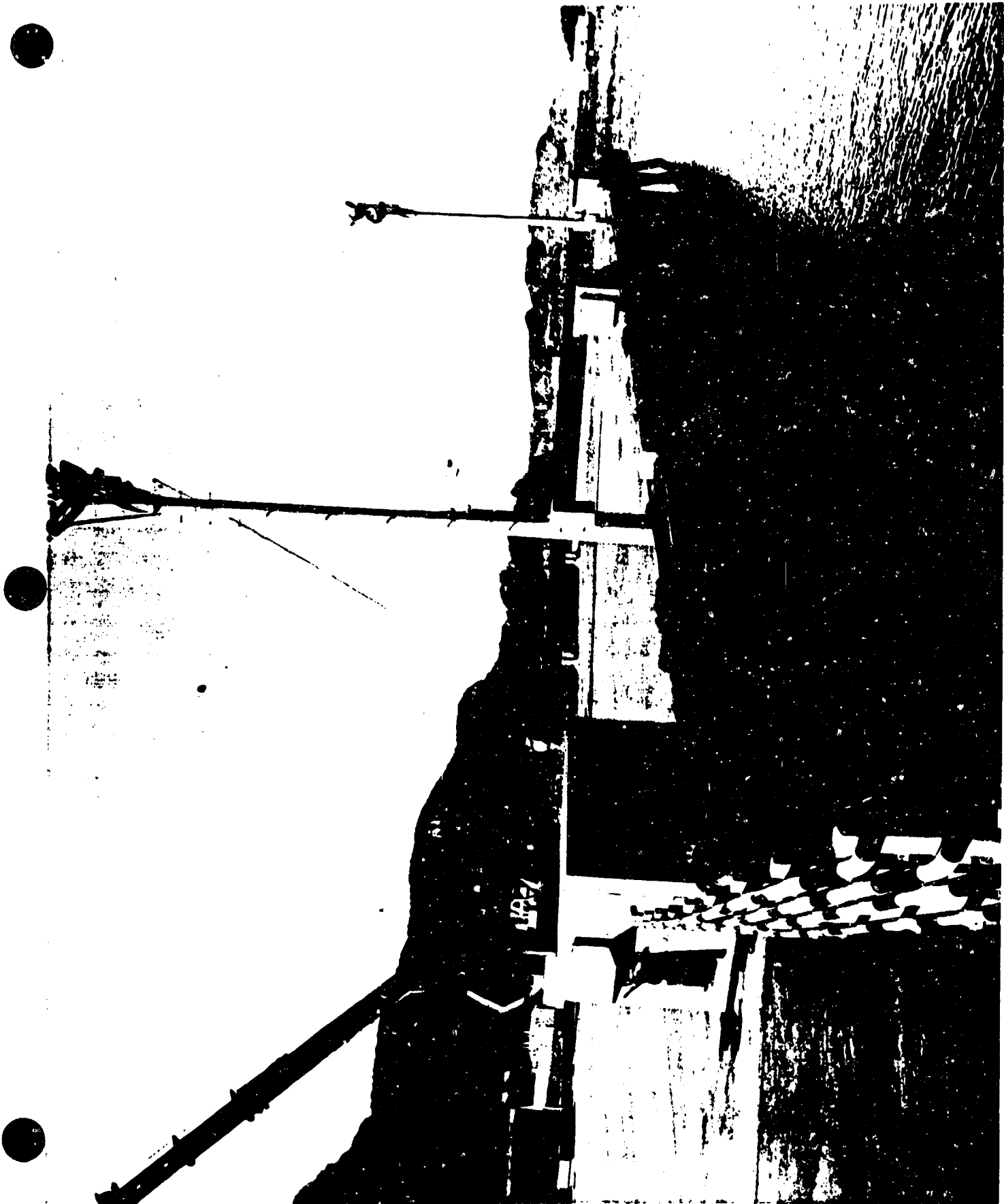


2000



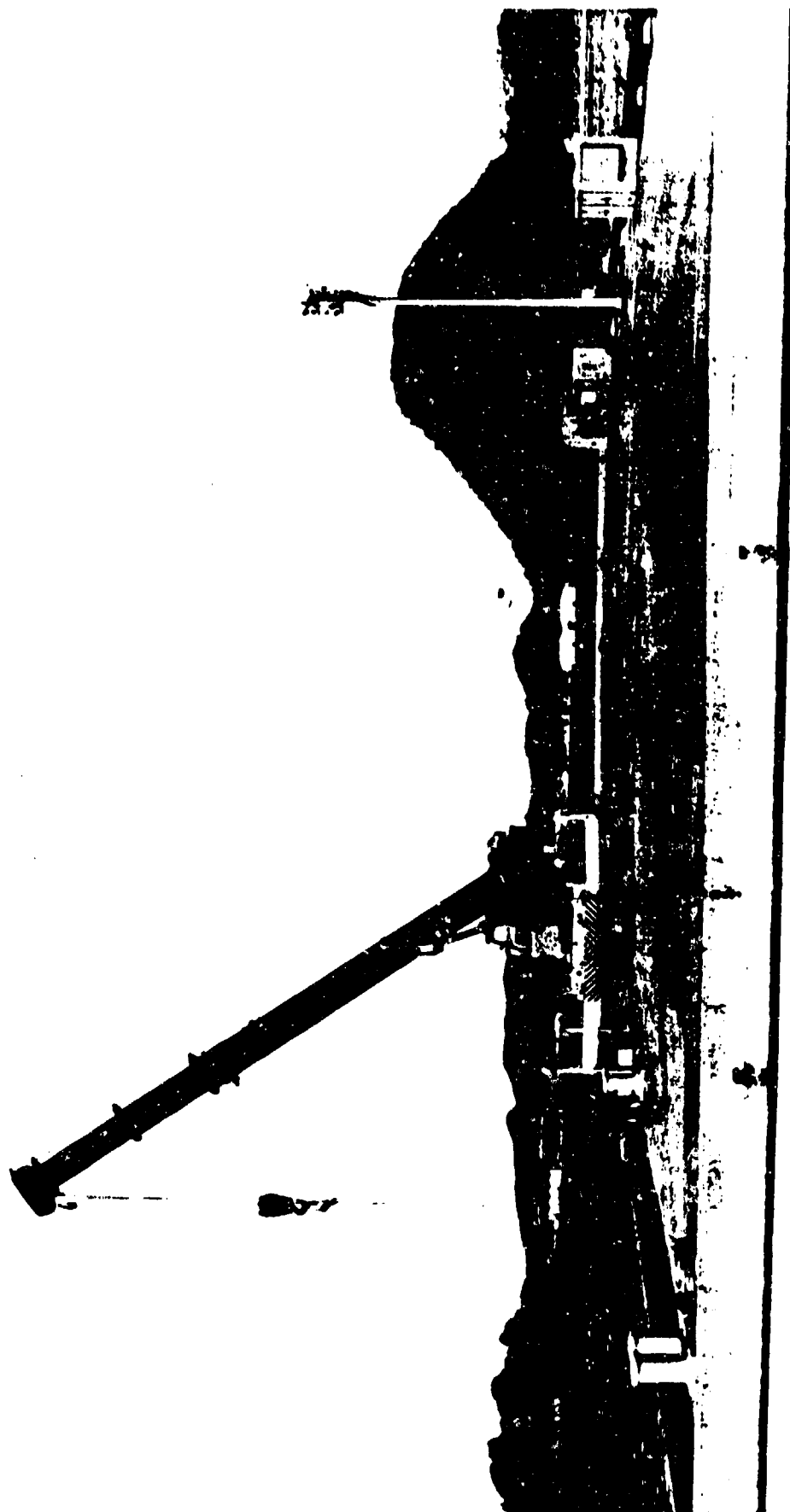
SASEBO WHARF

44



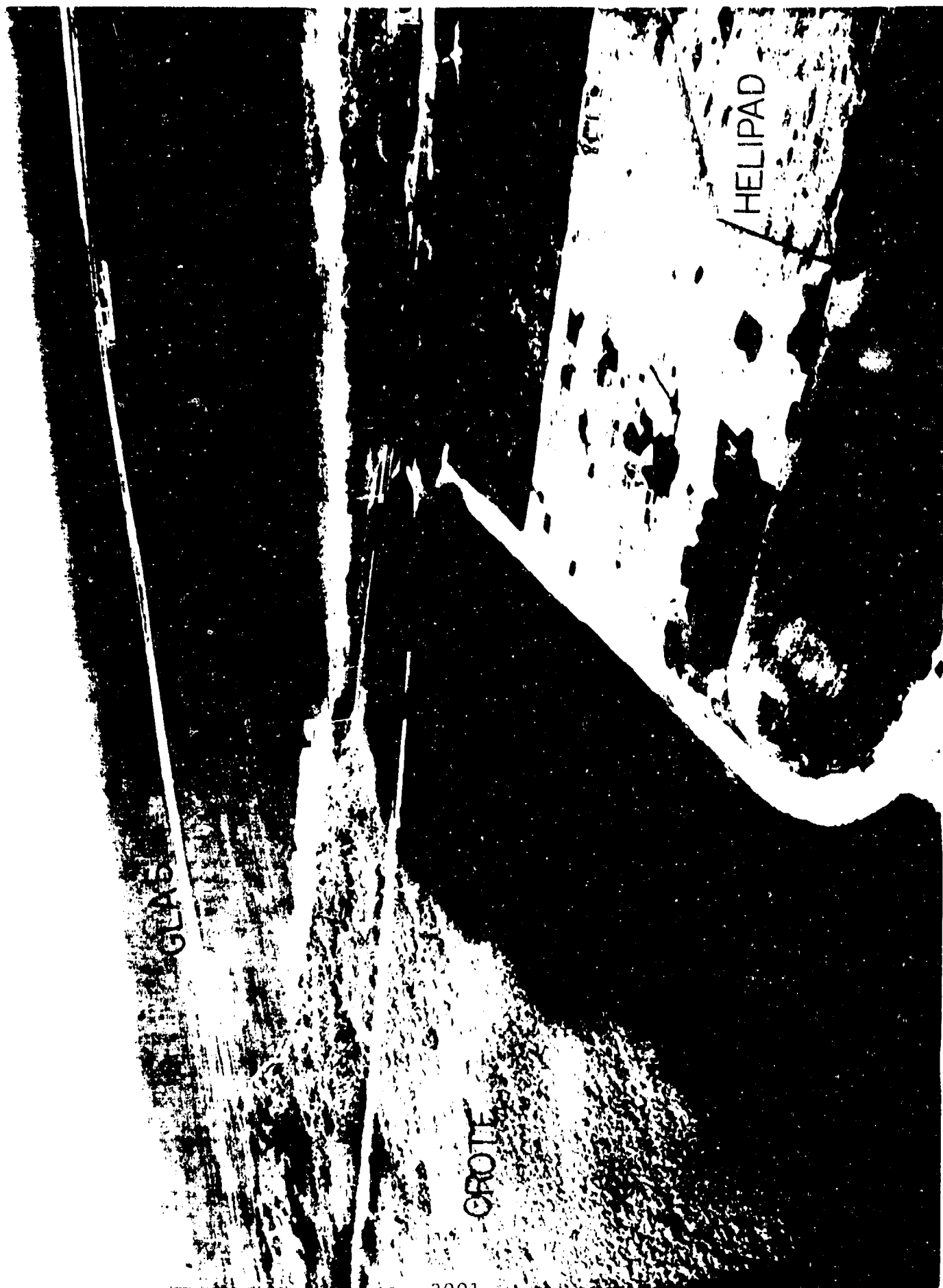
1999

2000

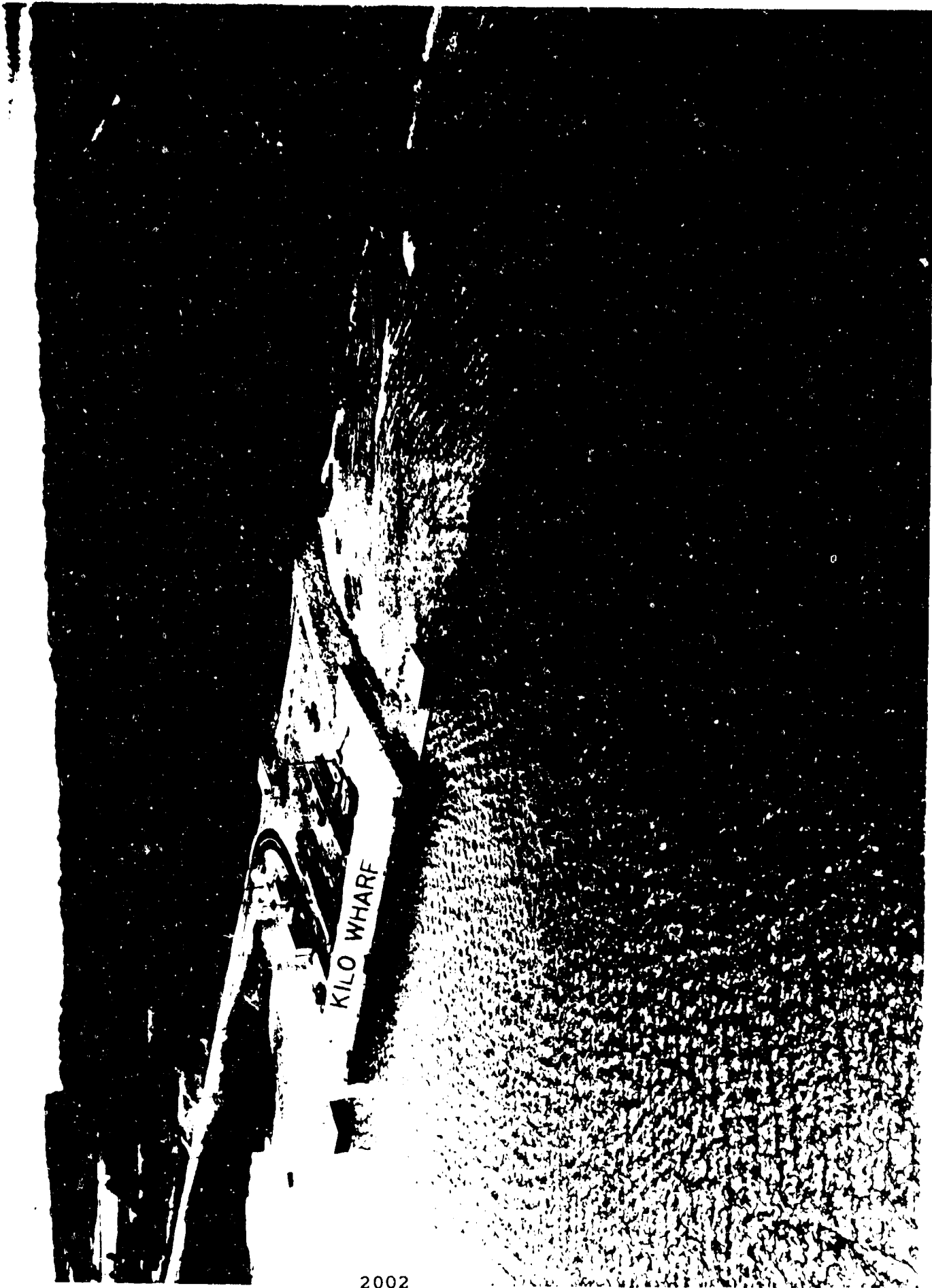


SASEBO WHARF

44



2001



WORLDWIDE PORT STUDY

- **MAY - JUN 90**
 - **PREPO OPERATIONS WERE CONDUCTED AT FLEET
ACTIVITY SASEBO AND AKIZUKI/HIRO FACILITIES**
 - **REVIEW OF ALTERNATE LOCATIONS WILL CONTINUE**

SOUTH KOREA



576,700 SHORT TONS



CHINHAE PIER



CHINHAE PIER



CHINHAЕ PIER

WORLDWIDE PORT STUDY CONCLUSION

- **THE PROCESS IS TO ESTABLISH:**
 - **CURRENT PORT CAPABILITIES/LIMITATIONS**
 - **VESSELS USED (FREQUENCY AND TONNAGES)**
 - **STORAGE CONFIGURATIONS AND NEW**
 - **EXPLOSIVES EFFECTS ON PORTS AND SURROUNDINGS**
 - **WAYS TO CONTROL/LIMIT THE MCE**
 - **CONTAINERIZATION/PACKAGING**
 - **STOWAGE/LOAD CONFIGURATIONS
SPACING/BUFFERING/SHIELDING**
 - **INSENSITIVE MUNITIONS**

WORLDWIDE PORT STUDY

ADDRESS:

**DIRECTOR, U.S. ARMY TECHNICAL CENTER
FOR EXPLOSIVES SAFETY, ATTN: SMCAC-ES,
SAVANNA, IL 61074-9639**

TELEPHONE:

COMMERCIAL	(815) 273-8802
DSN	585-8802
DATAFAX	585-8769

AUTOMATED EXPLOSIVE SITE PLANNER
A Software System for Siting Explosives

- by -

William Rieder
United States Air Force Logistics Command
Office of the Inspector General
Weapons Safety Division
(HQ AFLC/IGFW)

- and -

Captain Martin J. Barche Jr.
United States Air Force Logistics Command
Artificial Intelligence Support Center
(HQ ALD/JTI)

ABSTRACT

The AUTOMATED EXPLOSIVE SITE PLANNER (AESP) is a software system developed at Headquarters Air Force Logistics Command (HQ AFLC) to tackle many of the problems encountered with developing an explosives site plan and completing AFLC FORM 333, EXPLOSIVES AUTHORIZATION FOR SITED MUNITIONS FACILITY. This system consists of 3 separate, but coordinated, programs that:

- maintain a site database containing information on structures in and around the explosives storage area (ex: structure identification, type, location, etc).
- establish minimum quantity-distance separations (QDS) between the proposed structure and surrounding structures based on Air Force regulation 127-100, chapter 5.
- identify previously sited structures whose maximum net explosive weights must be reduced due to the introduction/placement of the proposed structure.
- complete AFLC FORM 333.

Programs 1 and 3 of this system were designed using "conventional" techniques and coded in a "conventional" programming language (TURBO Pascal). Program 2 employs artificial intelligence techniques and was coded using expert system development software (M.1).

This paper explains why this project was undertaken, how it was approached, and the rationale behind the approaches taken. It also provides a general discussion of the site planning process and detailed discussions on both program functions and system operation.

INTRODUCTION

The development of explosive site plans within the Air Force Logistics Command (AFLC) has always been shadowed by the ominous cloud of hidden errors that have somehow managed to circumvent the closest scrutiny of developers and reviewers alike. Although many of these errors can be categorized as quite insignificant, others have the potential to be catastrophic in terms of cost, facility damage, loss of life and/or impairment of mission capability during conflict. While we have learned from our mistakes, some lessons have been lost or forgotten due to personnel turnover, infrequent plan development, or random miscommunication.

In the late 1980's, AFLC instituted an initiative known as Total Quality Management (TQM) to improve products and processes throughout the command. Process action teams (PATs) were formed to examine selected processes and make recommendations on how to improve them. One such team was formed to examine the explosive site planning process. After analyzing the planning process and the problems typically encountered, the team determined that errors introduced into explosive site plans were primarily attributed to:

- the complexity of Air Force regulation (AFR) 127-100 (Explosive Safety Standards).
- misinterpretation of AFR 127-100 by the planner.
- misapplication of AFR 127-100 tables and footnotes.
- variations in training and experience levels of planners and reviewers.
- planner and reviewer proficiency deterioration due to the decreasing need to develop site plans.
- deficiencies in maps used in the planning process.

The PAT concluded that there were no "quick fixes" which would improve the planning process to meet the safety and operational needs of the Air Force; however, automating the planning process would solve the vast majority of the problems encountered.

Although efforts at HQ USAF and DOD levels were underway to design and develop a comprehensive automated site planner, the PAT concluded that AFLC could not wait several years for the system to materialize. In April 1989, the AFLC Weapons Safety Office (AFLC/IGFW) launched an effort to develop the Automated Explosive Site Planner (AESP). This system would focus exclusively on AFLC

explosive site planning and would complete AFLC FORM 333, EXPLOSIVES AUTHORIZATION FOR SITED MUNITIONS FACILITY (appendix 1).

System design and development efforts were limited by a variety of factors such as insufficient funding and a lack of manpower. These limits precluded a full-time design/development effort; therefore, AFLC/IGFW assets were used as available. During system design, it became evident that automating the process of establishing quantity-distance separations (QDS) using AFR 127-100 would be difficult, if not impossible, for IGFW personnel. Developing software to interpret and act upon the multitude of footnotes and exceptions found in this regulation was beyond their level of programming expertise. For this reason, help was requested from AFLC's Artificial Intelligence Support Center (AISC). The AISC provided system design and programming assistance on an ad hoc basis until October 1989 when they formally joined IGFW in the development effort.

GENERAL DISCUSSION

THE PLANNING PROCESS: Explosive site planning at Air Force Logistics Command (AFLC) bases is manually accomplished by weapons safety personnel working in cooperation with base civil engineers. This planning process can be divided into three phases:

1. PREPARATION: In the preparation phase, the proposed structure is tentatively plotted on a map depicting the explosives storage area and its surroundings. All structures within a radius specified by AFR 127-100 are located and classified by structure type (igloo, operating location, inhabited building, etc). Next, the closest existing structure of each type is identified and the shortest distance to the proposed structure is recorded. Finally, the orientation of each closest structure is established relative to the proposed structure.

2. QUANTITY-DISTANCE SEPARATION (QDS) DETERMINATION: In this phase, AFR 127-100 is used to establish the minimum QDS values between the proposed structure and the closest existing structure of each type (as established in phase 1). This is done for each explosive hazard class/division. QDS determination is always performed once, but may be performed twice:

- QDS values from existing potential explosion sites (PES) to the proposed structure are established for the closest PES of each structure type (igloo, module, etc).

- If the proposed structure will house explosives, a second set of QDS values is established by treating the proposed structure as the PES and all other structures as exposed sites (ES).

3. LIMITS DETERMINATION AND CONFLICT IDENTIFICATION: In this third and final phase, limits on the amount of net explosive weight (NEW) to be stored in the proposed structure are established. These maximum NEW values are calculated using the QDS values established by Program 2. Additionally, the QDS values are also used to calculate NEWs (where appropriate) for all existing structures involved in the site plan. These calculated NEWs are compared against their counterparts found in the existing structure's site plan (on file). If a calculated NEW is less than its counterpart on file, a conflict has occurred. (In other words, introduction of the proposed structure has reduced the NEW authorized for the previously sited structure). Identified conflicts are resolved by either moving the proposed structure so as to increase the distance between it and the existing structure, and/or by reducing the NEW authorized at the existing structure. After all conflicts are resolved, the NEWs calculated for the proposed structure are used to complete AFLC FORM 333.

PROBLEMS: As was mentioned previously, the opportunity for error abounds in this manual planning process...

- In the preparation phase, inaccurate maps, inaccurate measurements, and/or incorrect determination of the shortest distances are common sources of error. Problems have also arisen around determining the orientation of one structure to another as specified by AFR 127-100.
- In the QDS determination phase, discrepancies in AFR 127-100 chapter 5, misinterpretation of the regulation, misapplication of the various tables and footnotes, and skipping some possible ES/PES combinations have all caused problems at one time or another.
- With every repetition of the planning process due to conflict resolution, planner fatigue, confusion, and frustration increase the chances of missing conflicts and/or of making additional mistakes.
- When questions arise during the review of the site plan by AFLC/IGFW, it is difficult (and sometimes impossible) for the planner to recall exactly how AFR 127-100 was applied and footnotes/exceptions interpreted.

The AESP system addresses and resolves virtually all of the problems above by automating each of the site planning phases. In the next section, each of the 3 programs that comprise the AESP will be discussed individually. How they address the aforementioned problems will be described as well.

PROGRAM DESCRIPTIONS

PROGRAM 1: This TURBO Pascal program automates the preparation phase and resolves (or reduces) problems associated with it as described below:

- INACCURATE MAPS: All structure location information in the form of map coordinates will be placed into a site database. These coordinates will be provided by base civil engineers using their computerized map system. Program 1 provides menu-driven functions to create, maintain, and print/display this site database. For more information on the site database, please refer to appendix 2.
- INACCURATE MEASUREMENTS AND INCORRECT DETERMINATION OF SHORTEST DISTANCE: Using the coordinates in the database, Program 1 will mathematically determine the shortest distance between any 2 given structures.
- INCORRECT DETERMINATION OF STRUCTURE ORIENTATION: This program establishes the ES/PES orientations (front-to-side, rear-to-front, etc) using AFR 127-100 specifications.

PROGRAM 2: This M.1 program is the knowledge-based portion of the system and it automates the QDS determination phase of the site planning process. It reduces or eliminates the following problems normally associated with this phase:

- DISCREPANCIES WITHIN AFR 127-100: AFR 127-100 chapter 5 was methodically scrutinized during the development of Program 2. As a result, numerous discrepancies were identified and eliminated.
- MISINTERPRETATION OF AFR 127-100: Program 2 enforces the requirements of AFR 127-100 as interpreted by HQ AFISC/SEWV. Because AESP will be used to generate all site plans within AFLC, a uniform interpretation of the regulation is achieved.
- MISAPPLICATION OF AFR 127-100 TABLES/CHARTS: Program 2

determines the correct table/chart to use, when to use it, how to use it, and how to interpret and apply any referenced footnotes/exceptions. The planner is only prompted for necessary information, only at the time it's needed, and only when the information is not in the database. As long as the planner provides AESP with correct information, Program 2 will use the various tables and charts within AFR 127-100 correctly.

- INABILITY TO RECREATE THE PLANNING PROCESS: An audit log is kept of every footnote and/or exception that influences QDS value determination. When necessary, a transcript of the entire dialogue between Program 2 and the planner can be generated.

- SKIPPING POSSIBLE ES/PES COMBINATIONS: Program 1 "tells" Program 2 when to treat the proposed structure only as an exposed site (ES) and when to treat it as both an ES and a potential explosion site (PES). Program 2 checks all relevant ES/PES combinations.

PROGRAM 3: This third and final program, written in TURBO Pascal, automates the limits determination and conflict identification phase. If/when no conflicts are found, Program 3 completes AFLC FORM 333.

PROGRAM DESIGN RATIONALE

As mentioned in the program descriptions, the preparation and limits determination phases were automated using TURBO Pascal. TURBO Pascal was the "language of choice" for a variety of reasons:

- Both phases are very math oriented.
- Both phases are completed in a logical, methodical (ie: procedural) manner
- Turbo Pascal graphics capabilities supports diagram generation and display
- Turbo Pascal creates executable (.COM) programs that run on Z248s (or compatible). These programs can be distributed freely throughout the command (ie: no run-time costs involved).
- Turbo Pascal can allocate/release computer memory on the fly.
- Turbo Pascal was available; funds to purchase anything else were not!

Unlike the preparation and limits determination phases of the site planning process, QDS determination is neither math oriented nor procedural in nature. The emphasis in Phase 2 is on the interpretation of information as per AFR 127-100 rather than on data manipulation. A software package called M.1 (M1) was used to automate the QDS determination phase because:

- it is a rule-based, non-procedural language.
- M1 applications will run on the Z248 or compatible (as required by AFLC/IGFW).
- M1 was available and applications can be distributed freely throughout AFLC (ie: no run-time cost).
- M1 expertise was readily available.
- it uses a technique called "backward chaining" which is well suited to the problem of QDS processing. Backward chaining is advantageous for solving problems where it is easier to work backward rather than forward. For example, it is often easier to work from the center of a maze toward the outside than vice versa.

SYSTEM OPERATION

PRELIMINARY WORK: Before developing a site plan, the planner must use Program 1 to create and populate the site database. Program 1 prompts the planner for all needed structure information, much of which is obtained from the base civil engineer's computerized base mapping system. (See appendix 2 for the information required by the database.) Data on every structure in and around the explosives area must be entered. Additionally, every structure having an AFLC Form 333, Explosives Authorization for Sited Munitions Facility, on file will have the information on the form transcribed into the database. At present, this is a manual, time consuming process; however, it need only be done once. After initial data entry, Program 1 database maintenance functions can be used to add new structures, delete old structures, and/or change information in the database.

CREATING A SITE PLAN - PART(1): The creation of a site plan begins with the planner working with the base civil engineer (BCE) to tentatively plot the proposed structure on the BCE's computerized mapping system. Location information for the proposed structure (ie: map coordinates) provided by the BCE system will be needed by

Program 1. With this location information in hand, the planner starts the AESP system on his/her Z248 computer (or compatible). Program 1 is automatically started and a menu of options is displayed. The planner selects the option that allows him/her to develop a site plan. Next, the planner is prompted for information about the proposed structure. Once Program 1 has all of the information it needs, it performs preparation phase tasks which include:

- Determining the shortest distance between the proposed structure and all other structures (components) in the database. (See appendix 2 for an explanation of structure components.)
- Selecting the structure (component) of each AFR 127-100 structure type that is closest to the proposed structure.
- Establishing the orientations of the existing structure (component) and the proposed structure relative to each other.

Information about the proposed structure is placed in a STRUCTUR.NEW file. Similar information about all relevant existing structures (components) is written to a STRUCTUR.OLD file. Other information such a building orientation, "actual" (map) distances, etc. are written to other files so that this information is available to programs 2 and 3. With all of this accomplished, Program 1 ends and Program 2 takes over.

CREATING A SITE PLAN - PART (2): Program 2 begins by reading the STRUCTUR.NEW and STRUCTUR.OLD files. It takes one structure (component) at a time out of the STRUCTUR.OLD file, pairs it with the proposed structure to form an ES/PES set, and processes the ES/PES set to obtain QDS values for all explosive hazard classes. Next, it switches the ES/PES roles of the proposed and existing structures in an attempt to obtain a second set of QDS values. When all processing is complete, the next structure in the STRUCTUR.OLD file is paired with the proposed structure and the entire process repeats. This cycle continues until all components in the STRUCTUR.OLD file have been paired with the proposed structure.

At the beginning of every cycle, the proposed structure is treated as the ES and the existing structure (component) as the PES. (For the moment, let's assume that the existing structure will contain explosives and thus qualifies as a PES.) Initial AFR 127-100, Table 5-1 (Quantity-Distance Separation Criteria) row and column designations are assigned to the ES and the PES, respectively, based upon:

1. the structure classification assigned to them by Program 1

2. barricade information supplied by the planner.

Next, any footnotes referenced by Table 5-1 for the row number assigned to the ES are processed in order of appearance. Each footnote is a knowledge-based program that collects information from the database and/or the user as needed. When a footnote alters the ES designation, the new row number is assigned immediately and an annotation is made in an audit log. Both the footnote causing the change and the new row number being assigned are recorded. Processing of the footnotes associated with the new row then begins. This cycle continues until all footnotes for the given row have been processed and the ES designation has stabilized (ie: no other row changes occur). In cases where row footnotes create an infinite cycle, the original ES row designation is used.

Once a final ES designation (ie: row number) is established, the same type of processing occurs to arrive at a final PES designation (ie: column number). Program 2 uses these final Table 5-1 row/column designations to establish a default QDS value for hazard class 1.1 explosives by performing a simple table look-up. Next, any footnotes that affect the QDS value are applied. For every change to the QDS value, the footnote causing the change, and the change itself are recorded in the audit log.

After a final QDS value for hazard class 1.1 explosives is established for the given ES/PES set, the same methods are used to establish QDS values for all other hazard classes. All results are then written to a file for subsequent processing by Program 3.

When processing of the current ES/PES set is complete, or if the existing structure (component) was not a valid PES (ex: inhabited building, public traffic route, etc), the roles of the proposed structure and the existing structure are reversed. The proposed structure is treated as the PES and the existing structure (component) is treated as the ES. All of the processing described above will occur to generate a second set of QDS values only if 2 conditions are met:

- 1) The proposed structure is a valid PES.
- 2) Program 1 "informed" Program 2 that this role reversal should occur.

CREATING A SITE PLAN - PART (3): At the conclusion of Program 2, all relevant proposed/existing structure combinations have been evaluated and the QDS values for each have been written to a QDS file. Program 3 takes this information and begins the limits determination and conflict identification phase. Assuming that the proposed structure will house explosives (ie: acts as a PES), maximum net explosive weights (NEWs) are established for hazard classes 1.1 through 1.4 using the QDS values derived by Program 2

and the inter-structure distances calculated by Program 1. (REMEMBER! When 2 sets of QDS values are derived for a proposed/existing structure pair, the more restrictive of the 2 values is used.) Next, Program 3 calculates NEWS for all previously sited structures involved in the site plan and compares these calculated NEWS to their counterparts on file. Program 3 provides the planner with information on every conflict found (ie: when the calculated NEW is found to be less than the NEW on file). With this information in hand, the planner must take corrective action(s). This usually involves relocating the proposed structure and/or reducing the authorized NEW in the "offending" existing structure. After corrective action is taken, the AESP system must be run again using the new information.

REVISION NUMBER		EXPLOSIVES AUTHORIZATION FOR SITED MUNITIONS FACILITY			SITE PLAN NUMBER		ORGANIZATION		FACILITY NUMBER				
I. FACILITY DESCRIPTION													
A. TYPE CONSTRUCTION STANDARD: NON STANDARD - AT DEFINITIVE DWG NUMBER													
F. NUMBER OF ROOMS: BAT													
B. TYPE HEATING													
G. NUMBER OF EXITS													
C. TYPE OF ELECTRIC FIXTURES													
H. EXTENT AND TYPE OF BARRICAADING													
D. LIGHTNING PROTECTION													
I. DESIGN PURPOSE (MAINTENANCE, X-RAY, STORAGE, ETC.)													
E. DIVIDING WALLS (NUMBER, SIZE)													
J. SPECIAL FEATURES (OVERHEAD CRANE, MOIST, ETC.)													
II. COMPUTATION DATA													
NEAREST TARGET THAT REQUIRES	TARGET IDENTIFICATION	FROM (FPS) TO (FPS)	E FACTOR	DISTANCE	CL DIV 1.1	CLASS/DIVISION 1.2							
						(04) G	(08) H	(12) I	(16) J	CL DIV 1.3	CL DIV 1.4	OTHER	
MAGAZINE DISTANCE	4083	3	2.75/0.00	1376	500000	PMT CAP (4083)	PMT CAP (4083)	500000 (4083)	500000 (4083)	20842283 (4083)	PMT CAP		
INTERLINE DISTANCE	4067	3	18.00/0.00	1816	500000	PMT CAP (4067)	PMT CAP (4067)	500000 (4067)	500000 (4067)	47911252 (4067)	PMT CAP		
PTR DISTANCE	17	2	21.00/30.00	1530	186667	PMT CAP (17)	PMT CAP (17)	500000 (17)	500000 (17)	6995268 (17)	PMT CAP		
ING DISTANCE	4070	3	35.00/50.00	2393	170800	PMT CAP (4070)	PMT CAP (4070)	500000 (4070)	500000 (4070)	109627140 (4070)	PMT CAP		
OTHER	4071	3	0.00/0.00	2040	50	PMT CAP (4071)	PMT CAP (4071)	500000 (4071)	500000 (4071)	67917312 (4071)	PMT CAP		
OTHER													
III. REMARKS													
AUTHORIZATION													
CLASS/DIVISION 1.2													
CL/DIV 1.1		(04) B	(08) C	(12) D	(16) E	CL/DIV 1.3		CL/DIV 1.4		OTHER			
A		50	PMT CAP	PMT CAP	500000	6995268		PMT CAP		M			

PREVIOUS EDITION IS OBSOLETE

AFLC FORM 333 APR 89

APPENDIX 2
- The Site Database -

There is one entry (record) in the site database for every structure component that must be considered in the site plan as directed by AFR 127-100, when developing a site plan. One set of records will describe the components of the proposed structure, another set will describe the components of all surrounding structures (within the radius specified by AFR 127-100). Each record consists of the following fields:

COMPONENT ID: A unique identifier.

STRUCTURE TYPE: An integer code that identifies the type of structure (igloo, magazine, module, inhabited building, etc) the component belongs to.

COMPONENT SHAPE: An integer code that identifies the geometric shape of component (rectangle, triangle, circle, etc.)

COMPONENT COORDINATES: Cartesian coordinates of each endpoint on a polygonal component. Circular components have their center point and radius recorded.

COMPONENT ATTRIBUTE FLAG: This is a bit-mapped flag used to exchange information between the various parts/programs. Each bit of a 16-bit computer word has a predefined, binary meaning. For example, flag bit #1 indicates whether or not a structure is a non-standard structure (0 = no, 1 = yes).

STRUCTURE COMPONENTS: To simplify processing, irregularly shaped structures are represented as overlapping and/or adjoining triangular, rectangular, square, and/or circular components. Each component is treated as an individual structure during QDS value determination. Structures having a simple, regular shape are said to have one component. At present, breaking irregularly shaped structures into simple components is a manual process.

EXPLOSIVE SAFETY TRAINING

BARBARA J. OVERTON
CHIEF, CONVENTIONAL
AMMUNITION DEPARTMENT



"TRAINING FOR TOTAL QUALITY"



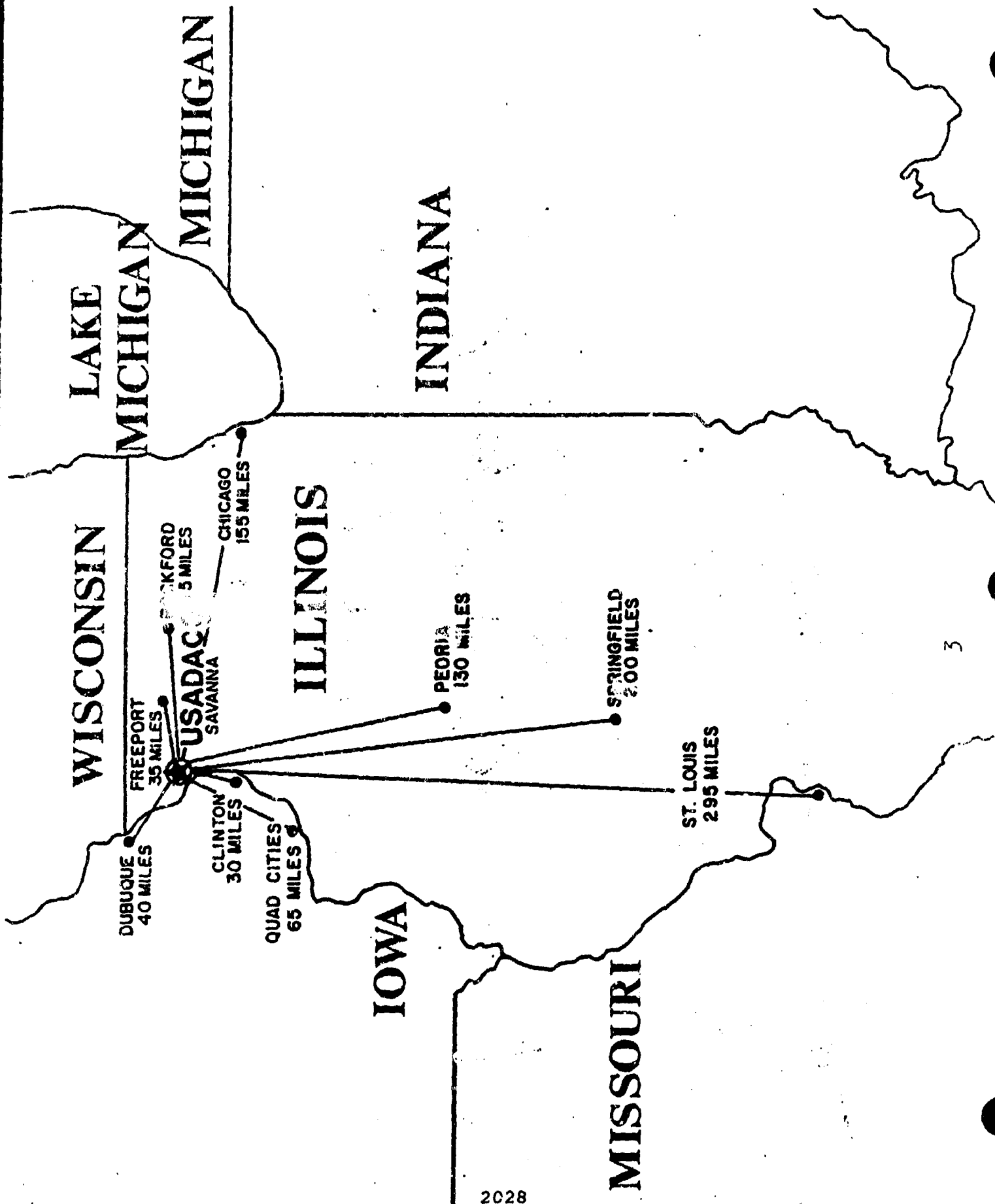
**U.S. ARMY DEFENSE AMMUNITION CENTER AND SCHOOL
SAVANNA ILLINOIS**

Mission Statement

The mission of the Ammunition School is to provide education and training for ammunition managers, specialists, and operating personnel required to perform conventional ammunition logistics missions IAW requirements of the Single Manager for Conventional Ammunition (SMCA) and of military services under provisions of DODD 5160.65. Additionally, it provides specialized training in support of Department of Defense (DOD) certification programs. A primary part of the Ammunition School mission is to recruit and train personnel for the Department of the Army (DA) Quality Assurance Specialist (Ammunition Surveillance) (QASAS) and Ammunition Manager (AM) Career Intern Programs.

Geographical Location

The U.S. Army Defense Ammunition Center and School is located in Illinois. at the Savanna Army Depot Activity. It is seven miles north of Savanna on the east bank of the Mississippi River, 155 miles west of Chicago, 65 miles north of Moline, and 40 miles south of Dubuque, Iowa. It is between the towns of Savanna and Hanover on Illinois Route 84, the Great River Road.



SOURCES OF STUDENTS

The U.S. Army Defense Ammunition Center and School (USADACS) conducts explosive safety training for a wide and varied clientele, crossing Service and Agency lines and even venturing into the private sector via government contractors.

Under the Department of the Army Explosive Safety Management Plan, the Ammunition School has responsibility for all Army explosive safety training. The Single Manager for Conventional Ammunition (SMCA) regulation, DOD 5160.65M, provides for the training for all the Services. Under a Memorandum of Agreement with the Department of the Navy, USADACS provides explosive safety training for both Navy civilians and military. Contractor personnel, non-DOD and international military students are provided explosive safety training on a space available basis.

SOURCES OF STUDENTS

ARMY

NAVY

AIR FORCE

MARINES

CONTRACTOR

OTHER FEDERAL AGENCIES

INTERNATIONAL MILITARY

TYPES OF TRAINING

- Explosive safety is an integral part of all courses taught at USADACS. Those courses to be discussed here can be classified into four broad categories:
- 1. Technical training required for operator/supervisor certification.
- 2. Training required to certify transportation of hazardous materials by surface, rail, air or sea modes under Department of Transportation (DOT) and Coast Guard and aviation regulations.
- 3. Non-technical training provided to safety and managerial personnel of the Army.
- 4. Non-technical training provided to safety and managerial personnel of the Navy.

TYPES OF TRAINING

- **OPERATOR/SUPERVISOR CERTIFICATION**
- **TRANSPORTATION CERTIFICATION**
- **ARMY EXPLOSIVE SAFETY**
- **NAVY EXPLOSIVE SAFETY**

OPERATOR/SUPERVISOR CERTIFICATION

2033

SPECIAL TECHNICAL AMMUNITION AMMO-C-9

- **PURPOSE:** This course provides basic training in the safety and fundamental aspects of ammunition and explosives for personnel directly involved in ammunition operations. It is primarily designed for non-supervisory wage grade employees, including wage leaders, requiring certification as required by AMCR 350-4, TRADOC-R 350-30, and FORSCOM-R 350-10.
- **SCOPE:** Course content will introduce the different classes of ammunition and explosives, stressing safe handling and explosive safety requirements during the receipt, storage, maintenance, production, demilitarization, or issue of ammunition at U.S. Army installations.
- **SPECIAL INFORMATION:** This course can also be presented onsite and may be tailored to meet Major Army Command (MACOM) requirements (AMMO-C-9-OS).
- **PREREQUISITES:** Nominees should be AMC civilian personnel having a need to become certified under provisions specified in AMCR 350-4.
- **SECURITY CLEARANCE:** None.
- **LENGTH:** 1 Week, 3 Days

Special Technical Ammunition
AMMO-C-9 - Length: 1 Week, 3 Days

Course Content

Orientation
Explosives, Propellants, and Chemical Agents
Packing and Marking
Small Caliber Ammunition
Artillery and Navy Gun Ammunition
Mortars
Rockets
Grenades, 40mm, and Pyrotechnics
Mines and Firing Devices
Bombs
Demolition Materials
Explosive Safety Standards
Standard Tools, Equipment, and Buildings
Storage
Transportation
Standing Operating Procedures
Operational Safety - Maintenance
Operational Safety - Demilitarization
Examination and Critique

SPECIAL TECHNICAL AMMUNITION FOR LOGISTICS ASSISTANCE REPRESENTATIVES (LARS) AMMO-C-24

- **PURPOSE:** This course provides training in the safety and fundamental aspects of ammunition and explosive for AMCCOM Logistics Assistance Representatives (LARS).
- **SCOPE:** Course curriculum will familiarize AMCCOM LARS with different types and classes of ammunition/explosive stressing safety, maintenance, packaging, marking, condition coding, restrictions, and malfunction reporting.
- **PREREQUISITES:** Nominees will be Logistics Assistance Representatives. This course is presented resident only.
- **SECURITY CLEARANCE:** None.
- **LENGTH:** 1 Week, 3 Days

**Special Technical Ammunition for Logistics
Assistance Representatives (LARS) - AMMO-C-24**

Length: 1 Week, 3 Days

Course Content

**Orientation
Sources of Information - Army
QASAS Responsibilities at a Using Unit
Explosives, Propellants, and Chemical Agents
Packing and Marketing
Small Caliber Ammunition
Artillery Ammunition
Mortars
Rockets
Grenades, 40mm, and Pyrotechnics
Mines and Firing Devices
Demolition Materials
Explosive Safety Standards
Malfunction Reporting
Examination**

TECHNICAL AMMUNITION

AMMO-C-3

- **PURPOSE:** This course provides basic training in the technical aspects of ammunition and explosives for personnel involved in ammunition related operations. The course provides a base for advanced study in the ammunition areas of maintenance, demilitarization, storage, supply, and inventory management. In addition, the course meets the requirements for certification of personnel under the provisions specified in AMCR 350-4, TRADOC-R 350-30, and FORSCOM-R 350-10.
- **SCOPE:** Course content includes Army, Navy, and Air Force references for ammunition and related operations, basic information on types of explosives and non-surety chemical agents, ammunition items description and functioning, quantity-distance consideration for explosive safety, and requirements for the storage and transportation of ammunition.
- **PREREQUISITES:** Priority acceptance will be for personnel requiring the course for certification IAW AMCR 350-4. Candidates selected for attendance should be working with ammunition or in related field.
- **SPECIAL INFORMATION:** This course is identified for attendance by international military students through provisions of AR 12-15. This course is presented resident only.
- **SECURITY CLEARANCE:** None.
- **LENGTH:** 7 Weeks, 3 Days

Technical Ammunition
AMMO-C-3 - Length: 7 Weeks, 3 Days

Course Content

Medium Caliber Artillery Ammunition and Fuzes
Mortar Ammunition
Large Caliber Artillery Ammunition
Navy Gun Ammunition
Rockets, Ratios, and Propellant Actuated Devices
Grenades
Aircraft Bombs and Dispenser Munitions
Demolition Materials and Disposal
Military Pyrotechnics
Mines and Firing Devices
DOD Explosives Safety Standards
Ammunition Storage
Transportation
Course Critique, Closeout, and Graduation

BASIC MISSILE OPERATIONAL SAFETY

AMMO-M-19-OS

- **PURPOSE:** This course provides the student with training in the basic operating principles of guided missiles and the functioning of missile Class V Components while stressing safe handling procedures and explosive safety requirements during storage, transportation, and maintenance of guided missile ammunition. It is primarily designed for non-supervisory, non-quality assurance wage grade employees requiring certification as defined by AMCR 350-4, TRADOGR 350-30, and FORSCOMR 350-10.
- **SCOPE:** Course includes generalized training on missile shop safety, Standing Operation Procedures (SOPs), blocking and bracing procedures, storage and outloading drawings, fire safety, grounding requirements, hazards of static electricity, and electromagnetic radiation.
- **PREREQUISITES:** None
- **SPECIAL INFORMATION:** This course can also be presented onsite at installations that store, issue, receive, maintain, test, inspect, and demilitarize guided missiles.
- **SECURITY CLEARANCE:** None
- **LENGTH:** 1 Week

Basic Missile Operational Safety
AMMO-M-19-OS - Length: 1 Week

Course Content

Orientation and Introduction
Guided Missile Operating Principles
Explosives and Class V Components
Operational Safety - Missile Maintenance
Operational Safety - Missile Demilitarization
**Operational Safety - Missile Transportation,
Storage, and Handling**

TECHNICAL CHEMICAL SURETY MATERIEL AMMO-M-8

- **PURPOSE:** This course is designed to provide current information and procedures regarding storage and handling of chemical surety agents and ammunition.
- **SCOPE:** Topics discussed include protective clothing, agent detection, decontamination, disposal, general safety, accident response, and the personnel reliability program. Meets the requirements for wage grade certification under AMCR 350-4, TRADOC-R 350-30, and FORSCOM-R 350-10.
- **PREREQUISITES:** This course is for those individuals who are enrolled in the Ammunition Management Intern program as defined in AR 690-950, and individuals requiring certification under the provisions of AMCR 350-4, TRADOC-R 350-30, and FORSCOM-R 350-10. Nominees should be assigned or have a planned assignment requiring knowledge of chemical agents/munitions. They must be capable of moderate exertion while wearing a protective mask and butyl rubber clothing. Students must be clean shaven as required by AMCR 385-131 for the duration of the course. Individuals are not required to be in the Chemical Personnel Reliability Program (CPRP), and no access to Chemical Surety Materiel is required. Federal Hazard Communication training is a prerequisite for U.S. students.
- **SPECIAL INFORMATION:** This course can also be presented onsite. (AMMO-M-8-OS)
- **SECURITY CLEARANCE:** None.
- **LENGTH:** 2 Weeks

**Technical Chemical Surety Materiel
AMMO-M-8 - Length: 2 Weeks**

Course Content

Orientation
Surety Agents
Chemical Munitions/Containers
Protective Clothing and Equipment
Detection and Identification
Decontamination
Disposal
Effects of Weather and Terrain
Surety Program
Safety Criteria for Agent Activities
Chemical Event Response and Assistance
Examinations

CHEMICAL HAZARD PREDICTION AMMO-M-7

- **PURPOSE:** This course provides current information relative to the prediction of downwind hazard areas resulting from the accidental release of toxic chemical agents.
- **SCOPE:** Course content is designed to provide current information on the chemical and physical properties, toxicity, and physiological effects of the toxic agents GB, VX, and HD and to provide descriptions and characteristics of toxic chemical munitions. Emphasis is on prediction of downwind hazard resulting from a release of toxic agents using personal computers. Maximum Credible Events (MCE), Safety Area, and Public Access Exclusion Distance (PAED) are discussed.
- **PREREQUISITES:** Nominees should be individuals who are enrolled in the QASAS Intern Program as defined in AR 690-950-20 or individuals assigned to a position which requires familiarity with the calculation of downwind hazard distances for toxic chemical releases. Examples include hazards analysis for safety submissions, calculation for agent releases for Chemical Accident/Incident Response and Assistance (CAIRA), and emission hazards for chemical operations. Individuals are not required to be in the Chemical Personnel Reliability Program, but must be employees of the U.S. Government. No access to chemical surety materiel is required. Prior completion of the Chemical Surety Materiel Course (AMMO-M-6), Technical Chemical Surety Materiel Course (AMMO-M-8), or equivalent, is recommended but not mandatory. This course is presented resident only.
- **SECURITY CLEARANCE:** None.
- **LENGTH:** 1 Week

Chemical Hazard Prediction
AMMO-M-7 - Length: 1 Week

Course Content

Orientation

Chemical Agents

Chemical Ammunition

Hazard Prediction Control

**Estimation of Chemical Hazard Distance
Examinations**

TRANSPORTATION CERTIFICATION

2046

21

GENERAL TRANSPORTATION OF HAZARDOUS MATERIALS AMMO-L-16

- **PURPOSE:** This course provides personnel from all Services with general information pertaining to the transportation of hazardous items.
- **SCOPE:** Course content includes emphasis on DOT and DOD regulations, planning, packaging, marking, labeling, compatibility requirements, placarding and documentation of hazardous material shipments by all modes of transportation. Emphasis placed on physical security of sensitive conventional arms, ammunition, and explosives during transportation. Satisfactory completion of this course meets the requirements of para 1-20b of AFR 71-4/TM 38-250/ NAVSUP PUB 506/MCO P4030.19E/DLAM 4146.3 for certification of DD Form 1387-2, and para 38-7a (1)(b) of AR 55-355/ NAVSUPINST 4600.7/AFR 76-2/MCO P4600.14B/DLAR 4500.3. This course will also cover the procedures necessary for preparing DD Form 1387-2. "Special Handling Data / Certification required for shipments of explosives and other hazardous materials by military air.
- **PREREQUISITES:** First priority is for those individuals requiring special certification for job performance. Candidates selected for attendance should be performing work in some phase of transportation of hazardous materials.
- **SPECIAL INFORMATION:** Personnel who successfully complete this course will be certified to accomplish the DD Form 1387-2.
- **SECURITY CLEARANCE:** None
- **LENGTH:** 1 Week

**General Transportation of Hazardous Material
Course - AMMO-L-16 - Length: 1 Week**

Course Content

Orientation

Related Organizations

**Regulations for Safe Shipment of Explosives and
Other Hazardous Materials**

Duties of Transportation Officer

**Definitions of Explosives and Other Hazardous
Materials**

**General Requirements for Safe Shipment of Explosives
and Other Hazardous Materials in Transportation**

**Shipping Paper Requirements for Safe Shipments of
Explosives and Other Hazardous Materials**

**Marking Requirements for Safe Shipment of Explosives
and Other Hazardous Materials**

**General Transportation of Hazardous Material
Course, Continued - AMMO-L-16 - Length: 1 Week**

Course Content

**Placard and Labeling Requirements for Safe Shipment
of Explosives and Other Hazardous Materials**

**Compatibility Requirements for Safe Shipment of
Explosives and Other Hazardous Materials**

**Containers Acceptable for Packaging of Explosives and
Other Hazardous Materials**

DOD Marking and Labeling Requirements

**Physical Security of Sensitive Arms, Ammunition, and
Explosives During Transportation**

**Safe Shipment of Explosives and Other Hazardous
Materials by Air**

Examination and Critique

TECHNICAL TRANSPORTATION OF HAZARDOUS MATERIALS AMMO-L-17

- **PURPOSE:** To provide personnel from all services detailed technical information pertaining to all phases of transportation of hazardous materials by all modes of transportation.
- **SCOPE:** Course content includes emphasis on regulation, planning, packaging, marking, labeling, compatibility requirements, placarding, and documentation of hazardous material shipments by all modes of transportation. Detailed instruction is given on outloading drawings necessary to properly block and brace explosives and other hazardous materials in various modes of transportation. Emphasis is placed on physical security of sensitive conventional arms, ammunition, and explosives during transportation. Course content also includes procedures necessary for preparing DD Form 1387-2, Special Handling Data/Certification, required for shipments of explosives and other hazardous materials by military air; instruction in the International Civil Aviation Organization (ICAO) regulations for safe shipment of hazardous materials by commercial aircraft; and special emphasis on radioactive waste relative to packaging, labeling, placarding, shipping papers, and monitoring requirements. This course meets the requirements for certification of personnel under the provisions specified in AMCR 350-4, TRADOCR 350-3, and FORSCOMR 350-10.
- **PREREQUISITES:** First priority is for those individuals who are enrolled in the QASAS Intern Program as defined in AR 690-250-20. Second priority is for those individuals requiring special certification for job performance. Candidates selected for attendance should be performing work in some phase of transportation of hazardous materials.
- **SPECIAL INFORMATION:** Satisfactory completion of this course meets the requirements of para 1-20b of AFR 71-4/TM 36-250/NA/6UP PUB 505/MCO P 4030.19E/DLAM 4145.3 for certification of DD Form 1387-2 and para 33.7 of AR 66-355/NA/8UPIN8T 4600.70-2/MCO P 4600.14B/DLAR 4500.3 (1)(b). This course meets the requirements for certification of personnel under the provisions specified in AMCR 350-4, TRADOCR 350-3, and FORSCOMR 350-10. This course can also be presented on-site. (AMMO-L-17-08).
- **SECURITY CLEARANCE:** None
- **LENGTH:** 2 Weeks

Technical Transportation of Hazardous Materials
AMMO-L-17 Course - Length: 2 Weeks

Course Content

Orientation
Related Organizations
Regulations for Safe Shipment of Explosives and
Other Hazardous Materials
Duties of Transportation Officer
Definitions of Explosives and Other Hazardous
Materials General Requirements for Safe Shipment
of Explosives and Other Hazardous Materials in
Transportation Shipping Paper Requirements for Safe
Shipments of Explosives and Other Hazardous
Materials Marking Requirements for Safe Shipment
of Explosives and Other Hazardous Materials
Placard and Labeling Requirements for Safe Shipment
of Explosives and Other Hazardous Materials
Compatibility Requirements for Safe Shipment of
Explosives and Other Hazardous Materials

**Technical Transportation of Hazardous Materials
AMMO-L-17 - Continued - Length: 2 Weeks**

Course Content

Containers Acceptable for Packaging of Explosives
and Other Hazardous Materials
Procedures for Safe Shipment of Unwanted
Radioactive Waste
DOD Marking and Labeling Requirements
Outloading Drawings - Field Trip
Physical Security of Sensitive Arms, Ammunition,
and Explosives During Transportation
Safe Shipment of Explosives and Other Hazardous
Materials By Rail
Safe Shipment of Explosives and Other Hazardous
Materials by Rail
Safe Shipment of Explosives and Other Hazardous
Materials by Motor Vehicle
Safe Shipment of Explosives and Other Hazardous
Materials by Water
Examinations and Critiques

INTERMODAL DRY CARGO CONTAINER CSC REINSPECTION AMMO-L-10

- **PURPOSE:** This course provides students with information required to reinspect intermodal dry cargo containers IAW the Convention for Safe Containers (CSC) standards.
- **SCOPE:** Course content includes survey of CSC test requirements; detailed analysis of reinspection criteria found in the CSC, U.S. Public Law, and Joint Service Regulations; orientation of container structural members; reporting requirements; and reinspection decal placement.
- **PREREQUISITES:** First priority is for those individuals who are enrolled in the QASAS Intern Program as defined in AR 650-950-20 and the Ammunition Management Intern Program as defined in AR 690-950. Other nominees should occupy, or be expected to occupy, a position which requires a knowledge of container reinspection standards.
- **SPECIAL INFORMATION:** Onsite training in the Intermodal Dry Cargo Container CSC Reinspection Course at various selected geographical locations is possible, provided such arrangements are made and approved through command channels. Personnel successfully completing the course will be certified as U.S. Army CSC Inspectors as required by TB 43-0241.
- **SECURITY CLEARANCE:** None
- **LENGTH:** 3 Days

**Intermodal Dry Cargo Container CSC Reinspection
AMMO-L-10 - Length: 3 Days**

Course Content

Orientation

Overview of Containerization

Structure of Containers

Inspection Criteria

ARMY EXPLOSIVE SAFETY

U.S. ARMY EXPLOSIVE SAFETY

AMMO-C-22

- **PURPOSE:** To provide U.S. Army safety specialist with training in ammunition explosive safety.
- **SCOPE:** Training includes review of publications, drawings, and other sources of information from which explosive safety technical data may be extracted; recognition of the characteristics of explosives, propellants, and chemicals and their impact upon safe operating procedures; identification of explosive hazard classes and item compatibility groups for safe storage and transport; application of explosive safety standards in determining explosive limits and computation of quantity distance requirements; evaluation of site plans and preparation of waivers and exemption requests; review of malfunction investigative procedures, explosive accident investigation and implementation of proper range procedures and safety; and identification of environmental requirements and hazard analysis procedures and their effects on explosive safety related areas.
- **PREREQUISITES:** Attendees will be U.S. Army Safety Interns and/or GS-08 and above safety specialists and engineers currently assigned to locations where explosive operations are ongoing.
- **SPECIAL INFORMATION:** This course can also be presented onsite.
- **SECURITY CLEARANCE:** NONE
- **LENGTH:** 2 Weeks, 3 Days

U.S. Army Explosive Safety
AMMO-C-22 - Length: 2 Weeks, 3 Days

Course Content

Orientation
Characteristics of Explosives and Propellants
Explosive Hazard Classification and Compatibility
U.S. and NATO Explosive Safety Standards
Site Plans, Waivers, and Exemptions
Handling and Operational Safety
Storage and Transportation Safety
Building Standards and Structure Inspection
Explosives Accident Prevention
Risk Assessment, Hazard Analysis and
Risk Management

NEW PLANT COMMANDERS SAFETY AND ORIENTATION AMMO-C-19

- **PURPOSE:** This course will provide general ammunition, safety, and logistics training for new plant commanders.
- **SCOPE:** The training will introduce the different classes of ammunition and explosives, stressing safe handling and explosive safety requirements. Items discussed in class will be material being produced at the installation student will be assigned to.
- **PREREQUISITES:** Students attending shall be Lieutenant Colonels coming into an assignment at an Army Ammunition Plant (AAP). Actual subcourses taught will be contingent on upcoming assignment of officers.
- **SPECIAL INFORMATION:** This course is presented resident only.
- **SECURITY CLEARANCE:** None.
- **LENGTH:** 1 Week

New Plant Commanders Safety and Orientation
AMMO-C-19 - Length: 1 Week

Course Content

Orientation
Explosives, Propellants, and Chemical Agents
Packing and Marking
Small Caliber & Artillery Ammunition (Including
Mortars and Rockets)
Grenades, 40mm, and Pyrotechniques
Mines and Firing Devices
Bombs
Storage and Transportation
Operational Safety for Disposal Operations
Explosive Safety Standards
Standing Operating Procedures
Environmental Requirements
General Safety
Accident Investigation and Reporting
Critique, USADACS Tour, and Closeout

NAVY EXPLOSIVE SAFETY

NAVAL MOTOR VEHICLE AND RAILCAR INSPECTION (HM)
S-000-0022 (Formerly ES-250)

- **PURPOSE:** This is the basic training course required by OP 2165 and OP 3681 to provide newly assigned inspection personnel with the up-to-date requirements, techniques, and procedures for inspection of motor vehicle and railcars for ammunition, explosives, and other related hazardous materials.
- **SCOPE:** Course provides students with instruction in DOT hazardous materials identification and communication procedures to include shipping paper preparation, marking, labeling, and placarding requirements; DOT packaging requirements; DOT loading and unloading requirements to include compatibility; DOT, DOD, and Navy transport equipment inspection procedures (hands-on) using DD Form 626, Motor Vehicle Inspection (Transporting Hazardous Material), and NAVSEA Form 802, blocking and bracing procedures; Navy transportation safety requirements; and security of sensitive conventional arms, ammunition and explosives. The requirements for Navy ammunition and explosive shipments are emphasized.
- **PREREQUISITES:** Candidates selected for attendance must be Navy or Marine personnel (military, civilian, and contractors) assigned functions of inspecting motor vehicles and/or railcars used for hazardous materials shipments or closely related positions.
- **SPECIAL INFORMATION:** This course can also be presented onsite (S-000-0022-OS).
- **SECURITY CLEARANCE:** None.
- **LENGTH:** 1 Week, 3 Days

**Naval Motor Vehicle and Railcar Inspection (HM)
S-000-0022 (Formerly ES-250) Length 1 Week, 3 Days**

Course Content

Orientation
DOT Requirements for Safe Shipment of Explosives and Other Hazardous Materials
DOD Marking and Labeling Requirements
Regulations and Forms Required to Assure Current Security Requirements are Correctly Implemented
Procedures and Practices Applicable to Loading and Securing of Hazardous Materials for Transportation by or to the Navy in Railcars, Trucks, and Trailers
Safe Shipment of Explosives and Other Hazardous Materials by Rail
Safe Shipment of Explosives and Other Hazardous Materials by Motor Vehicle
Examination, Critique, Graduation, and Departure

NAVAL MOTOR VEHICLE AND RAILCAR (HM) SHIPMENT REGULATIONS - S-000-0023 (Formerly ES-255)

- **PURPOSE:** This is a refresher course required by OP 2165 and OP 3681 in DOT and Navy regulations concerning the safe transportation of ammunition, explosives, and related hazardous materials and transport vehicle inspection.
- **SCOPE:** This course provides students with refresher training in DOT hazardous materials identification and communication procedures to include shipping papers, marking, labeling, and placarding requirements; DOT packaging requirements; DOT loading and unloading requirements to include compatibility; DOT, DOD, and Navy transport equipment inspection procedures; blocking and bracing procedures; and security of sensitive conventional ammunition and explosives in transportation.
- **PREREQUISITES:** Candidates selected for attendance must be Navy or Marine personnel (military, civilian, contractors) assigned functions of inspecting motor vehicles and/or railcars used for hazardous materials shipments or closely related positions.
- **SPECIAL INFORMATION:** This course can also be provided onsite (S-000-0023-OSO). This course must be successfully completed every two years for recertification.
- **SECURITY CLEARANCE:** None.
- **LENGTH:** 1 Week

6-9

Naval Motor Vehicle and Railcar (HM) Shipment Regulations S-000-0023 (Formerly ES-255) - 1 Week

Course Content

Orientation

**DOT Requirements for Safe Shipment of Explosives
and Other Hazardous Materials**

DOD Marking and Labeling Requirement

**Physical Security of Sensitive Conventional Arms,
Ammunition, and Explosives During Transportation
Blocking and Bracing of Ammunition, Explosives, and**

**Other Hazardous Materials in Railcar and Motor
Vehicles**

**Safe Shipment of Ammunition, Explosives, and Other
Hazardous Materials by Motor Vehicle and Railcar
Examinations, Critique, and Graduation**

EXPLOSIVE SAFETY FOR NAVAL FACILITY PLANNING

S-000-0024 (Formerly ES-305)

- **PURPOSE:** To emphasize the preparation and/or review of Navy site plans submitted for various explosive facilities.
- **SCOPE:** Course includes an in-depth review of DOD quantity distance standards and application of these standards in the form of a Facility Design Problems Workshop.
- **PREREQUISITES:** Attendees should be U.S. Navy/Marine Corps facility planners responsible for explosive facilities at shore installation, safety department personnel responsible for review of facility site plans and individuals who fall within the review chain of a typical Navy/Marine Corps facility site plan.
- **SPECIAL INFORMATION:** This course can also be presented onsite (S-000-0024-OS).
- **SECURITY CLEARANCE:** None.
- **LENGTH:** 4 1/2 Days

**Explosive Safety For Naval Facility Planning
S-0001-0024 (Formerly ES-305) Length: 4 1/2 Days**

Course Content

Orientation

Explosives and Propellants

Explosive Safety Standards

Site Planning

Facility Design Problems Workshop

Examination and Critique

BASICS OF NAVAL EXPLOSIVE HAZARD CONTROL

S-000-0025 (Formerly ES-310)

- **PURPOSE:** To provide basic introductory information as to safety practices described in OP 5 in a wide range of hazardous situations.
- **SCOPE:** Evaluation, classification, and control of hazards, safety in maintenance, demilitarization, transportation, and various handling operations will be covered. Characteristics of ammunition and explosives, storage compatibility, and quantity distance requirements will be introduced. An explanation of the Navy Safety and Qualification/Certification programs will be given. An examination is given on combined subcourse material.
- **PREREQUISITES:** Those attending must be Navy/Marine Corps personnel, responsible for safety in operations involving ammunition and explosives.
- **SPECIAL INFORMATION:** This course can also be presented onsite (S-000-0025-OS)
- **SECURITY CLEARANCE:** None.
- **LENGTH:** 1 Week

Basics of Naval Explosive Hazard Control
S-000-0025 (Formerly ES-310) - Length: 1 Week

Course Content

Orientation
Navy Explosive Safety Program
Characteristics of Ammunition and Explosives
Explosive Safety Principles
Safety Procedures for Storage and Handling
Operations
Transportation of Ammunition and Explosives
Maintenance and Disposal Operations
Examination and Critique

EXPENDABLE ORDNANCE MANAGEMENT (EOM) COURSE (NAVY)
S-4E-0001

- **PURPOSE:** To provide a mid-career course of training in the technical and managerial aspects of ammunition and explosives for Naval Officers O-3 to O-5 and civilian personnel involved in ammunition operations and provide a professional foundation in areas of maintenance, demilitarization, storage, supply, and inventory management of ammunition for personnel assigned to missions of receipt, storage maintenance, demilitarization, and issue of ammunition and related items. Additionally, this course will provide senior level ammunition management training to improve the capability of the ammunition manager, increase effectiveness in management of resources in ammunition operations, improve safety, and produce increased serviceability of assets.
- **SCOPE:** Course content includes specific Navy and Marine Corps Item Identification and functioning, sources of information available (primarily Navy but also DOD, Army, and Air Force), storage and transportation methods and requirements, and safety regulation requirements pertinent to ammunition operations. Management aspects of Planning, Programming, and Budgeting Systems, requirements determination, procurement and configuration management, and SMCA involvement as well as Systems Command responsibilities are presented.
- **PREREQUISITES:** Prospective attendees should be occupying key ammunition management positions at command locations, field organizations, weapons stations, air stations, or staff positions, or be in receipt of permanent change of station orders which include attendance TEMDUINS.
- **SECURITY CLEARANCE:** Secret.
- **LENGTH:** 6 Weeks

Expendable Ordnance Management (EOM) Course (Navy)
S-4E-0001 - Length: 6 Weeks

Course Content

Orientation

Sources of Information

Ammunition Organizations

Explosives, Propellants, and Non-Surety Chemical Materials

Fundamentals of Conventional Ammunition

U.S. and NATO Explosive Safety Standards (Quantity Distance)

Total Quality Management (TQM)

Ammunition Malfunctions and Investigations

Ammunition Maintenance and SOP Writing

Ammunition Demilitarization

Ammunition Supply

Expendable Ordnance Management (EOM) Course (Navy)
S-4E-0001 - Continued - Length: 6 Weeks

Course Content

Ammunition Inventory

Ammunition Storage

Ammunition Production, Planning and Control

Ammunition Transportation

Navy Explosives Safety Programs

Nuclear Weapons Safety and PRP Programs

Naval Industrial Funding

Environmental Issues

Basic Naval Weapons Station Organization

Ammunition Security

Labor Relations and Union Issues

1

TITLE OF PAPER: Twin-Screw Extruder Safety Demonstration Tests

AUTHORS: Dr. David R. Dillehay

ABSTRACT

Thiokol Corporation installed a Werner & Pfleiderer twin-screw extruder at the Longhorn Division in Marshall, Texas in 1988. A number of modifications to the installation have been made for safety and operational considerations. This paper will review the current installation and discuss some of the modifications and some of the processing results from operation of the system.

The facility has been used to process live composite propellant in the mixer mode including casting of samples and test motors. The latest work includes processing in the mixer mode for applications such as infrared decoy flare compositions. The facility is considered a state-of-the-art installation for continuous processing with broad capabilities and special consideration for processing energetic materials.

Introduction

Twin-screw extruders have been used for many years in Europe to process a wide variety of propellants and explosives. US interest in this processing technology has been under serious consideration for about the past 7 years. Most of the initial studies in the US were made with inert materials on Werner & Pfleiderer twin-screw extruders. Since then, several US facilities have processed live energetic compositions using either the W&P machines or an APV (the former Baker-Perkins) machine. These facilities include NSWC-White Oak, NOS-Indian Head, UPCO, UTC and, of course, Thiokol.

The initial studies of twin-screw extruder processing used Werner & Pfleiderer (W&P) twin-screw extruders of a modular barrel design. This modular design offered flexibility in setup since the barrel modules could be arranged to give any configuration of feed ports, process sections and vacuum ports desired. A major problem identified with this design concerned the problem of jamming of the screws due to feed problems. If the screws become jammed, the modular barrel design must be disassembled by disconnecting the screw shaft coupling and pulling the screws through the barrels with live material on the surfaces, or by unbolting each section of the barrel and pulling the barrel section over the shafts, again with live material on the surfaces. This was determined to be unacceptable practice under US safety standards. Thiokol worked with a W&P 30mm twin-screw extruder for over a year processing inert propellants. This background work developed the information to define the necessary changes to provide safety in operation. Hazards analyses from NOS-IH and Southwest Research Institute (for ARDEC) along with Longhorn developed process information were used in discussions with W&P to define the requirements for a safe twin-screw extruder design for processing energetic materials. W&P designed a split barrel extruder that could be remotely opened

in case of screw jamming and also incorporated many other design features specifically engineered for safety. After detailed review of the new design and additional requirement definition, W&P built the first twin-screw extruder designed specifically for energetic material processing for Longhorn.

The extruder has a nominal screw diameter of 58mm (2.3 in.) and a barrel length of 1440mm (56.7 in.) The length of the assembled screw elements on the shaft is 1440mm. This gives an L/D ratio of 24:1. Screw elements are available in several combinations of length and pitch. The elements are assembled on splined shafts and end caps are torqued to a minimum of 75 ft-lb.

There are three tempered zones in the extruder barrels and a fourth tempered zone in the die head when using direct extrusion. The tempered zones are temperature controlled by pumping heated water from Mokon hot water heaters through the barrel sections. The Mokons are capable of heating the water to 300 °F.

The top barrel section has four openings into the bore of the extruder. The first opening is near the back of the barrel for feeding polymers or slurries to the extruder. This port is approximately 0.25 in. in diameter. The second port is also near the back of the extruder and is a large (4x5 in.) opening for feeding solids to the extruder. This is followed closely by another liquid feed port, also 0.25 in. in diameter. Near the discharge end of the extruder, there is a large opening (4x8 in.) used for removing volatile solvents or gases from the composition. A vacuum vent is attached to this port and a water-seal vacuum pump is used to draw off volatiles.

The extruder is powered by a 50 HP General Electric DC motor. The barrels are split along the horizontal axis and can be remotely opened to clear a blockage or for inspection. There are three hydraulic cylinders to open and close the barrel halves. The cylinders are suspended from the top barrel and push the top up two screw diameters until reaching fixed stops. Continued application of hydraulic pressure causes the bottom barrel to be pushed down against four springs that serve as supports. When the barrels reach the full open position, a locking ring on the center cylinder snaps into place to hold the barrels open, even if hydraulic pressure is lost. When closing, the hydraulic pressure first opens the lock ring and then brings the barrel sections back to the closed position. All three cylinders have locking rings in the closed position to keep the barrels from opening if hydraulic pressure is lost during a run. Alignment pins assure that the barrel halves are positioned properly relative to the shafts and bearings.

The first live runs of energetic material were accomplished in August, 1989 using an aluminized composite propellant formulation. The runs led to the manufacture of over 500 lb of propellant for test and evaluation. Test motors and 70 lb BATES motors were cast and fired in the initial tests. All ballistic parameters were met and physical properties and compositional analyses were excellent. In a follow-on to the initial propellant work, over 500 lb of a thermoplastic elastomer propellant were processed on the extruder. Preliminary tests on this material showed nominal performance.

Infrared decoy flare composition is extremely hazardous to process by current methods. Figure 1. shows a block diagram of two actual processes for manufacture of flare composition and a third proposed process. The separate elements of the block diagram for the continuous processing have been demonstrated on the twin-screw extruder facility. Live flare composition was processed on the twin-screw extruder in the mixer mode and pressed into test pellets. The pellets were finished with normal production handling and tested in the test tunnel. Performance was excellent with all test parameters met. Reproducibility was excellent even though the material is in the mixer for only about 2 minutes. Future efforts will include developing criteria and techniques for processing in the extruder mode. One of the main safety features is the low amount of material in process at any time. The extruder is run starve-fed with approximately 2 lb of composition in the barrels at once. The solvent content of the flare composition can be reduced through the use of vacuum at the vacuum port. Figure 2. shows an artist's concept of a proposed remote processing concept for flare composition.

Safety Tests

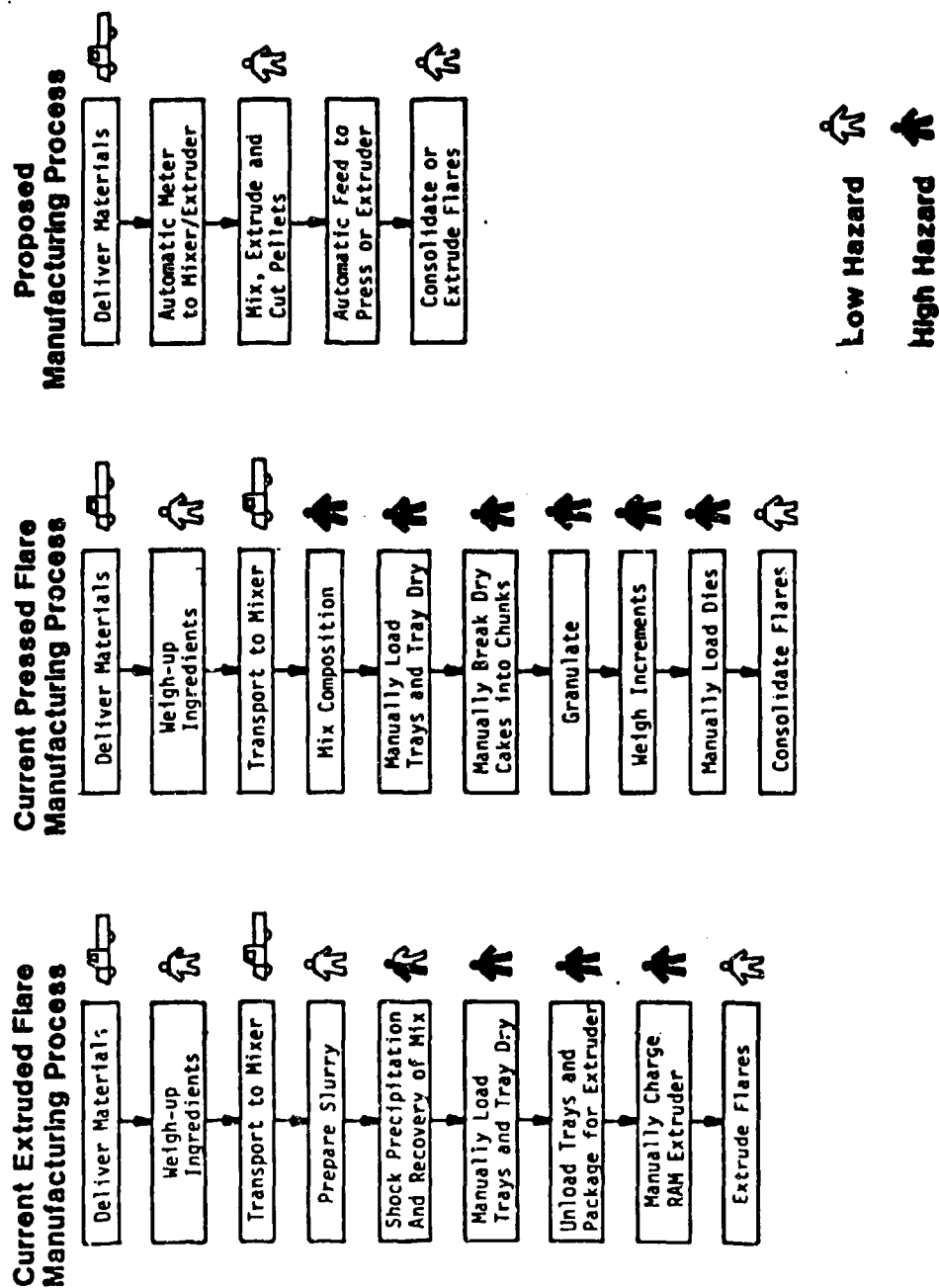
In all of the early work reported, there is no documented incident of an ignition in a twin-screw extruder while the machine was running. The few incidents that have been reported are generally of the "cook-off" variety or due to operator intervention with the product while the machine was stopped. In evaluating the new design for twin-screw extruders from Werner & Pfleiderer, Thiokol, Army and Navy hazards analyses posed concerns that certain operations could lead to ignition within the barrels while the extruder was in operation. Since there was no direct evidence to indicate how severe this incident would be, some tests were planned under the Thiokol IR&D program.

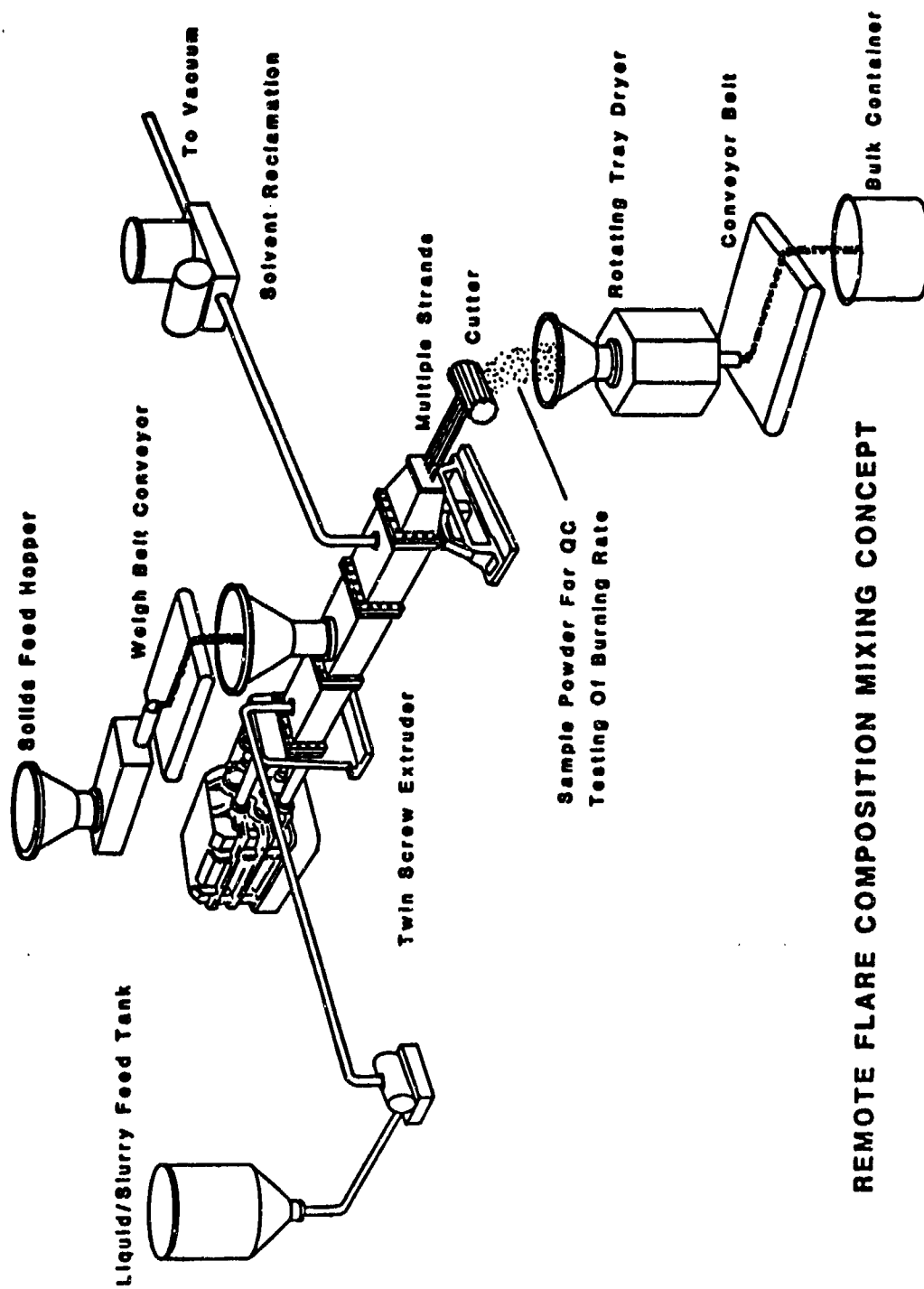
To prepare for these tests, arrangements were made with Werner & Pfleiderer to lease some old ZSK-53 extruder parts to build a mock-up of a twin-screw extruder. The ZSK-53 parts obtained included 8 barrel modules, a pair of screw shafts, and enough triple lobe screw elements to fill the shafts fully. A local contractor fabricated a drive unit utilizing a 9 HP air motor driving sprockets on the shaft ends with a "bicycle chain". A skid was built to hold the drive unit and support the barrels. No attempt was made to optimize the support and alignment system to prevent contact of the screws with the barrels. In these planned tests, the extruder was stopped and restarted with live material in the barrels to test the worst possible conditions.

The trials were run in an open field in one of the test areas at Longhorn. For the initial trials, the compositions were pre-mixed and charged into the extruder at the test site.

The first test consisted of an infrared decoy flare composition. A production formulation was chosen with known output characteristics and sensitivity. A standard mix was made and delivered to the test site. The extruder was set up about 75 feet from a bunker with air lines from a large compressor providing the air to drive the gears. The feed port was fitted with an aluminum pipe to serve as a feed funnel simulating the ZSK-58E. A die plate with a 1/2 in.

REDUCED HAZARDS FLARE MANUFACTURING





REMOTE FLARE COMPOSITION MIXING CONCEPT

diameter orifice was added to the extruder end to simulate the extrusion of the flare composition. Approximately 2 lb of the flare composition was loaded into the feed funnel and an aluminum follower plug was inserted to force the flare composition into the screws. The air motor was turned on from behind the bunker and the screw speed was adjusted to 20 rpm. When it was determined that flare composition was extruding through the die plate, an electric match was fired in a small bag of black powder to ignite the flare composition near the extrusion end of the barrels. The screws were kept turning during the entire test. The flare composition burned for approximately 20 seconds before reaching the funnel area. The confinement of the follower plug produced a surge in burning that blew the follower plug out of the funnel. It was found that the flame did not propagate through the die area and the extruded material did not ignite. The extruder was disassembled and inspected after the test and all of the parts were in satisfactory condition.

In the second test, a batch of LOVA propellant was produced in a vertical mixer for testing. LOVA is the acronym for Low Vulnerability Ammunition. It is a propellant designed to extinguish at atmospheric pressures to protect tank crews from their own propellant in the event of penetration of the ammunition in the tank. The test was set up the same as before. The LOVA propellant is a solvent-based system with ethyl acetate and ethyl alcohol solvents. When the igniter functioned, the solvents ignited and burned for about 2 minutes. When the solvent had burned away, the propellant did not ignite and the flame went out. This test went as expected, since the propellant does not sustain combustion under these conditions.

The third test was considered the most severe. A typical composite solid propellant was chosen for testing. This propellant is relatively energetic and has a known pressure exponent. It was sure to burn vigorously during the test. The propellant mix was made in a vertical mixer without the addition of the cure agent. This provided an extended pot life for testing. The funnel on the extruder was reduced in length and no follower plug was used with the propellant. The die plate was removed to simulate using the extruder in the mixer mode. Approximately 2 lb of propellant was placed in the funnel and the extruder screws were started. After it was observed that the propellant had filled the extruder barrels, the igniter was fired. The propellant quickly burned through the short distance to the extrusion end and ignited the propellant on the ground. After about 10 seconds, the flames progressed to the feed port and there was a muffled boom. Upon inspection of the extruder, it was noted that the aluminum plate used to hold the igniter had been bent significantly. It may be noted that the plate had been subjected to approximately 10 seconds of heating in a 5000 °F flame. When the extruder was cleaned and inspected, it was determined that the extruder parts were undamaged by the test.

The main point to be made by these tests was that there was no major damage or indication of severe hazard associated with ignition in the extruder while the screws were turning. This was considered an "overtest" since the ZSK-58E has provision for opening the split barrels and deluging the extruder. This would further mitigate the effects of an ignition. Automatic sensing of an anomalous temperature rise will be tested.

A fourth test was carried out to evaluate the effects of contamination of a propellant with particles that were too small to effectively screen out of the system. Screens capable of preventing the entry of nuts, bolts or other large contaminants into the extruder barrels have been incorporated in the system already. Since the clearance between screws and walls is nominally 787 microns and the clearance between screws is 787 microns, it was necessary to determine the effect of small particles on the hazards with contaminated propellant. The particle size distribution of the steel grit and sand used for these tests is shown in Table 1.

Table 1.
Particle Size Distribution

Screen	Opening (microns)	Cumulative Wt. %	
		Sand	Steel Grit
10	1910	13	0
16	1130	19	0
20	860	24	0
30	520	32	13
60	230	77	99
Pan	-	100	100

It is felt that 30 mesh screens would be the maximum that can be used for screening materials on a practical basis. If 16 mesh could be used for some materials, it would be a definite processing advantage. The remaining composite propellant used in the third test was chosen for this test. To evaluate the statistical probability of an ignition due to the incorporation of a small contaminant, 1% of sand and 1% of steel grit were added to the propellant. The propellant was then to be cycled through the extruder 20 times. Due to the age of the propellant, the viscosity had become very high and the material did not feed well in the extruder. There was a section of kneading blocks in the extruder to provide a "worst case" test. The propellant finally passed through the screws into a catch bucket. There was no ignition of the propellant during the first run, but due to the extreme difficulty in feeding, it was decided to terminate this test. The very high viscosity of this propellant caused the extruder to essentially granulate the mix. This resulted in a large surface area that would lead to a high rate of flame propagation. Under normal processing conditions, material would not be processed in this dry state.

It was decided that the ignition test would be conducted on this mix to assess the severity of the expected high burn rate on the extruder. The feed funnel was emptied of mixed propellant and 70 gm. of unground ammonium perchlorate was poured into the feed port. This was followed by 30 gm. of HTPB/Al slurry. The extruder was run for 30 sec to simulate the conditions expected at the feed port with unmixed propellant. An igniter was fired in the vacuum port to simulate an ignition. After approximately 1 second, there was a loud boom at the extruder. The aluminum feed funnel was split and ripped off the extruder. Two sections had closure plates blown out of the barrel. The skid the barrel

was mounted on allowed the downward force of the closure plate ejection to bend the barrel down and stretch the connecting bolts. Gaps were now visible between some of the barrel sections. The end caps that hold the screw elements on the shafts were elongated and cracked near the ends. Two screw elements had cracked at the interface to the next screw. The barrel sections were not severely damaged. New bolts and new screw element end caps were obtained and the two screw elements were machined off to eliminate the damaged sections. The extruder is now operational for additional testing. This is considered to have been a very severe test with contaminants covering a wide range of particle sizes in a mockup that permitted very harsh conditions to exist, including restarting the screws with live material in the barrels. It should be pointed out that this was a deliberate ignition of the system, and that the grit/sand mixture did not cause the ignition. In none of these severe condition tests was there an unintentional ignition of the energetic materials.

In conclusion, the tests conducted to date in the twin-screw extruder mockup have indicated that the original assumptions concerning the safety of the twin-screw extruder in processing energetics were justified. Future plans include more safety tests with the extruder mockup to gain more knowledge of possible failure modes and the results of accidental ignition.

"SPECIAL STUDY OF SAFETY IN PYROTECHNICS MANUFACTURING"

(OVERVIEW)

Presented By:

JOHN A. JOHNSON

**Chief, Development and Production
Explosives Safety Division**

U.S. ARMY TECHNICAL CENTER FOR EXPLOSIVES SAFETY (USATCES)

Savanna, IL

Presented to:

TWENTY-FOURTH DOD EXPLOSIVES SAFETY SEMINAR

28-30 August 1990

I. INTRODUCTION. In June 1989, a fire and deflagration occurred at one of the Army ammunition plants (AAPs). The plant was mixing an Infrared (IR) Decoy Flare composition in a mixing bowl when the incident occurred. The bowl contained 200 pounds of mixture which included magnesium, teflon, acetone, hycarb binder, and hexane.

A Board of Investigation (BOI) was formed immediately to identify a potential cause(s). As a result of the investigation, the BOI concluded that the most probable cause of the fire and deflagration was electrostatic discharge into the mixture.

As shown in figure 1, the plant was using a Cowles Dissolver System. The mixing bowl had been teflon coated to facilitate removing the mixture from the bowl as well as the clean-up process. However, the coating acted as an insulator and created some lack of grounding between the mixer bowl and the mixer shaft. A reading was taken of potential differences between the hexane dispenser tube and the mixer shaft and a net potential difference of 1,800 volts was found. A video tape taken of the operation at the time of the fire did, in fact, indicate a one-point initiation at precisely that location in the mixer bowl. A subsequent interview with one of the operators revealed that the flow of hexane into the mixer bowl had decreased that day by 50% as compared to the flow the day before.

The BOI deduced that the decreased hexane flow increased the vapors in the mixer bowl and an electrostatic discharge ignited the hexane vapors which then ignited the flare composition.

Within a week after the completion of the BOI, word was received at U.S. Army Technical Center for Explosives Safety (USATCES) that another Army activity was preparing to start a similar operation using basically the same materials and equipment. The USATCES representative, who had been a member of the BOI, was sent to observe the start-up of this operation and pass along lessons learned.

A review of the planned IR mixing operations revealed that the batch size would be considerably smaller (in the 5 pound range) and their Cowles mixer bowl was not teflon coated. A test was conducted to determine if electrostatic discharge was occurring here as it was at the other activity. The same problem of a high potential difference could not be duplicated.

From the results of the BOI and the subsequent visit to another activity, the following conclusions were made:

A. Non-standard Production Processes. Although the two activities were using similar technology, there were significant differences in procedures and equipment that were unique to each activity.

B. Fear of Losing "Proprietary Information." In some cases, the contractors managing the ammunition plants are in direct competition with other manufacturers and thus are protective of their procedures and equipment design and do not want to lose their advantages by revealing "Proprietary Information."

C. No exchange of "Lessons Learned." The exchange of "Lessons Learned" is almost non-existent. Problems uncovered during the BOI were discussed with other plants and they were totally unaware of the problems. In fact, some of the plants were not aware that a fire had occurred at another plant.

D. Production Schedules Not Known at Other Activities. Again, because of contractual concerns and a desire to keep some information confidential within an organization, the production schedules of specific plants are normally not known at other plants. There did not seem to be an effort to hide the information, but more likely a lack of interest or concern for what other plants were doing.

E. Safety Information Stops at Safety Office. During some comparisons, it was found that the Safety Offices at some plants were receiving accident/incident information and lessons learned and were promptly filing them away in their safety files without passing the information along.

F. Need to Get Information Down to The "Worker." In discussions with the workers, it was found they were not aware of previous accidents and the resulting fatalities and injuries. When asked about previous accidents and fatalities at their own plants, the workers were very vague as to when they occurred, why they occurred, and what the results were. Since these are the people who are most likely to suffer during an incident, they should be fully informed of the hazards involved and how they may prevent mistakes of the past.

II. PURPOSE OF USATCES STUDY. In August 1989, the Development and Production Explosives Safety Division of USATCES began a study of all pyrotechnic manufacturers to:

- A. Identify similarities and differences among Pyrotechnic processors.
- B. Identify the "best" ways of doing the same job.
- C. Look at the latest technologies being developed for pyrotechnic processes.
- D. Identify problems or potential problem areas.

III. ACTIVITIES VISITED. The USATCES planned to visit Government-owned, Government-operated (GOGO), Government-owned, contractor-operated (GOCO), and contractor plants in order to gain a broad perspective of policies and procedures in pyrotechnics manufacturing. Due to various causes, the contractor plants were not visited. However, the designers for both Navy and Army pyrotechnics were visited. One company was performing testing for the Army's Mixing, Granulating, and Drying (MIGRAD) systems and was visited to discuss their results of testing IR compositions. The Pyrotechnics Sub Group of the Joint Ordnance Commanders Group was visited to present preliminary findings of the USATCES study. The following were visited:

- A. Pine Bluff Arsenal (PBA)
- B. Longhorn Army Ammunition Plant (LHAAP)
- C. Lone Star Army Ammunition Plant (LSAAP)
- D. Lake City Army Ammunition Plant (LCAAP)
- E. Crane Army Ammunition Activity (CAAA)
- F. Naval Weapons Support Center (NWSC)
- G. U.S. Army Armament Research, Development and Engineering Center (ARDEC), Picatinny Arsenal
- H. Joint Ordnance Commanders Group (JOCG) Pyrotechnic Sub Group
- I. Sverdrup Corporation (Stennis Space Center)

IV. FINDINGS. There were several significant findings during the study. Because of curtailment of funding, some of the findings were not sufficiently studied to be included in this report. The following findings were observed or studied enough to be reported before completion of the overall USATCES study and final report.

A. Non-Standard Visitor Protection. The USATCES visits to the various plants revealed that the personal protective equipment (PPE) required of visitors was quite varied and not consistent with the types of areas visited.

(1) At one plant the visitors were required to wear basically the same clothing as the workers and were suited-up in cotton coveralls, conductive safety shoes, and safety eyewear.

(2) At another plant the visitors were required to wear only grounding straps over their street shoes.

(3) At another plant they were required to wear "NOMEX" shop coats and safety eyewear.

(4) The safety philosophies at the various plants varied significantly as to what visitors wore when visiting pyrotechnics facilities and how these visits were conducted.

B. Non-Standard Worker PPE. During the USATCES visits to the various plants, there was an obvious non-standard use of PPE.

(1) At one pyrotechnic manufacturer, the operators and supervisors were wearing cotton coveralls, conductive shoes, and safety eyewear.

(2) At another manufacturer, the operators were wearing "NOMEX" coveralls, conductive shoes, and safety eyewear while the supervisors wore "NOMEX" shop coats.

(3) At each location there were different safety philosophies on which PPE should be worn and how it was worn.

C. Non-Standard Use of Fire Suits. There were different safety philosophies on the use of fire suits.

(1) At one manufacturer the operators were wearing aluminized suits, hoods, and gloves over their cotton coveralls when handling magnesium powder.

(2) At another activity doing a similar type mix as above, the operator wore only a face shield in addition to cotton coveralls and conductive shoes when handling magnesium powder.

(3) When questioning the operators, they expressed a feeling of being safe. The operators wearing the aluminized suits felt they were protected from any fire as long as they were wearing the suit. However, from previous accidents and reports, we were able to determine that the IR composition fires occurred so fast that the operators were not properly protected.

(4) The USATCES representative looked at several existing self-cooled, heavy duty fire suits that had been purchased over the past fifteen years and observed that these suits were too heavy and bulky to be of real use in day-to-day operations. At all activities having these suits, the suits were stored out of the way.

(5) In questioning operators and supervisors, it was commonly believed that the cotton coveralls were static free. However, tests conducted by the Army and Navy have both proven that even cotton coveralls will have static buildup in low humidity conditions. Again, the operators had false beliefs that they were completely safe merely by wearing cotton coveralls.

D. MIGRAD.

(1) The MIGRAD is an abbreviation for the mixing, granulating and drying of pyrotechnic compositions. The line set up at PBA was a pilot plant model set up to test the concept of mixing, granulating, and drying of pyrotechnic composition in one operation. Plant systems will be 60 liters or 120 liters in capacity. The inert ingredients will be remotely charged into the mixing bowl and the bowl sealed with the exhaust vent to form one unit. Once the pyrotechnic composition has dried, the material will be pushed out of the system and slide down a chute into a velostat bag. An operator will personally remove the bag from the system.

(2) Sverdrup Technology Incorporated conducted testing at Stennis Space Center to determine which pyrotechnic compositions the MIGRAD would be able to handle. From their testing, they were able to determine that the MIGRAD could not handle certain "hot" items such as IR compositions.

E. Hazard Classification of IR Compositions.

(1) The USATCES found that there is not total agreement as to the hazard classification of IR compositions. The Army and Navy agree that the IR compositions should be hazard classified 1.3 when in the pressed state or in the final assembled state as an IR Decoy Flare. They also agree that the IR compositions in the wet state are 1.3. However, the Navy considers IR compositions to be 1.1 in the dry state while in process and the Army considers it to be 1.3. Classifying IR compositions as 1.1 vs 1.3 would have a significant effect on location of processing buildings because of the required separation distances. If a current operation/building is classified as 1.3 and the classification is changed to 1.1, then quantity distance (QD) would change and could cause some changes in location of the operation or shut down adjacent operations.

(2) During the USATCES study, it was found that the Army's tests to establish hazard classification did indicate that the IR compositions should be hazard classified as 1.3. However, later tests by the Navy and Sverdrup have shown that IR compositions react more violently than a mass fire and have indicated that additional test and studies do need to be conducted. As shown in figure 2, the accidents involving IR compositions since 1968 prove that processing of IR compositions has been deadly and costly. In that relatively short time, there have been 13 fatalities and over 30 serious injuries along with untold millions in property damages. In some cases, the entire plant operations were destroyed and were never restarted.

IV. CONCLUSIONS. The USATCES "Study of Safety in Pyrotechnics Manufacturing" is still in process and will be completed during fiscal year 1991. This paper has provided an overview of some of the findings of the study. The following conclusions are only a sampling of the total conclusions that will be included in the final report.

A. There is a definite need for the exchange of lessons learned among the AAPs and Activities. The workers on the line should be the recipients of these lesson learned so they will be aware of the hazards of their job and be better prepared to perform their daily tasks.

B. The PPE for visitors and workers at the various ammunition and explosives manufacturers and processors should be standardized.

C. The use of fire protection apparel should be standardized and the use of such equipment well defined in order to provide maximum protection to the worker.

D. IR compositions such as Magnesium-Teflon-Viton and Magnesium-Teflon-Binder (MTV/MTB) should be studied and tests conducted to determine the correct hazard classification of the compositions during processing in both the wet and dry states.

**"SPECIAL STUDY OF
SAFETY IN PYROTECHNIC MANUFACTURING"
(OVERVIEW)**

PRESENTED BY:

JOHN A. JOHNSON

**CHIEF, DEVELOPMENT AND PRODUCTION
EXPLOSIVES SAFETY DIVISION**

**U.S. ARMY TECHNICAL CENTER FOR
EXPLOSIVES SAFETY**

**TWENTY-FOURTH DOD EXPLOSIVES
SAFETY SEMINAR**

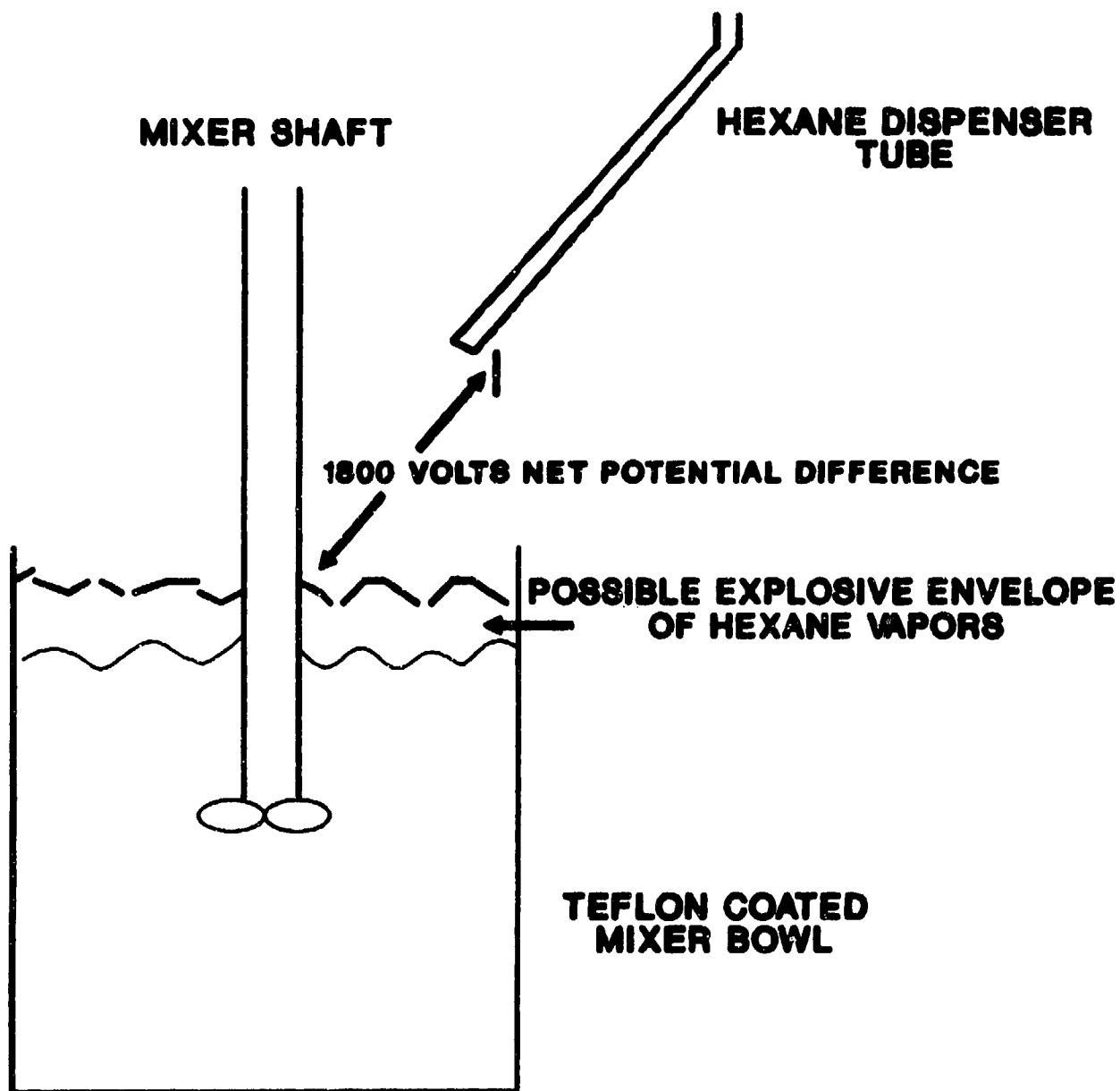
28-30 AUGUST 1990

DEVELOPMENT AND PRODUCTION DIVISION

BACKGROUND

- JUNE 1989 IR COMPOSITION MIXING FIRE
- JULY 1989 SIMILAR OPERATION BEGINS AT ANOTHER ACTIVITY

MEASUREMENT OF POTENTIAL DIFFERENCE



**FRONTAL VIEW OF
COWLES DISSOLVER SYSTEM**

DEVELOPMENT AND PRODUCTION DIVISION

CONCLUSION

- NON-STANDARD PRODUCTION PROCESSES
- FEAR OF LOSING "PROPRIETARY INFORMATION"
- NO EXCHANGE OF "LESSONS LEARNED"
- PRODUCTION SCHEDULES NOT KNOWN AT OTHER ACTIVITIES
- "SAFETY INFORMATION" STOPS AT SAFETY OFFICE
- NEED TO GET INFORMATION DOWN TO THE "WORKER"

DEVELOPMENT AND PRODUCTION DIVISION

PURPOSE OF USATCES STUDY

- IDENTIFY SIMILARITIES AND DIFFERENCES
- IDENTIFY "BEST" WAY TO DO THE JOB
- STUDY LATEST TECHNOLOGIES
- IDENTIFY PROBLEMS OR POTENTIAL PROBLEM AREAS

DEVELOPMENT AND PRODUCTION DIVISION

ACTIVITIES VISITED

- ✓ PINE BLUFF ARSENAL
- ✓ LONGHORN ARMY AMMUNITION PLANT
- ✓ LONE STAR ARMY AMMUNITION PLANT
- ✓ LAKE CITY ARMY AMMUNITION PLANT
- ✓ CRANE ARMY AMMUNITION ACTIVITY
- ✓ NAVAL WEAPONS SUPPORT CENTER (CRANE)
- ✓ ARDEC (PICATINNY ARSENAL)
- ✓ JOCG PYROTECHNIC SUB GROUP
- ✓ SVERDRUP CORPORATION (STENNIS SPACE CENTER)

DEVELOPMENT AND PRODUCTION DIVISION

FINDINGS

- NON-STANDARD VISITOR PROTECTION
 - COTTON COVERALLS, SAFETY SHOES, SAFETY EYEWEAR
 - STREET SHOES W/GROUND STRAP
 - NOMEX SHOP COATS
- NON-STANDARD PERSONAL PROTECTIVE EQUIPMENT (PPE)
 - COTTON COVERALLS
 - NOMEX SHOP COATS

DEVELOPMENT AND PRODUCTION DIVISION

FINDINGS (CONT)

- NON-STANDARD USE OF FIRE SUITS
 - ALUMINIZED FIRE SUIT
 - FACE SHIELD W/COTTON COVERALLS
- SIMILAR OPERATIONS
DIFFERENT LOCATIONS
- TOO MUCH FAITH IN ALUMINIZED SUITS
 - EXISTING SELF-COOLED SUITS TOO HEAVY AND BULKY
 - COTTON COVERALLS ARE NOT STATIC FREE
 - LOW HUMIDITY WILL ALLOW STATIC BUILDUP

DEVELOPMENT AND PRODUCTION DIVISION

FINDINGS (CONT)

- MIGRAD (MIXING, GRANULATING, DRYING)
- ARMY TESTING MATERIALS FOR
- WILL NOT ACCOMMODATE IR FLARE COMPOSITIONS
- OPERATOR MUST MANUALLY DISCHARGE MIX FROM SYSTEM

DEVELOPMENT AND PRODUCTION DIVISION

FINDINGS (CONT)

- HAZARD CLASSIFICATION OF IR COMPOSITIONS
 - ARMY CLASSIFIES AS 1.3 AT ALL TIMES
 - NAVY CLASSIFIES AS
 - 1.3 - FINISHED ITEM
 - 1.3 - WET STATE DURING PROCESSING
 - 1.1 - DRY STATE DURING PROCESSING

DEVELOPMENT AND PRODUCTION DIVISION

SUMMARY OF ACCIDENTS INVOLVING IR PYROTECHNIC COMPOSITIONS

<u>DATE</u>	<u>LOCATION</u>	<u>OPERATION</u>	<u>FATALITY</u>	<u>INJURY</u>
18 AUG 88	NWSC CRANE, BLDG 200	ASSEMBLY	3	1
18 DEC 88	NWSC CRANE, BLDG 198	EXTRUDER	1	1
13 NOV 75	CELESCO INDUSTRY	BLENDING	0	0
9 DEC 75	CELESCO INDUSTRY	MIXER	0	0
7 JAN 80	LONGHORN AAP	MIXER	1	1
19 DEC 83	TRACOR MBA, BLDG M-25	ASSEMBLY	2	19
18 JUL 85	BERMITE DIVISION	MIX/BLEND	0	0
8 AUG 85	TRACOR MBA	EMPTYING TUMBLER	3	5
19 MAY 86	DELA TEK	MIX/BLEND	1	2
28 AUG 86	KILGORE CORPORATION	DRYING ROOM	2	1
29 SEP 87	KILGORE CORPORATION	EXTRUDER	0	0
26 JUL 89	LONGHORN AAP	MIXER	0	0
9 NOV 89	TRACOR AEROSPACE	MIXING/DRYING	0	0
			<u>13</u>	<u>30</u>

SOURCE: JOINT ORDNANCE COMMANDERS GROUP (JOCG), SUB-GROUP FOR ORDNANCE
SAFETY REPORT OF CONVENTIONAL AMMUNITION AND EXPLOSIVES ACCIDENTS.

DEVELOPMENT AND PRODUCTION DIVISION

CONCLUSIONS

- NEED MORE AND BETTER EXCHANGE OF LESSONS LEARNED INFORMATION
- NEED TO STANDARDIZE WORKER AND VISITOR PPE
- NEED TO STANDARDIZE FIRE PROTECTION SUITS
- NEED TO REVIEW THE HAZARD CLASSIFICATION OF MTV/MTB IN DRY STATE DURING PROCESSING (1.1 VS 1.3?)

DESIGN AND INSTALLATION OF ULTRA HIGH-SPEED DELUGE SYSTEMS

ROBERT A. LOYD

**U.S. ARMY ARMAMENT
MUNITIONS AND CHEMICAL COMMAND**



**24th DEPARTMENT OF DEFENSE
EXPLOSIVES SAFETY SEMINAR
27-30 AUGUST 1990**

DESIGN and INSTALLATION of ULTRA HIGH-SPEED DELUGE SYSTEMS
for
ORDNANCE FACILITIES

I. Introduction:

1. The design and installation of ultra high-speed deluge systems for ammunition applications involves a technology which is substantially different from that associated with automatic sprinkler systems. Because, due the speed of water delivery from all of the nozzles, ultra high-speed deluge systems are highly dependent on the detection system, piping network, nozzles, and water supply characteristics, the design and the installation of ultra high-speed deluge systems must be performed by experienced designers and installers who thoroughly understand the limitations and capabilities of these systems.

2. Ultra high-speed deluge systems are sometimes installed with no thought or knowledge as to the hazards that they are to protect. Often, the system is designed or procured around specifications written for a completely different process. The lack of a complete definition of response time also effects the design of ultra high-speed deluge system.

3. This paper will discuss the following points:

- a. Brief description of an ultra high speed deluge system.
- b. Justification for ultra high-speed deluge systems.
- c. Proposed change to the definition of response time.
- d. Factors effecting water travel time from the nozzle to hazard.
- e. Changes to deluge system regulation.

II. The System.

1. Ultra high-speed deluge systems are used to protect personnel, process equipment, and buildings from the fire and thermal hazards presented by munition handling operations such as weighing, pressing, pelletizing, propellant loading, melting, extrusion, mixing, blending, screening, sawing, granulating, drying, and pouring. An ultra high-speed deluge system is designed to respond in ms by detecting a flame or ignition source in its incipient stage and by applying large volumes of water. A pre-primed, ultra high-speed deluge system utilizes the components listed below:

- Flame detector ultraviolet (UV) or infrared (IR)).
- Electronic controller (microprocessor).
- Valve (squib or solenoid operated).

- Pre-primed piping system with nozzles.
- Water supply.

2. See Appendix C for additional details.

III. Justification.

1. Ultra high-speed suppression has proven effective in prevention of propagation. For instance, during an explosive loading operation, the projectile being loaded initiated, and the deluge system was able to prevent propagation of the main explosive hopper. In cases of personal protection, there have been many cases where operators have been doused by water and serious burns were prevented. Total extinguishment has been accomplished many times in past incidents. Depending on the cost of the equipment, even if it is a remote operation, savings can be substantial if the fire is extinguished or not allowed to propagate.

2. The United States Department of Defense Ammunition and Explosives Safety Standards (DOD 6055.9-STD) states that, where exposed thermally energetic materials are handled that have a high probability of ignition and a large thermal output as indicated by a hazard analysis, they must be protected with an ultra high-speed deluge system. The system must suppress potential fires in their incipient state. Other publications such as AMCR 385-100 (U.S. Army Materiel Command Safety Manual), Navy Sea System Command OP 5 (Ammunition and Explosives Ashore), DOD 4145.26M (Contractor's Safety Manual), Military Handbook 1008 (Fire Protection for Facilities Engineering, Design, and Construction), and the National Fire Codes also provide guidance on ultra high-speed deluge systems.

3. Change 1 to AMCR 385-100 has clearly defined when a deluge system is required. An ultra high-speed deluge system is required when a potential fire and/or thermal hazard has a risk assessment code (RAC) of 1 or 2, as defined in AR 385-10, The Army Safety Program. See Figure 1.

IV. Response Time.

1. Response time criteria should be realistic and defined in a manner that will permit meaningful testing of the completed installation to ensure the performance criteria are met. There has been no common agreement on the definition of deluge system response time. This has caused confusion and prevented the development of a performance-type specification. This precludes the effective evaluation of ultra high-speed deluge systems.

2. In order to more precisely define response time requirements, it is necessary to understand the interrelationship between development of an incident and deluge system functions. The following outlines a way of breaking down the fire dynamics and deluge system functions into understandable segments:

a. Ignition Time T0: The start of ignition. Ignition of an item is defined as self-sustained deflagration.

b. Ignition To Sensing Threshold Time T1: The time from ignition until the buildup of energy reaches the sensing threshold of the detector saturation. This is dependent upon the configuration of the item being protected. For example, the ignition of propellant from the bottom of a hopper may require more than a second to reach the surface of the propellant where it can be sensed by a detector. If ignition occurred on the surface, the ignition to sensing threshold period would be in the ms range.

c. Ignition To Detector Response Time T2: The time from ignition to transmission of the signal to the controller.

d. Ignition To Controller Response Time T3: The time from ignition to transmission of signal to deluge valve squib or solenoid.

e. Ignition To Valve Opening Time T4: The time from ignition to the opening of the deluge valve permitting water to flow.

f. Ignition To First Water at the Nozzle Time T5: The time from ignition to the first flow of water from the critical nozzle(s). This is usually the nozzle(s) closest to the hazard or as determined by a hazard analysis.

g. Ignition To First Water on Target Time T6: The time from ignition to the first drops of water to strike the target from the critical nozzle(s). There is usually an initial stream of water, followed by a break in the flow, followed by a full flow pattern.

h. Ignition To Full Flow Water On Target Time T7: The time from ignition to a fully-developed spray of water strikes the target area.

i. Extinguishment Time T8: The time from ignition to termination of the deflagration.

3. There is no universally accepted agreement on the definition of deluge system response time. DOD 6055.9-STD, Ammunition and Explosives Safety Standards, and NAVSEA OP 5 Volume 1, Ammunition and Explosives Ashore, Safety Regulations for Handling, Storing, Production, Renovation, and Shipping discuss deluge systems but provide no guidance on response time. MIL-HDBK-1008A, Fire Protection for Facilities Engineering, Design, and Construction, cites a response time of 0.5 seconds (500 ms) but does not define response time. The U.S. Army Materiel Command Safety Manual, AMCR 385-100, provides the most complete definition of response time. It defines the response time for ultra high-speed deluge systems as: The sensing of a detectable event by the detector to the beginning of water flow from the critical nozzle(s) closest to the hazard or as determined by the hazard analysis (T1-T4). In lieu of testing, a small deluge system (design flow rate of 500 GPM or less) shall have a response time of 100 ms and large deluge system (design flow rate of more than 500 GPM) shall have a response time of 200 ms.

4. This definition does not consider the time required for the water to travel from the nozzles to the hazard being protected. This is the forgotten factor in the design of ultra high-speed deluge systems. It is not uncommon to see deluge systems that are specified for 100 ms response time, installed with nozzles 14 feet above the hazard. Applications like this are a waste of effort and provide an ineffective, unsafe system. The high-speed video tapes of the portable deluge tests at Tooele Army Depot and other tests conducted at various Army ammunition plants (AAPs) very graphically show the need to measure not only the time from detection to water at the nozzle but also from the nozzle to the target (hazard).

5. Deluge system response time should be redefined as total response time. This is the total time lapse from detector sensing threshold response to full flow of water on the target area (T1-T7). Total response time consists of two segments, detection time (T1-T4) and water delivery time (T4-T7). Detection time is the time from detector sensing threshold of the fire to the time that the signal is amplified and fires the primer in the water control valve or opens the solenoid valve (T1-T4). Water delivery time is the time required from primer firing or solenoid valve opening to the time a fully developed spray of water strikes the target (T4-T7). These will be discussed in more detail below.

6. Proposed definition: Response time is defined as the time from the sensing of a detectable event by the detector to a fully-developed spray of water striking the target/hazard from the critical nozzle(s) closest to the hazard or as determined by the hazard analysis. In lieu of testing, a small deluge system (design flow rate of 500 GPM or less) shall have a response time of XXX ms and large deluge system (design flow rate of more than 500 GPM) shall have a response time of YYY ms(T1-T7).

7. The actual times will need to be determined by testing and experience.

8. The total response time must be considered when designing deluge systems. The use of total response time provides a means to realistically evaluate the required response time of deluge systems. This will also provide a baseline for checking system response time during the annual flow tests and after a system has been inactive for an extended period of time, or a system has been modified.

V. Factors That Effect Water Travel Time.

1. Detection time is the time from detector sensing threshold of the fire to the time that the signal is amplified and fires the primer in the water control valve or opens the solenoid valve (T1-T4). The detection time is the fastest phase, and under ideal conditions, can be accomplished in as little as 10 ms. Although it is possible to shorten the detection time, the cost and increased chances of false activations usually make this impractical. Factors effecting detection time include:

- a. Distance between detector and target.

- b. Type of flame and amount of smoke.
- c. Signal processing time.
- d. Detector sensitivity.

2. Water delivery time is the time required from primer firing or solenoid valve opening to the time a fully developed spray of water strikes the target (T4-T7). It is the most time consuming portion of total response time. It is also the easiest to reduce both in terms of cost and system reliability. Water delivery time is dependent on several factors:

- a. Water pressure.
- b. The distance between the nozzle and hazard.
- c. Type of nozzle and piping configuration.
- d. The completeness of water prime of the piping system from the valve to the nozzles.

3. Research conducted by various agencies in the DOD establishment and private sector indicates there is a direct relationship between water travel time, water pressure, and nozzle type.

a. Preliminary tests at one facility indicated a definite relationship between pressure, water travel distance, and type of nozzle. With a target 12 inches from a nozzle, increasing the pressure from 75 to 150 psi resulted in a decrease of 13 ms (55 to 43 ms) for Nozzle A. The corresponding values for Nozzle B and C were 9 ms (46 to 37 ms) and 9 ms (56 to 47 ms) respectively. This pressure response relationship becomes more pronounced as the distance from the nozzle to the target is increased. With a target 36 inches from a nozzle, increasing the pressure from 75 to 150 psi resulted in a decrease of 20 ms (93 to 73 ms) for Nozzle A. The corresponding values for Nozzle B and C were 12 ms (91 to 79 ms) and 25 ms (116 to 91 ms) respectively. Figure 1 shows this relationship. While these distance/pressure relationships can vary somewhat depending on the type of nozzle and the basic relationship hold true for all systems. As can be seen by Figure 2 the difference in response times between the nozzles becomes greater as the pressure is increased.

b. Portable deluge tests conducted at Tooele Army Depot in March 1988 indicated there was a definite relationship between distance, pressure, and the type of nozzle. This relationship was observed during a review in the high speed video tape taken of the tests.

c. Several demonstrations at the 1984 Automatic Sprinkler Corporation Deluge Seminar indicated the following:

(1) The response times at 100 psi were approximately 20 ms faster than at 50 psi for both the squib and pilot types of systems. A pilot system was also tested twice at 150 psi. Surprisingly, the response times were the same as at 100 psi.

(2) A pilot system was activated four times, and the response times measured with a high-speed video camera. Detection time averaged 97 ms and water travel time from the nozzle to the target averaged 39 ms. The travel distances ranged from 15 inches to 24 inches. While four tests are not statistically valid, they provide an indication. See Figure 3.

d. Some tests done at Lone Star AAP in mid 1970's had similar results. A pilot type system was used with the nozzles set approximately 18 inches from the target. Tests were run at 75 and 100 psi. Water travel time was approximately 20 ms faster at the higher pressure. The type of nozzle also effected the water travel time.

4. Other items that can improve response time of systems.

a. Lone Star AAP:

(1) Lone Star AAP, operated by Day & Zimmermann Inc., has been a leader in the design of ultra high-speed deluge systems. For example, during the performance testing of two deluge systems, the design target of 100 ms could not be met. After analyzing the problem, three engineering changes were made: a looped water supply piping system in each bay; installation of a small pressurized surge tank; and removal of multiple 90-degree elbows. The response time was significantly reduced.

(2) A limited number of tests was conducted, and there was a problem with of erratic data caused by debris in system piping. This limits the credibility of test results; however, a reduction in response times of up to 60 percent indicated a need for more evaluation of the three design concepts for improved response times on ultra high-speed deluge systems.

(3) In one bay, the measured response time of a critical nozzle was reduced incrementally from 179 ms to 71 ms with the installation of the three modifications. That is a response time reduction of 60 percent. In another bay, a critical nozzle response time was improved from 124 to 70 ms after multiple 90-degree elbows were removed from the water supply line; however, the increase in response time of another critical nozzle from 109 to 225 ms indicates a possible problem with debris in the lines. After the looped pipe was installed, trash was found in the system. The trash was removed; however, the response time of 129 ms was still unacceptable. After installation of the surge tank, the response time of the critical nozzle dropped to 69 ms, which was acceptable. The surge tank had a capacity of 2 to 5 gallons. The tank was a standard bladder water pressure tank pressurized to approximately 26 psi. See figure 3. NOTE: All response times are detection to water at the nozzle.

(4) The general pattern of incremental reductions in response as each of the three modifications were completed indicates a need for further evaluation of the merits of looping the piping, installing the surge tanks, and removing the 90-degree elbows.

(5) The tests also indicate that trash and scale in deluge system piping can effect response time. This will become more of a problem as the water supply systems at ordnance facilities age. Many of these systems are more than 40 years old.

b. Research and experience have demonstrated the importance of removing all air trapped in the piping system of Primac Systems. An air pocket constituting 5 percent of the total volume of the system can cause a 100 percent increase in response time. An undetected small leak could result in the loss of water and entrance of air into the piping system which could drastically slow the system response time. One installation is evaluating a system for automatically removing trapped air and automatically adding water to the piping system whenever required.

VI. Changes to Deluge System Regulations.

1. The section on ultra high-speed deluge systems in AMCR 385-100 has been completely revised. The changes appear in Chapter 12 of Change 1, dated 16 March 1990. See Appendix 4 for details. The major changes include:

a. A potential fire and/or thermal hazard whose level of risk (RAC 1 or 2) is unacceptable will be mitigated by ultra high-speed deluge system, unless such a system will aggravate the hazard (reference AR 385-10 and AMCR 385-3).

b. Deluge systems will have a response time of 100 ms for small systems (design flow of 500 GPM or less) and 200 ms for large systems (design flow of more than 500 GPM).

c. Response time is defined as the time from the sensing of a detectable event by the detector (detector input) to the beginning of water flow from the critical nozzles.

d. Deluge systems shall be tested IAW the criteria of TM 5-825. Systems in laid-away or inactive facilities are exempt; however, they will be tested when put back into service. Records of the tests should be kept on file at the installation.

(1) A full operational flow test shall be conducted at intervals not to exceed 1 year, including measurement of response time. The results of the tests, or the use of the 100 or 200 ms response time will be retained on file by the installation for the life of the system.

(2) Detectors shall be tested and inspected for physical damage and accumulation of deposits on the lenses at least monthly.

(3) Controllers will be checked at the start of each shift for any faulty readings.

(4) Valves on the water supply line shall be checked at the start of each shift to ensure they are open.

e. Melt kettles and closed containers of molten explosives do not normally require the use of internal detectors or nozzles.

2. The AMCCOM Safety Office has submitted a completely new section on fire protection operations for ordnance operation and facilities for inclusion in the next revision of MIL-HDBK 1008. A copy is provided in Appendix E.

VII. Summary:

1. This paper provides an update on issues affecting the design and installation of ultra high-speed deluge systems. They include:

a. The need to redefine response time to include water travel time from the nozzle to the hazard.

b. Several ways that can improve system response time.

c. Changes to deluge system regulations.

2. Questions should be directed to Mr. Robert Loyd, U.S. Army Armament, Munitions and Chemical Command, ATTN: AMSMC-SFP, Rock Island, IL 61299-6000. Telephone: commercial (309) 782-2975/2182 and DSN 705-2975/2182.

VIII. Acknowledgment.

1. The technical reports in appendix A and the references in appendix B were utilized in the preparation of this paper.

2. The author greatly appreciates the technical assistance and material provided by the individuals below:

a. Mr. Gene Burns, Day and Zimmermann, Inc., Lone Star AAP.

b. Mr. Gary Fadorsen, Pyrotech International (formerly with Automatic Sprinkler Corporation).

c. Mr. Joe Priest, Grinnell Fire Protection.

d. Mr. Ken Klapmeier, Detector Electronics.

RISK ASSESSMENT CODE

Hazard Severity	Accident Probability			
	A	B	C	D
I	1	1	2	3
II	1	2	3	4
III	2	3	4	5
IV	3	4	5	5

Accident Probability

Description: Frequent
Level: A

Description: Probable
Level: B

Description: Occasional
Level: C

Description: Remote
Level: D

Hazard Severity

Category: 1
Description: Catastrophic

Category: II
Description: Critical

Category: III
Description: Marginal

Category: IV
Description: Negligible

FIGURE 1

AVE. RESPONSE TIMES FROM NOZZLE AT DIFFERENT DISTANCES

Distance from Nozzle to Target	12'	36'
--------------------------------------	-----	-----

75 p.s.i.
NOZZLE

A 40 degrees	55'	93'
B 90 degrees	46'	91'
C 120 degrees	56'	116'

125 p.s.i.
NOZZLE

A 40 degrees	44'	75'
B 90 degrees	41'	80'
C 120 degrees	48'	93'

150 p.s.i.
NOZZLE

A 40 degrees	42'	73'
B 90 degrees	37'	79'
C 120 degrees	47'	91'

Response Time (milliseconds)

FIGURE 2

EXAMPLES OF TOTAL RESPONSE TIME

TEST#	PRESSURE	WATER TRAVEL DISTANCE	DETECTION TIME	WATER TRAVEL TIME	TOTAL TIME
1	50 psi	18 in.	116 ms +	41 ms -	157 ms
2	175 psi	15 in.	91 ms +	33 ms -	124 ms
3	175 psi	21 in.	99 ms +	41 ms -	140 ms
4	175 psi	24 in.	91 ms +	41 ms -	132 ms

FIGURE 3

DESIGN IMPROVEMENTS

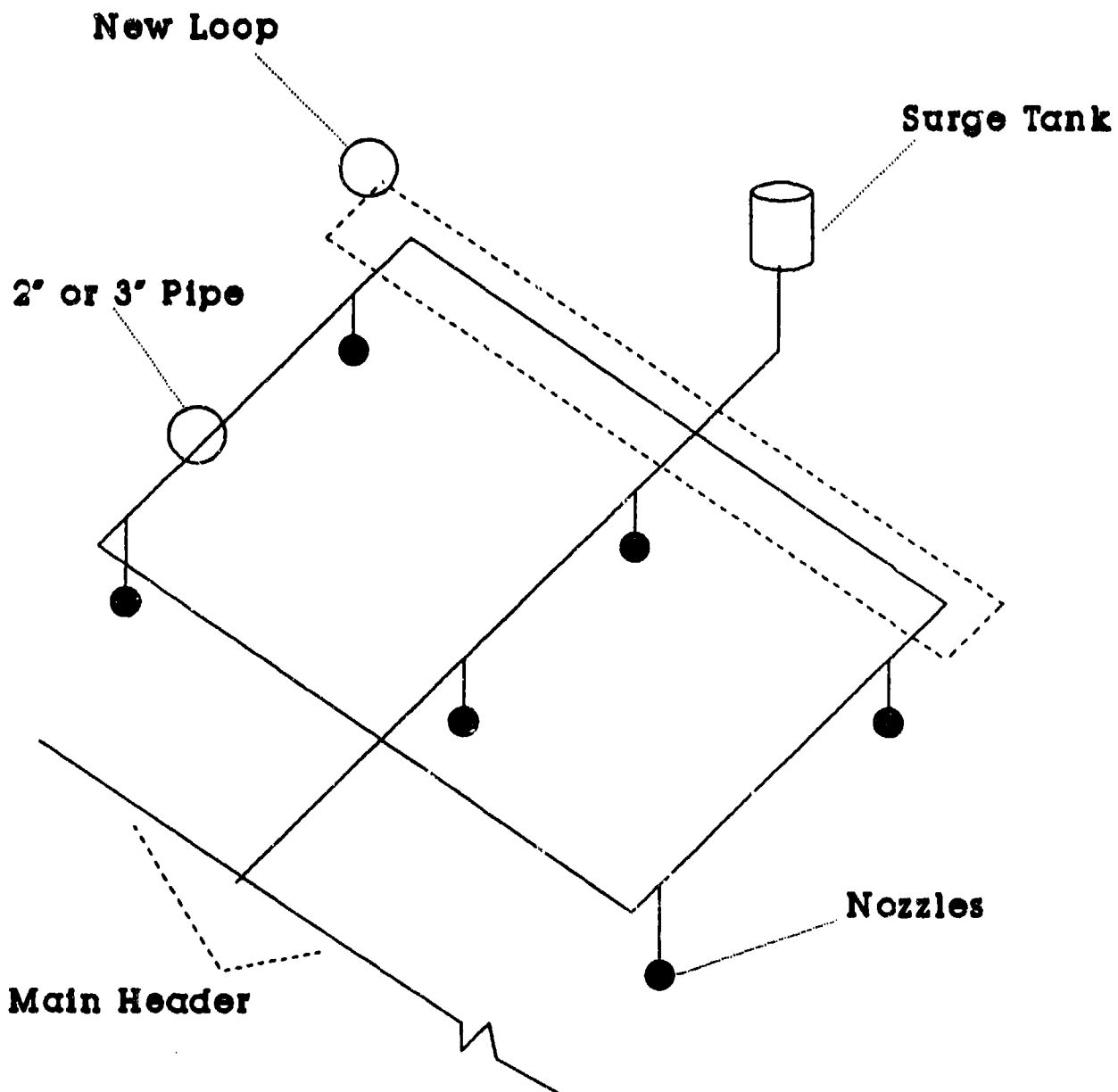


FIGURE 4

APPENDIX A

APPENDIX A

TECHNICAL REPORTS ON DELUGE SYSTEMS

1. Design of a Deluge System to Extinguish Lead Azide Fires, No. AD-E400 204, Aug 78, approved for public release (APR).
2. Evaluation of Pyrotechnic Fire Suppression System for Six Pyrotechnic Compositions, No. AD-E401 306, Mar 85, APR.
3. Engineering Guide for Fire Protection and Detection Systems at Army Ammunition Plants, Vol I (Selection and design), No. AD-E400 531, Dec 80, APR.
4. Engineering Guide for Fire Protection and Detection Systems at Army Ammunition Plants, Vol II (Testing & Inspection), No. AD-E400 874, Dec 82, Distribution limited to U.S. Government Agencies only - contains proprietary information.
5. On-site Survey and Analysis of Pyrotechnic Mixer Bays, No. AD-E401 141, Feb 84, APR.
6. Feasibility Study to Develop a Water Deluge System for Conveyor Lines Transporting High Explosives, Tech Rpt No. 4889, Aug 75, APR.
7. Development of a Water Deluge System to Extinguish M-1 Propellant Fires, No. AD-E400 217, Sep 78, APR.
8. Design of a Water Deluge System to Extinguish M-1 Propellant Fires in Closed Conveyors, No. AD-E400 216, Sep 78, APR.
9. Fire Suppression System Safety Evaluation, No. AD-E401 083, Dec 83, APR.
10. Dynamic Model of Water Deluge System for Propellant Fires, No. AD-E400 315, May 79, APR.
11. Deluge Systems in Army Ammunition Plants, prepared by Science Applications, Inc., for the U.S. Army Munitions Production Base Modernization Agency, 30 Jun 81.
12. Minutes of the Rapid Action Fire Protection System Seminar, U.S. Army Armament, Munitions and Chemical Command, 23-24 Oct 84.
13. Water Deluge Fire Protection System for Conveyor Lines Transporting High Explosives, No. AD-E400 034, Dec 77, APR.

14. Evaluation of an Improved Fire Suppression System for Pyrotechnic Mixes, No. AD-E401 569, Sep 86, Distribution limited to U.S. Government Agencies only.
15. Analysis of Mixer Bay Designs for Pyrotechnic Operations, No. AD-E401 602, Nov 86, APR.
16. Calculating Sprinkler Actuation Time in Compartments, Center for Fire Research, National Bureau of Standards, Mar 84.
17. Guidelines for a Thermochemical Kinetics Computer Program, Los Alamos National Laboratory, LA-10361-MS, May 85.
18. Mathematical and Numerical Methods Used in Thermal Hazards Evaluation, Naval Weapons Center China Lake, NWC TP 6510, Dec 86.
19. Technical Report on the Testing of Ultraviolet Actuated Deluge Systems Utilizing Solid State Controllers and Detonator-Actuated Valves to Extinguish Black Powder Fires, Day and Zimmerman, Lone Star Division, Nov 86.
20. Hazel - "A Computerized Approach to System Safety," Ken Proper, U.S. Army Defense Ammunition Center and School, Equipment Div, Aug 86.

Most of these reports can be ordered from the Defense Technical Information Center, Cameron Station, Alexandria, VA 22314. Their telephone number is AV 284-7633.

APPENDIX B

APPENDIX B

REFERENCES

1. AMC Safety Manual, AMCR 385-100, 1 Aug 85.
2. DOD Ammunition and Explosives Safety Standards, DOD 6055.9-STD, Jul 84.
3. Maintenance of Fire Protection Systems, TM 5-695 (Army)/FAC MO-117 (Navy)/AFM 91-37 (Air Force), Oct 81 with Change No. 1.
4. Military Handbook - Fire Protection for Facilities Engineering, Design, and Construction, MIL-HDBK-1008, 30 Apr 85.
5. National Fire Codes, National Fire Protection Association.

APPENDIX C

APPENDIX C

COMPONENTS OF AN ULTRA HIGH-SPEED DELUGE SYSTEM

I. Introduction.

1. Ultra high-speed deluge systems are used to protect personnel, process equipment, and buildings from the fire and thermal hazards presented by munition handling operations such as weighing, pressing, palletizing, propellant loading, melting, extrusion, mixing, blending, screening, sawing, granulating, drying, and pouring. An ultra high-speed deluge system is designed to respond in milliseconds by detecting a flame or ignition source in its incipient stage and by applying large volumes of water. A preprimed, ultra high-speed deluge system utilizes the following components:

- Flame detector (ultraviolet (UV) or infrared (IR)).
- Electronic controller (microprocessor).
- Valve (squib or solenoid operated).
- Preprimed piping system with nozzles.
- Water supply.

2. When a flame detector senses the radiant energy of a flame or ignition source within its field of coverage, it will respond within milliseconds, sending a signal to the electronic controller. The controller, in turn, sends a signal to the valve to open. Opening of the valve permits supply line water pressure to be applied to the priming water already in the pipe between the valve and the nozzles, causing water to flow from the nozzles suppressing the fire. At the same time, signals are sent to operate alarms and shut down process equipment. Approximately 500 preprimed, ultra high-speed deluge systems are used within the U.S. Army ammunition plant complex. We will discuss the components of an ultra high-speed deluge system in more detail later.

3. The ultra high-speed deluge system evolved from the conventional automatic sprinkler system. The conventional-type systems utilize closed heads with fusible links. It requires several minutes for the fusible links to melt and water to flow in the event of a fire. Next, came open head systems which were dependent upon heat actuated devices (HAD) to sense the fire and open a valve which permitted the water flow. Depending upon the HAD location, detection and water flow required 1 to 2 minutes. Finally, came the ultra high-speed deluge systems that use flame detectors (IR and UV), solid state electronic devices, explosively-actuated or solenoid-actuated valves, and the use of a preprimed piping system and nozzles to provide adequate water patterns and densities.

II. Detectors.

1. The flame detector is an optical device that responds to the radiant energy that is given off by a flame. When a flame or ignition source occurs within the field of view of the detector, the resulting electromagnetic radiation travels toward the detector at the speed of light. The detector responds to the radiant energy in milliseconds, sending a fire signal to the electronic controller.

2. The use of microprocessors now makes it possible to count and process the digital pulses from the UV detectors. Pulses no longer need to be stored in capacitors, but can be individually counted, entered into the registers of the microprocessor, stored in memory, and manipulated like any type of data processing information. This allows the design of flexible UV fire detectors using programmable memories and switches to provide an infinite number of combinations. Thus, we now have a marriage of UV detection devices with state-of-the-art microprocessors. Since the UV detector requires no signal processing other than comparing the radiation level to a present threshold, a very fast response time is achieved.

3. Ultraviolet detectors are ideally suited for applications where rapidly developing fires can occur in open areas. Ultraviolet detectors can be used to monitor ammunition assembly lines and renovation operations involving open mixing operation or open areas that are stocked with energetic materials awaiting processing. The UV detector is sensitive to welding arcs, lightning, gamma radiation, high electrostatic charges, and is easily obscured by contamination on the detector lens or in the atmosphere.

4. Typical applications for these high-speed IR detectors are characterized by strictly controlled, dark environments where a flash fire could originate. Conveyor belts passing through large covered ducts and closed explosive and propellant mixers are examples of the controlled environment necessary for proper application. However, high-speed IR sensors still must be carefully isolated from possible false alarm sources. Such sources include the sun and other blackbody radiation sources, high intensity light, flashbulbs, and fluorescent and incandescent lighting.

5. Typically, these systems are recommended to be used in combination with the appropriate UV systems, combining the advantages of UV for space protection with IR for enclosed areas. When dealing with an entire fire detection system that utilizes one or more than one type of detector, a detonator module greatly expands the flexibility and capability for the system. An individual detonator module can accept multiple input from UV and IR controllers, other detonator modules, manual alarm stations, heat sensors, smoke detectors, pressure sensors, or any contact closure device. In the event of a fire, any of these devices will cause the internal fire circuitry of the module to activate the detonator circuit, sound alarms, shut down process equipment, and identify the zone that detected the fire. When properly used, some detonator modules can add only a few milliseconds to the total system response time.

III. Valves.

1. Three types of ultra high-speed fire suppression systems are used in the U.S. Army ammunition plant/depot complex. They are the squib-actuated valve, the solenoid-actuated valve, and the explosive rupture valve.
2. The squib-operated valve uses an explosively-activated squib and a water-primed piping system in which, when the detection system senses the presence of radiant energy of an intensity and wavelength exceeding the detector's threshold, it sends an amplified electrical signal to the controller and detonator module which detonates the squib/primer in the control valve. The primer fires releasing a latch allowing the water supply line pressure to open the valve, thus, increasing the priming water pressure in the piping to the nozzle cap or rupture disk. The line pressure blows off the nozzle caps or bursts the rupture disk allowing water flow to the hazard.
3. The basic components of the solenoid-operated system are one or more IR or UV flame detectors, controller, pilot line solenoid, pilot control valve and nozzle, and supervisory test devices. In this system, the nozzle and associated valve is a pilot line-operated nozzle (relief) valve that is kept closed against the supply (fire) line pressure by the water pressure in the pilot line. This pilot line is normally connected to the water main as a source of pressure. The differential on the valve activating surface area (pilot line versus main water line pressure) maintains the nozzle valve in the closed position. The detector system may utilize IR or UV detectors. These detectors, upon responding to a fire, send an amplified signal to the controller, which, in turn, sends a signal to the pilot line solenoid-operated relief valve, causing it to open. This drops the pilot line pressure allowing the pilot control nozzle valves to open and main line water to flow. The pilot line is small enough to prevent the pilot pressure from being maintained with the relief valve in the open position. When pilot pressure is restored, the poppet reseats, even against fire main pressure.
4. A third type of ultra high-speed deluge system uses the explosive rupture disc. It has seen only limited use in the ammunition plant complex. It consists of preprimed piping with explosive rupture discs placed behind each nozzle. When a fire is detected, the squibs are fired, rupturing the disc, providing water at a very fast rate. This system can be preprimed at a much higher pressure than the squib valve. This type of system has been used on ammunition peculiar equipment.

IV. Preprimed Piping System with Nozzles.

1. An air pocket constituting 5 percent of the total volume of the system can cause a 100 percent increase in response time. An undetected small leak could result in the loss of water and entrance of air into the piping system which could drastically slow the system response time.
2. The pipe diameter, length, number of bends, and friction coefficient contribute to the volume of water that can be transported at an effective

pressure through the piping system. Pipe runs and bends should be kept to a minimum, and all horizontal runs should be sloped at least 1/4 inch per 10 feet of run, with air bleeders at all high points.

V. Water Supply.

1. The water density required will depend upon the type, quantity, and configuration of energetic material involved, process layout, and whether the goal is extinguishment, prevention of propagation, prevention of injury, or a combination of these. A commonly used density for preventing propagation and structural damage is 0.5 GPM/sq ft. The protection of personnel and process equipment, as well as the extinguishment of pyrotechnic fires, requires significantly higher density rates. These may be as high 3.0 GPM/sq ft for area coverage or 50 GPM/nozzle for point of operation coverage. Tests have shown that fires involving some pyrotechnic materials being mixed require a water flow of 200 GPM or more to extinguish. The only definitive guidance on water density requirements for ordnance facilities is Table 5-1, MIL-HDBK 1008. It specifies 0.5 gallons per square foot per minute.

2. An estimate of the maximum flow rate and pressure required by the deluge system should be made to determine water supply requirements. The capabilities of the existing water supply and distribution system to meet these requirements should be evaluated. A minimum static pressure of 45 to 50 pounds per square inch is usually needed at the building. If the required flow rate and pressure are not available, arrangements must be made to provide them. The water pressure required for proper functioning of an ultra high-speed deluge system must be available instantaneously, usually from an elevated tank or pressure tank. The instantaneous flow cannot be produced by starting a fire pump or jockey pump; however, a fire pump can be used to provide the required flow and pressure after the system has started to operate. Response time is directly related to water pressure, the higher the static pressure, the faster the response time. For most applications, the water supply should have a duration of at least 15 minutes. Water supply requirements for other deluge and sprinkler systems must also be considered. Since fires involving munitions are not normally fought, no allowance is required for fire department hose lines. However, the need for hose lines to protect nearby buildings from fires involving class 1.3 and 1.4 material and during cleanup should be considered.

APPENDIX D

DEPARTMENT OF THE ARMY
HEADQUARTERS UNITED STATES ARMY MATERIEL COMMAND
5001 EISENHOWER AVENUE, ALEXANDRIA, VA 22333-0001

AMC REGULATION
No. 385-100

1 August 1985

Safety

SAFETY MANUAL

12-18. Deluge Systems. a. The deluge system is an instantaneous response (millisecond) ultra-high-speed system controlled by flame detectors (usually ultraviolet or infrared). They are used primarily to protect personnel, process equipment, and buildings from the fire and thermal hazard presented by energetic material involved in high hazard explosive operations such as melting, mixing, blending, screening, sawing, granulating, drying, pressing, extrusion, and pouring. Deluge systems with heat actuated devices (HAD) are not ultra-high-speed deluge systems and should not be used for personnel protection.

b. The design and installation of ultra-high-speed deluge systems for ordnance applications involves a technology which is substantially different from that associated with automatic sprinkler systems. Due to the speed of water delivery from all the nozzles, ultra-high-speed deluge systems are highly dependent on the detection system, piping network, nozzles, and water supply characteristics; the design, specification, and installation of the deluge systems must be performed by experienced designers, engineers, and installers who thoroughly understand the limitations and capabilities of these systems.

c. Sequence of operation. When the flame detector senses a fire within its scanning range, notification that a fire condition exists is sent to the controller. The controller in turn sends an electrical impulse to open the valve. At the same time signals are sent to operate audible and/or visual alarms and to shut down process equipment. The deluge system consists of the following components:

(1) Detector. The most commonly used detector is the flame detector. It is an optical device that responds to the radiant energy that is given off by a flame. When a flame or ignition source occurs within the field of view of the detector, the resulting electromagnetic radiation travels toward the detector at the speed of light. The detector responds to the radiant energy in milliseconds, sending a signal to the electronic controller. Two types of detectors are commonly used in ultra-high-speed deluge systems: ultraviolet and infrared. The ultraviolet (UV) detector senses electromagnetic energy in the UV spectrum and is used primarily to observe open area operations such as ammunition assembly and renovation operations. The infrared detector senses energy in the infrared (IR) spectrum and is used primarily to observe operations in enclosed process equipment. The detectors should be constantly scanning and capable of responding and signaling when a flash or flame is detected. Each detector should have a method for automatically or selective remote verification of optical supervision and cleanliness. Detectors normally have about an 80 degree cone of vision. A third type of sensor is the fast acting (millisecond) pressure sensor. It responds to the pressure generated by a deflagration.

(2) Controller. The controller contains all the electronic circuitry for processing the signal from the detector to actuate the relays that control the deluge valve. The controller should be self-supervising with independent relay contacts, field adjustable sensitivity, plug-in modules and relays, and switches to put the system into a standby or bypass. The controller should have coded readouts of the system faults as they occur displayed prominently on the front panel. The controller should also contain the necessary instrumentation to monitor detectors, energize the audible and/or visual alarms indicating systems activation or malfunction, to transfer these signals to remote designated locations and to automatically stop the process equipment in the affected areas. The control panel should be located where it is easily accessible. A backup electrical power system should be provided. The backup system should be able to meet the electrical requirements of the system for 8 hours and still be capable of activating the deluge system.

(3) Valve. There are two common types of valves used in ultra-high-speed deluge systems. The squib operated valve uses an electrically fired explosive primer to open the valve permitting water to flow. The solenoid activated valve uses an electrically operated solenoid to open a poppet valve releasing pressure from the pilot line which permits the main valve to open and water to flow. A third type of valve is the electrically initiated rupture disc.

(4) Piping. The diameter, length, number of bends, and friction coefficient limits the effective flow rate of water that can be transported at an effective pressure by the piping system. Pipe runs should be kept to a minimum, and all horizontal runs should be sloped at least 1/4 inch per 10 feet of run, with air bleeders at all high points. The looping of deluge piping systems may improve response time by improving pressure and effective flow rate.

(5) Nozzle. The design of the orifice determines the dispersion pattern, water droplets, and turbulence of the water flow which in turn, directly affects the water velocity. Nozzles should be installed with priming water being held back at the nozzle with blowoff caps, rupture disc, or the poppet valve when utilizing pilot operated nozzles. Nozzle discharge rates and spray patterns should be selected to meet the hazard condition being protected.

d. Hazard analysis. All munition production, maintenance, renovation, and demil operations will be subject to hazard analysis in order to identify potential fire and thermal threats and to assess the level of risk. The hazard must be accurately defined. The risk assessment should include factors such as: initiation sensitivity; quantity of material; heat output; burning rate; potential ignition and initiation sources; protection capabilities (operational shields, clothing, etc.); personnel exposure (including respiratory and circulatory damage); munition configuration; process equipment; process layout; and building layout. A potential fire and/or thermal hazard whose level of risk (RAC 1 or 2) is unacceptable will be mitigated by a ultra-high-speed deluge system, unless such a system will aggravate the hazard. (Reference AR 385-10 and AMC-R 385-3).

e. Design. Once the hazard has been accurately defined, the deluge system can be properly designed. The design and installation of ultra-high-speed deluge systems for ordnance applications involves a technology which is substantially different from that associated with automatic sprinkler systems. Ultra-high-speed deluge systems are fire detection and suppression systems capable of water delivery from all nozzles in milliseconds following the detection of a fire. The deluge system is part of the total protection provided for an operation. Other protective features such as clothing, remote operations, protective construction, operational shields, venting, etc., must be considered. Factors such as water pressure, water density, water flow rate, pipe size, number of nozzles, nozzle design (spray pattern), pipe configuration, deluge valve location, water travel distance from nozzle to target detector location, number of detectors, and distance from detector to the hazard must be considered. Where no applicable data exists, experimental fire extinguishment should be performed in a safe location. Nozzles and detectors should be located as close as possible to the exposed energetic material to provide the best possible response time.

f. Performance. The deluge system must be capable of preventing propagation of a fire from the cell or bay to another. In conjunction with personal protective equipment required for workers at the operation, the deluge system shall prevent significant injury to the worker. The workers should not receive more than first-degree burns as the result of any thermal threat. The effectiveness of the deluge system shall be demonstrated by tests against actual or equivalent threat. These tests should be conducted with the maximum quantity of energetic material expected to be in the cell or bay. In lieu of testing, a small deluge system (design flow of 500 GPM or less) shall have a response time of 100 milliseconds and a large deluge system (design flow of more than 500 GPM) shall have a response time of 200 milliseconds or less, provided the hazard analysis indicates that a faster response time is not required. The results of tests or the use of the 100 or 200 milliseconds or less response time will be retained on file by the installation for the life of the system. Response time is defined below.

g. Density. The required density will depend upon the type of energetic material involved, process layout, and whether the aim is extinguishment, prevention of propagation, prevention of serious injury, or a combination of these. A commonly used density for preventing propagation and structural damage is 0.3 GPM/SQ FT. For protection of personnel and process equipment or extinguishment of pyrotechnic materials, significantly higher density rates may be necessary. These may be as high as 3.0 GPM/SQ FT for area coverage or 200 GPM for point of operation coverage.

h. Water supply. An estimate of the maximum flow rate and pressure that would be required by the deluge system should be made. The capabilities of the existing water supply and distribution system to meet these requirements should be evaluated. If the required flow rate and pressure is not adequate, arrangements must be made to provide the required flow and pressure. The water pressure necessary for proper functioning of a deluge system must be available instantaneously, usually from an elevated tank or pressure tank. The instantaneous flow cannot be produced by starting a fire pump; however, a fire pump can be used to provide the required flow and pressure after the system has started to operate. The water supply should have a duration of at least 15 minutes. No allowance is required for hose lines. All valves on water lines between the water main and the deluge systems will be supervised to ensure the valves are not accidentally closed.

i. Explosive vapors, gases, or dusts. When explosives vapors, gases, or dusts may enter nozzles and interfere with their operation, nonmetallic internally spring-held caps should be placed on the nozzles. The design must provide immediate release of the cap upon exertion of water pressure with the nozzle. Caps should be attached to the nozzles with small nonferrous chains to prevent their loss in equipment upon activation of the deluge system.

j. Manual activation. The deluge valve should be arranged for automatic and/or manual activation. Manual activation devices should be located at exits, in addition to the requirements of paragraph 5-9, and may be located at the operator's station when the hazard analysis determines the risk to the operator to be acceptable.

k. Response time. It is defined as the time in milliseconds from the presentation of an energy source to the detection system, to the beginning of water flow from the critical nozzle under test. The critical nozzle(s) is usually located closest to the hazard or as determined by a hazard analysis.

l. Measurement of response time. Two methods are commonly used to measure response time.

(1) Digit timer. A millisecond digital timer is started by a saturated UV source (IR for IR detectors) held directly in front of the detector and is stopped by the actuation of a water flow switch at the critical nozzle(s). This method does not measure the time lag of and water travel time from the nozzle to the target. It is normally used for routine testing.

(2) High-speed video recording system. A high-speed video camera and recorder (at least 120 frames/second) can be used as it permits very accurate measurement. The time from ignition to detection and water travel time from nozzle to target can also be measured. The video recording system can be used for contract compliance or when measurement of total response time is required.

m. Testing and maintenance. Deluge systems shall be tested and maintained per the criteria of TM 5-695 and para 12-18k. A good preventive maintenance program is required to reduce the number of false alarms and other system problems. Systems in laid-away or inactive facilities are exempt; however, they will be tested when put back into service. Records of the tests should be kept on file at the installation.

(1) A full operational flow test shall be conducted at interval not to exceed 1 year, including measurement of response time. The results of tests will be retained on file by the installation for the life of the system.

(2) Detectors shall be tested, inspected for physical damage and accumulation of deposits on the lenses at least monthly.

(3) Controllers will be checked at the start of each shift for any faults.

(4) Valves on the water supply line shall be checked at the start of each shift to ensure they are open. Unless the valve is secured in the OPEN position with a locking device or is monitored by a signaling device that will sound a trouble signal at the deluge system control panel or other central location.

n. Melt kettle and closed containers of molten explosives. They will normally not be equipped with internal flame detectors or deluge nozzles for the following reasons: The detector lenses or viewing ports are usually obstructed by molten explosives or moisture; the internal temperature of the kettle or container usually exceeds the maximum operating temperature of flame detectors (typically 150 degrees F.); the adverse and potentially violent reaction of water from leaks and condensation with molten explosives, especially those containing materials such as powdered aluminum and powdered magnesium; and the adverse effect of large quantities of cool water hitting the molten explosives. The exterior of the kettles and closed containers should be protected by ultra-high-speed deluge systems, especially openings where materials are placed in them. The hazard analysis requirements of paragraph 12-18d must be considered.

APPENDIX E

DRAFT

MIL HANDBOOK 1008 (FACILITIES FIRE PROTECTION)

4.4.2 Ordnance Facilities: The choice of fire suppression systems for ordnance facilities shall be based on the following considerations, which are listed in no particular order:

- a. Presence/absence of personnel.
- b. Exposed/unexposed energetic materials.
- c. Period of time exposed energetic materials are present.
- d. Process(es) involved.
- e. Physical properties of the energetic materials; i.e., rate of pressure rise, rate of decomposition/deflagration/detonation/initiation sensitivity, etc.
- f. Potential ignition and initiation sources.
- g. Quantities of energetic materials.
- h. Suppression goals (considering total extinguishment, prevention of propagation, equipment protection, personnel protection, and building protection).
- i. Survivability of the suppression/detection system.
- j. Physical properties of nonexplosive materials present; i.e., solvents, flammable liquids, combustible packaging materials.
- k. Lessons learned.
- l. Not used.
- m. Test data.
- n. Hazard analysis, safety assessment, and system safety assessment.
- o. Building construction.
- p. Type of process equipment and layout.
- q. Munitions configuration.
- r. Frequency of operation.
- s. Other protective measures such as clothing, equipment, shielding, and remote operations.
- t. Individual DOD service ordnance criteria.

4.4.2.1 Energetic material: Energetic materials includes any chemical compound or mechanical mixture which, when subjected to heat, impact, friction, detonation, or other suitable initiation, undergoes a very rapid chemical change with the evolution of large volumes of highly heated gases which exert pressures in the surrounding medium. The term applies to materials that either detonate or deflagrate and include explosives, propellants, and pyrotechnics. The paragraphs below provide guidance for facilities that contain energetic material. Use of competent engineering judgement is essential. All projects must conform to DOD 6055.9-STD, Ammunition and Explosives Safety Standards; Navy projects shall also conform to NAVSEA OP 5 Volume 1, Ammunition and Explosives Ashore; Army projects shall also conform to AR 385-64, Ammunition and Explosive Safety Standards; and Army Materiel Command projects shall also conform to AMCR 385-100, Safety Manual, and AR 385-64.

4.4.2.2 Ordnance facilities with exposed energetic material: These include ordnance production, assembly, maintenance, and surveillance facilities containing exposed energetic material. Typical procedures performed on exposed energetic materials (explosives, propellants, and pyrotechnics) include, but are not limited to: magnetic separation, visual inspection, screening, melting, machining, pressing, rocket motor assembly, projectile loading, drilling, defuzing, thread cleaning, propelling charge assembly, pouring, booster loading, blending, weighing, drying, mixing, grinding, pelletizing, igniter assembly, fuze assembly, depriming, flaking, washout/steamout, extrusion, casting, sawing, and granulating. Complete protection of such facilities is essential. Specific automatic sprinkler protection requirements for areas within these type of facilities are as follows:

a. Ultra-high-speed deluge systems are preprimed instantaneous response ultra-high-speed systems controlled by flame detectors which start to deliver water in milliseconds (ms). They are used primarily to protect personnel, process equipment, and buildings from the fire and thermal hazard presented by exposed energetic materials involved in ordnance operations and storage. Deluge systems with HADs (heat actuated devices) are not ultra high speed deluge systems due to their slow response times of 20 to 100 seconds. They provide little personnel protection. Refer to Table 10 in section 5, Water Demands for Sprinklered Facilities under the occupancy classification "Ordnance Plants (exposed energetic material)" to determine the sprinkler design criteria.

b. The design and installation of ultra-high-speed deluge systems for ordnance applications involves a technology which is substantially different from that associated with automatic sprinkler systems. Due to the speed of water delivery from all the nozzles, ultra-high-speed deluge systems are highly dependent on the detection system, piping network, nozzles, and water supply characteristics; the design, specifications, and installation of ultra-high-speed deluge systems must be performed by experienced designers, engineers, and installers who thoroughly understand the limitations and capabilities of these systems.

c. Sequence of operation. When the flame detector senses a fire within its scanning range, notification that a fire condition exists is sent to the controller. The controller in turns sends an electrical impulse to open the valve. At the same time signals are sent to operate audible and/or visual alarms and to shut down process equipment. The deluge system consists of the following components:

(1) Detectors - The most commonly used sensor is the flame detector, either ultraviolet (UV) or infrared (IR) is the flame detector. It is an optical device that responses to the radiant energy that is given off by a flame. Two types of detectors are commonly used in high-speed deluge systems. When a flame or ignition source occurs within the field of view of the detector, the resulting electromagnetic radiation travels toward the detector at the speed of light. The detector responds to the radiant energy and sends a signal to the electronic controller when the sensing threshold of the detector is reached. The UV detector senses electromagnetic energy in the UV spectrum. UV detectors are normally used to provide area coverage over and around process equipment. At least two detectors are normally used - one to cover the specific hazard and one to cover the bay. The IR detector senses electromagnetic energy in the IR spectrum. IR detectors are normally used in closed process equipment, vessels, and covered conveyors shielded from natural and artificial light. The detectors should be constant scanning and capable of responding and signaling when a flash or flame is detected. Each detector should have a method for automatically or selective remote verification of optical supervision and cleanliness. Detectors normally have about an 80-degree cone of vision. A third type of sensor is the fast acting (ms) pressure sensor. It responds to the pressure generated by a deflagration. Heat detectors are recommended for ordinary deluge systems. Smoke detectors are not usually used for ordnance facilities detection/suppression system. An exception to this is facilities that handle or process munitions containing smoke mixes, when the smoke could blind UV and IR detectors and a ms response time is not required.

(2) Controller - The controller contains all the electronic circuitry for processing the signal from the detector to actuate the relays that operate the deluge valve and other related outputs. The controller should be self-supervising with independent relay contacts, field adjustable sensitivity, plug-in modules and relays, and switches to put the system into a standby or by-pass. The control panel/rack assembly should have read-outs of the system faults as they occur displayed prominently on the front panel. The assembled panel/racks should also contain the necessary instrumentation to monitor detectors, controllers and flow control components, to energize the audible and/or visual alarms indicating system activation or malfunction, to transfer these signals to remote designated locations (fire department etc.) and to automatically stop the process equipment in the affected areas. The control panel should be located where it is easily accessible. A backup electrical power system should be provided. The backup system should be able to meet the electrical requirements of the system for 24 hours.

(3) Valve - There are two common types of valves used for high speed deluge systems. The squib operated valve uses an electrically fire explosive primer to open the valve permitting water to flow. The solenoid activated valve uses an electrically operated solenoid to open a poppet valve releasing pressure from the pilot line which permits the main valve to open and water to flow. A third type of valve is the electrically initiated rupture valve.

(4) Piping - The diameter, length, number of bends, and friction coefficient contribute to the volume of water that can be transported at an effective pressure by the piping system. Pipe runs should be kept to a minimum, and all horizontal runs should be sloped at least 3/4 inch per 10 feet of run, with air bleeders at all high points. Removal of all trapped air is very important. A very small air pocket can significantly increase response time.

(5) Nozzle - The design of the orifice determines the dispersion pattern, water droplets, and turbulence of the water flow which in turn, directly effects the water velocity. Nozzles should be installed with priming water being held back at the nozzle with blow-off caps, rupture disc or the nozzle poppet when utilizing pilot operated nozzles. Nozzle discharge rates and spray patterns should be designed to meet the hazard condition being protected. Nozzles should be located as close at the hazard as possible, but still protect the operator and all exposed energetic material.

d. Hazard analysis. All munition production, maintenance, renovation, and demil operations will be subject to hazard analysis or safety assessment in order to identify potential fire and thermal threats and to assess the level of risk. The hazard must be accurately defined. The risk assessment should include factors such as: initiation sensitivity; quantity of material; heat output; burning rate; potential ignition and initiation sources; protection capabilities (operational shields, clothing, etc.); personnel exposure (including respiratory and circulatory damage); munition configuration; process equipment; process layout; and building layout. A potential fire and/or thermal hazard whose level of risk is unacceptable will be mitigated by a high speed deluge system, unless such a system will aggravate the hazard.

e. Hazard. Once the hazard has been accurately defined, the deluge system can be properly designed. The deluge system is part of the total protection provided for an operation. Other protective features, such as clothing, remote operations, protective construction, operational shields, venting ect., must be considered. Factors, such as water pressure, water density, water flow rate, pipe size, number of nozzles, nozzle design(spray pattern), pipe configuration, deluge valve location, water travel distance from nozzle to target detector location, number of detectors, and distance from detector to the hazard must also be considered. Where no applicable data exists, experimental fire extinguishment should be performed in a safe location. Nozzles and detectors should be located as close as possible to the exposed energetic material to provide the best possible response time.

f. Performance. The deluge system must be capable of preventing propagation of a fire from the cell or bay to another. In conjunctions with personal protective equipment required for workers at the operation, the deluge system shall prevent significant injury to the worker. The workers should not receive more than first degree burns as the results of any thermal threat. Heat flux that an operator is exposed to should not exceed 0.3 calories per square centimeter per second with the operator wearing the proper protective clothing/equipment and taking turning-evasive action. The

effectiveness of the deluge system shall be demonstrated by tests against actual or equivalent threat. These tests should be conducted with the maximum quantity of energetic material expected to be in the cell or bay. In lieu of testing, a small deluge system (design flow rate of 500 gpm or less) shall have a response time of 100 ms and a large deluge system (design flow rate of more than 500 gpm) shall have a response time of 200 ms.

g. Density. The required density will depend on the type of energetic material involved, process layout, and whether the aim is extinguishment, prevention of propagation, prevention of serious injury, or a combination of these. A commonly used density for preventing propagation and structural damage is 0.5 gpm/sq ft. For protection of personnel and process equipment, or extinguishment of pyrotechnic materials, significantly higher density rates may be necessary. These may be as high 3.0 gpm/sq ft for area coverage or 200 gpm for point of operation coverage.

h. Water supply. An estimate of the maximum flow rate and pressure that would be required by the deluge system should be made. The capabilities of the existing water supply and distribution system to meet these requirements should be evaluated. If the required flow rate and pressure is not adequate, arrangements must be made to provide the required flow and pressure. A minimum static pressure of 45 to 50 psi is usually needed at the base of the riser. The water pressure necessary for proper functioning of a deluge system must be available instantaneously, usually from an elevated tank or pressure tank. The instantaneous flow cannot normally be produced by starting a fire pump, however a fire pump can be used to provide the required flow and pressure after the system has started to operate. The water supply shall be adequate to supply the total demand of the largest fire area at the specific residual pressure required by the system(s) plus an allowance for hose stream demand for a period of thirty minutes.

i. Explosive vapors, gases or dusts. When explosives, vapors, gases or dusts may enter nozzles and interfere with their operation, nonmetallic internally spring-held caps should be placed on the nozzles. The design must provide immediate release of the cap upon exertion of water pressure within the nozzle. Caps should be attached to the nozzles with small nonferrous chains to prevent their loss in equipment upon actuation of the deluge system.

j. Manual activation. The deluge valve should be arranged for automatic and/or manual actuation. Manual activation devices should be located at the exits, and may be located at the operators stations when the hazard analysis determines the risk to the operator to be acceptable.

k. Response time. It is defined as the time from the sensing of a detectable event by the detector to the beginning of water flow from the critical nozzle(s) closest to the target. This will normally be the nozzle(s) closest to the hazard or as determined by the hazard analysis. While the water travel time from the nozzle to the target is not included in the definition of response time, it must be considered in the design of ultra-high-speed deluge systems.

l. Not used.

m. Measurement of response time. Two methods are commonly used to measure response time.

(1) Digital timer - A ms digital timer is started by a saturated UV (IR source for IR detectors) held directly in front of the detector and is stopped by the actuation of a waterflow switch at the critical nozzle(s). This method does not measure the time lag from actual ignition to detector input and water travel time the nozzle to the target. It is well suited for routine measurement of response time by facility maintenance personnel. It is inexpensive, easy to operate, and quick to set up and tear down.

(2) High-speed video recording system - A high-speed video camera and recorder (at least 100 frames/second) is can used. It permits very accurate measurement. The time from ignition to detection and water travel time from nozzle to target can also be measured. It is used for determining compliance with specifications, system performance after major modifications, and research.

n. Testing. Deluge systems shall be tested IAW the criteria of the tri-service manual Maintenance of Fire Protection Systems (Army TM 5-695; Air Force AFM 91-37; and Navy NAVFAC MO-117). Systems in layed-away or inactive facilities are exempt, however they will be tested when put back into service. Records of the tests should be kept on file at the installation for the life of the system.

(1) A full operational flow test shall be conducted at intervals not to exceed 1 year, including measurement of response time.

(2) Detectors shall be inspected monthly for physical damage and accumulation of deposits on the lenses.

(3) Controllers will be checked at the start of each shift for any fault readings.

o. Ordinary deluge systems shall be provided in other areas or auxiliary sections of buildings which are not properly separated by fire-rated partitions (minimum 1 hour) from areas where exposed energetic material are routinely processed or stored exposed overnight. Refer to Table 10 in section 5, Water Demands for Sprinklered Facilities under occupancy classification "Ordinary Hazard Group 3" to determine the sprinkler design criteria.

p. Wet-pipe (dry-pipe in freezing areas) sprinkler systems shall be provided in other areas or auxiliary sections of buildings which are properly separated by fire rated partitions (minimum 1 hour) from areas where energetic materials are routinely processed or are stored exposed overnight. Such systems will also be provided where encased or enclosed energetic materials (not exposed) and munitions items are stored overnight in production, assembly maintenance, and surveillance facilities. Refer to Table 10, section 5, Water Demands for Sprinklered Facilities under the occupancy classification "Ordinary Hazard Group 3" to determine the sprinkler design criteria.

q. All electrical equipment, including fire detection and fire suppression equipment, in ordnance facilities shall be of the proper explosion classification. All electrical equipment, including fire detection and suppression equipment, in areas protected by deluge systems shall be suitable for wet locations.

r. Provide complete supervision of all sprinkler and detection systems so that any deficiency that develops that would affect the speed or reliability of operations will provide a distinctive alarm.

4.4.2.3 Melting Kettles: Melting units, melt-mix kettles and other equipment containing reservoirs of molten explosives shall be equipped with water deluge systems designed to completely and rapidly flood the equipment. The portions of the suppression piping within the equipment shall not be pre-primed with water and shall be protected by nonferrous or nonmetallic caps which will rupture or blow off and allow the water to flow. The valve shall be located outside the equipment and a weep hole shall be provided near the valve to guard against accidental leakage into the pipe. A 1-1/4 inch pipe under a head of at least 40 psi is recommended. The system shall be provided with automatic and manual activation. Detection devices (usually UV or IR detectors) shall be located to look into the interior of the kettle or reservoir during operation of the equipment. If a hazard analysis indicated detection is required only around the exterior the kettle or reservoir, then interior detection is not required.

4.4.2.4 Ordnance facilities with contained or encased energetic material: These include ordnance production, assembly, maintenance, and surveillance facilities with energetic material that is contained or completely encased in torpedo warheads, missile warheads, mines, rocket motors, projectiles, full up rounds (torpedo, missile, projectiles etc), and bulk energetic materials in fire resistant containers (e.g. metal but not fiberboard containers). Typical operations include but are not limited to: missile, torpedo, and projectile assembly, inspection, inprocess storage, laboratories, and packout. Specific automatic sprinkler protection requirements for areas within these type of facilities are as follows:

a. Wet-pipe (dry-pipe in freezing areas) or pre-action sprinkler systems are required. If electronic equipment is present, pre-action sprinkler systems are recommended. Refer to Table 10 in section 5, Water Demands for Sprinklered Facilities under the occupancy classification "Missile Assembly" to determine the sprinkler criteria.

b. Complete protection of such facilities is essential.

4.4.2.5 Test Cells: Missile and other weapon test cells shall conform to the requirements above for Explosive Operating/Assembly Buildings except that ordinary deluge systems (pre-primed or not pre-primed) should be installed in test cells if a rapid-spreading fire can be expected to occur as a result of a design basic accident. Exit doors shall be manually openable without requiring electric power.

4.4.2.6 Storage magazines: When constructed in accordance with definitive designs and used only for storage, storage magazines do not require automatic sprinkler protection.

4.4.2.7 Shipping/Receiving/Transfer/Handling/Segregation Facilities: In these facilities there should be no exposed energetic material, only finished ordnance items or energetic material that is total encased in project bodies, shipping containers, drums or boxes. They may remain in the facility overnight or short periods of time awaiting shipment. Refer to Table 10, in section 5, Water Demand for Sprinklered Facilities under the occupancy classification "Ordinary Hazard Group 3" to determine the sprinkler design criteria.

4.4.2.8 Automatic sprinkler and deluge systems in ordnance facilities shall be provided with flexible couplings and sway bracing similar to that provided for buildings in earthquake zones.

4.4.2.9 Ordnance facilities shall be provided with panic exiting hardware for personnel doors.

4.4.2.10 The provision of floor drainage should be considered for ordnance facilities protected by deluge systems. The run off water may be contaminated with explosive waste. This must be considered in the system design.

PRYO SUIT SYSTEM

STEPHEN J. ASTHALTER

Utility Safety Associates Inc.
103 Washington Street
Morristown, New Jersey 07960

Table of Contents

Foreword and Acknowledgements

Section One	Background Report: Pyrotechnic Safety Enhancement Program: Pyrotechnic Clothing Joseph Matura ARDEC
Section Two	Validation Picatinny Arsenal Tests 1987
Section Three	Overview Pyro Suit System Pyro Suit System Components
Section Four	Proper Donning Suit with Air Only Suit with Cooling Vortec Suit with Cooling Vortec and Vest Suit with Self Contained Breathing Apparatus
Section Five	Air Supply System Plant Air Air Supply System at Pine Bluff Arsenal Self Contained Breathing Apparatus
Section Six	Proper Suit Maintenance Suit Cleaning Faceshield Replacement Cooling System Air Hat System

● Foreword and Acknowledgements

This manual was written to help munition plants implement a pyrotechnic handlers suit program. The program involves an aluminized five piece pyro suit similar in design to firefighting clothing used at airports. However, due to the intense heat of a pyrotechnic fire, (often four times greater than a jet fuel fire), the fabrics used are substantially upgraded. The use of these fabrics allows the suit to be relatively thin and lightweight. The design incorporates an air line system, and an option permits the use of a self contained breathing apparatus. Cooling options are also available. The suit was developed by Mr. Olen Nelson, a manufacturer of safety clothing, in close cooperation with Tracor Aerospace. Stephen Asthalter, a consultant, worked with the U. S. Army Armament, Research Development & Engineering Center (ARDEC) at Picatinny Arsenal in Dover, NJ in testing and modifying the entire system. The suit, which the Army report reprinted in this manual refers to the second generation pyro suit, is commercially available.

The involvement of Tracor and the Army was in the area of testing and validation. Tests conducted at Tracor's facility in San Ramon, CA under the direction of Mr. Dan Barrios established the criteria for the fabric composition of the suit and basic design. The tests conducted at Picatinny Arsenal under the guidance of Mr. Joseph Matura validated the fabric composition for a 15 lb. magnesium sodium nitrate fire, but clearly pointed to the need for a redesign of the suit's hood to prevent the fire from getting inside. This redesign sealed the hood and thus required breathing air to be continuously supplied.

Mr. Matura's written report on the U.S. Army's testing and it's development of a pyrotechnic suit is found in Section One. A pictorial display with commentary of the testing conducted at Picatinny Arsenal is found in Section Two. This section is also designed to show employees who handle pyrotechnics the danger, and to motivate them to wear the pyro suit properly. Section Three will give an overview of the Pyro Suit System (the second generation suit) and a pictorial detailing of it's components. Section Four will discuss how plant air can be implemented and will show an excellent installation at Pine Bluff Arsenal. Sections Five and Six will demonstrate proper donning and maintenance respectively.

The initial introduction of the pyro suit to the U. S. Army was in March 1987. It should be noted that in a ten month period, the suit, was tested three times, redesigned once, presented to the Army ammunition plants for their input, and presented to the DODESB in Washington, D.C. The speed in which this was accomplished was the result of the cooperative spirit and a strong desire for an improved pyro suit program on the part of PBMA and ARDEC at Picatinny Arsenal, and the safety office for ARDEC at Rock Island, IL. The support and leadership of Jon Bomengen at PBMA and the advise and encouragement of Crane AAA, Pine Bluff Arsenal, and Longhorn and Lone Star AAP's was critical to the successful final outcome of this effort.

Section One: Background Pyrotechnic Safety Enhancement Program Protective Clothing

Joseph Matura
Acting Chief, Munitions Section
AAD, FSAD

As a result of accidents with pyrotechnic mixes, some involving fatalities, a comprehensive program was undertaken to enhance safety in these types of operations. One of the priority investigations was focused on designing protective clothing that would provide the best possible environment for an operator to survive accidental ignition in processing pyrotechnic mixes.

The initial approach to development of protective clothing was a joint effort of ARDEC and the Navy Clothing and Textile unit at Natick. This involved research into materials and individual testing of candidates utilizing unconsolidated pyrotechnic compositions. From this, we developed a one piece garment that was tested using instrumented mannequins arranged in a blending bay setting with loose pyrotechnic composition in a "mock up" blender. The instrumentation provided a means of measuring the temperature rise inside the garment on the surface of the mannequin, when the composition was ignited. The temperature of such an ignition was determined to be in the 5000 to 5500 degree F range. Measurement of the temperature rise on the surface of the mannequin was accomplished by the use of skin stimulants and thermocouples linked to a computer. The temperature rise was recorded at 30 degree F to 40 degree F indicating successful protection. The thermocouples were normally located at the head, chest (2 places) abdominal area, one arm and one leg. Subsequent to each of these test sequences the mannequin was photographed with the garment in place and then as the hood and main garment was removed, photographs were taken at each step to record the condition of clothing and mannequin. In addition, a white cotton undershirt was in place on the mannequin that would provide additional visual evidence of any temperature rise that would cause scorching of the cotton. As a result of the success of these tests, garments were manufactured and distributed to selected plants for their use and commentary.

The feedback data from the plants indicated dissatisfaction in certain areas. Specifically, the complaints centered on the difficulty of getting into and out of the one piece overall, the difficulty of cleaning the garment (complicated by some shrinkage) abrasion and tearing of the fabric, interference with free movement due to bulk and uncomfortable heat when worn in non-airconditioned areas. It is axiomatic that to provide protection against the type of event encountered, some restriction of movement and level of discomfort will probably be unavoidable. However, we evaluated each criticism and attempted to correct the situation. From this effort, a second generation garment evolved as a result of the cooperative effort of ARDEC and a commercial manufacturer of safety clothing that had developed a pyro fire safety suit for the private sector. The new garment is of a five piece design using the same basic protective material except that it is knitted rather than woven (to reduce bulk) and has an aluminized outer layer. The latter not only provides additional thermal protection but also provides for a reduced effort of cleaning. The garment was subjected to the identical test program discussed previously and was equally successful. The freedom of movement about the workplace has been enhanced by the reduced bulk and the level of effort to get into and out of the garment has been substantially reduced. In addition, we have provided a small, lightweight air conditioning unit that is now part of the breathing system.

At this juncture it is felt that the protective clothing discussed herein represents the best possible protection against accidental ignition of pyrotechnic compositions and the subsequent events. As near as can be currently determined, we have utilized state of the art materials and components that have resisted the test environment. By any objective standard, the level of protection provided by this garment is far superior to what is in current use, this being predicated on actual test data. All testing has been recorded on film, both still and motion and is being edited into an instructional and training film. Based on the data provided in this discussion, the protective clothing should be provided to the various plants at the earliest possible date.

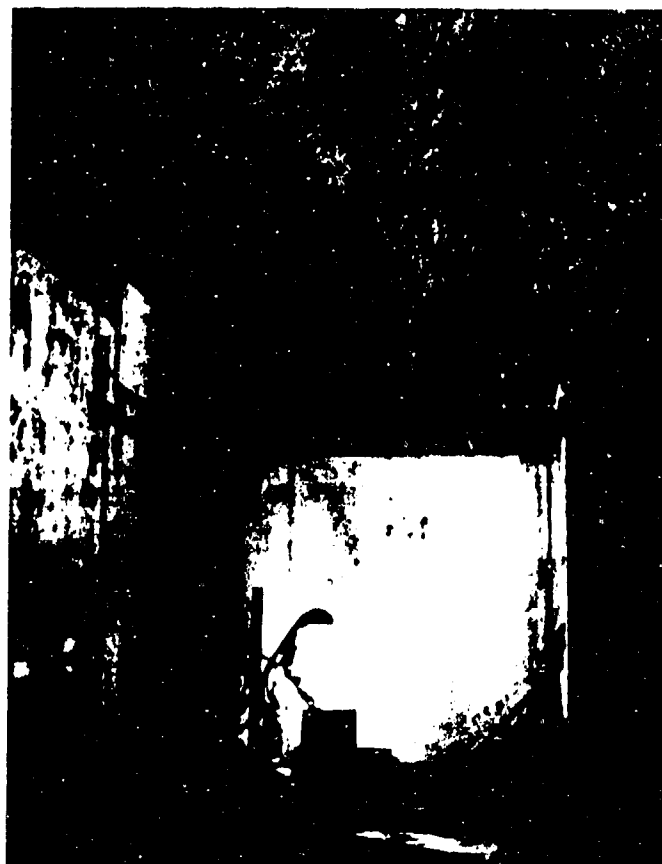
The following pages show the result of the test of the 2nd generation with all modifications included from the results of the testing.

Section Two: Validation: Picatinny Arsenal Tests 1987

The Pyro Suit System (second generation suit), was tested three times from April to August 1987. Using time lapse photograph the following pictures show how deadly this brief incident can be.



A mannequin is dressed in a test suit. A 15 lb. mix of magnesium sodium nitrate is in the drum.



The fire ball hits the mannequin squarely in the face in less than one tenth of a second.



In less than one-eighth of a second the mannequin is engulfed in a 5000 degree fire ball.



In less than two seconds molten magnesium rains down on the mannequin.

[illegible]

Section Three: Overview

Pyro Suit System

Pyro Suit System

The Pyro Suit System, referred to in Mr. Matura's report as the second generation suit, utilizes state of the art fire retardant fibers and unique fabrics which result in a lightweight and flexible aluminized suit. In addition, an air supply and cooling system has been built into the suit. Familiarity in five areas: fibers and yarns, fabric design, suit design and the air cooling system, is necessary to an understanding of the Pyro Suit System (PSS).

Fibers and Yarns

Fibers

P.B.I.: Polybenzimidazole, known as P.B.I., is considered the most fire resistant fiber made in the world today. P.B.I. is produced by the Hoechst Celanese Corporation. Despite its fire resistant characteristics, P.B.I. has a soft silky feel.

Kevlar: Kevlar has a temperature rating of 800° and is a very strong fiber. Kevlar is produced by Dupont.

Durvil: Durvil has a temperature rating of 400° and is comparatively inexpensive compared to PBI and Kevlar. The fiber is soft and adds wearing comfort to a fabric. Durvil is made by the Avtex Corporation.

Yarns

The characteristics of the fibers mentioned may be combined by blending them into yarns. A strong fire retardant yarn is produced when P.B.I. and Kevlar are blended. A soft yarn, that is also highly fire resistant, is produced when P.B.I. and Durvil fibers are blended.

Fabric Design

There are three basic types: wovens, knits and felts. In comparison with knits and felts, wovens are stiff and when aluminized are inflexible. By aluminizing a knit and a felt a great degree of flexibility is retained in the PSS fabrics.

The outer layer of the PSS is a highly fire retardant aluminized knit that is made with a yarn that contains 50% P.B.I. and 50% Durvil fibers. The middle insulation layer is an aluminized fire retardant felt that is made with yarns that are 40% P.B.I. and 60% Kevlar. The inner liner is the same base fabric as the outer liner but un-aluminized. The Durvil content added to the P.B.I. helps make it a comfortable fabric against the skin.

Suit Design

The basic suit consists of five pieces: a coat, hood, pants, gloves and spats. In contrast with a one piece coverall design, this multi piece design eases donning. However, it also creates a potential danger if the five pieces are not donned properly. It is critical that the hood inner bib be worn inside the coat to prevent a fire ball getting under the hood. The faceshield in the hood consists of two pieces, with an inner shield of clear polycarbonate and an outer shield of polycarbonate with gold coating for heat reflection.

In situations when a wearer cannot be attached to plant air, the back of the coat is expanded with a pouch to accommodate a self contained breathing apparatus.

Another advantage of the five piece design is economics. Individual components can be replaced as they wear out, reducing suit replacement costs.

Air Cooling System

Once the inner bib is placed under the coat, all air is cut off and an air source is required. A simple air supply tube attached to the hard hat in the helmet, and then attached to plant air as depicted in Section Four, provides the breathing air needed. A vortex can be added to this air line to cool the air. A vest can be added to the same air line to provide additional cooling. This system is depicted in Section Five.

The Pyro Suit System raises the level of protection against a 5500° pyrotechnic flash, which exceeds what is currently available. It must be worn in accordance with the instructions in this manual to provide protection.

Pyro Suit System Components



Pyro Coat



Pyro SCBA Coat



Pyro Hood



Pyro Pants



Pyro Gloves



Pyro Spats



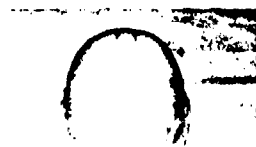
Suspenders



Gold Faceshield
Clear Faceshield



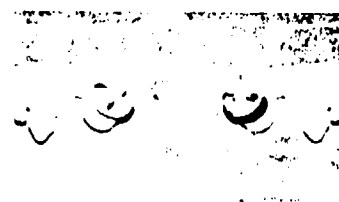
Hood Air Supply System



Air Hard Hat



Suspension



Faceshield Holders



Hood Air Supply Hose Assembly



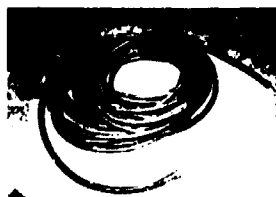
Male Plug



Belt Loop



Set of 3 Plastic Holders



Main Air Hose



Vortec Cooling Tube



Vortec Belt



Cooling Vest



Air Splitter Hose

Section Four: Proper Donning Suit with Air Only



1. The pants and spats are put on first.



2. The hood is then donned. Care is taken to flatten the front of the inner bib against the chest.



3. The outer bib is temporarily attached to the back of the hood by a velcro holding tab and the green tail that is attached to the back of the inner bib is turned down. This procedure is done keeping the inner bib inside the coat when the coat is put on.



4. At this point the air is connected and turned on.



5. The coat is now put on. The inner bib is securely placed inside the coat.

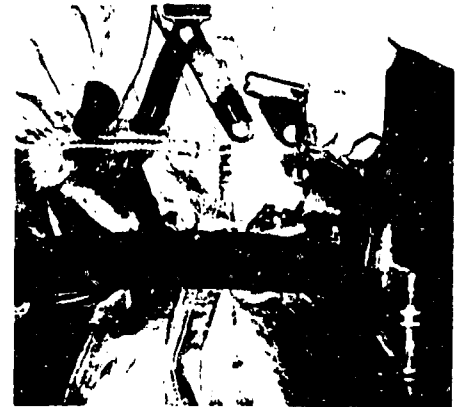


6. The coat is closed up. The inner bib is attached to the back of the hood by velcro. Straps attached to the back of the outer bib are placed under the arm and across the front of the outer bib.

● Suit with Cooling Vortec



1. The male plug is removed and the garden hose fitting is exposed.

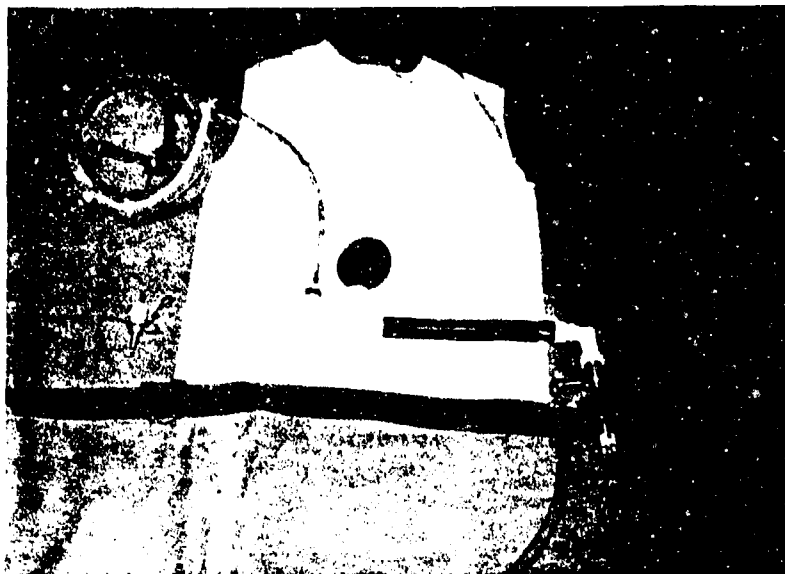


2. The male plug is attached to the loop on the suspenders. The vortec tube is put on.



3. The hood air supply hose is attached to the vortec. The main air supply hose is attached and turned on. The coat and gloves are now put on.

Suit with Cooling Vortec and Vest



1. This overview picture shows the complete air supply system with cooling.



2. The pants, spats and vest are now on. The inlet connection on the vest is being connected over the top of the pants.



3. The vest air hose splitter is attached to the air hose inlet.



4. The hood is now put on. The vest is attached to the air hose, and the hose is now attached to the rest of the suit is done.

Suit with 30 or 60 Minute Self Contained Breathing Apparatus (SCBA)



1. The pants and spats are put on. The SCBA unit is put on according to the SCBA's manufacturer's instructions.



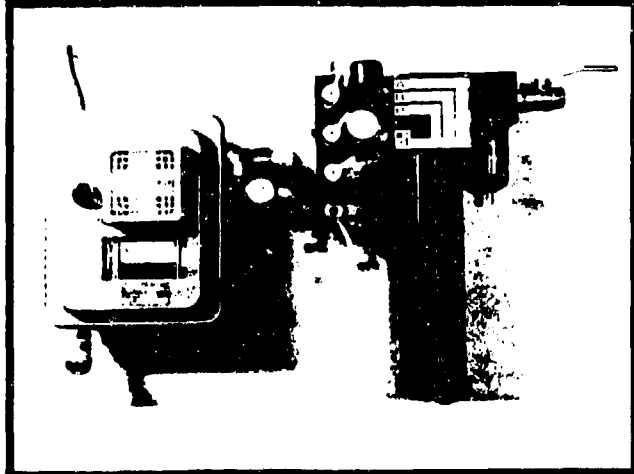
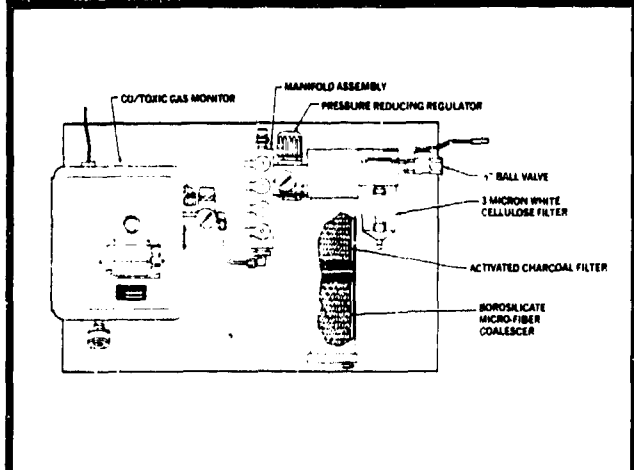
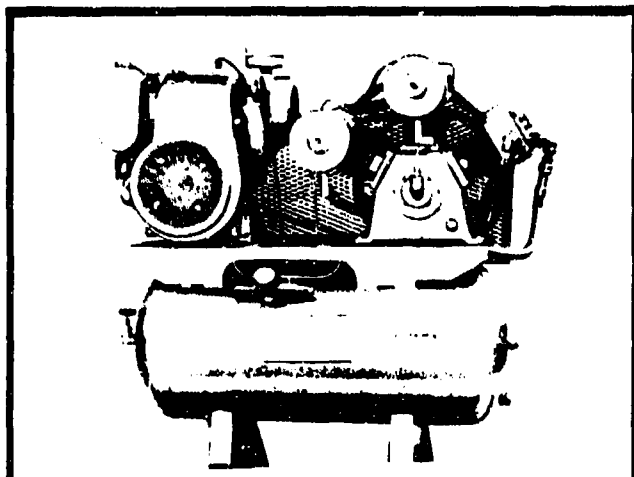
2. The hood is donned in normal fashion, and a coat, modified to be worn with SCBA's is put on. The gloves are then donned.



3. Another view of the fully donned suit with a 30 minute SCBA unit.

Note: The suit is designed to accept most SCBA's. Additional modifications can be made to accept any SCBA unit.

Section Five: Air Supply System Plant Air



Supplying Grade D Air.

Grade D breathing air needs to be supplied to the hood and cooling vest. A regular industrial air compressor may be used for this purpose if the air is filtered and continuously monitored for carbon monoxide and toxic gases.

1. Air Compressor

An air compressor must be able to deliver air at the following flow rates for each option found in the chart.

Option	PSI	CFM
Air Only	8	6
Vortec	41	6
Vortec with Vest	65	6

NOTE: 6 CFM must be maintained in the hood at all times.

2. Airline Monitor

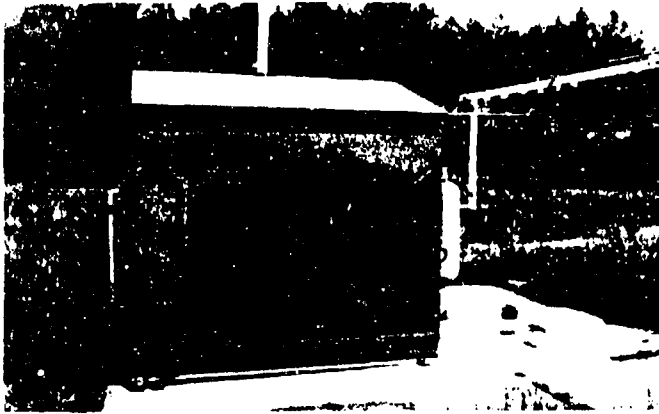
An electronic monitor, utilizing a solid state catalytic sensor is used to detect carbon monoxide and other toxic gases that may either be generated by the compressor or pulled in from the air surrounding the compressor. A warning horn and/or light may be built into this unit when unacceptable levels are indicated. (See picture #3) The air system can be wired to turn off when unacceptable air is being supplied to the hood.

A three stage filter system removes oil, dust and other liquids.

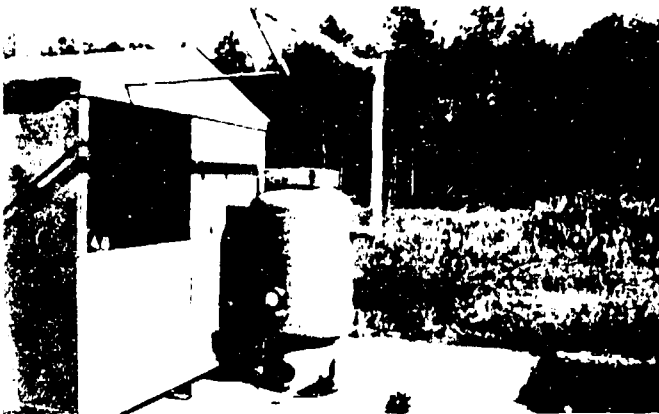
3. Maintenance

Airline monitors must be calibrated frequently. Sensors have a service life of five years and filters must be replaced on a need basis. The manufacturer of the system used will be able to give directions for their equipment.

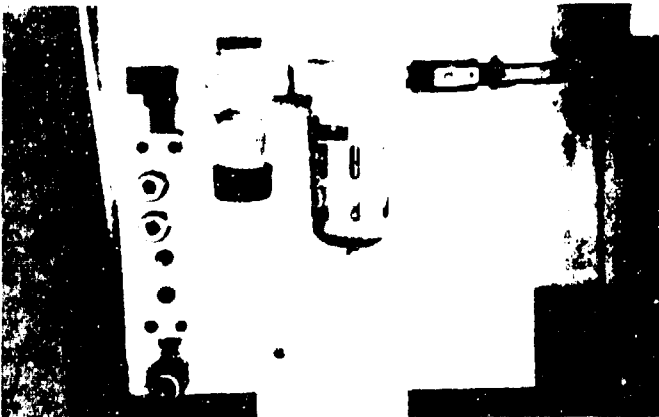
Air Supply System at Pine Bluff Arsenal



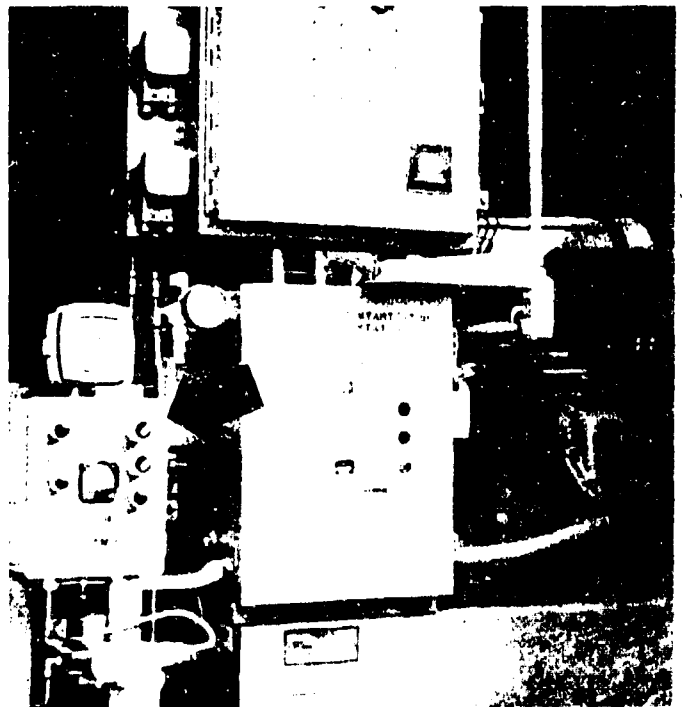
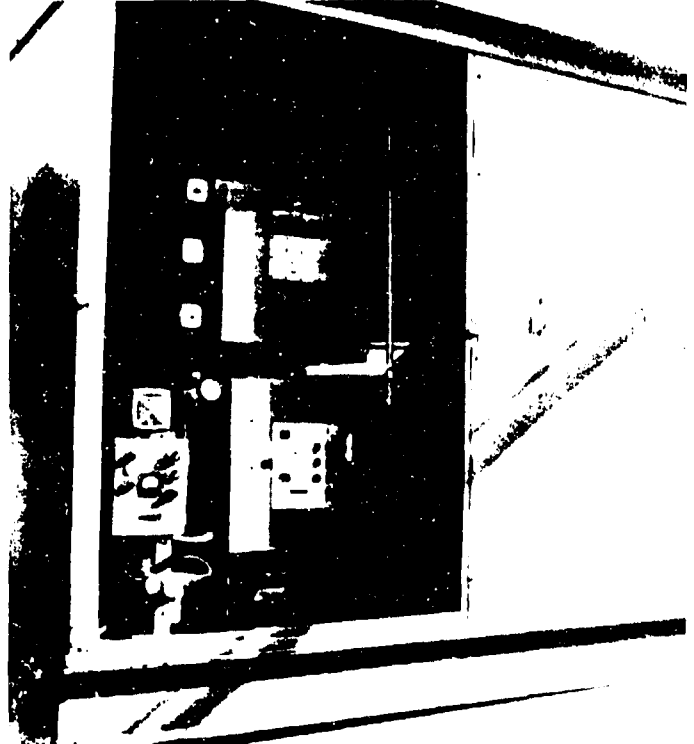
The air compressor is housed in a separate shed approximately 20 feet away from the building it serves.



The air is pumped into a pressurized holding tank and delivered through the piping that is marked breathing air. This is a dedicated breathing air system, an excellent practice.



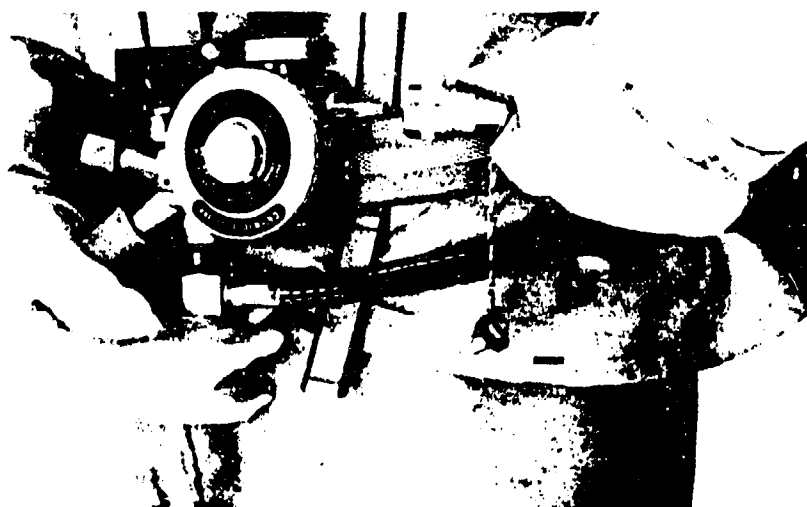
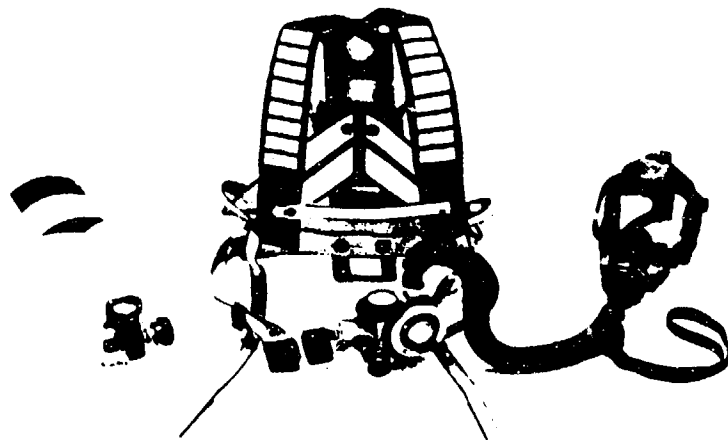
In this installation the air filtering system is separated from the monitoring system and close to the point of



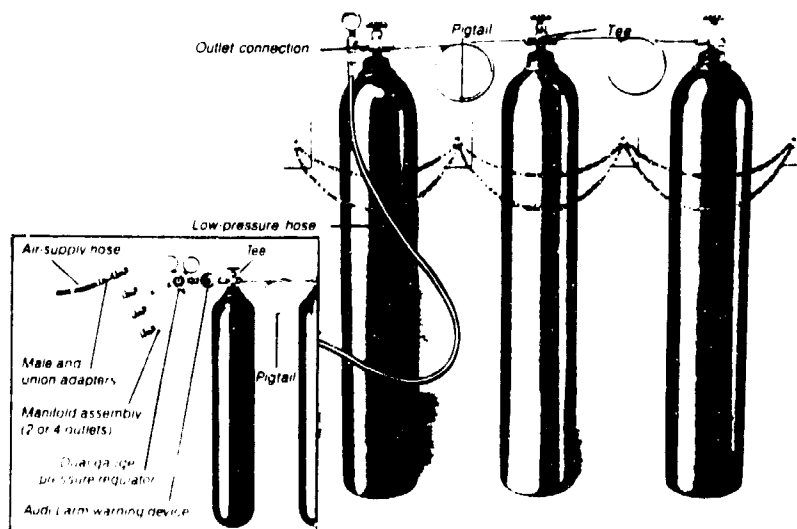
When the door is removed the compressor controls are evident, and the CO monitor, indicated by the arrow, is seen. The warning horn is mounted on top of the monitor.

Self Contained Breathing Apparatus

In situations where air to the hood can not be provided with an airline, or a worker could be trapped, a self contained breathing apparatus (SCBA) must be used. Units are available with 30 and 60 minute air supply bottles. The approximate weight of the 30 minute units available on the market is as low as 22 lb., and approximately 34 lb. for a 60 minute unit.



Several manufacturers of this type of equipment are providing dual purpose versions, combining a self contained breathing apparatus with the capabilities of an air line respirator. This option should be used in situations where workers can be trapped, but at the same time need to work in an area for more than 60 minutes. The picture to the left shows a man attaching the air regulator of a SCBA that he is wearing to an airline.



The air to the airline system mentioned above can be plant air, but it must be monitored and filtered as previously outlined. If plant air can not be provided, 300 cubic ft. bottles can be coupled together to provide the needed air. Each 300 cubic ft. bottle provides five hours of breathing air per wearer. Air bottles should only be used to supply an SCBA respirator discussed on this page, not the hood. The manufacturer's manual of the SCBA being used should be consulted in implementing this type of program.

Section Six: Proper Suit Maintenance

Suit Cleaning



1. It is recommended that the outer aluminized layer be hand cleaned with a soft brush and a mix of warm water and ordinary laundry detergent. **WARNING: DO NOT USE ANY SOLVENTS.**



2. The suit is then turned inside out and placed in an industrial washing machine. Regular laundry detergent is used in a warm wash. A cold rinse is recommended. **WARNING: CHLORINE OR ANY OTHER KIND OF BLEACH SHOULD NOT BE USED.**



3. In the event an industrial washing machine is not available the suit can be cleaned by blotting the inside with soapy warm water and then hosing the garment down with cold water.



4. The suit must be hung up to dry on coat hangers. **WARNING: DO NOT USE MECHANICAL GAS OR ELECTRIC LAUNDRY DRYERS TO DRY SUIT. DO NOT HANG THE SUIT ON PEGS — STRETCHING OF THE ALUMINIZED LAYER COULD OCCUR.**

Faceshield Replacement



1. To replace the double faceshield remove it from the air hard hat by unscrewing the faceshield holders



2. Place the hood on your lap with the faceshield opening facing you. Pull down the lower lip and slip the double faceshield out



3. The faceshield pocket is easy to see

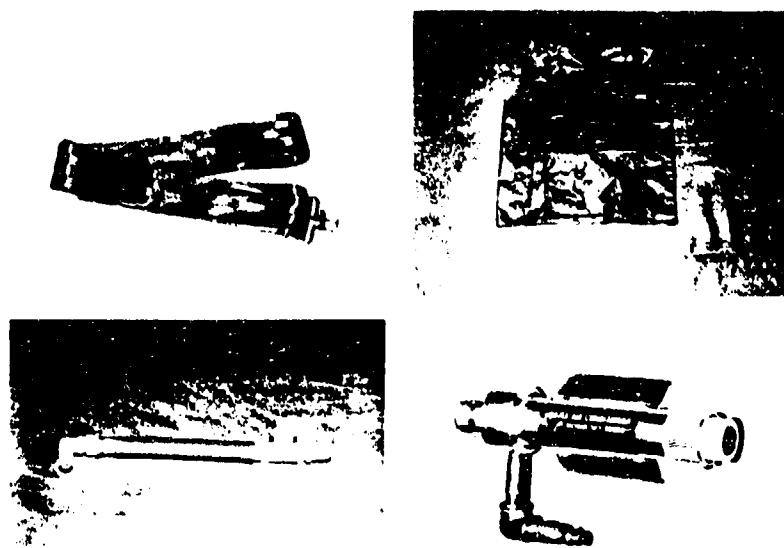


4. To replace the faceshield place the gold outer shield over the clear inner shield, and slide the lower edge into the bottom of the faceshield pocket



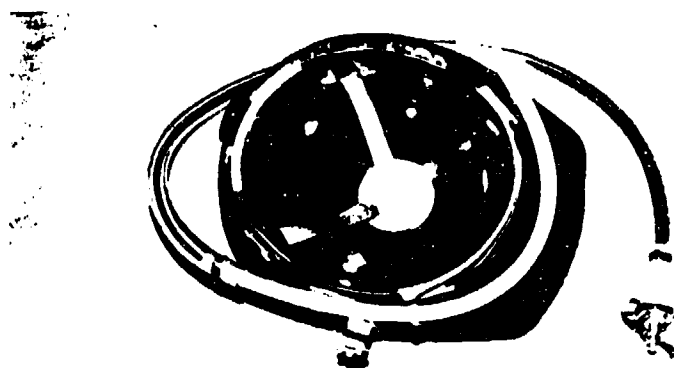
5. Slip the faceshield extensions into the slits in the upper corners of the pocket. Reattach the hat. **WARNING: MAKE SURE THE GOLD FACESHIELD IS IN THE OUTSIDE POSITION. THE FACESHIELD MUST BE IN THE POCKET COMPLETELY.**

Cooling System



The cooling system is to be wiped clean only. No maintenance is needed on the vortex.

Air Hat System



The recommended way of cleaning this unit is to keep it together and immerse it in a bucket of warm water and then rinse. The air hose can be removed by cutting the plastic strips. The suspension also slips out for replacement. To replace the air hose new plastic holders are needed.
WARNING: IF THE AIR HOSE IS REPLACED MAKE SURE THE HOLES ARE FACING DOWN.

PROCEDURES FOR THE ANALYSIS OF THE DEBRIS PRODUCED BY EXPLOSION EVENTS*

prepared by

Michael M. Swisdak, Jr.
Naval Surface Warfare Center
10901 New Hampshire Avenue
Silver Spring, MD 20903-5000

ABSTRACT

Questions often arise as to the proper procedures to apply to the collection and analysis of the debris produced by explosive events. This paper recommends a standardized set of collection and analysis procedures which should be applied to both the debris produced by accidental events and the debris produced by planned explosion tests. Sample calculations which demonstrate the methodology are presented.

BACKGROUND

At the request of the Department of Defense Explosives Safety Board (DDESB), the Naval Surface Warfare Center (NAVSWC) has established and proposes the methodology defined in this paper to "standardize" the analysis of debris for purposes of quantity-distance safety criteria analyses.

The goal of the debris analysis described here is the determination of the hazardous fragment distribution (density) and the maximum debris throw range. The DDESB defines a hazardous fragment density as "A density of hazardous fragments exceeding one per 600 sq. ft. (55.7 m²)"¹ A hazardous fragment is defined as "one having an impact energy of 58 ft-lb (79 Joules) or greater." A crucial question is the interpretation of one per 600 sq. ft. Is the 600 ft² measured along the ground surface, on vertical targets, or along a line which is normal to the trajectory?

Recent interpretations by the Secretariat of the DDESB have taken the 600 ft² to be measured trajectory-normal. This is difficult, if not impossible, to determine experimentally. Ground surface data, on the other hand, is straight-forward to obtain. To facilitate the computation of a "pseudo-trajectory-normal" density, the DDESB has proposed the following procedure: The number of hazardous debris pieces within a recovery zone will consist of the number of pieces of hazardous debris actually collected within the zone as well as the number of hazardous pieces passing through the zone and landing at a greater distance. For example, consider a 5° recovery sector which is divided into 100-foot increments. The total number of hazardous fragments in the sector between 500 and 600 feet would consist of the hazardous material found in that sector plus the hazardous material found beyond 600 feet; the next sector (600-700) would contain consist of all the material in that sector added to the material located beyond 700 feet.

* This work was sponsored by the Department of Defense Explosives Safety Board under Military Interdepartmental Purchase Requests E8789L036 and E8790L215.

TRAJECTORY-NORMAL VERSUS GROUND SURFACE PICK-UP

How valid is the procedure described above for generating a reasonable approximation to trajectory-normal data from ground surface pick-up? The two methods can be compared in two ways--through the use of experimental data and through the use of computer simulation. Unfortunately, the experimental data base is relatively limited. As part of warhead or weapons evaluation tests, fragmentation arenas are used to sample the near-field (within 100 feet of the point of the detonation) fragmentation patterns. When far-field collections are made, they have, predominately, relied on ground surface pickup. Thus, we are limited to computer simulations.

The computer program FRAGHAZ² was used to generate debris densities as a function of range for four systems: (1) Weapon A (based on an arbitrary number of MK 82 bombs), (2) Weapon B (based on an arbitrary number of 155 mm projectiles), (3) Weapon C (based on an arbitrary number of 5"/54 projectiles), and (4) Weapon D (based on an arbitrary number of 105 mm projectiles). The FRAGHAZ program uses near-field arena data and calculates individual trajectories for each fragment. Because complete trajectories are generated for each fragment, both the ground surface density and the trajectory-normal density can be determined.

Figure 1 graphically illustrates the problem of ground surface density versus trajectory-normal densities. Each graph has been normalized to its own maximum fragment range, and presents the ratio of the trajectory-normal densities to the ground surface densities. One would expect this density ratio to approach 1 as the range approaches the maximum range. Indeed, this is the case. However, even at the maximum range ($R/R_{\max} = 1.0$), the trajectory-normal densities are significantly higher than the ground surface densities. At ranges less than the maximum range $R/R_{\max} < 1.0$, the density ratio is much greater than 1. Hence the need to, somehow, estimate the trajectory-normal densities from the ground surface densities.

The same FRAGHAZ runs used to generate the data for Figure 1 were also used as input data for calculations of hazard range for both trajectory-normal and ground surface pickup (for these calculations, all fragments were considered hazardous). The procedures outlined in the following sections were used to calculate the debris range. The results are presented in Table 1. In each case, the pseudo-trajectory-normal densities (estimated from the ground surface data) over estimated the density by 8.1 to 15.9%--with an average 12.2%. Thus, this approximation technique appears valid--yielding realistically conservative estimates of the trajectory-normal densities.

GENERAL GUIDELINES FOR DEBRIS ANALYSIS

These guidelines can be broken down into two parts--(1) those that apply to planned tests--a part of which is debris collection and analysis and (2) those that apply to debris investigations of unplanned events.

Planned Tests

- (1) Survey 5° debris recovery sectors in each significant direction. Make sure these sectors are clear and smooth out to a distance of at least $50W^{1/3}$ feet, where W is the explosive weight in pounds ($19.8 Q^{1/3}$ meters, where Q is the explosive weight in kilograms). If the real estate is available, these sectors should extend out to $75W^{1/3}$ feet ($25.8 Q^{1/3}$ meters). A minimum of three directions is required.
- (2) Divide and mark each 5° sector into known range increments (a minimum increment of 5 meters is required; the maximum increment should not be greater than 30 meters). Each recovery sector should have a surface area of at least 100 m².
- (3) Provide sufficient high speed camera coverage to allow reliable estimation of fragment initial velocities and launch angles.
- (4) For each range increment of each 5° sector, where feasible, recover, bag, and label all the debris material found within the increment. If it is not feasible to recover particular debris pieces, treat them in the same manner as the material in Step (5).
- (5) Survey the locations of all significant debris pieces located outside the 5° sectors. For each piece record its location (range and azimuth from ground zero) as well as its description (length, width, thickness, mass, and type of material). A general rule of thumb is that if you can see it, then it is a piece of significant debris. Photographs of each significant piece may also be necessary.
- (6) Determine a minimum debris size for the particular test. For example, all material with a weight of less than 1.0 grams might be excluded; similarly, all material whose length, width, or thickness is less than 5 mm might be excluded. Screen all of the material collected in the recovery sectors. The material that is larger than the minimum debris size should be weighed and have its length, width, and thickness and type of material determined.
- (7) For each recovery sector, determine which debris pieces are hazardous. One method would be to utilize a series of trajectory calculations to determine the minimum debris size which could have an impact energy of 58 ft-lbs (or whatever energy threshold is decided upon).
- (8) Within each 5° sector, calculate the numbers of pseudo-trajectory-normal hazardous fragments. For a given recovery zone within a particular 5° sector, this is simply the number of hazardous fragments landing in that zone and in all zones beyond.
- (9) Once the numbers of pseudo-trajectory-normal hazardous fragments have been obtained, generate a function which gives the number of hazardous fragments per 600 ft² as a function of range. This function should be of the form :

$$D = Ae^{BR}$$

where D = Fragment Density (Number of hazardous fragments per 600 ft²)
 R = Range
 A,B = Fitting Constants.

Once this fit has been obtained, solve for the value of R which gives a fragment density, D, equal to one. This, then, is the debris hazard range for that particular set of data.

(10) Prepare two debris maps--one showing the locations of all debris and the second showing the locations of all hazardous debris. Show on these maps the computed debris hazard ranges.

(11) Prepare a computerized "debris catalog". This should contain an entry for every fragment that is recovered. This entry should include the location (range and azimuth from ground zero), description, and whether or not it was determined to be hazardous.

(12) Prepare a mass distribution (fragment/debris mass versus number of pieces with that mass or greater) based on the recovered debris.

Unplanned Events

(1) Obtain photographic coverage of the area; this should include photographs of all major pieces of debris.

(2) Determine the location of every piece of significant debris (If you can see it, then it is significant). For each piece, record its location (range and azimuth from ground zero) as well as its description (length, width, thickness, mass, and type of material).

(3) Prepare a computerized debris catalog and map of all recovered material.

(4) Set up analysis sectors on the computerized debris maps. Sufficient sectors should be chosen to show any azimuthal variations in debris density. These sectors should have a minimum width of at least 5°.

(5) Go to Step 7 for "Planned Events" and continue to analyze each 5° sector, paying special attention to those sectors with the highest concentrations of material.

SAMPLE CALCULATIONS

Two sets of data are presented as examples on the use of this methodology. Both are based on the results of accident investigations.

Processing Building Accident

At the 1988 DDESB seminar, results were presented on the analyses of the debris produced by a processing building accident.³ At the time, it was estimated that the accident was equivalent to the detonation of approximately 4200 pounds of TNT. Subsequent to the publication of the paper, the analysis procedures presented above were finalized and accepted by the Secretariat of the DDESB. Therefore, this data will be re-examined using the new procedures.

Table 2 presents the "raw data", as collected at the accident site. Each cell corresponds to a recovery area of 100' x 100'. The shaded area near the center represents the approximate location of the building itself. Where a fragment was found on the boundary between two cells, it was split between them.

Fifteen degree azimuth lines were overlaid on this data and the numbers of fragments along each azimuth were computed. Table 3 gives this data as a function of azimuth around the structure (0° corresponds to a direction of East) (Note: Trajectory calculations indicated that all debris should be considered as hazardous).

Table 4 presents the pseudo-trajectory-normal densities as a function of azimuth and range. These were calculated according to the procedures described above. The application and solution of the curve fitting procedures results in the information presented in Table 5 and Figure 2.

There were two features at this site that should have caused reductions in the debris range--a barricade (shadowing the areas between 225° and 285°) and a hill (between 345° and 45°). For reference, flat terrain was located between 135° and 195°. None of the data approach the current standard of 1250 feet. The flat terrain was 18% below this figure. However, if the flat terrain data is taken as a new standard, the reductions caused by the hill and the barricade can be computed. The range in the direction of the hill is reduced 36%, while in the direction of the barricade, the reduction is 42%.

1985 Radford Accident

NOTE: The following analysis was performed on data that was assembled by Paul E. Montanaro of the Naval Surface Warfare Center.

In February 1985, an accident occurred at the RADFORD Army Ammunition Plant, destroying a building. Debris maps of the area were prepared. However, a catalog giving the locations (range and azimuth or map coordinates) and descriptions of each individual piece was not prepared. The ranges and azimuths for each piece of debris was inferred from its location on the debris maps. It was further assumed that every piece was hazardous. Eight recovery sectors (45° apart) with widths of 30° were overlaid on the debris maps. With these assumptions, the raw data presented in Table 6 were prepared. When this information was analyzed with the procedures described above, the pseudo-trajectory-normal densities shown in Table 7 were obtained. The curve fitting procedures yielded the debris hazard ranges shown in Table 8 and Figure 3.

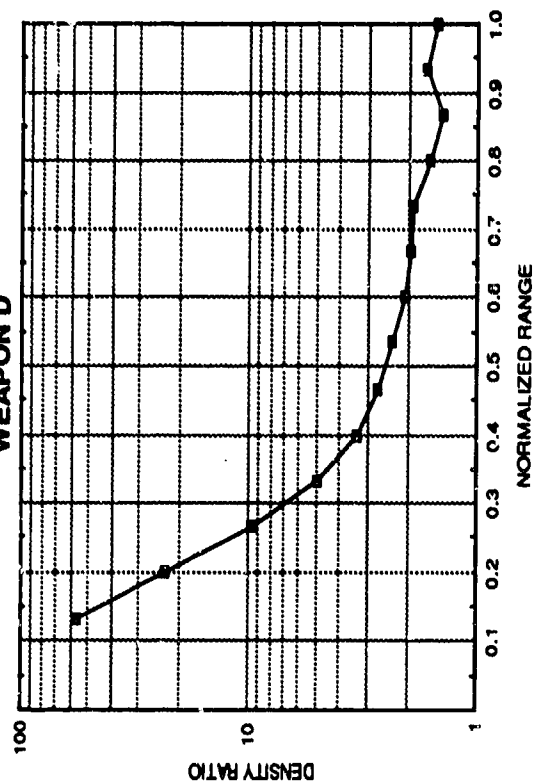
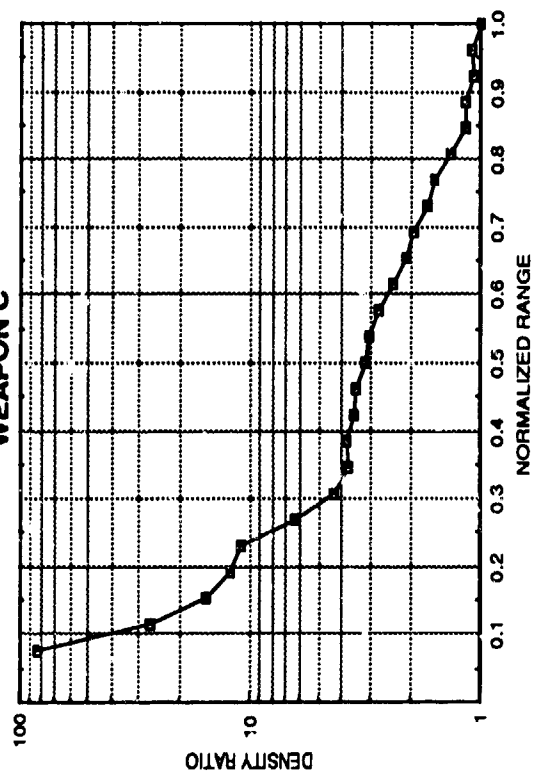
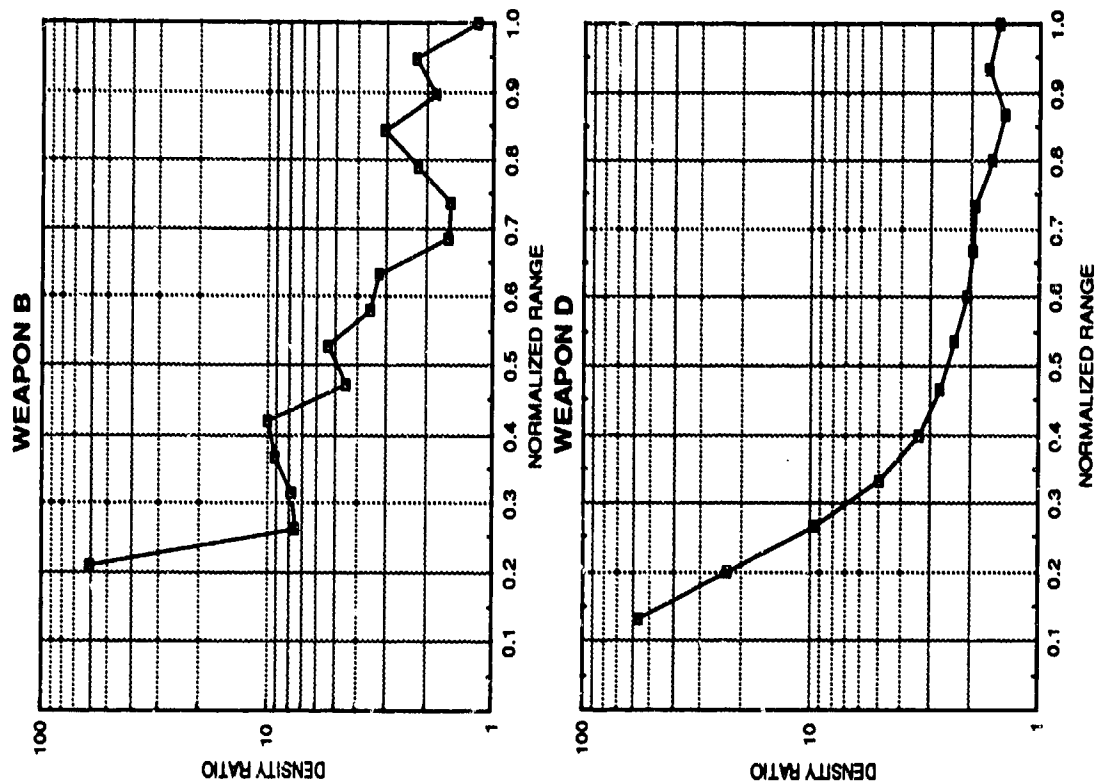
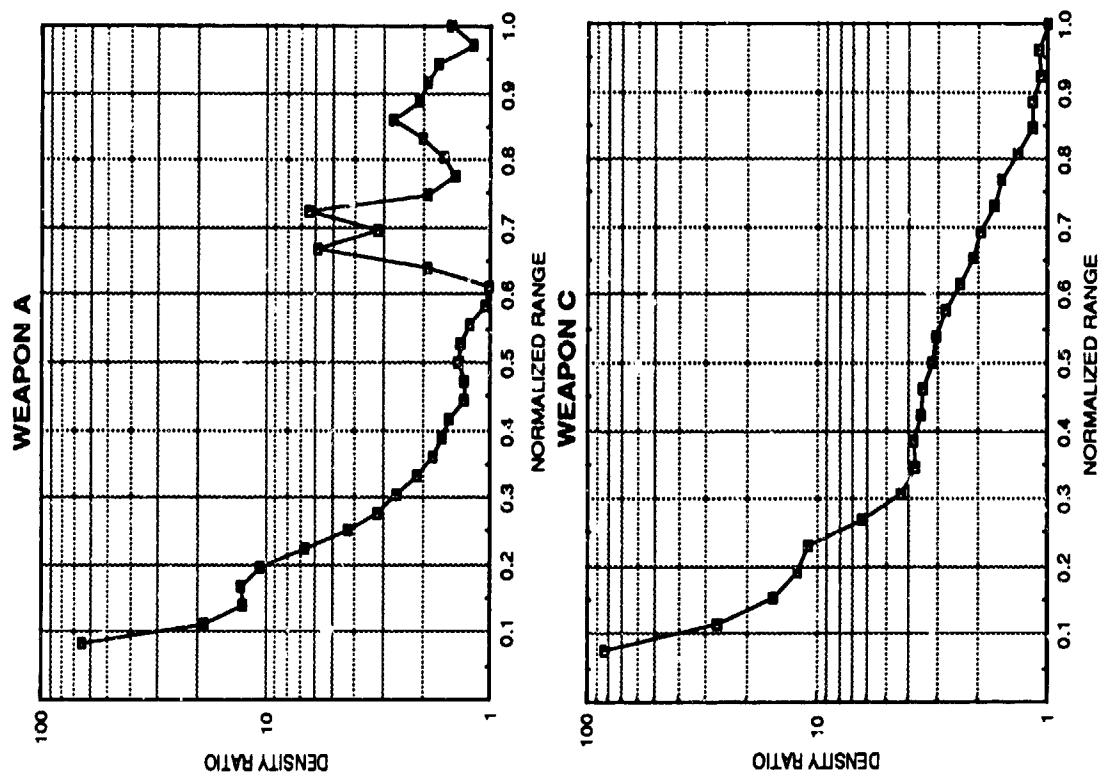
SUMMARY

A new procedure for approximating trajectory-normal densities from ground surface debris pickup is described and analyzed.

A set of standardized procedures have been developed for the analysis of explosion produced debris. The use of these procedures should greatly enhance the amounts and types of information which can be obtained from debris investigations.

REFERENCES

1. Department of Defense Ammunition and Explosives Safety Standards, DOD 6055.9-STD, First Amendment (Change 2), 28 October 1988.
2. McCleskey, F., "Quantity-Distance Fragment Hazard Computer Program (FRAGHAZ)," NSWC TR 87-59, February 1988.
3. Swisdak, Michael M., Jr., "Analysis of the Debris Produced By A Processing Building Accident," Minutes of the Twenty-Third Explosives Safety Seminar, 9-11 Aug 1988.



(NOTE: DENSITY RATIO=TRAJECTORY-NORMAL DENSITY/GROUND SURFACE DENSITY)

FIGURE 1 TRAJECTORY-NORMAL VERSUS GROUND SURFACE DENSITY

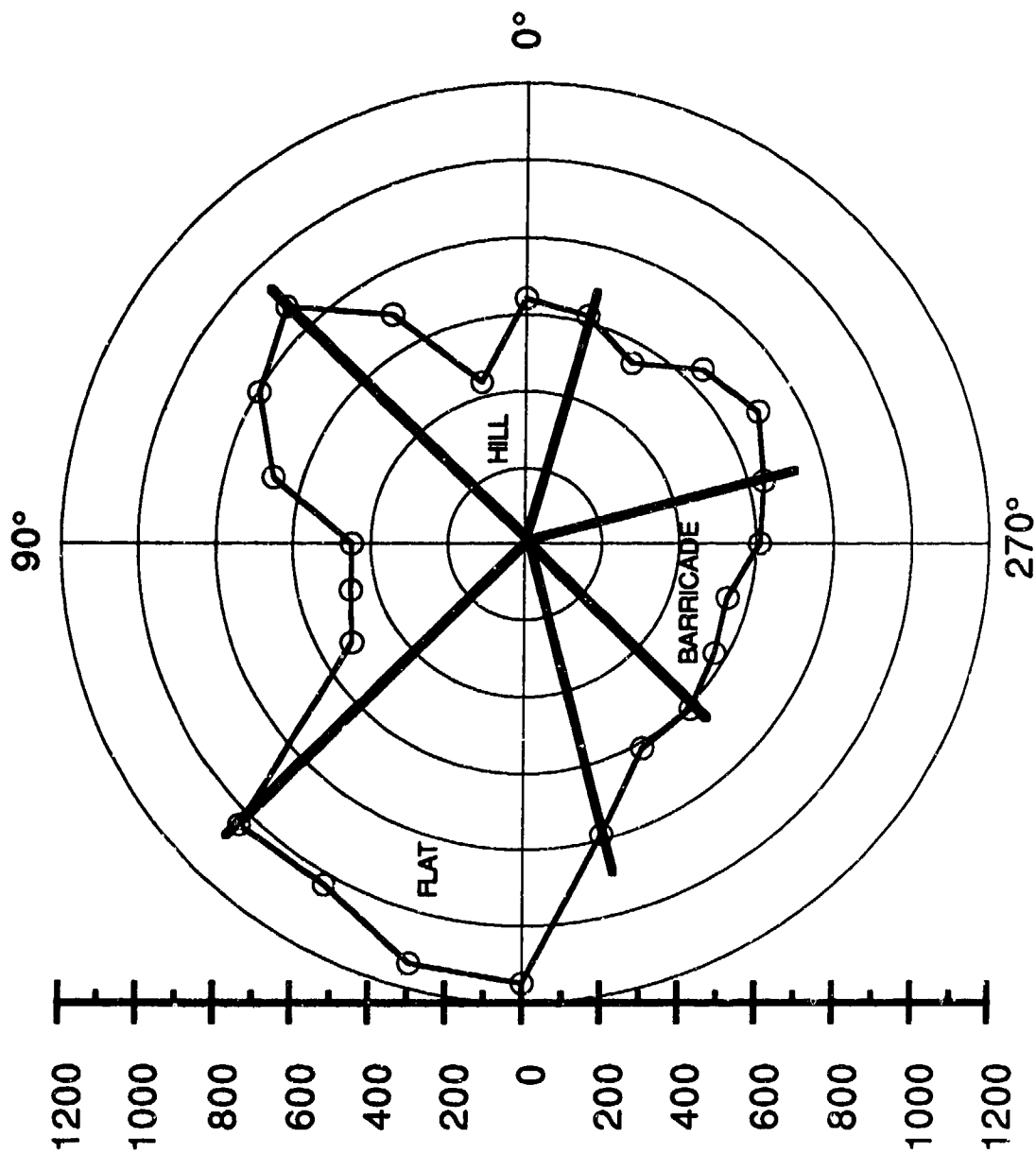


**FIGURE 2 PROCESSING BUILDING ACCIDENT--
DEBRIS HAZARD RANGE CONTOUR**

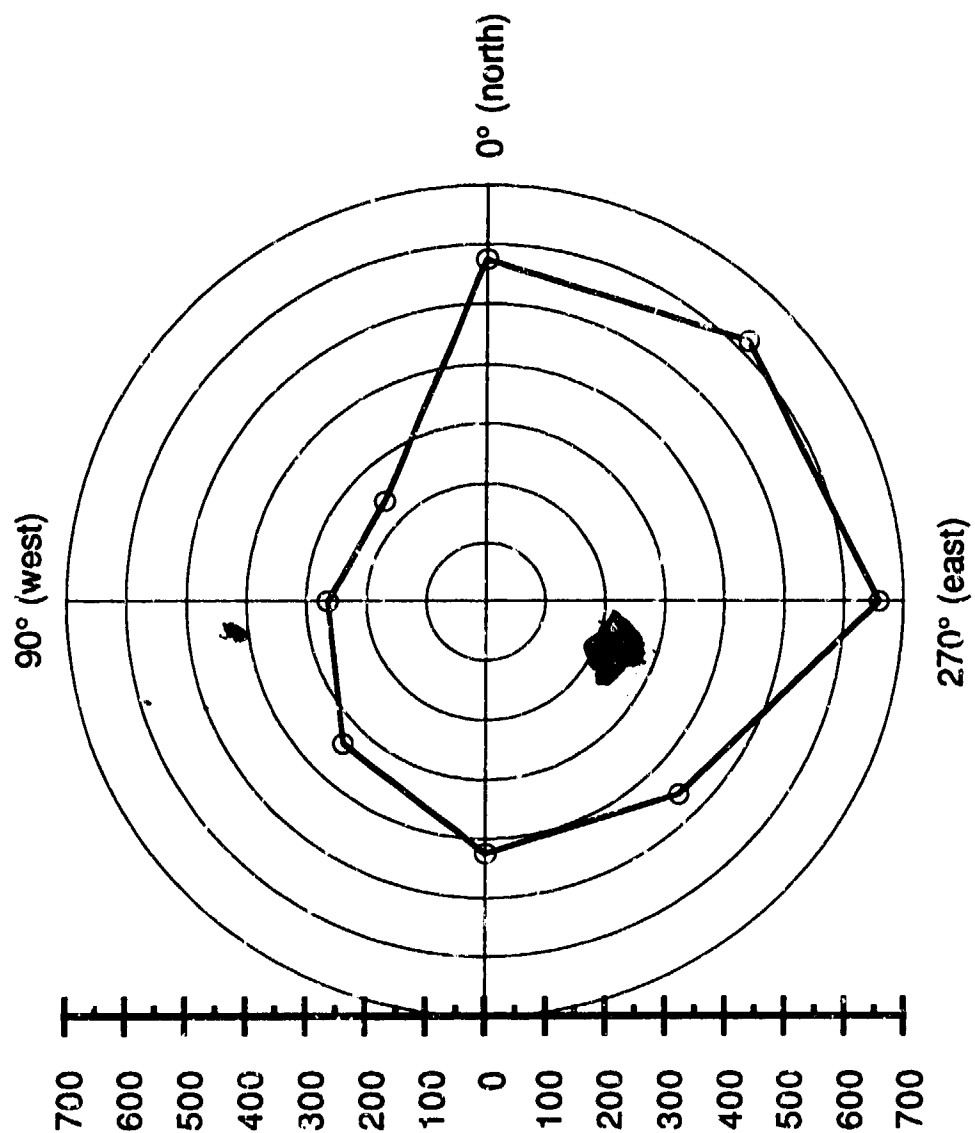


**FIGURE 3 RADFORD ACCIDENT--
DEBRIS HAZARD RANGE CONTOUR**

TABLE 1 COMPARISON OF TRAJECTORY NORMAL AND REVISED GROUND SURFACE PICKUP

WEAPON	RANGE TO A DENSITY OF 1 PER 600 FT ² (ft)		RANGE TO A DENSITY OF 1 PER 600 FT ² (ft)		PERCENT DIFFERENCE
	TRAJECTORY NORMAL		PSEUDO-TRAJECTORY-NORMAL		
A	1767 (1698-1835)*		2025 (1991-2059)*		14.60
B	1408 (1381-1434)*		1554 (1510-1599)*		10.37
C	1259 (1207-1309)*		1459 (1404-1515)*		15.89
D	718 (650-780)*		776 (716-835)*		8.08
AVERAGE PERCENT DIFFERENCE					12.23

*95% confidence interval

TABLE 3 PROCESSING BUILDING ACCIDENT--NUMBERS OF FRAGMENTS VERSUS RANGE AND AZIMUTH

Lower Radius (ft)	Upper Radius (ft)	AZIMUTH (°)						
		0°	15°	30°	45°	60°	75°	90°
200	300	6.00	13.40	14.80	14.50	12.80	10.56	17.00
300	400	5.00	16.40	12.56	9.08	10.40	20.32	11.00
400	500	11.00	9.70	7.80	11.00	8.52	15.70	19.00
500	600	6.00	0.53	5.00	6.86	6.12	4.12	6.00
600	700	4.00	1.43	3.88	2.98	6.84	4.08	
700	800	1.00	0.98	3.44	3.50	12.20	6.55	
800	900	4.00	0.68	5.78	4.92	7.74	5.09	
900	1000	5.00	1.12	7.18	6.98	4.64	2.20	
1000	1100	3.00	0.29	3.64	5.60	4.35	3.00	
1100	1200	0.00	0.58	0.68	5.40	3.02	1.04	
1200	1300	1.00				1.22		
1300	1400	0.50						
1400	1500							
1500	1600							

Lower Radius (ft)	Upper Radius (ft)	AZIMUTH (°)						
		105°	120°	135°	150°	165°	180°	195°
200	300	39.32	60.24	70.68	75.71	72.13	26.50	16.77
300	400	14.27	16.72	36.14	55.59	46.55	17.00	4.52
400	500	13.45	11.69	25.25	47.12	25.65	18.00	38.10
500	600	8.64	2.64	10.44	24.80	53.78	78.50	73.08
600	700	2.62	2.16	9.14	16.24	46.90	105.00	189.65
700	800		0.32	5.42	20.72	68.92	68.00	8.00
800	900		1.40	1.48	9.60	32.00	36.00	1.28
900	1000		0.40	4.74	12.46	24.88	36.00	1.34
1000	1100		1.44	2.28	5.16	9.90	6.00	1.38
1100	1200		0.64	2.60	5.05	11.80	13.00	1.00
1200	1300			3.32	3.22	7.64	9.00	
1300	1400			3.04	1.12	1.80	0.00	
1400	1500			3.75	2.10		2.50	
1500	1600			2.56	1.22			

Lower Radius (ft)	Upper Radius (ft)	AZIMUTH (°)						
		210°	225°	240°	255°	270°	285°	300°
200	300	12.24	13.48	10.30	27.40	27.00	26.88	28.84
300	400	3.70	14.08	9.88	28.20	59.00	27.64	14.65
400	500	13.08	15.28	8.40	16.16	32.00	30.68	8.80
500	600	23.08	3.76	8.44	22.14	15.50	17.56	16.54
600	700	16.08	2.30	0.72	1.58	9.00	10.40	9.12
700	800	12.94	7.38	3.80	1.48	5.00	4.72	7.40
800	900	2.56	3.34	3.58	0.82	3.00	3.32	9.84
900	1000	1.08	2.08	2.08	0.42	0.50	1.00	7.00
1000	1100	0.12	1.40	0.22	0.58		0.78	0.80
1100	1200		0.06	1.34			0.32	0.32
1200	1300							
1300	1400							
1400	1500							
1500	1600							

Lower Radius (ft)	Upper Radius (ft)	AZIMUTH (°)		
		315°	330°	345°
200	300	20.80	6.45	6.32
300	400	4.64	5.71	9.40
400	500	4.54	4.34	12.42
500	600	8.58	8.80	10.30
600	700	3.60	9.12	3.16
700	800	4.77	2.78	4.58
800	900	1.47	0.00	2.88
900	1000	0.48	1.62	2.06
1000	1100	2.00	1.60	1.40
1100	1200	0.88	0.52	1.06
1200	1300	1.42		0.20
1300	1400	1.22		0.32
1400	1500	0.68		
1500	1600			

TABLE 4 PROCESSING BUILDING ACCIDENT--PSEUDO-TRAJECTORY NORMAL DEBRIS DENSITY VS. AZIMUTH

RADIUS (ft)	AZIMUTH (°)											
	0°	15°	30°	45°	60°	75°	90°	105°	120°	135°	150°	165°
250	2.79	2.72	3.88	4.25	4.55	4.36	3.18	4.70	5.86	10.85	16.81	24.13
350	2.43	1.91	3.01	3.38	3.78	3.73	2.16	2.34	2.24	6.61	12.26	19.80
450	2.13	0.93	2.25	2.83	3.16	2.51	1.50	1.48	1.24	4.44	8.93	17.01
550	1.47	0.35	1.79	2.17	2.77	1.58	0.36	0.68	0.54	2.93	6.10	15.47
650	1.11	0.32	1.49	1.76	2.40	1.32		0.16	0.38	2.30	4.61	12.24
750	0.87	0.23	1.25	1.58	1.99	1.07			0.25	1.75	3.64	9.43
850	0.81	0.17	1.05	1.37	1.26	0.68			0.23	1.43	2.40	5.29
950	0.57	0.12	0.70	1.06	0.79	0.37			0.15	1.34	1.82	3.37
1050	0.27	0.05	0.27	0.66	0.52	0.24			0.12	1.05	1.07	1.88
1150	0.09	0.03	0.04	0.32	0.25	0.06			0.04	0.92	0.76	1.29
1250	0.09				0.07					0.76	0.46	0.58
1350	0.03									0.56	0.27	0.11
1450	0.03									0.38	0.20	
1550	0.03									0.15	0.07	

RADIUS (ft)	AZIMUTH (°)											
	180°	195°	210°	225°	240°	255°	270°	285°	300°	315°	330°	345°
250	25.17	20.11	5.09	3.79	2.93	5.93	9.06	7.41	6.20	3.30	2.46	3.25
350	23.46	19.10	4.36	2.98	2.31	4.28	7.44	5.80	4.47	2.06	2.07	2.67
450	22.44	18.83	4.14	2.14	1.71	2.59	3.90	4.13	3.59	1.78	1.73	2.30
550	21.36	16.54	3.35	1.22	1.21	1.62	1.98	2.29	3.06	1.51	1.47	1.56
650	16.65	12.16	1.97	0.99	0.70	0.29	1.05	1.23	2.07	0.99	0.94	0.94
750	10.35	0.78	1.00	0.86	0.66	0.20	0.51	0.61	1.52	0.78	0.39	0.75
850	6.27	0.30	0.23	0.41	0.43	0.11	0.21	0.33	1.08	0.49	0.22	0.48
950	4.11	0.22	0.07	0.21	0.22	0.06	0.03	0.13	0.49	0.40	0.22	0.30
1050	1.83	0.14	0.01	0.09	0.09	0.03		0.07	0.07	0.37	0.13	0.18
1150	1.47	0.06			0.08			0.02	0.02	0.25	0.03	0.09
1250	0.69									0.20		0.03
1350	0.15									0.11		0.02
1450	0.15									0.04		
1550												

TABLE 5 PROCESSING BUILDING ACCIDENT--DEBRIS RANGES

(NOTE: based on pseudo-trajectory normal densities)

AZIMUTH (°)	DEBRIS HAZARD RANGE (ft)	TERRAIN FEATURE	AVERAGE (ft)
345	617	HILL	653
0	642	HILL	
15	439	HILL	
30	691	HILL	
45	875	HILL	
60	796		1027
75	674		
90	447		
105	464		
120	514		
135	1037	FLAT	
150	1028	FLAT	
165	1136	FLAT	
180	1149	FLAT	
195	786	FLAT	
210	615		594
225	609	BARRICADE	
240	569	BARRICADE	
255	544	BARRICADE	
270	609	BARRICADE	
285	639	BARRICADE	
300	694		
315	647		
330	547		

FLAT TERRAIN : 1027 ±156 FEET

HILL: 653 ±146 FEET

BARRICADE: 594 ±37 FEET

NOTE: where not noted, the terrain is mixed and varied.

MIXED: 600 ±116 FEET

TABLE 6 RADFORD ACCIDENT--NUMBERS OF FRAGMENTS VERSUS RANGE AND AZIMUTH

LOWER RADIUS (ft)	UPPER RADIUS (ft)	AZIMUTH (°)							
		0	45	90	135	180	225	270	315
0	100	80	57	10	30	25	121	17	39
100	200	35	2	1	13	4	3	3	12
200	300	23	7	0	6	23	1	9	8
300	400	20	3	8	5	15	9	21	20
400	500	11	0	4	2	13	15	31	18
500	600	8	1	4	4	4	10	16	24
600	700	19	0	3	3	3	7	17	16
700	800	4	2	0	3	2	5	22	10
800	900	1	1	0	2	4	2	17	6
900	1000	6	0	0	0	0	3	7	1
1000	1100	2	0	0	0	1	1	6	4
1100	1200	1	0	0	0	1	0	4	4
1200	1300	0	0	0	0	0	0	2	4
1300	1400	3	0	0	0	0	0	1	0

TABLE 7 RADFORD ACCIDENT--PSEUDO-TRAJECTORY NORMAL DEBRIS DENSITY VERSUS AZIMUTH

AVERAGE RADIUS (ft)	AZIMUTH (°)							
	0	45	90	135	180	225	270	315
50	48.82	16.73	6.88	15.58	21.77	40.57	39.65	38.04
150	10.16	1.22	1.53	2.90	5.35	4.28	11.92	9.70
250	4.49	0.64	0.87	1.15	3.03	2.43	7.01	5.27
350	2.46	0.23	0.62	0.62	1.41	1.70	4.71	3.50
450	1.40	0.10	0.28	0.36	0.71	1.09	3.13	2.22
550	0.92	0.08	0.15	0.25	0.31	0.58	1.92	1.44
650	0.63	0.05	0.05	0.14	0.19	0.32	1.34	0.79
750	0.26	0.05		0.08	0.12	0.17	0.90	0.44
850	0.18	0.01		0.03	0.08	0.08	0.50	0.26
950	0.14				0.02	0.05	0.24	0.16
1050	0.07				0.02	0.01	0.14	0.13
1150	0.04				0.01		0.07	0.08
1250	0.03						0.03	0.04
1350	0.03						0.01	

TABLE 8 RADFORD ACCIDENT--HAZARDOUS DEBRIS RANGE

AZIMUTH (°)	DEBRIS HAZARD RANGE (ft)
0	574
45	240
90	264
135	337
180	424
225	458
270	658
315	620

Building Debris Hazard Prediction Model

by

Patricia M. Bowles
Charles J. Oswald

Southwest Research Institute
6220 Culebra Road
San Antonio, Texas 78228-0510

ABSTRACT

An analytical model has been developed to predict hazardous debris distances for accidental high explosive detonations within buildings constructed of various materials. The model was developed for the Department of Energy (DOE) to assist in siting buildings based on explosive amounts and construction types specific to DOE; however, it can be used to predict maximum hazardous debris distances using the high explosive contents of any building constructed of reinforced concrete, masonry (clay tiles or concrete masonry units), corrugated metal, or a combination of one or more of these materials. Verification and refinement of the model are currently being accomplished using data from an extensive test program funded by DOE. Full scale, half scale, and quarter scale walls of the above construction types were exposed to various loading conditions, including fully vented, partially vented, and closed configurations, and a range of charge amounts applicable to DOE facilities. Test results include debris velocities and trajectory angles from high speed film, debris grid summaries (including maximum debris distance and average debris mass), internal and external shock load measurements, internal gas load measurements, and wall failure sequence and breakup patterns from high speed film. The end result will be a flexible predictive model, verified with test data, which can be used to safely site explosive handling buildings according to predicted maximum debris distances instead of the current broad-ranged debris safety criteria.

1.0 Introduction

Safe separation distances required for Department of Energy (DOE) explosives handling facilities, as of July 1984, are determined using the fragment/debris hazard criteria in addition to the blast criteria outlined in the Department of Defense (DoD) "Ammunition and Explosive Safety Standards", DoD 6055.9. The current DoD guideline for inhabited building separation due to debris hazards is 570 feet for high explosive (HE) amounts up to 100 lbs and 1250 feet for HE amounts greater than 100 lbs up to 30,000 lbs. This change has caused great concern at existing DOE and DOE contractor facilities. Since structure siting at these facilities was based on blast protection alone prior to 1984, some of the now required separation distances exceed current boundaries or distances between existing structures at these facilities. Efforts to comply with the criteria have resulted in reduction of explosive amounts handled or processed, expansion of plant real estate, or hardening of existing structures (including the erection of barricades). In several cases, exemptions have been requested to allow operations to continue. However, granting an exemption for every siting violation is an undesirable solution to the problem. The ultimate cost and disruption of operations associated with any of these options have prompted the DOE safety community to question the applicability of the broad ranged DoD fragment separation criteria for siting DOE structures, many of which house relatively small quantities of HE compared to DoD facilities.

The need to provide safe clearance for hazardous debris which can evolve from accidental explosions or detonations of energetic materials is not disputed. However, more specific data to supplement the quantity-distance (Q-D) requirements for combinations of structure and explosive configurations found at DOE facilities is needed to establish new criteria which would allow many existing facilities to comply, without compromising the intended safety. DOE funded an extensive program to gather data, concentrating on the lower DOE charge amounts and building types, and to use it to supplement the existing criteria. The two main objectives of this program can be summarized as follows:

- development of a predictive model (a combination of computer programs and empirical correlations with data) which can be used to determine hazardous debris distances resulting from accidental explosions in DOE structures which handle HE, and
- verification and refinement of the predictive model using data from component tests of construction types and explosive amounts of interest for DOE facilities.

This paper presents a brief summary of the work conducted during the third of three tasks covering these overall objectives. The first two tasks (described in Reference 1) included an examination of the structures and explosives present at DOE facilities; a study of existing data on structural breakup caused by accidents; and the initial development of a predictive model for determining debris hazard distances. The focus of the third task has been to obtain data necessary to verify as many model

assumptions as possible within time and funding constraints and to refine the model accordingly. The end product will be a flexible, component based predictive model which, although tailored to specific DOE operations and facilities, can be adopted by DOE and DoD as a siting tool.

2.0 Supporting Test Program

An extensive test program was conducted to obtain data on debris characteristics and wall failure patterns for the wall types most commonly found in DOE facilities. The test program included full, half, and quarter scale tests of reinforced concrete, unreinforced masonry, and lightweight metal walls. Wall thickness, reinforcement details, and concrete strength were varied in the concrete wall tests. The masonry wall tests included tests of various geometries of clay tile walls and full and quarter scale concrete masonry unit (CMU) walls. The testing was highly concentrated on concrete and masonry wall breakup, but two corrugated metal walls and one metal stud wall were also tested. Although the metal walls were all tested in a fully vented (open air) configuration, three different loading conditions were used for the concrete and masonry walls: fully vented, partially vented, or closed. Three separate test fixtures were used to allow testing of different scales and loading conditions. The explosive charges used varied in amount from 0.2 lb to 25 lb TNT equivalent. The tests conducted are summarized in Reference 2. Further details of these tests and complete data summaries can be obtained from Reference 3.

3.0 General Description of Predictive Model

The predictive model refined during this program is a combination of steps to determine hazardous debris distance and, thus, proper siting distance between explosive handling facilities and inhabited buildings. The key steps involve the use of pre-existing computer codes, one of which has been modified based on the analysis of data from the test program conducted for this study. Other intermediate steps consist of making prescribed calculations which are based on test data analysis and observations from tests. The intermediate calculations are currently incorporated in a spreadsheet to simplify use of the model. These calculations are used to determine some of the input necessary for the computer codes.

A component based analysis procedure forms the predictive model to be used. The procedure includes the general steps listed below:

- loading prediction on internal surfaces,
- prediction of component breakup and determination of debris characteristics (mass, velocity, angle, drag),
- debris dispersion, and
- debris tumble after impact (ricochet and roll).

The analysis approach and general description of each of these steps is given in this section. More explicit steps on how to use the model are provided in Section 4.0. Complete documentary details can be found in Reference 3.

3.1 Loading Prediction on Internal Surfaces

Once the explosive threat (charge amount and location) and the wall and roof components of the donor structure have been defined, the first step of the model is to determine internal loads. Blast loading inside a confined space can be characterized by an initial shock phase followed by a gas or quasistatic phase loading. The shock phase consists of very short duration, high pressure pulses which load surfaces as the shock reverberates within the donor bay. The magnitude of the shock phase depends on the charge amount, the distance to the loaded surface, and the location of nearby reflecting surfaces. The magnitude of the quasistatic phase depends on the charge amount and the donor bay volume, with the duration also depending on available vent area and mass of vent covers. If the vent area is sufficiently large and the vent cover mass is small, the gas phase is essentially eliminated.

The SHOCK and FRANG computer codes are used to determine the shock and gas impulse on all components in the donor structure. The sum of the quasistatic impulse and the shock impulse is used in the next step of the model to determine maximum debris velocity. This proves to be an accurate treatment of the load based on comparisons to the test data generated during this program. SHOCK is based on a program originally written by Ammann & Whitney. The version currently used in the model was acquired, with modifications, from the Naval Civil Engineering Laboratory (NCEL). It is used to predict average shock phase loading on internal surfaces including the shock reflections off nearby surfaces. The program includes a reduced area option which allows determination of average shock impulse over a portion of a wall surface or at a single point on the wall. Thus, loads over a local area or at a point directly across from the charge can be determined. If a building has an exterior ramp or corridor which can also contribute to the debris hazard, the loads on these structural elements are determined using peak reflected air blast curves and the line-of-sight distance to the element. The impact distances determined for these debris are then added to the total debris dispersal predicted for the affected direction. Any quasistatic impulse caused by a detonation in a confined building is predicted using the computer code FRANG. This code was also acquired from NCEL and is the code which was used to develop the gas impulse curves in Reference 4.

3.2 Building Component Breakup and Debris Characteristics

Component breakup is predicted based on the applied load and the component type. This loading is described using only the applied effective impulse (shock plus quasistatic impulse as discussed in the previous section) and the loading duration for close-in loading. Two different loading realms are possible depending on the location of the explosive charge in relation to the loaded component: localized loading where the scaled charge standoff is $1.5 \text{ ft/lb}^{1/3}$ or less, and

loading at larger scaled standoff distances. The breakup exhibited under localized loading is characterized by small, low angle debris. A majority of the tests conducted during this program resulted in localized loading or a combination of localized and uniform quasistatic loading due to small standoff distances between the charge and the wall. For localized loading, the maximum velocity of the debris is determined, as shown in the steps in Section 4.0, by calculating the maximum motion of the wall directly opposite the charge, i/m , where i is the effective impulse and m is the mass per unit area of the wall, and applying a reduction factor, k , to the velocity. This reduction factor is based on fits to test data comparing maximum wall velocity (i/m) to maximum measured velocity. The factor is a function of the applied impulse and the load duration (and the concrete strength for reinforced concrete walls). Much more uniform loading is observed when the charge is located further from the wall (scaled standoff, $R/(\text{charge weight})^{1/3} > 1.5$). For reinforced concrete, wall response in this loading realm is characterized by the wall breaking along yield lines into several large debris and only 10 to 20 percent of the wall breaking into small pieces. The maximum velocity for debris for this case is predicted as the maximum wall velocity calculated assuming a single degree-of-freedom system at a specific failure criteria.

Maximum debris velocity of unreinforced masonry is calculated with the same procedure for both loading realms. For larger standoff distances, the reduction factor becomes 1.0 (no reduction). A more complete description of the methods used to predict wall important component breakup parameters, as well as the manner in which the methods were derived, is presented in References 3 and 5. Special attention was devoted to the maximum debris velocity here because it was found to have the dominant effect on debris dispersion.

High speed film coverage of both the response of the walls and the manner in which debris left the test fixtures provided data on component breakup and debris flight and impact characteristics. The extensive debris recovery effort provided data on debris size. These data have been used to refine the model procedures for determining characteristics for debris from reinforced concrete, unreinforced masonry, and lightweight metal walls. The following parameters are based directly on test data:

- average debris mass
- total destroyed mass of a wall
- initial angles at which debris leave a wall
- wall breakup (two or three dimensional)
- debris roll and ricochet upon impact.

Other characteristics such as debris velocities and drag coefficients are based on comparisons of prediction methods to test data. Wherever possible, statistical analysis provided the basis or verification of input recommendations for the debris dispersion code. All pertinent statistical correlations and complete data summaries are documented in Reference 3.

The breakup is predicted to provide input in a form compatible with the computer code MUDEMIMP used for debris throw. This code, which is discussed in Section 3.3, estimates the hazardous debris distance for each component of a building using input probability distributions to describe building breakup. Probability distributions for the following debris parameters are input into the code:

- debris mass
- initial debris velocity
- initial debris trajectory angle
- debris drag coefficient
- debris drag area factor.

The choice of input probability distribution to use for each of these parameters is based on statistical correlations with the test data. Statistical sampling of the measured data for mass, velocity, and angle for each test (including goodness of fit tests on each parameter) established the distributions to be used for these parameters. The recommended distributions are summarized in Section 4.0.

3.3 Debris Dispersion

The results of the component breakup and debris characteristics prediction are used to create input for another computer code. The MUDEMIMP code (Reference 6) for Multiple Debris Missile Impact Simulation is used to determine the hazardous debris distance and debris dispersion for a building. Originally written by Louis Huang at the Naval Civil Engineering Laboratory (NCEL), this code uses a probabilistic approach to include variations and uncertainties of launch/flight characteristics of each individual debris missile from an explosion. It uses the Monte-Carlo random sampling technique to select a set of launch/flight parameters for each debris piece. It then calculates the trajectory, impact range, and terminal kinetic energy of each piece based on the selected initial conditions. In addition to an output file containing all input and output parameters for every debris missile simulated, the code also outputs a histogram of the accumulated number of hazardous debris as a function of impact range. Hazardous debris are defined as those debris with impact kinetic energies exceeding a critical energy input by the user, e.g. 58 ft-lbs.

General input and output information is discussed in this section, but detailed input descriptions can be found in Reference 3. Five main launch/flight parameters are required to run the code: debris mass, initial velocity, initial trajectory angle, drag coefficient, and drag area factor. The actual input to the code is in the form of probability distributions which describe the possible range of values for each major parameter. Parameters for each individual debris piece are chosen

by the code randomly selecting from the probability distributions. Although the code allows the use of seven different probability density functions for each parameter, the following functions for the five main launch/flight parameters are recommended:

- exponential -- debris mass
- normal -- initial velocity
- normal -- initial trajectory angle
- uniform -- drag coefficient
- constant -- drag area factor (due to changes in code discussed below)

The drag coefficient for each individual debris simulation remains constant and is not allowed to vary with Mach number because most debris considered by the model fly in the subsonic speed region. These distributions are recommended based on extensive statistical sampling of the data from each test in this program. Complete documentation of the results of the statistical analysis is included in Reference 3. Other input includes initial height of debris and characteristic length. All debris are assumed to be launched from a single point.

As testing progressed, test data were used to compare to code predictions and to indicate where code modifications were necessary. Some of the code changes were the result of examining the characteristics selected randomly by the code for each individual debris simulation. The most significant of these changes was the method in which drag area and shape factors are assigned. Originally, the drag area for a particular debris piece was calculated using a randomly selected drag area factor or "k-factor", independent of the randomly selected debris mass. To simulate a more plausible trajectory, the code was modified to calculate a drag area factor for each debris piece for which one dimension, the thickness, was likely to be constant for all debris. The area calculation needs to correspond to the type of breakup expected, either two- or three-dimensional, so a new input parameter, BKUP, was introduced. The default value is 2 for two-dimensional breakup for which the thickness of each debris is assumed constant. This value is appropriate for masonry, metal, and metal stud walls. A value of 3 needs to be input if three-dimensional breakup is expected, as with reinforced concrete walls.

The input parameter "L" for characteristic fragment length should now be used to indicate wall thickness (or shell wall thickness for masonry walls). The use of the "k-factor" in randomly determining fragment drag area has been turned off for reinforced concrete and masonry debris by recommending it be a constant distribution with a value of 1.0. The k-factor can still be used to change the effective drag area by using a constant distribution set to some value other than 1.0, but this is only recommended when making a single fragment run or when all debris considered are similar in shape (like corrugated metal panels). The drag area will be calculated as the average of all six sides of an assumed rectangular solid for both types of breakup. For two-dimensional breakup, one of these sides will be assumed as fixed to a dimension "L" for all debris.

After a considerable analysis effort spent examining the debris data from the test program, a few additional modifications were made to MUDEMIMP and the recommended input for the code. A study was made of the manner in which the random deviates were determined for each of the debris launch/flight parameter distributions. Reference 3 should be reviewed for details of the study, but the main conclusion was that the number of random debris simulations should be large to establish accurate distributions for each of the launch/flight parameters. Numerous computer runs have been made to determine an acceptable number of simulations based on statistical accuracy and execution time. The final decision is that each MUDEMIMP analysis needs to use 5000 computer simulated debris, regardless of how many actual debris are expected from an accident. This number guarantees accurate distributions for each of the input variables and less than a 10 percent variation between separate 5000 fragment runs even though a completely random seed is used to select each distribution. This variation is a compromise between the variation expected between repeated tests (which is probably on the order of 20 to 30 percent) and the repeatability expected from a siting tool used for design purposes. One set of test conditions was repeated in the subject program and the results of maximum debris distance differed in the two tests by 25 percent. Maximum debris velocity differed by 10 percent. A fixed seed can also be used to begin each run if absolutely no variation in the predicted maximum distance is desired, i.e. any user running the same problem at any time will get the same results. For debris density calculations, the code internally adjusts the number of simulated debris to agree with the input effective destroyed mass. In this way, the user is assured of getting a desired number and total mass of debris regardless of the number of debris used in the simulation. A summary of guidelines for determining program input and using the model is provided in Section 4.0.

3.4 Debris Tumble After Impact (Ricochet and Roll)

If debris thrown from an explosion impacts the ground at a shallow angle, it may ricochet or roll after impact. Predicting the first impact location as the final resting place is very inaccurate and unconservative. Initially, logic for ricochet was incorporated in the MUDEMIMP code; however, the tests indicated the phenomenon was more of a rolling effect than the ricochet of debris. An empirical method has now been included in the code to include debris roll. The sequence of steps which led to this decision are described in this section.

The Naval Surface Warfare Center (NSWC) computer code FRAGHAZ (Reference 7) is a debris dispersion code which contains logic to handle ricochet effects, but not roll. This logic was examined to understand the method used to predict when ricochet occurs and what effect it has on the final impact location of debris. A soil constant is randomly selected (or it can be input if the appropriate value is known for the explosion site). For each debris trajectory, the angle at impact is compared to a critical angle for ricochet which is related to the soil constant. If ricochet is indicated, new initial launch conditions are calculated considering the kinetic energy lost and a new launch angle. The trajectory is then continued with the new parameters. The reported impact distance at the end of a run is then the total of each "leg" of the trajectory for a particular piece of debris.

This ricochet logic was used to create an equivalent code modification to MUDEMIMP. Comparisons to test data from Reference 8 (prior to the testing conducted during this task) indicated the most prevalent effect was that the debris distribution resembled a normal probability distribution over the impact range when ricochet was included, i.e. there were few debris stopping close to the wall or at the maximum impact distance, with most debris coming to rest at distances between these two extremes. These are logical results since debris making their first impact close to the wall generally impact at shallow angles, causing them to be launched at least one more time to come to rest at a greater distance. The debris landing near the maximum impact distance impact at higher angles and do not ricochet. The problem is that the debris impacting at higher angles can still roll, end over end, to a distance further than the trajectory calculations in MUDEMIMP will predict. This phenomenon was observed throughout the recently completed tests. The rolling of debris is not covered by the ricochet logic obtained from the FRAGHAZ code (Reference 7). That code was written to describe munition fragments such as those from bomb casings, and those fragments only exhibit ricochet characteristics, not roll. Thus, a method was needed to account for this rolling of debris.

Several possible methods in the literature were reviewed for determining roll, but none of them would result in a simple addition to the MUDEMIMP code. An entire research project is needed to adequately address roll as it applies to the debris generated in this test program. Some film coverage of rolling debris was obtained in some of the later tests, but there is not nearly enough data to aid in creating a sophisticated roll model. However, it was obvious from the test data obtained in this program that debris roll or tumble can play a significant role in determining the final resting points of debris from an accident. Some way of accounting for roll had to be added to the model. For single debris runs using the maximum velocity and a very small angle (approximately equal to the average angle of the fastest debris), a roll factor of 5.0 applied to the calculated distance of the first impact conservatively predicts the maximum measured distance for all the tests. It was found that the roll factor increased with increased debris velocity and, in general, the roll factor was larger for concrete debris than for masonry debris. However, debris leaving a wall at higher angles are not expected to exhibit the same roll characteristics as those leaving normal to the wall. Less roll results for the higher angle debris. For this reason, an empirically based step function has been included within the MUDEMIMP code to provide reasonable final impact distance predictions for all the debris simulated.

4.0 Guidelines for Using the Model

As illustrated in this paper, three computer codes -- SHOCK, FRANG, and MUDEMIMP -- are required to use the model. The versions of SHOCK and FRANG used during model development are the versions obtained from NCEL and are designed to run on a personal computer (PC). The MUDEMIMP code obtained from Louis Huang when he worked at NCEL was designed to run on a mainframe VAX computer. For much of the model refinement task, MUDEMIMP was run on a VAX 780 at SwRI so that the appropriate graphics routines (from a proprietary graphics package) could be utilized. A PC version of MUDEMIMP has been created which will provide the same

output except it has no graphics capability yet. The PC version does, however, create an extra output file containing the data necessary to create a final density histogram of number of hazardous debris as a function of distance in a form convenient for importing into a spreadsheet.

Step-by-step guidelines for using the model to determine proper siting distance for a building follow. More complete descriptions of the analysis used to establish these steps and the tests used to collect the backup data can be found in Reference 3.

1. Define the threat. Describe all the structural components which comprise the building. Define the explosive charge amount and location. Generally, for siting purposes, the charge location should be a plausible worst case location which would cause the worst case debris formation. Some trial and error may be necessary to define this location.
2. Determine vent areas and descriptions. Define both covered and open vent areas and the weight per unit area of the covered areas.
3. Calculate effective impulse load on each component. Run the SHOCK code to get the shock impulse, i_s , at a point directly across from the charge for each component. Run the FRANG code using the appropriate SHOCK predicted impulse for covered vent surfaces to get the gas or quasistatic impulse, i_g . Use the gas impulse at the code-defined critical venting time when obtaining gas impulse for a venting component. Use the total gas impulse for other components. The effective impulse, i , is the sum of i_s and i_g .
4. Calculate the maximum debris velocity expected. For close-in loading on concrete and both loading realms for masonry, calculate the maximum wall velocity as $(1/k)(i/m)$, where i is the effective impulse, m is the mass per unit area of the wall, and k is the appropriate empirical reduction factor. The reduction factor depends on whether the wall is locally or uniformly loaded. The equations and guidelines for calculating k are found in Reference 3. For far-range loading of concrete, use a simplified single degree-of-freedom approach called out in the model to calculate maximum debris velocity. Average debris velocity and debris velocity standard deviation are calculated directly from the maximum debris velocity.
5. Calculate the average debris mass. The empirically based equations for average debris mass, m_{avg} , are in the form

$$m_{avg} = k (\text{volume}) (\text{density})$$

where k is a factor based on fits to data.

The specific equations for reinforced concrete and masonry walls are shown below.

Concrete:

$$m_{avg} = 0.10 [(\text{rebar spacing})^2 (\text{cover thickness}) (\text{density})]$$

Masonry:

$$m_{avg} = (k) [(\text{shell face thickness})^3 (\text{density})]$$

where k is related to maximum debris velocity

6. Determine the effective destroyed mass of the wall. The MUDEMIMP code requires the input of the total destroyed mass of the wall. The main use of this input by the code is to help define the input mass distribution and establish the adjustment factor to get the appropriate number of debris (as adjusted from the 5000 simulations). The value used for this parameter is actually an effective destroyed mass and not necessarily the total mass expected to be destroyed. The reason is because the recommended value is based on data from tests in which debris which impacted very close in to the wall were not included in the data collection. These debris do not set either the maximum debris distance or the hazardous debris distance and, thus, were ignored in the analysis. They certainly are a real part of the actual total destroyed mass, but since the calculation procedure is based on test data which excludes those debris, the input value for this parameter should be considered an effective destroyed mass instead of a total destroyed mass.
7. Run MUDEMIMP to determine hazardous debris distance. The main input parameters are summarized below.

<u>Parameter</u>	<u>Density Function</u>	<u>Limits</u>
Mass	Exponential	m_{avg} total destroyed mass
Velocity	Normal	mean=average velocity, v_{avg} =0.6(max velocity) $sd^*=(\text{max velocity} - v_{avg})/3$.
Angle	Normal	mean=0 degrees $sd^*=1.4$ degrees(unrestrained roof) $sd^*=10$ degrees(restrained roof)
Drag Area Factor	Constant	1.0
Drag Coefficient	Uniform	0.8, 1.98

* sd = standard deviation

Other key input parameters in addition to the probability density functions include material density, launch height, wall thickness, type of breakup (two or three dimensional), and grid length for use in determining hazardous debris density (defaults to 24.5 feet for a full scale event to represent a 600 square foot bin).

The model is run for each component of a building, and input for all components can be run in the MUDEMIMP code as a multiple execution. The final outcome is either a histogram or tabulated data of number of critical debris as a function of distance for a given building.

5.0 The Model as a Siting Tool

A brief overview of the hazardous debris evaluation model has been presented in this paper. It is flexible in that several different construction types can be analyzed using the model. In many cases test data have been used to verify or establish code input or calculation procedures. The intent has been to make the model as accurate as possible without requiring the use of highly sophisticated procedures to determine the input and run the model. Because of this, hazardous and maximum debris distances are conservatively predicted, but less conservative than the current broad-ranged criteria. The model will be an effective siting tool for the types of buildings and explosive amounts commonly found in DOE facilities and should be equally useful to members of the DoD explosive safety community as well. All supporting documentation as well as example model calculations for current DOE safety exemption buildings will be included in Reference 3. The model is scheduled for presentation for technical approval by DOE in September. It will also be presented to the DDESB Secretariat at that time as a means of supplementing the existing debris criteria. Final presentation to the DDESB is scheduled for November 1990.

References

1. Bowles, P.M., Oswald, C.J., Whitney, M.G., and Baker, W.E., "Fragment and Debris Hazard Evaluation", SwRI Project 06-2362, prepared for Bernard Johnson Incorporated under Mason & Hanger -- Silas Mason Co., Inc. Contract H0760102, U.S. Government Contract DE-AC04-76DP-00487, April 1989.
2. Bowles, P.M., Oswald, C.J., and Vargas, L.M., "Building Debris Hazard Evaluation Test Program", paper presented at the Twenty-fourth Department of Defense Explosives Safety Seminar, St. Louis, Missouri, August 28-30, 1990.
3. Bowles, P.M., Oswald, C.J., Vargas, L.M., and Baker W.E., "Debris Hazard Evaluation, Task 3: Test Program and Predictive Model Refinement", Final Report in preparation for SwRI Project 06-2945, prepared for Bernard Johnson Incorporated under Mason & Hanger -- Silas Mason Co., Inc. Contract H0760103, U.S. Government Contract DE-AC04-76DP-00487, to be submitted September 1990.
4. "Structures to Resist the Effects of Accidental Explosions", Special Publication ARLCD-SP-84001, Volumes II, IV, and V, December 1986.
5. Oswald, C.J., "Development of Predictive Methods from Test Data For Breakup of Building Components Subjected to Close-in Explosive Loading", paper presented at the Twenty-fourth Department of Defense Explosives Safety Seminar, St. Louis, Missouri, August 28-30, 1990.
6. Huang, L.C.P., "Theory and Computer Program for the Multiple Debris Missile Impact Simulation (MUDEMIMP)", Naval Facilities Engineering Command, Naval Civil Engineering Laboratory, Program No. Y0995-01-003-331, June 1984.
7. McCleskey, F., "Quantity-Distance Fragment Hazard Computer Program (FRAGHAZ)", Kilkeary, Scott & Associates, Inc., prepared for Naval Surface Warfare Center and Department of Defense Explosives Safety Board, February 1988.
8. Vargas, L.M., Hokanson, J.C., and Rindner, R.M., "Explosive Fragmentation of Dividing Walls", prepared for ARRADCOM, SwRI Project 02-5793, August 1980.

Development of Predictive Methods from Test Data for Breakup of Building Components and Debris Roll

by

Charles J. Oswald

**Southwest Research Institute
6220 Culebra Road
San Antonio, Texas 78228-0510**

Abstract

A series of thirty-one tests on reinforced concrete, unreinforced masonry, and lightweight metal walls, was conducted in order to refine an existing model which predicts dispersion of building component fragments created by an accidental internal explosion. The tests, which were conducted at one-quarter scale, one-half scale, and full scale, consisted primarily of two types of loading, severe close-in loading and severe quasistatic loading. Test data used to refine the model includes the mass of debris collected after each test and debris velocities, angles, and size sampled off high-speed film.

The test data was used to refine methods to predict building component breakup parameters including debris mass, initial velocity, and initial trajectory angle. The test data was also used to refine the predictive method for debris roll and ricochet after first impact. Probability density distributions are predicted for each of the component breakup parameters. The predictive methods are primarily based on correlation of measured component breakup parameters and measured debris distances to measured test parameters. Many parameters were found to correlate well to the maximum measured debris velocity. This paper presents and discusses the predictive model refinements. The effect of test scale on test results is also discussed where it is observed that this factor is important.

1.0 Introduction

A series of thirty-one tests on reinforced concrete, unreinforced masonry, and lightweight metal walls was conducted in order to refine an existing model which predicts dispersion of building component fragments created by an accidental internal explosion. The model was recently developed by Southwest Research Institute in a Department of Energy (DOE) funded program. It consists of four major steps; 1) prediction of explosive loads on building components, 2) prediction of component breakup parameters (such as initial debris mass and velocity), 3) prediction of debris trajectory distance until first impact with the ground, and 4) prediction of final trajectory distance including debris roll and ricochet after impact. The output from each step is an input into the prediction method of the next step. A general description of the overall model ^{[1],[2]} and of the test series ^[3] are presented elsewhere. Existing prediction methods which are based on previous experimentation and research ^{[4],[5]} are used for steps 1 and 3 in the model. Data from the test series is used to refine the prediction methods for most of the parameters within steps 2 and 4. These prediction methods will be presented and discussed in this paper for reinforced concrete and unreinforced masonry components.

2.0 Data Reduction and Data Collection

Most of the data collected in the test series was on one-quarter scale concrete and masonry walls loaded at either close-in (less than 1.0 ft/lb³³) scaled standoff distances or with large quasistatic load. These two general types of loading conditions will cause the worst case debris distances. Other loading conditions, such as far-range loading without large quasistatic loading, will cause considerably less building component destruction. Therefore a conservative method of estimating debris dispersion (not based on extensive test data) is judged acceptable for these cases.

Data reduction consisted of sampling fragment velocity, angle, and size off high-speed film and collecting and weighing all fragments meeting the test collection criterion. During the first three months of the test series all debris with any dimension larger than 3/8 in. (for quarter-scale tests) were collected. It was then decided for practical reasons that the collection criterion should be doubled. The collection criterion was scaled up for larger scale tests. Also, for the half-scale and full-scale tests, only debris further than three wall heights from the wall were collected. This was necessary in order to limit the total collected debris weight to manageable limits. The debris collection criterion is important because DOD defines critical debris range in terms of fragment kinetic energy. It was found that the maximum critical debris range was usually very near the maximum debris range for all the tests conducted and there was no noticeable difference in this regard between tests with different collection criteria.

Fragment velocities, angles, and sizes were sampled off high-speed film at intervals of every tenth, fifth, or second fragment, beginning with the first fragment to appear on the film. The sampling interval was selected so that approximately fifty fragments would be sampled from each test. The camera was located downrange from the test wall so that fragments traveled five to ten feet before entering the camera field of vision. It is judged that the fragments did not slow down significantly before entering the camera field of vision and can therefore be considered as initial fragment velocities. However, significant angle change had clearly occurred within this distance for slower fragments. Therefore, measured angles were only considered as close estimates of initial fragment trajectory angles for the higher speed debris. Fragment size was measured against a background grid as the dimension

of an equivalent square which would approximately include the presented area of the fragment. This measurement is only used qualitatively to look for correlation between debris size and debris velocity and angle.

3.0 Refinement of Model Predictive Methods from Test Data

The test data were analyzed with the intent of refining the prediction methods of those parameters in the model which were not predicted with an adequate level of confidence and accuracy. These parameters were the building component breakup parameters, including debris initial velocity, initial trajectory angle, mass, and a parameter or method to account for debris roll and ricochet after first impact. These factors are very important to the model because debris dispersion is heavily dependent on the debris initial flight conditions during component breakup, particularly initial velocity, and on roll after first impact. Roll accounts for the majority of the total distance traveled by the debris from walls most typical of DOE buildings (walls not laterally restrained at the top). The resulting refined prediction methods for component breakup parameters consist primarily of curve-fits of loading parameters and component mass and strength to measured breakup parameters. Debris roll and ricochet were found empirically to be proportional to both initial debris velocity and initial distance to first impact.

Prior to analysis, a parameter study was undertaken to determine the parameters which have the largest effect on debris distance. Figure 1 summarizes the parameter study which investigated the change in trajectory distance caused by changes in each of four building component breakup parameters: initial velocity, initial trajectory angle, mass, and average drag coefficient. The figure shows that initial debris velocity has the largest effect on trajectory distance. For this reason, more analysis effort was expended on the prediction method for building component debris velocities than on other parameters. No account for debris roll and ricochet is included in this figure.

4.0 Component Breakup Prediction Methods

Building component breakup in the model is described in terms of probability density distributions of debris mass, velocity, trajectory angle, drag coefficient and drag area. For example, the velocities of the debris from a building component are described in the model by a normal distribution of velocities with a given mean velocity and a given standard deviation. Test data are used to determine both the type of distribution and the values defining the bounds of the distribution (such as the standard deviation and the mean) of debris initial velocities, initial trajectory angles, and masses for reinforced concrete and unreinforced masonry.

4.1 Probability Density Distributions Used to Describe Component Breakup

The sampled fragment velocities and angles from all tests for which a sufficient number of fragments were filmed were statistically analyzed to determine the distribution which best fit the data. Analysis of fragment trajectory angles was not performed on tests where it was determined that all fragments were filmed during downward flight. The distribution which best fits mass of all fragments collected for each test was also determined. Table 1 shows the results of this analysis. Each distribution

was checked for goodness of fit with the Kolmogorov-Smirnov test. The table shows the number of tests for which the data meets the goodness-of-fit criterion of each distribution at the 5% level of significance. Therefore, there is 95% confidence that the data was sampled from the distributions shown in Table 1. This information was used to determine the type of probability density distribution to be used in the model for initial debris velocity, trajectory angle, and mass. The distributions which were selected are shown in the last column of Table 1. An exponential distribution was chosen for mass because this distribution is considerably simpler to specify than a log normal distribution. The observed scatter in predictive methods for the average mass caused low confidence in the capability of possible predictive methods to determine the more numerous values needed to define a log normal distribution.

Table 1. Summary of Probability Density Distribution Fits to Test Component Breakup Data

Parameter	No. of Tests for Which Probability Density Distribution Fits Data ($p > 0.05$)					Distribution Selected for Model
	Normal	Log Normal	Exponential	Weibell	No Fit	
Debris Initial Velocity	16	1	0	1	1	Normal
Debris Mass	0	29	7	0	3	Exponential
Debris Initial Trajectory Angle	4	0	0	0	12*	Normal

*Normal was considered "best" fit

Figures 2,3, and 4 are scatterplots of sampled fragment velocity, angle, and size plotted against each other. Measured values from all reinforced concrete tests which were sampled are included in each plot. The plots for the unreinforced masonry tests are similar. All debris velocities and size are plotted relative to the largest debris velocity and size in the test from which they were sampled. These plots show that the measured debris initial launch conditions are not strongly correlated. This observation is in agreement with the current logic of the Monte-Carlo simulation in the MUDEMIMP code which randomly assigns initial velocity, mass, trajectory angle to each fragment from the input probability density distributions. The fact that there is not strong correlation is fortunate since a more complex procedure is required to model correlated inputs with a Monte-Carlo simulation.

Some trends, however, are evident in the figures. A reduction in measured angle with decreased velocity (indicating downward flight) is evident in Figure 2. This relationship is most probably caused by the sampling procedure (camera setup) discussed above. It is also evident from Figure 2 that most of the highest velocity fragments travel at a velocity very near zero degrees (along the horizontal). It is important to note that the plotted tests only include close-in loading and large quasistatic loading on

vertical walls which are restrained along the sides and the bottom but which are free along the top. It is probable that larger angles would have been measured among the fastest fragments for large quasistatic loading if the top of the wall had been restrained. High-speed films of the wall response showed that for close-in loading local response does not initially include the support conditions. Therefore, it is judged that the local response, and thus the behavior of the highest velocity fragments, was independent of the support conditions for close-in loading. In these figures, and in most other figures in this paper, the test data are plotted with a numeral corresponding to the inverse of the scale at which the test was conducted. Therefore, it will be evident if the scale factor is skewing the data. In Figures 2, 3 and 4 there is no evidence that the data is affected by the scale factor.

4.2 Values Used to Define Component Breakup Distribution Bounds

A mean and a standard deviation are necessary to define the values included in a normal distribution and a mean is required to define the values included in an exponential distribution. These values were determined for concrete and masonry components from curve-fits to data. The data analysis showed that maximum debris velocity is a good predictor of most parameters important to debris dispersion. Maximum debris velocity was found to correlate to the applied load and to the properties of the loaded component. Therefore, the expected maximum velocity can be determined initially after the applied load has been calculated and this value can then be used to determine other parameters for the predictive model. It is evident that the accuracy of the model is heavily dependent on an accurate prediction of maximum debris velocity. Separate prediction procedures are used to predict maximum debris velocity for close-in loading and for large quasistatic loading.

4.2.1 Prediction of Debris Velocity Mean and Standard Deviation for Close-in Loading

The close-in loading realm for the model includes all cases where the scaled standoff distance is less than $1.5 \text{ ft/lb}^{.33}$. Most of the tests in the test series were conducted with close-in scaled standoff distances between $0.5 \text{ ft/lb}^{.33}$ and $1.0 \text{ ft/lb}^{.33}$. Debris distribution mean and standard deviation values are predicted from the maximum debris velocity. Therefore, the predictive method for maximum debris velocity will be discussed first. For all the unreinforced masonry and reinforced concrete tests it was found that maximum fragment velocity could be taken as the peak theoretical velocity of the wall opposite the charge divided by a reduction factor. The peak wall velocity, which assumes all the applied impulsive energy is converted into kinetic energy, is calculated as i/m , where i = reflected specific impulse (impulse per unit area) at the point on the wall opposite the charge and m = wall specific mass. For masonry, the minimum specific mass through the thickness is used. This includes only the thicknesses of the face shells and any internal shells. Loads were not measured on the test walls, therefore all impulses were calculated using the computer program SHOCK^[4]. This program accounts for the impulse off adjacent reflecting surfaces.

For both material types the reduction factor was found to decrease linearly to a value of 1.0 (and therefore no reduction) as the applied impulse and as the loading duration increase. For concrete, it was also found that the reduction factor decreases to 1.0 as the concrete compressive strength decreases. Therefore, the maximum debris velocity approaches the peak wall velocity for larger applied loads

which overwhelm the wall, for longer duration loads, and for weaker strength walls. Figure 5 shows a plot of the reduction factor for concrete and Figure 6 shows a plot of the reduction factor for masonry. It is evident that significantly less energy loss occurs in masonry than in concrete for similar loading.

As mentioned previously, the figures show the curve-fit plotted against the applicable test data where the test data are plotted with a numeral representing the inverse of the scale at which the test was conducted. Consideration of test scale is important because the measured fragment velocities and overall test wall damage were found to be heavily dependent on the scale at which the test was conducted. Similar tests measured significantly more damage at larger scale. This same trend has been noted elsewhere^{[6],[7]}. This scale dependence is not evident in Figures 2 and 3 because the independent parameter (on the horizontal axis) varies with the scale factor in approximately the same proportion as the measured damage. Most often component response is found to be scale independent and response parameters and loading parameters are both expressed as scale independent parameters.

Mean and standard deviation values of the measured debris velocities off the high-speed film for each concrete and masonry test were normalized against the maximum debris velocity measured in the test. On the average, this ratio was equal to 0.6 for the mean and 0.16 for the standard deviation. The coefficient of variation about these averages was 0.16 for the mean and 0.3 for the standard deviation. The tests included a total of twenty concrete and masonry tests with both close-in and far-range loading, and tests ranging from full scale to one-quarter scale. The magnitude of the coefficients of variation is due, at least in part, to the difficulties in sampling fragments off the films. High debris densities near the average make it difficult to maintain the fragment sampling interval in this velocity range. Also intermittent dust clouds occasionally confound the sampling intervals. It was judged that the average debris velocity would be predicted with adequate accuracy for the model by taking it as six tenths of the maximum predicted debris velocity. The standard deviation is taken as the maximum debris velocity multiplied by 0.14 (rather than the average measured value of 0.16) since the sampling difficulties cited above would tend to exaggerate the standard deviation. Also, the value of 0.14 causes the maximum predicted velocity to differ from the average by three standard deviations. This is consistent with the fact that on the average, about 500 fragments were filmed for each test.

4.2.2 Prediction of Debris Velocity Mean and Standard Deviation for Far-Range Loading

Far-range loading includes all loads which are relatively uniform and applied with pressures which do not significantly exceed the dynamic compressive strength of the wall. For the model these are all loads which are dominated by impulse applied at a scaled standoff distance greater than 1.5 ft/lb³³.

For masonry, the maximum debris velocity prediction method for far-range loading is the same as that discussed above for close-in loading. The duration increases rapidly with increased scaled standoff so that the reduction factor goes to 1.0 for far-range loading. This trend matches well with limited test data in the far-range loading realm. For reinforced concrete, the maximum debris velocity for this loading realm is predicted as the maximum wall velocity at a specified failure criteria. The failure criteria will be three or four degrees hinge rotation of the wall calculated by a simplified

single-degree-of-freedom analysis. This portion of the model is not currently complete in its final form. For both concrete and masonry with far-range loading, the standard deviation and the mean will be calculated from the maximum debris velocity as discussed above.

4.2.3 Prediction of Debris Initial Trajectory Angle Mean and Standard Deviation

The average mean and standard deviation values of the measured debris angles off the high speed film for fourteen concrete and masonry tests were -0.7 degrees, and 2.4 degrees, respectively. The coefficient of variation of the means and standard deviations of the tests about the average values were 1.8 for the mean and 0.5 for the standard deviations. This indicates very considerable scatter from test to test about the average. Figure 7 shows that the mean angle approaches zero degrees as the average debris velocity measured during the test increases. This figure also shows that 1.4 degrees is a good estimate of the average standard deviation for the higher velocity tests. The fact both mean angle and standard deviation converge to a relatively uniform average value as average debris velocity increases shows that slower fragments sampled off the film during their downward flight are significantly affecting the data. Therefore, some judgement must be exercised in choosing values to be used in the model. The mean initial trajectory angle for the model is taken as zero degrees since the most reliable data, that from tests with high debris velocity, measure nearly this value. The standard deviation for the model is taken as 1.4 since this is a good approximation of the average standard deviation in Figure 7 among tests with higher velocities.

The quoted value of 1.4 degrees for the standard deviation of the normal distribution of debris angles applies to walls, as tested, with unrestrained roofs. This is the most common condition found in DOE facilities. Although no tests were conducted for walls with restrained roofs, data on the horizontal angles at which debris landed on the ground due to the restrained sides of the wall give some indication of the angles which should be used in the case of a wall with a restrained roof. For these cases, the mean is recommended to still be zero degrees with a standard deviation of 10 degrees.

4.2.4 Prediction of Mean Debris Mass

Figure 8 shows the variation in measured average mass with measured maximum debris velocity for all 13 masonry tests conducted where debris was collected. The point for each test is plotted with a "CM" indicating CMU (concrete masonry unit) or with "CT" indicating clay tile masonry. Average mass is normalized against the mass of a cubic fragment with the dimensions of the shell face thickness. Almost all masonry fragments included the full shell thickness. It is clear that average mass decreases as maximum debris velocity increases. There is also no difference evident between CMU and clay tile even though clay tile is considerably stronger. This may be because the collection criteria differed between these two types of walls. Almost all clay tile tests were conducted at full scale and therefore the larger fragments within 18 ft of the test wall, which would increase the average mean, were not collected. Almost all the CMU tests, on the other hand, were conducted at quarter scale and all debris from these tests were collected. This may, at least partially, explain why no difference in average mass relative to the mass of the shell thickness cubed is evident between these two types of masonry. The relationship in Figure 8 is used in the model to predict average debris mass since only that debris which travels more than 18 ft is of practical significance for most applications of the model.

Figure 9 shows a plot of measured average debris mass versus maximum measured debris velocity for all the reinforced concrete tests. Average debris mass is normalized against the mass of a piece of concrete with a thickness equal to the concrete cover thickness and an area equal to the area between the orthogonally spaced rebar. This mass is chosen because the rebar spacing limits the largest area any debris would be expected to have and the cover distance limits the thickness. No strong correlation is evident in Figure 9. No correlation between other parameters such as concrete strength, or scaled standoff was observed. Therefore, a value independent of maximum debris velocity near the center of the plotted data is used for the model. As shown in Figure 1, the debris distance predicted by the model is not very sensitive to debris mass.

4.2.5 Prediction of Total Effective Destroyed Mass

In all masonry tests the total test wall was destroyed. In all the concrete tests with close-in loading, a significant portion of the test wall remained in, or very near, the test fixture. In all concrete tests with large quasistatic loading the total wall was thrown downrange. For the cases with large quasistatic loading, a very large percentage of the wall was thrown in two or three large pieces. The MUDEMIMP code determines the total number of fragments as the quotient of the input total destroyed mass divided by the input average mass. All these factors were considered during refinement of this portion of the predictive model.

Figure 10 shows the total collected fragment mass normalized against the total test wall mass for each test. This parameter is plotted versus the maximum measured debris velocity. The masonry data includes only those tests (full scale) where the collection criteria limited debris collection to downrange fragments which were further than 18' from the test wall. The concrete data does not include large pieces (pieces comprising more than 1/4 of the total wall mass) thrown in the tests with large quasistatic loading. The figure shows that, in general, significantly more fragments are ejected downrange from masonry walls than from concrete walls for similar loading. It also shows that total measured fragment mass, within the limits of the test data and the collection criterion used, is linearly related to the maximum measured debris velocity for close-in loading. Total fragment mass, excluding large pieces, is relatively constant with maximum debris velocity for concrete tests with large quasistatic loading.

Total effective destroyed mass is used in the model where the term "effective" is used to only include fragments, other than large pieces of the component, which are transported a significant distance (more than 18') downrange. These exclusions are made because they are not expected to significantly affect downrange debris density distributions and they allow for a closer correlation between the model and the data. The total effective destroyed mass is calculated in the model using the linear relationships shown in Figure 10. For close-in loading the linear relationships are extrapolated up to 1.0, or a total effective destroyed mass equal to the total wall mass, because this is currently judged as the most logical approach. For concrete tests dominated by large quasistatic loading, the total effective destroyed mass is always taken as one-tenth of the total wall mass. This portion of the model is based on the trend in Figure 10 which shows that the wall breaks primarily into several large pieces for this type of loading regardless of the loading intensity.

5.0 Prediction of Debris Roll and Ricochet

Figure 11 shows a plot of a roll factor, which accounts for debris roll and ricochet, versus measured maximum debris velocity for each concrete and masonry test. The roll factor is calculated as the ratio of the maximum measured debris distance to the assumed distance to first impact of the furthest fragment. The initial impact distance is calculated for each test with a trajectory code assuming a velocity equal to the maximum measured debris velocity, an initial trajectory angle of 1.5 degrees, a launch height equal to the height of the charge from the ground, a mass equal to the average measured mass, and a drag coefficient of 1.4, which is considered an average value. The trajectory angle of 1.5 degrees does not represent a worst case for the roll factor but it does cause better correlation when applied to debris initial impact distances calculated with the MUDEMIMP debris dispersion code. For the recommended input angle probability density distributions, this code assigns initial trajectory angles near 1.5 degrees to debris with velocities at, or very near, maximum values.

Figure 11 shows that the roll factor for both concrete and masonry debris is linearly related to debris velocity. The considerable scatter is not unexpected based on the multitude of phenomena which can affect roll and ricochet. Figure 11 also shows that the roll factor for masonry debris is somewhat less than that for concrete debris.

In the model the initial debris distance before first impact is calculated in the MUDEMIMP code with logic lifted from a trajectory code. This initial calculated distance for each fragment in the simulation is multiplied by a roll factor calculated from the initial fragment velocity, the debris material, and the relationships shown in Figure 12. It is judged from limited data⁽⁸⁾ that less roll and ricochet result for fragments launched at high debris angles. Therefore, the model assumes a roll factor of two for all debris with angles larger than forty degrees and linearly interpolates a roll factor between that calculated from Figure 12 and a value of two for angles between ten degrees and forty degrees. A roll factor of two is considered to be conservative for high angle fragments⁽⁹⁾.

6.0 Summary

This paper presents and discusses the refinement of methods predicting component breakup and debris roll and ricochet after first impact. The refinement is primarily based on the correlation of measured component breakup parameters and measured debris distances to measured test parameters, primarily measured maximum debris velocity. The predictive methods are formulated as portions of an overall predictive model which predicts building debris dispersion based on known loading parameters and certain building component parameters. Therefore, the most important test of the predictive methods discussed in this paper is the correlation of predicted debris distance calculated with the predictive model to measured debris distances. Preliminary results indicate that good correlation is obtained. The combined effect of the scatter in the correlations presented here tends to be offsetting so that the error does not tend to accumulate through the model.

It must also be noted that the refinement of the predictive model is almost in its final form, but is not yet complete. The reader must refer to Reference 2 for a description of the model refinements in their final form. This report will be completed by the end of September 1990.

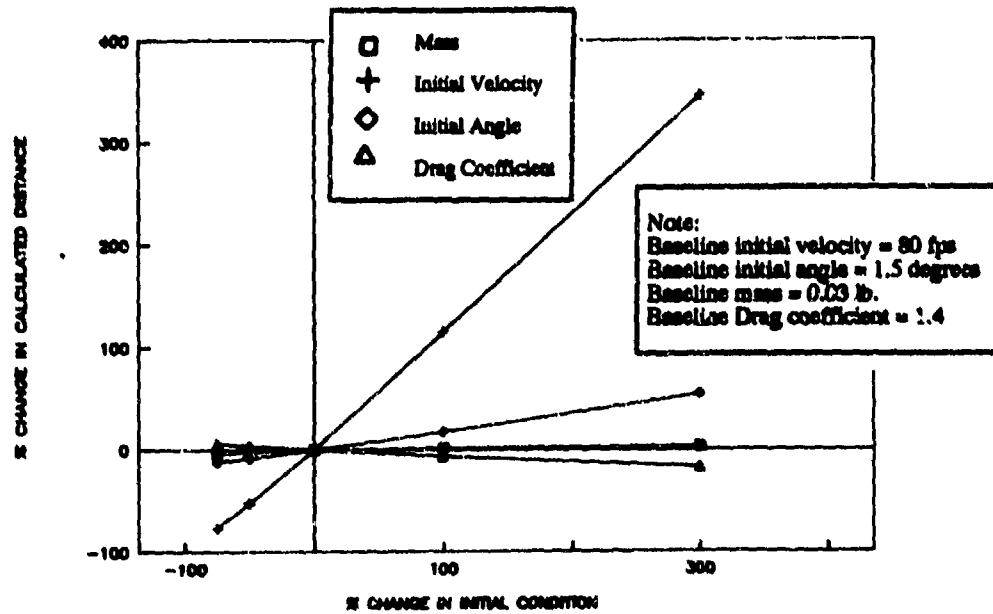


Figure 1. Effect of Debris Initial Conditions on Calculated Dispersion Distance

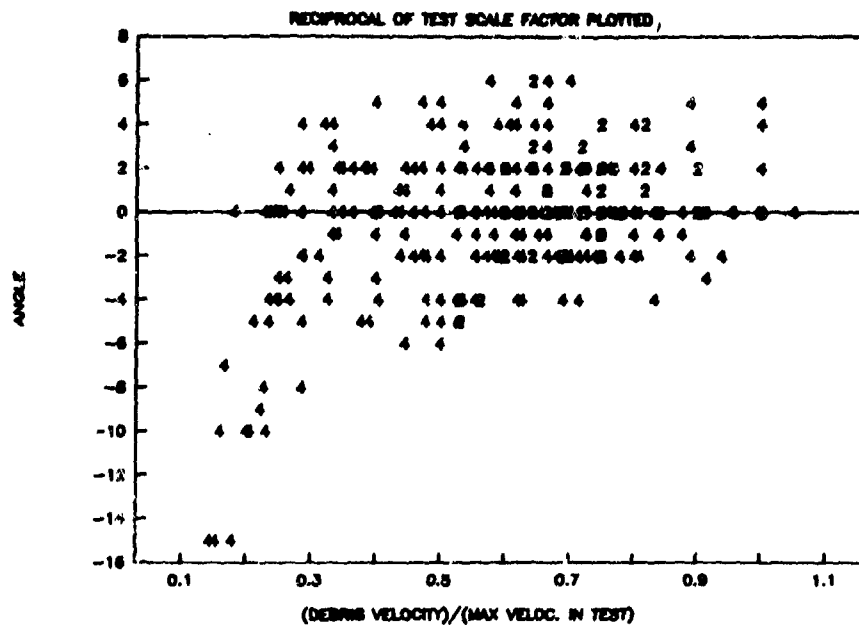


Figure 2. Scatterplot of Relative Debris Velocity vs. Debris Angle from Sampled Concrete Tests

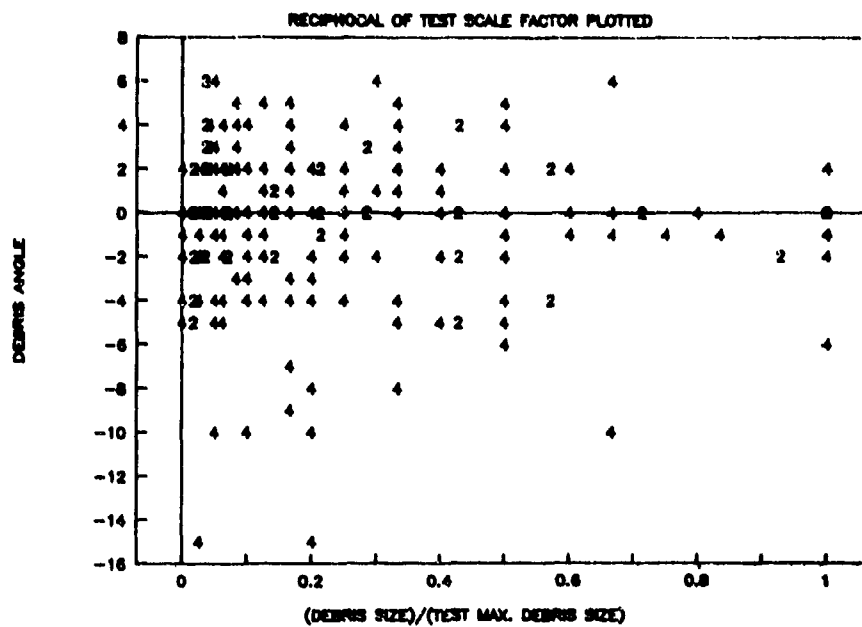


Figure 3. Scatterplot of Relative Debris Size vs. Debris Angle from Sampled Concrete Tests

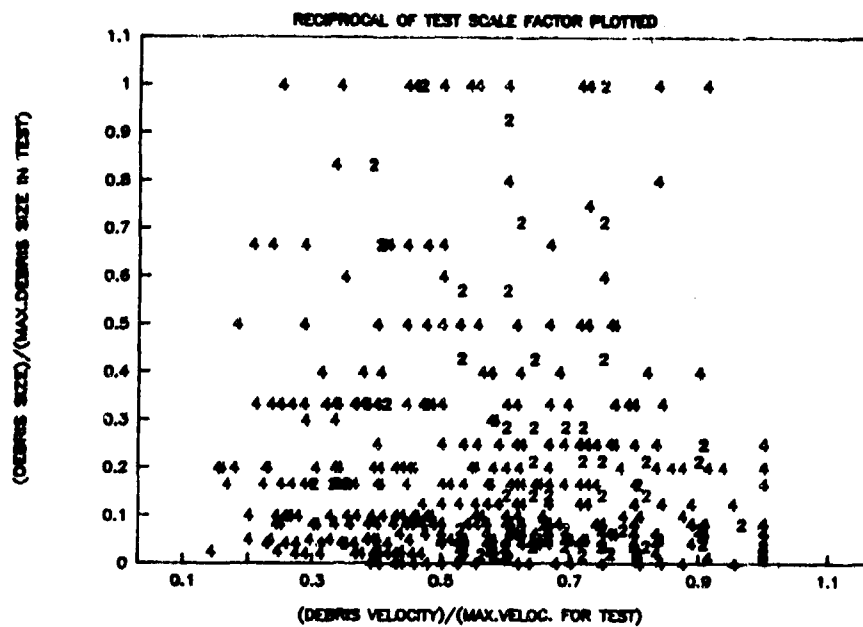


Figure 4. Scatterplot of Relative Debris Velocity vs. Relative Debris Size from Sampled Concrete Tests

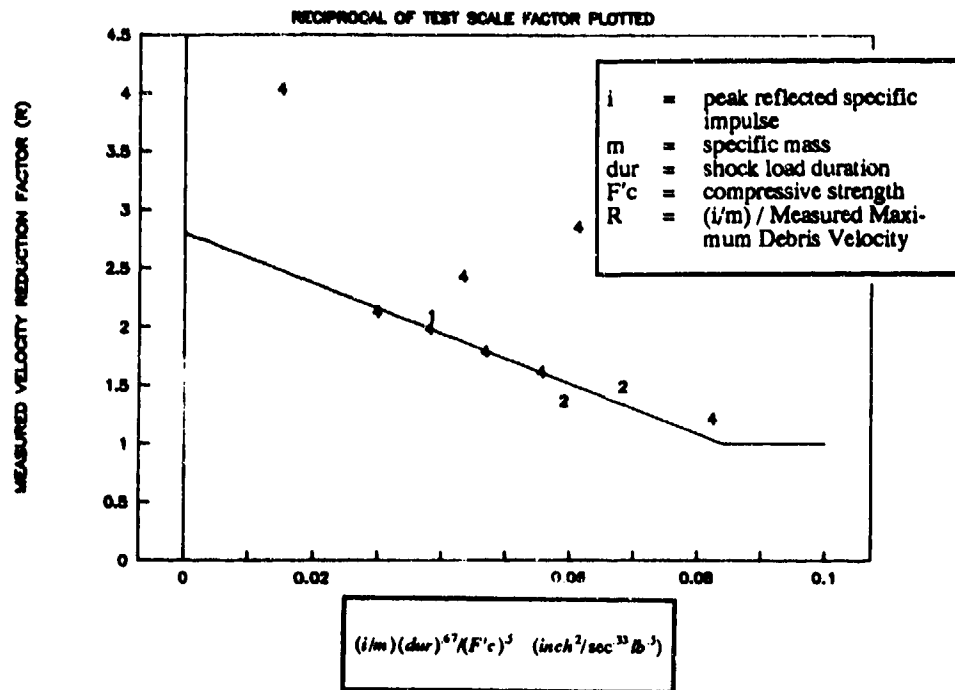


Figure 5. Reduction Factor for Maximum Debris Velocity of Concrete Walls with Close-in Loading

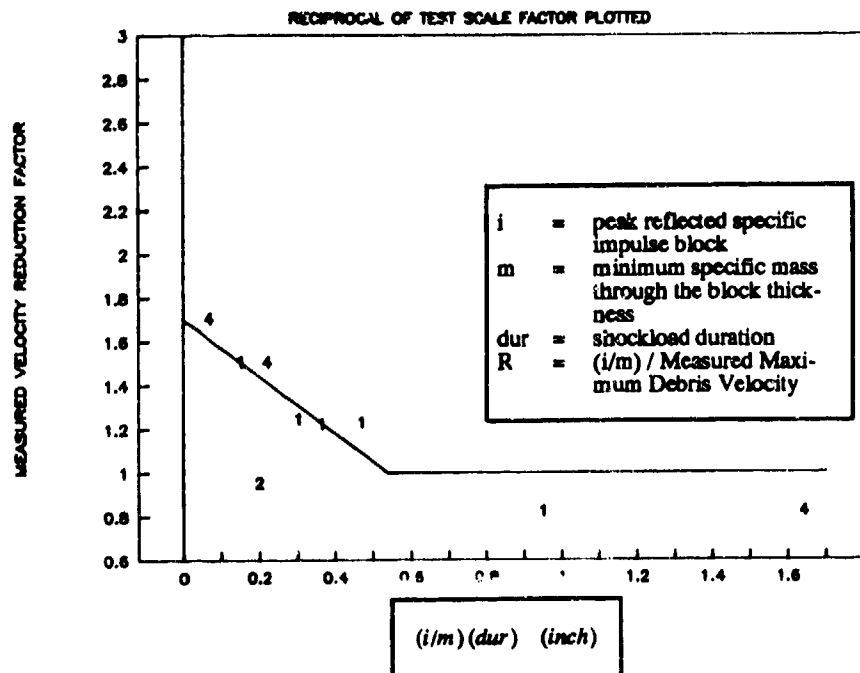


Figure 6. Reduction Factor for Maximum Debris Velocity of Unreinforced Masonry Walls

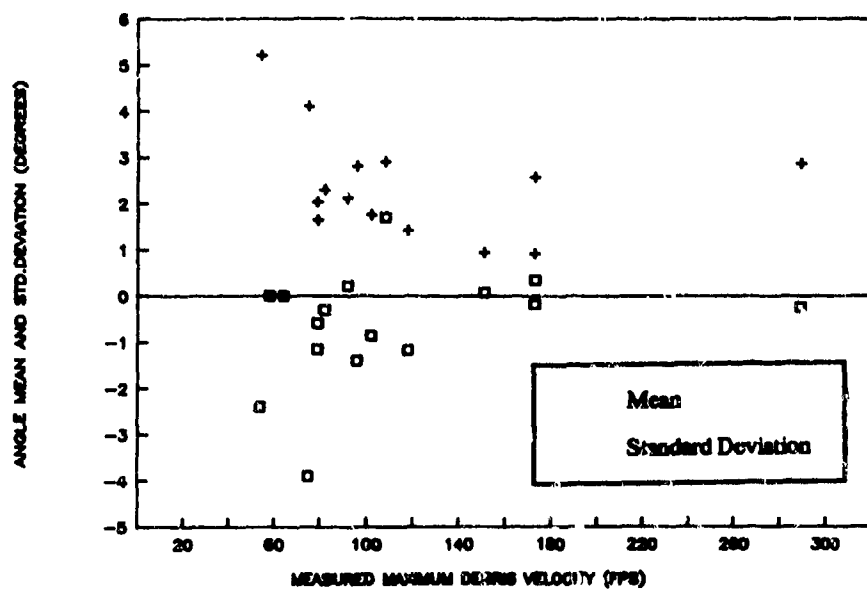


Figure 7. Measured Means and Standard Deviations of Debris Angle for Concrete and Masonry Walls

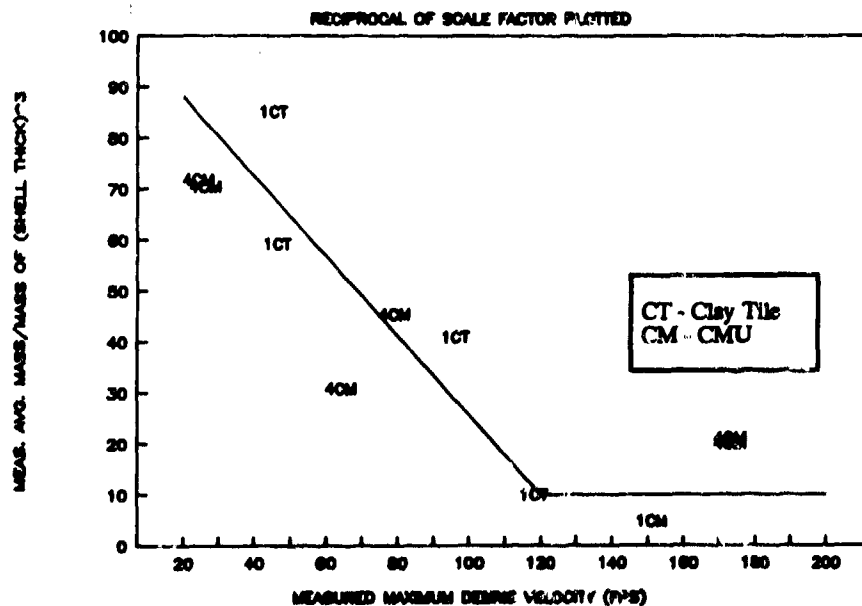


Figure 8. Normalized Average Debris Mass vs. Maximum Debris Velocity for Masonry Tests

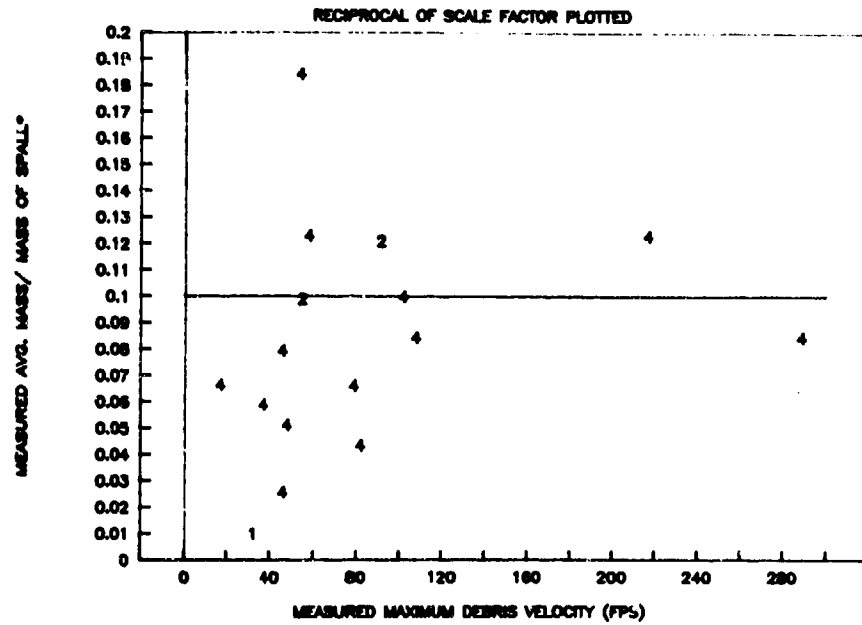


Figure 9. Normalized Average Debris Mass vs. Maximum Debris Velocity for Concrete Tests

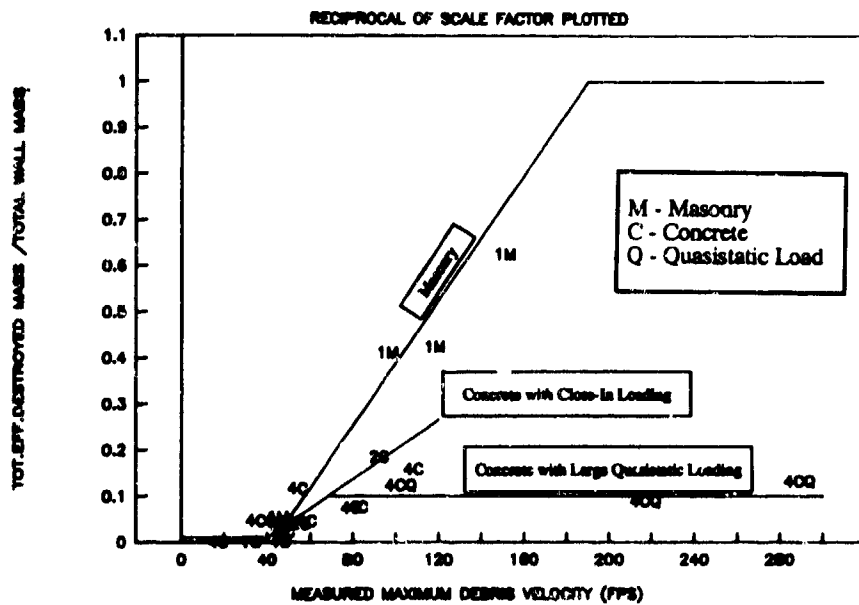


Figure 10. Normalized Total Effective Destroyed Mass vs. Maximum Debris Velocity for Concrete and Masonry Tests

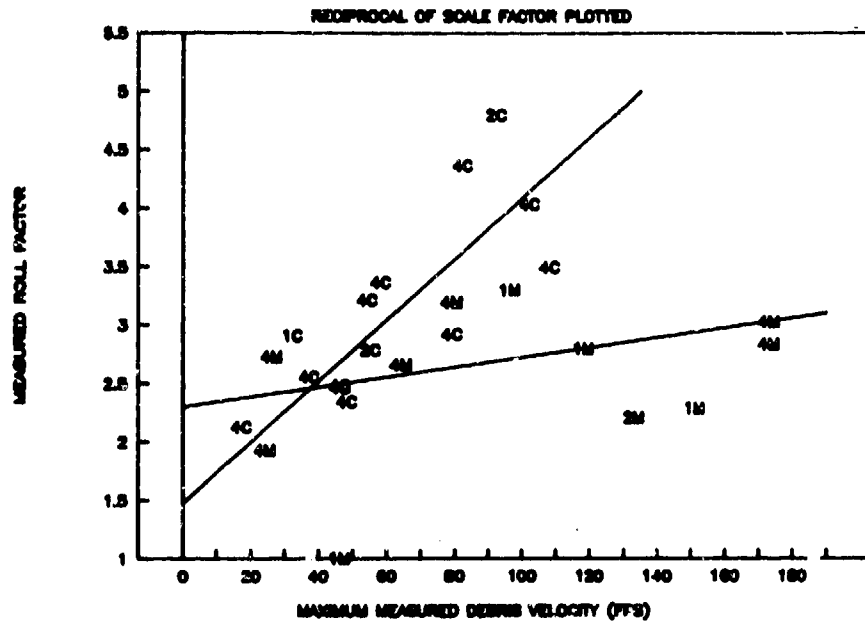


Figure 11. Roll Factor vs. Maximum Debris Velocity for Concrete and Masonry Tests

References

1. Bowles, P.M., Oswald, C.J., "Building Debris Hazard Prediction Model", paper presented at the Twenty-fourth Department of Defense Explosives Safety Seminar, St. Louis, Missouri, August 28-30, 1990.
2. Bowles, P.M., Oswald, C.J., Vargas, L.M., And Baker, W.E., "Debris Hazard Evaluation, Task 3: Test Program and Predictive Model Refinement", Final Report in preparation for Southwest Research Institute Project 06-2945, prepared for Bernard Johnson Incorporated under Mason & Hanger -- Silas Mason Co., Inc. Contract H0760103, U.S. Government Contract DE-AC04-76DP-00487, to be submitted September 1990.
3. Bowles, P.M., Oswald C.J., And Vargas, L.M., "Building Debris Hazard Evaluation Test Program", paper presented at the Twenty-fourth Department of Defense Explosives Safety Seminar, St. Louis, Missouri, August 28-30, 1990.
4. Ayvazyan, H.E., Dobbs N., Computer Program Impres, special publication ARLCD-SP-84001, prepared by Ammann & Whitney, New York, New York, for U.S. Army Armament Research and Development Center, Large Caliber Weapon Systems Laboratory, Dover, New Jersey.
5. Huang, L.C.P., "Theory and Computer Program for the Multiple Debris Missile Impact Simulation (MUDEMIMP):", Naval Facilities Engineering Command, Naval Civil Engineering Laboratory, Program No. Y0995-01-003-331, June 1984.
6. McVay, Mark K., "Spall Damage of Concrete Structures", Technical Report SL-88-22, U.S. Army Engineer Waterways Experiment Station, Vicksburg, Mississippi
7. Watson, A.J., Hobbs, B., Wright, S.J., "Scaling Explosive Damage to Reinforced Concrete Beams and Slabs", for the Proceedings of First International Conference on Structures Under shock and Impact, Cambridge, Massachusetts, July 1989.
8. Ward, J., et. al., Modeling of Debris and Air Blast Effects from Explosions Inside Scaled Hardened Aircraft Shelters, Research and Technology Department, Naval Surface Weapons Center, Dahlgren, VA, Silver Springs, MD, May 1985.
9. Kossover, David; Dobbs, Norval; and Caltagirone, Joseph, "Engineering - Quantity/Distance Analysis of Ammunition and Explosives Operations", paper presented at the Fourth International Symposium on the Interaction of Non-Nuclear Munitions with Structures, April 1989.

Building Debris Hazard Evaluation Test Program

by

Patricia M. Bowles
Luis M. Vargas
Charles J. Oswald

Southwest Research Institute
6220 Culebra Road
San Antonio, Texas 78228-0510

ABSTRACT

An extensive test program has been conducted to study the formation and subsequent throw of building wall debris subjected to internal high explosive detonations. The objective of the Department of Energy (DOE) sponsored program was to refine and verify an analytical model developed to predict maximum hazardous debris distances resulting from these internal detonations. Once appropriate approval has been obtained, DOE plans to use the model to aid in the safe siting of structures containing high explosives. The test program included full, half, and quarter scale tests of reinforced concrete, masonry, and metal walls. Loading conditions (fully vented, partially vented, and closed), charge amounts, and structural characteristics have been varied to understand their effects on the breakup of a building and the resultant debris spread following an accident. An overview of the tests and the manner in which the test data were used to refine the predictive model are included in this paper.

1.0 Introduction

An extensive test program was conducted to study the formation and throw of building wall debris due to an internal high explosive detonation. The objective of this Department of Energy (DOE) funded program was to refine and verify an analytical model developed to predict maximum hazardous debris distances and velocities resulting from internal detonations (Reference 1). Three different types of building wall construction were evaluated: reinforced concrete walls, masonry walls and lightly constructed walls, i.e., metal siding and metal stud walls. Tests were conducted using full scale, half scale and quarter scale wall sections with the wall sections supported on three sides. Tests were conducted in the open and in a vented quarter scale box reaction frame which could be completely closed allowing the generation of quasistatic loads. In order to model a number of actual in-plant loading conditions, several physical parameters were varied including: wall thickness, concrete strength, charge weights and standoff distances. Wall debris velocities, ranges and mass distributions were obtained for each test, and these data were used to refine the predictive model.

2.0 Design and Construction of Test Fixtures

This program involved the conduct of tests in three different test fixtures: 1) a quarter scale box reaction frame, 2) a full scale open air reaction frame, and 3) a quarter scale open air reaction frame. All of the tests were conducted at the SwRI Test Range with the exception of the tests performed using the full scale open air reaction frame which were conducted at a remote test facility. The following paragraphs describe the different test fixtures fabricated for this program.

2.1 Quarter Scale Box Reaction Frame

The quarter scale box reaction frame as shown in Figure 1 was designed for use in conducting closed and vented tests involving quarter scale models of walls 20 feet high by 20 feet wide which are typical of DOE facilities. The box fixture was constructed with inside dimensions of 5 feet by 5 feet by 7.5 feet and consisted of a rectangular inner and outer steel liner filled with concrete. The four sides of both the inner and the outer steel liners were fabricated using 5/8 inch steel plates welded together while the front and rear portions were fabricated using one inch plates. The front face was fabricated out of thicker steel to allow bolting of the wall test panel to the front face. The rear face was also fabricated using one inch plate to allow a solid steel plate to be bolted on for the closed tests. Nelson studs were welded to the inside surfaces of the inner and outer liners to assist in the development of the concrete and steel. Sections of hollow steel tubing were welded between the inner and outer liners to allow mounting of the pressure gages used to measure reflected pressure and quasistatic pressure for the various tests. A framework was designed for the front and rear of the box for clamping the test panels in place and for modeling typical wall connection strengths.

This framework was bolted directly to the front or rear faces of the box on two sides, and the base of the test panel was clamped using steel spacers which were inserted after the wall panel had been positioned.

2.2 Large Scale Open Air Fixture

The large scale open air fixture was designed to enable testing of half scale reinforced concrete panels and full scale CMU or clay tile panels. The fixture was also used to test frangible wall panels such as the corrugated metal "Butler" building panels. The test fixture dimensions were based on the previous one-sixth scale dividing wall tests (Reference 2). The fixture consisted of two vertical members used to clamp the wall panels at the two edges and two angles bolted to the base of the test fixture for clamping the base of the wall test panel. The vertical members were fabricated out of six inch heavy wall square tubing and the base angles were fabricated out of 1/2 inch angle. The vertical members and the base angles were bolted to a one inch steel base plate which was anchored to the concrete test slab. The vertical members were designed to be movable, allowing for testing of the six foot wide concrete panels as shown in Figure 2 as well as testing of the CMU panels, the clay tile panels and the "Butler" building type panels which were all ten foot wide. Figure 3 shows a CMU wall section in place prior to the test.

2.3 Quarter Scale Open Air Fixture

This quarter scale fixture was designed to test reinforced concrete panels and the quarter scale CMU wall panels in an open air configuration similar to tests conducted on one-sixth scale dividing wall panels tested in an earlier program (Reference 2).

3.0 Test Set-up

As previously mentioned, tests were conducted at the SwRI Test Range and at a remote test facility. The tests conducted at both sites involved the recovery of wall debris and the measurement of debris velocities. To aid in the debris recovery, SwRI personnel constructed debris recovery zones at both sites. The following paragraphs describe the test set-ups at both sites.

The recovery zone at SwRI consisted of an area approximately 150 feet long by 21 feet wide located directly in line with the box reaction test frame. This area was cleared and filled with a layer of washed sand approximately three inches deep. A removable grid was constructed using plastic pipe which was laid on top of the debris recovery area after a test to map the debris locations. The plastic grid was 21 feet wide by 9 feet long and consisted of three rows of seven grids each. After each test, the grid was initially positioned six feet from the edge of the box reaction frame and the debris in each square were identified and recovered. The grid was then moved farther down the test bed to the next location and the debris identified and recovered. This procedure was repeated until all of the debris of interest in the test bed were recovered. This debris recovery scheme was also used on the quarter scale open air tests which were conducted directly in front of the box reaction frame. Figure 4 shows a reinforced concrete panel in the quarter scale open air fixture. The tests conducted in the quarter scale box reaction fixture were instrumented with reflected pressure gages, quasistatic pressure gages and side-on pressure gages. Four reflected pressure gages

were mounted in the side of the reaction fixture and three quasistatic pressure gages were mounted on the box, one gage on each of the two sides of the box and one on the top side of the box. Two side-on pressure gages were located directly in front of the wall test panel at two different standoffs, 15 feet and 20 feet from the charge location. Two side-on gages were located on the back side of the box at 15 foot and 20 foot standoffs from the charge location for measuring the vent pressures. Two additional side-on pressure gages were placed perpendicular to the side of the box and in line with the front and rear faces for measuring the pressure as it wrapped around the box.

The debris recovery area at the remote test facility consisted of an area approximately 250 feet long by 80 feet wide which was graded to remove any vegetation and existing debris. The area was divided into 12 foot by 12 foot squares and the debris in each square were identified and recovered in a manner similar to that described for the SwRI Test Range setup.

Debris velocities were measured at both test sites using high speed cameras to record the debris in flight. A large elevation grid background was constructed from plywood and was located along one side of the recovery zone. Initially, two high speed cameras were used on the tests with both cameras recording the debris trajectories and velocities. After the sixth test, the decision was made to use one camera for measuring the debris velocities and to use the second camera to focus on the back face of the test wall for documenting the actual wall breakup. A third camera was added late in the program and was used to record the roll exhibited by the debris. The initiation of the explosive charges was performed remotely using RP-83 detonators which were actuated by a signal from one of the high speed cameras.

4.0 General Test Descriptions

4.1 Reinforced Concrete Tests

A total of 16 reinforced concrete tests were conducted during this program. Eight of the tests were conducted in the quarter scale box reaction frame using three different types of venting configurations: full venting which consisted of leaving the back wall of the box completely open, partial venting which involved placing a frangible material such as gypsum board across the back side of the box, and no venting which required complete closure of the back wall of the box. These eight tests were conducted at the SwRI Test Range. Three open air tests were conducted at the remote test facility using the full scale reaction frame, and five open air tests were conducted at the SwRI Test Range using the quarter scale reaction frame. The full scale reinforced concrete wall that was used as a baseline for the scaled tests was 9 foot x 9 foot x 12 inches with #4 reinforcing rods each face, each way positioned at 12 inch centers. The reinforcing steel had an ultimate strength of 90 - 95 Ksi. Grade 4 aggregate which had a maximum size of approximately 3/8 inch was used on all of the quarter scale walls. A range of scaled charge sizes were tested with the largest charge being a 25 pound TNT equivalent charge and the smallest charge being 0.4 pounds TNT equivalent charge. Since the scales tested were quarter, half, and full scale, the full scale equivalent charges ranged from 25 pounds to 200 pounds. The scaled charge standoff was also varied from 9 inches to 36 inches. Scaling of the walls was performed using replica scaling and scaling of the charge was performed using Hopkinson scaling.

4.2 Masonry Wall Tests

A total of 12 masonry wall tests were conducted during this program. Five of the tests conducted were full scale tests and were performed at the remote test facility. Four quarter scale masonry wall tests were conducted in the box reaction frame using either a full venting configuration, which consisted of leaving the back wall of the box completely open, or no venting which required complete closure of the back wall of the box. Two additional quarter scale masonry tests were conducted in the small open air test fixture. One test was performed using half scale tile blocks. This test was performed in the box reaction frame in the vented configuration. The full scale masonry blocks that were used included four different types: concrete masonry unit (CMU) blocks and three different geometries of clay tiles. The full scale CMU blocks were standard blocks 7.5 inches x 7.5 inches x 15.5 inches weighing 24.5 pounds. The full scale clay tiles ranged in size from 5.7 inches x 6.7 inches x 6.7 inches to 4.875 inches x 7.625 inches x 11.5 inches and in weight from 13.7 pounds to 16.8 pounds. The quarter scale CMU were 1.91 inches x 1.91 inches x 3.89 inches and weighed 0.57 pounds. The half scale clay tiles were 3.85 inches x 3.85 inches x 7.78 inches and weighed 5.0 pounds. A number of different charge amounts were used. Scaling of the walls was performed using replica scaling, and scaling of the charge was performed using Hopkinson scaling. The same debris recovery zones and recovery techniques used in the reinforced concrete tests were used in the masonry tests.

4.3 Lightly Constructed Wall Tests

A total of three lightly constructed wall tests were conducted during this program. Two tests were conducted on half scale corrugated metal "Butler" building walls, and one test was conducted on a half scale metal stud wall with a plaster and lathing cover. These tests were all performed at the remote test facility. Figure 5 shows one of the "Butler" building walls. The actual wall sections were 6 feet high and 10 feet wide. The structural members, sheet metal and sheet metal screws used on the "Butler" building walls were all scaled down to half scale. The metal stud wall used half scale structural members with the thickness of the lathing and plaster also scaled down. The first "Butler" building wall was exposed to the half scale equivalent of 200 pounds of TNT at a standoff of three feet from the wall and from the floor. A later test of this wall type used the same configuration at a larger wall standoff of six feet. The metal stud wall test examined the effects of a much smaller 5 pound TNT equivalent charge (40 pounds full scale) at the three foot standoff. Scaling of the walls was performed using replica scaling and scaling of the charge was performed using Hopkinson scaling. The same debris recovery zones and recovery techniques used in the reinforced concrete and the masonry wall tests were used in the lightly constructed wall tests.

5.0 Summary of Test Results

5.1 Reinforced Concrete Tests

As previously mentioned, 16 tests were conducted using scale model reinforced concrete walls. A summary of the physical characteristics of each of the walls is presented in Table 1 and includes the wall thickness, the concrete strength on the day the test was conducted, and the reinforcement ultimate and shear strengths for each test. Table 2 presents a summary of the test

results for each test including the maximum and average debris velocities, debris ranges and masses for each of the tests and the total number of debris recovered for each test. Figure 6 shows the damage sustained by one of the quarter scale concrete walls, (Test No. 1.2), which was a 3 inch thick wall mounted in the quarter scale open air fixture. Figure 7 shows the damage to a full scale concrete wall (Test No. 3.3) mounted in the open air test fixture, while Figure 8 shows the debris generated by Test 3.7 which involved a half scale concrete wall mounted in the open air fixture. A number of comparisons of the data presented can be made to determine the effects of scaling, venting, charge standoff and concrete strength. Selected comparisons will be presented here.

The effects of venting are evident in the data presented in Table 2. Test 1.3 was conducted in the quarter scale box reaction fixture in the vented configuration while Test 1.4 was conducted in the quarter scale box reaction fixture in the closed configuration (for this test, a substantial steel plate was bolted to the back side of the box). As can be seen in Table 2, the velocities and ranges for Test 1.4 are much larger than the velocities and ranges for Test 1.3 due to the effects of the quasistatic loads generated in the closed box. The number of wall debris is also larger for the closed test than for the vented test. The two tests performed using the steel plate to close the box, Tests 1.4 and 1.9, resulted in the largest debris velocities and ranges of all the tests performed. Tests 1.8 and 1.10 were also conducted in the closed configuration; however, for these tests, the back side of the box was closed using a frangible material that did not contribute as significantly to the development of the quasistatic loads as did the steel plate. Thus, lower debris velocities and ranges resulted.

The effects of concrete strength on the generation of debris and on the debris velocity and range can be seen in a comparison of Tests 3.1 and 3.2 which were both quarter scale open air tests. Test 3.1 had a concrete strength of 1600 psi as measured on the day of the test as compared to a concrete strength of 2900 psi for Test 3.2. As can be seen in Table 2, the debris range and both the maximum and average velocities are higher for Test 3.1 than they are for Test 3.2. The number of debris is also larger for Test 3.1 than for Test 3.2.

The effects of thickness on the debris and on debris velocity and range can be evaluated by comparing Tests 2.1 which involved a 2 inch thick wall and Test 2.2 which involved a 3 inch wall. As would be expected, the number of debris pieces, the debris range and the debris velocity are much higher for the thinner wall than for the thicker wall.

5.2 Masonry Wall Tests

As previously mentioned, 12 tests were conducted on standard concrete masonry blocks (Test 1.6), quarter scale CMUs (Tests 1.7, 1.7A, 2.9, 2.10, 2.11 and 2.16) and different clay tile geometries (2.15, 2.21, 3.8, 3.9 and 3.10). A summary of the test results is presented in Table 3 and includes data on the debris velocity, range and mass for each of the tests performed. Figure 9 shows the debris generated in Test 2.15 which was a full scale clay tile wall mounted in the open air fixture. Figure 10 shows the debris from Test 1.7 which was a quarter scale CMU test in the open air fixture.

The quarter scale CMUs were geometric scale models of the full scale CMU, however, their density was found to be greater than that of the full scale CMU. The densities of the quarter scale CMU and the clay tiles were very similar and, therefore, most of the data comparisons are made between the quarter scale CMU and the clay tile data. One observation can be made between the full scale CMU wall, Test 1.6 and the full scale clay tile wall, Test 2.21. As shown in Table 3, the debris from the concrete masonry blocks has a higher velocity and a larger range than the debris from the clay tiles. The actual number of debris, however, is less for the CMU blocks than for the clay tiles.

5.3 Lightly Constructed Wall Tests

Lightly constructed walls found at DOE facilities are typically either corrugated metal walls, as in "Butler" buildings, or metal stud walls consisting of a metal frame covered by a layer of plaster and lathing. Since reinforced concrete and masonry walls are more predominantly found in these facilities, the test program concentrated heavily on those components and less on the lightly constructed components. However, a procedure for estimating debris throw from these walls is included in the predictive model, so an effort was made to collect some data in an attempt to verify this area of the model. Two corrugated metal walls and one metal stud wall were tested as summarized in Table 4. While the data from these tests are not enough to verify the specific prediction procedure, the data did indicate important aspects of breakup of this type of wall. The first corrugated metal wall was tested in half scale with a 25 pound charge positioned 3 feet from the wall. The close standoff caused the wall to break into smaller pieces (less than a single metal panel) than seen in accidents in these type of buildings. None of the accident data reviewed, however, had the explosive source this close to the wall. A later test using identical test conditions except at a larger standoff produced larger debris sizes (half and quarter panels) as expected based on the accident data review. The one half scale metal stud wall tested indicated the plaster and lathing were blown out as debris, but none of the metal studs broke free. This is the type of breakup expected for the low loading conditions to which these walls are generally exposed.

6.0 Use of Test Data to Refine the Predictive Model

Although only brief descriptions of the tests conducted and a few comparisons of data from test to test have been presented in this paper, extensive analysis (including a statistical study) of the data has resulted in refinement of the model used to predict hazardous debris throw distance (References 1 and 3). The data have been used to verify loading prediction techniques and methods used to define debris characteristics such as debris mass, initial velocity, drag area, drag coefficient, and trajectory angle. In addition to verifying or modifying initial debris characteristics needed for input to the model, the data have been used to define the effect of debris roll or ricochet on debris distances and to devise a way to incorporate this effect within the dispersion code used in the model. Test data from this program have also been used to examine concepts such as velocity absorbed in the wall breakup process and "jetting velocity" of small debris pieces which can exceed the maximum predicted wall motion velocity. The data have been used to study scaling effects in reinforced concrete and masonry as well. Although all questions on scaling of breakup in these materials have

not been resolved, the method used to predict velocities and throw distances is conservative. All scaling aspects studied in the program have been well documented in Reference 1 so that further research in these areas can benefit from analysis already conducted.

The tests conducted as part of this DOE funded program provided much needed data for developing a flexible model for predicting hazardous debris distance. Once approved, the model will help solve DOE's compliance problems with the current broad-ranged hazardous debris siting criteria, but it will also become an important tool to be used in the siting of any explosive handling or processing facilities. The large amount of data collected in this program greatly contributes to the limited database available for updating DOE/TIC-11268 (Reference 4), a DOE blast and fragment loading prediction manual, as well. The update of this manual is expected to begin within the next year or two. Any other future programs examining the response of reinforced concrete or masonry walls or the distribution of debris from these construction types will also benefit from a careful review of Reference 1.

References

1. Bowles, P.M., Oswald, C.J., Vargas, L.M., and Baker W.E., "Debris Hazard Evaluation, Task 3: Test Program and Predictive Model Refinement", Final Report in preparation for SwRI Project 06-2945, prepared for Bernard Johnson Incorporated under Mason & Hanger -- Silas Mason Co., Inc. Contract H0760103, U.S. Government Contract DE-AC04-76DP-00487, to be submitted September 1990.
2. Vargas, L.M., Hokanson, J.C., and Rindner, R.M., "Explosive Fragmentation of Dividing Walls", prepared for ARRADCOM, SwRI Project 02-5793, August 1980.
3. Bowles, P.M. and Oswald, C.J., "Building Debris Hazard Prediction Model", paper presented at the Twenty-fourth Department of Defense Explosives Safety Seminar, St. Louis, Missouri, August 28-30, 1990.
4. Baker, W.E., et al., "A Manual for the Prediction of Blast and Fragment Loading on Structures", DOE/TIC-11268, Contract No. DACA87-79-C-0091, November 1980.

Table 1. Reinforced Concrete Data Summary

Test No.	Thickness (in)	Concrete Strength (psi)	Reinforcement	
			Ultimate (psi)	Shear (psi)
Full	12	4000	90000	60000
1.1	6	6400	95500	84000
1.2	3	5800	91470	72234
1.3	3	5000	91470	72234
1.4	3	5200	91470	72234
1.5	3	5200	91470	72234
1.8	3	7000	91470	72234
1.9	3	5200	91470	72234
1.10	3	5500	91470	72234
2.1	2	5400	91470	72234
2.2	3	5850	97750	89500
3.1	3	1600	91470	72234
3.2	3	2900	91479	72234
3.3	12	4500	70000	40000
3.4	3	5000	70000	N/A
3.5	2	2600	91470	72234
3.7	4	3300	95500	84000

Table 2. Summary of Test Results for Reinforced Concrete Walls

Test No.	Scale	Loading Condition	W (lbs)	R (ft)	Velocity (ft/sec)		Range (ft)		Mass ¹ (lbs)		Number of Debris
					Maximum	Average	Maximum	Average	Largest	Average	
1.1	1/2	Open Air	25	1.5	92	62	216	62	4.32	0.378	751
1.2	1/4	Open Air	3	0.75	54	25	55	12	1.03	0.072	312
1.3	1/4	Vented	2.5	0.75	58	25	70	6	1.17	0.016	2737
1.4	1/4	Closed	2.5	0.75	217	108	240 ²	64	1.21	0.016	5260
1.5	1/4	Vented	2.5	0.75	79	46	83	17	1.49	0.009	8263
1.8	1/4	Closed	2.5	2.5	37	35	45	10	2.36	0.023	1933
1.9	1/4	Closed	2.5	2.5	289	158	213 ²	85	3.34	0.011	11334
1.10	1/4	Closed	2.5	2.5	102	61	195	55	8.45	0.013	8936
2.1	1/4	Vented	2	0.75	82	45	134	25	1.46	0.034	1407

¹ The largest and average debris mass are very dependent on the minimum debris size collected and the extent of the collection. Pickup criteria varied for some tests.

² The maximum measured debris range for Tests 1.4 and 1.9 represents the final range of the furthest debris piece found. Both tests resulted in debris being thrown beyond the excavated test bed, making collection difficult.

Table 2. Summary of Test Results for Reinforced Concrete Walls (cont.)

Test No.	Scale	Loading Condition	W (lbs)	R (ft)	Velocity (ft/sec)		Range (ft)		Mass ¹ (lbs)		Number of Debris
					Maximum	Average	Maximum	Average	Largest	Average	
2.2	1/4	Vented	2	0.75	46	30	40	6	.06	0.01	171
3.1	1/4	Open Air	3	0.75	108	60	142	30	2.64	0.033	923
3.2	1/4	Open Air	3	0.75	46	27	20	8	1.15	0.031	208
3.3	Full	Open Air	25	1.5	32	26	48	30	1.27	0.25	15
3.4	1/4	Open Air	.4	0.375	17	15	10	4.5	0.05	0.026	3
3.5	1/4	Open Air	3	1.5	48	28	38	8	1.11	0.015	198
3.7	1/2	Open Air	24	3	55	38	78	19	7.75	0.232	180

Table 3. Summary of Test Results for Masonry Walls

Test No.	Scale	Loading Condition	W (lbs)	R (ft)	Velocity (ft/sec)		Range (ft)		Mass (lbs)		Number of Debris
					Maximum	Average	Maximum	Average	Largest	Average	
1.6	Full	Open Air	25	3	151	92	200	63	26.2	0.75	1822
1.7	1/4	Open Air	.4	0.75	26	18	21	6	7.88	0.267	315
1.7A	1/4	Open Air	.4	0.75	64	36	54	15	1.038	0.039	1309
2.9	1/4	Vented	1	0.75	173	98	200	43	15.1	0.08	2979
2.10	1/4	Vented	3	4.5	173	106	260	89	0.867	0.076	3311
2.11	1/4	Closed	.1875	0.75	79	41	125	31	9.2	0.172	1578
2.15	Full	Open Air	12	3	N/A	N/A	32	24	5.18	0.978	179
2.16	1/4	Closed	.1875	4.5	24	16	22	8	22.8	0.272	1041
2.21	Full	Open Air	25	3	96	56	174	43	31.8	0.47	2767
3.8	Full	Open Air	25	12	46	40	24	24	25.9	1.73	58
3.9	Full	Open Air	25	3	118	73	180	46	4.2	0.293	3495
3.10	1/2	Vented	3	1.5	133	64	126	N/A	N/A	N/A	N/A

Table 4. Summary of Test Results for Metal Siding and Metal Stud Walls

Test No.	Scale	Loading Condition	W (lbs)	R (ft)	Velocity (ft/sec)		Range (ft)		Mass (lbs)		Number of Debris
					Maximum	Average	Maximum	Average	Largest	Average	
2.17	1/2	Open Air	25	3	1660	796	324	134	1.34	0.084	654
2.20	1/2	Open Air	25	6	1120	624	252	112	6.74	0.278	255
2.18	1/2	Open Air	5	3	138	90	96	43	0.502	0.225	1535



Figure 4.10.10.1 Scale Box Reaction Frame -
Winch Concrete Wall Panel

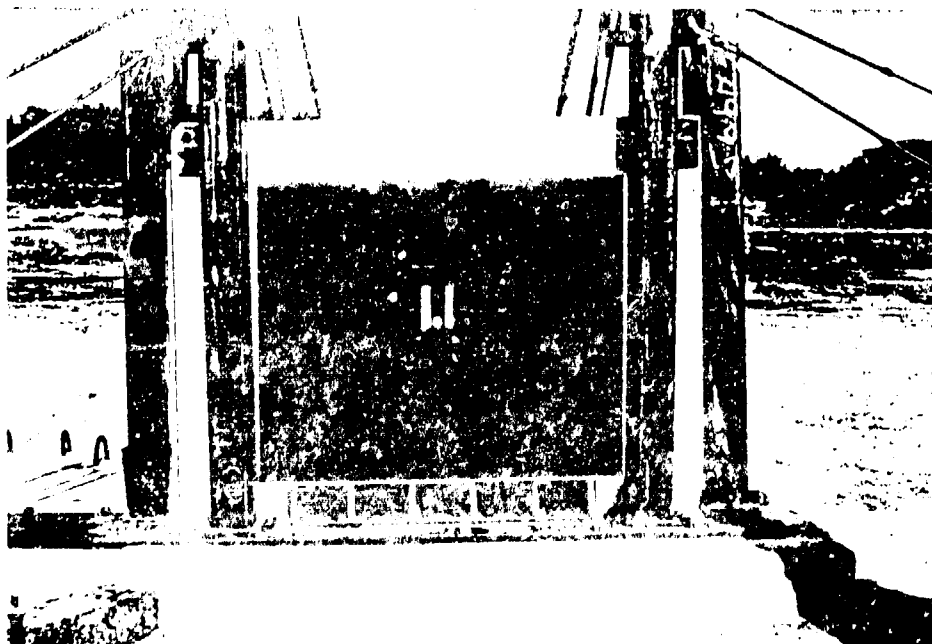


Figure 4.10.10.2 Scale Box Reaction Frame -
Winch Concrete Wall Panel

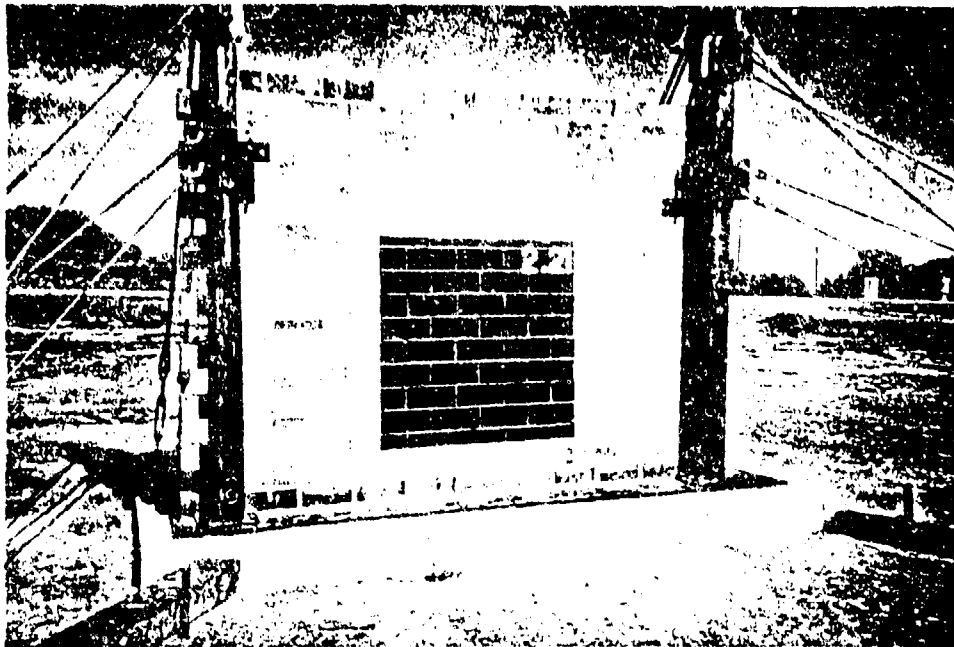


Figure 3. Full Scale Open Air Fixture -
Clay Tile Wall Panel

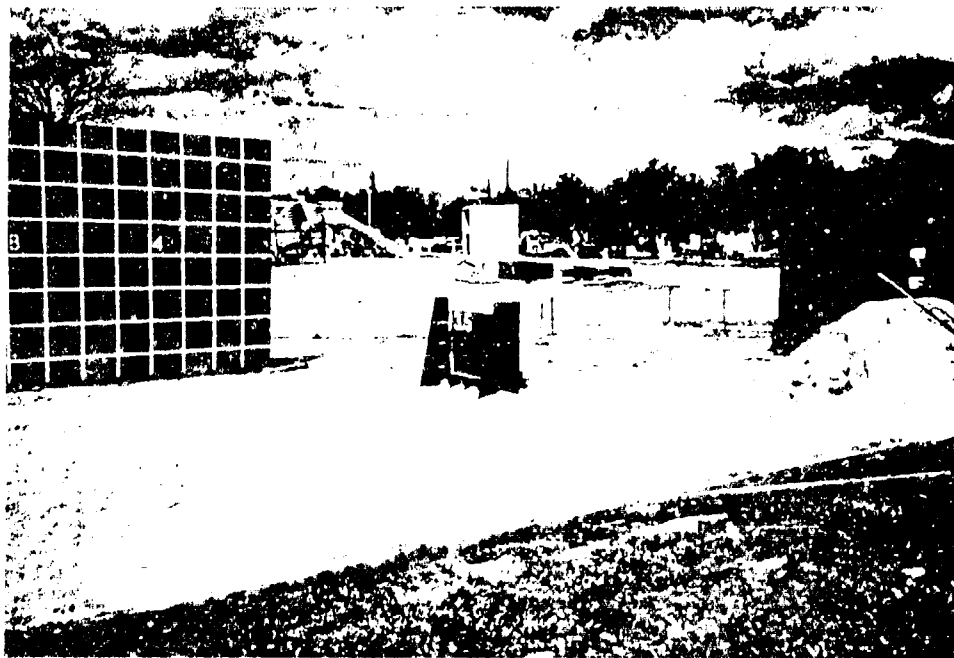


Figure 4. Quarter Scale Open Air Fixture -
2-inch Concrete Wall Panel

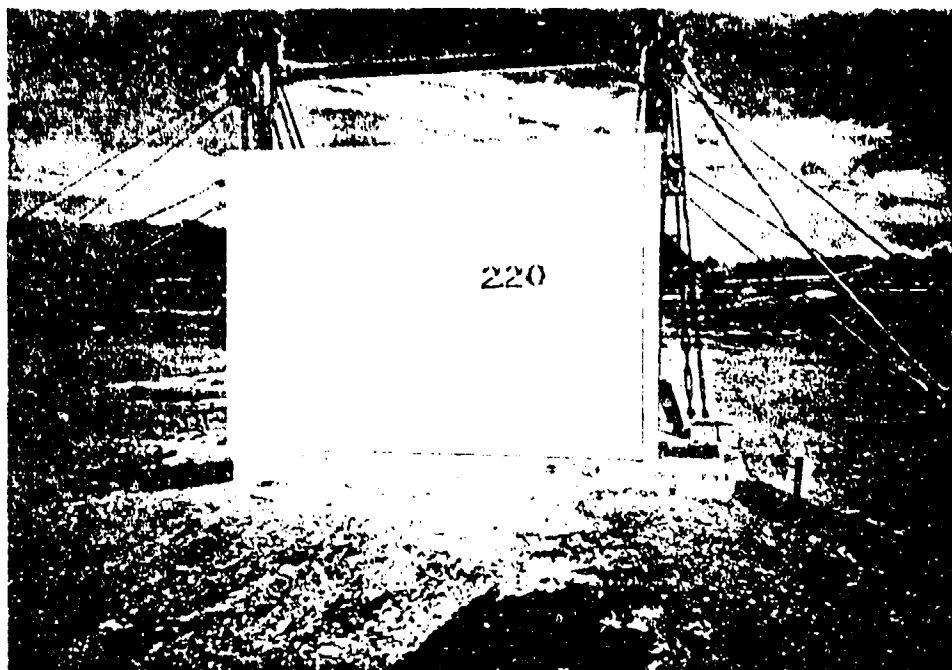


Figure 5. Full Scale Open Air Fixture -
"Butler" Building Wall Panel

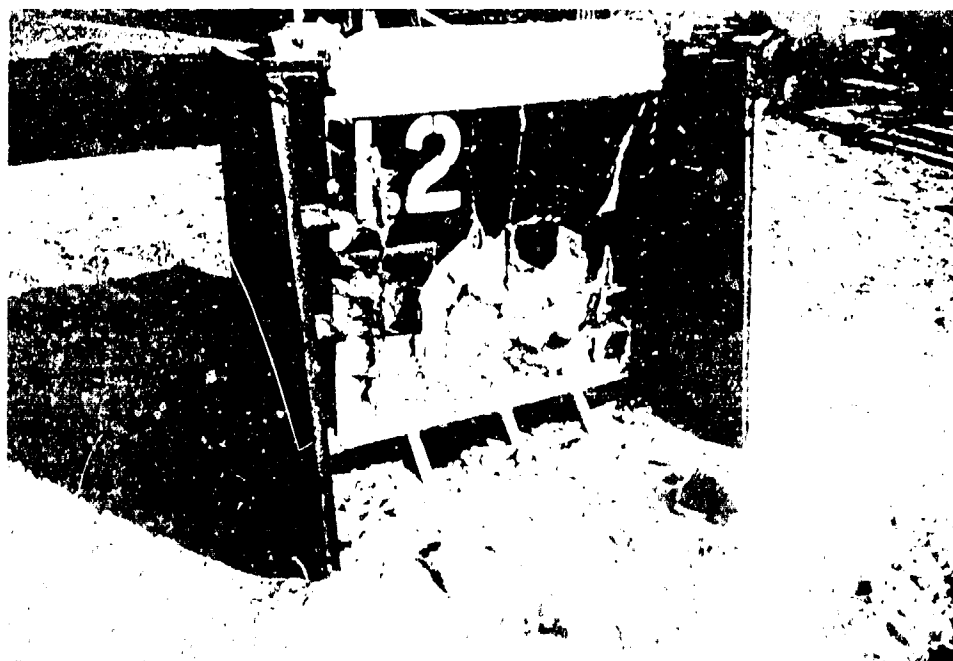


Figure 6. Open Air Fixture Sustained by Quarter Scale Cable

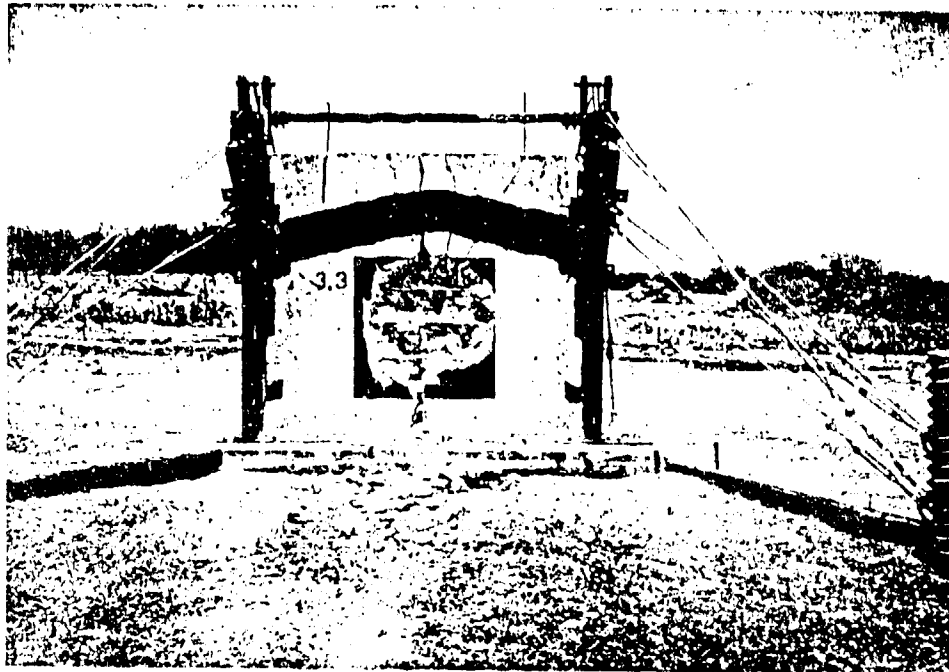


Figure 7 Damage Sustained by Full Scale Concrete Wall in Open Air Fixture

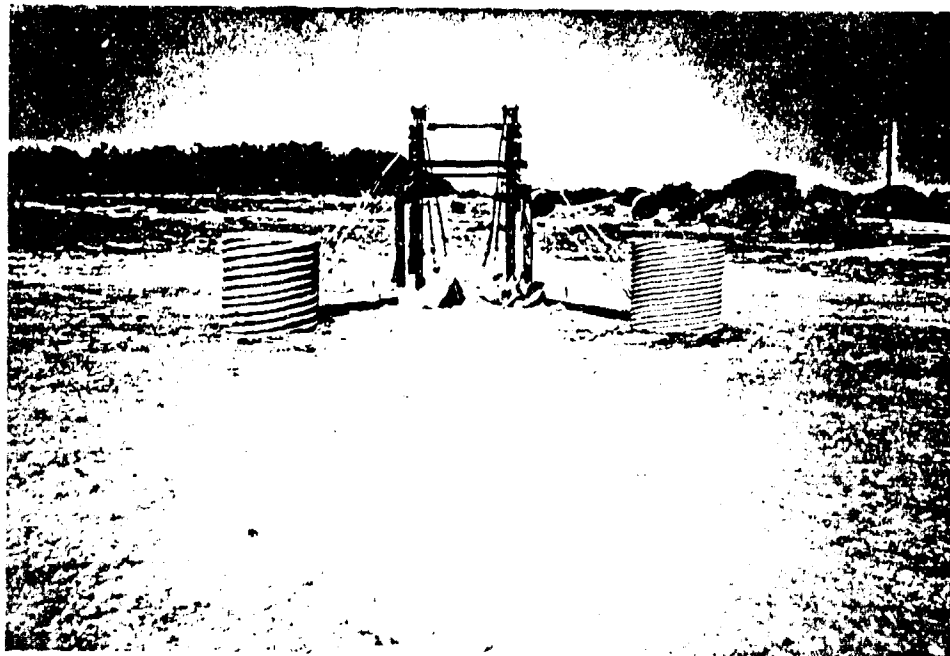


Figure 8. Debris From Half Scale Concrete Wall in Open Air Fixture

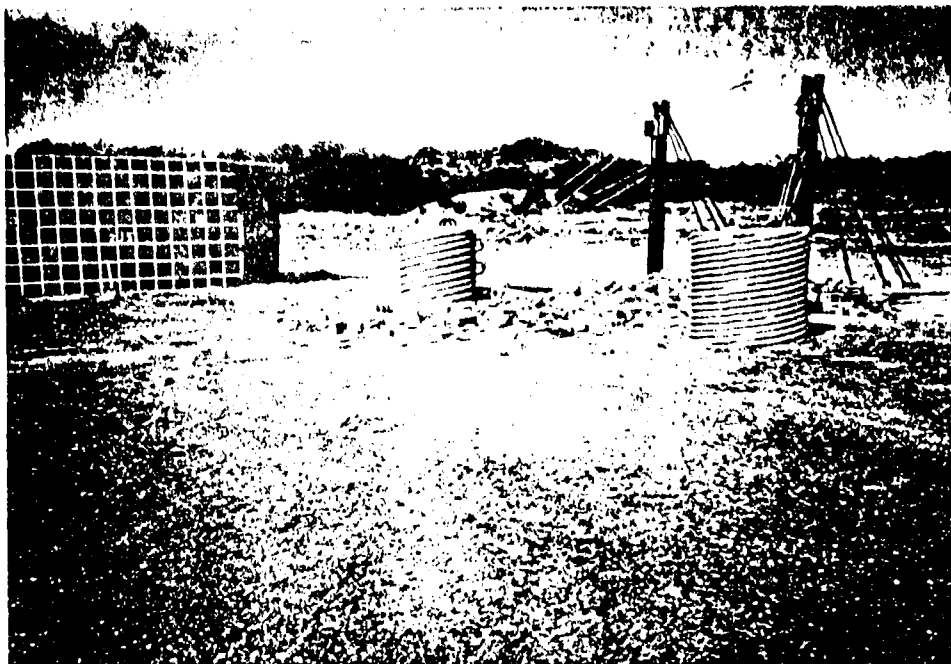


Figure 9 Debris from Full Scale Clay Tile Wall in Open Air Fixture



Figure 10 Debris from Quarter Scale CMU in Open Air Fixture

Twenty-Fourth DoD Explosives Safety Seminar

18-30 August 1990, Saint Louis - Missouri

**THE HAZARD OF AN EXPLOSION OF THE ARIANE 5 LAUNCHER-
THE RISKS FOR THE ASTRONAUTS SITTING ON THE EJECTOR SEATS**

BY

M. Rouzé, F. Laporte

Centre National d'Etudes Spatiales

18, Avenue Edouard Belin

31055 Toulouse Cedex - France

Abstract

Europeans will soon send inhabited missions into space with the Ariane 5 launcher and spaceshuttle Hermes combination. In case of an incident at launch, either on the pad or up to some speed after launch, it is proposed to eject the flight crew to safety on individual ejector seats. The risks which would be confronted by the astronauts have been studied.

This paper presents the development of a method for calculating the probability that a fragment of the launcher

hits an ejector seat either in flight or at ground level during the initial launch phase.

Introduction.

Despite a high confidence in the launcher's reliability, the risk of accidents exists ; the possibility of explosion of the launcher is not to be excluded.

With the projected inhabited missions of Ariane 5, ejection of the astronauts on individual ejector seats is proposed when its explosion risk has been «estimated» as excessive.

If the seats have been ejected successfully, accurate evaluation of the hazards is important to assure the safety of the astronauts after the explosion. These Hazards are known and are :

- the shock wave propagating through the air (gas dynamic problem...),
- thermal phenomenon due to the fireball (thermal exchanges, combustion, chemical kinetic problems...)
- fragment trajectories.

The last item is considered a danger due to the risk of launcher fragments hitting the astronauts on the ejector seats and is also the subject of this paper..

It is interesting to calculate whether there exists an «optimal» time, beyond which the hit probability is less than a given value.

Presented in the following is the current stage of our work in trying to solve this problem.

Ejection of the astronauts.

In all ejection situations, the mode of operation of the seat is the same. As the seat separates from the Hermes cabin, the drogue is deployed (the deployment can be delayed for ground level escape) and maintains the seats attitude during rocket burn. The parachute deployment phase will follow a

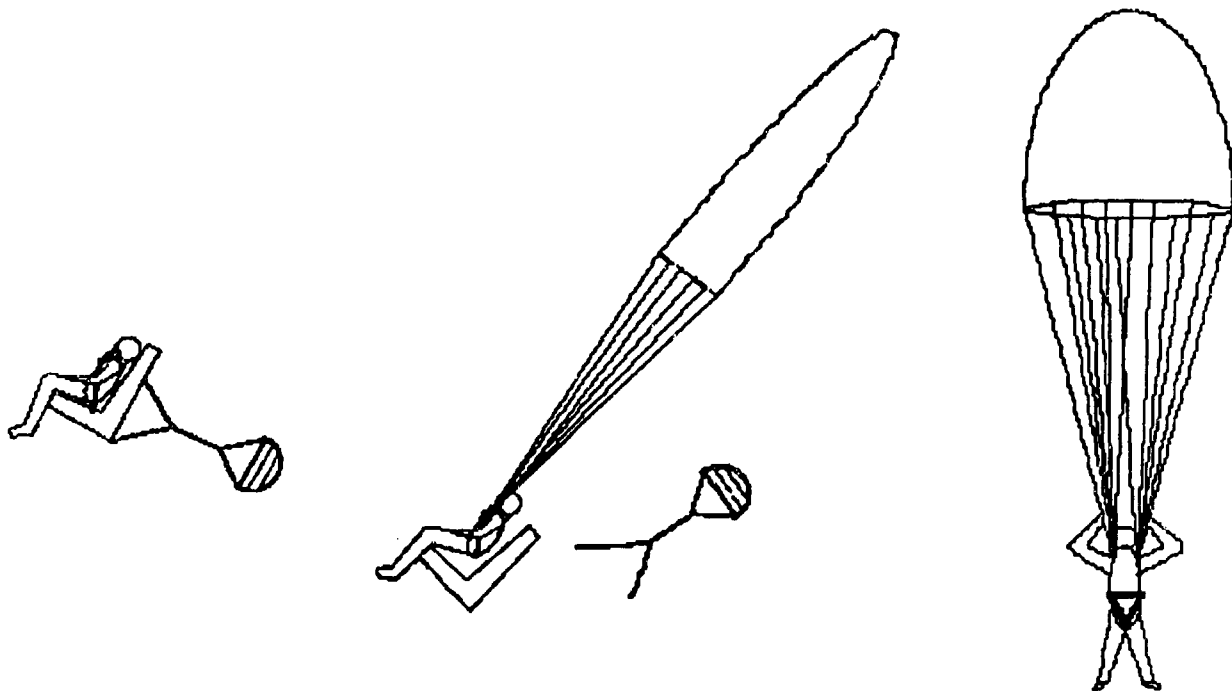


Fig. 1 - ejector seat sequence

conventional ejector seat sequence . Finally, the crewperson is pulled off the seat by the inflating parachute and descends with it.

Description of the Ariane 5 Launcher.

In its «HERMES» configuration, Ariane 5 consists of a cryogenic stage H155 (155 tonnes of liquid oxygen and liquid hydrogen) propelled by a HM60 Vulcain motor and two boosters with solid propellant P230 (230 tonnes of Ammonium Perchlorate).

Elements of the problem.

Accidents involving liquid propellant rockets have shown that they can generate violent explosions. We know however that while their potential explosive yield is very high, their actual yield is in fact

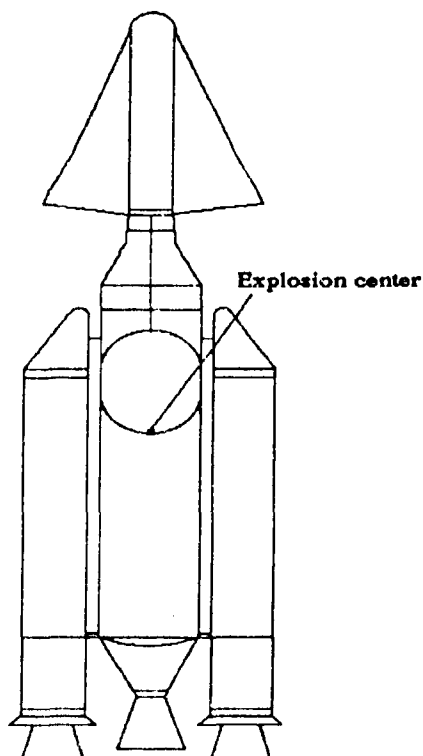


Fig 2 - Ariane 5 launcher

much lower.

The most likely causes of accidents are :

- failure of an interior bulkhead which separates fuel and oxidizer within the stage,
- excessive air-load on, and break-up of the launcher (malfunctioning of the vehicle...)
- destruct command (the launcher could be considered dangerous to the population...)
- others...

Before proceeding to the description of the model, we must specify that our approach is of the first order. That is to say that we only treat amongst the accident

scenarios those which will give the greatest explosion energy.

-A- Description of the model - The Launcher explosion - First model.

As described in [1,2], because the Liquid Oxygen/Liquid Hydrogen mixture is not hypergolic, mixing between these products can occur before explosion. As mentioned earlier, we will overestimate the reaction energy, so the T.N.T. equivalent «Y» is taken to be the upper bound as described in [1]. In fact we have a relation as :

$$Y = Y(W_p)$$

where W_p is the total propellant mass prior the explosion. With Y we may deduce the effective

reacting propellant mass W_R which has volume V_R and released energy E ([1]).

Classically, if we compare this explosion with a mechanical one (compressed gas reservoir), we

$$E = \frac{P V_R}{\Gamma - 1}$$

obtain the «pressure» P of the combustion gases by manipulating the relation :

where Γ is a generalized local adiabatic exponent.

Alternatively, we know that detonation (Chapman-Jouguet detonation) can occur after the ignition. Use of a code modelling thermochemical relations shows that the characteristics of the C-J detonation products for a stoichiometric mixture are :

- the products : H_2O , O_2 , H_2 , OH , H , O .
- detonation temperature : 4347 K.
- C-J pressure : 43770 Bars.

If, as a first approach, we suppose that the pressure, specific volume, temperature... profiles after the detonation shock are of the Taylor-Zeldovich type for a spherical propagation, we have the alternative initial condition for the gas pressure.

Calculation of the fragment velocities (a first approach).

In a first step, we «construct» the launcher. A launcher is composed of structures (propellant reservoirs for example...), of objects (cryogenic motors, Helium sphere...) and propellant. The explosion center may then be placed.

The ejection speed of a given fragment is assumed to be consistent with that of a «cone element» C_Ω , i.e. a cone defined by a solid angle Ω emanating from the explosion center. The structures and the unburnt propellant included in the cone C_Ω are all part of the fragments' «environment» (Fig. 3). Its mass W_i is concentrated on the surface of a thin spherical cap. A technique following that of Bessey's

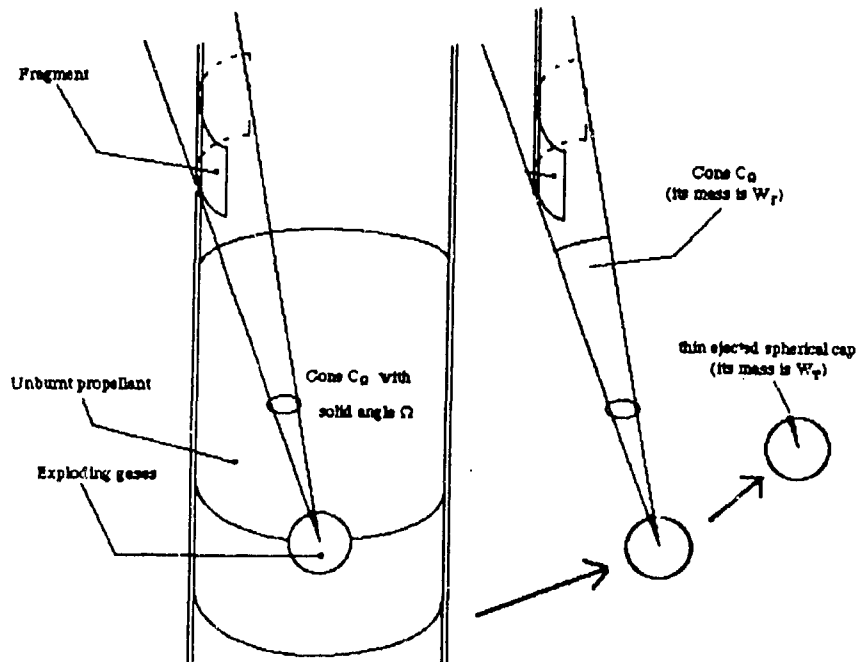


Fig. 3 - «cone element» C_n

([4]) may be used with a correct state equation ([27,45]) for the exploding gases to calculate the fragment velocities.

Calculation of the fragment velocities (a second approach).

Another method to compute (estimate) the ejection speed of a given fragment is to study the interaction between fluid and rigid moving bodies ([41,42]). In this case, we utilise the idealized cone environment described in the former paragraph.

The two-dimensional domain is discretized, and an algorithm for the advancement in time of the solution can be applied as follows :

- 1- the Euler partial differential equations are solved (finite differences) ; the «fragment» (with the mass W_f) is considered as a reflector,

- 2- we compute the body forces from the pressure field (no body moments),
- 3- we compute the acceleration of the fragment, and we move it by one time-step,
- 4- the grid is adapted,
- 5- we update the characteristics of the gas around the fragment,
- 6- back to -1-

Comparing the results between the above two methods, we have observed that the velocities are greater using the former method (up to 100% greater for small values of Ω [13]). Even though the former method gives seemingly erroneous results, similar results to the second method may be achieved by application of a modified discharge coefficient k . The former method then is quite useful as it is quicker than the latter at estimating the initial velocities and may be easily corrected.

Breakup of the booster P230.

We must consider a simultaneous explosion of the H155 and the two P230 ; the booster fragment velocities can be estimated following the same procedures outlined above.

Fragment trajectories.

These are calculated using the fourth order Runge-Kutta method. The drag coefficient of a fragment

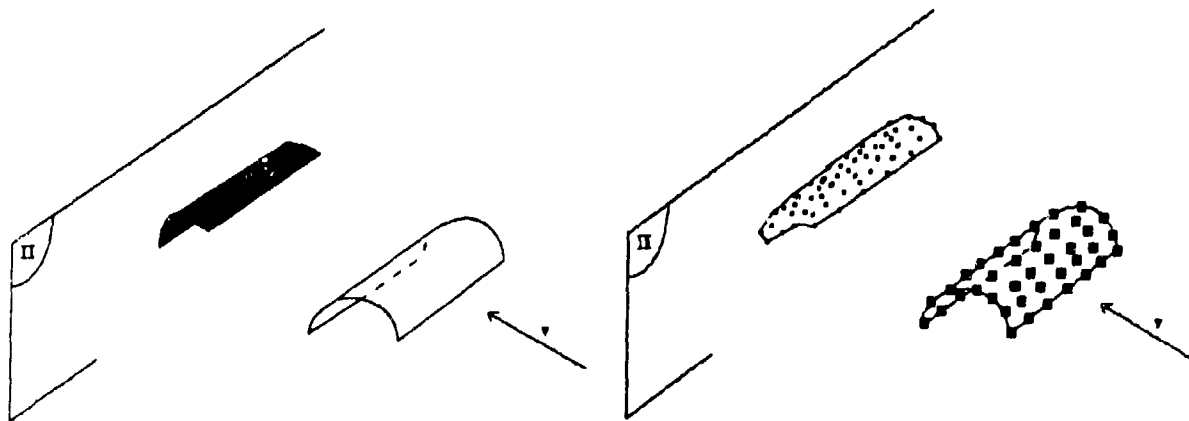


Fig 4 - Calculation of A_{max} and A_{av}

is a function of the two dimensionless parameters $A_r = A_{\max}/A_{\text{avg}}$ and Mach number ([43]). A_{\max} and A_{avg} are the maximum and average presented fragment areas. We suppose there is no lift, and the wind is a function of altitude (z) but there is no z component.

We can estimate A_{\max} and A_{avg} in the following way. If these two values are not «evident», we «discretize» the fragment (Fig. 4), then we project these points on to a plane. A_{\max} is the greatest area of the smallest polygon containing all the projected points when the projection direction is varying; A_{avg} is the average value.

-B- Description of the model - The Launcher explosion - second model.

Computational time in the first model is very important for fragment treatment. Replacing every costly (computational time) step in the first approach by an analytic (or quasi-analytic) formula reduces calculation time drastically.

Fragment velocities - Analytic formulation.

By studying the physical parameters needed in the iterative calculation of a fragment's velocity V ,

$$V = V\left(\Omega, \frac{W_T}{W_\Omega}\right)$$

it can be shown (with realistic simplifications and similitude theory) that V can be written :

W_T is the total mass ejected in the cone C_Ω with solid angle Ω , W_Ω is the compressed combustion gas mass in C_Ω . The above function $V(.,.)$ is determined by parameter estimation with the simplest suitable functions bases [8]. The parameter estimations may easily be computed using a computational system such as us «Mathematica». The result of this analytic approach compares well with the former computational algorithm ([8]).

Fragments trajectories - quasi analytic formulation [36].

The position and the velocity of the fragment must be determined on several points along the trajectory; we need intermediary results.

Before proceeding to the description of the problem's solution it is necessary to define the approximated physical environment :

- assume non-sphericity of the Earth for the impact point calculation,
- include effects of the Earth's rotation,
- the Earth's gravitational acceleration (g) varies with altitude,
- atmospheric effects; in this first study, in order to develop a method able to give results in real time, we considered drag effects only (atmospheric density and fragment drag coefficient are assumed to vary as a function of position). We assume that the effect of lift is averaged out by the fragments tumbling motion and there is no wind.

The results' accuracy must be consistent with the uncertainties related to the physical parameters:

- uncertainty in the main body state vector (i.e. position and velocity) at vehicle destruct time,
- uncertainty in destruct velocity imparted to the fragment,
- uncertainty due to effects of the atmosphere during freefall.

Our methodology is to solve the problem utilising a quasi-analytic approach. It's not possible to solve the complete governing equations of the system analytically, some approximations to these complete equations must be applied to determine achievable analytic solutions.

This is done by applying a uniform space partitioning technique. In each sub-space created we can simplify the physical framework and thus solve analytically the reduced equations. The new simplified theoretical framework within each sub-space becomes:

- plane movement,
- drag coefficient and atmospheric density are assumed to be constant,
- drag force direction is assumed to be constant,
- Earth's gravity is assumed to be constant.

Such a partitioning is defined by the triplet (dx , dz , da) where:

- dx is the length (overall free-fall range) of the sub-space,
- dz is the height (maximum altitude variation) of the sub-space,
- da is the maximum variation of the fragment velocity angle inside the sub-space.

Thus, the fragment impact point calculation consists of partitioning and making a sequence of elementary calculations inside each subsequent sub-space. The results of the calculations within each sub-space become the initial conditions of the next, with the constant parameters updated.

The final result accuracy is improved albeit at the expense of calculation time by finer partitioning. The choice of triplet (dx , dz , da) influences our method's operation and is a way to control response time or result accuracy.

In order to improve the method's performance, atmospheric effects beyond a certain altitude may be eliminated as air density reduces, as a result an analytic calculation taking only gravitational forces into account is performed.

The method has been tested for a wide range of realistic trajectories and comparison has been made with reference trajectories calculated by numerical integration. The computational time remains low even for accurate results i.e. in the case where the calculation error is of the same order as those due to the atmospheric parameter uncertainties (i.e. drag coefficients, atmospheric density, ...). The computational time can be up to 1000 times less than that of numerical integration; the average gain is usually of the order of 100 times.

To give an idea of the dimensions involved, the triplet for a partition could be : $dx = 50$ km, $dz = 1$ km, $da = 1$.

The main advantage of this method is that its control mode (dx , dz , da) can be chosen independently of the initial conditions. Computation time is only dependent on desired accuracy (i.e. chosen triplet) and not on the initial conditions. These characteristics are particularly useful for real time applications.

-C- Hit probability of the seats.

The above model is deterministic ; however some parameters are «uncertain». To account for this, we have created a model which utilises the Monte-Carlo method. The values for certain variables are

randomly selected for each fragment within «uncertain bounds». These are :

- Initial fragment velocity, because of the uncertainty of the propellant weight inside the cone C_n ,
- The attitude of the fragment,
- Drag coefficient ([43]).

Computation of hit probability is simple and classical ; if necessary, the trajectories of the fragments or the seats are approximated by cubic polynomials. Attitude, «configuration» (propulsed or with a parachute) of the seats and relative movement with the fragments are taking into account.

The fragmentation.

An important parameter in a Monte-Carlo approach is the number of hazardous fragments, their mass distribution and their location on the launcher.

At the moment, this is for us an unresolved problem.

We know that the number of fragments over a given mass may be predicted by a Mott equation ([2]) from which we have simply extrapolated for the Ariane 5 launcher.

Future work.

An obvious extension of our quasi-analytic trajectory calculation method will be to take into account lift and wind effects.

For the Monte-Carlo modeling, an obvious extension is the random choice of the T.N.T. equivalent parameter «Y», including multiple explosions, different explosion scenarios..., and an improved knowledge of the corresponding fragmentation.

Acknowledgments.

We are very grateful to Joseph Sasso for his attentive reading and remarks of this paper.

-References-

- [1] W.E. BAKER, J.J. KULESZ, R.E. RICKER, R.L. BESSEY, P.S. WESTINE, V.B. PARR, G.A. OLDHAM :
«Workbook for predicting pressure wave and fragment effects of exploding propellant tanks and gas storage vessels»,
NASA Report CR-134906, 1976.
- [2] W.E. BAKER, P.A. COX, R.L. BESSEY, V.B. PARR : «Assembly and Analysis of Fragmentation Data for Liquid
propellant Vessels», NASA Report CR-134538, 1974.
- [3] W.E. BAKER, J.J. KULESZ, R.E. RICKER, P.S. WESTINE, V.B. PARR, L.M. VARGAS, P.K. MOSELEY :
«Workbook for Estimating effects of Accidental Explosions in Propellant Group Handling and Transport Systems»,
contract NAS3-20497, 1978.
- [4] R.L. BESSEY : «Fragments Velocities from Exploding Liquid Propellant Tanks»; The shock and Vibration Bulletin,
N 44, Aug 1974.
- [5] R.L. BESSEY, KULESZ J. J. : «Fragments Velocities from Bursting Cylindrical and Spherical Pressure Vessels»
; Southwest Research Institute - San Antonio, Texas.
- [6] W. H. BOGGS : «Autoignition-A Liquid Propellant Explosive Potential Limiting Phenomena»
- [7] F. V. BRACCO : «Air Blast Parameters Close To A Liquid Propellant Explosion»
Wyle Laboratories-Research Staff ; Reporty WR 66-3 ; Jan. 1966.
- [8] M. CAMPS : «Logiciel SEDIA micro-vitesse d'éjection des fragments du corps central»
Note CNES TE/IS/MS/MN-90.188 ; Juin 1990.
- [9] R. CHERET : «La détonation des explosifs condensés» Masson-1988.
- [10] T. CHRISTOS, Y. MIRON, H. JAMES, H. PERLEE : «Combustion Characteristics Of Condensed-Phase
Hydrazine-Type Fuels With Nitrogen Tetroxide» J. Spacecraft, Vol. 4, N 9, pp 1224-1229.
- [11] W. DAIMON, M. TANAKA, I. KIMURA : «The Mechanisms Of Explosions Induced By Contact Of Hypergolic
Liquid Propellants, Hydrazine, And Nitrogen Tetroxide».
20th Symposium On Combustion/The Combustion Institute, 1984 ; pp 2065-2071.
- [12] M. DEFOURNEAUX : «Transfert d'Energie Dans La Propulsion Par Explosif» ; Publication ENSTA 1978.
- [13] F. DESCLAUX : Note CNES à paraître.

- [14] J. DONEA, S. GIULIANI, J.P. HALLEUX : «An arbitrary lagrangien-eulerien finite element method for transient dynamic fluid-structure interactions». Computer Methods in Applied Mechanics And Engineering 33 (1982) 689-723.
- [15] M. ECK, M. MUKUNDA : «Predicting the velocity and azimuth of fragments generated by the range destruction or random failure of rocket casings and tankage». IAF-88-523.
- [16] E. D. ESPARZA, W. E. BAKER : «Blast From Bursting Fragible Pressure Sphere» 1980.
- [17] E.A. FARBER, J.H. SMITH, E.H. WATTS : «Prediction of Explosive Yield and Other Characteristics of Liquid Rocket Propellant Explosions» ; contract N NAS 10-1255 ; 1973.
- [18] E.A. FARBER : «Critical Mass of Cryogenic Rocket Propellants»
- [19] E.A. FARBER, J. M. DEESE : «A systematic Approach For The Analytical Analysis And Prediction Of The Yield From Liquid Propellant Explosions» .
- [20] E.A. FARBER, R. L. SAN MARTIN : «Studies And Analyses Of The Mixing Phenomena Of Liquid Propellants Leading To A Yield-Time Relationship» ; New York Academy Of Sciences, Annals.
- [21] FLETCHER R.F. «Liquid-Propellant Explosion» ; Journal of spacecraft and rocket ; Vol 5.
Octobre 1968 ; Page 1227-1229.
- [22] FLETCHER R.F. «Explosion Of Propellant» ; AIAA Journal, vol. 4, Apr. 1966, pp 755-757.
- [23] FLETCHER R.F. «Characteristics Of Liquid-Propellant Explosions»
12th Technical Symposium, NASA Manned Spacecraft Center, Houston.
- [24] M. FINGER, H. C. HORNIG, E. L. LEE, J. W. KURY : «Metal Acceleration By Chemical Explosives»
Proc. Symp. Detonation, 5th, 1970.
- [25] H. D. GRUSCHKA, F. WECKEN : «Gasdynamic Theory Of Detonation» Gordon and Breach ; 1971.
- [26] A. HARTEN : «High resolution scheme for hyperbolic conservation laws»
Journal Of Computational Physics 49,357-393 (1983).
- [27] O. HEUZE «Contribution au calcul des caractéristiques détonation de substances explosives gazeuses ou condensées» Thèse de troisième cycle ; ENSMA Poitiers.
- [28] S.L. JEFFERS : «Fragment Velocity Measurements From Three Project Pyro Experiments »
Sandia Laboratories, Albuquerque ; SC-DR-69-329 ; JUIN 1969.
- [29] G. E. JONES, J. E. KENNEDY, L. D. BERTHOLF : « Ballistics Calculations Of R. W. GURNEY».
Am. J. Phys. 48(4), Apr. 1980.
- [30] A. M. KANURY : «Introduction To Combustion Phenomena» Gordon And Breach science publishers 1977

- [31] J. E. KENNEDY : «Explosive Output For Driving Letail» ; Behavior and Utilization of Explosives in Engineering Design. L. Davison et Al. EDS., ASME ; Albuquerque, N.M. 1972.
- [32] J. E. KENNEDY : «Gurney Energy of Explosives : Estimation Of The Velocity And Impulse Imparted To Driven metal» ; SC-RR-70-790 ; Decembre 1970.
- [33] G. F. KINNEY, K. J. GRAHAM : «Explosive Shocks In Air» ; Springer-Verlag ; 1985
- [34] J. J. KULESZ, L. M. VARGAS , P.K. MOSELEY : «Prediction of Fragment Velocities and Trajectories» ; Southwest Research Institute ; San Antonio, Texas.
- [35] J. W. KURY, H. C. HORNIG, E. L. LEE, J. L. McDONNELL, D. L. ORNELLAS, M. FINGER, F. M. STRANGE, M. L. WILKINS : «Metal Acceleration By Chemical Explosives» ; Proc. Symp. Detonation, 4th, Office of Naval Research, Rept ACR-126, pp 3-13.
- [36] F. LAPORTE : «Calcul des points d'impact-Présentation du modèle de PIAF»
Note CNES TE/IS/MS/MN/045 Février 1990
- [37] D.H. LEISTER, A.G. GIBBS, D.L. LESSOR : «A Study of Liquid Propellant Autoignition»
contract N NAS 10-8591 ; 1975.
- [38] M. LEMAITRE : «Hypothèse d'Instabilité De Combustion d'Origine Chimique»
Contrat CNES 74/1044, lot 38A
- [39] M. LEMAITRE : «Hypothèses relatives à La Formation Intermédiaire De Nitriles Lors De La Combustion N2O4/UDMH ; Contrat CNES 74/1044, lot 38C.
- [40] H.W. LIEPMANN, A. ROSHKO : «Eléments de la dynamique des gaz», Gauthier-villars ; 1962.
- [41] R. LOHNER : «Adaptive remeshing for transient problem with moving bodies» ; AIAA 88-3736-CP.
- [42] S. MADSEN «Stationing Report 1-12-88» Note CNES CT/DTI/MS/MN à paraître
- [43] MCCLESKEY : «Drag Coefficients for Irregular fragments» - Naval Surface Warfare Center.
- [44] S. B. MELLSEN : «Drag Measurements On Cylinders In Event Dial Pack»
- [45] H.N. PRESLES : communication personnelle.
- [46] W. A. RIEHL, L. J. ULLIAN : «Close-In Characteristics Of LH2/LO2 Reactions».
- [47] M. ROUZE «L'explosion du Lanceur ARIANE-Description des Phénomènes-Modélisation» .
Note CNES CT/DTI/MS/MN/108 ; Mars 1988.
- [48] M. ROUZE «Etude explosion ARIANE V-Eclatement au sol du P230 : domaine de retombée» .
Note CNES CT/DTI/MS/MN/316 ; Octobre 1988.

[49] E. STERNE : «A Note On The Initial Velocities Of Fragments From Warheads»

Report 648 ; Ballistic Research Laboratories ; Septembre 1947.

[50] R.A. STREHLOW, W.E. BAKER : «The Characterization and Evaluation of Accidental Explosions»; NASA-CR-134779 ; 1975.

[51] D.E. TAYLOR, C.F. PRICE : « Velocities of Fragments from Bursting Gas Reservoirs » ; Journal of engineering for industry, Vol. 43, Nov. 1971.

[52] R. R. WOLFE : «TNT Equivalency Study For Space Shuttle (EOS)»

Report N ATR-71(7233)-4, Vol I. The Aerospace Corporation, El Segundo, California.

[53] J. ZIEREP «Similarity Laws And Modeling» ; Gasdynamics, Volume 2 ; Marcel Dekker, 1971.

CRITICAL FAILURE OF CONCRETE SLABS DUE TO CONTACT CHARGES

R.J.M. van Amelsfort, J. Weerheijm and G. Opschoor
TNO Prins Maurits Laboratory

Abstract

Within the scope of a study on layered protective structures, experiments were performed to quantify the load on the construction caused by failure of the upper plate. In the experimental programme the failure of concrete slabs due to contact charges was examined. From earlier experiments performed at the TNO Prins Maurits Laboratory it is known that when the loading exceeds a certain critical value, a concentrated stream of high velocity particles is formed, originating from the crushed concrete. These particles penetrate and form a severe loading for the next layer. However, very little was known about the origin and properties of this particle stream.

The aim of the performed study was to gain more comprehension of the failure process of the concrete slab and to gather data to quantify the loading due to the particle stream.

The tests were focussed on mass, velocity, divergence and particle size distribution of the particle stream. Different experimental set-ups were developed to measure the various parameters.

With the obtained experimental data the total impulse of the particle stream can be calculated and the force that may be exerted by the stream on following layers can be estimated.

TWENTY-FOURTH DOD EXPLOSIVES SAFETY SEMINAR
28 - 30 AUGUST 1990, ST LOUIS, MISSOURI

CRITICAL FAILURE OF CONCRETE SLABS DUE TO CONTACT CHARGES

by

R.J.M. van Amelsfort, J. Weerheijm and G. Opschoor

TNO Prins Maurits Laboratory

P.O. Box 45, 2280 AA Rijswijk

The Netherlands

1 INTRODUCTION

From previous TNO-PML investigations, it appeared that layered structures, often comprising two concrete slabs with an intermediate layer of sand, have a critical thickness of the directly loaded (outer) slab of $d_c = 13.4 * W^{1/3}$ (mm) for 80 % PETN contact charges and 60 mm thick concrete slabs. Here W is the weight of the charge in grams (Weerheijm et al, 1984). The experiments showed that if the thickness of the slab is smaller than the critical thickness, a concentrated loading is created by the stream of particles which are ejected through the hole punched in the directly loaded slab. This concentrated load has a high energy content and dominates the failure process in the next layer(s).

Very little was known about the origin and properties of this particle stream. The aim of this study was to gain some insight into the failure process of the concrete slab and to gather data to quantify the loading due to the particle stream. To simulate this situation, experiments were performed with contact charges on concrete slabs. A short description of some theoretical aspects of the failure mode of concrete slabs is given.

To obtain information of the threat formed by the particle stream, numerical data with respect to the impulse or energy exerted by the particle stream, for instance, must be known. An experimental programme was carried out to obtain the parameters of interest. Numerical data of the velocity, divergence and total mass of this particle stream and the particle and size distribution itself, were determined for various charge weights. Using these data, the threat of the particle stream can be described. When more information on the threat is known, it becomes possible to take measures for protection. In the discussion of the experimental results, an attempt was made to join theory and experimental data together.

THE FAILURE MODE OF A CONCRETE SLAB

When a contact charge detonates, temperature and pressure increase to very high levels (of the order of 5000 to 7000 K and 10 to 20 GPa) and the concrete near the contact area melts and is completely crushed. The strength of the material is of minor importance because of the high pressure occurring in this region. The pressure wave expands in the slab and so the pressure decreases with increasing distance from the charge. With this decreasing pressure the influence of the strength of the materials involved increases. The pressure decreases and reaches a stress level at which the concrete can withstand the load.

2.1 The behaviour of concrete with increasing compression

Concrete is made from a mixture of sand and gravel embedded in a cement matrix. The latter is the ~~weakest link in the concrete and will crush first when the load increases. A crushing cement matrix~~ results in a decreasing internal cohesion and an increasing deformation of the material. If the load increase is continued, the cement matrix will be fully crushed and the sand and gravel particles are loaded directly. This results in an increase in the concrete strength. Further increase in the load results in crushing the filler particles as well. It is a generally accepted assumption that under the conditions of an instantaneously increasing pressure, concrete starts to lose its internal strength at a stress level of about 8 to 10 times the static compressive strength (Pahl, 1979).

2.2 Stress waves, crater formation and spalling

An extensive description of the stress waves and the process of crater formation and spalling is given in (Weerheijm et al, 1984). A summary will be given in this paragraph. The pressure in the contact area of the charge and the slab is of the order of 10 to 20 GPa. This stress level together with the shape of the stress wave determine the strength of the concrete, and this strength in its turn determines the propagation velocity of the stress wave. Figure 1 gives the stress-strain relation of concrete for hydrostatic pressure and volumetric strain. This stress-strain relationship governs the wave velocity (c) and the profile of the pressure wave.

Immediately after the explosion a stress wave corresponding with the high stress level (10 to 20 GPa) is initiated. The pressure rapidly decreases with increasing distance from the initiation point and the lower stress level causes a different shape of the stress wave. Below stress level C in Figure 1, the first load of the concrete is performed by the precursor or elastic wave with a stress level of about 8 to 10 times the static compressive strength. The stress level increases and the concrete is crushed behind this wave front.

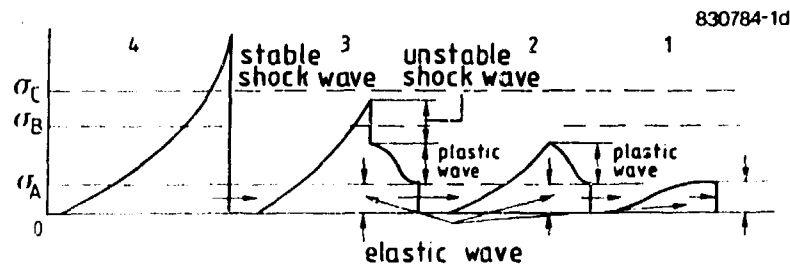
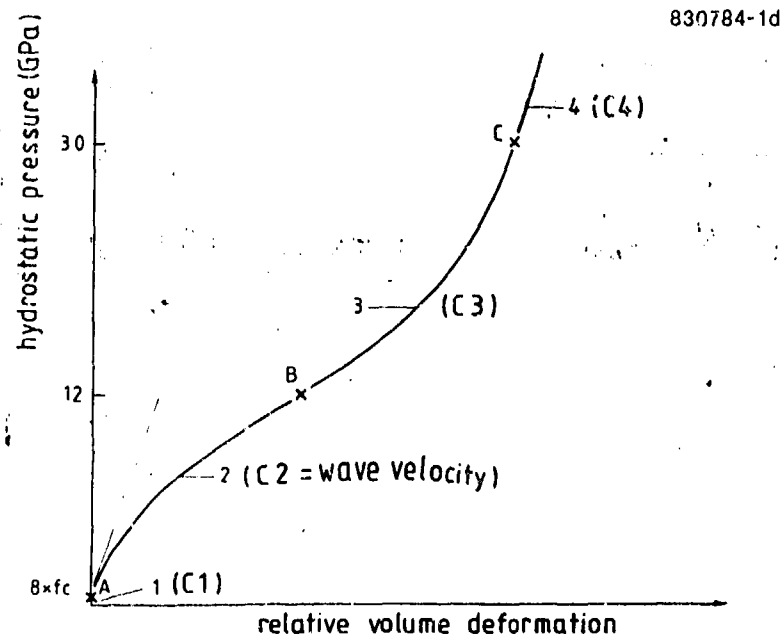


Figure 1 Relationship between pressure stresses and relative volume deformations and the variation in the profile of the pressure wave for the different regions

The velocity of expansion of the region in which the concrete is fully crushed appears to be smaller than the longitudinal wave velocity. This means that the cratering process in a concrete slab, which can only occur in the crushed zone, can be influenced and disturbed by the elastic waves reflected from the back of the slab as tensile waves. Figure 2 gives the trajectories of the tensile stresses. The consequences of this interference will be discussed later.

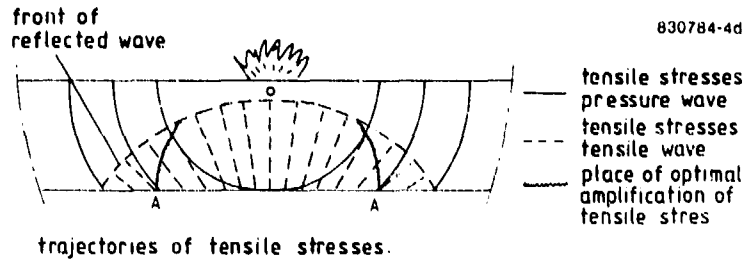


Figure 2 Trajectories of tensile stresses

The particle velocity u due to a plane stress wave is given by the quotient of the pressure P and the acoustic impedance (product of density ρ and longitudinal wave velocity c): $u = P / (\rho \cdot c)$.

For crushed material the particle velocity will increase due to the increasing stress and the decreasing impedance. The radial movement of the particles will be obstructed by less crushed material. When this resistance is sufficient, the radial trajectories are deflected, the crushed material is ejected and a crater is formed. As mentioned earlier, this cratering process can be partly disturbed by the reflected (tensile) stress waves. The interference of waves during the cratering process results in principal tensile and compressive stresses. Because of the small tensile strength of concrete, spalling can occur over nearly the whole area, covered by the reflected wave. The resistance of the material in front of the crushed zone to the movement of the particles in this zone decreases continuously by the expansion of the crushing zone and by spalling and cracking at the rear of the slab. When the reflected wave reaches the crushing zone in the concrete slab the particles are ejected downwards through a hole and cratering is stopped. Owing to the high stresses in the area around the charge, the energy of the concentrated particle stream can be very high. This process of forming a concentrated particle stream will occur above some critical charge weight.

To quantify this theory, detailed information on the levels of the tensile stresses is needed (Van Amelsfort and Weerheijm, 1987). This article however, emphasizes the necessary data to quantify the effects of the phenomena described above.

3 PROBLEM DEFINITION

In the previous section, a theoretical explanation is given of the origin of a concrete particle stream when a concrete slab is loaded with a contact charge greater than a critical charge. Also, the lack of knowledge about the particle stream properties has been mentioned. From previous experiments a severe loading was observed. To quantify the loading and to enlarge the knowledge about the process, the experimental programme was focussed on mass, velocity, divergence and particle size distribution of the particle stream. Various experimental set-ups were developed to measure the different parameters. When these parameters are known, quantities such as the impulse or energy of the particle stream can be calculated.

When the total impulse of the particle stream is known, the force that may be exerted by the stream on following layers, can be estimated.

4 EXPERIMENTAL RESULTS

All experiments were performed with 60 mm thick reinforced concrete slabs of laboratory quality B22.5. The 60 mm thickness was chosen to carry out experiments on plates of the same thickness as performed earlier with the layered structures. Another more practical reason concerns the weight and handling of the specimens.

Two types of experiments were performed. A vertical set-up was used to measure masses and particle sizes and to film the particle stream. A horizontal set-up was used to measure the load (impulse) exerted by the particle stream. The identifications horizontal and vertical refer to the direction of the particle stream. Figures 3 and 4 give a view of both set-ups. A more detailed description of both set-ups was given in (Van Amelsfort and Weerheijm, 1987). A total number of 40 experiments in the vertical set-up and 34 experiments in the horizontal set-up was performed, while all experiments were performed with hemispherical contact charges of high explosives with 80 % penthrite and 20 % inert material.

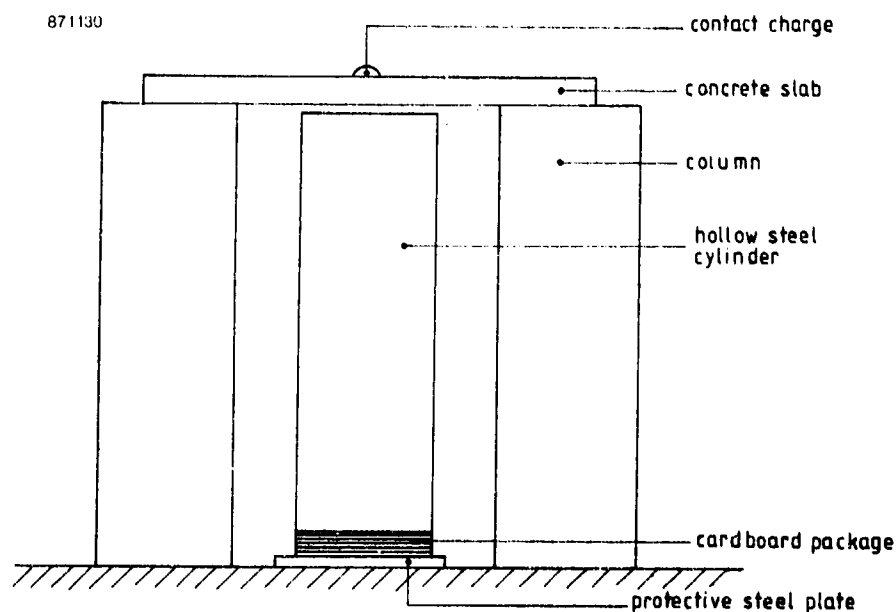


Figure 3 Front-view of vertical experimental set-up

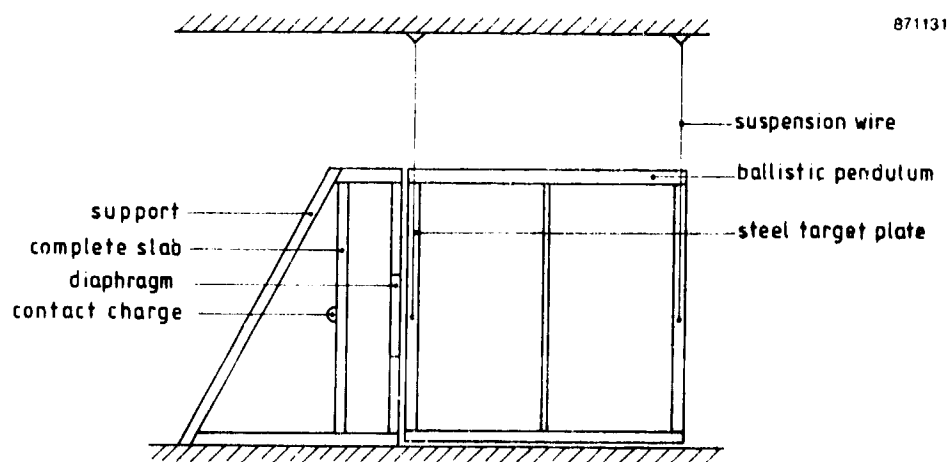


Figure 4 Side-view of horizontal experimental set-up

4.1 Determination of the critical value

Experiments in the vertical set-up with two concrete slabs on top of each other, supported at four corners and loaded in the centre of the top slab were performed. By comparing the results (both slabs perforated, first slab perforated and second slab not perforated, both slabs not perforated), it was concluded that the critical charge for 60 mm thick concrete slabs is about 85 g PETN (80 %). The formula given in (Weerheijm et al, 1984),

$$d_c = 13.4 * Q^{1/3}, \quad (1)$$

where d_c is the critical thickness in mm and Q is the weight of the charge in g, yields for a charge of 85 g a value for the thickness of $d_c = 58.9$ mm. This is in good agreement with the observed critical thickness for a charge weight of 85 to 90 grams used in the experiments (60 mm).

4.2 Determination of the crater dimensions

The results of all experiments, both in the vertical and horizontal set-up, were fitted by exponential functions for the crater diameter at the front side (d_f), the hole diameter (d), and the crater diameter at the back side (d_b) of the concrete slab (Figure 5).

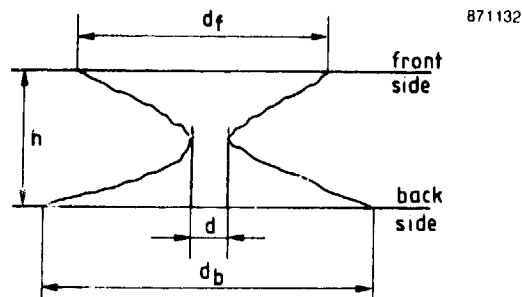


Figure 5 Crater and hole dimensions in a concrete slab loaded with a contact charge

If the charge Q is set in grams, these functions are:

$$\text{Crater diameter at the front side} : d_f = 58.7 * Q^{0.3} \quad (\text{mm}) \quad (2)$$

$$\text{Hole diameter} : d = 30.9 * Q^{0.36} \quad (\text{mm}) \quad (3)$$

$$\text{Crater diameter at the back side} : d_b = 78.3 * Q^{0.3} \quad (\text{mm}) \quad (4)$$

With a few exceptions these formulae result in crater dimensions within 10 % of the measured values.

4.3 Determination of the impulse of the particle stream

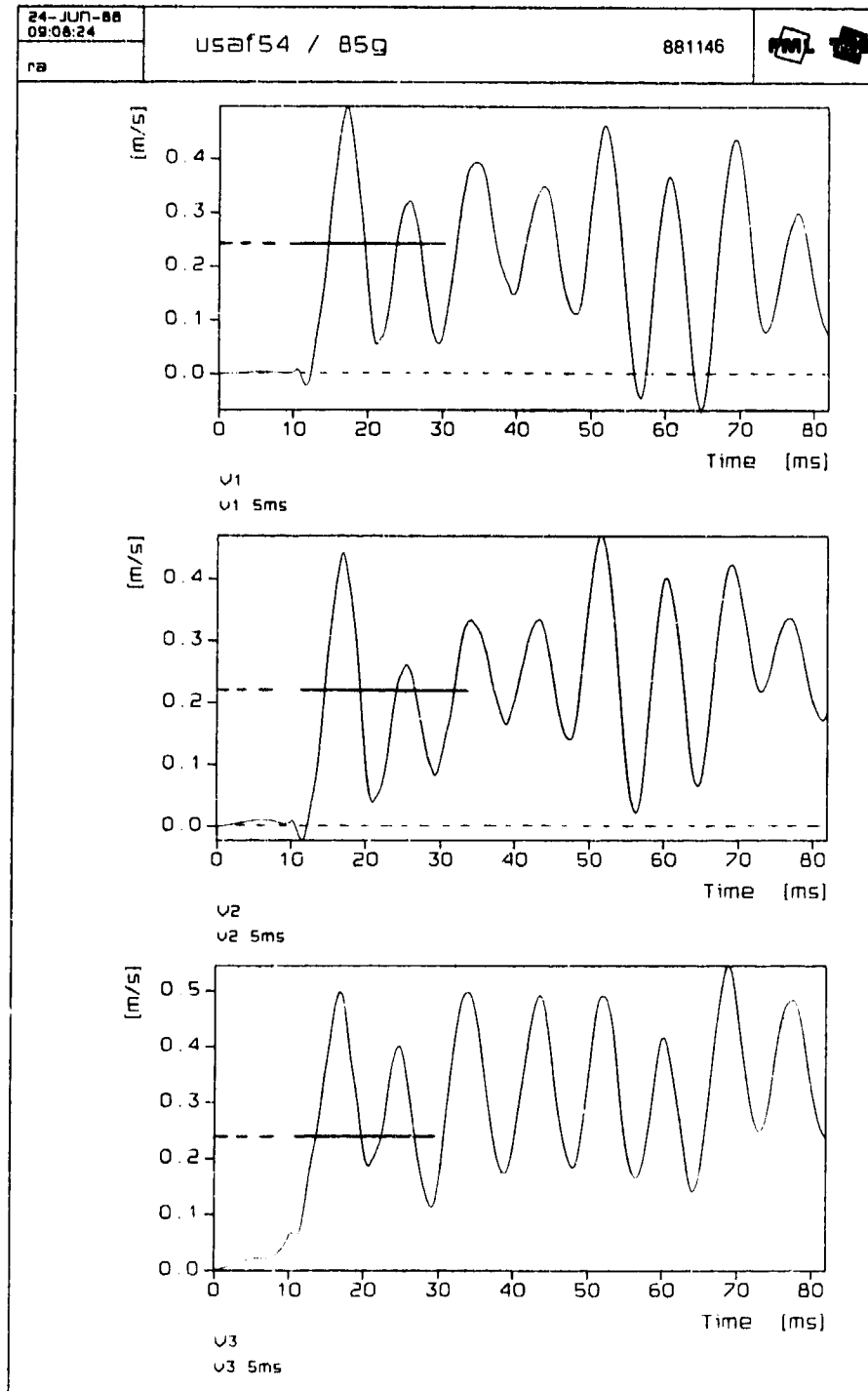
In order to get some information about the magnitude of the impulse of the particle stream several experiments were performed with both the horizontal and the vertical set-up (Van Amelsfort and Weerheijm, 1987). With a ballistic pendulum method (Kolkert and Van Amelsfort, 1982 and 1983) the impulse transferred to the pendulum by the particle stream can be derived. The particle stream hits a target plate fixed in the ballistic pendulum and gives the pendulum an initial velocity and a maximum amplitude. Two types of pendulum were used with three different distances between the back of the concrete slab and the front of the target plate fixed in the pendulum:

- Weight 245.5 kg, pendulum length 0.975 m, period 1.8 s, distance between slab and plate 1.05 m.
- Weight 519.0 kg, pendulum length 1.01 m, period 1.875 s, distance between slab and plate 0.245 m.
- Weight 519.0 kg, pendulum length 1.01 m, period 1.875 s, distance between slab and plate 0.557 m.

The initial velocity of the pendulum was measured/calculated in three ways:

- by filming the movement of the pendulum,
- by integrating the signals of acceleration transducers fixed on the pendulum, and
- by measuring the maximum magnitude of the deflection of the pendulum.

The acceleration signals are subjected to some treatments before and after the integration, such as filtering, offset and drift correction. These treatments did not affect the amplitude of the acceleration and velocity signals. Figure 6 is an example of the integrated signals of the acceleration transducers.



2252

Figure 6 Resulting signal of the acceleration transducers after filtering, offset correction, integration and drift correction

Multiplication of the results obtained for the initial pendulum velocity and the weight of the pendulum yields the impulse (I_t) transmitted to the pendulum. The order of magnitude for the impulse I_t transmitted to the pendulum obtained in these ways, amounts to about 50 kgm/s for the 50 g load, about 110 kgm/s for the 85 g load and about 220 kgm/s for the 170 g load. A fit of all obtained data results in (charge Q in grams):

$$I_t = .777 * Q^{1.1} \text{ (kgm/s)} \quad (5)$$

The reliability of this fit formula (and of all following fit formulae) is limited, because of the limited reproducibility of the loading and failure process in concrete.

At least for the first part of the trajectory of the particle stream (about 1 m), the impulse transmitted to the pendulum is not dependent on the distance between the slab and the target plate in the pendulum or on the type of pendulum.

4.4 Determination of the properties of the particle stream

To determine the properties of the particle stream, the vertical experimental set-up was used. The charge was varied from 20 to 170 g. By catching the concrete particles and weighting them, the next formulae could be derived (charge Q in grams):

$$\text{Mass with particle size greater than 1 mm diameter: } P_{g1} = 127.39 * Q^{-0.15} (\%) \quad (6)$$

$$\text{Mass with particle size greater than 4 mm diameter: } P_{g4} = 59.26 * Q^{-0.10} (\%) \quad (7)$$

$$\text{Mass with particle size smaller than 1 mm diameter: } P_{11} = 15.93 * Q^{0.175} = 100 - P_{g1} (\%) \quad (8)$$

For measuring the velocity of the particle stream itself in the experiments, a film technique appeared to be the easiest way (Van Amelsfort and Weerheijm, 1987). When studying the films it also appeared to be important whether the contact charge was placed just over the reinforcement or not. When the charge was placed over the reinforcement, the particle stream was divided into two particle streams, while the divergence remained very small. The measured values of this velocity were 120 m/s for a 50 g charge, 170 m/s for a 85 g charge and 275 m/s for a 170 g charge. When the charge was placed next to the reinforcement, the particle stream remains intact, the divergence was negligible and the velocity was obviously higher: 160 m/s for a 50 g charge, 225 m/s for a 85 g charge and 335 m/s for a 170 g charge. In this case, a fit of the obtained data results in (charge Q in grams):

$$V = 16.25 * Q^{0.587} \text{ (m/s)} \quad (9)$$

For the first metre of the concrete particle trajectory, the impulse transferred to the target plate was not dependent on the distance (see 4.3).

This means that for the calculation of the impulse by means of the product of data experimentally obtained for mass and velocity, average values for the velocity (tip velocity of the particle stream) and the total mass can be regarded as sufficient for a reliable value for the impulse.

Examples of the particle stream for both cases, contact charge over and next to the reinforcement, are given in Figures 7 and 8.

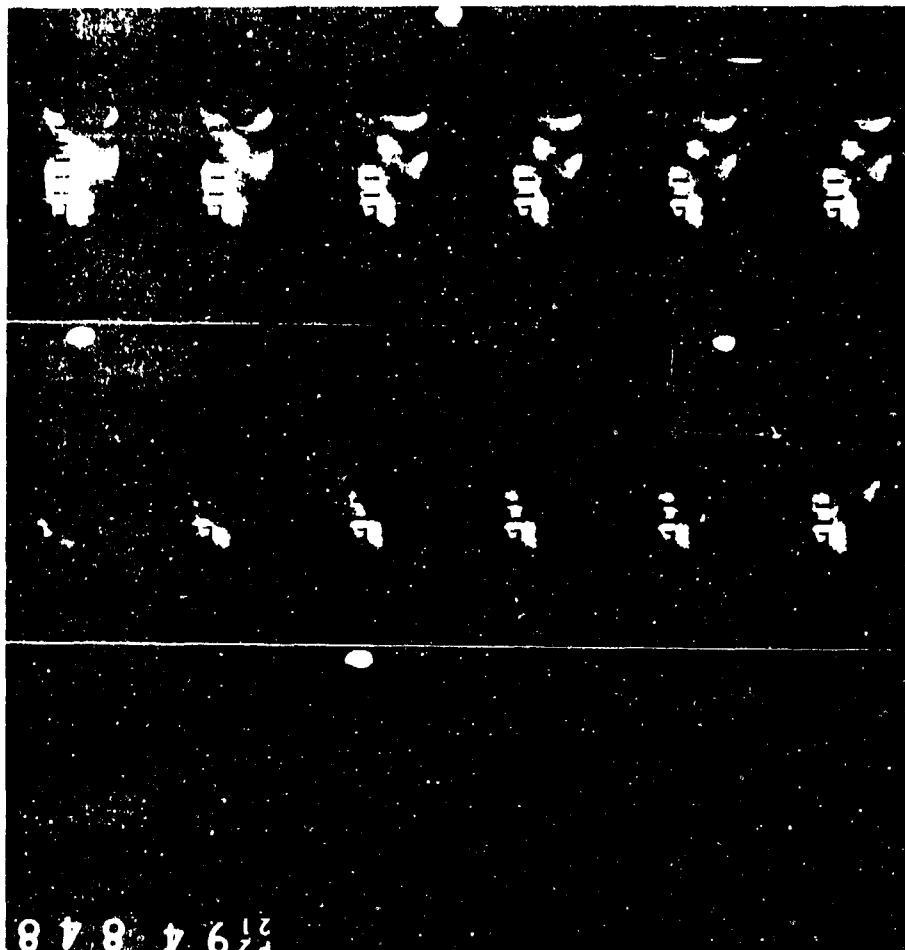


Figure 7 The formation of the concrete particle stream when the contact charge is placed next to the reinforcement (170 g charge)



Figure 8 The formation of the concrete particle stream when the contact charge is placed over the reinforcement (170 g charge)

5 DISCUSSION OF RESULTS

5.1 Critical charge

The experiments confirm the theory of a critical charge when a concrete slab is loaded with a contact charge, as described in (Weerheijm et al, 1984). Several phenomena can be observed for this critical charge, being 85 g of 80 % PETN for a 60 mm thick concrete slab:

- The crater dimensions give a point of inflection at the critical charge.
- The concrete mass retrieved after the experiments has a maximum at the critical charge. Since the crater dimensions increase with increasing charge, the volume and the mass should increase too. A maximum in the retrieved mass means that the amount of dust which cannot be caught increases with increasing charge.
- The percentage of retrieved mass particles with a particle size greater than 1 mm diameter decreases, and with particle size less than 1 mm diameter increases, with increasing charge. The retrieved concrete

mass with particle size greater than 1 mm diameter has a maximum at the critical charge, while the retrieved mass with particle size less than 1 mm increases with increasing charge.

This means that for charge weights above the critical threshold the unretrieved mass increases and consists of very small particles originating from the front crater, according to the theoretical description of critical failure.

The results justify the conclusion that other phenomena occur for contact charges above the critical charge.

5.2 Dominant force performed by the particle stream

When comparing the load performed by the particles originating from the crater at the back of the slab and the (small) particles ejected through the hole, the following considerations can be made. Assuming the crater diameter d_b is double the hole diameter d (see 4.2), the volume, and thus the masses of the particles of both origins differ by about a factor 2 in favour of the crater particles, if geometrical and material damping are neglected. The maximum velocity u of these particles can be calculated with: $u = 2.f_{cd}/(\rho.c)$, where f_{cd} is the dynamic compressive strength. This results in $u = 65$ m/s when f_{cd} is about ten times the static compressive strength, $\rho = 2200$ kg/m³, and $c = 3500$ m/s. Paragraph 4.4 shows velocities of the particle stream of around 200 m/s. Because of a factor of about 3 between these velocities, the difference between impulses in both cases is a factor 2/3 against the crater particles.

The durations of both loads determined by the quotient of half the slab thickness and the particle velocities also give a minimum factor of 3. The ratio of the squares of crater and hole equals a factor 4, owing to the double diameter. The average load performed by both types of loading can be calculated by dividing the impulses by the duration and the surface areas. This results in a factor 18 in favour of the particles ejected through the hole. So, when neglecting damping and using minimum particle velocities, the force of the load caused by the particle stream ejected through the hole is at least 18 times the force of the load caused by the spall particles. This means that for charges above the critical charge, the dominant force on following slabs is formed by the mass stream of small particles ejected through the hole that is punched in the slab, in accordance with the conclusions mentioned before (Weerheijm et al, 1984, Van Amelsfort and Weerheijm, 1987).

5.3 Impulse of the particle stream

By assuming the particle stream as a massive block with mass M and with an average velocity V multiplication of M and V (9) gives an estimate of the supplied impulse I_s to the pendulum. The average velocity V of the front was measured, and the mechanism indicates that the small particles perform

the dominant force. The experimentally retrieved mass with particle size less than 1 mm diameter appears to correspond with the mass M , as given below:

$$M = \pi/4 * d^2 * (1/2 h) * \rho * 10^{-6} \text{ (g)}, \quad (10)$$

with the hole diameter d and the slab thickness h (see Figure 5) in mm and the concrete density ρ in kg/m^3 .

By substituting the hole diameter (3) in (10) and after multiplication with V (9), an expression for I_s can be found:

$$I_s = 6.093 * h * \rho * Q^{1.307} * 10^{-6} \text{ (kgm/s)}, \quad (11)$$

with the slab thickness h in mm, the concrete density ρ in kg/m^3 and the charge Q in g. It should be noted that due to the fact the unretrieved mass beyond the critical charge level increases significantly, the formula (11) underestimates the impulse for the concentrated particle stream. This impulse is an ideal impulse while the particle stream delivers a non-ideal impulse. The equation leads to values for the supplied impulse of 135, 210, 270 and 660 kgm/s respectively for charges of 50, 70, 85 and 170 g (with $h = 60 \text{ mm}$, $\rho = 2200 \text{ kg/m}^3$). When these values of the impulse I_s are compared with the values of the impulse I_t transmitted to the pendulum (5) it appears that a part of the impulse is dissipated during the acceleration of the pendulum. The fitted formula (5) for I_t , yields in 57, 83, 103 and 221 kgm/s , respectively.

The quotient I_s/I_t is a measure for the loss of impulse during impact of the concrete particle stream onto the target plate in the pendulum. This loss is mainly caused by the non-ideality of the impulse delivered to the pendulum. The target load is not a solid mass with one velocity which hits the target plate, but a lot of (small) particles, each with its own velocity hitting the target plate at different times. Although the load of the pendulum is not ideal, the movement of the pendulum is like the movement of a mathematical pendulum, as already concluded in (Van Amelsfort and Weerheijm, 1987).

5.4 Load performed by the particle stream

For determining the threat (P) performed by the particle stream, the duration time of the load (t_d) must be known, because P is the quotient of the supplied impulse (I_s) and t_d . For a hemispherical charge Q (in grams) an expression for the total impulse due to the detonation pressure is given in (Pahl, 1979):

$$I_t^P = 1.2 * Q \text{ (kgm/s)} \quad (12)$$

This formula gives values of 60, 84, 102 and 204 kgm/s respectively for the above-mentioned charges. These values for the total supplied impulse correspond with our measured values for the transmitted impulse.

The total load F_b due to the detonation pressure (Pahl, 1979) is

$$F_b = \pi * R^2 * P_b, \quad (13)$$

where P_b is the dynamic strength (in Pa) equal to about ten times the static compressive strength, and R is the radius of the assumed load surface (in m). This means F_b is the load (in N) caused by the elastic precursory wave. The formula for R given by Pahl is

$$R = 10.1 * (Q / f_c)^{1/3}, \quad (14)$$

with the charge Q in g and the static compressive strength f_c in Pa. The values calculated for R varies from 0.12 to 0.19 m for charges from 50 to 170 g. When these values are compared with the measured diameters, it appears that R corresponds with the crater diameter at the back. Pahl evidently considered the load performed by the particles to originate from the crater. For a static compressive strength of 25 MPa these formulae result in values for the total load of 12.7, 15.8, 18.1 and 28.6 MN for 50, 70, 85 and 170 g contact charges, respectively.

Now the quotient of the total impulse I_s^P and the total load F_b , which gives the pressure duration time t_d for a block load, can be calculated. By assuming a value for the dynamic strength of ten times the static compressive strength and using the crater diameter at the back ($I_s = I_t$), the pressure duration times resulting from these calculations are lower limits. When using these duration times in combination with the experimental values of the supplied impulse (I_s) and those of the hole diameter, the loading can be calculated.

By assuming the same failure mechanism for charges below and above the critical charge, this will lead to over and underestimated values for this load. For small charges, the particle stream is less concentrated and the use of the hole diameter leads to an overestimated value of the load, while for greater charges the unretrieved mass increases, which leads to an underestimate of the impulse and thus of the load. For a block load assumption, the resulting stress levels, as shown in Table 1, are of the order of 2 to 3 GPa which is about 80 to 100 times the static compressive strength (25 - 30 MPa). This is an upper limit for the load supplied from the back of the concrete slab because the values for the duration time t_d are underestimated.

Table 1 Calculated upper limit of the load performed by the particle stream

Charge (g)	I_s^P (kgm/s)	F_b (MN)	t_d (μ s)	I_s (kgm/s)	I_s/t_d F(MN)	d (m)	$\pi/4 \cdot d^2$ A (m^2)	F/A P (GPa)
50	60	12.7	4.7	135	29	>0.131	>0.013	<2.2
70	84	15.8	5.3	210	40	>0.142	>0.016	<2.5
85	102	18.1	5.6	>270	48	0.157	0.019	>2.5
170	204	28.6	7.1	>660	93	0.199	0.031	>3.0

By considering the quotient of half the thickness of the slab (30 mm) and particle velocity, maximum values for the duration times can be calculated, resulting in minimum values for the load P. For the same assumptions and under the same restrictions, as mentioned for Table 1, stress levels of 55 to 235 MPa are obtained in this case, which is about 2 to 10 times the static compressive strength (Table 2).

Table 2. Calculated lower limit for the load exerted by the particle stream

Charge (g)	u (m/s)	td (μ s)	I_s (kgm/s)	I_s/t_d (MN)	A (m^2)	P (MPa)
50	160	190	135	0.7	>0.013	<55
70	200	150	210	1.4	>0.016	<88
85	225	130	>270	2.1	0.019	>110
170	340	90	>660	7.3	0.031	>236

Besides these methods of determining upper and lower limits of the load, another method can be used, by considering the crushed concrete in the concentrated particle stream as loose dry sand. With the use of equation $u = P/(\rho \cdot c)$ and the properties of concrete ($\rho = 2200 \text{ kg/m}^3$ and $c = 3500 \text{ m/s}$), respectively loose dry sand ($\rho = 1500 \text{ kg/m}^3$ and $c = 500 \text{ m/s}$), upper and lower limits for the load P can be calculated for both materials, as shown in Table 3.

Table 3. Calculation of the load performed by particle streams of concrete and loose dry sand by using $P = u \cdot \rho \cdot c$

Charge (g)	u (m/s)	Concrete P (GPa)	Loose dry sand P (GPa)
85	225	1.7	0.17
170	340	2.6	0.26

Concerning the quotient of the acoustic impedances ($p.c$) of concrete and loose dry sand, which equals a factor 10, the same factor is found for the load for both materials. This means that the 'concrete' value for P , as given in Table 3, is an overestimated one, because of the decreasing values for the density and wave velocity, when the concrete has been crushed. The 'sand' value for P on the other hand will probably be an underestimated one.

Weighting of both underestimated and both overestimated values for the load, a range for the stress level at the back of the concrete slab of 500 to 2000 MPa at critical charges is indicated.

6 CONCLUSIONS

The main goal of this study to indicate the magnitude of the force that may be exerted by the particle stream (initiated by contact charges on concrete slabs) on following layers, was reached. A review of the conclusions is given below:

- A critical slab thickness does exist, below which at a given load, phenomena like a concrete particle stream consisting of an increasing percentage of small particles of high energy occur.
- The assumption for the dynamic strength in instantaneous response to be 8 to 10 times the static compressive strength seems reasonable.
- The influence of the reinforcement of the concrete on the force of the particle stream is remarkable. When the charge is located just over the reinforcement, the velocity of the concrete particles reduces by about 25 %. This means that a reinforcement with small meshes will reduce the threat of the load for subsequent slabs by 25 %.
- The divergence of the concrete particle stream is negligible, so the distance between two successive slabs has no influence for the first metre at least (which was tested).
- The supplied impulse, calculated as the product of total particle mass and average particle velocity, amounts to about 2.5 to 3 times the measured transmitted impulse to the next plate. This can be explained by the inhomogeneity of the stream. The tail of the particle stream will contribute much less to the total impulse than the head of the stream.
- The main load for following layers at critical charges is formed by the concrete particles ejected through the punched hole. The range of the stress level at the back of the directly loaded slab is estimated to be about 500 to 2000 MPa.

ACKNOWLEDGEMENT

This research was sponsored in part by the European Office of Aerospace Research and Development (EOARD), London, England, Grant no. AFOSR-86-0340.

REFERENCES

Pahl, H.

Obererdische und erdversenkte Schutzbauten für Kriegshauptquartiere gegen die Wirkung konventioneller Waffen.

Bericht über das 100. Wehrtechnische Symposium Waffenwirkung und Schutzbauten, Mannheim, 1979.

Weerheijm, J., Karthaus, W., Opschoor, G.

The failure mode of layered concrete constructions due to contact charges.

21st DOD Explosives Safety Seminar, August 1984.

Amelsfort, R. van, Weerheijm, J.

The failure mode of concrete slabs due to contact charges.

Progress Report No.1, 30 Sept. 1986 - 27 Feb. 1987.

PML 1987-IN18, Grant AFOSDR-86-0340 DEF

Amelsfort, R. van, Weerheijm, J.

The failure mode of concrete slabs due to contact charges.

Interim Scientific Report, 30 Sept. 1986 - 29 Sept. 1987.

FML 1987-C146, Grant AFOSDR-86-0340

Kolkert, W., Amelsfort, R. van

Ballistic pendulum methodology to study armour/anti-armour interactions at oblique impact.

33rd Conference Aeroballistic Range Association, 1982.

Kolkert, W., Amelsfort, R. van

Study of armour/anti-armour interactions at oblique impact with a ballistic pendulum methodology.

7th International Symposium on Ballistics, 1983.

**Experiments Used for Comparison of Blast Damage to Full Scale
and One Fourth Scale Reinforced Concrete Structures.**

by
Rickard Forsén
Swedish Defence Research Establishment

for
24th DoD Explosives Safety Seminar
Saint Louis, MO, 28-30 August, 1990

ABSTRACT.

The advantages of using small scale models of blast loaded structures are obvious. The accuracy of the results of two types of setups have been investigated. Details of test setups and results of experiments will be presented.

Part I: Contact Charges

In order to determine the damage of concrete slabs due to contact charges experiments have been made in one fourth scale. Different sizes of charges have been used and some experiments have also been made in full scale.

Part II: Confined Explosions

Experiments have been made in order to determine the damage of dwelling houses due to confined explosions. Reinforced concrete confinements with loading densities of approximately 1 kg/m³ have been used both in one fourth scale and full scale.

**Experiments Used for Comparison of Blast Damage to Full Scale
and One Fourth Scale Reinforced Concrete Structures.**

by
Rickard Forsén

INTRODUCTION.

Two types of damage from high explosive charges have been investigated using 1:4 scale model experiments. The model scale experiments have been compared to full scale experiments and show good agreement.

The first test series concerned damage from contact charges to reinforced concrete slabs. The main task was to find a relation between charge weight and hole diameter in concrete slabs similar to floors in ordinary dwelling houses.

The second test series concerned damage from a confined explosion in a concrete building. The purpose was to determine the debris launch velocity when a General Purpose Bomb detonates inside an ordinary dwelling house. Both uncased and cased charges were used.

CONTACT CHARGES.

Background.

After an act of explosion sabotage or an explosion accident a question about the size of the charge is often raised. If the charge has been in contact with a concrete slab it is tempting to use formulas from design manuals for demolition of concrete or design manuals for protective structures and try to calculate the charge weight with data about the slab and the size of the hole. The problem is that these formulas often concern very strong structures. Another problem is that the formulas from design manuals for demolition of concrete are made to calculate a charge weight that with certainty will break the concrete slab and thus tend to overestimate the charge weight. On the other hand the formulas from design manuals for protective structures are made to calculate a slab that with certainty will withstand

a certain high explosive charge and thus tend to underestimate the charge weight. In order to find a true relation between charge weight and hole diameter in a concrete slab similar to slabs that are often used in ordinary Swedish dwelling houses a test series was made (Jonasson, 1990).

Experiments.

The thickness of the reinforced concrete slabs were .16 m in full scale and thus 0.04 m in the model scale experiments. The strength of the concrete was 40 MPa in full scale and 49 MPa in model scale. The reinforcement in the full scale slabs were 10 mm ϕ at 300 mm cc's Ks400 (410 MPa yield strength and 670 MPa ultimate strength) and thus 2.5 mm ϕ at 75 mm cc's in model scale experiments (450 MPa yield strength and 790 MPa ultimate strength) (Fig. 1). The same type of reinforcement as in the full scale (ribbed bars) couldn't be found in model scale so instead an annealed thread with smooth surface was used.

A military plastic explosive was used in all the experiments but three, where Dynamex (a commercial high explosive) was used as comparison. The charges were formed to hemispheres except for one experiment with a cube, one with a cylinder and one with a sphere. Altogether twenty experiments were made with different size of charges in contact with the slab. Four experiments were also made with a small distance between charge and slab surface.

Twentytwo of the experiments were made in one fourth scale and two in full scale.

After the detonations the diameter and the volume of the holes were measured and furthermore four parameters defining the shape of the crater on top and bottom of the slab (Fig. 2).

A summary of the test set ups and results is shown in Table 1.

Results.

The reinforced concrete slabs in full scale reacted similar to the model scale slabs. The reinforcement were often torn

out without breaking and no difference was noted between the smooth surface reinforcement in model scale and the ribbed bars in full scale.

Characteristic for the shape of the holes is a conical shaped crater both on top and bottom of the slabs. In the experiments with a slight distance between charge and surface of the slab however there is no crater on the top of the slab and it is interesting that the Dynamex charges in contact with the slab neither gave any top side crater (Fig. 3). An explanation could be that Dynamex has lower density and lower detonation velocity and consequently lower detonation pressure than the plastic explosive (see table below).

	Plastic explosive M/46	Dynamex M
Density (kg/m ³)	1770	1400
Detonation velocity (m/s)	6800	5000
Explosion energy (MJ/kg)	5.54	4.70
Detonation pressure (MPa)	20500	8750

The experiments with the spherical, cubical and cylindrical charges gave approximately the same results as the hemispherical charge shape.

A function has been adapted to the experiments with different sizes of plastic explosive charges in contact with the model scale slabs and it says that the diameter of the hole can be calculated as

$$D_{1/4} = -52 + 45 \cdot \ln(Q)$$

In which $D_{1/4}$ = diameter of hole (mm); Q = weight of charge (g).

If this function is transformed to full scale (the scale factor for length is four and the scale factor for weight is sixtyfour) the diameter of the hole can be calculated as

$$D = 0.28 + 0.18 \cdot \ln(Q)$$

In which D = diameter of hole (m); Q = weight of charge (kg). This last function is valid for a hemispherical charge of plastic explosive in contact with a 0.16 m thick reinforced concrete slab with reinforcement 10 mm ϕ at 300 mm cc's in both directions in the bottom side. This function agrees very well with the two full scale experiments (Fig. 4).

The function gives 0.21 kg as the lower limit of charge weight that penetrates the slab.

CONFINED EXPLOSIONS.

Background.

A confined or partially confined explosion in a building may cause severe damage to the building and to the inhabitants if the explosion originates from for example an aerial bomb, an artillery shell or a terrorists high explosive charge. In order to estimate the debris launch velocity caused by the detonation of a 250 kg General Purpose Bomb inside a concrete frame residential building a test series was made (Forsén, 1989). The loading density (i.e. the weight of the high explosive divided by the volume of the confinement) for such an event will be approximately 1 kg/m³. In the experiments a much smaller volume than the real building was used namely 8 m³, here called "full scale". The thickness of the walls (0.15 m) and dimensions of the reinforcement (ϕ 10 mm) however were the same as in a real building and the loading density was the same, 1 kg/m³. The scaled venting area (i.e. the area of venting openings divided by the volume) also was the same as in the real building namely 0.11 m⁻¹.

Experiments.

Two full scale experiments were made (Fig. 5). In the first experiment an uncased charge, a sphere of 8 kg Comp B, was detonated in the center of the confinement. In the second experiment a steel cased charge (13 kg Comp B inside a 21 kg steel case, considered to give approximately the same pressure as the uncased charge) were detonated also in the center of the confinement.

Four model scale experiments with all dimensions scaled to a fourth were also made. Two were made with uncased charges and two with cased charges. The type of reinforcement used was the same as in the experiments with contact charges.

In all the experiments the pressure was recorded inside the confinements. The velocity of the walls and floors were recorded with gages and the experiments were high speed filmed from several directions. After the experiments the concrete debris size and position were registered.

Results.

The debris launch velocity scattered rather much between different walls and also between the same wall in similar model scale experiments especially in experiments with cased charges. The tendency however is that the same answers about debris launch velocity can be gained in one fourth scale experiments as in full scale experiments.

The pressure also scaled very good (Fig. 6) but both pressure and impulse density (after scaling) are slightly lower in the model scale than in the full scale. An explanation to this can be that the location of the transducer wasn't scaled properly. In the full scale the transducer was mounted proportional closer to a corner than in the model scale experiments. This might give a higher influence of reflections and thus a higher recorded pressure in the full scale than in the model scale, but of course this doesn't effect the actual pressure on the walls and floors.

The resulting debris launch velocity of the walls was found to be approximately 35 m/s for the uncased charge and approximately 30 m/s for the steelcased charge. The velocity of the floors was slightly lower approximately 35 m/s for the uncased charge and approximately 25 m/s for the cased charge. The reason for lower velocity of the floors is probably the higher amount of reinforcement. The lower velocity in the experiments with cased charges is probably due to the fact that the shrapnels from the case break the walls very quickly and thus allows the pressure to escape which gives a lower impulse density than in the experiments with uncased charges where the walls are thrown away almost unbroken (Fig. 7).

A summary of the test results is shown in Table 2.

Most of the concrete debris was found very close to the normal of each wall (Fig. 8) especially in experiments with uncased charges. Within a sector of $\pm 5^\circ$ from the normal 85 % was found in the experiment with uncased charge in full scale and corresponding figures in model scale are 77 % and 82 %.

In the full scale experiment with cased charge 55 % was found within $\pm 5^\circ$ and corresponding figures in model scale are 40 % and 72 %.

The proportion of larger fragments is higher in experiments with uncased charges than in experiments with cased charges and this can be seen both in full scale and model scale experiments (Fig. 9).

CONCLUSIONS.

A function has been evaluated, using one fourth scale experiments, for calculating the hole diameter when a charge of plastic explosive detonates on a 0.16 m thick reinforced concrete slab. Two full scale experiments show excellent agreement with the formula.

For confined explosions the debris launch velocity scatters rather much both in experiments in different scale and in similar experiments. Both full scale and one fourth scale experiments indicate however that the velocity will be 35-40 m/s with an uncased charge, and 25-30 m/s with a cased charge detonating inside a concrete frame residential building when the loading density is 1 kg/m³.

REFERENCES.

- | | |
|------------------|--|
| Forsén
1989 | INITIALVERKAN. Verkan på byggnader av inneslutna explosioner. (INITIAL PHASE. Effects of Explosions in Buildings.) FOA Report C20747-2.6. February 1989. In Swedish. |
| Jonasson
1990 | KONTAKTVERKAN 1. Sprängladdningars kontaktverkan på armerade betongplattor. (CONTACT CHARGES 1. The Damage to Reinforced Concrete Slabs from Detonating High Explosive Charges in Contact.) FOA Report in preparation. In Swedish. |

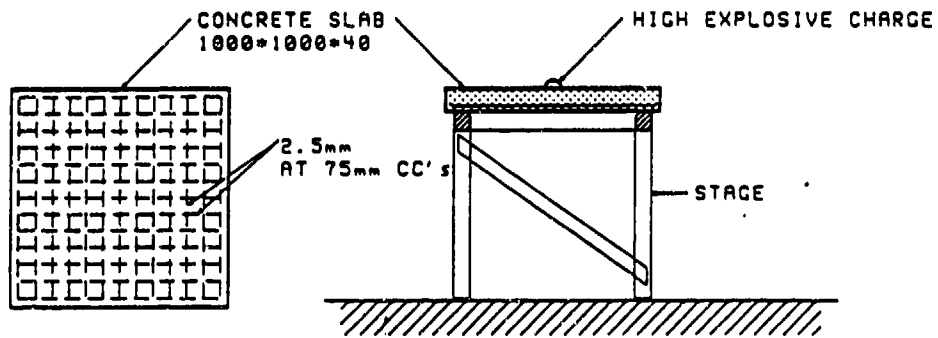


Figure 1. Concrete slab (one fourth scale) and test setup for the experiments with contact charges.

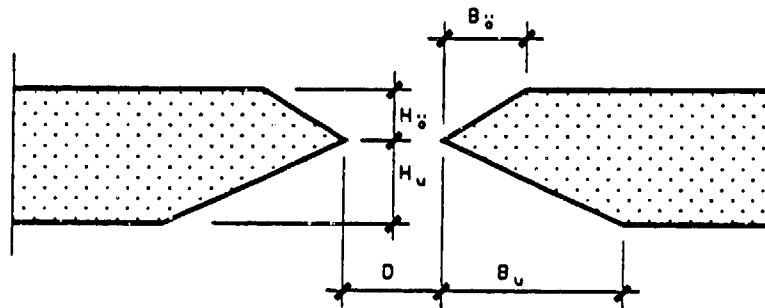


Figure 2. Measured parameters after the experiments.

		Charge data					Hole & crater dimensions					
Nr	Scale	Weight g	Diam mm	Stand off mm	Shape	High expl	Volume $10^{-6} m^3$	D mm	H _u mm	H _o mm	B _u mm	B _o mm
P1	1/4	23	39	0	hemi- sph.	pl.- expl.	370	97	24	17	37	26
P2	"	52	50	0	"	"	790	132	24	13	26	25
P3	"	150	70	0	"	"	1310	148	26	13	61	29
P4	"	250	90	0	"	"	1810	181	27	14	53	27
S1	"	14	34	0	"	"	300	72	28	12	49	37
S2	"	7	25	0	"	"	145	30	28	12	64	41
S3	"	1	--	0	blasting cap		0	0	0	7	0	10
S4	"	3.5	20	0	hemi- sph.	pl.- expl.	25/110	0	18	12	71	44
S5	"	500	103	0	"	"	2090	215	26	14	59	48
S6	"	125	65	100	"	"	2890	175	40	0	122	0
S7	"	125	65	300	"	"	0	0	0	0	0	0
S8	"	125	65	200	"	"	0	0	0	0	214	104
S9	"	125	41	0	cube	"	810	124	30	10	49	25
10	"	125	51	0	cyl.	"	810	129	27	13	45	17
11	"	125	52	0	sphere	"	985	130	27	9	49	14
12	"	125	65	0	hemi- sph.	"	1590	187	20	20	41	51
13	"	3.5	20	0	"	DYNA- MEX	0	0	0	8	0	27
14	"	125	65	0	"	"	1110	127	40	0	67	0
15	"	250	90	0	"	"	1530	160	40	0	73	0
16	"	125	65	0	"	pl.- expl.	1110	138	30	10	57	44
F1	1/1	3330	190	0	"	"	62000	510	81	81	218	134
F2	1/1	7000	243	0	"	"	88000	652	75	85	181	133
E1	1/4	1000	136	0	"	"	4040	280	27	20	48	48
E2	1/4	1000	136	170	"	"	----	345	40	0	48	0

Table 1. Data of all the experiments with contact charges.

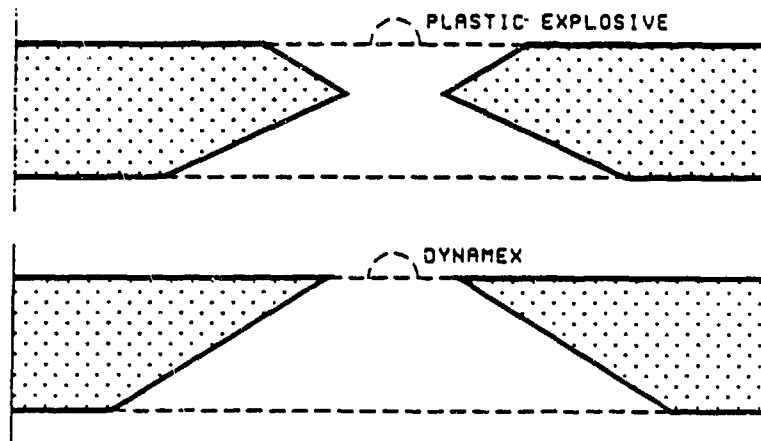


Figure 3. Plastic explosive gives a crater both on top and bottom of the slab but Dynamex only on the bottom.

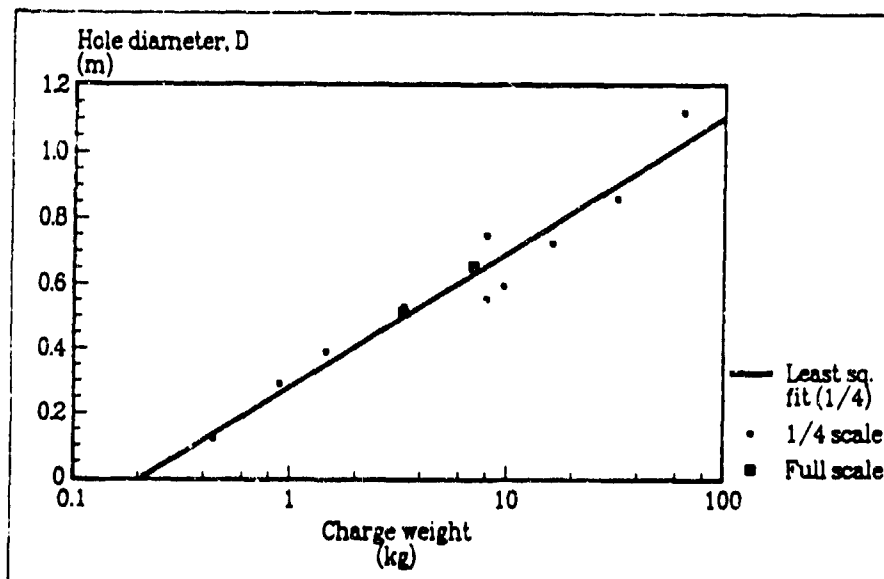


Figure 4. Test results and adapted function for the experiments with contact charges. For the results from the model scale the diameter is multiplied by four and the weight by sixtyfour.

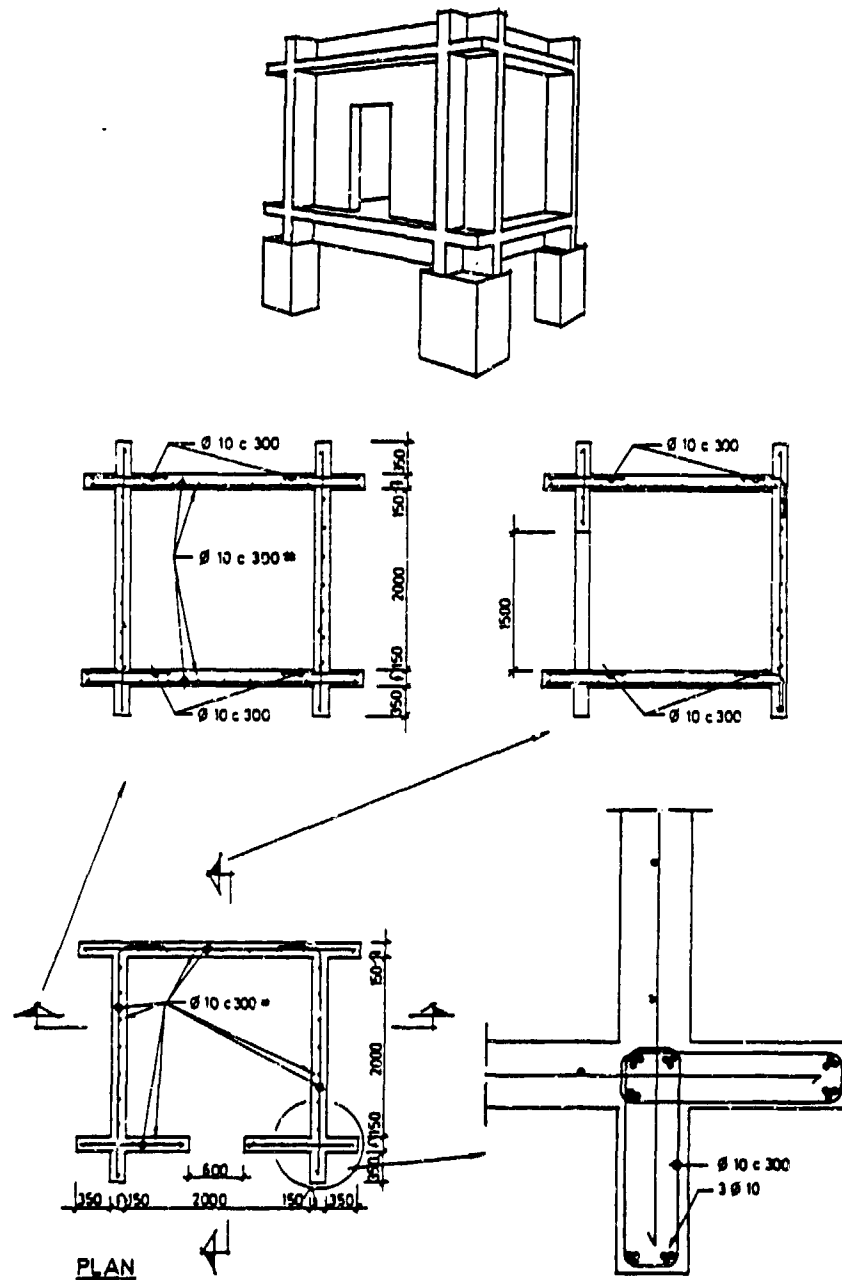


Figure 5. Test specimen used for the confined explosions. The figures and reinforcement concern full scale. All figures are in mm.

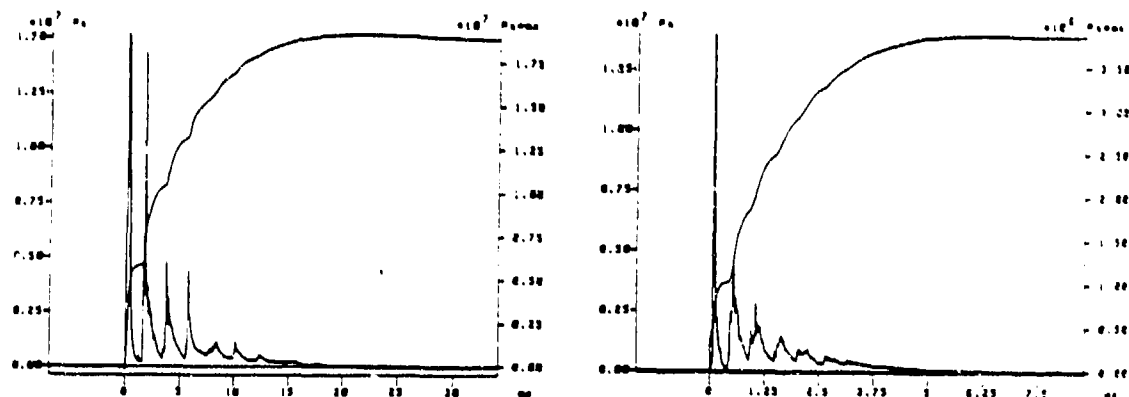


Figure 6. Recorded overpressure time history inside the confinement, full scale (left) and one fourth scale (right). Also shown are impulse densities.

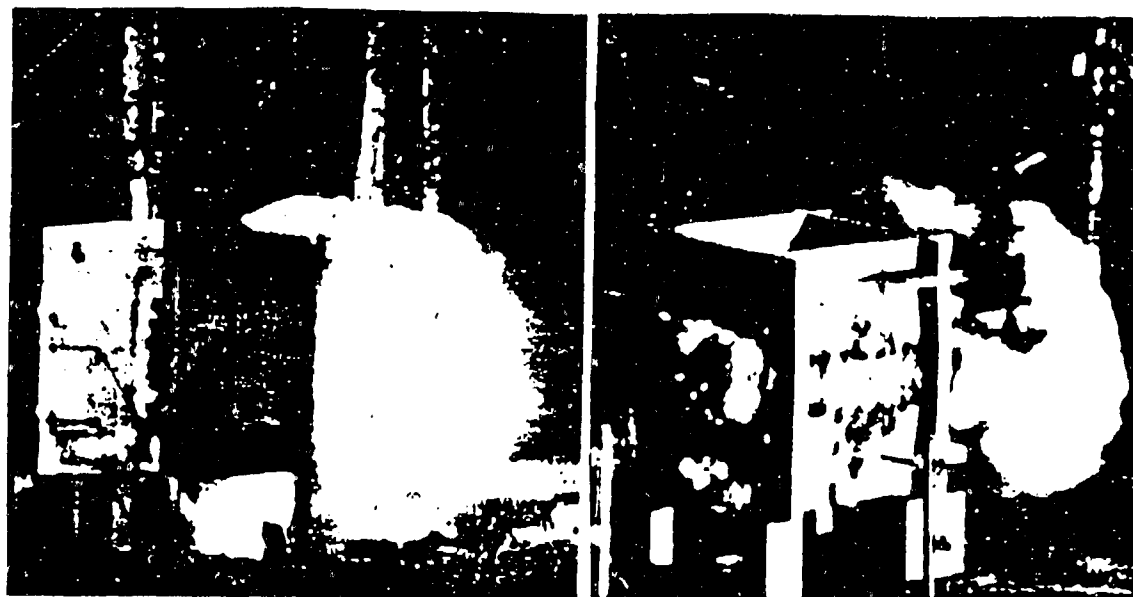


Figure 7. The walls didn't break the same way in the experiments with uncased charges (left) as they did in the experiments with cased charges (right).

	Uncased charge			Cased charge		
	Full scale	Model scale		Full scale	Model scale	
Shot nr	407	482	483	408	484	485
Velocity (m/s)						
side	40	36	34	25	29	32
front	37	37	37	33	21	32
floor	38	34	26	28	20	28
Impulse density I_+ (kPas)	19.3	15.4	15.5	12.4	11.9	12.1

Table 2. Summary of test results in experiments with confined explosions. Impulse densities are multiplied by four in the model scale experiments.

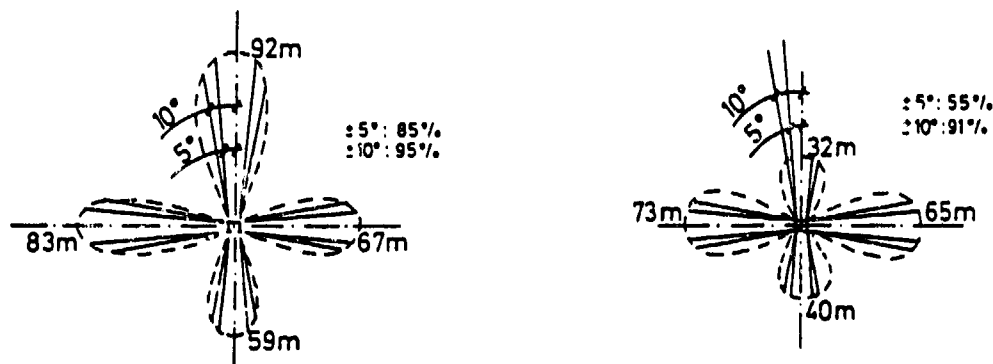
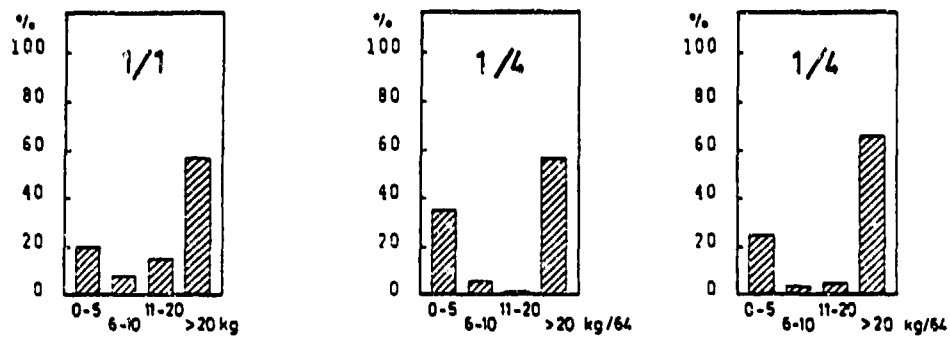
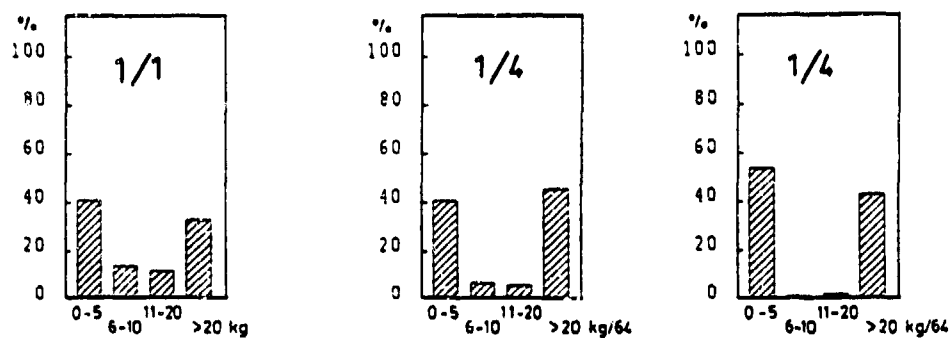


Figure 8. Scatter of concrete fragments in full scale experiments with uncased charge (left) and cased charge (right).



Uncased charges



Cased charges

Figure 9. Weight distribution of concrete fragments from the walls found after the experiments with confined explosions.

BEHAVIOUR OF CONCRETE UNDER HIGH VELOCITY IMPACT

BEHAVIOUR OF CONCRETE UNDER HIGH VELOCITY IMPACT

(R.A. Goel, S. Chandra, U.C. Chandola, A.K. Abrol & R. Kumar)

(Terminal Ballistics Research Laboratory, Defence Research & Development
Organisation, Chandigarh, India)

Abstract

Steel Fibre reinforced concrete (SFRC) has shown improved engineering properties such as Flexural strength and shattering resistance etc. in comparison to Plain or Reinforced Cement Concrete. This technique has been recommended for the construction of explosive/ammunition storage buildings and processing areas. Experimentation have been undertaken to investigate its behaviour against high velocity impact of projectiles. Specially designed model projectiles of calibre 30 mm were made to interact with different types of concretes such as PCC, SFRC and SFRC reinforced with steel rods, with varying velocities ranging from 50 to 450 m/s. Transient behaviour of the interaction has been recorded with high speed photography. In the process of high velocity impact concretes are damaged differently, showing cracking, spalling or scabbing or their combinations. Behaviour of various types of concretes against high velocity impact and their comparative performance have been discussed in this paper.

Introduction

Conventional plain cement concrete although in use for decades but has limited scope of application due to its low tensile strength and poor ductility. In practice, concrete is normally reinforced with steel bars or mesh to withstand tensile stresses. Advancement in material science and engineering

has led to the development of a composite construction material named Steel Fibre Reinforced Concrete. It consists of conventional concrete or mortar, reinforced by random disposal of short fine steel fibres of specific geometry. This concrete has better tensile strength, toughness and ductility vis-a-vis plain or reinforced concrete.

To study the behaviour of this concrete against high velocity impact of the projectile extensive work has been carried out at Terminal Ballistics Research Laboratory, Chandigarh, India and the detailed investigations are reported in the following paragraphs.

Experimental Set Up

Impact studies on concrete targets were carried out with specially designed projectiles of calibre 30 mm. The projectiles were of CRH value one and their length was 150 mm. These projectiles were hollow and filled with high explosive substitute. The projectiles were made of EN-24 material. They were in the weight group of 472 ± 4 gm. These projectiles were projected horizontally with 30 mm launcher at desired velocity. Velocity of the projectile was varied from 50 to 470 m/sec by changing the propellant weight. Figure 1 shows an assembled round alongwith its components.

Three types of concrete blocks i.e. PCC (Plain Cement Concrete), SFRC (Steel Fibre Reinforced Concrete) and SFRC reinforced with steel rods were used as targets. Although blocks of different types were having different compositions but they were of the same size i.e. 75 x 75 x 17.5 cm. Compressive strength of each block was measured by non-destructive method before firing and it was found to be in the range of 350 ± 20 Kg/Cm . Details of these blocks have been shown in Figures 2 (a,b,c).

Multiple Spark Photography was used for seeing the flight of the projectile in pre and post impact stages. The transient behaviour of the target during its interaction with the projectile was also recorded. A pair of screens connected with microsecond counter was placed in front of the block (target) for measuring the velocity of the projectile, just before impact. In every experimental trial concrete target was placed vertically, facing muzzle of the launcher. The projectile was allowed to hit at the centre of the block and only one trial was conducted on each block.

All experiments were conducted for normal attack only. Figure 3 shows the set up of the experiment.

Observation

After completion of each experiment the projectile was recovered and examined carefully for any damage sustained. In no case the projectile was found to have any type of damage. After each firing, the target was also examined and it was found to have inculcated a crater of almost conical in shape with circular base, on the front surface of the block and the apex inside. The damage was assessed in terms of the penetration i.e. the depth of the apex from the front surface, dia of the crater (mean of the two values measured at right angles) and the volume of the crater in each of the experiments. The data for different impact velocities of projectile have been given in Table I, II and III for PCC, SFRC and SFRC reinforced with steel rods, respectively. At lower velocities all the three types of concrete targets sustained damage on the front surface only and no effect on the rear was recorded. But as the impact velocity was increased a stage was reached when cracks were developed on the rear of the concrete targets. Figures 4, 5, 6 show the cracks developed on the rear of three types of blocks. For further

increase in the impact velocity, a scab was thrown off from the rear of the block. In between these two stages a critical stage was also observed where scab a big chunk was found hanging at the rear surface and was about to be detached. Figure 7 and 8 shows the critical stage of the scabbing. Fig 9 shows sequentially the scab flying away from the rear of the block. The scab was not one mass of concrete but shattered pieces leaving a crater of conical shape. These observations were similar for all types of concretes. Figure 10, 11 and 12 show the crater formed after the scab was thrown off from three types of blocks. It is evident from these figures that the crater were of different sizes for different types of concrete blocks. The dia of the crater on the rear was measured along two perpendicular axes and mean taken. It was a significant observation that the dia of the crater on the rear side was always bigger than the dia formed on the front side. Values of the depth and volume of the crater so formed on the rear of the three types of blocks were also recorded. The data has been given in Table IV.

Discussion

To evaluate the comparative behaviour of three types of concretes, based on the damage inculcated on them, graphs were plotted taking impact velocity on x axis and penetration, crater dia and volume of the crater formed on the front surface on Y axis. These have been shown in Figure 13, 14 and 15. It is evident from Figure 13 that SFRC reinforced with steel rods offered maximum resistance to penetration while PCC the minimum. But no marked difference in the penetration behaviour of three types of concrete was recorded upto a velocity of 160 m/sec. Figure 14 and 15 show the variation of crater dia and crater volume of three types of concretes with impact velocity of the projectile. These two graphs also show that for impact velocity upto 160

m/sec, the variation in these two parameters is almost the same for three types of blocks. It is only after this value of impact velocity the curves diverge from each other.

A close look to these graphs reveals that SFRC reinforced with steel rods offers maximum resistance to the impact of high velocity projectiles sustaining minimum damage on the front surface followed by SFRC and PCC in sequence.

Regarding, scabbing behaviour of concretes it has already been mentioned in observation column that the damage incurred due to scabbing on the rear surface for any concrete is always greater than its respective front surface damage. For having a comparison of the scabbing behaviour of three types of concretes histogram of recorded values of four parameters i.e. critical velocity of scabbing, volume, dia and depth of crater formed on the blocks after the scabs were thrown off were plotted. This has been shown in Fig 16. This histogram clearly shows that out of three types concretes, it is PCC which suffers scabbing most easily i.e. at the lower impact velocity than SFRC, and SFRC reinforced with steel rods, which follow in sequence. Damage caused due to scabbing also follows the same sequence and volume of the crater formed in three types of concrete i.e. SFRC reinforced with steel rods, SFRC and PCC are in the ratio 1:1.4:4.5 while dia bears up a ratio 1:1.8:2.3 and depth of penetration in 1:1.2:1.5.

Conclusion

Based on above investigations superiority of steel fibre reinforced concrete over PCC against impact of high velocity projectiles has been established. However, if this concrete is further reinforced suitably with steel rods, will provide more immunity against the said attack.

Acknowledgement

Authors pay their thanks to Dr. AK Bhalla, Director, Shri R Srinivasan, Joint Director, Directorate of Explosive Safety, New Delhi and Shri DS Murthy, Deputy Director, Terminal Ballistics Research Laboratory, Chandigarh for useful discussions and suggestions in this work. We are thankful to Dr. C Raj Kumar, Joint Director, Shri Rattan Lal, Scientist and Dr. Anil Kumar, Scientist, National Council for Cement and Building Materials, New Delhi for the design and fabrication of concrete blocks for this work.

We pay our solemn gratitude to our Director, Shri M Balakrishnan for his able suggestions during the course of work and permission to publish the paper in the Proceedings of the 24th Seminar on Explosive Safety.

TABLE I- DAMAGE DATA OF PCC TARGET

Sr.No	Impact Velocity (m/sec)	Penetration (mm)	Av.Dia. (cms)	Measured Volume (Cu.cc)
1.	44.69	8.8	2.75	30.62
2.	71.91	15.0	6.10	48.01
3.	78.98	15.9	6.25	57.11
4.	91.93	18.8	8.75	68.15
5.	105.11	25.0	11.75	120.03
6.	117.33	27.9	11.25	120.26
7.	128.40	29.5	11.25	128.31
8.	140.63	34.1	12.75	173.01
9.	149.69	35.8	13.50	233.11
10.	166.33	37.0	12.25	176.32
11.	215.02	55.25	17.50	554.63
12.	223.71	64.2	16.35	672.01
13.	225.30	62.5	20.35	666.83
14.	255.80	65.3	19.50	513.10
15.	319.50	80.0	23.00	1138.20
16.	300.07	86.2	19.00	1307.90
17.	337.12	91.7	22.75	1090.10
18.	347.86	90.5	24.00	1246.00 (Limiting case of scab)
19.	366.28	85.7	26.25	Scabbed

TABLE II - DAMAGE DATA OF SFRC TARGETS

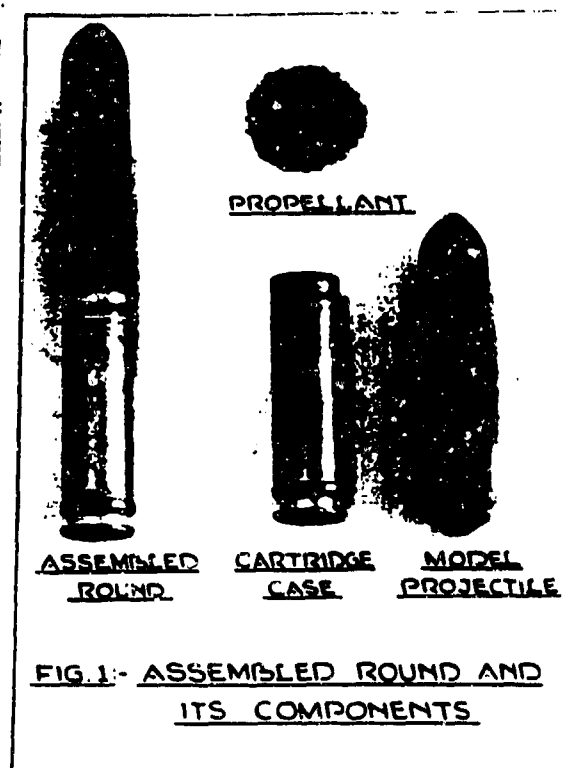
Sr.No	Impact Velocity (m/sec)	Penetration (mm)	Av.Dia. (cms)	Measured Volume (cu. cc)
1.	72.75	16.0	7.00	36.42
2.	86.31	19.2	8.75	45.50
3.	110.06	25.5	10.75	97.56
4.	160.18	36.7	12.75	326.19
5.	230.51	42.4	14.40	264.00
6.	269.33	59.0	17.00	461.50
7.	321.10	76.0	17.50	562.74
8.	374.33	90.5	18.00	461.50
9.	436.59	80.0	18.20	Limiting case of scab Scabbed

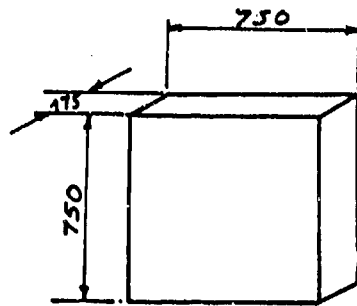
TABLE III - DAMAGE DATA OF SFRC TARGETS
REINFORCED WITH STEEL

Sr.No	Impact Velocity (m/sec)	Penetration (mm)	Av.Dia. (cms)	Measured Volume (cu. cc)
1.	60.00	14.5	5.25	21.50
2.	88.01	21.7	6.15	37.53
3.	114.89	28.4	10.00	136.59
4.	164.70	38.0	10.50	157.26
5.	223.25	48.5	15.75	413.93
6.	334.44	51.8	14.00	240.06
7.	235.32	59.3	15.25	703.60
8.	376.86	80.0	14.50	361.40
9.	423.96	90.3	13.50	531.45 (Limiting case of scab)
10.	462.35	114.0	26.00	Scabbed

TABLE IV - DATA OF DAMAGE DUE TO SCABBING ON
DIFFERENT TYPES OF CONCRETE

Sr.No	Type of Block	Scabbing Velocity (m/sec)	Dia.of Scab (cms)	Depth of Scab (cms)	Volume of scabbed portion (cu. cc)
1.	PCC	366.80	41.00	9.7	6374
2.	SFRC	426.59	32.75	8.0	1970
3.	SFRC + RC	462.55	18.00	5.6	1407





PCC

MIX PROPORTIONS (PCC)

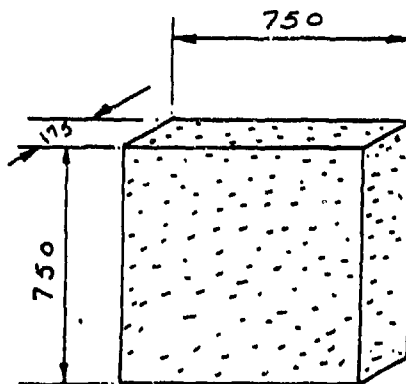
GRADE OF CONCRETE - M 30

QUANTITY OF MATERIALS PER

C.U.m OF CONCRETE

1. CEMENT - 530 Kg
2. SAND - 619.5 Kg
3. COARSE AGGREGATE $\left\{ \begin{array}{l} 309.7 \text{ Kg (PASSING THROUGH} \\ 10 \text{ mm \& RETAINED ON 4.75mm)} \\ 619.3 \text{ Kg (PASSING THROUGH} \\ 20 \text{ mm \& RETAINED ON 10 mm)} \end{array} \right.$
4. WATER - 219.7 LITRES
5. SUPER PLASTICIZER - 5.3 Kg. (1% BY WEIGHT OF CEMENT)

FIG 2(a) :- SKETCH SHOWING DETAIL OF PCC



SFRC

MIX PROPORTION (SFRC)

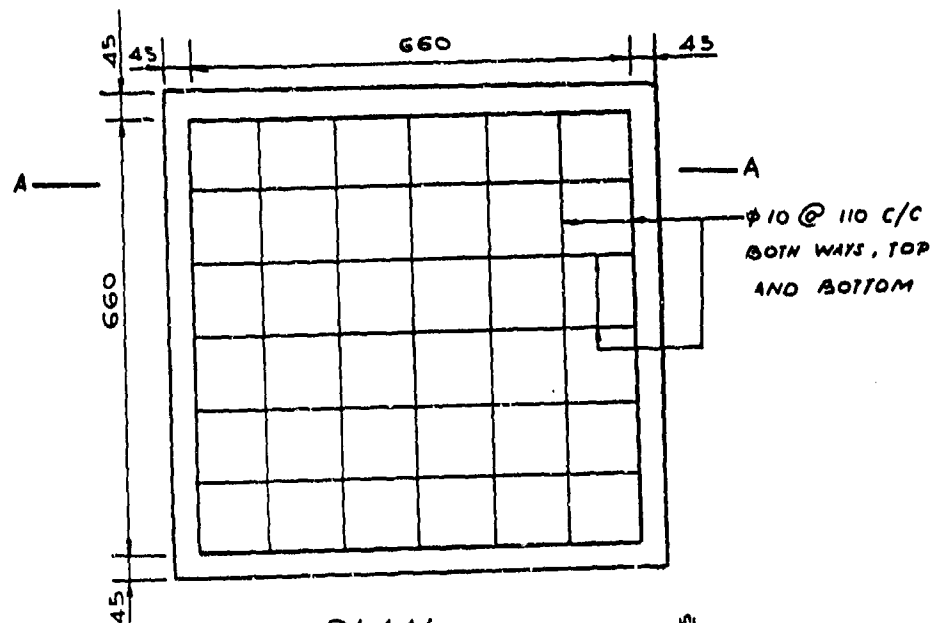
GRADE OF CONCRETE-M 30

QUANTITY OF MATERIALS PER CU.m
OF CONCRETE.

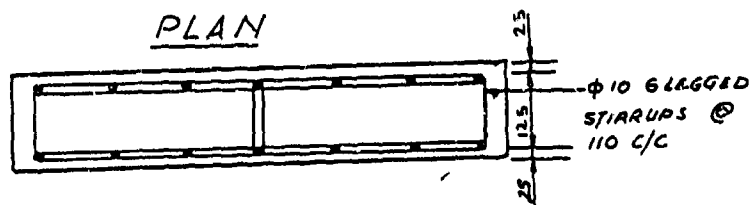
- | | |
|----------------------|--|
| 1 CEMENT | - 530 kg |
| 2 SAND. | - 603.5 kg |
| 3. COARSE AGGREGATE | <div style="display: inline-block; vertical-align: middle;"> 301.7 kg (PASSING THROUGH
10mm & RETAINED ON 10mm)
 603.5 kg (PASSING THROUGH
20mm & RETAINED ON 10mm) </div> |
| 4. WATER | - 220 LITRES. |
| 5. SUPER PLASTICIZER | - 5.3 kg . 1% WT. OF WATER |
| 6. STEEL FIBRE | <div style="display: inline-block; vertical-align: middle;"> 98.125 kg (1.25% BY VOLUME
ON CONCRETE)

 ASPECT RATIO - 80
 (LENGTH - 36mm, ϕ - 0.45mm) </div> |

FIG. 2(b).:- SKETCH²²⁸⁸ SHOWING DETAIL OF SFRC.



PLAN



SECTION AT A-A

FIG. 2(C) SKETCH SHOWING DETAILS OF SFRC
REINFORCED WITH STEEL RODS

DIMENSIONS IN mm

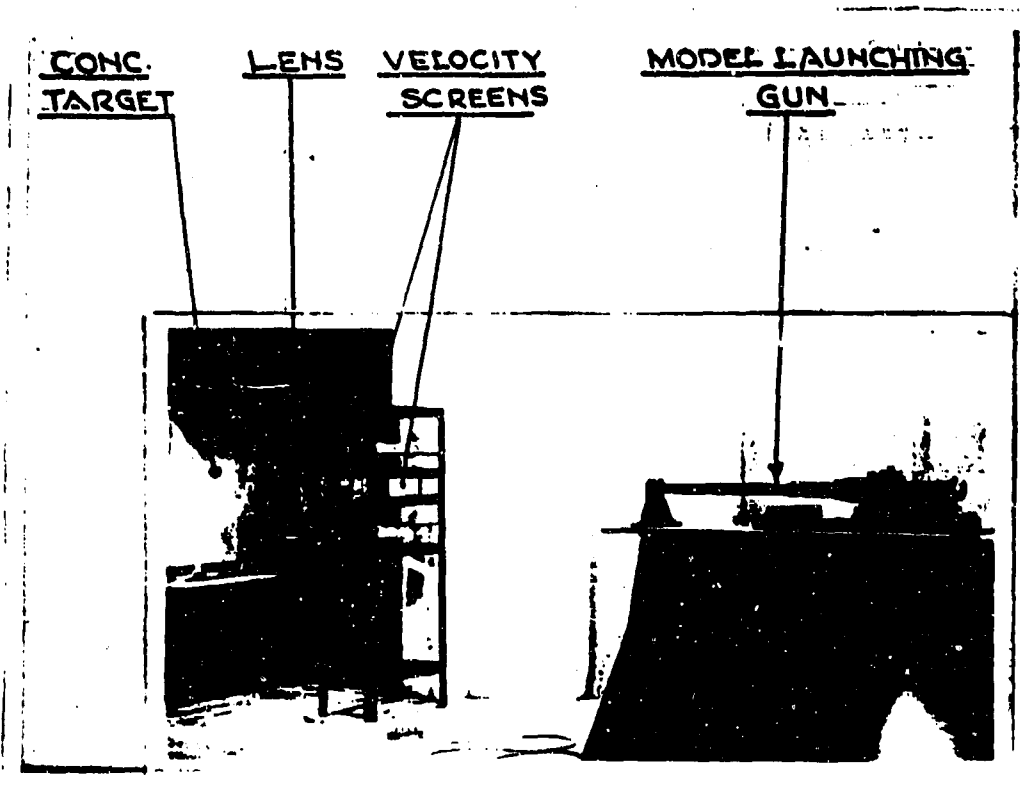


FIG.3 : EXPERIMENTAL SET UP

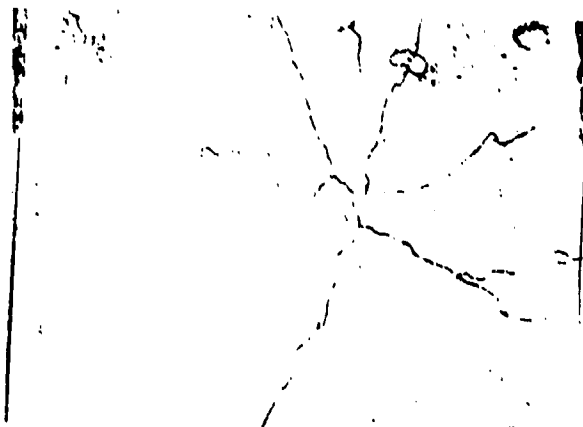


FIG.4. CRACKS DEVELOPED
ON THE REAR SIDE
OF PCC TARGET



FIG.5. CRACKS DEVELOPED
ON THE REAR SIDE
OF SFRC TARGET



FIG.6. CRACKS DEVELOPED
ON THE REAR SIDE
OF SFRC AND RE-
INFORCED WITH
STEEL RODS.

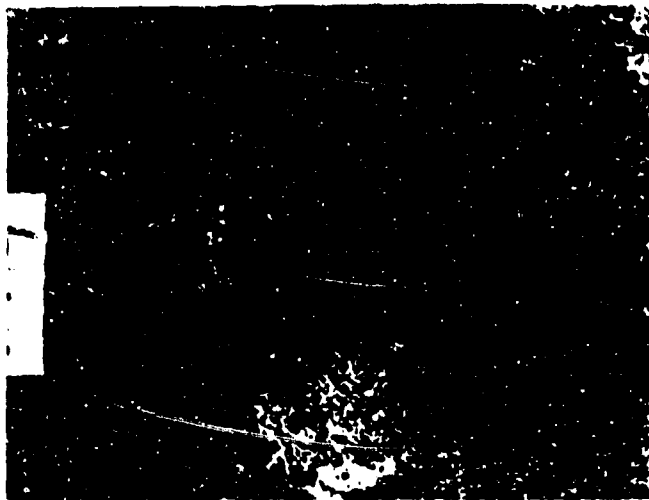


FIG.7. PROJECTILE STRUCK IN THE SFRC
TARGET AT THE CRITICAL STAGE
OF SCABBING



FIG.8. A SCAB ABOUT TO BE FLOWN OFF
FROM THE REAR OF SFRC TARGET

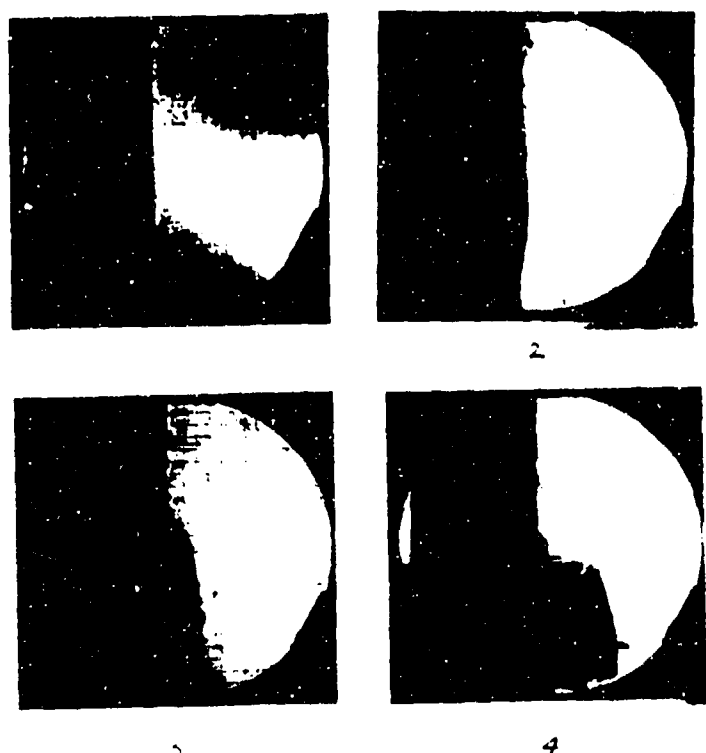


FIG.9. SEQUENTIAL RECORD SHOWING EMERGENCE OF SCAB FROM THE REAR OF TARGET No.AN-2(SFRC+RCC) WHEN HIT BY PROJECTILE WITH AN IMPACT VELOCITY OF 494.11 m/sec.

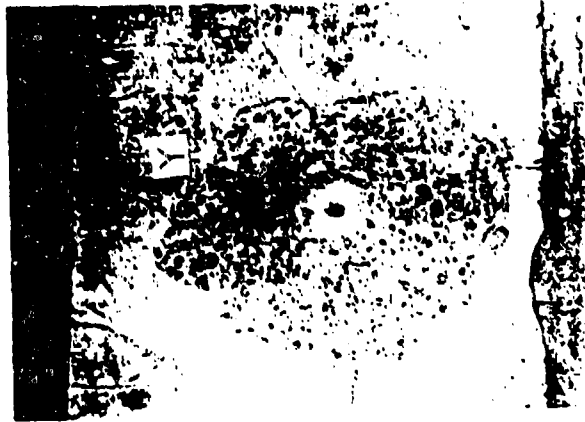


FIG. 10. CRATER FORMED ON
THE REAR SIDE OF
PCC TARGET AFTER
SCABBING.



FIG. 11. CRATER FORMED ON
THE REAR SIDE OF
SFRC TARGET AFTER
SCABBING.

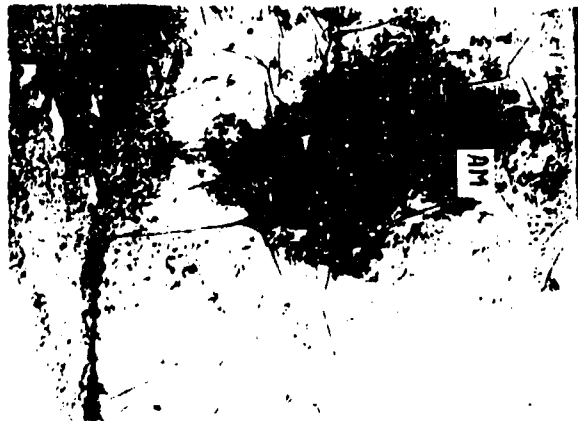


FIG. 12. CRATER FORMED ON
THE REAR SIDE OF
SFRC REINFORCED
WITH STEEL RODS
TARGET AFTER
SCABBING.

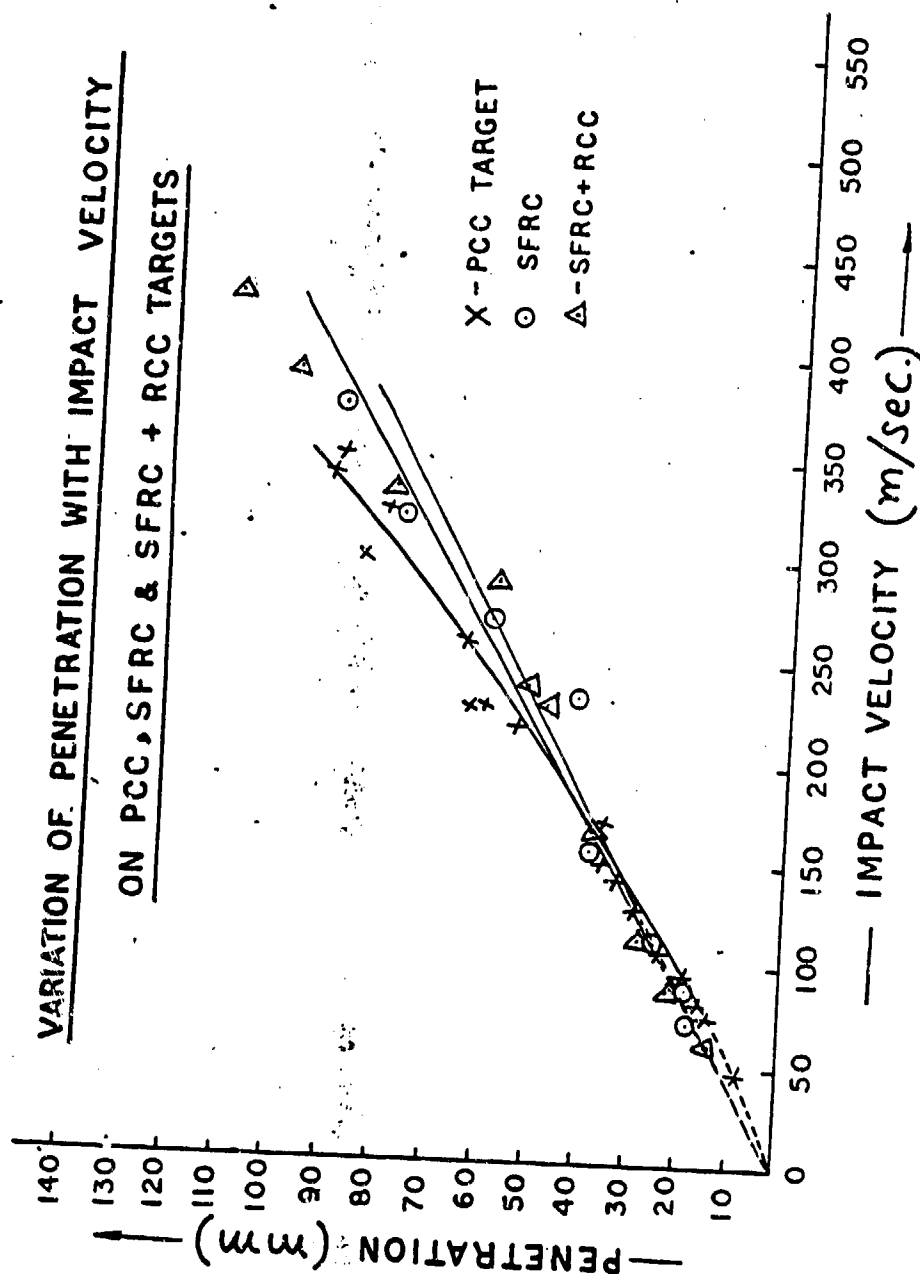


FIG. 13

**VARIATION OF CRATER DIA INCULCATED ON PCC, SFRC
& SFRC + RCC TARGETS WITH IMPACT VELOCITY**

X - PCC TARGET

○ - SFRC

△ - SFRC + RCC

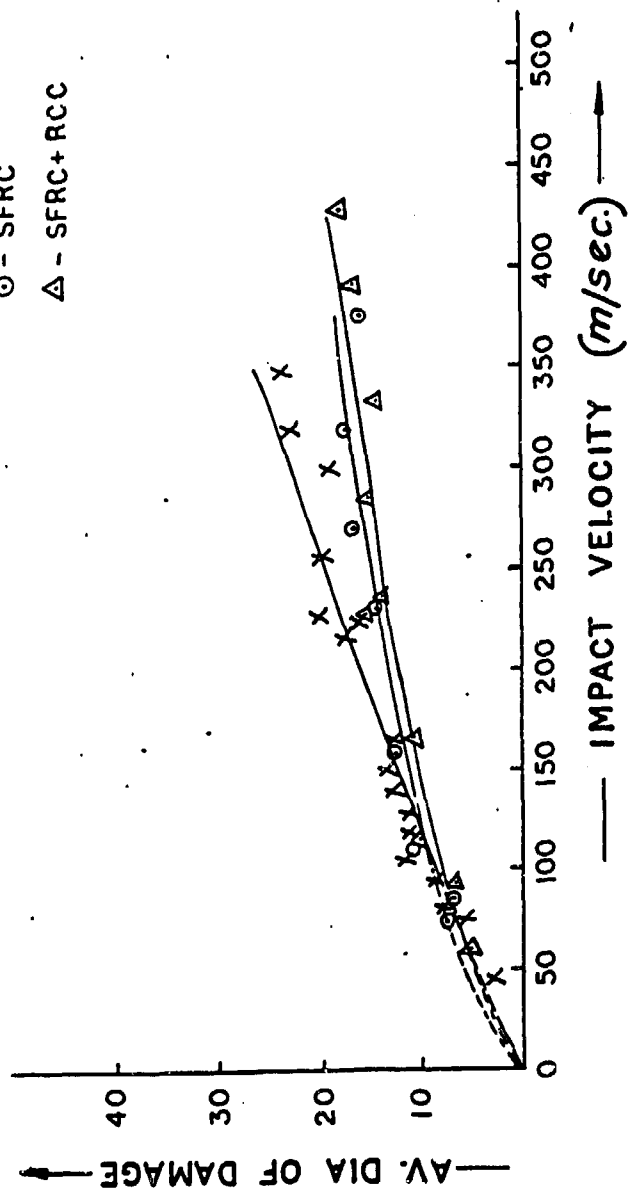
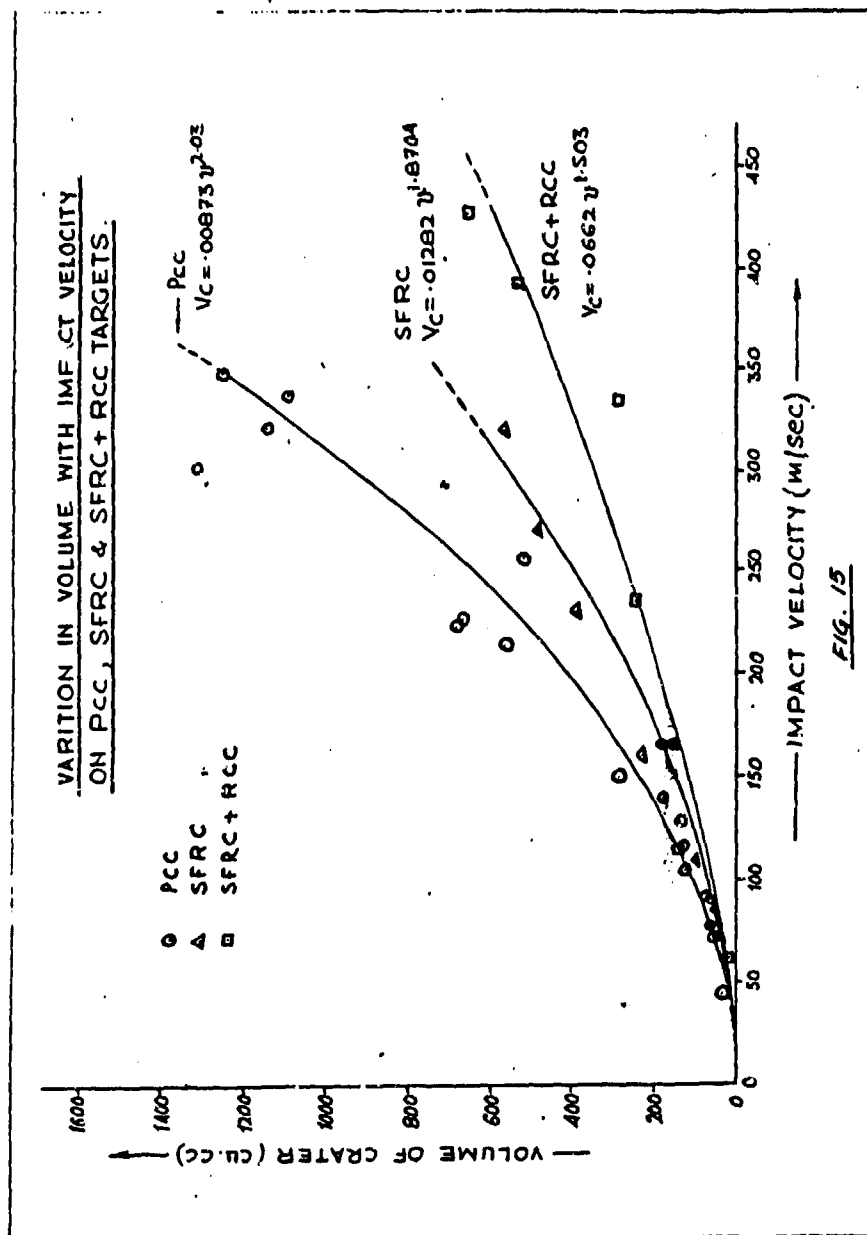


FIG. 1A



COMPARATIVE SCABBING BEHAVIOUR OF PCC, SFRC & SFRC+RCC TARGETS

SCABBING VELOCITY IN m/sec VOLUME OF SCABBED PORTION IN cm^3 CC
 AV DIA OF SCAB IN cm DEPTH OF SCAB IN cm

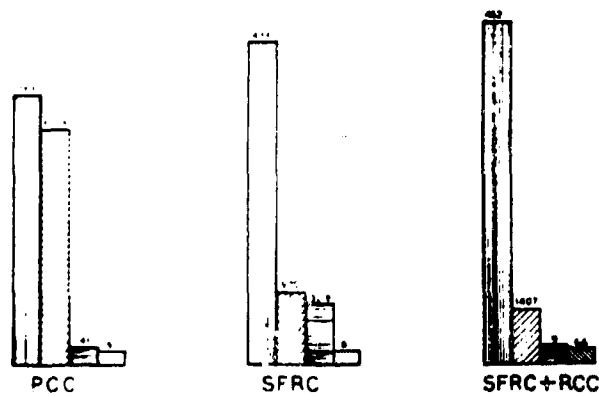


FIG.16. HISTOGRAM SHOWING COMPARATIVE SCABBING BEHAVIOUR OF PCC, SFRC AND SFRC REINFORCED WITH STEEL RODS.

PRESENTED AT THE TWENTY-FOURTH DOD EXPLOSIVE SAFETY SEMINAR
ST. LOUIS, MISSOURI, AUGUST 30, 1990

VULNERABILITY ASSESSMENT OF STRUCTURALLY DAMAGING
IMPULSES AND PRESSURES (VASDIP)

Frank B. Tatom
John W. Tatom

ENGINEERING ANALYSIS, INC.

Huntsville, Alabama

ABSTRACT

Based on the dimensionless pressure-impulse-damage contours developed by Southwest Research Institute, the Vulnerability Assessment of Structurally Damaging Impulses and Pressures (VASDIP) software has been developed by Engineering Analysis, Inc. For each of twenty-four different structural components (six concrete, eight steel, five masonry, and five wood or timber) the structural design engineer can specify eight to twelve design parameters associated with that particular type of component. VASDIP provides as output dimensional pressure-impulse-damage contours, and also five vulnerability parameters for use with the High Explosive Damage Assessment Model-Second Industrial Version (HEXDAM-B). Like HEXDAM-B, VASDIP is designed for use with minimal equipment, consisting of an IBM PC-XT/AT (or compatible), monochrome monitor and dot matrix printer. By means of VASDIP the structural design engineer can rapidly optimize a structural component to withstand a specified blast.

1.0 INTRODUCTION

The evaluation of the vulnerability of a group of structures to a blast wave from an explosive burst is a significant problem under serious consideration by a large number of organizations. According to current single-degree of freedom models, blast damage can be represented by **Pressure-Impulse (P-I) diagrams**, which are characterized by three regions: 1) pressure-sensitive, 2) impulse-sensitive, and 3) transition, as shown in Figure 1. Southwest Research Institute (SRI) recently developed a set of dimensionless pressure-impulse-damage contours, based on a combination of **single-degree-of-freedom theory** and **actual test data** [1]*. The SRI contours represent the most general method of carrying out vulnerability evaluation without resorting to finite element analysis. However, the procedure

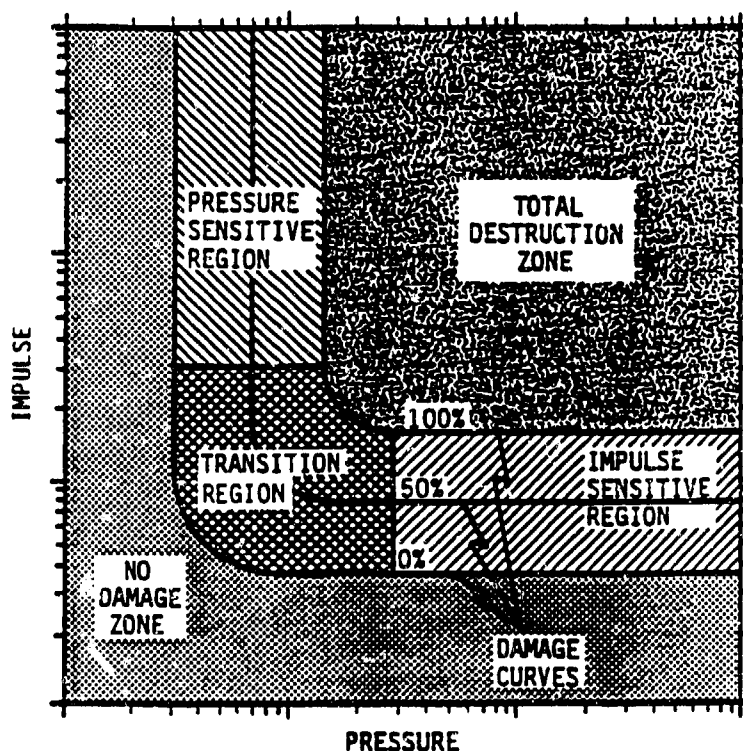


FIGURE 1. PRESSURE-IMPULSE DIAGRAM

*Numbers in brackets correspond to references cited in Section 8.0.

for converting the **dimensionless** contours into their **dimensional** counterparts, consistent with a set of design specifications, involves a number of manual computations, which can be both tedious and time-consuming.

In an effort to simplify this procedure, Engineering Analysis, Inc. (EAI) has developed the **Vulnerability Assessment of Structurally Damaging Impulses and Pressures (VASDIP)** software. VASDIP is based on the SRI pressure-impulse-damage contours, and automates the process of converting the dimensionless contours into the specific dimensional contours of interest to the user. Furthermore, as depicted in Figure 2, the output of VASDIP provides the **vulnerability parameters** required for use with the HEXDAM-B software [2]. As noted in subsequent discussion, VASDIP can analyze twenty-four different structural components.

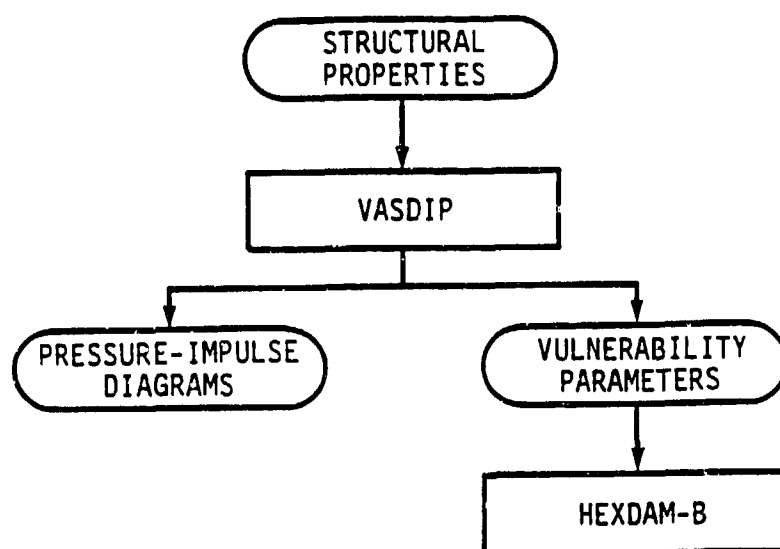


FIGURE 2. RELATIONSHIP BETWEEN VASDIP AND HEXDAM-B

2.0 CAPABILITIES/LIMITATIONS

VASDIP is a useful tool for assessing the vulnerability of structures or components of structures to blast effects. Table 1 provides a list of the 24 different structural components which can be analyzed. As described in Section 3, a set of design parameters are defined for each component and the user has the freedom to select any physically reasonable value for each such parameter. VASDIP is designed for use by structural design engineers. A general familiarity with structural design terminology is essential for its proper application. VASDIP deals only with pressures and impulses associated with blast effects. No thermal or fragmentation effects are included.

TABLE 1. VASDIP STRUCTURAL COMPONENTS

- | | |
|---|--|
| ● Reinforced Concrete Beams | ● Steel Corrugated Metal Decking |
| ● One-Way Reinforced Concrete Slabs | ● Steel Exterior Columns (Bending) |
| ● Two-Way Reinforced Concrete Slabs | ● Steel Interior Columns (Buckling) |
| ● Reinforced Concrete Exterior Columns (Bending) | ● Steel Moment-Resisting Frame Walls |
| ● Reinforced Concrete Interior Columns (Buckling) | ● One-Way Unreinforced Masonry Walls |
| ● Reinforced Concrete Moment-Resisting Frames | ● Two-Way Unreinforced Masonry Walls |
| ● Steel Beams | ● One-Way Reinforced Masonry Walls |
| ● Metal Stud Walls | ● Two-Way Reinforced Masonry Walls |
| ● Open Web Steel Joists (Tension failure in bottom chord) | ● Masonry Pilasters |
| ● Open Web Steel Joists (Web buckling) | ● Wood or Timber Stud Walls |
| | ● Wood or Timber Roofs |
| | ● Wood or Timber Beams (Bending) |
| | ● Wood or Timber Exterior Columns |
| | ● Wood or Timber Interior Columns (Buckling) |

2.1 BOUNDARY CONDITIONS

VASDIP is based on single-degree-of-freedom analysis with adjustments to take into account actual test data [1]. Among the characteristics which the user can input to the software are the boundary conditions of the components. For each such boundary condition, based on the Equivalent Single-Degree-of Freedom Principle, a boundary coefficient is specified, or computed within VASDIP. With different boundary conditions, different coefficients result.

2.2 STRUCTURE ORIENTATION

In addition to boundary conditions, the user also has two options pertaining to the orientation of each structural component as follows:

- side/rear-facing
- front-facing

As indicated in Figure 3, the side/rear-facing option applies for components which do not face the blast wave, or in cases where the angle between the unit normal to the surface of the component and the direction of blast wave propagation, ϕ , is greater than 45° . For components, which face the blast wave, or in cases where ϕ is equal to or less than 45° , the front-facing option is applicable. For cases involving the side/rear-facing option, the P-I diagram will involve **peak incident** overpressure and impulse. For the front-facing option, the P-I diagrams are expressed in terms of **peak reflected** overpressure and impulse. Throughout this discussion the term "pressure" will generally be used for "peak incident overpressure" and the term "reflected pressure" for "peak reflected overpressure".

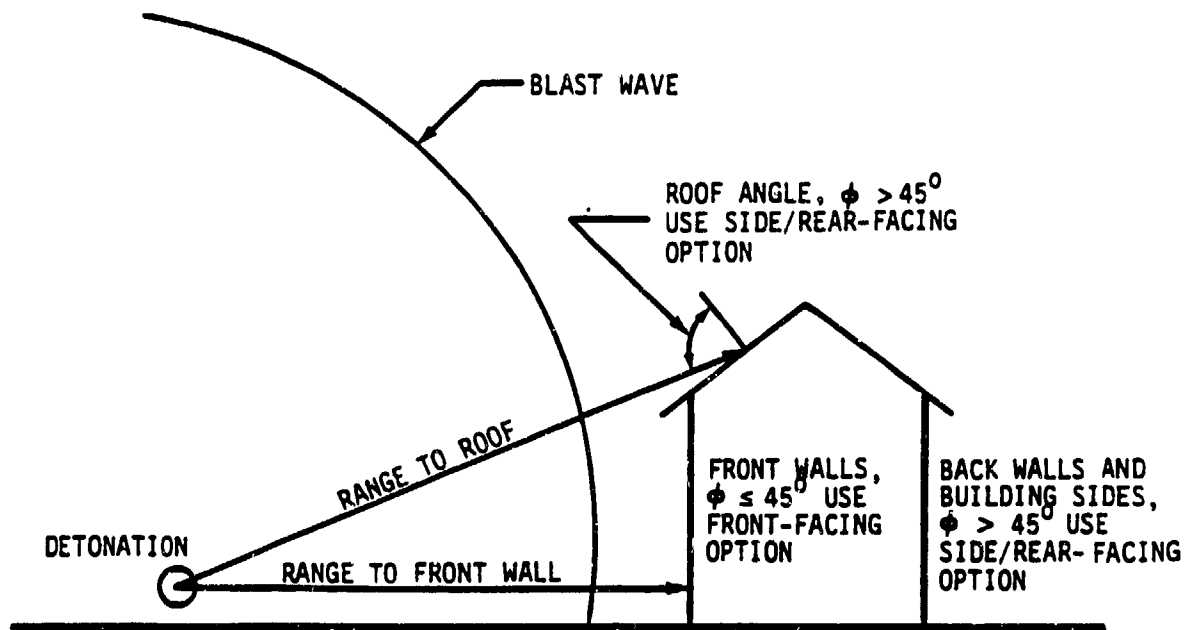


FIGURE 3. CRITERIA FOR USING FRONT-FACING OR SIDE/REAR-FACING OPTION

2.3 SYSTEM SPECIFICATIONS

VASDIP is designed for use with minimal equipment, consistent with the requirements for HEXDAH-B [2]. A summary of VASDIP equipment requirements is provided in Table 2.

TABLE 2. VASDIP EQUIPMENT REQUIREMENTS	
ITEM	DESCRIPTION
PROCESSING UNIT	IBM PC-XT/AT OR COMPATIBLE
DISK DRIVE	1 FLOPPY DRIVE AND/OR 1 HARD DISK DRIVE
PRINTER	(WITH GRAPHICS CAPABILITY)
MONITOR	MONOCHROME OR COLOR
GRAPHICS CARD	MONOCHROME, CGA, OR EGA
OPERATING SYSTEM	DOS 3.2 OR LATER
DEVICE DRIVERS	APPROPRIATE IBM OR GSS SOFTWARE
RAM	MINIMUM OF 512 KILOBYTES

2.4 SUGGESTED VALUES FOR STRUCTURAL PROPERTIES

In specifying the design parameters for a specific structural component the user will generally have some idea of the dimensions of the component and its general composition, configuration, orientation, and boundary conditions. The user may, however, be uncertain about certain parameters, especially involving spacings, densities, and strengths. For this reason, suggested values or equations for certain structural parameters are provided [3].

2.5 TYPICAL APPLICATIONS

In the design of structures, which may be exposed to a blast wave produced by an explosion, there is a general need for a means of rapidly computing the vulnerability of the structure to blast effects. Of special importance is the ability to determine how such vulnerability changes as structural design parameters are varied. For a given structural component, VASDIP is designed to provide the user with two basic items: P-I diagrams and vulnerability parameters.

P-I diagrams, such as shown in Figure 1, consist of three damage contours, corresponding to 0%, 50%, and 100% damage. Because of the hyperbolic shape of these contours, they can generally be divided into three segments or regions as follows:

- 1) Pressure-sensitive
- 2) Transition
- 3) Impulse-sensitive

If the user is aware of the magnitude of the pressures and impulses, which the component must be designed to withstand, he can vary the input parameters to VASDIP to generate a series of P-I diagrams. By such a procedure, he can optimize the design of the component, with respect to one or more parameters, to withstand specified pressures and impulses.

If the user is not certain as to the magnitude of the blast to which the structural component is exposed, he can use the vulnerability parameters generated by VASDIP to create a user-defined structure for input into HEXDAM-B [2]. He can then use HEXDAM-B to position the structural component at various ranges from a detonation (with a yield which can be varied over a range of values), and observe the resulting damage levels predicted by HEXDAM-B. By such a procedure, the user can establish how far from the detonation point, with a specified yield, a particular structural design is acceptable. As before, he can optimize the design with respect to one or more parameters by generating a number of different sets of vulnerability parameters for analysis with HEXDAM-B.

3.0 VASDIP INPUT PROCEDURES

The user supplies inputs to VASDIP by first selecting a specific type of structural component from the Master Menu, described in subsection 3.1, and then by responding to a series of prompts to provide the necessary structural specifications, as discussed in subsection 3.2. The user is also prompted concerning his choice of outputs, as discussed in subsection 3.3.

3.1 MASTER MENU

The Master Menu provides the user with a choice of the 24 different structural components identified in Table 1. These components consist of six concrete components, eight steel components, five masonry components, and five wood or timber components. After a particular component is selected and analyzed,

control is returned to the Master Menu to permit the user to select another component for analysis. When all analyses are complete, the user can exit the program by making the appropriate selection from the Master Menu.

3.2 STRUCTURE SPECIFICATIONS

For each of the twenty-four types of structural components, a special series of prompts is provided to permit specific details of a component to be input. **The units which the user should use in making his response are included in the prompt.** As noted in Section 2, the user is assumed to have some understanding of structural design. For certain parameters, suggested values are provided, as already noted [3]. For some parameters, reference to various handbooks [4-6] may be necessary.

The last three parameters to be input pertain to the damage thresholds or levels associated with "severe", "moderate", and "slight" damage. If the output of VASDIP is to be used with HEXDAM-B, these three damage thresholds should be set to 75%, 30%, and 5%, respectively.

3.3 OUTPUT OPTIONS

Immediately after selecting a structure component from the Master Menu, the user will be given the option of sending output to the printer. After the user has responded to all input prompts, a copy of all responses entitled "Structure Specifications" can also be output to the printer.

The user is given the option of generating pressure-impulse tables corresponding to 0%, 50%, and 100% damage. If he elects to generate these tables, the output can be sent to the printer, or can be displayed on the screen. The user is also given the option of generating a pressure-impulse plot, in the form of a hard copy, and/or a similar display on the monitor screen.

In all cases the user will be provided, either on the printer or on the monitor, with values for the vulnerability parameters used with HEXDAM-B. Further discussion of these outputs is included in Section 4.

4.0 VASDIP OUTPUT

The VASDIP output consists of four items

- Structure Specifications,
- Pressure-Impulse Tables,
- Pressure-Impulse Plots, and
- Vulnerability Parameters.

These outputs and the associated options are discussed in subsections 4.1 through 4.3.

4.1 STRUCTURE SPECIFICATIONS

The structure specifications represent a tabulation of all input parameters. An example of these specifications for a one-way reinforced concrete slab is provided in Figure 4.

```
ONE-WAY REINFORCED CONCRETE SLABS                      ** VASDIP **** EMI **
*****
                        STRUCTURE SPECIFICATIONS
*****
ORIENTATION                      : SIDE/REAR FACING
SLAB SPAN (FT)                   : 5.000000E+00
CROSS-SECTIONAL AREA OF SLAB SECTION (SQ.IN.): 3.60000E+001
TENSILE STEEL AREA (SQ.IN.)      : 4.30000E-001
SLAB SECTION WIDTH (IN)          : 1.20000E+001
DEPTH OF TENSILE REINFORCEMENT (IN) : 3.00000E+000
YIELD STRENGTH OF REINFORCEMENT (PSI) : 3.600000E+04
COMPRESSIVE STRENGTH OF CONCRETE (PSI) : 4.000000E+03
WEIGHT DENSITY OF SECTION (LBF/FT**3) : 1.500000E-02
BOUNDARY CONDITIONS               : FIXED-FIXED
SEVERE DAMAGE THRESHOLD (%)       : 7.500000E+01
MODERATE DAMAGE THRESHOLD (%)     : 3.000000E+01
SLIGHT DAMAGE THRESHOLD (%)       : 5.000000E+00
*****
```

FIGURE 4. EXAMPLE OF STRUCTURE SPECIFICATION OUTPUT

4.2 PRESSURE-IMPULSE TABLES AND PLOTS

For each damage contour (0%, 50%, 100%), a pressure-impulse table can be output, consisting of 500 values of pressure and impulse. In addition, VASDIP offers the user a P-I plot similar to Figure 1. An example of this plot, corresponding to the structure specifications shown in Figure 4 is presented in Figure 5.

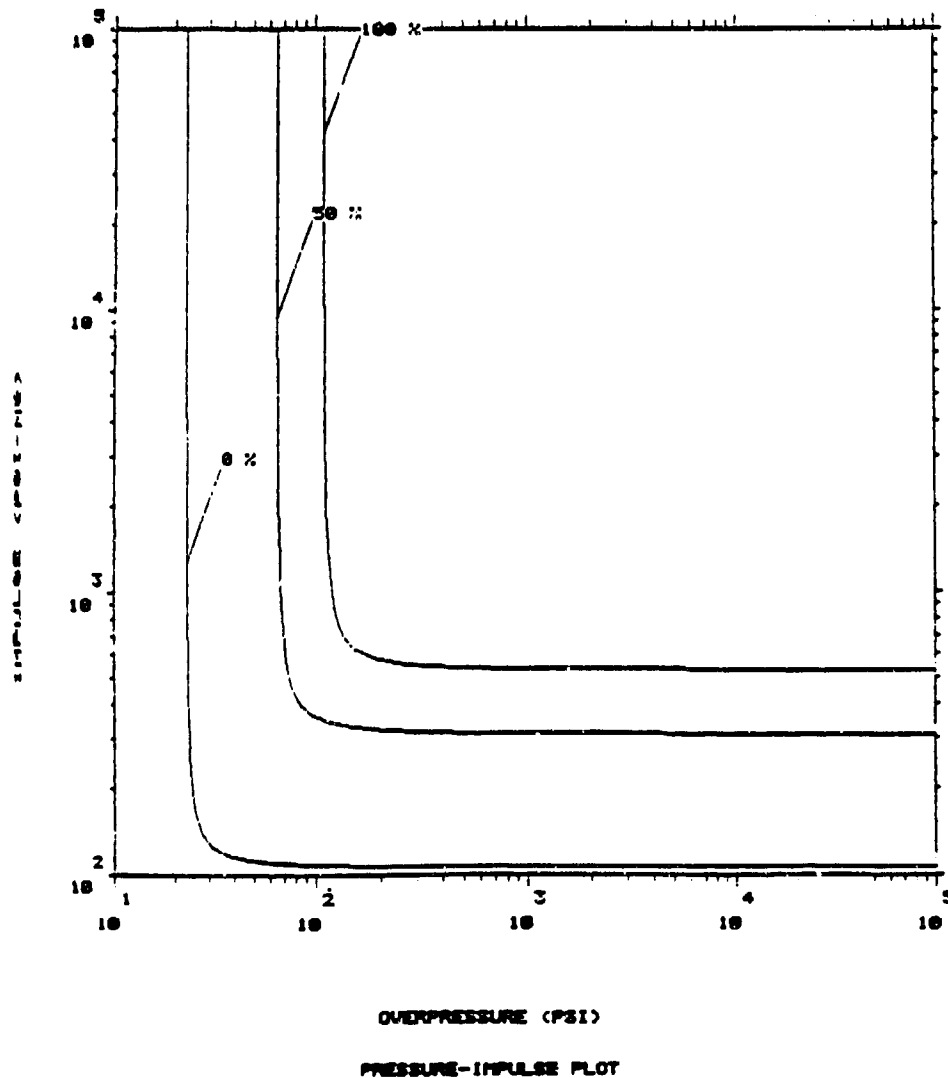


FIGURE 5. EXAMPLE OF PRESSURE-IMPULSE PLOT OUTPUT

4.3 VULNERABILITY PARAMETERS

For all cases, values for five vulnerability parameters are output either to the printer or the monitor, depending on the Print option selected. These five parameters are

- overpressure causing severe damage to a P-type structure, $P(S)$,
- overpressure causing moderate damage to a P-type structure, $P(M)$,
- pulse duration factor associated with severe damage, $K(S)$,
- pulse duration factor associated with moderate damage, $K(M)$ and
- reference yield above which structure is insensitive to impulse.

These five parameters are designed to be used as inputs in the construction of a User-Defined Structure Data File (UDSDF) for HEXDAM-B [2]. An example of the vulnerability parameters, corresponding to the case of a one-way reinforced concrete slab, as specified in Figure 4, is presented in Figure 6.

```
*****
***** VULNERABILITY PARAMETERS *****
*****
P(S)= 8.40404053E+001 PSI      K(S)= 4.058758000E-01
P(M)= 4.28725959E+001 PSI      K(M)= 2.022520000E-01
REFERENCE YIELD (LBS) = 1.463459E+05
*****
```

FIGURE 6. EXAMPLE OF VULNERABILITY PARAMETER OUTPUT

5.0 VALIDATION

For each of the twenty-four structural components covered by VASDIP, a comparison was made between hand calculations and the results using the software. For eight cases, these calculations were taken from examples in the original SRI report [1]. Five other cases were taken from SRI hand calculations associated with the validation of HEXDAM [7]. For those eleven cases not covered by either of the previous references, the hand calculations were performed by Engineering Analysis, Inc. personnel. Agreement between hand calculations and the VASDIP output was quite satisfactory.

6.0 SAMPLE PROBLEM

In order to demonstrate the application of VASDIP, a sample problem involving a lightweight reinforced concrete roof is presented in the paragraphs which follow.

The lightweight reinforced concrete roof is taken to be a 4" one-way reinforced concrete slab, as shown in Figure 7 with the following dimensions:

- slab section width, $b = 12$ in.
- slab section thickness, $T_c = 4$ in.
- slab section cross-sectional area, $A = 48$ in.²
- slab span, $\ell = 15$ ft.
- tensile steel area, $A_s = .2016$ in.²
- depth of tensile reinforcement, $d = 3$ in.

Structural properties are taken as follows [1]:

- compressive strength of concrete, $f'_c = 4000$ psi
- yield strength of reinforcement, $f_y = 50,000$ psi
- weight density, $\gamma = 150$ lb_f/ft³

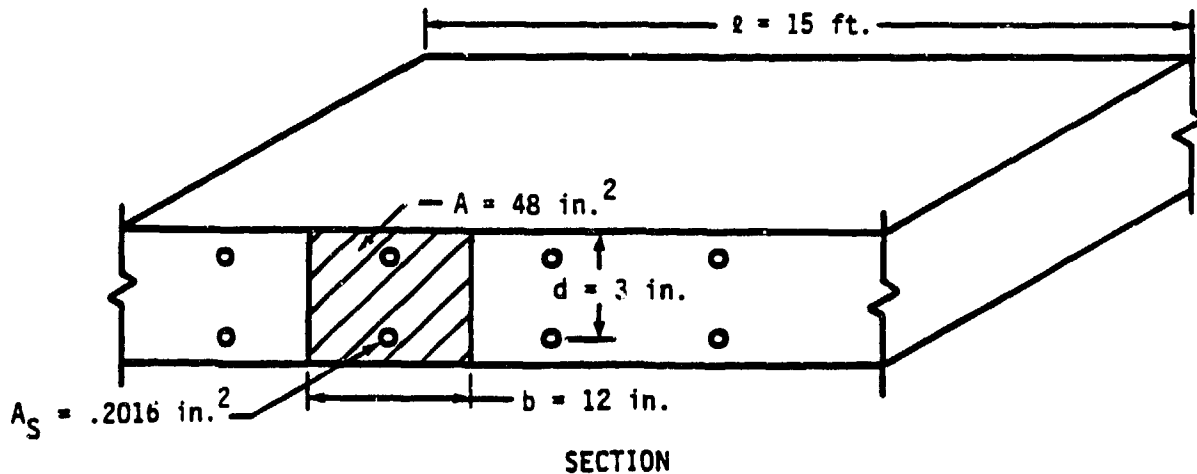


FIGURE 7. CONCRETE ROOF DIAGRAM, SAMPLE PROBLEM

The boundary conditions are assumed to be simple-simple and the orientation angle, ϕ , is assumed to be $< 45^\circ$, resulting in a front-facing orientation.

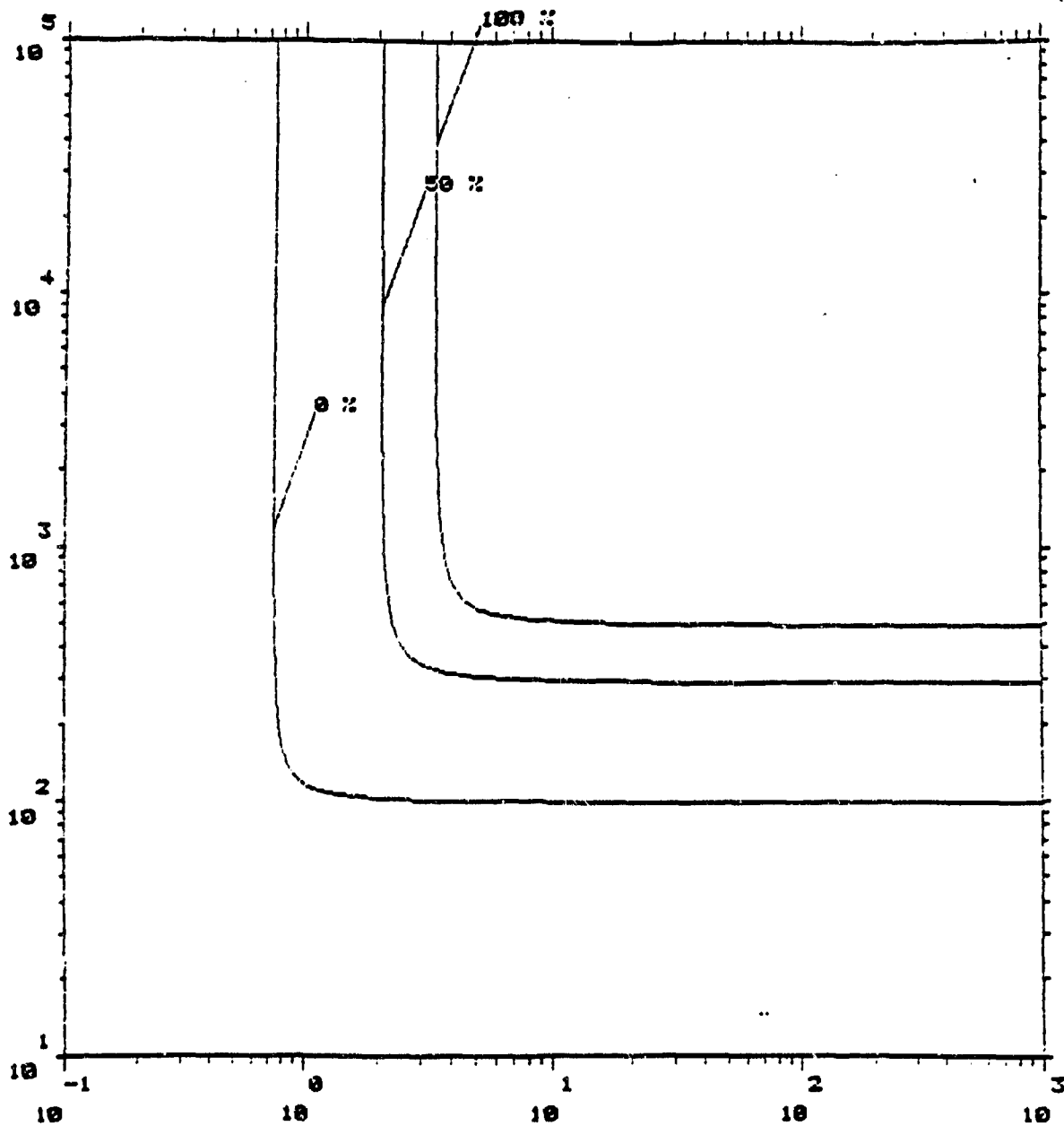
The corresponding inputs to VASDIP are presented in Figure 8. The resulting outputs, without the P-I tables, are presented in Figures 9 through 11.

```
* ONE-WAY REINFORCED CONCRETE SLABS *****
ENTER ORIENTATION (F FOR FRONT FACING OR S FOR SIDE/REAR FACING): F
ENTER SLAB SPAN (FT): 15
ENTER CROSS-SECTIONAL AREA OF SLAB SECTION (SQ.IN.): 48
ENTER TENSILE STEEL AREA (SQ.IN.): .2016
ENTER SLAB SECTION WIDTH (IN): 12
ENTER DEPTH OF TENSILE REINFORCEMENT (IN): 3
ENTER YIELD STRENGTH OF REINFORCEMENT (PSI): 5E4
ENTER COMPRESSIVE STRENGTH OF CONCRETE (PSI): 4E3
ENTER WEIGHT DENSITY OF SECTION (LBF/FT**3): 150
ENTER BOUNDARY CONDITIONS (S FOR SIMPLE-SIMPLE
OR F FOR FIXED-FIXED): S
ENTER SEVERE DAMAGE THRESHOLD (%): 75
ENTER MODERATE DAMAGE THRESHOLD (%): 30
ENTER SLIGHT DAMAGE THRESHOLD (%): 5
```

FIGURE 8. INPUT PROMPTS AND RESPONSES, SAMPLE PROBLEM

```
ONE-WAY REINFORCED CONCRETE SLABS                ** VASDIP **** EAI **
*****
                STRUCTURE SPECIFICATIONS
*****
ORIENTATION                                : FRONT FACING
SLAB SPAN (FT)                             : 1.500000E+01
CROSS-SECTIONAL AREA OF SLAB SECTION (SQ.IN.): 4.80000E+001
TENSILE STEEL AREA (SQ.IN.)                : 2.01600E-001
SLAB SECTION WIDTH (IN)                   : 1.20000E+001
DEPTH OF TENSILE REINFORCEMENT (IN)        : 3.00000E+000
YIELD STRENGTH OF REINFORCEMENT (PSI)      : 5.000000E+04
COMPRESSIVE STRENGTH OF CONCRETE (PSI)     : 4.000000E+03
WEIGHT DENSITY OF SECTION (LBF/FT**3)      : 1.500000E+02
BOUNDARY CONDITIONS                        : SIMPLE-SIMPLE
SEVERE DAMAGE THRESHOLD (%)                 : 7.500000E+01
MODERATE DAMAGE THRESHOLD (%)               : 3.000000E+01
SLIGHT DAMAGE THRESHOLD (%)                : 5.000000E+00
*****
```

FIGURE 9. STRUCTURE SPECIFICATIONS OUTPUT, SAMPLE PROBLEM



REFLECTED OVERPRESSURE (PSI)

PRESSURE-IMPULSE PLOT

FIGURE 10. PRESSURE-IMPULSE PLOT OUTPUT, SAMPLE PROBLEM


```

-----
VULNERABILITY PARAMETERS
-----
F(S)= 1.29724513E+000 PSI      K(S)= 1.371534000E-01
F(M)= 6.72633323E-001 PSI      K(M)= 7.290347000E-02
REFERENCE YIELD (LBS) = 1.574017E+08
-----

```

FIGURE 11. VULNERABILITY PARAMETERS OUTPUT, SAMPLE PROBLEM

7.0 CONCLUSION

The VASDIP software has been demonstrated to be a useful engineering tool in calculating the vulnerability of structures to blast overpressures and impulses. The software has been validated by comparison with hand calculations. VASDIP not only provides dimensional pressure impulse diagrams, but also provides the necessary vulnerability parameters for use as inputs to the HEXDAM-B software. By means of such software an engineer can rapidly evaluate a series of different designs for withstanding a specified explosion.

8.0 REFERENCES

1. Whitney, M.G., Ketchum, D.E., and Polcyn, M.A., "Blast Vulnerability Guide", Project No. 06-1473-040, Southwest Research Institute, San Antonio, Texas, October 1987.
2. Tatom, Frank B., "Enhanced High Explosive Damage Assessment Model - Second Industrial Version (HEXDAM-B) User's Manual", EAI-TR-89-003, Engineering Analysis, Inc., Huntsville, Alabama, June 1989.
3. Tatom, Frank B., "Vulnerability Assessment of Structurally Damaging Impulses and Pressures (VASDIP) Users Manual", EAI-TR-90-001, Engineering Analysis, Inc., Huntsville, Alabama, January 1990.
4. Manual of Steel Construction, American Institute of Steel Construction, 9th Edition. Chicago, Illinois, 1989.
5. Standard Specifications, Load Tables, and Weight Tables for Steel Joists and Joist Girders, Steel Joist Institute, Murrelle Beach, South Carolina, 1989.
6. Mark's Standard Handbook for Mechanical Engineers, 8th Edition, New York, New York, 1979.
7. Tatom, Frank B., "Evaluation of HEXDAM Damage Prediction Algorithm", EAI-TR-89-005A, Engineering Analysis, Inc., Huntsville, Alabama, November 1989.

CHARGE CALCULATION FOR UNDERWATER BLAST DEMOLITION AND ITS APPLICATION

He Chengzhi and Li Zheng
Engineering Design and Research Institute
P.O.Box 55, Beijing 100053, P.R.China

Wang Zhongqian
Academy of Railway Science
Beijing, P.R.China

ABSTRACT

It appears to be an effective method to demolish concrete containers or container-like structures by underwater blast. As compared with conventional blast by charge within drilled holes, underwater blast has advantages in some respects such as simplicity of work process, lower cost, lower noise, less effect of air blast wave and better control of fragments.

In this paper, equations for underwater blast charge calculation are analyzed and derived for cylindrical and rectangular structures on the basis of properties of underwater blast loading, strength and dynamic characteristics of structures, and two examples of application are given.

CHARGE CALCULATION FOR UNDERWATER BLAST DEMOLITION AND ITS APPLICATION

It appears to be a relatively effective method to demolish concrete containers or container-like structures by underwater blast. As compared with conventional blast by charge within drilled holes, underwater blast has advantages at least in some aspects as below:

1. Simplicity of work process;
2. Lower cost;
3. Lower noise;
4. Less effect of air blast wave;
5. Better control of direction and range of scattered fragments.

Thus, since 1978, research work on underwater blast demolition for application within urban area has started by organizations of railway engineering.

I. BLAST WAVE OF WATER PRESSURE

The demolition object with peripheric faces exposed above ground and footing underground may be considered as an one degree freedom structure, and according to D'Alembert's principle, the vibration equation for this structure with damping under dynamic load may be expressed as

$$m\ddot{y}(t) + \gamma\dot{y}(t) + Ky(t) = P(t) \quad (1)$$

if we substitute $\gamma = 2\xi m\omega$ into equation (1), we get

$$\ddot{y}(t) + 2\xi\omega\dot{y}(t) + \omega^2 y(t) = \frac{1}{m}P(t) \quad (2)$$

when $t > u$, the solution of equation (2) is

$$y(t) = \frac{1}{m\bar{\omega}} \int_0^t P(u) e^{-\xi\gamma\bar{\omega}(t-u)} \sin \bar{\omega}(t-u) du \quad (3)$$

where $y(t)$ --- displacement of vibration;

m --- mass;

K --- stiffness factor;

γ --- damping factor;

ξ --- damping ratio;

ω --- natural circular frequency without damping,

$$\omega = \sqrt{\frac{K}{m}};$$

$\bar{\omega}$ --- natural circular frequency with damping,

$$\bar{\omega} = \frac{\omega}{\sqrt{1 + \frac{1}{4}\gamma^2}};$$

$P(t)$ --- dynamic load.

Generally we call equation (3) as Duhamel Integral for system with damping, it may be used to calculate the response of one degree freedom system with damping under dynamic load of any type. Usually, when explosives being blasted underwater, the duration τ for blast wave of water is much less than that for air blast, the difference is about two order of magnitude. Also the charge weight needed for underwater blast is relatively small, therefore under general condition, $\tau < \frac{1}{4}T$ (T ---natural period of structure). Thus the demolish action of blast wave in water to a structure may be considered as the action of im-

pulse 1, as shown in Figure (1)

Since impulse I is expressed as

$$I = \int_0^{\infty} P(t) dt, \quad t \rightarrow 0, \quad P(t) \rightarrow \infty$$

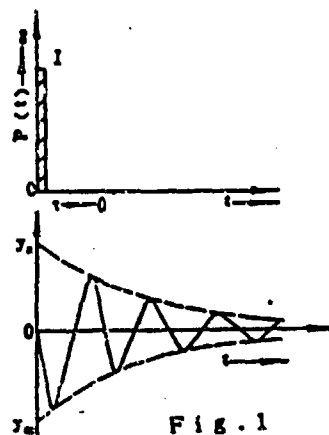
at this time, $y(t) = \frac{I}{m\omega} e^{-\gamma/\gamma_0 t} \times \sin \omega t$

$$y_m = \frac{I}{m\omega} e^{-\gamma/\gamma_0 t}, \quad t_m \approx \frac{1}{4} \bar{T}$$

$$y_1 = \frac{I}{m\omega} e^{-\gamma/\gamma_0 t}, \quad t_1 \approx \frac{3}{4} \bar{T}$$

$$\bar{T} = \frac{2\pi}{\omega}$$

$$P_{eq} = Ky_m = I\omega e^{-\gamma/\gamma_0 t}$$



where P_{eq} --- equivalent static load, under the action of this load, the max. displacement of structure is the same as that under the action of blast wave impulse 1.

Generally the internal damping is rather small for ordinary construction materials, $\gamma = 0.015$ for concrete, $\gamma = 0.015 \sim 0.018$ for reinforced concrete, therefore:

and $e^{-\gamma/\gamma_0 t} \approx 1$

$$\bar{\omega} = \frac{\omega}{\sqrt{1 + \frac{1}{4} \gamma^2}} \approx \omega$$

Therefore, equation (4) may be more simplified as

$$P_{eq} = I\omega \quad \text{kg/cm}^2 \quad (5)$$

For TNT of density 1.5 g/cm^3 , when being blasted underwater, the impulse I on unit area at distance R may be calculated by

$$I = 0.0588 Q^{1/3} \left(\frac{Q^{1/3}}{R} \right)^{0.49} \quad \text{kg.sec/cm}^2 \quad (6)$$

where Q --- charge wt., kg;

R --- distance from blast center to the loading face
of structure, m.

Substitute equation (6) into equation (5), we get the
equivalent static load of water pressure blast

$$P_{\text{eq}} = 0.0588 Q^{1/3} \left(\frac{Q^{1/3}}{R} \right)^{0.89} \omega \quad (7)$$

II. EQUATION OF CHARGE CALCULATION FOR UNDERWATER BLAST

In the application of underwater blast demolition, usually we deal with cylindrical and rectangular structures. Thus, the equations of charge calculation for underwater blast demolition of these two types of structure shape are discussed in this paper. For shapes that are nearly rectangular or cylindrical, they may be treated as cylindrical or rectangular by some simplification of shape.

1. Thin Wall RC Cylinder

The definition for a thin wall cylinder is that $\delta/R < 0.1$, where δ is the wall thickness, and R is the radius of cylinder.

The natural frequency of a cylinder is

$$\omega = \frac{c}{R} \quad (8)$$

where c --- velocity of sound wave within concrete, m/sec,
see Table 1;

R --- radius of cylinder, m.

Table 1 Values of R and c for Concrete

Mark No. of Concrete	100	150	200	250	300	350	400
R_t (kg/cm ²)	8.0	10.5	13.0	15.5	17.5	21.5	24.5
c (m/sec)	2760	3060	3260	3420	3500	3585	3670
$K_d R_t / 0.0588c$	0.069	0.082	0.095	0.108	0.119	0.142	0.159

For a thin wall concrete cylinder under uniform internal pressure, if the charge center is placed at the center of cylinder, then the stress of cylinder wall is

$$\sigma = \frac{P \cdot R}{\delta}$$

When this stress exceeds the strength of concrete, failure of the structure will occur. But for blast demolition, this stress will exceed the strength of concrete extremely, then a factor K_d is introduced, which is called the factor of damage degree for the structure after blast, thus we get:

$$\sigma = \frac{P \cdot R}{\delta} \geq K_d K_t R_t \quad (9)$$

Substitute equations (7) and (8) into (9), we get the equation for charge calculation of a thin wall concrete cylinder.

$$Q_{cyl} = \left(\frac{K_d K_t R_t}{0.0588 \times c} \right)^{1.39} \delta^{1.39} R^{1.41}, \quad \text{kg} \quad (10)$$

where K_d --- factor of increased dynamic strength for concrete, $K_d = 1.4$;

R_t --- static tensile strength of concrete, kg/cm²,

see Table 1;

δ --- wall thickness of cylinder, m;

K_b --- factor of damage degree for structure after blast

(1) Correction Factor for Reinforcement

Usually we have reinforcement in the wall of concrete cylinder, we may approximately treat this problem by changing the area of steel to area of concrete according to static tensile strength ratio of steel and concrete, then evaluate the factor K_s for reinforcement. The charge value from equation (10) should be multiplied by K_s to increase its value.

$$Q_c = K_s Q_{c0} \quad (11)$$

$$\text{where } K_s = 1 + \frac{K_{ds} R_s (\sum A_s)}{K_t R_t b \delta} \quad (11a)$$

and b --- unit width, $b=1\text{m}$;

K_{ds} --- factor of increased dynamic strength for steel,
 $K_{ds}=1.35$ for mild steel;

R_s --- static yield strength of steel, here we use $R_s=$
 3800 kg/cm^2 ;

$\sum A_s$ --- the total area of circumferential steel along
unit length b of longitudinal section, m^2

(2) Factor of Damage Degree, K_d

As for the requirement of blast demolition, the damage degree of structure exceeds by far that at plastic deformation stage, and may be expressed by factor of damage degree K_d .

K_d may be divided as three damage levels, and the value of

K_b for each level may be determined by previous data and simulated test.

Damage Level I ($K_b = 10$)

Cross pattern of breakage of concrete.

Spalling of surface layer.

Damage Level II ($K_b = 20$)

Partial failure of structure.

Concrete cracked into pieces, but most of them retained on steel reinforcement.

Some flying fragments.

Damage Level III ($K_b = 40$)

Complete failure of structure.

Most cracked pieces of concrete apart from steel reinforcement.

Many flying fragments.

(3) Correction Factor for Thick Wall Cylinder ($\delta \geq \frac{R}{10}$)

As equations (10) and (11) are suitable for thin wall cylinder, when used for thick wall cylinder, the charge value from equation (10) or (11) should be multiplied by K_1 to increase its value. K_1 is called correction factor for thick wall cylinder, as shown in Table 2.

Table 2 Correction Factor for Thick Wall Cylinder, K_1

d/R	0.2	0.4	0.6	0.8	1.0
K_1	1.16	1.38	1.64	1.92	2.22

2. Concrete Structure of Rectangular Shape

A structure of rectangular cross section is shown in Figure 2.

The natural circular frequency for a rectangular structure is

$$\omega = \frac{0.23\delta c\Omega}{l^2} \quad (12)$$

where δ --- wall thickness of concrete structure, m;
 c --- velocity of sound wave within concrete, m/sec;
 L --- length of one side of rectangular, m;
 Ω --- frequency factor, see Table 3.

Under uniform static pressure P_{eq} , the moment will be maximum at the corner of a rectangular structure, the stress at the corner will be

$$\sigma = \frac{6K_n P_{eq} l^2}{b\delta^2} \quad (13)$$

where K_n --- moment factor;
 b --- width of section, use 1m;

Substitute equations (7) & (12) into equation (13), and also considering the correction factor for reinforcement K_r from equation (11a), then the equation for charge calculation of reinforced concrete rectangular structure will be

$$Q_{rcc} = \left(\frac{K_r K_n R_t b}{0.0811 \times K_n \Omega c} \right)^{1.59} \delta^{1.59} R^{1.41}, \quad (14)$$

where R --- perpendicular distance from inner surface of wall to charge center, m.

The value of K_n and Ω for various length ratio are shown in Table 3.

Table 3 Values of K_n and Ω for Rectangular Structure

B/L	0.5	0.6	0.7	0.8	0.9	1.0	1.2	1.4	1.6	1.8	2.0
Ω	15.20	14.40	13.35	12.20	11.10	9.85	7.80	6.20	4.60	2.90	1.40
K_n	0.062	0.063	0.066	0.070	0.076	0.083	0.103	0.125	0.163	0.203	0.250
$K_n \Omega$	0.94	0.91	0.88	0.85	0.84	0.82	0.80	0.78	0.75	0.58	0.35

III. APPLICATION

Example 1

A trapezoidal hollow concrete block is shown in Fig 3, the volume of concrete is 1.02m^3 . This block is used in field experiment for mounting transducers for ground vibration measurement. The mark no. of concrete is 400. The wall thickness varies from 0.2--0.44m, take $\delta=0.3\text{m}$ as mean value.

For blast demolition, the block is overturned with hollow bottom up and filled with water. The charge bag is banged within water and covered with straw bags at top of block.

For simplification, the trapezoidal hollow space is treated as an equivalent rectangular, take $B/L=0.7$, from Table 3 we get:

$$K_n = 0.066, \quad \Omega = 13.35,$$

From Table 1 we get

$$K_d = 1.4, \quad R_t = 24.5 \text{ kg/cm}^2, \quad c = 3670 \text{ m/sec}$$

for concrete of mark no. 400.

And from the arrangement of reinforcement we get $K_s = 2.0$.

Three blocks were demolished by underwater blast with different charges, $Q_1=0.15\text{kg}$, $Q_2=0.30\text{kg}$ and $Q_3=0.80\text{kg}$.

Transform equation (14) into following form, and compute value K_s for charge Q_1 , Q_2 and Q_3 respectively, then to predict

the degree of blast damage.

$$K_b = \frac{0.0811 \times K_n \cdot \Omega \cdot c}{K_s \cdot R_t \cdot b \cdot \delta} \left(\frac{Q}{K_s} \right)^{0.43} R^{-0.39}$$

The calculated K_b and underwater blast results are shown in Table 4.

Table 4 Underwater Blast Results of Trapezoidal Concrete Hollow Block

Charge No.	Charge Wt.(kg)	Charge per Unit Volume	Calculated K_b	Blast Results
Q ₁	0.15	0.147	14.5	Cracked to form large pieces, basically the thick wall cracked at corners, and the thin wall broke into small pieces near around, no flying fragments
Q ₂	0.30	0.294	22.5	Broke into five large pieces, part of steel reinforcement separated, many small pieces, flying fragments within 10m.
Q ₃	0.80	0.784	42.0	Total concrete blasted to small pieces, part of steel reinforcement separated, flying fragments within 50m, ready for clear up.

Example 2

A reinforced concrete chamber is shown in Fig. 4. The chamber is used in field experiment as a measurement station.

The thickness of four side walls is 0.15m, and the thickness of top slab is 0.10m. The inner dimension is 4.0m in length, 2.0m in width and 1.8m in height. Mark no. of concrete is 200, with $\phi 12@180$ mesh and $\phi 8@180$ mesh steel reinforcement, one layer each respectively.

The charge wt. is calculated from equation (14).

As the blast was taken at spacious area, and there are no problems about safety distances, therefore we chose the factor of damage degree $K_s=30$.

From Table 1, for concrete mark no. 200, $K_c=1.4$, $R_c=13$ kg/cm², $c=2362$ m/sec, $\delta=0.15$ m.

For uniformity of wall damage, two charge bags are designed. The distance between bags is 2m, distance to end walls are 1m. As the front wall has wing wall extended on each end, the charge bag is a little nearer to the front wall, the distance is 0.95m, and the distance from bag to the rear wall is 1.05m. The average distance $R=1.0$ m is used in calculation. As there are two charge bags, the chamber may be considered as two squares, thus $B/L=1.0$. From Table 3, we have $K_n=0.083$, $\Omega=9.85$.

For steel of mark no. 3, $K_s=1.35$ and $R_s=3800$ kg/cm². The total steel area per unit length of concrete is $\Sigma A_s=9.05$ cm².

From equation (11a), we get $K_s=2.71$.

The calculated charge wt. for each bag will be

$$\begin{aligned}
 Q &= K_s \left(\frac{K_s K_c R_s b}{0.0811 K_n \Omega c} \right)^{1.59} \delta^{1.59} R^{1.41} \\
 &= 2.71 \left(\frac{30 \times 1.4 \times 13 \times 1}{0.0811 \times 0.083 \times 9.85 \times 2360} \right)^{1.59} \times (0.15)^{1.59} \times (1.0)^{1.41} \\
 &= 0.58 \text{ kg}
 \end{aligned}$$

In practice, the charge bags are made of powder TNT, the actual wt. for each bag is 0.65kg. The bag are 0.6m above bottom slab. The water height is about 1.5m.

After blast, the concrete break into pieces, most pieces are still hanging on the reinforcement steel mesh, with some flying fragments within 30m range. This result fulfills the blast requirement. The wing walls which have no contact with water are basically no damage, and as the wing walls attribute some stiffening to the front wall, the damage of front wall is somewhat lighter than other walls.

As the distance from charge bag to rear wall is 11% larger than that to front wall, the top slab of chamber is turned to the rear, and water flushed out from the opening between the top slab and front wall.

The result of blast is shown in Fig.5

CONCLUSION

The equations presented in this paper give satisfactory results in practice of blast demolition.

REFERENCES

1. J. Henrych, "The Dynamics of Explosion and Its Use" , 1979
2. R. W. Clough and J. Penzien, "Dynamics of Structures", 1975
3. R. H. Cole, "Underwater Explosions", Princeton University Press.

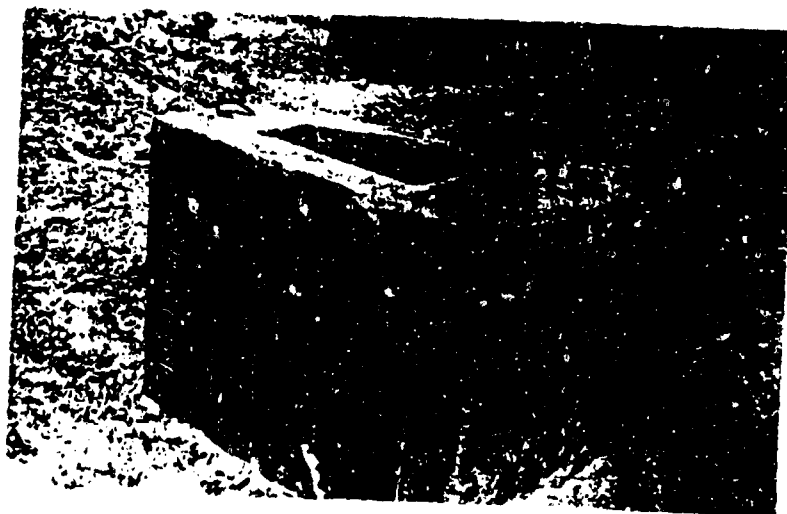


Fig. 3



Fig. 5

NOISE ABATEMENT AT FMC HOLLISTER SITE

Kathy H. Spivey
Wilfred Baker Engineering, Inc.

Dr. Wilfred E. Baker
Wilfred Baker Engineering, Inc.

ABSTRACT

FMC Corporation conducts extensive outdoor explosives testing at a test site near Hollister, California. There are two, well-separated firing areas on the site, plus a number of explosives storage magazines. Maximum amount of high explosive detonated in any test is about 25 pounds. The nearest property line to a test arena is 1,440 feet, while the nearest inhabited building is the site owner's ranch house, about 3,300 feet NNE of one test arena. However, new housing construction is taking place closer to the site and the problem of noise disturbance is increasing. FMC would like to preserve good community relations. Thus, a feasibility study for noise mitigation at the site was conducted.

This paper gives a review of the site visit and presents a number of options for noise abatement and control including use of suppressive shields, complete containment, variation on munition test structures, aqueous foam, computer-based meteorological focusing predictions and portable sound level measuring systems. It evaluates the options, gives approximate costs, and confidence levels of each option, and gives our conclusions and recommendations. It also includes pertinent references.

BACKGROUND

FMC Corporation requested that a feasibility study for noise mitigation at their test site near Hollister, California be conducted. FMC felt they had good community relations in Hollister, and did not want to jeopardize these relations. To assure that community disturbance was minimized, various methods of noise mitigation for their explosives testing were studied. Work included a visit to the Hollister site; discussions with FMC personnel regarding testing facility layout, arrangements, and constraints; and reporting of various mitigation techniques, availability of equipment, and success confidence levels for each technique.

There are two firing arenas on the site and a number of explosive storage magazines. All magazines conform to government explosives storage criteria, and are not of concern in noise mitigation. At the Hollister site, there are no off-site restrictions based on U.S. Government explosives safety regulations and standards (Quantity-Distance Standards) even with much greater than 25 pounds of explosive detonated at either firing arena. The city of Hollister is west of the site. Both areas are located in natural arroyos in the hilly countryside. The maximum amount tested has been 17 pounds of high explosive (HE). FMC wished to test up to 25 pounds total HE at either arena. There is no blast containment at any of the present firing sites, but there is extensive barricading.

Arena #1 has two firing pads and an explosives arena. One firing pad is arranged for flash x-ray and high-speed camera instrumentation of detonating hardware. There are protective barricades for the flash x-ray equipment and cameras. The other firing pad is used primarily for gun launch and impact testing. Much of the equipment tested or used for diagnostics is heavy, so forklift access to all parts of the arenas is a necessity. This arena also has an explosives loading room and a

well-barricaded firing bunker. Arena #2 is smaller and newer than Arena #1. It too, requires forklift access, has barricades to protect instrumentation, a loading room, and a personnel bunker for instrumentation and firing control.

A number of concepts for explosive noise mitigation were developed using previously analyzed and tested configurations. These were felt to be quite promising for control of off-site noise.

DESCRIPTION OF CONCEPT

Suppressive Shields

In 1968, an Edgewood Arsenal program resulted in the initial concept for suppressive shields (SS). The suppressive shield program was very active in the mid-1970's. Several concepts for fixed, vented panels and structures were developed, analyzed and tested (Refs. 1-13). These uniformly vented panels were intended to strongly attenuate air blast passing through them to a safe level at a prescribed distance, arrest high-speed fragments, and to reduce the diameter of the fireball generated by the explosion.

There is no doubt, from Ref. 1, that suitable suppressive shields can be designed and constructed of standard structural steel components to completely surround each firing site. A rectangular box structure would form the framework for the shield, and vented panels could consist of a number of layers of perforated plates, nested I-beams, or nested angles, as shown in Figure 1. One panel could be a full-height door, large enough for access of a fully-loaded forklift.

The closest safety-approved shield design is the Group 4 design, shown in Figure 2, including a cross-section through a vented panel. This shield has interior dimensions of 9.2 feet wide by 13.1 feet long by 9.3 feet high. It is designed for 10.6 pounds of TNT and a serious fragment hazard. It has been proof tested with 12.7 pounds of TNT in a heavy case.

Although this specific shield design is not large enough, nor does it have a large enough door opening for FMC test arenas, a slightly larger shield with a larger door can be designed and should prove quite adequate. Desired internal dimensions are 16 feet wide with a 6-foot opening full height door in the wall center, 10 feet high and 12 feet deep. Scaled test data summarized in Ref. 1 allow design of a suppressive shield to provide a range of blast wave attenuations.

A variation on the suppressive shields concept which could prove to be less expensive to build and more desirable for operations consists of a structure with a strong, welded I-beam framework, with walls filled with dropped-in railroad ties, as shown schematically in Figure 3a. The roof should probably be made of welded, interleaved I-beams, as shown in Figure 3b. The door should open outward for ease in operations, and could be of similar construction to either the walls or roof.

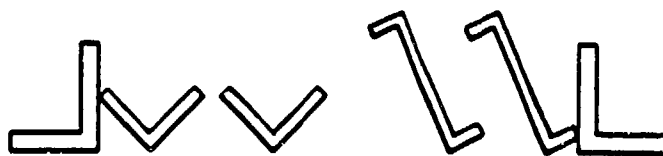
Variation on "Momentum Trap" Structure

Figure 4 is a schematic of the Eglin AFB "momentum trap" test structure. It consists of a pair of massive concrete piers topped by a welded steel I-beam and plate "roof," which is emplaced by a crane, and not tied to the piers. At either end of the internal volume, steel plates are hung from supports allowing the impulse from internal explosions to be converted to plate momentum. The plates are apparently massive enough that plate velocities are low, and plate swing is limited by gravity and air drag.

For tests with up to 25 lbs of HE and fragment impacts, this design would probably be inadequate for repeated tests, because of accumulated blast and fragment damage to the concrete piers. It is strongly suggested that the concrete piers be replaced by a double-walled steel



(a) Nested Angles



(b) Side-By-Side Angles or Zees



(c) Louvres



(d) Interlocked I-Beams

Figure 1. Cross-Sections for Some Vented Panel Designs for
Suppressive Shields

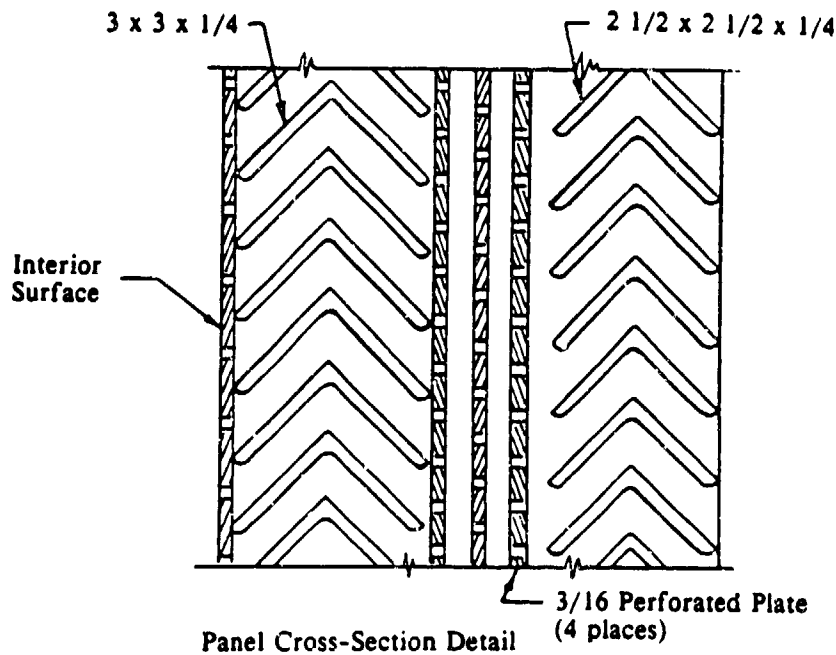


Figure 2. Group 4 Suppressive Shield (Ref. 1)

construction, filled with sand or gravel, as shown in Figure 5. The suspended steel plates could be replaced with woven wire rope blasting mats, which are more flexible and probably less easily damaged by fragment impacts. The "momentum traps" should also be larger than the openings between piers, to prevent them swinging into the interior volume of the structure.

Complete Containment Structures

A number of government and private agencies employ complete containment test fire chambers to mitigate noise from explosive tests. All of these chambers include many portholes and instrument lead passthroughs, so design of these accoutrements is straightforward. For example, U.S. Army Ballistic Research Laboratories use a 30-foot 3-inch thick, steel blast sphere which has an explosive limit of 500 lbs TNT (although it is limited to 20 lbs in repetitive testing); Battelle Memorial Labs uses a cylindrical reinforced-concrete structure with top and bottom domes, 40 feet in diameter and 30 feet in height, with an explosive limit of 50 lbs TNT; EG & G Mound uses a horizontal cylindrical steel chamber 10 feet in diameter and 25 feet in length, with 1-inch wall thickness, with an explosive limit of 10 lbs TNT; and Lawrence Livermore National Laboratory uses horizontal steel cylinders 10 feet in diameter and 25 feet in length, with 2- to 3-inch wall thickness, with an explosive limit of 22 lbs TNT.

The easiest type of blast chamber to analyze is a spherical structure with the explosive charge located in the center. This design does not lend itself to easy access of the facility or efficient utilization of space within the chamber. Complete containment structures have often been designed in pressure vessel geometry, as in Ref. 14, because spherical shells or cylindrical shells with domed ends are more efficient shapes for explosion containment than box-shaped structures. (Material is stressed primarily in tension, rather than bending.)

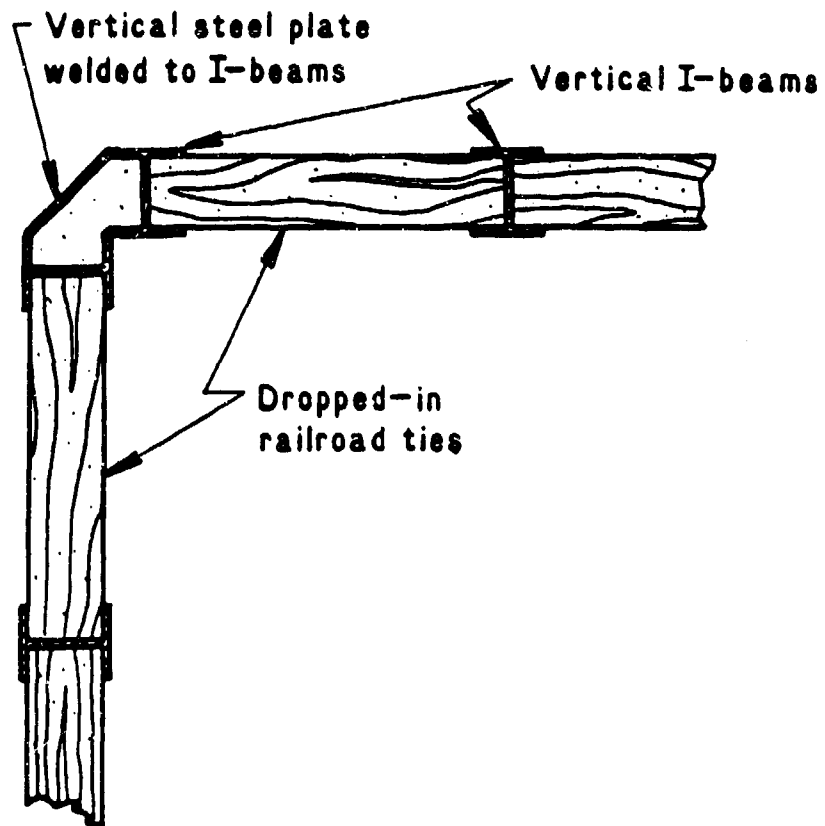


Figure 3A. Schematic Section for Walls of Variation on Suppressive Shields Option



Figure 3B. Section Through Interleaved I-Beam Roof for Suppressive Shield

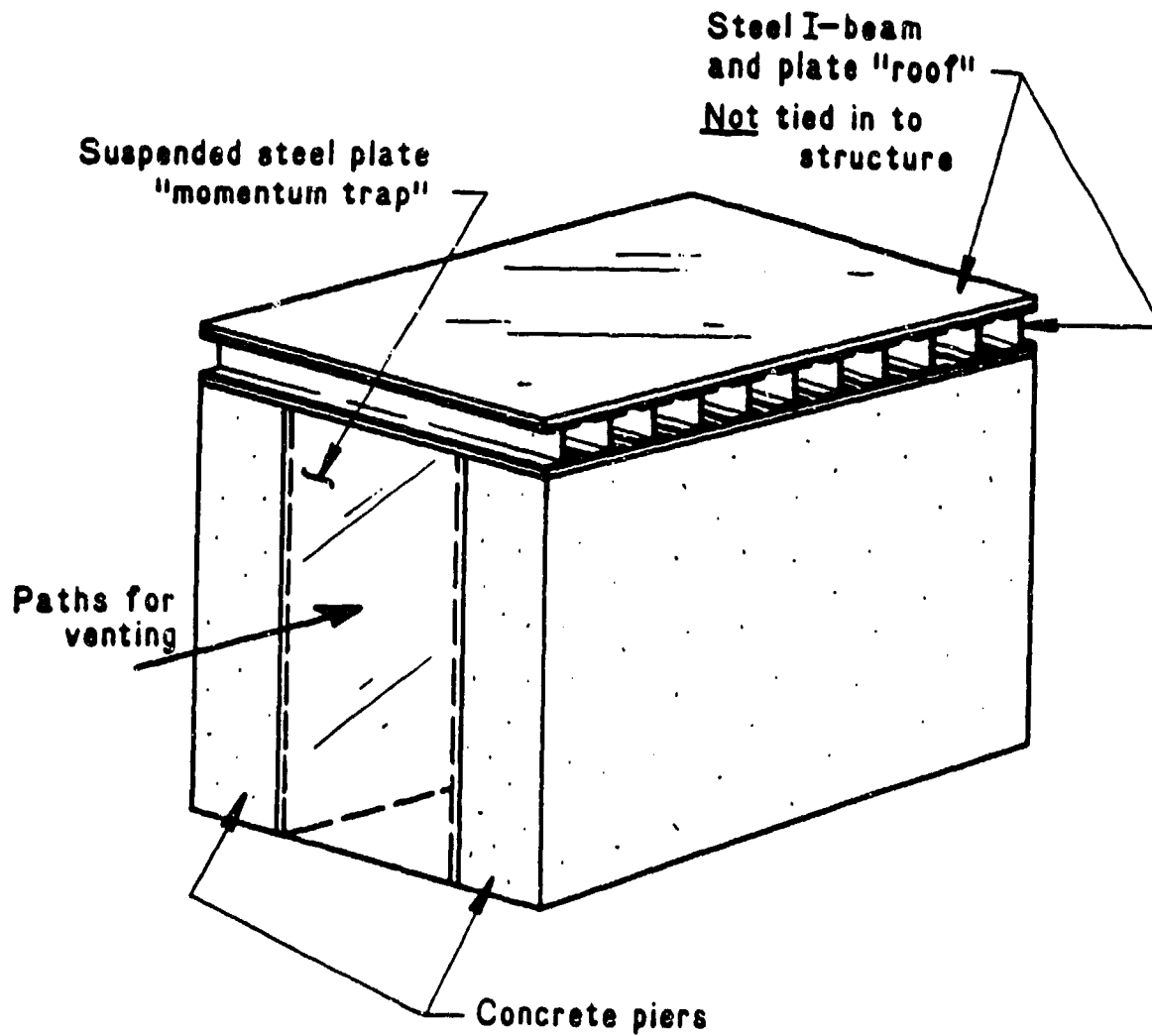


Figure 4. Eglin AFB "Momentum Trap" Test Structure

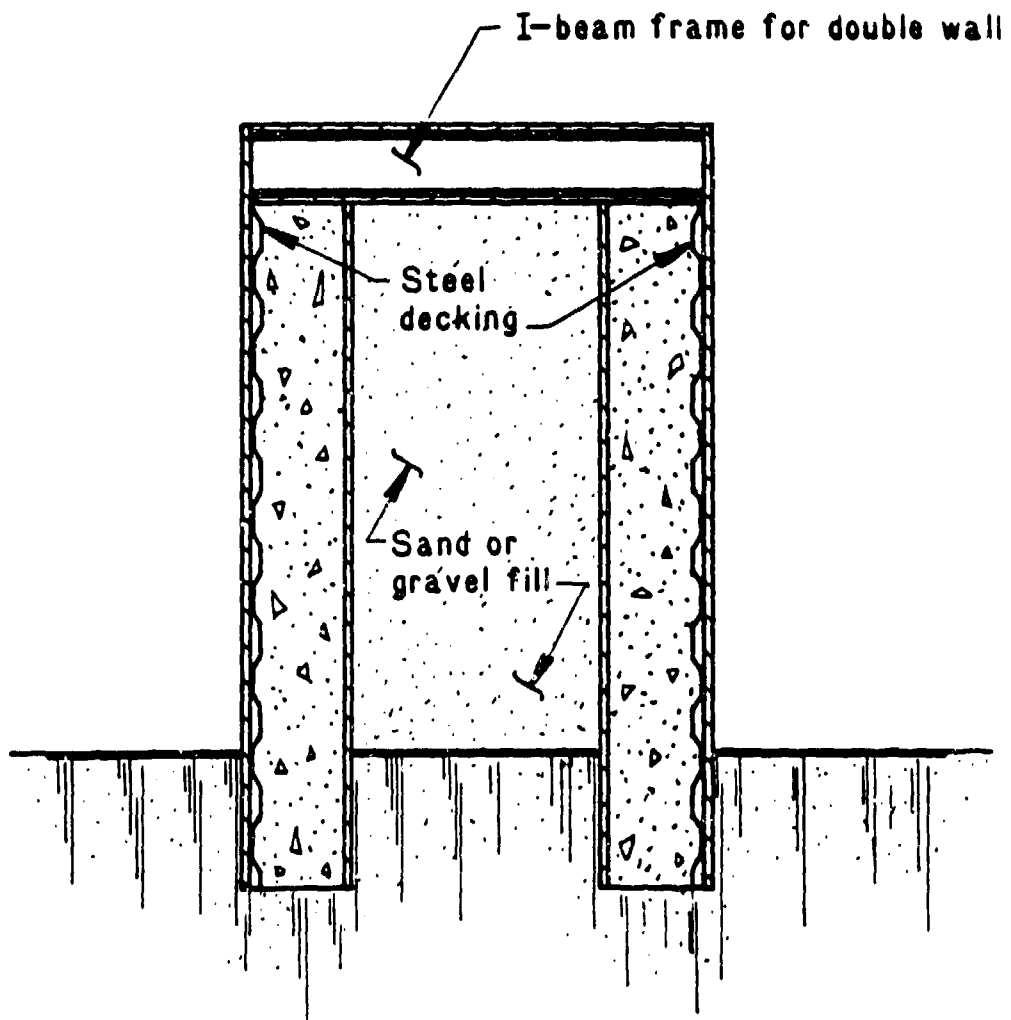


Figure 5. Section Through Filled Double Wall

However, box-shaped structures are usually preferable because of the operational and constructional problems encountered with a spherical or cylindrical blast chamber. Ref. 15 presents a compromise design which was conceived and tested for Battelle Columbus Labs using a circular building with a domed roof and foundation as illustrated in Figure 6. Over 300 charges had been fired of up to 60 lbs of dynamite at the time of reporting. Noise levels at a distance are minimal.

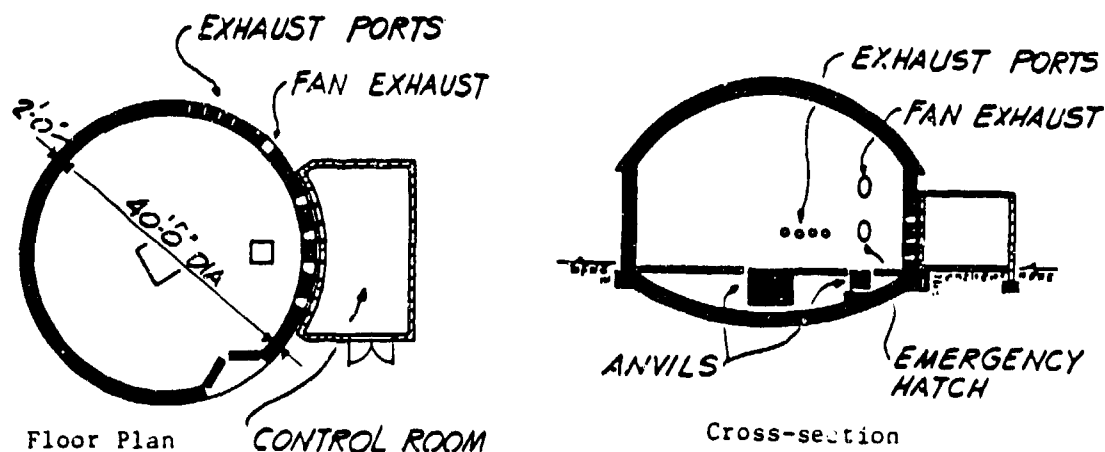


Figure 6. Circular Blast Chamber with Domed Roof and Foundation (Ref. 15)

Complete containment with complete pressure sealing will allow no external air blast from the detonation of an explosive charge within the chamber. Quasi-static pressure will decrease very slowly as heat from the high temperature explosion is transferred to the walls of the chamber, whereby cooling the interior gas and reducing the pressure.

However, complete pressure sealing is not always needed, and a containment can in fact be designed with a small amount of vent area to allow the long-term quasi-static pressure rise to decrease by exiting the chamber through the vent. A small amount of venting will not produce any significant air blast outside the containment (Ref. 16).

Aqueous Foam

Aqueous foams consist of thin sheets of water surrounding pockets of air. Different expansion ratios of the foam can be produced by increasing the surface tension of the water. There has been considerable work done on the attenuation of shock traveling through aqueous foam (Refs. 17 to 20). Possible causes of overpressure decrease are direct energy reduction by cooling of explosives' fireball by the foam through transfer of explosive energy into vaporizing the foam, interference with the explosive afterburn by the foam and the transfer of explosive energy into accelerating the foam surfaces, and shock attenuation by diffusion of the shock wave by multiple reflections from the foam surfaces, possibly diffusing the shock wave by lowering sound velocity, contribution of surface tension effects, and creation of waste energy due to the presence of higher heat capacity materials during expansion (Refs. 17, 21-29).

Blast Focusing Prediction

Certain atmospheric conditions can refract blast energy, which normally would have propagated upward, downward to the ground, causing a focusing effect in a specific area. To determine the focusing conditions one must know the temperature, wind speed, and wind direction as a function of altitude at the test site. Ref. 30 is a good guide for the evaluation of atmospheric effects on blast.

These data can be used for computer-based predictions of blast focusing or defocusing near the test site. Several computer programs have been written to predict blast-focusing and have been validated with test data (Refs. 31-33).

For this option to be viable, a system to launch and track sounding balloons with temperature sensors and telemetry to the surface would have to be purchased or leased. Weather runs should be made shortly before test times for these predictions to be accurate. Results would be the basis for the decision to give clearance to fire.

Less accurate, but perhaps adequate, use of this option would be to request the same detailed weather data which could be recorded at the test site from nearby Air Force bases, or perhaps commercial airports. Data for the closest source could be used in the same manner as data collected from a sounding system at the test site.

Portable Sound Level Monitoring System

One or more portable seismic and sound level monitoring systems could be located in or near areas around the test site where noise complaints could be expected. This type of monitoring system is used often in pre- and post-blast surveys to determine blast vibration effects, such as noise levels, for operations which involve detonations of explosives near populated areas. Monitoring systems could be set up in suspected noise problem areas prior to testing. A test charge much smaller than the main charge would be detonated at the site. Significant noise recorded at the monitoring equipment location would indicate blast focusing conditions which would postpone the main test. Insignificant noise level would indicate safe atmospheric conditions for main charge testing.

APPROXIMATE COSTS ESTIMATES AND CONFIDENCE LEVELS

Suppressive Shields

Construction of a Group 4 suppressive shield was estimated at \$105,000 in 1975 dollars. A somewhat larger shield would be needed for each firing site. Including design engineering costs, the larger size, and inflation, cost could be in the range of \$200,000-\$300,000 per shield.

With this option, design and construction methods are very well proven, so the shield should be sufficient for many repeated, largest size internal explosions, and should strongly attenuate air blast to any desired level. Confidence level for this option is very high.

"Momentum Trap" Structure

Methods for predicting shock and quasi-static pressure loads on this structure, as well as response of the momentum traps, are readily available in the literature. It is likely that the structure, with the piers designed as shown in Figure 5, would be less expensive than a suppressive shield. This option is estimated at \$150,000-\$250,000 per structure. Confidence level is not quite as high as for Option 1, because such structures have not been proof-tested for repeated firings or noise suppression.

Containment Structure

The cost for a complete containment steel box would probably not exceed the cost for a suppressive shield of the same size and containment capability. This option is estimated at \$200,000-\$300,000 per structure.

Confidence level for this option is higher than for Option 1, because no objectionable noise can be generated, as proven through a considerable amount of testing.

Aqueous Foam

Testing to prove this option and establish volume of foam needed to achieve desired attenuation levels would be essential. At least 10 tests should be run, with varying HE/foam combinations, and multi-channel air blast instrumentation. Such testing could cost as much as \$100,000. Foam equipment and supply costs are not yet known, but prices should be easy to obtain from fire-fighting equipment companies such as Ansul, or may already be available at the test site.

This option could substantially interfere with test objectives for many tests, and so may not be a viable option. The major disadvantage is that the explosive must be completely buried in foam for significant attenuation. This negates motion picture or video coverage of explosive events, but may have little effect on flash x-ray instrumentation. Emplacing foam and subsequent cleanup would also complicate testing. The need for a validation test program before the method can be applied with confidence also lowers its desirability. The confidence level for this option is rated at moderate.

Blast Focusing Prediction

Costs of the tracking equipment are not yet known, but radiosonde balloons are relatively inexpensive, about \$100 per balloon, including pressure and temperature recording and telemetry. Chance of successful balloon launch and tracking is 60-70%. The accuracy of the computer blast focus predictions is good, dependent of course on accurate input data.

Acquisition of the needed input data at nearby Air Force bases seldom fails, but the data are suspect for use at Hollister unless collected within several miles of the site. Also, data may not be available near test time.

No changes in present firing arenas are needed, but rather large capital investment in meteorological system and staff training in its use must be made. There is also the possibility of "weather holds" in firing with unfavorable weather conditions. Various uncertainties in this option render the confidence level only moderate.

Local Sound Level Monitoring

Portable monitoring equipment is readily available for lease or purchase. It is relatively inexpensive with the cost of leasing per unit at approximately \$600/month. A testing program to "calibrate" the units with small test charges would be essential, but should only cost about \$50,000. Operations are complicated somewhat with the necessity of pre-test small shots to establish safety for larger shots, but this method should interfere much less with operations than other options. Perhaps the most attractive feature is direct measurement of noise focus or defocus, at exactly the correct time and shot location.

The confidence level in this method is very high.

CONCLUSIONS AND RECOMMENDATIONS

We conclude that all six of the options have very good potential for noise control/abatement for explosives testing at the Hollister site. The order of confidence level for success of the six options, best to worst, is:

- Certain, Option 3
- Very high, Option 1
- Very high, Option 6
- High, Option 2
- Moderate, Option 4
- Moderate, Option 5

We could only make very approximate cost estimates for each option in this brief study. But, ranking from least expensive to most is probably:

- Least expensive, Option 6
- Relatively inexpensive, Option 5 (using public meteorological data)
- Relatively inexpensive, Option 4
- Moderately expensive, Option 5 (setting up meteorological system at Hollister)
- Expensive, Option 2
- Most expensive, Option 1
- Most expensive, Option 3

We recommend that Option 6 be tried first. It is probably by far the least expensive option, has very high confidence level once "calibrated," and could well have a positive effect on community relations because FMC would show interest in noise control for site testing.

Finally, simply scheduling firing at times of day when communities tend to have minimal response to "impulse noise" from explosions can minimize complaints. Ref. 7 is an excellent summary of this aspect of noise abatement.

REFERENCES

1. "Suppressive Shields Structural Design and Analysis Handbook," HNDM-1110-1-2, U.S. Army Corps of Engineers, Huntsville Division, Huntsville, AL, November 1977.
2. E.D. Esparza, "Estimating External Blast Loads from Suppressive Structures," EM-CR-76030, Report No. 3, Edgewood Arsenal, MD, November 1975.
3. W.E. Baker and P.S. Westine, "Methods of Predicting Blast Loads Inside and Outside Suppressive Structures," EM-CR-76026, Report No. 5, Edgewood Arsenal, MD, November 1975.
4. E.D. Esparza, W.E. Baker, and G.A. Oldham, "Blast Pressures Inside and Outside Suppressive Structures," EM-CR-76042, Report No. 8, Edgewood Arsenal, MD, December 1975.
5. R.N. Schumacher, C.N. Kingery and W.O. Ewing, Jr., "Airblast and Structural Response Testing of a 1/4 Scale Category I Suppressive Shield," BRL Memorandum Report No. 2623, USA Ballistic Research Laboratories, Aberdeen Proving Ground, MD, May 1976.
6. C.N. Kingery and G. Coulter, "Shockwave Attenuation by Single Perforated Plates," BRL Memorandum Report No. 2664, USA Ballistic Research Labs, Aberdeen Proving Ground, MD, August 1976.

7. F.H. Oertel, Jr., "Evaluation of Simple Models for the Attenuation of Shock Waves by Vented Plates," BRL Report No. 1906, USA Ballistic Research Labs, Aberdeen Proving Ground, MD, August 1976.
8. A. Ceimins, "Analysis of Category I Suppressive Shield Effectivity Data," BRL Report No. 1936, USA Ballistic Research Labs, Aberdeen Proving Ground, MD, September 1976.
9. R.N. Schumacher, "Airblast and Structural Response Testing of a Prototype Category III Suppressive Shield," BRL Memorandum Report No. 2701, USA Ballistic Research Labs, Aberdeen Proving Ground, MD, November 1976.
10. C. Kingery, R. Pearson, and G. Coulter, "Shock Wave Attenuation by Perforated Plates with Various Hole Sizes," BRL Memorandum Report No. 2757, USA Ballistic Research Labs, Aberdeen Proving Ground, MD, June 1977.
11. C. Kingery, G. Coulter, and R. Pearson, "Venting of Pressure Through Perforated Plates," Technical Report ARBRL-TR-02105, Ballistic Research Labs, Aberdeen Proving Ground, MD, September 1978.
12. W.E. Baker and G.A. Oldham, "Estimates of Blowdown of Quasi-Static Pressures in Vented Chambers," EM-CR-76029, Report No. 2, Edgewood Arsenal, MD, November 1975.
13. J.F. Proctor, "Blast Suppression/Predictive Model, WBE 4333," Monthly Technical Report, Naval Surface Weapon Center, White Oak, Silver Spring, MD, November 1975.
14. W.E. Baker and P.A. Cox, Jr., "Design Study of an Experimental Blast Chamber," *The Shock and Vibration Bulletin*, Bulletin 46, Part 3, pp. 227-250, August 1976.
15. R.S. Fling and V. Linse, "Design and Operation of a Blast Containment Structure," 12th Annual Symposium on Behavior and Utilization of Explosives in Engineering Design, 2-3 March 1972.
16. W.E. Baker and R.J. Hayes, "Design, Fabrication and Proof Testing of an Electrical Explosion Containment," *Minutes of the 23rd Explosives Safety Seminar*, August 1988.
17. Richard Raspet, "Use of Aqueous Foams to Mitigate Demolitions Noise," CERL TR N-112, USA CERL, Champaign, IL, September 1981.
18. R. Raspet, S.K. Griffiths, J.M. Powers, H. Krier, T.D. Panniczak, P.B. Butler, and F. Jahani, "Attenuation of Blast Waves Using Foam and Other Materials," USA-CERL TM N-89/01, U.S. Army Corps of Engineers Construction Engineering Research Laboratory, November 1988, AD-A203 148.
19. D.L. Evans, D.F. Jankowski, and E.D. Hirleman, "A Preliminary Investigation of Aqueous Foam for Blast Wave Attenuation," ERC-R-76050, College of Engineering and Applied Sciences, Arizona State University, Tempe, AZ, January 1979.
20. W.E. Baker, P.K. Moseley, W.A. Mallow, and R.E. White, "Determination of the State-of-the-Art of the Blast Wave Attenuation Characteristics of Expanded Aqueous Foam, SwRI Final Report No. 02-5338, for Naval Surface Weapons Center, Dahlgren Laboratory, Dahlgren, Virginia, October 1978.

21. F.H. Winfield and D.A. Hill, "Preliminary Results on the Physical Properties of Aqueous Foams and Their Blast Attenuating Characteristics," Technical Note No. 389, Defense Research Establishment, Suffield, Ralston, Alberta, August 1977.
22. D.A. Dudley, E.A. Robinson, and V.C. Pickett, "The Use of Foam to Muffle Blast from Explosion," Paper presented at the IBP-ABCA-5 Meeting, June 1976.
23. Personal communication between Dr. R. Raspet of CERL and Dr. D. Keefer of the University of Tennessee Space Institute, September 1978.
24. F.B. Porzel, "Introductions to a Unified Theory of Explosives (UTE)," NOL TR 72-209/AD758000, September 1972.
25. J.S. de Krasinski and A. Khosla, "Shock Wave Propagation and Attenuation in Foams," Fifth Australian Conference on Hydraulics and Fluid Mechanics, University of Canterbury, Christchurch, New Zealand, December 1974.
26. D. Keefer, "Conceptual Design of a Muzzle Blast Attenuator Based on Porzel's Unified Theory of Explosions," Final Report, Delivery Order 1371, Battelle Columbus Laboratories, Durham Operations.
27. V. Ramesh and J.S. de Krasinski, "Small Strength Shock Waves Speed and Attenuation in Liquid Foams," Report No. 75, University of Calgary, Canada, Department of Mechanical Engineering, March 1976.
28. J.S. de Krasinski and A. Khosla, "Shock Attenuation in Non-Homogeneous and Porous Media," Report No. 34, University of Calgary, Canada, Department of Mechanical Engineering, March 1972.
29. W. Anson and J.S. de Krasinski, "Field Experiments in the CIL Facilities of the University of Calgary," Department of Mechanical Engineering, March 1976.
30. "Estimating Air Blast Characteristics for Single Point Explosions in Air, With a Guide to Evaluation of Atmospheric Propagation and Effects," ANSI S2.20-1983, American National Standard, American Institute of Physics for the Acoustical Society of America, 1983.
31. J.W. Reed, "Explosion Airblast Predictions on a Personal Computer and Applications to the Henderson, Nevada, Incident," SAND88-0681C, with Addendum - "FORTRAN-77 Program BLASTO.FOR Interpretations and Instructions," Sandia National Laboratory, Albuquerque, NM, August 1988.
32. R.A. Lorenz, "Noise Abatement Investigation for the Bloodsworth Island Test Range: Description of Test Program and New Long Range Airblast Overpressure Prediction Method," NSCW TR 81-431, Naval Surface Weapons Center, Silver Spring, MD, November 1981.
33. D.A. Douglas, "Blast Operational Overpressure Model (BOOM): An Airblast Prediction Method," AFWL-TR-85-150, Air Force Weapons Laboratory, Kirtland Air Force Base, New Mexico, April 1987.

PREDICTION OF ACOUSTIC FOCUSING HAZARD IN THE ATMOSPHERE

Gil Smith
Material Research Laboratory,
Melbourne.
PO Box 50, Ascot Vale, Vic. 3032, Australia.

1. INTRODUCTION

Acoustic noise or blast energy can travel significant distances through the atmosphere where anomalous overpressures may cause damage or public irritant. These relatively low overpressures can present a structural damage hazard so that serious injury is possible due to the partial collapse of buildings or from glass fragments and debris. The purpose of this paper is to present a methodology which allows an assessment of acoustic focusing hazard in the atmosphere when detonating explosives. The method provides an ability to analyse or avoid these long range blast effects.

The method employs a graphical package (Smith, 1989) which can process weather data with the altitude profiles of (i) temperature, wind speed and wind direction as a minimum requirement, and (ii) pressure and relative humidity profiles for improved accuracy. The results are expressed in four graphs which can be consulted together in order to predict foci at ground level.

With the accumulation of accurate weather data before and during tests on explosive devices, routine ordnance deployment, and ordnance disposal, an assessment of the hazard risk can be investigated and appropriate measures taken to reschedule firing. Additionally, if records were kept of weather data and the time and location of explosives operations, the ability to evaluate such data could be of service if the possibility of litigation arose.

2. THE METHOD

A sound velocity profile is used to determine the type of acoustic refraction in the atmosphere. A ray trace graph is generated to indicate the convergence of acoustic rays. To eliminate the chance of ray trace artifacts and to evaluate convergences, the foci locations can be cross-referenced with graphs of range vs ray elevation angle (and/or ray arrival time vs ray elevation angle). A focus is indicated where these graphs show a near zero slope which corresponds to the arrival of a set of rays at the same range and arrival time. To enhance the focus, reflections and other ray angles can also be shown to exhibit the same range and arrival time on these graphs.

Calculations in this methodology assume acoustic propagation away from the shot site and are concerned with the prevailing weather conditions producing an acoustic lens within the layers of the atmosphere. This approach is taken because, remote from ground zero, overpressures are relatively low and may be regarded as perturbations in the ambient pressure so that the speed of a wave front is approximately acoustic (Cox, et al, 1952) and the front will follow the laws of acoustics.

3. FACTORS AFFECTING ACOUSTIC FOCUSING

3.1 RAYS AND ENERGY TUBES

It is convenient to indicate the direction of the energy flow by a series of acoustic ray paths of equal angular displacement which radiate out from the shot site and remain at all times normal to the blast front. An inhomogeneous atmosphere may be indicated by ray paths which deviate from straight radial paths diverging from the shot site (Figs 2 - 4). Because these rays are traced along the flow of energy, then energy radiating from the shot site within some solid angle remains within their bounds - this region may be called an energy tube (Sach, 1961). Although it is not anticipated that the energy within a tube will flow normal to the bounding rays of the tube wall, it is possible that two or more energy tubes may intersect to produce a focus. However, there is atmospheric attenuation within each energy tube due to viscosity, the exchange of translational and rotational energy between colliding molecules, and thermal heating and conduction effects particularly near the shot site where pressure gradients and wave velocities are the greatest.

3.3 ACOUSTIC REFLECTION

Reflection of the sound front normal to the boundary is a minimum between vertically adjacent atmospheric layers of similar sound velocities and acoustic impedances - e.g. cloud and meteorological discontinuities. Conversely, there is a maximum reflection of the sound front at the boundary between media of greatly different acoustic impedance - e.g. air and ground. Only reflections off the ground need be considered here.

3.4 ACOUSTIC DIFFRACTION

Diffraction of a sound wave would require very large overpressures found in shock fronts near ground zero to become significant in the dispersion of energy. However, at extended ranges the overpressures are relatively small and front velocities are approximately the speed of sound (Whitham, 1957). In the present study we therefore neglect the effects of diffraction.

3.2 ENVIRONMENTAL FACTORS AFFECTING SOUND VELOCITIES

Temperature Effects

The speed of sound in air is primarily dependant on temperature. Fig 1 shows a variation in the velocity of sound due to atmospheric temperature gradients. An increase in temperature will result in an increased sonic velocity.

Humidity Effects

The contribution to sonic velocity from humidity is below 1% at normal temperatures and may be neglected (Herman, 1983). The model used here includes humidity effects when required.

Wind Shear Effects

In a non-turbulent, moving atmosphere each medium has a wave velocity with respect to the ground so that sound wave velocity components and the corresponding wind velocity components may be summed vectorially (Fig 1). This means high winds may markedly alter acoustic velocities from very low to quite large sound velocities. Therefore, along with temperature profile effects, wind shear effects are a major contributor to the question of noise focusing in the atmosphere. The component of the wind velocity which is of interest is the one that moves along the path taken by the propagating sound front.

3.5 ACOUSTIC REFRACTION

Refraction of rays through the atmosphere is the cause of focused blast energies at extended ranges. All refracted sound rays in an atmospheric layer behave as follows:

K	Condition	Refraction	Fig No.
$K_i < 0$	$v_{i+1} < v_i$	Upward	Fig 2
$K_i = 0$	$v_{i+1} = v_i$	Not refracted	Fig 3
$K_i > 0$	$v_{i+1} > v_i$	Downward	Fig 4

Generally a ray will be turned toward regions where the sound velocity is lower according to a Huygens-Kirchhoff construction. Therefore ducting of sound toward the ground requires the presence of stratified atmospheric layers with sound velocity profiles such that :

- (i) some sound velocity is greater at a higher altitude than at the ground
- (ii) a collection of rays at various angles are incident at the same range, and arrive at the same time and in-phase (according to Fermat's principle of least time) so that they superimpose to produce a large overpressure.

Focusing requires a very sharp increase in the sound velocity profile with altitude or, more usually, an inversion structure. This is where the profile exhibits a sound velocity

greater than at ground zero, preceded by a smaller sound velocity than at some lower altitude.

4. ACOUSTIC FOCUS PREDICTIONS

4.1 REFFOCUS - A COMPUTERISED AID TO ACOUSTIC FOCI MODELLING

REFFOCUS, in Fortran 77 code, is a computerised aid to predict the location of acoustic foci in the air by acoustic refraction. Using meteorological/height data it calculates and, if appropriate, plots:

1. The maximum ray elevation angle, θ_{1crit} , which will turn over in the atmosphere.
2. The range, R, of rays at discrete angles from $\theta=0$ to θ_{1crit}
3. The time of arrival, T, of these rays from $\theta=0$ to θ_{1crit}
4. The sound velocity/height profiles.
5. The ray path followed by each angle from $\theta=0$ to θ_{1crit}
6. Multiple reflections of the Range, Time of arrival, and Ray paths for each angle from $\theta=0$ to θ_{1crit}
7. Tabulates data.

The program presently assumes:

1. Acoustic rather than shock wave behaviour over the entire range.
2. Surface blasts or noise generation - not restricted to sea level.
3. A locally flat earth without curvature or relief.
4. A horizontally homogeneous atmosphere where the weather conditions and sound velocities are stable.
5. Rays which return to earth at shot site level are reflected with 100% of their energy on a flat surface to return to earth at multiples of their initial range.

REFFOCUS is designed to be readily used by an inexperienced person. To facilitate input there is the option of a keyboard or data file input; meteorological or velocity profile data input; and a review option to allow a recapitulation of the data and graphs. For each azimuthal sound velocity profile the equations used by REFFOCUS in the calculation of refracted rays through n layers of atmosphere are detailed by Szith (1989).

4.2 EXPLOSION PROFILES

Figures 5 to 8 have been produced by REFFOCUS to illustrate the hazard prediction methodology. These figures are in addition to those simple profiles shown in figures 1 to 4. The graphs are generally in groups of four, each with the same figure number and with letters a,b,c or d. The nomenclature is as follows:

- a. - Sound velocity profile
- b. - Range vs initial ray angle
- c. - Time of arrival of sound ray vs initial ray angle
- d. - Ray traces

The REFFOCUS acoustic focus methodology can be applied to a number of explosive tests or accidents for which weather data, ground zero elevation and prevailing conditions are available. According to the information available to us, the following are graphical representations of their acoustic focus conditions. Where possible these were derived from weather data around the time of, and in close proximity to the explosive sites. Damages were claimed as a result of some of these incidents. Where data sources have quoted distances and altitudes in feet the calculations have been completed in the imperial system and also indicated in SI.

Medina Facility, San Antonio, USA

Date - 1100 CST, November 13, 1963.

Explosion - accidental detonation of 111,500 lb chemical HE, 145,000 TNT equivalent, distributed in a bunker.

Main Location of Damage - north-south band about 8 miles (12.9 km) east.

Ground Zero Elevation - 800 ft (240 m).

Met. Data - Easterly azimuth sound velocity profile.

Met. Data Location - Unknown

Data Time - Interpolated between balloon soundings at 0530 & 1130 CST.

Recorded Pressure Measurements - None.

Data Reference - Reed (Ref 8).

Discussion

Figure 5a is the sound velocity profile. It shows an inversion morphology up to 6000 ft. This corresponds to rays emanating from ground zero between $\theta_1=0^\circ$ and a maximum elevation angle, θ_{1crit} , of 14.4° . Figures 5b & c display zero slope at approximately 6° (arrival time 56s, range 60,000 ft (11.4 mls) or 18.3 km) and 14° (arrival time 39s, range 44,000 ft (3.3 mls) or 13.4 km). These correspond to convergences at the same distances in the ray trace, Figure 5d. Possible foci are therefore located at the two ranges : 13.4 km and 18.3 km. The first focus is close to the reported damage in a built up area at around 12.9 km east of the explosion.

With data limited to one direction of interest, the focus range was accurate to within 4% of measurements. Other comparisons are not available due to limited data.

Pepcon, Henderson, Nevada, USA

Date - 1157 PDT, May 4, 1988.

Explosion - Accidental series of explosions, the largest being 1500 tons Ammonium Perchlorate, equivalent to 0.5 kt HE surface burst estimated by ground zero phenomena or a 0.25 kt surface burst as estimated 2km away in a crosswind direction.

Main Location of Damage - 2 km at 285°, 2.7 km Northwest, 4.2 km Northeast, 4.3 km East Northeast (all encroaching residential areas), scattered damage in the northwest and westerly directions toward inhabited areas of Las Vegas and Henderson.

Ground Zero Elevation - 1900 ft (580 m)

Met. Data - Full meteorological data.

Met. Data Location - Desert Rock over 100 km north-west of Las Vegas.

Data Time - Balloon soundings at 0500 & 1700 PDT May 4, 0500 PDT May 5, and interpolated data between 0500 & 1700 PDT May 4.

Recorded Pressure Measurements - Estimations by window pane damage.

Data Reference - Reed (Nov., 1988)

Discussion

Figure 6a shows a sound velocity profile produced from the interpolated meteorological data and in a northerly direction. The data has been interpolated from 7 hrs before and 5 hrs after the explosion and so cannot guarantee adequate accuracy. This profile comes closest to, but still precludes, some ducting. Nor is ducting possible for any of the azimuthal directions in any of the data listed in the reference before or after the explosion. REFFOCUS does not attempt to graph range, time of arrival or ray traces because ducting of sound back to the ground is not indicated by the available data.

There is a lack of weather data between 0 and 500 m above ground where there remains the possibility of ducting between those levels. Reported damage did not provide a well defined pattern to establish any focus conditions, nor was the true extent of the explosive yield substantiated. To recognise acoustic focusing conditions more detailed data would be required not only at the lower altitudes but also closer to the time of the explosion.

The quality of the model predictions may not be evaluated because of the unavailability of sufficient weather data around the time of the accident.

Minor Scale, New Mexico, USA

Date - 1220 MDT, June 27, 1985.

Explosion - 4.8 kt Ammonium Nitrate-fuel oil (ANFO)

Main Location of Damage - Carrizozo, 60 km east.

Ground Zero Elevation - 5000 ft (1524 m).

Met. Data - Sound Velocity profile in Easterly direction.

Met. Data Location - Stallion site 28 km North of GZ, Jallen site 50 km South of GZ.

Data Time - completed at 1220 MDT (Stallion) & 1330 MDT (Jallen).
Recorded Pressure Measurements - Carrizozo - 297.5 Pa
overpressure with a 400 ms duration, 160 s after Minor
Scale.

Data Reference - Reed (Ref 10)

Discussion

Shot time balloon soundings occurred at balloon burst approximately 2 hrs (100,000 ft) after release. The shot time balloon sounding at Stallion site (28 km North of ground zero) showed an increase in sound velocity at higher altitudes than previous soundings that day. The sounding which was completed 1hr 25 mins later from Jallen site (50 km South of ground zero) showed a greatly increased sound velocity at higher altitudes and displayed focus conditions. The Jallen sounding was in mid-flight at shot time and sounding the altitudes where sound velocities were increasing. The profile produced by the Jallen site could therefor be seen to be more indicative of the prevailing conditions. This is one example where real time sounding by Doppler radar is warranted.

Using the Jallen site data at 1330 MDT: the sound velocity profile, figure 7a, in the direction of Carrizozo (87°) shows an inversion morphology up to 11000 ft. In the range graph, Figure 7b, the reflected rays first return to ground at 24 km (80,000 ft) and on their first reflection returned to ground between 44 km (145,000 ft) to 55 km (217,500 ft). The initial return to ground and its reflected return to ground are indicated by shallow slopes in the range graph, Figure 7b, and the time of arrival graph, Figure 7c. This indicates the rays very nearly arrive simultaneously and are in-phase resulting in some acoustic reinforcement as seen in the ray trace. The calculated range for the second reflection is close to the reported 60 km to Carrizozo. Significantly, the calculated time of arrival at Carrizozo is 164 s which is very close to the reported 160 s time of arrival and shows that the lower angle rays (the furthest travelled rays) were responsible for the response at Carrizozo. Range and time variations can be attributed to the variability of sound profiles over the intervening terrain including the 9000 ft Oscura Peak. The sound rays have been calculated to have just cleared the peak at around 11000 ft. Figure 7d is the ray trace including the climb over Oscura Pk and the following 2 reflections. Only the rays at ground zero with elevation angles between $\theta_1 = 0^\circ$ to 5.9° were ducted in the direction of interest to Carrizozo while the rest were refracted upward and lost to the atmosphere.

Similar sound velocity profiles were reported for other towns in the area without damage; however no sound velocity profiles were available to the author. Socorro (70 km North West), Tularosa (80 km South East), Alamogordo (100km South West), and Holloman AFB (100km South South West) were all probably outside the multiple returns to ground coinciding with

reflected sound rays. This accounts for their weak acoustic response.

The method is in good agreement with measurements. Range is within 9% and the time of arrival within 4% of measurements.

Larkhill 21Z, Royal School of Artillery, Great Britain.

Date - 2100 GMT January 20, 1981.

Explosion - 5 kg HE

Main Location of Damage - Unknown

Ground Zero Elevation - 10 m.

Met. Data - Met data including: height, wind speed and direction.

Met. Data Location - On site.

Data Time - 2100 GMT

Recorded Pressure Measurements - None

Data Reference - Sills (1981)

Discussion

The Larkhill weather data was taken from data used by Sills to introduce predictive methods designed to reduce noise damage and complaint against artillery practices at Larkhill. The sound velocity profile, Figure 8a, indicates an inversion morphology in the Southerly direction. This is confirmed by the Range, and Time of Arrival vs Elevation Angle graphs, Figures 8b & c. In these graphs, most rays between an elevation of $\theta_1=0$ and 12° would range close to 17.5 km (53 s arrival) to 19 km (57 s arrival). The curves are relatively flat here and show candidate focusing conditions if Larkhill had proceeded with a firing. Rays with angles from 12° to 18.5° also show some ducting shown by overlapping ranges and arrival times. For illustrative purposes this model atmosphere was terminated at 3000 m so that rays travelling above this ceiling were not plotted. These rays at elevation angles of $\theta_1>18.5^\circ$ would have ranged to 34 km and beyond. The focusing conditions here agree with Larkhill results.

4.3 SUMMARY

INCIDENT	SIZE (TNT)	DATA QUALITY	PREDICTION QUALITY
Medina	145 kt	Sound vel in 1 dir No time of arrival	Good-Range 4% error
Pepcon	0.25-0.5kt	Poor met data	Unable to apply
Minor Scale	4.8 kt	Good Met data	Good-Range 9% error -Time 3% error -Ray trace
Larkhill	Artillery	Limited met data	Good-agrees with larkhill predictions

5. CONCLUSION

Weather conditions may cause variations in the velocity of sound which allows the atmosphere to refract sound waves and act

as an acoustic lens. Certain weather conditions such as temperature inversions may allow an acoustic focus many kilometres away from an explosion.

Acoustic propagation from a noise producing installation has been mathematically modelled to locate anomalous overpressures by acoustic focusing. Additionally, M.R.L. has developed a computer model, REFFOCUS, to graphically illustrate foci in a vertically inhomogeneous, non-turbulent, moving atmosphere. The model uses sound velocity profiles derived from meteorological data.

The results obtained from the model have shown that the combined examination of these plots for a given set of weather conditions may be enough to infer the possibility of a focus by purely graphical means. This can be achieved by considering the angular spread of rays converging down range from the shot site. Acoustic foci may be predicted by the collaborated observation of:

1. an inversion type sound velocity profile,
2. a zero slope in the Range versus θ plot and,
3. a corresponding zero slope in the Time of Arrival versus θ plot and,
4. the relative density of rays at the convergence of rays when they return to ground in the Ray trace plot.

In this fashion, those installations which use explosives where there is a potential for shocked acoustic foci at extended ranges may base the decision to proceed according to REFFOCUS predictions using the prevailing weather data. REFFOCUS can therefore be used to minimise noise and larger overpressures and can be extended to confirm atmospheric weather data.

Where this method is used to analyse an accidental explosion the range and time of arrival graphs may also be used to decide the contribution to damage by reflected rays. For Minor Scale, the measured time of arrival indicated the overpressures experienced at Carrizozo were produced by the lower angle rays after their first reflection.

Irrespective of the method used to predict or analyse acoustic focusing, accurate and up-to-date weather profiles are of prime importance. Weather details can be made more accurate by using two weather balloons around shot time. One can be used at balloon burst to indicate prevailing conditions and to signal shot time, and the other arranged to be in mid-flight. Alternatively, real-time weather data soundings, by laser Doppler radar or acoustic and EM Doppler radar, would be of advantage. The latter is being investigated as a cheap and mobile option to aid weather soundings.

This acoustic focus model assumes noise generation in a vertically inhomogeneous atmosphere with stable weather and sound velocities at ambient pressure. In order to produce a working acoustic foci model we have assumed constant atmospheric composition and no earth curvature or relief. Further additions to the model may include blast weights and sonic attenuation in overpressure calculations using energy tubes or a finite element analysis.

5. ACKNOWLEDGEMENTS

I am grateful to Dr P. Ryan, Materials Research Laboratory, for his computer plotting subroutine which is used by REFFOCUS to model foci. Similarly, I would like to thank MRL colleagues D. Oliver who suggested the problem and also R. Borg, R. Kummer, and M. Chick for their useful suggestions.

6. BIBLIOGRAPHY

1. Baker, W. E.
Explosions in Air
University of Texas Press, Austin & London, 1973
2. Cox, E. F.; Plagge, H. J.; Reed, J. W.
Damaging Air Shocks At Large Distances From Explosions
Sandia Corporation, April 24, 1952.
3. Berning, W.
Investigation of The Propagation of Blast Waves Over
Relatively Large Distances and The Damaging Possibilities of
Such Propagation.
BRL Report No. 675. Aberdeen Proving Ground.
4. Braddick, H. J. J.
Vibrations, Waves and Diffraction
McGraw-Hill Pub. Co. Ltd, London, 1965
5. Herman, R. A.; Wessels and Carel; A. Velds
Sound Propagation In The Surface Layer Of The Atmosphere.
J. Acoust. Soc. Am. 74(1), July 1983
6. Kahler, J. P.
Focus - A Computerised Aid For Making Sound Propagation
Forecasts.
Staff Meteorology 6585th Test Group Hollman AFB, Jan 1979
Report No. ADTC-TR 79-8
7. Perkins, B.; Lorrain, P. H.; Townsend, W. H.
Forecasting The Focus Of Air Blasts Due To Meteorological
Conditions In The Lower Atmosphere.
BRL Oct 1960. Report No. 1118. Aberdeen Proving Ground.
8. Reed, J. W.
Evaluation Of Window Pane Damage Intensity In San Antonio
Resulting From Medina Facility Explosion n November 13, 1963
Test Effects Dept. 9150 Sandia Laboratories, Albuquerque.
Annals NY Academy of Sciences.
9. Reed, J. W.
Acoustic Wave Effects Project: Airblast Prediction
Techniques
Test Effects Dept. 9150 Sandia Lab., Albuquerque, May 1969.
10. Reed, J. W.
Damaging Distant Airblast From Minor Scale.
Ground Motion & Seismic Division - 7111
Sandia Nat. Lab., Albuquerque, NM, 1985.
11. Reed, J. W.
Climatological Assessment of Explosion Airblast
Propagations.
Ground Motion & Seismic Division - 7111
Sandia Nat. Lab., Albuquerque.
12. Reed, J. W.
Analysis Of The Accidental Explosion At Pepcon, Henderson,
Nevada, May 4, 1988
Ground Motion & Seismic Division - 7111
Sandia Nat. Lab., Albuquerque. Report SAND88-2902.UC-70 1988

13. Reed, J. W.
Explosion Airblast Predictions On A Personal Computer And
Applications To The Henderson, Nevada, incident
Ground Motion & Seismic Division - 7111
Sandia Nat. Lab., Albuquerque.
SAND88-0681C, DE88 014991 , 1988.
14. Sach, C. I.
Long Range Blast Pressure Prediction
Department Of Supply. Australian Defence Scientific Service
Defence Standards Laboratories. Technical Note 59, Mar 1961.
15. Sills, A. G.
The Prediction of Sound Intensity From an Explosive Source.
Applied Acoustics 15 (1982) 231-240
16. Smith, G. E.
Focusing Of Acoustic Waves In A Non-Uniform Atmosphere
Explosives Division, MRL Melbourne, Vic., Australia, 3032.
MRL Technical Report MRL-TR-89-10 , 1989.
17. Weinstock, R.
International Series In Pure and Applied Calculus Of
Variations.
McGraw-Hill Book Co. Inc., Y, 1952.
18. White, M. J.
Application Of The Parabolic Equation To Sound Propagation
In A Refractive Atmosphere
PhD. thesis, University Of Mississippi, 1988.
19. Whitham, G. B.
A New Approach To Problems Of Shock Dynamics. Part 1 Two-
Dimensional Problems.
J. Fluid Mech. Vol 2, 1957, pp 145-71

TWENTY - FOURTH D.O.D. EXPLOSIVES SAFETY SEMINAR
28 - 31 AUGUST SAINT LOUIS - U.S.A.

**AN OPERATIONAL PREDICTION FOR FAR FIELD
AIRBLAST EFFECTS :
PRACTICAL EXPERIENCE AT CAEPE.**

J. SAUVEL
DGA / CAEPE
BP N°2
33165 Saint Médard en Jalles - FRANCE -

J. VERMOREL
ISL
12 rue de l'Industrie
68300 Saint Louis - FRANCE -
present address :
DGA / E.T.B.S. route de GUERRY
18015 Bcurges - FRANCE -

abstract

During the firings of explosives or during the testing of solid rocket motors, detonation or deflagration generates high amplitude aerial shockwaves. Before performing a large-scale test, the commander of the facility must know what risks it can create for nearby populated areas according to local weather conditions : this corresponds to the French Z5 security zone.

The prediction system used at CAEPE is presented : the physical assumptions and numerical discretizations are reviewed. Key factors are studied and verifications are computed on two real situations. This prediction has been operationnally used since 1987 and this experience is summarized : the complexity of the numerical code is sufficient. However, the knowledge of weather conditions has to be improved in order to secure operational prediction.

Long range acoustic levels due to high noise generation is also discussed. An example for the noise of ARIANE 5 launcher is described.

KEYWORDS : Far-field focusing, shockwaves, Z5 limits, operational prediction, explosives, rocket motors, static firings.

1 - INTRODUCTION

1.1 - ENVIRONMENTAL NEEDS FOR A TEST CENTER

Any test center must know what potential environmental problems can be created before deciding to perform a new test. For example, static firings of solid rocket motors or of explosives can generate risks outside the facility area in the following fields :

- a) high aerial shockwave due to a detonation of a 1.1 pyrotechnical object or due to the pneumatical explosion of a highly pressurized volume (especially at the end of a firing)
- b) high noise due to the generation of sounds by the exhaust jet of combustion gases
- c) artificial cloud created by the combustion gases and pollutant species such as HCL
- d) X Ray propagation if a high generator is used during a firing in order to investigate combustion phenomena.

Other risks can happen such as fragment hazards or high thermal flux but they are restricted to the close surrounding of the test site.

The DGA/CAEPE - Centre d'Achèvement et d'Essais des Propulseurs et Engins - is a rocket test center under the authority of the «Délégation Générale pour l'Armement» - French Ministry of Defence. It is mainly responsible for static firings of rocket motors or for security tests of explosive systems. Twelve different test facilities are used. Figures 1 and 2 shows photographs of tests bays during and after explosions. In particular the facility for large security tests is designed for potential detonations up to 20 tons of 1.1 propellant or explosive and for a few hundreds tons of 1.3 pyrotechnical products.

The use of these facilities has implied CAEPE in the field of environmental predictions :

- the effect c) has been operationally predicted at CAEPE since 1980 because of the use of composite propellants containing a high content of hydrochloric acid.
- the effect d) has been solved with the use of huge blocks of concrete or sand.
- the effect b) has been studied at CAEPE since 1985 because of the increasing exhaust flowrate of combustion gases for large size motors.

1.2 - OBJECTIVE OF THE PRESENT PAPER

In the present article, the subject a) «Far-field airblast predictions» is studied and the following approach is considered :

- description of the obligations due to the French legislation and description of risk philosophy used at CAEPE (part 2 of the present paper).
- description of the general system of prediction used at CAEPE (part 3)
- description of the numerical model (part 4)
- checking of the model on real cases (part 5)
- uncertainties of the general system of prediction used at CAEPE (part 6)
- usefulness of improvements (part 7)

In the present paper, no new theoretical, computational or experimental development will be made compared to what has been already written in the scientific literature. In all the further paragraph, the emphasis will be put on practical comments and «every-day» uses.

The subject b) «far-field noise prediction» has many similarities with the airblast one. This similarity is presented in appendix and an example is described for firings of the motors of the launcher ARIANE 5 in French Guyana.

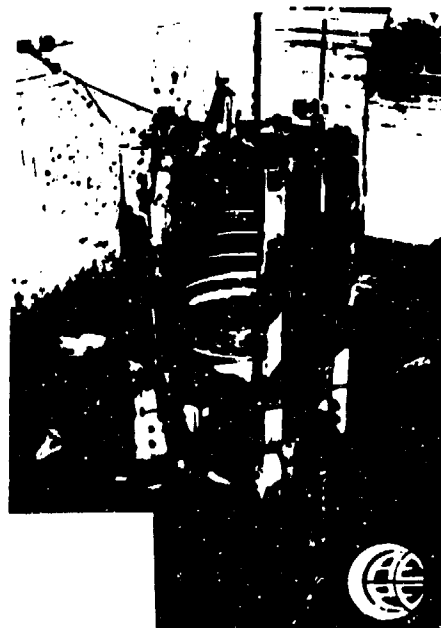
- Figure 1.a -
Explosion of a 1.3 motor



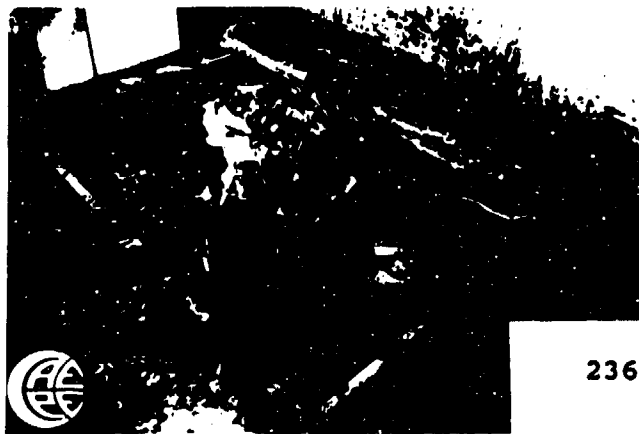
- Figure 1.b -
Close view of an explosion



- Figure 2.b -
Result after another explosion during a nozzle up
firing. The emission of shockwaves has been
mainly on a side of a motor



- Figure 2.a -
Result after an explosion



2 - FRENCH LEGISLATION OBLIGATIONS AND GENERAL PHILOSOPHY USED AT CAEPE FOR PREDICTING

2.1) FRENCH LEGISLATION

The French legislation about pyrotechnical safety has been thoroughly made uniform between 1979 and 1981 in order to be easily applied by any factory or test center (references 1, 2, 3). The area surrounding the pyrotechnical facility is classified in five safety areas (table 1) : the Z5 area correspond to light destructions of windows and to very unlikely injuries. The main hazards inside the limits Z1 to Z5 are due to aerial shockwave, fragments throwing and heat flux : the limits for each safety area are given in table 2. For Z5 area, over-pressure peaks are less than 50 hPa (0.7 psi).

Definition of safety zones

SAFETY AREA	Z1	Z2	Z3	Z4	Z5
Damages to human beings	Deadly wounds for more than 50 per 100	Important wounds which can be deadly	Wounds	Possibilities of wounds	Very unlikely possibilities of light wounds
Damages to materials	Very heavy damages	Heavy damages	Damages	Light damages	Very light damages

TABLE 1 (Table taken from reference 2)

Physical limits of safety zones

SAFETY AREA	Z1	Z2	Z3	Z4	Z5	OBSERVATIONS
Relative over-pressure peak (in hPa)	600	300	100	50		Higher values than these printed ones may be considered if duration of positive phase of over pressure signal is not above a certain value (of the order of 20 ms for the limits of Z1 and Z2 areas)
Energy of a flung fragment with no sharp corners (in Joule)	50	20	8			These values have to be reduced if the flung fragment has sharp or cutting parts
Heat flux (averaged density in Watt/cm ²)	1,5	0,6				This averaged density of heat flux has to be calculated over a duration according to the combustion conditions

TABLE 2 (Table taken from reference 3)

The reference 2 authorizes that the extent of Z5 area may be outside the test center perimeter. However, any crowded places such as hospitals, factories, schools or large buildings are not allowed inside the Z5 area.

The classification 1.1 correspond to pyrotechnical object which can detonate : their distances for Z1 to Z5 (on a flat ground and uniform weather conditions) are given by Table 3.

Safety distances for 1.1 pyrotechnical objects

SAFETY AREA	Z1	Z2	Z3	Z4	Z5
Distance from the charge whose weight is equal to Q	$0 < R_1 < 5 Q^{1/3}$	$< R_2 < 8 Q^{1/3}$	$< R_3 < 15 Q^{1/3}$	$< R_4 < 22 Q^{1/3}$	$< R_5 < 44 Q^{1/3}$

R : in meters

Q : in TNT - equivalent kilograms

TABLE 3 (Table taken from reference 3)

The text of reference 3 mentions that special conditions such as relief can induce variations of the limits Z1 to Z5. The variations of weather do not induce major changes for the extents of Z1 to Z4. The propagation of shockwaves whose peaks are above 50 hPa (0.7 psi) are not highly dependent of temperature or wind variations their prediction is relatively easy a long time in advance (with subcale studies or numerical computations). This can be performed for the primary safety analysis during the design of the test bay. The test site has to be sufficiently large to include the Z4 area. So there is no need for an operational and near-real time prediction for the limits of Z1 to Z4. However, under 50 hPa (0.7psi) aerial shockwave propagation depends highly on the weather stratification : focusing of shockwaves can happen during thermal inversion phenomena or (and) during strong vertical wind shear. So the extent of Z5 can vary according to the local weather conditions on the test day and there is a need for an operational prediction.

2.2) GENERAL PHILOSOPHY USED AT CAEPE

According to the weather conditions, the extent of Z5 can be quite large (e.g. several kilometers beyond CAEPE limits). So, the commander of a test center has the following solutions

Wrong solutions

- One possibility would be to try to reduce the shockwaves near its sources : the design of underground or indoor facilities is nearly impossible, because the combustion gases have a high flowrate (up to 0.3 tons per second at CAEPE). The only solution would be to build an expensive ejector tube and diffuser. This solution is performed only in altitude simulation facilities. For the other test bays, the costs are prohibitive.

- The use of barricades is efficient only for an horizontal distance equal to the height of the barricade multiplied by a factor of 4 (see reference 2). Beyond this distance, the use of barricades is useless in order to protect from aerial shockwaves.

- The purchase of additional ground surfaces is impossible for economical and political reasons.

Chosen solution

The knowledge of Z5 limits is mandatory before performing a large test with tons of 1.1 pyrotechnical products. The solutions chosen by CAEPE is to use the test facility according to the weather solution : before performing a firing, the CAEPE commander has to know where is located the Z5 extent in order to decide to do the firing or to postpone it until better weather conditions. This situation implies a reduction of the operational availability of the test bay but it is the easiest one to apply as far as predictions are not overly pessimistic.

For that reason, CAEPE has developed an operational prediction system which produces a map of the area surrounding its bay perimeter : the levels of shockwave amplitude and the densities of population are shown on this map.

However the commander of CAEPE (or of any large test center) do not care for precise predictions : his only worry is to be sure to clearly understand what are the maximum risks according to the local weather conditions. This implies a prediction of risks and not an accurate prediction of phenomena. The difference between these two aspects are the following :

- no detailed account for complex phenomena as far as their effects are maximized in the risk prediction
- a clearly readable map : to avoid a messy map, only two levels of pressure peaks are drawn
- 20 hPa : possible breakings of windows
 - 10 hPa : insignificant damages. (This means the end of the Z5 extent).
- time duration and integrated energies of shockwaves are commonly used to estimate potential damages. These factors are not taken in account. Only peak amplitude criteria is used.

In the present paper, the description of prediction system will only deal with predictions of risks. This will allow a lot of simplifications in the computations.

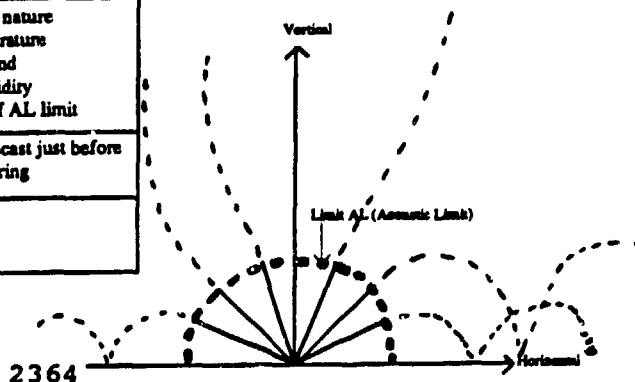
3 - PREDICTION SYSTEM

3.1) GENERAL VIEW

Table 4 gives a general view of the problem for aerial shockwave predictions. As indicated in paragraph 2.1, the close-field for aerial shockwave can be predicted independently to the weather conditions : this prediction is not easy but has to be done only once for every kind of tested pyrotechnical object (e.g. motor, military head...). For the far-field the prediction model is more simple but has to be used just before the test.

	HIGH-LEVEL SHOCKWAVE	SMALL-LEVEL SHOCKWAVE (summation of acoustic waves)
Model	non linear	linear (Frequencies are conserved during propagation)
Principal parameters to take in account	Source directivity Test bay relief Ground nature	Ground nature Temperature Wind Humidity Location of AL limit
Availability for prediction	Can be forecast a long time in advance	Can only be forecast just before the firing
Limit	Between 30 and 50 hPa (0.4 and 0.7 psi)	

Table 4 : General features for prediction of shockwaves
(For energy generated less than 200 TNT - equivalent tons)



3.2) SYNOPTIC OF THE SYSTEM USED AT CAEPE

Table 5 shows a synoptic of the prediction system used at CAEPE. The knowledge of the local weather conditions in the lower atmosphere are the first step. However, the key point is obtaining the map with critical danger areas. This is the result of a numerical prediction model which uses acoustic ray theory and which is detailed in paragraph 4. (The need for the knowledge of weather conditions depend on what are the inputs in the numerical code).

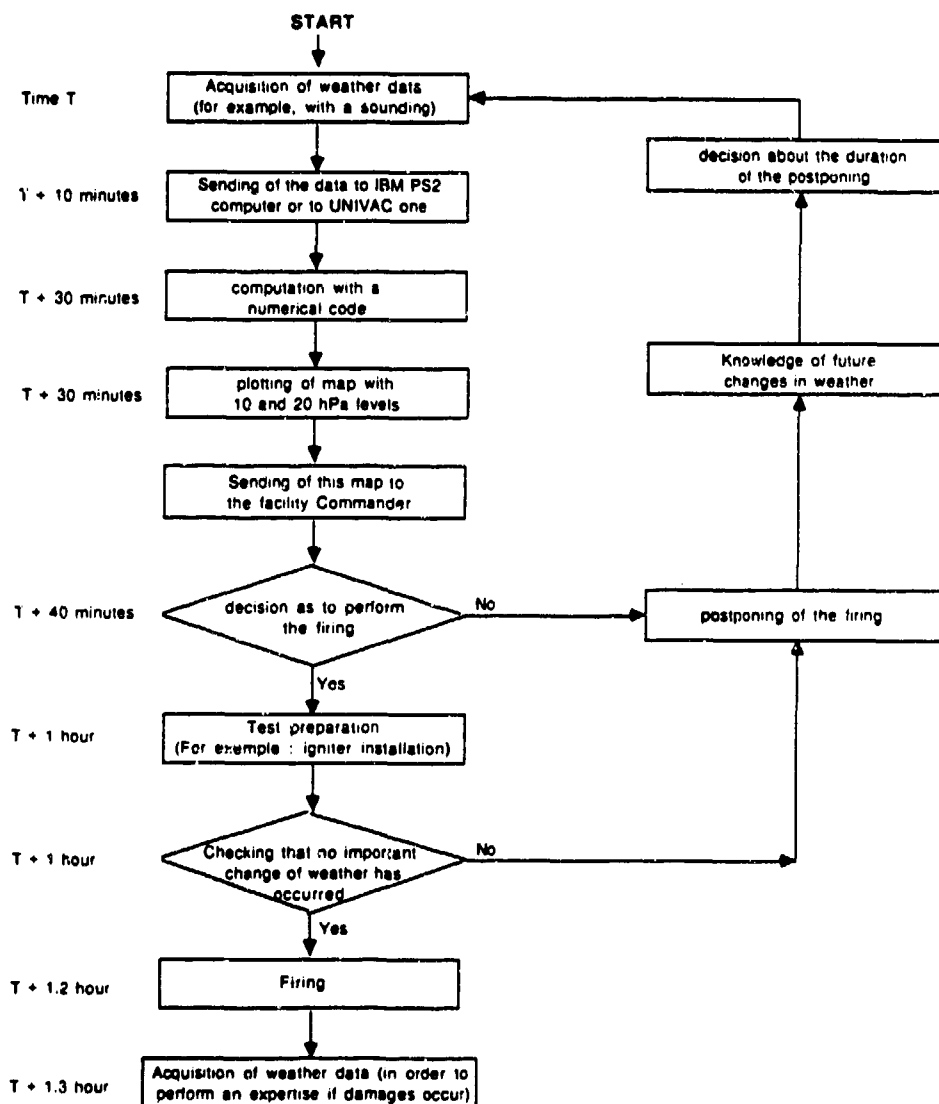


Table 5 : Synoptic of whole chain of decision. For small firings, some steps can be excluded. For complicated firing with a long preparation of the test equipment, weather sounding and predictions can be performed all along the day in order to allow an early postponing.

4 - NUMERICAL MODEL

4.1) STATE OF ART

Far field acoustic propagation has long been studied (see reference 4 for example). Predictions were highly dependent on poor capabilities of computers : in 1977, REED used a simple ducting criteria for sound velocity gradient in order to allow launching of TRIDENT 1C4 missiles from CAPE CANAVERAL. Nowadays, prediction uses mainly the two following methods :

- ray theory.

This assumes that sound propagation can be separated in small energy tubes with no interference between one and the others. So, the equations can be locally solved for each tube. The computation is performed with every tube along its path : this a lagrangian method.

For practical purposes (helicopter noise detection or road design), ISL and CSTB have recently developped models according ray theory (see references 6 and 7 for more details).

- parabolic method.

The equation for the whole field are solved : it is an Euler method. This method is more accurate than the ray theory method for low frequencies, but it needs a lot of computation time. ONERA has recently developped a model according to this theory, and has compared it with other models (references 8 and 9).

A lot of numerical work has also been performed for the study of long range propagation of noise in the underwater field because of the needs in discretion or detection of submarines. Most of this work can be applied in aerial acoustics.

4.2) MODEL USED AT CAEPE

4.2.1) Basic assumption

A shockwave can be considered as the sum of short duration sinusoidal "acoustic" waves (this is a simple Fourier transform). For small amplitude shockwaves, it is assumed that these acoustic waves can be studied independently : there are no interferences during their propagation. So, the propagation of small-amplitude shockwave can be modeled with summing the results of propagation of these independant acoustic waves. This "independance" assumption may be theoretically unsatisfying but it is enough for a risk prediction.

4.2.2) Choice of ray theory

Parabolic methods do better predictions in low frequencies than acoustic ray ones. However detailed comparisons between models show that small discrepancies in the case of focusing of acoustic energy. Figure 9 of reference 9 exhibits less 3 dB between ray and parabolic results at 80 Hz and 200 Hz.

- So the ray theory has been chosen by CAEPE. Its main advantages are the following :
- fast computations
 - ability to separate the following physical phenomena : i) geometrical propagation inside the air, ii) absorption by ambient, iii) rebounds on the ground. This allows the creation of codes with separated modules
 - an easy qualitative view of insight phenomena : the plotting of rays in a vertical plan enable to visualize where are the focusing areas.

4.2.3) Two-dimensional model

In case of transverse wind, the acoustic propagation can be curved, due to the term dV_e/dY ROSEN (reference 7) has studied this effect. Its Figure 11 (reference 7) shows that focusing areas are not so different with or without transverse wind : the difference in location is less than the order of 1 km at a distance of 10 kilometers from the source. This accuracy is beyond the scope of risk prediction (see paragraph 2.2). So, the model used at CAEPE is only two-dimensional and takes no account of effects of transverse winds.

Practically, for the geometrical propagation, this induce to solve the equations :

Ray paths :

$$\frac{d^2Z}{dx^2} = \frac{-1}{C + V_e} \left[\frac{dC}{dz} + \frac{dV_e}{dz} \right] \quad (1)$$

Z = vertical coordinate

X = horizontal coordinate

Y = horizontal coordinate perpendicular to «X»

C = modulus of sound velocity

V_e = modulus of wind velocity

In case of constant gradients, the equation (1) has parts of circles as solutions. These easy analytical solutions were used by scientists in the past before the improved performances of computers.

4.2.4) Source modelisation

The inputs for acoustic propagation are the shockwave field at the limit AL between short and long ranges areas of table 4. In CAEPE, we have simply taken 50 hPa for this limit even if this is not so clear in the scientific literature. The knowledge of the geographical position of this limit is taken in diagrams published for T.N.T explosions. At CAEPE, we use ISL diagrams (reference 10) for flat grounds with T.N.T - equivalent mass of explosives or propellants.

For simplification of computations, the energy is supposed to be uniform for the part of limit AL close to the ground with angle less than 20° . Actually, focusing computations use only the rays which creates rebounds. If one ray has no rebound (which means it goes straight up in the sky), the above rays will not rebound. So «uniform» assumption is necessary only for rebounding rays : these ones are located generally between the horizontal direction and an angle less than 20° .

4.2.5) Computation of energy levels

Equation (1) describes the propagation path of acoustic rays. Two situations can occur :

- a) - the rays impact the ground at a certain distance from the source and they rebound according to the nature of the soil and of the vegetation
- b) - the rays go up in the sky and no energy tube reach the ground.

Rebounds on the ground

For case a), the model used at CAEPE assume the conservation of energy in the acoustic tubes. This gives the equations (2) with notations explained in Figure 2

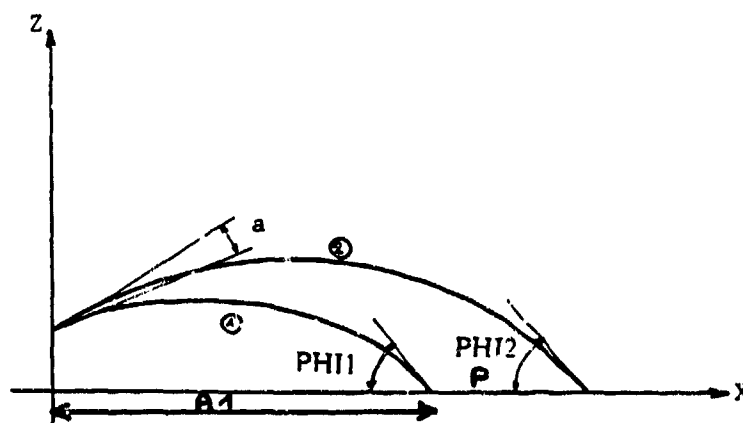
$$S = b (A2 - A1) \left(\frac{\sin \text{PHI1} + \sin \text{PHI2}}{2} \right) \left(\frac{A1 + A2}{2} \right) \quad (2)$$

$$I = \frac{W}{S}$$

with b = horizontal discretization angle

W = energy in the elementary tube

I = intensity of energy at the point on the ground level

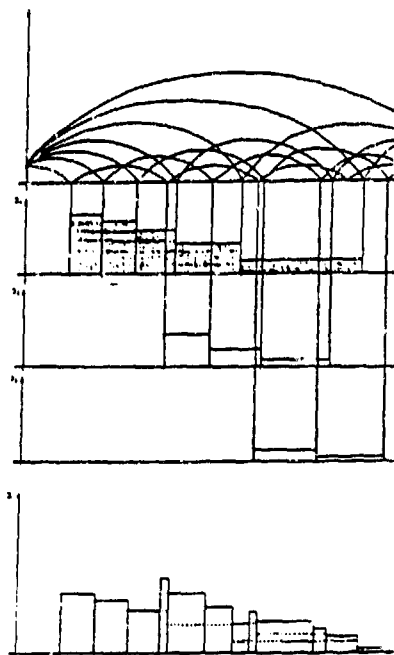


- Figure3 -
Elementary acoustic rays which are downwards

The summation of first rebounds from all acoustic tubes is a simple summation of the arithmetic modules of energy brought by each tube. As ever in this article, the phase aspect is not taken in account : the phase variations are complicated to compute; turbulence or local errors on the weather are important for these variations. So an easy maximization (see paragraph 2.2) is to suppose that all the waves are with the same phase.

The summation of all successive rebounds is performed in the same manner. This gives the scheme described in Figure 4.

- Figure 4 -
Summation of energy due to rebounds



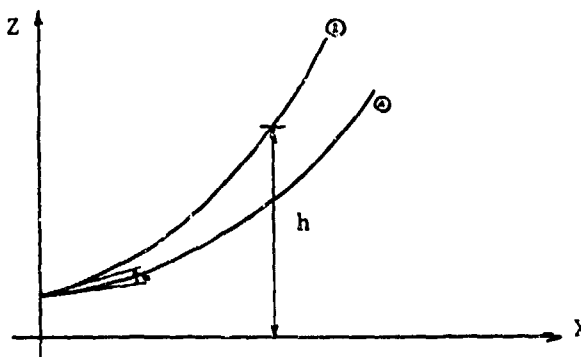
No rebound on the ground

For case b), ray theory indicates that no energy reaches the ground. So, no noise should be heard at the ground level. However, diffraction and diffusion effects induce a small amount of noise and they are not taken in account in ray theory. These phenomena are to be maximized by simple methods.

In addition, the case of atmospheric neutral conditions (no gradients of wind and temperature) is between cases a and b. It produce an hemispheric solution with a decrease law in $R^{1/2}$.

For a risk prediction, a maximization of case b) can be performed with the equations (3) with notations explained in Figure 5.

$$\left. \begin{aligned} I &= \frac{W}{S} \\ S &= h \times a \end{aligned} \right\} \quad (3)$$



- Figure 5 -
Elementary acoustic rays which are upwards

4.2.6) Atmospheric absorption

Humidity and temperature in the air can induce important attenuations of sound. In hot and humid weather, this induce a fast decrease of amplitudes of sound waves. To take in account this factor, CAEPE use tables from reference 11.

4.2.7) Absorption during reflection on the ground

This effect happens each time that there is a rebound of an acoustic path on the ground : the induced attenuation can be important on soft soils such as mud, damp, or snow and on thick vegetation.

In order to study this effect, CAEPE has used the simple theory which takes in account the acoustic ground impedance Z and the angle between the ground and the incident reflected ray. Values for Z were taken from references. The computations were performed only with amplitudes of sound waves and not with phases. After studies with the natures of soils around CAEPE, it was found to be no too pessimistic to use a perfect reflection ground. This induced a simplification of CAEPE model and was consistent with a risk prediction.

4.2.8) Raised relief effects

The CAEPE is located in the pine trees forest of LANDES near Bordeaux. It is the largest forest in France and its ground is flat : altitudes varies for less than 15 meters for distances in tens of kilometers. So, for CAEPE computations, the ground was supposed to be uniformly flat.

4.2.9) Necessary weather inputs

In order to run our numerical model, the following weather inputs are needed :

- vertical profile for temperature
- vertical profile for wind (direction and amplitude)
- averaged humidity

These values are needed locally. Because of its uniform nature of the LANDES area, weather conditions are taken as uniform for the area surrounding CAEPE. So, only one vertical sounding in a close location from the test site is considered. According to the hour of CAEPE firings, the sounding from the close BORDEAUX International Airport or from CAEPE own weather station is used. For less than 10 Tons of TNT-equivalent, only the first vertical 1000 meters are used as inputs for the prediction computations. Up to 200 Tons, the first 2000 meters are considered to be useful. The time delay between weather CAEPE firing has to be minimum. As described in table 5, this depends on the remoteness of the location of test site, on the performances of numerical program for prediction and on the preparation of the firing. In anti-cyclonic conditions, weather conditions can be quite steady in time. However, this is not the case during the passage of fronts. This matter will be discussed in paragraph 6.



5 - CHECKING OF THE CHOSEN MODEL

5.1) VERIFICATION OF THEORETICAL RAY PATHS

As explained in paragraph 4.2.3) these paths are relatively simple. The ones from CAEPE models were checked with the ones of Figures 20 to 23 of reference 12. In addition, the numerical stability was checked on the repeatability of curves after numerous rebounds.

5.2) SOUGE EXPLOSION

On the 21 November 1986, a large detonation occurred during the destruction of 1.5 Tons of old explosives in a site called SOUGE which is west from BORDEAUX. This phenomena created a few problems around. The larger damages happen in a factory located at place X in Figure 6. A strong «bang» sound was also heard in the dashed area.

Legend:  Villages where a strong "bang" was heard
 Location of the factory where the biggest damages occur.

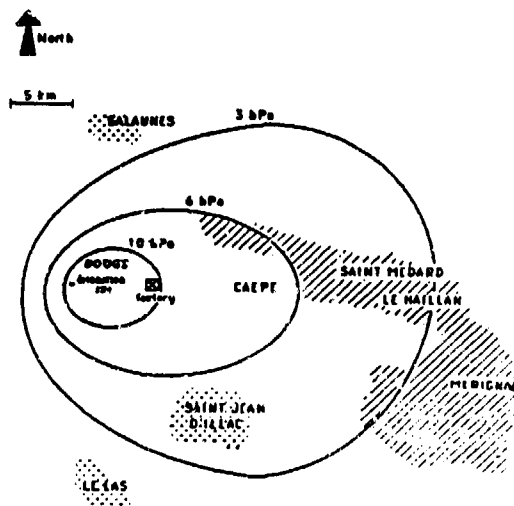


Figure 6

Map of the area around SOUGE detonation site
 Predicted overpressure contours are also shown

The explosion site was less than 10 kilometers away from BORDEAUX airport where was performed weather sounding at about the same time (an half hour) than the explosion. CAEPE prediction model was used with these data. Figure 6 shows an example of computation for 270° - 90° directions. Figure 7 show the predicted amplitude level for the area surrounding the sites. The predicted level 10 hPa (0.14 psi) is coherent with the phenomena encountered in the factory. The areas where the «bang» noise was heard, correspond with the predicted levels above 3 hPa (0.04 psi).

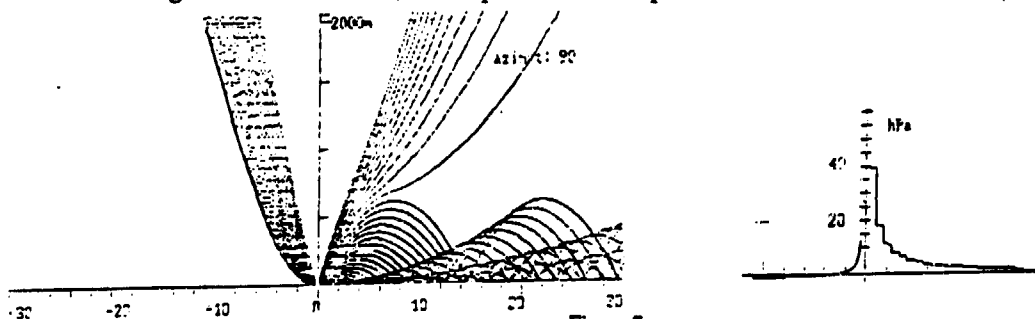


Figure 7

Example of prediction computation in a vertical plane

5.3) MEDINA EXPLOSION

On the 13 November 1963, a detonation of a huge quantity of chemical explosives happened at Medina facility, on the outskirts of San Antonio, Texas (Figure 8). Reference 13 describes the damages created by this accident and contains ray theory computations. The TNT equivalent was taken as 140 tons. The weather conditions were known because of temperature and wind sounding at the close San Antonio International Airport.

With the east-west wind and the temperature profiles described in reference 13, predictions were performed with CAEPE code. For example, Figure 9 shows ray paths for the 90° - 270° direction. The North-South component of the wind was supposed to be nul (Reference 13 indicated that the wind gradients were predominantly in the east-west direction).

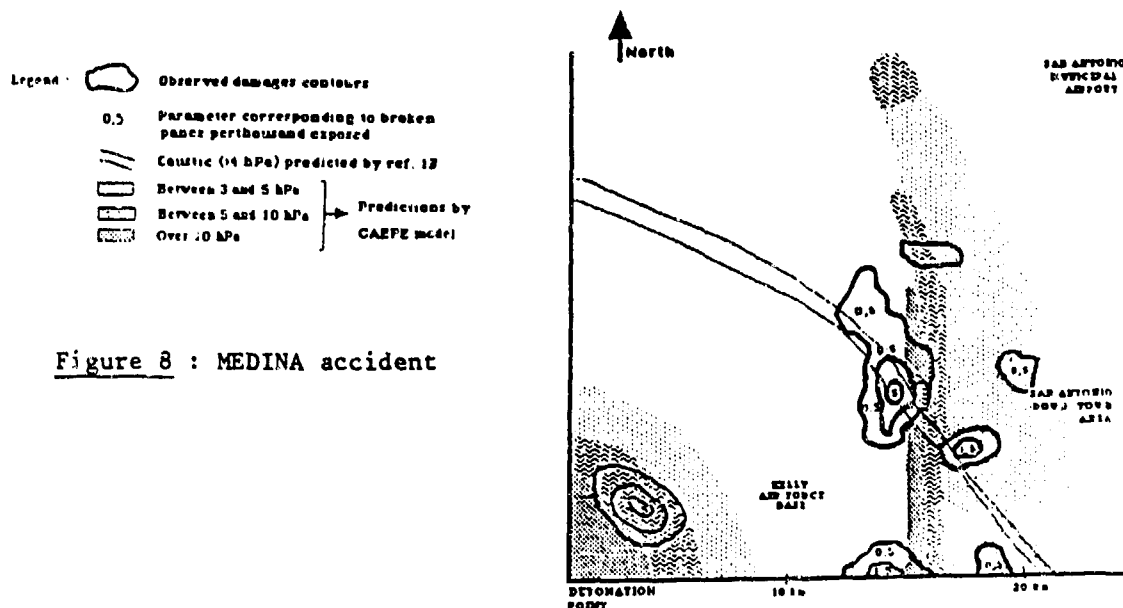
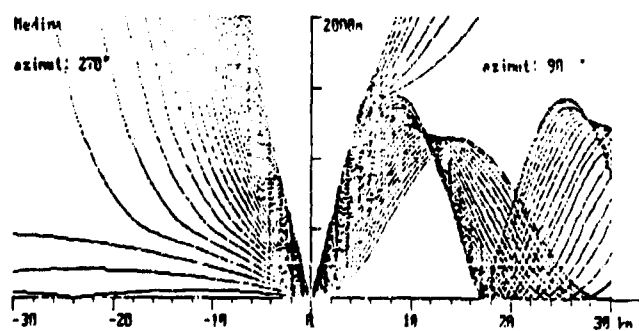


Figure 8 : MEDINA accident

Figure 8 shows CAEPE predictions. Its main features correspond with real observations (taken from reference 13) : a focusing due to the wind gradient occur 15 kilometers away from Medina site. The extent of this focusing area is about 3 kilometers large. The encountered levels range from 8 hPa (0.12 psi) to 3 hPa (0.04 psi) : these levels are enough to break glasses in an urban area. For directions close to the north one, larger discrepancies occur between CAEPE observations and reference 17 results : the planned obtention of North South component of the wind will perhaps enable to solve these discrepancies.

- Figure 9 -
Example of focusing for Medina explosion
(azimuth 270° - 90°)



6 - ESTIMATION OF UNCERTAINTIES

6.1) GENERAL COMMENT

The uncertainties and errors in CAEPE predictions are due to the following origins :

- physical phenomena which are not taken or badly taken in account by CAEPE model
- numerical imperfections of CAEPE code
- wrong estimation of weather conditions

These three problems are detailed in the next paragraphs.

6.2) PHYSICAL PHENOMENA WHICH ARE NOT TAKEN IN ACCOUNT BY CAEPE MODEL

6.2.1) Turbulence :

According to scientific literature (see ref 9, 12, 14 and 15 for example), turbulence modifies amplitudes and phases of acoustic waves. Reference 9 indicate variation of 10 dB over short periods, typically a few seconds. Sophisticated models can take in account turbulence, such as KE, Ke or higher order closure equations. However, this requires the precise knowledge of surrounding flowfield. This is beyond our operational capabilities.

For shockwaves prediction, the result is the summation of different acoustic waves (see paragraph 4.2.1.) Turbulence has a different effect on each wave according to its wavelength. So, turbulence effect is perhaps less important for shockwave levels than for mono-chromatic sounds. In addition, the loss of coherences for phases will induce a decrease in overpressure peak. This decrease is not predictable by CAEPE model.

6.2.2) Diffusion and diffraction

These effects are difficult to take in account. They have a weak importance for prediction of focusing levels. They are predominant in «silent» zones where no acoustic rays arrive, but they still induce very low level of noise. So, these effects can be neglected in an operational prediction.

6.2.3) Source directivity

The assumption of uniform emission for rays paths close to the ground (see paragraph 4.2.4) is certainly wrong. On a 1/50° subscale test of an open air test bay, ISL has performed measurement of pressure waves at the angle 5° and 10° all around the source (reference 16). Variations of only 20 % were found between all these measurements.

This result is satisfying because of the relatively small induced error. However this scheme can be wrong in case of peculiar accident : detonation in a rocket motor can start in an anormal way and can even be only partial. This can give peculiar diagrams of directivity.

6.2.4) Existence of caustic

When different ray paths merge at the border of a silent zone, this give a caustic curve where energy density is supposed to be infinite. This is obviously not true in reality, but considerable

enhancements of pressure peaks can nevertheless happen near this caustic. This effect is of prime importance in a risk prediction. A relatively correct account for this is to have a sufficient vertical angular discretization: this allow to simulate enough ray paths (see paragraph 6.3.2. for numerical details).

6.3) NUMERICAL IMPERFECTIONS

6.3.1) Horizontal angular discretization

The computation is performed for vertical planes with an angle b between each plane. Usually, the value for b is taken equal to 10° , 15° , 20° or 30° according to the needed accuracy. An angle of 15° is largely enough to detect dangerous situations. So, this discretization induces no important error in a risk prediction.

6.3.2) Vertical angular discretization

In a vertical plane, the computations are performed in order to show results similar to the outputs presented in Figure 7. The angle "a" between two beginnings of rays is a key point for computation time.

Focusing-case

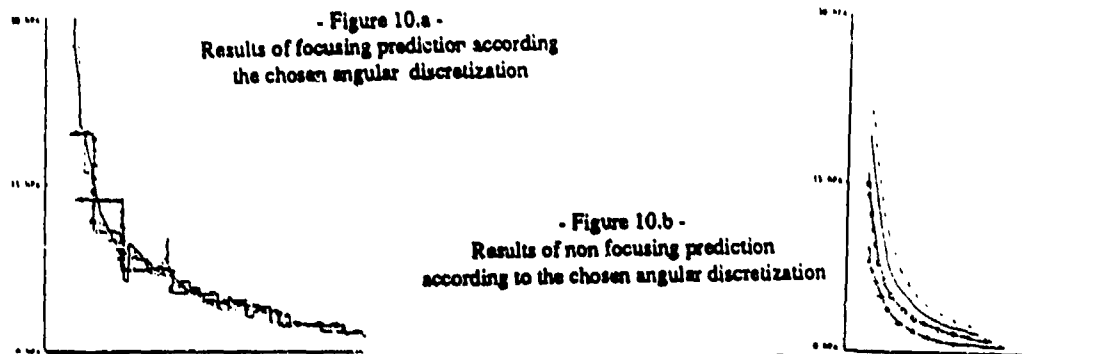
Figure 10 a shows results with "a" values equal to 0.1° , 0.3° , 1° , 2° for a focusing case. Obviously more detailed results are obtained for small angle increments (0.1° , 0.3°) than for large increments. Local increases of 4 hPa compared to a mean value of 8 hPa are observed. This is due to the close encounter of two adjacent rays (see previous discussion about caustics).

Non-Focusing case

The equation (3) is an artificial use of an extrapolation of results from neutral conditions. The angle "a" is the angular discretization. The path of the first ray above the horizontal (see Figure 4) is supposed to give the energy at ground level. The case of convex ray paths is most common for non-focusing rays. So, the rougher is the angular discretization, the higher is the «computed» value for pressure peak. This obvious feature is illustrated in Figure 10 b. This feature has no importance because the military perimeter around the test site is large enough to insert any non-focusing situation especially the neutral conditions ones.

6.3.3) General reliability of the numerical code

Some peculiar situations can happen if the software has not been fully analyzed. For example, rebounds close to the external corner near the external border (usually 15 or 30 kilometer) can stop the computation. Similar problems happen also if mistakes have been done during writing of code lines. This is a weak point for CAEPE code because it was written by engineers and not by specialists of software quality. This kind of worry are well known, in software development. They are beyond the scope of the present paper.



6.4) METEOROLOGICAL INPUTS

6.4.1) Errors in the sounding

Usual radio sounding give temperature, humidity and windspeed with a high rate of values in less than one hundred meters. However the results can be wrong if the gauges are badly calibrated or badly installed. In addition, the local sounding can be non-representative of the general conditions, for example with a sounding performed under a cumulo- nimbus.

In order to investigate these errors, various typical weather situations were studied with artificial variations. First, variations of temperature profile were introduced inside general conditions with no temperature inversion and a strong wind gradient. These conditions are shown in Figure 11 a. The result of computation with CAEPE code are shown in Figure 11b. Secondly, the same method was applied inside general conditions with a weak wind gradient and a strong temperature inversion (Figure 12a and b). Thirdly, variations of wind profile were introduced inside general conditions with a strong wind gradient and no thermal inversion (Figure 13a) ; the computation results are shown in Figure 13b.

These results show strong variations of pressure peaks. The order of magnitude of 6 dB corresponds to the multiplication of the signal by a factor equal to 2.

6.4.2) Time evolution of weather conditions

Table 5 indicates the synoptic of operations before a firing. About one hour happen between the obtention of radio sounding and the firing time. This delay can induce changes of weather. Some minor changes can happen without changing the general pattern of the risk prediction. However, others can be more important, especially during a front passage.

The only way to protect oneself against such strong changes is to have a precise weather forecast station. At CAEPE, the one from Centre d'Essais des Landes (D.G A /C.E.L.) is used : D.G.A/C.E.L. station is part of French National Weather Service (METEO FRANCE) and has a general code for all the Eastern North Atlantic and a detailed code with a local grid of 30 kilometers over BORDEAUX area.

6.5) SUMMARY : SYNOPTIC OF ERROR SOURCES

	ACCOUNT IN MODEL	INDUCED UNCERTAINTY
1 - Physical phenomena		
Turbulences	no account	large uncertainty
Diffusion + diffraction	no account	small in focusing cases
Rebound on ground	maximized	no uncertainty because of the maximization
application of ray theory to low frequencies	_____	small in focusing cases
Absorption by air	account	weak
2 - Numerical imperfections		
Horizontal angular discretization	_____	no large uncertainty with 10° to 20° angles
Vertical angular discretization	_____	large uncertainty for 1° and 2° angle weak uncertainty for 0.1° to 0.5° angles
3 - Weather account		
Input errors	_____	large uncertainties
Weather variations	no account	large uncertainties but can be planned with a good meteorological forecast.

Note 1 : these two effects were already discussed in paragraph 4 and have not been

6.6) OPERATIONAL APPLICATION

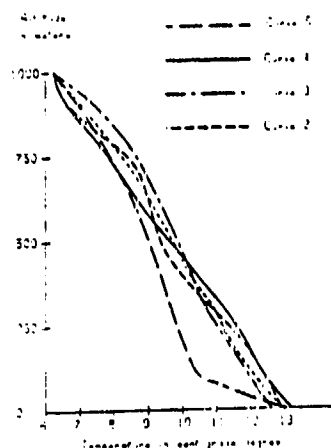
Except for strong turbulence situations or for a wrong use of radiosounding materials, the study described in previous paragraphs show that a realistic risk prediction can be performed : the assumed uncertainty is taken as equal to 5 hPa (0.07 psi) for a 15 hPa (0.22 psi) signal and to 3 hPa (0.04 psi) for a 7 hPa (0.1 psi) signal. So the levels 20 hPa (0.29 psi) and 10 hPa (0.15 psi) shown on the prediction map to CAEPE commander are actually the levels 15 hPa (0.22 psi) and 7 hPa (0.1 psi).

7 - CONCLUSION

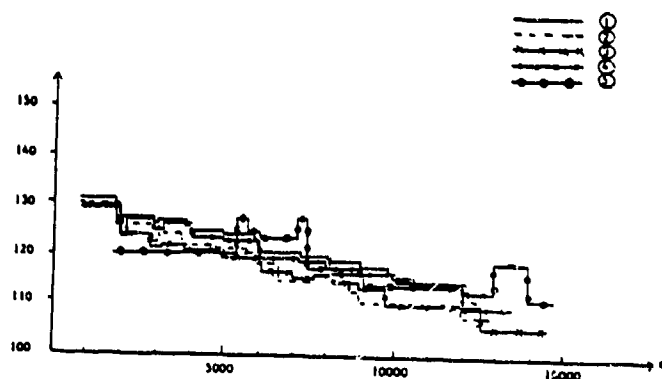
For a risk analysis, the code used at CAEPE is sufficient : the approximated areas of focusing and the order of magnitude of pressure peaks are relatively well predicted or at least maximized.

The main problems are due i) to the approximate values of sounding results and ii) to the time delay between weather sounding and actual test. With an IBM PS2 this delay is rather independent of minutes of computer time for map producing : it is partly due to the duration of operations and possible delays before and after the agreement of the commander to perform the firing.

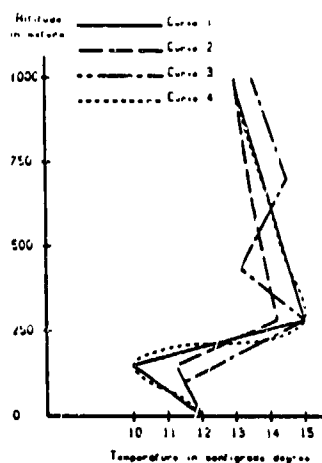
In order to improve our prediction, emphasis has to be put on immediate acquisition of weather data: even the best prediction model will perform a wrong output if its inputs are unreliable. Real time sounding apparatus have been developed in industrial world for the last ten years. For example, SODAR using acoustic diffraction gives real time wind profiles every minute. Presently, at CAEPE, a study is going on in order to modify our weather station. This will lead to an improved reliability of the prediction results.



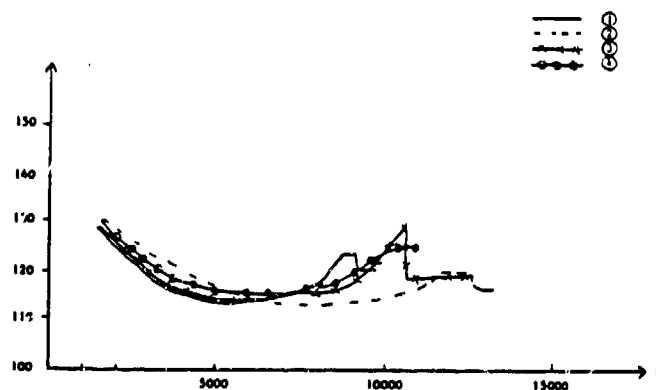
- Figure 11.a -
Different temperature profiles studied in case of
a strong wind gradient and no thermal inversion



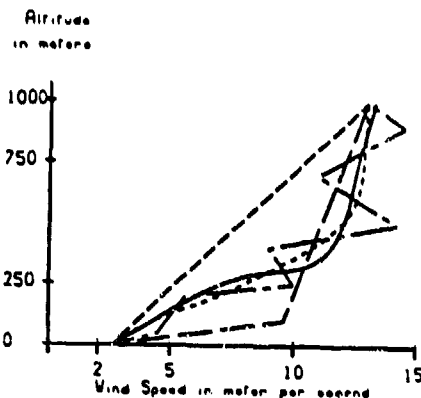
- Figure 11.b -
Long-range predictions with the temperature
profiles described in Figure 11.a



- Figure 12.a -
Different temperature profiles studied
in case of a strong thermal inversion

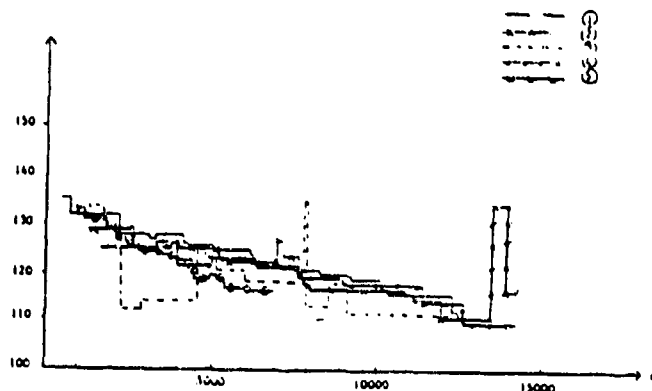


- Figure 12.b -
Long-range predictions with the
temperature profiles described in Figure 12.a



- Figure 13.a -

Different wind profiles studied in case of a strong wind gradient and no thermal inversion



- Figure 13.b -

Long-range predictions with wind profile described in figure 13.a

REFERENCES

- 1 - 1979 - "Décret N° 79-845 du 28.09.1979 portant règlement d'administration publique sur la protection des travailleurs contre les risques particuliers auxquels ils sont soumis dans les établissements pyrotechniques" - Journal Officiel du 2.10.1979 et rectificatif au Journal Officiel du 18.11.1979
- 2 - 1980 - "Arrêté du 28.09.1980 fixant les règles de détermination des distances d'isolement relatives aux installations pyrotechniques" - Journal Officiel du 2.10.1980
- 3 - 1981 - "Circulaire du 8.05.1981 relative à l'application de l'arrêté du 26.09.1980 fixant les règles de détermination des distances d'isolement relatives aux installations pyrotechniques"
- 4 - J.E. Piercy ; T.E.W. Embleton ; L.C. Sutherland - 1977 - "Review of Noise Propagation in the Atmosphere" - Journal of the Acoustical Society of America, 61 (6)
- 5 - J.W. Reed - "Blast Predictions for Trident Test Launches" - Sandia Laboratories - Albuquerque
- 6 - J. Vermorel - 1987 - "La propagation acoustique dans la basse atmosphère" Université de Haute Alsace - I.S.L. - Thèse R 126/87
- 7 - M. Rosen - 1986 - "Contribution à l'étude des effets du vent et d'un gradient de température sur l'efficacité des écrans acoustiques" - Thèse de Doctorat - CSTB - Université du Maine
- 8 - V. Malbéqui - Septembre 1989 - "Etude d'un réseau à pas variable et comparaison entre la méthode des rayons et l'équation parabolique dans le cadre de la propagation acoustique atmosphérique" - Rapport final N° 12/3641 PY
- 9 - S. Canard-Carvane, S. Lévy, J. Vermorel, G. Parmentier - 1990 - "Long Range Sound Propagation Near the Ground" - Noise Control Engineering Journal - May-June 1990
- 10 - M. Froboese - 1968 - "Fonctions de propagation des ondes de choc aériennes sphériques" - Rapport I.S.L. 3/68
- 11 - 1980 - AFNOR - Norme S 30.009 - "Atténuation du son dans l'air"
- 12 - J. Vermorel, G. Parmentier - 1986 - "Propagation acoustique dans la basse atmosphère - Etude expérimentale et modélisation par la méthode des rayons" - Communication présentée au 10ème Colloque d'Acoustique Aéronautique et Navale - Marseille
- 13 - J.W. Reed, B.J. Pape, J.E. Minor, R.C. DeHart - 1963 - "Evaluation of window pane damage intensity in San Antonio resulting from Medicine Facility explosion on November 13, 1963" - Annals New York Academy of Sciences
- 14 - P. Naz, G. Parmentier - 1990 - "Propagation du bruit des hélicoptères dans les basses couches de l'atmosphère" - Colloque de Physique - Colloque C2, supplément au N° 2, Tome 51, 1er Congrès Français d'Acoustique 1990
- 15 - J.D. Turton, D.A. Bennett, D.J.W. Nazer - 1988 - "The Larkhill noise assessment model - Part II: Assessment and use" - The meteorological magazine N° 1391 - June 1988 - Vol. 117
- 16 - G. Parmentier - 1989 - "Etude de la propagation des ondes de choc autour d'un banc d'essai de propulseurs à poudre à l'aide d'une maquette à l'échelle 1/50" - Rapport technique I.S.L. - RT 88024/69
- 17 - 1988 - "Arrêté du 20.08.1988 relatif aux bruits aériens émis dans l'environnement par les installations classées pour la protection de l'environnement" - Journal Officiel du 10.11.1988

APPENDIX

PREDICTION OF LONG DURATION HIGH NOISE

Table A1 shows a comparison between high noise predictions and shockwaves ones.

	SMALL SHOCKWAVE	HIGH NOISE
Legislation	rules about the areas with potential light damages (references 1,2,3)	no surrounding area over 160 dB Limited level over the whole year : integration of all noises during a year : (see reference 17)
Computations	ray theory for the far field	ray theory
Source	limit of shockwaves near 50 hPa	nearly a pinpoint source
Outputs	map in hPa	map in dB (for building response) and in dB a (for human response)

Table A1 : Comparison between high noise predictions and shockwave ones.

A version of CAEPE model inserts noise sources and produces maps with levels in dB and dBA. An example is given in Figure 14 : it shows the far field noise generated by the launcher ARIANE 5 before it lifts off from the ELA3 platform. The induced levels are very weak for the areas far from the launching pad : they are even weaker than the ambient normal noise.

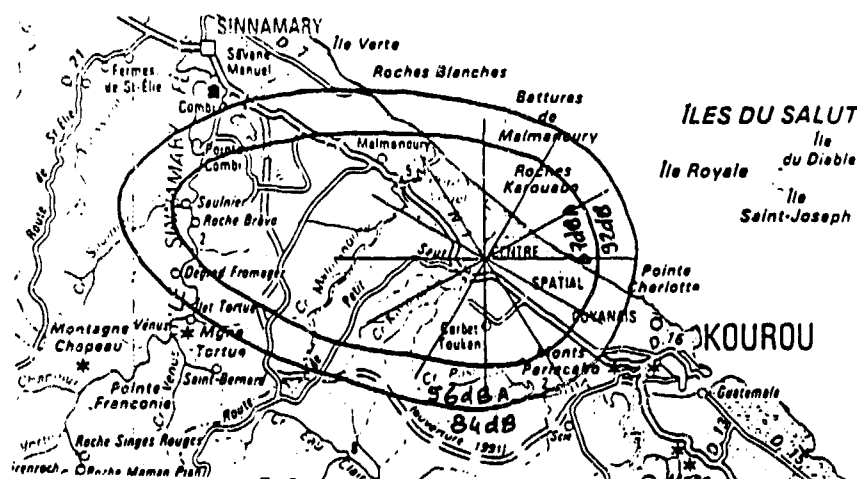


Figure 14 : Far field levels generated by the launcher ARIANE 5 before its lift off. This prediction work was performed on account of CNES/CSG.

(Curves in dB and dBA are normally not the same : the attenuation of sound due to air or to ground rebounds are different according to frequencies. However, for ARIANE 5 computations, these curves are only slightly different. So, on the map, each curve represent a level in dB and one in dBA).

PROGRAM "BLASTO" FOR WEATHER-DEPENDENT AIRBLAST PREDICTIONS.

Jack W. Reed
JWR, Inc.
Albuquerque, New Mexico

ABSTRACT

A test and evaluation draft version of BLASTO was described and demonstrated at the 23rd DOD Explosive Safety Seminar [1] in 1988. It produces overpressure-distance tables for a variety of input conditions of yield, ambient conditions, and height or depth of burst. When upper air weather observations are available, they allow directional, weather dependent adjustments to the overpressure-distance function, based on atmospheric refraction effects and propagation experiments.

Several individuals and agencies have tried it and provided their comments and questions. Some minor errors were uncovered, mostly traced to a history of translations from main frame through VAX to PC MS-DOS operation. BLASTO also needs to be more user-friendly; an expert in explosive effects, meteorology, and computers has little trouble in understanding or running it, but it appears that a more typical prospective user may lack one or more of these skills. A current up-dated version will be described in this report and suggestions will be solicited for further improvement.

INTRODUCTION

A personal computer program BLASTO, for weather-dependent airblast predictions, was introduced and described at the 23rd DOD Explosive Safety Seminar along with a report on the PEPCON accident at Henderson, Nevada [1]. Over one hundred copies were distributed in draft form for test and evaluation by the potential user community with IBM-compatible MS-DOS systems. There have been disappointingly few responses and comments about this disk program, and many of these have involved localized and corrigible troubles with disk loading or weather data file reading.

A few who have actually run BLASTO have found some minor bugs which have been corrected. Several incidents, however, have demonstrated elements of unfamiliarity with either computers, airblast phenomena, or meteorology. It thus appeared that a more user-friendly BLASTO was necessary and changes have since been made toward this goal. These will be demonstrated in this paper.

BACKGROUND

BLASTO accepts inputs of explosion yield and material, ambient pressure, and height-of-burst or depth-of-burst, and generates an equivalent nuclear explosive (NE) point yield. With distance scaling laws [2] and a reference standard explosion phenomenology [3-5], it produces an overpressure versus

distance function for the airblast wave in a calm, homogeneous atmosphere. Adjusted functions are then calculated for five typical categories of weather conditions of directed sound velocity versus height which may distort an airblast wave by refraction. Weather dependencies had been established by various experiments [6,7].

With shot-time weather available - usually radiosonde weather balloon observations (raobs) - effects of upper air temperatures on sound speeds and of winds aloft on directed sound velocities are used by BLASTO to estimate propagation enhancements or attenuations for specified directions. Azimuths for concern may be selected either in around-the-clock increments or toward specified target locations. A wide range of acceptable input units is allowed, but calculations are done and output is provided in metric units, with one exception allowed by special command.

BLASTO MOD 8.0

This high model number reflects 20 yr of BLASTO evolution, with major modifications required at each transition through a series of main frame computers and operating systems at Sandia, from IBM, CDC, Cray, and VAX systems to today's IBM-PCs. BLASTO now comes on two 5.25" standard density floppy disks, with almost 500 kbytes in 22 files. With a BLAST command, an introduction is brought to the screen (see Table 1) which describes various starting modes. If most needed information is already in archived files, the start command is BLASTO. If new test, shot point, target, or weather data are to be used, startup commands NEWTEST, NEWGZ, NEWTGT or NEWX are used for data entries.

NEWTST brings to screen a form (see Table 2) for entering all essential input test parameters. It is presented with filled out blanks as examples, but these are overtyped with new material. Results are translated, reformatted, and added to an archive file of test data for access by BLASTO. NEWGZ and NEWTGT bring to screen their respective archives of previous entries. Additional location names and coordinates are appended to these files.

NEWX takes a radiosonde observation in any of several commonly-used codes or formats (Table 3), translates it to proper format, and appends it to a weather archive file for access by BLASTO. When all new information has been entered, a BLASTO command starts an interactive session for selecting desired sets of input data for analysis. Throughout this interactive phase, each keyboard entry is checked for appropriateness, and typographical errors or out-of-range entries are immediately rejected with a call for a corrected entry.

The first selection (see Table 4) picks the test name to be used, followed by an opportunity to make temporary changes to any of the provided parameters. Next, a choice is allowed between AFWL-75 [3,4] and DNA-81 [5] Standard explosion models. Then a listing is shown of archived radiosonde data/times, from which one is chosen. If a test location and a target list is available (see Table 5), appropriate selections and opportunities for changes are presented. A choice of directions for analysis is also made at this time.

Provision is made for updating surface weather reports. Since raobs are usually taken only twice daily (at 0000 UT and 1200 UT) and at widely spaced locations (roughly 500 km separations), more timely and localized test conditions of wind and temperature will probably be required for real-time operational predictions.

The final interactive choice allows alternative English units for tabulations of directed wind components and sound velocities versus height. These may aid in pin-pointing upper wind and temperature levels that could be causing an unacceptably strong airblast prediction for a particular target. Then weather forecasters could be consulted about any likelihood of needed improvement in these particular features. Use of familiar English units may enhance this process.

RESULTS OUTPUT

On completion of calculations, BLASTO saves about five pages of tabulations in an output file BLASTO.DAT. This file may be read from a screen or given a PRINTER command. Portions of this output (see Table 6) include definition of units code numbers, a summary of input test parameters, and overpressure-distance values for six categories of weather-dependent propagation. Input weather reports are repeated as in Table 7, followed by tables of directed sound velocities and wind components. The bottom-line result, in Table 8, gives distances to selected overpressures in each specified direction.

IN CONCLUSION

An attempt has been made to give BLASTO, a program for weather-dependent airblast propagation predictions, user-friendly and goof-proof characteristics for operation by less-than-expert practitioners. This latest Model 8.0 has been proof-tested on three IBM-compatible personal computers operating in MS-DOS. It appears to work satisfactorily on Tandy 4000, AT&T 6300, and Leading Edge D machines.

Earlier versions of BLASTO, prepared before this author's retirement from Sandia National Laboratory, were non-proprietary and distributed with no charge, in hope of soliciting constructive response and commentary for improving its accuracy and effectiveness. Defense Nuclear Agency had expressed an intent to underwrite this subsequent BLASTO refinement project, for the general benefit of explosives operators. Unfortunately, this has not yet occurred because of ubiquitous DOD budget woes, so updates must be negotiated.

REFERENCES

1. Reed, J. W., "Explosion Airblast Predictions on a Personal Computer and Application to the Henderson, Nevada, Incident," in Minutes, 23rd DOD Explosive Safety Seminar, DOD ESB, Washington, DC, August 8-11, 1988.
2. Glasstone, S. and P. J. Dolan (Editors), The Effects of Nuclear Weapons, 3rd Ed., USGPO, Washington, DC, 1977.
3. American National Standards Institute, Estimating Air Blast Characteristics for Single Point Explosions in Air, with a Guide to Evaluation of Atmospheric Propagation and Effects, ANSI S2.20-1983, Acoustical Society of America, New York, NY, 1983.
4. Needham, C. E., M. L. Havens, and C. S. Knauth, "Nuclear Blast Standard (1 kt)," AFWL-TR-73-55 (Revd.), USAF Weapons Laboratory, Kirtland Air Force Base, NM, 1975.
5. Needham, C. E., and J. E. Crepeau, "The DNA Nuclear Blast Standard (1 kt)," DNA 5648T, S-CUBED, Inc., Albuquerque, NM, 30 January 1981.
6. Reed, J. W., "Climatology of Airblast Propagations from Nevada Test Nuclear Airbursts," SC-RR-69-572, Sandia Laboratories, Albuquerque, NM, December 1969.
7. Reed, J. W., "Project Propa-Gator Intermediate Range Explosion Airblast Propagation Measurements," in Minutes, 19th DOD Explosive Safety Seminar, DOD ESB, Washington, DC, September 9-11, 1980.

Table 1. Introductory Video Display of BLASTO Commands

BLASTO - AIRBLAST PREDICTIONS PROGRAM FOR EXPLOSIONS. Mod. 8.0

Jack W. Reed, JWR, Inc. Tel. (505) 265.6550
 5301 Central NE, Suite 220, Albuquerque, New Mexico 87108

 ***** Operations may be terminated at any time by typing CTRL+C *****

OPERATING MODE COMMANDS: BLASTO NEWX NEWTEST NEWTGT NEWGZ PRINTER

Type: BLASTO <CR>

This command starts Program BLASTO, and assumes that all necessary information has been previously entered into appropriate data files, or will be entered through keyboard interactions with BLASTO. Thus,

- a) Desired test parameters are listed in TESTS.DAT;
- b) Weather data (if needed) are listed in RAOBS.DAT;
- c) Desired shot point coordinates are listed in SHOTPTS.DAT;
- d) TARGETS.DAT contains the necessary target coordinates.

***** OTHERWISE *****

Type: NEWX <CR> - This command is used after entering a new coded upper air radiosonde observation in file named WXCODE.INP (Weather Code Input). It will start Program WXCODE for translating coded data into a format needed for running BLASTO. This new tabulation is appended to the weather data archive file RAOBS.DAT (and preserved for future recall). It may then be accessed by BLASTO following interactive entry of the appropriate date/time groups.

***** OR *****

Type: NEWTEST <CR> - This command opens a blank form NEW TEST DATA, for entering necessary parameters of a newly defined test into an archive test record file TESTS.DAT. It will be accessed by BLASTO through interactive selection of the appropriate test name.

***** OR *****

Type: NEWTGT <CR> - This command opens archive file TARGETS.DAT, for entering a target name and its related explosion site and coordinates. Entries may then be accessed by BLASTO.

***** OR *****

Type: NEWGZ <CR> - This command opens file SHOTPTS.DAT, for entering the new shot point name, test site, and GZ coordinates. Entries may then be accessed as requested by BLASTO.

***** OR *****

Type: PRINTER <CR> - This command sends calculations output file BLASTO.DAT to your printer.

***** MAKE A CHOICE, AND THEN *****

Type: BLASTO, NEWX, NEWTEST, NEWTGT, NEWGZ, or PRINTER, followed by <CR> or <CR> to EXIT.

Table 2. Form for Entering New BLASTO Explosion Parameters.

NEWTEST Entries for BLASTO Airblast Predictions

You should be in overtype mode (UNDERLINE cursor); if not (BLOCK cursor), toggle <INSERT> key. Move cursor with ARROWS and ENTER keys. Enter explosion test data in blanks; be sure to stay in underlined spaces and keep decimal points aligned as shown. Acceptable units are shown opposite their number codes in the following table:

ACCEPTABLE UNITS

CODE	LENGTH	PRESSURE	YIELD	EXPLOSIVE	TEMPERATURE	RAOB FILE	BLAST MODEL
1	M	PA	KG	NUCLEAR	K	NONE	AFWL 1975
2	KM	KPA	TONNES	HE(TNT)	DEG-C	RAOB.DAT	DNA 1981
3	FT	MB	LB	ANFO	DEG-F	RAOBS.DAT	
4	KFT	PSI	TONS				
5	MILES	IN.HG	KT				
6	NAUT.MI.	MM.HG	MT				

TEST DATA ENTRIES

```

TEST NAME           : 1-KT NE DNA STANDARD      (Must be unique in TESTS.DAT)
TEST SITE           : FREE AIR BURST             (Required if weather used)
ALTITUDE            : 1.0 1 Units above Mean Sea Level (Minimum 1.0 m)
TEST DATE           : 3/16/90      TIME: 1200 MDT Time Zone (Default=UTC)
BLAST YIELD          : 1.0 5 Units 1 Explosives
HEIGHT-OF-BURST     : 4000.00 3 Units above the surface (Default = 0.0 m)
DEPTH-OF-BURST      : 0.0 1 Units under G surface (Optional: G[round]
                    :                   - or W[ater])
HEST CAVITY PLAN AREA : 0.0 Square 1 Units (Enter only for HEST events)
AMBIENT PRESSURE     : 1.00 3 Units (1.0=Unknown; uses Standard
                    :                   - Atmosphere pressure at indicated altitude)
TEMPERATURE          : 15.0 2 Units (Default = 0.0 Deg-C; Optional)

IS UPPER AIR WEATHER INFO AVAILABLE? N Y(es) or N(o) If answer is YES, then
IS UPPER AIR INFO IN SINGLE REPORT FILE RAOB.DAT? (Enter X if appropriate)
OR IN ARCHIVE FILE RAOBS.DAT? ( ditto )

USE STANDARD EXPLOSION FROM DNA-81 (Default) OR FROM AFWL-75? 2 Code response.
*****

```

When all necessary entries have been made, EXIT editor with the following keys: <ESC> <F>iles <Q>uit <Y>es, to SAVE file named FORMB, which will be reformatted by Fortran program READER and appended to file TESTS.DAT.

Table 3. Some Typical Formats for Coded Upper-Air Weather Reports.

Blocks opened with TTAA contain altitude, pressure, temperature, humidity, and wind reports at "Mandatory" levels of 1000, 850, 700, 500, etc millibars.

Blocks opened with TTBB contain pressure, temperature, and humidity at "Significant" levels where temperature lapse rates change.

Blocks opened with PPBB contain wind reports at 1000-ft intervals to 10,000-ft MSL, 2000-ft intervals to 20,000-ft MSL, and 5000-ft intervals at higher altitudes.

NNNN

1238 01/10/90 1200 UTC
UJWU2 KAWN 251207

(EXAMPLE IN FORMAT "A")

TTAA 60121 72293 99001 12035 20006 00142 12456 19506 85555 19680
03505 70185 07080 13520 50587 09980 19513 40755 23180 23520 30958
39763 24532 25080 487// 25031 20226 547// 25034 15407 627// 25028
10650 725// 26029 88999 77999 51515 10164 00011 10194 06509 11011=

TTBB 6012/ 72293 00001 12035 11995 16464 22986 22080 33960 25680
44928 25280 55642 02280 66588 00580 77539 05180

PPBB 60120 72293 90012 20006 11516 06511 90346 02009 02007 06505
90789 11509 14514 14514 91246 13026 12520 15013 9179/ 16511 19512
92035 19515 21017 24021 93045 23026 26532 25530 936// 25031 9436/
25536 25028 95024 27521 25020 26029=

LAXSGLNKX

(EXAMPLE IN FORMAT "B")

TTAA00 KNKX 101200

72293 TTBB 6012/ 72293 00001 12035 11995 16464 22986 22080
33960 25680 44928 25280 55642 02280 66588 00580 77539 05180

PPBB 60120 72293 90012 20006 11516 06511 90346 02009 02007
06505 90789 11509 14514 14514 91246 13026 12520 15013 9179/
16511 19512 92035 19515 21017 24021 93045 23026 26532 25530
936// 25031 9436/ 25536 25028 95024 27521 25020 26029=

LAXSGLNKX

TTAA00 KNKX 101200

72293 TTAA 60121 72293 99001 12035 20006 00142 12456 19506
85555 19680 03505 70185 07080 13520 50587 09980 19513 40755
23180 23520 30958 39763 24532 25080 487// 25031 20226 547//
25034 15407 627// 25028 10650 725// 26029 88999 77999 51515
10164 00011 10194 06509 11011=

GLOBAL WEATHER DYNAMICS, INC.
COPYRIGHT 1989

(EXAMPLE IN FORMAT "C")

--> SKEWT 72293

TTAA 60121 72293 99001 12035 20006 00142 12456 19506
85555 19680 03505 70185 07080 13520 50587 09980 19513 40755
23180 23520 30958 39763 24532 25080 487// 25031 20226 547//
25034 15407 627// 25028 10650 725// 26029 88999 77999 51515
10164 00011 10194 06509 11011=

TTBB 6012/ 72293 00001 12035 11995 16464 22986 22080
33960 25680 44928 25280 55642 02280 66588 00580 77539 05180

PPBB 60120 72293 90012 20006 11516 06511 90346 02009 02007
06505 90789 11509 14514 14514 91246 13026 12520 15013 9179/
16511 19512 92035 19515 21017 24021 93045 23026 26532 25530
936// 25031 9436/ 25536 25028 95024 27521 25020 26029=

TTCC 68123 72293 70838 571// 29510 50051 583// 36008
30371 569// 08518 20631 527// 88999 77999 51515 10182=

TTDD 6812/ 72293 11971 547// 22859 589// 33765 555// 44393
607// 55199 527//=

EOF

Table 4. Video Sequence of Interactive Operations with BLASTO, Part 1.

BLAST CALCULATIONS FOR WEATHER-DEPENDENT EXPLOSION AIR BLAST PREDICTIONS

IF LISTED HERE, TYPE DESIRED TEST NUMBER AND ENTER;
OTHERWISE, ENTER A ZERO TO GET NEXT PAGE.

(7)
YOU HAVE SELECTED RAOB NUMBER

Table 5. Video Sequence of Interactive Operations with BLASTO, Part 2.

ARE TEST AND NEIGHBORHOOD COORDINATES AVAILABLE?

1 = YES, 2 = NO, 3 = ?

(1)

1 WHITE SANDS	M-P GZ
2 WHITE SANDS	HE-A1
3 WHITE SANDS	HE-A2
4 WHITE SANDS	HE-A3
5 WHITE SANDS	HE-B1
6 WHITE SANDS	HE-B2
7 WHITE SANDS	HE-B3
8 WHITE SANDS	HE-C
9 WSMR	M-G GZ
10 WHEREVER	ZERO
11 WHEREVER	ZERO
12 GREEN FARM	GUN
13 MODEL	A
14 MODEL	B
15 MODEL	C

IS THE SHOT POINT IN THIS LIST? 1=YES, NO=2

(1)

ENTER DESIRED SITE NUMBER.

(1)

ENTER ANY CORRECTIONS UNDER PROVIDED VALUES.

WHITE SANDS

M-P GZ

1062826.4280 W 333716.0188 N 7

<CR>

SELECT

1: 30-DEG INCREMENTED DIRECTIONS ONLY,
 2: INCREMENTED & TARGET DIRECTIONS, OR
 3: TARGETED DIRECTIONS ONLY.

(3)

TEST SITE	TARGET	X	Y	U
1 WHITE SANDS	MCDONALD RANCH	-42.5055	72.4569	7
2 WHITE SANDS	ADMIN PARK	-49.8700	72.9503	7
3 WHITE SANDS	OBSERVER POINT	-49.8667	75.4919	7
4 WHITE SANDS	STALLION	-00.0368	91.1428	7
5 WHITE SANDS	SAN ANTONIO	-00.0603	102.0222	7
6 WHITE SANDS	SOCORRO	-83.4011	116.0301	7
7 WHITE SANDS	CARRIZOZO	11.0914	72.3907	7
8 WHITE SANDS	TULAROSA	-2.0244	8.2967	7
9 WHITE SANDS	ALAMOGORDO	3.5092	-14.2432	7
10 WHITE SANDS	DEMING	-165.2986	-80.9848	7
11 WHITE SANDS	SILVER CITY	-213.0941	-25.0882	7
12 WHITE SANDS	RESERVE	-254.9545	79.1205	7
13 WHITE SANDS	QUEMADO LAKE	-231.0507	129.4207	7
14 WHITE SANDS	GRANTS	-166.5838	238.6981	7

HOW MANY TARGETS SHOULD BE ADDED? DEFAULT=0

<CR>

IS A SURFACE WEATHER OBSERVATION UPDATE AVAILABLE? Y(ES) OR N(O)=DEFAULT:

<CR>

SHOULD DIRECTED SOUND VELOCITY TABLES BE PRINTED IN SI METRIC UNITS?
 IF O.K., TYPE Y(ES)=DEFAULT, OTHERWISE TYPE E(GLISH) OR B(OTH),
 FOR OUTPUT UNITS.

<CR>

Stop - Program terminated.

Table 6. Selected excerpts from BLASTO output file BLASTO.DAT.

ACCEPTABLE UNITS				NUMBER CODES			
CODE	LENGTH	PRESSURE	YIELD	EXPLOS.	TEMPERATURE	RAOB FILE	BLAST MODEL
1	M	PA	KG	NE	K	NONE	1975
2	KM	KPA	TONNES	HE(TNT)	DEG-C	RAOB.DAT	1981
3	FT	MB	LB	ANFO	DEG-F	RAOBS.DAT	
4	KFT	PSI	TONS				
5	MILES	IN.HG.	KT				
6	NAUT.MI.	MM.HG.	MT				
7	LATITUDE, LONGITUDE IN DEGREES, MINUTES, & SECONDS						
8	LATITUDE, LONGITUDE IN DECIMAL DEGREES						

TEST DESCRIPTION

```

TEST EVENT      : MISTY PICTURE
DATE            : 5/14/87 AT 1000 MDT
RAOB AT        : DATE      : 3/19/90
                TIME       : 1200          UTC
SHOT AT        : PHETS GZ
YIELD          : 3904.167          TONS   HE(TNT)
CONW FACTOR    : .2000E-02        FOR CONVERSION TO KT NE UNITS.
YIELD          : .156E+02        KT NE AIRBURST EQUIVALENT
BURST AT HOB   : .000          FT/KT**1/3
BURST DEPTH AT : .000          M/KT**1/3
HEST AREA      : .000000E+00    SQUARE METERS
AMBIENT PRESSURE : 85140.0      PASCALS
YIELD SCALE FACTOR : 2.6483    x DISTANCE(1-KT NE FAB)
BURST AT       : 1503.0        METERS ABOVE MEAN SEA LEVEL.

```

PLANNING PREDICTIONS (NO CURRENT WEATHER)

OVERPRESSURE (PA) VS. DISTANCE (M) CURVE DATA

PROPAGATION CONDITIONS

DISTANCE(M)	STANDARD	+10M/S INV	+5M/S INV	-5M/S GRAD	-10M/S GRAD	CAUSTICS
100.0	5583560.0	5583560.0	5583560.0	5583560.0	5583560.0	5583560.0
200.0	846413.7	846413.7	846413.7	846413.7	846413.7	846413.7
400.0	158994.9	158994.9	158994.9	158994.9	158994.9	158994.9
700.0	51707.2	51707.2	51707.2	51707.2	51707.2	51707.2
1000.0	28039.7	28039.7	28039.7	28039.7	28039.7	28039.7
2000.0	9991.9	9991.9	9991.9	9991.9	9991.9	9991.9
4000.0	3951.6	3951.6	3951.6	3951.6	3951.6	5377.4
7000.0	1933.1	2003.2	1974.8	1902.1	1856.2	3673.2
10000.0	1239.9	1470.0	1366.5	1128.3	996.2	2880.9
20000.0	535.7	805.6	668.1	409.0	297.2	1796.8
40000.0	238.0	441.5	326.7	148.2	88.7	951.8
70000.0	125.6	271.7	183.3	65.3	33.4	502.4
100000.0	84.1	199.4	126.9	38.8	17.9	336.3
200000.0	39.0	109.3	62.0	14.0	5.3	155.9
400000.0	18.2	59.9	30.3	5.1	1.6	73.0
700000.0	10.0	36.9	17.0	2.2	.6	39.8
1000000.0	6.8	27.0	11.8	1.3	.3	27.1
2000000.0	3.2	14.8	5.8	.5	.0	12.9
4000000.0	1.5	8.1	2.8	.2	.0	6.2
7000000.0	.9	5.0	1.6	.0	.0	3.4

Table 7. Selected excerpts from BLASTO output file BLASTO.DAT.

PROVIDED WEATHER REPORT

INPUT RAOB- DATE: 3/19/90 TIME: 1200 UTC

ALTITUDE-MSL (M,KM,FT,KFT)	ALT. (1)	TEMPERATURE (K,C,F) (2)	ALT. (3)	DIRECTION (DEG) (4)	WIND SPEED (MPS,KPH,FPS,MPH,KTS) (5)	ALT. (6)
1620.0	0	2.8	0	90.	18.0	0
1677.2	0	2.8	0	94.	16.9	0
1800.0	0	2.5	0	105.	15.0	0
2100.0	0	1.6	0	110.	12.0	0
2191.0	0	1.4	0	108.	9.8	0
2400.0	0	0	0	95.	5.0	0
2700.0	0	-1.8	0	330.	3.0	0
2783.6	0	-2.3	0	316.	3.5	0
2872.0	0	-7	0	305.	4.3	0
3143.0	0	-1.3	0	290.	7.0	0
3300.0	0	-2.2	0	290.	12.0	0
3600.0	0	-3.8	0	285.	17.0	0
3798.6	0	-4.9	0	281.	19.9	0
4054.8	0	-7.1	0	277.	23.8	0
4167.3	0	-7.9	0	275.	25.5	0
4200.0	0	-8.1	0	275.	26.0	0
4230.6	0	-8.3	0	276.	25.7	0
4800.0	0	-11.9	0	290.	21.0	0
5018.4	0	-13.3	0	297.	20.5	0
5700.0	0	-18.8	0	320.	21.0	0
5740.0	0	-19.1	0	320.	22.0	0
999.0	0	0	0	0.	0	0

WIND COMPONENTS, W, AND DIRECTED SOUND VELOCITIES, V (M/S).

DIRECTION(DEG)	22.	87.	145.	150.
ALTITUDE(M)	W	V	W	V
1620.	0	333.2	0	333.2
1630.	-3.5	329.7	-9.2	323.9
1677.	-2.7	330.5	-8.6	324.6
1800.	-1.0	332.0	-7.3	325.7
2100.	-2	332.2	-5.7	326.8
2191.	-4	331.9	-4.7	327.6
2400.	-8	330.7	-2.5	328.9
2700.	-9	329.4	7	331.1
2784.	-7	329.3	1.2	331.2
2872.	-5	330.5	1.7	332.8
3143.	1	330.8	3.3	334.0
3300.	2	330.4	5.7	335.8
3600.	1.1	330.3	8.3	337.5
3799.	2.0	330.5	9.9	338.4
4055.	3.3	330.4	12.1	339.2
4167.	3.8	330.4	13.0	339.6
4200.	4.0	330.5	13.2	339.8
4231.	3.8	330.2	13.1	339.5
4800.	4	324.6	9.9	334.1
5018.	-9	322.4	9.1	332.4
5700.	-5.0	314.8	6.4	326.3
5740.	-5.3	314.4	6.7	326.4

Table 8. Selected excerpts from BLASTO output file BLASTO.DAT.

OVERPRESSURE ISOBAR RADII (METERS)							

MODE:		0		1		2	
PROPAGATION:		GRADIENT		INVERSION		CAUSTIC	
AZIMUTH (DEGREES) / DV(M/S)							
PROPN MODE:	0	2	2	2	1	1	1
DIRECTION(DEG)	22	87	145	150	219	241	273
V CHANGE (M/S)	-3.5	-9.2	-6.1	-5.6	5.8	8.1	9.3
OVERPRESSURE(PA)							
20000	1255.	1255.	1255.	1255.	1255.	1255.	1255.
10000	1999.	1999.	1999.	1999.	1999.	1999.	1999.
7400	2503.	2503.	2503.	2503.	2503.	2503.	2503.
4000	3964.	5950.	5950.	5950.	3964.	3964.	3964.
2160	6418.	14164.	14164.	14164.	6418.	6418.	6418.
1186	9882.	32936.	32936.	32936.	11668.	12254.	12584.
1000	11173.	37919.	37919.	37919.	13831.	14730.	15241.
700	14444.	50909.	50909.	50909.	19738.	21644.	22751.
400	21610.	81491.	81491.	81491.	34484.	39586.	42655.
200	35595.	147865.	147865.	147865.	68827.	83622.	92913.
100	58630.	272149.	272149.	272149.	137374.	176643.	202388.
70	75795.	374517.	374517.	374517.	196042.	259547.	302109.
40	113401.	620113.	620113.	620113.	342509.	474708.	566416.
AZIMUTH (DEGREES) / DV(M/S)							
PROPN MODE:	1	1	1	1	1	1	1
DIRECTION(DEG)	288	303	312	317	320	324	324
V CHANGE (M/S)	8.8	7.8	6.8	6.4	6.1	5.8	5.8
OVERPRESSURE(PA)							
20000	1255.	1255.	1255.	1255.	1255.	1255.	1255.
10000	1999.	1999.	1999.	1999.	1999.	1999.	1999.
7400	2503.	2503.	2503.	2503.	2503.	2503.	2503.
4000	3964.	3964.	3964.	3964.	3964.	3964.	3964.
2160	6418.	6418.	6418.	6418.	6418.	6418.	6418.
1186	12457.	12165.	11922.	11802.	11746.	11669.	11663.
1000	15044.	14592.	14220.	14036.	13951.	13833.	13824.
700	22322.	21348.	20555.	20167.	19988.	19742.	19723.
400	41457.	38779.	36644.	35614.	35141.	34496.	34445.
200	89252.	81225.	74988.	72032.	70686.	68863.	68718.
100	192149.	170132.	153456.	145688.	142185.	137466.	137092.
70	285102.	248894.	221826.	209331.	203720.	196189.	195593.
40	529499.	452121.	395450.	369662.	358162.	342808.	341597.

DRAG COEFFICIENT MEASUREMENTS FOR TYPICAL BOMB AND PROJECTILE FRAGMENTS

By

Miles C. Miller

U. S. Army Research, Development and Engineering Center
Aberdeen Proving Ground, Maryland 21010-5423

ABSTRACT

The FRAGHAZ computer program has been developed to predict the hazardous regions due to fragments produced by an accidental explosion of stored ammunition. Determination of these hazardous regions is based on computer simulations of fragment trajectories. Currently, the fragment drag coefficients used in the program are extrapolations of subsonic drag coefficients out to transonic and supersonic speed regimes. Errors in the Mach number effects of these fragments can influence the predicted range characteristics. This paper describes a series of wind tunnel and air gun tests conducted to measure the drag coefficients of representative bomb and projectile fragments over the entire Mach number range experienced in flight. Comparative trajectories are made to illustrate the differences between using the original and current drag coefficient data for the FRAGHAZ program.

ACKNOWLEDGEMENT

The author would like to thank Mr. Daniel C. Wise and Mr. Frank G. Wrede, Aerodynamic Research and Concepts Assistance Branch, for their assistance during this study. Mr. Wrede arranged and conducted the wind tunnel tests and Mr. Wise performed the air gun tests and trajectory calculations.

NOMENCLATURE

C_D	Drag coefficient - D/qS	V	Velocity
S	Reference Area	ρ	Air Density
D	Drag force	R_e	Reynolds number - Vd/ν
E	Flight path angle (to ground)	d	Reference length
q	Dynamic pressure - $\rho V^2/2$	ν	Air kinematic viscosity

INTRODUCTION

The FRAGHAZ computer program (Ref 1) has been developed to predict the hazardous regions due to fragments produced by an accidental explosion of stored ammunition. Determination of these hazardous regions is based on computer simulations of fragment trajectories. The trajectory calculations are a function of the drag coefficients derived from representative bomb and artillery projectile fragments. These drag coefficients depend on the fragment shape and the Mach number at which they fly through the air. Currently, the fragment drag coefficients are established by extrapolating measured subsonic drag coefficients out to transonic and supersonic speed regimes. Errors in the Mach number effects of these fragments could influence the predicted range characteristics.

This paper describes the initial results of wind tunnel and air gun tests to measure the drag coefficients of representative bomb and projectile fragments over the entire Mach number range experienced in flight. These data are used to compute comparative trajectories to illustrate the differences between using the original and current drag coefficient data for the FRAGHAZ program.

BACKGROUND

The FRAGHAZ program computes the trajectories of nominal fragment configurations using experimentally determined initial velocities and experimentally determined drag characteristics. A large number of parameters defining the physical conditions of the fragments and the initial blast effects can be simulated. Resulting fragment trajectories are computed using a Monte Carlo statistical technique and danger regions determined for any prescribed hazard constraints. The drag coefficients used in the FragHaz program are functions of the fragment shape and the Mach number at which they fly through the air. Initial fragment velocities depend on their size and weight, but are on the order of 5000 ft/sec (Mach 4.5).

The current version of the FRAGHAZ program uses an empirical method to define the drag coefficient for a particular class of fragments. This approach is based on a drag coefficient value for the fragment determined during previous experiments in a vertical wind tunnel. A particular fragment was placed in the test section of the tunnel and the upward directed air stream was adjusted until the fragment freely floated. The fragment thus assumed the same flight attitude to the free stream that it would have under free flight conditions. The tunnel velocity represented the fragment's terminal velocity and this value, along with the known fragment weight and size, allowed the drag coefficient to be computed. This method provided the experimental drag coefficient value for the actual flight attitude, but for a very low Mach number (on the order of Mach 0.1). This procedure was repeated for a large number of fragments and the data analyzed to develop a general empirical

method to determine the drag coefficient for any fragment over the entire Mach number range of interest. Using the single subsonic data point as a reference, the drag coefficient was estimated at specific Mach number "anchor points" to generate the general Mach number effects. This procedure is illustrated in Fig 1.

The goal of the current study was to experimentally determine the drag coefficient as a function of Mach number over the entire anticipated Mach number range. These data could then be compared to the previous empirical method to validate or improve the FRAGHAZ program.

FRAGMENT CONFIGURATIONS

The original fragment analysis considered a total of 96 representative fragments composed of half artillery projectile and half bomb type fragments. From these, 10 projectile and 10 bomb fragments were selected for analysis under this effort. These were chosen to represent various size, shape and texture characteristics. Since these fragments are part of a set of standard fragments which are being retained for future reference, it was not desirable to alter these fragments for wind tunnel mounting nor risk the chance of losing them during air gun firing. This problem was solved by making multiple duplicates of each fragment. A rubber based molding apparatus was constructed which allowed duplicate fragments to be molded out of CERABEND metal which is a low melting temperature alloy used by pipe fitters. Several different fragments could be made from a single mold as shown in Fig 2. The resulting fragments had the same size, shape and effective weight of the original and could be easily made by the dozens. Fig 3 contains an actual and a duplicate fragment.

WIND TUNNEL TESTS

Initially, a series of wind tunnel tests was conducted to measure the drag coefficients of selected fragments for validation of the FRAGHAZ program as well as to provide a comparative basis for the air gun tests. The full scale, duplicate fragment model was mounted to a sting type strut in a broadside orientation to the free stream air flow direction which is the attitude at which it is expected to have in free flight. An internal strain gage balance was located inside the strut to measure the drag force. The model was first tested in the ARCA Br 6 X 6-Inch Supersonic Wind Tunnel over a Mach number range from Mach 1.5 to Mach 4 (Ref 2). The same arrangement was then employed for tests in the ARCA Br 20 X 20-Inch Transonic Wind Tunnel for speeds of Mach .45 through Mach 1.2. Figs 4 and 5 show the model installed in the supersonic and transonic wind tunnels, respectively. A 1-Inch sphere model was tested using the same experimental setup to validate the experimental arrangement. The resulting data are shown in Fig 6 compared with data

from other sources. Fig 7 summarizes the drag coefficient as a function of Mach number for a nominal fragment as determined from these tunnel tests.

The supersonic wind tunnel has the capability of operating at fixed Mach numbers like conventional facilities. However, its asymmetrical nozzle block can be pneumatically shifted with time allowing the Mach number to be varied during a single test run. This permits supersonic data to be obtained in a relatively short time. Fig 8 compares drag data for the nominal fragment using these two tunnel testing techniques.

AIR GUN TESTS

A series of tests were conducted where the fragment was fired from the ARCA Br. 6-Inch spinning barrel air gun illustrated in Fig 9. A special sabot design was employed to launch the fragments from the 6 inch diameter gun as shown in Fig 10. Upon exiting the barrel, the two piece, polyethylene sabot separated from the fragment allowing the fragment to fly down range. Barrel spin provided a means of rapidly separating the sabot pieces and having them travel laterally away from the fragment flight path. The small amount of spin also reduced lateral dispersion of the fragment keeping it flying along its original heading. A ground based, doppler radar system tracked the fragment velocity as a function of time. From the deceleration data and the known fragment weight and size, the drag coefficient could be obtained over the flight Mach number achieved. This approach has the advantages over wind tunnel testing in that it obtains data over a large Mach number range very quickly and allows the fragment to assume its natural flight orientation.

Initially, air gun tests have been completed with a spherical projectile in order to evolve and validate the testing technique. Fig 11 shows data for a 1-Inch diameter sphere which was tested from the air gun and illustrates the complex interaction between Reynolds number and Mach number characteristic of a sphere. Only a few air gun tests have been completed with a fragment and these have been limited to transonic and subsonic velocities. Data for the nominal fragment are shown in Fig 12.

VELOCITY CALCULATIONS

Fig 13 summarizes the drag coefficient data obtained from this study with that generated by the current FRAGHAZ methodology for the nominal fragment. Note that the newer data possesses a slightly lower transonic drag coefficient and a slightly higher supersonic drag coefficient compared to the original data. The resulting velocity decay for these sets of data are contained in Fig 14 for a typical initial blast condition. The associated velocity with range for these same conditions are shown in Fig 15. Finally,

the resulting trajectory is contained in Fig 16. Note, that the newer data results in about a 5% increase in range compared to the older data. These data also include the results using the subsonic drag coefficient value only. This latter result indicates a 20% increase in range over the original FRAGHAZ approach. Even though the bulk of the flight is subsonic, the higher Mach number effects have an appreciable influence on the trajectory.

CONCLUSIONS

1. The use of duplicate fragments molded from CERABEND metal provides a large number of identical fragments for testing purposes.
2. The results of conventional wind tunnel tests have shown good agreement with the current FRAGHAZ fragment drag coefficient estimating technique.
3. Initial air gun firings of duplicate fragments have demonstrated the use of the special sabot and radar tracking methodology but have been limited to transonic and subsonic velocities.

REFERENCES

1. McCleskey, F., "Drag Coefficients For Irregular Fragments", NSWC TR 87-89, February 1988.
2. Miller, M. C., "Experimental Aerodynamic Facilities of the Aerodynamics Research and Concepts Assistance Section", CSL Special Report, ARCSL-SP-83007, February 1983.

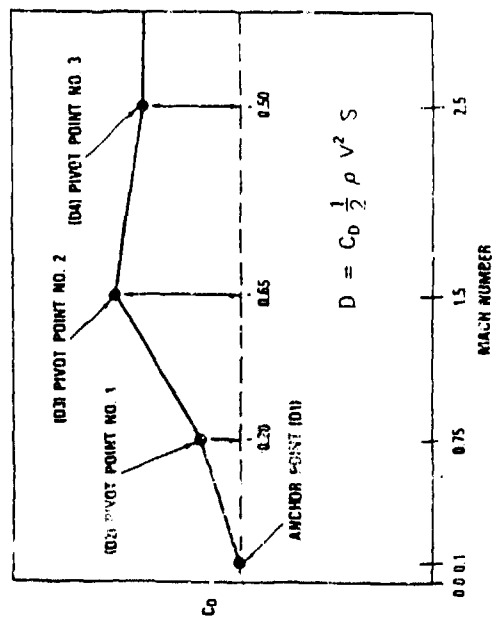


Fig. 1. FRAGHAZ Coefficient Method

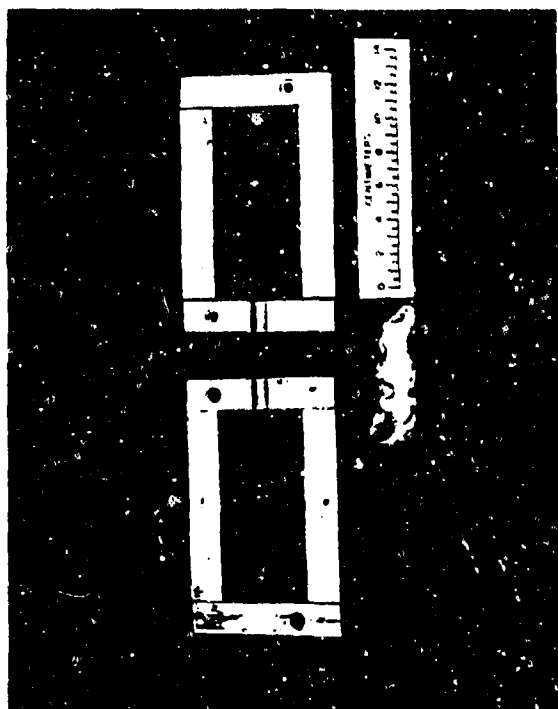


Fig 2. Duplicate Fragment Mold

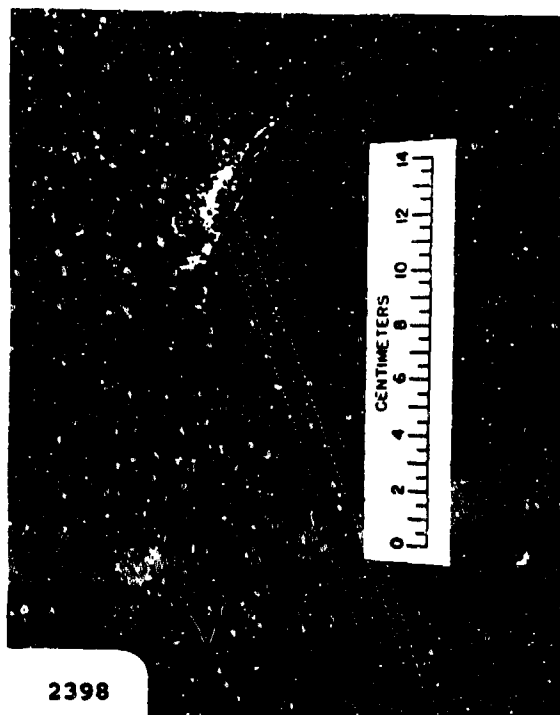


Fig 3. Duplicate and Actual Fragment

2398



Fig 4. Model Installed in Supersonic Wind Tunnel

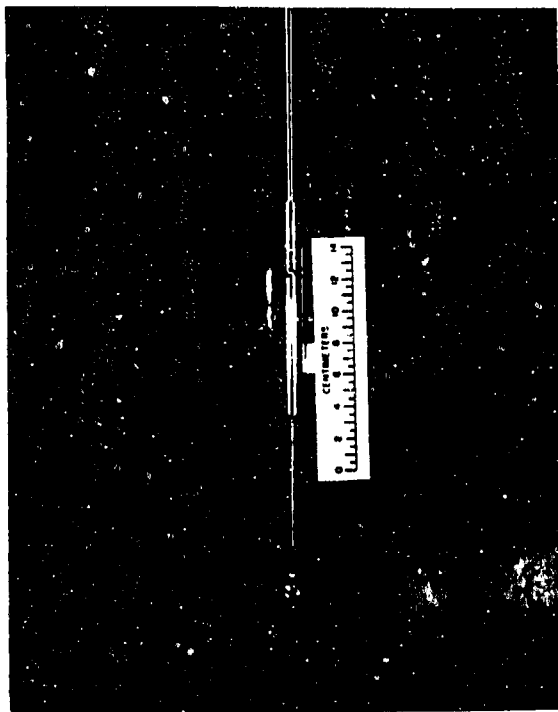


Fig 5. Model Installed in Transonic Wind Tunnel

2399

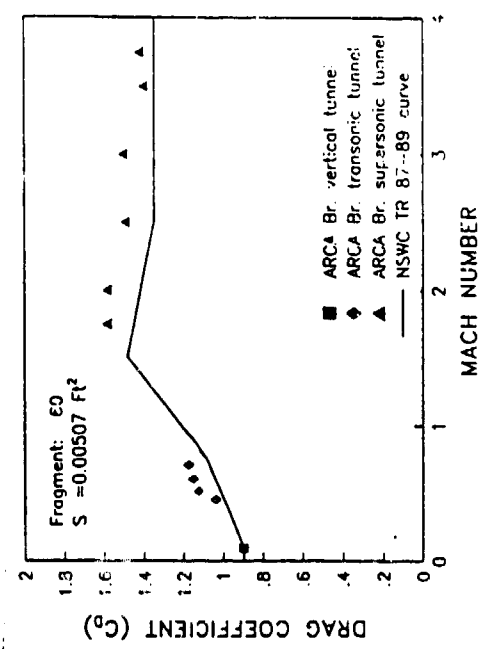


Fig 7. Wind Tunnel Data for Fragment

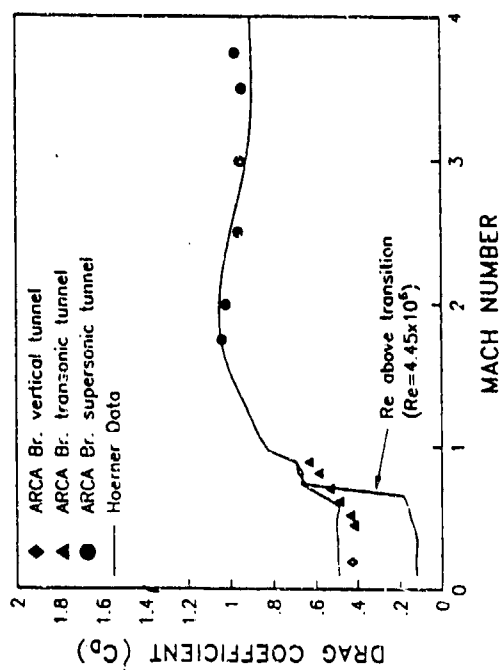


Fig 6. Wind Tunnel Data for Sphere

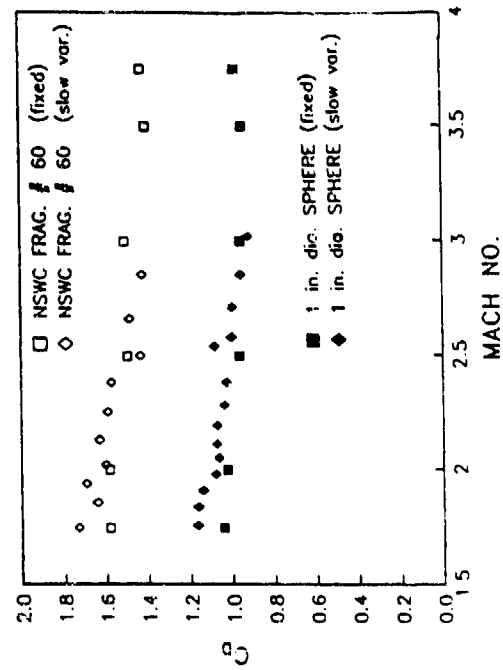


Fig 8. Variable Versus Fixed Mach Number Data

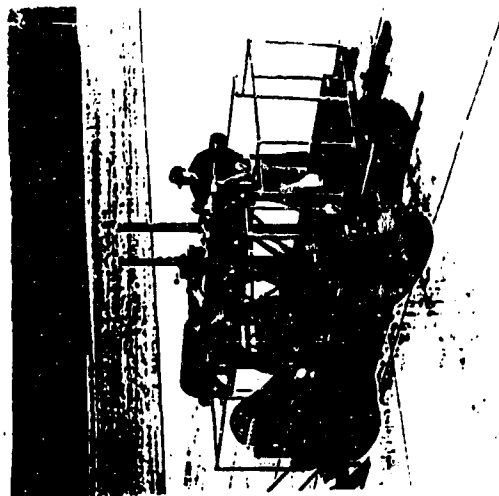


Fig 9. Spinning Barrel Air Gun

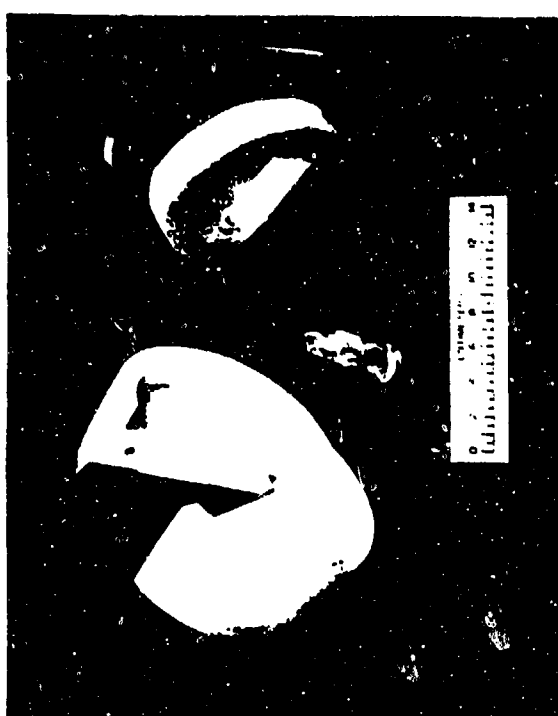


Fig 10. Fragment Sabot

2400

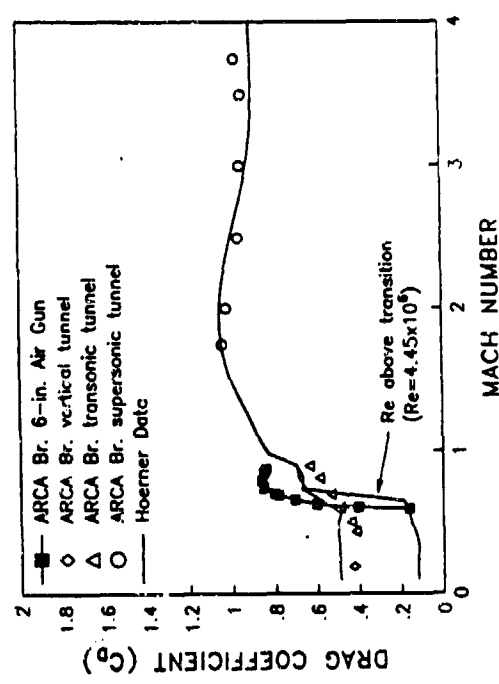


Fig 12. Air Gun Test Data for Fragment

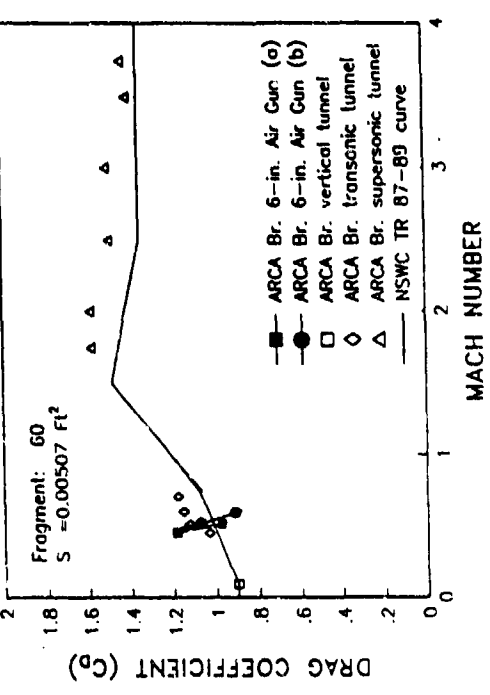


Fig 11. Air Gun Test Data for Sphere

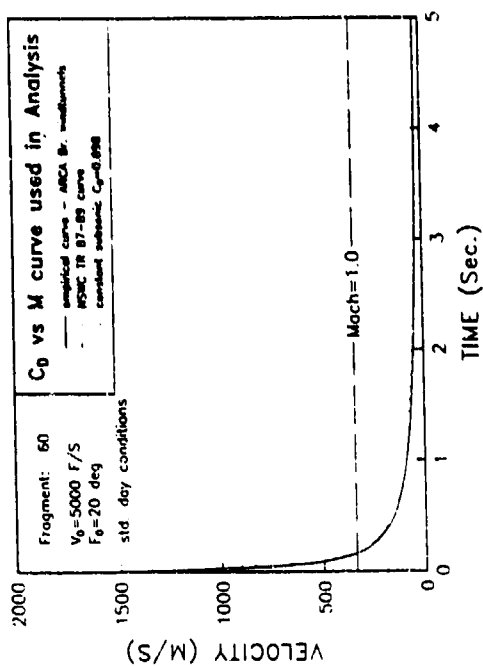


Fig 14. Computed Velocity Decay With Time

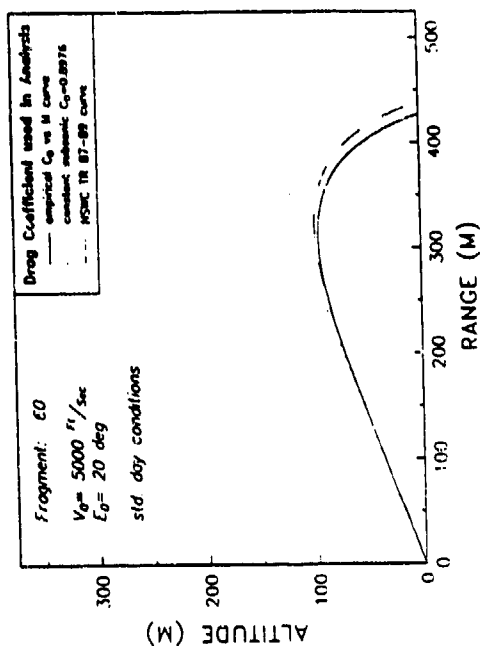


Fig 16. Computed Trajectories

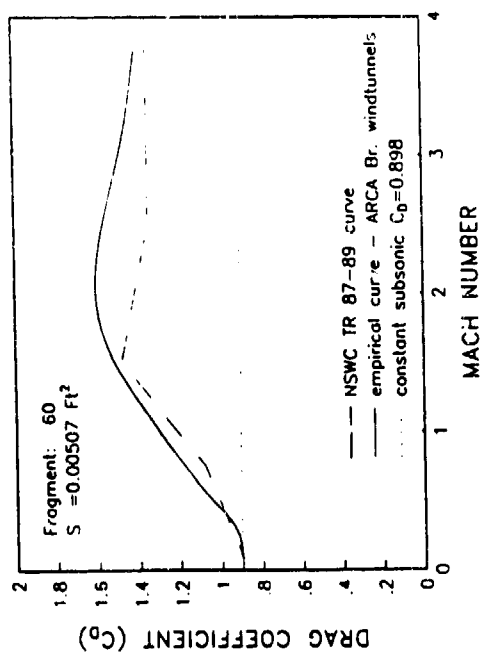


Fig 13. Comparison of FRAGHAZ and Test Data

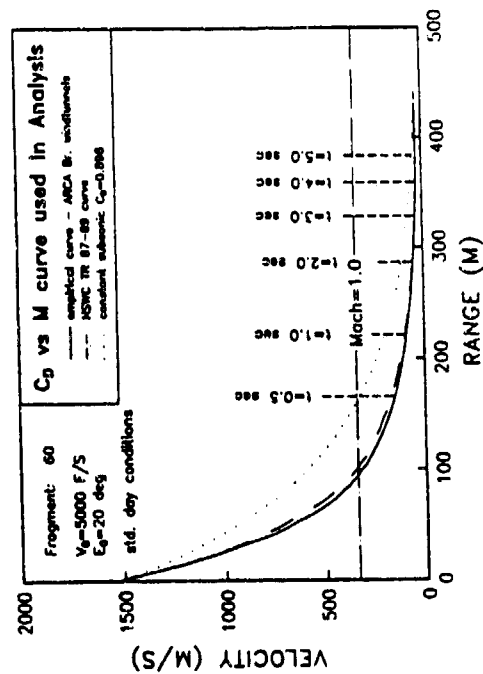


Fig 15. Computed Velocity Decay With Range

Fragment Mass Distribution of Debris

Manfred Held
Messerschmitt-Bölkow-Blohm GmbH
8898 Schrobenhausen - West Germany
for
Department of Defense
Twenty-four Explosives Safety Seminar
St. Louis, Missouri
27-30 August 1990

ABSTRACT

The equation established by the author for the mass distribution of the natural fragments of an explosive-filled projectile, or for that of secondary fragments behind one or several spaced target plates, can also be applied with very good results to the mass distribution of the debris from an exploded aircraft shelter.

The two constants required for this, namely, the scale parameter B and the shape parameter λ can be determined to a usually high confidence level, with a correlation coefficient close to 1, especially when the given total mass M_0 is changed to a "best mass" M_{0B} that best describes the actual fragment mass distribution.

1. INTRODUCTION

There are virtually no formulas available, at least not in unclassified published literature, that describe the mass distribution of debris from buildings, such as aircraft shelters, when several bombs have detonated inside.

The main cause of this is certainly the fact that only very few qualifield tests have been made where the mass distributions of such debris fragments have been thoroughly analyzed. The author had the opportunity of obtaining carefully recorded test results of minutely planned model aircraft shelter blasting trials <1>, and it was his intention to find out whether the mass distribution of such debris fragments could be described by a formula he had established earlier in context with the natural fragmentation of detonating high explosive shells.

It is demonstrated below that Held's formula, that had been established to adequately describe the mass distribution of the so-called natural fragments from high explosive projectiles, as well as that of secondary fragments (see <2> to <7>), can also be used to give a good description of the mass distribution of the debris fragments experimentally recorded in shelter blasting trials.

2. DISTRIBUTION FUNCTION

The Weibull distribution <8> can be applied to a great variety of technical problems. The distribution density of the 3-parameter Weibull distribution is as follows:

$$f(x) = \frac{\lambda(x-\mu)^{\lambda-1}}{\delta^{\lambda}} \cdot e^{-\left(\frac{x-\mu}{\delta}\right)^{\lambda}}, \quad x > 0 \quad (1)$$

with the 3 parameters

δ = scale parameter

λ = shape parameter

μ = location parameter

The 3-parameter Weibull distribution (1) reduces to a 2-parameter Weibull distribution, when the location parameter μ is set equal to 0; this is equivalent to a transformation to the new variable $x - \mu$:

$$f(x) = \frac{\lambda x^{\lambda-1}}{\delta^{\lambda}} \cdot e^{-\left(\frac{x}{\delta}\right)^{\lambda}}, \quad x > 0 \quad (2)$$

The 2-parameter Weibull distribution follows from (2) by an integration:

$$F(x) = 1 - e^{-\left(\frac{x}{\delta}\right)^{\lambda}}, \quad x > 0 \quad (3)$$

In some papers on fragment mass distribution, the 2-parameter Weibull distribution (3) is referred to as Rosin-Rammler-Speckling (RRS) distribution, which goes back to the description of the grain size distribution in grinding processes. Sometimes, the distribution of the "fragment masses" is also termed the RRS distribution.

In context with fragmentation and the distribution of fragment sizes, the Weibull distribution (3) has entered fragmentation ballistics since Mott (see <8>). With regard to this particular application it is therefore often refer-

red to as Mott distribution, and it is usually taken to describe the distribution of the "number of fragments".

One the basis of flash X-ray pictures that permit analyzing also smaller and finer fragments, Held <4> has made an experimental approach to represent the fragment mass distribution as a function of the number of fragments.

For comparison, the 3 formulas are given below:

$$\text{RRS : } M(m) = M_0 e^{-\left(\frac{m}{m_R}\right)^{\lambda_R}} \quad (4)$$

$$\text{MOTT : } N(m) = N_0 e^{-\left(\frac{m}{m_M}\right)^{\lambda_M}} \quad (5)$$

$$\text{HELD : } M(n) = M_0 (1 - e^{-Bn^{\lambda_H}}) \quad (6)$$

Where the symbols have the following meaning:

M_0	total mass of all fragments
$M(m)$	cumulative fragment mass, i.e. overall mass of all fragments whose mass is greater than or equal to a given mass m
$M(n)$	cumulative fragment mass, i.e. overall mass of the fragment number n , beginning with the largest fragment
m	mass of the n -th fragment
N_0	total number of fragments
$N(m)$	cumulative fragment number, i.e. number of all fragments whose mass is greater than or equal to a given fragment mass m
n	cumulative fragment number, beginning with the heaviest fragment
m_x, λ_x, B	constants.

The RRS formula is not related to the number of fragments at all, and the Mott formula requires a given number N_0 of fragments, whereas Held's formula does not need this. Any number of fine fragments may be added, even if they contribute virtually nothing to the overall mass M_0 .

3. DESCRIPTION OF MASS DISTRIBUTION WITH HELD'S FORMULA

The method of how to analyze mass distributions by means of Held's formula <4> and <5> is explained below. This formula, when applied correctly, gives an excellent description of the mass distribution of the natural fragments generated in the detonation of all high explosive projectiles examined <6>, even when filled with various types of explosives, and also of secondary fragments behind a target plate, or even behind a set of multiple spaced target plates <7>. The simple equation for this is:

$$M(n) = M_0 (1 - e^{-Bn^\lambda}) \quad (7)$$

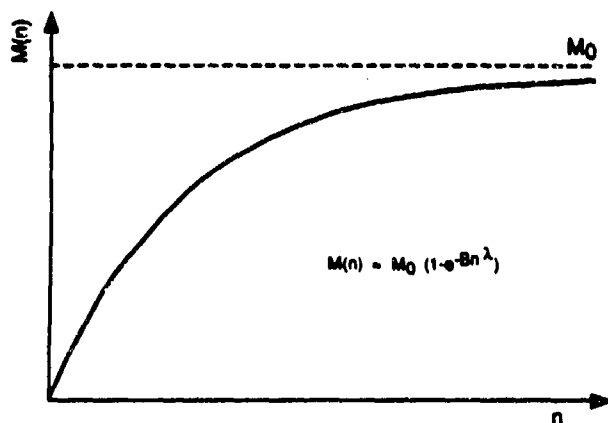
This equation is shown schematically in Fig. 1. The constants B and λ in equation (7) are readily found by isolating the exponential term in Eq. (7)

$$\frac{M_0 - M(n)}{M_0} = e^{-Bn^\lambda} \quad (8)$$

and then taking the natural logarithm of Eq. (8):

$$\ln \frac{M_0 - M(n)}{M_0} = -Bn^\lambda \quad (9)$$

For an easy determination of the values of B and λ it is convenient to again take the logarithm of Eq. (9) so

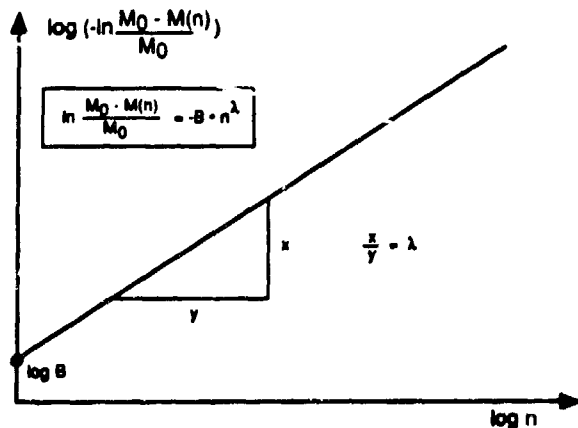


that in a logarithmic representation the point of intersection $n = 1$, or $\log n = 0$, will give the constant $\log B$ directly on the ordinate axis, and the exponent λ can be determined from the slope of the straight line (Fig. 2).

Fig. 1 Summed up mass over cumulative fragment number n .

$$\log \left(-\ln \frac{M_0 - M(n)}{M_0} \right) = \log \left(\ln \frac{M_0}{M_0 - M(n)} \right) = \log B + \lambda \cdot \log n \quad (10)$$

To this end, the value of $M(n)$ must be computed with the associated cumulative number of fragments, n , beginning



with the largest fragment. This value must then be subtracted from the total fragment mass, M_0 , and then be divided by M_0 . The corresponding logarithms can then be plotted in a log-log diagram.

Fig. 2 Easy determination of the constants B and λ from the log-log plot.

4. FRAGMENT MASS DISTRIBUTION OF AN 155 MM HE-ROUND

Table 1 gives the natural fragments generated by the detonation of an 155 mm HE-round filled with Composition B, arranged in mass classes. For the analysis according to Held, the fragment masses $M(n)$ must be summed up over the corresponding numbers, beginning with the largest fragment and the result must then be evaluated with Eq. (9). The total mass M_0 of the fragments is either the sum of all partial masses, which in this case is 18164 g or the total mass of the casing with 32151 g. The latter was used in the generation of the first diagram (Fig. 3).

The values obtained by the outlined method and plotted in a log-log-diagram, which is called the fragment mass distribution log-log-diagram or short FMD-log-log-diagram (Fig. 3, left) with a best-fit straight line, which gives a constant B of 0.089 and an exponent λ of 0.6531 with a correlation coefficient C of 0.9958.

Taking the derivative of Eq. (7) with respect to n gives the following equation (11) for the mass of the n -th fragment:

$$m = \frac{d M(n)}{dn} = M_0 B \lambda n^{\lambda-1} e^{-Bn\lambda} \quad (11)$$

This equation, when plotted in the diagram "mean fragment mass as a function of the cumulated number n ", or short MFM-diagram, with the given M_0 and with the constants B and λ calculated, shows a not too good agreement between the numbers of fragments and the mean fragment masses in the individual mass classes according to Table 1 and Eq. (11) (see Fig. 3, right).

Table 1

Fragment Classes	Number of Fragments	Weight of Fragments in each class (g)	n	M(n) (g)	x ₁	x ₂
(g)	n	(g)		(g)		
200-250	1	205	.1	205	0.99272	0.00731
150-200	1	156	2	361	0.98718	0.01290
125-150	2	260	4	621	0.97795	0.02230
100-125	6	666	10	1287	0.95430	0.04677
90-100	1	91	11	1378	0.95107	0.05016
80-90	2	175	13	1553	0.94486	0.05672
70-80	4	303	17	1856	0.93410	0.06817
60-70	15	977	32	2833	0.89941	0.10601
50-60	17	943	49	3776	0.86593	0.14395
40-50	40	1771	89	5547	0.80305	0.21934
30-40	60	1954	149	7501	0.73367	0.30970
20-30	116	2762	265	10263	0.63560	0.45319
15-20	116	2000	381	12263	0.56459	0.57166
14-15	47	683	428	12946	0.54034	0.61557
13-14	42	561	470	13507	0.52042	0.65313
12-13	59	734	529	14241	0.49435	0.70450
11-12	54	613	583	14854	0.47259	0.74953
10-11	76	801	659	15655	0.44415	0.81160
9-10	73	689	732	16344	0.41969	0.86825
8-9	100	857	832	17201	0.38926	0.94352
7-8	122	919	954	18120	0.35663	1.03107
6-7	175	1140	1129	19260	0.31615	1.15154
5-6	209	1142	1338	20402	0.27560	1.28880
4-5	310	1385	1648	21787	0.22642	1.48534
3-4	420	1455	2068	23242	0.17476	1.74433
2-3	642	1586	2710	24828	0.11845	2.13327
1.5-2.0	446	773	3156	25601	0.09100	2.39686
1.0-1.5	717	889	3873	26490	0.05944	2.82262
0.5-1.0	1102	888	4975	27378	0.02791	3.57883
0.0-0.5	4508	786	9483	28164	0	-

$$x_1 = \frac{M_0 - M(n)}{M_0}$$

$$x_2 = \frac{M_0}{M_0 - M(n)}$$

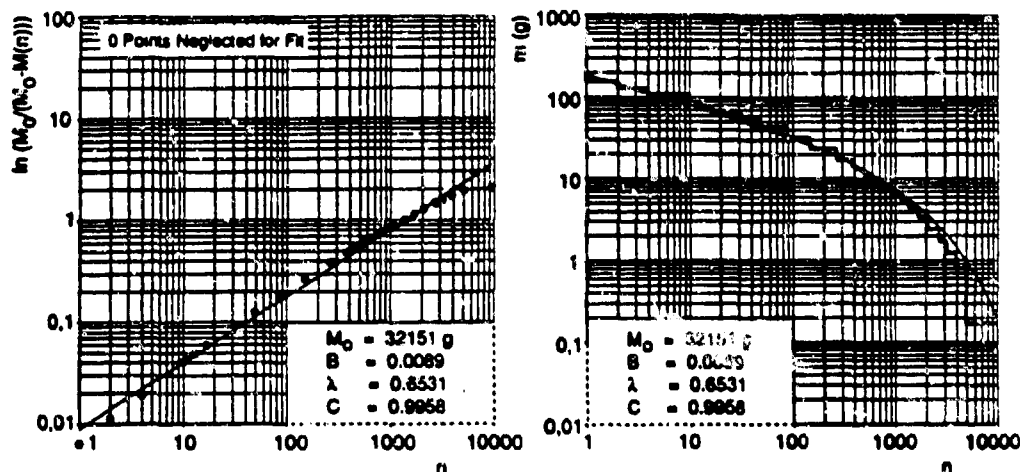


Fig. 3 Fragment mass distribution (FMD for short) log-log-diagram (left side) and mean fragment mass (MFM) (right side) as a function of the cumulative fragment number n for an 155 mm HB-projectile, filled with Composition B.

In the log-log-diagram, the straight line does not fit the measured data very well (Fig. 3 - left side). The first 4 fragments and the fragments over 4000, in particular, deviate from the straight line. Also the MFM-diagram (Fig. 3- right side) gives not a too good description of the found experimental distribution.

The agreement can be improved by adapting the overall mass M_0 as well as by neglecting some of the largest fragments which do not correlate with the fragment mass distribution of the shell casing, because they originate from the end plate and from the fuze adapter flange.

Using the constants B and λ as originally determined, one can now calculate an optimum mass M_{OB} , i.e. a total mass M_{OB} which best fits this set of equations:

$$M_{OB} = \frac{M(n)}{1 - e^{-Bn^\lambda}} \quad (12)$$

The new constants B_B and λ_B are now determined with this new total mass M_{OB} :

$$M(n) = M_{OB} \cdot (1 - e^{-B_B \cdot n^{\lambda_B}}) \quad (13)$$

With this new total mass $M_{OB} = 28318$ g, which is very near on the summed up mass of the found fragment masses of 28168 g, instead of $M_0 = 32151$ g, which in the example given means 12% less mass, the experimental data are much better described by the fitting of a straight line. The new constants are now $B_B = 0.0088$ (instead of $B = 0.0089$) and $\lambda_B = 0.6975$ (instead of $\lambda = 0.6531$), with a correlation coefficient of 0.9994 (instead of previously 0.9958) (Fig. 4, left). As can be seen in Fig. 4, right, the cumulative number n of fragments can now be described much better as a function of the mass classes, when these constants are used.

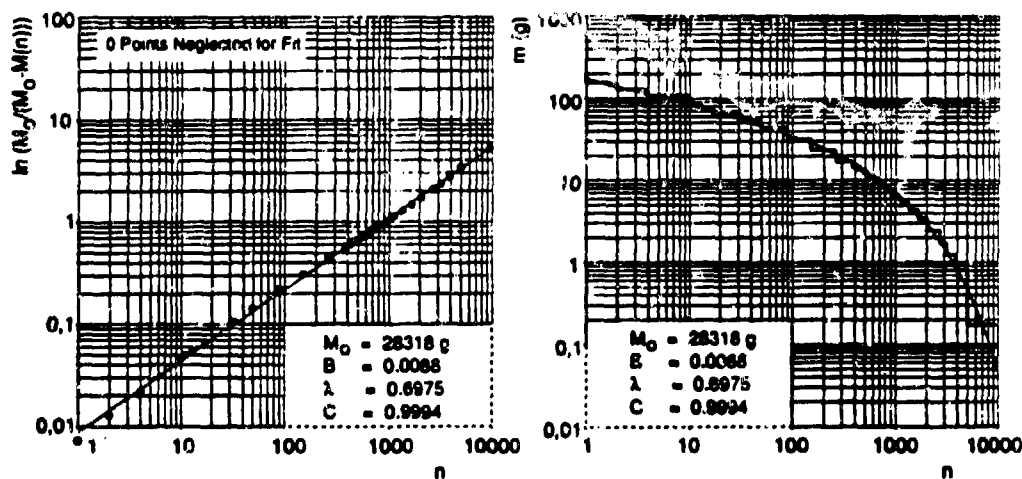


Fig. 4 FMD-log-log- and MFM-diagramm for an 155 mm HE-projectile with corrected mass compared to Fig. 3.

However, Fig. 4, left, shows that the individual points still fluctuate about the best-fit straight line, with the first 3 points - meaning the four largest fragments - deviating even more than the rest. These 4 fragments, with their random masses, must not be relevant to the fragment mass distribution.

When the first three points, corresponding to these four fragments, are omitted in this example, optimizing the mass M_0 now leads to a value of $M_{OB} = 28374$ g, and the constants become $B_B = 0.0100$ and $\lambda = 0.6763$, with a correlation coefficient of 0.9998. As can be seen in Fig. 5, left, all points - except for the three that have been purposely omitted - fit the calculated straight line rather well. Of course, the fragment mass equation with m as a function of the cumulative number of particles, n , averages the experimental values particularly well (Fig. 5, right).

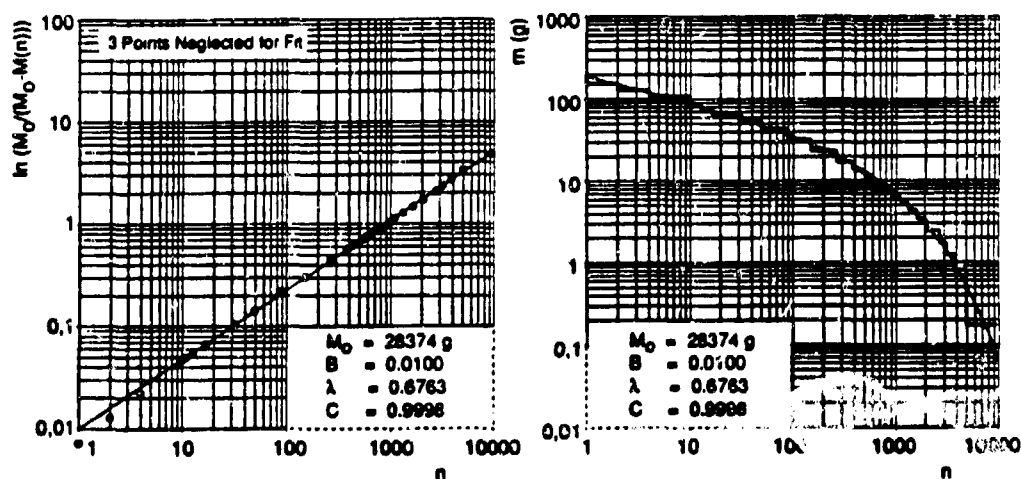


Fig. 5 FMD-log-log- and MFM-diagrams for an 155 mm HE-projectile with corrected mass, and neglecting the first 3 points (equivalent to the first 4 fragments).

3. MASS DISTRIBUTION OF DEBRIS FROM A SHELTER

The mass distribution of debris from 5 model-scale shelter trials is given in <1>, where tables 2 are presented showing the weight intervals and the associated numbers of fragments, the total weight without sieve data, and that with sieve data. As an example, Table 2 here shows Table 4-28 for the model 1 <1>.

All data presented in that paper have been analyzed using Meld's formula. In this, the mass had to be optimized in order that an adequate description of the debris distribution be obtained.

Figure 6 left, shows the logarithm of the mass ratio plotted against the cumulative number of particles, n , with the given initial mass M_0 equal to 37029 kg. It is obvious from this graphic representation that the initial mass was not correct, which results in a curved line representing the fragment distribution. A straight line reduced from this diagram cannot describe the fragment masses as a function of the cumulative number (Fig. 6 right).

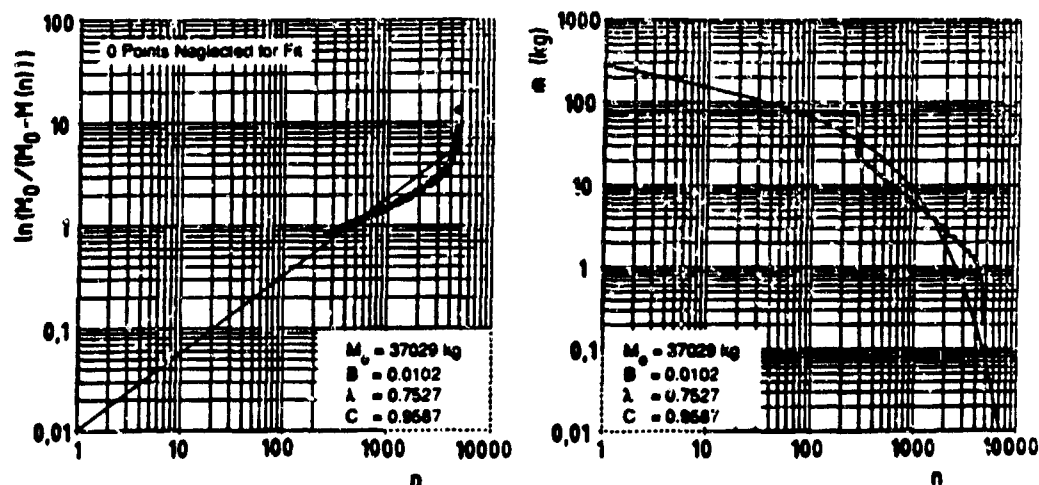


Fig. 6 FMD-log-log- and MFM-diagrams for model No. 1 without any correction.

Table 2

WEIGHT INTERVAL (LBS)			WITHOUT SIEVE DATA		WITH SIEVE DATA	
W1	-	W2	NUMBER	TOTAL WEIGHT	NUMBER	TOTAL WEIGHT
.25	-	.35	0	.00	234	73.37
.35	-	.45	31	13.67	3374	1365.94
.45	-	.55	2	.93	1294	615.95
.55	-	.65	1	.55	59	33.95
.65	-	.75	33	21.87	66	44.14
.75	-	.85	4	3.22	50	40.15
.85	-	.95	40	35.27	677	601.20
.95	-	1.05	0	.00	717	727.08
1.05	-	1.15	38	41.84	1401	1412.66
1.15	-	1.25	1	1.23	1044	1239.70
1.25	-	1.35	47	62.13	692	896.25
1.35	-	1.45	2	2.78	529	736.70
1.45	-	1.55	62	95.68	298	445.44
1.55	-	1.65	1	1.61	25	39.31
1.65	-	1.75	3	5.16	40	67.99
1.75	-	1.85	96	169.36	101	178.40
1.85	-	2.25	267	565.55	307	643.49
2.25	-	2.75	315	798.05	326	825.06
2.75	-	3.25	340	1011.48	342	1017.65
3.25	-	3.75	404	1412.13	408	1425.58
3.75	-	4.25	259	1051.65	260	1055.62
4.25	-	4.75	250	1124.14	250	1124.14
4.75	-	5.75	386	2028.23	388	2039.25
5.75	-	6.75	241	1515.13	244	1534.53
6.75	-	7.75	251	1819.89	262	1901.24
7.75	-	8.75	136	1126.12	136	1126.12
8.75	-	9.75	161	1490.10	161	1490.10
9.75	-	10.75	99	1013.62	99	1013.62
10.75	-	12.75	179	2093.33	179	2093.33
12.75	-	14.75	146	1998.09	146	1998.09
14.75	-	16.75	95	1491.29	95	1491.29
16.75	-	18.75	99	1752.39	99	1752.39
18.75	-	20.75	61	1204.03	61	1204.03
20.75	-	22.75	72	1563.89	72	1563.89
22.75	-	24.75	47	1119.02	47	1119.02
24.75	-	26.75	39	1004.29	39	1004.29
26.75	-	28.75	31	861.15	31	861.15
28.75	-	30.75	29	864.65	29	864.65
30.75	-	32.75	21	663.59	21	663.59
32.75	-	34.75	24	811.57	24	811.57
34.75	-	36.75	15	537.38	15	537.38
36.75	-	38.75	26	977.77	26	977.77
38.75	-	40.75	9	354.94	9	354.94
40.75	-	42.75	19	796.53	19	796.53
42.75	-	44.75	12	527.19	12	527.19
44.75	-	46.75	13	591.72	13	591.72
46.75	-	48.75	7	335.76	7	335.76
48.75	-	50.75	8	396.02	8	396.02
50.75	-	52.75	8	414.91	8	414.91
52.75	-	****	269	45864.77	269	45864.77
			TOTAL NB.	TOTAL WEIGHT	TOTAL NB.	TOTAL WEIGHT
			4699	81635.69	15013	89938.92

NOTE: 1 LB = 0.454 kg

If, however, the mass M_0 is optimized as outlined above, then the result is a straight line that excellently fits the measured. To this end, the total mass must be raised from 37029 kg to 40502 kg, i.e. by 8,6 % (Fig. 7, left). The resulting constants $B = 0.0641$ and $\lambda = 0.4312$ excellently describe the experimental fragment distribution, as can be seen in Fig. 7, right.

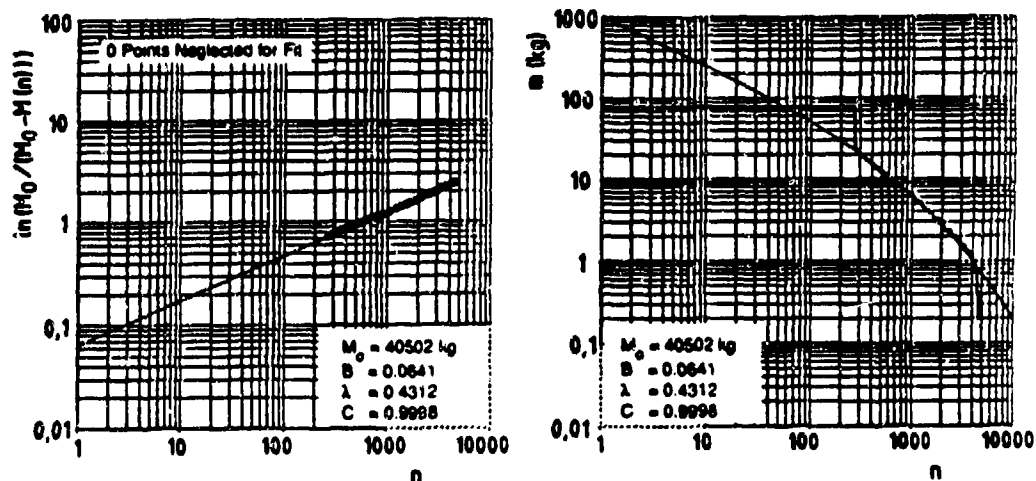


Fig. 7 FMD-log-log- and MFM-diagrams with mass correction from the data without any sieve.

With the sieve data, the mass difference is small, even though also here the initial mass M_0 of 40796 kg is not optimal (Fig. 8).

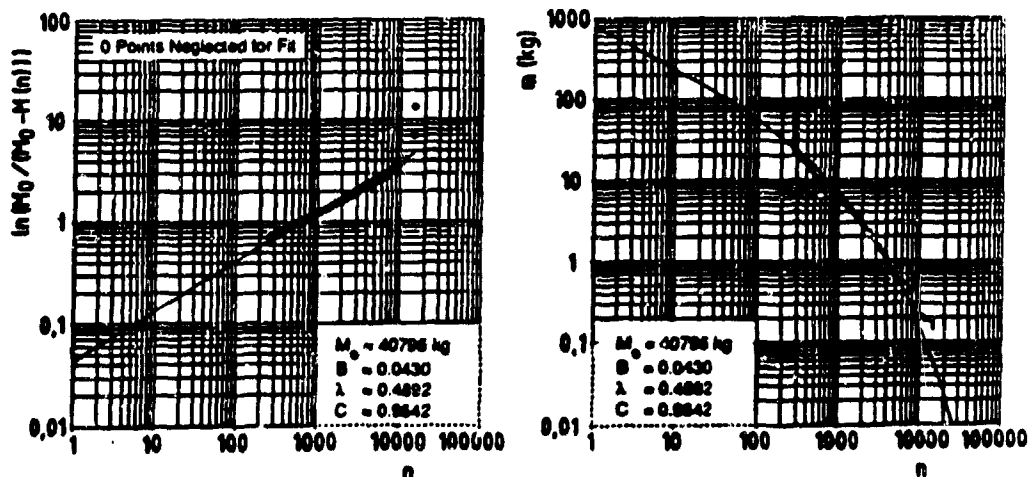


Fig. 8 FMD-log-log- and MFM-diagrams for model No. 1 with sieve data, without any correction.

An initial mass corrected by some 4 % again constitutes an optimum adaption to the mass distribution (Fig. 9).

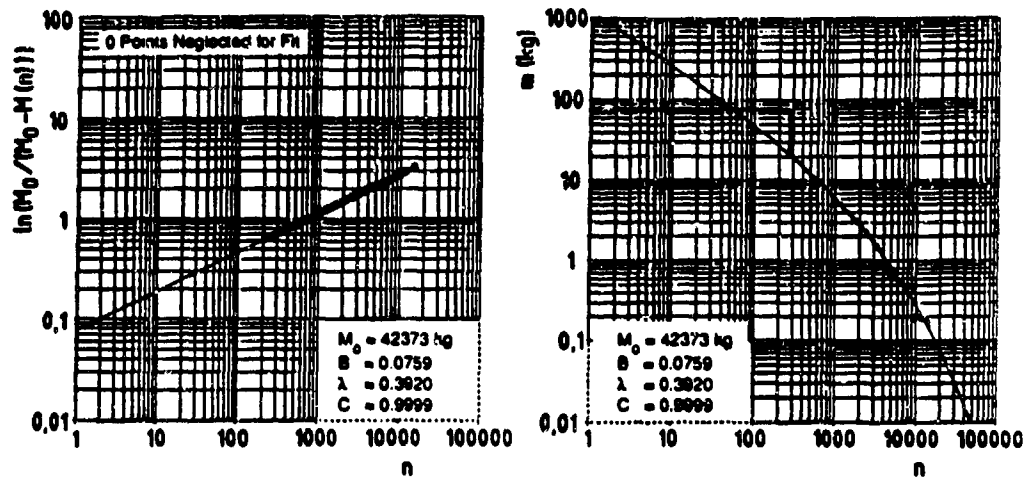


Fig. 9 FMD-log-log- and MFM-diagrams with only mass correction for the data with sieve.

With the smaller fragment masses, there is obviously an error in the analysis of the mass distribution with the sieve, which leads to a deviation of the curve fit for fragment masses of less than 0.6 grams. These small deviations exist in all analysis results with sieve data.

For reasons of space, the individual curves for the models 2 to 5 will not be presented here. With optimally selected M_0 values the curves for the fragment masses, as a function of fragment number for the 5 model tests without and with the sieving data, are compared in Fig. 10. They have indeed only relatively small deviations from one another. With the data without sieving, the mass correction is always greater than in the case with sieve data.

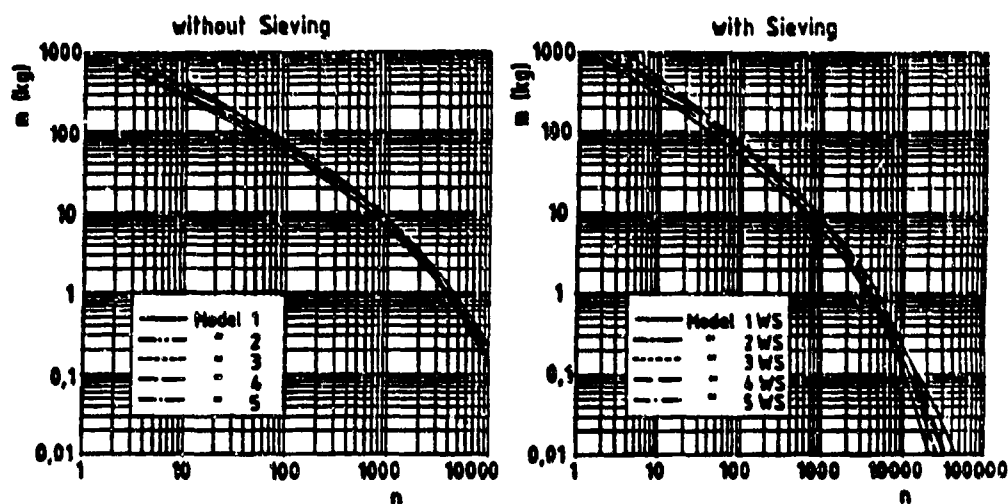


Fig. 10 Comparison of the mass distribution in the MFM-diagram for the fragment distributions of the model No. 1 to 5 without and with sieve data.

The table 3 lists the overall masses M_0 and the corrected masses $M_{0,Best}$ for the optimum fragment mass distribution, together with the constants B and λ and the correlation coefficients C , for the values without sieve data and with sieve data, for the five model tests.

Table 3

Model	M_0	$M_{0,Best}$	B	λ	C
1	37.020	40.502	0.0641	0.4312	0.9998
2	47.880	51.541	0.1363	0.3588	0.9999
3	50.582	52.874	0.0615	0.4608	0.9999
4	47.933	51.904	0.0602	0.4403	0.9999
5	41.975	44.859	0.0459	0.4932	0.9998
1	40.796	42.373	0.0759	0.3920	0.9999
2	50.644	51.461	0.1330	0.3630	0.9999
3	52.657	53.532	0.0665	0.4448	0.9999
4	50.891	51.763	0.0583	0.4458	0.9999
5	43.811	44.338	0.0404	0.5164	0.9998

Fig. 11 represents all the values of the table 3 in a graphical form. $M_{0, \text{Best}}$ varies relatively little. Also λ is fairly constant. The values of B are practically constant for tests 1, 3 and 4, but greater by a factor of 2 for test no. 2, and smaller by 30 % for test no. 5.

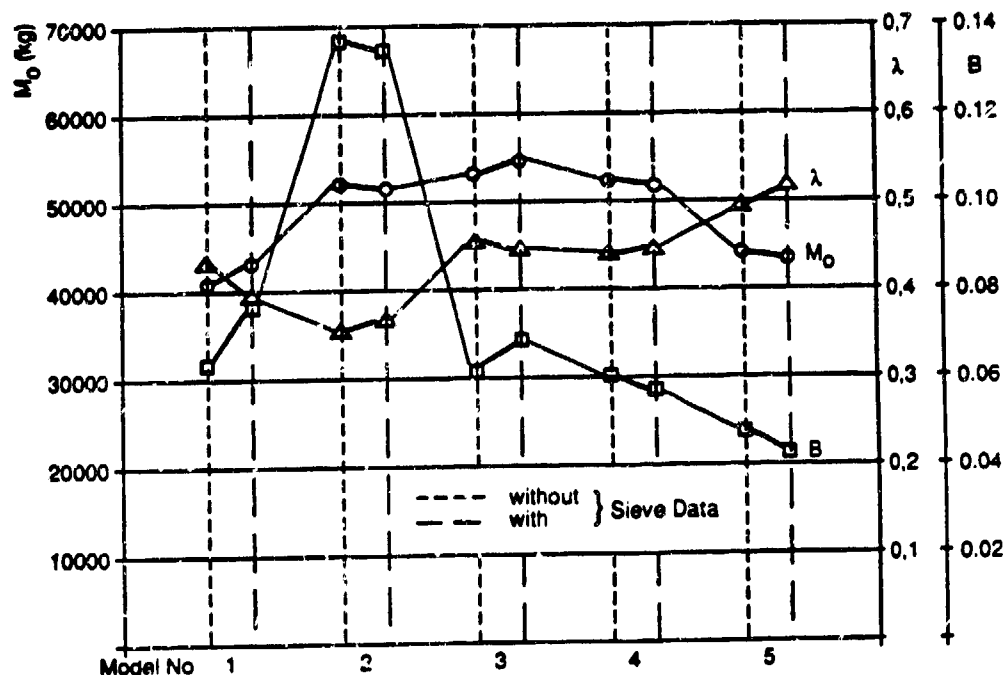


Fig. 11 The masses M_0 and the constants B and λ used for the description of the fragment mass distribution for the 5 model tests, with-out and with sieve data.

6. SUMMARY

The equation established by Held for the mass distribution of the natural fragments of an explosive-filled projectile can also be applied with very good results to the mass distribution of the debris from an exploded aircraft shelter.

The two constants required for this, namely, the scale parameter B and the shape parameter λ can be determined to a usually high confidence level, with a correlation coefficient close to 1, especially when the given total mass M_0 is changed to a "best mass" M_{0B} that best describes the actual fragment mass distribution.

The equation gives an even better description of the mass distribution of projectile - and this will show in a higher correlation coefficient - if the first, large fragments are omitted from the consideration. These fragments often do not belong into the fragment mass distribution. To omit means here that approximately 1 % to 2 % of the heaviest fragments will not be taken into consideration in the determination of the constants B and λ ; this is usually done on various but reasonable grounds. Omitting certain fragments is not necessary when the mass distribution of debris fragments from an aircraft shelter is to be described.

Such an optimization in the mass distribution of

- natural fragments of an explosive-filled projectile
- debris of e.g. an aircraft shelter

according to Held produces excellent results, with correlation coefficient that usually have four nines behind the comma.

REFERENCES

- <1> J.M. Ward, M.M. Swisdak, P.J. Peckham, W.G. Soper and R. Lorenz "Modeling of Debris and Airblast Effects from Explosions Inside Scaled Hardened Aircraft Shelters", NSWC TR 85-470, 1985
- <2> Oerlikon Taschenbuch, Para. 6.2.1.3 "Splittermassenverteilung" , pp. 210-216, 1981

- <3> M. Held, "Splitterballistik", Explosivstoff 15, 265-274, 1967; 16, 49-55; 73-78, 1968
- <4> M. Held, "Berechnung der Splittermassenverteilung von Splittermunition", Explosivstoffe 16, 241-244, 1968
- <5> M. Held, "Consideration to the Mass Distribution of Fragments by Natural Fragmentation in Combination with Preformed Fragments", Propellants and Explosives 1, 20-23, 1979
- <6> M. Held, "Fragment Mass Distribution of HE Projectiles", Propellants, Explosives and Pyrotechnics, In Preparation
- <7> M. Held, "Fragment Mass Distribution of Secondary Fragments", Propellants, Explosives and Pyrotechnics, In Preparation
- <8> R. Heiser, "Gesetze für die Massen- und Formverteilung von natürlichen Splintern", Handbuch der Munitionswertung, BWB WM VI 2, 302-312, 1979

A COMPARISON OF TWO PERSONNEL INJURY
CRITERIA BASED ON FRAGMENTATION

by

Frank McCleskey
Kilkeary, Scott and Associates
and
D. N. Neades
Ballistic Research Laboratories, Aberdeen Md.
and
R. R. Rudolph
Ketron, Inc.

FOR INFORMATION CONTACT:

Frank McCleskey
Rt. 3 Box 105
King George, VA 22485
703-775-7210
24th DOD Explosives Safety Seminar
28-30 August 1990

ABSTRACT

This paper includes a comparison of two Personnel Injury Criteria based on fragmentation. The first is the 58 ft-lb rule (Kinetic Energy Criterion) which has been in vogue since about 1900. The second is a new criterion, based on Kinetic Energy Density, which has been established by BRL over the last three decades. Both criteria are compared using four weapons for which suitable fragmentation data are available. The comparison is inconclusive as far as recommending one or the other criterion for use with the DDESB FRAGHAZ Computer Program. The paper contains recommendations to assist in making a choice between the two injury criteria.

The first 11 pages of this paper represent the presentation made by David Neades, Ballistic Research Laboratories, at the Explosives Safety Seminar held in Atlanta, Georgia in August 1988. It serves as background to pages 12-17 which comprise the paper for presentation by Frank McCleskey at the Explosives Safety Seminar held in St. Louis, Missouri in August 1990.

An Examination of Injury Criteria for Potential Application
to Explosive Safety Studies

D. N. Heades

U.S. Army Ballistic Research Laboratory
Aberdeen Proving Ground, Maryland 21005

R. R. Rudolph

Ketron, Inc.
Towson, Maryland 21204

1. Preface

The work described in this paper was sponsored and funded by the Department of Defense Explosive Safety Board (DDESB) in March 1983 under Project 4A665805M857.

2. Introduction

Present Department of Defense Explosive Safety Board (DDESB) doctrine establishes the acceptable fragmentation hazards to personnel exposed to accidental explosions. Presently, the acceptable limit is exposure to not more than 1/600 square feet of hazardous fragments. Current DDESB policy is to define a "hazardous fragment" as one which has at least 58 foot-pounds of kinetic energy. Clearly, the use of this, or any other injury criterion will effect the calculated distances required to limit personnel to the acceptable exposure limit.

Use of the 58 ft-lb criterion to define fragmentation hazards has been criticized in recent years because, 1) it is not based on any well defined injury classification scheme, 2) it is overly simplistic in nature, and 3) a general feeling that there must be something better available in light of all the research into wounding phenomena and effects that has taken place over the last several decades.

The objectives of this investigation were to review the literature on kinetic energy wounding, assess the state-of-the-art, determine the applicability of existing data and models to explosive safety studies, and if appropriate, recommend new criteria. In addition, since the far-field hazards relate mainly to large (ranging from a few grams to several kilograms), relatively slow moving fragments with speeds approaching their free-fall velocity, the range of variables over which the various criteria are valid was to be determined and methods for extrapolating to the mass range of interest considered. The discussion

- 2 presented here will focus on the major findings of the investigation with respect to the availability of a suitable 58 ft-lb law replacement candidate. Additional details concerning other important research not covered in this paper, along with the bibliography which resulted from the current study, can be found in a soon to be published BRL report.

3. Literature Search

The survey of the literature was conducted by a contractor, Ketrion, Inc. Several hundred technical reports and journal articles were compiled, reviewed, and analyzed with the above mentioned objectives in mind. A majority of the documentation was located by querying the DTIC (Defense Technical Information Center), NTIS (National Technical Information Service), TRIS (Transportation Research Information Service), BIOSIS (Biological Research Abstracts), and MEDLINE (Medical Literature Analysis and Retrieval Systems) automated data bases. In addition, a significant amount of relevant information was obtained through numerous informal discussions with various researchers in ballistics and related fields. A comprehensive bibliography containing 304 citations was compiled from the reviewed literature.

4. Penetrating Trauma

In the search for relevant literature, a natural division seemed to occur between penetrating injury and non-penetrating injury data. Accordingly, the documents reviewed were categorized as relating to either one or the other. The overwhelming majority of data and models located pertain to research into penetrating injury phenomena. The following discussion will focus on only a few of the criteria which were established as a result of this research.

4.1. 58 Ft-Lb Criterion

The literature abounds with references to the 58 ft-lb energy criterion. Rohne is usually given credit for establishing this criterion which was probably intended as nothing more than a rough rule of thumb. The date usually attributed to its origin is 1906. The actual quote, translated from the 1906 article¹ by Rohne is "To remove a human from the battlefield, a kinetic energy of 8 mkg is sufficient according to the prevailing view in the German artillery community;....". Actually, an earlier article by Rohne, written in 1896 under the same title, contains the same statement; in neither case does he cite any data, experimental or otherwise, to substantiate this view. Interestingly, in a subsequent paragraph, he states that "Horses require a larger impetus to incapacitate them. Colonel Langlois set forth a kinetic energy of 19 mkg in his report 'L'artillerie de campagne en liason avec les autres armes',... Again, it is unfortunate that the basis for these statements is not explained. Rohne, while not discussing the validity of the 58 ft-lb criterion, used it to determine ranges at which various military rifles ceased to be effective.

¹ Rohne, H.; Schiesslehre fur Infanterie, 1906.

3 While the exact origin and basis for the 58 ft-lb figure remains obscured, other researchers have considered its validity as a criterion with varying results. Sterne², for example, in 1955, suggested that Rohne's criterion applied to lethality rather than to a sublethal effect. Indeed, penetrating injury research shows that lethal injuries can occur at impact kinetic energy levels significantly less than 58 ft-lbs. Without giving additional consideration to other parameters such as missile shape, size, mass, and possibly impact location, energy based hazard assessments can be misleading.

4.2. Incapacitation Criteria

In the years since Rohne, numerous researchers have investigated projectile induced kinetic energy wounding usually in hopes of relating, in some fashion, some form of ballistic dose to the projectile's casualty producing potential. The U.S. Army's incapacitation criteria, which resulted from extensive research conducted over the last three decades, were established to predict the incapacitating effects of wounding by fragmenting munitions, bullets, and flechettes. Certain of these criteria have, on occasion, been applied to hazard type analyses, but in general they are used as effectiveness criteria in the context of weapon system analyses. Briefly, the approach taken to establish these criteria was as follows.

An initial set of four steel fragment simulators was chosen to represent the class of munition fragments of interest. The projectile masses and the velocities at which they were assessed are shown in the following table.

Table 4-1. Incapacitation Projectile Data Base

Projectile	Mass	Experimental Striking Velocities
0.85 gr, steel sphere	0.055 gram	305, 914, 1524 meters/second
2.1 gr, steel cube	0.136 gram	305, 914, 1524 meters/second
16.0 gr, steel cube	1.04 gram	305, 914, 1524 meters/second
225 gr, steel cube	14.58 gram	152, 305, 762 meters/second

Basically, for each of these mass-velocity combinations, firings were conducted against biological targets to generate actual wound data. The nature of the observed wounds was delineated by assigning to it a

² Sterne, T. E., and A. J. Dziemian; "Provisional Probabilities of Incapacitation by a Caliber 0.30 Rifle-Bullet, Ball M-2," BRLM 949, U.S. Army Ballistic Research Laboratory, Aberdeen Proving Ground, MD, Dec 1955.

- 4 wound class which related incapacitation to loss of arm and leg function.

The most widely applied criteria of this type are the curves published by Kokinakis and Sperrazza in 1965³. The correlation relates striking mass and velocity of an impacting steel fragment to the conditional expected level of incapacitation given a single random hit. The functional form of the relationship is:

$$P(I/H) = 1 - e^{-a(mv^A)^b}$$

where e = base of natural logarithm
 m = fragment mass (grains)
 v = fragment striking velocity (ft/sec)
 A, a, b, n = fitted constants which depend on tactical role, time after wounding, and body part hit.

Since these criteria are based upon the physical requirements and tactical functions related to infantry soldiers in the assault, defense, reserve, and supply roles, it would be inappropriate to apply them to situations involving threshold injury levels to non-military personnel.

4.3. Other Penetrating Trauma Models

In 1967, Kokinakis and Sperrazza⁴ published data on the ballistic limits of skin and clothing, based on experimental firings of steel projectiles. Until recently, this skin penetration criterion was used by the U.S. Army as the "official" safety criterion for assessing threshold fragmentation hazards. However, in 1978 Lewis⁵, et al developed an empirical formula for estimating the probability of skin penetration by various projectiles, including low density fragments. Of interest to

³ Kokinakis, W. and Sperrazza; "Criteria for Incapacitating Soldiers with Fragments and Flechettes," BRL Report 1269, U.S. Army Ballistic Research Laboratory, Aberdeen Proving Ground, MD, January 1965, (CONFIDENTIAL).

⁴ Sperrazza, J. and W. Kokinakis, "Ballistic Limits of Tissue and Clothing," BRL TN 1645, U.S. Army Ballistic Research Laboratory, Aberdeen Proving Ground, MD, January 1967.

⁵ Lewis, J. H., P. A. Coon, V. R. Clare, L. M. Sturdivan; "An Empirical/Mathematical Model to Estimate the Probability of Skin Penetration by Various Projectiles," ARCSL-TR-78004, U.S. Army Armament Research & Development Command, Chemical Systems Laboratory, Aberdeen Proving Ground, MD, 1978.

- 5 them was the environmental debris such as rocket motor fragments and other secondary projectiles that pose a hazard to personnel. Backblast debris from small rocket-motor launched weapons could include wood fragments from vegetation and structures, metal fragments from the weapon, rocklike fragments from stone or concrete structures and stones from the ground. Accordingly, they included in their investigation three sizes of wood cylinders having diameters and lengths equal to 0.5 inch (1.27 cm), 1.0 inch (2.54 cm), and 1.5 inch (3.81 cm) and irregular gravel weighing approximately 2 grams. Other missiles were 4 grain (0.259 gram), 16 grain (1.035 gram), and 64 grain (4.14 gram) steel cubes, a 0.85 grain (0.055 gram) steel sphere and a 16 grain (1.035 gram) tungsten cube. These projectiles were fired at sections of goat skin backed with 20 percent gelatin at 10 degrees C. Striking velocity was treated as a test variable.

One objective of the study was to determine the probability of complete skin perforation (full-thickness skin laceration) since the authors had equated this occurrence to a hazardous condition- the assumption being that given a complete penetration of the skin layer, the potential for deeper penetration into various parts of the body also exists. Since a fragment perforates or fails to perforate the skin, the Walker - Duncan Method⁶ could be used to estimate the probability in terms of a single variable X defined by some function of the test variables. In this instance, the authors selected for their model

$$X = \ln [(MV^2)/A]$$

where m = mass of the projectile (grams)
 v = velocity of the projectile (meters/sec)
 A = presented area of the projectile (sq cm).

The Walker-Duncan estimation is then given by

$$P = \frac{1}{1 + \exp [-(a + bx)]}$$

where: a and b are curve fitting constants
 and x is as defined above.

Employing curve fitting techniques, the authors determined a and b values for the targets shown in Table 4-2.

⁶ Walker, S. H. and D. B. Duncan; "Estimation of the Probability of an Event as a Function of Several Independent Variables", Biometrika 54:167-179, (1967).

Table 4-2 Logistic Function Coefficients

Target	a	b
Bare Skin	-28.42	2.94
Two-Layer Uniform	-48.47	4.62
Six-Layer Uniform	-50.63	4.51

Probability curves for skin penetration as a function of $\ln [(MV^2)/A]$ are shown in Figure 4.1.

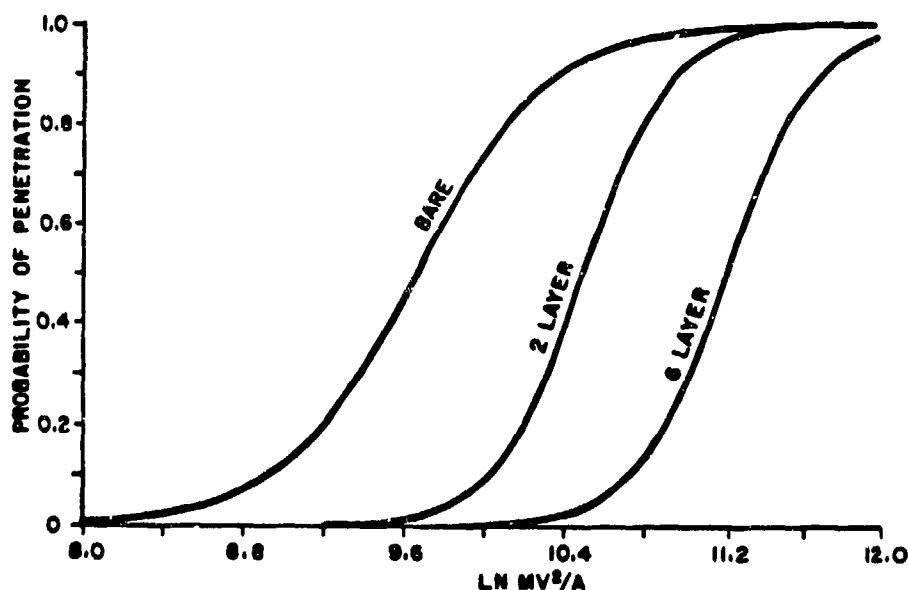


Figure 4.1 Walker-Duncan Curves Estimating the Probability of Skin Penetration as a Function of Projectile Parameters. (Reproduced from Reference 5).

5. Non-Penetrating Trauma

Although penetration is the primary damage mechanism of interest here, it was felt that the potential for injury from non-penetrating missiles exists as well. Non-penetrating injury, or blunt trauma, generally refers to any injury caused by a victim either striking or being struck by a non-piercing object. Objects causing projectile induced blunt trauma are characterized by their low velocity, lack of cutting and piercing features and size.

Most of the research pertaining to projectile-induced blunt trauma has occurred since the passage of The Omnibus Crime Control and Safe

7 Streets Act of 1968. Much of the research was sponsored by The National Institute of Law Enforcement and Criminal Justice and performed by multi-disciplined teams of researchers from the U.S. Army's Biophysics Laboratory located at Edgewood Arsenal (EA), Maryland and Land Warfare Laboratory (LWL) at Aberdeen Proving Ground Maryland, and various contractors.

The LWL team of Shank, Thein, Campbell and Wargovich conducted valuable research⁷ into the physiological response to the effects of non-lethal weapons. An interesting part of their work involved the classification system they established for measuring these responses.

With regards to the availability of injury criteria for non-penetrating missiles the four-parameter model of Clare, et al⁸, apparently represents the "state of the art" in blunt trauma modeling. Given knowledge of the input parameters, (projectile mass, velocity and diameter and target (body) mass) the model predicts the probability of lethality as a result of impact to the thorax. Their model is of the form:

$$P(r) = f(mv^2)/wD$$

where

$P(r)$ = probability of response (death, serious injury, etc)
 m = mass of projectile in grams.
 v = impact velocity of the projectile in meters/second.
 w = body mass of the animal in kilograms.
 D = diameter of the projectile in centimeters.

The same model, with appropriate adjustment of the discriminant line intercept, was extended by the authors to fracture/no-fracture data for the liver.

⁷ Shank, E. B., B. K. Thein, D. Campbell and M. J. Wargovich; "A Comparison of Various Less Lethal Weapons," LWL TR-74-79, U.S. Army Land Warfare Laboratory, Aberdeen Proving Ground, MD, June 1974.

⁸ Clare, V. R., J. H. Lewis, A. P. Michiewicz and L. M. Sturdivan; "Handbook of Human Vulnerability Criteria Chapter 9. Projectile-Induced Blunt Trauma," EB-SP-76011-9, Department of the Army, Headquarters, Edgewood Arsenal, Aberdeen Proving Ground, MD, May 1976.

- 8 As shown in figures 5.1 and 5.2, the model discriminates between low, medium, and high regions of response/no response. The authors emphasize that they consider the model to be provisional, pending availability of additional data for further validation.

6. Applicability to Explosive Safety

The relevancy of models described in the previous sections can be summarized from an examination of Figure 6.1. To facilitate comparisons of the various relationships, the masses and velocities corresponding to each model's predicted measure were determined. For example, for line B, the masses and velocities are those which correspond to a 50% probability of skin penetration (for steel cubes) according to the model of Lewis.

The presently employed 58 ft-lb law (line A) is shown in comparison with two pairs of penetrating injury relationships. The upper pair, represented by lines B and C, are based on the skin penetration model of Lewis et al. The test mass upper bound was 4.08 grams. Line B is for steel cubes; line C was derived assuming a spherical shape factor. The second pair of lines, represented by lines D and E describe the penetration law of Sperrazza and Kokinakis. The test mass upper bound was 15 grams. Line D is based on steel cubes; line E was derived assuming a spherical shape factor. In addition, the calculated DDESB mass interval of interest⁺ is shown in the shaded area.

The two lines labeled "G" represent the relationship of Clare, et al for threshold liver fracture. The bottom solid G-line most directly reflects the test data for which the average animal weight, w , was about, 11.3 kg. The upper dashed G-line is an extrapolation to a man's body weight of 70 kg. Both lines are for low density (average 1.31 g/cm³) projectiles and the mass test data interval was from 3 grams to 381 grams. Also shown is the LWL blunt trauma relationship for the first damage level (line F).⁺⁺ The LWL relationship was not discussed here since it is not directly applicable to humans. It is included because it corresponds to a low level of injury (LWL damage level 1) and is therefore of interest from an injury threshold perspective. Unfortunately, the model is not appropriate for human body weights. With the EA model, weight of the target is an input parameter.

⁺ The interval depicted represents a crude estimate of the relevant mass range based on 155 mm projectile data published by Feinstein, D. I., in "Fragmentation Hazards to Unprotected Personnel," IITRI J6176, Engineering Mechanics Division, IIT Research Institute, Chicago, IL for the Department of Defense Explosive Safety Board (DDESB), Washington, DC, January 1972.

⁺⁺ The LWL team of Shank et al used a six valued damage level grading system to describe the effects of blunt trauma wounds. Damage level 1, corresponds in general to superficial or slight damage. See reference 7 bottom of page 7.

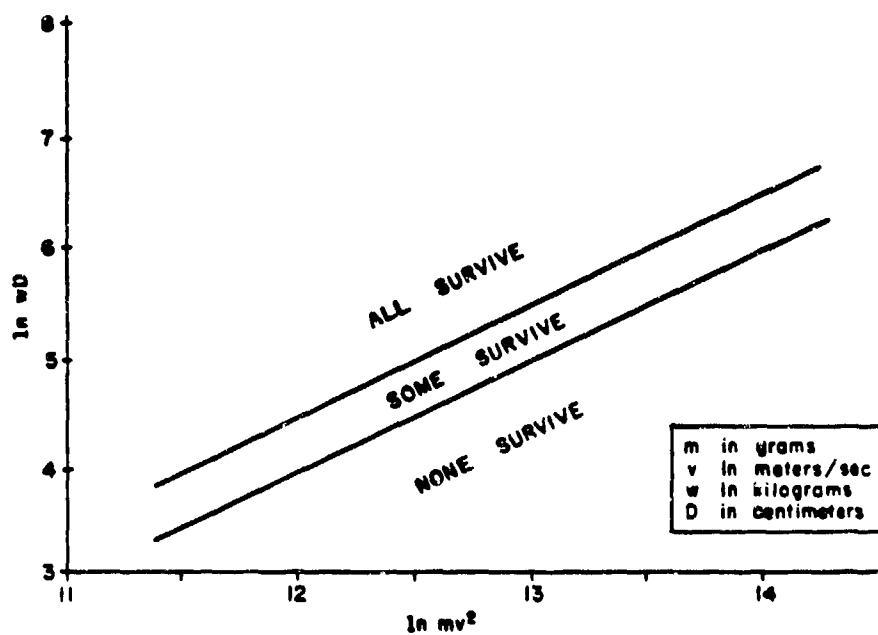


Figure 5.1 Lethal/Non-Lethal Discriminant Lines, Based on EA Four-Parameter Model Applied to Animal Blunt Trauma Data.

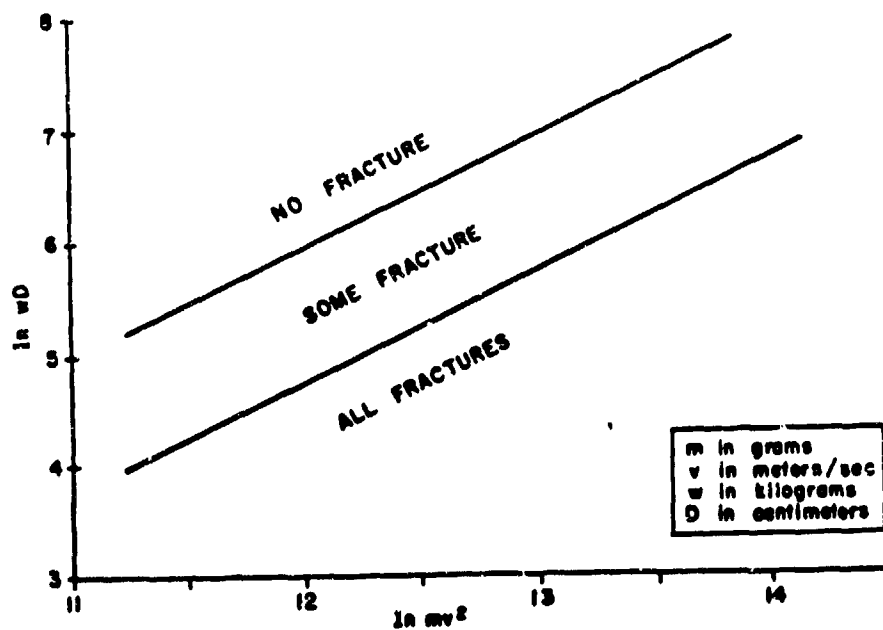


Figure 5.2 Liver Fracture/No Fracture Discriminant Lines, Based on EA Four-Parameter Model Applied to Blunt Trauma Data.

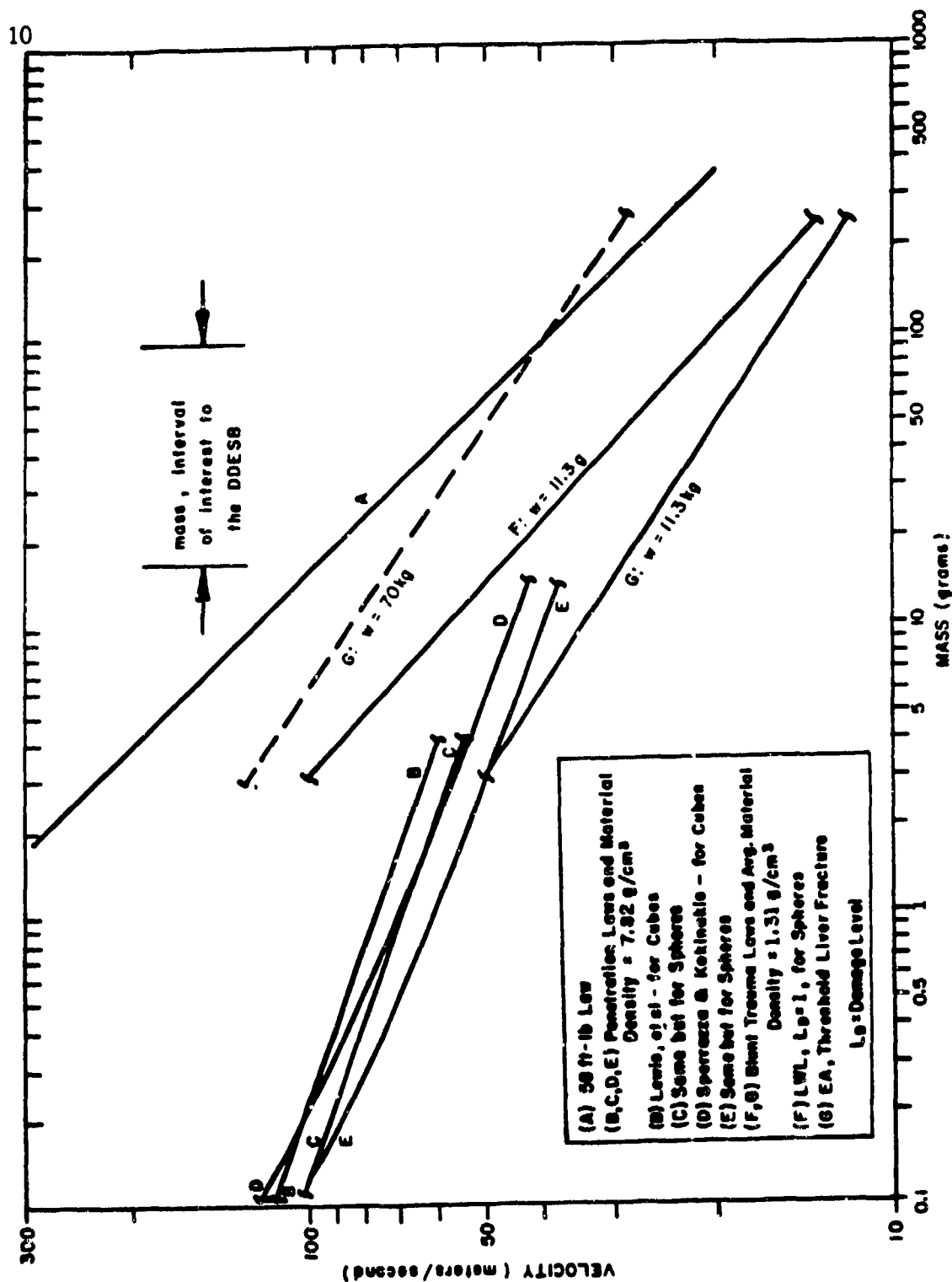


Figure 6.1 Lava, Mass Bounds on Data and DDESB Mass Interval of Interest.

11 7. Summary and Conclusions

In the attempt to locate criteria which represent an improvement over the currently used 58 ft-lb law, it became obvious that an accurate assessment of the hazards for typical far-field fragments by application of the various criteria located was not possible due to two noted shortcomings, namely:

- 1.) the lack of non-penetrating injury data for projectiles with densities greater than about 1.31 gm/cm³,
- 2.) the lack of penetrating injury data for projectiles with mass greater than about 15 grams.

The above deficiencies are a result of wounding/injury research being concentrated on the effects of small, high velocity, steel projectiles. Where investigations were conducted into non-penetrating trauma, the projectiles of interest were, by design, of low density materials. The assessments and comparisons made in the analysis then are, in some cases, based on severe extrapolations of the existing data bases. For example, in comparing Lewis's skin penetration model with the 58 ft-lb rule, it was necessary to assume the model was valid for fragment masses an order of magnitude larger than those upon which the model is based. Accordingly, there is a critical need to verify the skin penetration curves in the mass ranges of interest, and the blunt trauma relationship for high density materials. Given these model validations/modifications, it is felt that a viable solution to the problem of determining far-field fragment hazards to personnel could involve simultaneous application of the two models mentioned above to quantify the potential for both penetrating and non-penetrating injury. A hazardous condition would be indicated if either criterion was met.

A methodological change of this nature would of course require a concomitant change in philosophy as to just what constitutes an unacceptable hazard to personnel. The economic, social, and political implications of adopting the skin penetration model as a replacement for the 58 ft-lb rule have not been considered in this investigation. In conclusion, we find numerous arguments against the continued use of the 58 ft-lb criterion, the strongest of which concerns its inability to predict a well defined injury level on the basis of mass and velocity alone, and suggest that after further investigation, more meaningful criteria can be formulated by validating other scientifically based models by extending and/or modifying those models through additional experimentation and analysis.

8. Injury Criteria Comparisons

8.1 Background

Previous portions of this paper have discussed the 58 ft-lb personnel injury criterion and a number of other alternate criteria. These data were presented to the explosive safety community in the August, 1988 seminar held in Atlanta, Georgia.

The 58 ft-lb criterion is currently used by the Department of Defense Explosives Safety Board (DDESB) in the FRAGHAZ⁹ computer program to evaluate fragment hazards from stored munitions. Since 1988, the Ballistic Research Laboratories (BRL) have established and recommended the skin penetration model attributed to Lewis et. al. as a replacement for the 58 ft-lb criterion.

Since 1988, FRAGHAZ runs have been made using the two criterion with four weapons - MK 82 Bombs, 155mm Projectiles, MK 64 Projectiles and 105mm Projectiles. Fragmentation data for these four weapons are the only sets currently available for use with the FRAGHAZ computer program. This work was done to provide a quantitative estimate of the difference in results for the two personnel injury criteria. The two injury criteria are defined as follows:

8.1.1 58 Ft-Lb Kinetic Energy Criterion

$$KE = \frac{mv^2}{2g}$$

where

KE = Kinetic Energy (ft-lbs)

M = Mass of fragment (lbs)

V = Striking Velocity (ft/sec)

g = Acceleration due to gravity (32.174 ft/sec²)

In this criterion, a fragment is considered hazardous if it has at least 58 ft-lbs of kinetic energy when it strikes the target person. If the fragment has less than 58 ft-lbs of kinetic energy when striking the person, it is considered non-hazardous. This, then, is a threshold criterion, with no transition zone, having a probability of injury of either 0 or 1. As explained in the first part of this paper, the 58 ft-lb rule was developed around 1900 and does not specify the severity of the injury inflicted except to state something like.... "remove a soldier from the battlefield".

⁹McCleskey, Frank "Quantity - Distance Fragment Hazard Computer Program (FRAGHAZ)" NSWC TR 87-59, Naval Surface Warfare Center, Dahlgren, Virginia, Feb 1988

8.1.2 Continuous Probability of Injury Criterion (CPIC)

This is the criterion proposed by BRL as a replacement for the 58 ft-lb rule. It is based on the work of Lewis et. al. and involves bare skin penetration as the injury criterion. It is stated as a probability of injury as follows:

$$P_I = \frac{1}{1 + \text{EXP}(-(A + B \ln \frac{MV^2}{C}))}$$

where:

- P_I = Probability of Injury (skin penetration)
- EXP = Exponential (base e)
- A = Constant = -27.35
- B = Constant = 2.81
- ln = Natural Log (base e)
- M = Striking fragment mass (grams)
- V = Striking fragment velocity (meters/sec)
- C = Average fragment presented Area (cm²)

Note that the constants A and B are slightly different than those given previously. This resulted from the tests with 100 gram fragments which were completed since the 1988 paper. Since fragments always have a finite velocity at strike, the probabilities of injury are always greater than 0. Likewise at the other end of the scale, the probabilities of injury are always less than 1. This is truly a transitional criterion providing injury probabilities between 0 and 1. Also note that this criterion involves the average striking area (C) which is certainly a consideration for skin penetration. The 58 ft-lb rule ignores this variable.

8.2 Comparisons

Comparisons for the two personnel injury criteria are shown in Figures 8.1 and 8.2. Figure 8.3 shows the mass and impact velocity combinations for the two injury criteria.

Figure 8.1 shows comparisons for the three mass detonating munitions currently available for the FRAGHAZ computer program. Mass detonating implies near simultaneous detonation of a stack from 1 or more detonating donor munitions.

Figure 8.2 shows two comparisons for the non-mass detonating 105mm projectiles. Plot A is for 0-200 projectiles and Plot B is for 0-8000 projectiles. The two plots are required because of the number of projectile differences for the two injury criteria. Non-mass detonating implies sequential detonating that results when the stack is engulfed by fire. Detonations may be seconds, minutes, or even hours apart.

For both plots, sea level and no wind conditions apply. Hazard density in both cases is one hazardous fragment per 600 square feet (1/600 = .001667). The plots then show the number of munitions required to produce the hazard density (1/600) at the hazardous ranges indicated. Only hazardous fragments meeting the requirements shown in Figure 8.3 are included. The number of munitions apply to the 90th percentile currently specified by the DDESB. The 90th percentile implies that 10 percent of the time, hazard ranges will be greater than those shown.

Figure 8.1 - Injury Criteria Comparisons

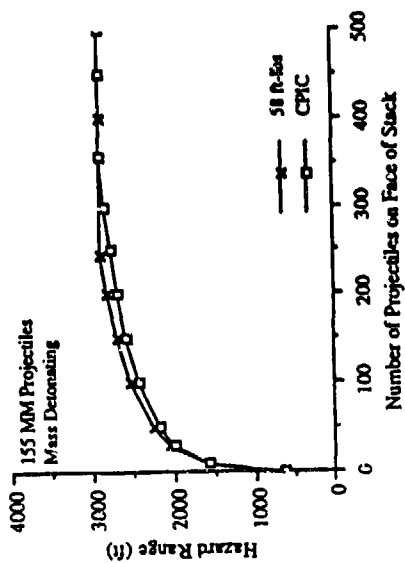
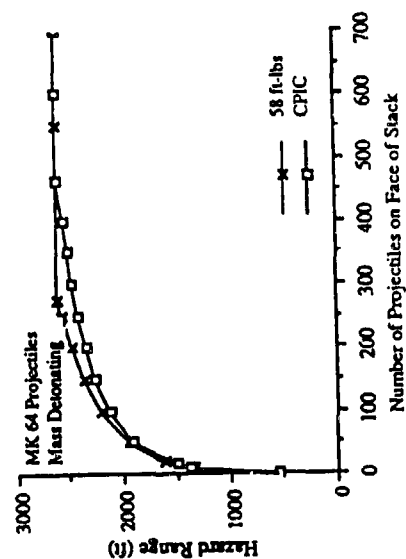
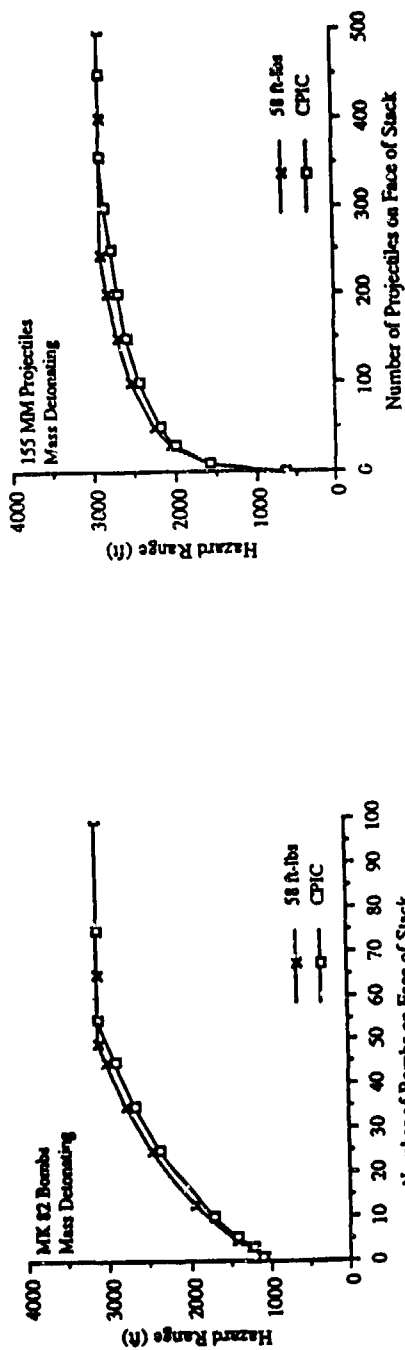
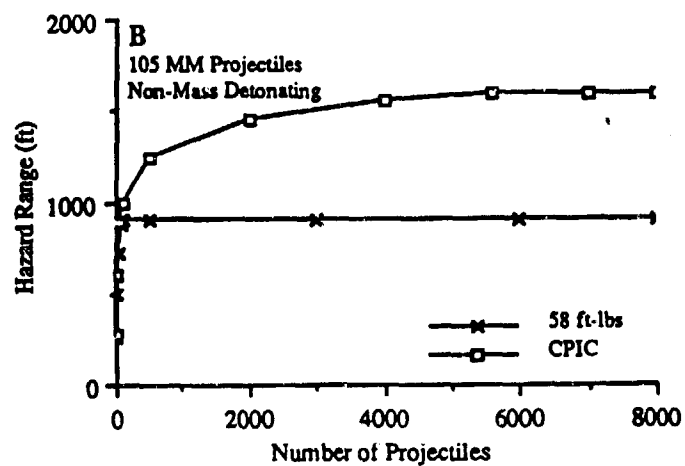
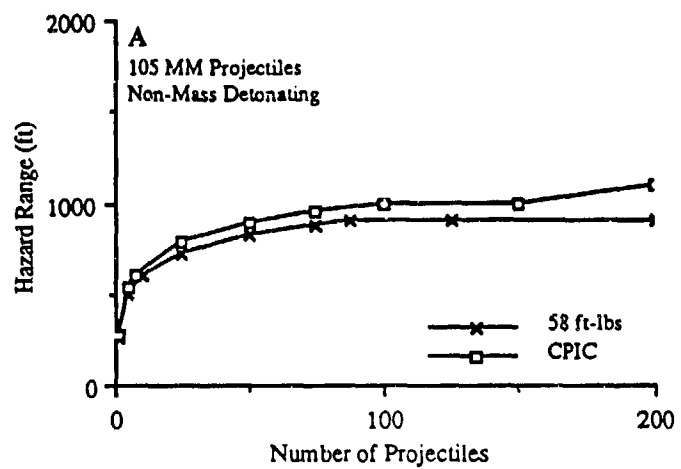


Figure 8.2 - Injury Criteria Comparisons

**Figure 8.3 - Personnel Injury Criteria Thresholds
(M, V Requirements)**

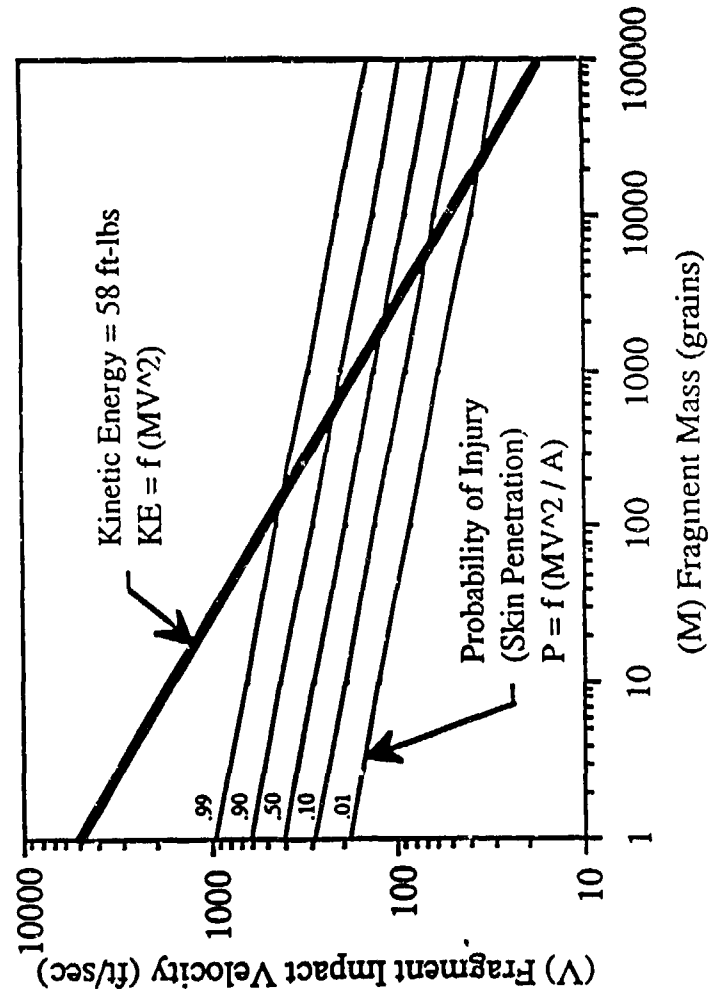


Figure 8.3 shows the threshold injury levels for the two injury criteria as a function of mass and velocity for an impacting fragment. The slopes for the two criteria are quite different, which could result in large differences, especially for small fragment masses.

8.3 Discussion

8.3.1 Figure 8.1 shows no significant difference for the two injury criteria for the three mass detonating munitions.

8.3.2 Figure 8.2 shows an A and B plot for non-mass-detonating 105mm projectiles. Plot A is for 0 to 200 projectiles and plot B is for 0 to 8000 projectiles. There is hardly any significant difference for 0 to 200 projectiles as shown in plot A. In plot B however, there is a significant difference when we exceed 200 projectiles. In plot B, the maximum hazard range for the 58 ft-lb criterion is 900 feet while the maximum hazard range for the CPIC (skin penetration) criterion is 1600 feet. This is due mainly to the fact that fragments going to the maximum range are less than 1000 grains. They do not meet the 58 ft-lb criterion but do produce a small probability of injury with the CPIC (skin penetration) criterion.

8.3.3 In figure 8.3 it is shown that the 58 ft-lb line crosses the .99 probability of injury line at about 100 grains. At the other end it crosses the .01 probability of injury line at about 20,000 grains. Oddly enough this is about the range of fragment weights for the four munitions investigated. Experimental verification for the 58 ft-lb rule is very limited while the CPIC (skin penetration) criterion has a very large quantity of experimental verification over a wide range of fragment masses.

8.4 Conclusions and Recommendations

8.4.1 Results currently available are not sufficient to make a definite recommendation for shifting from the 58 ft-lb criterion to the CPIC (skin penetration) criterion for use with the DDESB FRAGHAZ computer program. This is partly due to the uncertainty in the personnel, time and money required to change all the reports and manuals currently active in the DDESB files.

8.4.2 The DDESB should evaluate the conditions and requirements for non-mass-detonating munitions like the 105mm projectiles considered here. The reevaluation should include:

1. Time element - the successive detonations of non-mass-detonating munitions may go on for hours. A time limit expressed as a limiting number of projectiles should be considered to reflect a reasonable time exposure for the personnel target.
2. Projectile alignment - successive explosions will rearrange the alignment of projectiles with respect to the hazard area.

8.4.3 Figure 8.3 shows a marked departure of the 58 ft-lb line from the .99 probability of skin penetration below 100 grains. As such, an evaluation of the hazards from anti-personnel munitions should be conducted with the Army to compare the two injury criteria.

**AN INVESTIGATION
OF FRAGMENT STOPPING BARRICADES**

BY

**FRANK McCLESKEY (KILKEARY, SCOTT, AND ASSOC.)
LEE WILSON (ADVANCED TECHNOLOGY, INC.)
ROSE BAKER (NAVAL SURFACE WARFARE CENTER)**

FOR INFORMATION CONTACT:

**FRANK McCLESKEY
RT. 3 BOX 105
KING GEORGE, VA. 22485**

703-775-7210

**24th DOD EXPLOSIVES SAFETY SEMINAR
28 - 30 AUGUST 1990**

ABSTRACT

This paper describes a two-part investigation of the reduction in fragment hazards afforded by barricades. Also included is a description of the FRAGHAZ Computer Program used in the investigation. Part I is a general investigation of barricades to test the usefulness of the FRAGHAZ Program and to gain initial in-sight on barricades. Part II covers a specific investigation of the fragment hazard reduction capability of a natural hillside barricade in Taegu, Korea. The results of the investigation indicate that the configuration and positioning of the ammo stacks relative to the barricade are prime considerations in reducing fragmentation hazards.

PREFACE

This paper will be published as a Naval Surface Warfare Center report in the future. The tables to be published in the report have not been included in this paper. However, the more important aspects of the tables are included in the figures contained in this paper. References to the tables have been retained to indicate the scope of the investigation.

INTRODUCTION

This report is divided into two parts. Part I contains a general study of barricades; Part II involves a specific investigation of the barricade effects of hilly terrain in Taegu, Korea.

Barricades have been in use for many years in areas where explosive ordnance is stored. Barricades provide a means for stopping fragments produced by inadvertently detonated ammunition stacks. They may be artificial (man made) or natural obstacles such as hills. This report covers the study of both an artificial and a natural barricade.

All of the numerical results contained in this report were produced by the FRAGHAZ Computer Program.¹ In order to provide the reader with a basis for judging the validity of the numerical data contained herein, the general characteristics and capabilities of the FRAGHAZ Computer Program, together with the variables taken into account, are discussed in the following paragraphs.

FRAGHAZ COMPUTER PROGRAM DESCRIPTION

PURPOSE

The FRAGHAZ Computer Program was developed by the Naval Surface Warfare Center for the Department of Defense Explosives Safety Board (DDESB) to provide a method for predicting the fragment hazards produced by the inadvertent detonation of munitions. The computer program is designed such that it can be easily modified to handle a variety of specific problems like the barricade studies contained in this report.

HAZARD VOLUME

A relatively simple mathematical model is used in the calculation and accumulation of fragment hazard statistics. This hazard volume model is shaped like a narrow piece of pie with the sharp edge fixed to the face of the fragment producing ammunition stack. Down-range is divided into 100 ft sectors such that hazard statistics can be accumulated in 100 ft range increments. The height of the hazard volume is equal to the height of the target, the target in this report being a standing man. The standing man is represented as a three dimensional rectangular parallelepiped randomly located in the hazard volume. Since the hazard volume is shaped like a piece of pie, it diverges as range increases at an angle usually taken as 10 degrees. This 10 deg angle is commensurate with the 10 deg sectors used with actual fragment pickup in full-scale tests of ammunition stacks. This fragment pickup data will be discussed later under FRAGHAZ COMPUTER PROGRAM VALIDATION.

STACK FRAGMENTATION CHARACTERISTICS

The FRAGHAZ Computer Program uses actual fragmentation data from small-scale arena tests which can be scaled up to represent large ammunition stacks. The small-scale tests may consist of one or more pallets of a specific munition. When the individual munitions of a pallet are detonated simultaneously, or nearly so, jets are produced between adjacent munitions. For the FRAGHAZ program these jets are called interaction areas. These interaction areas contain the high

density and high velocity fragmentation which is used for safety purposes to calculate down-range fragmentation hazards. The fragment characteristics necessary to calculate individual trajectories for each fragment recovered in specified polar and azimuthal angle limits are obtained from the small-scale arena tests. For a pallet of Mk 82 bombs there are 260 fragments greater than 300 grains that define the fragmentation characteristics of a single interaction area. Fragments that weigh less than 300 grains do not go to far-field ranges and, even at the short ranges, they seldom possess the kinetic energy at impact to meet the threshold hazard kinetic energy criterion of the DDESB (58 ft-lbs).

FRAGMENT TRAJECTORIES

For each fragment recovered in the small-scale arena test, a complete trajectory is calculated using a fourth order Runge-Kutta procedure. As such, the velocity, displacement and trajectory angle in three dimensions can be calculated at any point along the trajectory. In practice we are mostly concerned with the portion(s) of the trajectory that lie within the Hazard Volume. It is only then that the fragment may impact the target. Since we know the complete dynamics of the fragment we can calculate hazard statistics such as hazard density and hazard probability of hit.

There are two types of trajectories considered: normal and ricochet. The normal trajectories have only one ground impact while the ricochet trajectories have two or more ground impacts. The ricochet equations are based on tests conducted by the Ballistic Research Laboratories in the late 1960s.²

Wind can be included in the trajectory calculations. For a tailwind, the added range due to wind is approximately equal to the time of flight times the wind speed. Since time of flight varies up to about 30 seconds, a tailwind of 60 ft/sec (41 MPH) can extend the range by about 1800 ft.

The fact that a separate and complete trajectory is calculated for each fragment permits the FRAGHAZ Computer Program to be used for a large variety of specific problems like the barricade studies contained herein. The program has also been used to determine hazards to vehicles on public traffic routes and hazards to ammunition stacks from fragments.

MONTE CARLO PROCEDURE

A Monte Carlo procedure is any mathematical technique which uses random numbers to simulate the uncertainty associated with one or more random variables affecting the outcome of the calculations. In FRAGHAZ there are seven random variables affecting the hazard calculations:

- Initial fragment elevation angle
- Initial fragment velocity
- Fragment drag coefficient curve³
- Height of fragment trajectory origin above the ground surface
- Soil constant for ricochet
- Wind speed
- Altitude of the ammunition stack site

In the Monte Carlo procedure, each replication represents one simulation of a full-scale test. For example the trajectories of the 260 fragments used to represent Mk 82 bomb pallets would constitute one replication. Each random variable associated with the fragments would have

a known or assumed range of uncertainty. Random numbers are then used to designate a particular value for each random variable. Any of the random variables may be set to a constant in FRAGHAZ. Trajectories would be calculated for each of the 260 fragments with an effective number of fragments associated with each trajectory commensurate with the number of munitions or interaction areas in the specific stack under consideration. Hazardous intersections with the target would be recorded and accumulated in the program for each 100 ft sector of the Hazard Volume. This would constitute one replication. Because of the uncertainty in the random variables, this would constitute only one possible outcome for the stack being considered. As a result, a second replication would be conducted with the 260 fragments using a new set of random numbers to define new values for the random variables. New outcomes for the 100 ft sectors of the Hazard Volume would be obtained and recorded. This procedure would continue for the number of replications selected, 60 for the data in this report. When all the replications are completed we are then in a position to calculate statistics, such as averages, for such measures of effectiveness as Hazard Density for each 100 ft range increment of the Hazard Volume.

For this report percentiles are important. In our example, we would have 60 distinct hazard densities for each 100 ft range increment. For each 100 ft range increment, we can sort the 60 values in ascending order from minimum to maximum. When sorted, the 54th highest value would be the 90th percentile value because only 6 values (ten percent of the total) would be equal to or greater than the 54th value. The 100th percentile would then coincide with the largest sorted value. We may interpret the percentile level as follows. If we are talking about a 90th percentile value, we may say that only 10 percent of the time should we expect the value to be greater than the 90th percentile value and we should not expect the value to be greater than the 100th percentile value.

HAZARD CRITERIA

In order to distinguish hazardous from non-hazardous fragments, hazard criteria must be specified beforehand. The following criteria represent the current specifications of the Department of Defense Explosives Safety Board (DDESB).

Kinetic Energy

A hazardous fragment is one that has at least 58 ft-lbs of kinetic energy when it strikes a personnel target. The DDESB is currently reviewing a criterion submitted by the Army which depends not only on mass and velocity but on the average presented area of the fragment on impact. This criterion, Continuous Probability of Injury Criterion (CPIC), which depends on skin penetration has a great deal of experimental data to support it. Some recent studies, however, indicate that the two criteria produce roughly the same results.

Hazard Density

Densities equal to or greater than one fragment per 600 ft² are considered hazardous provided all the fragments involved are hazardous in terms of the kinetic energy criterion given above. This density is predicated on a standing man having a frontal presented area of 6 ft². As such it is roughly equivalent to a probability of hazard hit of .01.

Other

Both wind and percentile level affect hazard density statistics. Currently the DDESB specifies zero wind and a 90th percentile levels for safety studies.

PROGRAM OUTPUT

The FRAGHAZ Computer Program has three basic outputs: Number of Final Ground Impacts versus Range, Hazard Density and Probability of Hit versus Range, and Number of Units Required to exceed the Density and Probability of Hit Hazard Criteria versus Range.

Number of Final Ground Impacts Versus Range

If we have 60 replications of 260 fragments then we will obtain 60 distinct distributions of final ground impacts versus range. This data can be sorted and, from it, we can obtain minimum, maximum, and average number of final ground impacts for each 100 ft increment of range. This data can be used to demonstrate the validity of the program as explained below under the FRAGHAZ COMPUTER PROGRAM VALIDATION heading.

Hazard Density and Probability of Hit

Hazard density is obtained by projecting the particular three dimensional 100 ft hazard sector, intersected by the fragment trajectory, into the plane perpendicular to the trajectory at the point of target impact. This can be done since we know the trajectory angle at all times. The projected target area is not calculated but is assumed to be a constant 6 ft² for a personnel target. The hazard density is then the number of hazard fragments associated with the particular trajectory divided by the projected area of the 100 ft hazard sector in the plane perpendicular to the fragment trajectory.

For probability of a hazardous hit, we use the hazard density calculated above and the presented area of the target in the plane perpendicular to the fragment trajectory. These two values are then used, with an appropriate equation, to calculate hazard probability of hit for the personnel target.

Since target presented area is not used in the calculation of hazard density, using the hazard density criterion will make the results look more hazardous than those calculated using a consistent probability of hazard hit criterion. This occurs because the hazard density criterion of one fragment per 600 ft² assumes the maximum presented area of a personnel target, 6 ft², which approximates a probability of hit of 0.01. With a probability of hit criterion, the presented area of the personnel target is taken into account and will almost always be less than 6 ft². In fact, it can be as low as 0.55 ft² when the fragment comes straight down on a standing man. As such, with a hazard density of 1/600, the probability of hit will almost always be less than 0.01.

Number of Units To Exceed the Hazard Criterion

Using the hazard density and probability of hit discussed above, the program can then be

used to calculate the number of units or interaction areas required to just exceed the hazard density criterion (1/600) or the hazard probability of hit criterion (.01).

FRAGHAZ COMPUTER PROGRAM VALIDATION

There is always a question with computer programs whether the predicted results obtained with the program actually match the results obtained with experimental tests. Two tests have been conducted, one with 36 pallets (288 rounds) of 155mm projectiles, and another with 1 pallet (6 bombs) of Mk 82 Bombs. After the explosion in each case, personnel were sent down-range to pick up all fragments greater than 300 grains. The terrain was marked off in 10 deg azimuthal sectors and these sectors, in turn, were marked off into 200 to 400 ft range increments. In this way each fragment could be identified with a particular azimuth sector and a range zone in the azimuth sector.

As mentioned above, the FRAGHAZ Computer Program can output the number of final fragment impacts as a function of 100 ft range increments for a particular azimuth sector. Since we had only one test for 155mm projectiles and six for Mk 82 bombs, we can not say whether the results per range increment were maximum or minimum values or some point in between. Since each replication of FRAGHAZ represents the results of an entire stack, and we run many replications (usually 60), we can obtain the minimum and maximum results expected in the actual tests. We therefore ask that the actual test results fall between the minimum and maximum values predicted by the FRAGHAZ Computer Program. In both cases there was good agreement between the predicted and actual test results.

SUMMARY

The FRAGHAZ Computer Program provides a flexible tool for predicting the fragment hazards of stacks of ammunition. The program has the inherent capability of considering the multidimensional problem posed by fragment hazards. The program is moderately large having about 1000 lines of code and over 200 variables, about 25 of which are prime variables directly affecting hazard values. Its modular characteristics make it relatively easy to modify for specific problems like the barricades considered herein. The essential characteristics of the program are summarized as follows:

- Individual three dimensional trajectories
- Two dimensional wind vectors (horizontal plane)
- Fourth Order Runge-Kutta trajectory calculations
- Fragment ricochet included for various soil types
- Incorporates three dimensional targets
- Can use different hazard criteria
- Air density and sound speed a function of altitude
- Storage sites may be at different altitudes
- Fragment drag coefficient a function of Mach Number and based on wind tunnel tests
- Predicts distribution of final fragment impacts in ground plane
- Predicts hazard density and hazard probability of hit as a function of range for different hazard levels such as minimum, maximum, average and specified

percentiles

- Predicts hazard distance values for different hazard levels (minimum, maximum, average and specified percentiles) as a function of number of units or interaction areas required to just exceed each of the two hazard criteria, density and probability of hit

PART I - GENERAL BARRICADE INVESTIGATION

PREFACE

This study was requested by the Department of Defense Explosives Safety Board (DDESB). The DDESB wanted to know if the FRAGHAZ Computer Program could be used to assist in the design and evaluation of barricades intended for use in stopping fragmentation produced by ammunition stacks. In the past, barricade studies were mostly qualitative and based on the long experience of investigators in general fragmentation characteristics.

A related purpose of the study was to demonstrate that meaningful measures of effectiveness could be produced by the FRAGHAZ program to assist in the design and evaluation of barricades. The FRAGHAZ Computer Program was modified to include the geometry and variables associated with the barricade defined below.

CONDITIONS

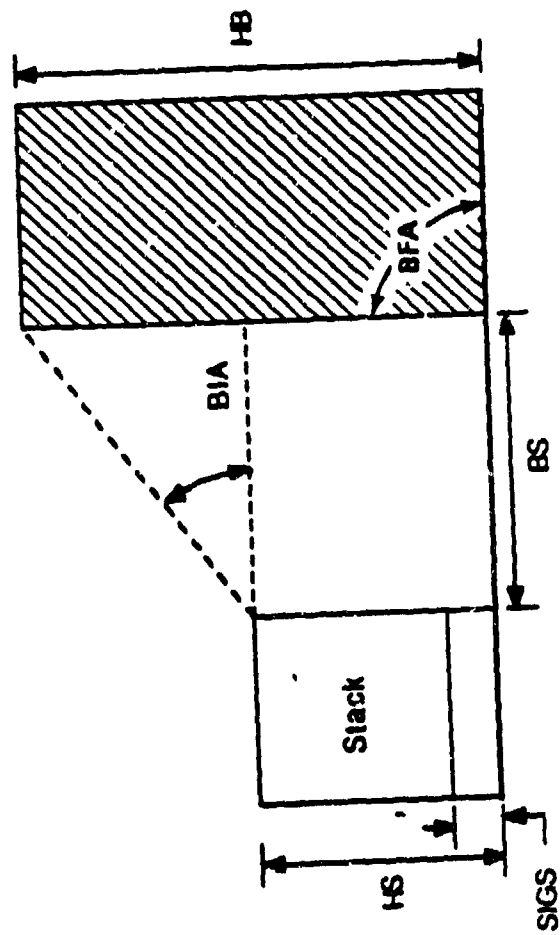
Barricade Model

The barricade model is shown in Figure 1. In keeping with the general nature of the study, the barricade used was a simple box type. The walls of the box barricade could be planks, the inside of which could be filled with dirt. The variables addressed in the study are also shown in Figure 1. The Stack Inert Ground Standoff is just the height of the pallet on which the munitions rest. The Barricade Face Angle determines the slope of the front face of the barricade. For this general study the front face of the barricade was vertical and the Barricade Face Angle was 90 degrees. All fragments which strike the barricade face, or the ground between stack and barricade, are considered stopped in the 0 to 100 ft range increment of the FRAGHAZ Hazard Volume. The Barricade Face Angle is too large to permit ricochet and, therefore, ricochet off the barricade was ignored. Under instruction of the DDESB, the complete or partial destruction of the barricade by the explosion of the munitions was not considered.

Munitions Selection

The two munitions selected were those for which there are fragmentation data appropriate to the FRAGHAZ Computer Program. These munitions were the Mk 82 bomb and the M107 155mm projectile. Of all the fragmentation data available, these two munitions are the most hazardous. Additionally, the Mk 82 bombs are stored horizontally while the 155mm projectiles are stored vertically. The fragmentation data available reflects this difference in storage attitude. Both sets of fragmentation data are for mass detonating munitions (Class 1, Division 1). For both munitions, only one pallet was used. For both munitions, the pallet height is approximately 2.5 ft including the pallet. As such, the barricade height is determined by this height and the values of Barricade Intercept Angle and Barricade Standoff as shown in Figure 1.

FIGURE 1
BOX BARRICADE



HS - Height of Stack
 SIGS - Stack Inert Ground Standoff
 BS - Barricade Standoff
 BIA - Barricade Intercept Angle
 BFA - Barricade Face Angle (90 deg)
 HB - Height of Barricade

Hazard Criteria

Throughout this study, the target was a standing man. The Continuous Probability of Injury Criterion (CPIC) was used. This criterion depends on skin penetration and was provided by the Ballistic Research Laboratories at Aberdeen, Maryland. It is currently under review by the DDESB. Unlike the 58 ft-lbs criterion, with the CPIC criterion all fragments are hazardous to some finite level of probability and, therefore, the maximum range and the maximum hazard range will be the same. This is an advantage for the measures of effectiveness selected as described below.

The current DDESB Hazard Density Criterion of at least one hazardous fragment per 600 ft² is used. In addition zero wind is used along with 90th percentile levels.

Measures of Effectiveness

The two measures of effectiveness and associated criteria used are described below:

- The first was maximum hazard range. Since we are using the CPIC Injury Criterion, all fragments are hazardous and the maximum fragment range coincides with the maximum hazard range. This is unlike the case with the 58 ft-lbs Injury Criterion where the fragment going to maximum range may have a kinetic energy less than 58 ft-lbs and therefore would not be considered hazardous by the program. As such, maximum range and maximum hazard range could be different.
- The second measure of effectiveness is Hazard Density. This is the measure currently specified by the DDESB. For a 100 ft range increment to be hazardous, the density must be at least one fragment per 600 ft² ($1/600 = 0.001667$) and all fragments making up the density must be hazardous. Since we are using the CPIC Injury Criterion, all fragments are hazardous to a finite probability and this probability is used in calculating the reduced, or effective, Hazard Density.
- The two measures of effectiveness were calculated using zero wind and 90th percentile levels. The barricade standoff (BS in Figure 1) was held constant at 4 ft, the practical minimum specified by the DDESB. Hazards will tend to increase as BS increases.

Monte Carlo Running Option

The Monte Carlo option was used in all cases. All runs contained 60 replications. The same seed (one for each munition) was used such that the same fragment trajectories were used for each Barricade Intercept Angle. In this way, the dispersion in results with different seeds was eliminated and only the effects of different Barricade Intercept Angles are seen.

Stack Top Fragmentation

Because of the physical dimensions of the munition pallets, a part of the fragmentation from the top of the stacks was included in the arena test recovery. The exact amount of the fragmentation from the stack tops, however, is unknown. For this initial study, it is not of much

consequence since the elevation angles involved would be greater than 70 degrees. In PART II, however, where stacks may be 6 pallets deep, stack top fragmentation must be taken into account.

RESULTS

Maximum Hazard Range

The Maximum Hazard Range as a function of Barricade Intercept Angle is shown in Figures 2 and 3 for 155mm Projectiles and Mk 82 Bombs respectively. The data on these two figures represent the 90th percentile level. Maximum Hazard Ranges for the no barricade condition are also shown for reference. Barricade heights are also shown for corresponding Barricade Intercept Angles given a stack height of 2.5 ft. If the stack height were increased, say to 3 pallets high or 7.5 ft, then the barricade heights would increase 5 ft for the given Barricade Intercept Angles.

The figures show a slow and steady decline in Maximum Hazard Range for increasing Barricade Intercept Angle. There are no abrupt changes except at zero deg Barricade Intercept Angle where we experience drops from the no barricade conditions. At these conditions, the barricade height is 2.5 ft and blocks the long range fragments. In actuality, the two curves will meet to the left of the ordinate at a Barricade Intercept Angle of about -32 degrees. Negative angles were not considered because of the need to take ricochet into account from the top of the barricade.

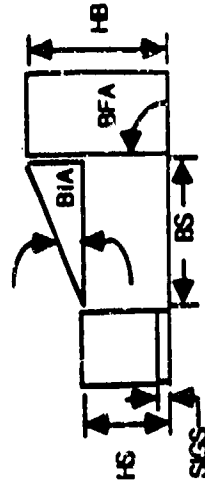
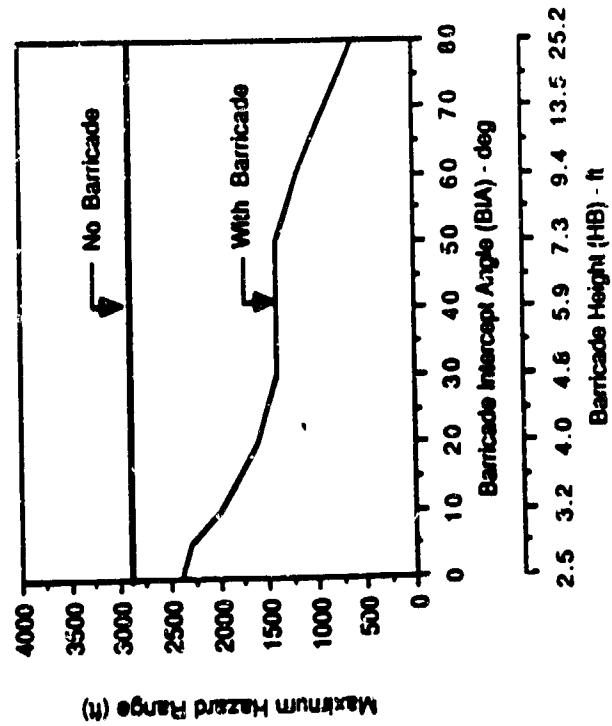
Note in Figures 2 and 3 that a small Barricade Intercept Angle (like the 2 degrees in DoD 6055.9 - STD) does not produce a drastic reduction in Maximum Hazard Range as might have been expected. The drops, however, are significant, about 500 ft for the 155mm projectiles and 950 ft for the Mk 82 bombs.

Table 1 gives Maximum Hazard Ranges for the 50th, 90th and 100th percentile levels.

TABLE 1
MAXIMUM HAZARD RANGE (ft) FOR BOX BARRICADES *

MUNITION	155mm PROJECTILE			Mk 82 BOMB			BARRICADE HEIGHT (FEET)
PERCENTILE	50	90	100	50	90	100	
NO BARRICADE	2300	2900	3200	2000	3300	3500	0
BIA = 0°	1900	2400	2400	1900	2400	2400	2.5
5°	1500	2300	2400	1900	2400	2400	2.9
10°	1400	2000	2400	1800	2300	2400	3.2
20°	1300	1600	2400	1700	2000	2400	4.0
30°	1200	1400	1600	1500	1800	2000	4.8
40°	1200	1400	1600	1200	1700	1800	5.9
50°	1100	1400	1600	1100	1300	1700	7.3
60°	900	1200	1500	900	1200	1400	9.4
70°	700	900	1000	700	800	1000	13.5
80°	400	600	600	300	300	400	25.2

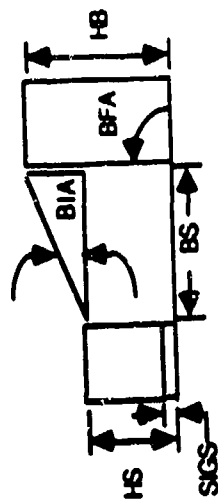
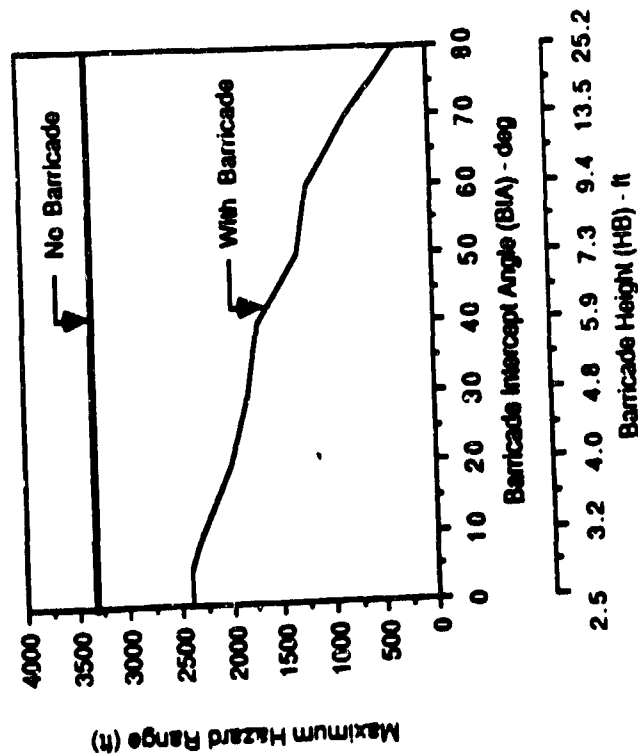
FIGURE 2
BARRICADE EFFECTIVENESS
M107 PROJECTILES (155mm)
MASS DETONATION (CLASS 1, DIVISION 1)
VERTICAL STORAGE



Height of Stack (HS) = 2.5 ft
 Stack Inert Ground Standoff (SGS) = 0.5 ft
 Barricade Standoff (BS) = 4.0 ft
 Barricade Face Angle (BFA) = 90 deg

Target: Standing Man
 Monte Carlo Option
 Replications = 60
 Seed = 8271
 Sea Level
 No Wind
 Continuous Probability of Injury Criterion
 90th Percentile

FIGURE 3
BARRICADE EFFECTIVENESS
MK 82 LOW DRAG BOMBS (500 lb)
MASS DETONATION (CLASS I, DIVISION 1)
HORIZONTAL STORAGE



Height of Slack (HS) = 2.5 ft
 Slack Inert Ground Standoff (SIGS) = 0.5 ft
 Barricade Standoff (BS) = 4.0 ft
 Barricade Face Angle (BFA) = 90 deg

Target: Standing Man
 Monte Carlo Option
 Replications = 60
 Seed = 17351
 Sea Level
 No Wind
 Continuous Probability of Injury Criterion
 90th Percentile

* Conditions for both munitions:

Height of stack = 2.5 ft
 Stack inert ground standoff = 0.5 feet
 Barricade standoff = 4.0 ft
 Barricade face angle = 90 degrees
 Barricade intercept angle = 0 - 80 degrees

Maximum Hazard Range provides a simple and efficient measure of barricade effectiveness. It does not depend on the number of munition in the stack as Hazard Density does.

Hazard Density

Hazard Density as a function of range and Barricade Intercept Angle is shown in Figures 4 and 5 for 155mm Projectiles and Mk 82 Bombs respectively. Again, the data in these figures represent 90th percentile levels. The current DDESB Density Criterion (1 frag / 600 ft²) is given on the figures for reference. Hazard Density depends on the number of munitions or interaction areas on the face of the stack toward the target area. The data shown on Figures 4 and 5 are for one interaction area. If Hazard Densities for more than one interaction area are desired, the values given in Figures 4 and 5 can be multiplied by the number of interaction areas in question. For example, in Figure 5 the Hazard Density at a range of 2000 ft and a Barricade Intercept Angle (BIA) of 0 degrees is approximately 0.00001. If a stack had 50 interaction areas on the face of the stack toward the target area, then the Hazard Density would be 0.0005 at a range of 2000 ft and a BIA of 0 degrees. If we wished to know how many interaction areas on the face of the stack toward the target area would result in a hazard density just greater than the DDESB criterion of 1 frag per 600 ft² (0.001667), we would divide the hazard criterion by the Hazard Density for one interaction area. For the case stated of a BIA of 0 degrees at a range of 2000 ft, this would be (0.001667 / 0.00001) or 167 when rounded up to the nearest whole number. Without the barricade, this number would be reduced to about (0.001667 / 0.00003) or 56 interaction areas which we might say is about three times more hazardous.

Hazard Density might be more properly called Injury Density when using the Continuous Probability of Injury Criterion (CPIC). The Hazard Density Criterion (1/600) is used to approximate the probability of hit criterion. The Hazard Density is defined as follows:

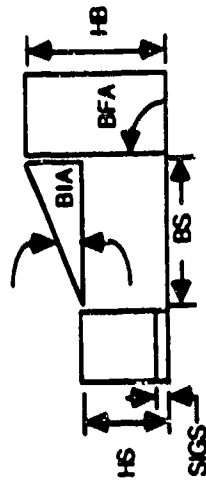
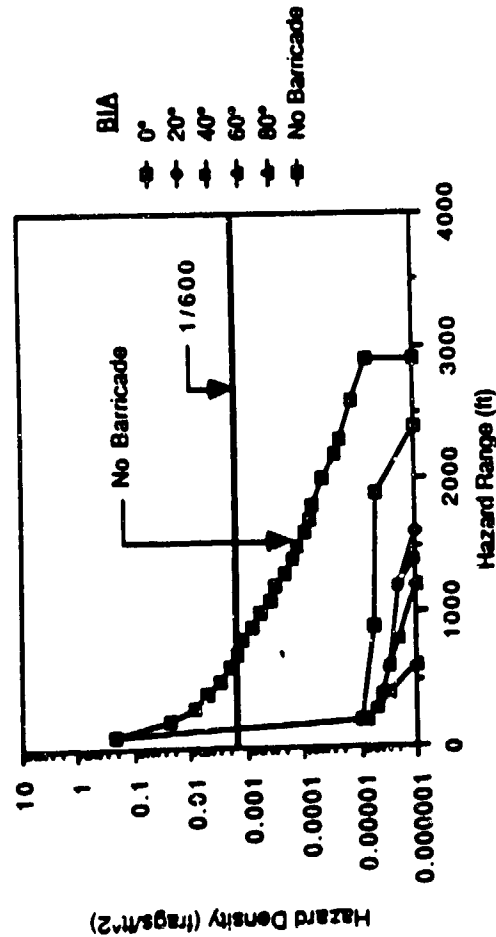
$$\text{Hazard Density} = (\text{NF} / \text{AT}) * \text{P} (\text{INJ} / \text{HIT})$$

where

NF	=	Number of hazardous fragments
AT	=	Presented area of the hazard volume of a 100 ft range segment in the plane perpendicular to the fragment trajectory
P (INJ / HIT)	=	Conditional probability of injury given a hit
*	=	Multiplication

With the 58 ft-lbs injury criterion, the probability of injury is either zero or one as the impacting fragment has less than 58 ft-lbs or at least 58 ft-lbs of kinetic energy respectively.

FIGURE 4
BARRICADE EFFECTIVENESS
M107 PROJECTILES (155mm)
MASS DETONATION (CLASS 1, DIVISION 1)
VERTICAL STORAGE

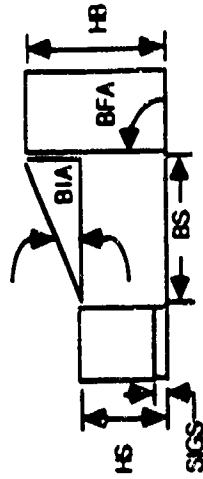
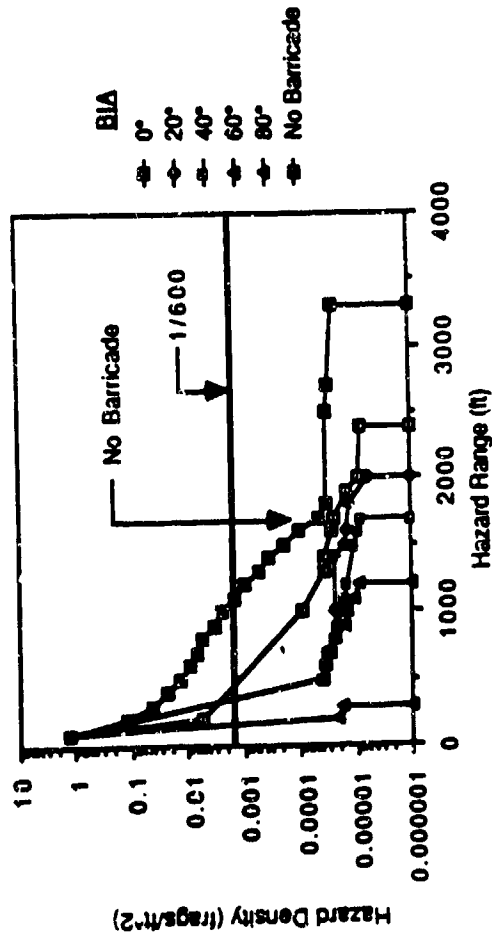


Height of Stack (HS) = 2.5 ft
 Slack Inert Ground Standoff (SIGS) = 0.5 ft
 Barricade Standoff (BS) = 4.0 ft
 Barricade Face Angle (BFA) = 90 deg
 Barricade Height (See Figure 2)
 Barricade Intercept Angle (BIA) = 0° - 80°

Target: Standing Man
 Monte Carlo Option
 Replications = 60
 Seed = 8271
 Sea Level
 No Wind
 Continuous Probability of Injury Criterion
 90th Percentile

One Interaction Area

FIGURE 5
BARRICADE EFFECTIVENESS
MK 82 LOW DRAG BOMBS (500 lb)
MASS DETONATION (CLASS I, DIVISION I)
HORIZONTAL STORAGE



Height of Stack (HS) = 2.5 ft
 Stack Inert Ground Standoff (SGS) = 0.5 ft
 Barricade Standoff (BS) = 4.0 ft
 Barricade Face Angle (BFA) = 90 deg
 Barricade Height (See Figure 4)
 Barricade Intercept Angle (BIA) = 0° - 80°

Target: Standing Man
 Monte Carlo Option
 Replications = 60
 Seed = 17351

Sea Level

No Wind

Continuous Probability of Injury Criterion
 90th Percentile

One Interaction Area

CONCLUSIONS

- The FRAGHAZ Computer Program can be adapted to evaluate the design and effectiveness of barricades.
- More complex barricade designs and effects of ricochet can be considered by the FRAGHAZ Computer Program.
- The FRAGHAZ Computer Program can be used to determine shapes and dimensions for barricades to meet specific design criteria. For example, it might be desirable to design a barricade to limit down-range hazardous fragments to the hazard blast radius for a specific ammunition stack.

PART II - SPECIFIC HILLSIDE BARRICADE INVESTIGATION

PREFACE

The investigation contained herein was conducted in response to a request made by the Air Force. The letter containing the request is reproduced in Appendix C. Correspondence subsequent to the request provided details on the site necessary to conduct the investigation. The site is located at Taegu Air Base in Korea.

The Air Force requested that the clear zone for fragments about a storage shed be reduced from 1250 ft to something nearer 800 ft because of a natural hill barricade surrounding the shed on three sides. Although the shed is used for handling a variety of munitions, it has been stated that six Mk 82 Bomb pallets (36 bombs) would be taken as the source of the maximum hazard for the investigation.

The FRAGHAZ Computer Program was modified to include the site geometry and munition fragmentation characteristics of Mk 82 Bomb pallets. The Mk 82 Bomb weighs 500 pounds.

CONDITIONS

Stack Configurations

Six stack configurations were used as shown in Figure 6. They were selected to provide minimum and maximum fragmentation hazards for both side and top interaction areas. Configurations 1 and 5 provide maximum and minimum hazards for side interaction areas respectively. Configurations 3 and 5 provide minimum and maximum hazards for top interaction areas respectively. The remaining configurations provide intermediate hazards which give information on transition from minimum to maximum hazards.

Information from the Air Force stated that a maximum of six Mk 82 Bomb pallets (36 bombs) could be stored in the shed (Building 230) at Taegu Air Base in Korea. The six configurations shown in Figure 6 represent rectangular parallelepiped stacking of the 6 pallets. Configurations where the number of pallets would differ in different tiers were not considered since they would only involve intermediate hazard conditions between the six configurations selected.

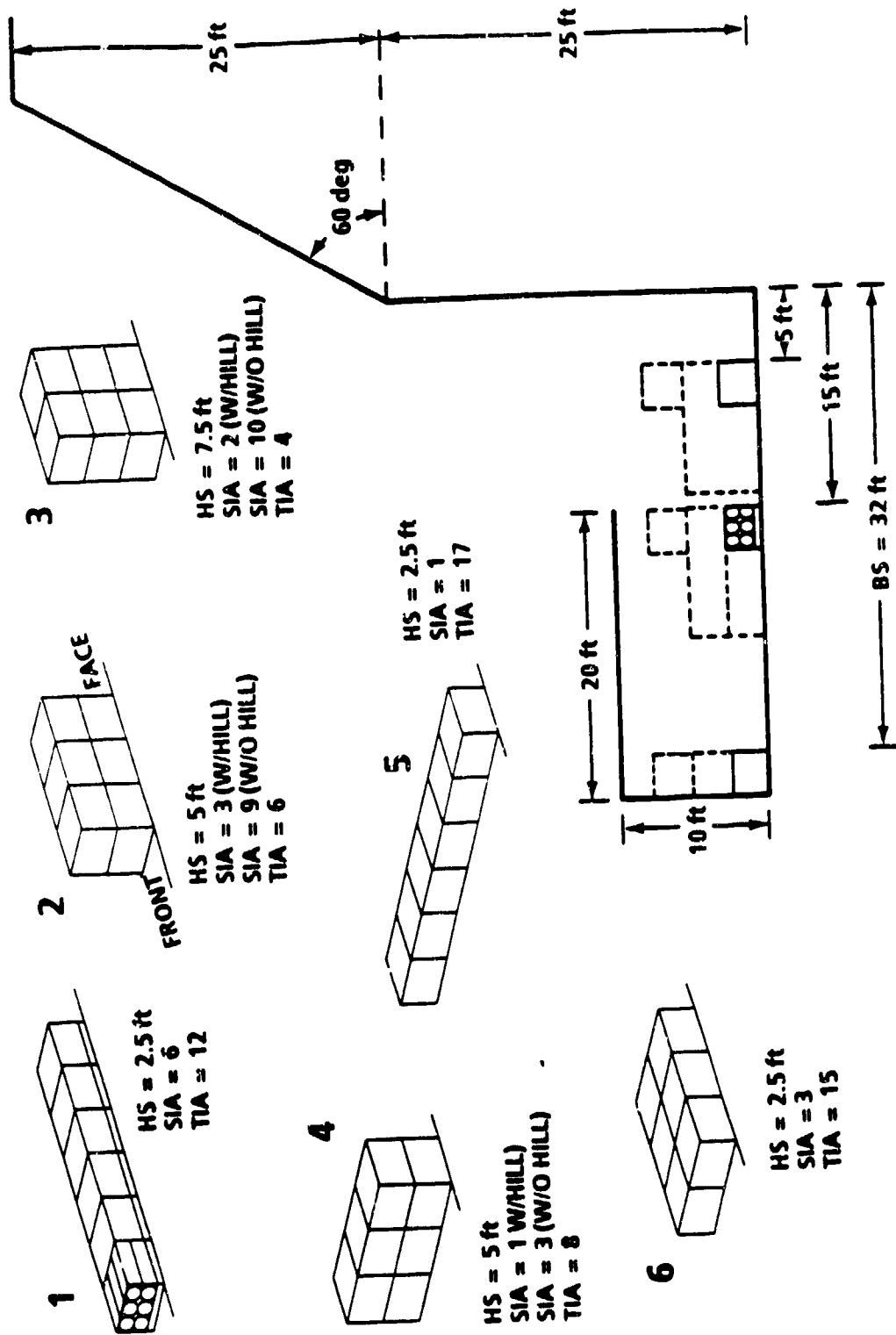
Since the height of the shed is about 10 ft, the maximum height of any stack was taken to be 7.5 ft; that is, 3 pallets high. The height of an individual pallet is about 2.5 ft.

The abbreviations associated with each stack configuration in Figure 6 are explained as follows:

HS = Height of stack.

SIA = Number of side interaction areas used in the calculation of Hazard Densities. With the hill barricade (w/hill), only the interaction areas of the top layer of the pallets are used. The fragmentation from the interaction

FIGURE 6
STACK CONFIGURATIONS
KOREAN HILLSIDE BARRICADE: TAEQU; BUILDING 230
6 PALLETES MK 82: 6 BOMBS PER PALLET



areas of lower layers will be stopped by the hillside barricade. The top layer includes not only the interaction area fragments from the bomb case zone A-B-C in Figure 7 but also fragmentation from the zone C-D. Without the hill (w/o hill), all interaction areas on the face of the stack, including those formed by adjacent pallets, are pertinent to the calculations. When pallets are stacked on top of one another, an additional interaction area is formed between pallets.

TIA = Number of interaction areas on the top of the stack including those formed by adjacent pallets. When pallets are positioned next to one another with long bomb axis to long bomb axis, then an additional interaction area is formed between pallets. If the pallets are positioned bomb base to bomb base, nose to nose, or nose to base then no additional interaction areas are formed.

The effects of blast pressures from any of the stacks were not considered in the hazard calculations.

Site Configuration

The essentials of the site configuration used for hazard calculations are shown in Figure 6. The hillside barricade consists of two legs, one vertical and one angled back at 60 degrees. Fragment ricochet was considered on the leg angled back at 60 degrees. A soil constant of 1.1 was used which is appropriate for cohesive soils supporting vegetative growth.

The effects of the shed structure on fragment trajectories were not considered. The effects are considered minor. Ignoring shed effects might even tend to err against the side of safety since the shed structure could be the source of additional fragments, although such fragments would probably have poor aerodynamic characteristics.

The site altitude used in the hazard calculations was 150 ft above sea level. Even if this altitude is off by a few hundred ft, the effects on the overall calculations would be negligible.

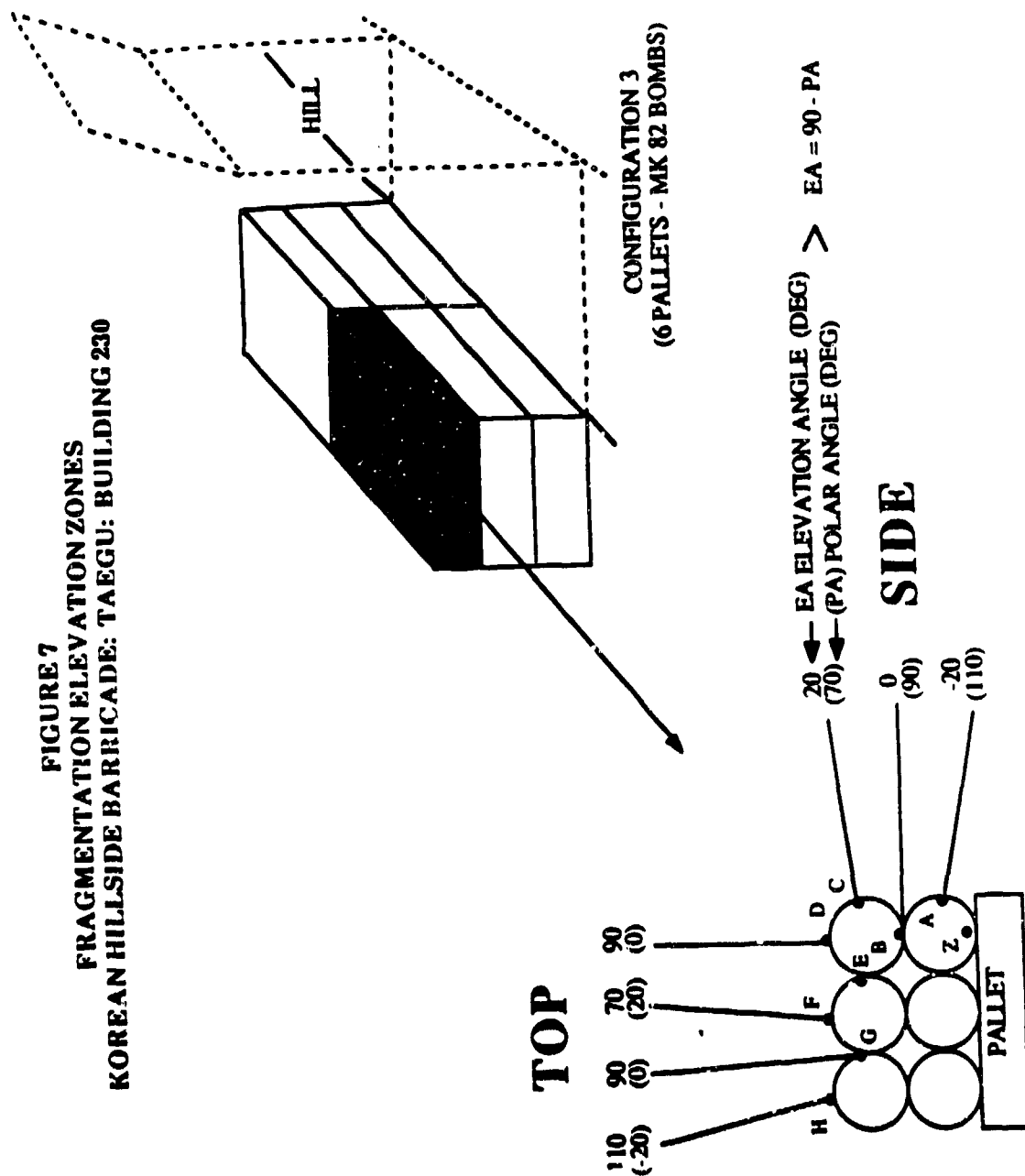
Three distances for positioning the stacks relative to the hillside were used. A barricade standoff (BS) of 32 ft as shown in Figure 6 corresponds to a stack position at the back of the shed. A BS of 15 ft is for a stack position at the front of the shed. The barricade standoff of 5 ft was used to determine whether a significant reduction in fragment hazards could be obtained that might justify a change in storage location.

Hazard Criteria

The target for this investigation was a standing man. The 58 ft-lbs Injury Criterion, currently specified by the DDESB, was used to distinguish hazardous from non-hazardous fragments. The Continuous Probability of Injury Criterion (CPIC) was used for comparison purposes. CPIC was provided by the Army and is currently under review by the DDESB.

A Hazard Density of one hazardous fragment per 600 ft², currently specified by the DDESB, was used as the limit above which Hazard Density is considered unacceptable for safety purposes by the DDESB.

FIGURE 7
FRAGMENTATION ELEVATION ZONES
KOREAN HILLSIDE BARRICADE: TAEGU: BUILDING 230



Zero wind and the 90th percentile level were also used as standard conditions for safety analysis as currently specified by the DDESB.

Side and Top Fragmentation

The zones for side and top fragmentation are shown in Figure 7. Side fragmentation comes from the bomb case portion labelled Z-A-B-C-D. The side interaction area is taken to come from A-B-C where the fragment densities and velocities are highest. In the arena test from which the fragmentation characteristics used in this investigation were taken, the pallet of Mk 82 Bombs was positioned so as to recover the fragmentation from the side area. At the time, it was assumed that all fragmentation going down-range came from the face of the stack toward the target area. Reviewing the arena test data, however, showed that fragments with interaction area velocities were recovered between polar angles 10 and 30 degrees. These fragments must almost certainly come from the top interaction area zone D-E-F. Whether some of this fragmentation might also have come from top interaction area zone F-G-H is unknown. Because of this uncertainty and for the sake of safety, the side and top fragmentation were taken to be exclusive of one another. That is, the fragmentation recovered in the arena test was taken to come from the bomb case zone Z-A-B-C-D only. Adopting such a procedure may result in some double counting of fragments but any error should tend to be on the side of safety.

The top fragment interaction areas were taken to be similar to the side interaction area A-B-C. In reality, much depends on where the stack is initiated. In the arena test, the middle bomb of the lower tier was the donor bomb making the interaction area A-B-C to be skewed upwards. In practice, the initiation point for a stack will be unknown. As such, we have used an average such that the bomb case zone A-B-C is taken to produce an interaction area between polar angle 70 and 110 degrees (elevation angles plus or minus 20 degrees). This zone then becomes the model for the top interaction areas. Each top interaction area is taken to be independent since we have no test data on the interaction of interaction areas. The arena test was conducted with only one interaction area, A-B-C. However, this same type of independence was used with 155mm projectiles which had six interaction areas in the arena test and good results were obtained.

The top interaction areas were defined by rotating the side interaction area, A-B-C, 90 degrees such that elevation angle -20 degrees became elevation angle 70, and elevation angle 20 degrees became elevation angle 110. The top interaction areas have a spread of 40 degrees like the side interaction area. When making such a 90 deg rotation, account must be taken of a diminished number of fragments which are applicable to the 10 deg Hazard Volume. When recovering fragments in the arena, the vertical extent of the recovery packs at any elevation angle between the 10 deg azimuthal limits is approximately:

$$H = 2 * R * \tan(5^\circ) * \text{ABS}(\cos(E))$$

where

H	=	Distance between azimuthal limits
R	=	radius of the arena
E	=	Elevation angle in degrees
*	=	Multiplication

When we rotate toward polar angle 0 (elevation angle 90), the distance between the azimuthal limits decreases, finally becoming zero at polar angle 0 degrees (elevation angle 90). Since only those fragments whose initial trajectories are constrained between the azimuthal limits will end up in the 10 deg Hazard Volume, we must take this into account by diminishing the number of fragments recovered from the polar zone 70 to 110 which we rotate 90 degrees to form top interaction areas. The reduction factors used were 0.25 for the 70 to 110 degree top interaction area elevation zone, and 0.1 for the 80 to 90 top interaction area elevation zone.

In the investigation, the Hazard Densities were calculated independently for the side and top fragmentation and then summed for total Hazard Density. Linear scaling was used for multiple interaction areas; that is, Hazard Densities were calculated for one interaction area and then multiplied by the number of interaction areas for the particular stack configuration to obtain total Hazard Densities.

Wind

The DDESB currently specifies zero wind for safety analysis. Two other wind conditions were used for reference. These were a 30 ft/sec tailwind (20.5 MPH) and 60 ft/sec tailwind (40.9 MPH). A tailwind tending to push the fragments directly down-range is almost always the most hazardous. A 30 ft/sec wind corresponds to fair weather gusting. A 60 ft/sec wind corresponds to gusting associated with electrical storms.

Monte Carlo Running Option

The Monte Carlo option of the FRAGHAZ Computer Program was used in all cases. All runs contained 60 replications. The same seed was used in all cases such that the same fragment trajectories were used for all six stack configurations and the alternate conditions studied. In this way, the dispersion in results with different seeds was eliminated and only the effects of the different stack configurations and alternate conditions were obtained.

RESULTS

The results of this investigation are given in the tables of Appendices A and B. In all cases, the measure of effectiveness is Hazard Density. The ranges given in these tables are the upper bound of the 100 ft sectors of the Hazard Volume; that is, a range of 300 denotes the 200 to 300 ft sector, a range of 1200 ft denotes the 1100 to 1200 ft sector and so forth. The tables of Appendices A and B represent a wide variety of conditions which are intended to lend scope to the investigation and provide a broad basis for evaluating the request made by the Air Force in Appendix C. In order to provide a graphic picture of the results, selected data from the tables of Appendix A and B have been plotted in Figures 8 through 15. These figures show the effect on results caused by changes in hazard criteria and other alternate conditions. When plotting these figures, the Hazard Densities for the 0 to 100 ft sectors have not been plotted. These densities are extremely large since they include the hazards from all the fragments stopped by the hill. A discussion of the results shown in Figures 8 through 15 is given below.

Figure 8: Baseline Hazard Densities

Figure 8 shows three curves, one for each of the three tailwind speeds (0, 30 and 60 ft/sec). The curve for a tailwind speed of 0 ft/sec is the baseline and will be the curve used as a basis of comparison for most of the succeeding curves. The baseline curve is considered the best estimate of Hazard Densities for Stack Configuration Number 3 (the least hazardous configuration given in Tables A-1 through A-9) under the hazard criteria and conditions currently specified by the DDESB as listed in Figure 8. Note that the barricade (hill) standoff is 32 ft which corresponds to the back of the shed. This position causes a slightly higher hazard than the other two standoffs - 15 and 5 ft. All the remaining curves in this figure and in Figures 9 through 15 are for comparison with this baseline curve and to lend scope to the investigation by showing the effects of different hazard criteria and conditions.

The baseline curve is taken from Table A-1, data column 6. The curve for 30 ft/sec tailwind is taken from Table A-4, data column 6. The curve for 60 ft/sec tailwind is taken from Table A-7, data column 6.

Note that the ordinate of Figure 8, and succeeding figures, is graduated with a log scale. Most of us are more accustomed to the usual linear scale graduations and this can be a problem when estimating how many times greater one point is than another. For example, the threshold safety hazard density (one fragment per 600 ft²) shown as a thick horizontal line at Hazard Density 0.001667 appears to be about 1.3 times greater than the baseline Hazard Density at 200 ft range. Actually the baseline Hazard Density at 200 ft range is 0.000449 from Table A-1 and, therefore, the threshold safety hazard density is $(0.001667 / 0.000449)$ or 3.7 times greater. The threshold safety hazard density appears about 2.4 times greater than the baseline Hazard Density at 1400 ft range while actually it is $(0.001667 / 0.000084)$ or 19.8 times greater.

Since we have always tended to err on the side of safety when we encountered uncertainties, the Hazard Densities for the baseline conditions represent a large factor of safety relative to the threshold safety hazard density. We might say from the above calculations that the factor of safety ranges from about 3 to 20 depending upon range. For the approximate safety range of 800 ft, requested in Appendix C, the factor of safety would be about 18.

From Figure 8, we can also see that tailwind speed does not have a very large effect relative to the threshold safety hazard density. The tailwind curves for 30 and 60 ft/sec are still well below the one fragment per 600 ft² (0.001667) threshold.

Figure 9: Minimum and Maximum Hazard Configurations

Figure 9 shows minimum and maximum Hazard Density curves for Stack Configurations 3 and 5 respectively. Actually, there is a crossover at about 1200 ft range due to the fact that Configuration 5 has half as many side interaction areas as Configuration 3 (see discussion on Figure 14 for side and top contributions). The Configuration 3 curve is taken from Figure 8 and Table A-1, data column 6. The Configuration 5 curve is taken from Table A-1, data column 10. Configuration 5, see Figure 6, represents a non-compact stack of 6 pallets and is somewhat analogous to scattering single pallets around the shed floor. Figure 9 indicates the need for arranging the pallets in compact stacks like Configuration 3, especially when hazard ranges of interest are less than about 1000 ft.

Figure 8

Baseline Hazard Densities

Korean Hillside Barricade : TAEGU : Bldg 230
Stack Configuration No. 3

Target - Standing Man : Injury Criterion - Kinetic Energy Threshold = 58 ft-lbs
Monte Carlo Option : Replications 60 : Seed 17351 : Site Altitude 150 ft
Stack Top Vertical Fragmentation Elevation Zone = 70 - 110 Deg
90th Percentile : Stack Barricade (Hill) Standoff = 32 ft

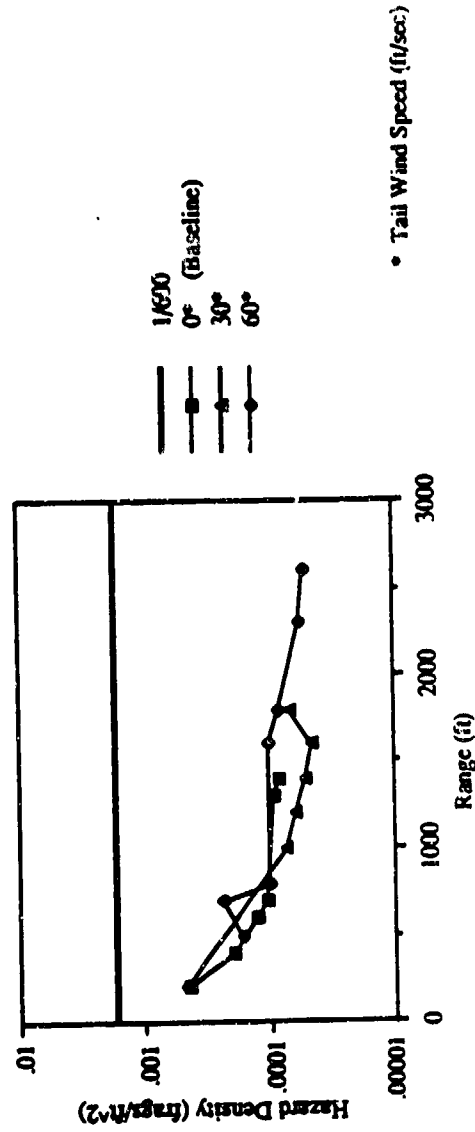


Figure 9

Minimum and Maximum Hazard Configurations

Korean Hillside Barricade : TAEGU : Bldg 230

Target - Standing Man : Injury Criterion - Kinetic Energy Threshold = 58 ft-lbs
 Monte Carlo Option : Replications 60 : Seed 17351 : Site Altitude 150 ft
 Stack Top Vertical Fragmentation Elevation Zone = 70 - 110 Deg
 90th Percentile : Stack Barricade (Hill) Standoff = 32 ft : Zero Wind

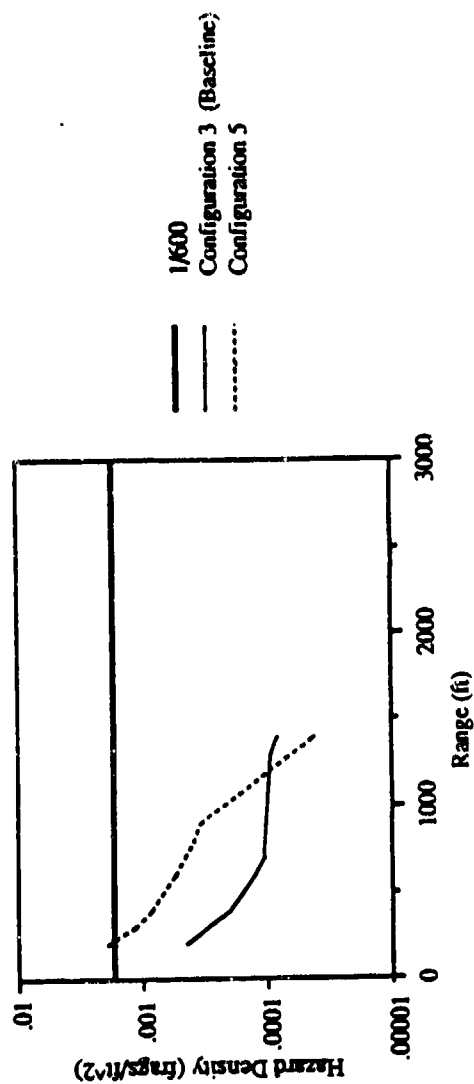


Figure 10: Hazard Densities for 58 ft-lbs and CPIC Injury Criteria

Figure 10 shows the baseline curve (Table A-1, data column 6) and a second curve (Table A-10, data column 6) for the same conditions except that the baseline personnel injury criterion of 58 ft-lbs has been changed to the Continuous Probability of Injury Criterion (CPIC). As shown in Figure 10, the effect of the change is small, both curves being well below the threshold safety hazard density of one hazardous fragment per 600 ft² (0.001667).

Figure 11: 90th Versus 100th Percentile Hazard Densities

Figure 11 shows results with the baseline Configuration 3 stack at two percentile levels, 90 and 100. The baseline curve is taken from Table A-1, data column 6. The 100th percentile curve is taken from Table A-1, data column 5. The 90th percentile curve represents the level of Hazard Densities which we expect to be exceeded only 10 percent of the time. Of that 10 percent of the time, the 100th percentile represents the maximum level expected. The curves are close and well below the threshold safety hazard density of one hazardous fragment per 600 ft² (0.001667).

Figure 12: Hazard Densities With and Without Hill

Figure 12 shows the results with Stack Configuration Number 3 for the case of no hill as opposed to the baseline case with the hill. The baseline data with the hill are taken from Table A-1, data column 6. The data for the case without the hill are taken from Table B-1, data column 2. The case without the hill implies a flat and horizontal plane extending from the stack down-range. The curve for the case of no hill shows Hazard Density exceeding the DDESB limit (one hazardous fragment per 600 ft²) out to about 1400 ft. Configuration Number 3, however, is not the best stack configuration for the case without the hill. Another study would have to be performed to define the stack configuration which would be best for open terrain. The use of Configuration Number 3 is for comparison but probably represents a near maximum hazard for open terrain.

In Appendix C, the Air Force stated that the storage shed is surrounded on three sides by the hill. The fourth is apparently open but blocked to some extent by an undefined barricade. Since Hazard Densities for the fourth side would probably fall between the two curves shown in Figure 12, calculations should be made when the stack-barricade geometry for the fourth side becomes available.

Figure 13: Hazard Densities for 0 and 58 ft-lbs Injury Criteria

Figure 13 shows the effect of an ultra-conservative personnel injury criterion. The baseline curve is taken from Table A-1, data column 6. The 0 ft-lbs injury criterion curve is taken from Table B-3, data column 2. With the 0 ft-lbs injury criterion, every fragment has a probability of injury of 1. Actually, every fragment has a kinetic energy greater than 0 at impact because the impact velocity is always greater than 0. Selecting 0 ft-lbs as the criterion insures that every fragment will be hazardous when we do not know the minimum kinetic energy at impact. This figure is designed to show an extreme point of reference.

Figure 10

Hazard Densities for 58 ft-lbs and CPIC Injury Criteria

Korean Hillside Barricade : TAEGU : Bldg 230
Stack Configuration No. 3

Target - Standing Man

Monte Carlo Option : Replications 60 : Seed 17351 : Site Altitude 150 ft
Stack Top Vertical Fragmentation Elevation Zone = 70 - 110 Deg
90th Percentile : Stack Barricade (Hill) Standoff = 32 ft : Zero Wind

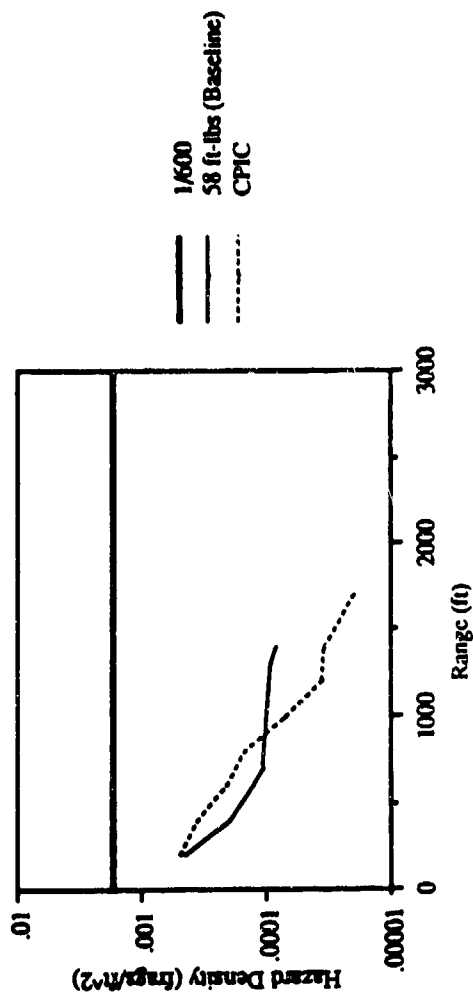


Figure 11

90th versus 100th Percentile Hazard Densities

Korean Hillside Barricade : TAEGU : Bldg 230
Stack Configuration No. 3

Target - Standing Man : Injury Criterion - Kinetic Energy Threshold = 58 ft-lbs
Monte Carlo Option : Replications 60 : Seed 17351 : Site Altitude 150 ft
Stack Top Vertical Fragmentation Elevation Zone = 70 - 110 Deg
Stack Barricade (Hill) Standoff = 32 ft : Zero Wind

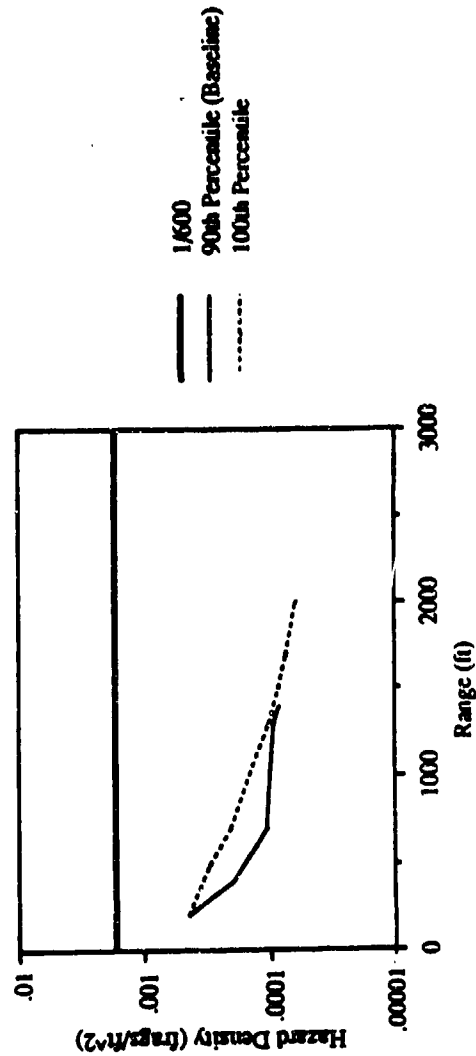


Figure 12

Hazard Densities With and Without Hill

Korean Hillside Barricade : TAEGU : Bldg 230
Stack Configuration No. 3

Target - Standing Man : Injury Criterion - Kinetic Energy Threshold = 58 ft-lbs
Monte Carlo Option : Replications 60 : Seed 17351 : Site Altitude 150 ft
Stack Top Vertical Fragmentation Elevation Zone = 70 - 110 Deg
90th Percentile : Stack Barricade (Hill) Standoff = 32 ft : Zero Wind

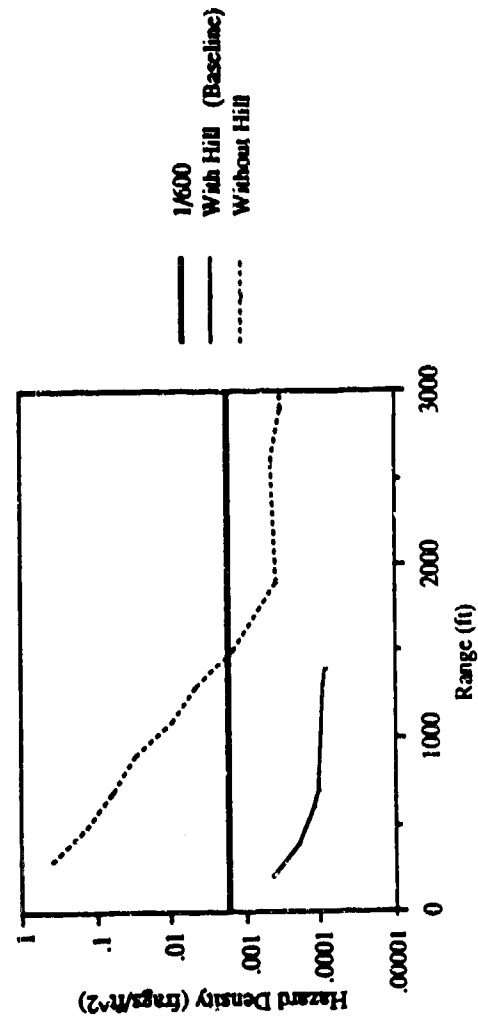


Figure 13

Hazard Densities for 0 and 58 ft-lbs Injury Criteria

Korean Hillside Barricade : TAEGU : Bldg 230
Stack Configuration No. 3

Target - Standing Man

Monte Carlo Option : Replications 60 : Seed 17351 : Site Altitude 150 ft
Stack Top Vertical Fragmentation Elevation Zone = 70 - 110 Deg
90th Percentile : Stack Barricade (Hill) Standoff = 32 ft : Zero Wind

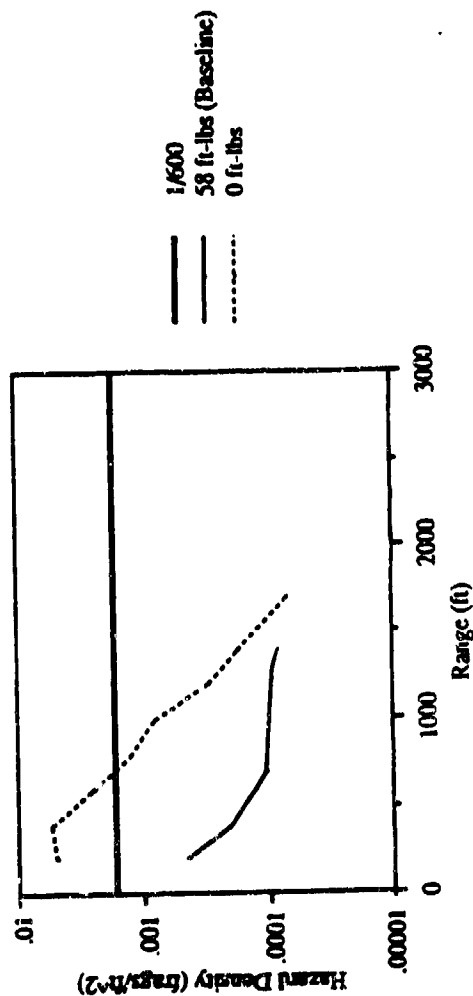


Figure 14: Hazard Density Contributions From Side and Top Fragmentation

The side fragmentation curve is taken from Table B-2, sheet 1, data column 3. The top fragmentation curve is taken from Table B-2, sheet 1, data column 4. It is interesting to note that the two contributions do not overlay in range. These two curves together form the baseline curve but shows a range gap. In the previous figures, the baseline curve showed these two regions connected to make a smooth, continuous curve. The figure shows that the hill is doing an excellent job of blocking the side fragmentation. See Figure 7 for a description of side and top fragmentation.

If the baseline curve had been calculated with the stack positioned at the front of the shed, the contribution from the side fragmentation would be zero beyond 100 ft range (see Table B-5, sheet 1, data column 6). As such, the baseline curve would terminate at 900 ft range, as shown in Table A-2, data column 6.

Figure 15: Hazard Densities For Vertical Fragmentation Elevation Zones 70 - 110 and 80 - 90 Deg

The 70 - 110 degree baseline elevation zone results are taken from Table A-1, data column 6. The 80 - 90 elevation zone results are taken from Table B-4, data column 2. In the fragmentation arena tests, only one interaction area was involved. In deriving the top fragmentation from the side fragmentation we do not know the elevation zone width for two or more interaction areas making up the top fragmentation. The two elevation zone widths shown in Figure 15 are the best estimates of the maximum and minimum zone width. From Figure 15, the selection of the 70 - 110 deg zone width for the baseline configuration should err on the side of safety. The reason that the two curves come together at approximately 1400 ft range is that beyond 900 ft range only the side fragmentation is involved and the total Hazard Density beyond 900 ft is therefore independent of the top fragmentation.

Probability of Hazard Hit

The Hazard Density threshold (one hazardous fragment per 600 ft²) was selected to produce a threshold probability of hazard hit of approximately 0.01 when the presented area of the personnel target was 6 ft². In this investigation with the hill, the angle of fall for all fragments is very steep and the presented area of the standing man is much less than 6 ft²; it is more nearly 1 ft². With the hill and with zero wind, a rough estimate of probability of hazard hit may be obtained by multiplying Hazard Density by 0.65. If a probability of hazard hit criterion were used, the results would have appeared much less hazardous. If, however, we had used a prone man instead of a standing man then the results would have appeared pretty much the same.

Positioning the Stacks

In terms of top fragmentation, there is very little effect due to the positions of the stacks relative to the hill. In terms of side fragmentation, however, there is some effect (see Table B-5). Positioning the stack near the front of the shed (BS = 15 ft) is better than positioning it at the back of the shed (BS = 32 ft). There is little or no advantage in positioning the stack outside the shed nearer to the hill.

Figure 14

Hazard Density Contributions From Side and Top Fragmentation

Korean Hillside Barricade : TAEGU : Bldg 230
Stack Configuration No. 3

Target - Standing Man : Injury Criterion - Kinetic Energy Threshold = 58 ft-lbs
Monte Carlo Option : Replications 60 : Seed 17351 : Site Altitude 150 ft
Stack Top Vertical Fragmentation Elevation Zone = 70 - 110 Deg
90th Percentile : Stack Barricade (Hill) Standoff = 32 ft : Zero Wind

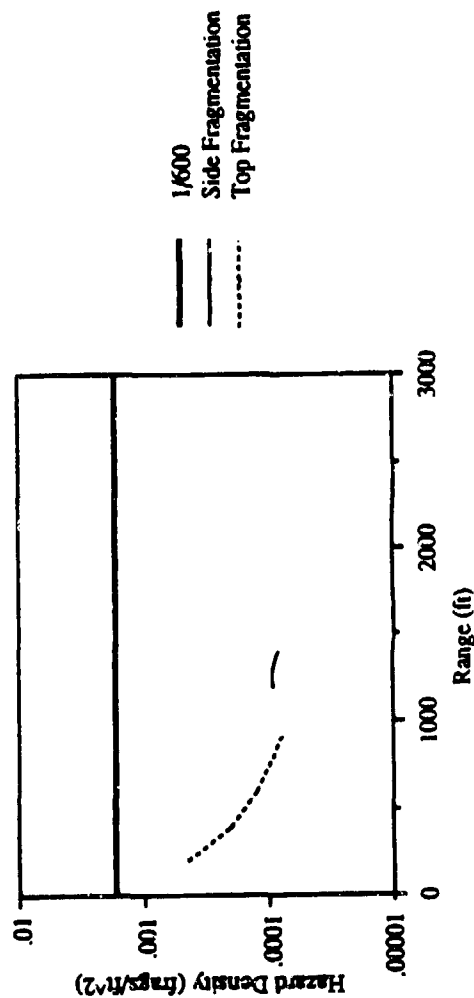
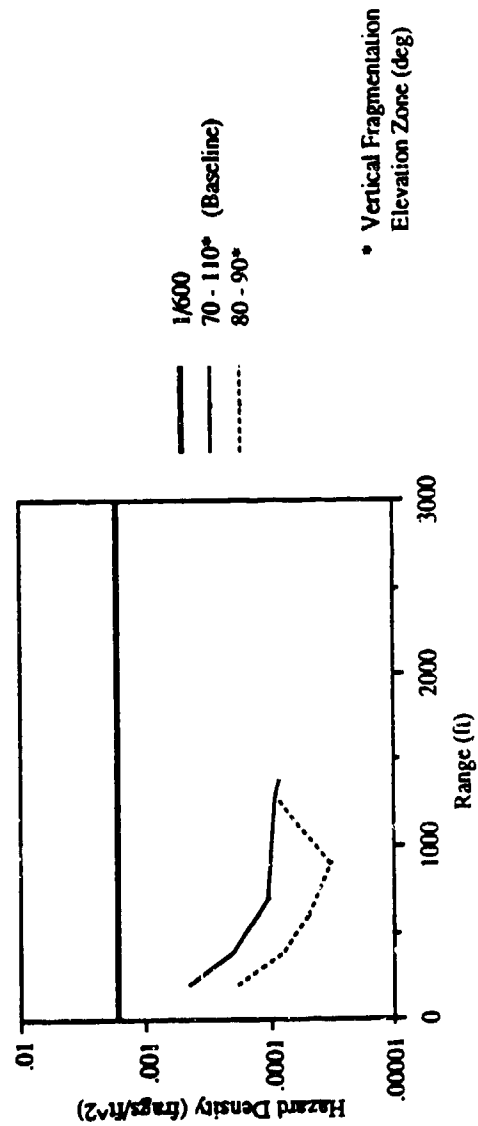


Figure 15

Hazard Densities for Vertical Fragmentation Elevation Zones of 70 - 110 and 80 - 90 Deg

Korean Hillside Barricade : TAEGU : Bldg 230
Stack Configuration No. 3

Target - Standing Man : Injury Criterion - 58 ft-lbs Kinetic Energy Threshold
Monte Carlo Option : Replications 60 : Seed 17351 : Site Altitude 150 ft
90th Percentile : Stack Barricade (Hill) Standoff = 32 ft : Zero Wind



CONCLUSIONS

The following conclusions may be drawn from the results of this investigation.

- The pallets of Mk 82 Bombs should be stacked in a compact configuration like Configuration Number 3 shown in Figure 6.
- The stack should be positioned as near to the front of the shed as practical. There is very little advantage in positioning the stack outside the shed and nearer to the hill (see Table B-5).
- The baseline Stack Configuration Number 3 provides a significant margin of safety (see Figure 8) under the hazard criteria currently specified by the Department of Defense Explosives Safety Board (DDESB). At 800 ft range, the margin of safety is about 18 for zero wind.
- The presence of tailwinds do not significantly alter the margins of safety (see Figure 8). The tailwind curves are still well below the threshold hazard of one hazardous fragment per 600 ft².
- Since the investigation tended to err on the side of safety when uncertainties arose, hazards are not expected to exceed those shown in Figures 8 through 15.
- The hill does an excellent job of stopping the fragmentation from the side of the stacks, especially when the stacks are positioned at the front of the shed (see Table B-5). The hill has little or no effect on the fragmentation coming from the top of the stacks.
- In the Air Force request, contained in Appendix C, it was stated that the storage shed was surrounded on three sides by a hill with the fourth side open and blocked by an undefined barricade. This fourth side should be investigated when detailed data on the stack-barricade geometry become available. It is possible that a compromise stack configuration may be necessary to minimize the overall hazard.

REFERENCES

1. McCleskey, Frank, Quantity Distance Fragment Hazard Computer Program (FRAGHAZ), Naval Surface Warfare Center, TR 87-59, February 1988
2. Reeches, Mark, Fragment Ricochet from Homogeneous Soils and Its Effects on Weapon Lethality (U), Army Material Systems Analysis Agency Technical Memorandum Number 79, August 1970 (CONFIDENTIAL)
3. McCleskey, Frank, Drag Coefficients for Irregular Fragments, Naval Surface Warfare Center, TR 87-89 February 1988

BLAST YIELD ESTIMATION FOR THE PEPCON AMMONIUM PERCHLORATE ACCIDENTAL EXPLOSIONS

**Willfred E. Baker
Quentin A. Baker
Kathy H. Spivey**

**Willfred Baker Engineering, Inc.
San Antonio, Texas**

ABSTRACT

An on-site accident investigation was conducted to determine the number and magnitude of explosions that occurred in May 1988 at the Pacific Engineering and Production Company of Nevada (PEPCON) ammonium perchlorate plant in Henderson, Nevada. Included in this investigation was measurement of damage to many metal structures and objects throughout the plant. The locations of explosion centers were determined from craters and the direction of structural deformation. The deformation and standoff data were the basis for calculations of blast yield for several explosions which occurred during the accident sequence. This paper discusses these "reverse engineering" methods of calculating accident explosion yields.

THE ACCIDENT

On May 4, 1988, a series of fires and explosions demolished the PEPCON ammonium perchlorate (AP) plant near Henderson, Nevada, in what was probably the most massive accidental explosion since the Texas City disaster in 1947. The event sequence was reconstructed from eyewitness reports and a video tape taken from Black Mountain about 2.3 miles southeast of the plant.

There was an initial fire in an AP batch dryer building. As the fire spread, a relatively small explosion followed. This first explosion caused local damage and spread burning firebrands throughout the plant. Fortunately, this explosion also triggered evacuation of both the PEPCON plant and the nearby Kidd marshmallow factory.

Extensive fires then engulfed most of the outdoor ammonium perchlorate storage areas. After several minutes, a massive explosion occurred in Storage Area 19, which had been burning fiercely. This was followed after some delay by two more explosions on a loading dock. There was a final, very large explosion in Storage Area 20.

The timing of the five major explosions follows:

<u>Event</u>	<u>Time</u>	<u>Location</u>
Fire detected	~11:45 a.m.	In batch dryer building
Explosion 1	~11:52 a.m.	North of batch dryer building
Explosion 2	11:56 a.m.	Storage Area 19
Explosion 3	11:58:31 a.m.	Loading dock
Explosion 4	11:58:37 a.m.	Loading dock
Explosion 5	12:00 noon	Storage Area 20

Both the PEPCON and Kidd plants were totally demolished by the explosions and fires.

ACCIDENT INVESTIGATION

A number of experts and investigative firms were engaged to help investigate the accident. The investigation is ongoing. Our primary role in the investigation is to determine blast yields for all explosions in the sequence, if possible.

We first visited and toured the site within two days of the accident, but were not allowed to take any measurements or photographs until the site was released by the local fire department in late June 1988. The site was carefully preserved, however, so we could measure and photograph many pieces of "bent metal" to use as damage indices for blast yield calculation. We also reviewed eyewitness reports, and injury reports. In all, we made five site visits.

ANALYSIS METHODS

The methods for estimating blast yields are essentially the reverse of methods used in blast resistant structural design and safe siting studies for explosives operations or storage. Usually, one postulates worst-case accidental explosions, calculates blast loads, and designs structures to be blast resistant via dynamic analysis, or establishes safety distances based on acceptable blast strengths for personnel. In calculation of blast yields for this accident, we determined what blast loads would have caused observed damage or injury, estimated distance from explosion center, and then used standard scaled TNT surface burst air blast curves to determine the cube root of the blast yield. The final blast yields are then obtained by cubing the result. Each single damage indicator then gives a single estimate of blast yield.

In a complex explosion sequence such as this one, one cannot always be certain which explosion caused observed damage (with the exception of ear and lung injuries, which were almost all caused by the second explosion). To discriminate, one usually calculates yields assuming that damage was caused by each of several explosions, and compares results. Usually, only one result will be rational, and others can easily be discarded. In this accident sequence, however, we could not accurately ascribe observed damage to Explosions 3 and 4 because they were located close to Explosion 5, which was much more powerful. Damage indicators for Explosions 1, 2 and 5 were clearly identified.

The best damage indicators are the simplest, i.e., pipes, beams and flat plate elements. We used a large number of such elements in our analyses. In some instances, we also used damage to more complex structures, when the damage was well defined.

We correlated damage or injury to corresponding blast wave properties using four techniques:

- 1) We ran repeated structural dynamic calculations for elastic-plastic structural responses using methods from Ref. 1 (automated by an in-house computer program named BIGGS (Ref. 2)), varying the dynamic loading until permanent deformation matched the observed deformation. This technique was used for relatively complex structures.

- 2) We used existing, scaled pressure-impulse (P-i) diagrams for maximum response of simple elements (Chapter 4 of Ref. 3). In some instances, we had to calculate new scaled P-i curves for larger deformations than were originally determined in Ref. 3.
- 3) We developed special solutions for structural deformations based on energy-balance methods.
- 4) We determined locations in the plant for injured employees from interviews, and compared to literature data on eardrum rupture and lung injury (Chapter 8 of Ref. 3).

As an example of the second procedure just enumerated, dimensionless P-i curves for beam strip elastic-plastic bending, such as Figure 1 (see Refs. 3 & 4) were used to develop dimensional P-i curves for deformations of end plates in cement hopper cars on a siding near the PEPCON plant. The "unscaled" curves corresponding to various permanent deformations are shown in Figure 2.

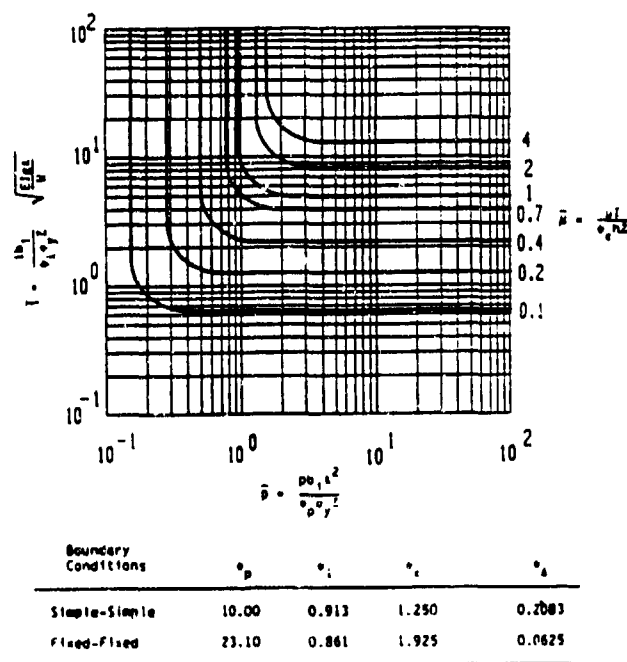


Figure 1. Dimensionless P-i Curves for Beam Bending, (Refs. 3 & 4)

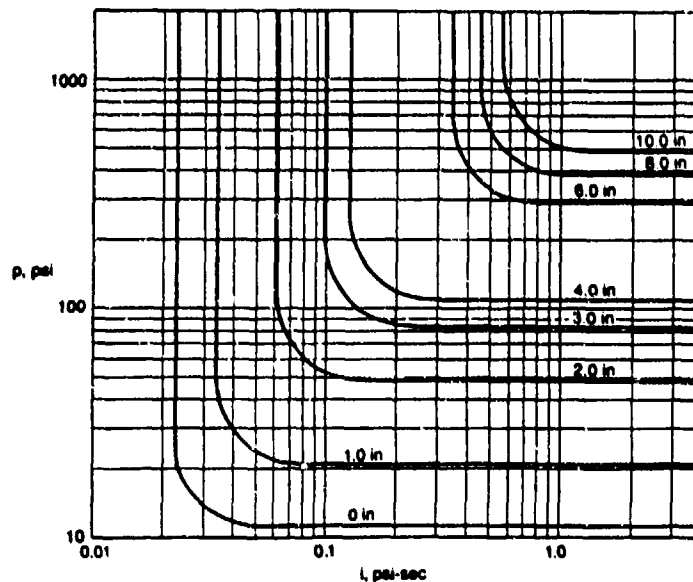


Figure 2. P-i Curves for Hopper Car End Panels

Actual deformations were then correlated with possible blast loads, from Explosion 5, with large impulses lying well to the right of the maxima in Figure 2. This showed that quasi-static dynamic response governed, and that reflected peak overpressure P_r could be used to define blast yield, when coupled with measured permanent deformations and distance from the explosion center.

As an example of the third procedure (energy balance methods), consider deformations of pipe fence posts around the employees' parking lot. There were 60 of these posts, and they provided the best estimates of blast yield from Explosion 2. Figure 3 shows a schematic of an unbent and a bent pipe, with dimensions, loads, and properties. We developed a special energy-balance solution, which applies only for large bend angles, long-duration blasts, and small-diameter pipes. These restrictions let us use the following simplifying approximations:

- 1) Plastic bending provides so much of the resisting force that elastic bending can be ignored.
- 2) Diffracted blast loads are inconsequential compared to drag blast loads, so peak pressure applied horizontally equals $C_D Q$, i.e., drag coefficient times peak dynamic pressure.
- 3) Blast load durations are much larger than pipe response times, so loading is quasi-static, and response is therefore determined by peak loads, and is independent of duration or impulse.

- 4) Pipe failure mode is pure plastic bending (plastic hinge) at the pipe base. (This is confirmed by the observed failure mode for all pipes.)

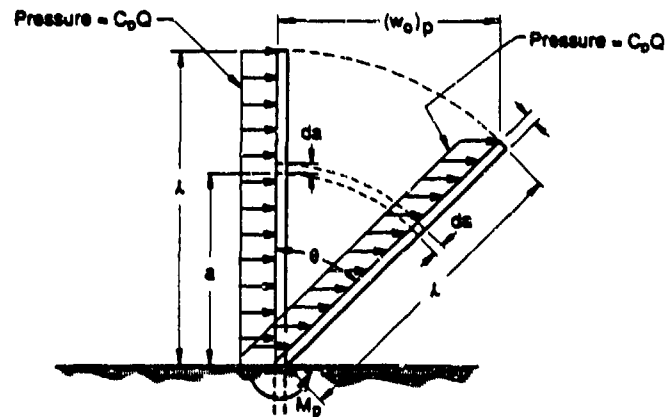


Figure 3. Schematic of Drag-Loaded Pipe Bending

Using the above assumptions, we calculated strain energy to deform the pipes and equated this to work done by the external pressure to cause the same permanent deformation. After considerable algebra, an explicit equation for scaled pipe tip deformation results, in terms of loading and pipe parameters. This equation is

$$\frac{(\omega_0)_p}{l} = \sin \left(\cos^{-1} \frac{2\sigma_y dZ}{C_p Q b l^2} \right) \quad (1)$$

It can be inverted to obtain peak dynamic pressure Q in terms of measured deformations and other parameters,

$$Q = \frac{2\sigma_y dZ}{C_p b l^2} \sec \left[\sin^{-1} \frac{(\omega_0)_p}{l} \right] \quad (2)$$

In this equation,

σ_{yd} = dynamic yield strength,

Z = plastic section modulus,

b = pipe width (diameter)

l = pipe length,

C_D = drag coefficient for slender cylinder,

and $(w_o) p$ = permanent tip deformation.

Once Q is known from measured pipe deflections, we can read a corresponding effective scaled distance from standard TNT air burst blast curves,

$$Z_e = \frac{R}{w_e^{1/3}} \quad (3)$$

Knowing distance R to an explosion center, we then get effective TNT charge weight

$$w_e = \left(\frac{R}{Z_e} \right)^3 \quad (4)$$

and account for ground reflection to finally get

$$w_{TNT} = \frac{w_e}{2} \quad (5)$$

RESULTS

Only four pieces of bent metal could be identified as clearly damaged by Explosion 1. They were primarily bent pipe stanchions for a protective railing north of the dryer building and quite close to the single tote bin which exploded in Explosion 1. So few data points did not allow statistical averaging. Estimated TNT equivalents cannot be given because of pending litigation.

Explosion 2 had the largest number of good damage indicators, including the fence pipes round the employees' parking lot, ear and lung injuries, damage to empty tote bins, damage to an electrical tower at the main electrical substation, damage to end plate on the

batch dryer drum, and damage to steel ducting. Distances for these damage indicators from explosion center ranged from 250 ft to 1,400 ft. The calculated yields for these damage indicators cannot be given because of pending litigation.

We could not unequivocally separate damage caused by either Explosion 3 or Explosion 4 from other blast damage. This is not surprising, because it is readily apparent from the Black Mountain tape that these were both much less energetic explosions than Explosion 2 or 5. Also, the loading dock where these explosions occurred had few nearby structures that could be used as damage indicators for Explosions 3 and 4.

The primary damage indicators for Explosion 5 were dished tops and end plates for seven railroad hopper cars located on a siding next to the plant. We obtained two measurements for each car top, because there were gradations of damage along the tops. Again, estimated blast yields cannot be given because of pending litigation.

DISCUSSION

Some general points regarding all "reverse engineering" explosion yield estimates are as follows:

- 1) The more structurally simple pieces of bent metal one uses, the better the blast yield estimates.
- 2) In accidents with multiple explosions, discrimination of effects for individual explosions can be difficult, but not impossible. Calculated yields can be determined with reasonable certainty.
- 3) Often, existing P-i diagrams or other aids in correlating damage with yield must be modified or extended based on observed damage in a particular accident.

Regarding this explosion, let us emphasize that there is a strong effect of distance on calculated blast yields shown in our calculations for Explosion 2. We interpret this effect as a shape effect, with the blast coming from a distributed explosive source rather than a spherical or hemispherical source. There are currently too few blast analyses or tests for distributed sources to correct for this effect.

REFERENCES

1. J. M. Biggs, Introduction to Structural Dynamics, McGraw-Hill Book Co., New York, NY, 1964.
2. "BIGGS Version 2.0 Users' Manual," Wilfred Baker Engineering, Inc., San Antonio, Texas, July 1990.
3. W. E. Baker, P. A. Cox, F. S. Westine, J. J. Kulesz, and R. A. Strehlow, Explosion Hazards and Evaluation, Elsevier Scientific Publishing Co., Amsterdam, 1983.
4. M. G. Whitney, C. J. Oswald, and M. A. Polcyn, "Blast Damage to Typical Structural Elements," in Structures for Enhanced Safety and Physical Security, ASCE, New York, NY, March 1989, pp. 389-411.

APPENDIX A

CHAIRMAN, DOD EXPLOSIVES SAFETY BOARD

CLOSING REMARKS

I want to congratulate all those who participated in making this Seminar a great success. We had an attendance of over 650 people, representing some eighteen nations. In particular, I thank those who took their own time and effort to organize and present the latest developments in the technology supporting our field of explosives safety. We sponsor a few of them, but others volunteer their services. We owe you all a lot. This Seminar could not exist without you.

As this Seminar draws to a successful end, remember we will be back again for the 25th Seminar somewhere on the West Coast in 1992. We look forward to hosting all of you at that time.

Now, it is my distinct pleasure to introduce Brigadier Robin Armstrong, Chairman of the Explosives Storage and Transport Committee in the United Kingdom, who has consented to make a few closing remarks.

24TH DOD EXPLOSIVES SAFETY SEMINAR

CLOSING REMARKS

by

BRIGADIER R C ARMSTRONG, CHAIRMAN EXPLOSIVES STORAGE AND

TRANSPORT COMMITTEE LONDON

Ladies and Gentlemen, we've covered a lot of ground in the last 3 days. It would be near impossible to summarize all the material that has been presented. Furthermore, I recognise that I am on borrowed time so I will keep it short.

Ms Millicent Woods made a very telling introduction when she regaled us with the catalogue of disasters that led to setting up of DD ESA. No doubt it was catastrophic events of the same kind in each of the countries represented here today that led to similar actions being taken. In the UK it was the explosion of a barge carrying gunpowder in the Regents Canal in London which led to the Explosives Act of 1875 being passed and which first introduced legislative

control into the manufacture and handling of explosives. It is a sad reflection that it needs such catastrophies to further the cause of safety. If we were still in any doubt as to the dangers of explosives and munitions these were graphically reinforced in the sessions Accidents I and Accidents II.

They remind us that there is no room for complacency.

They reinforce the point that we all, in this room, know; that is; if an accident can happen then someday it will happen.

We heard that accidents can happen through chemical degradation, or as an act of God, but more often as a result of human error. We cannot leave the human operator out of the chain. We may be able to automate the manufacturing process but at the end of the day it is the sailor, the soldier or the airman who must use the munitions. We must not forget that nearly all of our work is directed to serving them.

It is important that we remember this and balance the desire for total safety with what is realistic and

practicable.

We saw the need for this balance in the session on Range Safety. At some point we have to rely on effective drills and effective supervision. A good example was the description of the accident caused by double loading an 81mm Mortar. It is possible to fit a device to prevent double loading, the Soviets use one, but the increased safety is offset by a reduced rate of fire, ie a reduced operational capability.

It is up to us to give realistic advice, based on facts, which the decision makers will feel able to use.

We are living in an age when all aspects of safety are getting high public visibility. The public is realising that the State has an obligation to keep them safe, or failing that to compensate them. Why should they be put at risk by the activities of others, they ask. Also peoples' expectations of personal freedom have increased and the pressure on land grows. Why should the armed forces have so much land, they ask.

It all makes our task more difficult.

We must therefore get more efficient. It was encouraging to see so many steps during the Seminar leading in that direction.

- The work of the Klotz club on underground storage.
- The sharing of trials, their data and their costs to validate Q-D criteria. None of us can afford to go it alone.
- The work on Insensitive Munitions which as well as leading to safer munitions could result in lower hazard classifications and hence more efficient storage.
- The work on Risk Assessment techniques which will move us away from solely consequence based criteria, and take into account frequency of occurrence and probability of injury. This, hopefully, will lead to the more efficient use of land both for storage and on the firing ranges.

We must continue to pool our resources and work closely

together. It is the only sensible way forward.

Ironically, our very success in preventing accidents breeds complacency in the eyes of those who control the purse strings. But we all lack resources to do what we know needs doing in order to become more efficient and effective - it's a Catch 22 situation.

This conference has been so important because it has allowed us to pool our ideas. In this sense it has been a superb catalyst.

To give you my personal impression, as a first timer of this conference. I liken it to a jigsaw puzzle. At each session another piece of the jigsaw is put on the table and then in the margins people get together and start joining the pieces together and a picture begins to emerge. Unfortunately we will have to put it away unfinished, until the next time when we can continue the process. I congratulate the organisers in their foresight in giving us such wide margins.

Quite apart from the most valuable technical exchanges: what else has the Seminar achieved.

- It has reminded us that we are not alone, that our opposite numbers in other countries have similar problems; knowing that gives us strength to return to the fight.

- The exchange of views with like minded people fires us with enthusiasm to continue.

- As an added bonus we have all I am sure learnt more than we expected to. I congratulate all the presenters for making that possible.

Jack, may I congratulate you on a most successful Seminar.

- please continue with them.

- may I also congratulate you on an excellent selection of venue.

- finally a word on administration. We have a saying that one is only aware of bad administration. I know that an enormous amount of effort must have gone into organising this Seminar but I have not

been aware of it going on. May I congratulate your staff on their excellent behind the scenes work.

I would like to conclude by proposing a vote of thanks from all of us here and on behalf of all the nations represented to Col Jack Mathews and all the staff of the Department of Defense Explosives Safety Board for an excellent seminar - Jack, thank you.

ATTENDANCE LIST
Twenty-Fourth Explosives Safety Seminar
1990

24th DDESB EXPLOSIVES SAFETY SEMINAR
ATTENDANCE LIST

ABRISZ, Gary W.	USA Ammo Ctr & Sch, Savanna, IL 61074
ACKERMANN, Juergen	MOD Germany, Schneizlreuth, Germany
ADAMS, Arlie E.	Air Force Log Cmd, Wright-Patterson AFB, OH
ADAMS, Richard T.	Naval Sea Systems Command, Wash., DC 20362
ADAMSON, J.	Royal Ordnance Arm Div, Lancashire, England
AGEE, Midge	EOD Technology, Oak Ridge, TN 37831
AKEY, Williams, CWO	Air Command, Westwin, Manitoba
ALBRECHT, Ricky L.	Defense Nuclear Agency, Kirtland AFB, NM 87115
ALLAIN, Laurent A.	SNPE, France
ALLAN, Terry O.	Mason & Hanger Engr Inc., Lexington, KY 40504
ALLEN, John E.	BMO, Norton AFB, CA 92409
ALLES, John, CDR	Royal Netherlands Navy, Holland
AMIABLE, Rene, BRIG GEN	Chmn, French Explosives Board, France
ANASTOS, Ernest G.J.	Raytheon Msl Sys Div, Tewksbury, MA 01876
ANDERSON, Andrew W.	Argonne National Lab, Bel Air, MD 21014
ANDERSON, Mark C.	Wyle Laboratories, Norco, CA 91760
ANDERSON, Ray W.	Agabian Associates, Pasadena, CA 91105
ANDERSON, Robert G.	Tooele Army Depot, Tooele, UT 84074
ANNUZZIO, Joseph F.	Pacific Missile Test Ctr, Point Mugu, CA 93042
ANSPACH, Earl E.	Sverdrup Technology, Inc., Arnold AFB, TN 37389
ARCHAUX, Gilbert	French Defense Ministry, France
ARMSTRONG, Robin, BRIG, UK	Ordnance Board, London, England
ARNOLD, James I.	USATHAMA, Aberdeen Proving Ground, MD 21020
ARTAUD, Alain	French Defense Ministry, France
ATHEY, Ronald E.	Hercules, Inc., Wilmington, DE 19894
AUSTEN, Bryan S.	USAF Civil Engr Rsch Div, Kirtland AFB, NM
AUYER, Joseph L.	Aerojet ASRM Div, Orangevale, CA 95662-1270
AVEDISSIAN, Hagop A., LCDR	Defense Nuclear Agency, Kirtland AFB, NM 87115
BAJPAYEE, Tara S.	U.S. Bureau of Mines, Pittsburgh, PA 15236
BAKER, Charles (Joe) F.	Lawrence Livermore Nat Lab, Livermore, CA 94550
BAKER, Quentin A.	Wilfred Baker ENgr, Inc., San Antonio, TX 78209
BAKER, Wilfred E.	Wilfred Baker Engr, Inc., San Antonio, TX 78209
BARATTA, Gary A., CAPT	Hawthorne AAP, Hawthorne, NJ 89415
BARKER, Darrell D.	Mason & Hanger-Silas Mason Co., Amarillo, TX
BARKER, Donna	DoD Explosives Safety Board, Alex, VA 22331-0600
BARNES, Floyd M.	HQ AFSPACECOM, Peterson AFB, CO 80914
BARR, Michael J.	Los Alamos National Lab, Los Alamos, NM 87544
BATEMAN, David A.	ATF, Kansas City, MO 64106
BECK, Mervin L.	Umatilla Depot Activity, Hermiston, OR 97838
BEHAN, Carl R., CAPT	15th AF/SEW, March AFB, CA 92518
BELL, Jack L., CAPT	EOD, MCB Camp Pendleton, CA 92055
BELL, Kenneth C.	NM Engr Research Inst., Albq., NM 87131
BENDER, Urs S., MAJ GEN	DCOS Logistics General Staff, Bern, SW
BENGEL, John R.	Hercules, Inc., DeSoto, KS 66018-0549
BENNETT, George T.	1776 ABW, Andrews AFB, MD 20331
BERGBAUER, Daniel M.	Naval Ordnance Station, Indian Head, MD 20640
BERRY, Sharon L.	Naval Wpns Ctr, China Lake, CA 93555

BERTHIAU, Jean P.
 BERTOLI, Donald J., MSGT
 BESSON, Jacques C., COL
 BIBLE, William B.
 BISCOTTE, Michael N.
 BLAIR, Douglas R.
 BLAU, Sullivan E.
 BLOOM, Thomas
 BLOSE, Thomas L.
 BLOUNT, Wilson E.
 BLUNK, Steven R.
 BOATWRIGHT, John W.
 BOIMEL, Arie
 BOLES, Howard D.
 BONONES, James A., CAPT
 BONZON, Lloyd L.
 BOOM, J.G.
 BOONE, Robert D.
 BOONE, Timothy L., CAPT
 BOREL, Raywood W.
 BORSCH, Richard E.
 BOTTJER, Gary M.
 BOTTJER, Sandy
 BOVA, Kevin M.
 BOWLES, Patricia M.
 BOYLES, David J., LT.COL.
 BRISTOL, Greg W.
 BROWN, Warren R.
 BRUCE, William E., CAPT
 BRUCKER, David A.
 BRUNO, Fred A.
 BRYANT, William, COL
 BUCHHOLTZ, Walter C.
 BULLOCK, James W.
 BULTMANN, Edward, Dr.
 BUNCH, Kenneth D.
 BURCHETT, MSGT
 BURGESS, William P.
 CAESAR, Don E.
 CAHALANE, Patrick T.
 CAMMARATA, Richard C.
 CAMPBELL, Clarence J.
 CAMPBELL, Glen
 CAMPBELL, Jimmy F.
 CANADA, Chester, Dr.
 CANNON, Paul C.
 CAREW, Donald L.
 CARROLL, Donna S.
 CARSON, Robert C.
 CASE, James E., LT.COL.
 CASHIN, Richard H.
 CATES, Charles
 CAYERE, Paul J.

French Defense Ministry, France
 302 TAW, Peterson AFB, CO 80914
 French Minister of Defense, France
 Martin Marietta, Milan AAP, Milan, TN 38358
 Hayes, Seay, Mattern, Roanoke, VA 24034
 APO NY 09403
 Strategic Indus. Safety, Brigham City, UT 84302
 Quantic Industries, Inc., San Carlos, CA 94070
 Naval Weapons Center, China Lake, CA 93555
 HQAFISC, Norton AFB, CA 92409
 USA Ammo Ctr & Sch, Savanna, IL 61074
 Tri-State Mtr Transet, Joplin, MO 64801
 Israel Military Industries, NY, NY 10022
 Boeing Aerospace & Elec., Seattle, WA 98124
 TRADOC Mun Sys Mgr Ofc, Redstone AR, AL 35897
 Sandia Nat'l Lab, Albuquerque, NM 87185
 Ministry of Defense, Netherlands
 Hercules, Inc., Magna, UT 84044
 Weapons Laboratory, Kirtland AFB, NM 87117
 Naval Coastal Sys Ctr., Panama City, FL 32407
 NASA ODFL, Edwards, CA 93523
 HQ, AMC, Alexandria, VA 22333
 DoD Explosives Safety Board, Alex, VA 22331-0600
 Naval Weapons Sta Earle, Colts Neck, NJ 07722
 Southwest Research Inst., San Antonio, TX 78228
 HQ, AFISC/IGLW, Norton AFB, CA 92409
 CAPCO, Inc., Grand Junction, CO 81502
 Olin Corporation, Baraboo, WI 53913-5000
 96 BMW, Dyess AFB, TX 79607
 Ogden ALC Wpns Saf Ofc, Hill AFB, UT 84056
 McDonnell Douglas, Titusville, FL 32780
 DoD Explosives Safety Board, Alex., VA 22331
 Tyndall AFB, FL 32403-6001
 Physics Inter Co., San Leandro, CA 94577
 UNM/MMERI, Albq., NM 87131
 McDonnell Douglas, St. Louis, MO 63166
 2701 EODS, Hill AFB, UT 84056
 Naval Surface Warfare Center, Dahlgren, VA 22448
 Valentec Dayron, Orlando, FL 32814-0394
 US Dept. of Energy, Amarillo, TX 79120
 Booker Associates, St. Louis, MO 63101
 AMC Field Safety Activity, Charlestown, IN 47111
 Olin Corporation, Marion, IL 62959
 First Air Force, Langley AFB, VA 23665
 DoD Explosives Safety Board, Alex., VA 22331
 Thiokol Corp., Brigham City, UT 84302
 First Air Force, Langley AFB, VA 23665
 Webb, Murray & Assocs., Johnson Spc Ctr, TX
 McDonnell Douglas, St. Louis, MO 63166
 AFISC, Kirtland AFB, NM 87117
 Army Materiel Cmd, Picatinny AR, NJ 07806
 DoD Explosives Safety Board, Alex., VA 22331
 Physics International Co., San Leandro, CA

CENTENNIAL, Carl R.	Southwest Research Inst., San Antonio, TX 78228
CESSARIO, Thomas R.	Thiokol Corporation, Elkton, MD 21921
CHAFFIN, William A.	USA Corps of Engrs, Huntsville, AL 35807
CHAI, Peh Lien	CDC-Construction Development, Singapore
CHANDLER, Albert	Applied Ord Tech Inc., Arlington, VA 22202
CHANDLER, E. Fred	USA Def Ammo Ctr & Sch, Savanna, IL 61074
CHANG, Il Chol	Korea Explosives Co., Seoul, Korea
CHANG, Wel Shing	Bureau of Explosives, Short Hills, NJ 07078
CHASE, Ronald R.	436 MAW/SEV, Dover AFB, DE 19902
CHIA, Cake Han	Lands & Estates Organ, Singapore
CHICADO, Fred	Directorate of Distribution, Hill AFB, UT 84056
CHIZALLET, Maurice	Matra Defense, Cedex, France
CHOO, Chong	CDC-Construction Development, Singapore
CLAPP, Rodger C.	Martin Marietta Msl Systems, Orlando, FL 32855
CLARIDGE, Robert R.	Dyseaton Pty Ltd, Manuka ACT Australia 2603
CLARK, Dan D.	Olin Corporation, East Alton, IL 62024-1174
CLARK, Eugene	DoD Explosives Safety Board, Alex., VA 22331
CLARK, Ronald F.	Crane Army Ammo Activity, Crane, IN 47522
CLARK, Thomas P.	WESTNAVFACENGCOM, San Bruno, CA 94066
CLEMENTS, Lynn C.,	HQs, Forces Command, Ft. McPherson, GA 30330
CLINTON, Stephen P.	Hayes, Seay, Mattern&Mattern, Roanoke, VA 24034
CLOONAN, James J.	SM-ALC/SEW, McClellan AFB, CA 95652
CLYDE, David C., LT.COL.	Australian Defence Force, Canberra, Australia
COBB, Michael K.	AMCCOM, Rock Island, IL 61299
COCHRAN, Grover G.	Readiness Group, Fort Douglas, UT 84113
CODEMO, James A.	Olin Corp., East Alton, IL 62024
COLLIER, Richard S.	Electro Magnetic App., Lakewood, CO 80228
COLLIS, Dave	New Mexico Inst. of Mining & Tech, Socorro, NM
CONNELL, Malcolm	Property Svcs Agency, Croydon, UK
COOK, Johnnie, L.	Red River Army Depot, Texarkana, TX 75507
CORLEY, John D.	AF Armament Lab, Eglin AFB, FL 32542-5435
COSCO, Philip M.	Air National Guard, APG, MD 21010
COTE, Remi, MWO	Air Command, Westwin, Manitoba
COUCH, William A.	Sandia Nat'l Lab, Albq., NM 87185
COULSON, John R.	Coulson Consulting Corp., Wilmington, DE 19809
CRABLE, John M.	Hercules, Radford, VA 24141
CRAIG, James C.	David Taylor Rsch Ctr, Portsmouth, VA 23709
CROZIER, Charles O.	Charles O. Crozier, Inc., Marietta, GA 30062
CRUZ, Ignacio T.	Naval Weapons Station, Yorktown, VA 23691
CUEFF, Christian	French Defense Ministry, France
CUMMINGS, Melvin E.	DPRO-LASC, Marietta, GA 30063
CURRY, Ronald K., CDR	Naval Safety Ctr, Norfolk, VA 23511
DAHN, Carl J.	Safety Consulting Engrs, Inc, Rosemont, IL 60018
DALKE, William C.	2854 CES/DEEX, Tinker AFB, OK 73145
DALTON, Bruce	Naval Ordnance Station, Indian Head, MD 20640
DAVIDSON, Edward F.	U.S. Army Japan, APO San Francisco 96343-0054
DAVIES, Ian R., LT.COL.	Directorate of Ordnance, Canberra, Australia
DAVIS, Leah J.	USA Test & Eval, Somerville, AL 35670
DAVIS, Leland E.	Strategic Safety, Brigham City, UT 84302
DAY, Douglas M.	Radford AAP, Radford, VA 24141
DAYE, James O.	NAVSEACENLANT, Portsmouth, VA 23703
DAYWALT, Raymond A.	Naval Weapons Support Ctr, Crane, IN 47522
DENISON, Thomas S.	Honeywell, Inc., Minnetonka, MN 55343

DERICKSON, Jon D.
 DERR, Ronald L.
 DESHPANDE, Praalhad
 DEWITT, Gregory M., CAPT
 DIEHL, Dennis
 DILLARD, Don
 DILLEHAY, David R.
 DILTS, Chuck D.
 DITTMAN, Harry A.
 DODGEN, James E.
 DODY, Kevin
 DOMINGUEZ, Joseph F, SMSGT
 DORN, Dennis J.
 DOTTS, J.E.
 DOUTHAT, C. David
 DOVELL, Nigel C.
 DOWLING, Thomas P.
 DRAKE, James
 DRAKE, James L.
 DRILLEAU, Jean-Jacques
 DROLET, Jean Francois
 DROUX, Rolland
 DUA, Balbir S.
 DUARTE, Richard M.
 DUDLEY, Michael J.
 DUNAWAY, Thomas L.
 DUNCAN, Kendal M.
 DUNSETH, Clifford A.
 DUPUIS, Gardy J.
 DeSHAZO, James B.
 EARLY, Wilbert, MSGT
 EDDY, John R.
 EINERTH, Bengt
 ELLEDGE, James
 ELLIOTT, Jim E.
 ELMORE, Richard E.
 ENGLEBRETSON, Alfred, CWO
 ENGLISH, Thomas P.
 EPPERT, Franklin P.
 EYTAN, Reuben
 FAHY, Francis A., CAPT
 FANNIN, Gerald F.
 FARR, Allen M.
 FATZ, Ray
 FELLER, Shaul, Dr.
 FENG, Kuo K.
 FENNESSY, Richard A.
 FERRARO, Carlo
 FEY, Klaus G., LT.COL.
 FICK, Rudi, CAPTAIN
 FLORY, Robert A.
 FLOYD, James Q.
 FORSEN, Rickard B.

Hoes Engineering, Inc., Davis, CA 95616
 NWC, China Lake, CA 93555
 Ex-Dy. Gen Mgr, Pune, India
 Defense Nuclear Agency, Kirtland AFB, NM 87115
 Olin Corporation, Marion, IL 62959
 Olin Corporation, Marion, IL 62959
 Thiokol Corporation, Marshall, TX 75671
 McDonnell Douglas, Titusville, FL 32780
 DCMR Cleveland, OH 44199
 Dodgen Engr Co, Colorado Springs, CO 80906
 Olin Corporation, Marion, IL 62959
 HQAFISC, Norton AFB, CA 92409
 The Nathan Hale Group, Chantilly, VA 22021
 Sandia Nat'l Lab, Albq., NM 87185
 USA Corps of Engrs, Huntsville, AL 35807
 Property Services Agency, Surrey, England
 Inst. of Makers of Explo, Wash, DC 20036
 DoD Explosives Safety Board, Alex., VA 22331
 Applied Research Assoc., Vicksburg, MS 39180
 Societe Nat des Poudres ET Explosifs, France
 Def Research Estb., Valcartier, Canada
 C.E.A., Paris, France
 Day & Zimmermann, Kansas AAP, Parsons, KS 67357
 USA Corps of Engrs, Kansas City, MO 64106
 DCMR LA-QS, El Segundo, CA 90245
 US DOT Fed Highway Admin, Atlanta, GA 30367
 Arm Resch Dev & Engr Ctr, Picatinny AR, NJ 07806
 HQDA, Army Safety Office, Ft. Rucker, AL 36362
 McChord AFB, WA 98374
 Explosion Dynamics Br, Dahlgren, VA 22448-5170
 1st Tact Fighter Wing, Langley AFB, VA 23665
 Defense Nuclear Agency, Alex., VA 22310
 Nat'l Inspectorate of Explosives, Sweden
 United Technologies, San Jose, CA 95161
 Safety Office, Picatinny Arsenal, NJ 07806-5000
 NSWC, Dahlgren, VA 22448
 Nat'l Defense Hqs, Ottawa, Canada
 Nav Coastal Sys Ctr, Panama City, FL 32407
 Booker Associates, St. Louis, MO 63101
 Eytan Building Design, Ltd., Tel Aviv, Israel
 Weapons Laboratory, Kirtland AFB, NM 87117
 OC-ALC, Tinker AFB, OK 73145
 AFDTIC, Eglin AFB, FL 32542
 HQDA, DACS-SF, Pentagon, Wash., DC 20310
 Israel Armanent Dev Auth, Israel
 Canadian Explosives Rsch Lab, Canada
 Milsearch Pty. Limited, Canberra, Australia
 Chief of Naval Operations, Wash., DC 20350
 Amt fur Studien und Ubungen der Bundeswehr, GE
 FMOD Armed Forces Staff, Bonn, Germany
 Applied Research Associates, Alex., VA 22314
 Warner Robins Air Log Ctr, Robins AFB, GA 31098
 Swedish Defence Research Estab, Sweden

FORSYTHE, Frank J.
 FOULK, David W.
 FOWLER, Norman L.
 FRAGA, Don M.
 FRANCIS, Anna N.
 FRANKS, Andrew P., Dr.
 FRECK, Stanley G.
 FREIMANIS, Alvis
 FRIEDMAN, Gary
 GALLAGHER, Richard N.
 GARAY, Frank A.
 GARCIA, Felipe A.
 GARDNER, Charles C.
 GAUBE, William H.
 GEITZ, William C.
 GIBSON, James A.
 GILBERT, Archaux
 GLAZNER, Frederick E.
 GLOVER, Robert, CAPT
 GOLIGER, Jean G.
 GORDON, Walter W.
 GORMAN, Daniel J.
 GOULD, Les R., SQUAD LDR
 GRACE, Paul J.
 GRAHAM, Alan C., COL
 GRAHAM, Kenneth J.
 GRAVE, Alain
 GREENBERG, Paul L, MAJ GEN
 GREENFIELD, Gary R.
 GREENWADE, Edward R.
 GROSMAN, Boaz
 GUTHRIE, Mitchell A.
 HAI, Lim Kim, CAPT
 HAINES, Robert O.
 HALSEY, Carl C.
 HAMILTON, Glen D.
 HAMILTON, Jerry
 HAMMITT, Donald K.
 HANSEN, Niels J.
 HARMANNY, Ake
 HARRIS, Robert A.
 HARRIS, Robert E., MAJ
 HARRIS, Theodore E.
 HART, Richard, LT.COL.
 HARTMAN, Gerald A.
 HARTZOG, SMSGT
 HARVEY, Harry E.
 HASH, Harmon H.
 HAUGE, Einar
 HAYES, John R.
 HAYES, Kenneth T., MSGT
 HEATH, C. Luckey
 HEATH, Joel H.

Uniroyal Chem Co. Joliet AAP, Joliet, IL 60434
 USA Def Ammo Ctr & Sch, Savanna, IL 61074
 HQ AFESC/DEMM, Tyndall AFB, FL 32403
 RJO Enterprises, Inc., Lanham, MD 20706
 AMSMC-SFP, Rock Island, IL 61299
 AEA Technology Safety & Reliability, England
 BDM International, McLean, VA 22102
 Knight Arch Engr Planners, Chicago, IL 60606
 Naval Surface Weapons Ctr, Dahlgren, VA 22448
 Defense Plant Rep, Boeing, Seattle, WA 98124
 NSWSES, Port Hueneme, CA 93043
 Naval Coastal Sys Ctr., Panama City, FL 32407
 RAAP-Hercules Inc., Radford, VA 24141
 Omaha District Corps of Engrs, Omaha, NE 68101
 Atmospheric Rsch Systems, Palm Bay, FL 32905
 HQ, Mil Traffic Mgmt Cmd, Falls Church, VA 22041
 Ministry Francais Dela Defense, France
 USA Msl Command, Redstone Arsenal, AL 35898
 DoD Explosives Safety Board, Alex., VA 22331
 SNPE, France
 Strategic Wpns Fac, Kings Bay, GA 31547
 EG&G Mound Applied Tech., Miamisburg, OH 45343
 DoD, Air Force Ofc, Australia
 Aerojet Propulsion Div, Sacramento, CA 95813
 HQAFISC, Norton AFB, CA 92409
 Atlantic Research Corp., Gainesville, VA 22065
 Aerospatiale, Div Engins Tactiques, France
 AMCCOM, Rock Island, IL 61299
 SRI International, Menlo Park, CA 94025
 Pan Am World Services, Patrick AFB, FL 32925
 Israel Military Industries, Israel
 Kilkeary, Scott & Assocs., Arlington, VA 22202
 Republic of Singapore Air Force, Singapore
 Dept. of Army, Iowa AAP, Middletown, IA 52638
 Naval Wpns Ctr, China Lake, CA 93555
 Olin Corp., Lake City AP, Independence, MO 64051
 Vitro Corporation, Silverdale, WA 98383
 Beech Aircraft Corp., Wichita, KS 67201
 DEMEX Consulting Engrs., Denmark
 Stuvex Benelux, Belgium
 Cmbt Development, Ft. Leonardwood, MO 65473
 Nuclear Supt Ofc, Kirtland AFB, NM 87117
 Naval Surface Wpns Ctr, Dahlgren, VA 22448
 Sunflower AAP, DeSoto, KS 66018-0640
 Wyle Laboratories, Norco, CA 91760
 2701st EOD, Hill AFB, UT 84056
 Hercules, Inc., DeSoto, KS 66018-0549
 Cmbt Systems Test Acty, APG, MD 21005
 Raufoss A/S, Raufoss, Norway
 USA Constr. Engr Rsch Lab, Champaign, IL 61853
 AF Special Oper Cmd, Hulburt Field, FL 32544
 Thiskol Corporation, Ogden, UT 84401
 FORSCOM HQS, Fort McPherson, GA 30330

HELES, Gregory S.	USA Ammo Ctr & Sch, Savanna, IL 61074
HELLE, Charles J.	CIA Brasileira de Cartuchos, Brazil
HELLMANN, Steven P., MAJ	HQ, USAF, Ft. Detrick, MD 21701
HENDERSON, James	Naval Plant Rep Ofc, Sunnyvale, CA 94088
HENDERSON, Jonathan	Ministry of Defence, England
HENDERSON, William H.	Naval Surface Warfare Ctr, Dahlgren, VA 22448
HENRY, Guy	Olin Corporation, Marion, IL 62959
HEPLER, Jonny	Hqs, Tech Air Cmd, Langley AFB, VA 23665
HERCHBERGER, Chester K.	Defense Logistics Agency, Anaheim, CA 92812
HERRBACH, Allan M.	1606 ABW, Kirtland AFB, NM 87117
HERRON, Roger A.	Safety & Health Phy Ofc, APG, MD 21005
HESSLER, George R.	McDonnell Douglas, St. Louis, MO 63146
HEWKIN, David J., Dr.	ESTC Risk Analysis Study Team, London, England
HIGH, Harvey T.	HQ TRADOC, Fort Monroe, VA 23651
HIGHLANDS, William	Atmospheric Rsch Systems, Palm Bay, FL 32905
HILL, Daniel B.	Tooele Army Depot, Tooele, UT 84074
HILL, Don	Olin Corporation, Marion, IL 62959
HITES, Walter G.	317 TAW/SEV, Pope AFB, NC 28308
HLIWA, Ron	Olin Corporation, Marion, IL 62959
HOES, Charles F.	Hoes Engineering, Inc., Davis, CA 95616
HOFFMAN, Edward J.	HQ V Corps, APO 09079-0701
HOFFMAN, Norman H.	Technical Ordnance Inc., Waconia, MN 55387
HOLM, Matthew M.	Defense Nuclear Agency, Alex., VA 22310
HOMB, Hans Frode	Raufoss A/S, Raufoss, Norway
HONG, Kwang Woong	Korea Explosives Co., Seoul, Korea
HOUCHINS, William D.	Naval Surface Warfare Ctr, Dahlgren, VA 22448
HOWARD, Charles	NSWSES, Port Hueneme, CA 19304
HOWELL, Edward Dale	DoD Explosives Safety Board, Alex., VA 22331
HUDSON, Melvin C.	Naval Ordnance Station, Indian Head, MD 20640
HUDSON, Ron	Olin Corporation, Marion, IL 62959
HUEHN, Wilfried, LT.COL.	Materialamt der Bundeswehr, W. Germany
HUMPHREY, James E., LT.COL.	HQAFISC, Norton AFB, CA 92409
HUNT, Eddie T.	USASDC, Huntsville, AL 35807
HUNTER, Dennis M.	New Mexico Inst. of Mining & Tech, Socorro, NM
HUTTON, Judith A., WO	FAC Maintenance, 29 Palms, CA 92278
INDIHAR, Gary	USA Missile Command, Huntsville, AL 35898
INGALLS, Morrie J.	Nav Coastal Sys Ctr, Panama City, FL 32407
IRELAND, John P.	Explosives Educational Svcs, Wyckoff, NJ 07481
JACKSON, Ron E.	Mason & Hanger Engr Inc., Lexington, KY 40504
JACKSON, Ronnie L.	Texas Instruments, Inc., Dallas, TX 75265
JACKSON, Sherry S.	Accudyne Corporation, Janesville, WI 53545
JACOBS, Edward M.	Integrated Sys Analysts, Ft. Walton Beach, FL
JACOBS, Raymond L.	Wright-Patterson AFB, OH 45433
JASCHKE, Vernon M.	MDMSC, St. Louis, MO 63166
JEHN, Christopher	Assistant Secretary of Defense, Wash, DC
JENSSSEN, Arnfinn	Norwegian Defence Constr Svc, Oslo, Norway
JOACHIM, Charles E.	USA Engr Waterways Exp Sta, Vicksburg, MS 39180
JOE, Donald Y.	Sandia Nat'l Lab, Albq., NM 87185
JOHNSON, John A.	USA Ammo Ctr & Sch, Savanna, IL 61074
JOHNSON, Paul M.	Naval Surf Warfare Ctr, MD 21771
JONASSEN, Kjell	Norwegian Defence Constr Svc, Oslo, Norway
JONES, Donovan J.	Talley Defense Systems, Mesa, AZ 85234
JONES, Peter	British Defense Staff, Wash., DC 20008

JORGENSEN, Carl L.
 JOSEPHSON, Carl H.
 JOSEPHSON, Larry H.
 JOYNER, Taylor
 KATSANIS, David J.
 KEEFE, Robert L.
 KEFNAN, William A.
 KELLER, Bill H.
 KELLEY, Philip G.
 KENNEDY, Lynn
 KERKER, Daniel L, SMSGT
 KERNS, Avery J.
 KERR, Gordon S.
 KERR, Larry W., MSGT
 KILFER, Deborah J.
 KILLEEN, Roger A., GP CAPT
 KIM, Kyong In
 KIM, Young-Yun
 KING, Cecile D., Dr.
 KING, Jane F.
 KITA, Terry J.
 KLAPMEIER, Kenneth M.
 KLEIHAUER, Dennis M.
 KNAPP, Kenneth P.
 KOELKER, Dave
 KONGEHL, Helmut F., LT.COL.
 KOON, Cecil L.
 KOROPCHAK, John
 KOSTERMANS, G.S.M.
 KRACH, Fred G.
 KRAUSE, Bill C.
 KREPS, Raymond E.
 KRESS, Jack A.
 KRITZ, Terry E.
 KRISTOFF, Francis T.
 KRONICK, Richard A.
 KRUPKO, Edmund J.
 KRYAK, Gregory D.
 KUMMER, Peter O.
 KUNKLE, Ronald
 KWAK, Solim S.W., Dr.
 KYLEN, Deverle
 LAHTONEN, Jan C.
 LAINE, Pekka
 LANNEN, Wesley L.
 LAPORTE, Francois
 LARSON, Ronal W.
 LAWRENCE, William
 LEANDER, Richard C.
 LEATHAM, Scott D.
 LEATHAM, Scott D.
 LEATHERMAN, Barry, SGT
 LECHNER, Charles A.

Dugway Proving Ground, UT 84022
 Ensign Bickford Aerospace, Simsbury, CT 06070
 Naval Weapons Center, China Lake, CA 93555
 New Mexico Inst. of Mining & Tech, Socorro, NM
 Shielding Tech Inc., Pylesville, MD 21132
 Hercules, Inc., DeSoto, KS 66018-0549
 Naval Civil Engr Lab, Port Hueneme, CA 93003
 Naval Ord Test Unit, Cape Canaveral, FL 32920
 Mason & Hanger-Silas Mason Co., Amarillo, TX
 Maxwell Laboratories, Albq., NM 87106
 HQ AFISC, Norton AFB, CA 92409
 Biazzi S.A., New York 13801
 Talley Defense Systems, Mesa, AZ 85234
 HQ SAC, Offutt AFB, NE 68113
 Seneca Army Depot, Romulus, NY 14541
 Australian Ordnance Council, Australia
 Korea Explosives Co., Seoul, Korea
 Poongsan Corporation, Seoul, Korea
 DCMR, Dallas, TX 75202
 3d Space Supt Wing, Peterson AFB, CO 80914
 Federal Cartridge Company, Anoka, MN 55303
 Detector Electronics Corp., Mpls, MN 55438
 DLA, DCMO, St. Louis, MO 63103
 2721 Mun Maint & Test, Hill AFB, UT 84056
 Olin Corporation, Marion, IL 62959
 Bundesminister der Verteidigung (MOD), FRG
 DoD, DLA, DCMR Atlanta, Marietta, GA 30060
 Olin Corporation, Marion, IL 62959
 Royal Netherlands Army, Netherlands
 Mound Applied Technologies, Miamisburg, FL 45343
 United Technologies, San Diego, CA 92121
 Eastern Space & Msl Ctr, Patrick AFB, FL 32925
 Safety Dept, NWSO, Crane, IN 47522
 USA Depot System Cmd, Chambersburg, PA 17201
 RAAP-Hercules Inc., Radford, VA 24141
 Lockheed Msl & Space Co., Charlestown, IN 29411
 Thiokol Corporation, Huntsville, AL 35816
 Olin Corp., East Alton, IL 62024
 Ernst Basler & Partners, Ltd., Switzerland
 HQ AFOTEC, Kirtland AFB, NM 87117-7001
 USA Ammo Ctr & Sch, Savanna, IL 61074
 2721st Mun Maint & Test, Hill AFB, UT 84056
 Federal Cartridge Company, Anoka, MN 55303
 Technical Research Centre of Finland
 Naval Weapons Station, Concord, CA 94520
 CNES, Toulouse, France
 Electro Magnetic App., Lakewood, CO 80228
 BRL, Aberdeen Proving Ground, MD 21005
 Thiokol Corporation, Marshall, TX 75671-1059
 DCMR, St. Louis, MO 63103
 DPRO Thiokol, Brigham City, UT 84302
 Cmbt Development, Ft. Leonardwood, MO 65473
 USA Toxic & Haz Mat Agency, APG, MD 21010

LEDERER, John M.
 LEE, Edward L.
 LEE, Robert A.
 LEMKE, John C.
 LEWIS, Bud
 LIM, Chee Hiong
 LINCK, Richard P.
 LIND, Larry
 LIPP, Curtis A.
 LISKA, Walter B.
 LITTLE, Lyn
 LOBER, Christine B.
 LONG, EVERETT A.
 LONG, L.J.
 LOOMIS, Richard L.
 LORENZ, Richard A.
 LORGE, Bryan A.
 LOVE, Jim
 LOVETT, David E.
 LOWE, William F.
 LOYD, Robert A.
 LUKUC, Ray
 LURK, Paul W.
 LYNAM, Edmond O.
 LYNCH, Robert D.
 LaHOUD, Paul M.
 Le CHENADEC, Roger
 MADSEN, Niels K.
 MAHER, John J.
 MAHONEY, Patricia L.
 MAIRANTZ, Benjamin Z.
 MAIRSON, William R.
 MANTHEY, James P.
 MARKSON, Ralph
 MARS, Larry
 MARTINEZ, Pat A.
 MASSABKA, Farid
 MATHEWS, Jack, COL
 MATTERN, Steven F., CAPT
 MATTHEWS, Roy A., CAPT
 MAURER, Heinz G.
 MAURITS, William, Dr.
 ME-BAR, Yoav
 MEADOR, Delbert L.
 MEIERAN, Sigmund
 MERRIFIELD, Roy
 MERRILL, Claude
 MESSERICH, Kenneth P.
 MEYER, Bill
 MEYER, Horst
 MEYER, Wallace M.
 MIHALYI, Harry
 MILLER, Miles C.

Weapons Laboratory, Kirtland AFB, NM 87117
 Lawrence Livermore Nat'l Lab, Livermore, CA 94550
 Thiokol, Louisiana Div, Shreveport, LA 71130
 DoD Saf & Occupational Safety, Wash., DC 20301
 Kansas AAP, Parsons, KS 67357
 Lands & Estates Organ, Singapore
 Booker Associates, St. Louis, MO 63101
 Redwood City, CA
 Aerojet Propulsion Co., Sacramento, CA 95813
 Ofc of Proj Mgr for Ammo Logs, Picatinny AR, NJ
 USA Ammo Ctr & Sch, Savanna, IL 61074
 Huntsville, AL 35814
 USN Weapons Ctr, China Lake, CA 93555
 McDonnell Douglas, St. Louis, MO 63166
 Directorate of Distribution, Hill AFB, UT 84056
 Boeing Defense & Space Group, Seattle, WA 98124
 USA Missile Cmd, Redstone Arsenal, AL 35898
 Aerojet Propulsion Div, Sacramento, CA 95813
 Naval Submarine Base, Kings Bay, GA 31547
 AF Armament Laboratory, Eglin AFB, FL 32542
 USA Muns & Chem Cmd, Rock Island, IL 61299
 Olin Corporation, Marion, IL 62959
 USATHAMA, Aberdeen Proving Ground, MD 21010
 Teledyne McCormick Selph, Hollister, CA 95024
 Atlantic Research Corp., Gainesville, VA 22065
 Huntsville Corps of Engrs, Huntsville, AL 35805
 French Defense Ministry, France
 DEMEX Consulting Engrs., Denmark
 Australian Defence Industries, Australia
 Los Alamos Nat'l Lab, Los Alamos, NM 87545
 14. Achi-meir St., Tel Aviv, Israel
 Sandia Nat'l Lab, Albq., NM 87185
 USA Corps of Engrs, Huntsville, AL 35807
 Airborne Research Assocs., Weston, MA 021193
 Sverdrup Tech, Inc, Stennis Space Ctr, MS 39529
 Aerojet, Sacramento, CA 95813
 Sverdrup, Arlington, VA 22209
 Chairman, DoD Explosives Safety Board, Alex, VA
 Wright-Patterson AFB, OH 45433
 2895 Distr Squadron, Robins AFB, GA 31098
 Polaris Msl Fac Atl, Charleston, SC 29408
 DoD Explosives Safety Board, Alex., VA 22331
 Rafael Ballistics Center, Haifa, Israel
 930 TFG/Safety, Grissom AFB, IN 46971
 Pacific Msl Test Ctr, Point Mugu, CA 90462
 Health & Safety Exec, Bootle, Merseyside, England
 Astronautics Lab, Edwards AFB, CA 93523
 AMC Field Safety Acty, Charlestown, IN 47111
 Olin Corporation, Marion, IL 62959
 BWB, Postfach 7360, Koblenz, Germany
 General Dynamics, Ontario, CA 91261
 DCMAO Dallas, Dallas, TX 75250
 USA Chemical Rsch Ctr, APG, MD 21010

MILLER, Stephen J.
 MILLS, John L.
 MISCHLER, Marston R.
 MIXON, Larry G.
 MONTANARO, Paul
 MOORE, Harold D., LT.COL.
 MOORE, K.
 MOORE, Verence D.
 MORAN, Edward P.
 MORCOS, Michael
 MOREAU, Bernard
 MORGAN, G.D.
 MORLAND, Henri C.
 MORONEY, Rick A.
 MORRISON, George E.
 MOSIER, Kent D.
 MOXLEY, Robert
 MULKEY, Robert J.
 MUREAUX, Les
 MURPHY, David J.
 McAFEE, John M.
 McALLISTER, Donald H.
 McCLESKEY, Francis
 McCUBBIN, Melvin J.
 McDONALD, Jack L.
 McELHINNEY, William J., CDR
 McFALL, Larry L.
 McGINNISS, John
 McGRAW, Richard P.
 McHALE, James M.
 McINTYRE, Frederick L.
 McLAIN, John P.
 McNEILL, Robert E.
 McQUEEN, Jerry
 NAPADENSKY, Hyla S.
 NASH, Keith A., MSGT
 NATANI, Kirmach
 NEEDHAM, Charles
 NEFF, Ronald A.
 NETT, Dal M.
 NEWBERN, Robert
 NEWBY, Lewis R.
 NEYRINCK, Ronny G., CDT
 NICHOLSON, Edwin P., CAPT
 NICHOLSON, Tom E.
 NICKERSON, Howard D.
 NOLL, Gary A.
 NORTON, Edward S.
 NORTUNEN, Larry R.
 NOUGUEZ, Bruno M.
 ODENBRING, Tor, LT.COL.
 OLSON, Douglas B.
 OLSON, Eric T.

Universal Propulsion Co., Phoenix, AZ 85027-9801
 LTV Missiles & Electronics, Camden, AR 71701
 Trident Refit Facility, Kings Bay, GA 31547
 Naval Coastal Sys Ctr., Panama City, FL 32407
 Naval Sur Warfare Ctr, Silver Spring, MD 20903
 HQ FORSCOM, Ft. McPherson, GA 30330
 Rockwell International, Downey, CA
 NAV SWC, Silver Spring, MD 20903
 DDESB, Alex., VA 22331
 Pacific Msl Test Ctr, Point Mugu, CA 93041
 SNPE, Paris, France
 McDonnell Douglas, St. Louis, MO 63166
 Aerospatiale, France
 Texas Instruments, Lewisville, TX 75067
 LGW, Langley AFB, VA 23665
 Texas Instruments, Redstone AR, AL 35808
 Kelly AFB, TX
 Mason & Hanger-Silas Mason Co., Amarillo, TX
 S.N.I. Aerospatiale, France
 Lockheed Missile & Space Co., Santa Cruz 95060
 Los Alamos Nat Lab, Los Alamos, NM 87545
 Naval Wpns Station, Seal Beach, CA 90740
 Kilkeary, Scott & Assoc, King George, VA 22485
 Naval Wpns Ctr, China Lake, CA 93555
 DCMAO, San Antonio, TX 78294
 Naval Surface Warfare Ctr, Dahlgren, VA 22448
 HQ, LABCOM, Adelphi, MD 20783
 Naval Surface Weapons Ctr, Dahlgren, VA 22448
 Ensign Bickford Aerospace, Simsbury, CT 06070
 Talley Defense Systems, Joliet, IL 60435
 Sverdrup Tech, Inc, Stennis Space Ctr, MS 39529
 New Mexico Inst. of Mining & Tech, Socorro, NM
 USA Missile Command, Redstone AR, AL 35898
 Motorola, Inc., Scottsdale, AZ 85252
 Napadensky Energetics, Inc., Evanston, IL 60202
 Arnold AFB, TN 37389
 McDonnell Douglas, St. Louis, MO 63146
 Maxwell Laboratories, Albq., NM 87106
 Milan AAP, Milan TN 3835-5000
 USA Cmbt Sys Test Acty, APG, MD 21005
 DoD Explosives Safety Board, Alex., VA 22331
 Sandia Nat'l Lab, Albq., NM 87185
 Belgium Army, Zwyndrecht, Belgium
 Naval Ordnance Station, Indian Head, MD 20640
 Aerojet Electronic Sys Div, Azusa, CA 91702
 Naval Facs Engr Cmd, Alex., VA 22332
 63 Military Airlift Wing, Norton AFB, CA 92409
 UK Ordnance Board, Columbia, MD 21044
 USA Def Ammo Ctr & Sch, Savanna, IL 61074
 SNPE, France
 Forsvarets Materielverk, Karlstad, Sweden
 New Mexico Tech, Socorro, NM 87801
 AMC Field Safety Ofc, Charlestown, IN 47111-9669

OLSON, Leonard S., CAPT
 OLSON, Ransley K.
 OPEL, Mervin C.
 OPSCHOOR, Gerard
 OVERLAY, Larry W.
 PACE, George E.
 PACEWITZ, Gary J.
 PAKULAK, Mary S.
 PAPP, A.G.
 PARHAM, Ken
 PARKES, David A.
 PARSONS, Gary
 PATRICK, Gwyn C.
 PATTESON, Macon G.
 PAZELL, Tom M.
 PELCHAT, Andre J., CAPT
 PELTIER, Michael A.
 PENA, Steven, MSGT
 PEPPERS, Charlene C.
 PEREZ, Anthony L.
 PERRY, Robert B.
 PETERS, Charles R.
 PEYTON, Roger K.
 PHILLIPS, R.W.
 PICKETT, J.W.
 PIPER, Charles J.
 PITTS, Larry R.
 PLUMB, Russell H., MSGT
 POE, Robert S.
 POGUE, George B.
 POLINS, Stan
 PORRITT, Rick J., LT.COL.
 POTTRATZ, Bill
 POWELL, Thomas J., LT.COL.
 PRESCHERN, HORST
 PREVOST, R. John
 PRICE, Paul D.
 PRICE, William A.
 PRUSACZYK
 QUIGLEY, Robert P.
 RAGAN, E. Wayne
 RANKIN, James T.
 RAPP, Mark A.
 REDMAN, Harold
 REED, Jack W.
 REES, Norman, Dr.
 REEVES, Harry
 REITMEYER, Gregory A.
 REYNOLDS, Keith B.
 RICH, Max S.
 RICHARD, Philippe J.
 RICHARDSON, David E.
 RIEDER, William E.

Crane Army Ammo Activity, Crane, IN 47522
 Aerojet ASRM Div, Orangevale, CA 95662-1270
 ICI Americas Inc., Charlestown, IN 47111
 Prins Maurits Laboratory, Netherlands
 Cmbt Sys Test Activity, APG, MD 21005
 AF Regional Civil Engrs, Norton AFB, CA 92409
 NASA DFRF, Edwards, CA 93523
 Naval Weapons Center, China Lake, CA 93555
 Mason & Hanger-Silas Mason Co., Amarillo, TX
 USA Def Ammo Ctr & Sch, Savanna, IL 61074
 Black & Veatch, Kansas City, MO 64114
 Wyle Laboratories, Norco, CA 91760
 USA Test & Eval Cnd, APG, MD 21005
 Naval Surface Weapons Center, Dahlgren, VA 22448
 HQAFISC, Norton AFB, CA 92409
 Nat'l Defense Hqs, Ottawa, Canada
 DCMO Twin Cities, St. Paul, MN 55116
 TAW/SEV, Little Rock, AR 72099
 HQ, AMCCOM, Rock Island, IL 61299
 Day & Zimmermann, Kansas AAP, Parsons, KS 67357
 Prog Mgr for Chemical Demil, APG, MD 21010
 US Armament, Mun & Chem Cnd, Picatinny AR, NJ
 NSWC, Dahlgren, VA 22448
 Sandia National Lab, Livermore, CA 94550
 Olin Corporation, East Alton, IL 62024-1174
 Quantic Industries, Inc., San Carlos, CA 94070
 AF Armament Lab, Eglin AFB, FL 32542-5435
 7AF, SEW, APO San Francisco, CA 96570
 Naval Ordnance Station, Indian Head, MD 20640
 Motorola, Inc., Scottsdale, AZ 85252
 LTV Msl & Electronics, El Paso, TX
 Nat'l Defense Hqs, Ottawa, Canada
 USA Missile Command, Huntsville, AL 35898
 HQUSAFE, Germany
 AVL, Austria
 Southwest Research Inst., San Antonio, TX 78228
 HQAFISC, Norton AFB, CA 92409
 Vitro Corporation, Silver Spring, MD 20906
 Olin Corporation, Marion, IL 62959
 Hercules Aerospace Co., Bacchus, Magna, UT 84044
 2750 ABW/Safety, Wright-Patterson AFB, OH 45433
 Wright Patterson AFB, OH 45433
 Oklahoma City Air Log Ctr, Tinker AFB, OK 73145
 EOD Technology, Oak Ridge, TN 37831
 JWR, Inc., Albuquerque, NM 87108
 MOD UK, Orpington, Kent, England
 New Mexico Inst. of Mining & Tech, Socorro, NM
 Nav Coastal Sys Ctr, Panama City, FL 32407
 Thiokol, Inc., Brigham City, UT 84302
 Thiokol Corporation, Brigham City, UT 84302
 Dimensions, Saint-Aubin, France
 Hercules, Inc., Magna, UT 84044
 AFIC, Wright Patterson AFB, OH 45433

RIEF, George W.
 RIVERS, Douglas A.
 ROBB, David R.
 ROBERTSON, Thomas R.
 ROBINSON, Kim W., CAPT
 ROBINSON, Ralph D.
 ROBSON, William J.
 RODLAND, Harold M.
 ROLLINS, Charles H.
 ROOT, George L.
 ROSE, Warren W.
 ROSENOW, John M.
 ROSS, Boyce L.
 ROUZE, Michel
 ROZINKA, Mike J.
 RYLANDER, J.
 RYTZ, Hansjorg E.
 SANAI, Mehsen
 SANCHEZ, Felipe B.
 SAWYER, Ray B.
 SAYLORS, James A.
 SCARDINO, Philip J.
 SCHAFF, Michele
 SCHAICH, Eberhard, MAJ
 SCHIESEK, Erwin A., LT.COL.
 SCHIRF, Gregory A.
 SCHNEIDER, Bruce A.
 SCHOOLER, James S.
 SCHULTEN, Ernest R.
 SCHUM, Robert R.
 SCHWARTZ, Robert M.
 SEAL, Warren G.
 SEIWELL, Robert S.
 SERENA, Joseph M.
 SEXSTONE, Peter A., COL
 SEYMOUR, Richard B.
 SHANNAN, Joe E.
 RACHEL, Charles K.
 SHEEHAN, John W.
 SHELNUTT, Emily H., Dr.
 SHEPPE, Elizabeth M.
 SHIN, Chang-Soon
 SHIPE, Richard B.
 SHOPHER, Kenneth R.
 SHRIVER, Jerry R.
 SHULTS, Richard H.
 SIEGER, M.L.
 SIERRA, Gabriel
 SILER, Ken A.
 SINAI, Joseph
 SINGH, Ashok K.
 SISK, Wayne E.
 SKOGMAN, David P.

AF Flight Test Ctr, Edward AFB, CA 93523
 3M Corporate Safety Dept., St. Paul, MN 55144
 HQ AFRES, Robins AFB, GA 31098
 Explosives Division, Ottawa, Canada
 Tulsa Air Nat'l Guard, Tulsa, OK 74115
 Defense Nuclear Agency, Albq., NM 87115
 United Technologies, San Jose, CA 95161
 HQ, ATC, Randolph AFB, TX 78150
 United Technologies, San Jose, CA 95161
 Jet Prop. Lab, Edwards Fac, Edwards, CA 93523
 Bristol Aerospace Limited, Winnipeg, Canada
 Sandia National Lab, Livermore, CA 94551
 USA Corps of Engrs, Huntsville, AL 35807
 CNES, Toulouse, France
 Thiokol Corporation, Brigham City, UT 84302
 Northrop Corporation, Perry, GA 31069
 Swiss Fed DoD, Switzerland
 SRI International, Menlo Park, CA 94025
 Naval Surface Wpns Ctr, Dahlgren, VA 22448
 DDESB, Alex., VA 22331-0600
 Bernard Johnson Inc., Houston, TX 77056
 Defense Contract Mgmt Cmri, Kirtland AFB, NM
 Accudyne Corporation, Janesville, WI 53545
 Materialamt der Bundeswehr, W. Germany
 German Army Material Cmd, GE
 Naval Ordnance Station, Indian Head, MD 20640
 New Mexico Engr Rsch Inst., Albq., NM 87131
 Red River Army Depot, Texarkana, TX 75507
 Naval Submarine Base, Kings Bay, GA 31547
 DCMO Twin Cities, St. Paul, MN 55116
 Day & Zimmerman, Phil., PA 19103
 Naval Weapons Ctr, China Lake, CA 93555
 Webb, Murray & Assocs., Johnson Spc Ctr, TX
 USA Corps of Engrs, Huntsville, AL 35807
 Secretary ESTC, London, England
 Martin Marietta, Denver, CO 80201
 Mason & Hanger-Silas Mason Co., Middletown, IA
 Technical Analysis Inc., Huntsville, AL 35816
 Wright-Patterson AFB, OH 45433
 Naval Surf Warfare Ctr, White Oak, MD 21771
 Air National Guard, Andrews AFB, MD 20331
 Poongsan Corporation, Seoul, Korea
 USA Combat Sys Test Acty, APG, MD 21005
 Yucaipa, CA 92399
 Defense Logistics Agency, Sacramento, CA 95852
 Atlantic Research Corp., Gainesville, VA 22065
 McDonnell Douglas, St. Louis, MO 63166
 Union Espanola de Expl, Madrid, Spain
 Def Quality Assur Mgmt Supt Ofc, Marietta, GA
 Israel Military Industries, NY, NY 10022
 CRSS, Station B, Greenville, SC 29606
 USA Toxic & Haz Mat Agency, APG, MD 21010
 AMSMC-SF, Rock Island, IL 61299

SLATTERY, Kerry T.	Washington Univ in St. Louis 63130
SMALL, James W.	101st Ordnance Battalion, Schwaebisch Hall, GE
SMITH, Dennis R.	Martin Marietta, Redstone AR, AL 35808
SMITH, Drexel L.	Wyle Laboratories, Norco, CA 91760
SMITH, Earle L.	HQAFISC, Norton AFB, CA 92409
SMITH, Mark H.	Naval Weapons Station, Concord, CA 94520
SMITH, Matthew J.	USA Ammo Ctr & Sch, Savanna, IL 61074
SMITH, Obie	Central Ammo Mgmt Ofc, Ft. Shafter, HI 96858
SMITH, Samuel L.	Honeywell, Inc., Joliet, IL 60434
SOLEAU, Edward W.	LTV Msl & Electronics Group, Dallas, TX 75265
SOLES, Barry L.	Naval Weapons Sta Earle, Colts Neck, NJ 07722
SONG, So-Young	Agency for Defense Development, Korea
SPERLING, Michael B.	Aerojet-ASRM Div, Iuka, MI 38852
STALL, Linda	Safety Dept, NWSC, Crane, IN 47522
STANCKIEWITZ, Charles	Indiana Army Ammo Plant, Charlestown, IN 47111
STATON, James W.	AFSC/IGFA, Andrews AFB, MD 20335
STEDEM, Donald L.	Allied-Signal Aero Co., Kansas City, MO 64131
STEELE, John A.	AMCFSA, Charlestown, IN 47111
STENSLAND, Per	Norwegian Navy Material Cmd, Norway
STEWART, Edger K.	USA, ARDEC, Picatinny AR, NJ 07806
STILSON, Robert L.	NAVSEACENLANT, Portsmouth, VA 23702
STOREY, Robert	Directorate of Distribution, Hill AFB, UT 84056
STRATMAN, George E.	USAF, Hill AFB, UT 84056
SUEKER, Wayne R.	Honeywell, New Brighton, MN 55112
SUTHERLAND, John D.	Martin Marietta, Denver, CO 80201
SUTTON, Scott M.	Ethyl Corporation, Baton Rouge, LA 70801
SWISDAK, Michael M.	Naval Surface Wpns Ctr, Silver Spring, MD 20903
SYMONDS, Peter C., GROUP CAPT	Ofc of Inspector of Explosives, London, England
SZELOG, John P.	Selfridge ANGB, MI 48045
TANCRETO, James E.	Naval Civil Engr Lab, Port Hueneme, CA 93003
TATOM, Frank B., Dr.	Engineering Analysis, Huntsville, AL 35801
TENBRINK, Wayne A.	Weapons Station Concord, CA 94520
THOMAS, Chester A.	Hughes Aircraft Co., Tucson, AZ 85734
THOMAS, William B.	Thiokol Corp., Huntsville, AL 35815
THOMPSON, Gary B.	Hercules Aerospace Co., Bacchus, Magna, UT 84044
THOMPSON, Kenneth A.	USA Ord Msl & Mun Ctr & Sch, Redstone AR, AL
TIDWELL, Ray W.	Ogden Air Log Ctr, Hill AFB, UT 84056
TINKLER, William	MOD UK, Orpington, Kent, England
TOTZKE, Mark	USAES, DCD, MLSD, Ft. Leonard Wood, MO 65473
TRAMMELL, Steven R.	United Technologies, San Jose, CA
TRIPP, Brian A.	100 AD/SE, Whiteman AFB, MO 65305
TUAN, Chris Y.	Wilfred Baker Engr, Inc., San Antonio, TX 78209
TUOKKO, Seppo S.	Ministry of Defense, Helsinki, Finland
UNDERWOOD, Phil	Olin Corporation, Marion, IL 62959
UTLEY, Patricia T.	Calspan Corp., Arnold AFB, TN 37389
VAIDYANATHAN, H.	Dept Nat'l Def, Ottawa, Canada K1A 0K2
VALDEZ, Denise	Sunflower AAP, DeSoto, KS 66018-0640
VALENTINE, Ronald F.	Robins AFB, GA 31098
VAN NAME, Donald G.	USA Ammo Ctr & Sch, Savanna, IL 61074
VAN RIPER, Edwin E	Safety & Health Phy Ofc, APG, MD 21005
VARACALLI, Nick	Olin Corporation, Marion, IL 62959
VIALI, Charles C., COL	DDESB, Alex., VA 22331
VICKERS,	Australian Defence Industries, Australia

VICKERS, Marvin E.
 VOSTEEN, James R.
 VRETBAD, Bengt E., Dr.
 WAGMAN, James H.
 WALKER, Lee R.
 WALSH, James H.
 WARD, Jerry, Dr.
 WARWICK, B.W.
 WEBER, Michael E.
 WEBSTER, Larry D.
 WEST, Buddy
 WESTERDAHL, Carolyn A.
 WESTON, Albert M.
 WHEELER, Ron H.
 WHITE, Charles A.
 WHITE, Dale A.
 WIJDEMANS, Jan, MAJ
 WILBOURNE, Joseph C.
 WILCOX, Robert G.
 WILKAITIS, Norm
 WILKIE, Lynne
 WILLIAMS, Doyle G.
 WILLIAMS, Earl H.
 WILLIAMSON, George E.
 WILLS, Arthur G.
 WILSON, Ted, CWO
 WINDSOR, Joan C.
 WINGATE, Mark A.
 WINKLE, Billy W.
 WINTLE, Fred L., CAPT
 WOLF, Jack D.
 WOLFF, Vernon E.
 WOODARD, Don
 WOODS, Millicent
 WORRELL, Aurelie A.
 WRIGHT, Terry P.
 WU, Da-Lih
 WUENNENBERG, Thomas C.
 WYSOWSKI, John R., LT.COL.
 YADAVA, Om P.
 YAMAMOTO, Akihiko
 YOUNG, See Wee
 YUHAS, John C.
 YUTMEYER, William P.
 ZAKRZEWSKI, Peter H.
 ZAUGG, mark M.

NAVSEACENPAC, San Diego, CA 92186
 Monroe Electronics, Inc., Lyndonville, NY 14098
 Swedish Fortification Administration, Sweden
 Weapons Lab (AFSC), Kirtland AFB, NM 87117
 AF Communications Cmd, Scott AFB, IL 62225
 Naval Ord Msl Test Sta, White Sands, NM 88002
 DoD Explosives Safety Board, Alex., VA 22331
 Lockheed Msl & Space Co., Sunnyvale, CA 94088
 Atlas Powder Company, Dallas, TX 75248
 DDESB, Alexandria, VA 22331-0600
 AF Development Test Ctr, Eglin AFB, FL 32542
 Army Insensitive Mun Ofc, Picatinny AR, NJ 07806
 Lawrence Livermore Nat'l Lab, Livermore, CA 94550
 SSI Services, Inc., Arnold AFB, TN 37389
 AF Special Oper Cmd, Hulburt Field, FL 32544
 AMSMC-SFS, Rock Island, IL 61299
 Royal Netherlands Air Force, Netherlands
 Naval Ordnance Station, Indian Head, MD 20640
 USA Corps of Engrs, Huntsville, AL 35807
 Olin Corporation, Marion, IL 62959
 McDonnell Douglas, St. Louis, MO 63166
 Louisiana AAP, Shreveport, LA 71130
 USA Corps of Engrs, Huntsville, AL 35805
 Health & Safety Exec, Bootle, Merseyside, England
 USAF HQ 22AF, Travis AFB, CA 94535
 Range Control, MCB, Camp Pendleton, CA 92055
 USA ARDEC, Picatinny Arsenal, NJ 07806
 Olin Corp., Lake City AAP, Indep., MO 64051
 Hercules, Inc., DeSoto, KS 66018-0549
 51 TFW, SF, CA 96366
 Boeing Military, Wichita Br, Kansas 67277
 Hercules, Inc., Wilmington, DE 19894
 Olin Corporation, Marion, IL 62959
 Deputy Assistant Secretary of Defense, Wash, DC
 Crane Army Ammo Activity, Crane, IN 47522
 NSWSES, Port Hueneme, CA 93043
 Bechtel National, San Francisco, CA 94119-3965
 Booker Associates, St. Louis, MO 63101
 HQAFISC, Norton AFB, CA 92409
 Ordnance Factory Board, Govt of India
 Nippon Oil & Fats Co., New York, NY 10166
 Repoulic of Singapore Air Force, Singapore
 Technical Ordnance Inc., Waconia, MN 55387
 AMC FSA, Charlestown, IN 47111-9669
 Def Contract Mgmt Region, St. Louis, MO 63103
 Tooele Army Depot, Tooele, UT 84074